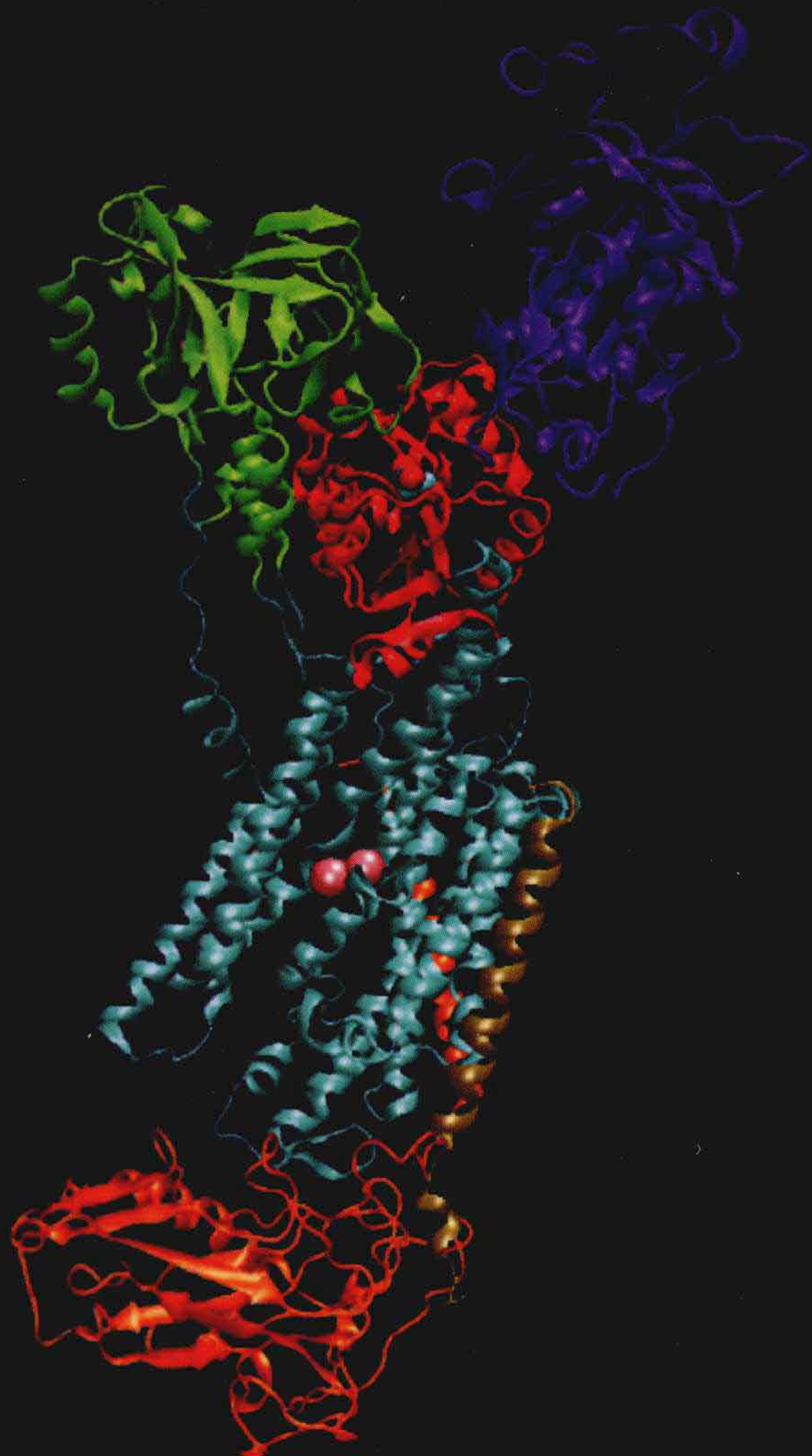
生命科学名著



细胞生理学手册（原书第四版）

——膜生物物理学精要

Cell Physiology Sourcebook:

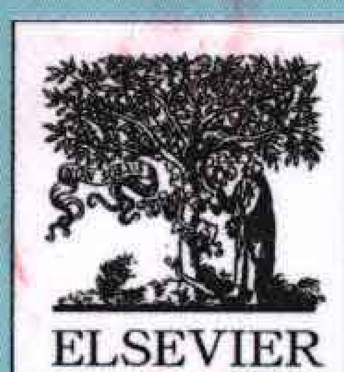
Essentials of Membrane Biophysics

下册

FOURTH EDITION

〔美〕N.斯皮尔莱克斯　主编

张志鸿　导读



原版引进



科学出版社

(Q-3129.0101)

封面设计 / 美光设计

本书的评价

《细胞生理学手册》于1996年（第一版）及1998年（第二版）被美国图书馆协会的期刊“精选”（CHOICE）列入优秀学术书籍的名单。

“细胞生理学领域的权威性书籍，无疑是当今最具综合性有效信息的手册之一。”

— CHOICE

“……一本细胞生理学的核心教科书……，有充分的理由表明拥有这样一本书很有必要，它实现了其客观的卓越性。在信号转导、膜生物学、离子通道、神经与肌细胞生理学等学科内容方面特别强……，它在其领域中是一本精深的教科书……”

— DOODY'S PUBLISHING REVIEWS

“第二版《细胞生理学手册》对学习细胞生理学、细胞生物物理学、电生理学的高年级本科生、研究生以及对众多领域中的生物科学家都非常有用。该书特别适合于引导接受物理科学训练的学生学习细胞生理学、引导生物学背景的学生学习细胞生物物理学。”

— BIOPHYSICAL JOURNAL

《细胞生理学手册》的特点

第四版《细胞生理学手册》提供了内容全面、权威性的信息。它是主要为高年级本科生和研究生编写的教材，也可供研究者做参考。此包含多种学科的出版物为对细胞生理学、膜生物物理学、电生理学和细胞信号感兴趣的科学家、研究者和学生提供了坚实的基础。本书在确立为该领域的一流教材的同时也是经典医学生理学教材的极好补充读物。

主要特色：

- 由多领域的一流研究者撰写
- 清晰、简明及全面地包含从基础概念到进展的细胞生理学所有方面

主要包含的论题：

- 蛋白质的物理化学
- 膜的分子结构与特性
- 膜受体与第二信使
- 离子与非电解质的主动运输
- 离子通道的结构与运转
- 膜兴奋与传播
- 作为毒素、药物与疾病靶的离子通道
- 感觉转导机制
- 突触传递
- 光合作用与生物发光
- 原生动物与细菌的生理学

www.sciencep.com



科学出版中心 生物分社
联系电话：010-64012501
E-mail：lifescience@mail.sciencep.com
网 址：http : // www.lifescience.com.cn



销售分类建议：生物学／生物物理

定价：148.00元

生命科学名著

细胞生理学手册

——膜生物物理学精要（下）

（原书第四版）

Cell Physiology Sourcebook：

Essentials of Membrane Biophysics

（Fourth Edition）

〔美〕·N. 斯皮尔莱克斯　主编

张志鸿　导读

科学出版社

北京

图字：01-2012-5510 号

内 容 简 介

本书内容极其丰富，包含了动物、植物等各种细胞内发生的重要生命事件的分子基础、物理化学的机制、发现的历史渊源、数学上的定量描述、生理学功能、病理变化和疾病的关系，以及近代进展和展望等方面的详细内容和原始文献，具有作为“手册”的重要参考价值。全书分为七个部分，共 52 章 970 页。

本书内容适于作为高等院校和科研单位生理学、生物物理学、细胞生物学、分子生物学、生物化学、医学、药理学等学科研究生及高年级本科生的教材或阅读参考书，从事生命科学研究的工作者或其他交叉学科对生命科学感兴趣的师生和学者也可参考和阅读。

This is an annotated version of
Cell Physiology Sourcebook：Essentials of Membrane Biophysics（Fourth Edition）
Edited by Nicholas Sperelakis

ISBN：978-0-12-387738-3

图书在版编目(CIP)数据

细胞生理学手册：膜生物物理学精要（下）＝Cell physiology sourcebook：essentials of membrane biophysics：第 4 版：英文/(美) 斯皮尔莱克斯（Sperelakis，N.）主编．张志鸿导读．—北京：科学出版社，2013.5

（生命科学名著）

ISBN 978-7-03-037526-1

Ⅰ.①细… Ⅱ.①斯…②张… Ⅲ.①细胞生理学－手册－英文
Ⅳ.①Q25－62

中国版本图书馆 CIP 数据核字（2013）第 105199 号

责任编辑：李　悦／责任印制：钱玉芬
封面设计：美光设计

科学出版社 出版
北京东黄城根北街 16 号
邮政编码：100717
http://www.sciencep.com
源海印刷有限责任公司 印刷
科学出版社发行　各地新华书店经销
*
2013 年 5 月第　一　版　开本：787×1092　1/16
2013 年 5 月第一次印刷　印张：29 1/2
字数：701 000

定价：148.00 元

（如有印装质量问题，我社负责调换）

导　读

张志鸿
（复旦大学生命科学学院，上海 200433；
E-mail：zhzhang@fudan. edu. cn）

细胞是生命的基本单元。单细胞是最简单的生命形式，高等生物则是多细胞的社会，依靠细胞之间在时间、空间上结构与功能的复杂、有序和动态的相互作用网络，展现出各种多姿多态的生命现象。虽然生命形式多种多样，但自然界的生物进化还是赋予所有生命具有共同的特性：都是由同样一些化学分子组成、细胞结构上有类似的组织原理、其行使类似功能的生物大分子往往有高度同源性的结构，更为重要的是这些生命活动都遵循同样的物理学和化学的基本定律。因而，虽然在自然界中它们表现出惊人的生物多样性，但基本的细胞功能，特别是细胞内外的物质交换、遗传规律、能量转换、细胞对内外环境的感受与响应、细胞内的信号转导、细胞间的通讯、细胞内各种内环境的恒定性、细胞运动等重要方面都有着同样的规律和基于类似的结构基础。其中的不少生命过程都是在生物膜（包括细胞表面的质膜和各细胞器上的内膜）的舞台上进行和展现的，本书即以此为出发点，根据这些重要生命活动的基本物理学和物理化学规律进行相当详实的阐述。

本书主编 Nicholas Sperelakis 教授现是美国辛辛那提大学医学院退休荣誉教授，曾长期担任该学院的主任和弗吉尼亚大学生理学教授，主要从事神经与肌肉的电生理学和生物物理学研究。他在膜生物物理学、磷酸化和环核苷酸等多种因子对离子通道的调控、离子通道的发育变化、心肌与平滑肌中兴奋的传播机制等方面开展了不少独创性研究，发表了550 多篇科学论文。2002 年正式退休关闭实验室后，他用电子电路仿真软件 PSpice 继续深入进行研究。Nicholas Sperelakis 教授非常热爱和敬业于教学，他善于用容易理解的方式对学生讲授一些理解困难的概念。他的课程深受学生的欢迎，多次被学校学生评为“最佳讲授”。

本书的第一版出版于 1995 年，以后随着“细胞生理学”领域研究的快速发展以及新概念与成果的不断出现，至 2001 年又改版了 2 次。本书多年来已成为不少学校研究生和高年级本科生的教材以及生理学研究工作者经常查阅的范本。本书第四版则是 Nicholas Sperelakis 教授花费了一年半时间全身心集中编著而成。细胞生理学涵盖的内容极广，是我们了解“生命逻辑”、整合及系统生理学等方面的基础。这样一本巨著仅靠几位作者是难以完成的，因此 Nicholas Sperelakis 教授还邀请了其他 63 位具有不同专长的国际一流学者共同撰写了第四版《细胞生理学手册》。

本书内容极其丰富，包含了动物、植物等各种细胞内发生的重要生命事件的分子基础、物理化学的机制、发现的历史渊源、数学上的定量描述、生理学功能、病理变化和疾病的关系，以及近代进展和展望等方面的详细内容和原始文献，具有作为“手册”的重要参考价值。全书分为七个部分，共 52 章 970 页，各部分内容的简介如下。

第一部分　生物化学、代谢、第二信使与超微结构　根据生理溶液的物理化学特性

（热力学、化学平衡、反应动力学、运输过程、表面现象、分子结构与波谱学等），阐明活细胞中水分子的三种结构与功能、水与离子的相互作用、离子间的相互作用、溶质运输及膜电位等；蛋白质的分子结构、测定技术、结构与功能的关系；生物膜基本结构研究的历史沿革、膜脂质与膜蛋白、细胞膜的流动镶嵌模型、膜上脂质与蛋白质的相互作用、脂筏的膜微区结构、平面脂质双分子层膜上各种离子载体对离子选择性的通透；用多种光镜和电子显微镜技术获得的各种细胞器的超微结构；细胞内信号转导网络的普遍原理、19 种主要通过膜上 G 蛋白偶联受体和受体酪氨酸激酶介导的细胞内信号途径、调节生理学过程的主要几种信号途径；小分子化学介体（Ca^{2+}、cAMP、cGMP、DAG、IP_3等）的第二信使作用、质膜及细胞内膜上的膜蛋白（离子通道、运输交换体、离子泵）对细胞内 Ca^{2+} 的调节、Ca^{2+} 信号的产生、Ca^{2+} 主要通过细胞内三种分子（钙调蛋白、钙结合蛋白、蛋白激酶 C）的介导机制进行信号转导。

第二部分　膜蛋白、运输生理学、泵与交换体　物质跨膜扩散与通透的物理化学；决定细胞内离子浓度的主要因子（Na^+-K^+偶联泵、Ca^{2+}-Na^+交换反应、Ca^{2+}泵）、细胞膜的等效电路分析、细胞静息膜电位的起源及定量描述（Goldman-Hodgkin-Katz 恒场方程、弦电导方程）；细胞内不通透性荷电大分子导致的跨膜 Gibbs-Donnan 平衡电位；膜上载体蛋白介导的运输（易化扩散、协同运输与逆向运输）及其热力学、动力学模型分析；跨膜主动运输离子泵（Na^+、K^+-ATPase、Ca^{2+}-ATPase、H^+、K^+-ATPase 等）的结构及其运输机制；膜上 Na^+-Ca^{2+}交换体的结构、功能、系统发育及离子交换的乒乓机制；水跨膜通透及细胞内环境的恒定性（氯离子的调节、细胞容积的调节、细胞内 pH 的调节）。

第三部分　膜兴奋与离子通道　神经纤维、骨骼肌纤维等的生物电缆特性、动作电位通过膜上局部回路电流方式的快速传播；神经、肌肉和内分泌细胞的膜兴奋性；动作电位的产生机制及其特性、Hodgkin-Huxley 分析、膜片钳技术（常规膜片钳方法、自动膜片钳系统）；通过生物化学纯化方法、重组 DNA 技术、突变技术、X 射线晶体学等分子结构的测定技术，详细研究电压门控离子通道的结构及其功能；可兴奋细胞中的电突触、间隙连接的结构与特性；细胞膜上离子通道的各种调节机制：环核苷酸依赖性磷酸化的调节、GTP 结合蛋白的调节、与细胞骨架相互作用的调节；发育过程中离子通道的类型、数目和动力学特性的改变；众多离子通道呈现的机械敏感性。

第四部分　作为毒素、药物与遗传疾病靶的离子通道　用毒素分子探究不同组织中的特异性离子通道异构体、用行为分析确认可能有神经活性的新毒素；毒素分子和通道蛋白的相互作用；靶向 2 种心脏离子通道（电压门控 Ca^{2+}离子通道和电压门控 Na^+离子通道）的分子药理学；基于离子通道分子结构设计的药物分子能特异性地和通道蛋白中关键的位点结合，从而起到对离子通道功能调节的作用；几种离子运输异常的遗传性疾病（家族性偏瘫偏头痛、囊性纤维化、长 QT 综合征、肌强直与骨骼肌周期性麻痹、恶性高热、利德尔综合征、巴特综合征）、基因突变对蛋白质结构与功能的影响、减轻或治愈病人症状的治疗方法。

第五部分　突触传递与感觉转导　神经递质配体（乙酰胆碱、谷氨酸、GABA、甘氨酸等）门控及细胞内配体（Ca^{2+}、环核苷酸、ATP、IP_3等）门控的 2 大类配体门控离子通道；配体门控离子通道的分子结构及三个基本特性：门控、电导及离子选择性通透；化

学突触的结构与功能、突触整合及放大、突触传递的调节；肽激素和神经递质分泌过程中的“兴奋一分泌偶联”、此过程中细胞骨架与跨膜信号的相互作用；依靠“刺激一响应偶联”，代谢感觉细胞中特化细胞内受体能感受循环代谢原料水平、代谢废物水平、细胞周围的离子组成、器官中张力等的变化，其中不少是通过 K^+ 通道的协调实施的；环核苷酸（cGMP 或 cAMP）门控离子通道在心脏起搏、视觉、嗅觉以及脑中突触可塑性等重要生理过程中起重要作用；一些感觉（电、机械力、盐觉、酸觉）受体是膜上的离子通道，另一些感觉（化学、光）则间接地通过特化的受体蛋白作用于离子通道；声转导与视觉转导；红外线感觉器官；通过受体系统动物有探测电场和磁场的能力。

第六部分　肌肉与其他收缩系统　骨骼肌和平滑肌细胞膜上离子通道的不同类型和不一样的兴奋性；心脏动作电位的产生、窦房结处起搏细胞的自发去极化；骨骼肌中兴奋一收缩偶联、T 管上的二氢吡啶受体（DHPR）和肌质网膜上雷诺定受体（RyR）之间的相互作用、三联体处 DHPR 四聚体的胞质段和 RyR1 四聚体物理相互作用以及相临 RyR1 彼此之间的协同作用、兴奋一收缩偶联的调节机制；肌肉收缩的滑动肌丝理论和横桥理论、肌肉能力学；非肌肉运动系统（鞭毛、纤毛、基于肌动蛋白和基于中心体蛋白）的运动、细胞迁移和黏着、生物弹簧；电鱼的电细胞中特化的膜蛋白不对称分布造成兴奋时的跨细胞不对称电流，这是电鱼的电器官产生强电发射的基础。

第七部分　原生动物与细菌　原生生物的生理学多样性、分子多样性、细胞器多样性、细胞多样性；一些未知功能的结构；原核生物细胞学、细菌细胞的能力学（底物水平磷酸化和化学渗透偶联）、细菌细胞中的物质运输与代谢策略、细菌对环境的响应及其机制、细菌致病的生理学。

第八部分　特化过程：光合作用与生物发光　光合细菌反应中心的组成及分子排列、反应中心的电子传递、光合作用的进化、叶绿体及碳同化的生物化学、叶绿体中光驱动的电子传递和质子跨膜运输、化学渗透假说及 ATP 的合成、光合作用的调节；生物发光的酶促机理、荧光素与萤光素酶、生物发光的意义（防御、进攻与通讯）、生物发光的调节机制。

本书内容的特点是：①以“手册”的要求，简明、全面地阐明了细胞内发生的重要生理学事件，介绍了其历史发展、近代进展和研究展望，同时对一些重要的方法学也进行了详细介绍。在知识水平上处于当前学科的最前沿；②侧重从膜生物物理学的角度、结构与功能的关系、仿真和数学定量等方面分析；③大多数章节开篇都有摘要，对公式和方程式有详细的由来说明、推导和演算，这些都大大方便了读者学习和理解；④主编 Nicholas Sperelakis 教授有长期教学的经验、本书的各撰写人也都是本学科相关领域的国际一流专家，经过四版修订后本书更趋完善。

目前，国际上已有几本在分子水平上介绍细胞内各种生命活动及其机制的细胞分子生物学教科书被广泛采用并得到一致的好评，它们主要是将近年来分子生物学、分子遗传学、结构生物学等学科迅猛发展取得的成果应用于阐述细胞生物学中的分子事件。本书则主要依据物理学和物理化学的概念和理论，从生物膜的舞台展示和分析分子水平上整个细胞全局的生理功能，其着眼点已从溶液中发生的生物化学变化拓展到一个活的生命机体。因此，在这个意义上本书和其他细胞分子生物学教科书在内容上能很好地互补和相互参

考。正是本书的这种有别于传统生理学和其他细胞分子生物学的新颖特点，自 1995 年第一版发行以来很快得到学术界和教育界的好评，次年即被美国图书馆协会评列为优秀学术教科书。时隔仅三年后的第二版几近一半的内容又得到了更新和补充，可见主编和撰写人的重视和努力。更令人赞叹的是当 Nicholas Sperelakis 教授 80 岁高龄时仍为了满足教学的需要，和出版社一起广泛听取社会的反馈意见和建议完成了这本第四版。在新一版中内容增加了许多重要的新材料，大多数章节进行了全面的修订，删除了一些在其他细胞生物学等教科书中常见的重复内容，各个章节的组织机构更为统一，同时为易于高年级大学本科生的理解而在正文中略微降低了水平（一些理解难度较大的热力学分析、重要方程的推导等内容放在相应章节后的附录中）。这些改进使得本书更加完善，特点更加突出。

本书内容适于作为高等院校和科研单位生理学、生物物理学、细胞生物学、分子生物学、生物化学、医学、药理学等学科研究生及高年级本科生的教材或阅读参考书，从事生命科学研究的工作者或其他交叉学科对生命科学感兴趣的师生和学者也可参考和阅读。

献　辞

谨以本书献给地球及所有为拯救与保护环境，为使海洋、湖泊、河流、饮用水、空气及土壤免遭污染，为保护农田，为稳定世界人口，为保护野生生命，为保护动物生存权，以及为全球人权奋斗而孜孜不倦工作的机构。我也要感谢我的家庭给予的挚爱和支持，他们是我的夫人 Dolores，子女 Mark Demitri（已亡故）、Christine M.、Sophia A.、Thomas A.、Anthony J.，儿媳 Sherri，孙辈 Demetra、Gregory、Nina-Nicole。特别要感谢克利夫兰诊所的小儿科主任医学博士 David Magnuson 的贡献、技艺、智慧及博爱。非常感谢！

纪　　念

Hugo Gonzalez-Serratos 博士于 2011 年 4 月 1 日逝世。Hugo 是位于巴尔的摩的马里兰大学生理学教授。他于 1960 年中期在伦敦大学学院是诺贝尔奖获得者 Andrew F. Huxley 教授的研究生。Gonzalez-Serratos 博士在肌肉生理学领域是公认的顶级科学家。我们大家都将永远怀念他。Gonzalez-Serratos 教授是本书的一名撰写人，永远缅怀他！

第一版序言

承蒙好意，我的朋友 Nicholas Sperelakis 的这本出色的书和本人的《普通生理学教材》(*A Textbook of General Physiology*) 很相近。在本人的书第一版的前言中，我表达了希望能和 Bayliss 的《普通生理学原理》(*Principles of General Physiology*) 相比较的愿望。本书的组织和部分撰写都是由像 William Bayliss 爵士和我一样与伦敦大学学院(Sperelakis 教授在此度过一年学术休假) 有关联的学者完成的，因此若要做比较的话还是非常恰当的。我非常高兴地回忆起在伦敦大学学院初次遇见 Nicholas 时的情景，我还记得，我们讨论了关于他在眼睛跨晶状体电位方面的开拓性研究。

和内容不相关的是本书有着不一样的书名，我想这是因为“一般”与“普通”生理学之间的差别已变得界限模糊，以至需要更合适的书名。在本人所著教科书第一版的前言中，我提出普通生理学的定义应为：研究活体根据物理学和化学定律做出的即时反应。之后，我担忧该定义过于狭窄，于是提出可用“研究所有生命形式的共同特性”来取代。但无论我们选择何种定义，对我来说相当满意的是，实质上 Nicholas 这本新书的各部分标题都和我自己的书上基本一致。

如果让我进一步追忆，我经常怀疑一名积极从事研究的科学家如何能撰写这样一本内容广泛的新书。自第二次世界大战结束后 2 年我才开始写书的，此后有好几年（在英国长达 10 年）很少见到有原创性学术生理学和新研究结果的发表。这样，才有可能浏览相当长时期的原始文献，而不至于淹没在快速接连出现的新发现中，否则我的任务几乎是不可能完成的，其命运就像西西弗斯（古时希腊的暴君——译者注）一样。今天，这种任务更加难以完成，所以，我非常惊叹 Nicholas 只和几位合作者就写出了这本宏伟的书。

Hugh Davson

1995 年

第二版序言

在《细胞生理学手册》第一版序言中，Hugh Davson 认定该书与他本人众所周知、被高度赞誉的《普通生理学教材》为一个系列。仍由 Nicholas Sperelakis 主编的《细胞生理学手册》第二版继续着同样的传统。虽然第一版由于其内容的深度和广度受到了细胞生理学界的热烈欢迎，但自出版以来在此快速发展的领域出现了很多重要的进展。通过修订论题以及在第一版的所有部分中加入一些章节，第二版涉及了这些新进展。这些在各个部分加入的新论题包括：脂质结构、线粒体生理学、细胞对激素的响应、红细胞运输、神经细胞生理学、离子通道的发育变化、声转导、兴奋一收缩偶联、电板细胞。此外，新版还很有价值地增加了两部分新内容，其一是“原生动物与细菌”，内含两章有关这些有机体的生理学；另一部分是“细胞分裂与细胞凋亡”，包含的章节为细胞分裂的调节、癌细胞、细胞凋亡、电离辐射效应。第二版中这些大的修改及新材料的补充将本书提升到一个新的水平。

在生物学中具有重要地位的细胞生理学产生于许多更为传统的领域，因而其文献也涉及广泛。《细胞生理学手册》的重要价值在于它把该领域中内容丰富的诸种现代章节聚集在一起，各章都呈现统一的表现形式和写作水平，由此再加上内容清晰的表达，使得本书非常适于作为高年级学生或研究生水平的细胞生理学课程教材。第二版中更为广泛的内容也使它被选作为细胞生物物理学、膜生物学及生物医学工程等课程的教材很有吸引力，同样本书也可以作为教材用于离子通道结构及生理学的导论课程。

我非常高兴和荣幸应我同事 Nicholas Sperelakis 之邀写此《细胞生理学手册》第二版序言。本书清晰地给出了优秀的新标准。

Thomas E. Thompson

1997 年

第三版序言

当 Nicholas Sperelakis 诚邀我写此序言之时，我曾怀疑我是否能跟随 Hugh Davson 的脚步。我在伦敦大学学院学习生理学时正值他的不朽著作《普通生理学教材》一书出版之时。伦敦大学学院是那时身为一个学生的非凡之地。这不仅是因为 Hugh Davson 打下了他那特别的学科奠基石，而且也因为 Leonard Bayliss 那时也正在修订他父亲的著名《普通生理学原理》一书。这些书使我确信自己能成为生理学的研究学者，而细胞生理学是入门之地。同时，Davson 和 Bayliss 还担负着吸引医学学科的学生对生理学研究引起兴趣的责任。之后，我记得在成为伦敦大学学院的青年讲师时我曾问过 Hugh Davson 为何他未经常给学生讲授。他简单地作了这样的回答："Denis，我已将所有的都写下来了。告诉他们去阅读!"事实上也正是这句话唤起我阅读该书的兴趣。那本书现在仍在我的藏书室里，并且保存很好，还经常查阅。

本书亦将成为新一代生理学家经常查阅的范本，这将是对 Nicholas Sperelakis 和他同事们的工作的最大赞誉。新一代生理学家将踏入这门令人激动的学科，因为细胞生理学是我们了解整合与系统生理学所有方面的基础。因而，对所有想渴望了解终究何为"生理学"名词含意和根源的"生命逻辑"的我们来说，本书将是必不可少的资料源。当然，生命没有单一的"逻辑"。将一些其本质已被发现、公认的物理化学机制相互结合及交叉地用于阐明即使形成最简单细胞功能的各种缠绞在一起的过程时，我们惊奇地发现自然界的分子机制经常反复地在不同场合重现。基因密码能将与生命特性紧密相关的逻辑代代相传，因此我们称这种创新策略为"基因舞蹈"。逻辑是生理学的而非遗传学的。分子生理学家 Sydney Brenner 最近的文章（发表于诺华公司的题为"生物学中还原论的局限性"的学术讨论会）对此简明地阐述为："基因只是赋予它们编码蛋白质的特有性质，而系统的任何一种整合特性必须是它们之间的相互作用'计算'出来的。"我们正是认同了这样的观点：了解这些相互作用足以使生理学上升为能解决所遇到各种问题的定量分析科学。Brenner 意味深长地继续评论：这为仿真分析提供了框架。仿真实质上也已成为分析的一种必要工具，这是我们科学已走向成熟的标志。

这也是细胞生理学的范围现在更为广泛的标志。内容的广度是本书最大亮点之一，各个章节包含绝大多数重要的分子和细胞系统，因而它完全和其"手册"的书名相吻合。

Denis Noble

第四版序言

我很高兴为《细胞生理学手册》第四版写序言。Hugh Davson 教授在他的不朽著作《普通生理学教材》第四版后不再继续改版。可能，他意识到生理学的知识已变得太广，再要像以前那样单靠他一个人撰写出涵盖所有方面的受高度赞誉的教科书已不太可能了。

那么，什么原因使 Nicholas Sperelakis 教授能后继 Davson 写此教材巨著呢？他决定邀请更多的专家，这些人允诺与他合作，因为他们十分敬重他在细胞生理学领域中做出的重要贡献。虽然 2002 年 Sperelakis 教授关闭了实验室正式退休，但他还是和辛辛那提大学电子和计算机工程系的 L. Ramasamy 博士合作继续发表论文。Sperelakis 教授甚至花时间熟悉了 PSpice 中的技术，这是一种用以电路设计和分析的电子工程软件程序，其中的一些电学参量（如电阻、电容等）可用来代表生理学的参数。他在学习这一新方法时非常兴奋，并用 PSpice 仿真主要在《理论生物学和医学模型及生物医学工程》在线刊物上发表了约 10 篇论文。因第一篇论文概述了主要的概念，这里我仅列出这一篇完整的文献：N. Sperelakis and L. Ramasamy，*Propagation in Cardiac Muscle and Smooth Muscle Based on Electric Field Transmission at Cell Junctions：An Analysis by PSpice*. IEEE—EMB 21，177—190，2002。

Nicholas Sperelakis 教授在 20 世纪 60 年代有一些较有争论的研究发现。1977 年他与合作者数学家 James E. Mann 共同报道：心肌细胞之间闰盘的狭窄缝隙中产生的强电场能使兴奋从心肌中的一个细胞传递至下一个。由此，他们认为心肌中的兴奋传播可不必需要任何心肌细胞之间相连的间隙连接通道的参与。他们论证闰盘膜上快速 Na^{+} 通道的密度要大于表面肌纤维膜上的，这表明闰盘处的兴奋性同样地较大。我很高兴发现 Sperelakis 教授的电场假说已不再是孤立的，因为该假说已独立地被日本学者的论文所证实（K. Tsumoto，T. Ashihara，R. Haraguchi，K. Nagazawa，and Y. Kurachi，*Role of Subcellular Na Channel Distributions in the Mechanism of Cardiac Conduction*. Biophysical Journal 100，554—563，2011）。

本书第三版充实了有关细胞生理学和膜生物物理学领域各方面的重要信息。最为突出的是有多位在本人专长领域（收缩机制及兴奋—收缩偶联）中的著名专家的参与，这给我很深的印象。自《细胞生理学手册》第一版以来，以后的几个版本中接连有新的撰写人加入，我相信第四版亦是如此。我总是非常高兴接到 Nicholas Sperelakis 教授的电话，他是如此兴奋于研究、如此激动于发现。这种热忱也正是我们如此敬重他的一个原因。可能也正是这种热忱，他的妻子 Dolores 形容他仍似他们 51 年前结婚时那样的年轻和充满智慧。按弗吉尼亚医学院主任 Diomedes Logothetis 教授的说法，非常出色的学生是被生理学“病毒”过度兴奋的。因而，我想这也同样发生在如 Sperelakis 教授这样的成功科学家

身上。

当我写此序言之时，Nicholas Sperelakis 教授正在庆祝他的 81 岁生日。值此特殊的周年纪念日，许多希腊人会高喊“chronia polla”，它可不严格地翻译为“许多许多年”或“许多快乐再来”。我们不仅向 Sperelakis 个人，同时也为他的新版《细胞生理学手册》祝福。

Alexandre Fabiato

里士满，弗吉尼亚州

2011 年 3 月 8 日

第四版前言

从前，一位 80 岁退休的大学教授正过着安静和隐居的生活。然而，2010 年春天的某一天，突然，Academic Press 的高级策划 Janice Audet 联系他，她说许多学院仍使用我们第三版的“细胞生理学手册”作为他们细胞生理学课程的教科书，即使此第三版出版的年份（2001 年）已久。

事实上，我已意识到第三版已被许多学院采用。大约 2 年前，一名佐治亚州立大学的研究生和我联系，告知他们将我的书作为他们细胞生理学课程的教材，然而他买不到新书，因为该书已不再印刷。他请求我能把本人的那本寄给他，他允诺会很好保护并在课程结束时返回给我。他甚至提出驱车到辛辛那提我的家来取。这位学生显然对该书非常渴望，因而就此问题我和我之前的编辑 Noelle Gracy 通了话。她安排了使用该教材的电子版作为替代品。问题解决了！

Janice 想知道我是否对出第四版感兴趣。在我给她确切回复之前我请她在全国范围内向若干位课程负责人调查一下他们是否喜爱或不喜爱该书的第三版，理由是什么。从反馈来看，一致的意见是我们的书从总体上来说对于修读细胞生理学课程的低年级的研究生（或高年级大学本科生）来说水平过高；另一些建议是我们应该剔除前三版书中详述的有关细胞生物学的章节/论题，如细胞分裂、细胞凋亡等；我们应该采用彩图；应当在每一章加一个摘要的小节；虽然完成起来不易，但我们还是应当将这么多作者撰写的各章在格式上更趋一致。

我同意进行第四版的工作，重点集中在将这些建议采纳进新版。这一版的一些变化包括：删除约 14 章、合并几章，同时请撰写人将他们分担的章节内容定在研究生水平。新增了约 10 位新的撰写人负责一些专门的学科领域。我相信，最后定下的这些撰写人都是顶级的，我非常感谢他们的参与。

此项目需要我付出极大的努力，而且是在健康状况不是很好之时。那么我为何同意呢？是为了财富或金钱？绝对不是！那是微乎其微的。是为了名声或赞誉？不，现在要从这方面得益我已太老了。况且，我已主编了该书的三个版本。是对教学的奉献？是的，正是如此！我已将毕生奉献给教学，我相信我具有独到的能力可以将晦涩难懂的概念以容易理解的方式讲授出来。例如，我在伊利诺斯大学的学生时代，我们四名学生在一起学习准备隔天的遗传学考试。我解答了小组中提出的诸多问题，其中一位同学当时说：“Nick，你可以当这门课的老师了。”在我的教学生涯中，我也多次因最佳讲授被辛辛那提大学生理学系的研究生授予“金苹果”奖。

还有一个值得提及的例子。Michael Palmer 是一位医学奥秘畅销书的作者，在他 2009 年发行的《二次诊断》小说中使用了我的姓。我的儿子 Thomas 问 Palmer 博士怎么会起“Sperelakis”的姓？要知道这在希腊后裔中它是非常少见的。Palmer 博士的回答是：1960 年代中期在他还是凯斯西储大学的一名医学学生时，他选读了我的神经与肌肉电生理学的课程。他说我是他上过的所有课程中最喜欢的基础科学教师，当时他们给我起了“spike”（神经动作电位的术语）的绰号。你能否相信经过约 45 年后 Palmer 博士仍记得我以及我

的绰号？奉献于教学！对此确有些不可思议，因为我自 10 岁至今有严重的口吃（虽然现在已轻得多）。

在本书第一版出版之前，我意识到在细胞生理学和膜生物物理学领域确实需要一本好的、权威性的教材。这样一本大学科范围的书要像我的朋友 Hugh Davson 那样单靠一人撰写的时代已过去。一本权威性教材要涵盖众多的学科专长，看来它只能由聚集一群分别涉及各个领域的专家的多作者撰写，在所有四个版本中我们都遵循这一原则。本教材的第一版、第二版及第三版分别出版于 1995 年、1998 年和 2001 年。第一版和第二版因其优秀被美国图书馆协会授予“精选奖”。

伦敦大学学院的 Hugh Davson 写了第一版的序言。自他的《普通生理学教材》出版后 Davson 教授很有名，这本书多年来确实是所有研究生的“圣经”。我初次遇见 Hugh 是 1965～1966 年我在伦敦大学学院度学术休假时。他是一位迷人的家伙，我们间建立了亲近的友谊。那个时候，伦敦大学学院是非常合适之地。诺贝尔奖获得者 A. F. Huxley 是生理学系的主任，之后的诺贝尔奖获得者 Bernard Katz 是生物物理学系的主任。诺贝尔奖获得者 A. V. Hill 仍每周 1～2 次来到他在生物物理学系的办公室，他那时已 90 岁了！简直难以相信！顺便提及，伦敦大学学院也是我初次和本书的一位撰写人 Hugo Gonzalez-Serratos 相识之地。

Thomas E. Thompson 撰写了第二版的序言。他是我在弗吉尼亚大学工作时的生物化学系主任。他在平面及球形脂质双分子层膜领域是位一流的研究者。Tom 也是位出色的老师，我曾请他参与我的研究生课程。他曾任生物物理学会的主席。

牛津大学的 Denis Noble 撰写了第三版的序言。Denis 是心脏电生理学领域的一流研究者和理论家。一次，他请我在牛津举行的会议上作报告，诺贝尔奖获得者 Alan Hodgkin 爵士主持了那次分会。那时我双腿一直在打颤！

我决定请我长期的老友弗吉尼亚医学院的 Alexandre Fabiato 教授写此第四版的序言。Alex 是一位在心肌领域杰出的科学家。他在钙致钙释放机制上的研究非常有名，经常被引用。1989 年他获得了声誉很高的美国心脏协会研究成就奖。他是在法国接受培养成为一名心脏病学家的，是 Edouard Coraboeuf 教授（法国，奥赛，巴黎大学）和 Silvio Weidmann 教授（瑞士，伯尔尼大学）的研究生，这二位导师都是心肌生理学领域的一流开拓者和巨匠。我很自豪和高兴，Alex 允诺写序言。

在准备本书的道路上不是没有一些大的颠簸的，有时似乎是难以克服的路障。对教学的奉献以及人们对本书的渴望，鼓舞着我去完成它。而且，我也感到这是一种对诸位撰写人的强烈责任心，一些撰写人在本修订版之初业已花费了时间和精力。再一次，我不知如何来强调我对他们努力的赞颂，以及我是多么自豪他们能参与本书的撰写。我们全体共同希望本教科书能深受欢迎、非常成功。

Nicholas Sperelakis

2011 年 5 月

Dedication

This book is dedicated to Planet Earth and to all those organizations that are working tirelessly to save and protect the environment, to stop pollution of our oceans, lakes, rivers, drinking water, air, and soil, to preserve the farmlands, to stabilize world population, to protect and preserve wildlife, to promote animal welfare, and to fight for human rights around the globe.

I also want to acknowledge the love and support of my family: my wife Dolores and children Mark Demitri (deceased), Christine M., Sophia A., Thomas A., and Anthony J., daughter-in-law Sherri, and grandchildren Demetra, Gregory and Nina-Nicole.

A special thanks to David Magnuson, M.D., Chairman of Pediatric Surgery at Cleveland Clinic, for his great dedication, skills, wisdom and humanity. Efharisto para poli, aka "Εύχαριστω παρά πολύ".

Contents

Section III
Membrane Excitability and Ion Channels

Section IV
Ion Channels as Targets for Toxins, Drugs, and Genetic Diseases

Section V
Synaptic Transmission and Sensory Transduction

In Memoriam

Dr Hugo Gonzalez-Serratos passed away on April 1, 2011. Hugo was Professor of Physiology at the University of Maryland in Baltimore. He was a graduate student of Professor Andrew F. Huxley, Nobel laureate, at University College London in the mid-1960s. Dr Gonzalez-Serratos achieved great recognition as a top scientist in the field of muscle physiology. He will be greatly missed by all of us. Professor Gonzalez-Serratos was a contributing author to this book. May his memory be eternal!

Contributors

Francisco J. Alvarez-Leefmans MD, PhD, Professor, Department of Pharmacology and Toxicology, Boonshoft School of Medicine, Wright State University, Dayton, Ohio, USA

Clive M. Baumgarten, Professor of Physiology and Biophysics, Biomedical Engineering and Medicine (Cardiology), School of Medicine, Virginia Commonwealth University, Richmond

Kenneth M. Blumenthal, Professor and Chairman, SUNY Department of Biochemistry, School of Medicine and Biomedical Sciences, Buffalo, New York, USA

John H.B. Bridge, Research Professor of Medicine, Division of Cardiology, University of Utah Health Sciences Center, Nora Eccles Harrison Cardiovascular Research and Training Institute, University of Utah, CVRTI, Salt Lake City, Utah, USA

Bruce A. Carlson, Washington University, St Louis, Missouri, USA

Laura Conforti, Department of Internal Medicine, University of Cincinnati, Cincinnati, Ohio, USA

John R. Dedman, Professor and Ohio Eminent Scholar, Department of Cancer & Cell Biology, Department of Molecular and Cell Biology, University of Cincinnati, Cincinnati, Ohio, USA

Neil D. Detweiler, Department of Pharmacology and Toxicology, University of Arkansas for Medical Sciences, Little Rock, Arkansas, USA

Istvan Edes, Institute of Cardiology, University of Debrecen, Debrecen, Hungary

Robert A. Farley PhD, Professor Physiology and Biophysics, Biochemistry and Molecular Biology, Departments of Physiology and Biophysics, and Biochemistry and Molecular Biology, Keck School of Medicine, University of Southern California, Los Angeles, California, USA

Joseph J. Feher PhD, Professor of Physiology and Biophysics, School of Medicine, Virginia Commonwealth University, Richmond, Virginia, USA

Darrell Fleischman, Adjunct Associate Professor, Department of Biochemistry and Molecular Biology, Boonshoft School of Medicine, Wright State University, Dayton, Ohio, USA

Michael S. Forbes Ph.D., Department of Pediatrics, University of Virginia School of Medicine, Charlottesville, Virginia, USA

Kenneth W. Foster, Professor, Physics Department, Syracuse University, Syracuse, New York, USA

Jeffrey C. Freedman, Associate Professor, Neuroscience and Physiology, SUNY Upstate Medical University, Syracuse, New York, USA

Andrew S. French, Professor of Physiology and Biophysics, Department of Physiology and Biophysics, Halifax, Nova Scotia, Canada

Nicole Gallo-Payet, Professor and Research Chair of the Faculty of Medicine and Health Sciences, Departments of Endocrinology, and Medicine, University of Sherbrooke, Sherbrooke, Quebec, Canada

Hugo Gonzalez-Serratos, Professor, Physiology, University of Maryland, School of Medicine, Baltimore, Maryland, USA

Anthony L. Gotter, Division of Human Genetics, The Children's Hospital of Philadelphia and the Joseph Stokes Jr Research Institute, Philadelphia, Pennsylvania, USA

Michael S. Grace, Associate Professor, Biological Sciences Department, College of Science, Florida Institute of Technology, Melbourne, Florida, USA

Steven M. Grassl, Associate Professor, Pharmacology, State University of NY Upstate Medical University, Syracuse, New York, USA

Dennis W. Grogan, Professor, Department of Biological Sciences, University, College of Arts and Sciences, University of Cincinnati, Cincinnati, Ohio, USA

Judith Heiny, Associate Professor, Department of Molecular and Cellular Physiology, University of Cincinnati, Cincinnati, Ohio, USA

Aldebaran M. Hofer, Associate Professor of Surgery & Research Health Scientist, VA Boston Healthcare System and the Department of Surgery, Brigham and Women's Hospital and Harvard Medical School, Massachusetts, USA

Atsushi Inanobe, Department of Pharmacology, Graduate School of Medicine and The Center for Advanced Medical Engineering and Informatics, Osaka University, Osaka, Japan

Marcia A. Kaetzel, Department of Cancer and Cell Biology, University of Cincinnati, Cincinnati, Ohio, USA

Robert S. Kass, Alumni and David Hosack Professor of Pharmacology and Chair, Columbia University College of Physicians and Surgeons, New York, USA

Sujay V. Kharade, Department of Pharmacology and Toxicology, University of Arkansas for Medical Sciences, Little Rock, Arkansas, USA

Takeshi Kobayashi, Assistant Professor, Department of Cellular Physiology and Signal Transduction, Sapporo Medical University School of Medicine, Sapporo, Japan

Evangelia G. Kranias, Chair, Department of Pharmacology & Cell Biophysics, Distinguished University Professor, Co-Director, Cardiovascular Center of Excellence, Department of Pharmacology and Cell Biophysics, University of Cincinnati, Cincinnati, Ohio, USA

Yoshihisa Kurachi, Department of Pharmacology, Graduate School of Medicine and The Center for Advanced Medical Engineering and Informatics, Osaka University, Osaka, Japan

Stephen Lambert, Associate Professor of Medicine, College of Medicine, University of Central Florida, Health Sciences Campus at Lake Nona, Orlando, Florida, USA

Michael Levandowsky, Research Scientist, Adjunct Professor of Biology, Haskins Laboratories, Pace University, New York, USA

Simon Rock Levinson, Professor, Department of Physiology and Biophysics, University of Colorado School of Medicine, Aurora, Colorado, USA

Daniel C. Marcus, Program Director, KSU COBRE grant; Professor, Anatomy and Physiology, College of Veterinary Medicine, Kansas State University, Manhattan, Kansas, USA

Gerhard Meissner, Professor, Departments of Cell and Molecular Physiology, and Biochemistry and Biophysics, The University of North Carolina at Chapel Hill School of Medicine, Chapel Hill, North Carolina, USA

Stan Misler, Associate Professor, Internal Medicine, Cell Biology and Physiology, Washington University in St Louis School of Medicine, St Louis, Missouri, USA

Catherine E. Morris, Senior Scientist, Neuroscience, Ottawa Hospital Research Institute; Professor, Department of Medicine, Division of Neurology, University of Ottawa, Ottawa, Ontario, Canada

Michela Ottolia, Department of Physiology, Cardiovascular Research Laboratories, David Geffen School of Medicine at UCLA, Los Angeles, California, USA

Richard J. Paul, Professor, Director, PhD Program in Systems Biology and Physiology, Department of Molecular and Cellular Physiology, College of Medicine, University of Cincinnati, Cincinnati, Ohio, USA

Asif R. Pathan, Department of Pharmacology and Toxicology, University of Arkansas for Medical Sciences, Little Rock, Arkansas, USA

Marcel Daniel Payet, Professor, Department of Physiology and Biophysics, Faculté de Médecine, Université de Sherbrooke, Sherbrooke, Quebec, Canada

Matthew Pincus, Professor, Clinical Pathology, SUNY Downstate Medical Center in Brooklyn; Chief, Department of Pathology & Laboratory Medicine, New York Harbor VA Medical Center, Brooklyn, New York, USA

Tracy J. Pritchard, Department of Pharmacology and Cell Biophysics, University of Cincinnati, Cincinnati, Ohio, USA

Robert W. Putnam, Professor, Department of Neuroscience, Cell Biology and Physiology, Boonshoft School of Medicine, Wright State University, Datyton, Ohio, USA

Seth Robey, Department of Pharmacology, College of Physicians and Surgeons, Columbia University, NY, New York, USA

Stephen D. Roper, Professor, Department of Physiology and Biophysics, University of Miami Miller School of Medicine, Miami, Florida, USA

Nancy J. Rusch, Professor and Chair, Department of Pharmacology and Toxicology, University of Arkansas College of Medicine, University of Arkansas for Medical Sciences, Little Rock, Arkansas, USA

Kevin J. Sampson, Department of Pharmacology, College of Physicians and Surgeons, Columbia University, NY, New York, USA

William A. Sather, Associate Professor, Department of Pharmacology, University of Colorado Denver, Aurora, Colorado, USA

Nicholas Sperelakis, Department of Physiology and Biophysics, College of Medicine and Division of Pharmaceutical Sciences, College of Pharmacy, University of Cincinnati, Cincinnati, Ohio, USA

Anup K. Srivastava, Department of Pharmacology and Toxicology, University of Arkansas for Medical Sciences, Little Rock, Arkansas, USA

Janusz B. Suszkiw, Professor, Department of Molecular and Cellular Physiology, University of Cincinnati, Cincinnati, Ohio, USA

Timothy C. Tricas, Professor, Department of Zoology & Hawaii Institute of Marine Biology, University of Hawaii at Manoa, Honolulu, Hawaii, USA

Noritsugu Tohse, Professor, Department of Cellular Physiology and Signal Transduction, Sapporo Medical University School of Medicine, Sapporo, Japan

Päivi H. Torkkeli, Professor of Physiology and Biophysics, Department of Physiology and Biophysics, Dalhousie University, Halifax, Nova Scotia, Canada

Natalia S. Torres, Nora Eccles Harrison Cardiovascular Research and Training Institute, University of Utah, Salt Lake City, Utah, USA

Kenneth R. Tovar, Vollum Institute, Oregon Health and Science University, Portland, Oregon, USA

Richard D. Veenstra, Department of Pharmacology, SUNY Upstate Medical University, Syracuse, New York, USA

Gordon M. Wahler, Professor, Physiology, Midwestern University, Downers Grove, Illinois, USA

Gary L. Westbrook, Senior Scientist and Co-Director, Vollum Institute Dixon, Professor of Neurology Oregon Health and Science University Portland, OR USA

J. Woodland Hastings, Professor of Natural Sciences, Department of Molecular and Cellular Biology, Harvard University, Cambridge, Massachusetts, USA

Hisashi Yokoshiki, Associate Professor, Department of Cardiovascular Medicine, Hokkaido University Graduate School of Medicine, Sapporo, Japan

Anita L. Zimmerman, Professor and Vice Chair, Molecular Pharmacology, Physiology and Biotechnology, Brown University, Providence, Rhode Island, USA

Foreword to the First Edition

It was kind and generous of my friend Nicholas Sperelakis to relate this excellent book so closely to my own, *A Textbook of General Physiology.* In the preface to the first edition of my book, I had expressed the hope that it might be compared with Bayliss' *Principles of General Physiology.* If this comparison is valid, it is very appropriate that the present book be organized and partly written by one who is, along with Sir William Bayliss and myself, associated with University College London (Professor Sperelakis having spent a sabbatical year there). It is a pleasure to recall that it was there that I first met Nicholas, and I remember discussing his pioneering study on the potentials across the crystalline lens of the eye.

For reasons that I think bear no relation to its scope, this book has a different title; I presume it is because the distinction between "ordinary" and "general" physiology has become sufficiently blurred to demand something more appropriate. The definition of general physiology that I had proposed in the preface to the first edition of my textbook was "the study of those aspects of living material that show some immediate prospect of being described in terms of the known laws of physics and chemistry." Later, I had misgivings as to the narrowness of this definition, and I then suggested that it might be replaced by "the study of those features of life that appear to be common to all forms." Whatever definition we choose, however, it is of immense satisfaction to me that this new book, essentially, has been fitted into the same sectional headings that I employed in my own book.

If I may be permitted to reminisce further, I have wondered frequently how a single scientist, actively engaged in research, could write a new book of such wide scope. The answer is that I wrote the book during the 2 years immediately following the end of World War II. Thus, for several years – in Great Britain for as many as 10 years – very little original academic physiology and new research had been published. This made it possible to survey the original literature of a lengthy period without being overwhelmed by a rapid succession of new discoveries that would have rendered my task nearly impossible, a fate similar to that of Sisyphus. Today, this task would be impossible, and it only surprises me that Nicholas has been able to produce this magnificent book with so few collaborators.

Hugh Davson
1995

Foreword to the Second Edition

In his Foreword to the first edition of the *Cell Physiology Sourcebook*, Hugh Davson established it as the lineal descendent of his own well-known and highly respected work *The Textbook of General Physiology.* The second edition of the *Cell Physiology Sourcebook,* again edited by Nicholas Sperelakis, continues in this same tradition. Although the first edition was enthusiastically received by the cell physiology community because of its depth and breadth of coverage, considerable important progress has been made in this rapidly developing area since its publication. The second edition deals with these new developments by a thorough reworking of topics and by the inclusion of new chapters in all sections covered in the first edition. The new topics introduced into the various sections include lipid structure, mitochondrial physiology, cell responses to hormones, red blood cell transport, neuron physiology, developmental changes in ion channels, sonotransduction, excitation-contraction coupling, and electroplax cells. In addition, the scope of the new edition has been valuably broadened by the inclusion of two entirely new sections. One titled *Protozoa and Bacteria* covers the physiology of these organisms in two chapters. In the other, *Cell Division and Programmed Cell Death,* there are chapters on the regulation of cell division, the cancer cell, apoptosis, and the effects of ionizing radiation. The extensive revisions and the new material in the second edition raise it to a new level.

Cell physiology, an area of central importance in biology, has grown out of a number of more traditional fields, and as a result, the literature continues to be widely dispersed. The great value of the *Cell Physiology Sourcebook* is that it gathers together under a single cover a broad range of up-to-date chapters that, taken together, define the field. The various chapters exhibit a uniformity of style and level of presentation that are a credit to the editor. Because of this and the scope and clarity of the presentations, this book can serve exceptionally well as an advanced undergraduate or graduate level text for cell physiology courses. The broad coverage of this second edition also makes it very attractive for use in cell biophysics, membrane biology, and biomedical engineering courses. It can serve equally well as a textbook for introductory courses in ion channel structure and physiology.

I was pleased, and indeed proud, to be asked by my colleague Nicholas Sperelakis to contribute the Foreword to the second edition of the *Cell Physiology Sourcebook.* This book clearly sets a new standard of excellence.

Thomas E. Thompson
1997

Foreword to the Third Edition

When Nicholas Sperelakis kindly invited me to write this foreword, I wondered how I could possibly follow in the footsteps of Hugh Davson. I studied physiology at University College London (UCL) at the time when his monumental *Textbook of General Physiology* was published. UCL was an extraordinary place in which to be a student at that time. Not only was Hugh Davson laying his particular cornerstone of the subject, but Leonard Bayliss was also reworking his father's famous *Principles of General Physiology*. These were the books that convinced me to become a research physiologist and that cell physiology was the place to begin. Between them, Davson and Bayliss were responsible for seducing generations of medical students to discover the challenge and delights of physiological research. Later, as a young lecturer at UCL, I remember asking Hugh Davson why he didn't lecture very much to the students. He simply replied: "Denis, I've written it all. Tell them to read!" Actually, that remark inspired me to reread his books. My copies are still in my library, and they are well and truly thumbed.

It will be the greatest tribute to the work of Nicholas Sperelakis and his colleagues that the pages of their book will also become the well-thumbed bible of a new generation of physiologists. They will be entering the discipline at an exciting time, for cell physiology is the base on which our understanding of all aspects of integrative and systems physiology must rest. This book, therefore, will be an essential source for all of us who aspire to understand the "logic of life," which is, after all, the meaning and origin of the word "physiology." Life has no single "logic," of course. Unraveling the physicochemical mechanisms that nature has discovered, fashioned, combined, and interwoven into the tangled skein of processes that form the function of even the simplest cell is a process full of surprises as we discover with awe the audacity with which nature's molecular mechanisms are reused again and again in different contexts. One might call this audacity the "dance of the genes" were it not for the inanimate and unthinking nature of these bits of code that transmit the logic from one generation to another. The logic is physiological, not genetic. The molecular biologist Sydney Brenner put the point succinctly when he wrote recently (in a Novartis symposium titled The Limits of Reductionism in Biology) that "Genes can only specify the properties of the proteins they code for, and any integrative properties of the system must be 'computed' by their interactions." We are approaching the point at which our understanding of those interactions is deep enough for physiology to aspire to become the quantitative analytical discipline it needs to be to solve the problems it tackles. Brenner went on to remark, significantly, "This provides a framework for analysis by simulation." It is a sign of the maturity of our science that simulation is indeed also becoming an essential tool of analysis.

It is further such a sign that the scope of cell physiology is now so wide. The breadth of this book is therefore one of its greatest strengths. The chapters encompass the great majority of important molecular and cell systems, so that it does indeed justify its title as a *sourcebook*.

Denis Noble

Foreword to the Fourth Edition

It is my pleasure to write a Foreword for the fourth edition of this textbook, entitled *Cell Physiology Sourcebook*. Professor Hugh Davson did not continue after the fourth edition of his monumental *A Textbook of General Physiology*. Perhaps he realized that the knowledge of physiology had become too broad for him to continue to cover the entire field alone, as he had done for his highly respected textbook.

So what permitted Professor Nicholas Sperelakis to write a noteworthy successor to Davson's formidable textbook? He decided to call upon an increasing number of specialists, and these prestigious specialists accepted to collaborate with him because they highly respected him as one of the major role models in Cell Physiology. Instead of really retiring when he closed his laboratory in 2002, Professor Sperelakis continued to publish articles, generally in collaboration with Dr L. Ramasamy from the Department of Electrical and Computer Engineering of the University of Cincinnati. Professor Sperelakis took the time to familiarize himself with the techniques used in PSpice, an electrical engineering software program (for circuit design and analysis), in which one substitutes electronic equivalents (e.g. resistances, capacitances, etc.) for physiological parameters. He was very excited while learning this new methodology. They have published about 10 articles using the PSpice simulations primarily in Theor Biol & Med Modelling and BioMed Eng Online. Since the first article summarizes the main ideas, I shall give complete reference only to this one, namely *N. Sperelakis and L. Ramasamy, Propagation in Cardiac Muscle and Smooth Muscle Based on Electric Field Transmission at Cell Junctions: An Analysis by PSpice. IEEE-EMB* **21**, *177-190, 2002.*

Professor Nicholas Sperelakis had some rather controversial research findings in the 1960s. In 1977, he reported with his mathematician collaborator, James E. Mann, that the transmission from one cell to the next one can occur in the myocardium by the development of an intense electric field in the narrow clefts of the intercalated disks. They stated, therefore, that propagation in myocardium can occur without the need of any gap-junction channels connecting the myocardial cells. They demonstrated that the density of fast Na^+ channels is greater in the intercalated-disk membrane than in the surface sarcolemma, which means that the excitability is likewise greater at the intercalated disks. I am glad to find that Professor Sperelakis is no longer alone in his Electric Field Hypothesis ever since that hypothesis was independently confirmed in the article by a Japanese group, namely *K. Tsumoto, T. Ashihara, R. Haraguchi, K. Nagazawa, and Y. Kurachi, Role of Subcellular Na Channel Distributions in the Mechanism of Cardiac Conduction. Biophysical Journal* **100**, *554-563, 2011.*

The third edition is packed with important information about the various aspects of the field of cell physiology and membrane biophysics. Most notably, I am impressed by the exceptional quality of the contributors relating to my field of expertise, namely the contractile mechanism and excitation–contraction coupling. Since the first edition of the *Cell Physiology Sourcebook*, new contributors were added for the subsequent editions, and I am certain that such will be the case for the fourth edition. It is always a pleasure to receive a telephone call from Professor Nicholas Sperelakis. He is so excited about his research, so vibrant with his passion for discovery. This enthusiasm is just one of the reasons why we respect him so much. Perhaps it is this passion to which his wife Dolores refers when she says that he is still as youthful and intellectually active as the young man she married 51 years ago. According to Professor Diomedes Logothetis, Chairman of our department at the Medical College of Virginia, the exceptionally good students are being hyperexcited by the "virus" of physiology, and I think that this happens also to established scientists such as Professor Sperelakis.

Professor Nicholas Sperelakis is celebrating his 81st birthday as I write this Foreword. For such a special anniversary, many Greeks add a "chronia polla" exclamation, which loosely translated is "many more years" or "with many happy returns". We wish that blessing, not only to Professor Sperelakis personally, but also for the new edition of his *Cell Physiology Sourcebook*.

Alexandre Fabiato
Richmond, VA
March 8, 2011

Preface

Preface to the Fourth Edition

Once upon a time, an 80-year-old retired university professor was leading a quiet and secluded life. Then one day in the spring of 2010, out of a clear blue sky, he was contacted by Janice Audet, Senior Acquisitions Editor for Academic Press. She said that a number of colleges were still using our third edition of *Cell Physiology Sourcebook* as the textbook for their courses in cell physiology, even though the third edition came out long ago, namely, in 2001.

In fact, I was aware of the use of the third edition in a number of colleges. About 2 years earlier, I was contacted by a graduate student from Georgia State University saying that they were using my book as the textbook for their class on cell physiology, but that he could not buy a copy because it was out of print. He asked me to send him my personal copy of the book. He said he would treat it well and return it to me at the end of the course. He even offered to drive to my home in Cincinnati to pick it up. This student was obviously desperate, so I talked to Noelle Gracy, my former editor, about the problem. She arranged for the class to have access to the e-book version of the textbook. Problem solved!

Janice wanted to know if I was interested in doing a fourth edition. Before I could give her a definitive answer, I wanted her to sample a number of course directors around the country to learn what they liked and what they didn't like about the third edition of the book. The consensus was that our book, in general, was pitched at too high a level for beginning graduate students (or senior undergraduates) taking a course in cell physiology. Some other suggestions were that we should eliminate some chapters/topics that are well-covered in the three textbooks available on cell biology, such as cell division, apoptosis, etc; we should improve the figures by using color; we should add a summary section at the beginning of each chapter; and, although difficult to achieve with so many contributing authors, we should try to make the various chapters more uniform in style.

I agreed to work on the fourth edition, and focused on incorporating the suggestions into the new edition. Some of the changes made to this edition include the omission of approximately 14 chapters, combining a few chapters, and asking contributors to try to pitch their chapters at the graduate student level. About 10 new contributors were recruited for specific expertise in the subject area. I believe that the final slate of contributors is top-notch, and I am extremely grateful for their participation.

So why did I agree to carry out this project that would require tremendous effort on my part, while in precarious health at that? Was it fortune/money? Absolutely not! That is miniscule. Was it fame/recognition? No, I'm too old to benefit from that now. Besides, I already edited three editions of the very same book. Was it dedication to teaching? Yes, that's what it was! I have dedicated my life to teaching, and I believe that I have the unique ability to present difficult concepts in an easily understandable way. For example, during my student days at the University of Illinois, four of us were studying together for an exam in genetics the next day. I was answering questions that the group had when one of them said, "Nick, you should be the one teaching this class." In the course of my career, I had also received multiple "golden apple" awards from graduate students in the Department of Physiology at the University of Cincinnati for the best teaching in our graduate courses.

One final example is worth mentioning. Michael Palmer, a best-selling author of medical mysteries, used my last name in one of his novels, "The Second Opinion", which came out in 2009. My son, Thomas, asked Dr Palmer how he came up with the name "Sperelakis", which is very uncommon in persons of Greek heritage. Dr Palmer replied that he was a medical student at Case-Western Reserve University in the mid-1960s, and he took my lectures on electrophysiology of nerve and muscle. He said that I was the favorite instructor in basic science of his entire class, and that they gave me the nickname of "Spike" which is jargon for a nerve action potential. Can you believe that Dr Palmer would remember me and my nickname after about 45 years? Dedication to teaching! My dedication to teaching is more amazing because I was a severe stutterer throughout my life, beginning at age 10 and continuing to the present (although now much less severe).

Before the first edition of this book was published, I saw a real need for a good, authoritative textbook in the area of cell physiology and membrane biophysics. The days when a single individual, like my friend Professor Hugh Davson, could cover such a broad area are gone. To cover the wide-ranging expertise necessary for an authoritative textbook, there seems to be no alternative other than arranging a multi-authored textbook by assembling a group of experts in the various topics to be covered. We used this principle in all four editions. The first edition, second edition, and third edition of this textbook came out in 1995, 1998, and 2001. The first and second editions received awards from the American Library Association for being outstanding, namely receiving their "Choice Award".

The Foreword to the first edition was written by Professor Hugh Davson of University College London (UCL). Professor Davson became very famous because of his textbook on cell physiology. It was indeed the "Bible" for all graduate students for a number of years. I first met Hugh when I was there on sabbatical leave in 1965–66. He was an amazing guy and we struck up an immediate friendship. In those days, UCL was quite the place. A.F. Huxley, Nobel Laureate, was head of the Physiology Department, and Bernard Katz, future Nobel Laureate, was head of the Biophysics Department. A.V. Hill, Nobel Laureate, was still coming to his office in the Biophysics Department about once or twice a week at age 90! Unbelievable! Incidentally, UCL is also where I first met Hugo Gonzalez-Serratos, a contributor to this book.

The Foreword for the second edition was written by Thomas E. Thompson. Tom was head of the Biochemistry Department at the University of Virginia while I was there. He was a leading investigator in the area of planar and spherical lipid bilayer membranes. Tom was an excellent teacher, and I had him participate in my graduate courses. Tom served as President of the Biophysical Society.

The Foreword for the third edition was written by Denis Noble of Oxford University. Denis became a leading investigator and theorist in the field of cardiac electrophysiology. One time, he asked me to give a lecture at a meeting being held at Oxford, and Sir Alan Hodgkin, Nobel Laureate, was chairing the session. I was shaking in my boots!

I decided to ask a long-time good friend, Professor Alexandre Fabiato of the Medical College of Virginia, to write the Foreword for this fourth edition. Alex is an outstanding scientist working on cardiac muscle. He is very well known and highly cited for his Ca-induced Ca release mechanism (CICR). He received the very prestigious Research Achievement Award from the national American Heart Association in 1989. Alex was trained as a cardiologist in France, and he was a graduate student with Professor Edouard Coraboeuf (University of Paris, Orsay, France) and Professor Silvio Weidmann (University of Bern, Switzerland), both leading pioneers and giants in the field of electrophysiology of cardiac muscle. I am proud and pleased that Alex agreed to do it.

The roadway along the book preparation trail was not without some large bumps and, at times, seemingly insurmountable roadblocks. Dedication to teaching, along with the great need for this textbook, kept me inspired to finish it. In addition, I felt a strong obligation to the Contributors, some of whom already had spent time and effort in beginning their revision. Again, I cannot stress how much I appreciate their efforts and how proud I am that they contributed to this book. We all hope that this textbook will be well received and highly successful.

Nicholas Sperelakis
May 2011

目　录

第三部分　膜兴奋与离子通道

第四部分　作为毒素、药物与遗传疾病靶的离子通道

第五部分　突触传递与感觉转导

第六部分　肌肉与其他收缩系统

Section V

Synaptic Transmission and Sensory Transduction

Chapter 31

Ligand-Gated Ion Channels

Kenneth R. Tovar and Gary L. Westbrook

Chapter Outline

I. SUMMARY

Ligand-gated ion channels are membrane proteins that are fundamental signaling molecules in neurons. These molecules are localized in the plasmalemma and on intracellular organelles and can be gated by both intracellular and extracellular ligands. The neurotransmitter-gated ion channels discussed in this chapter mediate fast excitation and inhibition in the nervous system and have now been well characterized by physiological and molecular studies. Studies using the technique of voltage and patch-clamp recording have examined the three basic features of an ion channel: gating, conductance and selective permeability. In general, ligand-gated ion channels can be described by kinetic models involving binding of two or more ligand molecules that induce a conformational change in the protein. As a result, a central, water-filled pore opens and conducts ions at very high rates of up to 10^7 ions per second. Channel activity is terminated when the channel closes or when it enters a non-conducting (desensitized) state. In vertebrates, acetylcholine (Ach) and glutamate receptors are cation channels, whereas γ-aminobutyric acid (GABA) and glycine receptors are anion channels. The ACh, GABA and glycine receptors constitute the Cys-loop receptor superfamily that presumably evolved from a common ancestral gene. Glutamate receptors comprise a separate protein family. The ligand-binding domain of glutamate channels shares homology with bacterial amino acid binding proteins, whereas the pore shares homology with the pore of voltage-dependent ion channels.

Each of the neurotransmitter-gated channels appears to be comprised of a hetero-oligomeric complex of closely related subunits surrounding a central ion pore. For each receptor type there are a number of possible subunit combinations that can form functional channels. AChR subunits have four transmembrane domains with the second transmembrane domain lining the pore. Charged amino acid residues near the mouth of the pore are important in determining the selectivity and conductance of the individual channel types. The glutamate subunits have three transmembrane domains and a re-entrant loop domain that forms a portion of the pore. The recent availability of crystal structures of a homomeric Cys-loop receptor and a glutamate receptor will allow atomic level resolution of the conformational movements involved in binding and gating of these channels.

II. INTRODUCTION

Ion channels are fundamental signaling molecules in virtually all cells. Studies of ion channel in the plasmalemma of excitable cells have provided the foundation for our knowledge of these important molecules. In the nervous system, voltage-gated ion channels mediate action potentials (APs) and trigger neurotransmitter release, whereas ligand-gated channels are responsible for chemical signaling mediated by classical fast-acting transmitters. Neurotransmitters also trigger slower synaptic responses that are mediated by G-protein-coupled receptors.

Until the 1980s, the molecular properties of ion channel proteins were largely inferred from physiological and biophysical studies (Hille, 2001). In retrospect, many of the predictions from early biophysical studies have been

Cell Physiology Sourcebook. DOI: 10.1016/B978-0-12-387738-3.00031-7

confirmed and extended following the elucidation of the amino acid sequence of voltage- and ligand-gated ion channels by molecular cloning. However, the increasing knowledge of the three-dimensional molecular structure of ion channels and their homologs in lower organisms now permit sophisticated correlations of protein structure with function (Sine and Engel, 2004; Mayer, 2005). These advances have dramatically increased our understanding of the molecular operation of these prototypic membrane proteins. These molecules have captured the interest of many outstanding scientists whose studies of ion channel function and structure have led to several Nobel Prizes (Neher, 1992; Sakmann, 1992; McKinnon, 2004). Neurological disorders can also be caused by mutations in ion channels, the so-called "channelopathies" (Kullmann, 2010) and by autoimmune mechanisms that target ligand-gated ion channel proteins (Graus et al., 2010).

A biophysical approach to ion channels was pioneered by studies of voltage-gated ion channels in squid axon. These studies established that a conductance change was associated with the AP and that this conductance change could be attributed to selective increases in the membrane permeability to Na^+ and K^+ ions, with the energy for the process derived from the transmembrane ion gradients created by the Na^+, K^+-ATPase. These findings suggested that there were discrete pores in the membrane that accounted for the Na^+ and K^+ conductance. However, it was not until the 1970s that the existence of ion channels as discrete membrane proteins was confirmed, first by measurements of the statistical properties of currents through populations of ion channels, a technique called *fluctuation* or *noise analysis*. Later, this conclusion was refined by the introduction of *patch-clamp recording*, which allowed measurement of the current through single ion channels (Neher, 1992; Sakmann, 1992). Patch-clamp recording revolutionized the study of ion channels because it allowed detailed biophysical studies of the electrical activity of single molecules. Protein purification and molecular cloning revealed that ion channels are a large and diverse group of membrane proteins. Although ligand-gated ion channels vary in structural details, they share a common basic structure in that they are composed of multiple subunits arranged around a central water-filled pore. Each subunit is a polypeptide encoded by a separate gene. Generally, there are a large number of possible subunit combinations; thus, the particular subunits expressed in a certain class of neurons can result in channels with distinct functional characteristics.

This chapter is divided into three topic areas. In the first, the categories of ligand-gated ion channels are briefly reviewed. The basic physiological properties and general molecular structure of ligand-gated channels are then discussed using the muscle nicotinic acetylcholine receptor (AChR) and the N-methyl-D-aspartate (NMDA)-type glutamate receptor as the prototypes. In the third section, the features of neurotransmitter-gated channels that are responsible for fast synaptic transmission are discussed with an emphasis on their distinctive characteristics. Channels gated by acetylcholine (ACh), γ-aminobutyric acid (GABA), glycine and glutamate are included as representative examples. Related topics on ion channels are discussed in other chapters in Sections III through V of this book. The reader is also referred to the excellent monographs and reviews listed in the references for further details.

III. CLASSES OF LIGAND-GATED ION CHANNELS

Ligands that activate ion channels in nerve cell membranes can be roughly divided into two major categories, neurotransmitters and intracellular ligands (Table 31.1). The neurotransmitter-gated ion channels involved in fast chemical synaptic transmission have been extensively studied. These include ACh, which is the transmitter at the vertebrate neuromuscular junction and in autonomic ganglia and the amino acids, L-glutamate and GABA, which mediate the majority of fast excitatory and inhibitory synaptic transmission, respectively, in the vertebrate central nervous system. Each of these ligands also activates receptors that are coupled to second messengers via GTP-binding (G) proteins. G-protein-coupled receptors generally mediate slower and neuromodulatory transmembrane signaling. Other neurotransmitters that activate ligand-gated ion channels in various cell types include serotonin, glycine, histamine and adenosine triphosphate (ATP). For example, the $5HT_3$ receptor activated by serotonin is a ligand-gated ion channel (Julius, 1991). ATP is released from nerve terminals in several pathways and activates the P2X family of channels (Burnstock, 2007; Browne et al., 2010). The transient receptor potential (TRP) channels provide a particularly large and diverse group that are activated not by classical neurotransmitters, but rather by diverse chemical as well as physical stimuli (Wu et al., 2010).

In addition to neurotransmitter-gated ion channels, increasing attention has focused on ligand-gated ion channels that are activated by intracellular ligands. These ligands include Ca^{2+}, cyclic nucleotides, ATP and inositol trisphosphate (IP_3). Intracellular ligands can increase (Ca^{2+}, cAMP, IP_3) or decrease (cGMP, ATP) activity of the associated channel. These channels play important roles in cell function. For example, Ca^{2+}-dependent potassium, chloride and non-specific cation channels modify the excitability of the nerve cell membrane and thus can alter the AP and release of transmitter from nerve terminals. The cyclic nucleotide (cAMP, cGMP)-gated channels mediate sensory transduction in the visual and olfactory system. Light results in the closing of cGMP channels in vertebrate

TABLE 31.1 Ligand-Gated Ion Channels

Ligand	Receptor	Ion Selectivity[a]
Neurotransmitters		
Acetylcholine	Muscle, neuronal AChRs	NS
Glutamate	AMPA, kainate, NMDA	NS
GABA	$GABA_A$	Cl
Glycine	GlyR	Cl
Serotonin	$5HT_3$ receptor	NS
ATP	P2X receptor	NS
Intracellular Ligands		
Calcium	Calcium-dependent channels	K, Cl, NS
Cyclic nucleotides	cGMP and cAMP receptors	NS
ATP	ATP-dependent channel	K
IP_3	Calcium release channel	Ca

[a]Abbreviations for ion selectivity are: NS: non-selective cation permeability, some with calcium permeability; Cl: permeable to chloride; K: permeable to potassium; and Ca: permeable to calcium.

photoreceptors whereas odors trigger the opening of cAMP-gated channels in olfactory receptor neurons. (See Chapters 35 and 39 for more discussion of channels gated by cyclic nucleotides.)

IV. BASIC PHYSIOLOGICAL FEATURES

Patch-clamp techniques allow investigators to define the three fundamental properties of any ion channel – *conductance*, *selective permeability* and *gating* – in molecular terms. In addition to these fundamental properties, *modulation*, *channel block* and *desensitization* are processes that alter the activity of ligand-gated ion channels and are important in shaping the impact of channel activity on membrane excitability. The biophysical basis of these properties will be discussed first and then the structural features of ligand-gated channels that control these properties will be considered.

Conductance reflects the flux of charged ions through the channel and is measured in picoSiemens (pS). Most ligand-gated ion channels have a conductance of 5–50 pS, which corresponds to the movement of more than 1×10^6 ions per second through the channel pore. These high flux rates initially suggested that ligand-gated channels must contain a water-filled pore, because this rate is much higher than that predicted for other transport mechanisms, such as pumps or exchangers. The size of the single-channel conductance (γ) is characteristic for a given channel. Several openings of a glutamate-activated channel in a hippocampal neuron are shown in Fig. 31.1. The conductance of the open channel is usually near 50 pS, but drops occasionally to subconductance states of 8, 35, 40 and 45 pS. The conductance of a channel increases as the permeant ion concentration is raised, but eventually saturates at concentrations well above physiological levels. This behavior can be described by Michaelis–Menten kinetics, suggesting that ions bind to sites within the pore rather than simply obeying the laws of free diffusion. Most permeant ions have a low K_m of approximately 100 mM (K_m is the concentration at which the conductance is half-maximal, as defined by the Michaelis–Menten equation); thus the ions bind for only a microsecond or so before continuing through the pore.

The current carried by the opening of a single-channel is measured in picoamperes (pA) with the single-channel current given by:

$$i = \gamma(V - Veq) \qquad (31.1)$$

where V is the membrane potential and Veq is the equilibrium potential, at which no net current is measured. This equation is simply Ohm's law, where (V–Veq) is the electrochemical driving force for ions that can pass through the channel. For example, if the extracellular and cytoplasmic concentrations of permeant ions are equal, then Veq is 0 mV. Thus, as the membrane potential changes, the size of the single-channel current also changes; a plot of this relationship is called a current–voltage or I-V plot. For channels, such as the muscle AChR, that are permeable to

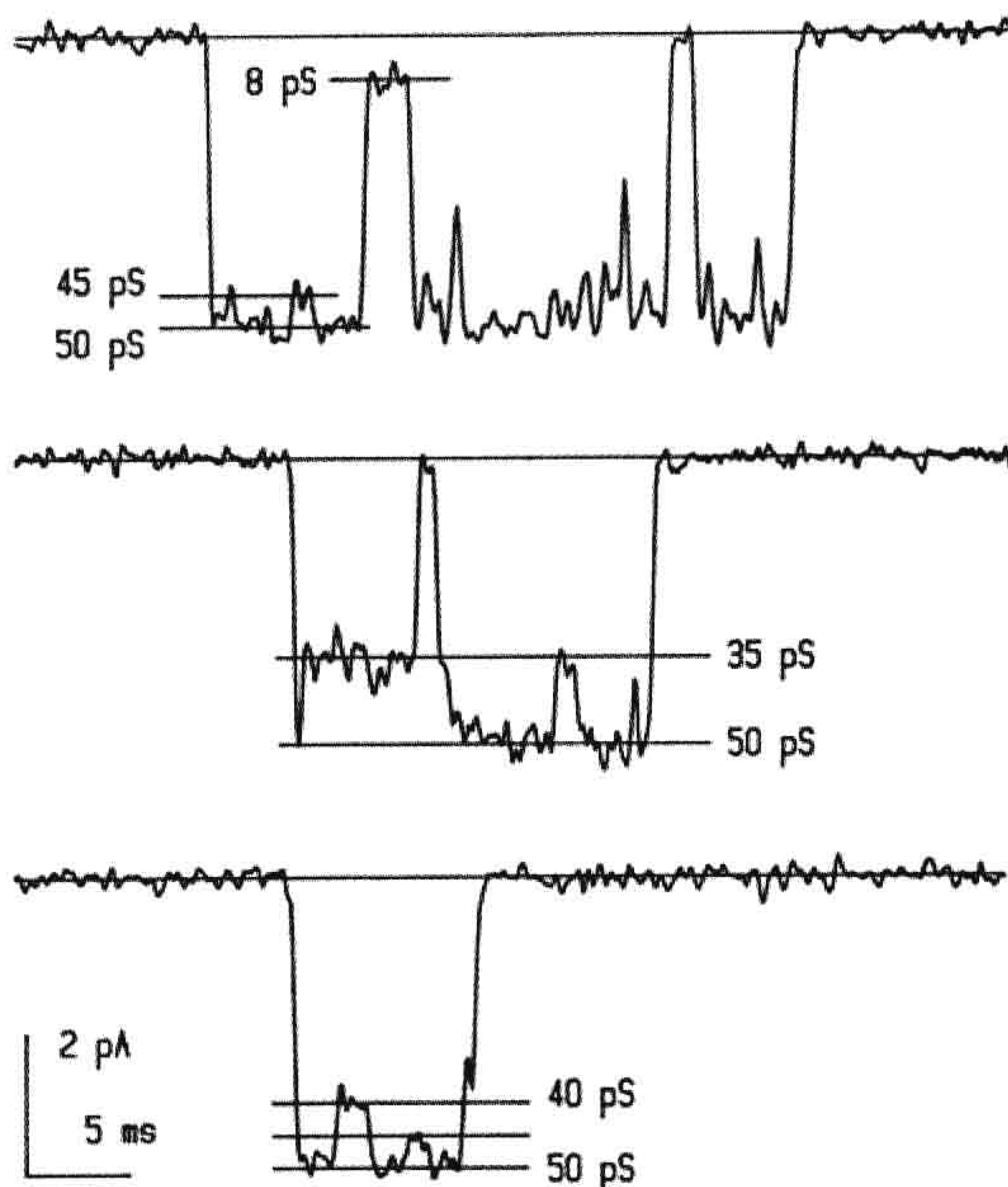


FIGURE 31.1 Activity of single ligand-gated channels as measured by patch-clamp recording. Examples of NMDA-type glutamate channel recording in an outside-out membrane patch obtained from a cultured hippocampal neuron. Downward deflections indicate opening of the channel in the presence of ligand (in this case, 20 μM NMDA). The channel usually opens to the 50 pS level, but may switch to lower levels of 8, 35, 40 or 45 pS before closing to the baseline level. *(Modified with permission from Jahr and Stevens (1987). Nature. 325, 522–525. Copyright 1987 by Macmillan Magazines Limited.)*

Na^+ and K^+, the reversal potential is 0 mV and the I-V curve is nearly linear. However, some channels deviate from linear behavior and show inward or outward rectification (i.e. the channel passes current in one direction better than in the other), analogous to the behavior of some voltage-gated K^+ channels.

Channels are not equally permeable to all ions, i.e. they exhibit selective permeability. As listed in Table 31.1, most ligand-gated ion channels are permeable to either monovalent cations or anions. The selective permeability of channels is partly due to the physical size of the pore. For example, the muscle AChR is permeable to cations with diameters up to about 6.5 Å. In general, cationic ligand-gated ion channels are less selective than voltage-gated ion channels, which are highly selective for Na^+, K^+ or Ca^{2+}, but more selective than gap junction channels, which are permeable to small molecular weight molecules such as cyclic nucleotides as well as to ions. Because anions and cations are approximately the same size, it is obvious that the pore dimensions cannot totally account for selective permeability. As discussed later, positively- and negatively-charged amino acid residues at the entrances to the channel and within the pore provide a means for this discrimination. Selective permeability is extremely important in considering the function of an ion channel. For example, channels that are permeable to Na^+ and K^+ do not significantly alter the ion concentrations on either side of the membrane but, instead, provide an electrical signal that depolarizes the neuron and brings the membrane potential closer to the threshold for AP generation. However, channels with significant Ca^{2+} permeability can transiently increase the cytoplasmic Ca^{2+} concentration and thus act as a biochemical signal. The relative Ca^{2+} permeability of ligand-gated channels, such as the NMDA receptor and some nicotinic receptors, is an important aspect of their role in neuronal function. The reader is referred to the monograph by Hille (2001) for a full discussion of channel permeability and its measurement.

Channel gating refers to the conformational change in the ion channel protein that is triggered by ligand binding. The conformational change results in a rapid switch between conducting (open) and non-conducting (closed) states of the channel. The gating behavior of channels has many parallels with the allosteric behavior of enzymes, with the binding of ligand providing the free energy necessary to maintain the channel in the open conformation. Gating between the open and closed configuration is extremely rapid (approximately 10 μs) and thus is beyond the resolution of standard recording methods. Each channel opening usually lasts a few milliseconds, but can, on some occasions, last up to several hundred milliseconds. Binding of more than one agonist molecule is usually necessary to open a channel. The binding of multiple agonist molecules creates a sigmoidal dose–response relationship, characteristic of the cooperative binding of substrates to enzymes. The steep activation created by sigmoidal kinetics prevents the channel from opening in the presence of a low concentration of agonist, which could be quite important in preventing desensitization of synaptic receptors. In general, the higher the binding affinity of the agonist, the longer the channel will remain open. This is because the channel can remain open (or reopen) until the agonist dissociates.

The gating of ligand-gated ion channels can be described by multistate kinetic diagrams as shown in Fig. 31.2A. Such state diagrams have been developed for many ligand-gated ion channels, based on the analysis of open and closed time distributions obtained in single channel recording. For example, the presence of two exponentials in an open time histogram implies the existence of two open states. The minimal kinetic model for a ligand-gated channel usually has at least four states, including closed and unbound, closed and bound, open and bound and non-conducting (desensitized). For the case shown in Fig. 31.2A and B, note that the channel opens only when two agonist molecules are bound. For fast-acting neurotransmitters, the concentration of transmitter in the

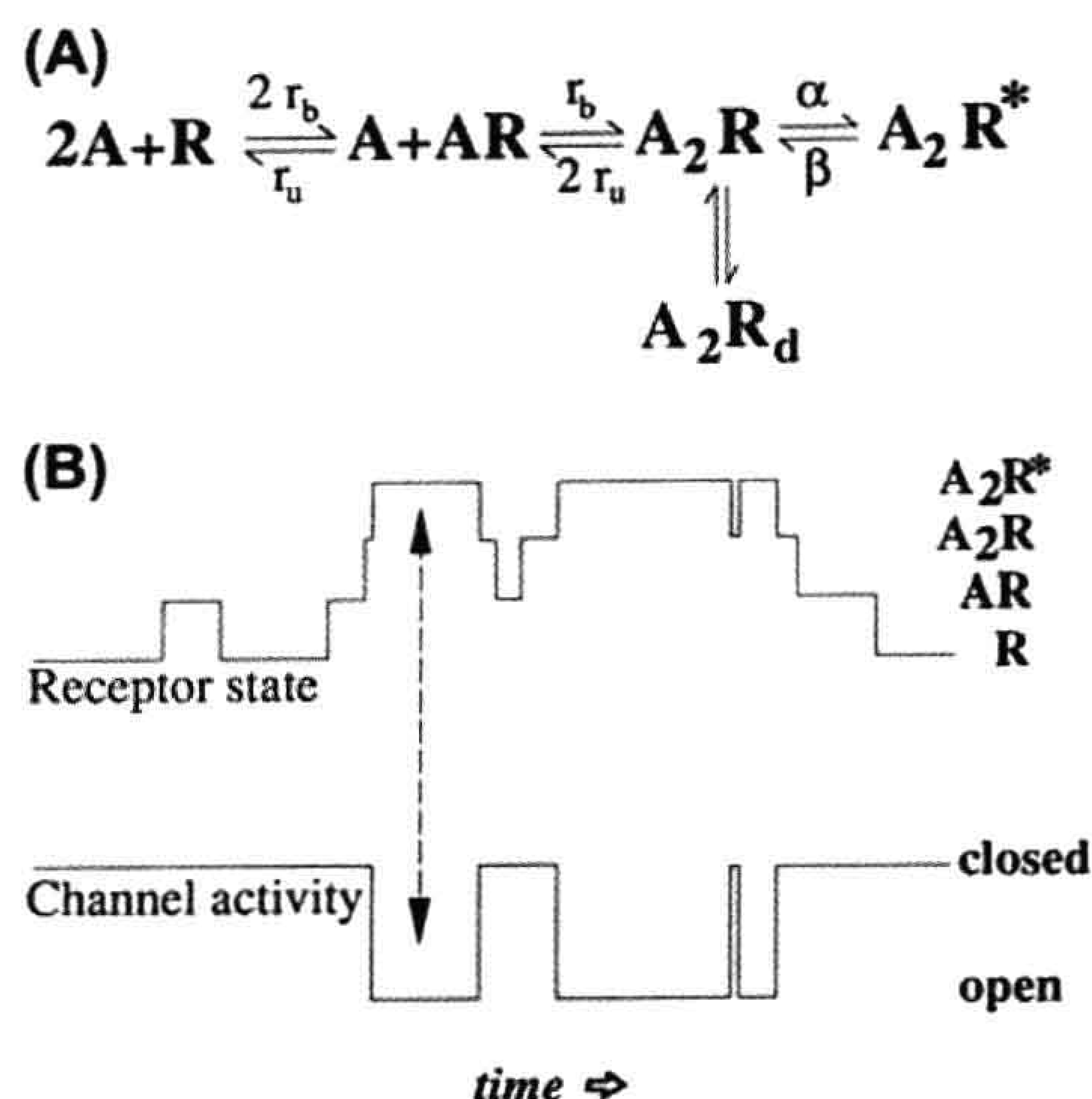


FIGURE 31.2 Kinetics of ligand-gated channels. (A) Example of a four-state kinetic scheme used to describe the behavior of ligand-gated ion channels. In this example, two agonist molecules (A) must bind before the channel can open (A_2R^*) or enter a non-conducting desensitized state (A_2R_d). The rate constants for agonist binding and unbinding are designated r_b and r_u, and the rate constants for channel opening and closing are designated as β and α. (B) Relationship of the state of the receptor to the open and closing of the channel. The channel opens only when the receptor is in the A_2R^* state as indicated by the arrows.

synaptic cleft is typically very high for a brief period. At high concentrations of agonist the receptors quickly reach the fully liganded but closed state because transition to this state is determined by the concentration of agonist as well as the binding rate, r_b. Thus, the rising and falling phase of the synaptic response largely reflects the unbinding rate, r_u, the channel opening and closing rates (β and α) and, in some cases, the rates in and out of the desensitized state, R_d. Classical pharmacological terms can be interpreted in terms of these kinetic schemes (Colquhoun, 1998). Agonists open the channel, whereas antagonists bind, but apparently do not cause a sufficient conformational change in the channel protein to open the channel. The fraction of time the bound channel spends in the open state is called the *open probability* and may differ between agonists – an agonist that activates the channel with higher probability therefore has a higher efficacy in the nomenclature of classical receptor pharmacology.

Earlier studies of the activity of ligand-gated channels were generally limited to equilibrium measurements because of the limits in the speed of application of agonists to cells or cell-free patches. Such equilibrium measurements are difficult to interpret in terms of state diagrams such as that shown in Fig. 31.2. In addition, the duration of fast-acting transmitters such as glutamate is generally brief, suggesting that the synapse itself operates under non-equilibrium conditions. However, the development of rapid solution exchange techniques allowed agonists to be applied within several hundred microseconds to membrane patches, usually in the "outside-out" configuration to allow agonist in the bath to access the extracellular face of the receptor. Such approaches appear to more closely resemble conditions at synapses and are particularly useful in evaluating the role of channel modulation, channel block and desensitization on synaptic responses. An example of the response of a membrane patch from a hippocampal neuron to a brief application of glutamate is shown in Fig. 31.3.

In general, the conductance and selective permeability of ligand-gated channels are not subject to regulation. However, a number of allosteric control mechanisms can profoundly affect gating (Changeux and Edelstein, 1998). These mechanisms can be manifest as *desensitization*, *channel block* and *allosteric modulation*. Desensitization refers to the loss of the response during the continued presence of agonist and was first noted in studies of the muscle AChR. At the single-channel level, desensitization reflects a non-conducting state of the channel. This phenomenon has now been seen for most ligand-gated channels and can be described by including an extra bound, but non-conducting, state in the kinetic scheme (see Fig. 31.2A). Depending on the channel, the non-conducting state may be accessible from either the closed state (A_2R) or the open state (A_2R^*). Desensitization represents a distinct conformation of the receptor as has been demonstrated by structural studies of AMPA receptors (see below). Very rapid desensitization may play a role in terminating the neuronal response to neurotransmitters at some synapses, whereas slower desensitization may actually prolong synaptic responses as channels re-enter open states after transiting through desensitized states (Jones and Westbrook, 1996).

Ligand-gated channels can be plugged by ions or drugs, a phenomenon referred to as *channel block*. If the blocking particle is charged, such as a large ion, the block will be influenced by the voltage across the membrane. Thus, the reduction in channel activity will be more pronounced at some membrane potentials. The voltage-dependent block of NMDA-type glutamate channels by extracellular Mg^{2+} is an example of this phenomenon (Ascher and Nowak, 1987). At the single channel level, channel block is usually seen as rapid interruptions ("flickers") of the open state as illustrated in Fig. 31.4A and B. A characteristic feature of most forms of channel block is that the blocker is only effective when the channel is open. Thus, the binding site for the blocker resides within the pore of the channel, or at least at a site that is only available in the open conformation of the channel. Channel block is the mechanism of action for a number of drugs, such as the local anesthetic lidocaine and psychoactive compounds, such as phencyclidine (PCP).

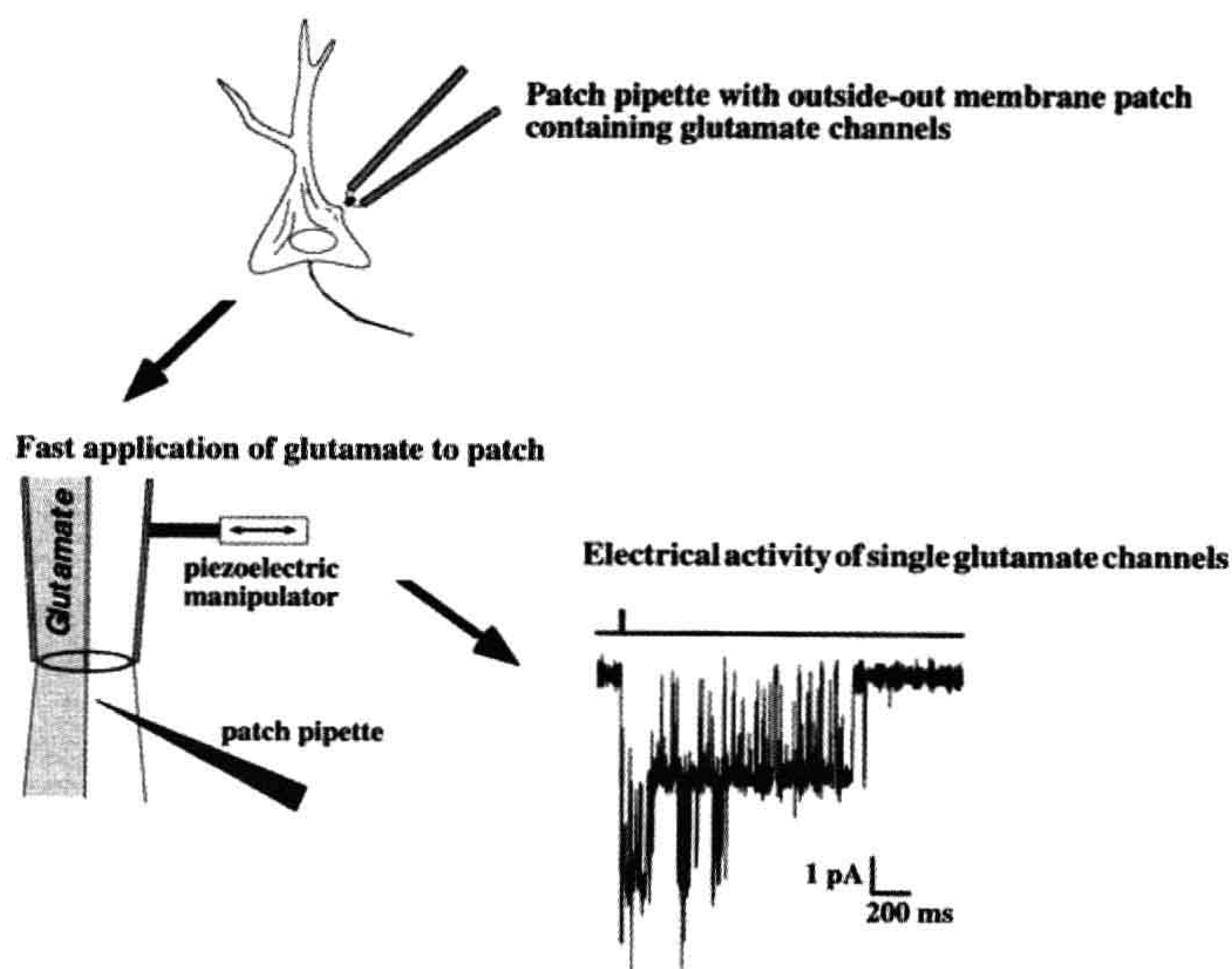


FIGURE 31.3 Use of rapid application methods to study kinetics of ligand-gated channels. The patch-clamp technique allows small membrane patches to be removed from a cell, such as a hippocampal neuron, with the extracellular side of the membrane facing the bath (outside-out configuration). The tip of the pipette is then placed in the interface of two rapidly moving streams of solution. A piezoelectric manipulator moves the solutions to change the solution flow over the patch in less than 1 ms, which mimics what occurs at glutamate release sites. The response, recorded as the opening of glutamate channels of the NMDA type, greatly outlasts the brief application of agonist. The bar above the channel activity indicates the duration of the glutamate application.

Channel gating is also subject to *modulation* by either covalent modification, such as phosphorylation (Swope et al., 1999), or via the non-covalent binding of modulators to the channel. Most ligand-gated channels undergo phosphorylation of intracellular portions of the channel protein; however, the resulting effect on channel function is dependent on the specific channel and the type of kinase involved. Phosphate groups are highly charged and thus can modify interactions in local regions. For example, phosphorylation of the AChR enhances desensitization and may also be important in clustering of AChR molecules at sites of innervation. The list of non-covalent modulators is long and includes Ca^{2+}, toxins, drugs and some endogenous substances such as protons and steroid hormones. These modulators usually act in a non-competitive manner, i.e. they do not directly interfere with ligand binding. Most of these

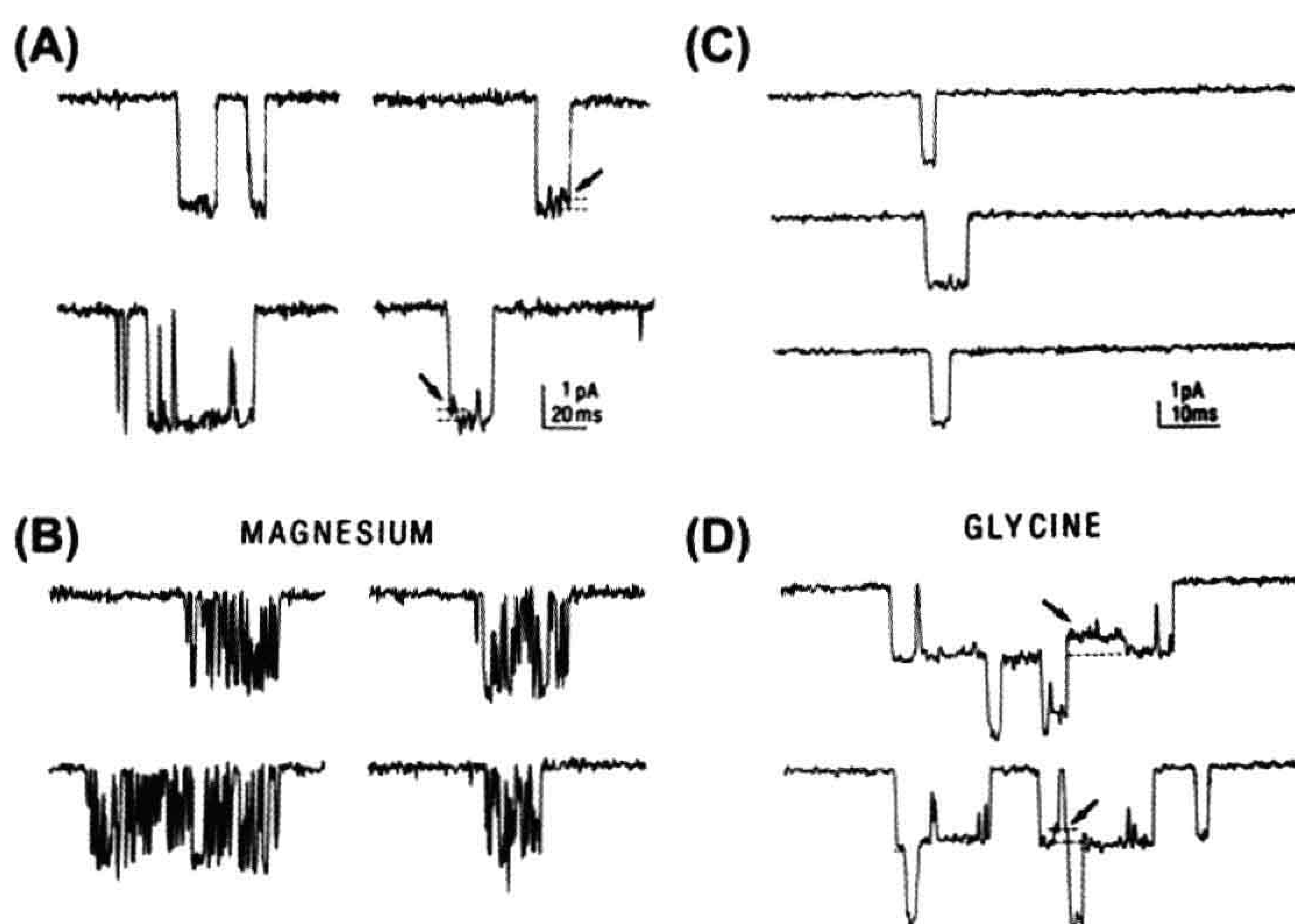


FIGURE 31.4 NMDA-type glutamate receptors illustrate two common mechanisms of channel regulation: channel block and allosteric modulation. (A and B). Channels activated by NMDA in a membrane patch from a hippocampal neuron in the absence of extracellular Mg^{2+} remain open (downward deflection) for several milliseconds before closing (A). However, in the presence of Mg^{2+} (B), the openings are interrupted by brief closures due to plugging of the pore by Mg^{2+} ions. (C and D) The frequency of NMDA channel opening is increased in the presence of extracellular glycine (D) compared to glycine-free solutions (C). The stepwise increase in current in part D indicates that at least two channels were present in the membrane patch. Because glycine is required for NMDA channel opening, the occasional openings in part C probably reflect contamination of the solution with low levels of glycine. *(Modified with permission from Ascher, R. and Nowak, L. (1987). Trends Neurosci. 10, 284–288.)*

reagents affect gating by altering the rate of channel opening or the time spent in the open state. For example, glycine binds to the NMDA channel and results in an increased probability of opening (see Figs. 31.4C and D). This is a dramatic example of allosteric regulation because the channel will not open unless both glycine and the transmitter (glutamate) are bound. A less profound, but equally important, example is the upregulation of $GABA_A$ receptor activity by benzodiazepines (Olsen and Sieghart, 2009).

V. MOLECULAR STRUCTURE

The ligand-gated ion channels can be divided into three main structural classes: the Cys-loop receptors, the glutamate receptors and the P2X receptors. Channels in these three families are formed as combinations 5, 4 and 3 subunits, respectively (Fig. 31.5). We discuss here structural information on the pentameric Cys-loop receptor superfamily that includes the nicotinic, $GABA_A$, glycine and 5-HT3 receptors, and the tetrameric glutamate receptor family that includes the AMPA, kainate and NMDA receptors. For the Cys-loop and glutamate receptor families, structural studies are providing a more and more detailed understanding of the main functional features of

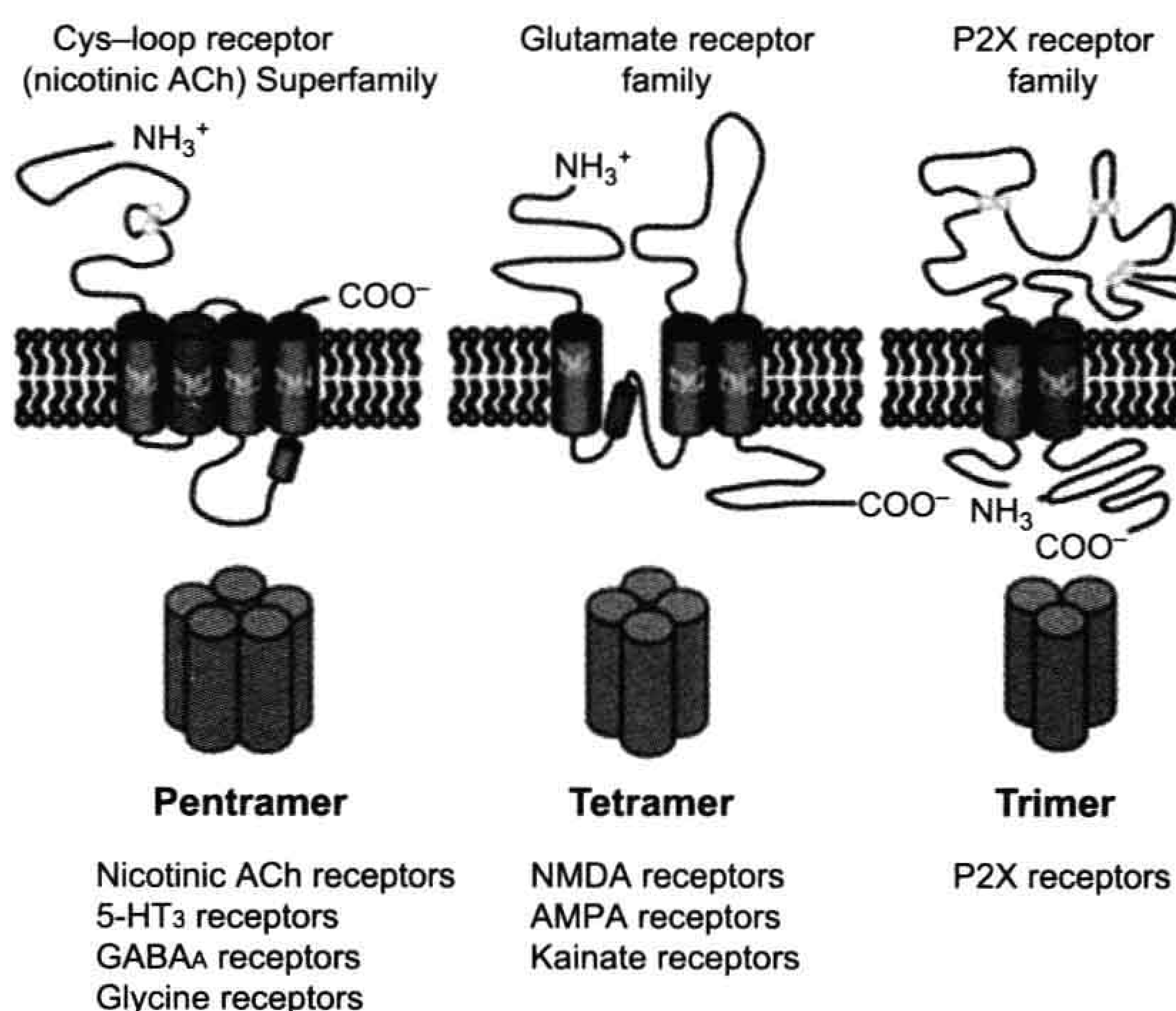


FIGURE 31.5 The topology of the three families of ligand-gated ion channel subunits. The general topologies of ligand-gated receptor subunits for each of the main receptor families are shown in the upper row. The stoichiometry of subunits in an assembled receptor are shown in the lower row. The Cys-loop family of receptors are pentameric, whereas the glutamate receptors are tetrameric and P2X receptors are trimeric. The three protein families also differ in the general structure of extracellular, intramembrane and intracellular domains. The red cylinders indicate the intramembrane pore region through which ions flow, M2 (TM2) in the case of Cys-loop and P2X receptors and the P loop for glutamate receptors. *(Modified with permission from Collingridge, G.L., Olsen, R.W., Peters, J., Spedding, M. (2009). Neuropharmacology. 56, 2–5.)*

ligand-gated ion channels: binding of ligand, the gating and ion selectivity of the channel and the coupling of ligand binding to channel gating. For information on the unique structure of the trimeric P2X receptors activated by ATP, see Browne et al. (2010).

The AChR led the way in determining the molecular structure of ligand-gated channels, beginning with biochemical studies of the muscle-type receptor (Karlin, 1991). This analysis took advantage of the high density of AChRs in the electric organ of the ray (*Torpedo californica*) and the high-affinity snake toxin, α-bungarotoxin, that binds to muscle-type AChRs. Protein purification revealed an approximately 250-kDa complex with two α-bungarotoxin binding sites per complex and separation on denaturing gels revealed polypeptides of 40, 50, 60 and 65 kDa designated as the α, β, γ and δ subunits. Because of the molecular weight of the complex and the binding of toxin molecules, a pentameric structure with two α subunits and single copies of β, γ and δ was proposed. Using the partial amino acid sequence of the purified subunits, the cDNAs encoding AChRs in the *Torpedo* electric organ were cloned and sequenced in the early 1980s. Incorporation of the purified protein complex in lipid bilayers or expression of AChR mRNA in *Xenopus* oocytes demonstrated channels activated by acetylcholine, confirming the identity of the molecule. Consistent with the proposed combination of subunits in intact receptors, the expression of AChRs in oocytes was much greater when all four subunit mRNAs were included. The α subunit was essential in order to obtain responses to acetylcholine.

Based on the hydrophobicity of amino acid residues in the primary sequence, the proposed transmembrane topology included four putative transmembrane domains (M1–M4), large N-terminal domain and short C-terminal extracellular domains and two cytoplasmic loops – a short one between M1 and M2 and a longer loop containing phosphorylation sites between M3 and M4. The early evidence that M2 lines the pore came from amino acid substitutions within that domain. In addition, a 23-amino-acid peptide fragment containing the M2 region of the *Torpedo* δ AChR subunit formed a cation channel when incorporated into lipid bilayers. The analysis of the primary amino acid sequence gives limited information about three-dimensional protein structure. Subsequently, two-dimensional crystals of AChRs from the *Torpedo* electric organ were analyzed with the electron microscope (Miyazawa et al., 1999), providing a good first estimate of the overall shape and structural features of the AChR.

Yet it was identification and high-resolution crystal structure of an acetylcholine-binding protein (AChBP) from the freshwater snail (*Lymnaea stagnalis*) that provided the next level of resolution (Smit et al., 2001; Brejc et al., 2001). Thc AChBP is a pentamer of identical subunits that is homologous to the extracellular ACh-binding

portion of the AChR and thus provided improved molecular resolution of ligand-binding domain. Combining AChBP with two-dimensional arrays of *Torpedo* channels began to reveal the relationship of the extracellular binding domains and the structural movements that lead to opening of the intramembrane channel (Unwin, 2005). Crystal structures of two full length homomeric channels related to the Cys-loop family now allow the first glimpse of the structure of an entire protein of this class. Interestingly, these structures are not those of well-studied members of the Cys-loop family, but rather include a pentameric ligand-gated channel from bacteria (Hilf and Dutzler, 2009) and a glutamate-gated chloride channel from *C. elegans* (Hibbs and Gouaux, 2011).

Each of the two binding pockets in the Cys-loop receptors is composed of hydrophobic and aromatic amino acid residues contributed by discontinuous segments of an α and a non-α subunit. The Cys-loop receptors get their name from an N-terminal 13 amino acid sequence flanked by cysteines that form a disulfide bond and make a closed loop in the extracellular domain. The binding pocket is capped by the "C-loop" contributed by the alpha subunit, which must be open for agonist access and is locked in place when the agonist is bound and thus fully enveloped. The structure also suggests a mechanism by which agonist binding can result in channel opening through linkers that connect to the first transmembrane domain. The new Cys-loop receptor crystal structures promise a much clearer picture of the conformational movements that underlie the open, closed and desensitized states.

As with the Cys-loop receptors, the proposed quarternary structure of glutamate channels involves multisubunit complexes surrounding a central pore (Fig. 31.6). However, cloning of the glutamate channels revealed that they differed substantially from the Cys-loop receptors in their primary amino acid sequence (Nakanishi, 1992; Hollmann and Heinemann, 1994). Notable differences include the much longer N-terminal domain (approximately 500 residues). In addition, the second hydrophobic domain of the glutamate subunits is a re-entrant loop that enters and exits the membrane from the cytoplasmic side without fully traversing the membrane. This "P" loop shows homology to the P loop of voltage-gated channels that lines the channel pore and controls ion selectivity and conductance. A prokaryotic glutamate receptor may provide an evolutionary link between the voltage-gated potassium channels and glutamate receptors (Chen et al., 1999). Secondly, the region between the third and fourth hydrophobic domains is extracellular in glutamate subunits whereas it is cytoplasmic in the AChR subunits. Finally, the C-terminus of the glutamate subunits is cytoplasmic. These unique features provided important clues to the location of the transmitter binding site(s), the behavior of the channel pore and sites of interaction with proteins that anchor and/or localize glutamate receptor subunits at synapses.

The extracellular component of glutamate receptors constitutes two separate domains (see Fig. 31.6). The amino terminal domain (ATD) of approximately 380 amino acids is involved in subunit assembly. The agonist-binding domain is discontinuous, being formed from the first extracellular region (D1) and the extracellular loop between the second and third transmembrane regions (D2). Both of these domains are homologous to bacterial proteins that bind amino acids. This homology led to a proposed model for the

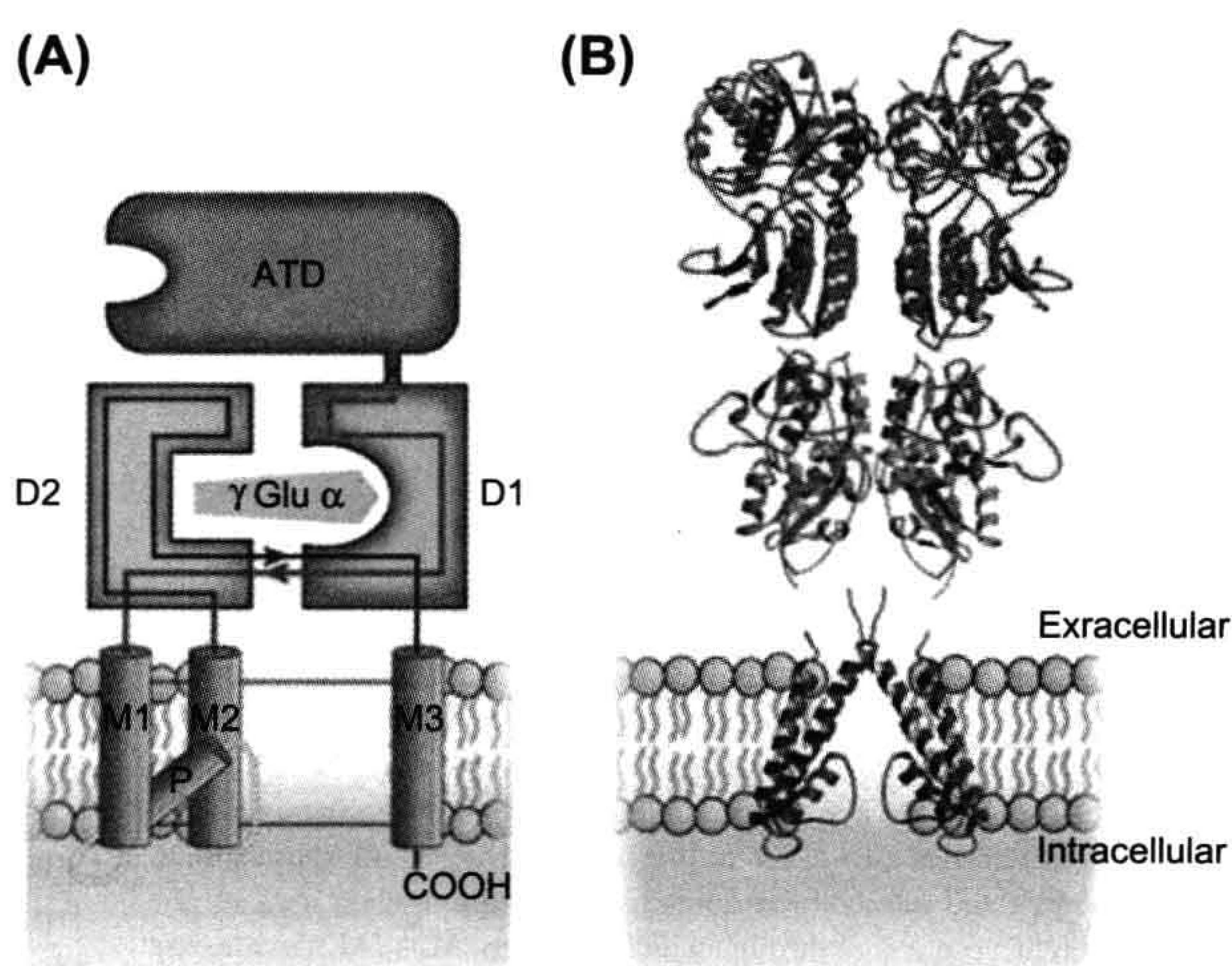


FIGURE 31.6 The domain organization of glutamate receptor subunits. (A) As shown in this schematic diagram, the extracellular region contains two domains, the ATD shown in green and the agonist-binding domain show in orange and blue surrounding an agonist molecule. The hydrophobic transmembrane domains M1, M2 and M3 as well as the P loop of the pore are shown in lavender. The intracellular domain is truncated in this schematic (-COOH). (B) A glutamate receptor assembles as a dimer of dimers. One representative dimer is shown here based on the crystal structures. The color-coded domains illustrate the secondary structure of α-helices and β-sheets that contribute to each domain. *(Modified with permission from Mayer, M.L. (2006). Nature. 440, 456-462.)*

glutamate binding site based on the crystal structure of the bacterial periplasmic binding proteins and subsequently confirmed based on chimeric receptors with domains from two glutamate subunits with distinct pharmacology (Stern-Bach et al., 1994). In GluN1, glycine occupies the agonist-binding domain instead of a glutamate, which binds to the GluN2 subunit. Selectivity for glycine over glutamate is conferred by the volume of the agonist-binding cavity resulting from steric constraints from residues present only in GluN1 (Furukawa and Gouaux, 2003).

Unlike AMPA or kainate receptors, which can form homomeric channels, functional NMDA channels are heteromeric, requiring two GluN1 and two GluN2 subunits. The general tetrameric organization of glutamate receptors was confirmed with the solving of a homomeric AMPA receptor structure (Sobolevsky et al., 2009). Unlike Cys-loop receptors, agonist binding in glutamate receptors occurs in a subunit-autonomous manner, requiring no inter-subunit interactions. The ligand binding regions of NMDA receptors are arranged as dimeric pairs (see Fig. 31.6B). Within a subunit, ligand binding occurs at the D1/D2 interface, which results in the closure of this structure in a clamshell fashion. These domain movements are thought to be associated with channel gating behavior, specifically, opening, closing and desensitization.

VI. NEURONAL ACETYLCHOLINE RECEPTOR CHANNELS

Studies of acetylcholine receptors began with the skeletal muscle isoforms (Steinbach, 1989), but AChRs are also expressed in neurons. The embryonic muscle AChR consists of an $\alpha_2\beta\gamma\delta$ pentamer, but later in development the γ subunit is replaced by an ε subunit. A much greater heterogeneity of receptor subunits is involved in the expression of AChRs at central synapses. (Dani and Bertrand, 2007). Neuronal AChRs mediate excitatory synaptic transmission in autonomic ganglia and at the recurrent collateral synapse of spinal motoneurons onto Renshaw cells (inhibitory interneurons). The functional role of nAChRs in the central nervous system was more difficult to establish despite the well-known action of nicotine (via cigarette smoke) on human behavior. nAChRs differ in several respects from muscle AChRs. First, α-bungarotoxin blocks muscle AChRs, but not most nAChRs. However, α-bungarotoxin binding sites represent a distinct subtype of nAChRs that have faster kinetics and a higher calcium permeability than other nAChR subtypes. The Ca^{2+} permeability of some nAChRs and changes in channel properties during synaptogenesis suggest that various nAChR subtypes play a role in synaptic plasticity and development. The activity of nAChRs are also modulated by phosphorylation. The kinase activation can be due to the actions of neuropeptides, such as vasoactive intestinal peptide and substance P, that are co-released with acetylcholine at some synapses.

Perhaps even more than for other ligand-gated channels, the cloning and characterization of subunit genes greatly accelerated studies of the structure and function of nAChRs (Role, 1992). Unlike the muscle AChRs, the nAChR pentamer is composed of only two classes of subunits, aptly named α and β. Subunits with cysteines at residues 192 and 193 are designated as α; subunits lacking these cysteines are called β. The genes for nine α (α_{2-10}) and three β (β_{2-4}) subunits have been cloned from rat and chick brain cDNA libraries. The stoichiometry of each channel molecule can be either homo-oligomeric (five alpha subunits) or heteromeric (usually with two α and three β subunits). Expression of single subunits and combination of subunits in *Xenopus* oocytes narrowed the possible combinations of subunits in functional channels. For example, α_{2-6} and β_{2-4} form heteromeric channels, whereas α_7, α_8 and α_9 do not. Combinations of subunits differ in their single-channel properties, ligand affinity and sensitivity to antagonists such as α-bungarotoxin. The $\alpha_4\beta_2$ receptor is a common heteromer in the CNS. It has a relatively high affinity for nicotinic agonists and thus is a principal target of the nicotine in tobacco smoke. Homo-oligomeric α_7 channels have a relatively low affinity for ACh and rapidly desensitize. This subunit has the closest homology to the snail AChBP and has been used to probe the structural substrates of channel properties such as desensitization, ion flux and selectivity. Homo-oligomeric α_7, α_8 and α_9 channels are sensitive to α-bungarotoxin, but α_7 is the predominant subunit of these three in brain. Presynaptic homomeric α_7 receptors with their high calcium permeability can enhance the release of glutamate and other transmitters. The α_9 subunit is unique due to its limited expression in the outer hair cells of the cochlea as well as its mixed muscarinic/nicotinic pharmacology.

Many central neurons have responses to exogenous application of nicotinic agonists and there is a wide distribution of nAChR subunit genes as revealed by in situ hybridization. However, there is a reasonable correlation between pathways with functional nAChRs (e.g. the cholinergic input to the hippocampus and medial habenula from the medial septum and diagonal band), the presence of nicotinic binding sites and the expression of nAChR subunits. Studies of nAChRs in different neuronal cell types have revealed a spectrum of channel properties and pharmacological characteristics, suggesting that individual neurons express several combinations of nAChR subunits. For example, *in situ* hybridization studies of neurons in the medial habenular nucleus have revealed two α and three β subunit genes. As for many classes of ligand-gated channels, the role of specific nAChR subunits has been investigated using genetically-engineered knockout and knock-in mice to investigate subunit-specific functions.

Interest in the nAChRs has been further fueled by studies indicating that mutations in α_4 or β_2 subunits cause a genetic form of human epilepsy.

VII. γ-AMINOBUTYRIC ACID AND GLYCINE RECEPTOR CHANNELS

Synaptic inhibition in the central nervous system (CNS) is mediated largely by $GABA_A$ and glycine receptors. These ligand-gated receptor channels are selectively permeable to anions, principally Cl^- under physiological conditions. GABA-gated Cl^- channels are designated $GABA_A$ receptors to distinguish them from the G-protein-coupled $GABA_B$ receptor (Padgett and Slesinger, 2010). $GABA_A$ and glycine receptors are members of the Cys-loop receptor family. Unlike other mammalian Cys-loop receptors that are non-selective cation channels, $GABA_A$ and glycine channels are selectively permeable to anions.

Virtually all CNS neurons have $GABA_A$ receptors, whereas the anatomical distribution of glycine receptors is generally restricted to the brainstem and spinal cord. $GABA_A$ receptors are often localized on proximal dendrites of central neurons, but also are expressed on axon initial segments and distal dendrites. Because the Cl^- equilibrium potential in many neurons is more negative than the resting potential, the opening of $GABA_A$ or glycine channels hyperpolarizes the cell membrane potential and reduces excitability. In addition to hyperpolarizing the membrane potential, the opening of large numbers of these channels lowers the membrane electrical resistance. Thus $GABA_A$ channels at proximal dendrites effectively "shunt" excitation traveling down the dendrite from excitatory synapses on more distal dendritic branches. In some neurons, particularly during early development, the Cl^- equilibrium is more positive than the resting potential, resulting in depolarizing $GABA_A$ or glycine responses. Depolarizing $GABA_A$ responses occurring in axons can increase excitability and neurotransmitter release. Finally, some inhibitory synapses in the spinal cord and brainstem contain both $GABA_A$ and glycine receptors. Analysis of unitary release events at these sites indicates that single synaptic vesicles contain both GABA and glycine and that a subpopulation of postsynaptic sites contains both receptor types (Jonas et al., 1998). As with other ligand-gated neurotransmitter receptors, molecular studies have revealed anchoring and regulatory proteins that interact with glycine and $GABA_A$ receptors, such as gephyrin (Fritschy et al., 2008) and GABA receptor-associated protein (GABARAP; Mohrluder et al., 2009). Gephyrin was identified as a cytoplasmic protein that interacts directly with glycine receptors. Gephyrin also interacts with tubulin and the actin-binding protein profilin and thus acts as a bridge between glycine receptors and the cytoskeleton. Gephyrin is also co-localized with $GABA_A$ receptors at postsynaptic sites but, unlike glycine receptors, has not been shown to bind to $GABA_A$ receptors. GABARAP interacts with many $GABA_A$ receptor subtypes, as well as binding to gephyrin and tubulin. Interaction with these cytoplasmic factors may alter the localization and trafficking of $GABA_A$ and glycine receptors as well as create zones of localized signal transduction.

The behavior of single $GABA_A$ and glycine channels can be described by a kinetic scheme similar to that of the nAChR with the binding of two agonist molecules required for channel opening (Macdonald and Twyman, 1992). Analysis of the openings and closings of single $GABA_A$ channels suggests that the channel may open briefly following the binding of a single $GABA_A$ molecule and into two longer-lived open states from the doubly liganded configuration. Comparison of the total open duration of singly- and doubly-liganded receptors demonstrates that occupancy of both agonist sites results in many more channel openings. Channels may close and re-enter longer-lived open states before the agonist dissociates from the receptor. These so-called *bursts* are composed of short closings interrupting a series of openings and they can last tens of milliseconds. Desensitization of $GABA_A$ channels results in long closed intervals that are grouped with bursts into *clusters* lasting up to several hundred milliseconds. These clusters are important in determining the duration of inhibitory postsynaptic potentials at some synapses (Jones and Westbrook, 1996).

The drugs that act on $GABA_A$ and glycine channels comprise a fascinatingly rich assortment of clinically important compounds (Olsen et al., 1991). Because these channels underlie synaptic inhibition in the CNS, enhancement or reduction in their activity can lead to profound changes in brain function, including amnesia (increased $GABA_A$ activity) or seizures (decreased $GABA_A$ activity). Antagonists for these receptors include strychnine, which inhibits glycine receptors; bicuculline, which inhibits $GABA_A$ receptors; and picrotoxin, which inhibits both receptor types. The $GABA_A$ receptor is also the target of sedative-hypnotic drugs, such as the benzodiazepines and barbiturates. Benzodiazepines (BDZ) increase the probability of channel opening, whereas barbiturates appear to act by prolonging long channel openings (bursts). The pharmacology of benzodiazepine modulation of the $GABA_A$ receptor is particularly interesting, because compounds either can enhance channel opening (BDZ agonists), reduce channel opening (BDZ inverse agonists) or block the effects of BDZ agonists (BDZ antagonists). $GABA_A$ receptor activity is also modulated by alcohol, volatile anesthetics, such as isoflurane, and some steroid anesthetics (or their endogenous equivalents, the neurosteroids).

Using benzodiazepines and strychnine as selective ligands, $GABA_A$ and glycine receptors were purified as

multimeric protein complexes, each with molecular weights of approximately 50–60 kDa. The solubilized receptor complex had a molecular weight of approximately 250 kDa, suggesting that, as for the AChR, five subunits constitute a receptor. Subsequent molecular cloning identified a series of receptor subunits for both receptors. The glycine subunits include the strychnine-binding subunit (α) of which four have been cloned and a single β subunit, with a stoichiometry of $(\alpha)_2(\beta)_3$ for receptors from mature animals. Interestingly, the immature form of the glycine receptor contains only α subunits. Gephyrin binds to the β subunit, thus the interaction between gephyrin and glycine receptors is limited to the adult form. Nineteen $GABA_A$ subunits have been identified and grouped according to sequence similarity. These include six α, three β, three γ, three ρ subunits and single δ, ε, π, and Θ subtypes (Wisden and Seeburg, 1992; Olsen and Sieghart, 2009). In heterologous systems, expression of single $GABA_A$ or glycine receptor subunits can result in functional homomeric receptors. However, given the broad co-expression patterns of many $GABA_A$ and glycine receptor subunits and the functional heterogeneity of native receptors, homomeric receptors probably occur rarely. The large number of $GABA_A$ receptor subunits provides a formidable challenge in determining which combinations form functional receptors in neurons. $GABA_A$ and glycine receptor subunit expression also varies during development and with neuronal cell type. Based on pharmacology, expression, biochemistry and subcellular localization, at least 26 different types of native $GABA_A$ receptors have been identified in CNS neurons (Olsen and Sieghart, 2009).

Subunit composition can have a strong influence on the biophysical and pharmacological properties of $GABA_A$ and glycine receptors. The GABA and benzodiazepine binding sites reside at the interface between an α subunit and a β or γ subunit (usually γ_2), respectively. The γ_2 subunit is broadly and highly expressed in the CNS and genetic deletion greatly reduces BDZ binding sites in the brain. Interestingly, the α_6 subunit has a low affinity for BDZ agonists, but still can bind BDZ inverse agonists or antagonists, which may explain benzodiazepine-insensitive $GABA_A$ receptors in some neurons. Homomeric receptors composed of the $GABA_A$ receptor ρ subunit are bicuculine-insensitive, weakly antagonized by picrotoxin and insensitive to BDZs, barbiturates and neurosteroids. These channels also show distinct gating properties and conductances compared to other $GABA_A$ receptors. They were initially referred to as $GABA_C$ receptors. However, due to their sequence similarity and proposed structure, they are currently thought of as a subtype of $GABA_A$ receptors. The three ρ subunits ($\rho1$, $\rho2$ and $\rho3$) are expressed throughout the CNS but expression is predominantly in several cell types in the retina.

VIII. GLUTAMATE RECEPTOR CHANNELS

Although it was known from the early 1950s that L-glutamate was a neuroexcitant, it was not until the 1980s that the role of glutamate-gated ion channels in central synaptic transmission was widely accepted (Collingridge and Lester, 1989; Westbrook and Jahr, 1989). It is now clear that glutamate receptor channels mediate a substantial portion of fast excitatory transmission in the brain and spinal cord through the simultaneous activation of two types of ion channels co-localized at excitatory synapses. Characterization of this family of ligand-gated ion channels was initially based on selective activation by the exogenous amino acid ligands: NMDA, kainate and quisqualate. AMPA (α-amino-3-hydroxy-5-methyl-4-isoxazole proprionic acid) replaced quisqualate as one of the prototypic ligands because quisqualate also activates a G-protein-coupled receptor. It soon became apparent that NMDA receptors were distinct from kainate and AMPA receptors, but for some time it was debated whether kainate and AMPA (i.e. non-NMDA) responses arose from the same or different receptors. It is now clear that AMPA and kainate receptors are distinct molecular entities, although kainate can activate both classes of receptors.

Initial studies of native AMPA/kainate receptor channels demonstrated many of the same features as AChRs. In hippocampal pyramidal neurons, AMPA receptor activation leads to brief openings (1–5 ms) of monovalent cation channels that show little or no voltage dependence. However, in some neurons, particularly interneurons, AMPA receptors have a higher calcium permeability and are inwardly rectifying. AMPA receptors rapidly desensitize when gated by glutamate and agonist dissociation (unbinding) and desensitization (agonist still bound but the channel is non-conducting) can contribute to the decay of the synaptic current. The behavior of AMPA channels seems well suited to the rapid relay of information that characterizes the fast component of excitatory postsynaptic potentials in the brain.

The NMDA channel provides perhaps the best example of the linkage between fundamental properties of ion channels and the electrical activity of single cells and complex behavioral phenomena (Bekkers and Stevens, 1990; McBain and Mayer, 1994). This linkage is primarily based on three features of NMDA channels: (1) voltage-dependent block of the open channel by extracellular Mg^{2+}; (2) a relatively high permeability to Ca^{2+}; and (3) slow channel kinetics resulting in long-lasting channel activity. Because Mg^{2+} ions are positively charged and thus sense the membrane electric field, they are drawn into the open NMDA receptor channel at negative membrane potentials. Mg^{2+} binds in the channel pore and impedes the flow of permeant ions, even though the agonists (glutamate and glycine) remains bound. However, during synaptic

activity as the cell membrane depolarizes, Mg^{2+} falls out of the channel and permeant cations flow through the channel. Thus, ion flux through the channel is voltage dependent. This mechanism differs from other voltage-dependent ion channels, such as the sodium or calcium channel, where voltage dependence results from an intrinsic conformational change in the channel protein. However, the end result is the same; current flows through the NMDA receptor channel more effectively with depolarization and thus acts as a positive feedback on synaptic activation.

Unlike many AMPA channels, Ca^{2+} contributes a substantial fraction of the flux through NMDA channels. However, the rate of flux of Ca^{2+} through the NMDA channel is slower than Na^{+} because Ca^{2+} transiently binds with higher affinity to sites within the channel (*energy wells*). Thus most of the current through open NMDA channels is due to Na^{+}, which is present in 50-fold excess in the extracellular space compared to calcium. Nonetheless, the 5–10% of the current that is carried by Ca^{2+} is sufficient to act as a biochemical signal for such processes as the induction of long-term potentiation in the hippocampus, an experimental model of associative learning. Excessive activation of glutamate receptors may also cause neuronal damage, presumably through elevations of intracellular Ca^{2+} concentration and subsequent activation of proteases and free radical formation. This mechanism, called *excitotoxicity*, has been implicated in brain damage due to prolonged seizures, following strokes and may also contribute to loss of neurons in several degenerative neurological diseases.

Because no high-affinity ligands were available for purification of glutamate receptors, molecular biologists were forced to use the somewhat laborious task of expression cloning to isolate cDNA clones for glutamate receptor subunits. The first AMPA receptor subunit (GluA1) was isolated by this technique in 1989 and the first NMDA receptor clone (GluN1) was also isolated by expression cloning in 1991. Using these initial AMPA and NMDA clones to screen for homologous sequences, 16 related glutamate receptor subunits were isolated from rat and mouse cDNA libraries. On the basis of glutamate receptor sequence homology and the characteristics of the expressed receptors, the subunits can be grouped into three categories: four AMPA subunits (GluA1-4, formerly called GluR1–4 or A–D), five high-affinity kainate subunits (GluK1–5, formerly GluR5–7, KA-1, KA-2) and seven NMDA subunits (GluN1, GluN2A–D, GluN3A–B, formerly NR1, NR2A–D, NR3A–B). GluD1 and GluD2 have significant homology to glutamate receptor subunits yet they do not bind glutamate agonists. They are referred to as orphan subunits and their function remains unclear. The GluD2 subunit is particularly intriguing because a mutation in the gene encoding this protein is responsible for the neurological phenotype of the *Lurcher* mouse. Relatively little is known about GluN3 subunits and it is unclear whether neurons make NMDA receptors that contain NR3 subunits. Curiously, when GluN1 and GluN3A or GluN3B are co-expressed in heterologous cells, they form excitatory channels that are gated by glycine rather than glutamate.

Some AMPA receptor subunits can combine to form functional homo-oligomeric receptors and this has revealed some interesting and curious phenomena. For example, the genes for GluA2, GluK1 and GluK2 code for a glutamine in the P loop region. However, the mRNA undergoes editing such that the expressed protein has an arginine residue at this site. This switch has a profound effect on the behavior of the channel. The current evoked by homo-oligomeric expression of unedited subunits shows marked inward rectification and an increased permeability to Ca^{2+}. The edited versions have a linear current–voltage relationship and are permeable only to monovalent cations (Na^{+} and K^{+}). Because the synaptic response mediated by AMPA receptors in hippocampal pyramidal cells has a linear current–voltage relationship, most AMPA receptors in these neurons contain one or more edited copies of GluA2. However, in interneurons in cortex and hippocampus as well as in dorsal horn neurons of the spinal cord, AMPA receptors lacking edited GluA2 subunits show inward rectification and increased permeability to Ca^{2+}.

Glutamate channels, particularly NMDA channels, are regulated by a variety of allosteric mechanisms and by phosphorylation. The most dramatic are the actions of glycine as a *co-agonist* that is required for the opening of NMDA channels and extracellular Mg^{2+} that blocks NMDA channels. Binding of two molecules of glutamate and two molecules of glycine are required to activate an NMDA channel. Because glutamate channels are tetramers, it is thought that each subunit contributes to agonist binding. The glycine concentration in cerebrospinal fluid exceeds the EC_{50} for the glycine site, thus it is likely that the glycine site is tonically saturated. Recent evidence indicates that endogenous D-serine may also bind to the glycine site, with approximately the same affinity and efficacy as glycine. Although AMPA receptor channels do not require a co-agonist, given their homology with NMDA receptor channels, four molecules of glutamate are probably necessary to activate AMPA channels (Rosenmund et al., 1998). Other regulatory factors that affect NMDA channel activity include extracellular protons, Zn^{2+}, polyamines, redox potential and intracellular Ca^{2+}. The ability of these factors to affect NMDA receptors can depend on subunit composition. For example, the GluN1/GluN2A receptors are almost 100-fold more sensitive to Zn^{2+} than GluN1/GluN2B receptors. There are numerous phosphorylation sites on the C-terminal domains of AMPA and NMDA receptor subunits that can be regulated by protein kinase A and C, tyrosine kinases and Ca^{2+}/calmodulin-dependent

kinase (Chen and Roche, 2007). Kinase activation can alter any of a number of channel properties including gating and membrane trafficking. Phosphorylation of AMPA and NMDA receptors can also affect receptor trafficking that can then govern the ability of synapses to respond to stimuli that trigger long-term changes in synaptic efficacy. Activation of the NMDA receptor itself and the subsequent Ca^{2+} influx can result in PKC activation, which can then alter AMPA receptor trafficking. The impact of these regulatory mechanisms on synaptic function is a continuing area of investigation (Lee, 2006).

As with other neurotransmitter receptors, glutamate receptors are clustered in the postsynaptic membrane at synaptic sites. Recent studies have revealed a number of proteins that are involved in the clustering and localization of glutamate receptor channels. Glutamate channels are imbedded in the postsynaptic density (PSD) that contains receptors, regulatory proteins and cytoskeletal proteins. Biochemical studies suggest that calmodulin and cytoskeletal proteins can interact with C-terminal domains of several NMDA receptor subunits at domains that are involved in the regulation of NMDA receptor desensitization, suggesting an intriguing link between dynamic regulation of channel activity (e.g. by compartmentalized regulatory proteins) and structural features, such as channel anchoring or localization at synapses. A family of proteins with a PDZ domain are involved in interactions with AMPA and NMDA subunits (Ehlers et al., 1996; Sheng and Pak, 2002). TARPs (transmembrane AMPA receptor regulatory proteins) are a family of proteins that share homology with auxiliary subunits of voltage-gated calcium channels. TARPs alter the gating and pharmacological sensitivity of AMPA receptors (Milstein and Nicoll, 2008) and thus are considered auxiliary AMPA receptor subunits (Mayer, 2005). Other recently identified proteins, like CKAMP44, may have similar regulatory actions on AMPA receptors. The interactions between glutamate receptors and their associated proteins is important in receptor lateral mobility and trafficking, synapse development and the dynamic regulation of activity of ligand-gated channels in a broad range of brain functions including learning and memory.

BIBLIOGRAPHY

Ascher, P., & Nowak, L. (1987). Electrophysiological studies of NMDA receptors. *Trends Neurosci, 10*, 284–288.

Bekkers, J. M., & Stevens, C. F. (1990). Computational implications of NMDA receptor channels. *Cold Spring Harbor Symp Quant Biol, 55*, 131–135.

Brejc, K., van Dijk, W. J., Klaassen, R. V., et al. (2001). Crystal structure of Ach-binding protein reveals the ligand-binding domain of nicotinic receptors. *Nature, 411*, 269–276.

Browne, L. E., Jiang, L. H., & North, R. A. (2010). New structure enlivens interest in P2X receptors. *Trends Pharmacol Sci, 31*, 229–237.

Burnstock, G. (2007). Physiology and pathophysiology of purinergic neurotransmission. *Physiol Rev, 87*, 659–797.

Changeux, J.-P., & Edelstein, S. J. (1998). Allosteric receptors after 30 years. *Neuron, 21*, 959–980.

Chen, B. S., & Roche, K. W. (2007). Regulation of NMDA receptors by phosphorylation. *Neuropharmacology, 53*, 362–368.

Chen, G. Q., Cui, C., Mayer, M. L., & Gouaux, E. (1999). Functional characterization of a potassium-selective prokaryotic glutamate receptor. *Nature, 402*, 817–821.

Collingridge, G. L., & Lester, R. A. (1989). Excitatory amino acid receptors in the vertebrate central nervous system. *Pharmacol Rev, 41*, 143–210.

Collingridge, G. L., Olsen, R., Peters, J., & Spedding, M. (2009). A nomenclature for ligand- gated ion channels. *Neuropharmacology, 56*, 2–5.

Colquhoun, D. (1998). Binding, gating, affinity and efficacy: the interpretation of structure-activity relationships for agonists and of the effects of mutating receptors. *Brit J Pharmacol, 125*, 923–947.

Dani, J. A., & Bertrand, D. (2007). Nicotinic acetylcholine receptors and nicotinic cholinergic mechanisms of the central nervous system. *Annu Rev Pharamacol Toxicol, 47*, 699–729.

Ehlers, M. D., Mammen, A. L., Lau, L. F., & Huganir, R. L. (1996). Synaptic targeting of glutamate receptors. *Curr Opin Cell Biol, 8*, 484–489.

Fritschy, J. M., Harvey, R. J., & Schwarz, G. (2008). Gephyrin: where do we stand, where do we go? *Trends Neurosci, 31*, 257–264.

Furukawa, H., & Gouaux, E. (2003). Mechanisms of activation, inhibition and specificity: crystal structures of the NMDA receptor NR1 ligand-binding core. *EMBO J, 22*, 2873–2885.

Graus, F., Saiz, A., & Dalmau, J. (2010). Antibodies and neuronal autoimmune disorders of the CNS. *J Neurol, 257*, 509–517.

Hibbs, R. E., & Gouaux, E. (2011). Principles of activation and permeation in an anion-selective Cys-loop receptor. *Nature*, May 15 [Epub ahead of print].

Hilf, R. J., & Dutzler, R. (2009). A procaryotic perspective on pentameric ligand-gated ion channel structure. *Curr Opin Struct Biol, 19*, 418–424.

Hille, B. (2001). *Ionic Channels of Excitable Membranes* (3rd ed.). Sunderland, MA: Sinauer Associates Inc.

Hollmann, M., & Heinemann, S. (1994). Cloned glutamate receptors. *Annu Rev Neurosci, 17*, 31–108.

Jahr, C. E., & Stevens, C. F. (1987). Glutamate activates multiple single channel conductances in hippocampal neurons. *Nature, 325*, 522–525.

Jonas, P., Bischofberger, J., & Sandkühler, J. (1998). Corelease of two fast neurotransmitter at a central synapse. *Science, 281*, 419–424.

Jones, M. V., & Westbrook, G. L. (1996). The impact of receptor desensitization on fast synaptic transmission. *Trends Neurosci, 19*, 96–101.

Julius, D. (1991). Molecular biology of serotonin receptors. *Annu Rev Neurosci, 14*, 335–360.

Karlin, A. (1991). Explorations of the nicotinic acetylcholine receptor. *Harvey Lectures, 85*, 71–107.

Kullmann, D. M. (2010). Neurological channelopathies. *Annu Rev Neurosci, 33*, 151–172.

Lee, H.-K. (2006). Synaptic plasticity and phosphorylation. *Pharmacol Therapeut, 112*, 810–832.

Macdonald, R. L., & Twyman, R. E. (1992). Kinetic properties and regulation of $GABA_A$ receptor channels. *Ion Channels, 3*, 315–343.

MacKinnon, R. (2004). Nobel lecture. *Potassium channels and the atomic basis of selective ion conduction Biosci Rep, 24*, 75–100.

Mayer, M. L. (2005). Glutamate receptor ion channels. *Curr Opin Neurobiol, 15*, 282–288.
Mayer, M. L. (2006). Glutamate receptors at atomic resolution. *Nature, 440*, 456–462.
McBain, C., & Mayer, M. (1994). N-methyl-D-aspartic acid receptor structure and function. *Physiol Rev, 74*, 723–759.
Milstein, A. D., & Nicoll, R. A. (2008). Regulation of AMPA receptor gating and pharmacology by TARP auxiliary subunits. *Trends Pharmacol Sci, 29*, 333–339.
Miyazawa, A., Fujiyoshi, Y., Stowell, M., & Unwin, N. (1999). Nicotinic acetylcholine receptor at 4.6 A resolution: transverse tunnels in the channel wall. *J Mol Biol, 288*, 765–786.
Mohrluder, J., Schwarten, M., & Willbold, D. (2009). Structure and potential function of gamma-aminobutyrate type A receptor-associated protein. *FEBS J, 279*, 4989–5005.
Nakanishi, S. (1992). Molecular diversity of glutamate receptors and implications for brain function. *Science, 258*, 597–603.
Neher, E. (1992). Ion channels for communication between and within cells. *Science, 256*, 498–502.
Olsen, R. W., Sapp, D. M., Bureau, M. H., Turner, D. M., & Kokka, N. (1991). Allosteric actions of central nervous system depressants including anesthetics on subtypes of the inhibitory gamma-aminobutyric $acid_A$ receptor-chloride channel complex. *Ann NY Acad Sci, 625*, 145–154.
Olsen, R. W., & Sieghart, W. (2009). $GABA_A$ receptors: subtypes provide diversity of function and pharmacology. *Neuropharmacology, 56*, 141–148.
Padgett, C. L., & Slesinger, P. A. (2010). $GABA_B$ receptor coupling to G-proteins and ion channels. *Adv Pharmacol, 58*, 123–147.
Role, L. W. (1992). Diversity in primary structure and function of neuronal nicotinic acetylcholine receptor channels. *Curr Opin Neurobiol, 2*, 254–262.
Rosenmund, C., Stern-Bach, Y., & Stevens, C. F. (1998). The tetrameric structure of a glutamate receptor channel. *Science, 280*, 1596–1599.
Sakmann, B. (1992). Nobel lecture. Elementary steps in synaptic transmission revealed by currents through single ion channels. *Neuron, 8*, 613–629.
Sheng, M., & Pak, D. T. (2002). Ligand-gated ion channel interactions with cytoskeletal and signaling proteins. *Annu Rev Physiol, 62*, 755–778.
Sine, S. M., & Engel, A. G. (2004). Recent advances in Cys-loop receptor structure and function. *Nature, 440*, 448–455.
Smit, A. B., Syed, L. I., Schaap, D., et al. (2001). A glial-derived acetylcholine-binding-protein that modulates synaptic transmission. *Nature, 411*, 261–268.
Sobolevsky, A. I., Rosconi, M. P., & Gouaux, E. (2009). X-ray structure, symmetry and mechanism of an AMPA-subtype glutamate receptor. *Nature, 462*, 745–756.
Steinbach, J. H. (1989). Structural and functional diversity in vertebrate skeletal muscle nicotinic acetylcholine receptors. *Annu Rev Physiol, 51*, 353–365.
Stern-Bach, Y., Bettler, B., Hartley, M., Sheppard, P. O., O'Hara, P. J., & Heineman, S. F. (1994). Agonist selectivity of glutamate receptors is specified by two domains structurally related to bacterial amino acid-binding proteins. *Neuron, 13*, 1345–1357.
Swope, S. L., Moss, S. J., Raymond, L. A., & Huganir, R. L. (1999). Regulation of ligand-gated ion channels by protein phosphorylation. *Adv Second Messenger Phosphoprotein Res, 33*, 49–78.
Unwin, N. (2005). Refined structure of the nicotinic acetylcholine receptor at 4 A resolution. *J Mol Biol, 346*, 967–989.
Westbrook, G. L., & Jahr, C. E. (1989). Glutamate receptors in excitatory neurotransmission. *Sem Neurosci, 1*, 103–114.
Wisden, W., & Seeburg, P. H. (1992). $GABA_A$ receptor channels: from subunits to functional entities. *Curr Opin Neurobiol, 2*, 263–269.
Wu, L. J., Sweet, T. B., & Clapham, D. E. (2010). International Union of Basic and Clinical Pharmacology. LXXVI. Current progress in the mammalian TRP ion channel family. *Pharmacol Rev, 262*, 381–404.

Chapter 32

Synaptic Transmission

Janusz B. Suszkiw

Chapter Outline

I. SUMMARY

The transmission of synaptic signals is mediated by chemical neurotransmitter substances. Neurotransmitters are synthesized in presynaptic terminals and stored in synaptic vesicles. Transmitter release is evoked by presynaptic action potentials (APs), which activate influx of Ca^{2+} into terminals and trigger a Ca^{2+}-dependent exocytosis of transmitter from synaptic vesicles into the synaptic cleft. Once released, neurotransmitters activate specific receptor-gated channels in the postsynaptic cell and elicit a transient change in the membrane permeability to cations or anions. Fast synaptic transmission is mediated by ionophoric receptors. Slow synaptic transmission is mediated by G-protein-coupled receptors. Excitatory postsynaptic potentials (EPSPs) are associated with transmitter-induced increase in Na^+ and K^+ conductance of the synaptic membrane, resulting in net entry of positive charge carried by Na^+ and membrane depolarization. Inhibitory postsynaptic potentials (IPSPs) are associated with transmitter-activated influx of Cl^- and membrane hyperpolarization. The EPSPs at the skeletal neuromuscular junction are called end-plate potentials (EPPs). In a healthy neuromuscular junction, the EPPs are always large enough to depolarize the muscle membrane to threshold and trigger muscle APs. The EPSPs generated at any single neuro-neuronal synapse are usually too small to depolarize the postsynaptic neuron to threshold. Synaptic signals converging onto a neuron are normally integrated through summation of EPSPs and IPSPs and an AP is triggered only when the resultant membrane potential reaches or exceeds the threshold. Chemical synaptic transmission is subject to modulation by intrinsic and extrinsic factors, including frequency and pattern of AP firing, which can either facilitate or depress the transmission across any given synapse.

II. INTRODUCTION

The function of nerve cells is to receive, process and transmit information. Intercellular transfer of signals among neurons or from neurons to effector cells is

Cell Physiology Sourcebook. DOI: 10.1016/B978-0-12-387738-3.00032-9

accomplished at specialized intercellular junctions called *synapses* and is by and large chemically mediated. A characteristic feature of a chemical synapses is the presence of a 20–100 nm wide extracellular space, the *synaptic cleft*, which separates the *presynaptic* (transmitting) and *postsynaptic* (receiving) elements of the synapse. This physical discontinuity prevents efficient transfer of current between the cells and necessitates intervention of a diffusible chemical transmitter substance. The fundamental aspect of chemically-mediated transmission is the transduction of voltage signal into the release of neurotransmitter from the presynaptic neuron and transduction of transmitter binding to a specific receptor into voltage change in the postsynaptic cell.

The basic principles of chemical neurotransmission have been elaborated in a series of seminal experiments conducted on the vertebrate skeletal neuromuscular junction by B. Katz and his collaborators in the 1950s and 1960s (Katz, 1966). At about the same time, the pioneering work by J.C. Eccles and his coworkers on spinal motor neurons showed that the general principles of chemical transmission established at the vertebrate neuromuscular junction also apply to central synapses (Eccles, 1964). Since then, new insights into the mechanism of synaptic transmission have been gained on the molecular level through the application of contemporary techniques of molecular biology and electrophysiology.

This chapter focuses on chemical synaptic transmission; however, the reader should be cognizant of another form of signal transfer, referred to as *electrical transmission*. Electrical transmission is mediated by the *gap junctions* (Bennett, 1997). Gap junctions consist of channel aggregates that bridge the closely apposed cell membranes and thus provide electrical continuity between the communicating cells. Unlike the chemical synapses, gap junctions and the electrical coupling they mediate are not unique to the nervous system but are also found in many other tissues. Gap junctions and electrotonic transmission are discussed in greater detail elsewhere in this volume.

III. STRUCTURE AND FUNCTION OF CHEMICAL SYNAPSES: AN OVERVIEW

Based on their morphofunctional characteristics, synaptic junctions may be classified as directed, fast-acting or non-directed, slow-acting synapses. Although the configurations of synaptic junctions can vary considerably, all share common features (Fig. 32.1). The presynaptic element, usually an axon terminal bouton or axon varicosity, is characterized by the presence of membrane-bound spherical organelles, the *synaptic vesicles*, which store the transmitter prior to its release. A subset of synaptic vesicles clusters near the presynaptic *active zone*, a structural specialization of the presynaptic membrane for synaptic vesicle docking and exocytosis. The juxtaposed postsynaptic membrane contains specific receptors for the transmitter released from the presynaptic terminal. A thickening of postsynaptic membrane, the *postsynaptic density*, is frequently observed and thought to play a role in localizing the neurotransmitter receptors at the synaptic membrane. The width of the synaptic cleft at highly directed (point-to-point), fast-acting synapses typically varies from about 20–50 nm but can be considerably wider at non-directed, slow-acting synapses. The synaptic cleft contains proteinaceous material, including various cell adhesion molecules (Hall and Sanes, 1993), thought to serve as an adherent for stabilizing the synapse. The junction is enveloped by glial elements, which insulate the synapse as well as perform other functions such as, for example, transmitter removal from the synaptic cleft. For a detailed discussion of synaptic ultrastructure, the student may wish to consult the articles in Pappas and Purpura (1972) and a more recent review by Burns and Augustine (1995).

Transmission at chemical synapses is *unidirectional* from the presynaptic to postsynaptic element. The presynaptic terminals are specialized for transmitter biosynthesis, packaging of transmitter into the synaptic vesicles and vesicular transmitter exocytosis. The transmitter receptors in the postsynaptic membrane transduce transmitter binding into ionic current which generates the *postsynaptic potential* (PSP). Postsynaptic potentials at fast synapses are generated by activation of *ionophoric*, or channel-forming, receptors. The synaptic potentials are typically fast in onset and last for only a few milliseconds. The generation of the postsynaptic potentials is, however, not instantaneous but rather registers 0.3–0.5 ms after the arrival of the action potential at the presynaptic terminal. This *synaptic delay* is a characteristic feature of chemical synapses and reflects, for the most part, the time required for the molecular events associated with the transmitter release. At non-directed, slow synapses, channels are not directly transmitter-gated but rather are coupled to the receptor via G protein and second messenger systems. These receptors are referred to as *metabotropic*. The synaptic potential generated by activation of the metabotropic receptors is slower in onset and longer lasting.

The process of chemical neurotransmission involves (1) synthesis and vesicular uptake of neurotransmitter in presynaptic terminal, (2) exocytotic release of vesicular transmitter into the synaptic cleft, (3) diffusion and binding of transmitter to postsynaptic receptors and generation of synaptic potential and (4) termination of synaptic activity. As indicated above, transmitters are synthesized in the nerve ending of the presynaptic neuron and are concentrated and stored in synaptic vesicles. The intravesicular packet or *quantum* of transmitter that is stored in the vesicles is released by Ca^{2+}-dependent exocytosis. Exocytosis is triggered when an AP in the presynaptic

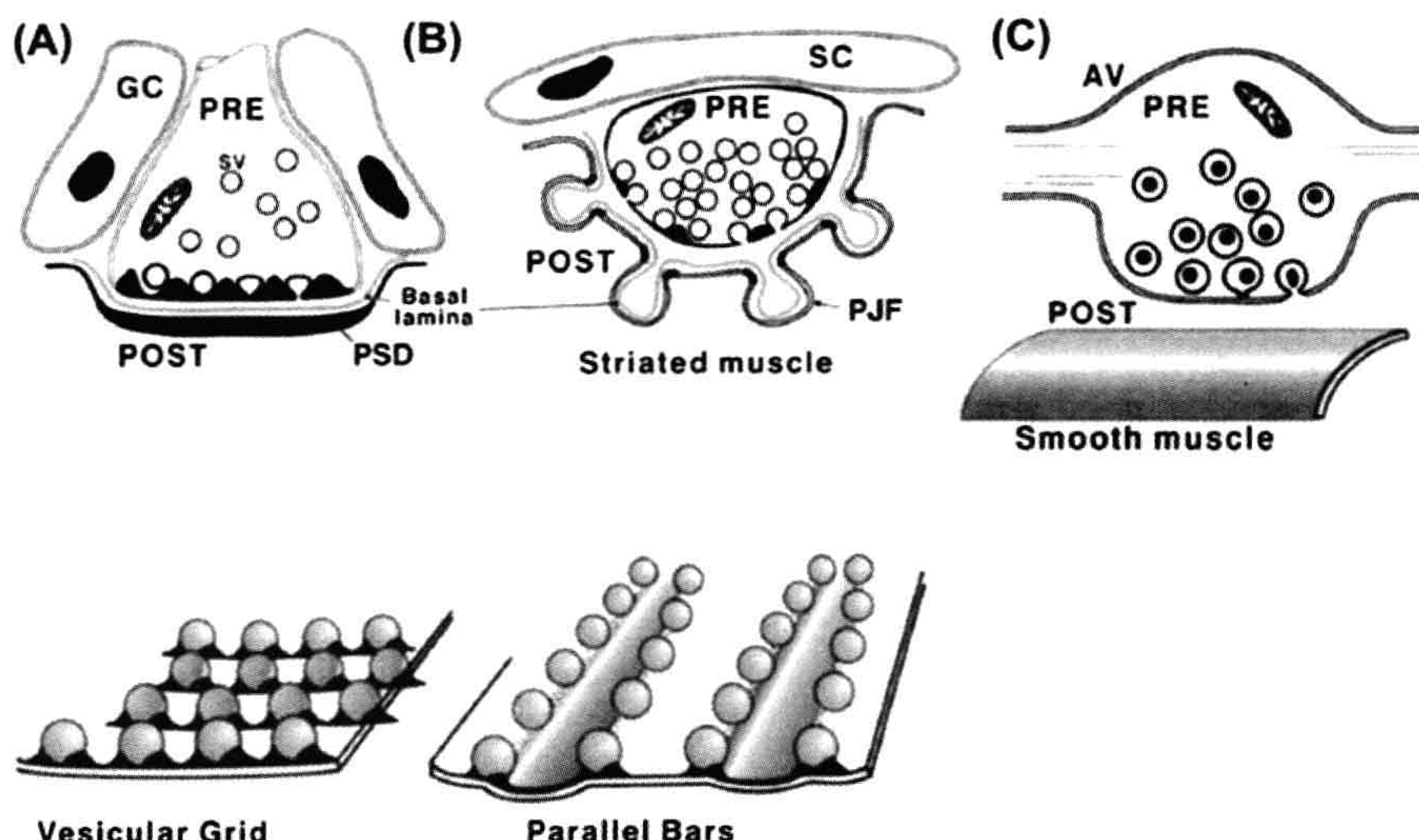


FIGURE 32.1 Schematic representations of neuro-neuronal and neuro-effector synaptic junctions. (A) A directed neuro-neuronal synapse subserving fast synaptic transmission in the CNS. The presynaptic terminal bouton contains mitochondria (M), clear-cored, about 40 nm in diameter, synaptic vesicles (SV), a subset of which is seen docked at the presynaptic vesicular grid. The receptors are localized in the juxtaposed thickening of postsynaptic membrane, the postsynaptic density (PSD). The presynaptic vesicular grid together with the juxtaposed PSD define the active zone of the synapse. The synaptic cleft is typically about 20 nm wide and contains dense material, with filamentous structures seen sometimes to span the cleft from pre-to-postsynaptic membrane. Glial cells (GC) cap and insulate the synapse. (B) The vertebrate skeletal neuromuscular junction (NMJ), a directed synapse subserving fast transmission from motor neuron to striated muscle. These large terminals are filled with many clear-cored, acetylcholine-containing synaptic vesicles. A few dense-cored vesicles can be also seen. A subset of clear-cored synaptic vesicles aggregate at the presynaptic active zone, which is defined by the presence of the presynaptic density. The presynaptic density appears to have the configuration of a bar defined by parallel rows of intramembrane particles, thought to represent the calcium channels, with two rows of vesicles attached on either side of the bar (bottom). The receptors for acetylcholine (AChR) are localized in the crests of the postjunctional folds (PJF) directly opposite the presynaptic active zones. The synaptic cleft at the vertebrate NMJ is typically 50 nm wide. The basal lamina within the synaptic cleft contains AChE, an enzyme that degrades ACh released into the synaptic cleft. The junction is insulated by Schwann cell (SC) processes. (C) A non-directed, slow-acting synapse between a presynaptic axon varicosity (AV) of a sympathetic neuron and smooth muscle. The varicosity contains large (>60 nm) dense-core, norepinephrine-containing vesicles. This synapse is characterized by the absence of distinct active zone structures and a variable but usually wide (>100 nm) separation between the presynaptic and postsynaptic elements of the junction.

neurons invades and depolarizes the nerve terminal, thereby opening the presynaptic voltage-gated Ca^{2+} channels and allowing influx of Ca^{2+} into the terminal. The resulting transient rise in $[Ca^{2+}]_i$ triggers fusion of synaptic vesicles with the plasmalemma and transmitter exocytosis. The requirement for Ca^{2+} influx is absolute. In absence of Ca^{2+}, the presynaptic AP will fail to trigger release.

Following its release into the synaptic cleft, transmitter combines with specific receptors in the postsynaptic membrane, causing a change in its permeability to specific ions. Change in membrane permeability to ions gives rise to synaptic current which, depending on ions involved, depolarizes or hyperpolarizes the postsynaptic membrane (Fig. 32.2). The depolarizing potential is called an *excitatory postsynaptic potential* (EPSP) because it tends to bring the cell membrane potential toward the threshold for an AP. EPSPs are associated with a change in the postsynaptic membrane permeability to Na^+ and K^+ ions and a net influx of positive charges (inward current carried by Na^+). The hyperpolarizing potential is called an *inhibitory postsynaptic potential* (IPSP), because it tends to move or hold the membrane potential away from the threshold, thus decreasing the likelihood of an AP being fired. The IPSPs elicited by activation of ionophoric receptors at fast synapses are associated with an increase in the postsynaptic membrane permeability to Cl^-. PSPs associated with activation of metabotropic receptors usually involve change in membrane permeability to K^+ ions.

Transmitter release normally terminates within less than 1 ms. As the presynaptic AP decays and the terminal repolarizes back toward the resting potential, the depolarization-activated calcium channels reclose, Ca^{2+} influx ceases and $[Ca^{2+}]_i$ is rapidly lowered to the prestimulus level. Transmitter action on the receptors in the postsynaptic membrane is terminated by diffusion and enzymatic degradation into an ineffective substance or clearance from the synaptic cleft by reuptake into the nerve terminals and/or glial cells. Reuptake and subsequent catabolism is the primary route of transmitter inactivation for most transmitters. The exception is acetylcholine, in

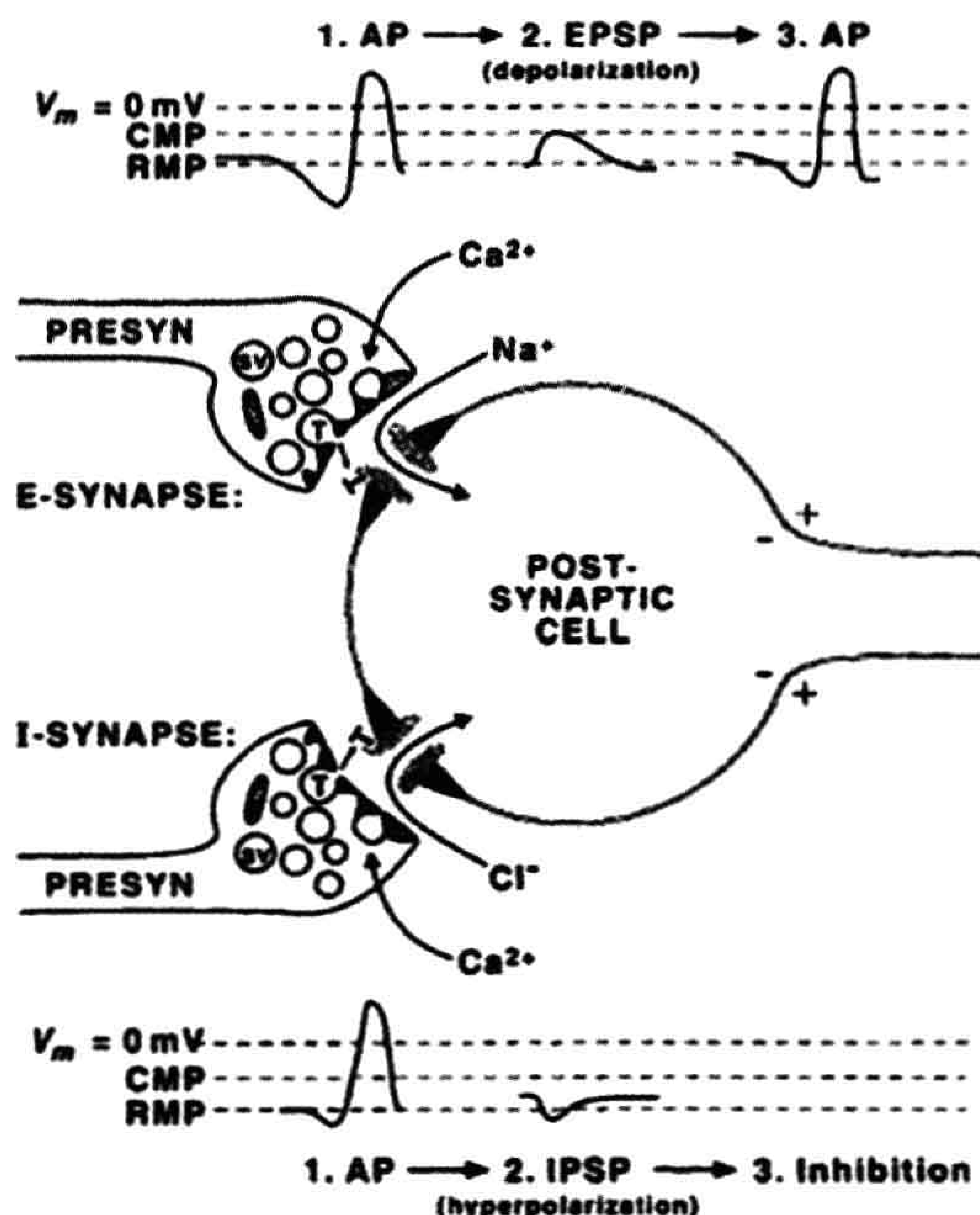


FIGURE 32.2 Fast excitatory versus inhibitory synaptic transmission. At an excitatory (E) synapse, the presynaptic action potential releases transmitters that activate cationic channels, resulting in an inward synaptic current carried by Na^+ ions and depolarizing potential, the excitatory postsynaptic potential (EPSP). EPSPs increase the likelihood of an action potential (AP) being fired by the postsynaptic cell. At an inhibitory (I) synapse, the transmitter activates receptor-gated chloride channels and influx of Cl^- ions, resulting in hyperpolarizing potential, the inhibitory postsynaptic potential (IPSP). The likelihood of an AP is diminished by activation of I-synapses because IPSPs hold or move the membrane potential of the postsynaptic cell away from the threshold. RMP, resting membrane potential; CMP, critical membrane potential (threshold) at which an AP is triggered.

which case inactivation is primarily by means of extracellular degradation of ACh to inactive acetate and choline.

IV. NEUROTRANSMISSION

IVA. Neurotransmitters and Neurotransmitter Receptors

Several criteria define a chemical substance as a neurotransmitter. (1) The biosynthetic enzymes for the synthesis of the substance must be present in the identified presynaptic neuron to catalyze the synthesis of transmitter in the nerve terminals. (2) The substance must be released by stimulation of the presynaptic neuron in a Ca^{2+}-dependent manner. (3) Application of the substance to the postsynaptic cell must mimic the actions of the neurally released substance. (4) A specific mechanism for inactivation of the transmitter substance, such as a selective uptake system in the presynaptic terminals or the presence of degradative enzyme(s), must be demonstrated at the synapse investigated.

Amino acid glutamate is the major excitatory neurotransmitter and γ-aminobutyric acid (GABA) and glycine serve as inhibitory transmitters in the CNS. Acetylcholine (ACh), dopamine (DA), norepinephrine (NE), epinephrine, serotonin (5-HT), histamine and ATP are all recognized as neurotransmitters or neurotransmitter candidates. Acetylcholine and norepinephrine are the established transmitters in the peripheral nervous system. In addition, there is good evidence that in the vascular smooth muscle, ATP is co-released and acts as a co-transmitter with NE. Neurons may also co-store and co-release various peptide hormones. These may act as co-transmitters or modulate the synaptic actions of conventional transmitters. Common low-molecular-weight transmitter substances and their chemical structures are shown in Fig. 32.3.

Neurotransmitter receptors (Table 32.1) are integral membrane proteins containing the transmitter recognition site and the transducer site. Ionophoric or channel-forming receptors include the muscle and neural nicotinic acetylcholine receptors; three pharmacologically distinguishable glutamate receptors that are selectively activated by analogs of glutamate – kainate, α-amino-3-hydroxy-5-methylisoxazole-4-propionic acid (AMPA) or N-methyl-D-aspartic acid (NMDA); the $5HT_3$ serotonin receptor; and

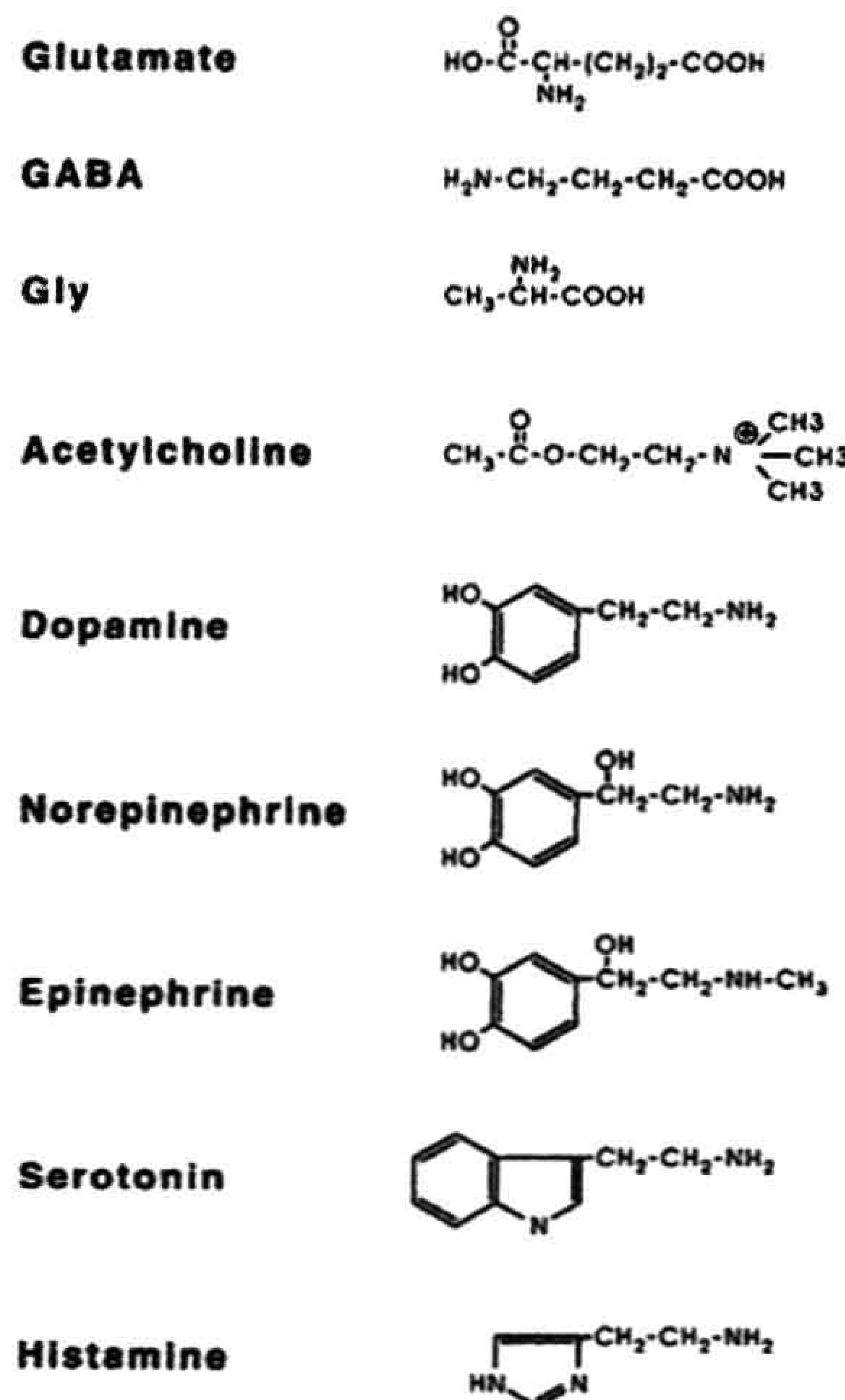


FIGURE 32.3 Structural formulas of common neurotransmitters.

TABLE 32.1 Common Neurotransmitters and Major Receptor Types

Transmission type	Neurotransmitter	Receptor[a]
Amino acidergic	Glutamic acid	**Kainate, AMPA, NMDA**, mGluR
	Gamma-aminobutyric acid (GABA)	**$GABA_A$**, $GABA_B$, **$GABA_C$**
	Glycine	**Gly-R**
Cholinergic	Acetylcholine	**nAChR**, mAChR
Aminergic	Dopamine	D_1, D_2
	Norepinephrine	α_1, α_2, β_1, β_2
	Serotonin	$5HT_1$, $5HT_2$, **$5HT_3$**
	Histamine	H_1, H_2, H_3
Purinergic	ATP, adenosine	P_1, **P_{2x}**, P_{2y}

[a] *Ionophoric or channel-forming receptors are indicated in bold. Regular lettering indicates metabotropic or G-protein-coupled receptors.*

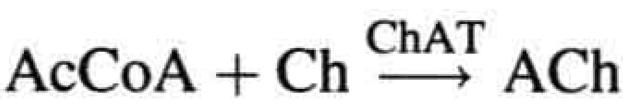
the P_{2x} purinoceptor for ATP. These relatively non-specific cationic channels permit passage of Na^+, K^+ and, in some cases, Ca^{2+} ions, but exclude anions. The anionic (Cl^-) channel-forming receptors include the $GABA_A$ and $GABA_C$ receptors and the glycine receptors (Gly-R).

Metabotropic receptors transduce the transmitter binding into a physiological response via G-protein/second messenger-coupled mechanisms. The synaptic actions of monoamines, dopamine, norepinephrine, epinephrine, serotonin and histamine are exerted via the G-protein/second messenger-coupled mechanisms systems. The G-protein-coupled receptors also include the muscarinic ACh receptors, metabotropic glutamate receptor (mGluR), $GABA_B$ and several receptors for adenosine and ATP. Ligand-gated and G-protein-coupled channels are discussed elsewhere in this volume.

IVB. Biosynthesis, Storage and Inactivation of Neurotransmitters

Conventional, low-molecular-weight neurotransmitters are synthesized locally in the nerve terminals and packaged into synaptic vesicles (SV) prior to release. The local synthesis of transmitter in the nerve terminals assures that transmitter is available for refilling the vesicles after they have released their contents into the synaptic cleft. The vesicular uptake of transmitters is mediated by specific transporters and is driven by an electrochemical gradient generated by electrogenic proton pump in the vesicular membrane (McMahon and Nicholls, 1991). Following release, the synaptic neurotransmitter action is terminated by diffusion, reuptake into presynaptic terminals or glial cells and degradation. Reuptake of transmitters from the extracellular space is energetically coupled to a transmembrane Na^+ gradient and is mediated by specific high affinity transporters that are distinct from the vesicular transporters. Two families of plasmalemmal transporters have been identified. The carriers for excitatory amino acids require the presence of extracellular Na^+, whereas the carriers for biogenic amines, GABA and glycine require both Na^+ and Cl^- for uptake (Fig. 32.4). (Amara and Arriza, 1993; Sonders and Amara, 1996.)

The key enzyme(s) involved in transmitter synthesis are selectively expressed in the neurons and define their neurotransmitter phenotype. Choline acetyltransferase (ChAT) is the marker enzyme for cholinergic neurons where it catalyzes the synthesis of acetylcholine (ACh) from acetyl coenzyme A (AcCoA) and choline (Ch):



$$AcCoA + Ch \xrightarrow{ChAT} ACh$$

Acetyl coenzyme A derives from the tricarboxylic acid (TCA) cycle whereas choline is transported into nerve terminals from the extracellular medium by the sodium-dependent, high-affinity carrier system that is localized in the presynaptic terminals. Transport of choline and synthesis of ACh are tightly coupled and both the rate of choline uptake and ACh synthesis increase during activity, ensuring adequate supply of the transmitter. The vesicular

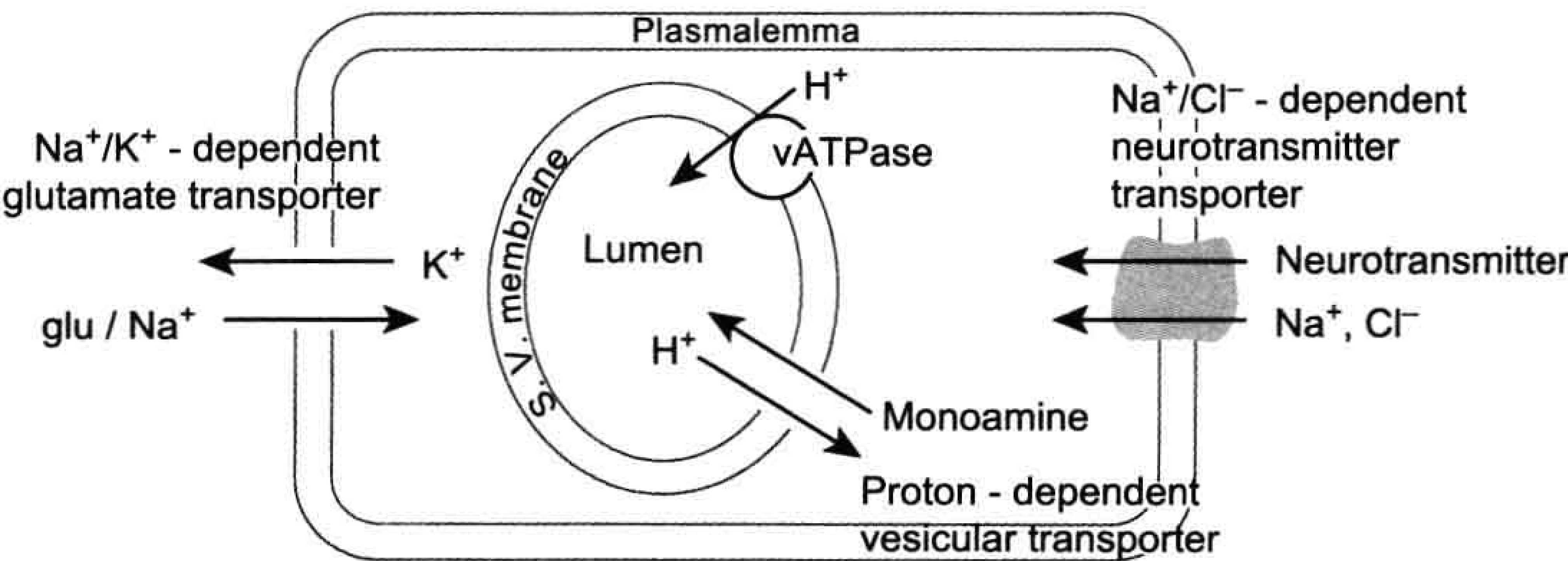
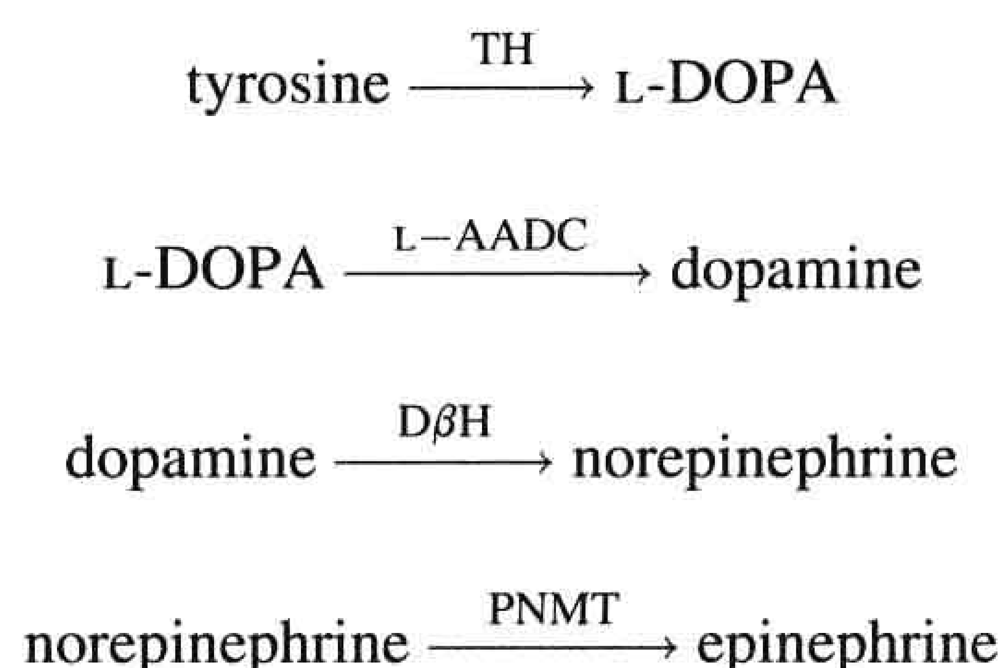


FIGURE 32.4 Neurotransmitter transport systems in vesicular and plasmalemmal membranes. *(Based on Amara and Arriza, 1993.)*

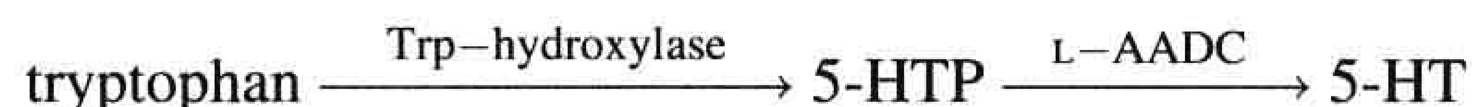
ACh transporter (VAChT) mediates uptake of ACh from the cytosol into synaptic vesicles. The plasmalemmal Ch uptake is selectively inhibited by a chemical hemicholinium-3 (HC-3) whereas vesamicol blocks vesicular uptake of ACh. Either of these drugs will cause depletion of ACh and failure of cholinergic transmission. Following its release, the synaptic action of ACh is terminated by diffusion and acetylcholinesterase (AChE)-catalyzed hydrolysis to inactive acetate and choline. Much of the choline is recaptured by the nerve terminals and reutilized in new ACh synthesis.

Catecholaminergic neurons and their synaptic connections comprise dopaminergic, noradrenergic (norepinephrine) and adrenergic (epinephrine) systems. The rate-limiting step in catecholamine biosynthesis is the tyrosine hydroxylase (TH)-catalyzed hydroxylation of tyrosine to L-dihydroxyphenylalanine (l-DOPA), which is then decarboxylated by a non-specific aromatic l-amino acid decarboxylase (L-AADC) to dopamine. Dopamine is taken up into synaptic vesicles and serves as a transmitter at dopaminergic synapses. In noradrenergic nerve endings, dopamine is further converted to norepinephrine by intravesicularly localized dopamine-β-hydroxylase (DβH). Methylation of norepinephrine to epinephrine at adrenergic synapses is catalyzed in cytosol by phenylethanolamine-N-methyltransferase (PNMT) in a reaction requiring S-adenosylmethionine as methyl donor:


$$\text{tyrosine} \xrightarrow{\text{TH}} \text{L-DOPA}$$
$$\text{L-DOPA} \xrightarrow{\text{L-AADC}} \text{dopamine}$$
$$\text{dopamine} \xrightarrow{\text{D}\beta\text{H}} \text{norepinephrine}$$
$$\text{norepinephrine} \xrightarrow{\text{PNMT}} \text{epinephrine}$$

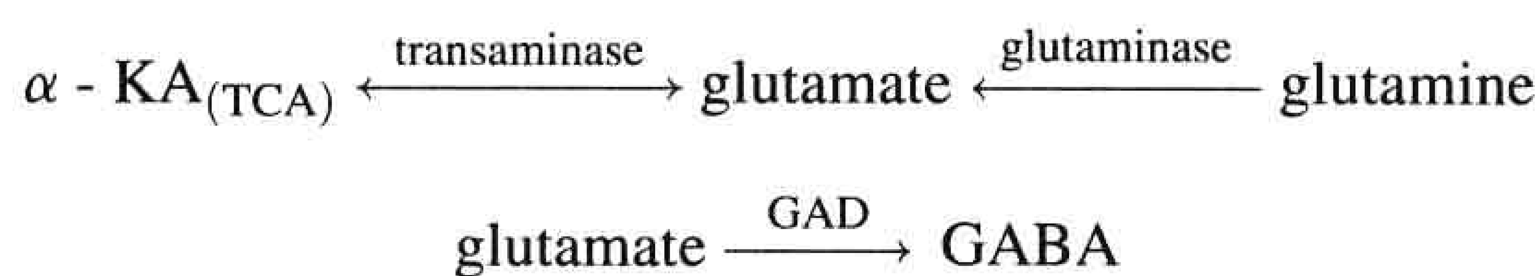
Vesicular monoamine transporters (VMATs) mediate the uptake of catecholamines into synaptic vesicles. Reserpine inhibits the VMATs and thereby depletes vesicular stores of catecholamines. Synaptic actions of catecholamines are terminated by high-affinity neuronal reuptake followed by intracellular degradation or reuptake into synaptic vesicles. The plasmalemmal catecholamine transporters are distinct from VMATs. Plasmalemmal reuptake is insensitive to reserpine but is blocked by psychoactive drugs, such as cocaine and amphetamine, which thereby increase extracellular levels of catecholamines. The major catabolic pathway for catecholamines involves the mitochondrial monoamine oxidase (MAO)-catalyzed oxidative deamination to aldehydes followed by their rapid conversion by hydrogenases and reductases to corresponding acids and alcohols.

Serotonergic neurons utilize serotonin as the transmitter. Serotonin, an indoleamine, is formed by tryptophan hydroxylase-mediated hydroxylation of tryptophan to 5-hydroxytryptophan (5-HTP), followed by l-AADC-mediated decarboxylation of 5-HTP to 5-hydroxytryptamine (5-HT, serotonin):


$$\text{tryptophan} \xrightarrow{\text{Trp-hydroxylase}} \text{5-HTP} \xrightarrow{\text{L-AADC}} \text{5-HT}$$

Uptake of serotonin into synaptic vesicles appears to be mediated by the same or a closely related VMAT that mediates vesicular transport of catecholamines. The synaptic action of serotonin is terminated primarily by neuronal sodium-dependent reuptake, mediated by a transporter that is homologous to the plasmalemmal transporters for catecholamines. Following reuptake, serotonin is degraded by MAO-catalyzed oxidative deamination to 5-hydroxyindole acid aldehyde and 5-hydroxyindole acetic acid.

Glutamic acid, GABA and glycine are the major amino acid neurotransmitters in the CNS. Because glutamic acid and glycine are common constituents of amino acid pools found in all cells, their use as neurotransmitters at glutamatergic and glycinergic synapses implies subcompartmentation within the respective nerve terminals. This subcompartment in all likelihood corresponds to synaptic vesicles (SV), which presumably selectively accumulate glutamic acid and glycine from the cytosol and release them during synaptic transmission. The amino acid neurotransmitters are synthesized in nerve terminals from intermediates of the tricarboxylic acid (TCA) cycle. Glutamate is formed by transamination of α-ketoglutaric acid (α-KA) and GABA is formed from glutamate in a reaction catalyzed by glutamic acid dehydrogenase (GAD), a marker enzyme for GABAergic neurons. Inactivation of synaptic actions of glutamate and GABA is through reuptake into nerve terminals as well as the glial cells, where both amino acids are converted to glutamine, which is in turn exported to the nerve terminals and reutilized in the formation of glutamate:


$$\alpha\text{ - KA}_{(\text{TCA})} \xleftrightarrow{\text{transaminase}} \text{glutamate} \xleftarrow{\text{glutaminase}} \text{glutamine}$$
$$\text{glutamate} \xrightarrow{\text{GAD}} \text{GABA}$$

IVC. Transmitter Release

Transmitter release is evoked by arrival of an action potential at the presynaptic terminal. Depolarization of the nerve terminal membrane activates (opens) the plasmalemmal voltage-gated Ca^{2+} channels, allowing influx of extracellular Ca^{2+} into the terminal. The resultant transient increase of Ca^{2+} concentration near the plasmalemmal

release sites triggers a cascade of biochemical events that culminate in synaptic vesicle–plasmalemma fusion and exocytosis of transmitter into the synaptic cleft. The process terminates upon nerve terminal repolarization when the Ca^{2+} channels deactivate (close), Ca^{2+} entry ceases and intracellular Ca^{2+} returns to prestimulus levels.

IVC1. Quantal-Vesicular Hypothesis of Transmitter Release

The evolution of the current understanding of the mechanism of transmitter release began with the formulation of the *quantal-vesicular hypothesis* of transmitter release by Bernard Katz and his collaborators (Fatt and Katz, 1952; delCastillo and Katz, 1954). Katz and colleagues observed that, in the resting neuromuscular junction, i.e. in the absence of stimulation, nerve terminals spontaneously release ACh, giving rise to small depolarizations that occur at random intervals and average about 0.5 mV in amplitude (Fig. 32.5A). These small potentials behaved in all respects as miniature replicas of the end-plate potential (EPP) evoked by presynaptic APs (Fig. 32.5B) and therefore were called miniature end-plate potentials (MEPPs). The crucial insight into the relationship between MEPPs and EPPs was provided by the observation that when evoked release was reduced in low-Ca^{2+}/high-Mg^{2+} solutions, the size of EPPs fluctuated in a random manner (Fig. 32.5C) such that the EPP amplitudes appeared to be made up of integral multiples of the average MEPP amplitude and could be described by Poisson distribution (Fig. 32.6). Katz concluded that transmitter release is a stochastic process, consisting of random release of multimolecular packets or quanta of ACh each producing a unit response (MEPPs) and that the EPP is a summation of many quantal units released nearly synchronously by a presynaptic AP.

For detailed discussion of the statistics of transmitter release, the interested reader is referred to Martin (1977). For the present purpose, it suffices to state that transmitter release can be described by a simple statistical expression:

$$m = nP$$

The parameter m is the average number of quanta released per presynaptic impulse when a large number of trials are performed and is called the *quantal content* of the EPP. The parameter n represents the number of quanta immediately available for release and most likely corresponds to either the population of synaptic vesicles associated with the presynaptic active zones or the number of release sites. P is the probability of any single quantum being released and primarily reflects the probability of a productive Ca^{2+}-dependent vesicle fusion with the plasmalemma as a function of Ca^{2+} concentration at the release sites. Reducing the availability of Ca^{2+} to enter terminals would reduce P, thus accounting for a reduction of transmitter release in low-Ca^{2+}/high-Mg^{2+} media. Conversely, increasing the concentration of Ca^{2+} at or near the release sites would tend to enhance the probability of exocytosis, i.e. facilitate transmitter release.

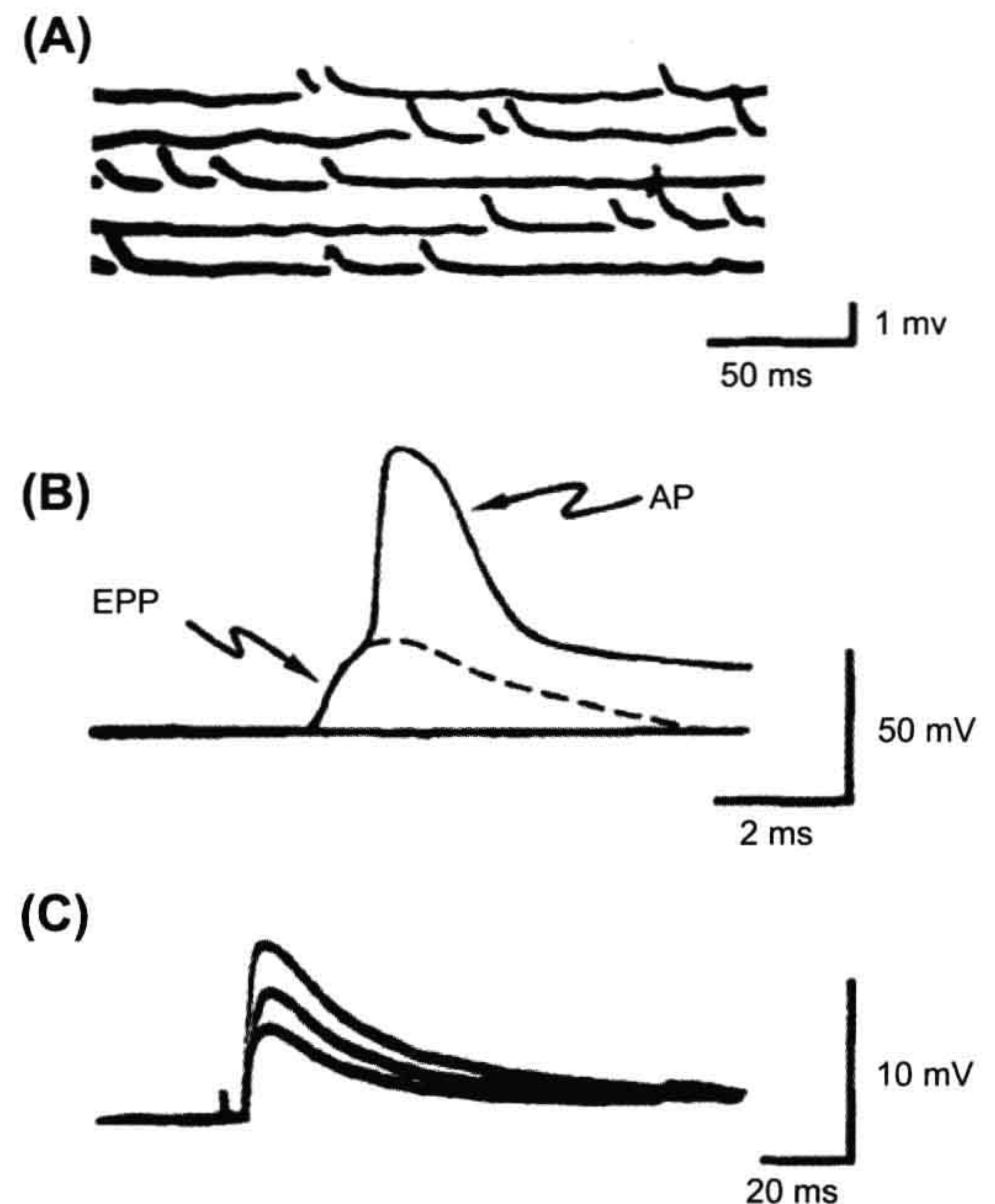


FIGURE 32.5 Intracellular recordings from the frog end-plate. (A) Spontaneous, miniature end-plate potentials (MEPPs) recorded from resting (not stimulated) junction. Note that these small depolarizing potentials are less than 1 mV in amplitude and occur randomly. (B) Postsynaptic response to a presynaptic action potential. The initial hump on the recorded waveform is the end-plate potential (EPP) elicited by ACh released by the presynaptic AP. Note that the EPP is a large depolarization (>40 mV), sufficient to bring the end-plate to threshold and trigger a muscle AP. (C) Fluctuations in EPPs when transmitter output has been reduced by adding 10 mM Mg^{2+} to the bathing medium. *(Adapted from Fatt and Katz, 1952, and delCastillo and Katz, 1954.)*

IVC2. Essential Role of Ca^{2+} in Depolarization-Release Coupling

The voltage-gated calcium channels in the presynaptic plasma membrane couple membrane depolarization to transmitter exocytosis. The essential role of Ca^{2+} influx in transmitter release was demonstrated by Katz and Miledi (1967), who showed that depolarization of presynaptic terminals failed to evoke transmitter release when Ca^{2+} was absent or its entry into nerve terminals was prevented by high Mg^{2+} concentration in the extracellular medium (Fig. 32.7). In subsequent experiments carried out at the squid giant synapse, where it is possible to make intracellular recordings from both pre- and postsynaptic cells simultaneously, Miledi (1973)

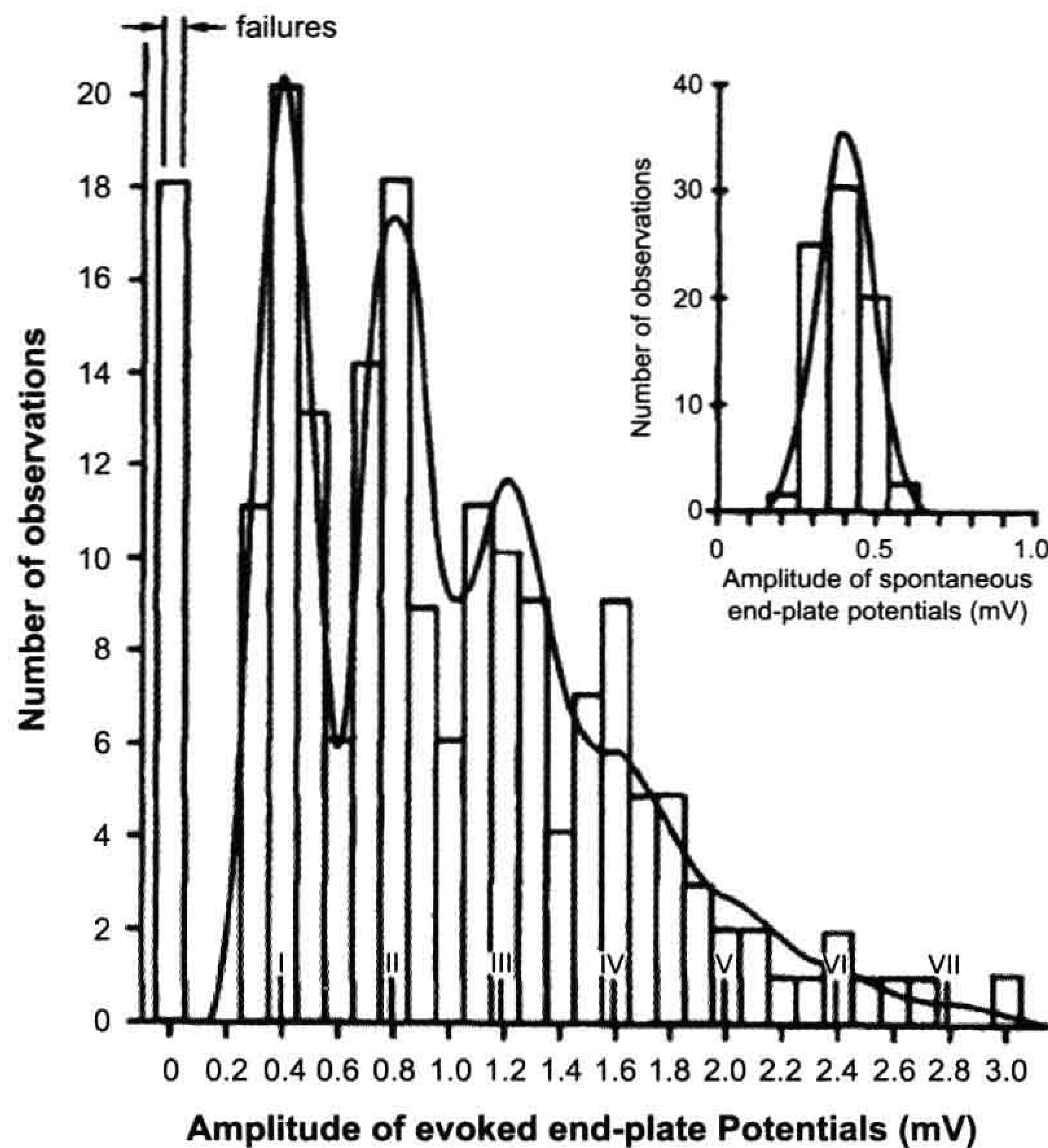


FIGURE 32.6 Distribution of EPP amplitudes recorded from mammalian end-plate under conditions of reduced transmitter release in high (12.5 mM) Mg^{2+}. The inset shows a histogram of spontaneous potentials (MEPPs) recorded from resting junction. Note that EPP amplitudes group around multiples of mean MEPPs amplitude and the number of experimentally observed failures (0 quanta released) and single, double, triple, or more quantal responses, fit the theoretical distribution (solid curve) calculated from the Poisson equation. *(From Boyd and Martin, 1956.)*

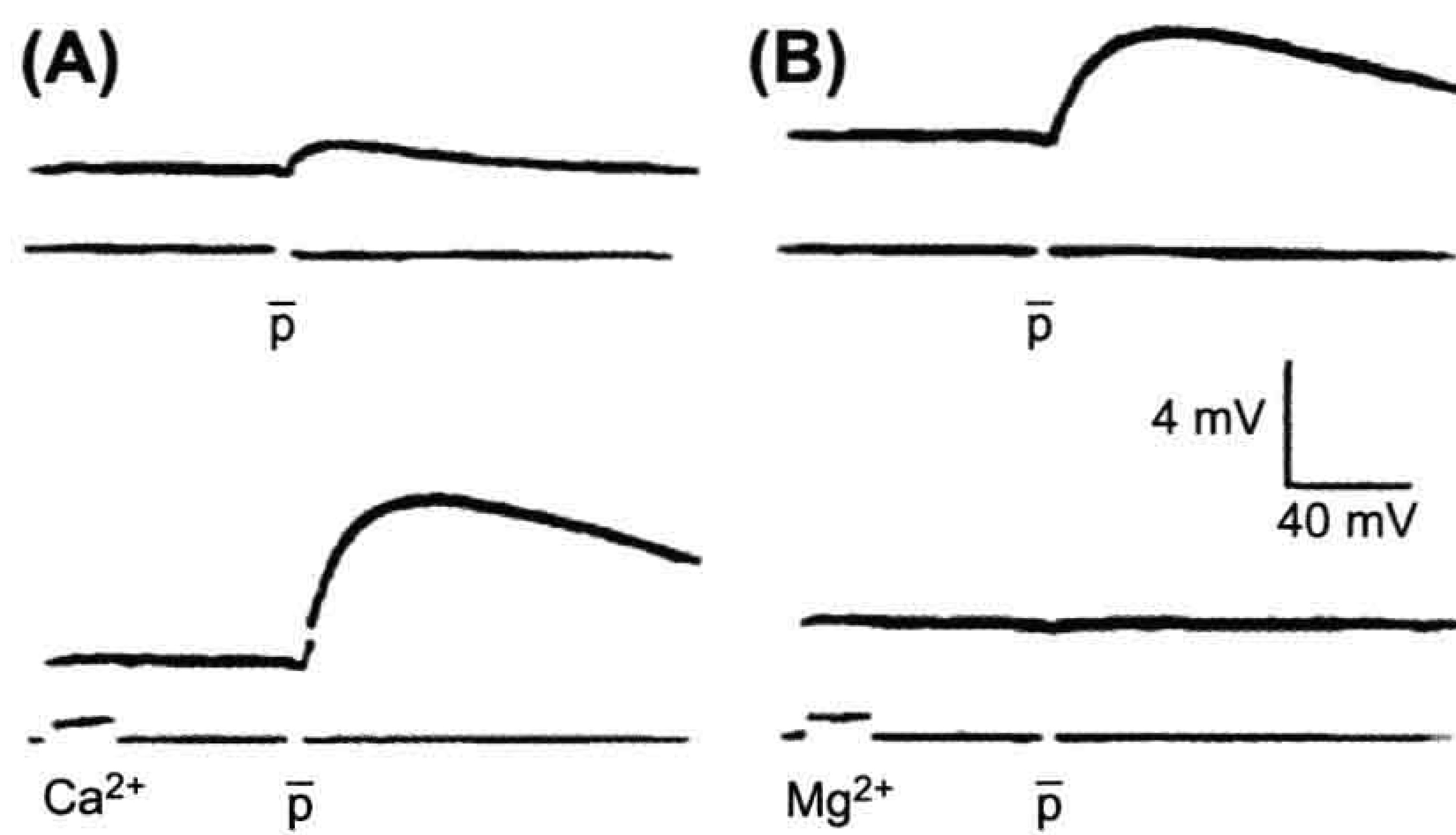


FIGURE 32.7 Calcium is required for transmitter release evoked by depolarization of nerve terminals. In the absence of Ca^{2+}, a depolarizing pulse (p) applied to a presynaptic nerve fails to evoke transmitter release and the postsynaptic response is nearly absent (A, top). Application of a pulse of Ca^{2+} to the neuromuscular junction shortly before applying stimulus (p) to the presynaptic nerve enables transmitter release as shown by the appearance of a postsynaptic response (A, bottom). The normal postsynaptic response in Ca^{2+}-containing media (B, top) is blocked by applying a pulse of high Mg^{2+} prior to the depolarizing pulse (p) (B, bottom). The failure to elicit transmitter release in the presence of high Mg^{2+} is due to block of Ca^{2+} influx into the terminals. *(Adapted from Katz and Miledi, 1967.)*

showed that injection of Ca^{2+} into presynaptic terminals elicited transmitter release, thus providing direct evidence that a rise in intracellular Ca^{2+} alone is sufficient for activation of the release process. Furthermore, using voltage-clamping to control the membrane potential of the presynaptic terminals at the squid giant synapse, Llinas (1977) showed that the quantity of synaptic transmitter released, monitored as the size of the postsynaptic potential, is related to the size of the presynaptic calcium current which, in turn, depends on the extent of nerve terminal depolarization (Fig. 32.8).

The presynaptic calcium channels that couple membrane depolarization to transmitter release at fast synapses appear to be strategically localized near the release sites (Robitaille et al., 1990). Opening of these channels results in domains of calcium entry, giving rise to localized subplasmalemmal calcium concentrations that may reach 0.1 mM or higher very rapidly and for a very brief duration (Smith and Augustine, 1988). These subplasmalemmal calcium transients represent more than a thousand-fold increase of $[Ca^{2+}]$ relative to the resting cytosolic calcium level of about 0.1 μM and provide a powerful trigger for focal synaptic vesicle exocytosis. The relationship between intracellular calcium concentration and the rate of exocytosis investigated in the terminals of goldfish retinal bipolar neurons indicates half-saturation at about 200 μM and cooperative interactions involving at least four calcium ions in activation of synaptic vesicle exocytosis (Heidelberger et al., 1994). Transmitter release occurs within about 60 μs following calcium entry into presynaptic terminals, indicating that Ca^{2+}-triggered exocytosis involves activation of a preassembled vesicle–plasmalemma docking/fusion complex (Bruns and Jahn, 1995; Sabatini and Regehr, 1996).

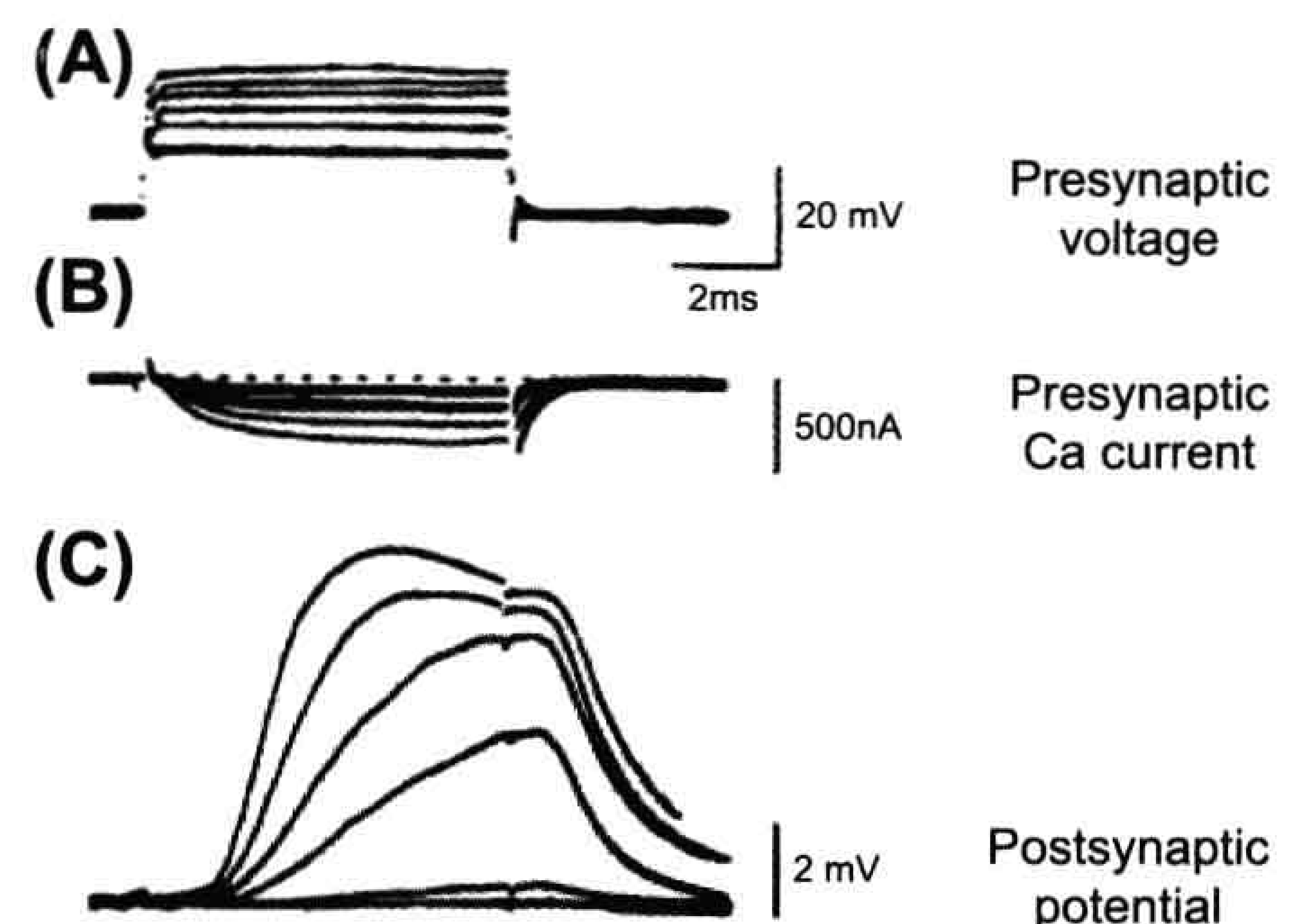


FIGURE 32.8 Experiments in the squid giant synapse illustrating the relationship between magnitude of presynaptic Ca^{2+} current and transmitter release monitored by recording postsynaptic potentials. Graded depolarizations of presynaptic terminals (A) evoke graded inward Ca^{2+} currents (B) that correlate with graded postsynaptic potentials (C), which reflect the amount of transmitter released. *(Adapted from Llinas, 1977.)*

IVC3. Exocytosis and Recycling of Synaptic Vesicles

The active zones in the presynaptic nerve terminals provide plasmalemmal specializations for synaptic vesicle docking and exocytosis. In ingenious experiments, Heuser and coworkers (1979) employed a specially constructed quick-freeze apparatus that enabled them to capture images of vesicle exocytosis at the active zone of the frog neuromuscular junction (Fig. 32.9). The comparison of the number of exocytotic pores captured in the quick-freeze experiment correlated with the estimated number of quanta released under similar conditions of stimulation, providing the most direct, structural evidence that exocytosis of synaptic vesicles at the active zone region is the likely mechanism of quantal transmitter release.

Synaptic vesicles within the terminal are distributed among the so-called readily available and reserve pools. The *readily available pool* is thought to correspond to the vesicles docked at the active zone and immediately available for release, whereas the *reserve pool* comprises the vesicles distributed within the terminal at some distance from the active zone. It is evident that, in order to maintain the availability of quanta for release, exocytosis must be accompanied by mobilization of new vesicles from the reserve pool within the terminal to the plasmalemmal release sites. Mobilization of vesicles is thought to involve alteration in vesicle cytoskeleton interactions that are regulated by phospho-dephosphorylation of synaptic vesicle-associated proteins, synapsins. Dephosphorylated synapsin seems to stabilize vesicle–cytoskeletal interactions and inhibit vesicle mobilization, whereas phosphorylation of synapsin by the Ca^{2+}-calmodulin-dependent protein kinase II is thought to promote vesicle mobilization (Llinas et al., 1991; Greengard et al., 1993).

The mechanism of vesicle docking and initiation of exocytosis by Ca^{2+} has not been yet completely worked out; however, remarkable progress has been made since the early 1990s. Studies initially conducted in model systems such as mast cells or chromaffin cells and then extended to synaptic preparations indicate that secretion is accompanied by a stepwise increase in cell capacitance, consistent with fusion of secretory granules with the cell membrane. Electrical measurements further suggest that the first event in exocytosis may be the formation of a pore that connects vesicle lumen with the extracellular space and may provide a channel for the release of soluble contents into the synaptic cleft and/or promote collapse and complete fusion of vesicle with the plasma membrane (Lindau and Almers, 1995; Matthews, 1996).

Beginning with the identification and cloning of synaptic proteins in the early 1990s (reviewed in Südhof, 1995), extraordinarily rapid progress has been made during the last few years in defining the molecular machinery of exocytosis. Current evidence indicates that the synaptic exocytotic apparatus makes use of constitutive membrane fusion machinery that has been placed under control of

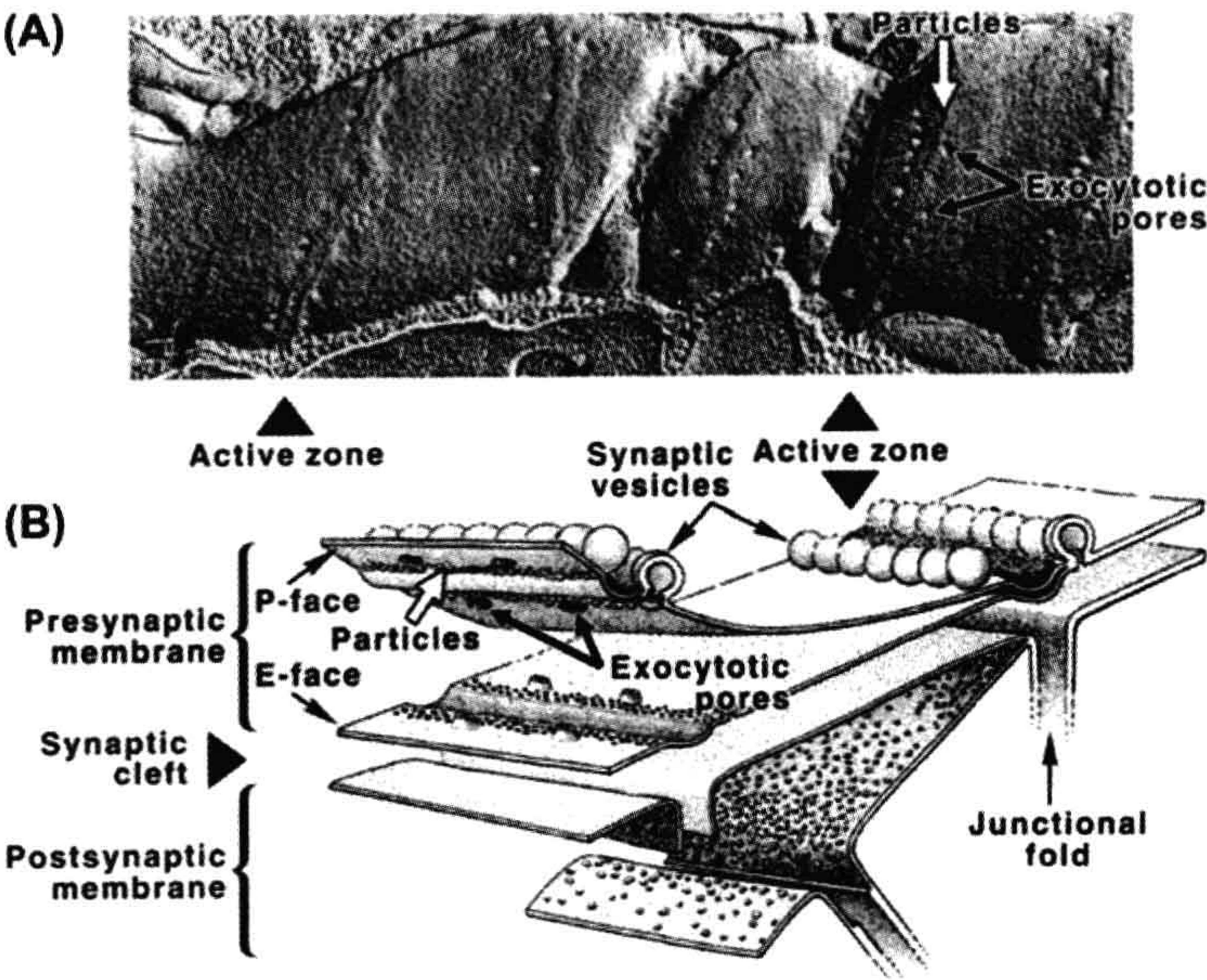


FIGURE 32.9 Synaptic vesicle exocytosis captured by a rapid-freezing technique. (A) P-face of freeze-fractured replica of a stimulated and rapidly frozen nerve terminal showing images of synaptic vesicles caught in the process of exocytosis at the active zones. The junction was activated in presence of 1 mM 4-aminopyridine to enhance the level of transmitter release per single presynaptic impulse. (*Adapted from Heuser et al. (1979). J Cell Biol. 81, 275–300.*) (B) Three-dimensional representation of pre- and postsynaptic membranes in relation to the freeze-fracture image above. The freeze-fracture splits membrane bilayers into protoplasmic (P-face) and extracellular (E-face) leaflets of the bilayer. The rows of intramembrane particles seen in P- and E-faces are thought to be the presynaptic Ca^{2+} channels. The openings in the P-face and their craterlike continuations in the E-face are the exocytotic pores formed when synaptic vesicles fuse with the plasmalemma along the parallel bars of the active zone. (*Adapted from Heuser et al. (1979). J Cell Biol. 81, 275–300.*)

a calcium sensor. The elements of the constitutive docking–fusion apparatus at synapses are the synaptic vesicle membrane-associated protein (VAMP) synaptobrevin and the plasma membrane proteins syntaxin and SNAP-25 (25-kDa, synaptosome-associated protein). The VAMP, syntaxin and SNAP-25 belong to a class of highly conserved membrane-targeting proteins that serve as SNAP (soluble NSF attachment protein) receptors and hence are referred to as SNAREs (Söllner et al., 1993a,b). The SNAREs have been shown to associate into a stable, 7-S core complex that links the apposed vesicle and plasma membranes through formation of parallel bundles of four interacting α-helices, with syntaxin and synaptobrevin each contributing one helix and SNAP-25 contributing two helices (Sutton et al., 1998). The evidence for the crucial role of SNARE complexes in exocytosis has been provided by the observation that selective proteolysis of either VAMP, syntaxin or SNAP-25 by clostridial neurotoxins prevents formation of the complex and inhibits transmitter release (Niemann et al., 1994; Hayashi et al., 1994). Biochemical studies indicate that the core complex is primed by ATP-dependent, SNAP-assisted binding of NSF (N-maleimide-sensitive factor). NSF is an ATPase whose activation is thought to play an important role in fusion by inducing a conformational change in syntaxin and disassembly of the SNARE complex (Whiteheart et al., 1994; Hanson et al., 1997). The synaptic vesicle membrane protein synaptotagmin 1, whose cytosolic domains contain two Ca^{2+}-binding C2 motifs homologous to the C2 regulatory domain of protein kinase C, is believed to serve as the Ca^{2+}-sensor of exocytosis (Brose et al., 1992; Shao et al., 1977). Biochemical experiments indicate that Ca^{2+} activation of synaptotagmin is associated with simultaneous binding of its C2 domains to the membrane phospholipids and the SNARE complex. The kinetics of synaptotagmin–Ca^{2+}–core complex interactions occur on a microsecond time scale consistent with its postulated function as Ca^{2+}-trigger receptor of exocytosis (Davis et al., 1999). Another protein that has been implicated in exocytosis is neurexin (Petrenko et al., 1991), a plasmalemmal protein that provides a target for α-latrotoxin, a component of black widow spider venom that induces massive Ca^{2+}-independent transmitter exocytosis. Through its capacity to associate with synaptotagmin, neurexin could somehow modulate interactions between synaptotagmin and SNAREs. A simplified model of a vesicle docking–fusion complex is illustrated in Fig. 32.10. Several other synaptic vesicle- and plasma membrane-associated proteins have been identified that are likely to have either accessory or regulatory functions in vesicle exocytosis/endocytosis (Südhof, 1995); however, their precise function and mechanism of action still remain by and large unresolved.

Following the release of transmitter, exocytosis may be terminated in at least two ways. One is simply through reclosure of the pore and fission of vesicles at the active zone. These postexocytotic vesicles may then refill with locally synthesized transmitter and, by virtue of being already positioned close to or at the active zone, release the newly formed transmitter in preference to the reserve pool. This could explain the well-documented phenomenon of the preferential release of newly synthesized transmitter. A more generally accepted idea is that, following fusion and exocytosis, vesicle membrane collapses into the

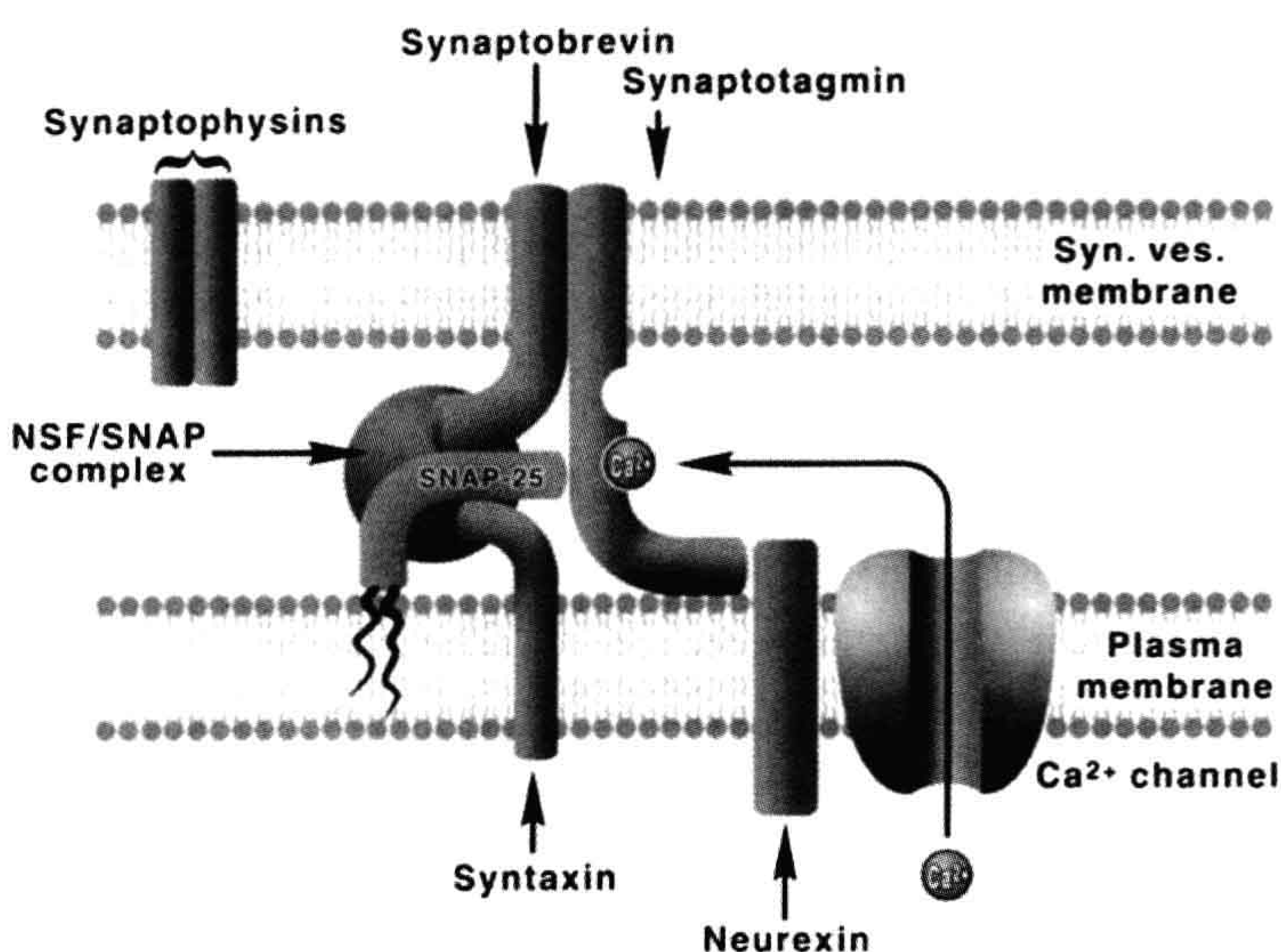


FIGURE 32.10 A simplified model of a vesicle docking–fusion complex. The model incorporates interactions among the proteins of synaptic vesicles (synaptobrevins and synaptotagmins), plasma membrane proteins (syntaxins, SNAP-25, neurexin) and the soluble elements of constitutive fusion machinery (NSF, SNAP). Synaptobrevin, syntaxin and SNAP-25 form a stable, 7-S core complex to which SNAP and NSF (an ATPase) bind to form a 20-S complex. Activation of NSF ATPase leads to disassembly of the complex, perhaps assisting in the final step of membrane fusion. The complex is thought to form in close proximity to the plasmalemmal calcium channels, with synaptotagmin serving as the key Ca^{2+} sensor. The plasma membrane protein neurexin interacts with synaptotagmin and may modulate its interactions with the core complex.

presynaptic plasmalemma to be retrieved in a series of transformations starting with clathrin-mediated endocytosis followed by endosomal fusion-budding and reformation of functional vesicles (Fig. 32.11). It is likely that both types, the rapid exo-endocytosis as well as the slower, clathrin-mediated endocytosis occur, but the extent to which one predominates over the other depends on the rate of presynaptic stimulation and possibly other factors. The evidence for local recycling of synaptic vesicles in the nerve terminals has been provided by the observation that vesicles become labeled with high-molecular-weight markers such as horseradish peroxidase (HRP) or dextrans when motor nerve terminals are stimulated with these markers in the extracellular medium (Ceccarelli et al., 1973). More recent evidence for vesicle recycling has been provided by tracking the movement of fluorescent-labeled synaptic vesicles during stimulation of motor nerve terminals at the frog neuromuscular junction (Betz and Bewick, 1992) and in other synaptic preparations (Ryan et al., 1993; Lagnado et al., 1996).

Vesicles undergoing local recycling within the nerve terminals are progressively degraded and replaced by vesicles that are formed de novo in the cell body and transported to the nerve terminals by fast axoplasmic transport. The half-life of vesicles has been estimated at 7–14 days. Evidently, synaptic vesicles can undergo numerous cycles of transmitter release-reloading before being replaced with new ones.

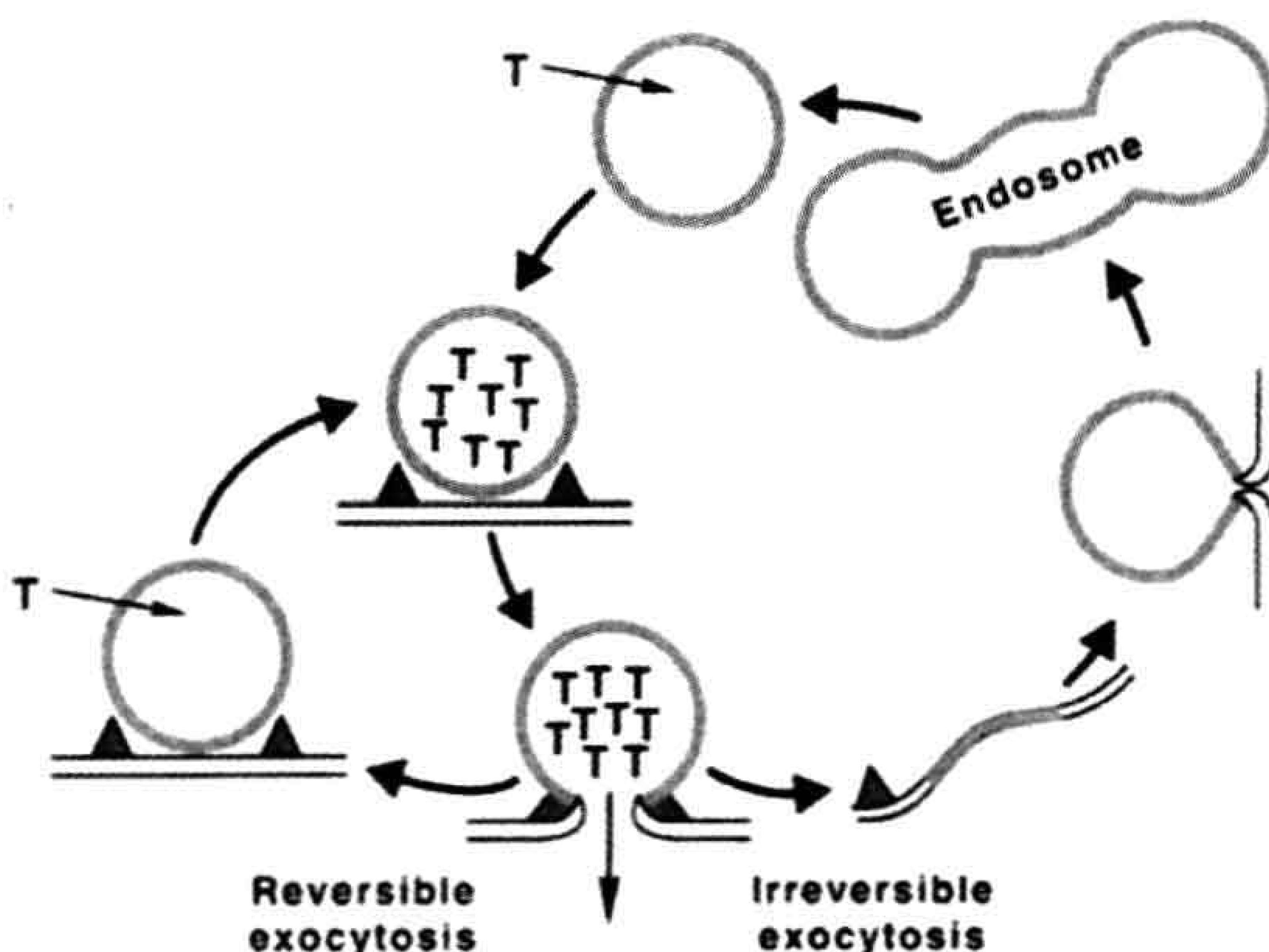


FIGURE 32.11 Synaptic vesicle cycling in nerve endings. Following vesicle docking and fusion, synaptic vesicles can recycle through a short or long pathway. The short pathway (left) involves transient fusion between vesicle and plasma membrane, followed by fission and recharging of the emptied vesicle with new transmitter (T). In the long pathway (right), vesicle membrane collapses into the plasmalemma to be eventually retrieved and reformed via a sequence of steps, then reloaded with new transmitter.

IVD. Generation of Postsynaptic Potentials at Fast Synapses

The nature of postsynaptic responses is determined by the type of receptor-gated ionic conductances that are activated in the postsynaptic membrane. At excitatory synapses, the transmitters activate receptor-gated channels that conduct cations, principally Na^+ and K^+. The net current through the synaptic channels is inward and carried by Na^+ ions, causing a depolarization of the postsynaptic membrane, or EPSP. The EPSPs generated at the skeletal neuromuscular junction are called end-plate potentials (EPPs) and those at other peripheral synapses, e.g. at nerve–smooth muscle junctions, are frequently referred to as excitatory junctional potentials, or EJPs. At inhibitory synapses, transmitters activate receptor-gated channels that conduct Cl^- ions. Influx of chloride ions through the synaptic channels tends to increase the negativity of the cell interior and hyperpolarizes the postsynaptic membrane. The hyperpolarizing postsynaptic potentials are called inhibitory postsynaptic potentials (IPSPs) because they tend to move the membrane potential away from the threshold.

IVD1. Synaptic Current and Synaptic Equilibrium Potential

The synaptic current (i_S) flowing through a single transmitter-activated channel is determined by the channel conductance (γ_S) and the electrochemical driving force ($V_m - E_s$) acting on the ions moving through the channel:

$$i_S = \gamma_S(V_m - E_S) \quad (32.1)$$

where V_m and E_S are membrane potential and the synaptic equilibrium potential, respectively.

In resting synapse, most of the receptor-gated channels are closed and the conductance of the postsynaptic membrane to ions is very low. When transmitter is released by presynaptic impulse, it binds to its receptors in the postsynaptic membrane and opens the associated channels for a short, 1–2 ms duration. The resultant total synaptic current, I_S, is a sum of currents through all opened channels:

$$I_S = n\gamma_S(V_m - E_S) = g_S(V_m - E_S) \quad (32.2)$$

where n is the number of active channels and g_S is the total synaptic conductance ($n\gamma_S$).

At excitatory synapses, the transmitter-activated channels permit the passage of both Na^+ and K^+ ions with about equal ease and the excitatory postsynaptic current $I_{S(E)}$ is the sum of Na^+ and K^+ currents:

$$I_{S(E)} = I_{Na} + I_K = g_{Na}(V_m - E_{Na}) + g_K(V_m - E_K) \quad (32.3)$$

where g_{Na} and g_K are Na^+ and K^+ ion conductances and E_{Na} and E_K are the Na^+ and K^+ equilibrium potentials, respectively. The direction and magnitude of ion flux is determined by the electrochemical driving forces ($V_m - E_i$). Because g_{Na} $(V_m - E_{Na}) > g_K(V_m - E_K)$, i.e. $I_{Na} > I_K$, the net synaptic current is always inward and carried by Na^+ ions, resulting in membrane depolarization. As the membrane potential (V_m) becomes depolarized, the term ($V_m - E_{Na}$) decreases and ($V_m - E_K$) increases until equilibrium is reached, where the inward Na^+ current is exactly equal to the outward K^+ current:

$$I_{Na} = -I_K \quad (32.4)$$

or

$$g_{Na}(V_m - E_{Na}) = -g_K(V_m - E_K) \quad (32.5)$$

The membrane potential V_m at which this occurs is the synaptic equilibrium potential (E_S). By solving for V_m, it is seen that E_S is a weighted average of sodium and potassium equilibrium potentials:

$$E_S = (g_{Na}/(g_{Na} + g_K))E_{Na} + (g_K/(g_K + g_{Na}))E_K \quad (32.6)$$

E_S is the limiting potential to which the postsynaptic membrane can be depolarized during the transmitter action. Any further depolarization beyond this point would result in $I_K > I_{Na}$ and reversal of net synaptic current from inward to outward direction. Therefore, the E_S is also called a *reversal potential* (E_r).

It is evident that activation of receptor-gated Cl^- channels at inhibitory synapses results in the synaptic current given by:

$$I_{S(I)} = g_S(V_m - E_S) \quad (32.7)$$

where the equilibrium potential E_S is the chloride equilibrium potential, E_{Cl}. This is the limiting potential to which a synaptic membrane can be hyperpolarized during the action of transmitter at inhibitory synapse.

IVD2. Relationship Between Synaptic Currents and Postsynaptic Potentials

The relationship between the synaptic current and postsynaptic potential can be analyzed in terms of an equivalent electrical circuit consisting of parallel synaptic and non-synaptic branches, as is illustrated for an excitatory synapse in Fig. 32.12. The synaptic branch represents the synaptic receptor-gated conductance (g_S) in series with the synaptic battery of the synaptic equilibrium potential E_S. The non-synaptic branch consists of membrane capacitance C_m and leakage channels (g_m) in series with the battery of the resting membrane potential, E_m.

During the synaptic action of transmitter at the E-synapses, the synaptic current (I_S) flows inward through the synaptic branch and outward through the parallel capacitive and resistive elements of the non-synaptic branch as I_C and I_m. The direction of current flow at the I-synapses is a mirror image of that at excitatory synapses.

$$I_{S(E)} = -(I_C - I_m) \quad (32.8a)$$

and

$$-I_{S(I)} = -(I_C + I_m) \quad (32.8b)$$

where

$$I_C = C_m dV_m/dt \quad (32.9)$$

and

$$I_m = g_m(V_m - E_m) \quad (32.10)$$

At the onset of synaptic action most of the synaptic current flows through the capacitive branch because the outward driving force ($V_m - E_m$) on current flow through the non-synaptic channels (g_m) is small. Once the membrane capacitance is discharged (depolarization) or charged (hyperpolarization) to its final value, all synaptic current exits through the leakage channels (g_m). Thus, at the peak of synaptic activation, $I_C = 0$ and

$$I_{S(E)} = -I_m \quad (32.11a)$$

$$-I_{S(I)} = I_m \quad (32.11b)$$

at E- and I-synapses, respectively.

Substituting Equations 32.2 and 32.10 into Equation 32.11 and solving for V_m yields the expression for the postsynaptic membrane potential at the peak of synaptic activation:

$$V_m = (g_S/(g_S + g_m))E_S + (g_m/(g_S + g_m))E_m \quad (32.12)$$

Equation 32.12 shows that the value of membrane potential (V_m) at the peak of synaptic activation is a weighted average of E_S and E_m, where the weighting factors are the relative magnitudes of synaptic (g_S) and non-synaptic (g_m) conductances. During peak activation of synaptic channels, $g_S > g_m$ and the membrane potential will tend toward the E_S but the amplitude of PSP (i.e. $V_m - E_m$) will be influenced by g_m of the non-synaptic membrane.

IVD3. Time Course of PSPs

The synaptic potentials are electrotonic potentials: they decay passively as a function of time and distance. The time course of the rising phase of the synaptic potential is determined by both active and passive properties of the membrane. As the synaptic channels spontaneously reclose, the PSP decays in an exponential fashion. The decay of the PSP is purely a passive process whose time course is a function of the membrane time constant, τ. The membrane time constant is the time required for an

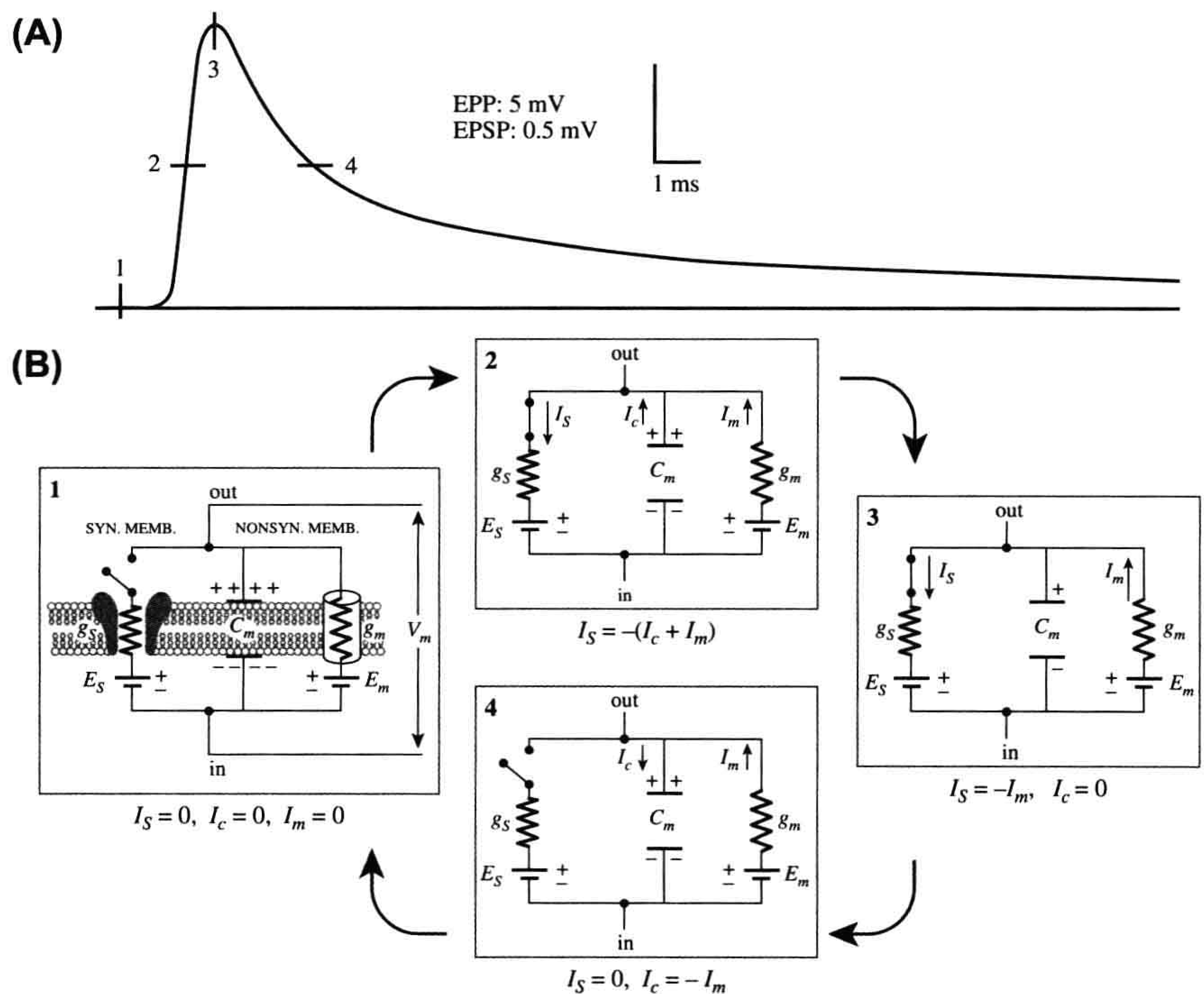


FIGURE 32.12 Equivalent electrical circuit description of excitatory synaptic potential. Four phases of the postsynaptic potential (A) and the corresponding equivalent circuit representations (B) are illustrated. (1) At rest, the transmitter-gated synaptic channels are closed (circuit open; no current flow; $dV/dt = 0$). (2) Onset of synaptic action (active phase). Synaptic channels are opened by transmitter binding to the receptor (the synaptic switch is closed) and I_s flows inward through the synaptic branch (g_s) and outward as I_c and I_m through the non-synaptic branch. (3) At the peak of synaptic action, capacitance C_m has discharged to its final value, $I_c = 0$ and $I_s = -I_m$ ($dV/dt = 0$). (4) Passive decay phase. Synaptic channels have reclosed (synaptic switch open) and $I_s = 0$. The current through the non-synaptic membrane consists of outward I_m and inward I_c, which recharges the membrane capacitance and repolarizes the membrane back to the prestimulus membrane potential. *(Based on Kandel et al. (2000). Principles of Neural Science. McGraw-Hill, New York. Reproduced with permission of The McGraw-Hill Companies.)*

electrotonic potential to decay to 1/e or 37% of its peak value. The time constant of neurons is in the range of 1−20 ms. The amplitude of the synaptic potentials decreases exponentially from the maximum recorded focally at the synapse as a function of the membrane length constant, γ. The length constant is the distance at which electrotonic potentials decay to $1/e$ or 37% of their amplitude at the point of origin. The length constant of dendrites is typically in the range 0.1 to 1 mm.

IVE. Slow Synaptic Transmission Mediated by G-Protein-Coupled Receptors

In contrast to fast synaptic potentials mediated by directly transmitter-gated channels, slow synaptic responses are mediated by a distinct family of proteins that transduce the transmitter binding into cellular responses through activation of GTP-binding regulatory proteins or G proteins. Binding of a transmitter to a specific receptor transforms the associated G protein into an active form that modulates activity of ionic channels at some distance from the receptor either through direct interaction with the channel and/or through second messenger systems. The slow synaptic transmission may involve either increase or decrease in postsynaptic membrane conductance due to a channel opening or channel closure, respectively. For example, activation of muscarinic receptors in heart muscle causes a G-protein-mediated opening of a certain class of voltage-gated K^+ channels and relatively long-lasting (seconds) membrane hyperpolarization. Similar, G-protein modulated potassium channels K(G) are present in central neurons, where they mediate slow IPSPs. In contrast, activation of a muscarinic receptor in sympathetic ganglion neurons and certain neurons in the central nervous system is associated with a second-messenger-mediated closure of K^+ channels and membrane depolarization. The responses

to transmitter activation of G-protein-coupled receptors need not be limited to modulation of ionic channels but also involve modifications of other regulatory proteins resulting in long-term modifications of the postsynaptic cell's physiology. For a more detailed discussion of G proteins and second messengers in slow synaptic actions of neurotransmitters, the reader is referred to Schulman and Hyman (1999).

IVF. Synaptic Integration versus Amplification

Central neurons can receive from several dozens to several thousand excitatory (E) and inhibitory (I) synaptic connections converging on the target neuron from a variety of other neurons in the brain. Whether or not a neuron discharges a propagated AP is determined by the number of E-synapses and I-synapses active at any one time. It should be noted that, even in absence of IPSPs, activation of a single excitatory synapse would be insufficient to discharge an AP, because individual PSPs generated at central synapses are very small, usually in the range of 0.5–2 mV in amplitude. Therefore, summation of several EPSPs is usually necessary to bring the membrane of the postsynaptic neuron to the threshold potential.

The postsynaptic neurons integrate the synaptic potentials by adding the EPSPs and subtracting the IPSPs from the membrane potential at any instant of time. Algebraic summation of two or more topographically separated synapses that are activated nearly simultaneously is called *spatial summation*. The effectiveness of spatial summation depends on the membrane space constant which, it will be recalled, is the distance at which electrotonic potentials decay to 37% of their amplitude at the point of origin. Clearly, synaptic inputs separated by a distance smaller than the space constant can sum together more effectively than those that are separated by distances larger than the space constant. When a presynaptic neuron fires at a rate such that the interval between successive presynaptic APs is less than the duration of the PSP, each succeeding PSP adds to its predecessor. This process is referred to as *temporal summation*. Effectiveness of temporal summation depends on the membrane time constant (i.e. the time required for an electrotonic potential to decay to 37% of its peak value). The larger the time constant, the longer is the duration of the PSP and thus the greater the opportunity for summation of successive PSPs to occur. A propagated action potential will be triggered only if the net current is of sufficient magnitude to depolarize the neuronal membrane to the threshold. An action potential is normally triggered at the initial segment of an axon, the region of the neuron with the lowest threshold. Since summation of synaptic currents at the initial segment is the principal determinant of whether or not an AP will be fired, the initial segment is referred to as the *integrative zone* of the neuron.

In contrast to the integrative activity at central synapses, the function of the neuromuscular junction is to transfer without failure the AP from the presynaptic motor neuron to the postsynaptic muscle fiber. In this case, the excitatory postsynaptic potential referred to as the endplate potential (EPP) is normally always suprathreshold and sufficient to trigger the muscle AP. It may be noted that because the nerve terminal is very small in diameter compared with the muscle fiber it innervates, even if these two membranes were contiguous, the current generated during the invasion of presynaptic terminal by an AP would be insufficient to depolarize the postsynaptic membrane to threshold due to impedance mismatch between the two membranes; i.e. the small nerve terminal cannot provide enough action current to depolarize the large-diameter skeletal muscle fiber much more than about 1 mV. Thus, the function of transmitter at the neuromuscular junction is to amplify the presynaptic signal.

IVG. Modulation of Synaptic Transmission

The efficacy of signal transmission at chemical synapses can be modulated by extrinsic and intrinsic factors, including the pattern of ongoing activity as well as history of previous activity. The efficacy of transmission may be altered by mechanisms that affect the dynamics of presynaptic transmitter release and/or modify the postsynaptic receptor-mediated events. This modification may be short lasting or may persist for some time. Thus, synaptic modulation provides for fine-tuning of ongoing synaptic activity as well as for longer lasting changes that are likely to play an important role in learning processes.

IVG1. Depression

Depression or fatigue of synaptic transmission refers to progressive reduction in the amplitudes of postsynaptic potentials in the course of prolonged, relatively high-frequency activation of presynaptic neurons, reflecting progressive depletion of releasable transmitter stores. Recovery from fatigue may take from minutes to hours.

IVG2. Facilitation

Facilitation is a frequency-dependent increase in the amplitude of postsynaptic potentials evoked by closely spaced presynaptic action potentials. The increase in the amplitudes of succeeding PSPs reflects the progressively larger amount of transmitter released with each nerve impulse in the course of stimulation. The mechanism is thought to involve build-up of ionized Ca^{2+} within the

terminals. That is, when presynaptic neuron is stimulated at certain frequency, the diffusion and clearance of Ca^{2+} from the release sites begins to lag and the residual Ca^{2+} adds to the Ca^{2+} transient evoked by the next arriving impulse. Build-up of Ca^{2+} increases the probability (P) of transmitter quanta being released. Facilitation is a relatively short-lived process that lasts for a few seconds.

IVG3. Post-Tetanic Potentiation

When the nerve is activated with relatively prolonged and/or high-frequency (tetanic) bursts of impulses, the quantity of transmitter is increased upon subsequent stimulation, even after a relatively long intervening rest period. This phenomenon is known as post-tetanic potentiation. In contrast to facilitation, post-tetanic potentiation may last for minutes and sometimes hours, suggesting a long-term modification of presynaptic function secondary to increase in cytosolic Ca^{2+} levels.

IVG4. Long-Term Potentiation

Long-term potentiation (LTP) refers to a long-lasting increase in EPSP following tetanic stimulation in the presynaptic neurons. It is distinguished from post-tetanic potentiation (PTP) in that the latter is a strictly presynaptic phenomenon, whereas induction and expression of LTP involves both postsynaptic and presynaptic elements. LTP was first described (Bliss and Lomo, 1973) and analyzed most extensively in the hippocampus. In the CA1 region, the LTP involves a special glutamate receptor subtype, the NMDA receptor. The NMDA receptor-gated channel is normally blocked by Mg^{2+}, but can be activated by glutamate when the postsynaptic neuron is sufficiently depolarized so that the Mg^{2+} blockade of the channel is relieved. The induction of LTP appears to be associated with influx of Ca^{2+} and activation of Ca^{2+}-dependent protein kinases CaM kinase II and protein kinase C, and possibly other protein kinases in the postsynaptic dendritic spine, which leads to increased efficacy of synaptic transmission that may last for days to weeks. It is thought that while induction of LTP involves the postsynaptic events, the maintenance of LTP may be associated with long-term increase in the probability of transmitter release, a presynaptic event.

IVH. Presynaptic Receptors and Transmitter Release

Receptors for neurotransmitters are not confined to postsynaptic sites, but are also found on presynaptic nerve terminals. The modulation of transmitter release by presynaptic receptors that respond to transmitter released by another neuron is referred to as *heterosynaptic modulation*. Heterosynaptic modulation may involve either inhibition or facilitation of transmitter release. In addition, certain presynaptic autoreceptors recognize the cell's own neurotransmitter. In this case, the neuron's transmitter may modulate its own release by interacting with these receptors. This is called *automodulation*. For example, many cholinergic neuron terminals possess muscarinic autoreceptors and ACh released from these terminals acts on the autoreceptors to inhibit its own release. Although the physiological role of presynaptic receptors has been a subject of debate, it is evident that they provide a potential mechanism for fine-tuning of transmitter release.

BIBLIOGRAPHY

Amara, S. G., & Arriza, J. L. (1993). Neurotransmitter transporters: three distinct gene families. *Curr Opin Neurobiol, 3*, 337–344.

Bennett, M. V. L. (1997). Gap junctions as electrical synapses. *J Neurocyt, 26*, 349–366.

Bennett, M. K., & Scheller, R. H. (1993). The molecular machinery for secretion is conserved from yeast to neurons. *Proc Natl Acad Sci USA, 90*, 2559–2563.

Betz, W. J., & Bewick, G. S. (1992). Optical analysis of synaptic vesicle recycling at the frog neuromuscular junction. *Science, 255*, 200–203.

Bliss, T. V. P., & Lomo, T. (1973). Long-lasting potentiation of synaptic transmission in the dentate area of the anaesthetized rabbit following stimulation of the perforant path. *J Physiol, 232*, 331–356.

Boyd, I. A., & Martin, A. R. (1956). The end-plate potential in mammalian muscle. *J Physiol, 132*, 30–38.

Brose, N., Petrenko, A. G., Südhof, T. C., & Jahn, R. (1992). Synaptotagmin: a calcium sensor on the synaptic vesicle surface. *Science, 256*, 1021–1025.

Bruns, D., & Jahn, R. (1995). Real-time measurement of transmitter release from single synaptic vesicles. *Nature, 377*, 62–65.

Burns, M. E., & Augustine, G. J. (1995). Synaptic structure and function: dynamic organization yields architectural precision. *Cell, 83*, 187–194.

Ceccarelli, B., Hurlbut, W. P., & Mauro, A. (1973). Turnover of transmitter and synaptic vesicles at the frog neuromuscular junction. *J Cell Biol, 54*, 30–38.

Davis, A. F., Bai, J., Fasshauer, D., Wolowick, M. J., Lewis, J. L., & Chapman, E. R. (1999). Kinetics of synaptotagmin responses to $Ca^{2+}$and assembly with the core SNARE complex onto membranes. *Neuron, 24*, 363–376.

delCastillo, J., & Katz, B. (1954). Quantal components of the end-plate potential. *J Physiol, 124*, 560–573.

Dreyer, F., Peper, K., Akert, K., Sandri, C., & Moor, H. (1973). Ultrastructure of the "active zone" in the frog neuromuscular junction. *Brain Res, 62*, 373–380.

Eccles, J. C. (1964). *The Physiology of Synapses*. New York: Academic Press, Inc.

Fatt, P., & Katz, B. (1952). Spontaneous subthreshold activity at motor nerve endings. *J Physiol, 117*, 109–128.

Greengard, P., Valtorta, F., Czernik, A. J., & Benfenati, F. (1993). Synaptic vesicle phosphoproteins and regulation of synaptic function. *Science, 259*, 780–784.

Hall, Z. W., & Sanes, J. R. (1993). Synaptic structure and development: the neuromuscular junction. *Neuron, 72*(suppl.), 99–121.

Hanson, P. I., Roth, R., Morisaki, H., Jahn, R., & Heuser, J. E. (1997). Structure and conformational changes in NSF and its membrane receptor complexes visualized by quick-freeze/deep etch electron microscopy. *Cell, 90*, 523–535.

Hayashi, T., McMahon, H., Yamasaki, S., et al. (1994). Synaptic vesicle fusion complex: action of clostridial neurotoxins on assembly. *EMBO J, 13*, 5051–5061.

Heidelberger, R., Heinemann, C., Neher, E., & Matthews, G. (1994). Calcium dependence of the rate of exocytosis in a synaptic terminal. *Nature, 371*, 513–515.

Heuser, J. E., Reese, T. S., Dennis, M. J., Jan, Y., Jan, L., & Evans, L. (1979). Synaptic vesicle exocytosis captured by quick freezing and correlated with quantal transmitter release. *J Cell Biol, 81*, 275–300.

Kandel, E. R., & Siegelbaum, S. A. (2000). Signalling at the nerve-muscle synapse: directly gated transmission. In E. R. Kandel, J. H. Schware, & T. M. Jessell (Eds.), *Principles of Neural Science* (pp. 187–206). New York: McGraw-Hill.

Katz, B. (1966). *Nerve, Muscle, and Synapse*. New York: McGraw-Hill Book Co., Inc.

Katz, B., & Miledi, R. (1967). The timing of calcium action during neuromuscular transmission. *J Physiol, 189*, 535–544.

Kuffler, S. W., & Nicholls, J. G. (1977). *From Neuron to Brain: a Cellular Approach to the Function of the Nervous System*. Sunderland: Sinauer Associates, Inc.

Lagnado, L., Gomis, A., & Job, C. (1996). Continuous vesicle cycling in the synaptic terminal of retinal bipolar cells. *Neuron, 17*, 957–967.

Lindau, M., & Almers, W. (1995). Structure and function of fusion pores in exocytosis and ectoplasmic membrane fusion. *Curr Opin Cell Biol, 7*, 509–517.

Llinas, R. R. (1977). Calcium and transmitter release in squid synapse. In W. M. Cowan, & J. A. Ferrendelli (Eds.), *Approaches to the Cell Biology of Neurons, Society for Neuroscience Symposia, II* (pp. 139–169). Bethesda: Society for Neuroscience.

Llinas, R. R., Gruner, J. A., Sugimori, M., McGuinness, T. L., & Greengard, P. (1991). Regulation by synapsin I and Ca^{2+}-calmodulin-dependent protein kinase II of transmitter release in squid giant synapse. *J Physiol, 436*, 257–282.

Martin, R. A. (1977). Junctional transmission II. Presynaptic mechanisms. In *Handbook of Physiology. The Nervous System, Vol. I* (pp. 329–355). Bethesda: American Physiological Society.

Matthews, G. (1996). Synaptic vesicle exocytosis and endocytosis: capacitance measurements. *Curr Opin Neurobiol, 6*, 358–364.

Maycox, P. R., Hell, J. W., & Jahn, R. (1990). Amino acid neurotransmission: spotlight on synaptic vesicles. *Trends Neurosci, 13*, 83–87.

McMahon, H. T., & Nicholls, D. G. (1991). The bioenergetics of neurotransmitter release. *Biochim Biophys Acta, 1059*, 243–264.

Miledi, R. (1973). Transmitter release induced by injection of calcium ions into nerve terminals. *Proc Roy Soc, 183*, 421–425.

Niemann, H., Blasi, J., & Jahn, R. (1994). Clostridial neurotoxins: new tools for dissecting exocytosis. *Trends Cell Biol, 4*, 179–185.

Pappas, G. D., & Purpura, D. P. (Eds.), (1972). *Structure and Function of Synapses*. New York: Raven Press Publishers.

Petrenko, A. G., Perin, M. S., Davletov, B. A., Ushkaryov, Y. A., Geppert, M., & Südhof, T. C. (1991). Binding of synaptotagmin to the a-latrotoxin receptor. *Nature, 353*, 65–68.

Robitaille, R., Adler, E. M., & Charlton, M. P. (1990). Strategic location of calcium channels at transmitter release sites of frog neuromuscular junction. *Neuron, 5*, 773–779.

Ryan, T. A., Reuters, H., Wendland, B., Schweizer, F. E., & Smith, S. J. (1993). The kinetics of synaptic vesicle recycling measured at single presynaptic boutons. *Neuron, 11*, 713–724.

Sabatini, B., & Regehr, W. G. (1996). Timing of neurotransmission at fast synapses in the mammalian brain. *Nature, 384*, 170–172.

Schulman, H., & Hyman, S. E. (1999). Intracellular signaling. In M. J. Zigmond, F. E. Bloom, S. C. Landis, J. L. Roberst, & L. R. Squire (Eds.), *Fundamental Neuroscience* (pp. 269–316). San Diego: Academic Press.

Shao, X., Davletov, B. A., Sutton, R. B., Südhof, T. C., & Rizo, J. (1997). Bipartite Ca binding motif in C2 domains of synaptotagmin and protein kinase C. *Science, 273*, 248–251.

Smith, S. J., & Augustine, G. J. (1988). Calcium ions, active zones and synaptic transmitter release. *Trends Neurosci, 11*, 458–464.

Söllner, T., Bennett, M., Whiteheart, S., Scheller, R., & Rothman, J. (1993a). A protein assembly-disassembly pathway in vitro that may correspond to sequential steps of synaptic vesicle docking, activation and fusion. *Cell, 75*, 409–418.

Söllner, T., Whiteheart, S. W., Brunner, M., et al. (1993b). SNAP receptors implicated in vesicle targeting and fusion. *Nature, 362*, 318–324.

Sonders, M. S., & Amara, S. G. (1996). Channels in transporters. *Curr Opin Neurobiol, 6*, 294–302.

Spray, D. C., Scemes, E., & Rozental, R. (1999). Cell-cell communication via gap junctions. In M. J. Zigmond, F. E. Bloom, S. C. Landis, J. L. Roberts, & L. R. Squire (Eds.), *Fundamental Neuroscience* (pp. 317–343). San Diego: Academic Press.

Südhof, T. C. (1995). The synaptic vesicle cycle: a cascade of protein-protein interactions. *Nature, 375*, 645–653.

Sutton, R. B., Fasshauer, D., Jahn, R., & Brunger, A. T. (1998). Crystal structure of a SNARE complex involved in synaptic exocytosis at 2.4 Å resolution. *Nature, 395*, 347–353.

Whiteheart, S. W., Rossnagel, K., Buhrow, S. A., Brunner, M., Jaenicke, R., & Rothman, J. E. (1994). N-ethylmaleimide-sen-sitive fusion protein: a trimeric ATPase whose hydrolysis of ATP is required for membrane fusion. *J Cell Biol, 126*, 945–954.

Excitation–Secretion Coupling

Nicole Gallo-Payet and Marcel Daniel Payet

Chapter Outline

I. SUMMARY

The first step in the secretory process for peptide hormones and neurotransmitters involves synthesis, modification and sorting of the molecules to be secreted. These secretory molecules are packaged in secretory granules or vesicles, which are then transported to the cell periphery, where they are released in the extracellular space by fusion with the plasma membrane. This complex process is named *exocytosis*. Exocytosis is an all-or-none phenomenon in which Ca^{2+} plays a pivotal role.

Interaction of cytoskeletal structures with transmembrane signaling is an important feature of excitation–secretion coupling. Actin-binding proteins are in large part responsible for cytoskeleton–receptor interactions. In resting cells, more than 95% of the phosphatidylinositol bisphosphate ($PtdInsP_2$) may be complexed with profilin. This interaction promotes actin polymerization. Following receptor activation, phospholipase C activity increases to a level where profilin protection can be overcome, resulting in $PtdInsP_2$ hydrolysis. In resting cells, the bulk of gelsolin is cytosolic. When the cell is activated, there is a transient rise in $[Ca^{2+}]_i$ due to $InsP_3$ action and/or Ca^{2+} influx, which activates gelsolin, causing a 200-fold increase in its affinity for actin. This results in rapid filament side-binding, followed by severing and capping, inducing a dramatic disruption of existing actin network structure in the vicinity of $[Ca^{2+}]_i$ elevation.

Dynamic changes in the cytoskeletal network are required for exocytosis. The subplasmalemmal area of secretory cells is characterized by the presence of a highly organized cytoskeletal network where F-actin, together with specific actin-binding proteins, forms a dense viscoelastic gel. Some actin-associated proteins, such as fodrin,

Cell Physiology Sourcebook. DOI: 10.1016/B978-0-12-387738-3.00033-0

caldesmon, gelsolin and scinderin, exist on secretory granule membranes, linking actin microfilaments to secretory granules. Caldesmon and synapsin I are other proteins that are associated with synaptic vesicles. Synapsin I binds to spectrin and actin microfilaments and may serve as an anchor between synaptic vesicles and the cytoskeleton. Synapsin I phosphorylation results in the release of synaptic vesicles from their anchoring site on the cytoskeleton, allowing the vesicles to move to the active synaptic zones.

Secretion is a process that requires (1) the movement of secretory vesicles toward the plasma membrane, (2) the fusion of vesicles with the plasma membrane and (3) subsequent release of secretory contents into the cell exterior. The process of secretion is mediated by contractile elements either associated with secretory vesicles or present elsewhere in the cell. As microfilaments (F-actin) are preferentially localized in the cortical surface of the chromaffin cell, F-actin may act as a barrier to the secretory granules, impeding their contact with the plasma membrane. Upon stimulation, fodrin rearranges into patches beneath the plasma membrane. Such a redistribution could be related to the clearing of exocytotic sites at the level of the plasma membrane. Scinderin is a cytosolic protein that shortens actin filament length when Ca^{2+} is present in the medium. Stimulation induces both redistribution of scinderin from the cytosol to the cell cortex and F-actin disassembly, which precedes exocytosis. Docking of granules on the plasma membrane is an important step in exocytosis. Several proteins are involved in this process: synaptobrevin, syntaxin and SNAP-25, which form the SNAP receptor (SNARE). Priming of the granules is also a pivotal step in exocytosis. N-ethylmalimide-sensitive fusion protein (NSF) primes the granule through ATP hydrolysis; once primed, an increase in $[Ca^{2+}]_i$ triggers the release. All these processes require the presence of Ca^{2+} in the extracellular medium. Therefore, only secretagogues that induce Ca^{2+} entry are able to produce these effects.

In regulated exocytosis, fusion of secretory granules with the plasma membrane is triggered by an appropriate signal. Every time a secretory granule fuses with the plasma membrane, the total capacitance of the cell increases by a value proportional to the surface of the new membrane added to the existing cell membrane. Capacitance step values generally range from 1 to 30 fF, corresponding to granule diameters of 0.2 to 1 pm. Freeze-fracture images of exocytosis reveal the presence of narrow pores formed between the granules and the plasma membrane called *fusion pores*. The size of the pore increases as fusion progresses, allowing for the release of vesicle contents.

Control of exocytosis occurs not only in electrically excitable cells, but also in non-excitable systems in response to receptor activation. The regulatory pathways that couple stimulation and secretion vary widely among cell types. In many cells, Ca^{2+} is the key signal for triggering exocytosis. Ca^{2+} influx from the external medium is crucial for secretion, but internal Ca^{2+} release from internal stores also plays a pivotal role, depending on cell type. In some cases, Ca^{2+} alone is not able to trigger secretion, but the presence of a guanine nucleotide together with Ca^{2+} is necessary and sufficient for exocytosis.

II. INTRODUCTION

The process of excitation–secretion coupling is completely different depending on the peptide/amine or lipid nature of the secretory products. The secretory process for peptide and amine molecules begins with the synthesis, modification and sorting of the molecules to be secreted. Synthesis occurs in the rough endoplasmic reticulum (RER) and sorting occurs in the Golgi complex. The secretory molecules are packaged in secretory granules or vesicles, which are then transported to the cell periphery before they are released in the extracellular space by fusion with the plasma membrane. This complex process is named *exocytosis* or *reverse pinocytosis* and can be operated either by a constitutive or a regulated mechanism. Constitutive secretion is unregulated and closely follows the rate of synthesis of the secretory products. This form of secretion occurs in many cell types, including lymphocytes, hepatocytes and pancreatic β cells. In regulated secretion, fusion of the secretory granules with the plasma membrane is initiated by a specific signal (ligand-receptor coupling), triggered by an increase in cytosolic calcium concentration ($[Ca^{2+}]_i$). In steroid-secreting cells (adrenal cortex, ovary, testis), the process of synthesis begins with cholesterol stored in lipid droplets followed by subsequent steps occurring in mitochondria and smooth endoplasmic reticulum. It is generally assumed that steroids are free to diffuse throughout the aqueous cytoplasm and lipid phase of the plasma membrane. Secretory vesicles are not present and secretion and/or release of steroids is tightly coupled to steroid synthesis.

Although the process of synthesis differs, stimulation of secretion of peptide hormones, neurotransmitters and steroids involves similar cascades of molecular events. After binding to their specific receptors, the stimuli activate second messenger production, several cascades of phosphorylation/dephosphorylation of intracellular proteins, cytoskeleton reorganization, synthesis of new products and release of secretory products. Cytoskeleton and Ca^{2+} ion are certainly the most important players involved in this excitation–secretion coupling. However, while disruption of the actin network is necessary to trigger fusion of secretory vesicles with the cell membrane, a well-preserved organization seems important for steroid release.

III. CELLULAR COMPONENTS INVOLVED IN EXCITATION–SECRETION COUPLING

IIIA. Interaction of Cytoskeletal Structures with Transmembrane Signaling Molecules

The cytoskeletal elements are described in Chapter 5. Therefore, the brief descriptions given here on microfilaments and microtubules are aimed at understanding the mechanisms involved in excitation–secretion coupling (Schmidt and Hall, 1998). In the living cell, actin filaments, F-actin (consisting of two staggered, parallel rows of monomers, G-actin, non-covalently bound and twisted into a helix), interact with several proteins, such as vinculin, α-actinin, villin and fodrin, which cross-link and bundle microfilaments into a well-organized three-dimensional network. They can also cross-link myosin, forming a contractile network, or form a very dense network at the cell periphery, the cell cortex (Figs. 33.1A and 33.2A). This dynamic organization of microfilaments depends on a large and diverse group of actin-binding proteins, including profilin and caldesmon (which bind G-actin) and gelsolin and scinderin (which cap and sever F-actin). On the other hand, polymerization, stabilization and modulation of microtubules depend on several microtubule-associated proteins (MAPs) that adorn the tubulin-containing core of the tubules. The complete cell cytoskeletal network includes interaction between microfilaments, microtubules and intermediate filaments (see Figs. 33.1 and 33.2 and Chapter 5).

Association of cell surface molecules with the cytoskeleton is widely believed to be one of the earliest consequences of cellular activation for many systems. These cell surface molecules include not only receptors, but also *integrins*, the receptors of the components of extracellular matrix. Appropriate stimulation of receptors and integrins has immediate and profound effects on the organization and activity of the microfilaments (Aplin et al., 1998). Several studies have shown that microfilament disruption (with cytochalasins) or microtubule disruption (with colchicine or vinblastine) increased exocytosis (i.e. peptide or amine secretion), although steroid hormone secretion is decreased or abolished. In other words, these observations indicate that cytoskeleton is a barrier in the former, but a requirement for the latter. In both cases, microfilaments are active players in the process of excitation–secretion coupling. Several studies indicate that receptors (either G-protein-coupled or tyrosine kinase types), α subunits of heterotrimeric G proteins (α_i, α_s, α_q), monomeric G proteins (Rho, Rac, Cdc42), second-messenger-activating enzymes (adenylyl cyclase, phospholipase C [PLC]), Ca^{2+}, K^+ or Cl^- channels (see Chapter 31) and proteins up or downstream from second messenger production (phosphatases, protein kinase C [PKC], mitogenic associated protein kinase [MAPK]) are associated with microfilaments. For example, anchoring of PKC-e to F-actin is required for glutamate release in nerve endings of neuronal cells (Janmey, 1998). In general, these associations occur mainly via acting-binding proteins, which bind effectors or phosphoinositides through specific domains, called plecktrin homology domains, (PH domains). PH domains are essential for the membrane recruitment of several proteins that contain them and are frequently accompanied by other motifs (Src homology domains SH2 and SH3 and proline-rich, Dbl homology [DH], or GTP exchange domains), indicating that the recruitment of the PH domain protein would nucleate sites on the membrane for protein complex assembly (Inglese et al., 1995; Janmey, 1998; Martin, 1998). In addition, close functional association between G proteins and microtubules has also been extensively described (Popova et al., 1997). Such observations indicate that the cytoskeleton operates as a matrix improving the efficiency of the signal transduction cascade and that actin-binding proteins are in large part responsible for these cytoskeleton–membrane receptor interactions.

IIIB. Actin-Binding Proteins Important in Signaling

The physical properties of actin networks depend on the length of microfilaments and the architecture of the three-dimensional network formed by interaction between actin and several actin-binding proteins. The aim of this section is to point attention to the F-actin cross-linking proteins which may be regulated by Ca^{2+} and thus involved in the process of excitation–secretion coupling (Schmidt and Hall, 1998).

Profilin was the first actin-binding protein described in signaling. Profilin also contains a $PtdInsP_2$ binding site and binding of $PtdInsP_2$ to this site triggers the dissociation of profilin from actin, promoting actin polymerization (see Fig. 33.1A). $PtdInsP_2$ molecules bind to profilin with a stoichiometry of about 8:1. This 8:1 association of $PtdInsP_2$:profilin complexes protects $PtdInsP_2$ from cleavage by phospholipase C_γ (PLC_γ). In a similar fashion, also in resting conditions, PLC_γ may also bind profilin. However, when PLC_γ becomes tyrosine phosphorylated (by appropriate ligand activation), its affinity for $PtdInsP_2$ increases to a level where profilin protection can be overcome, resulting in $PtdInsP_2$ hydrolysis. Hydrolysis of one or two of the eight $PtdInsP_2$ molecules bound to each profilin leads to a rapid decrease in $PtdInsP_2$ affinity and release of the remaining profilin-bound $PtdInsP_2$ molecules (see Fig. 33.1B). Thus, the binding of profilin to $PtdInsP_2$ not only liberates polymerization-competent G-actin, but also affects hydrolysis of $PtdInsP_2$ by PLC_γ (Forscher, 1989; Janmey, 1998).

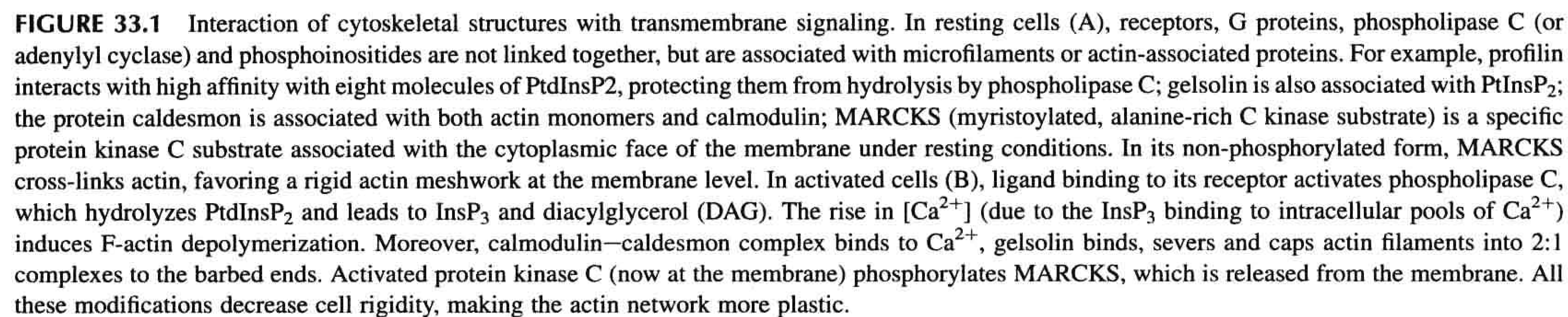


FIGURE 33.1 Interaction of cytoskeletal structures with transmembrane signaling. In resting cells (A), receptors, G proteins, phospholipase C (or adenylyl cyclase) and phosphoinositides are not linked together, but are associated with microfilaments or actin-associated proteins. For example, profilin interacts with high affinity with eight molecules of PtdInsP2, protecting them from hydrolysis by phospholipase C; gelsolin is also associated with $PtInsP_2$; the protein caldesmon is associated with both actin monomers and calmodulin; MARCKS (myristoylated, alanine-rich C kinase substrate) is a specific protein kinase C substrate associated with the cytoplasmic face of the membrane under resting conditions. In its non-phosphorylated form, MARCKS cross-links actin, favoring a rigid actin meshwork at the membrane level. In activated cells (B), ligand binding to its receptor activates phospholipase C, which hydrolyzes $PtdInsP_2$ and leads to $InsP_3$ and diacylglycerol (DAG). The rise in $[Ca^{2+}]$ (due to the $InsP_3$ binding to intracellular pools of Ca^{2+}) induces F-actin depolymerization. Moreover, calmodulin–caldesmon complex binds to Ca^{2+}, gelsolin binds, severs and caps actin filaments into 2:1 complexes to the barbed ends. Activated protein kinase C (now at the membrane) phosphorylates MARCKS, which is released from the membrane. All these modifications decrease cell rigidity, making the actin network more plastic.

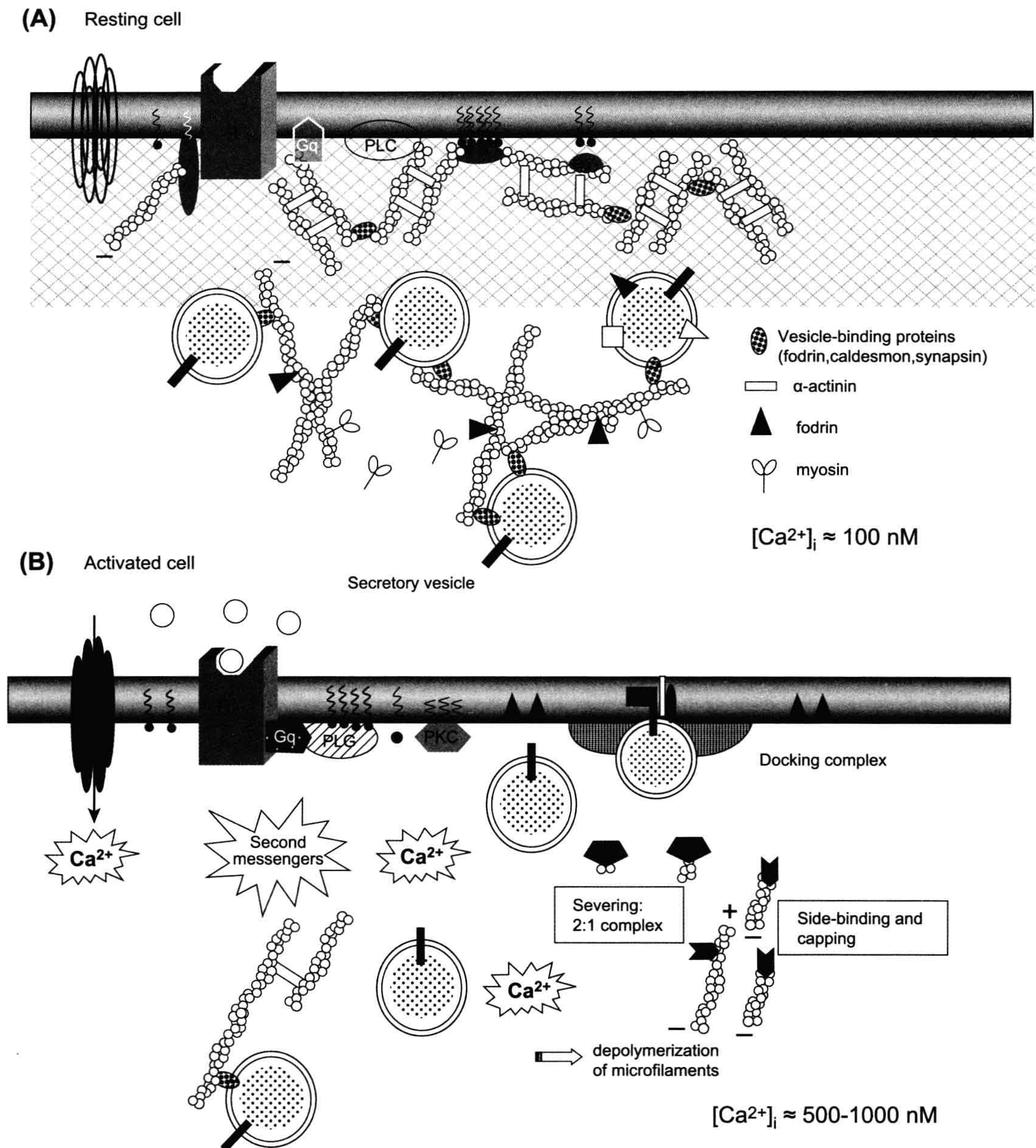


FIGURE 33.2 Dynamic changes in cytoskeleton during exocytosis. In resting cells ($[Ca^{2+}]_i$ ≈100 nM) (A), microfilaments interact with several proteins (including fodrin and α-actinin) that cross-link and bundle microfilaments into a well-organized three-dimensional network. In vesicle-secretory cells, microfilaments can also cross-link myosin, forming a contractile network, or form a very dense network at the cell periphery, the cell cortex. Activation of cells by appropriate stimulation (B) is associated with a reduction in the cell cortex rigidity, due to characteristic changes in cytoskeletal properties from "gel" (solid) to "sol" (liquid) states. These changes are primarily under the control of Ca^{2+}, which cooperates with phospholipid messengers to induce microfilament disruption. An increase in intracellular calcium ($[Ca^{2+}]_i$ (≈0.5–1 μM) induces several cellular modifications. In addition to capping and severing of the actin microfilaments (see Fig. 33.1), there is dissociation of actin from actin-associated proteins, such as fodrin, patching of fodrin along the plane of the plasma membrane (docking site) and dissociation of caldesmon from secretory vesicles. These events result in a decrease in viscosity, which favors movement of granules toward the plasma membrane releasing sites. Actin–myosin interactions could facilitate granule displacement in cytosol.

Gelsolin is a Ca^{2+}-dependent F-actin severing molecule which, along with villin, fragmin, adseverin and scinderin, is able to sever actin filaments. These proteins bind to actin filaments and bend and cleave them in a Ca^{2+}-dependent manner and afterwards cap the barbed filament ends. Severing actin filaments promotes cell cortex transition from a "gel" state to a "sol" state upon addition of Ca^{2+}. Gelsolin contains two spatially separate binding sites: a G-actin Ca^{2+}-sensitive site in the C-terminal domain and a PtdIns-sensitive site closer to the N-terminal portion. In resting cells ($[Ca^{2+}]_i \approx 100$ nM), the bulk of gelsolin is cytoplasmic and a small proportion is $PtdInsP_2$-associated. Gelsolin has little affinity for actin under these conditions and is in an actin-free state (see Fig. 33.1A). When the cell is activated, there is a transient rise in $[Ca^{2+}]$ due to $InsP_3$ action or Ca^{2+} influx that then activates gelsolin, causing a 200-fold increase in its affinity for F-actin. This results in rapid filament side-binding, followed by severing and capping of any free barbed filament ends, inducing a dramatic disruption of existing actin network structure in the vicinity of Ca^{2+} elevation (see Fig. 33.1B). The activities of these severing proteins are inhibited by binding to $PtdInsP_2$.

In the absence of PtdIns turnover, much of the $PtdInsP_2$ is likely to be tightly associated with profilin and thus unavailable to gelsolin. If gelsolin is activated under these conditions (e.g. by an increase in $[Ca^{2+}]_i$, independent of the PtdIns turnover), severing of actin networks is observed, but without subsequent actin reassembly. This leads to two possible modes of gelsolin activation: (1) calcium influx produced by activation of PtdInsP-independent pathways (i.e. voltage- or agonist-gated Ca^{2+} channels) leads to actin severing and capping only; (2) in contrast, activation of these same Ca^{2+} channels concomitant with PtdInsP turnover results in severing and capping followed by actin polymerization, i.e. actin remodeling (Forscher, 1989; Janmey, 1998).

In summary, association of actin-binding proteins with phosphoinositides causes opposite effects to those observed upon association with Ca^{2+}. In the former, such associations (profilin: $PtInsP_2$) promotes actin polymerization, favoring the cortical actin "gel" near the plasma membrane, while increased Ca^{2+} concentration favors association of actin-binding proteins (profilin, gelsolin) with Ca^{2+}, inducing depolymerization and thus "sol" state of actin filaments.

Caldesmon is a calmodulin-dependent actin-binding protein that, at low Ca^{2+} concentrations (100 nM), binds and cross-links actin monomers, inhibiting actin polymerization. Under these conditions, caldesmon interacts reversibly with secretory granules. At greater concentrations of Ca^{2+} (μM ranges), Ca^{2+}-calmodulin complex binds to caldesmon and reverses this inhibition. The flip-flop regulation of caldesmon may be important for secretory vesicle function during the changes in intracellular Ca^{2+} levels observed upon stimulation (see Figs. 33.1 and 33.2).

MARCKS (myristoylated, alanine-rich C kinase substrate) is a specific protein kinase C substrate that is targeted to the membrane by its amino-terminal binding domain. In resting cells, MARCKS associates with the cytoplasmic face of the membrane. In its non-phosphorylated form, MARCKS cross-links actin, favoring a rigid actin meshwork at the membrane level (see Fig. 33.1A). Activated protein kinase C phosphorylates MARCKS, which remains associated with actin filaments, but can no longer cross-link actin fibers, making the actin network more plastic (see Fig. 33.1B). In addition, an increase in intracellular Ca^{2+} concentration promotes binding of calmodulin to MAR-CKS, inhibiting its actin cross-linking activity, again resulting in a less rigid actin meshwork. Thus, PKC induces a local destabilization of the actin skeleton through the phosphorylation of MARCKS. MARCKS is phosphorylated when synaptosomes are depolarized, suggesting a role in secretion (Arbuzova et al., 1998).

Several newly identified proteins, such as the focal adhesion molecule ($p125^{FAK}$), paxillin and the small GTP-binding protein Rho are also closely implicated in actin polymerization after hormonal stimulation. Tyrosine phosphorylation of $p125^{FAK}$ and paxillin and their association with cytoskeleton and $\beta\gamma$ subunits of G proteins have been recently identified as early events in the action of several growth factors and G-protein-coupled receptors (such as angiotensin II and vasopressin). However, to date, their role has been ascribed to regulating cell adhesion, motility or proliferation rather than secretion (Inglese et al., 1995; Tapon and Hall, 1997; Hall, 1998).

IIIC. Interaction between Microtubules and Microtubule-Associated Proteins in Signaling

As mentioned earlier, polymerization, stabilization and plasticity of microtubules depend on several microtubule-associated proteins (MAPs), which differentially cross-link microtubules (Matus, 1988). Recent studies have shown that some MAPs could be implicated in the secretory process (Gundersen and Cook, 1999). MAPs are substrates for several protein kinases, including a Ca^{2+}-calmodulin-dependent kinase, a cAMP-dependent kinase, tyrosine kinases and protein kinase C. Both cAMP (via protein kinase A) and Ca^{2+} (via Ca^{2+}-calmodulin kinase) lead to phosphorylation of MAP-2. Moreover, MAP-1 and MAP-2 are responsible for binding secretory granules to microtubules, either in cells from the anterior pituitary gland, the β cells of the endocrine pancreas or in synaptic vesicles of neurons. These results strengthen the probable role of MAPs in secretory processes.

IIID. Actin-Binding, Docking and Fusion Proteins of the Secretory Granules

Granule vesicles for peptides or amine products not only allow secretory tissues to store large amounts of secretory products in a relatively small volume, but also protect this material from intracellular degradation while providing a very efficient means for transporting and releasing fixed quantities of secretory material.

IIID1. Actin-binding Proteins Associated with Secretory Granules

Induction of exocytosis is associated with a loss in the cell cortex rigidity, due to characteristic changes in cytoskeletal properties from "gel" to "sol" states. These changes are primarily under the control of Ca^{2+}, which cooperates with phospholipid messengers to induce microfilament disruption (see Figs. 33.1B and 33.2B) (Tchakarov et al., 1998). Moreover, several pieces of evidence indicate that microfilaments, rather than microtubules or intermediate filaments, are responsible for the mechanical changes initiated by Ca^{2+}. Chromaffin cells of the adrenal medulla and mast cells from the immune system synthesize and, along with neuronal synaptic vesicles, store and secrete large amounts of neurotransmitters or neuropeptides. These cells contain numerous electron-dense secretory granules which discharge their contents into the extracellular space by exocytosis. The subplasmalemmal area is characterized by the presence of a highly organized cytoskeletal network. F-actin seems to be exclusively localized in this area and, together with specific actin-binding proteins, forms a dense viscoelastic gel.

Fodrin, vinculin, α-actinin and caldesmon, four actin-binding proteins, as well as gelsolin and scinderin, two actin-severing proteins, are found in the plasmalemmal region. Moreover, fodrin, caldesmon and α-actinin binding sites also exist on secretory granule membranes, indicating that actin filaments can also link to secretory granules (see Fig. 33.2A). Chromaffin granules can be entrapped in this subplasmalemmal lattice and thus the cytoskeleton acts as a barrier preventing exocytosis (Burgoyne, 1995; Burgoyne and Morgan, 1998a).

Synapsin I, a phosphoprotein and a substrate for protein kinase A and calmodulin-dependent protein kinase II (CaM kinase II), is associated with synaptic vesicles. Synapsin I also binds to spectrin and actin microfilaments and may serve as an anchor between synaptic vesicles and the cytoskeleton. The affinity of synapsin I for synaptic vesicles is decreased by phosphorylation and neurotransmitter release is preceded by a reversible phosphorylation of synapsin I. Therefore, synapsin I phosphorylation results in the release of synaptic vesicles from their anchorage sites on the cytoskeleton, thus allowing the vesicles to move to the active exocytosis zones.

IIID2. Docking and Fusion Proteins

In addition to the actin-binding proteins, several proteins from the secretory vesicle membrane, the plasma membrane and the bulk cytosol interact together to form the core complex (or a *docking complex*) with docking, priming and fusioning properties (or *budding properties*). The most important of these properties are described next (Südhof, 1995; Fernandez-Chacon and Südhof, 1999).

The vesicular proteins synaptobrevins (or vesicle-associated membrane proteins, VAMPS) and the plasma membrane proteins syntaxin and synaptosome-associated protein (SNAP-25, M_r 25 kDa) form the three complex membrane proteins (called the core complex) essential to the regulated exocytosis machinery in neurons and neuroendocrine and endocrine cell types. Moreover, the potential involvement of the cytosolic proteins, N-ethylmalimide-sensitive fusion protein (NSF) and the soluble NSF attachment proteins (SNAPs) (α, β, γ isoforms), was demonstrated by the discovery that all these proteins interact to form a complex named SNARE (for SNAP receptor) (Fig. 33.3). Based on in vitro studies, a model for neurotransmitter release was proposed in which synaptic vesicles become docked at the plasma membrane by a specific pairing of VAMP (the vesicle membrane, v-SNARE) with syntaxin 1 and SNAP-25 (the target membrane, t-SNARE). The proposed sequence for docking and priming is described hereafter (Südhof, 1995; Aroeti et al., 1998; Burgoyne and Morgan, 1998a). Before and/or during docking, syntaxin is bound to Munc 18 and synaptophysin to synaptobrevin. These two complexes, syntaxin–Munc18 and synaptophysin–synaptobrevin, must dissociate in order for the core complex to be formed. Formation of this complex is considered to be the first step of vesicle priming. Syntaxin and SNAP-25 (t-SNARE) can then bind tightly together to form a high-affinity site for synaptobrevin (v-SNARE) located on the vesicle membrane; the core complex has a stoichiometry of 1:1:1. The trimeric core complex serves as a receptor (SNARE) for the soluble SNAPs (not related to SNAP-25). NSF will only interact with SNAPs (α, β) bounded on the trimeric complex. The NSF-SNAP receptor forms a multisubunit particle that sediments at 20S; it may form the core of a generalized apparatus catalyzing bilayer fusion (Söllner et al., 1993). NSF is a trimeric protein that cross-links multiple core complexes into a network. The core complex is then disrupted by enzymatic activity of NSF under ATP hydrolysis. Botulinum A and tetanus toxins are toxin proteases able to digest synaptobrevin, SNAP-25 and syntaxin. When entering in the nerve terminal, they irreversibly inhibit exocytosis. However, the number of docked granules is not decreased by the toxins, indicating that the primary function of the core complex is fusion and not docking. Hydrolysis of ATP by NSF is followed by

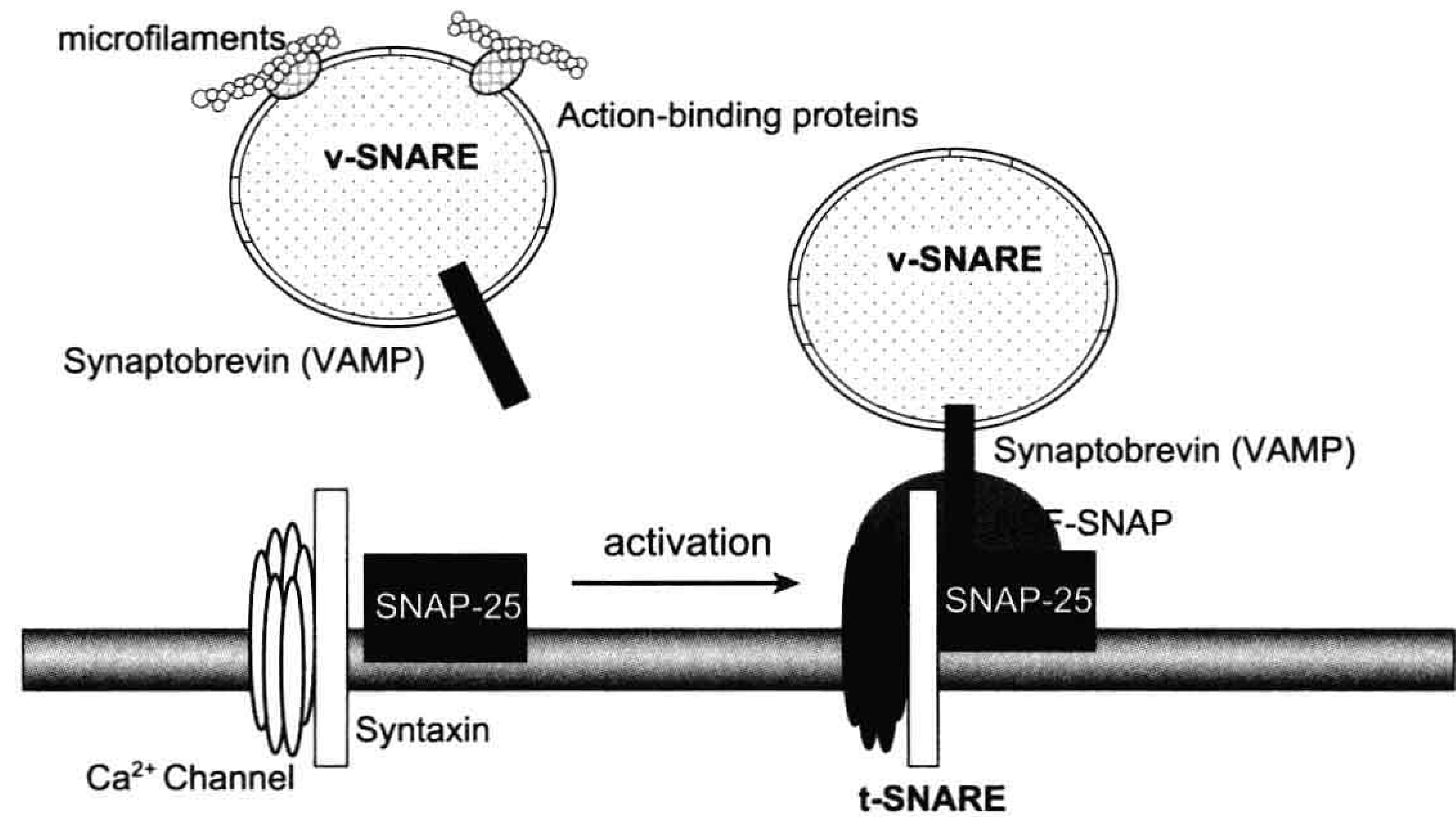


FIGURE 33.3 SNARE, the receptor involved in docking and fusion. The 20S particle that forms the core complex contains several interacting proteins. v-SNARE, related to synaptobrevin (VAMP) and located on the vesicle, binds to t-SNARE, related to syntaxin and SNAP-25 and located on the plasma membrane, to form the SNARE or SNAP receptor. SNAPs and NSF can then bind to the receptor to complete the core complex. Numerous SNARE-related proteins, each specific for a single kind of vesicle or target membrane, ensure vesicle-to-target specificity. Binding of synaptobrevin relies on the inhibition of the Ca^{2+} channel.

ATP-independent steps (see later) sensitive to temperature, H^+ and Ca^{2+}. The last step is Ca^{2+}-sensitive and likely involves a Ca^{2+} sensor at the site of exocytosis.

Synaptotagmins (Syt) are membrane glycoproteins found in brain secretory vesicles of which eight forms have been cloned. One of these, synaptotagmin I (Syt I), plays a pivotal role in the Ca^{2+}-triggered neurotransmitter release as a Ca^{2+} sensor (Südhof and Rizo, 1996; Goda and Südhof, 1997; Burgoyne and Morgan, 1998b). The functional implication of multiple synaptotagmins is unknown. Syt I binds Ca^{2+} cooperatively and undergoes a Ca^{2+}-dependent conformational change; the coefficient of cooperativity (4) is similar to that observed for Ca^{2+}-triggered release. Syt I also binds phospholipids as a function of Ca^{2+} with high affinity (half maximal binding, 5−6 μM). Syntaxin, one of the proteins of the core complex, in addition to its role in the docking and fusion process of the vesicle, controls the entry of Ca^{2+} by the voltage-dependent Ca^{2+} channels (L- and N-type). Indeed, binding of syntaxin to the Ca^{2+} channel prevents the opening of the channel by membrane depolarization. When the vesicle docks to the membrane by binding to syntaxin and SNAP-25, the inhibition of syntaxin on the channel is relieved, allowing voltage-dependent opening of the channel (see Fig. 33.3) (Geppert and Südhof, 1998).

In addition to phospholipids and syntaxin, Syt I binds to neuroxins, a family of neuronal cell surface proteins, and to AP-2, a protein complex involved in synaptic vesicle endocytosis. In addition to a Ca^{2+} sensitivity similar to Ca^{2+}-triggered release, the role of Syt I as a Ca^{2+} sensor has been illustrated in several ways. Knockout mice for Syt I have impaired Ca^{2+}-triggered transmitter release, but release can still be obtained by Ca^{2+}-independent agents, such as hypertonic sucrose or the excitatory neurotoxin α-latrotoxin (the receptor for α-latrotoxin belongs to the neuroxin family). Synaptotagmin *Drosophila* mutants show a severe but incomplete block of neurotransmission with an altered Ca^{2+}-dependence in some mutants. Injection of synaptotagmin peptide in squid nerve terminal inhibits release and vesicles accumulate possibly by competing for a common effector. Synaptotagmins are also able to interact with non-neuronal syntaxin, indicating that they can play a role in a variety of cell types from endocrine and immune systems.

Synaptophysin and the related protein synaptogyrin are major integral membrane proteins of small presynaptic vesicles. The presence of phosphorylation sites for tyrosine kinase of the Src family could indicate that phosphorylation modulates protein activity. The primary structure was deduced from the cDNA sequence, leading to the proposition that synaptophysin and synaptogyrin span the membrane four times with N- and C-terminals located in the cytoplasm. Ubiquitous isoforms of these two proteins are co-expressed in all cells and could represent invariant components of trafficking organelles.

The annexin family includes several Ca^{2+}- and phospholipid-binding proteins with conserved structure. Two of these are thought to be involved in the mechanism of exocytosis. Synexin (annexin VII) is a calcium-binding protein (47 kDa) with four transmembrane domains. This protein demonstrates a voltage-dependent Ca^{2+} channel activity. Synexin is able to induce the aggregation of chromaffin vesicles in the presence of Ca^{2+}. A model for the synexin-driven Ca^{2+}-dependent membrane fusion has been proposed in which synexin monomers polymerize as the concentration of Ca^{2+} increases. The polymerized synexin forms a hydrophobic bridge between the two membranes. Annexin II (calpactin) is located on the cytoplasmic side of the plasma membrane in chromaffin cells. Sites of phosphorylation for protein kinase C and camp- and calmodulin-dependent protein kinases have been localized within the N-terminal domain; phosphorylation

of these sites could inactivate the protein. A possible role for annexin II could be to link the granule with the plasma membrane (docking) and/or to induce fusion (Burgoyne, 1991).

Exocytotic fusion mechanisms also involve PtdIns transfer protein, PtdIns 4-kinase (PI4K), and PI5K to promote formation of $PtIns4,5P_2$ on the vesicle membrane (Martin, 1998).

IV. CELLULAR AND MOLECULAR EVENTS IN CHROMAFFIN, MAST CELLS AND NEURONAL SYNAPTIC VESICLES

Exocytosis is an all-or-none phenomenon in which Ca^{2+} plays a pivotal role. Ca^{2+} is required for second messenger activity, for the control of cytoskeletal dynamics and for the vesicle–plasma membrane fusion process. In neurons, neuroendocrine cells and some endocrine cells, the electrical activity of the cell, the action potential, leads to the opening of voltage-dependent Ca^{2+} channels with a subsequent increase in cytosolic Ca^{2+}. Neurotransmitter release at synaptic and neuromuscular junctions, peptide hormone secretion and catecholamine release by the adrenal medulla all belong to this class. In non-excitable cells, the triggering Ca^{2+} signal is provided by release of Ca^{2+} from intracellular stores after appropriate stimulation. Depletion in Ca^{2+} from these intracellular pools activates an influx of Ca^{2+}, which is responsible for the sustained increase in $[Ca^{2+}]_i$ observed in many cell types. Moreover, this Ca^{2+} influx provides Ca^{2+} ions for the replenishment of internal stores.

IVA. Dynamic Changes in the Cytoskeletal Networks are Required for Exocytosis

Secretion is a process that requires (1) the movement of secretory vesicles toward the plasma membrane, (2) the fusion of vesicles with the plasma membrane, and (3) subsequent release of secretory contents in the cell exterior.

As explained before, in resting conditions, actin filaments (F-actin) are preferentially localized in the cell surface and act as a barrier to the secretory granules, impeding their contact with the plasma membrane (Trifaró et al., 1992). Stimulation of chromaffin or mast cells as well as neuronal synaptic vesicles produces disassembly of the actin network and removal of the barrier (Tchakarov et al., 1998) (see Fig. 33.2). Several observations support this concept: (1) direct evidence for an actin barrier has come from the use of drugs that affect actin assembly and disassembly. Cytochalasin B and DNase I prevent actin assembly and drive the system toward net disassembly and increased secretion in permeabilized chromaffin cells. (2) Studies using fluorescent rhodamine-labeled phalloidin (a drug that stabilizes actin filaments in vitro and stops actin disassembly on stimulation) and actin antibodies have shown, in resting cells, a strong cortical fluorescent ring of filamentous actin. Cholinergic receptor stimulation produces a fragmentation of the fluorescent ring, leaving cell cortical areas devoid of fluorescence. These changes are accompanied by a decrease in F-actin associated with a concomitant increase in G-actin (Tchakarov et al., 1998) (Fig. 33.4). (3) Results from the use of toxins also support the concept of a cortical actin barrier. Botulinum C2 toxin,

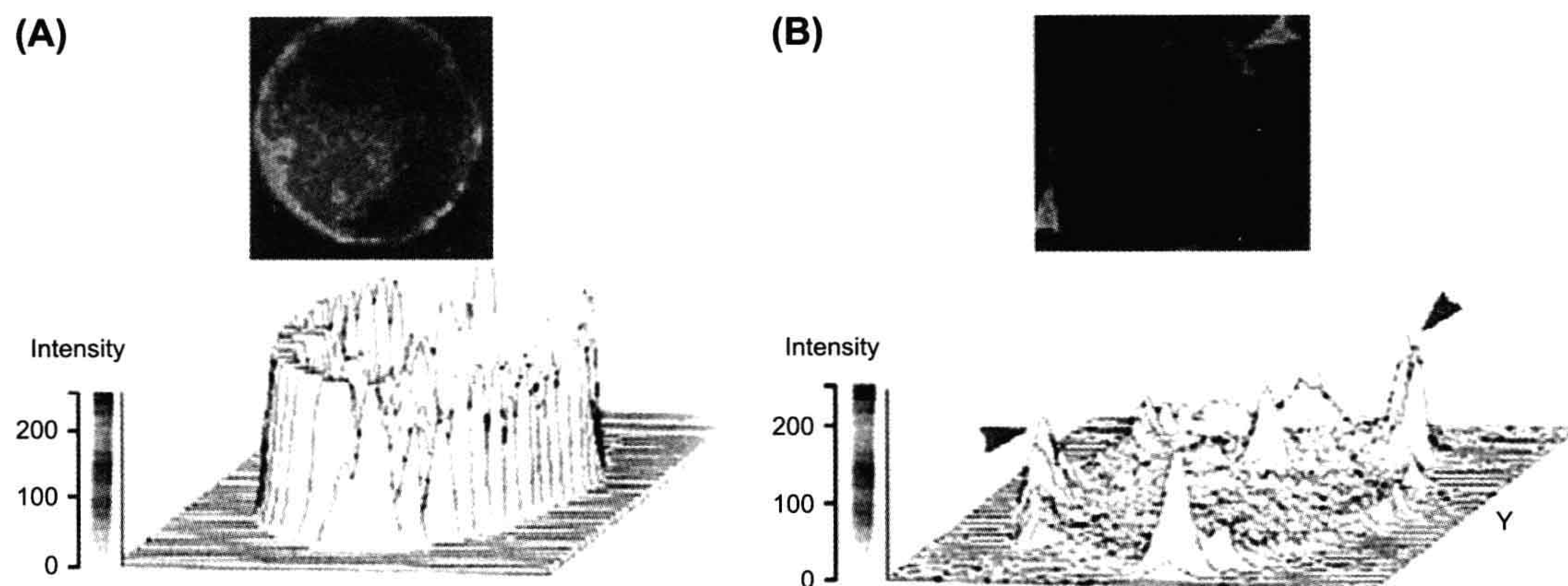


FIGURE 33.4 Rhodamine–phalloidin fluorescence of chromaffin cell cytoskeleton. Cultured chromaffin cells were incubated for 40 s in Locke's solution in the absence (A) or in the presence (B) of 10 μM nicotine. Cells were fixed and processed for fluorescence studies. Resting chromaffin cells showed a bright and continuous cortical fluorescent ring (A), while nicotinic-receptor-stimulated cells showed disruption in the cortical fluorescent ring. Some fluorescent patches are shown by arrowheads (B). Three-dimensional image analysis of the same patterns is shown below each cell. In control cells, there is a uniform cortical fluorescence intensity pattern, whereas in stimulated cells, the cortical fluorescent intensity pattern shows irregularities such as valleys and peaks. These peaks correspond to the patches observed in cells. *(Adapted with permission from Tchakarov et al., 1998.)*

which ADP-ribosylates actin and inhibits actin polymerization, enhances secretion in PC12 cells. In contrast, tetanus and botulinum A toxins, which block actin disassembly, inhibit exocytosis upon cholinergic stimulation.

Several actin-binding proteins present in the cell cortex undergo changes upon stimulation. In a resting cell, fodrin is localized in the cell cortex. On stimulation, it rearranges into patches beneath the plasma membrane. This redistribution could be related to the clearing of exocytotic sites at the plasma membrane. Scinderin is a cytosolic protein that shortens actin filament length when Ca^{2+} is present in the medium. Stimulation induces both redistribution of scinderin from cytosol to cell cortex and F-actin disassembly, which precedes exocytosis. Thus, stimulation-induced redistribution of scinderin and F-actin disassembly produce subplasmalemmal areas of decreased cytoplasmic viscosity and high secretory vesicle mobility. All these processes require the presence of Ca^{2+} in the extracellular medium. Therefore, only secretagogues that induce Ca^{2+} entry are able to produce these effects (see Fig. 33.2B).

In isolated chromaffin cells, stimulation with nicotinic agonists can result in secretion of about 30% of the total catecholamine. Electron microscopic observations show that a small number of granules lie within the exclusion zone of the cell cortex. This demonstrates the importance of changes in cortical actin to allow movement of the bulk of the granules involved in a full secretory response. Nevertheless, low levels of exocytosis, due to these granules in the cortical exclusion zone, could occur without generalized changes in cortical actin. Thus, in a physiological situation, where relatively few exocytotic events occur per stimulus, changes in cortical actin may not be necessary for the initial wave of exocytosis, but are required for the movement, into the cortical exclusion zone, of granules ready for the next stimulus. A similar picture has emerged from studies on the nerve terminal cytoskeletal phosphoprotein, synapsin I, which is believed to cross-link synaptic vesicles and release them following depolarization and phosphorylation of the synapsin I.

IVB. Physical Events Associated with the Fusion of Vesicles to Plasma Membrane

In regulated exocytosis, fusion of the secretory granules with the plasma membrane is triggered by an appropriate signal. The fusion process, following the triggering signal, can be very fast, such as in mammalian nerve terminals, with delays of less than 0.2 ms between the action potential and exocytosis. In some cells, however, delays of 0.2 s (chromaffin cells) to 50 s (mast cells) are observed. This delay is thought to be caused by the time required for production of second messengers possibly involved in exocytosis and removal of the cytoskeletal barrier that immobilizes the vesicles. However, the physical interactions between the granule membrane and the plasma membrane remain similar whether the exocytotic delay is fast or slow. Accordingly, the following fusion events will be described along general lines based on a sequence proposed by Almers (1990).

IVB1. Capacitance Jump

Each time a secretory granule fuses with the plasma membrane, the total capacitance of the cell increases by a value proportional to the surface area of the new membrane added to the existing cell membrane. Assuming that biological membranes have a constant specific capacitance of about 1 $\mu F/cm^2$ allows a simple calculation of the granule size. Upon fusion of a single vesicle, the capacitance value increases abruptly to a new stable value as the membrane of the vesicle and the plasma membrane become continuous and the vesicle lumen opens into the extracellular space. Figure 33.5 illustrates the equivalent circuitry of a resting cell (Fig. 33.5A) and that of a cell undergoing exocytosis (Fig. 33.5B). During degranulation, several granules fuse with the plasma membrane, which produces a typical staircase recording (Fig. 33.5C). Degranulation in three different cell types are presented in Fig. 33.6: human neutrophil (Fig. 33.6A), guinea pig eosinophil (Fig. 33.6B) and horse eosinophil (Fig. 33.6C). Note that the amplitude of the individual step capacitance is lower in human neutrophil than in horse eosinophil, reflecting the different sizes of the vesicles. A capacitance step amplitude histogram is built by measuring the step height of a large number of individual events. An example of this is illustrated in Fig. 33.6D for neutrophils. The capacitance step amplitudes range from 1 to 6 fF (1 to 6×10^{-15} F), with a greater number of events having an amplitude of 2 fF. Assuming a spherical shape, the diameter of the granule can be calculated from the step change in capacitance, δC_m in fF, by the relation:

$$\delta C_m = \pi d^2 \qquad (33.1)$$

The frequency distribution of the sizes of the granules obtained from the capacitance step amplitude histogram is represented in Fig. 33.6E for guinea pig eosinophils. The distribution is fitted (smooth line) by the sum of two Gaussian curves with means of 520 and 590 nm (Lindau and Gomperts, 1991). This size distribution fits in well with the morphometric data obtained by direct microscopic observation of the secretory vesicles. Capacitance step measurements have been achieved in a variety of cell types, including adrenal chromaffin cells, mast cells, pancreatic acinar cells, neutrophils, eosinophils, basophils, pituitary lactotrophs and nerve terminals derived from the posterior pituitary. Capacitance step values generally range between 1 and 30 fF, corresponding to granule diameters of 0.2 to 1 μm.

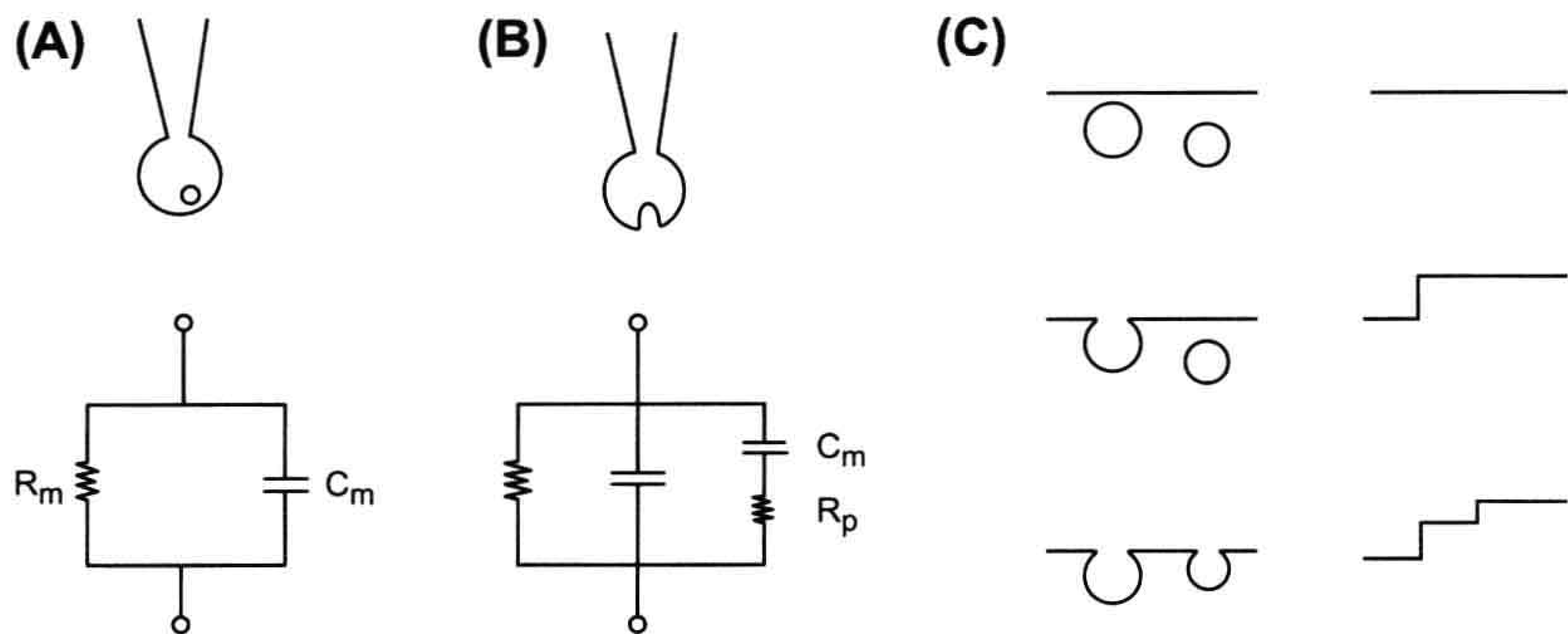


FIGURE 33.5 Capacitance measurement and equivalent electrical circuit. (A) The cell is patch-clamped in the whole-cell configuration. The cell is at rest and an unfused granule is shown near the plasma membrane. The equivalent circuit is represented by membrane resistance R in parallel with membrane capacitance C_m. The series resistance due mainly to the micropipette has been omitted for clarity. (B) Once the granule has fused with the plasma membrane, its capacitance C_v, proportional to the surface of membrane added, is added to the total capacitance of the cell. R_p is the fusion pore resistance, which will rapidly decrease as the pore dilates. (C) The fusion of a granule with the plasma membrane increases the capacitance by step. Granules of identical sizes induce the same increases in capacitance.

Giant vesicles with diameters ranging from 1 to 5 μm are found in mast cells from a strain of genetically defective beige mice (strain C57BL/6J-bg^j/bg^j). In these mice, mast cells and other granulocytes are unable to limit the size of their secretory vesicles; mast cells contain 10 to 40 giant vesicles that can easily be observed under photonic microscopy. These cells thus provide an ideal material for exocytosis studies and, for this reason, have been extensively used. The capacitance method offers the possibility to study degranulation in real time online; time analysis of the secretory process reveals that the granules fuse sequentially, one by one, with the plasma membrane. However, in mast cells, capacitance step analysis demonstrates the presence of step values greater than 60 fF, which could not be produced by the fusion of a single vesicle. A detailed analysis of the capacitance step histogram reveals a multimodal distribution of granule size, which indicates that the larger granules could be formed by the fusion of two to five single granules with each other.

IVB2. Capacitance Flickering

The pattern of the staircase increase in capacitance during degranulation demonstrates that each step builds upon the previous one, indicating that the fusion event is irreversible. However, closer observation of capacitance jumps in

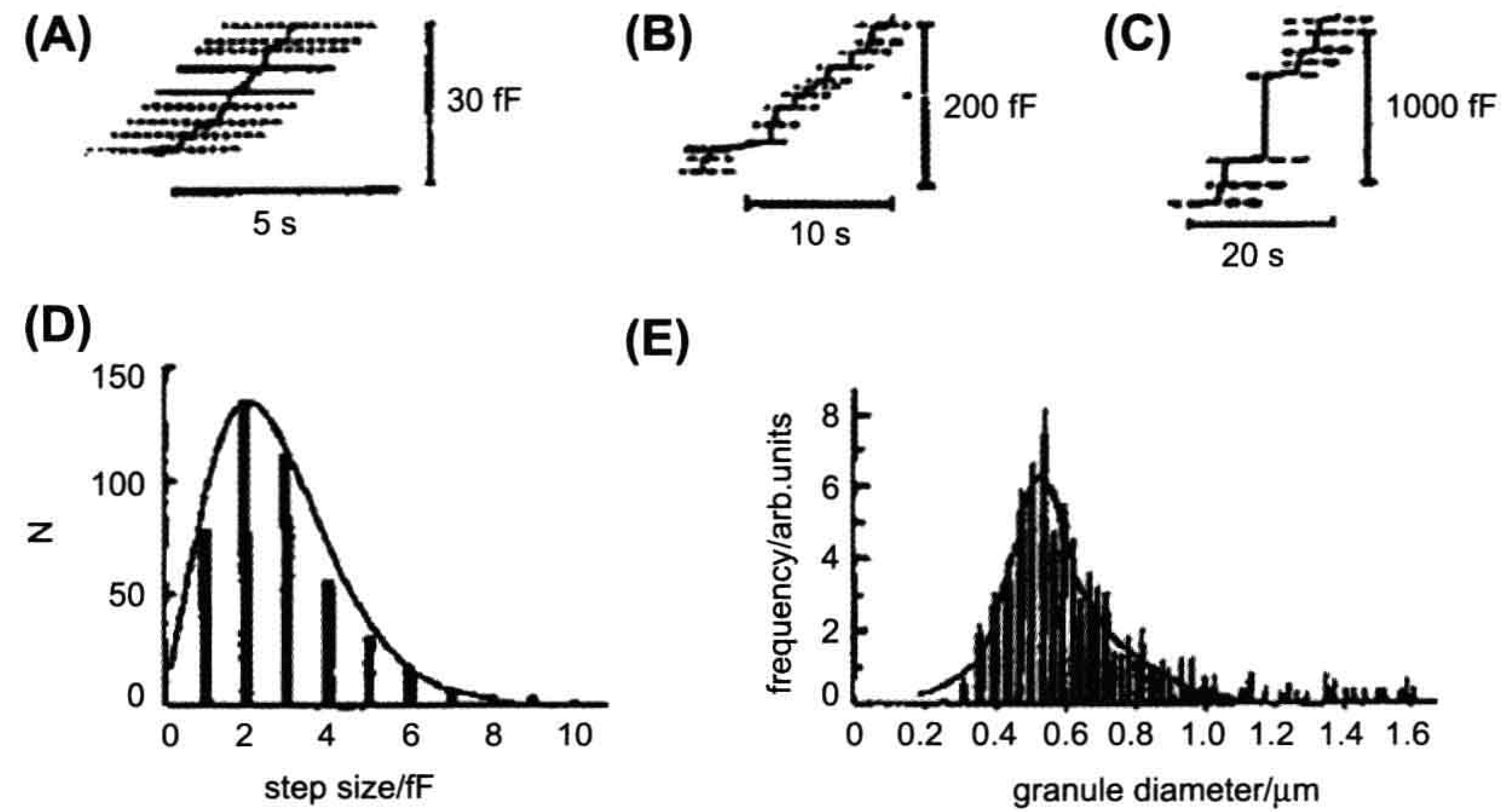


FIGURE 33.6 Analysis of step capacitance. Capacitance recordings obtained from different cells: (A) human neutrophils, (B) guinea pig eosinophils, (C) horse eosinophils. Note the staircase appearance of the recordings, which reflects the sequential fusion of individual granules and the size of the step capacitances, which are proportional to the size of the granules. (D) Frequency distribution of step sizes for human neutrophils. (E) Distribution of granule size for guinea pig eosinophils derived from capacitance measurement. *(Adapted with permission from Lindau and Gomperts, 1991.)*

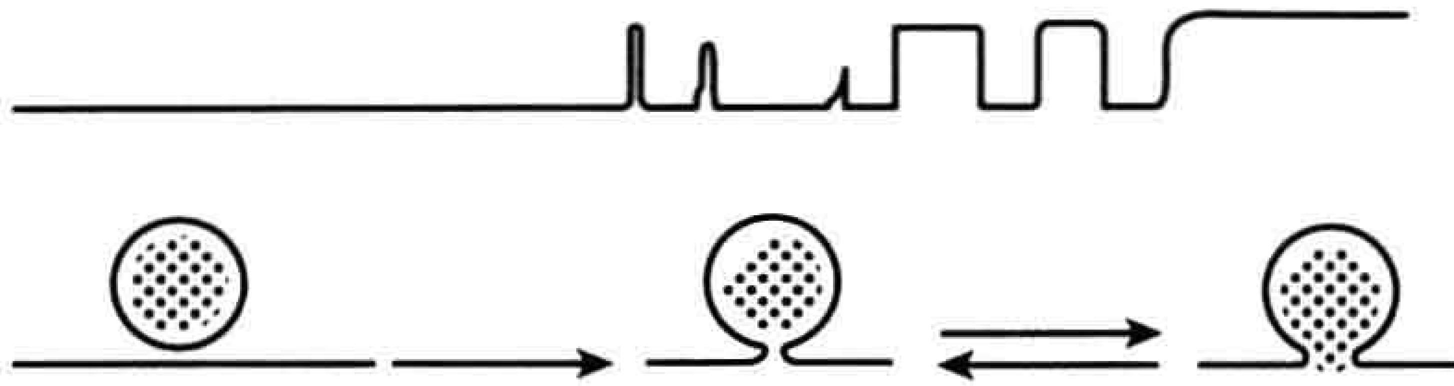


FIGURE 33.7 Flickering of the membrane capacitance. Fusion of the granule is reversible and can oscillate between an unfused state and a fused state. Each time the granule fuses with the plasma membrane, the capacitance of the cell increases by a step. If the fusion pore closes, the capacitance recovers its initial value; incomplete recovery indicates very brief closures exceeding the speed of the recording system. Eventually, a stable fused state can be reached.

mast cells reveals the existence of "on" and "off" steps. The "on" step is produced by the opening of a small-diameter pore, called a *fusion pore*, which adds the surface of the vesicle to that of the cell. Once opened, the fusion pore can close quickly and reopen (Fig. 33.7). Rapid oscillation between open and closed states gives the appearance of a flickering of the capacitance (Almers, 1990). Size distribution of capacitance steps during the flickering period shows that large steps are absent and that all steps remain in the range of values expected for single vesicle fusion events. The size of the fusion pore is proportional to its conductance. An unexpected result is that the reclosing of the pore occurs, not only in small-diameter pores (low conductance), but also in larger-sized pores having a conductance of several nS. Capacitance flickering is rather frequent in mast cells, but very few have been observed in eosinophils. This raises the question of the undetectable presence of flickering during the fusion of all vesicles before the irreversible fused state is attained. Indeed, the initial phase of fusion is a very fast process which cannot be faithfully recorded by the speed of the recording techniques used. The earliest steps as well as short-lived flickering are certainly missed.

IVB3. Fusion Pore

Freeze-fracture images of exocytosis in mast cells and neutrophils reveal the presence of narrow pores formed between the granules and the plasma membrane. The size of the pore increases as fusion progresses, allowing the release of vesicle contents. The presence of pores joining two secretory vesicles is also observed (Lindau and Gompertz, 1991). Electrically, the first opening of the fusion pore generates a brief transient current from which several parameters can be deduced.

Size of Fusion Pore

The conductance of the fusion pore can be calculated from the current transient produced by movement of the charges between two differently charged membranes, i.e. the plasma membrane and vesicle membrane. The initial value of the current, I_0, is related to the initial pore conductance, g_0, by the relationship:

$$g_0 = I_0/(E_c - E_v) \quad (33.2)$$

where E_c is the potential across the plasma membrane and E_v the potential across the vesicle membrane.

The initial conductance of the fusion pore in mast cells was found to be 230 pS. The corresponding pore diameter was calculated assuming a resistivity of 100 Ω-cm and a pore length of 15 nm. The abrupt increase in conductance corresponds to the all-or-none opening of a pore having an inner diameter of less than 2 nm. For comparison purposes, gap junction channels have conductances that vary from 80 to 240 pS and a diameter of approximately 2 nm. It can thus be proposed that the fusion pore is a large protein spanning across two membrane thicknesses and having a structure and function resembling that of a channel. Data obtained from electron microscopic observations reveal that the smallest pores that can be observed have diameters between 30 and 50 nm, values far higher than the values reported from conductance measurements. A rapid dilatation of the pore soon after its formation might explain this discrepancy. Once the pore has been formed, the conductance increases abruptly to a value near 250 pS. Thereafter, the pore begins to dilate, possibly by infiltration of lipid molecules between the subunits of the protein structure, followed by an increase in conductance. The pore conductance increases from 500 pS to 3000 pS in about 25 ms; a plateau is reached after 150 ms, corresponding to a pore diameter of more than 16 nm.

Does the Fusion Pore Leak?

Once established, the diameter of the fusion pore is similar to that of the gap junction, between 1.5 and 2 nm. Since gap junctions allow the intercellular passage of molecules weighing up to 1.9 kDa, the question can be asked as to whether granule contents can leak through the fusion pore. In guinea pig eosinophils, the irreversible fusion of the granule with the plasma membrane is occasionally preceded by a long-lived fusion pore having a conductance of 70–250 pS. When granules were loaded with the fluorescent dye quinacrine, no release of the dye in the extracellular medium could be observed during the life of the fusion pore. Only after the fusion pore had completely dilated and the vesicle had reached its irreversible state of fusion was the dye released. These results indicate that the fusion pore is too narrow for the release of granule contents.

However, computations based on the diffusion of a small molecule such as histamine predict that a granule with a diameter of 0.8 mm should release its contents rapidly through the opening of the fusion pore. Experimental proof was provided by Neher and collaborators

using bovine chromaffin cells (Chow et al., 1992). Secretion was measured by voltametry, while cells were studied by voltage-clamp. The cells were stimulated by depolarizing the membrane from a holding potential of −60 mV to a step potential of +10 mV for 25 ms to activate the Ca^{2+} channels. The amperometric signals, which represent the detection of the released catecholamine molecules by the carbon electrode (potential of 800 mV), were transient with a fast or slow rising phase and variable amplitudes. A histogram of integrals of current transient amplitude obtained on several cells showed that the mean charge transfer had a value of 0.76 pC, which is equivalent to the release of 2.36×10^6 molecules of catecholamine. Sometimes, larger events were detected, presumably corresponding to multigranular exocytosis. One interesting and surprising feature was that the majority of the fast-rising events were preceded by a small "foot" or "pedestal," as illustrated in Fig. 33.8A. The mean duration of the foot was 8.26 ms and the mean charge 34 fC, equivalent to 1.05×10^5 molecules (Fig. 33.8B). The foot was interpreted as reflecting a slow leakage of catecholamine molecules through the fusion pore formed during the early step of the fusion process. A second important result of this study was the discovery and quantification of a long latency period between the end of the stimulus and catecholamine release. The majority of the secretory events occurred 5 to 100 ms after the end of the electrical stimulus, which is rather long when compared to nerve endings, where the delay is about 1 ms. A complex cascade of intracellular events triggered by the increase of cytosolic Ca^{2+} concentration could be responsible for this long latency.

IVB4. Membrane Tension as a Driving Force for Fusion

As previously described, flickering is characterized by the opening and closing of the fusion pore. In some cases, it has been shown that after a period of flickering, the capacitance of the plasma membrane declines to a value lower than its initial value (Monck et al., 1990). Figure 33.9A shows that this decrease in capacitance is paralleled by an increase in the conductance of the fusion pore (Fig. 33.9B), thus establishing a relationship between the dilatation of the pore and decreased plasma membrane capacitance. Once the flickering stops, the conductance recovers its initial value but the whole-cell capacitance remains lower. These results are interpreted as reflecting a decrease of the plasma membrane surface due to a net transfer of material to the granule membrane. The difference between the "on" and "off" steps (found in one-half of the transient fusions with values between −2 to −4 fF) is proportional to the duration of contact between the plasma membrane and the secretory vesicle (Fig. 33.9C). The rate of cell surface area reduction

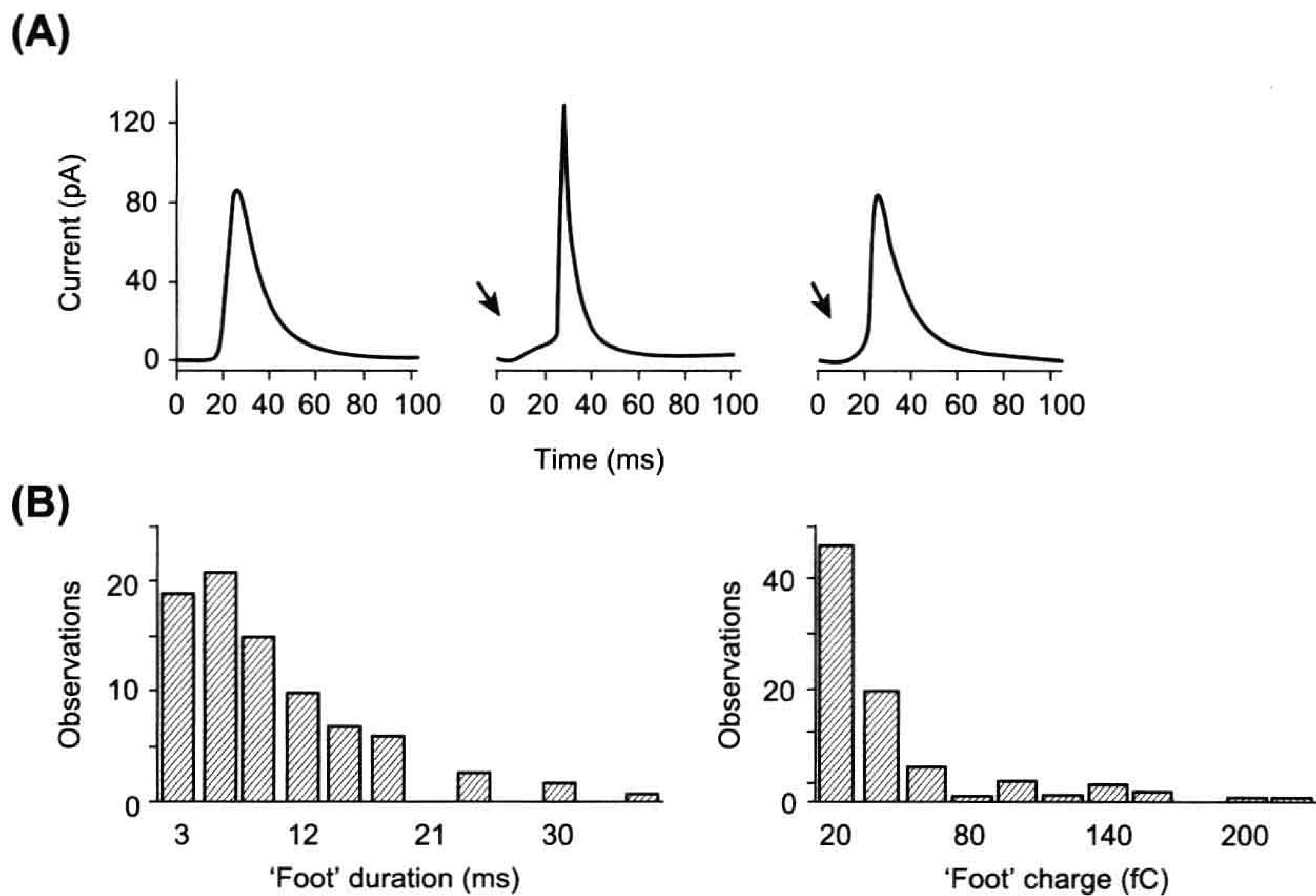


FIGURE 33.8 Amperometric current recorded in chromaffin cells. (A) The amperometric signal recorded with the voltametry method shows a fast rising phase followed by a slower decrease. Occasionally, the rising phase is preceded by a pedestal or foot. The foot signal is thought to be due to the leak of catecholamine by the fusion pore before its complete dilatation. (B) Histogram of the foot signal duration (left panel) and histogram of the charge of the foot signal (right panel), with a mean of 34 fC corresponding to 1.05×10^5 molecules. *(Adapted with permission from Chow et al. (1992). Nature. 356, 60–63. Copyright 1992 Macmillan Magazines Limited.)*

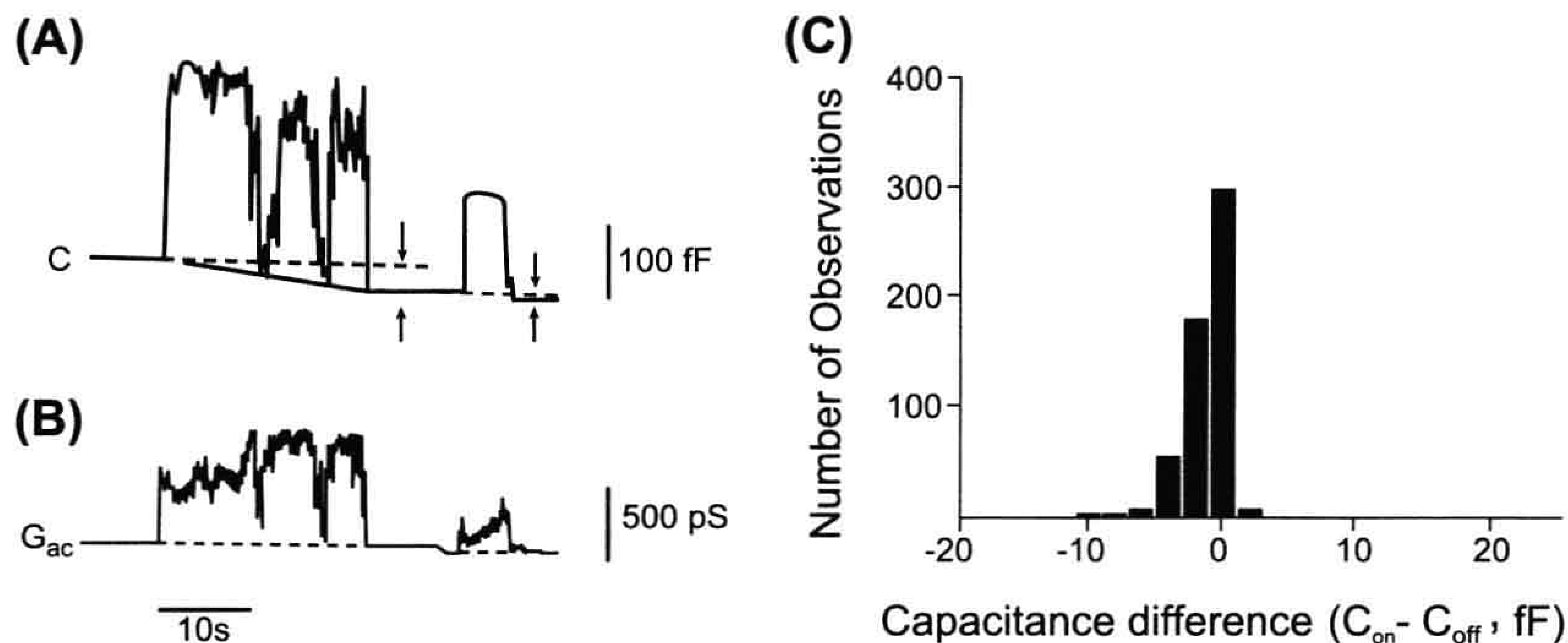


FIGURE 33.9 Decrease of total membrane capacitance after fusion. Capacitance (A) and conductance (B) measurements during transient fusion of a giant secretory granule from beige mouse mast cell. Capacitance and conductance increase on fusion. The fusion pore closes twice with a decrease in conductance and capacitance. Note that the conductance returns to its initial level but that the capacitance of the cell is lower than its initial value. This indicates a reduction of the surface of the plasma membrane due to a leak of lipid molecules toward the granule membrane. (C) Histogram showing the size distribution of the capacitance difference measured after transient fusion in mast cells. *(Reproduced with permission from Monck et al. 1990.)*

is $0.16\ \mu m^2 \cdot s^{-1}$. The transfer of membrane is facilitated by the fact that the membrane of the secretory vesicle is under tension. Upon fusion, a movement of phospholipid molecules occurs from the plasma membrane to the granule membrane. A possible mechanism for generating tension in the granule membrane is osmotic swelling. However, fusion can proceed in isotonic, hypotonic or hypertonic solutions with no change in the kinetics of capacitance increase.

IVB5. Fusion Steps

Several lines of evidence favor the hypothesis that a pore-forming protein could be involved in the fusion process. The abrupt opening of the fusion pore with an initial conductance of 250 pS, similar to the conductance of the gap junction channel and the occurrence of rapid flickering are the strongest arguments. Prior to their fusion, secretory granules are docked to the plasma membrane. In synaptic nerve endings, docking is localized to a restricted region and, upon stimulation, yields localized secretions. Docked granules have been observed in a variety of systems, including chromaffin cells. In these cells, localized secretion was also reported, depending on the applied stimulus.

IVC. Control of Exocytosis

Exocytosis occurs in a variety of electrically excitable and non-excitable systems in response to receptor activation. The regulatory pathways that couple stimulation and secretion vary widely among cell types. In the following section, analysis of the factors controlling exocytosis mainly focuses on two well-studied systems: the chromaffin cell from the adrenal medulla, which belongs to the class of excitable cells, and the mast cell from the immune system, a non-excitable cell.

IVC1. Effectors of Exocytosis

Calcium Signaling and Sources of Calcium

In many cells, Ca^{2+} is the key signal for triggering exocytosis. In chromaffin cells, the resting Ca^{2+} concentration has a value ranging between 50 and 100 nM. Chromaffin cells can be stimulated by two different classes of acetylcholine receptors. The nicotinic receptor has a channel-like structure consisting of five transmembrane subunits. The binding of two acetylcholine molecules opens the channel, which leads to a large net influx of Na^+ ions. This influx causes a membrane depolarization which can activate voltage-dependent Ca^{2+} channels. The nicotinic receptor channel is also permeable to K^+ ions and, to a lesser extent, Ca^{2+} ions. The muscarinic receptor belongs to the family of the seven-span transmembrane domain receptor proteins, which utilizes the G protein cascade pathway as its signal-transducing mechanism. Stimulation of chromaffin cells with the cholinergic agonist nicotine induces a rapid rise in $[Ca^{2+}]_i$ (measured with Ca^{2+}-sensitive fluorescent dye) up to 1 μM; this $[Ca^{2+}]_i$ increase is followed by F-actin disassembly (see Fig. 33.4) and exocytosis. Muscarinic stimulation of chromaffin cells also increases $[Ca^{2+}]_i$ but does not induce secretion.

In a Ca^{2+}-free external medium, secretion is abolished regardless of the stimulus. This observation reinforces the fact that Ca^{2+} influx from the external medium is crucial for secretion in chromaffin cells. Several voltage-dependent Ca^{2+} channels have been described in chromaffin cells, namely: (1) the L-type dihydropyridine-sensitive channels; (2) the N-type ω-conotoxin-sensitive

dihydropyridine-insensitive Ca^{2+} channels; and (3) the dihydropyridine-sensitive facilitation Ca^{2+} channels. Electrical depolarization, K^+ depolarization and nicotinic stimulation open the Ca^{2+} channels, allowing an immediate influx of Ca^{2+} ions from the external medium. The video-imaging technique allows the recording of $[Ca^{2+}]_i$ with good spatial definition. As shown in Fig. 33.10 (right panel), the increase in $[Ca^{2+}]_i$ is restricted to the immediate vicinity of the plasma membrane after activation of Ca^{2+} channels. The requirement of high Ca^{2+} concentration for exocytosis implies that secretory granules are stored near the Ca^{2+} channels. Recent experimental evidence confirms that when Ca^{2+} channels are activated, the concentration of Ca^{2+} at the secretory sites could range from 10 to 100 pM, creating a Ca^{2+} microdomain (Neher, 1998).

In chromaffin cells, internal Ca^{2+} release is provided by two different pools: the $InsP_3$-sensitive pool and the Ca^{2+}-induced Ca^{2+} release pool (CICR). The activation of the PtdIns-specific phospholipase C by the G_q-protein-coupled receptor or by cytosolic Ca^{2+} elevation induces the hydrolysis of $PtdInsP_2$, thus generating two messengers: $InsP_3$ and diacylglycerol (DAG) (see Figs. 33.1 and 33.2). The binding of $InsP_3$ to specific sites on the endoplasmic reticulum induces Ca^{2+} release. $InsP_3$ receptors were also

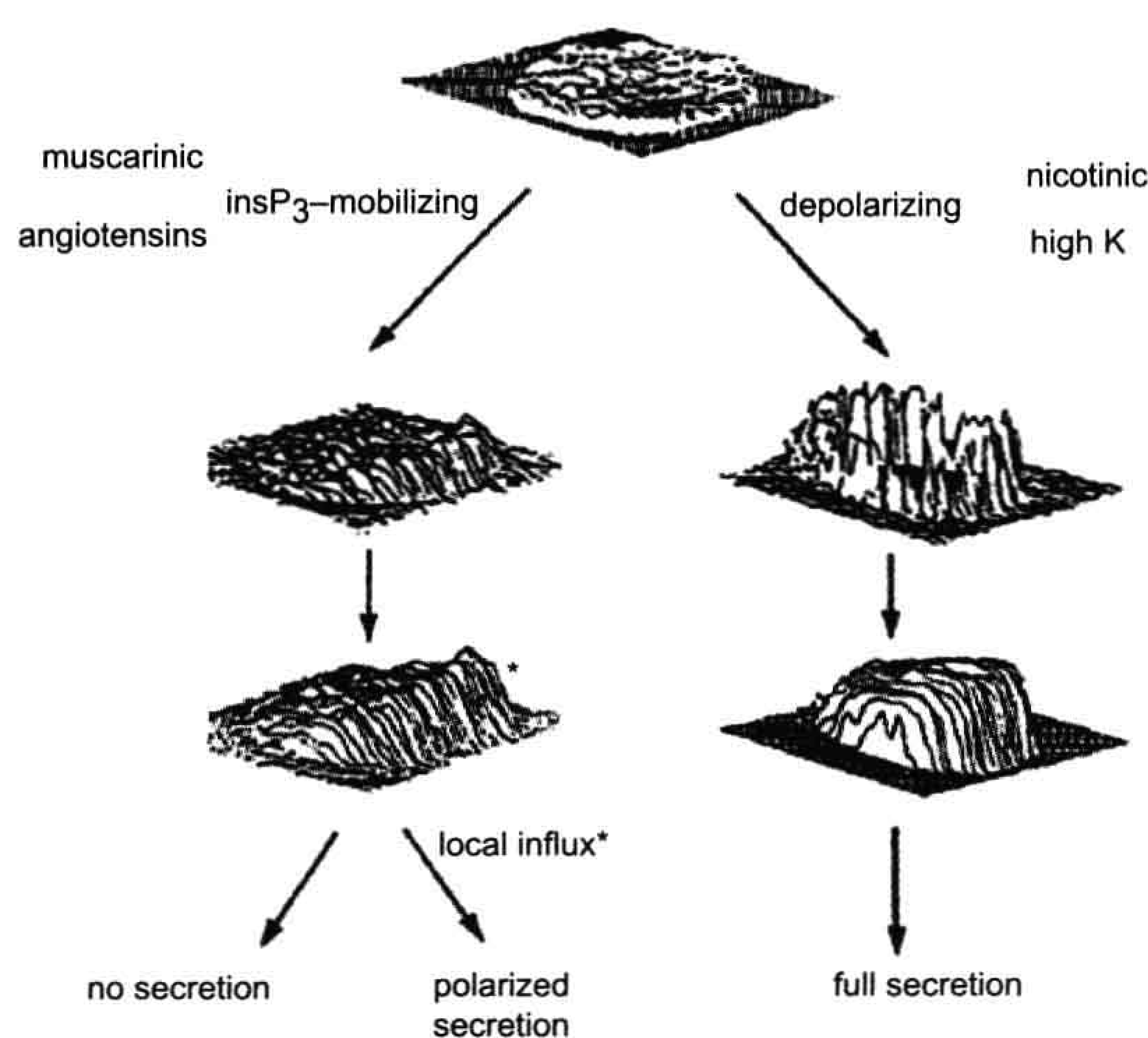


FIGURE 33.10 Ca^{2+} signal in a chromaffin cell in response to various agonists. The distribution of $[Ca^{2+}]_i$ is obtained by video-imaging. The figure illustrates the fact that level and distribution of $[Ca^{2+}]_i$ are important for full secretion. The right portion of the figure shows that a depolarization of the plasma membrane, induced by high $[K^+]_o$ or nicotinic agonist, opens voltage-activated Ca^{2+} channels with an immediate and high $[Ca^{2+}]_i$ increase at the periphery of the cell. Afterwards, $[Ca^{2+}]_i$ increases in the entire cell due to release of Ca^{2+} from internal stores; a full secretion is obtained. The left portion of the figure shows that release of Ca^{2+} from the IP_3-sensitive pool is not sufficient to induce secretion, although some localized secretion can be obtained in the region of the cell where $[Ca^{2+}]_i$ increase was the highest. *(Adapted with permission from Burgoyne, 1991.)*

found in secretory granules of endocrine and neuroendocrine cells. Their activation by $InsP_3$ induces the release of Ca^{2+} ions from the granules and provides a localized increase of $[Ca^{2+}]_i$. Ca^{2+} ion alone or caffeine can trigger the release of Ca^{2+} from the second pool (CICR). The muscarinic receptor induces the release of Ca^{2+} from the $InsP_3$-sensitive store without Ca^{2+} channel activation. The observed Ca^{2+} increase is low and sometimes localized to one pole of the cell (Fig. 33.10, left panel). Despite this $[Ca^{2+}]_i$ increase, there is little or no stimulation of secretion at the site where $[Ca^{2+}]_i$ has increased. A more uniform $[Ca^{2+}]_i$ increase can be generated by release from the Ca^{2+}-induced Ca^{2+} release pool by caffeine or from the $InsP_3$ pool by introduction of GTP-γS into the cell. However exocytosis still remains unstimulated. These results conclusively demonstrate that, in chromaffin cells, only a considerable rise in Ca^{2+} concentration in the proximity of the plasma membrane is able to trigger exocytosis. This highly localized $[Ca^{2+}]_i$ increase can only be achieved via the Ca^{2+} channels and not by a small increase due to release from internal stores.

Mast cells are able to synthesize, store and secrete histamine. However, Ca^{2+} alone is not able to trigger histamine secretion. There is a requirement for a guanine nucleotide together with Ca^{2+} for exocytosis. Mast cells are stimulated by antigenic binding on cell surface IgE receptors or by compound 48/80. A sudden rise in Ca^{2+} concentration (released from $InsP_3$-sensitive pool) is observed, reaching a level of up to several micromolar. The signal is transient and $[Ca^{2+}]_i$ declines within several seconds to its original baseline value. Degranulation begins soon after this transient response. Two important features should be noted concerning $[Ca^{2+}]_i$ and secretion in mast cells: (1) the $[Ca^{2+}]_i$ transient is not dependent on the presence of Ca^{2+} in the external medium; and (2) simultaneous recording of capacitance and membrane conductance reveals that conductance is constant throughout the duration of exocytosis. These results indicate that Ca^{2+} entry through Ca^{2+} channels is not a required signal for exocytosis, but rather its release from internal stores. A Ca^{2+} current, called I_{CRAC} (calcium-release activated calcium), was described in mast cells (Hoth and Penner, 1992); I_{CRAC} is activated by the depletion of intracellular Ca^{2+} pools. The role of I_{CRAC} in non-excitable cells could be to maintain a high $[Ca^{2+}]_i$ and to replenish empty Ca^{2+} stores after stimulation. A possible direct role in exocytosis has not yet been shown.

One conclusion is that Ca^{2+} release from internal stores is sufficient for exocytosis in mast cells. However, intracellular application of $InsP_3$ induces a transient $[Ca^{2+}]_i$ increase but does not trigger secretion, emphasizing that the signal is more complex. Application of the non-hydrolyzable GTP analog GTP-γS (100 μM) inside a mast cell (via a patch pipette) induces a transient

$[Ca^{2+}]_i$ increase, after a delay of 10–20 s, followed by an increase in capacitance. GTP-γS activates G proteins, including the G_q protein coupled to PLC, with a resulting production of $InsP_3$ and DAG. Ca^{2+} is released from the $InsP_3$-sensitive pool by the same mechanism as with the direct application of $InsP_3$ described above. However, in this case, exocytosis is stimulated, leading to the conclusion that GTP-γS activates a G protein that plays a crucial role in exocytosis.

Guanine Nucleotides

As seen earlier, Ca^{2+} and a guanine nucleotide are necessary and sufficient effectors to ensure secretion in mast cells. The stable analog GTP-γS is the commonly used guanine nucleotide, although any ligand that binds to G protein is able to stimulate secretion. In chromaffin cells, two types of observations have been recorded: (1) GTP-γS increases the Ca^{2+} sensitivity of secretion in permeabilized cells; and (2) GTP analogs stimulate secretion in a Ca^{2+}-independent manner (Morgan and Burgoyne, 1990). GTP analogs do not enhance the secretion induced by high Ca^{2+} concentration (10 μM), which indicates that the two stimuli (GTP and Ca^{2+}) act on the same exocytotic pathway.

Evidence for the involvement of a GTP-binding protein in secretion has been obtained from a variety of cells: neutrophils; platelets; parathyroid; pituitary lactotroph, gonadotroph and melanotroph; insulin-secreting cells; and pancreatic acinar cells. Various effects have also been observed in these cells: GTP or GTP analogs behave as effectors able to trigger a Ca^{2+}-independent secretion, or as modulators that increase Ca^{2+} sensitivity, or more surprisingly as inhibitors that block the exocytotic pathway at a late stage. The exact nature of the G proteins is not yet known, although some analogy can be made with GTP proteins involved in vesicular traffic (Rothman and Orci, 1992).

The small Ras-like GTPases are involved in the formation, transport and fusion of vesicles. In yeast, the small Ras-related GTP-binding protein SEC4 is required for targeting and/or fusion of vesicles to the plasma membrane. Rab3A from the rab family of proteins has been located in the membrane of neurosecretory vesicles. More than 30 Rabs have been identified. They have a regulatory role in secretion. In its GTP-bound form, Rab3A inhibits secretion, possibly by stabilizing a fusion-incompatible conformation. Under an appropriate signal, GTP is hydrolyzed to GDP with the help of GAP (a GTPase-activating protein); this exchange of GTP for GDP releases the inhibition. The fusion can then proceed to subsequent steps. Two accessory proteins are involved in the cycle: rabphilin-3A, which binds to the GTP-Rab3A form, and GDI (a GDP-dissociation inhibitor), which binds to the GDP-Rab3A form. Rabphilin is phosphorylated by many kinases and contains binding sites for Ca^{2+} and phospholipids. In endocrine cells, Nac2 binds GTP-Rab3A; this protein has a high similarity to the Rab3A-binding domain of rabphilin, but lacks the Ca^{2+} binding sites and phospholipids. GDI binds to Rab3A in its GDP form and removes it from the membrane. After dissociation of the GDI-GDP-Rab3A complex, GTP-Rab3A can bind again to another vesicle. Thus, rabphilin-3A and GDI control the Rab3A cycle but do not directly participate in the fusion (Südhof, 1995; Geppert and Südhof, 1998).

IVC2. Modulators of Exocytosis

ATP

Permeabilized cells rapidly lose their secretory response to agonists unless ATP is present in the medium. However, the sequence of exocytosis can be separated in an early phase that requires MgATP to proceed and a late phase that is MgATP-independent. ATP could act at various levels of the secretory response, acting as a substrate for protein phosphorylation or modulating various kinases involved in secretion. The last ATP-requiring steps in exocytosis have been identified; they involve ATPase, NSF and the formation of $PtdInsP_2$. NSF forms a large (20S) complex with the attachment proteins (SNAPs) and SNAP receptors (SNAREs), which has been proposed to be the fusion particle (see Fig. 33.3). The hydrolysis of ATP by NSF is thought to produce energy for the fusion (priming step). The formation of $PtdInsP_2$ by phosphatidylinositol 4-phosphatase-5-kinase and a phosphatidylinositol transfer protein requires the presence of ATP. $PtdInsP_2$ is thought to be involved in the interaction between cytoskeleton and secretory granules (docking step). Docking and priming of secretory granules are thus ATP-dependent. During vesicle transport through the Golgi, ATP hydrolysis by NSF occurs after docking, but in granule secretion no such evidence exists.

Cyclic Nucleotides

In chromaffin cells, cAMP concentration increases after cholinergic stimulation, leading to the hypothesis that cAMP could have a role in exocytosis. In pancreatic β cells, the cAMP-dependent protein kinase A enhances secretion. However, contradictory results have been reported on the effects of high and low cAMP concentrations on secretion modulation, i.e. inhibition and potentiation, respectively. Nicotinic-induced secretion in chromaffin cells is inhibited by high cGMP concentration, whereas low concentrations potentiate the secretory response.

Calmodulin

A calmodulin-binding protein of 65 kDa, called 65-CMBP or p65, has been found in several secretory vesicles, such as synaptic, neurohypophyseal, chromaffin, platelets and pancreatic islet granules. This protein also binds to

phospholipids with high affinity. A possible role of calmodulin in exocytosis was investigated by blocking its action. The calmodulin antagonist calmidazolium inhibits secretion from intact chromaffin cells. Antibodies raised against calmodulin inhibit the Ca^{2+}-dependent binding of calmodulin to vesicle membrane by acting on the docking and/or fusion steps of exocytosis. However, some reports indicate that the less specific calmodulin inhibitor trifluoperazine (TFP) has no effect on permeabilized cells. At present, it appears that calmodulin is not essential for Ca^{2+}-dependent exocytosis, although interaction between calmodulin and cytoskeletal proteins should nevertheless be considered.

Protein Kinase C

A role for PKC in secretion could be inferred from the fact that any agonist that stimulates secretion also induces activation of PKC. PKC has a modulating role in Ca^{2+} affinity, by decreasing Ca^{2+} requirements for exocytosis. Inhibition of PKC by staurosporine or through down-regulation partially inhibits secretion. However, in gonadotrophs, PKC-stimulated luteinizing hormone exocytosis is independent of Ca^{2+}. Obviously, the role of PKC in exocytosis is not yet completely understood. It is possible that PKC is not essential for Ca^{2+}-dependent exocytosis (modulator), but that a second Ca^{2+}-independent pathway could coexist in which PKC acts as an effector of secretion. Indeed, it has been recently shown in chromaffin cells that PKC acts at a late stage in exocytosis before the final Ca^{2+}-sensitive step. The role of PKC would be to increase the size of the readily releasable pool (RRP) of secretory granules by speeding their maturation after they dock with the plasma membrane. Moreover, direct stimulation of PKC by the phorbol ester PMA (phorbol 1,2-myristate-1,3-acetate) leads to a disruption of the actin network near the plasma membrane, which increases the number of docked granules. Several proteins involved in the regulation of the cytoskeleton are substrates for PKC: annexin I, annexin II and MARCKS (see Fig. 33.1).

Phospholipase A2 and Arachidonic Acid

A possible fusogen role of arachidonic acid was inferred from the fact that, in vitro, granules aggregated by synexin and Ca^{2+} fuse together if arachidonic acid is added to the medium. As previously mentioned for PKC activation, arachidonic acid is produced each time secretion is stimulated. Inhibition of phospholipase A2 and arachidonic acid metabolism inhibits secretion of chromaffin cells due to a blockage of Ca^{2+} entry.

IVC3. Secretory Granule Pools

In bovine chromaffin cells, increase in $[Ca^{2+}]_i$ triggers secretion at various rates: ultrafast secretion (time constant <0.5 s), fast secretion (time constant 3 s) and slow secretion (time constant 10 to 30 s). Nevertheless there is a weak correlation between the rate of secretion and $[Ca^{2+}]_i$ levels, the three types of responses are mainly observed for 10 to 50 μM, above 80 μM and around 170 μM $[Ca^{2+}]_i$, respectively. The time constant of the increase in membrane capacitance can be considered as a measure of the hormone released from a particular store. This indicates that the secretory granules are in various states of releasability. The ultrafast response comes from vesicles docked to the plasma membrane and immediately available for release by an increase in $[Ca^{2+}]_i$; they belong to the immediately releasable pool (IRP). A second pool of granules are located near the membrane in a nearly releasable pool (NRP) and can be released within seconds of a rise in $[Ca^{2+}]_i$; the fast response originates from this pool. Finally, the slow response originates from vesicles from a depot store in the bulk cytoplasm (Neher and Zucker, 1993). Movement of granules from the NRP to the IRP is Ca^{2+}-dependent and could involve calpactin in the docking process. However, not all the docked granules are available for the last steps, opening of the granule induced by Ca^{2+}. The fastest response, the exocytotic burst, mobilizes only one-tenth of the docked granules, which indicates that, after docking, granules undergo a maturation process in the IRP. Figure 33.11 describes a possible sequence for exocytosis in endocrine cells. PKC and ATP hydrolysis are involved in the docking and priming steps. Thereafter, three steps have been proposed based on their sensitivity to temperature, blockage by acidification and Ca^{2+} ion (three or four ions) triggering; PKC is thought to play a role in this sequence. The pivotal role of ATP in secretion has been outlined, however, a large pool of granules can be released in the absence of ATP by an increase in $[Ca^{2+}]_i$. This indicates first, that ATP hydrolysis by NSF is an early step in the priming process and, second, that if the energy of hydrolysis powers fusion, it remains stored in the core complex until $[Ca^{2+}]_i$ increases (Parsons et al., 1995; Gillis et al., 1996).

V. HORMONE RELEASE IN ENDOCRINE CELLS

VA. Polypeptide and Thyroid Hormones

Most of the events described previously could be applied for most of the endocrine secretory cells.

VA1. Secretion of Insulin

Insulin secretion by the pancreatic β cells provides an excellent example of a cellular activity that requires direction. Insulin is packaged in secretory vesicles which have to migrate to the plasma membrane and fuse with it to release the entrapped insulin. Both microscopic and

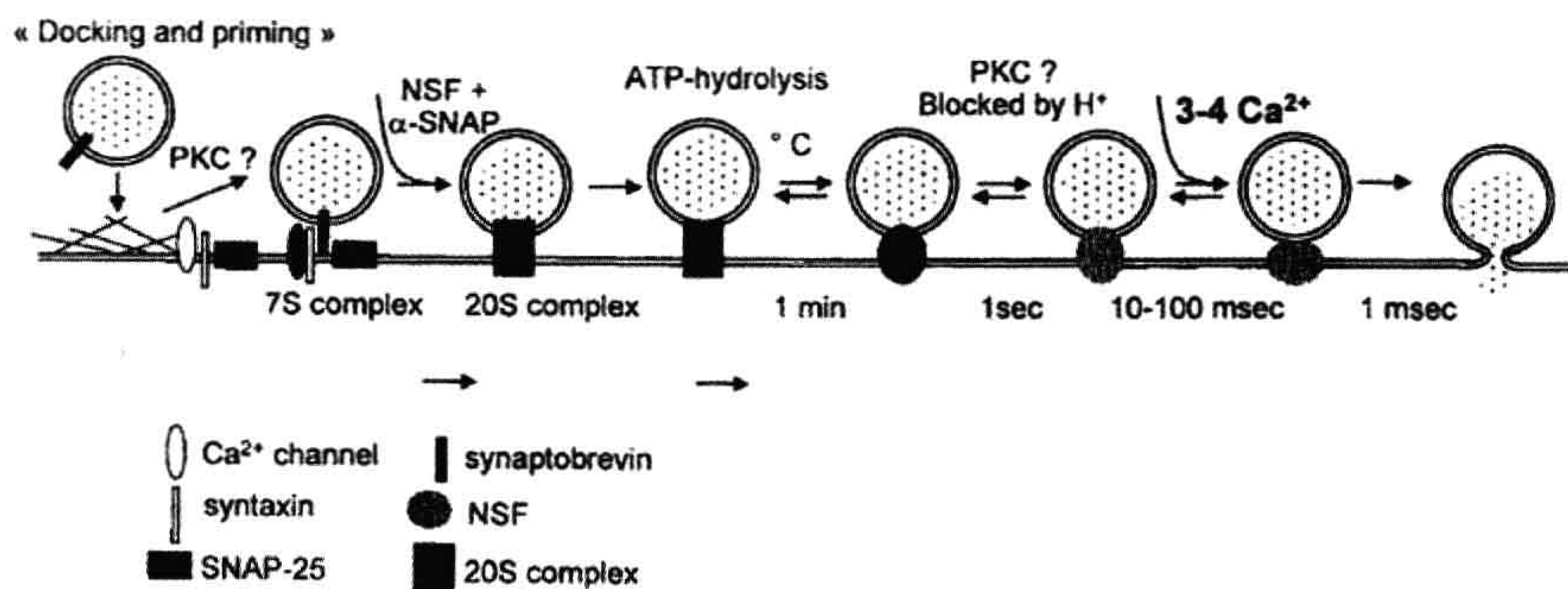


FIGURE 33.11 Docking and fusion of secretory granules in endocrine cells. Docking of vesicles involves the proteins synaptobrevin and syntaxin/SNAP-25. In the first step of docking, protein kinase C (PKC) could have a role in the disruption of the actin barrier. ATP hydrolyzed by NSF is thought to produce energy for fusion. Several steps have been identified after the ATP-dependent step based on their temperature, H^+ and Ca^{2+} dependence. PKC could be involved before the final Ca^{2+}-dependent step. *(Adapted with permission from Parsons et al., 1995 and Gillis et al., 1996.)*

biochemical studies have shown that secretory granules are linked to microtubules which direct attached vesicles to the cell surface. However, a cortical band of fine microfilaments is consistently observed in β cells. Alteration of this cell web by cytochalasin B is associated with an enhancement of glucose-induced secretion of insulin by isolated islets. This microfilamentous web plays an important role in the exocytosis of insulin secretory granules by controlling access to the cell membrane via a mechanism probably similar to that previously described for chromaffin cells. Ca^{2+} appears to initiate the cascade of events by which microtubules facilitate the displacement of granules toward the cell membrane. Glucose metabolism increases intracellular concentration of ATP, which closes the ATP-sensitive K^+ channels, consequently inducing cell depolarization and Ca^{2+} influx, while cAMP modifies the intracellular distribution of Ca^{2+} by increasing the cytosolic pool at the expense of Ca^{2+} bound to intracellular organelles. Protein kinase C also appears to be involved in the secretion of insulin.

VA2. Secretion of Pituitary Hormones

Anterior pituitary cells, in their diversity and heterogeneity, provide a rich source of models for secretory function. Secretion of the pituitary hormones is controlled by both specific hypothalamic-releasing peptides and neurotransmitters. Upon binding to their receptors, these agonists activate both Ca^{2+} influx by different types of Ca^{2+} channels (voltage-activated channels, ligand-activated channels and second messenger-activated channels) and second messenger production, thus resulting in hormone secretion. As a second messenger, cAMP appears to be as potent as $InsP_3$ and PKC in interacting with Ca^{2+} to trigger secretion. As for insulin secretion, cytoskeletal structures are tightly associated with hormone release. Purified secretory granule membranes co-sediment with microtubules, MAPs being involved in this association. This suggests that microtubules facilitate the movement of secretory granules from the Golgi apparatus to the plasma membrane, by providing tracks along which the granules can move. The granule membrane can then dissociate from the microtubules and fuse with the cell membrane, followed by exocytosis and release of the hormone into the circulation. Moreover, actin and microtubules are cross-linked by MAPs, forming three-dimensional networks. This cross-linking activity can be inhibited if MAPs are heavily phosphorylated. These observations suggest that MAPs might play an important role in the binding of secretory granules to tubulin and actin. Binding of actin to secretory granules suggests a role for actin in the final steps of exocytosis, as described previously.

VB. Stimulation of Steroid Synthesis and Secretion

While disruption of the actin network is necessary to trigger fusion of secretory vesicles with the cell membrane, a well-preserved organization seems important for steroid release. Several studies have shown that microfilament disruption (with cytochalasins) or microtubule disruption (with colchicine or vinblastine) decreases or blocks second messenger production and steroid secretion, either from the adrenal cortex or gonads. In contrast with peptide hormones, steroids are not packaged in vesicles. Steroid hormones are synthesized from cholesterol contained in lipid droplets. The process of steroidogenesis begins in the mitochondria, where cholesterol is converted to pregnenolone, from which others steroids are synthesized. Stimuli induce rapid increase in the production and secretion of steroids, without cytoplasmic storage. More recent biochemical analysis and fluorescence studies indicate

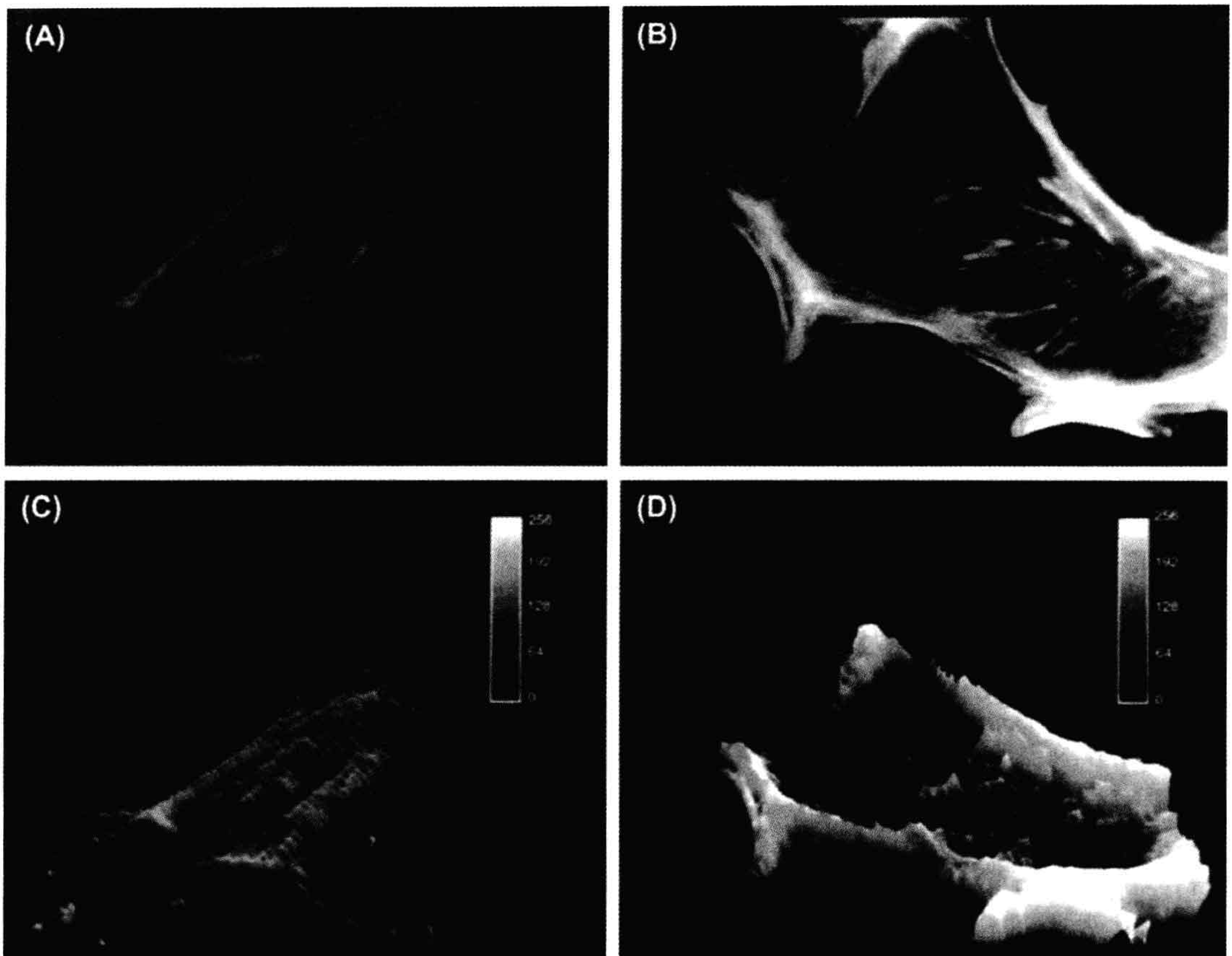


FIGURE 33.12 Effect of Ang II on immunofluorescence labeling of actin in rat glomerulosa cells. Rat glomerulosa cells were cultured for 3 days on plastic coverslips and then incubated without (A) or with (B) 100 nM angiotensin II for 1 min. After formaldehyde fixation and permeabilization with 0.1% Triton X-100, cells were processed for immunofluorescence labeling of actin using rhodamine-phalloidin. (C) and (D) represent the same images as (A) and (B) after computer analysis. Bars represent 13 μm. *(Adapted from Côté et al., 1997.)*

that ligand-receptor interaction induces a rapid polymerization of actin, demonstrated by a rise in the proportion of F-actin over G-actin and by an increased interaction of F-actin with the membrane (Fig. 33.12A and B versus C and D). Moreover, $G_{q/11}$ protein localization overlaps F-actin distribution and cell activation is accompanied by a rapid translocation of $G_q/_{11}$ and F-actin from the cytosol to the membrane, an association essential in promoting phospholipase C activation (Côté et al., 1997).

It has been shown that microfilaments are strictly required for both spontaneous and stimuli-induced corticosteroid secretions, including those utilizing the cAMP-dependent pathways (ACTH, serotonin and vasoactive intestinal peptide), as well as those utilizing the phosphoinositide pathway (angiotensin II and acetylcholine). They are involved in a common and probably late step of steroidogenesis (translocation of the DOC from RER to mitochondria). In contrast, microtubules seem involved in an early step in the mechanism of hormone action, probably at the level of their interaction with the α subunit of the G protein. Microtubules and microfilaments are closely associated with the plasma membrane. That colchicine and vinblastine stimulate basal steroidogenesis may be explained by the fact that most of the tubulin is linked to cholesterol, in lipid droplets. Thus, by acting on tubulin, antimicrotubular drugs could release cholesterol, causing an increase in basal steroid secretion (Feuillolley and Vaudry, 1996). Moreover, in adrenocortical cells, findings suggest that intermediate filaments could facilitate or increase the transport of cholesterol to mitochondria in response to ACTH and cAMP. Figure 33.13 summarizes the role of the three types of

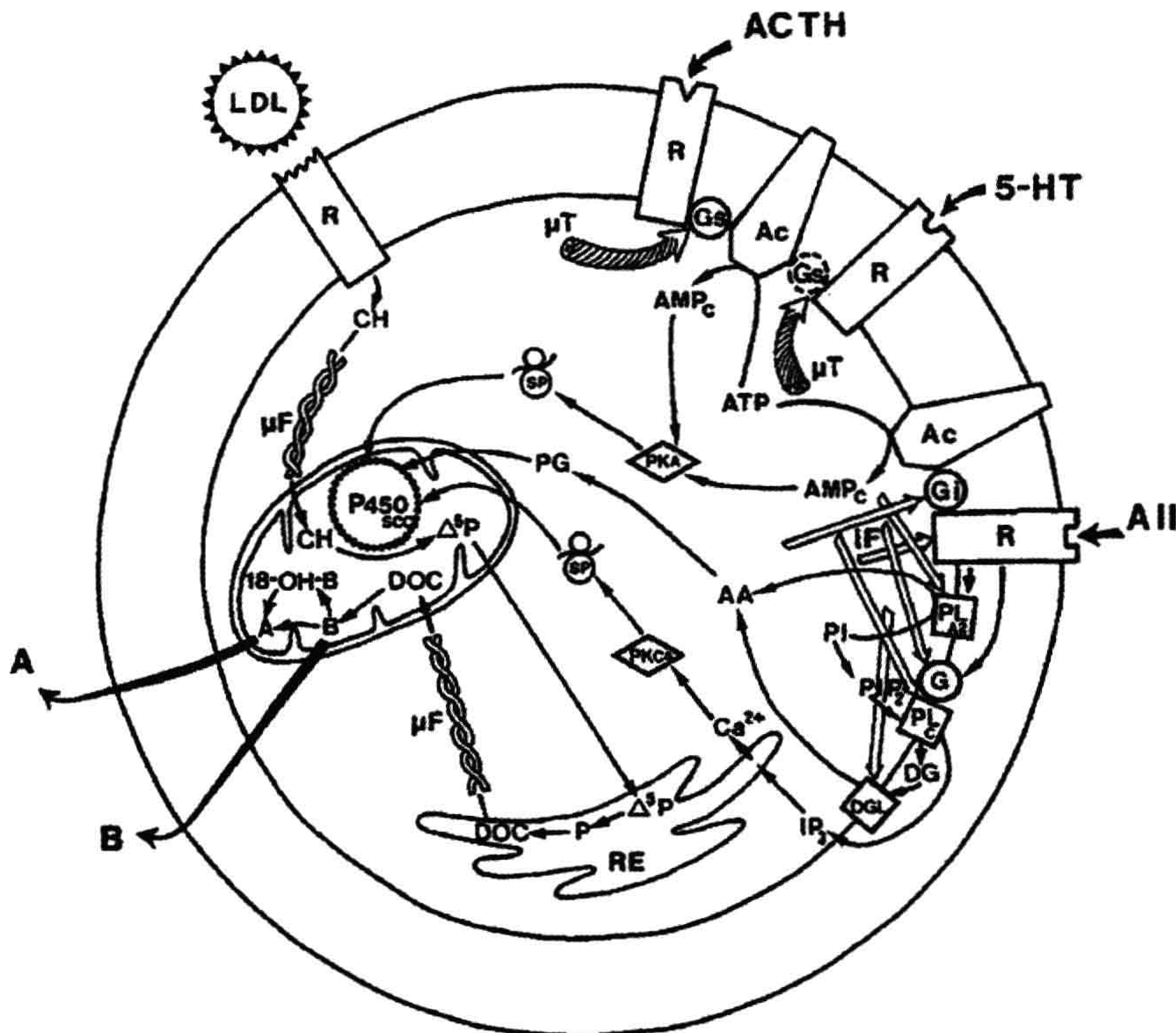


FIGURE 33.13 Cytoskeleton implication in adrenal corticosteroidogenesis. Microtubules (μT) are implicated in the action of ACTH and serotonin (5-HT), probably at a level of G_s protein. Microfilaments (μF) control the transfer of steroid precursors (cholesterol from lipid droplets or membrane low-density lipoproteins to mitochondria and from mitochondria to endoplasmic reticulum). Intermediate filaments (IF) appear to be implicated in the action of angiotensin II (AII), between hormone-receptor coupling and second messenger production. A, aldosterone; AA, arachidonic acid; AC, adenylyl cyclase; cAMP, cyclic adenosine monophosphate; ATP, adenosine triphosphate; B, corticosterone; DAG, diacylglycerol; DOC, 11-deoxycorticosterone; 18-OH-B, 18-hydroxycorticosterone; P, progesterone; P450scc, P450scc cytochrome; Δ^5P, pregnenolone; PG, prostaglandins; PI, PtdIns; PIP_2, $PtdInsP_2$; PKA, protein kinase A; PKCa, protein kinase Ca^{2+}-dependent; PLA_2, phospholipase A_2; PLC, phospholipase C; PS, protein synthesis. *(Reproduced with permission from Feuilloley et al., 1989.)*

cytoskeletal fibers in the steroidogenic effects of the main stimuli of corticosterone and aldosterone secretions (Feuillolley and Vaudry, 1996).

ACKNOWLEDGMENTS

The authors thank Dr Mylène Côté for critical review of the revised version and fruitful discussions and Dusan Chorvat, Jr, from the International Laser Center, Bratislava (Slovakia), for image analysis.

BIBLIOGRAPHY

Almers, W. (1990). Exocytosis. *Annu Rev Physiol, 52*, 607–624.

Aplin, A., Howe, A., Alahari, S., & Juliano, R. (1998). Signal transduction and signal modulation by cell adhesion receptors: the role of integrins, cadherins, immunoglobulin-cell adhesion molecules, and selectins. *Pharmacol Rev, 50*, 197–263.

Arbuzova, A., Murray, D., & McLaughlin, S. (1998). MARCKS, membranes, and calmodulin: kinetics of their interaction. *Biochim Biophys Acta, 1376*, 369–379.

Aroeti, B., Okhrimenko, H., Reich, V., & Orzech, E. (1998). Polarized trafficking of plasma membrane proteins: emerging roles for coats, SNAREs, GTPases and their link to the cytoskeleton. *Biochim Biophys Acta, 1376*, 57–90.

Burgoyne, R. D. (1991). Control of exocytosis in adrenal chromaffin cells. *Biochim Biophys Acta, 1071*, 174–202.

Burgoyne, R. (1995). Mechanisms of catecholamine secretion from adrenal chromaffin cells. *J Physiol Pharmacol, 46*, 273–283.

Burgoyne, R., & Morgan, A. (1998a). Analysis of regulated exocytosis in adrenal chromaffin cells: insights into NSF/SNAP/SNARE function. *Bioessays, 20*, 328–335.

Burgoyne, R., & Morgan, A. (1998b). Calcium sensors in regulated exocytosis. *Cell Calcium, 24*, 367–376.

Chow, R. H., Von Rüden, L., & Neher, E. (1992). Delay in vesicle fusion revealed by electrochemical monitoring of single secretory events in adrenal chromaffin cells. *Nature, 356*, 60–63.

Côté, M., Payet, M.-D., Dufour, M.-N., Guillon, G., & Gallo-Payet, N. (1997). Association of the G protein α_q/α_{11}-subunit with cytoskeleton in adrenal glomerulosa cells: role in receptor-effector coupling. *Endocrinology, 138*, 3299–3307.

Fernandez-Chacon, R., & Südhof, T. (1999). Genetics of synaptic vesicle function: toward the complete functional anatomy of an organelle. *Annu Rev Physiol, 61*, 753–776.

Feuillolley, M., & Vaudry, H. (1996). Role of the cytoskeleton in adrenocortical cells. *Endocr Rev, 17*, 269–288.

Forscher, P. (1989). Calcium and polyphosphoinositide control of cytoskeletal dynamics. *Trends Neurosci, 12*, 468–474.

Geppert, M., & Südhof, T. (1998). RAB3 and synaptotagmin: the yin and yang of synaptic membrane fusion. *Annu Rev Neurosci, 21*, 75–95.

Gillis, K. D., Mössner, R., & Neher, E. (1996). Protein kinase C enhances exocytosis from chromaffin cells by increasing the size of the readily releasable pool of secretory granules. *Neuron, 16*, 1209–1220.

Goda, Y., & Südhof, T. (1997). Calcium regulation of neurotransmitter release: reliably unreliable? *Curr Opin Cell Biol, 9*, 513–518.

Gundersen, G., & Cook, T. (1999). Microtubules and signal transduction. *Curr Opin Cell Biol, 11*, 81–94.

Hall, A. (1998). Rho GTPases and the actin cytoskeleton. *Science, 279*, 509–514.

Hoth, M., & Penner, R. (1992). Depletion of intracellular calcium stores activates a calcium current in mast cells. *Nature, 355*, 353–356.

Inglese, J., Koch, W., Touhara, K., & Lefkowitz, R. (1995). G beta gamma interactions with PH domains and Ras-MAPK signaling pathways. *Trends Biochem Sci, 20*, 151–156.

Janmey, P. (1998). The cytoskeleton and cell signaling: component localization and mechanical coupling. *Physiol Rev, 78*, 763–781.

Lindau, M., & Gomperts, B. D. (1991). Techniques and concepts in exocytosis: focus on mast cells. *Biochim Biophys Acta, 1071*, 429–471.

Martin, T. (1998). Phosphoinositides as signaling molecules. *Annu Rev Cell Dev Biol, 14*, 231–264.

Matus, A. (1988). Microtubule-associated proteins: their potential role in determining neuronal morphology. *Annu Rev Neurosci, 11*, 29–44.

Monck, J. R., Alvarez de Toledo, G., & Fernandez, J. M. (1990). Tension in secretory granule membranes causes extensive membrane transfer through the exocytotic fusion pore. *Proc Natl Acad Sci USA, 87*, 7804–7808.

Morgan, D., & Burgoyne, R. D. (1990). Stimulation of Ca^{2+}-inde-pendent catecholamine secretion from digitonin-permeabilized bovine adrenal chromaffin cells by guanine nucleotide analogues. Relationship to arachidonate release. *Biochem J, 269*, 521–526.

Neher, E. (1998). Vesicle pools and Ca^{2+} microdomains: new tools for understanding their roles in neurotransmitter release. *Neuron, 20*, 389–399.

Neher, E., & Zucker, R. S. (1993). Multiple calcium-dependent processes related to secretion in bovine chromaffin cells. *Neuron, 10*, 21–30.

Parsons, T. D., Coorssen, J. R., Horstmann, H., & Almers, W. (1995). Docked granules, the exocytic burst, and the need for ATP hydrolysis in endocrine cells. *Neuron, 15*, 1085–1096.

Popova, J. S., Garrison, J. C., Rhee, S. G., & Rasenik, M. M. (1997). Tubulin, Gq, and phosphatidylinositol 4,5-bisphosphate interact to regulate phospholipase $C\beta_1$ signalling. *J Biol Chem, 272*, 6760–6765.

Rothman, J. E., & Orci, L. (1992). Molecular dissection of the secretory pathway. *Nature, 355*, 409–415.

Schmidt, A., & Hall, M. (1998). Signaling to the actin cytoskeleton. *Annu Rev Cell Dev Biol, 14*, 305–338.

Söllner, T., Whiteheart, S. W., Brunner, M., et al. (1993). SNAP receptors implicated in vesicle targeting and fusion. *Nature, 362*, 318–323.

Südhof, T. C. (1995). The synaptic vesicle cycle: a cascade of protein-protein interactions. *Nature, 375*, 645–653.

Südhof, T., & Rizo, J. (1996). Synaptotagmins: C2-domain proteins that regulate membrane traffic. *Neuron, 17*, 379–388.

Tapon, N., & Hall, A. (1997). Rho, Rac and Cdc42 GTPases regulate the organization of the actin cytoskeleton. *Curr Opin Cell Biol, 9*, 86–92.

Tchakarov, L., Zhang, L., Rose, S., Tang, R., & Trifaro, J. (1998). Light and electron microscopic study of changes in the organization of the cortical actin cytoskeleton during chromaffin cell secretion. *J Histochem Cytochem, 46*, 193–203.

Trifaró, J.-M., Vitale, M. L., & Rodriguez Del Castillo, A. (1992). Cytoskeleton and molecular mechanisms in neurotransmitter release by neurosecretory cells. *Eur J Pharmacol, 225*, 83–104.

Chapter 34

Stimulus–Response Coupling in Metabolic Sensor Cells

Stan Misler

Chapter Outline

I. INTRODUCTION

The term *sensory receptor* is usually applied to a limited group of cells, located near the surface of the organism, designed to transduce stimuli from the external environment (e.g. photons of light or air or water-borne molecules or pressure disturbances) into the release of a chemical transmitter, which ultimately signals neurons that project into the central nervous system. However, to maintain a "steady state," organisms must also detect changes in their internal environment. To do this, specialized internal receptors must sense changes (1) in the levels of circulating metabolic fuels (e.g. nutrient metabolites and O_2); (2) in the levels of metabolic wastes (e.g. CO_2); (3) in the ionic composition of the extracellular lymph-like fluid which bathes the cells; and (4) in the internal or lumenal tension in hollow tubular organs (e.g. blood vessels and gut).

Currently, among the internal receptors, those sensitive to metabolic changes are better understood than those responding to changes in ionic composition or lumenal tension. In this chapter, we shall examine, in some detail, sensory transduction by five types of *metabolic sensor cells*.

1. *Pancreatic islet cells:* these cells sense changes in the levels of several circulating metabolites, especially glucose and amino acids, and respond with secretion of the hormone insulin and glucagon. Insulin promotes the uptake of glucose and its storage as glycogen in muscle and liver and maintains fat stores in adipocytes, while glucagon mobilizes fat and glycogen stores.
2. *Cardiac and skeletal myocytes and some neurons:* these cells curtail their excitability during hypoxia and substrate deprivation, thereby saving themselves from severe hypometabolic injury.
3. *Chemoreceptor cells of carotid body:* these cells sense changes in the O_2 and CO_2 content of blood and synapse onto sensory nerve fibers which project into the central nervous system (CNS) and help shape respiratory drive.

Cell Physiology Sourcebook. DOI: 10.1016/B978-0-12-387738-3.00034-2

4. *Vascular smooth muscle cells:* these cells sense local changes in O_2 tension and respond by regulating their tone, thereby locally controlling blood flow.
5. *Hypoxia-secreting renal interstitial cells and liver Ito cells:* in response to hypoxia, these cells secrete erythropoetin, the hormone critical for maturation and release from bone marrow of oxygen-carrying erythrocytes.

The first four types of metabolic sensor cells share a common property; each makes use of K^+ channels specially attuned to metabolic changes to transduce stimuli. Some also use the metabolic intermediates to modulate more distal processes in their scheme of *stimulus–response coupling*. The fifth cell makes use of what might be called *stimulus–synthesis coupling*. Familiarity with different patch-clamp recording configurations and basic concepts of excitation–secretion coupling in nerve cells is assumed (see Chapters 20 and 33).

II. STIMULUS–SECRETION COUPLING IN THE PANCREATIC ISLET CELLS

The pancreas consists of islands of endocrine tissue, islets of Langerhans, that regulate metabolite uptake, storage and release by liver, adipocytes and skeletal muscle, surrounded by a sea of exocrine tissue, acini and their ducts, that secrete alkaline digestive juices into the duodenum. Each islet contains about 1000 cells. Roughly 65% are insulin-producing β cells, triggered by an increase in serum glucose. These are the largest of the islet cells and have distinct crystals in their secretory granules. Roughly 20% are glucagon-producing α cells, largely triggered by a decrease in serum glucose. The remaining 15% are δ or PP cells secreting somatostatin or pancreatic polypeptide. After dispersal of the islet into single cells, α cells can be separated from β cells on the basis of their smaller size and decreased NAD^- autofluorescence. Though isolated islet cells secrete in response to appropriate stimuli, they secrete best when they are in clusters containing representatives of each cell type. Beta cells are electrically coupled. Alpha, beta and delta cells all "talk" to each other via paracrine interactions; glucagon enhances stimulus-induced insulin secretion, whereas somatostatin inhibits it. Insulin, glucagon and somatostatin all inhibit glucagon secretion.

The study of how a rise in plasma glucose leads to rapid secretion of insulin by β cells has provided fertile ground for the interaction of a wide range of disciplines in cell physiology. Since the mid-1970s, it has been widely appreciated that the release of insulin, which is stored in secretory granules, is dependent on extracellular Ca^{2+} concentration $[Ca^{2+}]_o$ (the *calcium hypothesis*), requires oxidative metabolism of glucose or other metabolite fuels (the *fuel hypothesis*) and follows the onset of complex electrical activity in the β cells (the *depolarization–secretion coupling hypothesis*). These features were first established using techniques of islet perifusion and radioimmunoassay of secreted insulin (Fig. 34.1A). In these experiments, islets are mounted on a filter and exposed to a continuous flow of solution able to trap secreted insulin. Timed aliquots of solution are collected and the insulin content is measured by radioimmunoassay, i.e. the ability of the secreted insulin to displace radioactively labeled insulin bound to an anti-insulin antibody. Note that insulin secretion induced by raising glucose from preprandial levels of 2–3 mM to levels above 5 mM occurs in two phases, a transient "first phase" and a sustained "second phase." In vivo, the "first phase" may saturate hepatic insulin receptors, as it is often not readily detected in assays of peripheral insulin levels. Note that the "second phase" of release is reversibly reduced by (1) transient reduction of the Ca^{2+} concentration of the perifusing solution or (2) addition of an inhibitor of glucose metabolism, in this case, sodium azide (NaN_3), an inhibitor of the mitochondrial respiration (see Fig. 34.1A). In parallel experiments, it was found that islets bathed in preprandial levels of glucose rapidly released insulin in response to exposure to high $[K^+]$, provided adequate extracellular Ca^{2+} was present.

When the *fuel hypothesis* was extensively tested, insulin release was found to be (1) stimulated by amino acids, glycolytic intermediates and ketone bodies shown to be metabolized by β cells but (2) inhibited by substances that specifically block uptake and metabolism of these substrates or by general inhibitors of mitochondrial function. The *calcium hypothesis* and the *depolarization–secretion coupling hypothesis* were tested with intracellular recording from islet cells in intact and perifused islets. Beta cells were found to maintain resting potentials of about −60 mV at fasting glucose concentrations. The resting potential varies with $[K^+]_o$ according to the Nernst equation, hence suggesting that it is largely due to K^+ permeability (P_K). Within several minutes of exposure to "secretagogue" concentrations of fuel metabolites, these cells depolarize, coincident with a decline in resting membrane conductance and shortly thereafter exhibit bursts of action potentials whose overshoots are a function of $[Ca^{2+}]_o$. In cells loaded with a Ca^{2+} indicator, "spikes" of cytosolic Ca^{2+} coincide with bursts of action potentials (see Fig. 34.1B).

From these observations emerged an early critical unifying hypothesis: *fuel metabolism → reduced P_K → electrical activity → Ca^{2+} entry → insulin release.* It is worth mentioning that this scheme also accommodates the actions of a class of hypoglycemic agents, called sulfonylureas. Though not related to fuel metabolites, and themselves not metabolized, sulfonylureas potentiate the

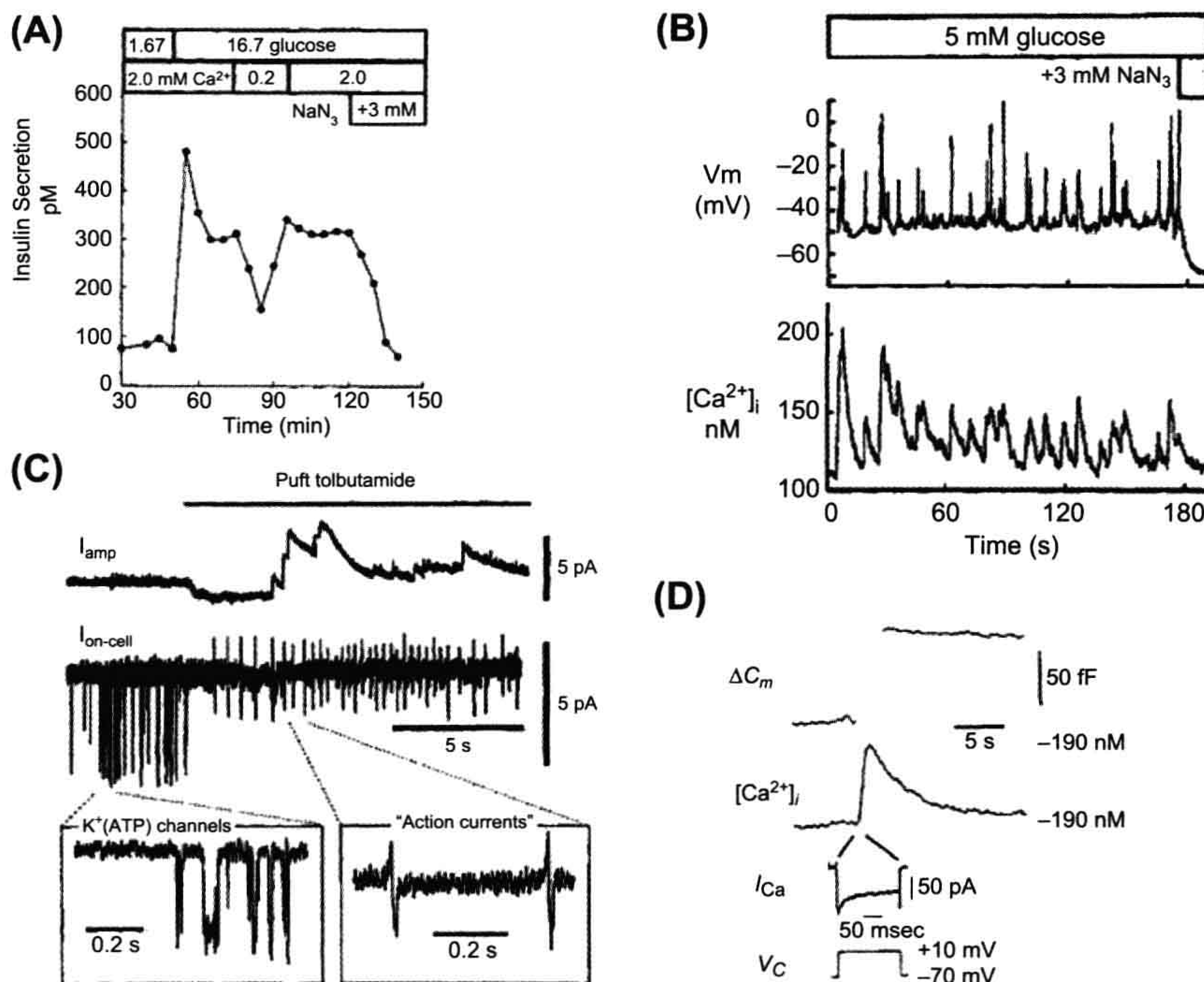


FIGURE 34.1 Overview of basic evidence supporting "fuel hypothesis," "calcium hypothesis" and "depolarization–secretion coupling hypothesis" of glucose-induced insulin release from pancreatic β cells. (A) Insulin secretion, measured by radioimmunoassay, from isolated intact human pancreatic islets of Langerhans. Note the rapid onset of biphasic insulin secretion on increasing glucose from 1.67 to 16.7 mM, the interruption of the plateau phase by reduction in extracellular [Ca^{2+}] from 0.2 to 2.0 mM and the termination of secretion by the addition of sodium azide (NaN_3), an inhibitor of electron transport by mitochondrial cytochromes. Leucine, glyceraldehyde and acetoacetate produce similar patterns of secretion in the presence of Ca^{2+}. (B) Simultaneous recording of electrical activity and cytosolic Ca^{2+} transients from single cryopreserved/thawed human β cells loaded with Ca^{2+} indicator FURA-2. Note that in the presence of 5 mM extracellular glucose, the cell fires individual or short trains of action potentials and that even single action potentials are sufficient to induce a Ca^{2+} transient. Subsequent addition of NaN_3 abruptly hyperpolarizes the cell to ≈ -70 mV and blocks the appearance of Ca^{2+} transients. (Unpublished experiments by D. Barnett and S. Misler.) (C) Single cell exocytosis detected by amperometry and capacitance. Simultaneous cell-attached patch recording and amperometry from small clamp of islet cells preloaded with serotonin. The amperometric electrode was positioned at the confluence of cells. In 2 mM glucose, the $I_{on\text{-}cell}$ trace shows single-channel openings, which will later be identified as those of ATP-sensitive K^+ channels (K^+(ATP)). After addition of tolbutamide, single channels close and "action currents" develop. After several impulses have fired, amperometric events are noted on the I_{amp} trace. Those events, slower than those observed when recording for single isolated cells, probably reflect simultaneous exocytotic discharge at several sites, each distant from the electrode. (D) Simultaneous-monitoring membrane capacitance and cytosolic Ca^{2+} from a voltage-clamped β cell. Note that a 200-ms depolarization from -70 to $+10$ mV increases global cytosolic [Ca^{2+}] by an estimated 100 µm and membrane capacitance by 75 fF. This corresponds to the fusion of 30–60 insulin granules, given that the C_m increase per granule is estimated at 1.25–2.5 fF.

action of glucose even when glucose metabolism is modestly inhibited. They reduce resting P_K, depolarize the cell, set off action potentials and stimulate insulin secretion even at preprandial levels of glucose. As we shall discuss in short order, these substances have been found to block directly the K^+ conductance that is physiologically gated by cell metabolism.

Critical clues to the validity and the molecular details of this hypothesis have been provided by (1) patch-clamp recording plus molecular biology of channels (cloning and site-directed mutagenesis) and (2) single-cell, real-time monitoring of exocytosis (or fusion of the granule membrane with the plasma membrane). In patch-clamped β cells, the workings of ATP-inhibited K^+ channels, whose closure underlies cell depolarization, have been analyzed in great molecular detail, in large part due to the identification of this molecule as the β cell's major sulfonylurea receptor. In patch-clamped β cells, depolarization-induced exocytosis can be measured electrically as an increase in membrane capacitance *(C_m)*, while agonist- (e.g. sulfonylurea-) induced release can be monitored electrochemically as release of packets of native insulin or the false transmitter serotonin previously loaded into insulin granules (see Fig. 34.1C). Using either measure, exocytosis

is found to be graded with the amount of Ca^{2+} entry induced by depolarization.

(Here it is worth recalling that exocytosis involves simultaneous fusion of the membrane of the secretory granule with the plasma membrane as well as the release of the granule content into the extracellular space. The membrane fusion event, an increase in plasma membrane surface area, is usually detectable as an increase in plasma membrane capacitance. Membrane capacitance is estimated from the ability of the membrane circuit to "phase shift," or displace in time, a sine wave of voltage excitation. The release of a packet of transmitter [or hormone] can be detected "biologically," by a receptive patch of membrane, or "electrochemically," at the surface of an electrode held at a potential sufficient to oxidize or reduce a component of the granule content. In either case, a brief spike of current is produced. When dealing with cells with large secretory granules, one can be more adequately convinced that exocytosis has occurred when it is possible to demonstrate the following points: (1) the jumps in C_m thought to represent single granule fusion events have amplitudes predictable from the surface area of the granule; (2) the single electrochemical spike [or "amperometric event"] coincides in time with jumps in C_m and represents the release of at least many tens to hundreds of thousands of molecules that are either native to the granule or else preloaded as a marker. In the case of β cells, the preloaded marker is serotonin. It is worth remembering that capacitance and amperometry are complementary techniques; capacitance monitors net increase in total membrane surface area [exocytosis minus endocytosis], whereas amperometry often permits direct counting of quantal release, albeit from a fraction of the cell surface.)

On the basis of these and other experiments, over the past decade a more detailed "consensus hypothesis" has emerged for glucose-induced insulin secretion from β cells (Fig. 34.2, right-hand side). Uptake of glucose (predominantly via a Glut-2 type transporter) provides glucose entry into glycolysis (via glucokinase, a low affinity hexokinase) and the mitochondrial Krebs cycle results in the generation of ATP and consumption of ADP (Step 1). This leads to the closure of ATP-inhibited K^+ channels, here abbreviated as *K^+(ATP)* (Step 2). Against a background of tonic activity of non-selective cation channels that pass Na^+ inward, K^+(ATP) channel closure results in the depolarization of the β-cell membrane (Step 3). When V_m reaches the threshold for activating voltage-dependent Ca^{2+} and Na^+ channels, electrical activity and voltage-dependent Ca^{2+}

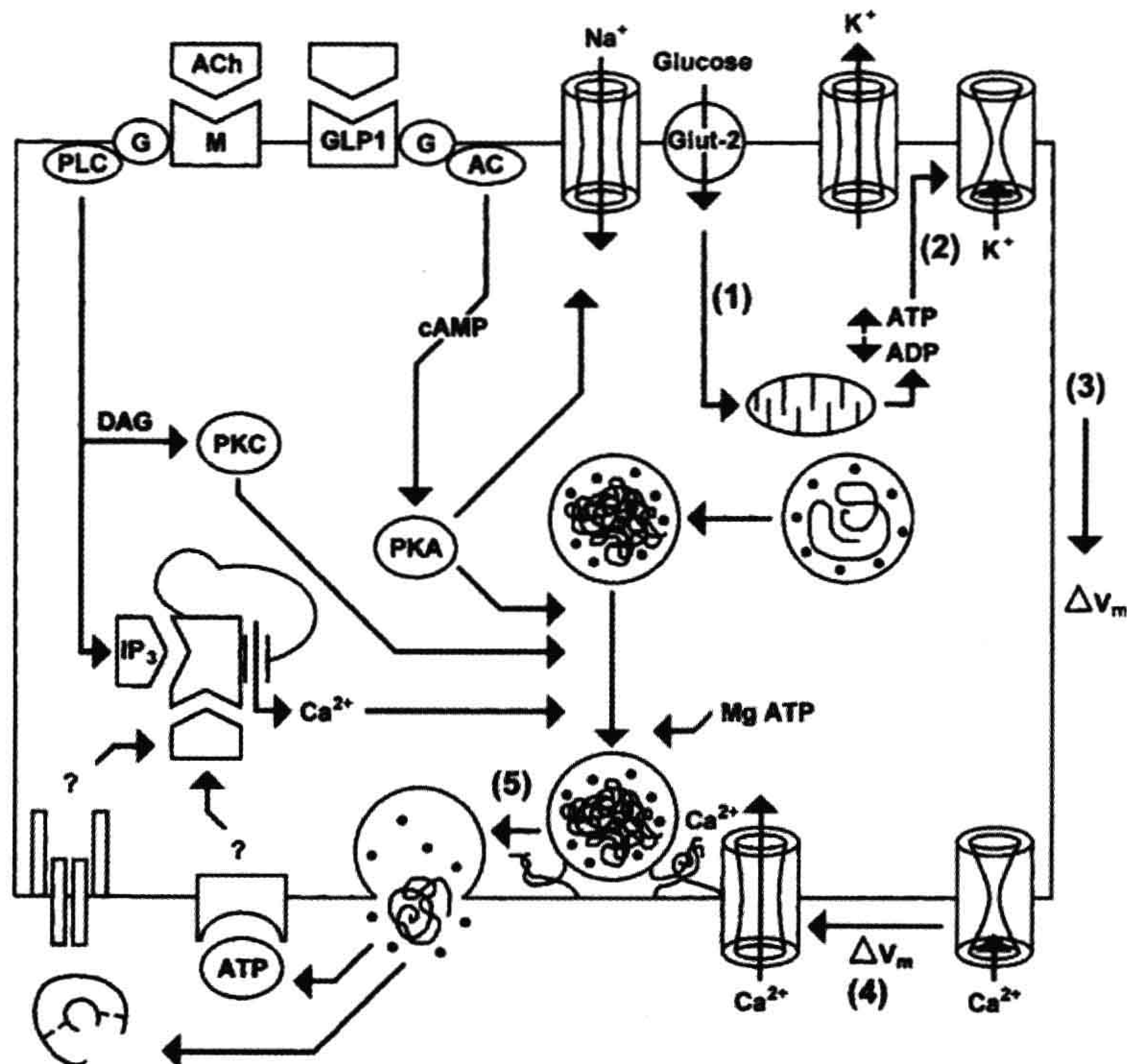


FIGURE 34.2 Overview of stimulus—secretion coupling in the pancreatic β cell. The right-hand side shows (1–5) a "consensus scheme" of stimulus—secretion coupling: glucose transport and phosphorylation (1),→ to intermediate metabolism, ATP production/ADP consumption and K^+(ATP) channel closure (2), → membrane depolarization (3), → opening of voltage-dependent Ca^{2+} channels (4) and, finally, Ca^{2+} binding to granule docking complex and granule fusion (5). Non-selective cation channels that form the counterweight to K^+(ATP) channels at rest are shown to the left of the Glut-2 transporter. Further to the left are the G-protein-linked receptor cascades for muscarinic, cholinergic agonists and the incretin GLP-1. The latter two "priming" compounds produce second messengers capable of releasing Ca^{2+} from intracellular stores and/or activating protein kinases to modulate channel activity and granule mobilization. Lastly, the contents of the secretory granule, namely insulin and ATP, may "feed back" on the β cell via cell surface receptors and complex signaling cascades.

entry begins (Step 4). The resultant rise in cytosolic Ca^{2+} triggers Ca^{2+}-dependent fusion of insulin granules with the plasma membrane (Step 5). Steps 4 and 5 are reminiscent of the process of depolarization–secretion coupling, well studied at nerve terminals and other electrically excitable endocrine cells (adrenal chromaffin cells, pituitary lactotropes and melanotropes and terminals of the supraoptic nucleus cells), with subtle differences that shall be discussed later.

However, this scheme does not answer some rather old questions. (1) How do enhancers of cAMP serve to restore stimulus–secretion coupling in metabolically and electrically active but non-secreting β cells? (2) How, aside from possibly depolarizing the β cell, do anticipatory or modulatory factors such as gut hormones and acetylcholine work? The anticipatory–modulatory pathways of receptor-mediated stimulus–secretion coupling, as well as possible autocrine effects of insulin and ATP released by exocytosis, are outlined on the left of Fig. 34.2 and also will be discussed later. In fact, it may be possible that, under very extreme conditions, modulatory pathways may result in some secretion independent of an inciting Ca^{2+} current or a detectable rise in global cytosolic Ca^{2+}. This might occur through the combination of a very localized rise in cytosolic Ca^{2+} with a vastly increased readiness of the secretory apparatus. However, it should never be forgotten that the "sui generis" of the β cell remains metabolic regulation of cell electrical activity via K^+(ATP) channels.

IIA. Role of ATP-Sensitive K^+ Channels in Coupling Metabolism to β-Cell Depolarization

How do fuel metabolites produce β-cell depolarization? Early patch-clamp experiments, using the cell-attached mode of recording, revealed the presence of a very interesting K^+ channel that was open at fasting levels of extracellular glucose (2–3 mM), but rapidly closed on raising ambient glucose concentrations to those encountered after a meal (5–7 mM). Usually, channel closure is followed closely by the onset of electrical activity. This channel is open at the cell's resting potential and its activity is not dependent on membrane voltage. However, the channel is inward rectifying (i.e. single channels pass inward flow of potassium better than outward). These channels have many features predictable from the fuel metabolism hypothesis: addition to the bath of any metabolized fuel closes the channel, yet the channel is reopened subsequently by the addition to the bath of inhibitors of metabolite transport or oxidation. The time course and relative change in channel activity seen in a cell-attached patch during a variety of metabolic maneuvers closely parallels the changes in whole-cell resting conductance (G_m), monitored as the change in membrane potential in response to a given test pulse of current applied (Fig. 34.3A, B). The latter strongly suggested that the activity of this channel, which tends to move V_m to a level near the potassium equilibrium potential, E_K, critically controls the cell's resting potential. Since this channel population is the predominant type open at rest, its closure

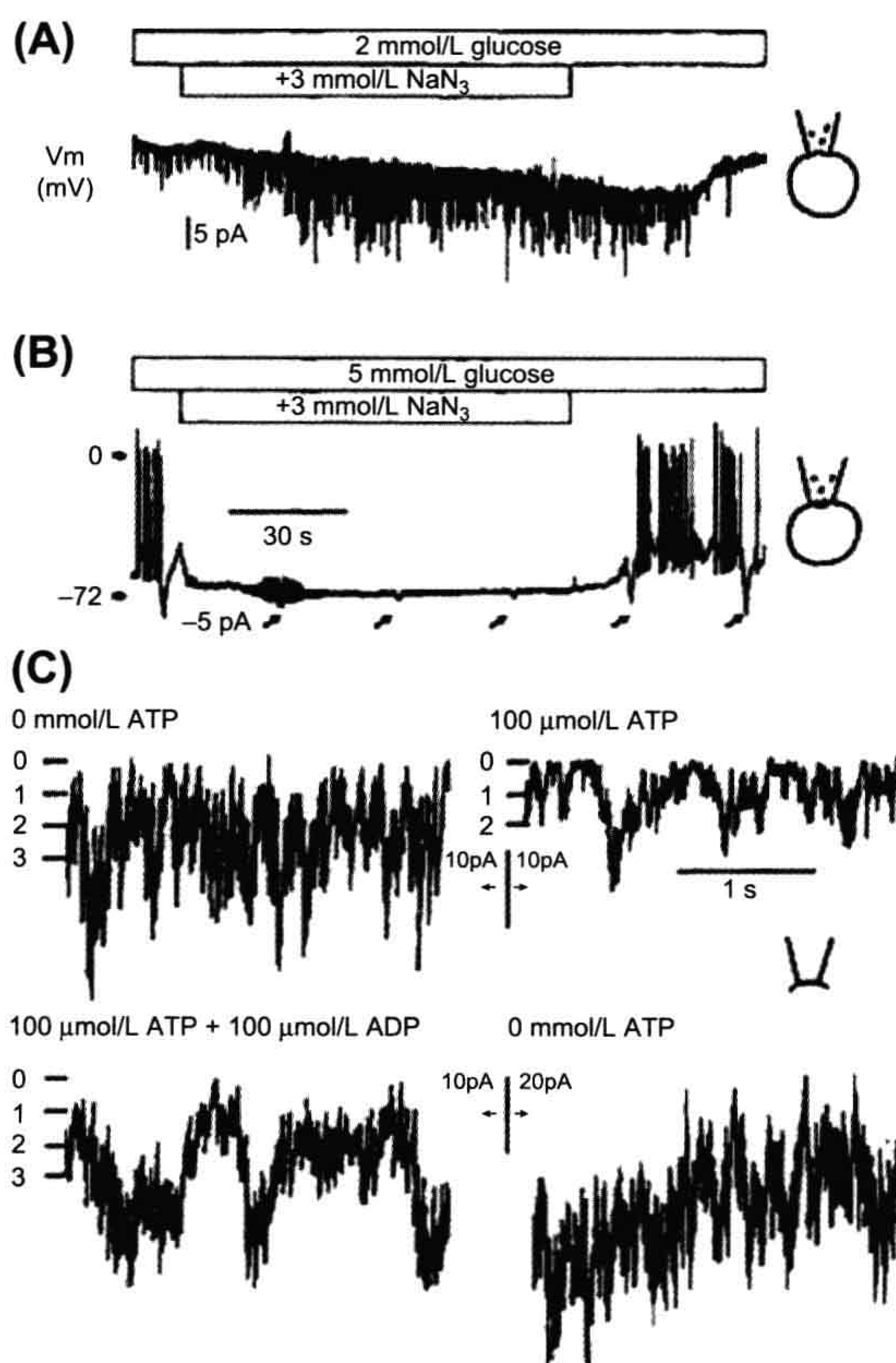


FIGURE 34.3 ATP-sensitive K^+ channels and electrical activity in canine pancreatic islet β cells. (A) A cell-attached patch was formed with the pore-forming antibiotic nystatin in the pipette. Shortly thereafter, ion-channel activity was recorded before, during and after application of sodium azide (NaN_3, 3 mM) to the low-glucose bath. (B) Electrical activity recorded 20 minutes later. By that time, the patch of membrane encompassed by the pipette had been permeabilized by insertion of nystatin channels, thereby permitting recording of membrane current or voltage from the whole cells. Reapplication of NaN_3 results in membrane hyperpolarization, abolition of electrical activity and increased membrane conductance (signified by the reductions in transient hyperpolarizations accompanying −5 pA currents applied at arrows). V_m denotes cell membrane potential. (C) Nucleotide gating of K^+(ATP) channel activity in the excised patch. Addition of 100 micromolar ATP (100 μM) reduces channel activity by threefold (C, upper right panel); further addition of ADP restores channel activity (C, lower left panel), whereas washout of ATP and ADP results in overshoot of channel activity (C, lower right panel) *(D.M. Pressel and S. Misler, unpublished data).*

en masse would be needed to make the K^+ conductance of the cell comparable to that of other conductance pathways operative at rest. The latter are non-selective cation conductance channels and anion conductance channels with estimated equilibrium potentials of 0 or ≈ -30 mV respectively. This would permit V_m to depolarize to the threshold for activating cell electrical activity (≈ -45 mV). Another hint of the importance of this type of channel was that it is closed by oral hypoglycemic agents.

How is this channel gated? In the cell-attached patch-recording configuration, in which the exterior of the channel was isolated from bath glucose by a very tight pipette-to-membrane seal, it is safe to assume that the channel is gated by one or more metabolic intermediates. A priori, cell metabolism might affect a host of metabolic intermediates, ranging from high-energy phosphate compounds (e.g. ATP and ADP), to redox equivalents, to cytosolic H^+ or Ca^{2+}. Early experiments (see Fig. 34.3C) showed that after excision of the patch, in an inside-out excised patch configuration, the metabolite-regulated K^+ channel was avidly gated by ATP at its inner surface, hence the name K^+(ATP) channel. Free concentrations of ATP, or its non-hydrolyzable analogs (e.g. AMP-PNP) as low as 10 μM reduce channel activity by half even in the absence of Mg. This suggests that ATP closes this channel by directly "gating" it rather than "phosphorylating" it. In parallel with this, in whole-cell patch experiments where ATP dialyzes out of the cell (due to the absence of ATP in the pipette), resting G_m increases and the cell hyperpolarizes. Interestingly, ATP inhibition of channel activity in the excised (inside-out) patch can be partially reversed by addition of MgADP to the bath. Hence, changes in the relative concentrations of ATP and ADP, which usually change in a reciprocal fashion as metabolism is altered, should be an important factor in physiological channel gating. In most cells, ATP concentrations change little with metabolism, but percentage-wise, ADP levels change more dramatically. Hence the channel may have been misnamed. To be sure, the activity of the K^+(ATP) channel is also altered by other potential intermediates whose cytosolic concentrations change with metabolic stimulation (e.g. NADH/NAD ratio, H^+ and Ca^{2+}), but these effects are much smaller and require changes beyond the physiological range.

A puzzling question regarding the function of this channel is how its low K_d value (μM) for ATP-induced channel closure in the excised membrane patch can be reconciled with the millimolar-range concentration of ATP in the cytosol. Several factors mitigate this discrepancy:

1. *Complex effects of ADP on channel activity.* ADP competition for an ATP binding site, combined with allosteric action of ADP at an independent binding site, adjusts the half-maximal effective concentration (K_d) of ATP, measured in the presence of ADP, closer to the mM range.
2. *Compartmentation of the ATP and steep ATP gradients from source to sink.* It is likely that the overwhelming majority of ATP is of mitochondrial origin: mitochondrial inhibition totally prevents glucose-induced channel closure, while ketone bodies, amino acids and their deamination products (e.g. leucine and ketoisovalerate), which directly enter mitochondria, stimulate channel closure even in the face of inhibition of glycolysis. In addition, given the random localization of these channels over the surface of cultured cells, it is likely that the channels are interspersed among ATPases. Hence, steep cytoplasmic gradients of ATP and ADP, due to en passant consumption of ATP and concomitant local production of ADP by neighboring plasma membrane ATPases, should make the ATP/ADP available to the channel different from the average cytosolic concentrations actually measured.
3. *Modulation of gating by other metabolic intermediates* such as long chain fatty acids.
4. *Artifactual enhancement of channel sensitivity to ATP in the excised patch by progressive washout of intrinsic channel inhibitors* such as anionic lipids (phosphoinositol phosphates), from the exposed membrane. Polyanionic molecules might specifically compete with ATP for binding to the channel or else contribute to a negative surface charge at the inner surface of the plasma membrane, thereby electrostatically repelling soluble anions.

Two features of the metabolite-regulated K^+(ATP) channel proved critical to its cloning and structure–function analysis. (1) The channel functions as an inward rectifier K^+ channel and hence could be cloned as a member of that family. (2) The channel is the major locus of action of hypoglycemic (glucose-lowering) sulfonylureas and could be cloned as a sulfonylurea receptor (SUR). The sulfonylureas (e.g. *tolbutamide* and *glyburide* [glibenclamide]) enhance glucose-induced insulin release by β cells and are useful in the treatment of non-insulin-dependent diabetes mellitus, in which β cells produce significant quantities of insulin, but release it out of synchrony with the appearance of the glucose load. At concentrations equal to free plasma levels that enhance glucose-induced electrical activity and insulin secretion in intact animals, the *sulfonylureas* close K^+(ATP) channels in cell-attached or excised patches alike, while leaving voltage and calcium gated K^+ channels unaffected. Curiously, though K^+(ATP) channels in myocytes show similar conductance, kinetics and ATP sensitivity, they have greatly reduced sulfonylurea sensitivity.

To reconstitute channel activity in a naive cell (e.g. *Xenopus* oocyte or clonal cell), it was necessary to transfect or inject the cell with cDNA or mRNA coding for

(1) a standard inward rectifier type subunit (Kir6.2), comprised of two membrane-spanning domains separated by an H loop dipping into the bilayer, and (2) the SUR from β cells (SUR1) (Fig. 34.4A, B). SUR 1 is a complex protein with multiple transmembrane domains (hydropathy plot analysis suggests 17!). Structurally, it contains two motifs resembling those of the ATP-binding cassettes of members of the ABC transporter superfamily, the most famous of which are the cystic fibrosis gene product, CFTR, and the multidrug resistance p-glycoprotein. SUR1 has two distinct cytoplasmic loops (or facettes) that bind nucleotide di- and triphosphates in the presence of Mg (NBFs). The channel itself is likely to be an octamer consisting of an inner ring of four Kir6.2 subunits (the confluence of the four H loops forming the ion selective pore) and an outer ring of four SUR1 subunits. The two types of subunits are needed to chaperone each other into the membrane as well as to provide full channel gating; without SUR1, Kir6.2 is not expressed. Clinically, mutations in SUR1 have been identified in persistent hyperinsulinemic, hypoglycemia of infancy, a disease where K^+(ATP) channel activity is not detected even after metabolic inhibition and β cells are persistently depolarized and secreting. Point mutations to NBF result in channels that are closed by ATP in excised patches, but are not reopened by MgADP, while more extensive mutations result in the absence of channel activity under any test circumstance. In contrast, a C-terminal truncated mutant of Kir6.2 (Kir6.2ΔC26) forms K^+ channels gated by ATP in the absence of Mg. These channels have lower affinity for ATP ($K_d \approx 10\ \mu M$ in the absence of Mg) than the native or Kir6.2/SUR1 cloned channel ($K_d \approx 100\ \mu M$) but show similar need for ATP cooperativity in channel gating ($n = 4$). However, these channels lack both inhibition of activity by sulfonylureas and enhancement of activity by MgADP. Hence, while Kir6.2 might be considered the ATP gating subunit, SUR1 with its NBFs is the ATP-hypersensitizing subunit as well as the subunit endowing the channel with special sensitivity to drugs and MgADP. A schematic model of K^+(ATP) channel gating is presented in Fig. 34.4C. SUR might have a natural ligand, a cytoplasmic protein called endosulfine, recently demonstrated to displace sulfonylureas from SUR binding sites.

Analysis of mutant channels has also elucidated the origin of a number of previously puzzling effects. One example is the "refreshment effect" of MgATP. That is, rapid wash-in and wash-out of MgATP, even in concentrations of 10–100 μM, can restore channel activity that otherwise would run down in time in its absence (see Fig. 34.3C). This effect can now be partially explained by the finding that small concentrations of MgATP as well as MgADP activate the channel by binding to a "Walker motif"

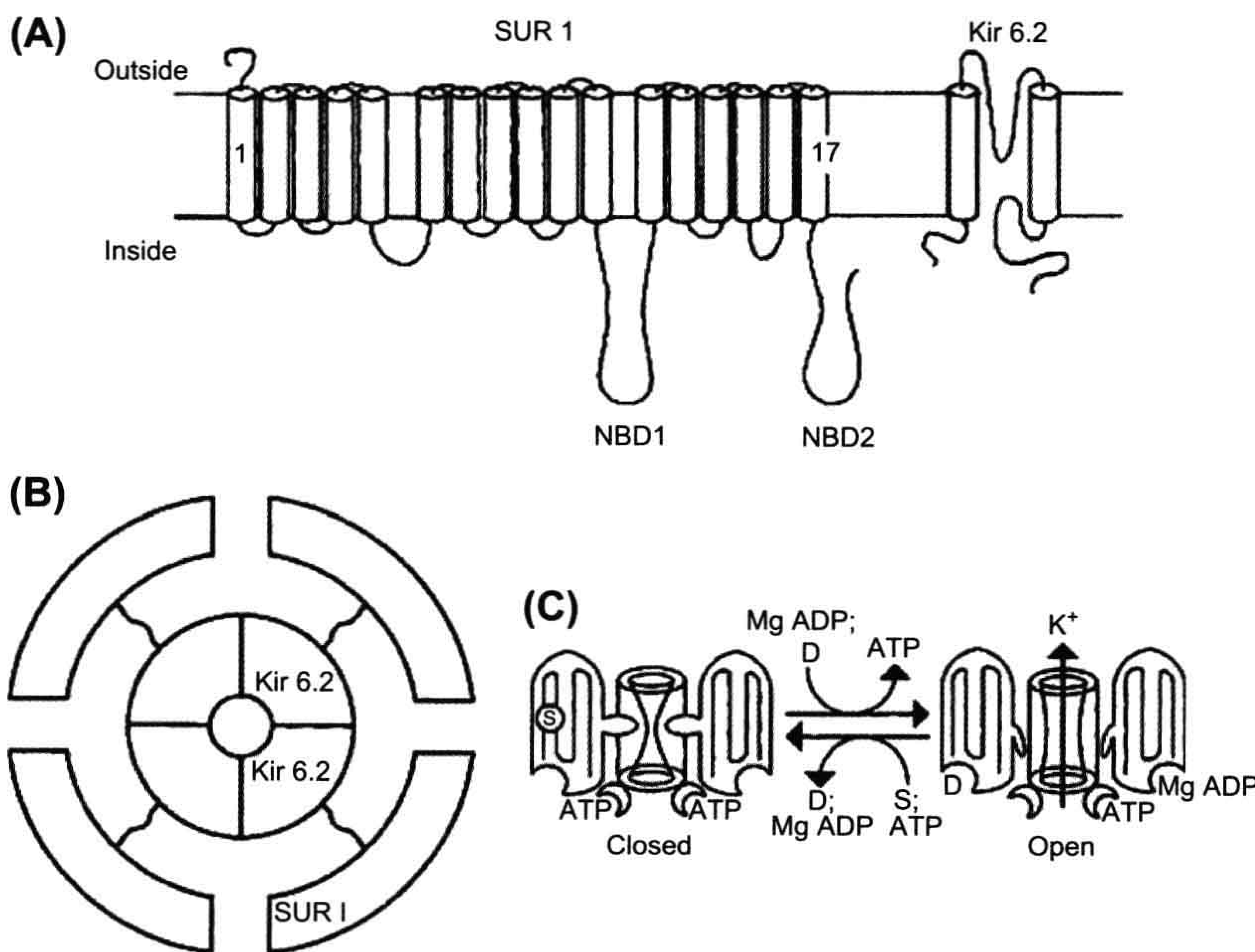


FIGURE 34.4 Illustrations depicting K^+(ATP) channel structure and function. (A) Transmembrane orientations of SUR1 and Kir6.2 subunits based on structural homology, hydropathy and site-directed mutagenesis. (B) Proposed octamer array of SUR1 and Kir6.2 subunits. (C) Simplified reaction scheme in channel gating.

of the NBF in native forms of SUR1 but not in those SURs whose NBFs have been mutated. Likewise, channel modulation by Mg-guanidine nucleotides also occurs at these sites, suggesting that there is no need to invoke G proteins in GTP or GDP modulation of channel gating (though G-protein-coupled receptors may independently modulate channel activity). Both effects require hydrolyzable nucleotides and Mg, suggesting that some phosphorylation reaction may be involved. A second example is the ability of certain vasodilator drugs, such as diazoxide, to open K^+(ATP) channels, hyperpolarize the β cell and inhibit glucose-induced insulin secretion. These drugs also bind to the "Walker motif". A third example is the differential sulfonylurea sensitivity of K^+(ATP) channels in β cells as compared with those in cardiac myocytes. While both channels have similar Kir6.2 subunits, their SURs differ. Replacing transmembrane domains 13–16 of cardiac SUR (SUR2) with the corresponding region of SUR by engineering of a chimeric SUR restores sulfonylurea sensitivity.

Is this finely tuned coupling of cell metabolism to K^+(ATP) channel activity used as a sensory mechanism by the two other major glucose receptor cells of the body, namely the *satiety center* of the hypothalamus and the peripheral sweet *taste receptors*? Recently, K^+(ATP) channels have been sought in glucose-receptive (GR) neurons of the ventromedial nucleus (VMN) whose activity is associated with suppression of food intake. In these neurons, reduction of bath glucose or addition of the glycolytic inhibitor mannoheptulose results in hyperpolarization and cessation of electrical activity accompanied by an increase in resting G_m; oppositely, tolbutamide produces excitation. In cell-attached patch recordings, cessation of electrical activity is associated with increased activity of a K^+-selective channel, which is voltage-insensitive. After excision of the membrane patch, the latter channel is inhibited by cytoplasmic ATP. However, this K^+ channel is quite distinct from the K^+(ATP) channel in β cells: under identical excised patch recording conditions, the K_i for ATP inhibition is 2.3 mM (rather than 20 μM in β cells) and the singlechannel conductance is 135 pS (rather than 55–65 pS in β cells). One very interesting feature of this channel is that it is opened and the cell is hyperpolarized by leptin, a protein released by adipocytes, or fat-storing cells, in proportion to their triglyceride storage. Leptin also opens K^+(ATP) channels in β cells and appears to do this in a manner dependent on activation of PI-3 kinase. Does leptin serve as a negative feedback hormone, that is signaling adequate energy stores by downregulating both appetite-induced caloric intake and insulin-dependent depot storage? One indication of this comes from obese, hyperphagic, hyperinsulinemic and hyperglycemic db/db rats, where leptin has little influence on the firing rate of VMN neurons.

In peripheral taste receptors, glucose chemoreception may occur through G proteins and a second messenger cascade. In these cells, application of sucrose or saccharin reduces the amplitude of a voltage-dependent outward K^+ current. This effect can be mimicked by application of membrane-permeable analogs of cAMP. In excised patches, K^+ channels with similar features are closed by exposure of the patch to ATP and cAMP-dependent protein kinase, but not by exposure to ATP alone, suggesting that this K^+ channel is "gated" by phosphorylation.

IIB. Metabolic Regulation of Depolarization–Secretion Coupling?

Recall that closure of K^+(ATP) channels only depolarizes the cell. Calcium must enter the cells and insulin granules must be ready to be released. Does metabolism alter the "calcium trigger" or maintain the "readily releasable pool" of insulin granules?

IIB1. The "Ca Trigger"

When β cells, exposed to sufficient glucose, a cAMP enhancer and near physiological temperature, are depolarized for many tens to hundreds of milliseconds, they exocytose in a Ca^{2+}-entry-dependent manner. Under these conditions, several studies have shown an approximately 3rd power dependence of exocytosis, as measured by amperometry or capacitance, on the total Ca^{2+} entering the cell (i.e. the integral of the Ca^{2+} current). Though most of the Ca^{2+} current is carried by L-type Ca^{2+} channels, in a subset of human β cells, where they are present in sufficient density, lower threshold T-type Ca^{2+} channels also support exocytosis. We might expect changes in cell metabolism to affect the gating of Ca^{2+} channels via phosphorylation or lipidation. To date, data supporting the hypothesis that enhanced glucose enhances Ca^{2+} channel activation or slows inactivation have been inconsistent. Another paradigm, however, which illustrates other aspects of depolarization–secretion coupling may provide some other clues.

Beta cells in intact islets secrete pulses of insulin that are time-linked to "bursts" of electrical activity. Longer "bursts" evoke larger pulses of insulin. Contrary to the situation at most nerve terminals and despite quite sizeable Ca^{2+} currents, it is very rare to see an isolated action potential, or a brief depolarization (10–50 ms in duration), provoke quantal release (here measured by amperometry). However, when the depolarization is extended out to many tens to several hundreds of milliseconds, release routinely commences in the course of the depolarization and often continues for several seconds after Ca^{2+} entry ceases, while cytosolic Ca^{2+} is falling (Fig. 34.5). These data suggest that Ca^{2+} might have to "jump through a few hoops" before triggering secretion and that it might set up a "chain reaction" that outlasts the peak Ca^{2+} concentration (Fig. 34.6).

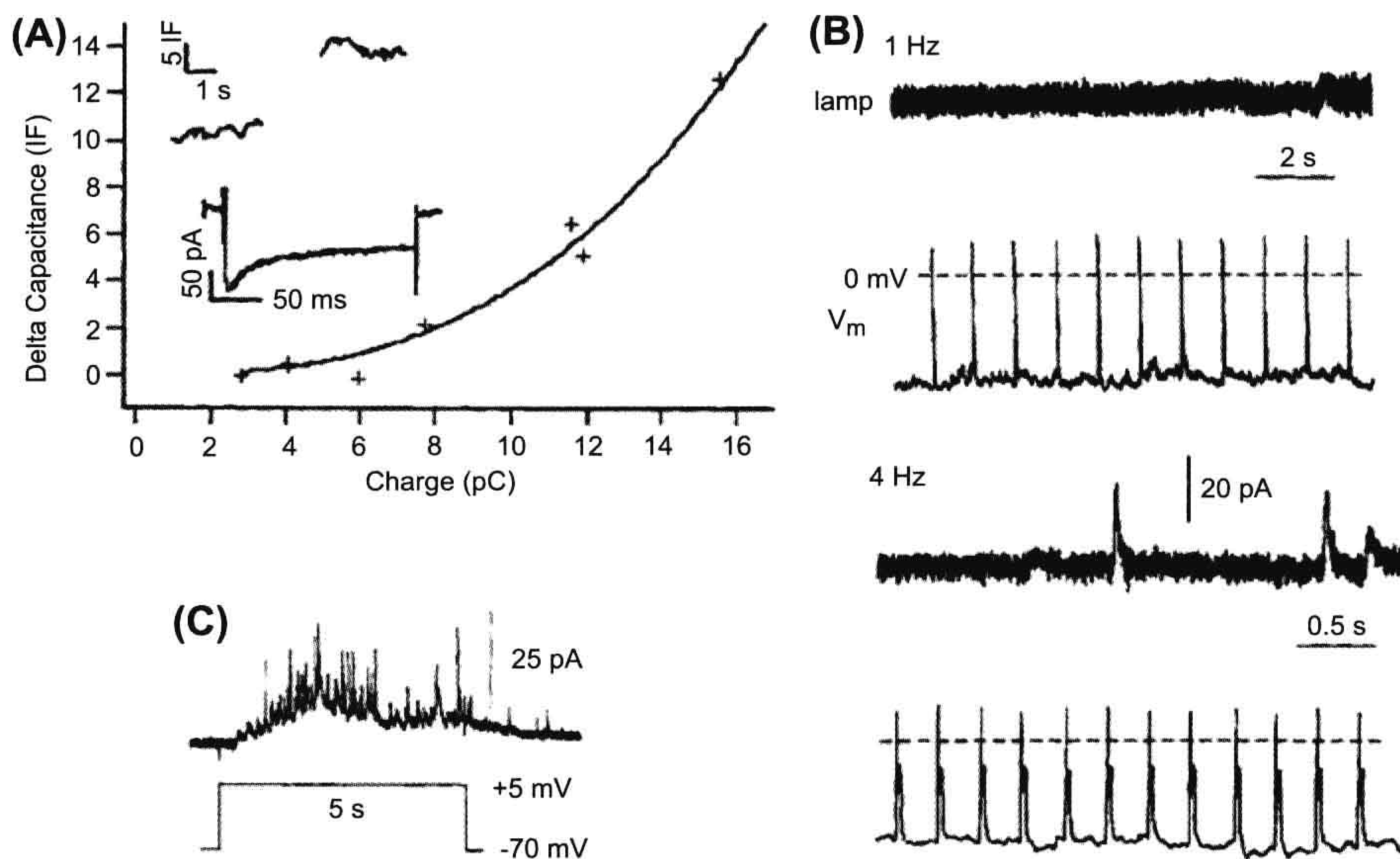


FIGURE 34.5 Aspects of Ca^{2+} dependence of exocytosis in β cells (A) Relationship of capacitance increase to total Ca^{2+} entry (integral of Ca^{2+} current Q_{Ca}) during β-cell depolarization. Ca^{2+} entry was altered by changing the membrane potential to which the cell was voltage-clamped for the 200-ms test stimulus *(unpublished data by D. Barnett and S. Misler)*. (B) Time course of amperometric events during trains of action potentials stimulated at 1 Hz (upper panel) and 4 Hz (lower panel) Note that none of the 11 action potentials occurring at 1 Hz stimulation results in quantal release, while at 4 Hz stimulation quantal release begins after several action potentials. (C) Time course of amperometric events recorded during continuous depolarization to +10 mV, where Ca^{2+} entry is maximal. Note that the first release event is seen ≈ 120 ms after start of voltage-clamp pulse, while release events continue, albeit at a low frequency, for nearly 3 s after depolarization is completed *(unpublished data by Z. Zhou and S. Misler)*.

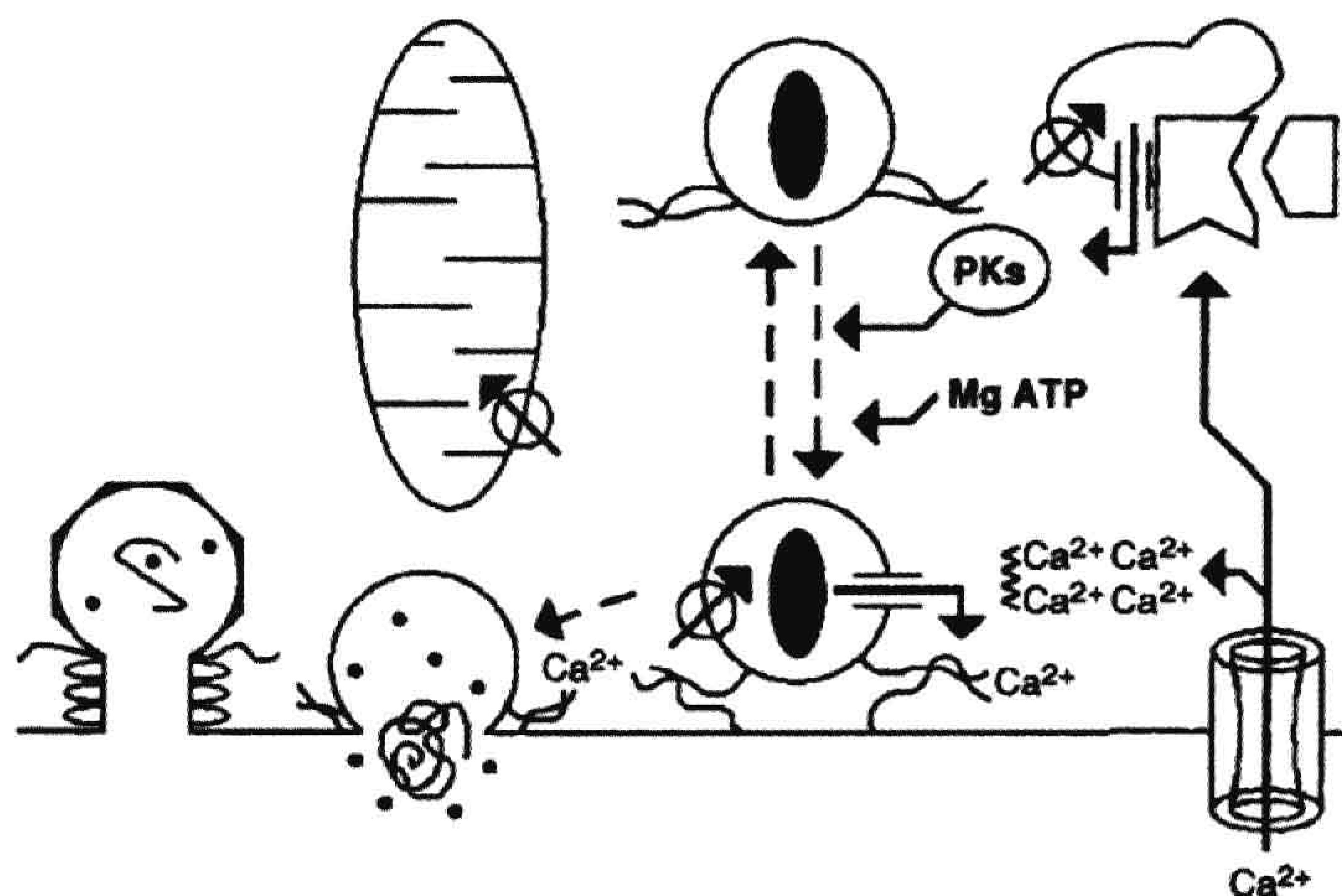


FIGURE 34.6 Calcium metabolism in β cells: potential sites for modulation of depolarization–secretion coupling. After calcium enters the cytoplasm, it is likely that much of it rapidly binds to either fixed or mobile buffers, the latter perhaps resembling the tetra-clawed EGTA. Some of the bound Ca^{2+} unbinds to diffuse further. Diffusing Ca^{2+} may then bind to one of the following: (1) a Ca^{2+}-binding protein (e.g. synaptotagmin) that is part of the docking complex that anchors a granule to the membrane and thereby directly triggers exocytosis, (2) a protein kinase, whose activity enhances the movement of granules along "motorized" tracks, (3) a binding site on Ca^{2+}-gated channels in Ca^{2+} storage organelles, including the secretory granule itself, which thereby triggers Ca^{2+}-induced Ca^{2+} release. Calcium uptake into organelles (granules, mitochondria and ER) is probably slower (on the time scale of hundreds of milliseconds to seconds). After fusion with the plasma membrane, granule membrane may be retrieved piecemeal by a local "pinch off" mechanism, by using dynamin, or as part of a large endocytic "slurp".

Several possibilities for this "slow-to-start, slow-to-stop" pattern of secretion are currently under investigation. First, with large-sized granules that are not clustered in any regular array, Ca^{2+} channels and granule release sites may not be all that closely co-localized. To be sure, the interspersed cytosol has many Ca^{2+}-buffering molecules. Hence, if the site where Ca^{2+} triggers exocytosis were, on average, a distance of 1–2 granule radii

(say 200–300 nm) from the inner mouth of the Ca^{2+} channel site, local cytoplasmic buffers would need to be saturated before Ca^{2+} could appear at the release site. This would cause a slight delay in the onset of exocytosis. At this distance, during continuous Ca^{2+} entry there might be good spatial equilibration of Ca^{2+} so that the Ca^{2+} concentration at the release site might closely follow the average Ca^{2+} concentration of the cell. This is in no way counterintuitive because it is well appreciated that Ca^{2+} and cytosolic Ca^{2+} concentrations as low as 1.5 μM evoke respectable rates of release (Fig. 34.7B). Conversely, once Ca^{2+} no longer enters the cell, the buffer might serve as a continuing source for Ca^{2+} and support a "secretagogue" level of free cytosolic Ca^{2+} for some time. This feature has been examined and modeled extensively in adrenal chromaffin cells but has only been explored in a cursory manner in β cells.

Second, Ca^{2+} entry might be causing regenerative release of Ca^{2+} from some intracellular stores, thus providing a sort of propagating Ca^{2+} wave, while the increase in cytosolic Ca^{2+} might be stimulating Ca^{2+} uptake by other stores for later use. To date, while it is well appreciated that Ca^{2+} can be released from ER stores by the generation of IP_3, blockade of Ca^{2+} release from ER stores has yielded only small changes in depolarization-induced rises in cytosolic Ca^{2+} or exocytosis. However, the picture may be more complex in other situations. For example, when GLP-1 is applied to voltage-clamped β cells in the presence of 20 mM Ca^{2+}, "spontaneous" spikes of cytosolic Ca^{2+} occur between depolarizations. To be sure, there are multiple stores of intracellular Ca^{2+}, aside from the IP_3-releasable ones in ER. For example, mitochondria- and hormone-containing granules might be expected to release as well as "mop-up" Ca^{2+}, but little is known about their release and uptake rates during various patterns of electrical stimulation or exposure to hormones and transmitters. Some recent evidence suggests that depletion of the Ca^{2+} content of the acidic compartment of cytoplasmic organelles, which includes secretory granules, reduces depolarization-induced Ca^{2+} release. In a metabolically stimulated cell where the Krebs cycle intermediates, NAD-derived redox equivalents and local ATP concentrations may be changing, it would not be surprising that changes in cell Ca^{2+} metabolism in response to Ca^{2+} influx might be a very dynamic feature.

Third, entering Ca^{2+} might rapidly recruit granules into a small, "readily releasable pool" waiting to be triggered.

IIB2. The "readily releasable pool" (RRP)

In cells designed for rapid secretion, it is convenient to assume that vesicles are lined up against the plasma membrane and ready to fuse as soon as the appropriate level of second messenger is achieved in the cytoplasm. Morphologically, in β cells, this does not appear to be the case (see Fig. 34.6). When viewed under the electron microscope, very few of the ≈ 10 000 granules in the β cell are within one granule diameter of the membrane. Physiologically, experiments with single cells reveal that secretion is actually quite "wimpy" unless "revved up" by other maneuvers; with repeated depolarizations, exocytosis "poops out" and may take many tens of seconds to recover. This suggests that the RRP of available granules is actually

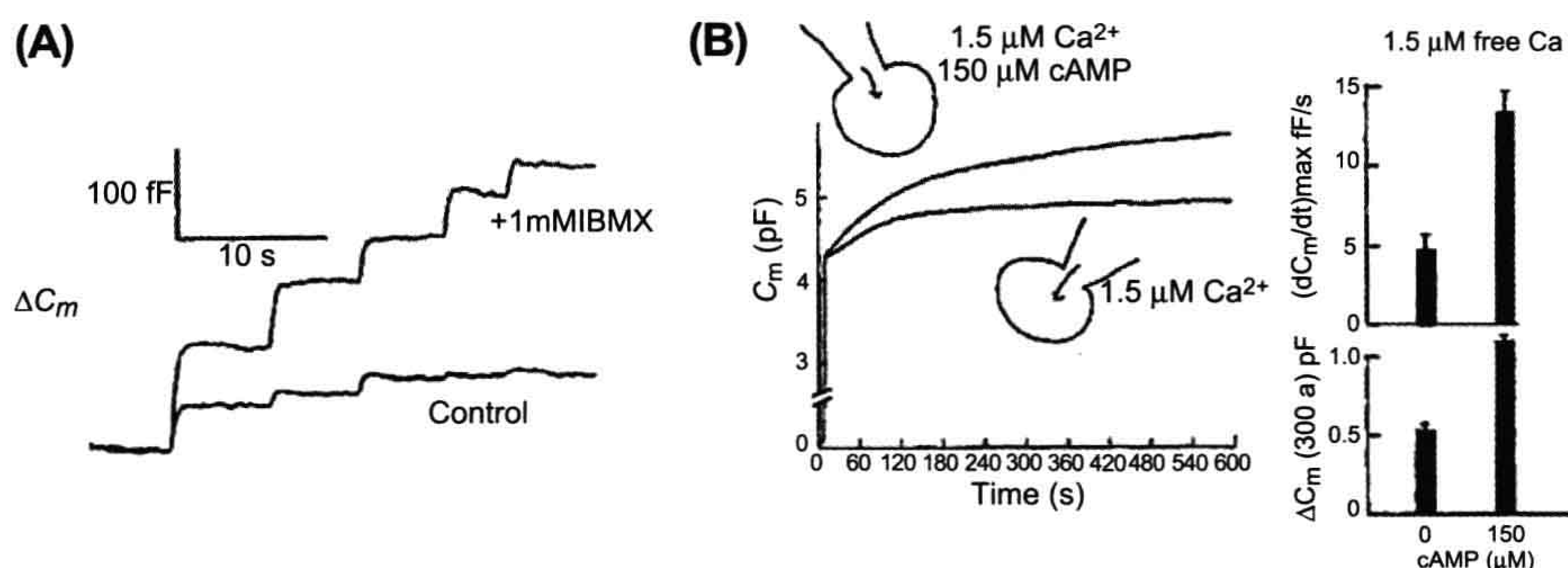


FIGURE 34.7 Enhancement of cytosolic cAMP appears to increase the pool of readily releasable granules. Test by repetitive stimulation. (A) Note that in the "control," repetitive depolarization produces rapid rundown of capacitance response so that by the fourth depolarization there is no evidence of further net exocytosis. In contrast, after addition of membrane permeable cAMP or a phosphodiesterase inhibitor, isobutylmethylxanthine (IBMX), not only is the response to initial depolarization enhanced, but response to 4th depolarization is nearly as large as the response to the 1st depolarization in the "control". In this cell, total Ca^{2+} entry over the entire series of depolarizations differed by less than 15% across the two runs. Perforated patch recording from rat β cell. Test by cell dialysis. (B) Cells with similar baseline capacitance (4–6 pF at break-in to the cell at time 0) were dialyzed against pipette solutions containing 1.5 μM Ca^{2+} versus 1.5 μM Ca^{2+} + 150 μM cAMP. Note that, in the presence of cAMP, not only was the maximum rate of rise of capacitance, abbreviated (dC_m/dt) max, on average nearly 2.5-fold greater, but the total capacitance increase over the entire 6 min of recording was on average nearly twofold greater.

quite small and that maintaining it under high output demand is a non-trivial matter. However, in β cells, two ideal sources of "physiological revving" of secretion are (1) activation of protein kinases (A and C) and (2) the provision of ATP by enhanced substrate metabolism. *Protein kinases* are well known to facilitate the attachment of a variety of granules to tracks (microtubules, actin filaments) that bring them in close proximity to the membrane. In β cells, during feeding, insulin secretion is "primed" even before serum glucose rises, by release of two substance that activate protein kinases, acetylcholine from vagal fibers and incretins (e.g. glucagon-like peptide [GLP-1]) from enterochromaffin cells. Activation of muscarinic ACh receptors results in activation of phospholipase C and production of IP_3 and diacylglycerol. Activation of incretin receptors results in activation of protein kinase A pathway and enhanced cytosolic cAMP levels. These ACh and GLP-1 pathways might enhance distal processes in excitation–secretion coupling, along with increasing the rate of β-cell depolarization in response to glucose, by affecting ATP-sensitive K^+ channels and/or the non-selective cation channels. Hence both background electrical activity and insulin release- and metabolite-induced electrical activity and insulin release could be enhanced. Changes in *cytosolic MgATP* would be expected to alter the fueling of vesicle transport processes as well as the molecular motors (e.g. NSF) that untwine paired attachment proteins (SNAREs) on granules and the target membrane. The latter permits SNAREs subsequently to intertwine with their cohorts on the complementary membrane, thereby accomplishing vesicle docking. In β cells, glucose is known to enhance insulin secretion evoked by elevated $[K^+]_o$ even when K^+(ATP) channels are already closed, while metabolic inhibition can block insulin secretion, even as cytosolic $[Ca^{2+}]$ rises into the micromolar range.

Experiments monitoring exocytosis from single β cells support the motion that the RRP is small, easily depletable and requires constant replenishment by processes that are cAMP, MgATP and temperature dependent. Three approaches have been used. In the first approach, the cell is rapidly depolarized, in the presence versus absence of a modulator, until there is no further increase in capacitance. An estimate of the total number of granules exocytosed provides a measure of RRP, while the time to recovery of full response provides a measure of the refilling rate. Then, a rough estimate of size and dynamics of vesicle pools, in the presence versus absence of a modulatory factor, is obtained by examining the time course of release after introduction of a given concentration of Ca^{2+} into cell. A final approach is to measure the capacitance increase, in the presence versus absence of the modulator, in response to instantaneous "uncaging," by flash photolysis, of Ca^{2+} bound to a chelator introduced into the cytosol, or "uncaging" a fraction of the modulator, now bound to a chelator, in the presence of a fixed level of cytosolic Ca^{2+}. Sample experiments demonstrating that stimulators of cytosolic cAMP enhance initial Ca^{2+}-entry-dependent, depolarization-evoked release, as well as maintain release with repeated depolarization, all with little attendant change in Ca^{2+} entry are shown in Fig. 34.7A. Sample experiments demonstrating that cAMP enhances both the initial maximum rate of exocytosis and the total exocytosis in cells dialyzed against a pipette with fixed concentrations of Ca^{2+} are shown in Fig. 34.7B. More recently, similar experiments using all three approaches have been performed at varying cytosolic levels of MgATP. ATP appears to modulate RRP as well.

Lastly, to be sure, anticipation of future high rates of release requires activity-stimulated, energy-dependent insulin synthesis followed by processing in specialized membrane compartments. With prolonged continuous stimulation, β cells undergo several phases of insulin release; after an initial spurt of release lasting several minutes, insulin secretion wanes and then, beginning 10–15 min later, rises to a plateau that is sustained for hours. Also, islets rechallenged with glucose several hours after an initial brief bout of secretion display greater "peak" insulin release on the second round of stimulation and do this with newly synthesized insulin. Thus islets display a crude but effective form of "memory" for previous stimulation. As activity-stimulated protein synthesis can be triggered by changes in cell Ca^{2+}, cAMP and ATP levels, their relative contributions to synthesis of competent new insulin granules is receiving intense scrutiny.

IIC. The Paradox of Stimulus–Secretion Coupling in the Glucagon-Secreting α Cell

Alpha cells secrete glucagon at preprandial levels of glucose (2–3 mM); secretion is further enhanced by amino acids such as arginine and depressed by higher levels of glucose. Curiously, under some conditions, the glucagon secretion is stimulated by tolbutamide and inhibited by diazoxide, both at concentrations that alter insulin secretion from β cells. So, do α cells have K^+(ATP) channels and, if so, do these channels contribute to α-cell function?

In the presence of 0–3 mM glucose, α cells generate spontaneous Na_o^+- and Ca_o^{2+}-dependent action potentials from their resting potential of ≈ −60 mV. They hyperpolarize on their exposure to increased glucose (5–20 mM); they depolarize and show enhanced spike frequency on exposure to 10 mM arginine. Under voltage-clamp control, depolarization of the α cell results in Ca^{2+}-entry-dependent increases in cytosolic Ca^{2+} and increases in membrane capacitance, the latter enhanced by agents that increase cytosolic cAMP (e.g. β2 adrenergic agonists).

Single-channel and whole-cell patch-clamp recording from α cells reveals inward rectifier K^+ currents that have

similar single-channel conductance and kinetics to those in β cells as well as similar K_d for inhibition by ATP and activation by MgADP and PIP_2. In situ hybridization identifies Kir6.2 and SUR1 subunits of characteristic of β-cell K^+(ATP) channels on glucagon-bearing cells; in fact, the densities of these subunits are even higher than those in β cells.

With apparently functional K^+(ATP) channels in place, the α cell's inability to respond to glucose or metabolic inhibition is probably related to their extraordinarily high cytosolic [ATP] and [ATP]/[ADP] ratio that remains virtually unchanged after increases in extracellular glucose. (α Cells are much less efficient transporters and metabolizers of glucose than are β cells.) In contrast, the α cell's response to arginine may be related to the depolarizing effect of the electrogenic transport of this cationic amino acid coupled to the low threshold for excitability of this cell type (i.e. low resting membrane conductance and abundance of low-voltage-activated [T-type] Ca^{2+} channels). (Arginine also depolarizes β cells without closing K^+(ATP) channels, although it usually does not enhance electrical activity unless suprathreshold concentrations of glucose are also present.) However, the crucial element of physiological regulation of the α cell, the inhibition of its electrical activity and secretion by glucose, remain unexplained on the basis of K^+(ATP) channel activity. It is possible that the inhibitory effect of glucose results largely from a paracrine interaction within the islet. α Cells display a robust γ-aminobutyric acid (GABA) activated Cl^- current which, when stimulated, can abolish arginine-enhanced electrical activity. β Cells are known to secrete GABA along with insulin. Hence secretagogue-induced β-cell exocytosis might be the "suppressor" of α-cell activity.

IID. Implications for Pathophysiology and Therapeutics

Diabetes mellitus, a disease characterized by hyperglycemia and dysregulation of metabolite use and culminating in multiorgan system damage, comes in two general varieties. The insulin-dependent, ketosis-prone variety (IDDM) is usually an autoimmune disease of rapid onset, characterized by destruction of β cells as a result of massive assault by antibodies and cytokines. In contrast, the non-insulin-dependent, non-ketosis-prone variety (NIDDM) is a spectrum of diseases characterized by increasing insulin resistance coupled with poorly timed, inadequate insulin secretion. One of its earliest indicators of this condition is the loss of the transient "first phase" of glucose-induced insulin secretion, thought to be "primed" by acetylcholine released by the vagus nerve and GLP-1 released by enterochrommaffin cells. Accompanying this is a "compensatory" increase in insulin release during the prolonged "second phase." Unfortunately, this contributes to downregulation or "tonic tune out" of insulin receptors. Possible defects in NIDDM have been proposed for every link along the β-cell's stimulus–secretion coupling cascade (i.e. from reduced affinity of glucose transporters to reduced efficiency of intracellular handling of Ca^{2+}). A recently explored model for NIDDM features insulin resistance of the β cell with chronically decreased release of Ca^{2+} from intracellular (ER) stores. No doubt, the single cell approaches outlined above will be increasingly brought to bear to dissect out cellular mechanisms underlying NIDDM.

Those approaches may be expected to spur the development of more "physiologically targeted" pharmacotherapy for NIDDM, including carefully timed, pre-prandial administration of (1) GLP-1 and other gut-secreted incretins and (2) highly selective sulfonylurea-type agents of shorter onset and duration of action than those currently marketed. To be sure, two realizations, (1) that α cells contain sulfonylurea-inhibited K^+(ATP) channels possibly of identical structure, and (2) that constant activation of α cells coupled with waning of β-cell function, may contribute to the progressive sulfonylurea insensitivity, are now promoting synthesis of hypoglycemic drugs more selectively targeted at β-cell function.

It is worth noting that sulfonylureas also modify the gating of some Cl^- conductance channels in β cells as well as the activity of Na^+-K^+ ATPase and the efficacy of depolarization–secretion coupling in a manner similar to the effects of protein kinase C enhancement. As mentioned above, the NBFs of SUR resemble those of CFTR. Spare CFTR subunits appear to interact with a variety of Cl^- channels and even with the epithelial Na^+ channel (EnaC) in epithelial cells. Do spare SUR subunits likewise interact with integral membrane or membrane associated proteins in β cells to modulate a variety of events in stimulus-secretion coupling?

III. METABOLIC SENSING AS PROTECTION FROM HYPOMETABOLIC INJURY

The hyperpolarization and increased K^+(ATP) channel activity displayed by β cells exposed to metabolic inhibitors that reduce cytosolic [ATP]/[ADP] suggests that a safeguard against hypoxic damage of an excitable cell might be hypoxia-induced opening of K^+(ATP) channels. This mechanism appears to apply to skeletal and cardiac myocytes and to some neurons. As in β cells, in these cells metabolically sensitive channels are very often K^+(ATP) channels consisting of Kir and SUR subunits, though often the SUR subunit (SUR2) has much lower affinity for some sulphonylureas than does SUR1. In addition, in skeletal myocytes, which produce lactate under hypoxic conditions, the K^+(ATP) channel displays pH_i sensitivity that is the reverse of K^+(ATP) channels in β cells; in these myocytes,

intracellular acidosis vigorously opens K^+(ATP) channels even at fixed [ATP]/[ADP]. Recent evidence suggests that, in highly active regions of the brain, those cell types with higher density of K^+(ATP) channels show most rapid excitability block in response to hypoxia and survive it best. However, what may be an adaptive feature to individual cells may have disastrous consequences for the entire organism. In skeletal muscle, a drop in tension development by some motor units results, via spinal reflex, in recruitment of other less active motor units. More extended fatigue due to inexcitability may preserve enough ATP to maintain sarcolemmal integrity and avert leak of myoplasmic contents such as myoglobin. (The latter condition, known as rhabdomyolysis, is the chief cause of extended incapacity and systemic illnesses, such as with acute renal failure, seen after intense bouts of exercise.) However, in contrast, in cardiac ventricle, block of excitability or excitation contraction coupling in one part of the electromechanical syncitium may predispose to an arrhythmia or severely dyskinetic contraction, while in neurons, excitability block can result in a depressed level of central consciousness and even coma.

As an example of hypoxia-induced excitation block, let us examine block of excitation–contraction coupling in the cardiac ventricular myocyte. Historically, this phenomenon was key to the original discovery of the K^+(ATP) current. In these cells, deprivation of substrate or oxygen, or inhibition of substrate metabolism, was found to result in shortening of Ca_o^{2+}-dependent plateau phase of the action potential with attendant abbreviation or block of generation of contractile force. This was found to have occurred prior to detectable changes in membrane potential or voltage-dependent Na^+ and Ca^{2+} currents and it was accompanied by major augmentation of resting K^+ conductance. Critically, plateau phase shortening and reduced contraction were reversed by intracellular injection of MgATP. As shown in Fig. 34.8, the key to this phenomenon is very basic. The plateau phase of the ventricular action potential represents a delicate moment-to-moment balance between two opposing tendencies. These are (1) the "depolarizing tendency" of the voltage-dependent, but slowly inactivating Ca^{2+} conductance and (2) the "repolarizing tendency" of the sum of a variety of K^+ currents that are either slowly activating or slowly emerging from "inward rectification" (i.e. polyamine or Mg block). Increases in background K^+ current provided by opening of K^+(ATP) channel tip the balance in favor of repolarization, as soon as the huge inward Na^+ current, underlying the rapid upstroke of the action potential, wanes. However, shortening of the broadly propagating action potential may reduce the refractory period and promote local impulse re-entry or rebound excitation. In addition, the period of reoxygenation may enhance arrhythmogenicity by promoting large transient inward currents (I_{ti}) which result in spontaneous

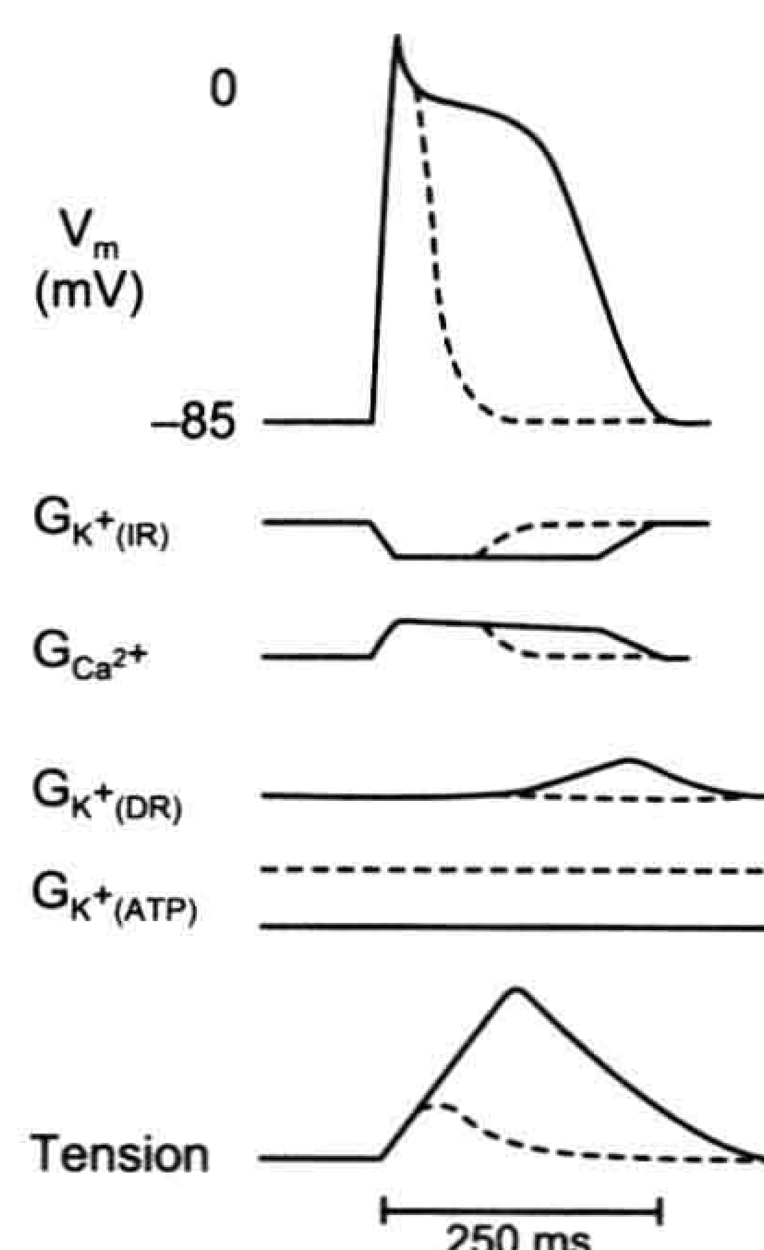


FIGURE 34.8 K^+(ATP) channels and cardiac excitability. A steady-state enhancement of K^+(ATP) conductance ($G_{K^+(ATP)}$), resulting from metabolic inhibition, shortens the time courses of the ventricular action potential and twitch tension and alters the time courses and magnitudes of the underlying ionic conductances. Solid lines indicate control; dashed lines indicate effects of metabolic inhibition.

depolarizations. Hence, it would appear to be better for the ventricle to anticipate rather than react to metabolic deprivation. Physiologically, this is exactly what happens: ventricular hypoxia results in dilation of coronary arterioles leading to greater supply of oxygen and metabolites (see Section VA). However, as often happens in critical physiological processes, there is yet another factor at work. Short bouts of hypoxia, with opening of K^+(ATP) channels, may actually "precondition" myocytes and ameliorate some of the effects of subsequent, more prolonged bouts. In that case, does prevention of hypoxia-induced opening of K^+(ATP) channels, as might occur in the presence of a sulfonylurea, predispose to hypoxia-induced cell injury? Controversy still surrounds this issue.

It is worth mentioning other mechanisms that might contribute to ischemia-induced contractile failure. These include (1) altered $[Ca^{2+}]_i$ "homeostasis," (2) changes in the binding affinity of the contractile apparatus for Ca^{2+} induced by accumulation of acid equivalents and (3) activation of other K^+ channels, such as muscarinic and G-protein gated K^+ channels, by metabolic intermediates generated during hypoxia.

IV. STIMULUS–SECRETION COUPLING IN CAROTID CHEMORECEPTOR CELLS

Neural control of respiratory drive is critical in maintaining physiologic levels of plasma O_2, CO_2 and H^+. In the rhythmic, neuromuscular process of breathing, trains of action potentials, generated by pacemaker cells in the CNS,

trigger motor neurons and activate periodic contractions of the inspiratory muscles (diaphragm and intercostal muscles). This action expands the chest, thereby sucking air of high-O_2, low-CO_2 content into the lungs. Gas exchange consists of net CO_2 diffusion from capillary to adjacent lung air spaces (alveoli) and net O_2 diffusion from alveoli to the capillary. Relaxation of inspiratory muscles, sometimes combined with the contraction of expiratory muscles, expels the air of high CO_2, low O_2 content from the lungs. A major stimulus for altering the pattern of respiratory drive is a drop in the partial pressure of O_2 dissolved in plasma (i.e. plasma pO_2); a secondary stimulus is a rise in plasma pCO_2 or a fall in pH. The carotid body is the organ that senses changes in plasma pO_2, pCO_2 and pH and mediates changes in CNS respiratory drive. Located at the bifurcation of the carotid artery, a branch of the aorta, the carotid body consists of a central core of *chemoreceptor* (or *glomus*) *cells*; these originate from the neural crest. Glomus cells synapse on dendritic endings of sensory nerve fibers that comprise the carotid sinus nerve travelling into the CNS. The glomus cell core is surrounded by more superficial glial, or sustentacular, cells, as well as by a dense network of highly porous capillaries. The glomus cell is the site of transduction of changes in plasma pO_2, pCO_2 and pH into changes in electrical activity of the afferent carotid sinus nerve. Decreases in pO_2, as well increases in pCO_2 or decreases in pH, lead to an increase in release of dopamine and probably to an increase in as-yet-unidentified transmitters from glomus cells, as well as to an increased action potential frequency in the dopamine-sensitive carotid sinus nerve. This contributes to increased respiratory drive.

IVA. Role of O_2-Sensitive K^+ Channels in Transduction of the Hypoxic Stimulus

Two divergent views have emerged concerning chemotransduction of hypoxia by glomus cells (Fig. 34.9A). The first theory proposed that hypoxia induces cell depolarization, followed by opening of voltage-gated Ca^{2+} channels, Ca^{2+} influx and synchronized exocytotic release of dopamine. This might give rise to sufficiently large excitatory postsynaptic potentials in the dendritic regions of single sinus nerve fibers to trigger propagating action potential. An alternative view proposed that hypoxia induces quantal release of transmitter in a Ca^{2+}-dependent manner that is independent of voltage-gated Ca^{2+} entry but dependent on the discharge of Ca^{2+} from intracellular stores. The latter should increase asynchronous quantal release of transmitter, generating a rise in the frequency of miniature excitatory postsynaptic potentials and should enhance ongoing electrical activity in the low-threshold carotid sinus nerve fiber. These contrasting viewpoints have arisen from data generated with different preparations from different species.

There are several lines of evidence supporting the classical scheme for "depolarization—secretion coupling" in glomus cells. First, glomi are electrically excitable sensory cells and contain HVA Ca^{2+} currents, delayed rectifier K^+ currents and, in some cases, voltage-dependent

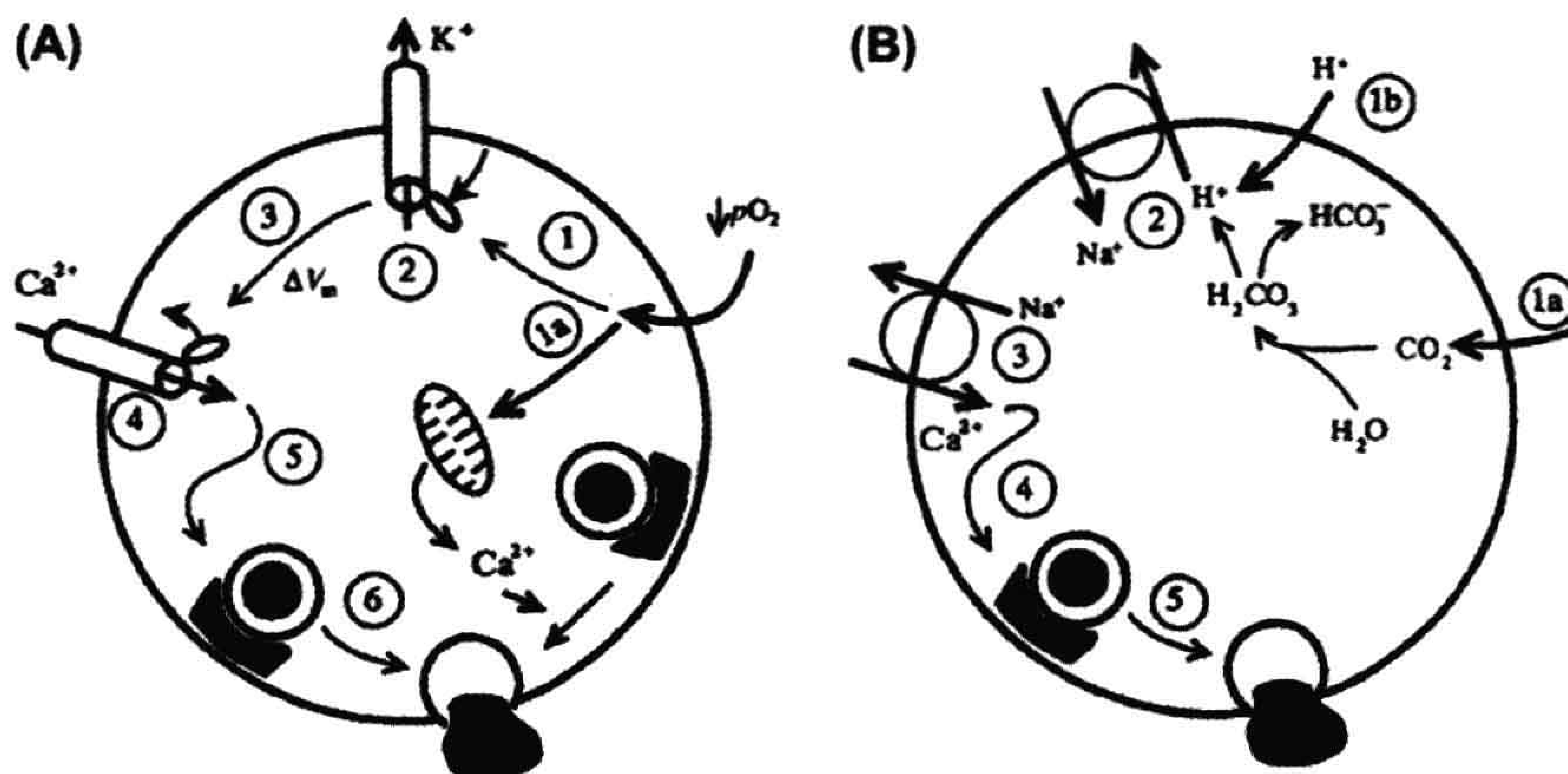


FIGURE 34.9 Stimulus—secretion coupling in carotid chemoreceptor cells. (A) O_2-induced transmitter release. Key steps in classical scheme of depolarization—secretion coupling are outlined. Decreased pO_2 results in decreased O_2 binding to the intracellular receptor coupling to a specific voltage-dependent K^+ channel (1). This results in the closure of the channel (2), cell depolarization (3), increased probability of the opening of HVA Ca^{2+} channels (4), increased calcium entry (5) and the enhanced rate of fusion of dopamine-containing vesicles with the plasma membrane (6). Alternatively (see path beginning with 1a), hypoxia-induced rundown of the mitochondrial proton gradient might result in reduced ATP generation, slow release of Ca^{2+} from mitochondria or other stores and, ultimately, a slow rise in spontaneous quantal release. (B) CO_2 and H-induced transmitter release. Increased pCO_2 or H entry (1b) results in decreased cytosolic pH and stimulation of the Na^+-H exchanger (2). The resultant influx in Na^+ stimulates the Ca^{2+}-Na^+ exchanger (3). This, in turn, increases Ca^{2+} influx (4) and Ca^{2+}-dependent exocytosis (5).

Na^+ currents. Second, in some isolated cell preparations, glomus cells respond to hypoxia by depolarizing and generating action potentials. (However, in other preparations, glomus cells fire action potentials only in response to current injection or release of the cell from sustained hyperpolarization. These cells show no change in passive electrical activity in response to hypoxia.) Third, in glomus cells that fire in response to hypoxia, depolarization increases both cytosolic Ca^{2+}, measured with intracellular dyes, and dopamine release, measured by amperometry. In these cells, depolarization–secretion coupling is reduced by exposure to blockers of the HVA-type Ca^{2+} channels or by reduction in extracellular Ca^{2+}.

A very exciting development in chemoreceptor physiology consistent with the depolarization–secretion coupling scheme outlined above is the discovery that, in whole-cell recordings, lowering ambient pO_2 selectively and reversibly reduces the outward K^+ current flowing through delayed rectifier K^+(DR) channels of the glomus cells. Reducing pO_2 from 160 mmHg to 90 mmHg reduces peak K^+(DR) current by ≈30%. This effect is not dependent on the concentrations of ATP (0–3 mM) or Ca^{2+} (<1 nM–0.5 mM) in the pipette. In outside-out patches of membrane, reduced ambient pO_2 reversibly decreases the probability of opening (P_o) of a 20-pS K^+(DR) type channel (Fig. 34.10). The first reports suggested that in vitro this channel was most responsive to changes in O_2 over the range of pO_2 values between 110 and 150 mmHg, in contrast to the intact carotid sinus nerve that actually fires optimally at pO_2s <70 mmHg. However, the O_2 sensitivity of the channel can be shifted into a more physiological range by the addition of a membrane-permeant analog of cAMP and recent data have shown K^+(DR)-type channel activity pO_2s ranging from 20 to 150 mmHg. In whole-cell, current-clamp recordings, the effect of a reduction in pO_2 is (1) an increase in the rate of cell depolarization on release from maintained hyperpolarization, (2) an increase in the frequency of spike activity in the resultant short train impulses and (3) an increase in AP overshoot. Hence, in glomus cells with some intrinsic spontaneous electrical pacemaker activity, O_2-dependent changes in K^+ current could alter the frequency of action potentials and large Ca^{2+} transients, thereby increasing [Ca^{2+}]-dependent transmitter release onto the afferent nerve. In glomus cells with little automaticity that maintain resting potentials of between −50 and −40 mV, closure of K^+(DR)-type channels could still cause steady-state depolarization "generator potential" and trigger electrical activity de novo. More extensive perforated-patch recordings will be needed to determine the range of electrical activity patterns exhibited by these cells.

These data suggest that O_2 maintains the activity of a delayed rectifier type K^+ channel through a novel gating mechanism. Several possibilities for the molecular mechanism of O_2 transduction and its relationship to channel gating have been suggested, but there is no definitive evidence for any of them. The first is that a heme protein, analogous to a subunit of the O_2-carrying protein hemoglobin, is attached to the channel, or to a functional subunit

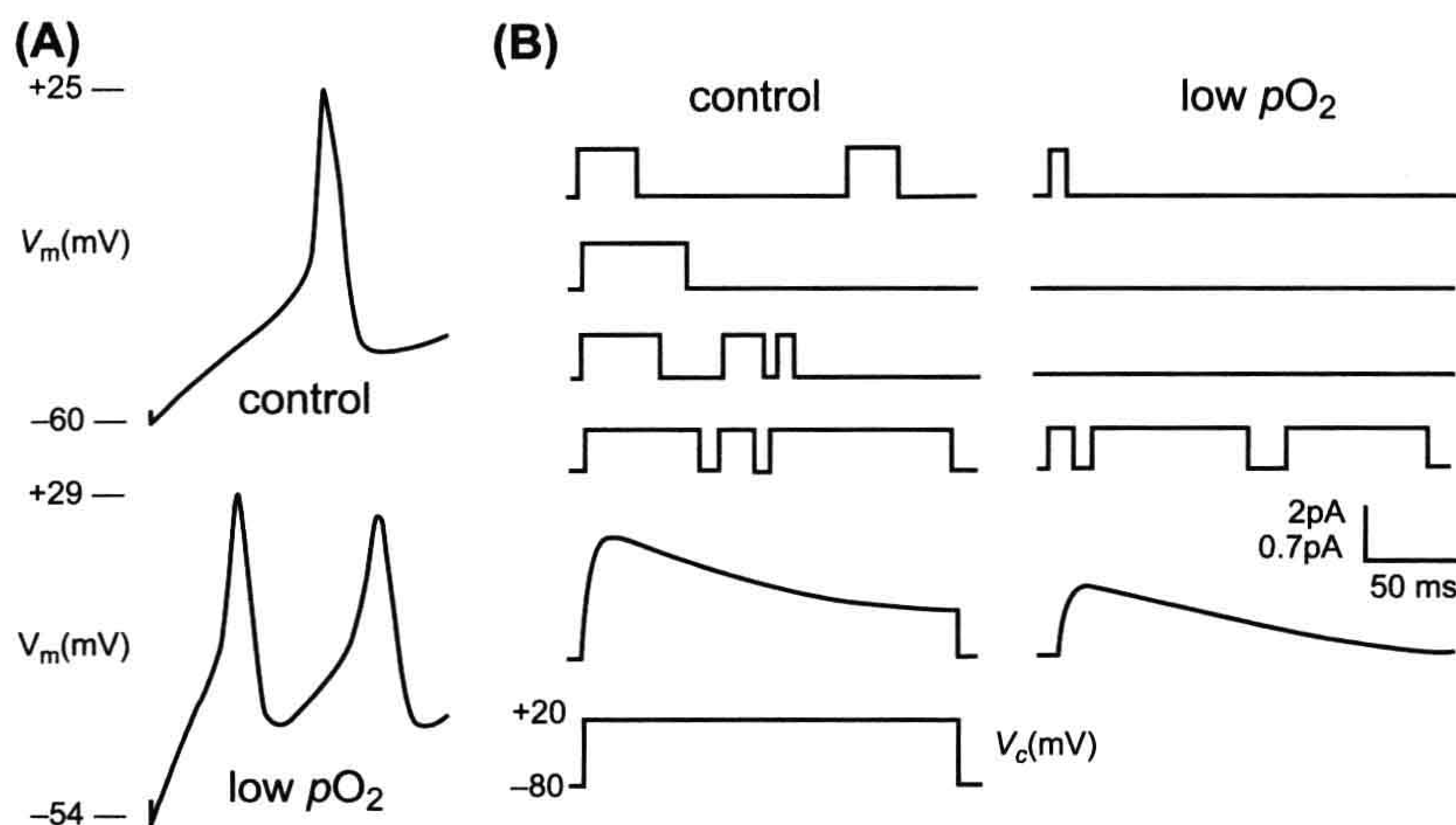


FIGURE 34.10 Origin of low-pO_2-induced enhancement of electrical activity in carotid glomus chemoreceptors. (A) Reduction in ambient pO_2 results in increased frequency of spontaneous AP activity, partly due to reduced rate of repolarization of the AP. Hence, any background depolarizing current might be more effective in raising the membrane potential toward threshold for firing a spike. *(Reproduced from* The Journal of General Physiology, *1989, Vol. 93, p. 979, Fig. 14. By permission of the Rockefeller University Press.)* (B) Reduction in ambient pO_2 reduces the probability (P_o) that a K^+(DR) channel will open on depolarizing the cell from −80 to +20 mV. Lowest traces in each column represent the average of many individual channel current traces. *(Idealized traces adapted from Ganfornina and Lopez Barneo, 1991.)*

of the channel. In this way, a change in configuration of the protein, on losing O_2, would alter channel gating. The second is the presence of an oxidase which, on reduction of cytosolic pO_2, produces less hydrogen peroxide (H_2O_2), consequently altering the concentration of redox intermediates and thereby of channel conformation.

The alternative view of chemotransduction of hypoxia in glomus cells is that the rise in intracellular Ca^{2+} necessary for dopamine secretion is due to Ca^{2+} release from intracellular stores and that voltage-activated currents play only a secondary role, perhaps allowing replenishment of intracellular Ca^{2+} stores. This hypothesis has arisen from data generated from both isolated glomus cells and in situ carotid cell bodies. Mitochondrial poisons, such as cyanide, produce a condition known as *histotoxic hypoxia*, which mimics true hypoxia in stimulating carotid body nerve activity and respiratory drive. These poisons produce increases in intracellular Ca^{2+} that are unaffected by pharmacologic maneuvers designed to abolish or enhance the action potential, hence suggesting that increases in cytosolic Ca^{2+} arise from intracellular stores. Hypoxia and mitochondrial poisons produce a rise of cell NAD(P)H. Additionally, studies from in situ carotid bodies have shown (1) that action potentials induced in carotid sinus nerve by hypoxia are not blocked by drugs that block outward K^+ currents and (2) that whole cell glomus membrane resistance is not changed in response to hypoxia. A proposed mechanism whereby hypoxia induces intracellular Ca^{2+} release is that low O_2 decreases mitochondrial efficiency, perhaps slowing electron transfer in the respiratory chain, and reducing the proton gradient across the mitochondrial inner membrane. A consequence of this could be the release of Ca^{2+} from mitochondria or decreased ATP production, resulting in slow Ca^{2+} release from other intracellular stores (e.g. the ER). For this mitochondrial-based hypothesis to work, it might be necessary that O_2-trapping properties of mitochondrial cytochrome oxidase and Ca^{2+}-storage properties of mitochondria in glomus cells differ significantly from their counterparts in other tissues.

IVB. Transduction of Increased pCO_2 and Decreased Plasma pH

Glomus cells rapidly equilibrate pH_i and pH_o. Hence, it is probable that with acidic stimuli the cell is actually sensing a fall in pH_i. But how does an increase in $[H^+]_i$ result in Ca_o^{2+}-dependent transmitter release, especially as H_i^+-induced release is insensitive to blockers of HVA Ca^{2+} channels and HVA Ca^{2+} channels are often inhibited by reduction in pH_i? The proposed link between increased $[H^+]_i$ and Ca^{2+} entry in promoting dopamine release is that increased $[H^+]_i$ activates an Na_o^+-H_i^+ exchanger which, in turn, elevates Na^+ and recruits a Na^+-Ca^{2+} exchanger. The activity of the latter exchanger is often augmented by cell depolarization; this may, in fact, occur because a drop in pH_i reduces K^+(DR) type K^+ current much as a drop in pO_2 does. An increase in background "spontaneous" quantal release of dopamine, which is not phase-linked to action potential activity, could increase steady-state depolarization of carotid nerve fibers and, perhaps, augment on-going impulse activity (see Fig. 34.9B). In considering this scheme, it should be cautioned that thus far, good evidence exists only for activation of an Na^+-H^+ exchanger.

To be sure, respiratory drive varies significantly according to age and physiologic status. Human fetuses do not exhibit regular respiratory movements in utero, whereas newborn infants often display periodic breathing different from breathing patterns seen in older children and adults. Disease states produce abnormal breathing patterns, such as Cheyne–Stokes breathing, the diamond-shaped changes in respiratory excursions followed by a period of non-breathing (apnea), seen in stroke, congestive heart failure and chronic hypoxia. In infants, prolonged apnea despite persistent hypoxia or hypercarbia can culminate in sudden infant death syndrome (SIDS). Recent data suggest that carotid body glomus cells from animals raised under hypoxic conditions show blunted electrophysiologic responses to hypoxia compared to cells from healthy animals. Disorders of breathing such as apnea and SIDS are seen in higher frequency in infants at increased risk for chronic hypoxia due to conditions such as prematurity or second-hand cigarette smoke exposure. Studies on the mechanism of changes in carotid body chemoreception in normal development and in various disease states should be a fruitful area for further inquiry.

V. STIMULUS–CONTRACTION COUPLING IN VASCULAR SMOOTH MUSCLE CELLS

VA. Hypoxic Vasodilation of Coronary and Mesenteric Vessels

Smooth muscle cells of resistance arterioles are very sophisticated metabolic sensors. In fact, they encompass a complete vasodilator reflex system in a single cell. In response to a drop in ambient pO_2, these cells reduce their tension generation. This results in vessel relaxation and the local redistribution of O_2 supply to O_2-consuming tissue. As in the case of the cardiac myocyte, a key to the explanation of this phenomenon is the increase in K^+ conductance and membrane hyperpolarization, which precedes the fall in tension.

It is well appreciated that resistance vessels in the coronary and mesenteric (gut) circulation display resting tone. Their myocytes maintain a resting potential of -40 to -50 mV and have an abundance of K^+(ATP) and

L-type (HVA) Ca^{2+} channels. In fact, in smooth muscle of mesenteric artery, the K_d value (μM) for ATP-induced closure of K^+(ATP) channels is roughly double that in cardiac myocytes, in principle making K^+(ATP) channels of these myocytes more sensitive to hypoxia than the K^+(ATP) channels in the heart. Under these circumstances, small changes in resting potential would be expected to affect resting tone. A small depolarization (of 5–10 mV) caused by closure of K^+(ATP) channels should result in increased opening of HVA Ca^{2+} channels and subsequent vasoconstriction (Fig. 34.11A). In contrast, a small hyperpolarization of 5–10 mV, affected by addition of a K^+(ATP) channel opener or a dihydropyridine Ca^{2+} channel antagonist, should reduce resting tone and result in vasodilation. These predictions have been borne out experimentally. A modest drop in microenvironment pO_2, insufficient to affect cardiac excitation–contraction coupling, is sufficient to reduce cytosolic ATP in vascular smooth muscle cells, open K^+(ATP) channels and cause vasodilation. (In bulk cardiac muscle in situ, preferential opening of smooth muscle K^+(ATP) channels might be further augmented by the release of adenosine by active cardiac tissue; extracellular adenosine has been shown to activate K^+(ATP) channels via a G-protein-dependent mechanism.) Hence preferential hypoxia-induced arteriolar dilation, with its attendant increases in local O_2 delivery, may spare cardiac myocytes the risk of hypoxia-induced alterations in excitation–contraction coupling. This scheme might work for the regulation of local blood supply to the brain and gut as well as to the heart.

VB. Hypoxia-Induced Vasoconstriction of Pulmonary Vessels

In contrast to coronary, mesenteric and cerebral vessels, pulmonary artery and its smooth muscle constrict in response to a drop in pO_2. This hypoxic pulmonary vasoconstriction (HPV) constitutes an adaptive response in the lung bed because it ensures that areas of the lung that are poorly oxygenated will receive less blood flow; the extra blood flow is "redirected" towards better oxygenated areas to optimize gas exchange. HPV is critical in fetal pulmonary development when the maturing air spaces are filled with secreted fluid rather than inspired air. Under these conditions, HPV maintains the relatively high pulmonary vascular resistance that shunts venous return around the low flow pulmonary bed, through the ductus arteriosus of the cardiac septum and into the left heart. With inflation of the newborn's lungs to air containing substantially higher pO_2, O_2-induced pulmonary vasodilation occurs, thereby promoting blood flow through the pulmonary circulation. In the adult, HPV is useful in maintaining moment-to-moment matching of local ventilation to perfusion; this reduces the risk of hypoxia that can occur when a portion of the lung is poorly inflated. However, when the areas of local poor ventilation are widespread, or with chronic hypoxia (such as at high altitudes), chronic HPV is accompanied by

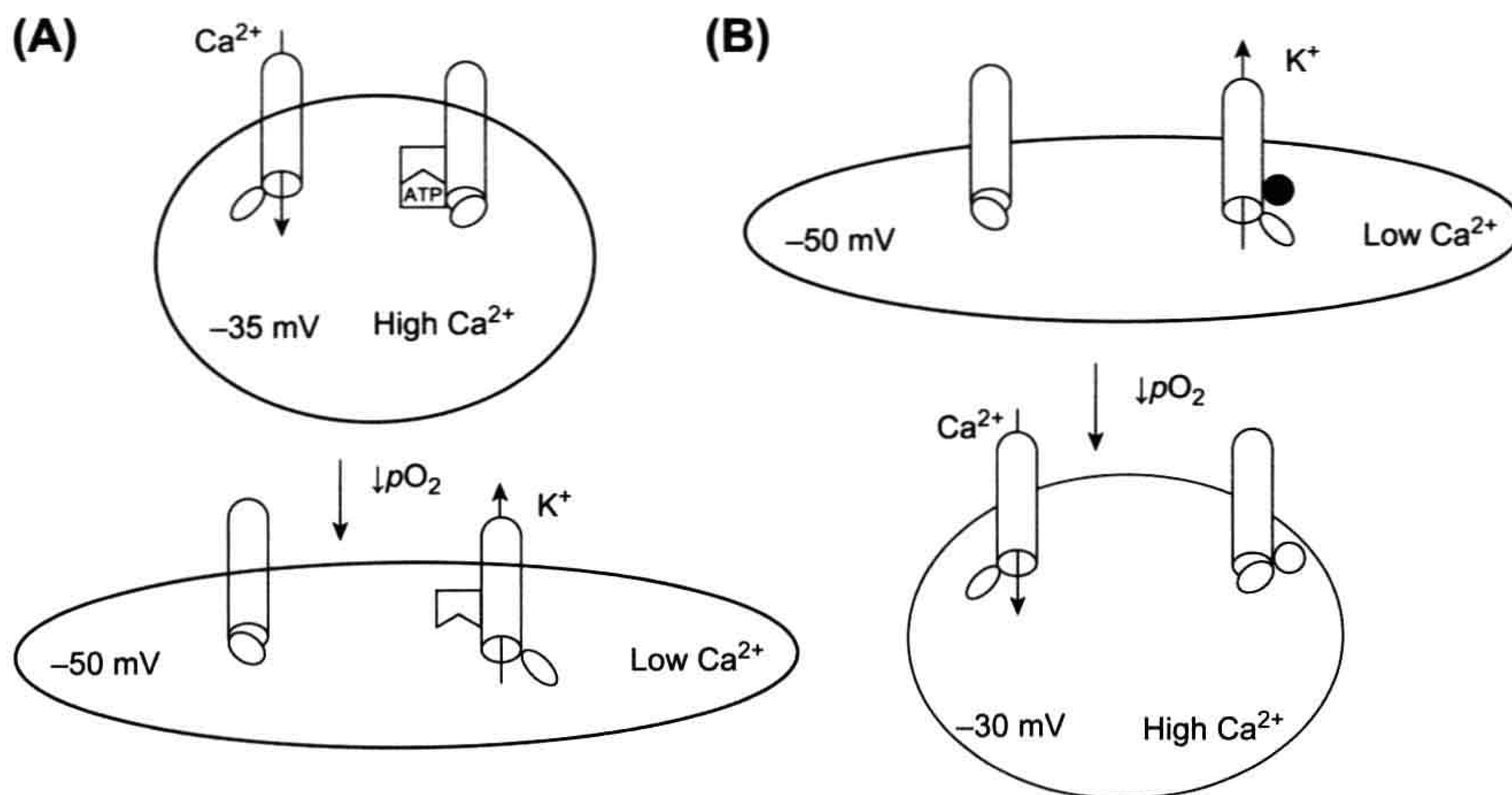


FIGURE 34.11 Hypoxia alters stimulus–contraction coupling in vascular myocytes. (A) Model of hypoxia-induced vasodilation in cardiac, cerebral and mesenteric vessels. In normoxic conditions, K^+(ATP) channels are largely closed, but voltage-dependent Ca^{2+} channels are open, $V_m \approx -35$ mV, and cytosolic Ca^{2+} is low. With a decrease in pO_2, cytosolic ATP levels drop, resulting in the opening of K^+(ATP) channels, repolarization to ≈ -50 mV, closure of Ca^{2+} channels, a drop in cytosolic Ca^{2+} and myocyte relaxation. (B) Model of hypoxia-induced vasoconstriction in pulmonary arteries. In normoxic conditions, $V_m \approx -50$ mV, O_2-sensitive K^+ channels are largely open and voltage-dependent Ca^{2+} channels are largely closed. Hence, cytosolic Ca^{2+} levels are low and there is little resting tension. With a decrease in pO_2, O_2-sensitive K^+ channels close, resulting in depolarization, opening of Ca^{2+} channels, Ca^{2+} entry and myocyte contraction.

smooth muscle proliferation (i.e. "work hypertrophy of muscle"). The end result is the development of increased resistance and pressure in the total pulmonary vascular bed. This "pulmonary artery hypertension" imposes an increased "afterload" on the right ventricle, thus becoming a stimulus for its hypertrophy.

What cellular mechanisms support HPV? Pulmonary artery myocytes maintain a low resting tension, a V_m of ≈ -40 mV and a resting cytosolic $[Ca^{2+}]$ of <100 nM. They respond to progressive hypoxia (e.g. a slow fall in pO_2 from 150 to 15 mmHg) with a 15-mV depolarization, which is not affected by changes in $[Ca^{2+}]_o$, followed by Ca_o^{2+}-dependent increases in both cytosolic Ca^{2+} and tension. Given that V_m in these cells shows a Nernstian relationship to $[K^+]_o$, these results suggest that membrane depolarization is due to a large decrease in Ca_o^{2+}-independent resting membrane conductance (e.g. GK). However, depolarization ultimately results in a small increase in G_{Ca}. This is sufficient to provide entry to trigger contraction. Tension is maintained so long as Ca^{2+} entry through voltage-gated Ca^{2+} channels exceeds Ca^{2+} efflux via the Na^+-Ca^{2+} exchanger. Whole-cell voltage-clamp experiments have provided good evidence that a voltage-activated, delayed rectifier type K^+ current seen at V_m values positive to -50 mV and, hence, open at rest, is significantly inhibited by hypoxia. Depolarization of a few mV would be sufficient to open HVA Ca^{2+} channels and result in vasoconstriction (see Fig. 34.11B). Hence, as in the carotid chemoreceptor, hypoxia-induced reduction in the activity of K^+(DR) type channels in a cell with a very low background G_m, appears to be responsible for depolarization and stimulus–response coupling.

An important paradox, which remains to be explained, is how pulmonary artery myocytes manage to "hide" K^+(ATP) channels, known to be present in the sarcolemma, during hypoxia. In these cells, K^+(ATP) channel openers abort high $[K^+]_o$-induced tension increase, while sulfonylureas enhance tension generation, as they do in resistance vessels, yet hypoxia does not open these channels. Are mechanisms similar to those in pancreatic α cells at play here?

VI. COUPLING OF OXYGEN SENSING TO RED CELL PRODUCTION BY ERYTHROPOIETIN-SECRETING CELLS

The ultimate metabolic sensors are the erythropoietin-(epo-) secreting cells of the renal interstitium and liver. These modified fibroblasts respond slowly to hypoxia by increasing their synthesis and constitutive secretion of epo which, in turn, serves as a maturation factor for erythrocyte precursors in bone marrow. Epo binds to a membrane receptor, which serves as a scaffold for the activation of numerous growth and division signaling pathways including JAK/STAT and ras/MAP kinases; epo also increases the expression of Bcl-Xl, an anti-apoptotic peptide. Mature erythrocytes are virtually cytoplasmic bags of hemoglobin (Hb) which bind O_2. In high pO_2 and pH environs (arterioles), Hb binds O_2, while at lower pO_2 and pH environs, Hb gives off its O_2. In this way Hb ferries O_2. The net effect of this receptor–effector cell pair is that hypoxia can ensure an increase in blood O_2 carriage for up to 120 days, the life span of an erythrocyte. A clue to the mechanism of O_2-reception epo-producing cells is that their exposure to cobalt, nickel and manganese mimics the effects of hypoxia, whereas exposure to metabolic (mitochondrial) inhibitors such as cyanide cannot. This suggests that the O_2 sensor is an Hb-type molecule, which can be locked into a deoxygenated form, rather than a molecule involved in red-ox transfer, which uses O_2 as the final acceptor. The epo gene has been cloned and its *cis*-regulatory element has been found to bind a hypoxically inducible factor (HIF) that can transfer from the cytoplasm into the nucleus (Fig. 34.12A). Epo regulation is

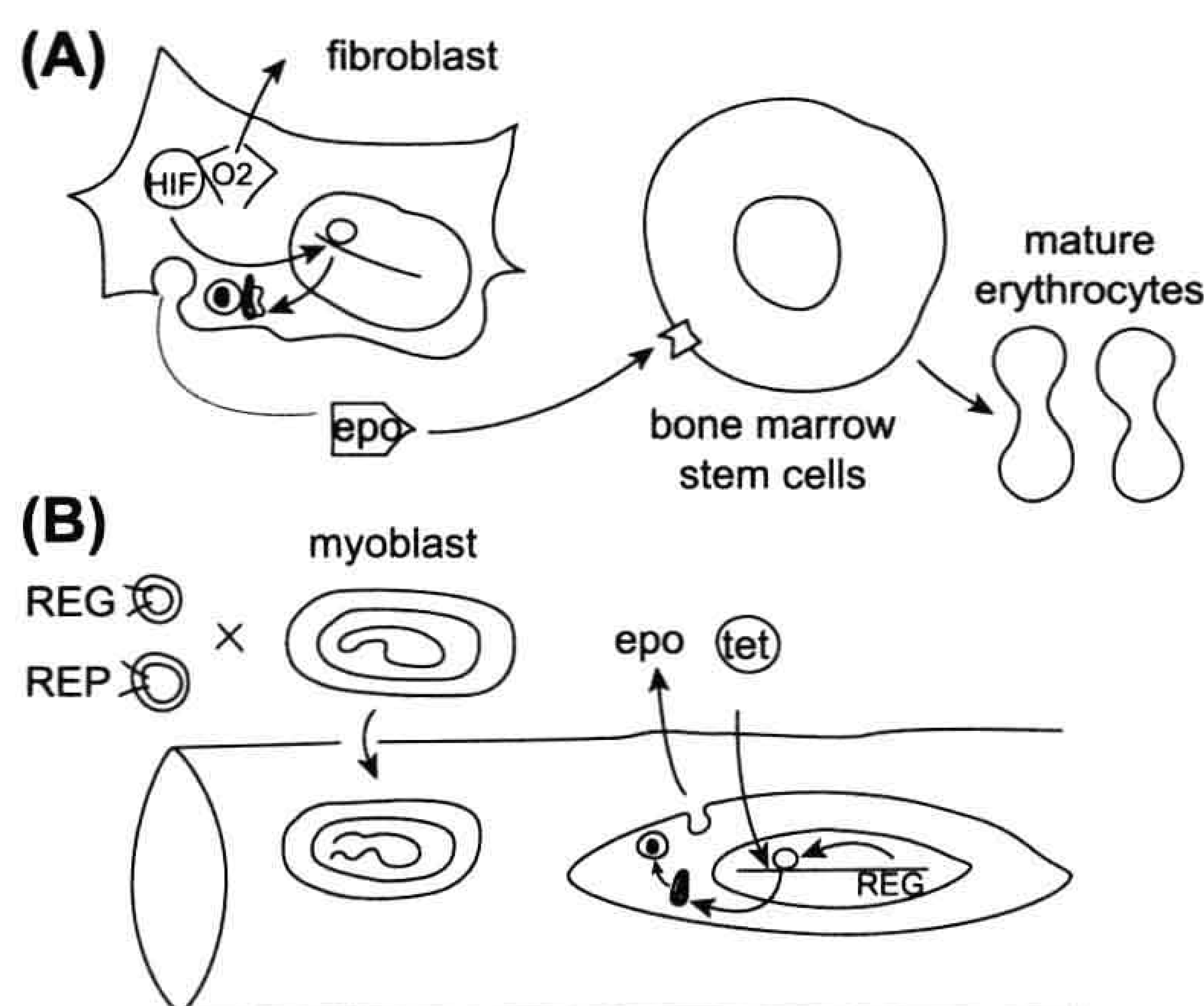


FIGURE 34.12 Native and bioengineered stimulus–synthesis coupling in erythropoietin production. (A) Stimulus–synthesis coupling in renal interstitial fibroblasts and hepatic Ito cells likely consists of triggering of epo gene transcription by a hypoxically induced factor (HIF), which is freed to enter the nucleus after O_2 dissociates from a heme pigment receptor. Newly synthesized epo is packaged and constitutively released. The kidneys are an excellent primary site for an O_2 sensor because under control conditions they are perfused with $\approx 20\%$ of the cardiac output. Circulating epo binds to erythroblasts (erythrocyte stem cells) in bone marrow and triggers their proliferation and maturation to enucleated erythrocytes that circulate as hemoglobin-packed, O_2 carrying sacs for an average of 120 days. (B) Genetically engineered stimulus–synthesis coupling for epo production in skeletal myocytes. Myoblasts are co-transfected with (i) a regulator gene (REG) under the control of mature muscle cells and (ii) a reporter gene (REP) coding for epo and under control of a tetracycline-sensitive product of the regulator gene. These co-transfected myoblasts are injected into muscle where they fuse with multinucleated myocytes. Under the control of exogenously added tetracycline (tet), myocytes are induced to synthesize and secrete epo.

an example of a widespread system for gene induction by O_2; this system includes pathways for induction vascular growth factors and changing isoforms of glycolytic enzymes in metabolically active cells.

Erythropoietin production wanes in chronic renal failure, as scar tissue replaces metabolically active cells. While epo can be replaced by weekly injection, the recombinant molecule is costly. To circumvent this, significant effort has recently been made to engineer cells that might tonically secrete epo on exposure to a simple, gene-activating stimulus. Primary myoblasts are co-transfected with two retroviruses and then injected into muscle where they fuse with mature, multinucleated myocytes. One of the transfecting retroviruses contains a regulator, or reverse transactivation, gene (REG) designed to be under the control of a promoter only activated in mature myocytes. The second retrovirus contains the reporter gene (REP), coding for epo, but under control of both the protein coded by REG and tetracycline (tet). Once in the mature muscle, the REG protein and tet control can tonically activate the epo gene. Significantly, when mice are injected with these engineered myoblasts, epo secretion can be switched on and off over months, depending on the availability of tet in the drinking water.

ACKNOWLEDGMENTS

Original data traces shown here were obtained in our laboratory through the support of NIH grant DK37380. I thank Todd Owyoung for preparing Figures 34.2 and 34.6, David Bryant for preparing Figures 34.9–34.11 and Drs David Pressel and David Barnett for sharing insights and delicate turns of phrase during the preparation of a prior version of this chapter.

This chapter is dedicated to the memory of Golda Hazak, wit and sage of Kiryat Yam.

BIBLIOGRAPHY

Ashcroft, F. M., & Grimble, F. M. (1999). K-ATP channels and insulin secretion; their role in health and disease. *Diabetologia, 42*, 9039–9196.

Ashcroft, F. M., & Rorsman, P. (1989). Electrophysiology of the pancreatic Beta cell. *Prog Biophys Mol Biol, 54*, 87–143.

Bohl, D., Naffakh, N., & Heard, J. M. (1997). Long-term control of erythropoietin secretion by doxycycline in mice transplanted with engineered primary myoblasts. *Nat Med, 3*, 299–304.

Bokvist, K., Olsen, H. L., Hoy, M., et al. (1999). Characterisation of sulphonylurea and ATP-regulated K^+ channels in rat pancreatic A-cells. *Pflügers Arch Eur J Physiol, 438*, 428–436.

Ganfornina, M. D., & Lopez-Barneo, J. (1991). Single K channels in membrane patches of arterial chemoreceptor cells are modulated by O_2 tension. *Proc Natl Acad Sci USA, 88*, 2927–2930.

Gonzalez, C., Almaraz, L., Obeso, A., & Rigual, R. (1992). Oxygen and acid chemoreception in the carotid body chemoreceptors. *TINS, 15*, 146–157.

Gromada, J., Holst, J. J., & Rorsman, P. (1998). Cellular regulation of islet hormone secretion by the incretin hormone glucagon-like pep-tide 1. *Pflügers Arch Eur J Physiol, 435*, 583–594.

Harvey, J., McKay, N. G., Walker, K. S., Van der Kay, J., Downes, C. P., & Ashford, M. L. J. (2000). Essential role of ohosphoinosotide 3-kinase in leptin induced K-ATP channel activation. *J Biol Chem, 275*, 4660–4669.

Inagaki, N., Gonoi, T., Clement I.V, J. P., et al. (1995). Reconstitution of I-K^+(ATP): an inward rectifier subunit plus the sulfonylurea receptor. *Science, 270*, 1166–1169.

Johnson, J. D., & Chang, J. P. (2000). Function– and agonist-specific Ca^{2+} signalling: the requirement for and mechanism of spatial and temporal complexity in Ca^{2+} signals. *Biochem Cell Biol.*, (in press).

Klingauf, J., & Neher, E. (1997). Modeling buffered Ca diffusion near the membrane: implications for secretion in neuroendocrine calls. *Biophys J, 72*, 674–690.

Misler, S., Barnett, D. W., Pressel, D. M., & Gillis, K. D. (1992). Electrophysiology of stimulus-secretion coupling in human betacells. *Diabetes, 42*, 1220–1227.

Nichols, C. G., & Lederer, W. J. (1991). Adenosine triphosphatesensitive potassium channels in the cardiovascular system. *Am J Physiol, 261*, H1675–H1686.

Nichols, C. G., Shyng, S.-L., Nestorowicz, A., et al. (1996). Adenosine diphosphate as an intracellular regulator of insulin secretion. *Science, 272*, 1785–1787.

Ratcliffe, P. J., Ebert, B. L., Ferguson, D. J. P., et al. (1995). Regulation of the erythropoietin gene. *Nephrol Dial Transplant, 10*, 18–27.

Rorsman, P., Ashcroft, F. M., & Berggren, P. O. (1991). Regulation of glucagon release from pancreatic A-cells. *Biochem Pharmacol, 41*, 1783–1790.

Seino, S., Inagaki, N., Namba, N., & Gonoi, T. (1996). Molecular biology of the beta-cell ATP-sensitive K channel. *Diabetes Rev, 4*, 177–190.

Weir, E. K., & Archer, S. L. (1995). The mechanism of acute hypoxic pulmonary vasoconstriction: the tale of two channels. *FASEB J, 9*, 183–189.

Wollheim, C. B., Lang, J., & Regazzi, R. (1996). The exocytotic process of insulin secretion and its regulation by Ca and G-proteins. *Diabetes Rev, 4*, 276–297.

Zawar, C., & Neumcke, B. (2000). Differential activation of ATP-sensitive potassium channels during energy depletion in Ca_1 pyramidal cells and interneurones of rat hippocampus. *Pflügers Arch Eur J Physiol, 439*, 256–262.

Zhou, Z., & Misler, S. (1996). Amperometric detection of quantal secretion from patch-clamped rat pancreatic beta-cells. *J Biol Chem, 271*, 270–277.

Chapter 35

Cyclic Nucleotide-Gated Ion Channels

Anita L. Zimmerman

Chapter Outline

I. SUMMARY

Cyclic nucleotide-gated (CNG) channels are directly activated by the binding of cGMP and/or cAMP, which are controlled by G-protein enzyme cascades. Their cousins, the hyperpolarization-activated, cyclic nucleotide-gated (HCN) channels, are voltage-gated, but their voltage sensitivity is regulated by the binding of cAMP. Both CNG and HCN channels are members of the superfamily of voltage-gated cation channels. CNG channels have established roles in sensory transduction, but they are also found in many non-sensory tissues. HCN channels are best known for their pacemaking role in the cardiac sinoatrial node. Both CNG and HCN channels are excitatory, since their opening allows Na^+ and Ca^{2+} entry. In the brain, both CNG and HCN channels are implicated in synaptic plasticity and other excitation processes, in addition to their pacemaking role in rhythmic neurons. There continues to be fast-moving research on these channels in the areas of structure/function, physiological roles, modulation, gating, permeation and development of pharmacological tools.

II. INTRODUCTION

Cyclic nucleotides have long been known as intracellular second messengers that regulate cell function by controlling the activity of protein kinases which, in turn, control many other cellular proteins. However, in 1985, Fesenko and his colleagues made a startling discovery that changed our view of the physiological role of cyclic nucleotides. These investigators found that the ion channel mediating the electrical response to light in retinal rod cells was directly opened by the binding of guanosine 3′,5′-cyclic monophosphate (cGMP); no phosphorylation reaction was required. Now the rod channel is considered to be a member of a special class of ion channels — the *c*yclic *n*ucleotide-*g*ated (CNG) channels, which are actually part of the superfamily of voltage-gated cation channels (reviewed in Yu et al., 2005). These channels are discussed in many recent reviews (Kaupp and Seifert, 2002; Barnstable et al., 2004; Broillet and Firestein, 2004; Bradley et al., 2005; Hofmann et al., 2005; Craven and Zagotta, 2006; Pifferi et al., 2006; Biel, 2009; Biel and Michalakis, 2009; Mazzolini et al., 2010; Cukkemane et al., 2011).

Since the discovery of CNG channels, a related class of ion channels has been found to underlie pacemaker currents (usually referred to as I_h or I_f) in the heart and brain (reviewed in Gauss and Seifert, 2000; Kaupp and Seifert, 2001; Craven and Zagotta, 2006; Biel, 2009; Wahl-Schott and Biel, 2009; DiFrancesco, 2010). These channels are called HCN channels, which stands for *h*yperpolarization-activated, *c*yclic *n*ucleotide-regulated channels. Their structure is similar to that of CNG channels, but they are mainly gated by voltage, with their voltage activation regulated by the direct binding of cyclic nucleotides. This chapter will focus mainly on CNG channels, but will make comparisons with HCN channels as well. Finally, although cyclic nucleotide binding domains have been found in Eag-like (ether à-go-go) K^+ channels and plant K^+ channels, the functional role of cyclic nucleotide binding to these channels remains under investigation and these channels will not be discussed here.

Cell Physiology Sourcebook. DOI: 10.1016/B978-0-12-387738-3.00035-4

Why would Nature directly gate or regulate ion channels with cyclic nucleotides? When a cyclic nucleotide regulates a kinase, it is also in effect regulating all the proteins controlled by that kinase and by substrates of the kinase. Regulating ion channels is similar in that, like kinases, ion channels have diverse physiological effects. For example, the opening of non-selective cation channels (such as those opened by cyclic nucleotides) depolarizes the cell membrane (via Na^+ entry) and also allows the entry of Ca^{2+}, another important second messenger. Membrane depolarization opens voltage-gated Ca^{2+} channels, further increasing the entry of Ca^{2+}. Many cell functions are controlled by membrane potential and/or intracellular Ca^{2+}, including nerve impulses, muscle contraction, gene transcription and the secretion of neurotransmitters and hormones. Finally, depolarization and intracellular Ca^{2+} open K^+ channels, which repolarize the membrane and thereby contribute to the termination of the cellular response. Thus, there are numerous possibilities for control of cell function by cyclic nucleotide-gated, and cyclic nucleotide-regulated, ion channels. In addition, ion channel gating and permeation are much faster than phosphorylation reactions. Thus, changes in cyclic nucleotide levels could have fast effects mediated by ion channels, followed by slower, longer lasting effects mediated by protein kinases.

III. PHYSIOLOGICAL ROLES AND LOCATIONS

Since their discovery in retinal rods, and their subsequent purification and cloning, CNG channels have been identified in many other types of cells. They have been implicated generally in sensory transduction, as they also have been found in retinal cones, olfactory cells, invertebrate photoreceptors and pineal gland cells (reviewed in Kaupp and Seifert, 2002). Furthermore, mRNA probes against the rod CNG channel have revealed its expression in cells of the heart, brain, muscle, liver, kidney and testis. In the brain, both CNG and HCN channels have been implicated in synaptic plasticity (reviewed in Barnstaple et al., 2004, Biel, 2009; Wahl-Schott and Biel, 2009). The CNG channels have been studied most thoroughly in vertebrate photoreceptors and olfactory cells and, therefore, the CNG channels from these cells are discussed in the most detail here.

In rods and cones, CNG channels are key players in visual transduction (discussed in Chapter 38). It is these channels that conduct the so-called *dark current* and whose closure generates the hyperpolarizing response to light, which decreases the secretion of glutamate onto bipolar cells at the rod–bipolar synapse. The physiological second messenger in the photoreceptors is cGMP, which is at relatively high cytosolic concentration in the dark and decreases in the light after hydrolysis by a phosphodiesterase (PDE). Activation of PDE occurs when a photon is absorbed by a G-protein-coupled-receptor (a GPCR, which in this case is the photopigment rhodopsin), which then triggers a G-protein cascade. A similar system operates in cone visual transduction. An overview of the enzyme cascade controlling the level of cGMP is given in the next section, with more detail provided in Chapter 38.

Rods and cones are particularly well suited to patch-clamp studies of CNG channels, since the plasma membranes of their light-sensitive outer segments contain no other type of ion channel (although Na^+:Ca^{2+},K^+ exchange carriers are present; see Section V and Chapter 38). Furthermore, the rod outer segment plasma membrane has an extremely high density of CNG channels – hundreds per square micrometer – allowing as much as nanoamperes of current to be recorded from a single excised patch (with blocking divalent cations removed; see Section VB below). Such large currents are especially useful in studying pharmacological agents and modulators. In contrast, cone outer segments have relatively low channel densities, allowing the study of single-channel kinetics in patches containing only one channel. However, rods and cones actually have about the same total number of CNG channels because of the much larger plasma membrane area in cone outer segments (a consequence of the characteristic infolding of this membrane that forms "sacs" rather than the internal "disks" found in rods; see Chapter 38).

Olfactory receptor cells use CNG channels in sensing odorants (reviewed in Chapter 39). In this system, however, there are numerous odorant-activated GPCR types. Furthermore, adenosine 3′,5′-cyclic monophosphate (cAMP) is the physiological second messenger and the stimulus triggers cAMP *production* by adenylate cyclase, rather than its degradation by a PDE. Thus, in response to an odorant, the CNG channels open and the olfactory receptor cell depolarizes, increasing the probability of generation of an action potential. In addition, the Ca^{2+} that enters through the CNG channels activates Ca^{2+}-activated Cl^- channels, whose opening further depolarizes the cell (note that for these cells, unlike most other cells, the Cl^- concentration is higher inside than outside the cell, which is why its flow through the channels depolarizes the cell).

Like rods and cones, the olfactory cell has its CNG channels concentrated in a specialized region: the olfactory cilia and ciliary knob. Although the channels have been studied in excised patches from olfactory cilia (Nakamura and Gold, 1987), such experiments are extremely difficult because of the small diameter of a cilium. Luckily, the knob is larger and some CNG channels are also located (at lower density) in the membrane of the soma. Furthermore,

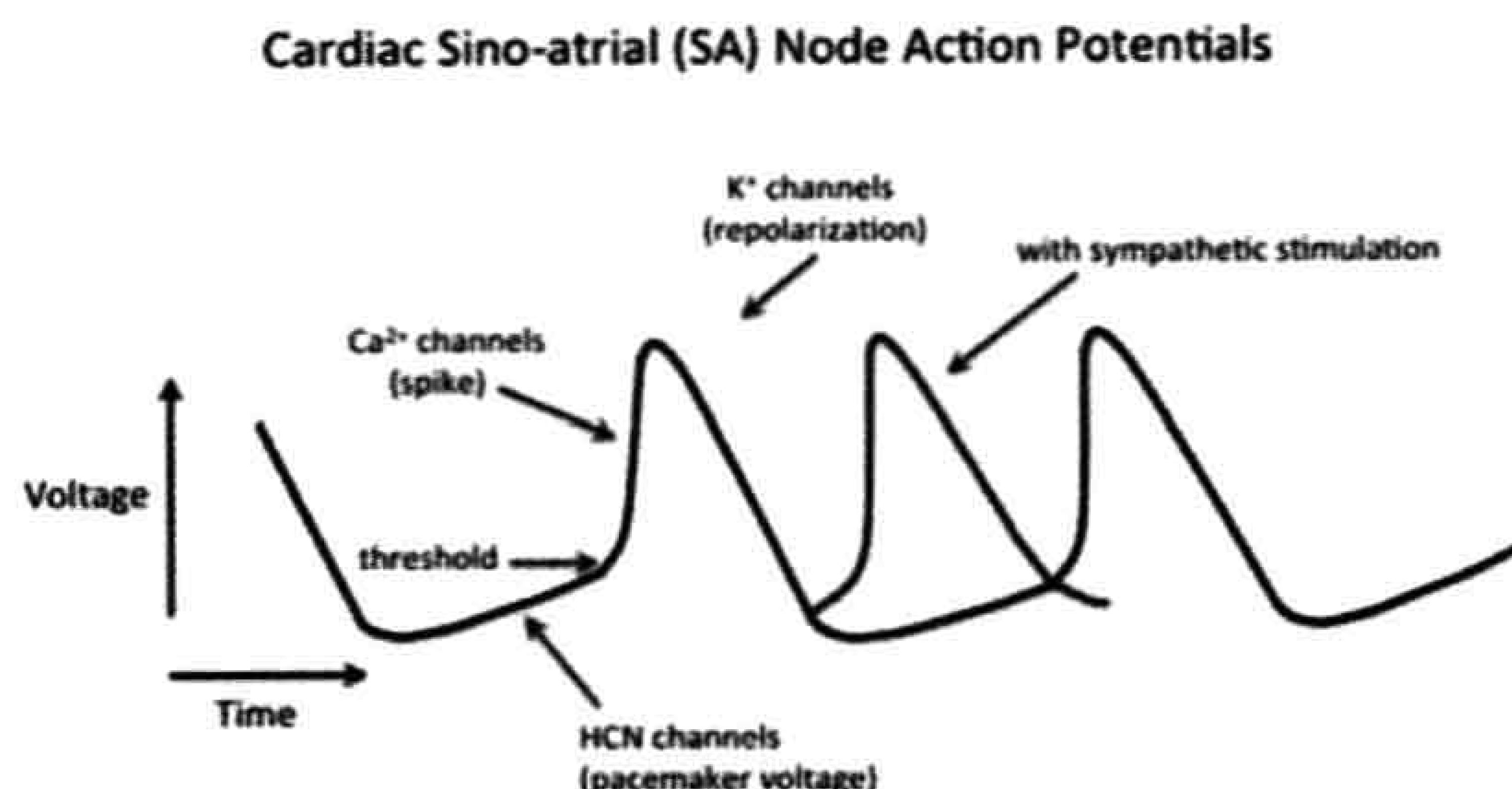


FIGURE 35.1 The role of HCN channels in the cardiac SA node action potential. The HCN channels are activated by hyperpolarization at the end of an action potential and their opening causes a slow depolarization that drives the membrane potential to threshold to trigger the next spike. Voltage-gated Ca^{2+} channels are responsible for the upstroke and voltage-gated K^+ channels repolarize the membrane. The inward pacemaker current through HCN channels is called I_h or I_f and is carried mainly by Na^+ under physiological conditions, despite the relatively high K^+ selectivity of HCN channels. Red trace: sympathetic agonists (e.g. norepinephrine) speed the heart by increasing the concentration of cAMP, which makes the HCN channels open more quickly (increased slope of pacemaker depolarization) and at less negative voltages, so that the next spike occurs sooner.

whole-cell patch-clamp methods have yielded considerable information on the olfactory CNG channels.

HCN channels were first studied in the sinoatrial (SA) node of the heart, where their opening produces the pacemaker current (I_h) that sets the heart rate by giving the initial slow depolarization at the beginning of the SA node action potential (Fig. 35.1; reviewed in DiFrancesco, 2010). Since the initial studies, HCN channels have been found in many other tissues as well, most notably in the brain, where they appear to play a role in synaptic plasticity, dendritic integration and maintenance of resting membrane potential (reviewed in Biel, 2009; Wahl-Schott and Biel, 2009). HCN channels also have been found to play a role in rhythmic activity in the central nervous system, especially in the thalamus (reviewed in Gauss and Seifert, 2000).

IV. CONTROL BY CYCLIC NUCLEOTIDE ENZYME CASCADES

Like cyclic nucleotide-regulated protein kinases, CNG and HCN channels are sensors of the local concentration of cyclic nucleotides. Stimulus-induced changes in cyclic nucleotide levels are mediated by GTP-binding proteins (G proteins). The stimulus-activated receptor interacts with a G protein, causing it to release GDP and bind GTP and to dissociate into two components: an α subunit and a $\beta\gamma$ subunit complex. The α subunit of the G protein, now bound to GTP, stimulates either adenylate cyclase (in olfactory receptors and cardiac SA node cells) or a cGMP-specific phosphodiesterase (in rods and cones). For the photoreceptors, the stimulus that activates the receptor is a photon, whereas for olfactory cells, the stimulus is an odorant molecule that acts as a receptor ligand, and for the SA node cells, the typical stimulus is a sympathetic agonist (e.g. norepinephrine) acting on a β-adrenergic receptor. A cyclic nucleotide enzyme cascade is diagrammed in Fig. 35.2 for a rod photoreceptor and in Fig. 35.3 for an olfactory cell. The cascade in cones is similar to that in rods, except that all the membrane-associated players are located on the plasma membrane, since cones lack internal disks (see Chapter 38). For the cardiac SA node cells, the cascade resembles that of the olfactory cell, however, cAMP does not activate the HCN channel, but rather makes the channel's activation by voltage occur sooner (i.e. at less negative voltages) and more quickly. This gives a speeding of the heart, since the SA node action potentials that set the timing of the heartbeat come more frequently. Activation of a muscarinic receptor by a parasympathetic agonist decreases [cAMP] and thereby slows the heart.

Cyclic nucleotide enzyme cascades are not fixed in their behavior. Instead, they are regulated by feedback systems, some of which involve CNG channels. For example, in rods, the Ca^{2+} that enters through CNG channels has been found to modulate the cGMP cascade. There is evidence that Ca^{2+} (in association with Ca^{2+} binding proteins) inhibits guanylate cyclase and inhibits the shutoff of rhodopsin (see Chapter 38). In olfactory receptors, Ca^{2+} appears to be involved in both excitation and adaptation (reviewed in Pifferi et al., 2006 and Chapter 39).

In addition to such feedback regulatory systems, there are the standard shutoff mechanisms employed in cyclic nucleotide cascades (e.g. see Chapter 38). These include phosphorylation of the receptor (e.g. the phosphorylation of rhodopsin, followed by its binding to arrestin), GTPase activity of the G protein (converting it back to the GDP-bound, inactive form), cessation of the stimulus and competing hydrolysis or synthesis of the cyclic nucleotide. There also are hints that the ability of the channels to respond to the cyclic nucleotide may be modulated (see Section VI).

V. FUNCTIONAL PROPERTIES

VA. Channel Gating

CNG channels are very sensitive detectors of the local concentration of cyclic nucleotides and they appear designed to work in the physiological concentration range of their respective agonists. Dose-response curves (e.g. Fig. 35.4) for activation of rod channels by cGMP give half-saturating concentrations ($K_{1/2}$ values) ranging from about 5 to 100 μM, which is within the expected physiological concentration range. The rather wide range of values of $K_{1/2}$ may reflect functional modulation of the channels by other factors (see Section VI).

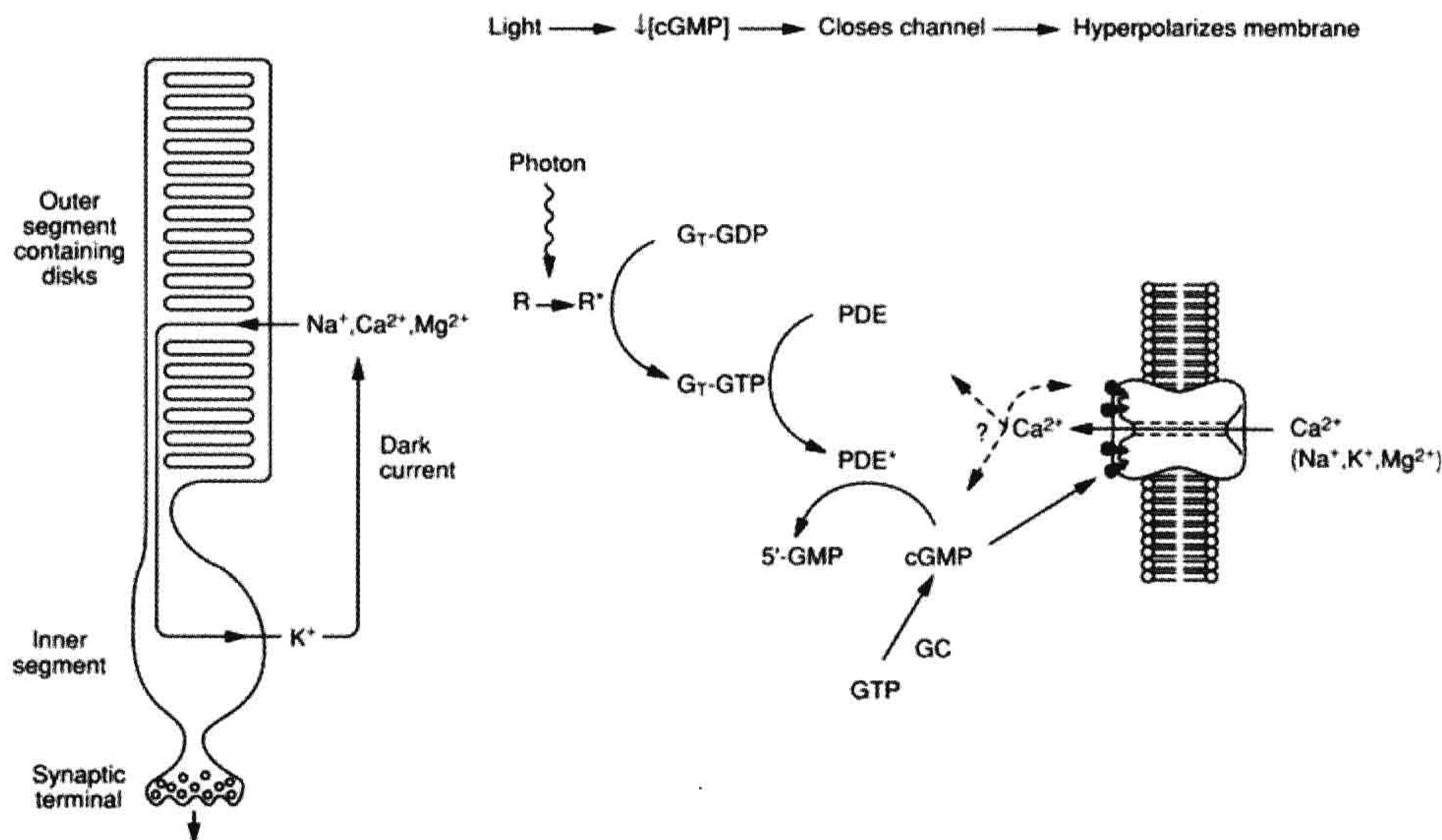


FIGURE 35.2 The cyclic nucleotide cascade controlling CNG channels in rods. R, R*, rhodopsin in its inactive and active forms, respectively. G_T, G protein ("Transducin"), bound to either GDP or GTP. PDE, PDE*, phosphodiesterase in its inactive and active forms, respectively. GC, guanylate cyclase. Calcium ions entering through the CNG channels are thought to modulate the function of several players in the cascade, including the channels themselves. A similar cascade operates in cones.

The form of the dose–response curve is well-described by the Hill equation:

$$\frac{r}{r_{max}} = \frac{[\text{cGMP}]^n}{K_{1/2}^n + [\text{cGMP}]^n}$$

where r is the response to cGMP (e.g. the cGMP-activated component of the membrane current measured in a patch-clamp experiment), r_{max} is the maximum response (obtained with a saturating concentration of cGMP to activate all channels in the patch) and n is the Hill coefficient. Reported Hill coefficients have ranged between about 1.5 and 4, suggesting that several molecules of cGMP typically bind to each channel to open it. As discussed later, a channel seems to consist of four subunits, each with a cyclic nucleotide binding site (reviewed in Bradley et al., 2005; Craven and Zagotta, 2006; Biel, 2009). Because the dose–response curve for channel activation is so steep, small changes in the concentration of cAMP or cGMP produce very large changes in channel open probability. Furthermore, unlike most ligand-gated ion channels, CNG channels do not desensitize in the continued presence of agonist (reviewed in Mazzolini et al., 2010).

Activation of olfactory CNG channels is similar to that of rod and cone channels except for relative cyclic nucleotide sensitivities and efficacies. Rod and cone channels are much less sensitive to cAMP than to cGMP, with a $K_{1/2}$ for activation by cAMP of about 1.5 mM. Native olfactory CNG channels are more sensitive to both cyclic nucleotides than are photoreceptor channels, but they are only two to five times more sensitive to cGMP than to cAMP, with most $K_{1/2}$ values for activation by cGMP in the range of 1 to 5 μM (and a few as high as 20 μM; see Nakamura and Gold, 1987). Furthermore, cAMP acts as only a partial agonist for the rod channel: even at saturating concentrations, it gives only a fraction of the open probability obtained with saturating cGMP (see Fig. 35.4). However, both cAMP and cGMP are full agonists for the olfactory channel. This difference in agonist efficacy can be explained by assuming that cGMP is a more effective agonist than cAMP for both channels, and that after agonist binding, the olfactory channel opens more easily than does the rod channel (i.e. the olfactory channel's opening conformational change is more energetically favored) (Gordon and Zagotta, 1995). Interestingly, HCN channels prefer cAMP to cGMP by about a factor of ten (reviewed in Craven and Zagotta, 2006).

Although some voltage-activated channels (e.g. HCN and Eag-like K^+ channels) are regulated by cyclic nucleotides, channels that are primarily activated by cyclic

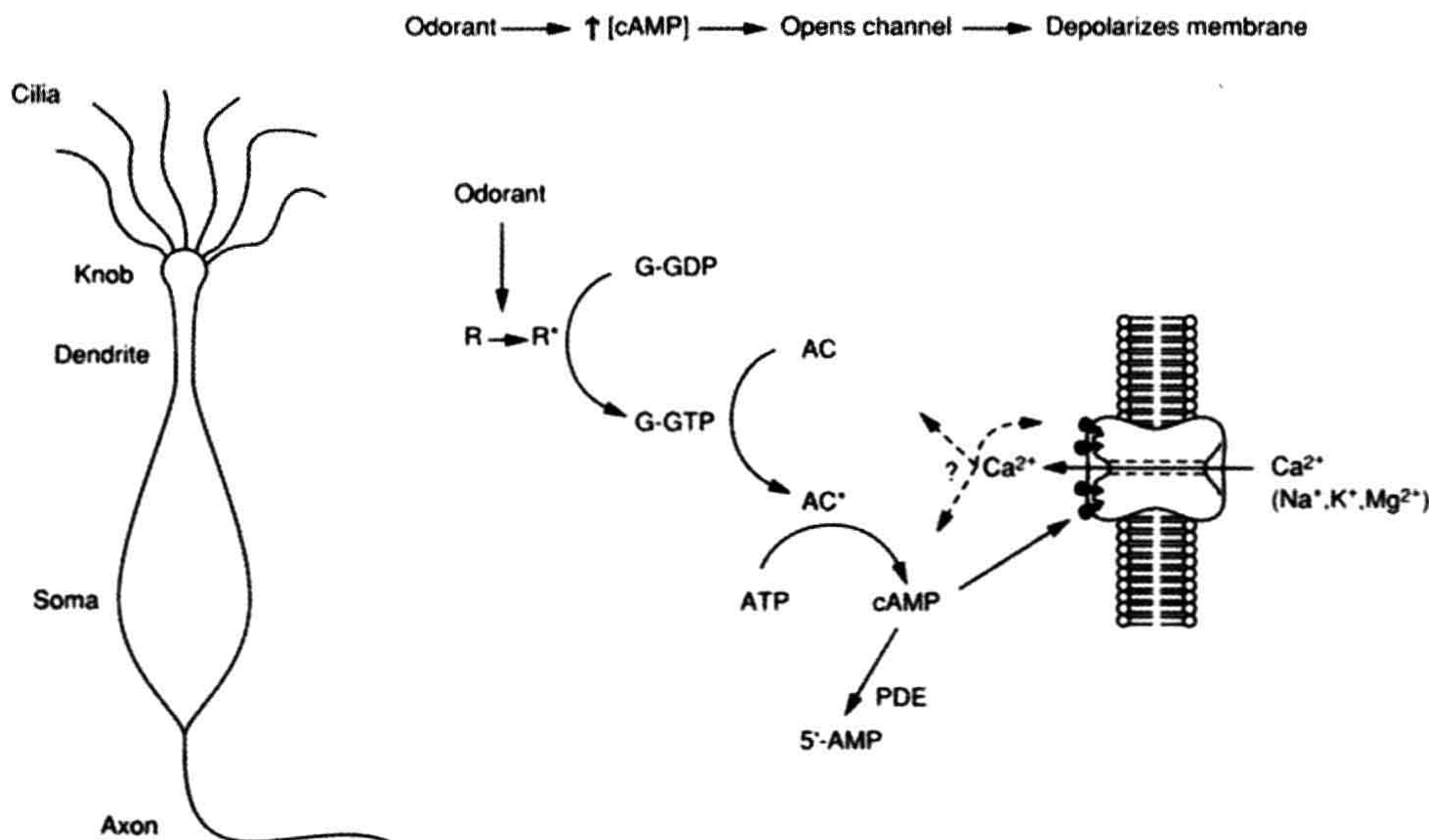


FIGURE 35.3 The cyclic nucleotide cascade controlling CNG channels in olfactory cells. R, R*, odorant receptor in its inactive and active (odorant-bound) forms, respectively. G, G protein, bound to either GDP or GTP. AC, AC*, adenylate cyclase in its inactive and active forms, respectively. PDE, phosphodiesterase. Here, as in photoreceptors, entering Ca^{2+} appears to modulate the cascade, including the CNG channels. The Ca^{2+} that enters through the CNG channels also opens Ca^{2+}-activated Cl^- channels (not shown), which further depolarize the cell.

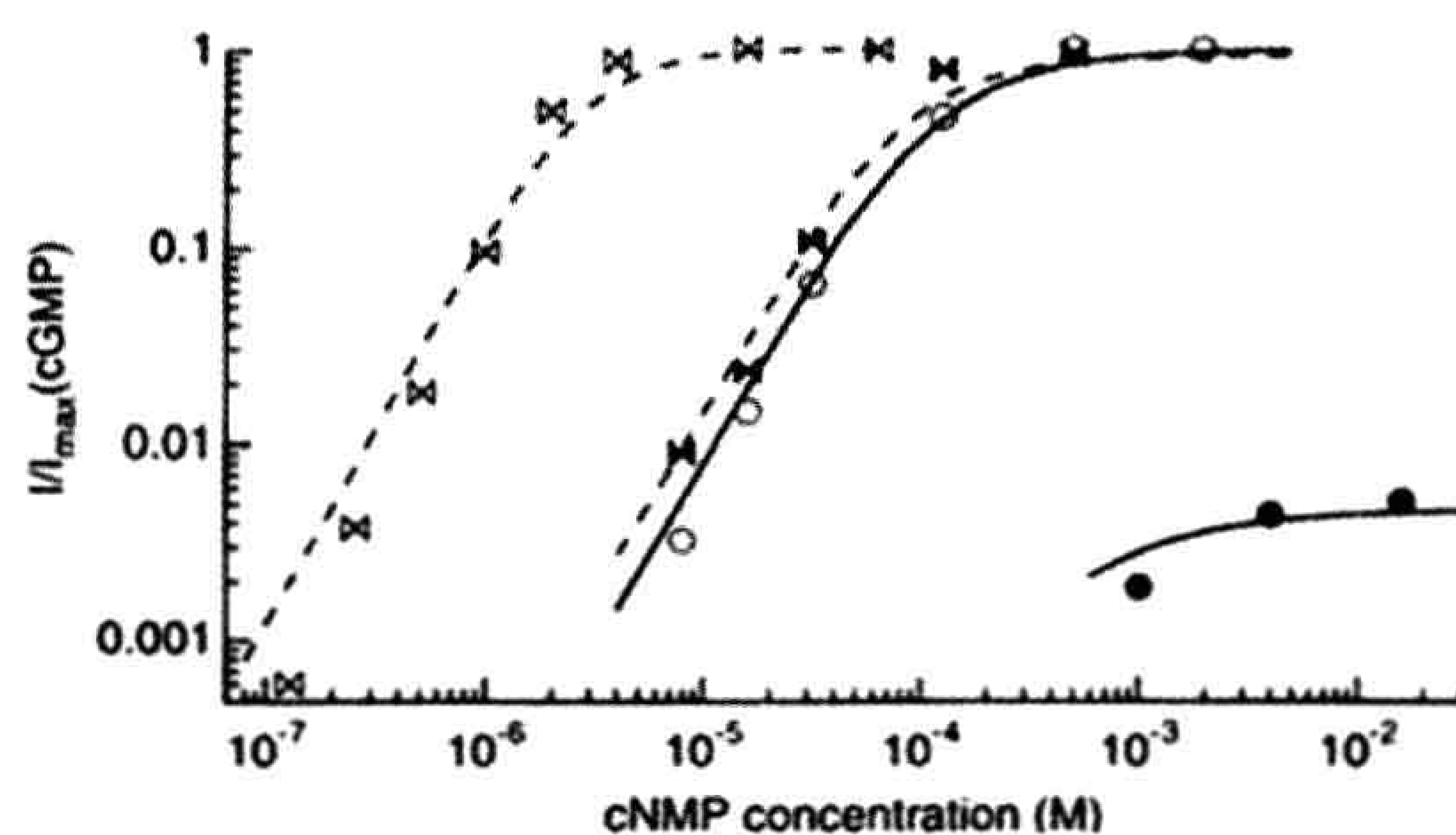


FIGURE 35.4 Dose–response curves for activation of cloned rod (circles) and olfactory (bows) α-homomultimeric channels. Both CNG channels show a higher apparent affinity (lower $K_{1/2}$) for cGMP (open symbols) than for cAMP (filled symbols), but for the rod channel cAMP appears to be a partial agonist, giving only a fraction of the current produced by a saturating concentration of cGMP. The smooth and dashed curves were calculated using a model in which the only difference between the results with cGMP and those with cAMP is that cGMP more effectively triggers the opening conformational change of the channels after it is bound. Currents were measured in response to voltage pulses of +100 mV from a holding potential of 0 mV and normalized to the current obtained in saturating cGMP (I_{max}). *(Reproduced with permission from Gordon and Zagotta, 1995. Copyright 1995 Cell Press.)*

nucleotides (CNG channels) are only weakly voltage dependent, with no voltage-dependent inactivation. In current–voltage (I-V) relations from excised patches, the voltage dependence of CNG channel gating is most obvious at low cyclic nucleotide concentrations, where it introduces significant non-linearity (e.g. see Fig. 35.7D). High concentrations of cyclic nucleotides overcome the voltage dependence of gating, driving the channels (by mass action) toward high open probabilities at all voltages and linearizing the I-V curves. Note, however, that much of the CNG channel rectification seen in intact cells probably results from voltage-dependent channel block by Ca^{2+} and Mg^{2+}, as discussed in Section VB below. The end result of both forms of non-linearity is that current is relatively independent of voltage in the physiological voltage range (for rods and cones, this would be about −40 to −80 mV). Thus, sensory CNG channels are able to transduce their stimulus faithfully in the face of changes in membrane potential that originate at either the transducing region or elsewhere in the cell, where there are many kinds of voltage-dependent ion channels.

Since CNG channels have voltage-sensing S4 segments, it is surprising that they have only very weak voltage

sensitivity. It has been proposed that glutamate residues in the vicinity of S4 contribute negative charges that may neutralize the effects of the positively-charged arginine and lysine residues of S4 that are thought to confer voltage sensitivity to the channel (Wohlfart et al., 1992; Tang and Papazian, 1997). Perhaps even more surprising is the fact that HCN channels, which also have S4 regions, have a voltage dependence that is the opposite of that found in most other voltage-dependent channels – HCN channels are activated by hyperpolarization, rather than by depolarization. Like CNG channels, most HCN channels do not inactivate with voltage. The one known exception is the spHCN channel from sea urchin sperm, which inactivates in the absence of cAMP (reviewed in Kaupp and Seifert, 2002; Hofmann et al., 2005; Craven and Zagotta, 2006; Biel and Michalakis, 2009).

Single-channel studies demonstrate that CNG channels have particularly fast open-shut transitions in the native membrane. This flickery behavior is striking in the cell-attached and excised-patch recordings obtained from toad rods by Matthews and Watanabe (1987) (Fig. 35.5).

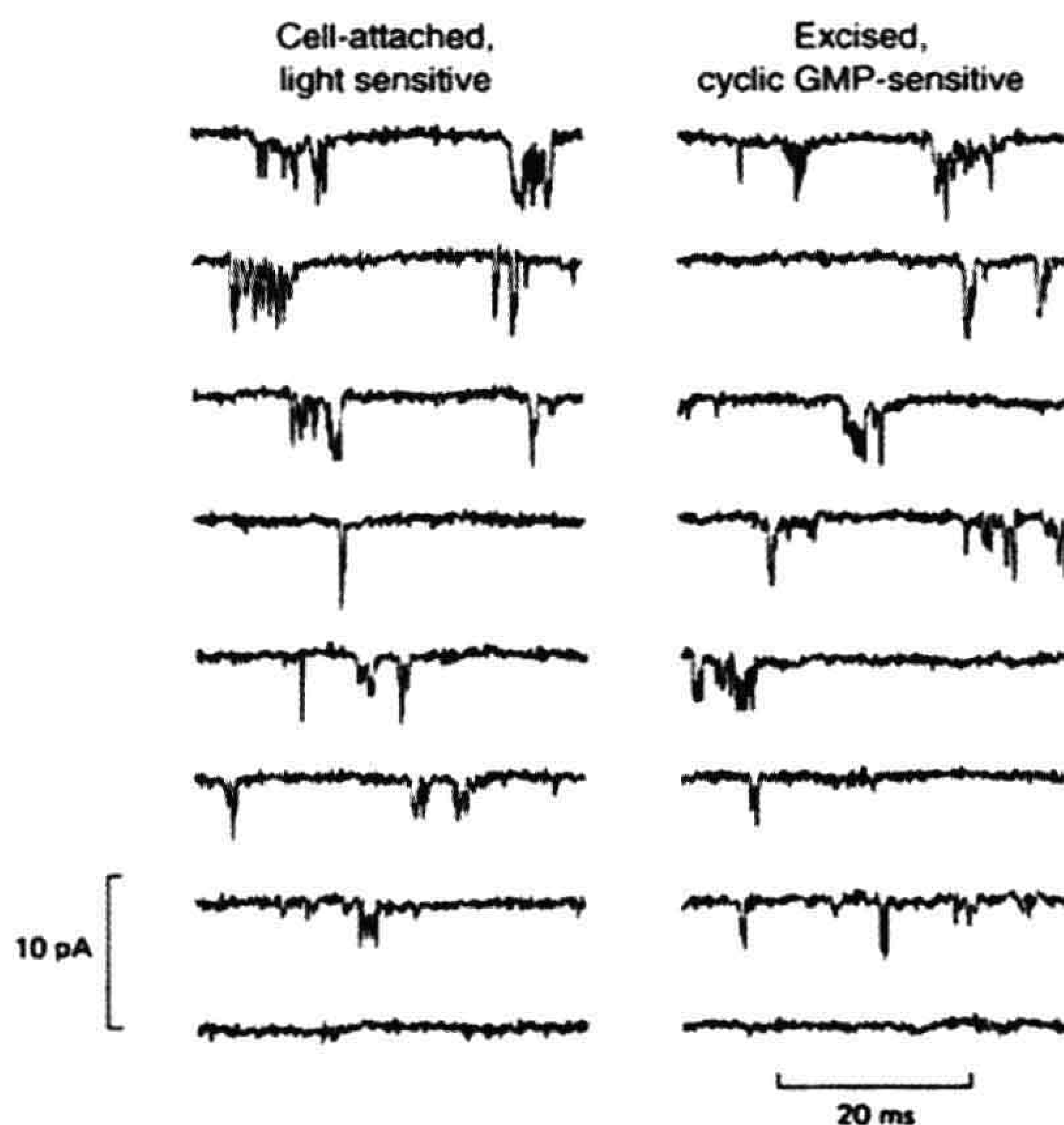


FIGURE 35.5 Single-channel recordings of CNG channels in native rod outer segment membranes demonstrate such rapid gating kinetics that many open-shut transitions are poorly resolved. Channel openings give downward deflections; holding potential −148 mV. Left: cell attached patch from toad rod outer segment; the bottom trace was obtained in a saturating light and all others in darkness. To prevent channel block, the pipette was filled with a solution lacking Ca^{2+} and Mg^{2+}. Right: the same patch after excision, with the intracellular surface bathed in either no cGMP (bottom trace) or 10 μM cGMP (all other traces); both pipette and bathing solutions lacked Ca^{2+} and Mg^{2+}. *(Reproduced with permission from Matthews and Watanabe, 1987.)*

However, when purified and reconstituted, or cloned and heterologously expressed, the channels were initially found to have much slower gating kinetics that are more typical of many other ion channels. Although Ca^{2+} and Mg^{2+} produce flicker block of these channels, the flickery gating behavior persists even in the absence of these ions. Furthermore, the transitions are too fast to reflect the binding and unbinding of cyclic nucleotides and they also apparently do not simply reflect block by protons. Accumulated evidence suggests that the flickery gating pattern of the native rod CNG channel results partly from the presence of a second channel subunit that was missing in the original reconstitution and expression studies, in which only one kind of subunit was identified (see Section VI below). This additional subunit also gives the channel its characteristic sensitivity to L-*cis*-diltiazem. Unlike the α subunit, the β subunit (also called *subunit 2*) does not produce cyclic nucleotide-activated currents when expressed alone.

For the olfactory channel, a second subunit (CNGA4, previously called r0CNC2) not only gives more flickery gating kinetics, but also increases the apparent affinity for cyclic nucleotides, giving more channel activity at low cyclic nucleotide concentrations (Fig. 35.6) (Bradley et al., 1994; Linman and Buck, 1994). Like the rod β subunit, this subunit also does not appear to produce cyclic nucleotide-activated currents when expressed alone. However, it is possible to obtain currents by treating the channel with nitric oxide (reviewed in Broillet and Firestein, 2004). With both rod and olfactory CNG channels, there still seem to be discrepancies between the behavior of the channels in vivo and in expression systems. Some of these differences may result from effects of channel modulators (see Section VI).

Although there remains disagreement over the detailed mechanism of activation (reviewed in Craven and Zagotta, 2006), it is clear that CNG channels can open with fewer than four ligands bound, but have highest open probabilities with all four sites occupied. Some studies suggest that a channel gate resides with the pore, at or near the selectivity filter (Karpen et al., 1993; Contreras et al., 2008). Certain mutations in this region switch the channel from ligand gated to voltage gated (Martinez-Francois et al., 2009). Innovative methods have been very useful in dissecting the molecular mechanism of gating. These include: covalent activation (reviewed in Kaupp and Seifert, 2002), polymer-linked cGMP dimers (reviewed in Brown et al., 2006), chimeras of different channel types (e.g. Gordon and Zagotta, 1995) and the use of modulatory substances, such as Ni^{2+}, to discern subunit interactions (reviewed in Kaupp and Seifert, 2002).

The cyclic nucleotide binding domain (CNBD) in HCN channels is thought to function as an autoinhibitory domain, causing the channel to require relatively large

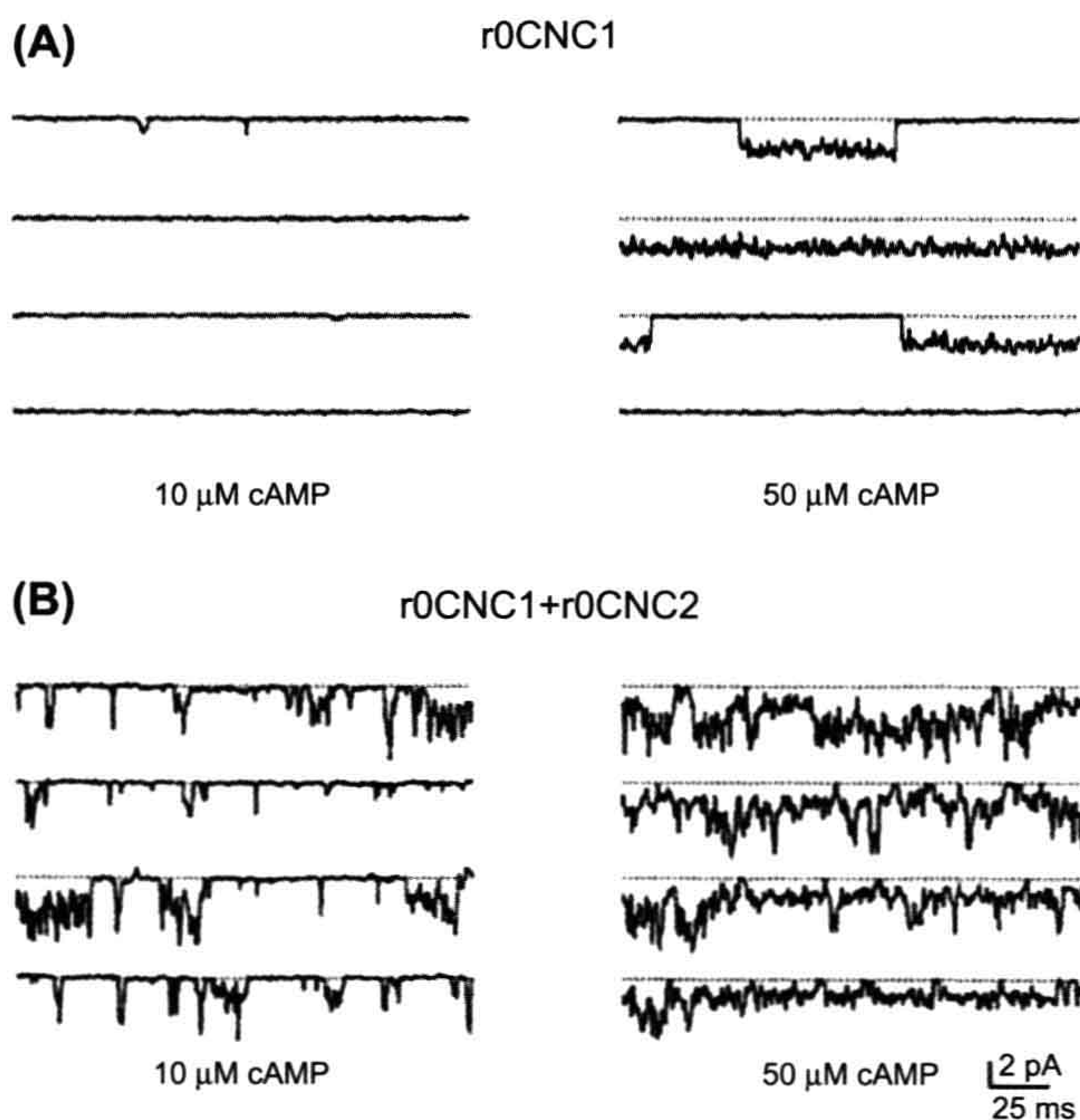


FIGURE 35.6 Increased cAMP sensitivity and flickery gating produced by co-expressing the second olfactory CNG channel subunit (rOCNC2; now called CNGA4) with the first (rOCNC1; now called CNGA2). When the first subunit is expressed alone (A) there are very few channel openings in 10 μM cAMP and the openings with 50 μM cAMP are much less flickery than those seen in (B), where both subunits are expressed in the same cell. Holding potential is −80 mV. *(Reproduced with permission from Liman and Buck, 1994. Copyright 1994 Cell Press.)*

negative voltages to activate (reviewed in Biel, 2009; Wahl-Schott and Biel, 2009). The binding of cAMP to the CNBD relieves that inhibition, allowing the channel to open at less negative voltages. The binding of cAMP also accelerates channel opening, leading to a steeper upstroke in the SA node action potential. Another function of cAMP in the SA node cells is activation of cAMP-dependent protein kinase, which phosphorylates voltage-dependent Ca^{2+} channels, facilitating their opening and further contributing to the increased frequency of SA node action potentials.

VB. Permeation, Selectivity and Block

CNG channels are relatively non-selective cation channels with no significant anion permeability. Thus, reversal potentials for most CNG channels studied under normal ionic conditions are about +5 to +20 mV. The monovalent alkali cation permeability sequence for the rod channel has been reported to be $Li^+ \geq Na^+ \geq K^+ \geq Rb^+ \geq Cs^+$ and Ca^{2+} and Mg^{2+} ions appear to be more permeant than the monovalent cations (reviewed in Kaupp and Seifert, 2002).

Cone and olfactory CNG channels also poorly discriminate among monovalent alkali cations, although their exact permeability sequences and ratios are not identical to those of the rod CNG channel. Strict comparisons are difficult because there is some variability in reported permeability ratios for each channel type. Relative permeabilities obtained may depend on whether the channels are studied in the intact cell, in excised patches, or in reconstitution or expression systems. The permeabilities may also depend on intracellular factors controlling functional modulation of the channels (see Section VI). In intact rods, the relative currents carried by monovalent and divalent cations have been found to depend on the concentration of cGMP (reviewed in Kaupp and Seifert, 2002). This finding, along with the dependence of subconductance states on cGMP (see below), suggests that the functional properties of CNG channels may change with the number of ligand molecules bound. If so, this may reflect a very interesting feature of these channels and one with tremendous potential for modifying physiological responses.

HCN channels differ from CNG channels in being significantly more selective for K^+ over Na^+ and having much lower Ca^{2+} permeability. Consistent with this high K^+ selectivity, the pore of an HCN channel contains the amino acid sequence, GYG (glycine-tyrosine-glycine) that is the hallmark of K^+-selective channels. Nevertheless, under physiological conditions (i.e. physiological concentration gradients and membrane potential), the main ion flowing through these channels is Na^+. Thus, under normal conditions, the opening of HCN channels, like that of CNG channels, produces a membrane depolarization.

Under physiological conditions, the rod CNG channel is occupied by Ca^{2+} or Mg^{2+} most of the time and these ions prevent the passage of Na^+ and K^+, which pass through the pore much more rapidly. Thus, these divalent cations behave as "permeant blockers". As a result of the very slow transport rate of the divalent cations, the mean single-channel conductance is extremely low – only about 0.1 pS in rods studied under physiological conditions. The channels can be blocked from either side but, under physiological conditions, they are mostly blocked by extracellular Ca^{2+} and Mg^{2+}. To resolve single-channel currents, one must reduce the concentration of divalent cations to the micromolar range. In the absence of divalent cations, the single-channel conductance is as high as tens of picosiemens. The extremely low single-channel conductance in physiological solutions gives an excellent signal-to-noise ratio for photon detection by rods, since the random openings and closings of individual channels produce only very tiny fluctuations in the dark current. The absorption of a single photon elicits the closure of hundreds of channels, giving a smooth, stereotypical waveform. If all those channels had single-channel conductances in the range of tens of picosiemens, the rod cell would have to contend with the consequences of a huge influx of Na^+ and Ca^{2+}. Cones and olfactory cells would have a similar problem, since their transducing regions also contain many CNG channels.

In the absence of divalent cations, *I-V* relations for CNG channels (with saturating cyclic nucleotide concentrations) are linear or nearly so (Fig. 35.7A and D, upper curve). Divalent cations introduce extreme non-linearity in the *I-V* relations (Fig. 35.7B and C). When the rod channel is studied in the presence of physiological concentrations of divalent cations, its *I-V* relation is very outwardly rectified.

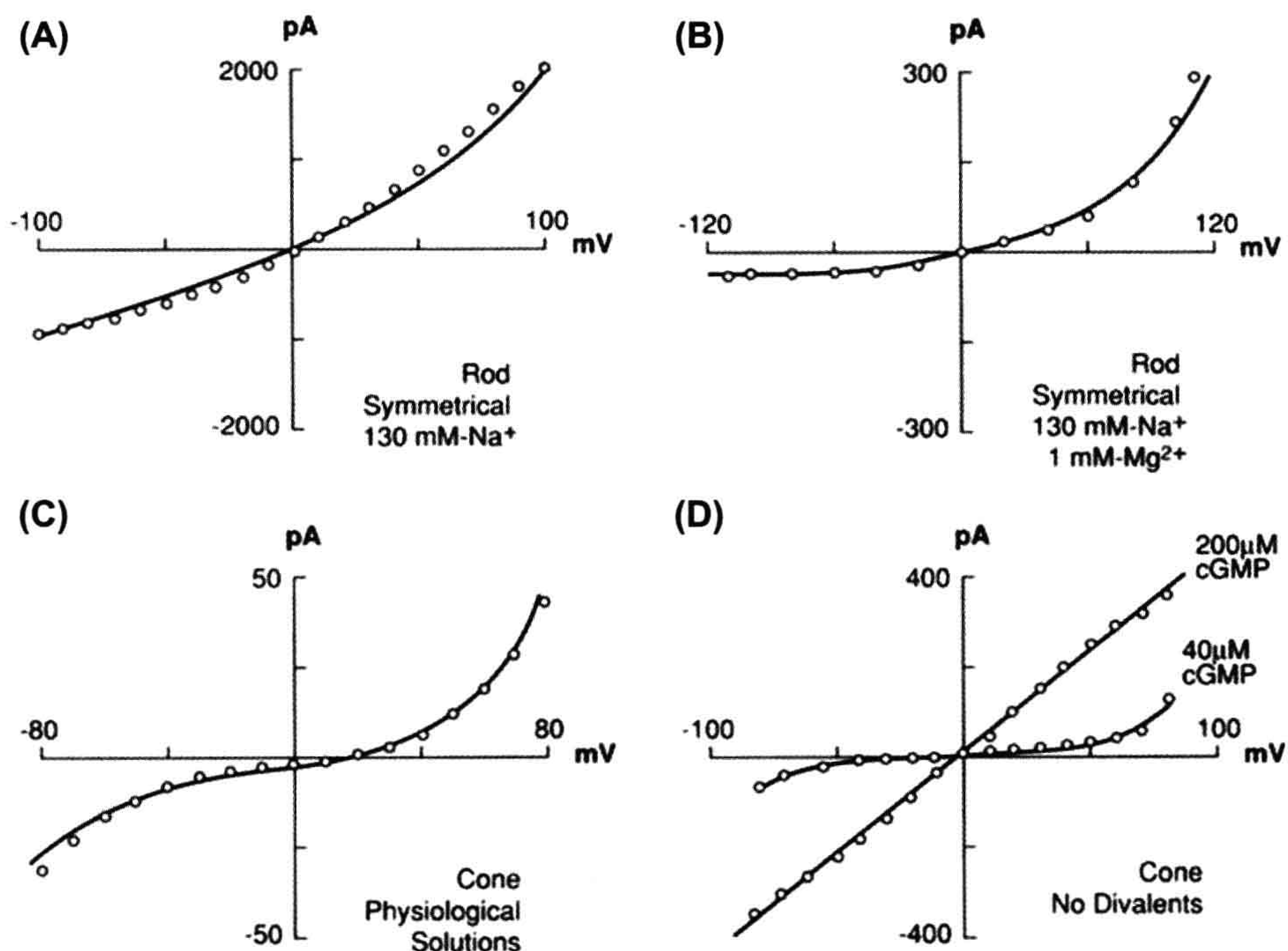


FIGURE 35.7 Current-voltage relations for photoreceptor cyclic GMP-activated currents from multichannel, excised patches. (A) The rod CNG channel relation is almost linear with saturating [cGMP] and no divalent cations. Olfactory CNG channels demonstrate a similar relation (not shown). (B) The addition of millimolar Mg^{2+} to both sides of the membrane gives strong outward rectification. Similar outward rectification has been reported for olfactory CNG channels. (C) Cone CNG channels show both outward and inward rectification in the presences of physiological (millimolar) levels of Mg^{2+} and Ca^{2+}. (D) The *I-V* relation for cone CNG channels is approximately linear with saturating [cGMP] and no divalent cations (top curve). Decreasing [cGMP] produces a non-linear *I-V* relation (bottom curve), because gating is slightly voltage dependent. Voltage-dependent gating of rod CNG channels also produces a very non-linear *I-V* relation [resembling that in (B)] in the absence of divalent cations, at low [cGMP]. *(Redrawn with permission from Zimmerman and Baylor, 1992 (A) and (B); from* Nature, *Haynes and Yau, 1985, Copyright 1985 Macmillan Magazines Limited (C); and Picones and Korenbrot, 1992 (D) Reproduced from The Journal of General Physiology, 1992, 100, 647–673, by copyright permission of The Rockefeller University Press.)*

Although some of this rectification is a consequence of the weak voltage dependence of channel gating described earlier, much of it results from channel block by Ca^{2+} and Mg^{2+}. Thus, at negative membrane potentials in the physiological range (about −40 to −80 mV), external Ca^{2+} and Mg^{2+} are drawn into the pore, reducing Na^{+} entry and giving an approximately flat *I-V* relation over a wide range of voltage. This very low, voltage-independent conductance in the physiological voltage range allows light-triggered outer segment voltage changes to travel relatively unattenuated to the inner segment to regulate synaptic transmission and also prevents the outer segment photon-sensing mechanism from fluctuating with voltage.

I-V relations of the olfactory channel, with and without divalent cations, are essentially indistinguishable from those of the rod channel, but surprisingly, the *I-V* relation for the cone channel is rather different. Whereas cone *I-V* curves from excised patches are linear in the absence of divalent cations, they are almost S-shaped when divalents are present (see Fig. 35.7C). Although the functional significance of this difference between cone CNG channels and those in rod cells and olfactory receptors is not clear, structurally, it may reflect a different location of the dominant ion-binding site within the cone channel. At subsaturating concentrations of cyclic nucleotides (which are closer to the physiological concentrations), the cone channel *I-V* relation is much more flat in the physiological range of membrane potential even in the absence of divalent cations (see Fig. 35.7D, lower curve). Similarly, the rod channel *I-V* curve shows increasing outward rectification as the cGMP concentration is lowered (not shown).

Single-channel recordings of the rod CNG channel in the absence of divalent cations have revealed at least two conductance states: one of about 25 to 30 pS and the other with a conductance about one-third as large. However, it has been suggested that the channel has at least one more, and perhaps many more, conductance levels. Because of the extremely rapid gating kinetics of this channel, numerous open-closed transitions are no doubt unresolved in the single-channel records. Thus, it is difficult to determine the exact number of distinct conductance states. It is also not clear whether these states are characterized by truly different ion transport rates or merely by different (incompletely resolved) open times, giving the appearance of different conductance levels. In the absence of divalent cations, the olfactory and cone CNG channels demonstrate major single-channel conductances around 45 to 50 pS, also with apparent subconductance states. Some results suggest a switching of the rod CNG channel from low to high conductance states with increasing ligand occupancy (reviewed in Kaupp and Seifert, 2002). The single-channel conductance of HCN channels is currently unresolved because there is a wide range of reported values — from 1 to 30 picoseimens. This large variability probably reflects variation in recording methods and types of cellular preparations (reviewed in Wahl-Schott and Biel, 2009).

Many pharmacological agents have been tested on CNG and HCN channels. Since CNG channels have a strong affinity for Ca^{2+}, various calcium channel blockers, such as verapamil and diltiazem, have been tested. Most block only weakly or not at all, but a few (e.g. L-*cis*-diltiazem and an amiloride analogue, 3′,4′-dichlorobenzamil) have been found to block effectively from the cytoplasmic surface of the membrane, with K_i values in the micromolar range. CNG channels also have been found to be blocked by a variety of other pharmacological agents (reviewed in Brown et al., 2006), but none have been found to bind with sufficient affinity and specificity. This also has been true for pharmacological agents against HCN channels, where the focus often has been K^{+} channel blockers.

VI. MOLECULAR STRUCTURE

Although CNG channels are ligand-gated channels, their molecular structures place them in the superfamily of voltage-gated cation channels, along with the HCN channels. The members of this family are characterized by a repeating structural motif, like that shown in Fig. 35.8, containing six putative membrane-spanning segments,

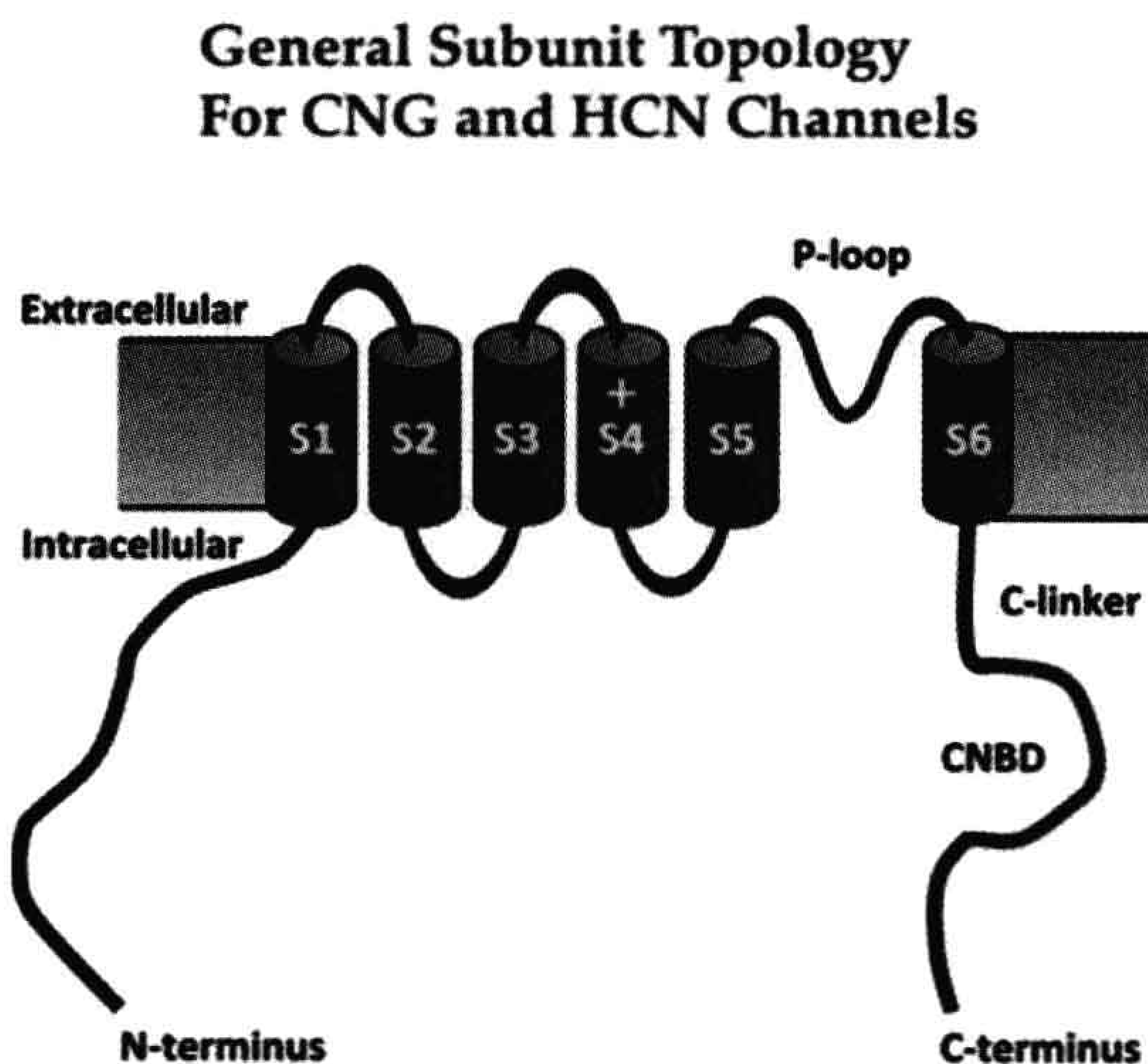


FIGURE 35.8 A model for the general organization of a CNG or HCN channel subunit. The model is based on information from many studies. Like typical voltage-gated K^{+} channel subunits, CNG channels are characterized by intracellular N- and C-termini, six transmembrane segments (S1−S6) and a region called the P-loop that lies between S5 and S6 and forms the selectivity filter through which ions pass. Cyclic nucleotide monophosphates, like cAMP and cGMP, bind in the cyclic nucleotide binding domain (CNBD) of the intracellular C-terminus. The C-linker region is thought to connect cyclic nucleotide binding at the CNBD to the allosteric opening transition involving movement of S6.

located between the hydrophilic N- and C-terminal regions that project into the cytosol. Also characteristic of these channels is a putative pore region (P-region) and an S4 transmembrane segment that contains many basic residues and is thought to be a voltage-sensing region. Of course, the channel region that best distinguishes CNG and HCN channels from a typical voltage-gated cation channel is the C-terminal cyclic nucleotide binding domain (CNBD), which resembles that found in other cyclic nucleotide-regulated proteins (e.g. cGMP-dependent protein kinase). A region often referred to as the C-linker, that connects the CNBD with the last transmembrane segment (S6), has been proposed functionally to link the cyclic nucleotide binding event to the allosteric opening transition of the channel (reviewed in Craven and Zagotta, 2006).

When the first subunit of the bovine rod CNG channel was cloned, the channel was proposed to consist of multiple identical subunits, each with a cGMP-binding site located in the C-terminal region. It now seems clear that the rod channel is a tetramer consisting of α and β subunits (CNGA1 and CNGB1, respectively; reviewed in Hofmann et al., 2005) and that there is a variety of other subunits that can associate to form functional CNG channels. The following subunit types have been identified in vertebrates: CNGA1, CNGA2, CNGA3, CNGA4, CNGA5, CNGB1 and CNGB3. The most recent addition to the list is CNGA5, which so far has only been found in the brain and pituitary of the zebrafish (Tetreault et al., 2006; Kahn et al., 2010). Functional homomeric channels can be made from all α subunits except CNGA4, but not from any β subunits. The subunit stoichiometry that has been proposed for rod, cone and olfactory CNG channels is as follows: in rods, three CNGA1s and one CNGB1; in cones, two CNGA3s and two CNGB3s; and in olfactory receptor cells, two CNGA2s, one CNGA4 and one CNGB1b (an alternatively spliced variant of CNGB1) (reviewed in Zimmerman, 2002; Bradley et al., 2005). Subunit stoichiometry and order remain to be determined for CNG channels in other cell types.

The known vertebrate HCN subunit types are HCN1, HCN2, HCN3 and HCN4. Each type has been found to form functional homomeric channels. Although some combinations have been identified in specific tissues and species (e.g. the rabbit heart SA node contains heteromeric channels that consist of HCN1 and HCN4), the subunit stoichiometries and arrangements have not been determined in any preparation. Outside the vertebrate world, an interesting HCN channel from sea urchin sperm (spHCN) has unusual gating properties that have provided some recent insights into voltage-dependent activation of HCN channels (reviewed in Wahl-Schott and Biel, 2009).

In addition to having two types of subunits, the rod CNG channel is part of a larger molecular complex. The rod β subunit (CNGB1) contains a very long glutamic acid-rich peptide (GARP) near its N-terminus. This GARP region connects with structural molecules on the rod cell's disk rims (see Chapter 38), giving it a potential role not only in channel function, but also in the structural stability and development of the rod cell and its internal disks. Free GARP molecules also have been found to inhibit the rod CNG channel (Michalakis et al., 2011). Furthermore, the rod CNG channel α subunits (CNGA1s) are tightly associated with Na^+:Ca^{2+},K^+ exchange carriers (see Chapter 38). The nature of the interactions of the rod CNG channel with these other molecules, and their functional consequences, are still under investigation.

There are currently no available crystal structures of an entire CNG or HCN channel. However, the CNBD has been crystallized for HCN2 and for a bacterial CNG channel, MloK1 (Zagotta et al., 2003; Schünke et al., 2011; reviewed in Craven and Zagotta, 2006). Although these structures have provided important information, numerous structural questions remain to be answered for both CNG and HCN channels, especially since crystal structures are static and since the CNBDs in those structures were disconnected from other channel regions. For example, despite extensive structure—function research, we still know only a few of the molecular details regarding interactions between subunits and between N- and C-terminal domains. In olfactory CNG channels, the latter interaction seems to be autoexcitatory and is disrupted by Ca^{2+}-calmodulin, which strongly inhibits channel opening (reviewed in Trudeau and Zagotta, 2003). It is also not known why the rod CNG α subunit is post-translationally cleaved *in vivo*, so that before its insertion into the rod membrane its molecular weight is reduced from 78 kilodaltons to 63 kilodaltons, with the loss of the end of its N-terminal tail (reviewed in Kaupp and Seifert, 2002). It also is not known exactly what structural changes occur in converting the binding of cyclic nucleotide at the C-terminus to the opening of the channel, how the selectivity filter is involved in this, or how the action of channel modulators (see following) is structurally linked to changes in channel gating. Finally, the nature of the regulation of HCN channels by cyclic nucleotides remains a mystery: although all HCN subunits have CNBDs, cAMP has a large effect on HCN2 and HCN4, but very little effect on HCN1 and HCN3. Mutational studies suggest this difference may be explained by the presence or absence of some type of "silencing" region outside the CNBD (reviewed in Wahl-Schott and Biel, 2009).

VII. FUNCTIONAL MODULATION

New information suggests that CNG channels may be modulated in ways that are only beginning to be elucidated. As mentioned above, there are hints that the ionic selectivity of the rod CNG channel may vary with the amount of cyclic nucleotide bound. There is also now evidence that the cGMP sensitivity of the rod channel may be tuned up or

down by phosphorylation and reduced by calmodulin in the presence of Ca^{2+} (reviewed in Kaupp and Seifert, 2002). It has not been determined whether other channel properties are also altered by these modulators. Protons modulate the rod CNG channel, increasing its open probability, while reducing its single-channel conductance (Gavazzo et al., 1997). Transition metal divalent cations, such as Ni^{2+}, also modulate CNG channel gating (reviewed in Kaupp and Seifert, 2002); interestingly, 10 μM Ni^{2+} increases the open probability of the rod channel, but decreases the open probability of the olfactory channel. Higher concentrations of Ni^{2+} block the pores of both rod and olfactory channels. Finally, there is mounting evidence that, in rods, the CNG channel interacts with Na^+:Ca^{2+},K^+ exchange carriers (see Chapter 38). The detailed functional significance of this interaction remains to be determined but, at the very least, it would allow the Ca^{2+} that enters through the CNG channels to be expelled more rapidly than if this tight association did not exist. Functional modulation of the rod CNG channel may help explain the large variability in reported cGMP affinity and cooperativity and may play a role in some aspects of visual transduction.

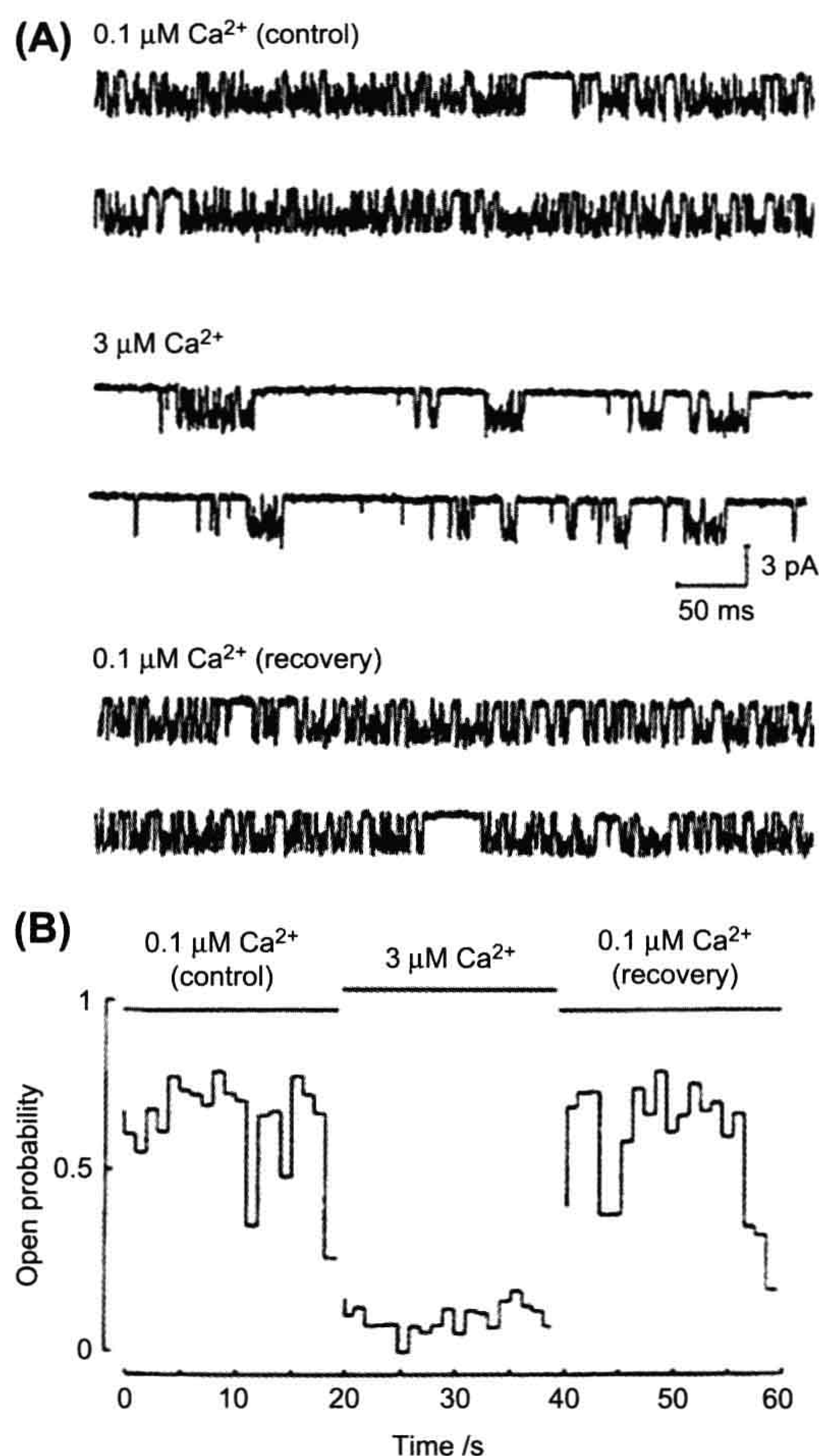


FIGURE 35.9 Modulation of an olfactory CNG channel by Ca^{2+}. Raising the Ca^{2+} concentration from 0.1 to 3 μM at the intracellular surface of an excised patch produced a reversible increase in channel closed time, resulting in a decrease in channel open probability. The cAMP concentration was 100 μM and the holding potential was −60 mV. Channel opening gives a downward deflection in current. *(Reproduced with permission from Zufall et al., 1991.)*

The gating of olfactory CNG channels has been found to be dramatically modulated by intracellular Ca^{2+}. Fig. 35.9 (Zufall et al., 1991) shows single-channel recordings obtained from an excised patch of olfactory dendritic membrane. When the concentration of Ca^{2+} bathing the intracellular surface of the patch was increased from 0.1 to 3 μM, there was a striking increase in channel closed time, giving a decrease in open probability. This modulation also has been found to involve calmodulin and, possibly, an endogenous Ca^{2+} binding protein distinct from calmodulin (reviewed in Pifferi et al., 2006 and Chapter 39). Research on cloned olfactory CNG channels suggests this inhibition results from disruption of an autoexcitatory interaction between the channel's N- and C-termini (reviewed in Trudeau and Zagotta, 2003).

HCN channels have been found to be modulated by a variety of factors, including protons, phosphoinositides, phosphorylation enzymes and Cl^-. These channels also appear to be regulated by interactions with a variety of proteins, including scaffolding proteins and other auxiliary proteins. Evidence suggests that such functional regulation of HCN occurs within elaborate intracellular molecular complexes (reviewed in Wahl-Schott and Biel, 2009).

BIBLIOGRAPHY

Barnstable, C. J., Wei, J. Y., & Han, M. H. (2004). Modulation of synaptic function by cGMP and cGMP-gated cation channels. *Neurochem Int, 45*, 875–884.

Biel, M. (2009). Cyclic nucleotide-regulated cation channels. *J Biol Chem, 284*, 9017–9021.

Biel, M., & Michalakis, S. (2009). Cyclic nucleotide-gated channels. *Handb Exp Pharmacol, 191*, 111–136.

Bradley, J., Li, J., Davidson, N., Lester, H. A., & Zinn, K. (1994). Heteromeric olfactory cyclic nucleotide-gated channels: α subunit that confers increased sensitivity to cAMP. *Proc Natl Acad Sci USA, 91*, 8890–8894.

Bradley, J., Reisert, J., & Frings, S. (2005). Regulation of cyclic nucleotide-gated channels. *Curr Opin Neurobiol, 15*, 343–349.

Broillet, M.-C., & Firestein, S. (2004). Cyclic nucleotide-gated channels: multiple isoforms, multiple roles. *Adv Mol Cell Biol, 32*, 251–267.

Brown, R. L., Strassmaier, T., Brady, J. D., & Karpen, J. W. (2006). The pharmacology of cyclic nucleotide-gated channels: emerging from the darkness. *Curr Pharm Des, 12*, 3597–3613.

Contreras, J. E., Srikumar, D., & Holmgren, M. (2008). Gating at the selectivity filter in cyclic nucleotide-gated channels. *Proc Natl Acad Sci USA, 105*, 3310–3314.

Craven, K. B., & Zagotta, W. N. (2006). CNG and HCN channels: two peas, one pod. *Annu Rev Physiol, 68*, 375–401.

Cukkemane, A., Seifert, R., & Kaupp, U. B. (2011). Cooperative and uncooperative cyclic-nucleotide-gated ion channels. *Trends Biochem Sci, 36*, 55–64.

DiFrancesco, D. (2010). The role of the funny current in pacemaker activity. *Circ Res, 106*, 434–446.

Fesenko, E. E., Kolesnikov, S. S., & Lyubarsky, A. L. (1985). Induction by cyclic GMP of cationic conductance in plasma membrane of retinal rod outer segment. *Nature, 313*, 310–313.

Gauss, R., & Seifert, R. (2000). Pacemaker oscillations in heart and brain: a key role for hyperpolarization-activated cation channels. *Chronobiol Int, 17*, 453–469.

Gavazzo, P., Picco, C., & Menini, A. (1997). Mechanisms of modulation by internal protons of cyclic nucleotide-gated channels cloned from sensory receptor cells. *Proc Biol Sci, 264*, 1157–1165.

Gordon, S. E., & Zagotta, W. N. (1995). Localization of regions affecting an allosteric transition in cyclic nucleotide-activated channels. *Neuron, 14*, 857–864.

Haynes, L., & Yau, K.-W. (1985). Cyclic GMP-sensitive conductance in outer segment membrane of catfish cones. *Nature, 317*, 61–64.

Hofmann, F., Biel, M., & Kaupp, U. B. (2005). International Union of Pharmacology. LI. Nomenclature and structure-function relationships of cyclic nucleotide-regulated channels. *Pharm Rev, 57*, 455–462.

Karpen, J. W., Brown, R. L., Stryer, L., & Baylor, D. A. (1993). Interactions between divalent cations and the gating machinery of cyclic GMP-activated channels in salamander retinal rods. *J Gen Physiol, 101*, 1–25.

Kaupp, U. B., & Seifert, R. (2001). Molecular diversity of pacemaker ion channels. *Annu Rev Physiol, 63*, 235–257.

Kaupp, U. B., & Seifert, R. (2002). Cyclic nucleotide-gated ion channels. *Physiol Rev, 82*, 769–824.

Khan, S., Perry, C., Tetreault, M. L., et al. (2010). A novel cyclic nucleotide-gated ion channel enriched in synaptic terminals of isotocin neurons in zebrafish brain and pituitary. *Neuroscience, 165*, 79–89.

Liman, E. R., & Buck, L. B. (1994). A second subunit of the olfactory cyclic nucleotide-gated channel confers high sensitivity to cAMP. *Neuron, 13*, 611–621.

Martínez-François, J. R., Xu, Y., & Lu, Z. (2009). Mutations reveal voltage gating of CNGA1 channels in saturating cGMP. *J Gen Physiol, 134*, 151–164.

Matthews, G., & Watanabe, S.-I. (1987). Properties of ion channels closed by light and opened by guanosine 3′5′-cyclic monophosphate in toad retinal rods. *J Physiol, 389*, 691–715.

Mazzolini, M., Marchesi, A., Giorgetti, A., & Torre, V. (2010). Gating in CNGA1 channels. *Pflügers Arch Eur J Physiol, 459*, 547–555.

Michalakis, S., Zong, X., Becirovic, E., et al. (2011). The glutamic acid-rich protein is a gating inhibitor of cyclic nucleotide-gated channels. *J Neurosci, 31*, 133–141.

Nakamura, T., & Gold, G. H. (1987). A cyclic nuceotide-gated conductance in olfactory receptor cilia. *Nature, 325*, 442–444.

Picones, A., & Korenbrot, J. I. (1992). Permeation and interaction of monovalent cations with the cGMP-gated channel of cone photoreceptors. *J Gen Physiol, 100*, 647–673.

Pifferi, S., Boccaccio, A., & Menini, A. (2006). Cyclic nucleotide-gated ion channels in sensory transducion. *FEBS Lett, 580*, 2853–2859.

Schünke, S., Stoldt, M., Novak, K., Kaupp, U. B., & Willbold, D. (2011). Solution structure of the Mesorhizobium loti K1 channel cyclic nucleotide-binding domain in complex with cAMP. *EMBO Rep, 10*, 729–735.

Tang, C. Y., & Papazian, D. M. (1997). Transfer of voltage independence from a rat olfactory channel to the Drosophila ether-a-go-go K^+ channel. *J Gen Physiol, 109*, 301–311.

Tetreault, M. L., Henry, D., Horrigan, D. M., Matthews, G., & Zimmerman, A. L. (2006). Characterization of a novel cyclic nucleotide-gated channel from zebrafish brain. *Biochem Biophys Res Commun, 348*, 441–449.

Trudeau, M. C., & Zagotta, W. N. (2003). Calcium/calmodulin modulation of olfactory and rod cyclic nucleotide-gated ion channels. *J Biol Chem, 278*, 18705–18708.

Wahl-Schott, C., & Biel, M. (2009). HCN channels: structure, cellular regulation and physiological function. *Cell Mol Life Sci, 66*, 470–494.

Wohlfart, P., Haase, W., Molday, R. S., & Cook, N. J. (1992). Antibodies against synthetic peptides used to determine the topology and site of glycosylation of the cGMP-gated channel from bovine rod photoreceptors. *J Biol Chem, 267*, 644–648.

Yu, F. H., Yarov-Yarovoy, V., Gutman, G. A., & Catterall, W. A. (2005). Overview of molecular relationships in the voltage-gated ion channel superfamily. *Pharmacol Rev, 57*, 387–395.

Zagotta, W. N., Olivier, N. B., Black, K. D., Young, E. C., Olson, R., & Gouaux, E. (2003). Structural basis for modulation and agonist specificity of HCN pacemaker channels. *Nature, 425*, 200–205.

Zimmerman, A. L. (2002). Two B or not two B? Questioning the rotational symmetry of tetrameric ion channels. *Neuron, 36*, 997–999.

Zimmerman, A. L., & Baylor, D. A. (1992). Cation interactions within the cyclic GMP-activated channel of retinal rods from the tiger salamander. *J Physiol, 449*, 759–783.

Zufall, F., Shepherd, G. M., & Firestein, S. (1991). Inhibition of the olfactory cyclic nucleotide gated ion channel by intracellular calcium. *Proc R Soc London Ser B, 246*, 225–230.

Chapter 36

Sensory Receptors and Mechanotransduction

Andrew S. French and Päivi H. Torkkeli

Chapter Outline

I. INTRODUCTION

While most living cells can detect and respond to a variety of changes in their external physical and chemical environments, we usually reserve the term *sensory receptor* for those cells that transmit information about such changes to the animal's nervous system. Even this classification must be qualified. For example, the heart and other hollow organs have localized, mainly autonomous, nervous systems that allow sensory receptors to produce very local functional changes. Moreover, some of the mechanisms that cells use to detect external events seem to be very similar as we move from unicellular animals to the complex sensory organs of humans. With these caveats in mind, this chapter is restricted to those cells (usually neurons) that transmit sensory information into one or more divisions of the central nervous system.

Several general principles can be applied to all sensory receptors. The concept of *modality* means that each sensory cell transmits information about only one type of environmental stimulus. Photoreceptors detect light but are insensitive to touch, while stretch receptors do not respond to odorant molecules. Within the modalities there are further specializations, so that cold temperature receptors do not respond to hot stimuli and sweet taste receptors do not respond to bitter substances. Each type of receptor seems to produce specific molecular machinery for detecting just one type of stimulus. An exception to this rule is provided by the cutaneous polymodal pain receptors (McGlone and Reilly, 2009) which respond to mechanical, thermal or chemical stimuli.

Neurons carrying information into the nervous system form *labeled lines* that signal specific modalities and specific locations. Artificially stimulating a sensory nerve by electrical or mechanical stimulation produces a sensation that reflects the modality and location of the sensory ending, not the artificial stimulus. Another general principle is that the intensity of the stimulus is encoded as the amplitude of the electrical signal passing along the sensory neuron. In most cases, this means the action potentials propagating along the sensory axon, with more action potentials per second representing a stronger stimulus. In some cases, the stimulus produces a decrease in ongoing neuronal activity. However, there are several situations where the primary sensory cell does not produce action potentials at all, but a graded change in membrane potential that is conducted decrementally along the cell. Graded potentials can usually be propagated for only very short distances (a few millimeters at most), so such cells are

Cell Physiology Sourcebook. DOI: 10.1016/B978-0-12-387738-3.00036-6

generally small. Well-known examples are the rods and cones of the retina and the hair cells of the inner ear.

II. SENSORY TRANSDUCTION

Sensory cells respond to an external stimulus by changing their membrane potential, although several processes may occur before and after this *transduction* step. This change in membrane potential is called a *receptor potential* and it is a graded potential, increasing and decreasing with the intensity of the stimulus. Non-sensory neurons are insensitive to external stimuli, such as mechanical stress, temperature or light, unless these reach such intensity as to threaten the cell's normal function or integrity. Therefore, sensory receptors must have specializations to detect external stimuli (Fig. 36.1). Conceptually, the simplest receptors are the electroreceptors, which use an external electrical current to change their own membrane potential by direct current flow. Although the concept is simple, these cells are highly specialized to maximize their electrical sensitivity. Current flows through resting membranes by the passage of ions through ion channels that are open at rest. The salt taste receptors of the tongue and mouth also rely on direct ion flow through ion channels. In this case, the channels are selective for Na^+ and can be blocked by amiloride, so that placing a small amount of amiloride in the mouth removes the ability to taste salt. Na^+ diffuses through these channels to depolarize the taste cell membrane. An additional level of complexity is illustrated by sour taste receptors, where cation channels are believed to be closed by external hydrogen ions, reducing outward K^+ current and depolarizing the cell. However, the sour taste receptor has not yet been identified.

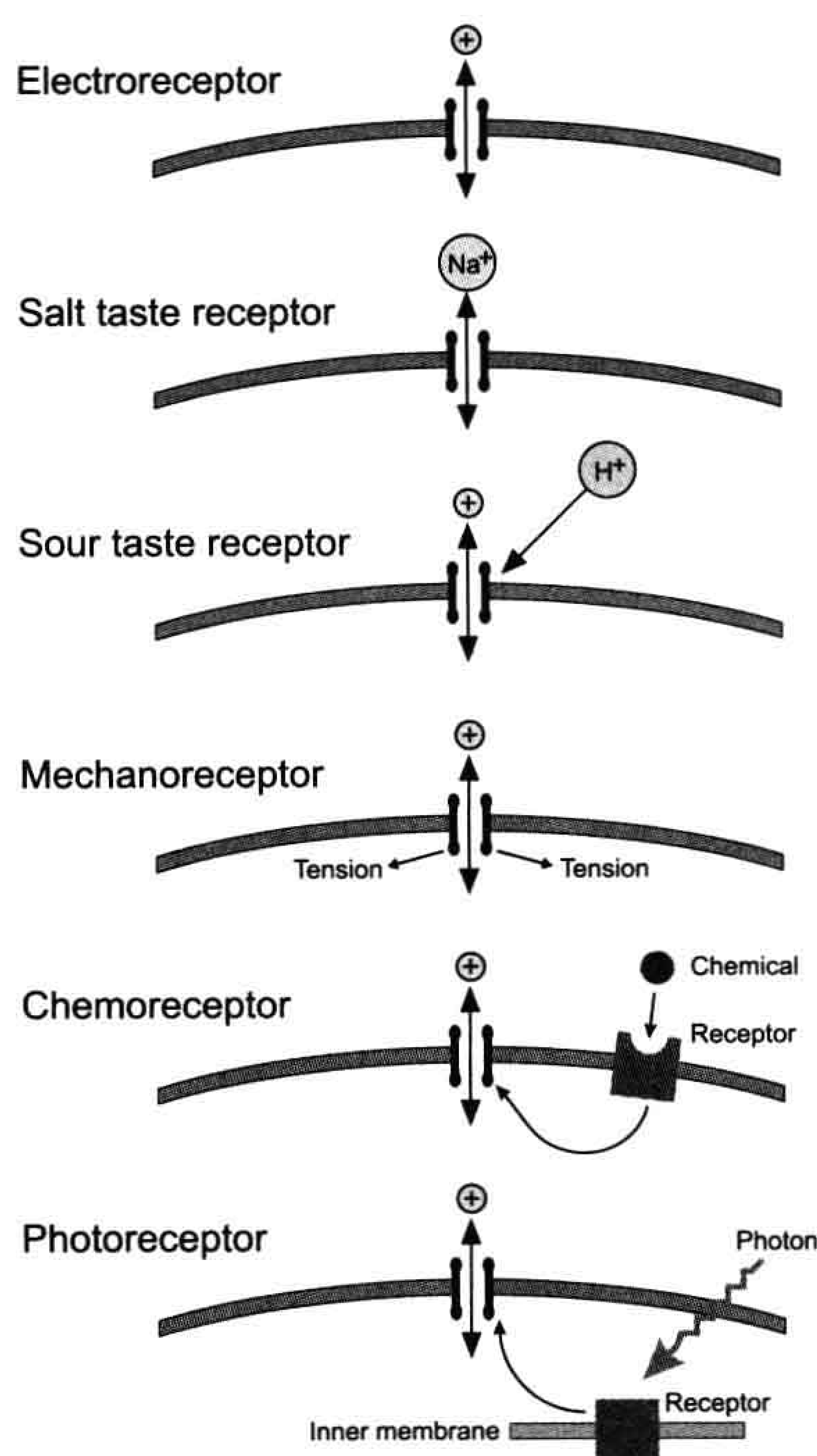


FIGURE 36.1 Mechanisms of sensory transduction organized by level of complexity. In each case the cell has specialized ion channels that produce a receptor current. Modulation of the current is achieved by changing the electrochemical force for the permeant ion in the cases of electroreceptors and salt taste receptors. In other receptors, the external stimulus changes the channel open probability, either by acting directly on the channel protein or via a second messenger cascade. Chemoreceptors have receptor proteins in the cell membrane. In vertebrate rods, the light-sensitive pigments, rhodopsins are in the internal disk membranes, but cones and invertebrate photoreceptors have their photopigments in invaginated cell membranes.

The fundamental transduction step in mechanoreceptors is not well understood, but is assumed to involve mechanically activated ion channels. These channels are believed to be either directly gated by forces acting on the plasma membrane or by tethers that connect the channel to the cytoskeleton or extracellular matrix (Christensen and Corey, 2007). If either model is true, this is another case where the external stimulus acts directly to open or close an ion channel. Finally, there are cases where the external stimulus acts indirectly through intermediate membrane receptors. In many chemoreceptors, specialized receptor proteins in the outer cell membrane activate ion channels through a second messenger cascade when they bind an appropriate stimulus molecule. In the case of rod photoreceptors, light activates specialized light-sensitive pigments in internal cell membranes, producing a second messenger cascade that eventually closes ion channels in the external membrane. Some models of mechanotransduction also suggest that a conformational change in a distant force-sensing component is communicated to the mechanotransduction channel by a second messenger (Christensen and Corey, 2007). It is not known which types of sensory receptor mechanisms evolved first, but it is clear that several, if not all, of these processes have close parallels in other non-sensory tissues, such as the Na^+ channels of epithelia, the mechanically activated channels of muscle and the second messenger cascades of synapses and secretory cells. It seems likely that the evolution of different sense modalities has taken advantage of pre-existing cellular mechanisms.

III. SENSORY ADAPTATION

Sensory receptors often have to deal with wide ranges of stimulus amplitudes. Therefore, they need high sensitivity to detect weak stimuli, plus the ability to reduce their sensitivity if the stimulus is strong. In some cases, the maximum sensitivity approaches the limits imposed by

physics or chemistry. Human rod photoreceptors and some arthropod photoreceptors can detect single photons arriving in the eye, which is clearly the physical limit. The human ear can detect air movements of about 0.01 nm, close to the diameter of a hydrogen atom (Hudspeth, 2005). In such cases, the sensory cells must amplify the initial signal considerably, which at least partly explains the complex morphologies of human rod photoreceptors and the cochlea.

The reduction in sensitivity following an increase in stimulus is called *adaptation*. It may be seen as a decrease in receptor potential with time during a constant stimulus, or as an increase in the strength of stimulus required to produce a constant response. All sensory receptors adapt to some extent, but there is a wide range of adaptation speeds and amounts. At one extreme are receptors such as Pacinian corpuscles (Loewenstein and Mendelson, 1965) and spider slit sensilla (French et al., 2002), which fire only one or two action potentials with even a strong, continuous stimulus. At the other extreme are Ruffini endings (Malinovsky, 1996), which continue to fire steadily for long periods. The type of adaptation is always appropriate to the function of the receptor. Muscle and joint receptors that signal limb position would not be useful if they adapted to silence in a few seconds, because the sense of limb position, or *proprioception*, would vanish if one did not keep moving. On the other hand, photoreceptors must function under a wide range of light intensities and it is essential that they can adjust their sensitivity to the ambient light level. The rapid adaptation of Pacinian corpuscles makes them ideally suited for detecting vibration, since a rapidly changing stimulus will repeatedly excite the receptor, while a steady stimulus will produce little response.

The mechanisms of adaptation vary widely and may occur at different stages of the process. Some involve components outside the sensory cell, such as the mechanical creep of the muscle in muscle spindles or the movements of screening pigments in insect eyes. Others may involve chemical signals within and between cells, as found in photoreceptors and olfactory receptors. Mechanical adaptation by the capsule of the Pacinian corpuscle is very well known from the pioneering work of Loewenstein and Mendelson (1965), who described the dramatic reduction in receptor potential adaptation that can be achieved by removing most of the capsule (Fig. 36.2). Unfortunately, many descriptions stop at this point, leaving the impression that mechanical adaptation dominates Pacinian corpuscle behavior, but Loewenstein and Mendelson showed that, even after decapsulation, the receptor will only fire one or two action potentials in response to a prolonged step stimulus (Fig. 36.2C). They described this as electrical adaptation and it now seems probable that many receptors use voltage- or calcium-activated ion channels in their membranes to produce electrical adaptation by raising the threshold for action potential production. This has been clearly established in several arthropod and vertebrate mechanoreceptors and is likely to occur in other types of receptors that use action potentials to encode the sensory signal (French and Torkkeli, 1994).

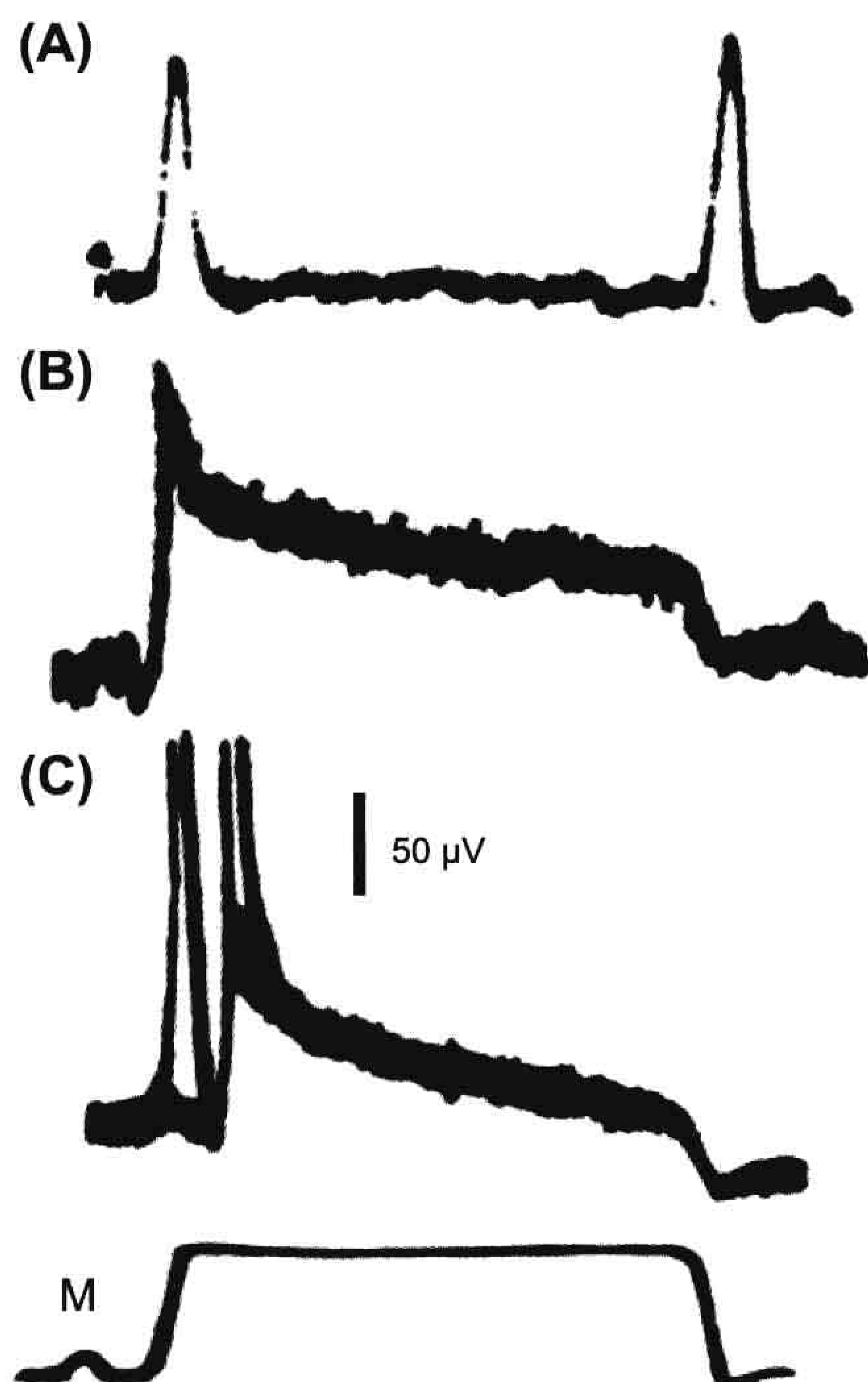


FIGURE 36.2 Adaptation in the mammalian Pacinian corpuscle occurs in two stages. (A) Stimulating a normal receptor with a mechanical step (M: bottom) causes rapidly adapting receptor potential responses at the start and end of the step. (B) Removing most of the lamellae surrounding the sensory ending (decapsulation) eliminates most of the adaptation to reveal a slowly adapting receptor potential. (C) Suprathreshold stimulation of a decapsulated receptor still produces only two action potentials, showing that there is rapid adaptation in the conversion of receptor potential to action potentials. *(Redrawn from Loewenstein and Mendelson, 1965.)*

IV. INFORMATION TRANSMISSION BY SENSORY RECEPTORS

Nervous systems and individual nerve cells deal with information. Cells with long axons transmit information over considerable distances and we assume that all nerve cells process information to some extent. Unfortunately, it is usually difficult to decide what the nature of the information is and how it is being processed, except in general terms. Sensory cells have been particularly important in trying to understand quantitatively how information is encoded and transmitted by nerve cells because it is usually

easier to define the input signal of a receptor neuron than other nerve cells. For example, the intensity and wavelength of light entering a photoreceptor or the length of a muscle spindle receptor can be accurately controlled while the output of the receptor in terms of receptor or action potentials is recorded.

Quantitative investigations of information flowing through sensory neurons have been based on ideas developed by engineers for dealing with artificial communication systems, such as telephone or television signals. Widespread use of digital communications has made the concept of *information transmission rate* (usually in bits per second, or bps) familiar. If we know the nature of the information being transmitted, we can measure the actual rate of transmission, but even if nothing is known about the kind of information being transmitted, it is possible to calculate the theoretical maximum rate that could be achieved by an optimum encoding scheme. This is called the *information capacity* of the system and it is closely related to the inherent noise in the system. The basic idea is that inherent noise limits the amplitudes and bandwidths of the signals that can be received unambiguously and thus the amount of information that can be transmitted and received in a given time. Note that when a noisy neuron fires action potentials the noise appears primarily as variability or randomness in the timing of the action potentials.

If a system behaves linearly, its information capacity can be calculated from the signal-to-noise ratio. This approach has been used in most estimates of receptor cell information capacity. Although relatively few measurements have been made, it is clear that cells using action potentials to transmit information have lower information capacities than those that do not. Spiking mechanoreceptors in cricket cercal mechanoreceptors and spider slit sensilla had capacities of 300 bps and 200 bps respectively, compared to values of 1650 bps for fly photoreceptors and 2240 bps for the receptor potential in spider slit sensilla before encoding (Juusola and French, 1997). However, it was possible to transmit information at rates up to 500 bps for short periods using a defined encoding scheme in a cockroach mechanoreceptor (French and Torkkeli, 1998), so we must be cautious about these estimates until we understand the actual encoding schemes that neurons use.

These findings support the concept that nerve cells use action potentials to transmit information faithfully over long distances, but there is a significant cost in information capacity. This probably explains why some sensory systems have elaborate neural structures located peripherally, close to the primary sensory neurons. A familiar example is the vertebrate retina, with two layers of non-spiking cells and complex synaptic interactions before the spiking ganglion cells. This arrangement presumably allows important information processing to take place on the high capacity input from the photoreceptors before it is encoded into the lower capacity ganglion cell axons.

V. MECHANORECEPTORS

VA. Vertebrate Mechanoreceptors

Vertebrate mechanoreceptors have such a wide variety of shapes and functions that classification is difficult. Many receptors bear the names of their original discoverers or re-discoverers, such as Meissner corpuscles and Ruffini endings. A variety of classification schemes have been used, based on features such as the morphology of the sensory ending and its associated tissues, rates of adaptation and location in the body. The hair cells of the vertebrate auditory and vestibular systems have been studied extensively (Hudspeth, 2005; Fettiplace, 2009), and are described in Chapter 37. Mammalian cutaneous mechanoreceptors have their sensory endings in the skin and their cell bodies in the dorsal root or trigeminal ganglion (Tsunozaki and Bautista, 2009). Figure 36.3 shows a classification of these mechanoreceptors according to the embryonic origin of the tissues associated with the sensory ending and the complexity of the sensory ending itself (Malinovsky, 1996). Type I receptors are associated with tissues of mesodermal origin (connective tissues and muscle) and include the Ruffini endings of the joints and skin, the Golgi tendon organs and the muscle spindles. Type II receptors are transitional between type I and type III and are associated with tissues of endodermal or ectodermal origin. They include the Merkel endings, where each sensory ending is closely apposed to a specialized

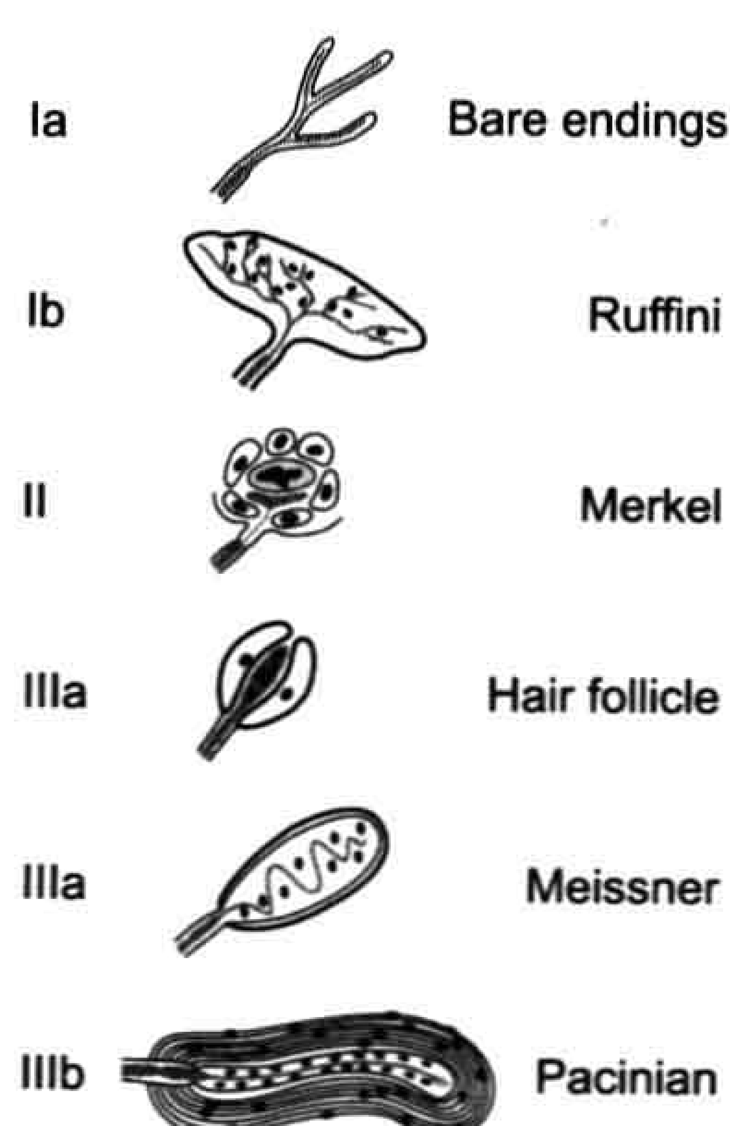


FIGURE 36.3 Classification of vertebrate mechanoreceptors by embryonic origin of associated tissues and complexity of ending; showing major examples. Type I are associated with tissues of mesodermal origin, type II with endodermal or epidermal and type III with epidermal. Subtypes (Ia, Ib, etc.) indicate morphological complexity. *(Redrawn from Malinovsky, 1996.)*

Merkel cell that is derived from epidermal lineage. Type III receptors are clearly associated with tissues of ectodermal origin and comprise a wide range of receptors including the bulbous endings found in hair follicles, the Meissner corpuscles and the Pacinian corpuscles. This classification broadly accompanies a functional shift from slowly adapting receptors (such as Ruffini endings) in the type I group to rapidly adapting receptors in the type III groups (such as Pacinian corpuscles). Phylogenetically, type I and type II receptors are found in all classes of vertebrates from fish to primates, while type III receptors are unknown in fish, start to occur in amphibia and become increasingly common in higher vertebrates (Malinovsky, 1996).

Vertebrate mechanoreceptors and nociceptors can also be classified based on myelination, conduction velocity of the afferent nerve fibers and whether they have low or high threshold as shown in Table 36.1 (Tsunozaki and Bautista, 2009). A further classification is based on the receptive field of the low threshold receptors; Meissner corpuscles and Merkel disks are located close to the skin surface and have small receptive fields while Pacinian corpuscles and Ruffini endings are located deeper in the dermis and have large receptive fields (McGlone and Reilly, 2009). Although most unmyelinated C-fibers originate from nociceptors that respond to one or more types of painful stimuli, one type of C-fiber is purely a touch receptor. These tactile C-fibers are only found in hairy skin and respond to slowly moving mechanical stimuli (McGlone and Reilly, 2009).

VB. Invertebrate Mechanoreceptors

Arthropods, especially insects, spiders and crustaceans, have provided important preparations for the investigation of mechanoreceptor function. Their receptors can be divided into two major groups, cuticular and multipolar, sometimes called type I and type II mechanoreceptors. *Cuticular receptors*, as the name implies, are generally associated with the arthropod cuticle and have their cell bodies in the periphery, close to the sensory ending. This arrangement is very different than most vertebrate and other invertebrate mechanoreceptors, which have their cell bodies in the central nervous system, distant from the sensory ending, and it allows recordings to be made close to the site of mechanotransduction. In addition, many

TABLE 36.1 Mammalian Cutaneous Sensory Fiber Types

	Fiber Group	Diameter (μm)	Fiber Type	Sensory Ending	Sensation	Conduction Velocity (m/s)	Von Frey Threshold (mN)
Myelinated	Aα	20	Proprioceptors from muscles and tendons		Proprioception	120	
	Aβ	5–12	Low threshold, rapidly adapting	Pacinian, Meissner	Touch	>10	1.0
			Low threshold, slowly adapting	Merkel, Ruffini	Touch	>10	1.5
	Aδ	2–5	Low threshold	Hair	Touch	2–10	<0.5
			Aδ mechanoreceptor	Free nerve ending	Mechanonociception	2–10	5
Unmyelinated	C	0.3–1.3	Polymodal	Free nerve ending	Mechano- heat- and chemonociception	<1.5	10
			Uni- or multimodal	Free nerve ending	Mechano- and/or heat- and/or cold-nociception	<1.5	6
			Silent[1]	Free nerve ending	Mechano- and/or heat-nociception	<1.5	N/A
			Low threshold	Free nerve ending	Touch	<1.5	<0.5

Approximate measurements are from cat.
[1] *Silent fibers activate only after sensitization (Kress, M., Koltzenburg, M., Reeh, P.W. and Handwerker, H.O. (1992). Responsiveness and functional attributes of electrically localized terminals of cutaneous C-fibers in vivo and in vitro. J Neurophysiol. 68, 581-595).*
Based on McGlone and Reilly, 2009; Smith, E.S. and Lewin G.R. (2009). Nociceptors: a phylogenetic view. J Comp Physiol A. 195, 1089-1106.

arthropod receptor cells are relatively large, allowing penetration by microelectrodes, which is impossible in most vertebrate receptors.

There are three major groups of cuticular receptors (Fig. 36.4). *Hair-like* receptors are found all over the outer surfaces of most arthropods in a variety of shapes and sizes from long, thin hairs to short pegs. The hair is supported by flexible cuticle within a socket and moves relative to the skin. In insects, a single mechanoreceptor neuron is closely apposed to the base and its sensory ending contains microtubules that end in a dense tubular body. It is assumed that movement of the hair compresses the ending, with the tubular body perhaps adding a rigid structure that the compression can work against. Crustacean and spider hairs are similar, but with two to four mechanosensory neurons in each hair. All arthropod hair types can contain other sensory neurons in addition to the mechanoreceptors, such as chemoreceptors in taste hairs. *Campaniform* (bell-shaped) sensilla are found in insects, where they detect stress in the cuticle. The stress leads to compression of a dendritic tip containing a tubular body by squeezing the bell as it is pushed downwards. Arachnids have analogous stress-detecting receptors called slit sensilla, where the neurons are located in cuticular slits. *Chordotonal* receptors are generally found further beneath the integument, although they can be connected to the integument by attachment structures. They serve a variety of functions, including hearing and joint movement detection. They generally lack tubular bodies but have dense scolopale structures surrounding the dendrite and can have multiple mechanosensory neurons.

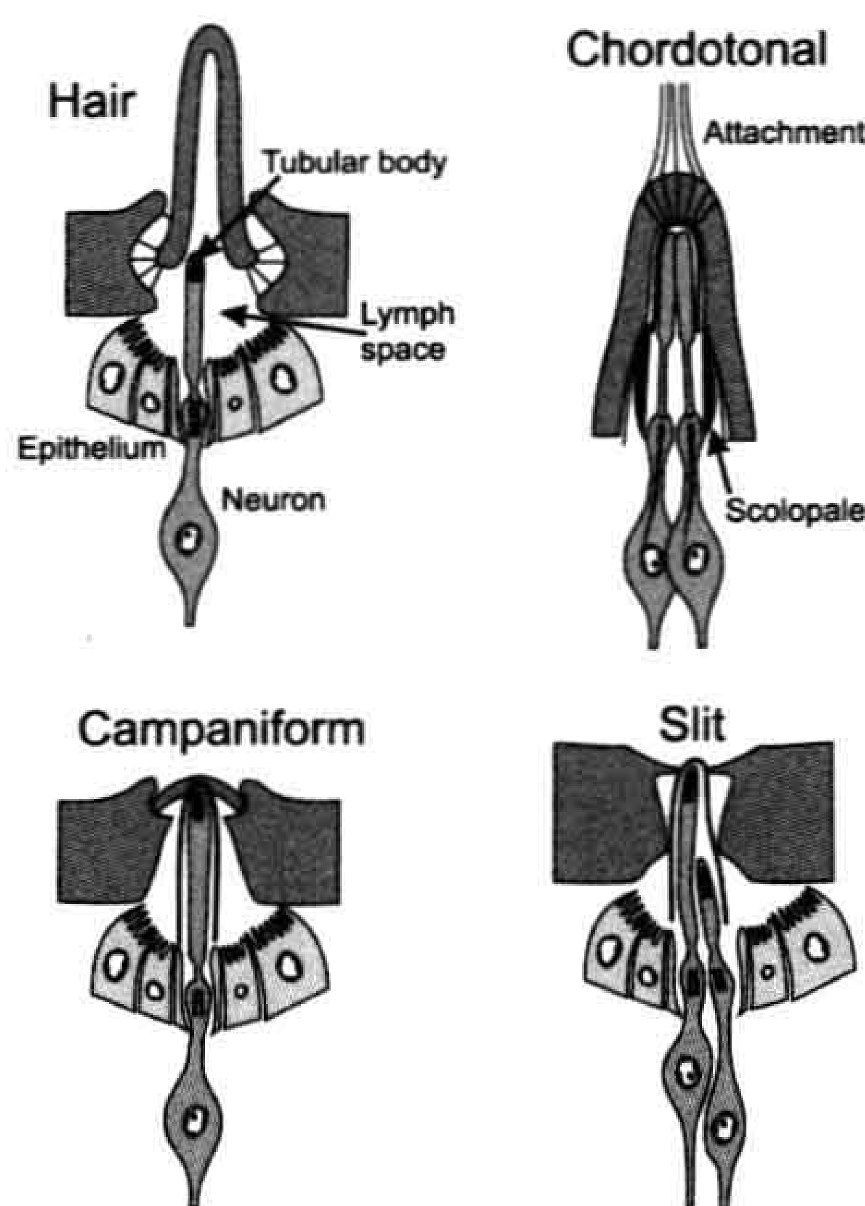


FIGURE 36.4 Four common types of ciliated arthropod cuticular mechanoreceptors. Hair receptors of various shapes are prevalent in many arthropods. Chordotonal receptors are found in insects and crustaceans, campaniform sensilla in insects and slit sensilla in arachnids. Sensory dendrites are usually surrounded by a dense sheath and often contain tubular bodies formed from microtubules embedded in electron-dense material. Epithelial layers connected by tight junctions form a lymph space surrounding the dendrite. Chordotonal sensilla feature dense scolopale rods surrounding sensory dendrites and may have an attachment to another structure, such as a joint.

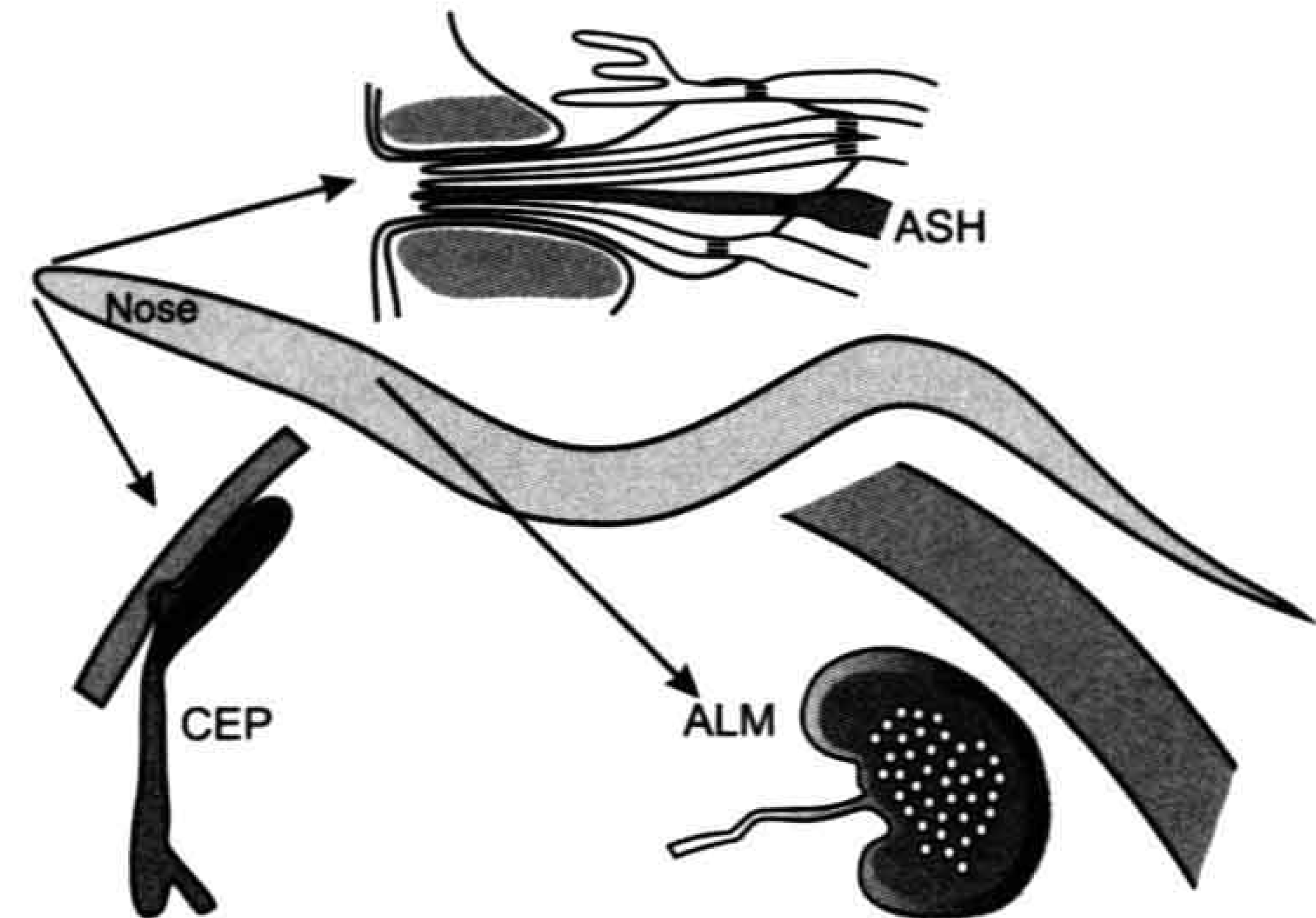


FIGURE 36.5 Mechanoreceptors of the nematode *C. elegans*. Ciliated amphid (ASH) and cephalic (CEP) sensory neurons are found in the nose of the animal; ASH neurons are with a group of chemosensory neurons in the labial region and CEP neurons are closely apposed to cuticle. Gentle touch of the body is detected by anterior lateral microtubule (ALM) neurons, which contain many microtubules and are surrounded by extracellular matrix. *(Based on Chalfie, 2009.)*

The nematode *Caenorhabditis elegans* also provides important models of mechanotransduction (Fig. 36.5). Its mechanoreceptors can be divided into three groups based on the specialization of their cytoskeleton. The first group has ciliated sensory endings, some of which abut to the cuticle while others, such as the polymodal sensory neuron in the nose, are located in channels that are open to external environment. Mechanoreceptors in the second group, including the gentle touch receptor neurons, are not ciliated but have large diameter microtubules in their sensory processes that are surrounded by an extracellular matrix, the mantle. The third group, including the harsh touch receptor, do not have specialized cytoskeleton. As the morphological differences suggest, research involving genetic manipulations combined with patch-clamp recordings have shown that several different mechanisms are involved in *C. elegans* mechanotransduction (O'Hagan et al., 2005; Chalfie, 2009; Kang et al., 2010).

VC. Muscle Mechanoreceptors

One of the best-known arthropod mechanoreceptors is the crayfish stretch receptor, which has interesting similarities to vertebrate muscle spindles (Fig. 36.6). These receptors are found on many muscles in crustaceans and are multipolar or type II arthropod mechanoreceptors. The large cell bodies are located in the periphery and the sensory endings consist of finely divided dendrites that cover part of the muscle surface. Unlike muscle spindles, crayfish stretch receptors

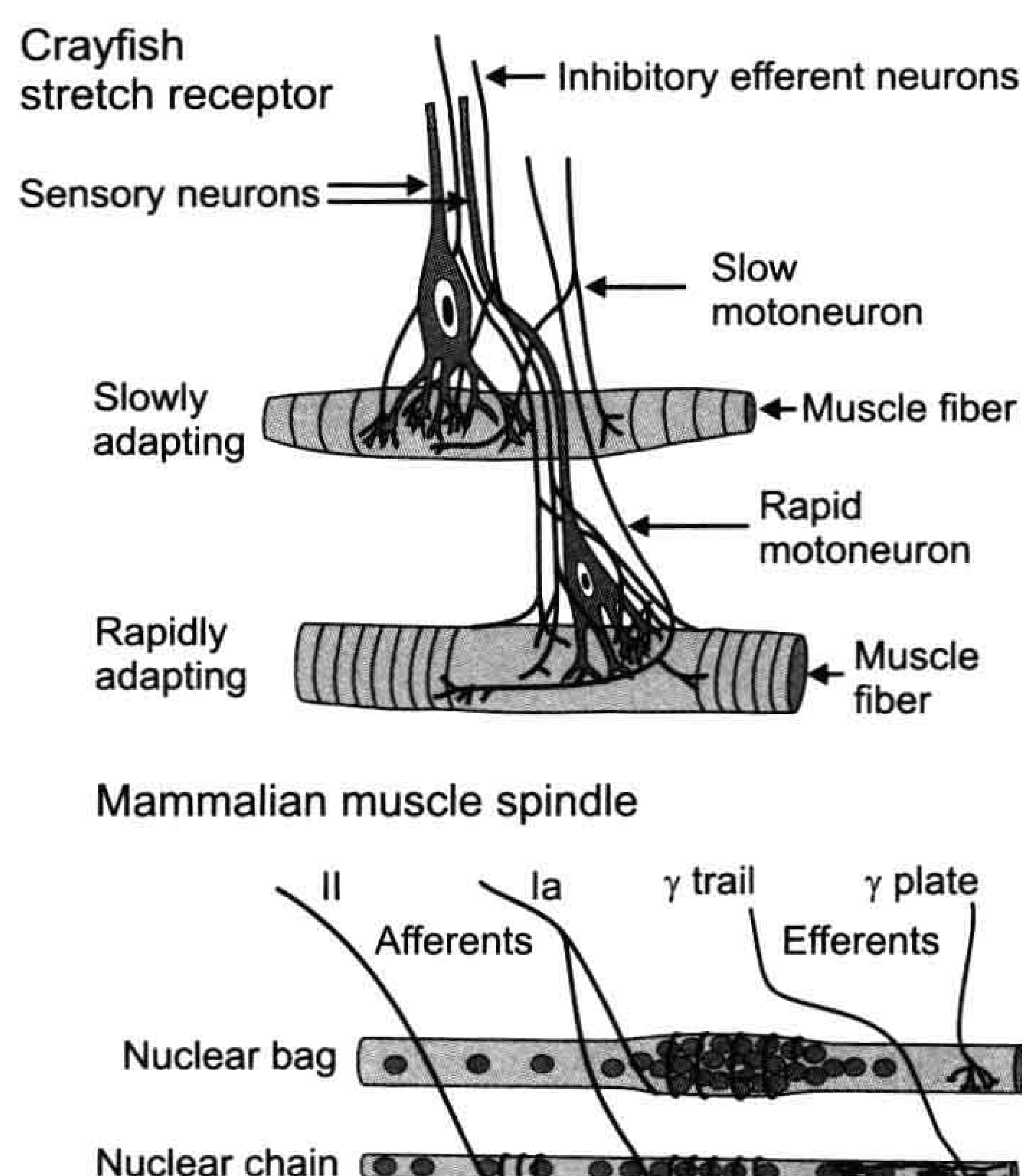


FIGURE 36.6 Invertebrate and vertebrate muscle mechanoreceptors. Crustacean stretch receptors are multipolar mechanoreceptors with many fine dendrites embedded in muscle fibers. There are two types of sensory neurons with different adaptation properties. Efferent GABAergic inhibitory neurons synapse onto the sensory neurons as well as the muscle fibers. *(Partly based on Rydqvist et al., 2007.)* Mammalian muscle spindles are modified muscle cells located within the main muscle and contain two types of fibers (nuclear bag and nuclear chain) with their own efferent innervation via two types of γ-motoneurons (γ-plate and γ-trail) that are activated separately from the main muscle fibers. There are also two types of sensory endings (Ia and II) with different adaptation characteristics. A whole muscle may contain hundreds of the much smaller muscle spindles.

are located on the main, force-producing muscle, and so are directly excited by passive stretch of the muscle or activation of motoneurons. This opens stretch activated ion channels that are permeable to Na^+, K^+ and Ca^{2+}. Crayfish stretch receptors also receive presynaptic γ-aminobutyric acid (GABA) -ergic innervation to the sensory neuron directly, as well as the muscle (Rydqvist et al., 2007).

Vertebrate muscle spindles are prominent and numerous mechanoreceptors that detect muscle stretch and are believed to be crucially involved in the control of muscle activation. However, they also make a major contribution to the senses of body position and movement (proprioception and kinesthesia) because appropriate artificial stimulation of muscle spindles gives sensations that the limbs are moving or in incorrect positions. Mammalian muscle spindles are small, modified muscle fibers located between the main, force-producing muscle fibers. Two types of sensory endings contact the spindle fibers and detect their length using mechanically activated cation channels. Spindle fibers are innervated by separate γ-motoneurons that allow the central nervous system to adjust their length, and hence the sensitivity of the receptors.

Closely associated with muscle spindles are the Golgi tendon organs. Located at the insertion of muscle fibers into the skeletal muscle tendons, these receptors use mechanically activated cation channels to detect muscle tension, rather than length, and contribute to reflex control of muscle activity.

VI. EXPERIMENTAL MECHANORECEPTOR PREPARATIONS

The complicated structures of many mechanoreceptor preparations make it challenging to record the receptor potential or receptor current, particularly while providing mechanical stimulation. Depending on the accessibility of the sensory neurons, various methods have been used (Fig. 36.7). *Decremental conduction* relies on insulating the sensory axon from the extracellular fluid as close as possible to the sensory ending, usually with a non-conducting substance, such as paraffin wax, petroleum jelly or sucrose solution, before leading it to a separate conducting solution. As the receptor is stimulated, some of the receptor current flows decrementally along the axon but cannot follow its normal path to the extracellular solution because of the insulation. It can only return through the second bath, where it is measured. This method has been used to observe the receptor potential in Pacinian corpuscles, muscle spindles and insect cuticular receptors. It allows a relatively stable preparation, because the receptor is not very disturbed and fine positioning is not needed after the initial setup. However, only a relatively small fraction of the total receptor current can usually be observed and the decremental conduction causes a selective loss of high-frequency signals through the membrane capacitance to ground, so that the observed receptor potential is attenuated and filtered. It is generally difficult to estimate accurately the amplitude and waveform of the original receptor potential.

Arthropod cuticular receptors have the sensory neurons so close to the surface that it is possible to observe part of the current flowing through the neuron from the exterior. For a hair receptor, a small pool of conducting solution can be placed in the hair socket and an electrode of some sort (glass, wire, wick) measures the potential in the pool. These *transepithelial* measurements rely on the high-resistance epithelium that surrounds cuticular receptor neurons (see below) and the relatively low resistance of the thin, flexible socket. A similar technique is used for cuticular chemoreceptors, where it is common to cut the hair and place the tip of an electrode over the cut end to obtain even better electrical contact. This is more difficult for mechanoreceptors, where the hair must be moved to stimulate transduction. However, this method has been successfully used to record mechanotransduction currents in *Drosophila* bristle hairs, an experimental preparation that also allowed electrophysiological testing of mechanoreceptive mutant

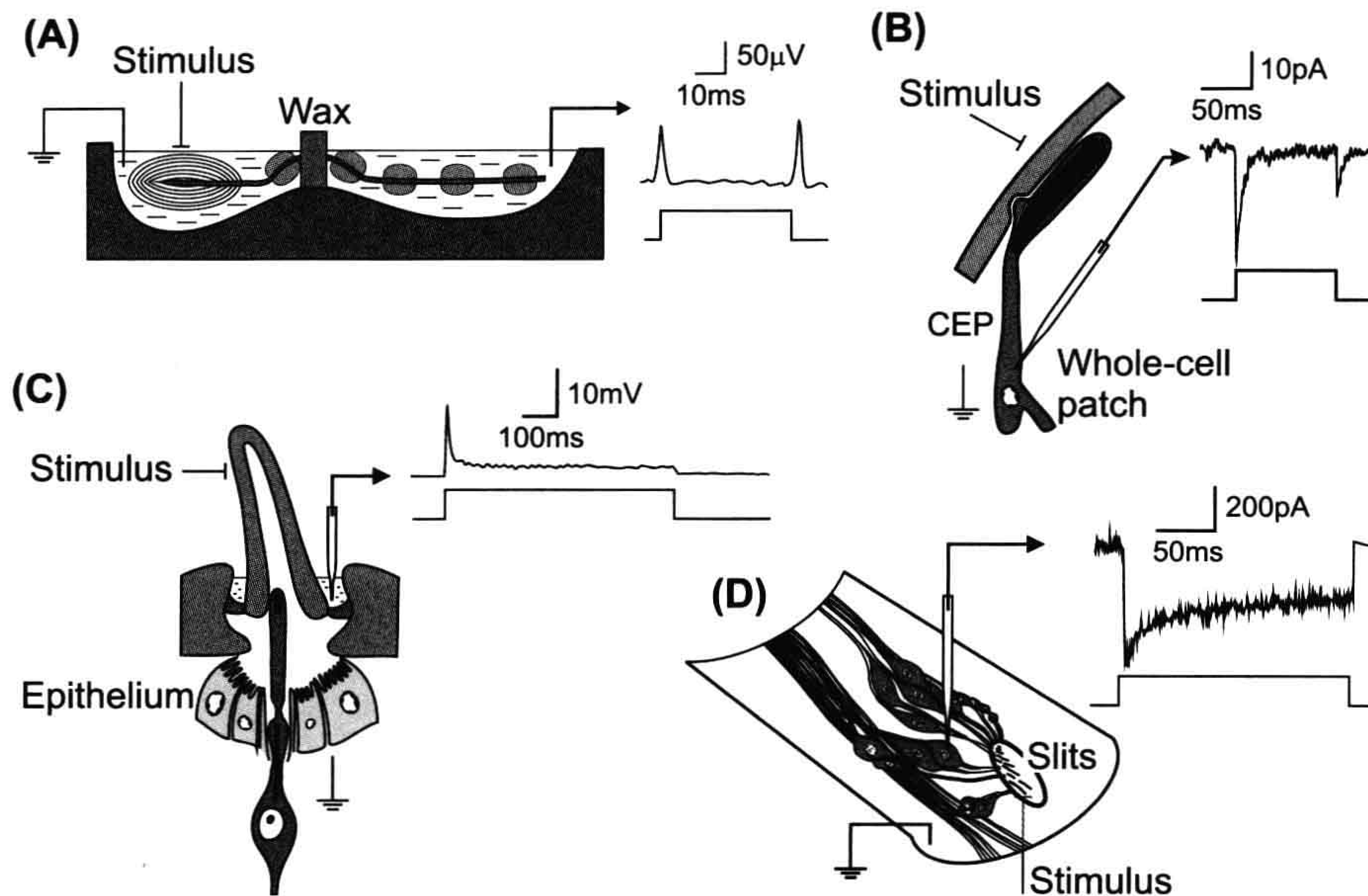


FIGURE 36.7 Examples of four methods that have been used to observe the receptor current and potential in mechanoreceptors. (A) Decremental conduction measures the current flowing along the sensory axon from a Pacinian corpuscle by insulating the axon as close as possible to the receptor. This prevents receptor current from reaching ground, except via the measuring bath. (B) Whole-cell patch-clamp of a CEP mechanosensory neuron beneath the nose cuticle of *C. elegans* while stimulating the external cuticle. (C) Transepithelial measurement of an arthropod hair receptor by sampling the voltage as close as possible to the lymph space surrounding the sensory ending and relying on the high resistance of the epithelium. (D) Intracellular recording from a neuron in the spider slit sensillum during mechanical stimulation of the slits from below. *(Redrawn in part from French et al., 2002; Kang et al., 2010.)*

flies (Walker et al., 2000). Transepithelial measurements allow a relatively stable recording situation, but the high-resistance access pathway attenuates the signal and emphasizes high frequencies, which can pass more easily through the cuticle. Here again, it is difficult to estimate the original receptor potential amplitude and time course with accuracy.

Intracellular recording close to the site of sensory transduction is clearly desirable if it can be accomplished. However, it requires stable penetration of a small neuron while the sensory ending is moved nearby and has only been successfully achieved in a few preparations. Even more useful is *voltage-clamp* of the sensory receptor membrane, since this allows the voltage across the ion channels to be controlled while the current flowing through them is recorded. Crustacean stretch receptors are relatively easy to penetrate, even with two microelectrodes, and have been used for pioneering studies of the mechanotransduction and other currents that contribute to the electrical properties of the neurons during sensory transduction (Rydqvist et al., 2007). However, the transduction currents probably originate in very fine endings embedded in the muscle (see Fig. 36.7) so that accurate voltage-clamp of this current is difficult. Voltage-clamp of arthropod cuticular receptors was first performed in the cockroach tactile spine (Torkkeli and French, 1994). A more successful cuticular preparation is that of spider slit sensilla, where it is possible to clamp the receptor potential close to the sensory ending while stimulating the slits (French et al., 2002).

Whole-cell patch-clamp recordings of *C. elegans* touch receptor neurons during mechanical stimulation have recently become possible (see Figs. 36.5 and 36.7) providing preparations where receptor currents and potentials can be studied in an animal model that also allows genetic screening (O'Hagan et al., 2005; Kang et al., 2010). Patch-clamp recordings from rat dissociated dorsal root ganglion neurons that detect touch and pain are also possible (Hu and Lewin, 2006; McCarter and Levine, 2006). However, dissociated neurons in culture lack the components that normally connect the physical stimulus to the membrane of the sensory neurons (Hu and Lewin, 2006).

VII. STEPS IN MECHANORECEPTION

Mechanoreception can be viewed as a three-stage process comprising *coupling*, *transduction* and *encoding* (Loewenstein and Mendelson, 1965). The stimulus is first mechanically coupled from its origin to the membrane

of the sensory cell where it is transduced into a receptor potential and, in cells with long sensory axons, this is encoded into action potentials that propagate to the central nervous system.

VIIA. Coupling

Living cells are not normally exposed to the outside surface of an animal, so most, if not all, external mechanoreceptors have some kind of tissue between them and the source of the mechanical input. In some cases, these surrounding tissues are elaborate and obviously designed to modify the input signal by affecting its amplitude and possibly its dynamic properties. Internal mechanoreceptors also have a variety of surrounding tissues with presumably similar functions. The morphology of these structures varies so strongly between different mechanoreceptors that it is widely used for classification, as described above (see Figs. 36.3 and 36.4). The Pacinian corpuscle is probably the most illustrated vertebrate mechanoreceptor, with its complex lamellar structure, but it represents only one extreme of a wide range of vertebrate mechanoreceptor endings. Invertebrate mechanoreceptors also display many morphological forms, including the well-known hair receptors that cover the outside surfaces of insects and spiders and the stretch receptors of crayfish and lobsters. Although we generally assume that these elaborate extracellular structures modify the spatial and temporal sensitivities of the receptors, there is relatively little quantitative information about these functions.

In many cases, the external structures attenuate the stimulus, so that the displacement of the receptor cell membrane is much smaller than the original movement. For example, hairs on the human skin can be moved by several millimeters, but the resulting movements of the follicle receptors are only a few micrometers. Estimates of this attenuation have been made in some cases. For the Pacinian corpuscle, it has been suggested that the pressure reaching the inner capsule is attenuated by about two orders of magnitude (100) compared to the pressure on the outer lamellae (Bell et al., 1994), but this force may already be greatly reduced compared to the initial stimulus at the skin. An attenuation of about 100 was also reported for insect hairs, based on the morphology of the sensory structure and the location of the moving elements (French, 1992). Estimates of attenuation during coupling also allow us to estimate the *threshold*, or minimum amplitude of movement at the cell membrane that leads to sensation. For Pacinian corpuscles, movements of 1–10 nm at the capsule are probably adequate to produce action potentials at the optimum vibration frequency of about 250 Hz and sinusoidal movements of about 0.3 nm can stimulate auditory hair cells (Hudspeth, 2005). For insect cuticular hair receptors, threshold estimates of 4 nm and 3 nm were obtained for bee and cockroach (French, 1992). Estimates of the mechanical force required at the surface of the animal for transduction vary more, from about 25 μN in spider slit sensilla to more than 10 mN in mammalian glabrous skin (Goodman and Schwarz, 2003), which probably reflects the wide range of coupling structures involved.

The few attempts that have been made to quantify the mechanical effects of coupling over a range of input movements indicate that it can have significant temporal effects and be substantially non-linear. The mechanical properties of crayfish stretch receptors have been studied thoroughly (Rydqvist et al., 2007) and require non-linear springs plus at least one dashpot (or Voigt element) to account for the passive properties of the receptor without any muscular activity. No mechanical description is available that includes active contraction. Muscle spindles also have strongly time-dependent mechanical properties, with probably more complex dynamic behavior during γ-motoneuron activation. The viscoelastic properties of Pacinian corpuscles are assumed to be responsible for most of the time dependence of the receptor current, but have not yet been quantified.

VIIB. Transduction

Transduction in mechanoreceptors probably involves mechanically activated ion channels in the receptor cell membrane (see Chapter 27 and recent reviews by Christensen and Corey, 2007; Chalfie, 2009; Árnadóttir and Chalfie, 2010; Lumpkin et al., 2010). Identification of these channels has only been made in a small number of mechanosensory neurons. The mechanotransduction channels in *C. elegans* gentle touch receptor neurons belong to the DEG/ENaC/ASIC (degenerin/epithelial sodium/acid sensitive ion channel) family (O'Hagan et al., 2005), while the pore-forming subunit in the ciliated touch receptors in *C. elegans* nose belong to the transient receptor potential (TRP) family (Kang et al., 2010). This TRP-4 protein is a member of the TRPN (or NompC) subfamily, and the NompC protein is also needed for mechanotransduction in *Drosophila* bristle hairs (Walker et al., 2000). Several members of the TRP and DEG/ENaC/ASIC families are expressed in mammalian mechanoreceptors, but it is not known if any of them are directly or indirectly involved in mechanotransduction (Tsunozaki and Bautista, 2009; Árnadóttir and Chalfie, 2010; Lumpkin et al., 2010).

The complex structures of the mechanoreceptor cells and the small numbers of mechanotransduction channels per cell mean that we do not yet have definitive single-channel recordings in intact, normally functioning mechanoreceptors. Single mechanically activated ion channels have been seen in crayfish stretch receptor neurons

(French, 1992) and in tissue-cultured moth antennal mechanoreceptor neurons (Torkkeli and French, 1999), but these channels were not located on the fine sensory endings where transduction is thought to occur. The crayfish channels had maximum conductance to K^+ (≈ 70 pS) but were also permeable to other cations. The moth channels were also permeable to K^+ with a conductance of ≈ 40 pS, but their selectivity has not yet been established. Single channel conductance is better characterized in auditory and vestibular hair cells, with a range of at least 100–300 pS and wide cation permeability (Fettiplace, 2009; also see Chapter 37).

Although single-channel data are sparse, we have significant information about some transduction channels, including ionic selectivity, ionic conductance, blocking chemicals and the numbers of transduction channels in each receptor cell (Fig. 36.8). In Pacinian corpuscles, muscle spindles, crayfish stretch receptors, spider slit sensilla and *C. elegans* gentle touch receptors, mechanotransduction current is carried by Na^+ ions. However, a variety of other cations can pass through most of these channels. (French, 1992; Bell et al., 1994; French et al., 2002; O'Hagan et al., 2005; Rydqvist et al., 2007). The mechanotransduction channels in *C. elegans* ciliated mechanoreceptor neurons (Kang et al., 2010) and in cultured rat dorsal root ganglion neurons (McCarter and

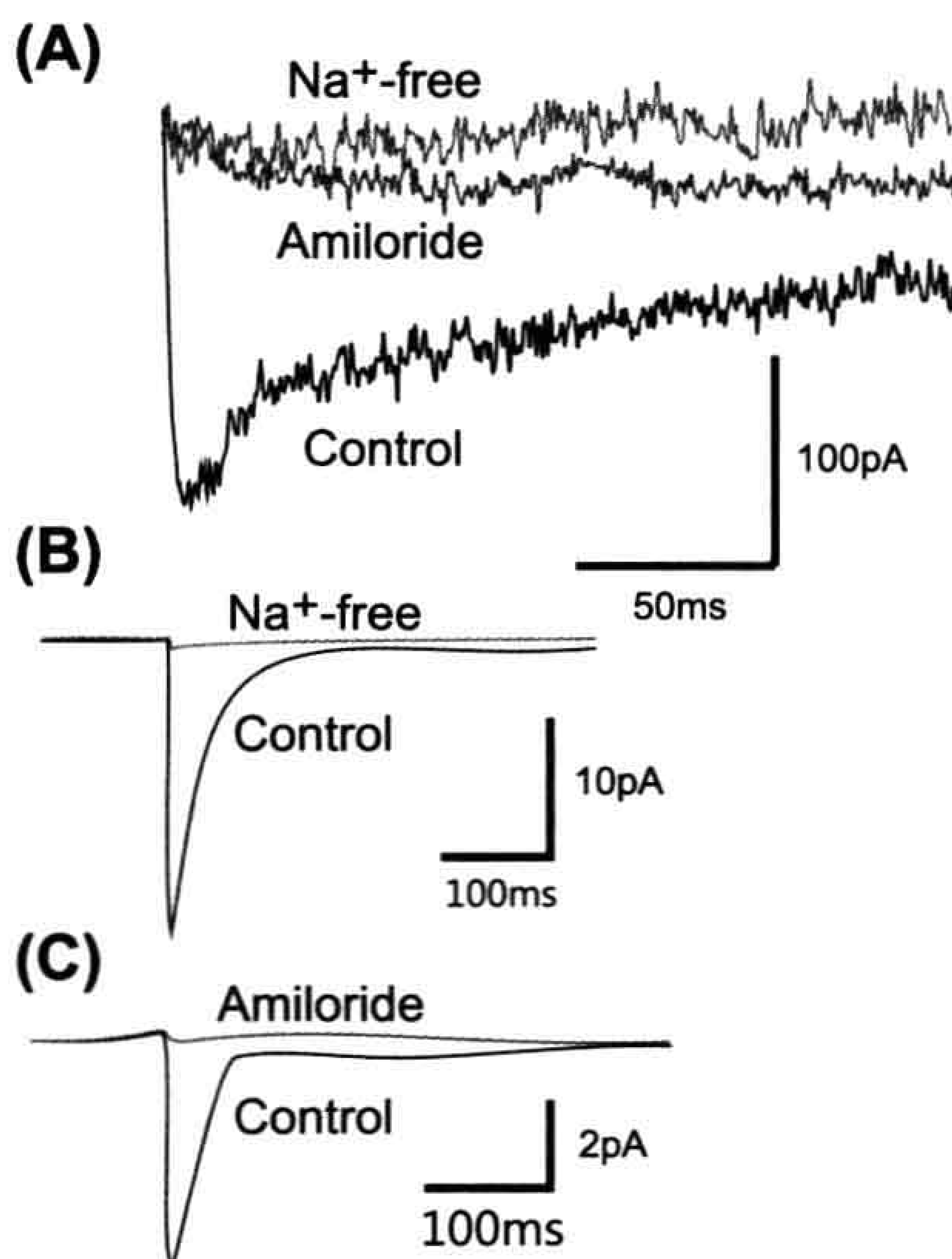


FIGURE 36.8 Sodium selectivity and block of receptor current by amiloride in two mechanoreceptors. (A) Step movements of a spider slit sensillum activate an inward current that is reduced to zero by replacing the Na^+ with impermeable choline or by adding 1 mM amiloride to the bath. (B and C) Sodium removal or application of 200 μM amiloride reduce the receptor current in whole-cell recordings from *C. elegans* PLM neurons. *(Redrawn from French et al., 2002 and O'Hagan et al., 2005.)*

Levine, 2006) are non-selective cation channels. In mouse dorsal root ganglion cells, the selectivity varied in different cell types so that slowly adapting current was non-selective to cations, while the rapidly adapting current was Na^+ selective (Hu and Lewin, 2006).

In several of these cells, the sensory ending is surrounded by an elevated Na^+ concentration and Na^+ entry during transduction causes a graded depolarization that leads to action potentials if the stimulus is strong enough. In vertebrate auditory and vestibular hair cells, the mechanotransduction channels are preferably permeant to divalent cations, such as Ca^{2+} and Mg^{2+}. However, in the inner ear, the hair bundles are bathed in endolymph that has high K^+ concentration and the transduction current is mainly carried by K^+ with a minor contribution from Ca^{2+} (Fettiplace, 2009). Similarly, in insect cuticular mechanoreceptors, the sensory ending is surrounded by lymph that is rich in K^+ and has a positive electrical potential relative to the normal hemolymph (French, 1992). The cases where K^+ is used to carry the receptor current generally rely on separating two regions of the sensory neurons by embedding them in an epithelial layer with tight junctions so that a K^+ concentration gradient, usually combined with an electrical gradient, can drive K^+ through the cell, depolarizing the membrane; similar arrangements exist for some of the Na-dependent systems. Cells with non-selective mechanotransduction channels may also receive a significant Ca^{2+} flux during transduction, because the inward Ca^{2+} electrochemical gradient is usually high.

Like many other ion channels, mechanotransduction channels can be blocked or closed by several chemicals. Gadolinium blocks mechanically-activated currents in several preparations including the crayfish stretch receptor (Rydqvist et al., 2007), the spider slit sensilla (French et al., 2002), cultured mouse dorsal root ganglion neurons (Hu and Lewin, 2006) and cochlear hair cells (Fettiplace, 2009). Sensitivity to gadolinium is sometimes used as an indicator that mechanically-activated channels are involved in a physiological process, but Gd^{3+} also blocks many Ca^{2+} channels, as well as some ligand- and voltage-gated cation channels. Amiloride is a well-known blocker of epithelial Na^+ channels and it blocks mechanotransduction current in the *C. elegans* gentle touch receptor neurons that are members of this family (O'Hagan et al., 2005) and in the spider slit sensilla (French et al., 2002) (see Fig. 36.8). The mechanotransduction current in ciliated touch receptor neurons in *C. elegans* nose are insensitive to amiloride, indicating that the TRP-4 channels are not sensitive to this blocker (Kang et al., 2010). Mechanically-activated currents in the cultured mouse dorsal root ganglion neurons (Hu and Lewin, 2006) and crayfish stretch receptors (Rydqvist et al., 2007) are also insensitive to amiloride, but it is not known which gene family these channels belong to. Interestingly, the mechanotransduction current

in vertebrate cochlear hair cells is blocked by amiloride, even though there is no evidence that this channel is a member of the ENaC family (Fettiplace, 2009). Some local anesthetics have also been used to block the receptor current in the crayfish stretch receptor (Rydqvist et al., 2007) and certain antibiotics as well as La^{3+}, ruthenium red, FM1-45 and Ca^{2+} are known to block transduction in auditory hair cells (Fettiplace, 2009).

The acid sensitive ion channel (ASIC) family has been associated with some mechanosensitive neurons and several members of the DEG/ENaC channel family are known to be opened by low pH (Árnadóttir and Chalfie, 2010). Mechanical sensitivity was enhanced by low pH in spider slit sensilla (French et al., 2002) although there was no evidence of direct acid activation.

Whole cell mechanotransduction currents have been recorded in some cells and noise, or fluctuation, analysis has been used to estimate single-channel conductance and the numbers of channels per cell in several cases. *Noise analysis* relies upon the idea that receptor channels opening and closing create variance in the mean receptor current, because all known channels regulate their average conductance by switching rapidly between open and closed states. Therefore, the variance is minimal when all receptor channels are either fully open or fully closed and maximal when the mean open probability is 0.5. Assuming that the noise variance is due to the summation of currents flowing through many independent, identical channels that are randomly opening and closing, it is possible to quantify the relationships between the membrane potential, total cell membrane current variance, total current, number of channels, single-channel conductance and mean channel open probability. In a few cases, noise analysis measurements in non-receptor systems have been confirmed by single-channel experiments. Noise analysis measurements are challenging because of the inherent difficulty of making good recordings of membrane currents in mechanoreceptor cells. However, the cases where they have been made have produced rather consistent results. In statocyst cells of the snail *Hermissenda*, noise analysis gave values of 5 pS for the single-channel conductance and 40 channels per cell (French, 1992). In vertebrate hair cells, the corresponding values were 12 pS and 280 channels per cell (Hudspeth, 2005) and in spider slit sensilla neurons, 7.5 pS and 300 channels per cell (French et al., 2002). In *C. elegans* gentle touch receptor neurons, the single channel conductance was 25 pS and the number of channels per cell was estimated to be 14 to 25 (O'Hagan et al., 2005) while the ciliated touch receptor neurons had 21 channels per cell with a conductance of 16 pS per channel (Kang et al., 2010). These single-channel conductances are all at the low end of the range of known mechanically-activated ion channels and significantly lower than the single-channel measurements described above. The total membrane conductances due to mechanotransduction channels observed during these measurements agree with several estimates made in other mechanosensory neurons, and would provide enough current to depolarize the neurons to produce action potentials. Therefore, it seems likely that the number of channels in each cell is limited to a few hundred at most, raising difficulties for electrophysiological, molecular and histological attempts at localization or characterization.

Another interesting property of mechanotransduction channels is their *temperature sensitivity*. This has been measured in at least six invertebrate and vertebrate preparations with activation energy values in the range of 12–22 kcal/mol ($\approx$50–100 kJ/mol) (French et al., 2002). These energy values are similar to those required to break chemical bonds and significantly more than the energy barriers associated with ionic diffusion or conductance through ion channels. Little is known about the activation energy of mechanically-activated ion channels, but it seems likely that some crucial stage in the link between membrane tension and ion channel opening leads to this relatively high energetic barrier.

VIIC. Encoding

Most mechanoreceptors use action potentials to transmit information to the central nervous system. The action potentials are produced by conventional combinations of voltage-dependent Na^+ and K^+ channels. Accurate characterization of these currents and other currents involved in the control of membrane excitability relies on voltage-clamp recordings, which have only been possible in a few cases. *Tetrodotoxin-sensitive Na^+ channels* are clearly responsible for the action potential upswing in Pacinian corpuscles (Loewenstein and Mendelson, 1965), lobster and crayfish stretch receptors (French, 1992; Rydqvist et al., 2007), the cockroach tactile spine (Torkkeli and French, 1994) and spider slit sensilla (French et al., 2002). The distribution of these channels in the cell membrane determines where the receptor potential is converted to action potentials. Voltage-gated Na^+ channels are present and the action potentials initiated at the first node of Ranvier under the lamellae of the Pacinian corpuscle (Pawson and Bolanowski, 2002). In the slowly adapting crayfish stretch receptor, the channels are located on the axon and the cell body but, in the rapidly adapting receptor, the channels are restricted to the axon itself (Rydqvist et al., 2007). In spider slit sensilla, Na^+ channels are more evenly distributed, with a significant concentration on the sensory dendrite and the soma, with action potentials initiated in the dendrite (French et al., 2002). An additional slow component of Na^+ inactivation was needed to model the firing behavior of lobster stretch receptors and is probably present in the slowly adapting crayfish stretch receptor (Rydqvist et al., 2007) and the cockroach tactile spine (French and

Torkkeli, 1994). *C. elegans* neurons do not have voltage-gated Na^+ channels, but transmit signals as graded or plateau potentials that are believed to be carried by Ca^{2+} (Lockery and Goodman, 2009).

Delayed-rectifier K^+ currents seem to be responsible for action potential repolarization in all of the mechanoreceptors studied, but other types of K^+ currents are found in different receptors. Transient K^+ currents resembling the A-type current have been described in the slowly adapting cockroach tactile spine (Torkkeli and French, 1994) but not in spider slit sensilla that adapt significantly faster (French et al., 2002). The slowly adapting crayfish stretch receptor neuron has two components of delayed rectifier K^+ current and an A-current (Rydqvist et al., 2007). *Ca^{2+}-activated K^+ currents* were found in the cockroach tactile spine (Torkkeli and French, 1995) and vertebrate auditory hair cells (Hudspeth, 2005). An *inwardly rectifying K^+ current* is present in the slowly adapting lobster stretch receptor (French, 1992) but has not been described in other mechanoreceptors.

Ca^{2+} currents are present in vertebrate auditory neurons and negative feedback from depolarization-induced Ca^{2+} entry to hyperpolarization via Ca^{2+}-activated K^+ current has been suggested to cause frequency tuning (Hudspeth, 2005). Ca^{2+} currents are also present in spider slit sensilla (French et al., 2002) and increased intracellular Ca^{2+} modulates both the receptor current and firing rate (Höger et al., 2010). *Electrogenic Na^+ pumping* is well established in crayfish stretch receptors and contributes to adaptation of action potential discharge by repolarizing the cell after Na^+ entry. There is also evidence for its contribution to adaptation in the cockroach tactile spine neuron (French, 1992).

The terms *rapid adaptation* and *slow adaptation* are qualitative and have been used to describe a wide range of time dependence. However, some mechanoreceptors adapt so rapidly that only one or a few action potentials are produced in response to a step stimulus (Fig. 36.9) and so can truly be called "rapidly adapting". Rapid adaptation generally infers a cessation of activity soon after the start of a constant stimulus, but many rapidly adapting mechanoreceptors can fire action potentials as long as the stimulus is moving, which makes them excellent vibration detectors (Fig. 36.9). It has been known for many years that the encoding stage of the Pacinian corpuscle limits its response to one or two action potentials (Loewenstein and Mendelson, 1965), although the ionic basis for the effect is not known. In the cockroach tactile spine, removal of the rapidly deactivating K^+ A-current increased the overall rate of firing, but the receptor continued to adapt, while removal of the Ca^{2+}-activated K^+ current removed most of the adaptation (Torkkeli and French, 1994, 1995). However, blockade of these currents does not affect the shape of individual action potentials because their rapid repolarization is due to the delayed-rectifier current. Rapid

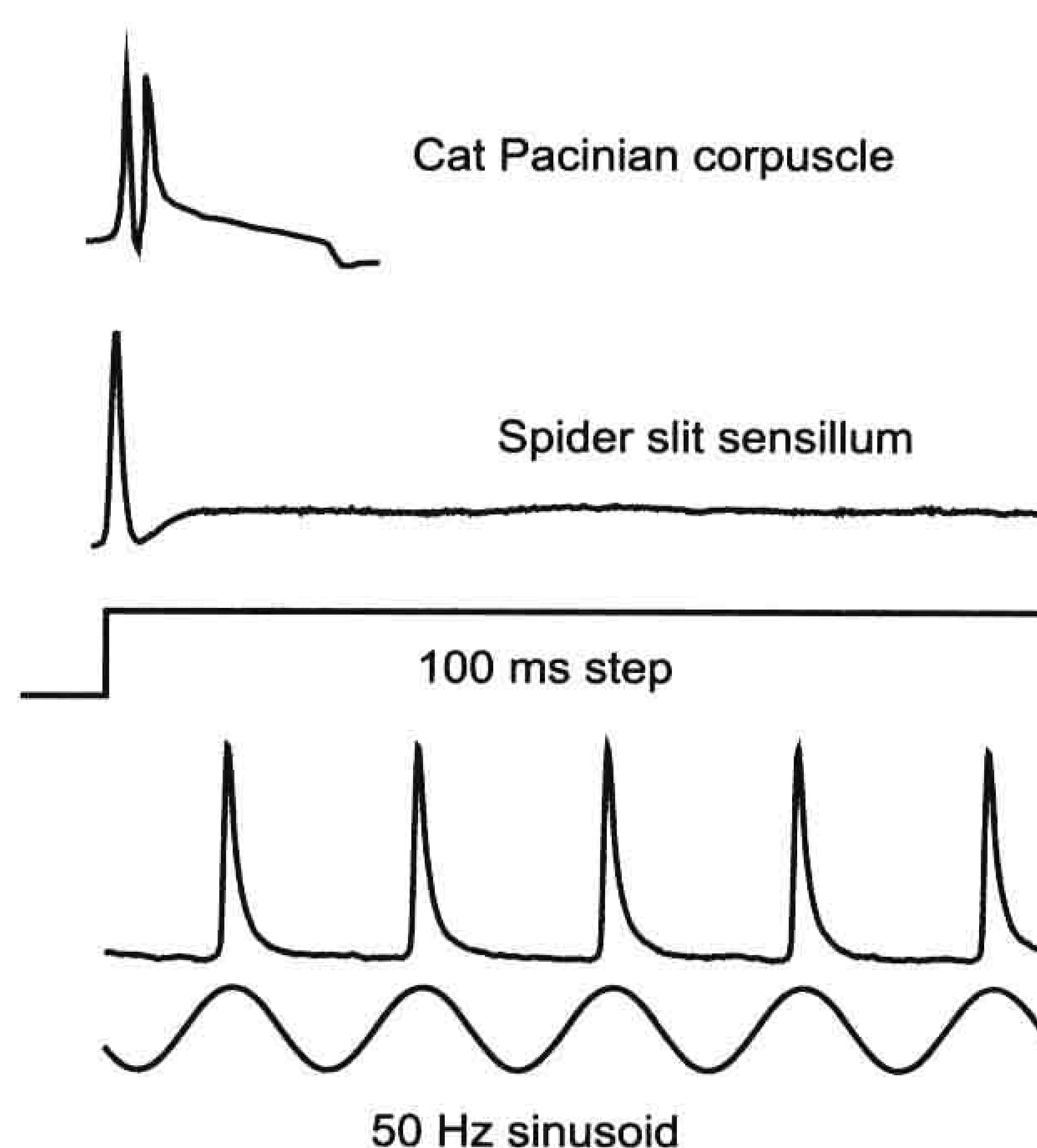


FIGURE 36.9 Rapid adaptation in vertebrate and invertebrate mechanoreceptors. A Pacinian corpuscle and a spider slit sensillum neuron each fire one or two action potentials in response to a step deformation and are then silent. But such receptors usually respond strongly to oscillating stimuli, making them good vibration detectors. Lower traces show a slit sensillum neuron firing 50 action potentials per second with sinusoidal mechanical stimulation. *(Partly redrawn from French and Torkkeli, 1994.)*

adaptation in spider VS-3 neurons seems to be partially due to the slow recovery of voltage activated Na^+ channels from their normal rapid inactivation (French et al., 2002).

Following the encoding stage, action potentials propagate into the central nervous system along nerve axons. In vertebrates, the cell bodies of the neurons are located in the dorsal root ganglia of the spinal cord and the axons enter via the dorsal roots. Cell bodies of the cranial mechanoreceptor nerves are located in the trigeminal ganglion. The major transmitter at the first central synapse is probably the excitatory amino acid glutamate. Arthropod mechanoreceptors have their cell bodies in the periphery and send axons into the central nervous system via nerve roots of the segmental ganglia, which are sometimes fused into larger structures. Conduction velocities are typically 1−5 m/s. The dominant transmitter for arthropod mechanoreceptors is acetylcholine (Burrows, 1996), although several spider mechanosensory neurons also contain histamine (Fabian et al., 2002). Relevant information about crustacean muscle, including the unique innervation, is given in the Appendix to Chapter 47.

VIII. EFFERENT CONTROL OF MECHANORECEPTORS

All mechanoreceptors receive inhibitory efferent innervation close to the output synapses of their centrally located axon terminals. Other well-known examples of efferent control are the gamma innervation of muscle spindles

(see Fig. 36.6) and presynaptic inhibition of peripheral mechanoreceptors and pain receptors (Rudomin, 2009). Presynaptic inhibition of mechanosensory neurons is remarkably similar in all vertebrate and invertebrate species studied so far (Burrows, 1996; Torkkeli and Panek, 2002; Rudomin, 2009). In addition to the GABAergic inhibitory control of axon terminals, most mechanosensory neurons are also regulated by other chemical agents. In many cases, the sensory endings and cell bodies also receive synaptic input from efferent neurons or accessory cells. Transmitter receptors are found in the somata of vertebrate dorsal root ganglion neurons (Robertson, 1989) and in the nerve fibers inside the Pacinian corpuscles (Pawson et al., 2009).

Merkel cells form synaptic contacts with mechanosensory afferents and, although Merkel cells have recently been shown to be necessary for the light touch responses, it is still not clear whether these cells are mainly modulatory or the actual sites of mechanotransduction (Lumpkin et al., 2010). Keratinocytes of the skin epidermis are also believed to perform signaling roles to mechanosensory endings (Tsunozaki and Bautista, 2009; Lumpkin et al., 2010). Modulation of vertebrate cutaneous mechanoreceptors and pain receptors by circulating factors has also been recognized for a long time. For example, sympathetic efferents have modulatory effects on muscle spindles, Pacinian corpuscles, several types of low-threshold skin mechanoreceptors and pain receptors, and these neurons express adrenergic receptors (Birder and Perl, 1999). Rohon–Beard neurons, which are developmentally early amphibian and fish touch receptors, have serotonergic efferent innervation and 5-HT is believed to alter their sensitivity to mechanical stimuli by inhibiting both low- and high-voltage-activated Ca^{2+} currents (Sun and Dale, 1997).

Arthropod mechanosensory neurons are modulated by biogenic amines, especially octopamine, the invertebrate analog of norepinephrine (Burrows, 1996). The dorsal unpaired median neurons of locust, which secrete octopamine, have terminals in the periphery, closely associated with the dendrites of mechanoreceptors that are modulated by octopamine. Similarly, octopamine-containing efferent neurons innervate spider mechanosensory afferents, which have octopamine receptors and are modulated by octopamine (Torkkeli et al., 2011). Although octopaminergic modulation in arthropods is probably the most thoroughly studied neuromodulatory system, there are no clear conclusions about the mechanisms involved. Octopamine may increase or decrease spiking frequency, even in the same mechanosensory neuron and it may act by increasing intracellular Ca^{2+} or cAMP concentration or both (Torkkeli et al., 2011).

The most conclusive evidence that peripheral regions of mechanoreceptors receive efferent innervation comes from immunocytochemical findings in arachnid and crustacean mechanoreceptors (see Figs. 36.6 and 36.10). Both types of receptors have dense efferent innervation, forming several types of synapses on all parts of the sensory neurons, including their somata and dendrites (Fabian-Fine et al., 2002). Spider cuticular mechanoreceptors have at least four different types of synaptic structures on the efferent terminals. In addition to octopamine, the efferent neurons contain GABA, glutamate and acetylcholine and all of these agents modulate the excitability of mechanosensory

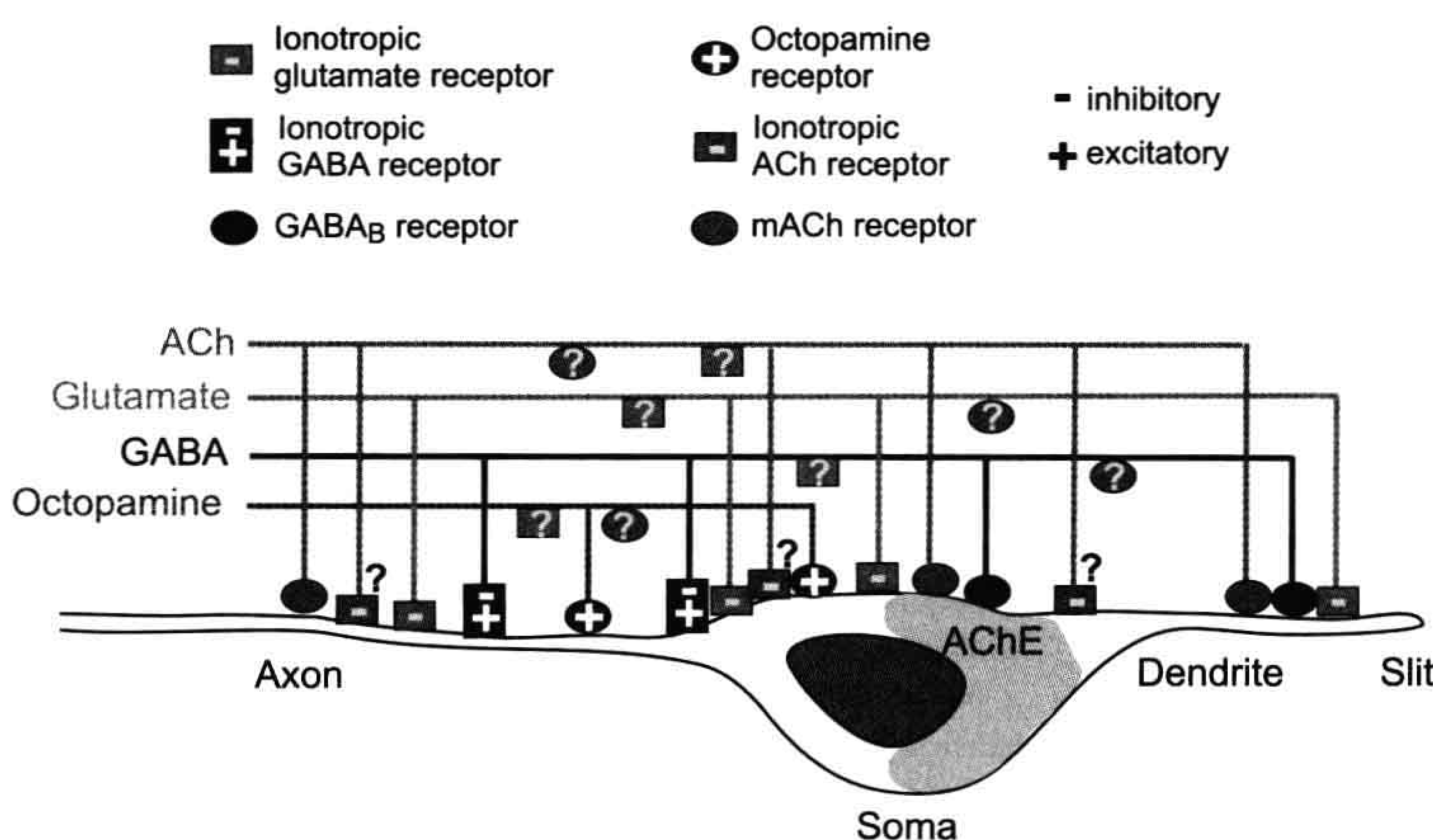


FIGURE 36.10 A schematic diagram showing the transmitter receptors on spider mechanosensory neurons and the efferent fibers innervating these neurons. At least three GABAergic, one glutamatergic and one octopaminergic efferent fiber have been identified by immunocytochemistry. In addition, choline acetyltransferase (ChAT) activity was present in one efferent fiber. Ionotropic inhibitory glutamate receptors (I_{Glu}) are located in all parts of the sensory neurons. Excitatory G-protein coupled octopamine receptors are only found in the axons and proximal parts of the somata. Ionotropic inhibitory-excitatory GABA receptors are probably also only present in the axons and somata. In contrast, the metabotropic $GABA_B$ receptors were found only at the distal parts of the soma and the dendrites. Ionotropic inhibitory ACh receptors are only present in the very rapidly adapting subgroup of VS-3 neurons (type A), but their distribution in these cells has not been determined, therefore these receptors are indicated with question marks. Muscarinic ACh receptors (mAChR) are present on all parts of the sensory neurons. AChE activity was present only in the type A VS-3 neuron and concentrated on the distal parts of the somata. I_{Glu} and mACh receptors are also found on some of the efferent neurons, but these have not been identified and therefore the receptors are indicated by question marks. *(Fabian-Fine et al., 2002; Widmer et al., 2006; Pfeiffer et al., 2009; Torkkeli et al., 2011).*

neurons, which have a variety of receptors to these transmitters (Widmer et al., 2006; Pfeiffer et al., 2009; Torkkeli et al., 2011). It is clear that the central nervous systems can control the sensitivity of mechanosensory neurons, although the full extent of this control is not yet completely understood.

IX. CONCLUSIONS

The large variety of morphological forms of mechanoreceptors indicates that the external components surrounding the sensitive endings play important roles in controlling the receptor behavior. Most of this control is assumed to involve coupling of initial movement into deformation of the membrane containing mechanically-activated channels. However, the mechanism involved has not been thoroughly decoded in any receptor and there may be other schemes involved, such as chemical modulation of excitability. Characterization of mechanically-activated channels is proceeding, but it is important to realize that no single-channel recordings have yet been unequivocally linked to mechanotransduction in any mechanosensory neuron. Therefore, it may yet emerge that an unknown family, or several different families, of channel proteins is responsible for this function in true mechanoreceptors. The encoding of action potentials from receptor current and the general control of receptor excitability involves voltage- and Ca^{2+}-activated ion channels, similar to those in other excitable cells, and complete models of encoding in some receptors are now available. Adaptation and general dynamic properties of mechanoreception involve both the coupling and encoding stages of the process. There may also be significant dynamic behavior of mechanotransduction channels, but this will not become clear until the channels themselves are better known. Efferent control of transduction and adaptation in mechanoreceptors is common but only well described in a small number of preparations.

Mechanoreception is a widespread and crucially important process for many physiological functions. Recent developments in electrophysiological techniques and new experimental preparations have provided important information about each stage of mechanoreception from initial deformation to action potential production, but much remains to be learned. In particular, the lack of vertebrate preparations that would allow voltage-clamp of receptor currents at the intact sensory ending or detailed examination of action potential encoding is a major problem. When the molecules responsible for mechanotransduction are known, it should be possible to discover how they are linked to other cellular components to confer mechanical sensitivity and from there to complete models of mechanoreception in intact sensory cells.

BIBLIOGRAPHY

Árnadóttir, J., & Chalfie, M. (2010). Eukaryotic mechanosensitive channels. *Annu Rev Biophys, 39*, 111–137.

Bell, J., Bolanowski, S., & Holmes, M. H. (1994). The structure and function of Pacinian corpuscles: a review. *Prog Neurobiol, 42*, 79–128.

Birder, L. A., & Perl, E. R. (1999). Expression of α_2-adrenergic receptors in rat primary afferent neurones after peripheral nerve injury or inflammation. *J Physiol, 515*, 533–542.

Burrows, M. (1996). *The Neurobiology of an Insect Brain*, Oxford: Oxford University Press.

Chalfie, M. (2009). Neurosensory mechanotransduction. *Nat Rev Mol Cell Biol, 10*, 44–52.

Christensen, A. P., & Corey, D. P. (2007). TRP channels in mechanosensation: direct or indirect activation? *Nat Rev Neurosci, 8*, 510–521.

Fabian-Fine, R., Seyfarth, E.-A., & Meinertzhagen, I. A. (2002). Peripheral synaptic contacts at mechanoreceptors in arachnids and crustaceans: morphological and immunocytochemical characteristics. *Microsc Res Tech, 58*, 283–298.

Fettiplace, R. (2009). Defining features of the hair cell mechanoelectrical transducer channel. *Pflügers Arch, 458*, 1115–1123.

French, A. S. (1992). Mechanotransduction. *Annu Rev Physiol, 54*, 135–152.

French, A. S., & Torkkeli, P. H. (1998). Information transmission at 500 bits/s by action potentials in a mechanosensory neuron of the cockroach. *Neurosci Lett, 243*, 113–116.

French, A. S., & Torkkeli, P. H. (1994). The basis of rapid adaptation in mechanoreceptors. *News Physiol Sci, 9*, 158–161.

French, A. S., Torkkeli, P. H., & Seyfarth, E.-A. (2002). From stress and strain to spikes: mechanotransduction in spider slit sensilla. *J Comp Physiol A, 188*, 739–752.

Goodman, M. B., & Schwarz, E. M. (2003). Transducing touch in *Caenorhabditis elegans*. *Annu Rev Physiol, 65*, 429–452.

Hu, J., & Lewin, G. R. (2006). Mechanosensitive currents in the neurites of cultured mouse sensory neurones. *J Physiol, 577*, 815–828.

Hudspeth, A. J. (2005). How the ear's works work: mechanoelectrical transduction and amplification by hair cells. *C R Biol, 328*, 155–162.

Höger, U., Torkkeli, P. H., & French, A. S. (2010). Feedback modulation of transduction by calcium in a spider mechanoreceptor. *Eur J Neurosci, 32*, 1473–1479.

Juusola, M., & French, A. S. (1997). The efficiency of sensory information coding by mechanoreceptor neurons. *Neuron, 18*, 959–968.

Kang, L., Gao, J., Schafer, W. R., Xie, Z., & Xu, X. Z. (2010). *C. elegans* TRP family protein TRP-4 is a pore-forming subunit of a native mechanotransduction channel. *Neuron, 67*, 381–391.

Lockery, S. R., & Goodman, M. B. (2009). The quest for action potentials in *C. elegans* neurons hits a plateau. *Nat Neurosci, 12*, 377–378.

Loewenstein, W. R., & Mendelson, M. (1965). Components of receptor adaptation in a Pacinian corpuscle. *J Physiol, 177*, 377–397.

Lumpkin, E. A., Marshall, K. L., & Nelson, A. M. (2010). The cell biology of touch. *J Cell Biol, 191*, 237–248.

Malinovsky, L. (1996). Sensory nerve formations in the skin and their classification. *Microsc Res Tech, 34*, 283–301.

McCarter, G. C., & Levine, J. D. (2006). Ionic basis of a mechanotransduction current in adult rat dorsal root ganglion neurons. *Mol Pain, 2*, 28–40.

McGlone, F., & Reilly, D. (2009). The cutaneous sensory system. *Neurosci Biobehav Rev, 34*, 148–159.

O'Hagan, R., Chalfie, M., & Goodman, M. B. (2005). The MEC-4 DEG/ENaC channel of *Caenorhabditis elegans* touch receptor neurons transduces mechanical signals. *Nat Neurosci, 8*, 43–50.

Pawson, L., & Bolanowski, S. J. (2002). Voltage-gated sodium channels are present on both the neural and capsular structures of Pacinian corpuscles. *Somatosens Mot Res, 19*, 231–237.

Pawson, L., Prestia, L. T., Mahoney, G. K., Guclu, B., Cox, P. J., & Pack, A. K. (2009). GABAergic/glutamatergic-glial/neuronal interaction contributes to rapid adaptation in Pacinian corpuscles. *J Neurosci, 29*, 2695–2705.

Pfeiffer, K., Panek, I., Höger, U., French, A. S., & Torkkeli, P. H. (2009). Random stimulation of spider mechanosensory neurons reveals long-lasting excitation by GABA and muscimol. *J Neurophysiol, 101*, 54–66.

Robertson, B. (1989). Characteristics of GABA-activated chloride channels in mammalian dorsal root ganglion neurones. *J Physiol, 411*, 285–300.

Rudomin, P. (2009). In search of lost presynaptic inhibition. *Exp Brain Res, 196*, 139–151.

Rydqvist, B., Lin, J. H., Sand, P., & Swerup, C. (2007). Mechanotransduction and the crayfish stretch receptor. *Physiol Behav, 92*, 21–28.

Sun, Q. Q., & Dale, N. (1997). Serotonergic inhibition of the T-type and high voltage-activated Ca^{2+} currents in the primary sensory neurons of *Xenopus* larvae. *J Neurosci, 17*, 6639–6649.

Torkkeli, P. H., & French, A. S. (1994). Characterization of a transient outward current in a rapidly adapting insect mechanoreceptor neuron. *Pflügers Arch, 429*, 72–78.

Torkkeli, P. H., & French, A. S. (1995). Slowly inactivating outward currents in a cuticular mechanoreceptor neuron of the cockroach (Periplaneta americana). *J Neurophysiol, 74*, 1200–1211.

Torkkeli, P. H., & French, A. S. (1999). Primary culture of antennal mechanoreceptor neurons of *Manduca sexta*. *Cell Tissue Res, 297*, 301–309.

Torkkeli, P. H., & Panek, I. (2002). Neuromodulation of arthropod mechanosensory neurons. *Microsc Res Tech, 58*, 299–311.

Torkkeli, P. H., Panek, I., & Meisner, S. (2011). Ca^{2+}/calmodulin dependent protein kinase II mediates octopamine-induced increase in sensitivity in spider VS-3 mechanosensory neurons. *Eur J Neurosci.*, (in press).

Tsunozaki, M., & Bautista, D. M. (2009). Mammalian somatosensory mechanotransduction. *Curr Opin Neurobiol, 19*, 362–369.

Walker, R. G., Willingham, A. T., & Zuker, C. S. (2000). A *Drosophila* mechanosensory transduction channel. *Science, 287*, 2229–2234.

Widmer, A., Panek, I., Höger, U., Meisner, S., French, A. S., & Torkkeli, P. H. (2006). Acetylcholine receptors in spider peripheral mechanosensilla. *J Comp Physiol. A, 192*, 85–95.

Chapter 37

Acoustic Transduction

Daniel C. Marcus

Chapter Outline

I. SUMMARY

The exquisite sensitivity of our sense of hearing results from the concerted action of many subsystems. The auditory peripheral organ, the cochlea, contains specialized cells for amplifying and sensing the mechanical auditory stimulus and other cells to create and maintain the unusual ionic environment in the cochlear lumen that powers and enables the transduction process. Function of these cells depends on specific gene expression patterns. A number of gene mutations are known to underlie specific clinical syndromic and non-syndromic hereditary hearing loss. It is perhaps surprising that most of these clinically important genes are located in the cells that engage in ion transport rather than the auditory sensory and neural cells. Major aspects of hearing and deafness can be understood as an integration of the many cellular processes that comprise the auditory organ.

II. INTRODUCTION

The detection of sound by mammals depends on a series of biological systems beginning with the collection of sound pressure waves by the external ear, followed by the mechanical transmission through the middle ear ossicles to the *cochlea* of the inner ear (Fig. 37.1). The sound pressure waves in the cochlea induce motion of the basilar membrane to which the sensory organ, the *organ of Corti*, is attached. The organ of Corti is comprised of the sensory *inner and outer hair cells* (Fig. 37.2), which are surrounded by Deiters' cells, pillar cells and Hensen's cells. Motion of the organ of Corti with respect to another structure (tectorial membrane) causes movements of the sensory cilia (hairs) on the hair cells and modulation of the flow of current through these hair cells, leading to modulation of the rate of firing of the afferent auditory nerve fibers, which synapse to the base of the hair cells. The nerve fibers carry the auditory information to the brain where the signal undergoes central processing, leading to the perception of sound. Peripheral auditory processing is modulated by efferent signals originating from the brain. This chapter focuses on the cellular aspects of acoustic transduction in the auditory periphery. Much of what we know about the cellular physiology of the mammalian cochlea is derived from experiments performed on

Cell Physiology Sourcebook. DOI: 10.1016/B978-0-12-387738-3.00037-8

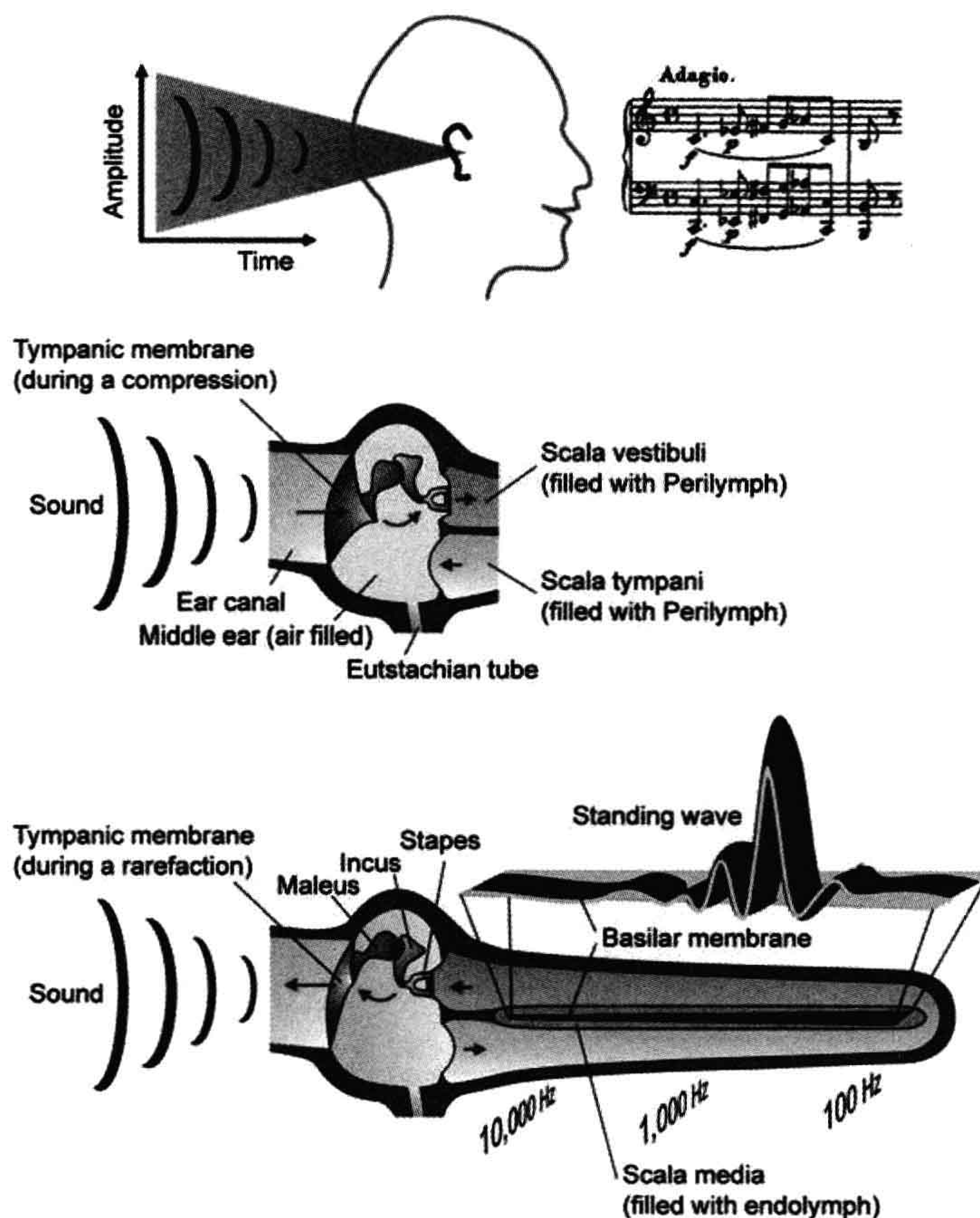


FIGURE 37.1 Diagrams of the physical pathway and effects of sounds from the environment to the cochlea. (Upper panel): Sound waves enter the outer ear and (middle panel) are transmitted by the tympanic membrane to the middle ear bones (ossicles: maleus, incus, stapes). The sound waves are then transmitted to scala vestibuli of the inner ear through the oval window. Acoustic energy enters the cochlea (lower panel; diagrammed uncoiled) where the frequency content of the sound waves is analyzed by the creation of standing waves along the basilar membrane and excites receptors and associated neurons at locations that code for the frequencies comprising the sound. *(Reproduced with permission from Marcus and Wangemann, (2009). In F.J. Alvarez-Leefmans and E. Delpire, eds), Physiology and Pathology of Chloride Transporters and Channels in the Nervous System – From Molecules to Diseases, pp. 425–437. Elsevier, New York.)*

preparations from the vestibular labyrinth of mammals, birds and amphibians, and from the cochlea of birds. There are strong homologies between the cochlea and vestibular labyrinth which are reviewed elsewhere (Lee and Marcus, 2008; Marcus and Wangemann, 2009, 2010; Kim and Marcus, 2011).

III. MAMMALIAN INNER EAR STRUCTURE

The transduction apparatus is part of an *epithelium* forming the *cochlear duct* and separating two distinct cochlear fluids, *endolymph* and *perilymph*. The composition and importance of these fluids is related later. A diagram of a cross-section of the mammalian cochlear duct is shown in Fig. 37.2. A mechanically stiff apical surface of the organ of Corti, the *reticular lamina*, is formed by cuticular plates just under the apical membrane of these cells. The organ of Corti sits on the *basilar membrane*, a fibrous sheet that transmits the acoustic stimulus.

In the medial direction from the organ of Corti, the duct is comprised of inner sulcus cells and interdental cells of the spiral limbus. The *tectorial membrane* is a gelatinous, acellular structure in the cochlear lumen apparently secreted by the interdental cells. Lateral from the organ of Corti, the cochlear duct consists of outer sulcus cells, spiral prominence cells and *marginal cells* of the *stria vascularis*. Reissner's membrane forms the remaining wall of the triangular-shaped cochlear duct and is comprised of a thin, avascular sheet of epithelial cells.

The apical and basolateral membranes of all of these cells are separated by tight junction complexes near the endolymphatic surface, which serve to join each cell to its neighbor and to complete the barrier between endolymph and the fluid bathing the basolateral membranes. The basolateral fluid is perilymph for all cell types except strial marginal cells, as described later. The cochlear duct is closed at the apex of the cochlea and is joined at the base of

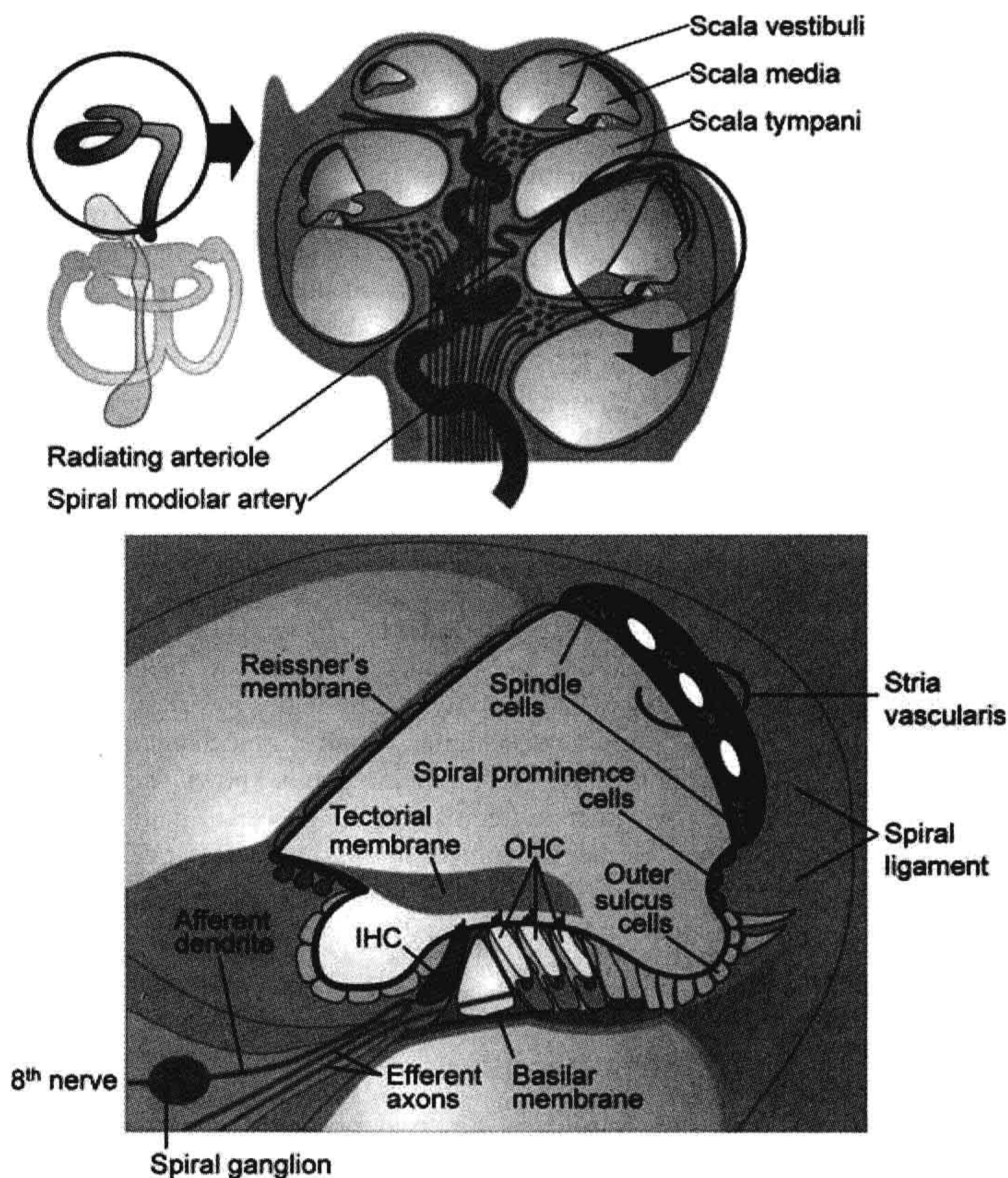


FIGURE 37.2 Diagram of a cross-section of a coiled cochlea. Upper panel shows the membranous structures of the inner ear (left) with the cochlea in the circle and a cross-section of the entire cochlea (right). Lower panel shows a cross-section of one turn of the cochlear lumen, scala media (pink), which is filled with endolymph, an unusual extracellular fluid that is high in K^+ and low in Na^+ and Ca^{2+} content. The composition of this fluid is maintained by the epithelial cells bounding the lumen that include the stria vascularis in the lateral wall, Reissner's membrane and organ of Corti that contains the sensory inner hair cells and the outer hair cells that provide amplification of the sound-induced mechanical vibrations of the basilar membrane. *(Reproduced with permission from Kim, H. M. and Wangemann, P. (2011) Epithelial cell stretching and luminal acidification lead to a retarded development of stria vascularis and deafness in mice lacking pendrin. PLoS.One. 6(3):e17949; Griffith, A. J. and Wangemann P. (2011) Hearing Loss Associated with Enlargement of the Vestibular Aqueduct: Mechanistic Insights from Clinical Phenotypes, Genotypes, and Mouse Models. Hear Res, doi:10.1016/j.heares.2011.05.009; Marcus and Wangemann, (2009). In (F.J. Alvarez-Leefmans and E. Delpire, eds), Physiology and Pathology of Chloride Transporters and Channels in the Nervous System—From Molecules to Diseases, pp. 425—337. Elsevier, New York.)*

the cochlea via a constriction in the epithelial lumen (ductus reuniens) to the vestibular system. Cellular physiologists have focused much of their attention on the strial marginal cells, which provide the energy source for the transduction process, and on the sensory hair cells themselves. In recent years, the contributions of other cell types bordering the cochlear lumen to endolymph ion homeostasis have been determined and are under continuing investigation.

IV. CELL PHYSIOLOGY OF ENDOLYMPH HOMEOSTASIS

IVA. Composition

Even in the absence of an acoustic stimulus, the cochlea is highly active, maintaining the electrolyte composition of endolymph (Table 37.1) and a standing current analogous to the "dark current" of photoreceptors (see Chapter 38) (Marcus and Wangemann, 2010). The transduction current from endolymph through the hair cells is carried predominantly by K^+ and so depends on the high concentration of that ion in endolymph. A low concentration of Ca^{2+} in endolymph is regulated by several cells types; this ion maintains the integrity of tip links between stereocilia of hair cells and enters the transduction channels of hair cells to modulate transduction processes. Gross changes in endolymph composition by a tear in *Reissner's membrane*, by drug action or by genetic interference in K^+ secretion led to degeneration of the hair cells with subsequent degeneration of the synapsing afferent auditory nerve (Vetter et al., 1996). The dimensions of the gelatinous tectorial membrane are sensitive to the levels of K^+, Na^+, H^+ and Ca^{2+} as well as to unknown chemical factors (Shah et al., 1995). Swelling has been associated with substitution of Na^+ for K^+ and with decreases of Ca^{2+}. Maintenance of the tectorial membrane structural properties is needed for normal hearing since it is one of the physical structures coupling the acoustic stimulus to hair cells.

TABLE 37.1 Approximate Ion Composition and Electrical Potential of Cochlear Endolymph and Perilymph[a]

Ion	Endolymph	Perilymph
Potassium (mM)	157	4.2
Sodium (mM)	1.3	148
Calcium (mM)	0.02	1.3
Chloride (mM)	132	119
Bicarbonate (mM)	31	21
Protein (mg/dL)	38	178
pH	7.5	7.3
Potential (mV)	+80	0

[a]Reproduced by permission from D.C. Marcus and P. Wangemann (2010). Inner ear fluid homeostasis. In P.A. Fuchs, ed.), The Oxford Handbook of Auditory Science: The Ear, pp. 213–230. Oxford University Press, Oxford.

IVB. Cellular Basis of Endolymphatic Ion Homeostasis

The ion composition of fluid compartments in the body is maintained by epithelial ion transport. The known epithelial domains in the ear responsible for K^+ and Na^+ transport are shown in Fig. 37.3A. Homeostatic imbalance leads to swelling or collapse of the cochlear lumen (Fig. 37.3B), as observed in Pendred syndrome or Scheibe's deformity, respectively.

Transepithelial transport is accomplished through expression of a special constellation of specific ion channels, transporters and pumps in the apical and basolateral membranes. The influx and efflux pathways for Na^+ and K^+ in the cochlea are illustrated in Fig. 37.3A. K^+ is taken up by the *stria vascularis* from the *spiral ligament* in the lateral wall and secreted into endolymph. K^+ enters the hair cells through *mechanosensitive transduction channels* in the apical stereocilia and this entry flux is modulated by the acoustically-gated mechanosensitive channels. K^+ then leaves the hair cells across their basolateral membranes via K^+-selective ion channels. The accumulated K^+ in the extracellular fluid surrounding the hair cells returns to the spiral ligament by diffusion. Three alternate pathways have been proposed and are described in Fig. 37.4. K^+ reaching the spiral ligament is then returned to the endolymph by the stria vascularis. Additional descriptions of K^+ transport by the stria vascularis and of the transduction process are given below.

Endolymphatic [Na^+] is maintained below electrochemical equilibrium with the perilymph; it "leaks" into the cochlear lumen and so must be actively removed. Two types of transport have been identified and described (reviewed in Kim and Marcus, 2011) (see Fig. 37.3B, C). The outer sulcus cells and the hair cells possess nonselective cation (NSC) channels in their apical membranes (small-conductance NSC channels and the large mechanosensitive transduction channels, respectively). Na^+, as well as K^+, enters the cells via these channels and are removed from the cells into perilymph by basolateral Na^+, K^+-ATPase (the Na^+-pump) in parallel with K^+ channels. The outer sulcus cells thereby act as a parasensory K^+ pathway in addition to their function as a Na^+ extrusion mechanism. This parasensory Na^+ and K^+ efflux is modulated by luminal ATP via P2X ionotropic receptors (Chapter 31).

A second, and perhaps more significant, Na^+ efflux pathway is through Reissner's membrane epithelium (reviewed in Kim and Marcus, 2011). These cells utilize apical epithelial Na^+ channels (ENaC) to mediate Na^+ absorption. ENaC activity can be under a variety of intracellular and extracellular control mechanisms. Na^+ absorption by Reissner's membrane is known to be stimulated by glucocorticoids via a genomic pathway and appears to be controlled by luminal ATP. ATP would increase the Na^+ absorption via ligand-gated NSC channels (P2X receptors) and decrease Na^+ absorption via signalling from P2Y4 receptors.

IVC. Stria Vascularis

The stria vascularis has two primary known functions: secretion of K^+ and generation of the lumen-positive *endocochlear potential* (EP; ca. +80 mV). The high endolymphatic K^+ concentration provides the carrier of the transduction current. The driving force for that current consists almost exclusively of the voltage across the transduction channels in the stereocilia (see Section VI) and that voltage is the sum of the intracellular potential of the hair cells and the EP. The large EP therefore heightens the sensitivity of the cochlear transduction process compared to vestibular organs, which do not have this high transepithelial electrical polarization. The cellular transport model by which the stria vascularis secretes potassium and generates the EP is shown in Fig. 37.4 and described next. Recall that all epithelial cells that produce a vectorial transport of substances do so by virtue of different membrane properties of their apical and basolateral membranes.

IVC1. Division of Function between Marginal and Basal Cell Barriers

The stria vascularis consists of two barriers formed by the marginal cells and the basal cells. Each barrier consists of a continuous sheet of cells joined by tight junction

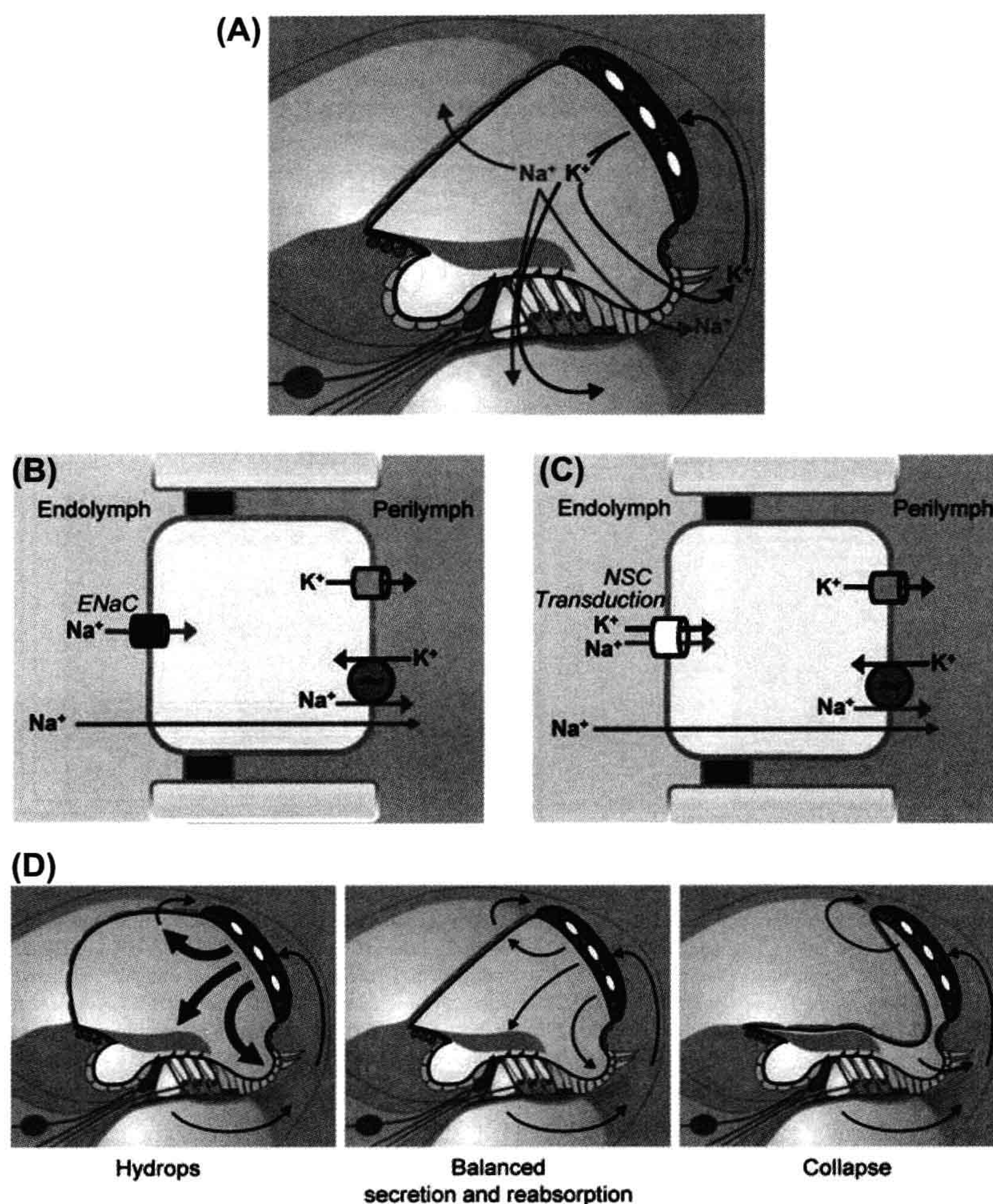


FIGURE 37.3 Schematic cross-sections through one cochlear turn illustrating inner ear ion and water transport. (A) K^+ secretion by stria vascularis (SV) and absorption by sensory cells in the organ of Corti and outer sulcus cells; Na^+ absorption by Reissner's membrane, hair cells and outer sulcus cells. Cell models of transepithelial Na^+ absorption via Na^+-selective epithelial Na^+ channels (ENaC) (B) or non-selective cation channels (C), including the non-selective transduction channels of hair cells. (D) Effects of hypoabsorption and/or hypersecretion (hydrops) of balanced transport (normal cross-section) and of hyperabsorption and/or hyposecretion (collapse). (C). *(Reproduced with permission from Kim, S.H. and Marcus, D.C. (2011). Regulation of sodium transport in the inner ear. Hear Res. 280, 21–29, and Wangemann, P. (2002). Adrenergic and muscarinic control of cochlear endolymph production. Adv Otorhinolaryngol. 59, 42–50, and Marcus and Wangemann, (2009). In (F.J. Alvarez-Leefmans and E. Delpire, eds), Physiology and Pathology of Chloride Transporters and Channels in the Nervous System—From Molecules to Diseases, pp. 425–437. Elsevier, New York).*

complexes (see Fig. 37.4). Between these barriers is the intrastrial space with the capillary bed for which the tissue is named and a discontinuous layer of *intermediate cells*. The basal cells are joined via *gap junctions* (see Chapter 22) to the intermediate cells and to fibrocytes in the adjacent connective tissue, suggesting a level of cooperation among these three cell types (Kikuchi et al., 2000). Unlike most sheets of epithelial cells, strial marginal cells are not coupled to each other nor to other cells by gap junctions (Takeuchi and Ando, 1998; Kikuchi et al., 2000). The physiological significance of this functional independence of marginal cells is not known.

The basal cell/intermédiate cell syncytium produces and supports the endocochlear potential and the strial marginal cells secrete K^+. In spite of the distinct cellular functions, the two processes are closely tied together through the composition of the intrastrial space. For example, inhibition of K^+ secretion by the marginal cells

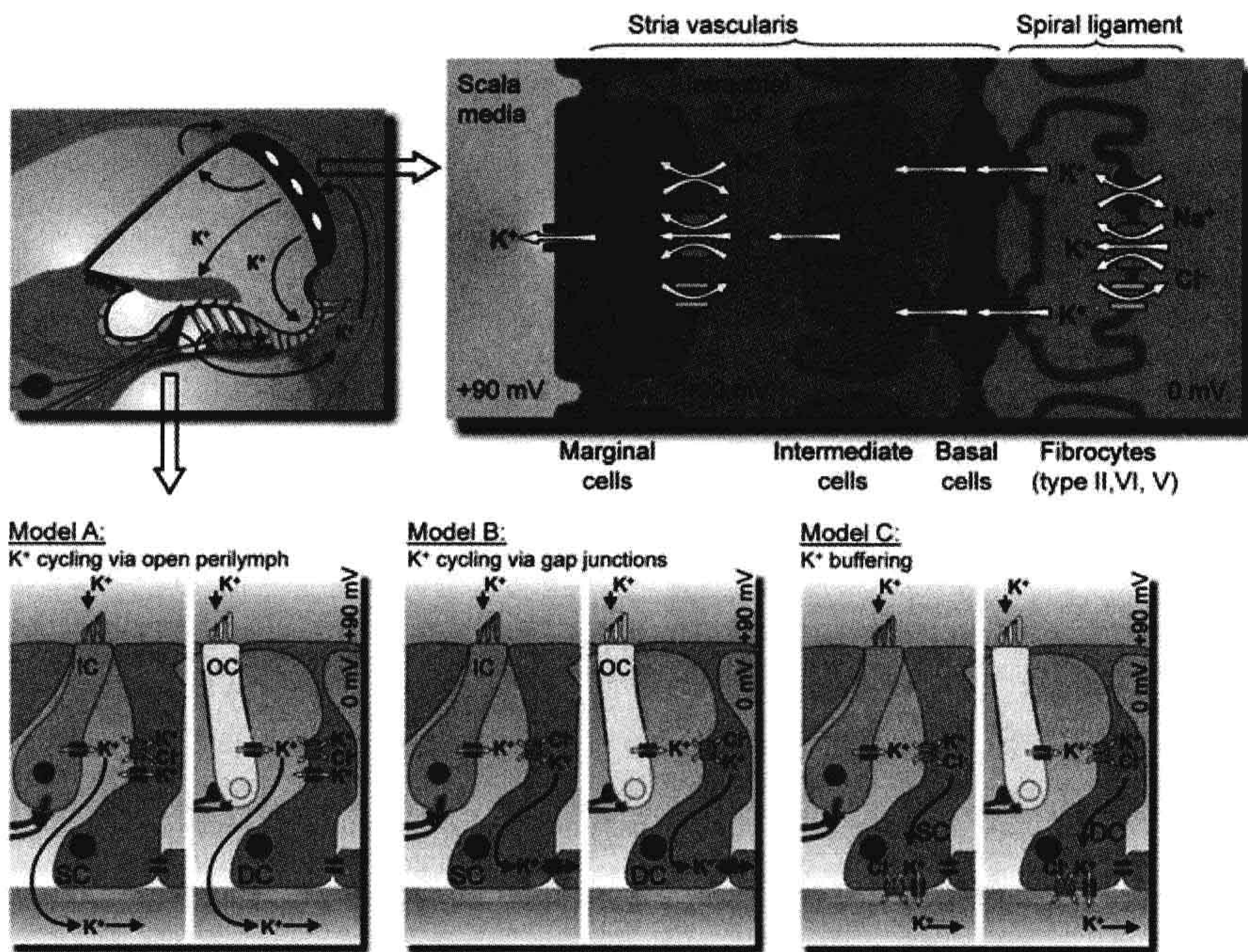


FIGURE 37.4 Overview of the stria vascularis and its K^+ transport mechanisms and three models of K^+ pathways that remove K^+ from the hair cells. (Inset) Cochlear cross-section. (Top panel) The stria vascularis consists of three distinct cell types: marginal, intermediate and basal cells. Intermediate cells are connected via gap junctions to basal cells which, in turn, form gap junctions with underlying fibrocytes. Gap junctions among the fibrocytes are not shown. (Bottom panel) Model A: postulates that K^+ released from hair cells cycles back to the stria vascularis through the open perilymph space; Model B: entails K^+ recycling through inner phalangeal cells, marked as supporting cells (SC) by the inner hair cells (IC) or Deiters' cells (DC) by the outer hair cells (OC); Model C: the supporting cells act as a K^+ buffer. Note that these three models are not mutually exclusive. *(Reproduced with permission from Zdebik, A.A., Wangemann, P. and Jentsch, T.J. (2009). Potassium ion movement in the inner ear: insights from genetic disease and mouse models. Physiology (Bethesda.) 24, 307–316, and Marcus and Wangemann, (2009). In (F.J. Alvarez-Leefmans and E. Delpire, eds), Physiology and Pathology of Chloride Transporters and Channels in the Nervous System—From Molecules to Diseases, pp. 425–437. Elsevier, New York.)*

leads to a decline of the endocochlear potential. This would occur by a rise in intrastrial K^+ concentration upon cessation of K^+ uptake by the marginal cells and the consequent depolarization of the K^+-selective intermediate cell membrane (see below). Several lines of evidence, including histochemical, biochemical, electrophysiological and flux studies, have strongly suggested that the stria vascularis is responsible for secretion of K^+ into the cochlear lumen and for production of the EP (reviewed in Marcus and Wangemann, 2010).

IVC2. K^+ Secretion by Strial Marginal Cell Epithelium

Active K^+ secretion in the cochlear duct has been demonstrated by flux measurements of radiolabeled K^+ introduced in either the perilymphatic or vascular space and its appearance in endolymph (Konishi et al., 1978; Sterkers et al., 1982). These fluxes were inhibited by transport blockers and anoxia. The stria was assumed to be the site of secretion since the flux was nearly the same when the radiotracer was added to either scala vestibuli or scala tympani; possible contributions by the spiral limbus were disregarded.

More recently, the stria was isolated from the cochlear duct, a K^+-selective self-referencing probe was placed near the tissue in vitro and a K^+ gradient was found directed away from the luminal surface (Wangemann et al., 1995) (Fig. 37.5A). The marginal cell layer of the stria vascularis produces this K^+ flux using the constellation of transport processes shown in Fig. 37.4. K^+ is taken up across the *basolateral membrane* from the *intrastrial space* fluid by two transporters: the *Na^+,K^+-ATPase (Na^+ pump)* and the *NKCC1 Na^+-K^+-Cl^- co-transporter*. The first is a primary active process, which uses the energy from cytosolic adenosine triphosphate (ATP) and the second is secondary active and uses the large Na^+ concentration gradient between extracellular and intracellular compartments created by the Na^+,K^+-ATPase. Na^+ and Cl^- taken up by the co-transporter are removed from the cytosol by the

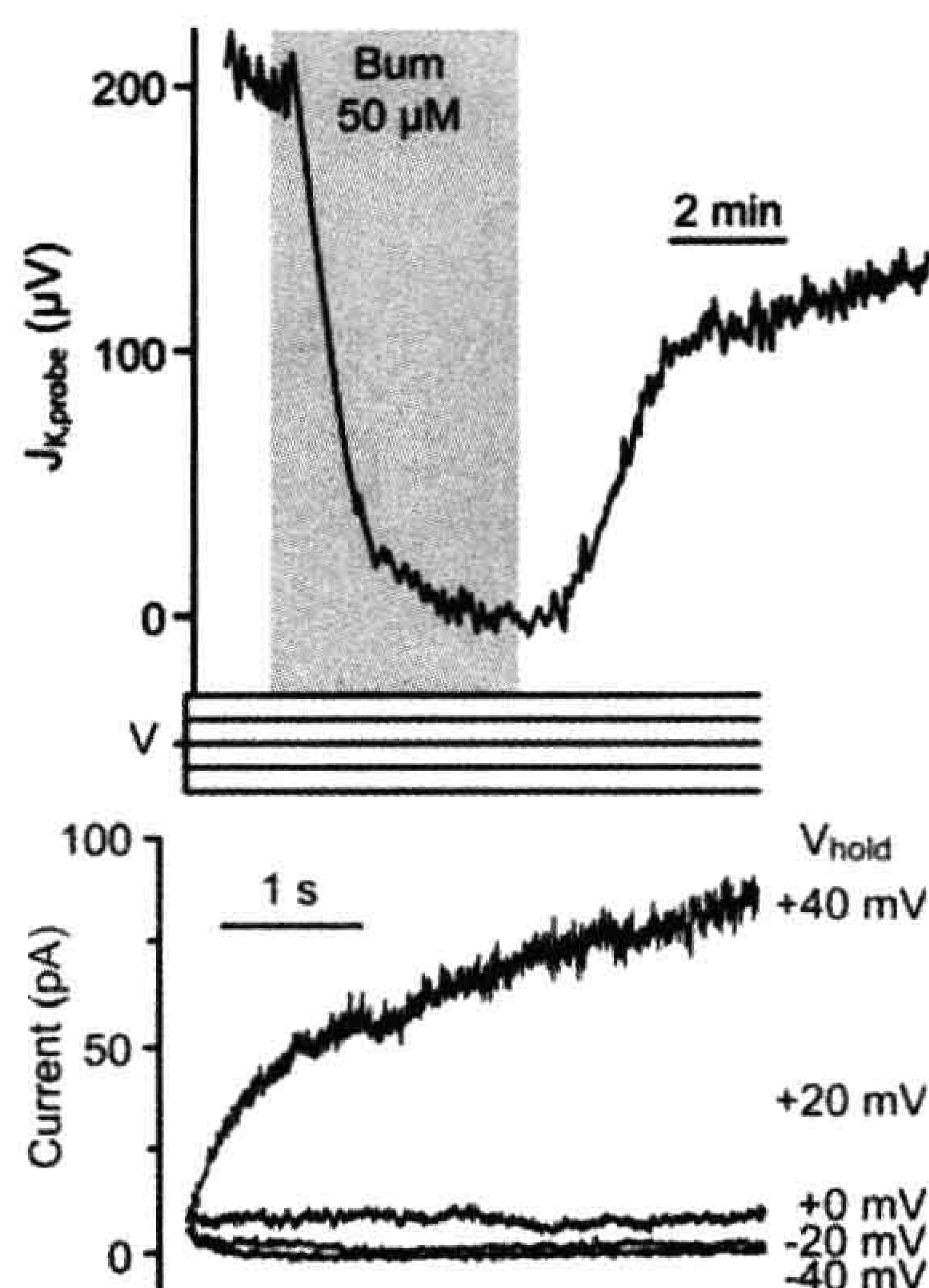


FIGURE 37.5 Transepithelial K^+ flux and apical membrane K^+ currents via KCNQ1/KCNE1 K channels. (A) K^+ secretory flux from stria vascularis measured with a K^+-selective self-referencing probe. The ordinate is the flux expressed as the difference in microvolts measured at the two positions of the probe. Flux was decreased by basolateral perfusion of the inhibitor of Na^+-K^+-Cl^- co-transport, bumetanide (Bum). *(Adapted from Wangemann, P., Liu, J. and Marcus, D.C. (1995). Ion transport mechanisms responsible for K^+ secretion and the transepithelial voltage across marginal cells of stria vascularis in vitro. Hear Res. 84, 19–29, Copyright 1995 with kind permission of Elsevier Science-NL, Sara Burgerhartstraat 25, 1055 KV Amsterdam, The Netherlands.).* (B) Patch-clamp currents from the apical membrane of a strial marginal cell, on-cell configuration. Sustained depolarizations activate the current slowly over several seconds, characteristic of KCNQ1/KCNE1 K^+ channels. *(Reproduced with permission from Shen, Z., Marcus, D.C., Sunose, H., Chiba, T. and Wangemann, P. (1997). I_{sK} channel in strial marginal cells: voltage-dependence, ion-selectivity, inhibition by 293B and sensitivity to clofilium. Auditory Neurosci. 3, 215–230.)*

Na^+,K^+-ATPase and basolateral *ClC-K/barttin (/BSND) Cl^- channels*, respectively (Marcus and Wangemann, 2010).

K^+ secretion occurs passively via channels in the apical membrane (see Figs. 37.4 and 37.5). These channels are products of the genes KCNQ1 and KCNE1, which code for the pore-forming α subunit and the regulatory β subunit of the channel, respectively. The KCNQ1/KCNE1 channels are characterized by slow activation (over seconds) in response to depolarization of the cell membrane and have a single-channel conductance of about 14 pS under in vivo-like conditions (see Fig. 37.5B) (Marcus and Shen, 1994; Shen et al., 1997; Marcus and Wangemann, 2010). The essential contributions to K^+ secretion of the apical K^+ channel and of the basolateral co-transporter have been demonstrated with gene knockout mice. Individual deletion of KCNQ1, KCNE1 or NKCC1 (Slc12a2) resulted in a collapsed lumen in knockout mice.

IVC3. Production of Endocochlear Potential by Strial Intermediate and Basal Cells

Two key genes expressed in the stria vascularis are at the heart of EP generation: those that code for the tight junction protein claudin-11 and the KCNJ10 K^+ channel. Tight junctions are formed from an assemblage of a number of proteins and the family of claudin isoforms provides definition to the permeability characteristics of each junction. The basal cell barrier contains claudin-11 and the connections among these cells are the only location for claudin-11 in the inner ear. An important demonstration of the importance of claudin-11 to EP generation was the observation that the EP collapsed in claudin-11 knockout mice, while K^+ secretion continued since marginal cell function was unimpaired (Gow et al., 2004).

The KCNJ10 K^+ channel (also known as Kir4.1) is expressed in the membrane of intermediate cells (see Fig. 37.4). Intracellular K^+ is maintained high by uptake from perilymph by fibrocytes in the spiral ligament and diffusion via gap junctions into basal cells and intermediate cells (see Fig. 37.4) (Kikuchi et al., 2000). Intrastrial K^+ is maintained at an unusually low level in the intrastrial space by the marginal cells. The membrane potential of the intermediate cells is dominated by the KCNJ10 conductance. Normally, one would then expect the intermediate cells to be highly negative, as observed in symmetrical cells that are dominated by a membrane K^+ conductance. However, the basal cells are highly depolarized, perhaps by non-selective cation channels, and the high density of gap junctions between basal cells and intermediate cells effectively "grounds" the cytosol of the intermediate cells. With the intermediate cells near zero with respect to the extracellular fluid of the spiral ligament (perilymph), the intrastrial space (electrically isolated from the perilymph by the claudin-11-containing tight junctions of the basal cells) is highly positive. That high positive potential appears in the endolymph as the EP. The marginal cell layer generates very little contribution to the EP, similar to the K^+-secreting vestibular dark cell epithelium which is a monolayer without the intermediate cell/basal cell layer. The importance of the KCNJ10 channel to EP generation is supported by the observation that KCNJ10 knockout mice have no EP, but maintain an elevated endolymphatic [K^+].

The general scheme of strial function shown in Fig. 37.4 was first supported by observations of the electrical and K^+ profile of the stria obtained with double-barrel electrodes (Salt et al., 1987). In the spiral ligament, the potential was taken as zero and the K^+ concentration was a few millimolar (Fig. 37.6). As the electrode was advanced, a region was found where the K^+ concentration was also low but the

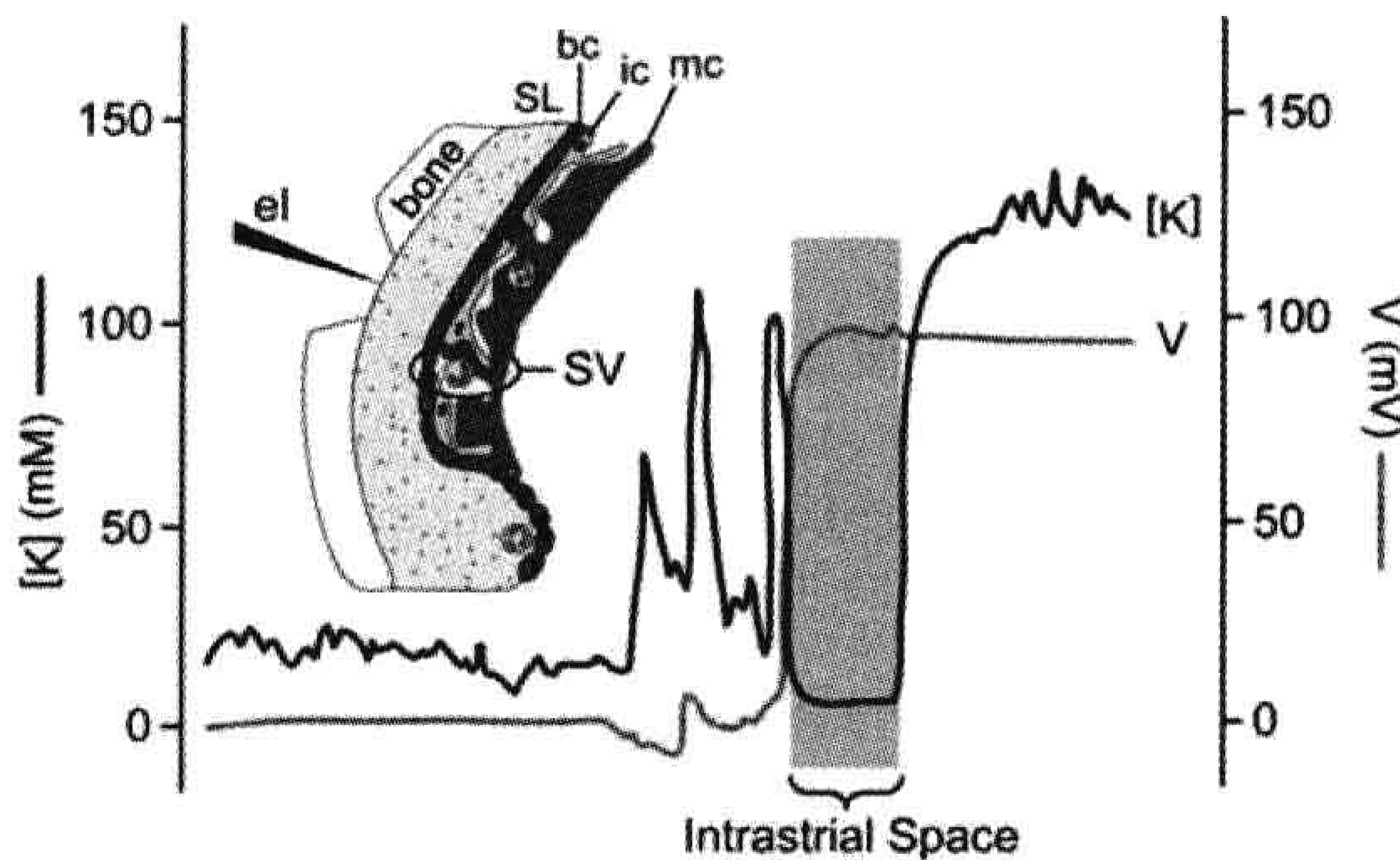


FIGURE 37.6 Recording of profiles for voltage (orange line; right axis) and K^+ concentration (blue line; left axis) during penetration of the stria vascularis (SV). A region was found where the voltage with respect to perilymph was highly positive but the K^+ concentration was low; this region was interpreted to be the intrastrial space. SL, spiral ligament; bc, basal cell; ic, intermediate cell; mc, marginal cell; el, penetrating electrode advanced from left to right. Horizontal axis is time/distance of electrode advancement. *(Adapted with permission from Salt, A.N., Melichar, I. and Thalmann, R. (1987). Mechanisms of endocochlear potential generation by stria vascularis. Laryngoscope. 97, 984-991, and (inset) from Dallos, P. (1996). Overview: Cochlear neurobiology. In (P. Dallos, A.N. Popper, and R.R. Fay, eds), The Cochlea, pp. 1–43. Copyright 1996 by Springer-Verlag.)*

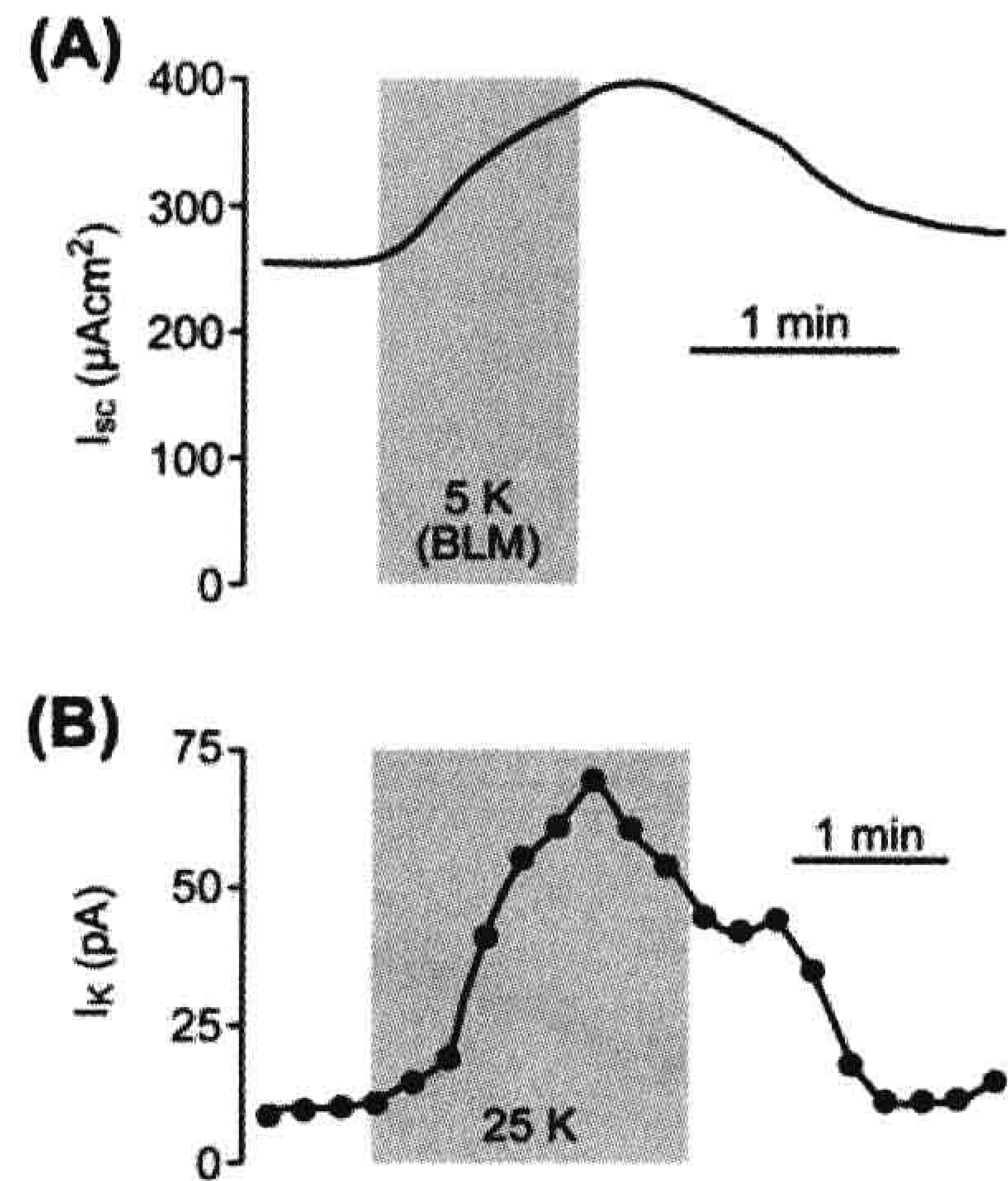


FIGURE 37.7 Stimulation of (A) short circuit current (I_{sc}) and (B) K^+ current through the apical KCNQ1/KCNE1 K^+ channels (I_K) on K^+ concentration in vestibular dark cells, the homologs to strial marginal cells. Basolateral [K^+] was increased from 3.6 mM to 5 mM (A) or 25 mM (B). *(Adapted from Wangemann, P., Shen, Z., and Liu, J. (1996). K^+ induced stimulation of K^+ secretion involves activation of the IKs channel in vestibular dark cells, Hear Res. 100, 201–210. Copyright 1996 with kind permission of Elsevier Science-NL, Sara Burgerhartstraat 25, 1055 KV Amsterdam, The Netherlands.)*

potential had risen to about +80 mV. This was interpreted as being located in the intrastrial space. Further penetration led to a jump of the K^+ concentration to that commonly found in endolymph with no appreciable change in the potential. The voltage gradient was therefore largest across the basal cell layer and the K^+ gradient largest across the marginal cell layer.

IVC4. Regulation of Ion Transport in Strial Marginal Cells

Every cell type encounters perturbations and signals by systemic variables, such as by hormones and/or neurotransmitters, osmotic strength and extracellular [K^+] and pH (pH_o), and by cytosolic variables, such as intracellular Ca^{2+} and pH (pH_i). K^+ secretion in the inner ear is altered in response to many such stimuli.

Basolateral [K^+] and Apical pH

The increase in flow of K^+ through hair cells in response to acoustical stimulation is known to increase the concentration of K^+ in the perilymph surrounding the basolateral membranes of the hair cells and the nerve endings. The rate of basolateral uptake of K^+ in strial marginal cells and of its secretion through the apical K^+ channel has been found to be exquisitely sensitive to the concentration of perilymphatic K^+ (Fig. 37.7). This K^+ sensitivity is believed to play a significant role in regulating the recirculation of K^+ back into endolymph (Wangemann et al., 1996) (see Fig. 37.7). Extracellular pH and [Ca^{2+}] of the lumen is under cellular control in the cochlea (see below). The luminal pH can control key ion transporters in the stria vascularis and other cells. Of particular importance is the stimulation of KCNQ1/KCNE1 K channel activity and the inhibition of TRPV5/6 Ca^{2+} channel activity by extracellular pH (see below).

Hormones

There is no innervation of the stria vascularis, but these cells contain receptors coupled to ion transport for several local or systemic hormones, including catecholamines, ATP and adrenocorticosteroid hormones (Table 37.2). Vasopressin (antidiuretic hormone) affects the EP and longitudinal K^+ concentration gradient (Mori et al., 1989; Julien et al., 1994), but the cells with vasopressin receptors have not yet been identified. Basolateral perfusion in vitro of the β-adrenergic agonist isoproterenol caused maximal increases in I_{sc} of 40–75% in strial marginal cells (Wangemann, 2002).

β-Adrenergic receptors

β-Adrenergic receptors are commonly coupled via G proteins to adenylate cyclase (see Chapter 6). Indeed, an increase of cytosolic cAMP in strial marginal cells by direct stimulation of adenylate cyclase, by perfusion of a membrane-permeable cAMP analog, or by inhibition of phosphodiesterases that catalyze the breakdown of

TABLE 37.2 Hormones and Signal Pathways Regulating KCNQ1/KCNE1 Current

Hormone/Signal	Stimulate	Inhibit
β-Adrenergic agonist		
Basolateral	X	
Purinergic agonist		
Apical	Transient	X
Basolateral		X
cAMP	X	
Phospholipase C		X
Protein kinase C		X
Cytosolic Ca^{2+}	X	
Cytosolic pH	Transient	X
Cell swelling	X	

cAMP, all lead to an increase of I_{sc}. The stimulation of K^+ secretion by adrenergic agonists was found to be mediated by β-adrenergic receptors through determination of the potency order of specific antagonists and by demonstration of the presence of transcripts for this subtype in cochlear tissue.

In isolated strial marginal cell epithelium, both apical and basolateral perfusion of micromolar ATP significantly alter I_{sc} (Fig. 37.8) (Lee and Marcus, 2008). Apical ATP and analogs monotonically downregulate I_{sc}, whereas basolateral ATP and analogs transiently increase I_{sc} followed by downregulation. The data are consistent with the presence of purinergic receptors of the $P2Y_4$ subtype on the apical membrane and $P2Y_2$ subtypes on the basolateral membrane. Additional purinergic receptors may also play a role.

P2Y receptor subtypes are known in other cells to be coupled to G proteins that stimulate phospholipase C (PLC). PLC catalyzes the breakdown of membrane phospholipid to produce both inositol trisphosphate (IP_3) and diacylglycerol (DAG) (see Chapter 6). It is most common that the IP_3 branch of the PLC pathway regulates ion channel activity through the cytosolic level of free Ca^{2+}. However, it was shown that the apical $P2Y_4$ receptor downregulates K^+ secretion primarily via the DAG-protein kinase C (PKC) branch (Lee and Marcus, 2008) even though inositol phosphate production is increased in the cochlear lateral wall in response to P2Y agonists (Ogawa and Schacht, 1995).

Basolateral muscarinic receptors (M_3 and/or M_4) were observed to inhibit K secretion by strial marginal cells, but the lack of direct innervations led to the speculation that

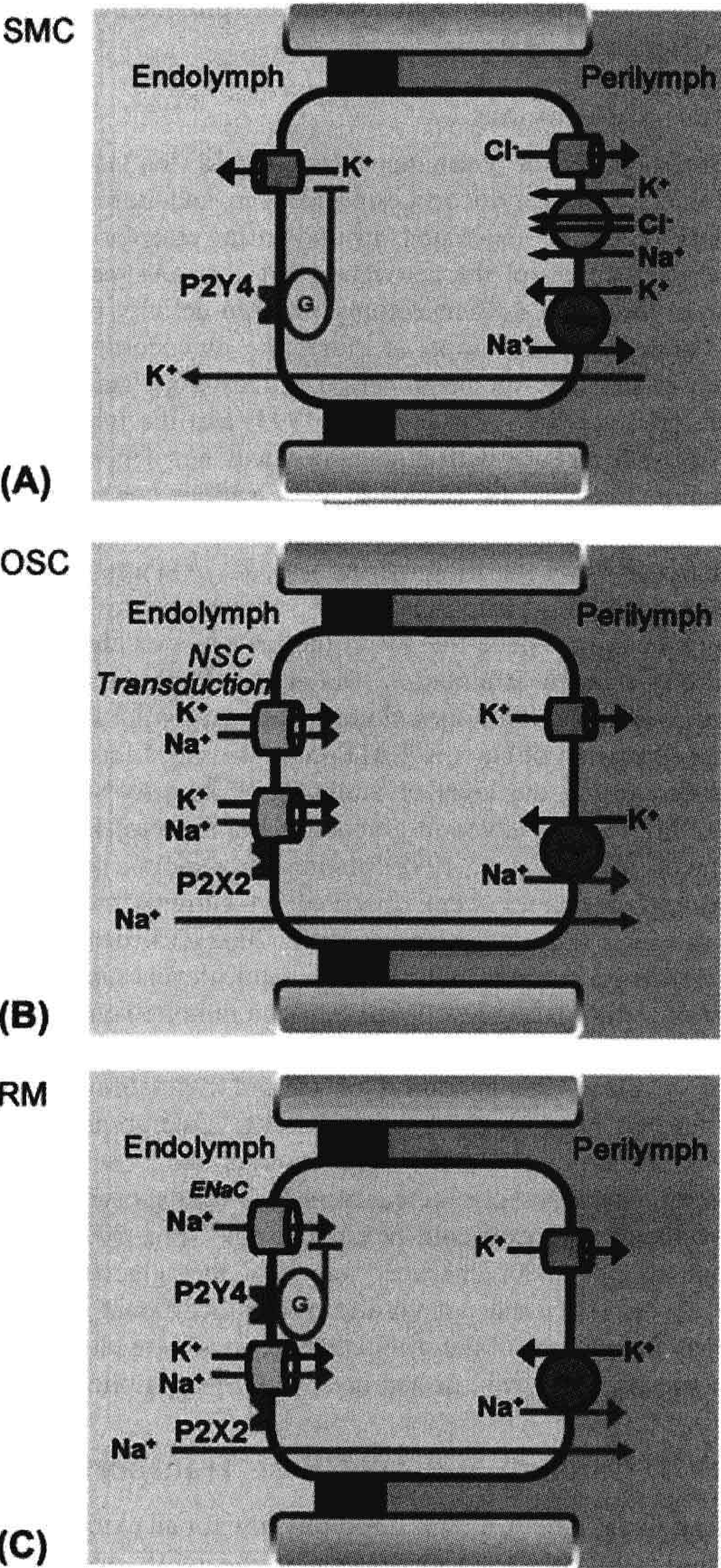


FIGURE 37.8 Purinergic signaling in the cochlear epithelium. (A) stria vascularis marginal cells; activation of P2Y4 receptors in the apical membrane reduce secretory K^+ flux via a G-protein (G) signal cascade (Lee and Marcus, 2008). There are additional purinergic receptors on the basolateral side (Lee and Marcus, 2008). (B) Outer sulcus cells; activation of apical P2X2 receptors open the associated non-selective cation channels (Lee and Marcus, 2008). (C) Reissner's membrane epithelial cells; activation of P2Y4 receptors (membrane location unknown) reduces ENaC-mediated Na^+ absorption, and activation of apical P2X2 receptors open the associated non-selective cation channels. *(Reproduced by permission from Kim, S.H. and Marcus, D.C. (2011). Regulation of sodium transport in the inner ear. Hear Res. 280, 21–29, and Lee, J.H., and Marcus, D.C. (2008). Purinergic signaling in the inner ear. Hear Res 235, 1–7.)*

circulating hormone might conceivably provide the agonist (Wangemann, 2002).

Steroid Hormones

Binding sites for both glucocorticosteroid (ten Cate et al., 1993) and mineralocorticosteroid (Yao and Rarey, 1996) have been demonstrated in the stria vascularis. Both corticoids control the activity of Na^+, K^+-ATPase in the stria vascularis (adrenalectomy reduced activity 60% and systemic administration of either the glucocorticosteroid dexamethasone or the mineralocorticosteroid aldosterone restored activity) (Curtis et al., 1993) and the increase in Na^+, K^+-ATPase with aldosterone was not dependent on major changes in blood plasma cation concentration (ten Cate et al., 1994). However, in spite of the strong dependence of the EP on strial Na^+, K^+-ATPase, a reduction of adrenocorticosteroids by adrenalectomy did not significantly reduce the EP in the presence or absence of strong acoustic stimulation (Ma et al., 1995). In addition, glucocorticoid hormones alone apparently do not stimulate the formation of Na^+, K^+-ATPase in the inner ear since no difference in the level of antibody binding to Na^+, K^+-ATPase was observed in glucocorticoid receptor knockout mice (Erichsen et al., 1998). Acute, non-genomic actions of steroid hormones were observed on currents from stria vascularis (Lee and Marcus, 2001, 2002). Corticosteroids stimulated currents only at therapeutic levels and not at normal circulating levels and estrogen inhibited currents at concentrations only found during the end of pregnancy.

A clear demonstration of steroid regulation of ion transport in the cochlea is on Reissner's membrane. Both Na^+ absorption and the expression of the α subunit of ENaC are markedly increased after 24 h exposure to the synthetic glucocorticoid dexamethasone (Fig. 37.9). This action of dexamethasone was via the glucocorticoid receptor (GR) and not via the mineralocorticoid receptor (MR) since both of the stimulatory actions were blocked by a specific GR inhibitor and not by an MR inhibitor.

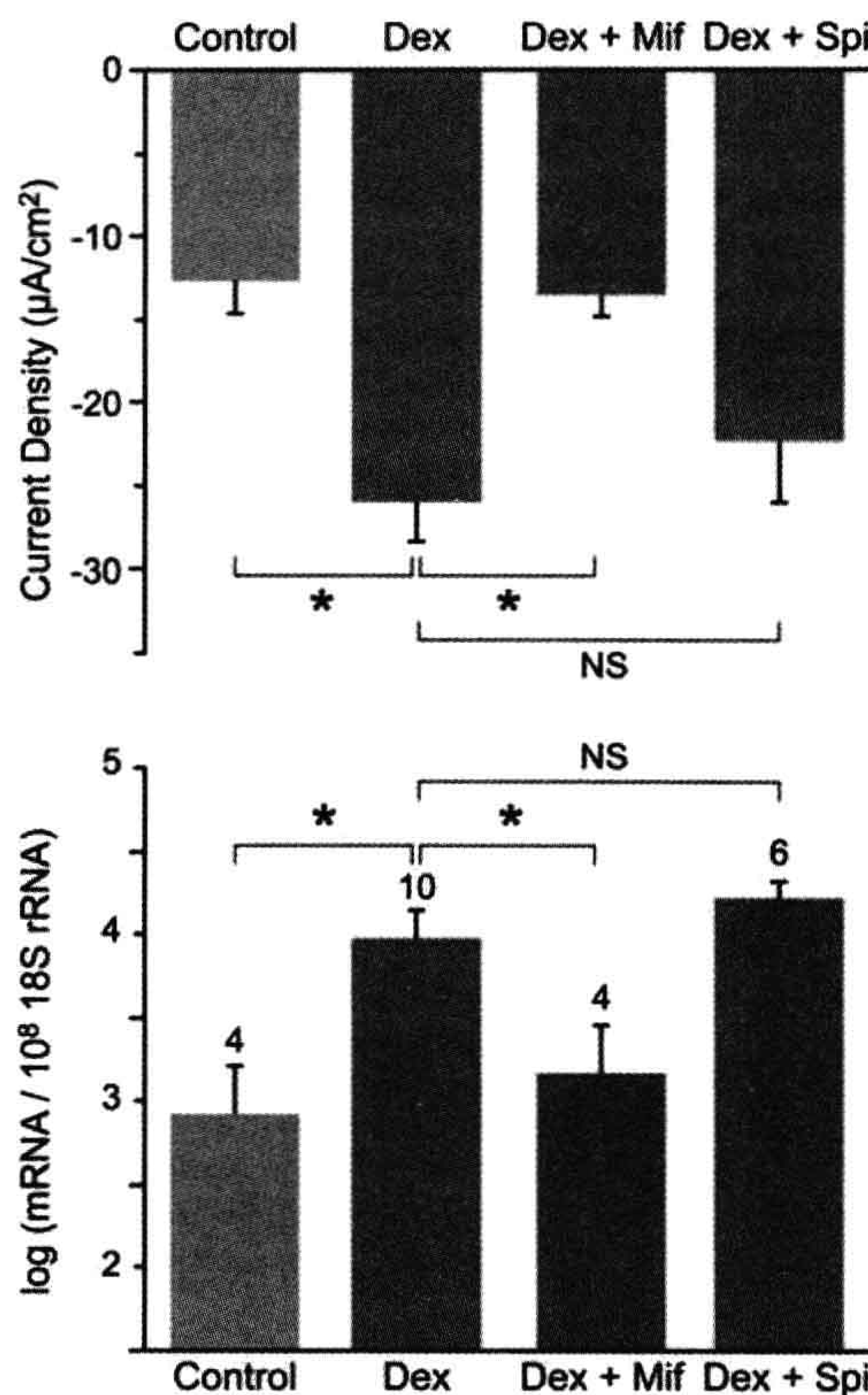


FIGURE 37.9 Stimulation of transepithelial sodium absorption by glucocorticoid, mediated by glucocorticoid receptor. (A) Changes of current density from Reissner's membrane under control conditions (gray bar), dexamethasone (blue bar; 100 nM, 24 h), dexamethasone + the glucocorticoid receptor antagonist mifepristone (orange bar; Mif, 100 nM), and dexamethasone + the mineralocorticoid receptor antagonist spironolactone (2nd blue bar; Spi, 100 nM). (B) qRT-PCR evaluation of transcript expression of the α subunit of ENaC under the same conditions as in (A). $*P < 0.05$; NS, not significant. *(Reproduced with permission from Kim, S.H., Kim, K.X., Raveendran, N.N., Wu, T., Pondugula, S.R. and Marcus, D.C. (2009). Regulation of ENaC-mediated sodium transport by glucocorticoids in Reissner's membrane epithelium. Am J Physiol Cell Physiol. 296, C544–C557.)*

IVD. Calcium and Acid/Base Transport

Endolymphatic $[Ca^{2+}]$ is unusually low for an extracellular fluid (see Table 37.1) and its level is apparently maintained at its set point by a "push-pull" system. Ca^{2+} is secreted ("pushed") into endolymph by the plasma membrane Ca^{2+}-ATPase PMCA2, which is located in the stereocilia of hair cells and likely also in Reissner's membrane (Yamoah et al., 1998; Kim et al., 2009; Marcus et al., 2011). Gene deletion/mutation of PMCA2 leads to a reduced level of endolymphatic $[Ca^{2+}]$ (Wood et al., 2004). An acid-sensitive Ca^{2+} absorptive system ("pull") is expressed in the cochlea and its gate-keeper apical channels, TRPV5 and TRPV6, are located in the inner and outer sulcus cells and have also been observed in marginal cells (Yamauchi et al., 2010).

Endolymphatic acid/base balance is apparently also a "push-pull" system. H^+ secretion from stria vascularis has been observed with self-referencing pH electrodes (Miyazaki, Wangemann and Marcus, unpublished observations). In addition, HCO_3^- secretion occurs via the Cl^-/HCO_3^- exchanger pendrin (*Slc26a4*), which is expressed in the apical membrane of strial spindle cells, spiral prominence and outer sulcus epithelial cells (Wangemann et al., 2004, 2007; Griffith and Wangemann, 2011). Pendrin, and likely other HCO_3^- transporters, maintain endolymph alkaline with respect to perilymph (see Table 37.1). Deletion of *Slc26a4* leads to an acidification of endolymph (Wangemann et al., 2007).

V. GENETIC BASIS OF DEAFNESS

Nearly 50% of profound hearing loss results from hereditary factors (Nance, 2003; Bayazit and Yilmaz, 2006; Morton and Giersch, 2010). Genetic causes of hearing loss are classified and identified in several ways. Clinical manifestations that are solely hearing-related are "non-syndromic" and those with pathologies in the ear plus one or more other organs are "syndromic". The chromosomal loci of non-syndromic hereditary DeaFNess are designated with DFN numbers, such as DFNA1 or DFNB 1. The A and B refer to autosomal dominant and autosomal recessive transmission of hearing loss and cases without A or B are X-linked; 80% of cases are of DFNB type (Bayazit and Yilmaz, 2006). Additional forms of deafness occur from mutations of the mitochondrial genome.

Several on-line sources of information on hereditary hearing loss include:

- the American Hearing Loss Foundation (http://www.american-hearing.org/disorders/congenital-deafness/)
- Dr Timothy C. Hain (http://www.dizziness-and-balance.com/disorders/hearing/cong_hearing.html)
- Hereditary Hearing Loss by Dr Guy Van Camp and Dr Richard Smith (http://hereditaryhearingloss.org/)
- Laboratory website of Dr Karen Avraham (http://www.tau.ac.il/~karena/overview-genetics.html).

DFNB1 is the most common DFNB and results from mutations of the gap junction gene coding for connexin-26, GJB2. Gap junctions between epithelial cells and between fibrocytes of the lateral cochlear wall and among fibrocytes, strial basal cells and strial intermediate cells (see Fig. 37.4) are crucial to acoustic transduction. The physical properties of junctions composed of heteromeric connexin-26 and connexin-30 as occur in the cochlea continue to be investigated (Change et al., 2008; Hoang et al., 2009).

Two of the important syndromic hearing losses are Jervell and Lange-Nielsen (JLN) syndrome and Pendred syndrome. JLN results from mutations of the KCNQ1/KCNE1 K channel in either of the subunits. It is "syndromic" because this K channel plays a prominent role in cardiac function as well as providing the sole route of K efflux from strial marginal cells (see above). Pendred syndrome results from mutations of the Cl^-/HCO_3^--exchanger coded by Slc26a4. As mentioned above, deletion of this gene in mice results in an acidic shift of endolymphatic pH, as expected from a HCO_3^--secretory transporter. The effects of pendrin mutation, however, go far beyond this relatively obvious consequence. A series of recent studies (reviewed in Griffith and Wangemann, 2011) has found that hearing loss results from a constellation of events.

Without normal levels of expression of functional pendrin during late embryonic and early postnatal development, there is tremendous expansion of the developing cochlea (10-fold increase in luminal cross-sectional area) that leads to enlargement and acidification of cochlear endolymph, which spread the effect from pendrin-expressing cells to many other cell types. The result is a delayed development of the stria vascularis and a fluctuating local oxidative stress in the stria. This oxidative stress results in downregulation of expression of the KCNJ10 K channel in the intermediate cells (Fig. 37.10). KCNJ10 expression is known to be especially sensitive to oxidative stress and its downregulation compromises the EP, which was proposed to be a factor leading to fluctuating hearing loss (Griffith and Wangemann, 2011).

VI. CELL PHYSIOLOGY OF ACOUSTIC TRANSDUCTION

The mammalian cochlea has an exquisite sensitivity, being able to detect sound pressure fluctuations of less than one millionth atmospheric pressure. At the threshold of hearing, the organ of Corti vibrates less than 1 nm. This sensitivity

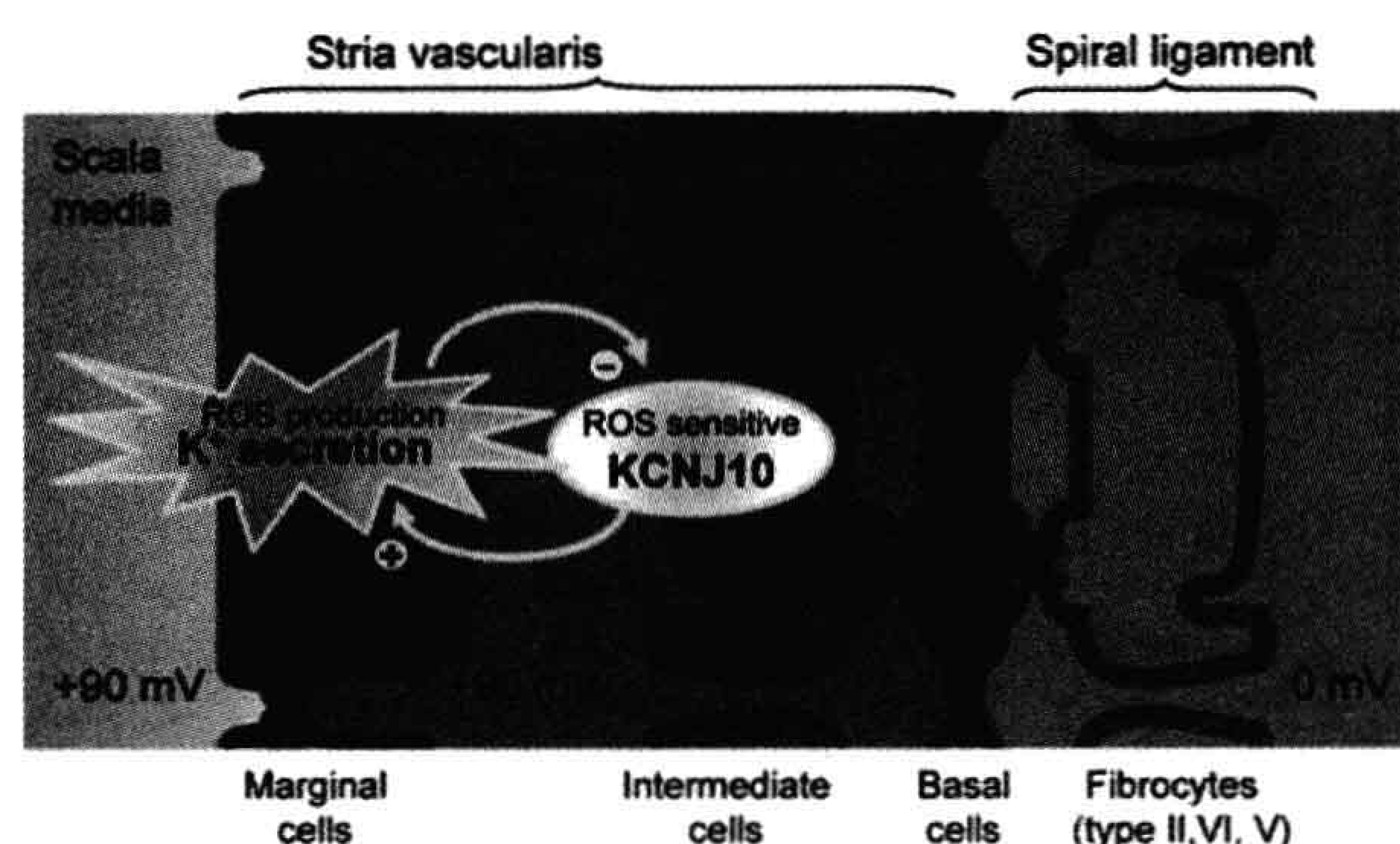


FIGURE 37.10 Proposed mechanism for fluctuating hearing loss. Diagram of the stria vascularis illustrating a feedback mechanism that leads to fluctuating loss of the K^+ channel that generates the endocochlear potential, KCNJ10. An increased rate of K^+ secretion related to the enlarged scala media generates increased levels of reactive oxygen species (ROS) in marginal cells. ROS diffuses to intermediate cells, where they downregulate expression of KCNJ10 channels (−). Reduced KCNJ10 decreases the EP and hearing and also reduces K^+ flux to the intrastrial space, thus limiting K^+ secretion by marginal cells; metabolic activity of marginal cells is reduced and ROS production drops. KCNJ10 expression is restored and the cycle repeats. Fluctuating loss of the endocochlear potential can thereby be expected to lead to fluctuating loss of hearing. *(Reproduced with permission from Griffith, A.J. and Wangemann, P. (2011). Hearing loss associated with enlargement of the vestibular aqueduct: mechanistic insights from clinical phenotypes, genotypes, and mouse models. Hear Res. doi:10.1016/j.hedres.2011.05.009.)*

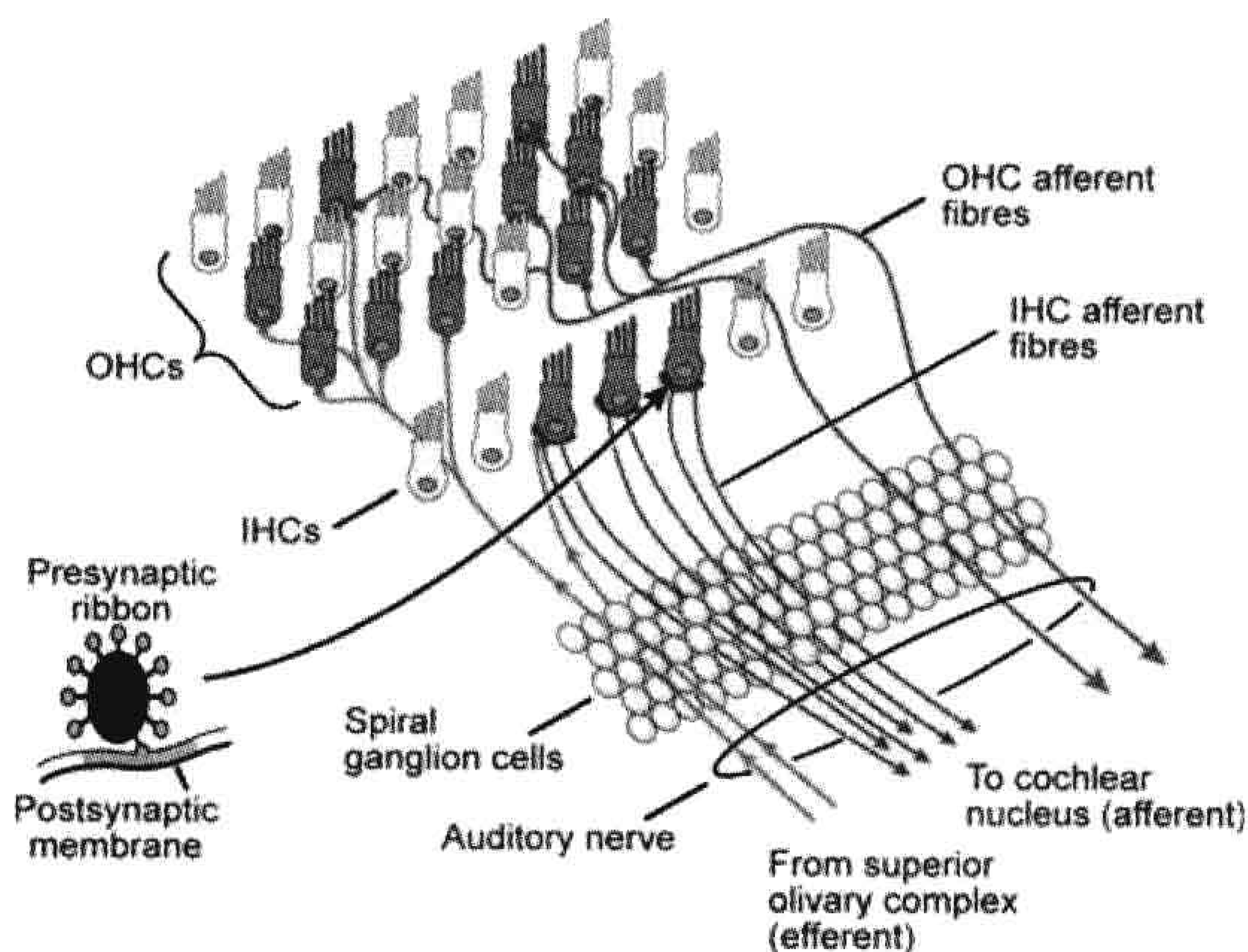


FIGURE 37.11 The organization of the cochlear inner and outer hair cells (IHCs and OHCs) and their (afferent and efferent) innervations. Each inner hair cell is innervated by 5–30 dendrites. The inset shows the schematic profile of the ribbon found at each afferent contact between the hair cells and the postsynaptic afferent terminal. *(Adapted with permission from Hackney, C. (2002). From cochlea to cortex. In D. Roberts, (ed.), Signals and Perception—the Fundamental Human Sensation, p. 31. Palgrave Macmillan Press, New York.)*

includes a gain of 100–1000 due to active mechanical amplification by the outer hair cells of the organ of Corti (but, see Ashmore et al., 2010). In spite of the delicacy of this process, the dynamic range for the amplitude detected by the cochlea is about one million to one due to compression of the response (Patuzzi, 1996).

The organization of the inner and outer hair cells and their innervations is depicted in Fig. 37.11. Afferent synapses to the inner hair cells account for most (95%) of the neural transmission from the cochlea to the brain. Each inner hair cell is innervated by 5–30 dendrites (Meyer and Moser, 2010). The remaining afferent fibers originate from the three rows of outer hair cells. Feedback occurs through an efferent neural supply that synapses with inner hair cell afferent fibers and directly with the body of outer hair cells (Elgoyhen and Fuchs, 2010). A local GABAergic innervation among outer hair cells has also been described (Thiers et al., 2008).

VIA. Transduction Channels

The mechanosensitive organelle of the sensory cells is the hair bundle (Fig. 37.12), which consists of 30–300 *stereocilia* arranged in rows of increasing height. Motion of the hair bundle modulates the fractional open time (open probability P_o) of the *mechanosensitive transduction channels* near the tips of the stereocilia. Modulation of P_o leads to corresponding fluctuations of the current through the apical membrane and to changes in the membrane potential of the hair cell. These changes in the membrane voltage are referred to as the *receptor potential*, the primary event to modulate synaptic transmission.

Bundle movement is believed to be the result of direct interaction of the outer hair cell stereocilia with the tectorial membrane and of the inner hair cell stereocilia with flowing endolymph pumped back and forth in the channel under the tectorial membrane (see Fig. 37.12). The cytoskeleton of the stereocilia is formed by a rigid matrix of actin filaments cross-linked by fimbrin. Deflection of the hair bundle results in a rotation of the individual cilia about a pivotal region at their base, which causes a shearing motion between the ciliary tips. Shear resulting from movement of the hair bundle in the direction of the tallest stereocilia increases P_o of the transduction channels from the resting activity of about 5–15%, whereas movement of the hair bundle in the opposite direction decreases P_o (see Figs. 37.12 and 37.13) (Hudspeth and Gillespie, 1994). Motion in the stimulatory direction is caused by the rarefaction phase of the external acoustic pressure wave. The asymmetric position on the receptor potential-stimulus transfer function of the stereocilia under unstimulated conditions (zero displacement in Fig. 37.13) leads to larger changes in the receptor potential with a given stimulatory displacement than for the same size inhibitory displacement. This asymmetry is a primary cause of distortion, which generates many of the non-linear properties of the auditory system, such as distortion products and otoacoustic emissions (see later section on reverse transduction).

The shear between stereocilia is posited in the *gating-spring model* of hair cell function to transmit a mechanical force through an elastic element (the gating spring) to the mechanosensitive gate of each transduction channel (Hackney and Furness, 2010). Increased tension on the spring increases P_o and decreased tension reduces P_o. The most widely accepted hypothesis is that the fine extracellular links (called tip links) that run between the tips of shorter stereocilia and the sides of taller ones constitute the elastic element of the model. The location of the transduction channels with respect to the attachment of the tip links remains somewhat equivocal, but the channels are apparently near the tips of sterocilia (Hackney and Furness, 2010).

Tip links are thought to be maintained under tension (see next section on adaptation), which is either increased or decreased by motion toward or away from the stimulatory direction. The time constant for response of the receptor current to a step stimulus has been found in saccular hair cells of the bullfrog to be in the range of 100–500 μs at 4°C and to become faster at higher temperatures (Corey and Hudspeth, 1983). This time course is substantially faster than can be accounted for by typical enzymatic or second messenger pathways and points to a direct mechanical coupling between the stimulus and the gate of the transduction channel.

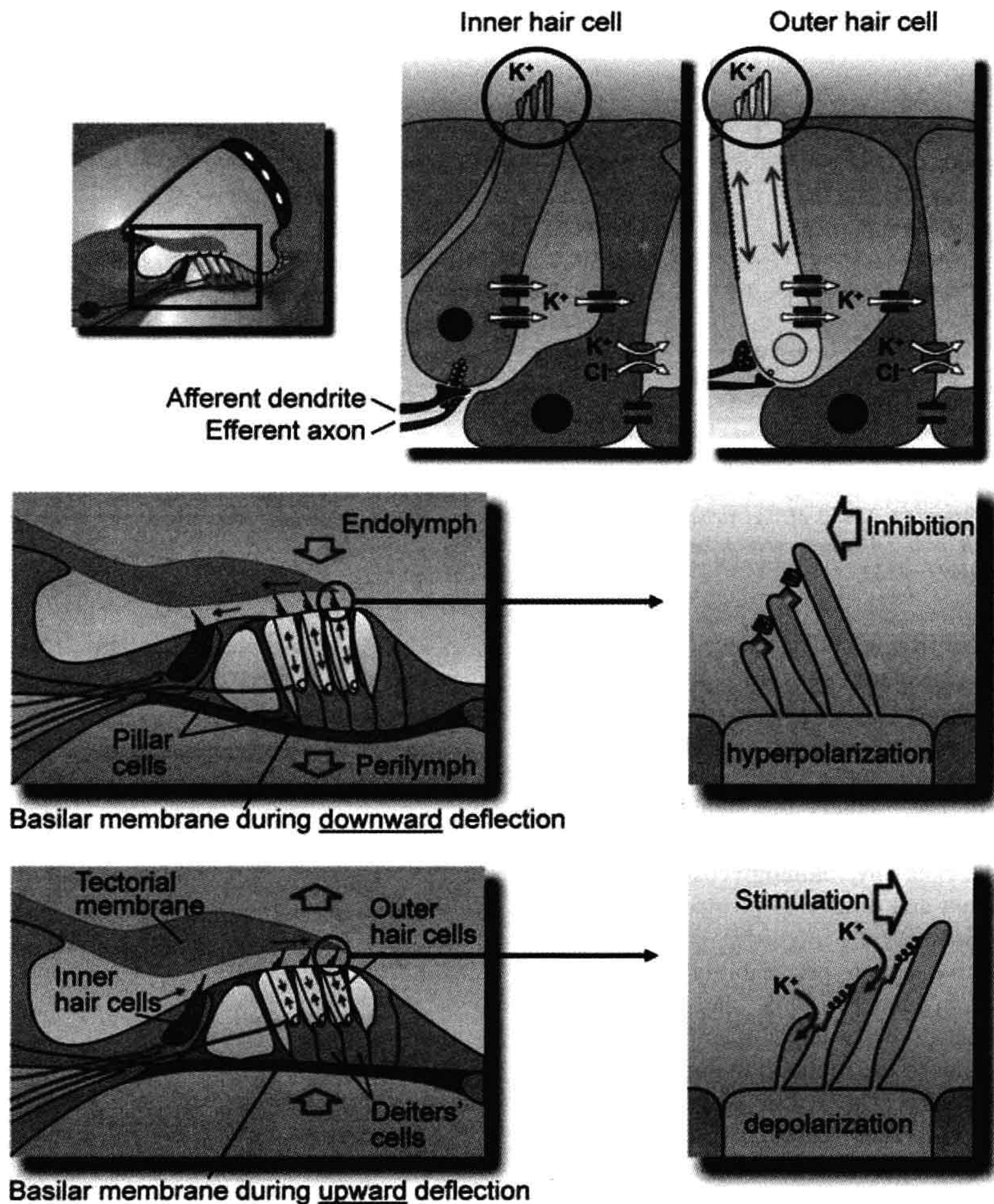


FIGURE 37.12 Diagram of the cochlear sensory structure, the organ of Corti and its inner and outer hair cells. (Top panel) The location of the organ of Corti (rectangle; left) and partial detail of an inner hair cell with supporting cell (middle) and an outer hair cell with supporting Deiters' cell (right). Stereocilia at the apical membrane of the hair cells tip links and transduction channels are circled; channels and transporters involved in putative K^+ buffering are described in the text and Fig. 37.4. (Middle panel) Downward deflection of basilar membrane (left) in response to sound is shown with medial movement of the outer hair cell stereocilia (right), leading to hyperpolarization of the hair cells (reduced afferent nerve transmission and elongation of the outer hair cell). (Bottom panel) Upward deflection of basilar membrane (left) in response to sound is shown with movement of the outer hair cell stereocilia (right), leading to depolarization. Arrows indicate movements of tectorial membrane, subtectorial fluid, basilar membrane (open arrow), K^+ flux through transduction channels at the tips of stereocilia and length changes in outer hair cells. *(Reproduced with permission from Marcus, D.C. and Wangemann, P. (2009). In (F.J. Alvarez-Leefmans and E. Delpire, eds), Physiology and Pathology of Chloride Transporters and Channels in the Nervous System — From Molecules to Diseases, pp. 425–437. Elsevier, New York.)*

The *conductance of the transduction channel* has been estimated from patch-clamp records to be on the order of 300 pS under in vivo conditions (Kros, 1996). The channel is permeable to cations including monovalent, divalent and small organic cations such as tetraethylammonium while selecting against anions (Corey and Hudspeth, 1979). Because potassium and calcium in endolymph are above electrochemical equilibrium with respect to the hair cell cytosol, it is primarily these two cations that flow through the transduction channel. Potassium carries the bulk of the current due to its high concentration, whereas entry of Ca^{2+} through the transduction channel is thought to control adaptation (see below). It was found that Ca^{2+} carries a surprisingly high fraction of the current through the

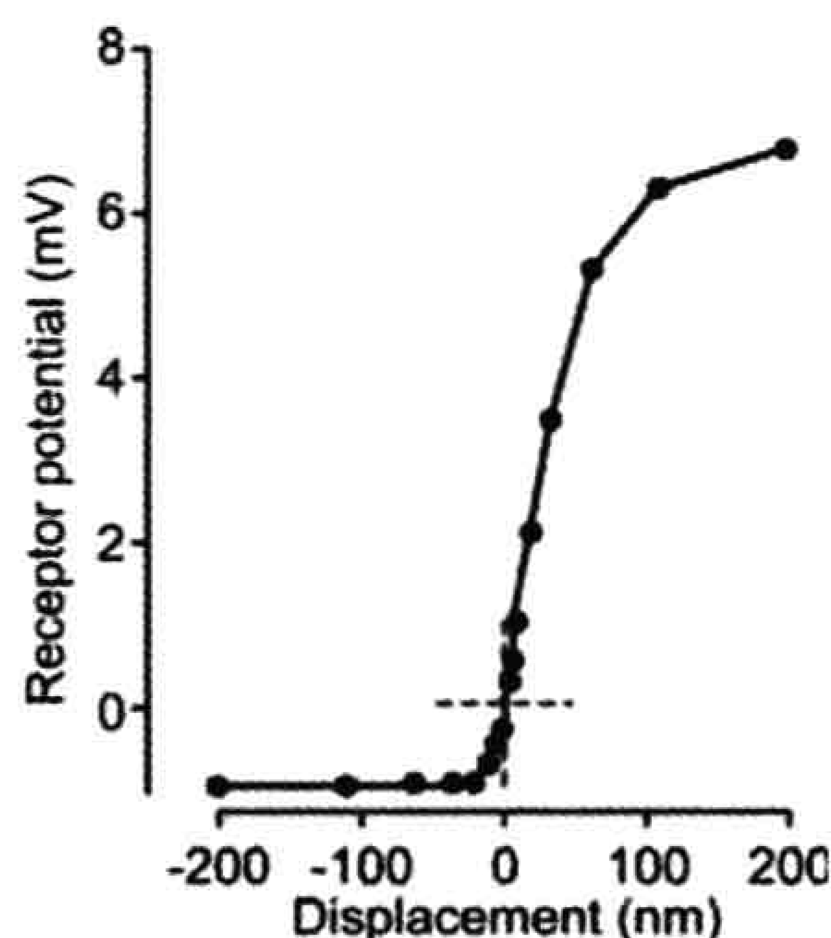


FIGURE 37.13 Response function of the receptor potential of outer hair cells to mechanical displacement of the stereocilia. The asymmetrical position of the quiescent point is indicated by dashed cross-hairs. *(Adapted with permission from Russell, I.J., Koessi, M. and Richardson, G.P. (1992). Nonlinear mechanical responses of mouse cochlear hair bundles. Proc R Soc London Ser B. 250, 217–227.)*

transduction channel (Ricci and Fettiplace, 1998) – about 20% (whereas the concentration of Ca^{2+} in endolymph is only about 0.01% that of K^{+}; see Table 37.1). This apparent anomaly may be due to the behavior of the transduction channel like a multi-ion pore in which the different ions interact. Sufficient Ca^{2+} enters the stereocilia to drive adaptation despite its low concentration. The channel is known to be blocked by aminoglycoside antibiotics (multivalent cations) and amiloride (a blocker of several Na^{+} transport processes).

The non-selective cation permeability of the transduction channel, in concert with the basolateral K conductance and negative basolateral membrane potential, in hair cells is similar to the situation in outer sulcus cells. Therefore, an efflux of Na^{+} from endolymph can be expected through hair cells, especially outer hair cells which are greater in number and have a greater basolateral membrane potential than inner hair cells. The molecular identity of the channels is different among the cell types, but the constellation is favorable for Na^{+} absorption (Kim and Marcus, 2011).

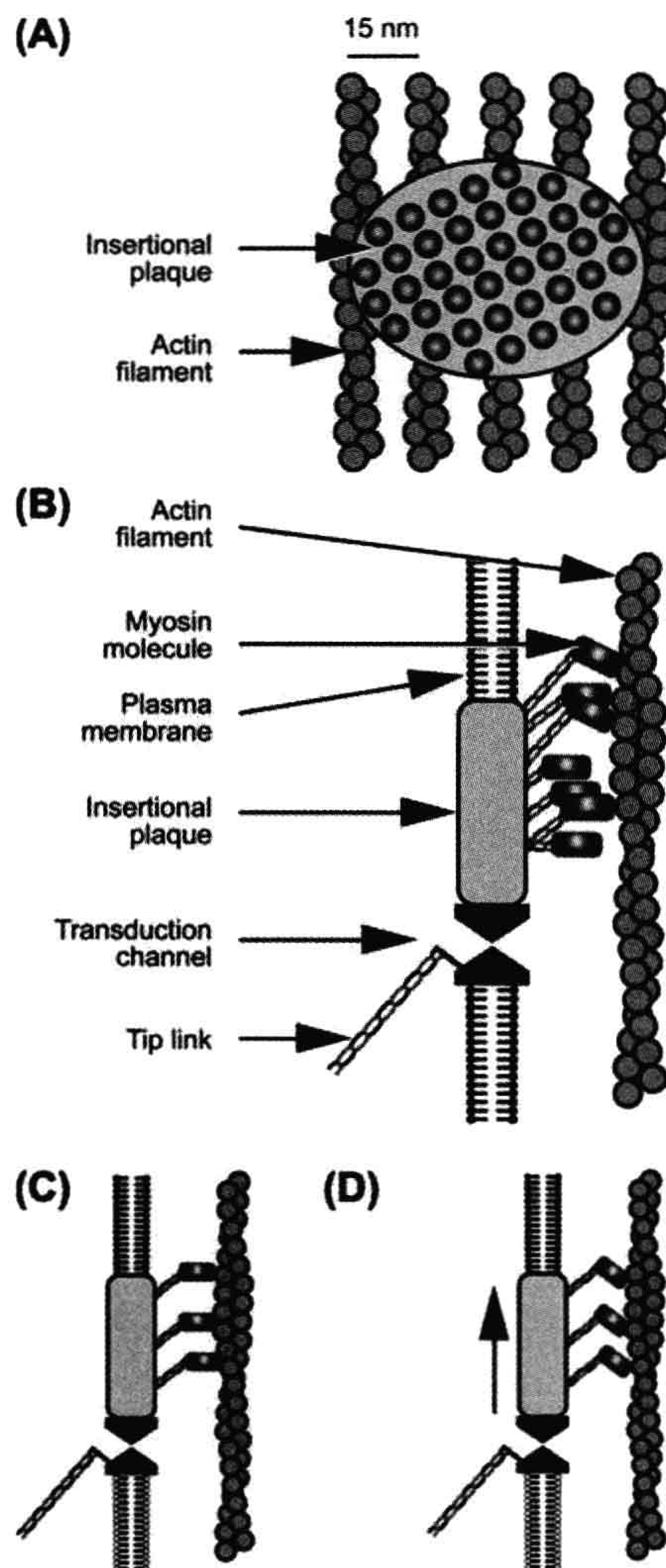


FIGURE 37.14 Proposed mechanism of adaptation: (A) frontal view of insertional plaque on actin filaments; (B) side view of insertional plaque with associated mechanosensitive transduction channel in cell membrane; and (C and D) power stroke of actin–myosin complex. *(Reproduced with permission from Hudspeth and Gillespie, 1994. Copyright 1994 by Cell Press.)*

VIB. Adaptation

When a sustained displacement is applied to hair cells, the transduction current is first stimulated but then relaxes in the continued presence of the stimulus with a complex characteristic time course, processes referred to as fast- and slow-adaptation (Hackney and Furness, 2010). The mechanism underlying slow adaptation is thought to be an active process in which myosin motors in the insertional plaque maintain tension within the tip link through a balance of climbing and slipping (Fig. 37.14). The tip link slackens when there is a deflection in the inhibitory direction but tension is soon re-established as the motor climbs along actin filaments within the taller stereocilium of each pair. Deflection in the stimulatory direction increases tension in the tip links, opening the mechanosensitive transduction channel. Ca^{2+} coming in through the channel is thought to bind to calmodulin, a myosin regulatory protein found to be concentrated in the tips of stereocilia which, in turn, promotes the dissociation of myosin from the actin filaments, allowing the plaque with the motors to slip. Fast

adaptation is thought to be a direct, calcium-dependent effect on the transduction channel.

The physiologic significance of adaptation is clear for vestibular hair cells where prolonged static displacements naturally occur during which sensitivity to transient stimuli must be maintained. However, the function of adaptation in the mammalian cochlea is less obvious (Kros, 1996). The adaptation process has been estimated to have an upper frequency limit of about 160 Hz, limiting its potential usefulness as a response to normal acoustic stimuli. Physiological significance in the cochlea may lie more with homeostasis of the system in the face of small readjustments of the position and/or size of cells during normal changes in systemic osmolarity and local metabolic processes or during development. There may also be a significant importance in controlling the response to infrasound, which gains attention with regard to insults by machinery such as wind turbine generators (Salt and Hullar, 2010).

VIC. Basolateral Membrane Channels

Although there are differences among hair cell types, they all contain a major basolateral K^+ conductance, comprised of voltage-dependent and Ca^{2+}-activated K^+ channels and voltage-gated Ca^{2+} channels (Fuchs, 1992; Kros, 1996). The K^+ channels serve to shape the receptor potential initiated by the acoustically-gated transduction channels and the Ca^{2+} channels to initiate transmitter release at the presynaptic sites, respectively. The presence of voltage-gated Ca^{2+} channels alone would be expected to lead to regenerative depolarization during acoustic stimulation, however, the basolateral voltage-gated K^+ channels provide an active repolarizing influence in the mature cochlea. Interestingly, immature inner hair cells have a different complement of channels including excitable Na^+ channels and a relatively slow K^+ channel, which lead to spontaneous and evoked action potentials. During development (see Chapter 25), a large, fast K^+ channel is expressed that greatly speeds up the membrane time constant, preventing action potentials (Kros et al., 1998).

The Ca^{2+} channels in hair cells appear to be of the L type, which are characterized by activation at depolarized membrane potentials, little or no inactivation, and block by dihydropyridines such as nifedipine. In inner hair cells, the Ca^{2+} currents are activated above −60 mV and peak near −20 to 0 mV, a range that correlates well with that of receptor potentials found in recordings made in vivo and with predictions from in vitro experiments (Kros, 1996). These Ca^{2+} channels are therefore well poised to participate in the graded release of neurotransmitter at the basolateral synapses to type I afferent fibers in the auditory nerve. The kinetics of channel activation have been estimated to be sufficiently fast so as not to limit accurate following of nervous discharge rates to the acoustic stimulus (Kros, 1996). By contrast, the Ca^{2+} currents in outer hair cells are activated only above −30 mV, a range that is far removed from the resting membrane potential near −80 mV found in vivo and never reached by receptor potentials, which apparently saturate at 15 mV (Kros, 1996). There is therefore no evidence at this time for a function of these voltage-gated Ca^{2+} channels in outer hair cells; there are also no measurements of neural activity in the type II afferent fibers in the auditory nerve that synapse exclusively to the outer hair cells.

In inner hair cells, the K^+ currents are activated by depolarization in the range of −60 to −20 mV, a range that correlates well with that of the resting and receptor potentials found in recordings made in vivo and with that of the voltage-gated Ca^{2+} channels described earlier. The resting potential of inner hair cells in vivo is about −40 mV, which reflects a compromise of the highly negative EMF from the basolateral K^+ channels by the depolarized EMF of the non-selective cation conductance in the apical membrane (Dallos, 1986).

VID. Synaptic Release of Vesicles

A comprehensive description of the afferent synapse is given in Ashmore (2010) and a diagram is in Fig. 37.11. Depolarization by acoustic stimulation leads to Ca^{2+}-dependent release of neurotransmitter at the 30–40 synapses with the afferent fibers at the base of each inner hair cell. This process can be monitored in vitro as changes in *membrane capacitance*. Opening of Ca^{2+} channels during depolarization raises the local free Ca^{2+} concentration to tens or hundreds of micromolar (Roberts, 1994), which is thought to trigger synaptic exocytosis of the neurotransmitter glutamate (Ashmore, 2010) (see Chapter 32). Depolarization led to increases in membrane capacitance (up to 5% of the initial value) that continued for up to 2 s. It was estimated that this was sufficient to exhaust more than five times the number of vesicles initially in close apposition to the plasma membrane at active zones, suggesting that hair cells are capable of rapidly replenishing vesicles at release sites (Parsons et al., 1994). Capacitance returned during repolarization toward its prestimulus level with a time constant of about 14 s, but only in perforated-patch recordings (see Chapter 20), suggesting that membrane retrieval depends on a diffusible intracellular factor.

VIE. Reverse Transduction: Cochlear Amplifier

Discrimination of frequency information in acoustic signals is performed broadly at an initial level by mechanical tuning of the basilar membrane as a function of position

along the cochlea. In lower vertebrates, frequency discrimination is accomplished by tuning the electrical properties of the hair cells. The exquisite sensitivity and fine frequency discrimination of mammalian hearing depends on amplification of the incoming sound within the organ of Corti (Ashmore, 2010; Iwasa, 2010). It is widely held that the outer hair cells sense displacements caused by sound and feedback forces that enhance the basilar membrane motion by reducing the inherent damping of the cochlear partition. In support of this hypothesis, outer hair cells show membrane potential-induced length changes at acoustic rates. This process has been termed *reverse transduction* by the *cochlear amplifier*. This property of the organ of Corti leads to an epiphenomenon called *otoacoustic emission* in which mechanical fluctuations are generated by the inner ear, resulting in sounds emanating from the ear (Kemp, 2010).

Reverse transduction occurs by somatic and/or ciliary motility, the former due to a high concentration of the motor molecule prestin (Slc26a5) (Iwasa, 2010) (current opinions: Ashmore et al., 2010). Outer hair cells shorten and lengthen by up to 5% when depolarized and hyperpolarized, respectively. Longitudinal motions of the outer hair cells (see Fig. 37.12) are assumed to be transmitted in vivo to the whole organ of Corti via the tectorial membrane by the rigid reticular lamina at the top and by the Deiters' cell bodies at the base, mechanically coupled to the basilar membrane. Shortening in vivo would cause an upward pull on the basilar membrane and/or a downward pull on the reticular lamina (see Fig. 37.12). The latency is less than 0.1 ms and can be driven to frequencies in excess of 22 kHz (measurement of upper frequency limited by instrumentation) (Dallos and Evans, 1995). This response is driven by membrane potential and is associated with an apparent non-linear capacitance. The presence of non-linear capacitance suggests that the motors act by conformational changes of the protein rather than by electrostatic repulsion between separate elements within the plane of the lipid bilayer.

Myosin in the stereocilia is estimated to be sufficiently plentiful and powerful to account for ciliary-driven amplification by the organ of Corti. However, if the stereociliary motion were modulated by Ca^{2+} rather than membrane potential, activation of stereociliar myosin by Ca^{2+} would not be restricted by the membrane's time constant. It remains to be determined whether these motors can operate at the highest frequencies detected by the mammalian cochlea (Ashmore, 2010; Iwasa, 2010).

Deiters' cells were previously thought to offer only a passive support to the outer hair cells and a mechanical connection to the acoustic stimulus at the basilar membrane. However, evidence suggests that these cells have a Ca^{2+}-dependent motile response. Increases in cytoplasmic Ca^{2+} caused an extension of the head of the phalangeal process away from the body by 0.5 to 1 μm within a few hundred milliseconds and the stiffness of the phalangeal process increased by 28 to 51% (Dulon, 1995).

VIF. Receptors and Neurotransmitters

A number of receptors for neurotransmitters and neuromodulators have been identified on cochlear hair cells (Ashmore, 2010; Elgoyhen and Fuchs, 2010). Some are known to mediate synaptic transmission while the physiological significance of others has not yet been identified.

VIF1. Outer Hair Cells

Receptors for several neurotransmitters and neuromodulators (Table 37.3) have been identified on outer hair cells by histochemical and electrophysiologic observations (Elgoyhen and Fuchs, 2010). The efferent synapses on the outer hair cells release acetylcholine (ACh) and γ-aminobutyric acid (GABA) as neurotransmitters from two populations of fibers and may co-release ATP with ACh. There is evidence for the presence of both ionotropic and metabotropic receptors for ATP and ACh and for the ionotropic $GABA_A$ receptor (Housley et al., 1995). Ionotropic receptors are coupled directly to ion channels, whereas metabotropic receptors act via G-protein pathways that ultimately regulate ion channel activity and/or other cellular processes (see Chapter 6). Cochlear Ach receptors contain the unusual α_9-receptor isoform subunit. Activation of ACh receptors causes membrane hyperpolarization apparently through an ion channel permeable to cations including Ca^{2+}. The entry of Ca^{2+} activates Ca^{2+}-dependent K^+ channels, likely the SK type (Elgoyhen and Fuchs, 2010), leading to hyperpolarization. Ionotropic ATP receptors depolarize the hair cell by opening associated non-selective cation channels permeable to Ca^{2+} as well as monovalent cations. The channels associated with the ionotropic ATP and ACh receptors admit Ca^{2+} into the cell, leading to a relatively slow elongation (a process referred to

TABLE 37.3 Effects of Outer Hair Cell Receptors on Fast and Slow Motility, Membrane Potential, and Calcium Concentration

	Fast	Slow	Vc	$[Ca^{2+}]_i$
ACh	x	x	Hyper.	x
ATP		x	Depol.	x
GABA			Hyper.	No
Substance P			Hyper.	No
CGRP				No, but potentiates ACh response

as slow motility or adaptation; see above). In addition to its effects on slow motility, ACh has been found to control the gain and magnitude of fast motility in outer hair cells (Sziklai et al., 1996). ACh evokes an increase in magnitude and gain of electromotility, which is sensitive to the muscarinic blocker atropine.

Receptors have also been found on outer hair cells for the peptides substance P and calcitonin gene-related peptide (CGRP). Substance P hyperpolarizes these cells by downregulating the non-selective cation conductance in the lateral wall via a pertussis toxin-insensitive G protein (Kakehata et al., 1993). CGRP had no effect on the resting cytoplasmic Ca^{2+} concentration but potentiated by about threefold the increase in Ca^{2+} caused by ACh stimulation in chick hair cells (Shigemoto and Ohmori, 1990).

VIF2. Inner Hair Cells

Inner hair cells have been found to have both metabotropic and ionotropic receptors for extracellular ATP (Sugasawa et al., 1996). At submicromolar ATP concentrations, the metabotropic receptors raise intracellular Ca^{2+} concentration, which hyperpolarizes inner hair cells via Ca^{2+}-sensitive K^{+} channels. The ionotropic receptors are non-selective cation channels activated at higher ATP concentrations and which mainly have a depolarizing effect on the inner hair cells. Although the source of agonist for these receptors has not yet been identified, Ca^{2+}-dependent release of ATP from the organ of Corti has been observed (Wangemann, 1996) and ATP release from cochlear cells via connexin/pannexin hemichannels has been reported to reduce outer hair cell motility via purinergic receptors (Zhao et al., 2005).

VIG. Echolocation

Bats can capture flying prey by echolocation (biosonar) even among vegetation and other bats. Sounds are vocalized by the bat at frequencies near 60 kHz (the upper range of human hearing is about 20 kHz) and typically consist of a constant-frequency tone pulse for 10–100 ms followed by a shorter period of dropping frequency. The pulse is reflected from surfaces in front of the bat and is returned and heard before the end of the emitted pulse. Several characteristics of the returned sound pulse are interpreted by the bat as an acoustic image. A Doppler shift of the frequency of the returned sound from that of the emitted sound carries velocity information (the rate of closure on a target). For example, a Doppler shift from 61 to 62 kHz corresponds to 6.3 miles per hour. The delay of the echo gives the distance to the target such that a 1-ms echo delay corresponds to a target distance of 17 cm. Temporal delay acuity has been reported to be as fine as 10 ns (Simmons et al., 1990), a surprisingly short time span for recognition by a biological system. It has been suggested, however, that bats may not respond directly to processing of the time delay but rather to spectral processing, which would require only a resolution of about a few kilohertz (Neuweiler and Schmidt, 1993; Simmons, 1993; Simmons et al., 1996; Fuzessery et al., 2011).

The fine tuning of hearing used in echolocation is mostly achieved by mechanical specializations of the cochlea, which spread out the physical mapping of the biosonar frequencies over a full half turn of the cochlea. There is also an amplifying reverberation of the acoustic wave traveling on the basilar membrane, which is due either to reflections at a discontinuity of the basilar membrane thickness or to different radial oscillation modes of the basilar membrane (Russell and Koessl, 1995). As in other mammalian cochleae, the tuning (and the bat's special reverberation) is thought to depend on active processes in the outer hair cells. Tuning of auditory nerve fibers, and therefore likely tuning of basilar membrane motion, to acoustic stimuli is amazingly high in the bat with Q10 values (center frequency/bandwidth 10 dB from the tip) as high as 610 in comparison to typical values of 1 to 10 for non-echolocating animals (Russell and Koessl, 1995). Processing by central neural pathways of the detected echoes has been reviewed by Fuzessery et al. (2011). An interesting specialization of the bats' prey has been found in the dogbane tiger moth, which apparently emits clicks when a bat approaches in order to interfere with the sonar echoes, thereby jamming the signal and averting becoming a meal (Fullard et al., 1994)!

VII. CONCLUDING REMARKS

The exquisite sensitivity of our sense of hearing results from the concerted action of many subsystems. Sound is conducted from our environment through the outer ear canal at the end of which it is conducted through the middle ear by the three ossicles to the oval window of the inner ear. Sounds can also reach the inner ear by bone conduction. This auditory peripheral organ transduces the mechanical stimulus into nerve impulses that travel to central auditory pathways in the brain where we interpret the impulses as sounds.

This chapter has focused on the cellular processes in the cochlea that support auditory transduction. In particular, several cell types contribute specific ion transport modalities to the creation and maintenance of the ionic composition of the cochlear luminal fluid, endolymph. The potassium, sodium, calcium and pH levels that comprise this unique extracellular environment all serve to power and support the transduction process performed by the sensory inner hair cells and the cochlear amplifier

embodied in several cell types in the organ of Corti and especially the outer hair cells.

All of these cellular processes depend on specific gene expression patterns; a number of gene mutations are known to underlie specific clinical syndromic and non-syndromic hereditary hearing loss. The only "surprise" has been that most of these clinically important genes are located in the cells that engage in ion transport rather than the auditory sensory and neural cells. Current and future areas of investigation include extending our knowledge of ion transport function to early developmental times, development of gene therapy and drug delivery techniques and discovery of cochlear "repair" through new extrinsic nerve stimulation paradigms and/or cochlear cell replacements.

ACKNOWLEDGMENT

This work was supported by NIH grant R01 - DC00212.

BIBLIOGRAPHY

Ashmore, J. (2010). The afferent synapse. In P. A. Fuchs (Ed.), *The Oxford Handbook of Auditory Science: The Ear* (pp. 259–282). Oxford: Oxford University Press.

Ashmore, J., Avan, P., Brownell, W. E., et al. (2010). The remarkable cochlear amplifier. *Hear Res, 266*, 1–17.

Bayazit, Y. A., & Yilmaz, M. (2006). An overview of hereditary hearing loss. *Otorhinolaryngol Relat Spec, 68*, 57–63.

Chang, Q., Tang, W., Ahmad, S., Zhou, B., & Lin, X. (2008). Gap junction mediated intercellular metabolite transfer in the cochlea is compromised in connexin30 null mice. *PLoS One, 3*, e4088.

Corey, D. P., & Hudspeth, A. J. (1979). Ionic basis of the receptor potential in a vertebrate hair cell. *Nature, 281*, 675–677.

Corey, D. P., & Hudspeth, A. J. (1983). Kinetics of the receptor current in bullfrog saccular hair cells. *J Neurosci, 3*, 962–976.

Curtis, L. M., ten Cate, W. J., & Rarey, K. E. (1993). Dynamics of Na, K-ATPase sites in lateral cochlear wall tissues of the rat. *Eur Arch Otorhinolaryngol, 250*, 265–270.

Dallos, P. (1986). Neurobiology of cochlear inner and outer hair cells: intracellular recordings. *Hear Res, 22*, 185–198.

Dallos, P., & Evans, B. N. (1995). High-frequency motility of outer hair cells and the cochlear amplifier. *Science, 267*, 2006–2009.

Dulon, D. (1995). Ca^{2+} signaling in Deiter's cells of the guinea-pig cochlea: active process in supporting cells? In A. Flock, D. Ottoson, & M. Ulfendahl (Eds.), *Active Hearing* (pp. 195–208) New York: Elsevier Science.

Elgoyhen, A. B., & Fuchs, P. A. (2010). Efferent innervation and function. In P. A. Fuchs (Ed.), *The Oxford Handbook of Auditory Science: The Ear* (pp. 283–306). Oxford: Oxford University Press.

Erichsen, S., Stierna, P., Bagger-Sjoback, D., et al. (1998). Distribution of Na, K-ATPase is normal in the inner ear of a mouse with a null mutation of the glucocorticoid receptor. *Hear Res, 124*, 146–154.

Fuchs, P. A. (1992). Ionic currents in cochlear hair cells. *Prog Neurobiol, 39*, 493–505.

Fullard, J. H., Simmons, J. A., & Saillant, P. A. (1994). Jamming bat echolocation: the dogbane tiger moth Cycnia tenera times its clicks to the terminal attack calls of the big brown bat Eptesicus fuscus. *J Exp Biol, 194*, 285–298.

Fuzessery, Z. M., Razak, K. A., & Williams, A. J. (2011). Multiple mechanisms shape selectivity for FM sweep rate and direction in the pallid bat inferior colliculus and auditory cortex. *J Comp Physiol A Neuroethol Sens Neural Behav Physiol, 197*, 615–623.

Gow, A., Davies, C., Southwood, C. M., et al. (2004). Deafness in Claudin 11-null mice reveals the critical contribution of basal cell tight junctions to stria vascularis function. *J Neurosci, 24*, 7051–7062.

Griffith, A. J., & Wangemann, P. (2011). Hearing loss associated with enlargement of the vestibular aqueduct: Mechanistic insights from clinical phenotypes, genotypes, and mouse models. *Hear Res*, doi:10.1016/J.heares.2011.05.009.

Hackney, C. M., & Furness, D. N. (2010). Hair bundle structure and mechanotransduction. In P. A. Fuchs (Ed.), *The Oxford Handbook of Auditory Science: The Ear* (pp. 231–258). Oxford: Oxford University Press.

Hoang, D. E., Ahmad, S., Chang, Q., Tang, W., Stong, B., & Lin, X. (2009). Diverse deafness mechanisms of connexin mutations revealed by studies using in vitro approaches and mouse models. *Brain Res, 1277*, 52–69.

Housley, G. D., Connor, B. J., & Raybould, N. P. (1995). Purinergic modulation of outer hair cell electromotility. In A. Flock, D. Ottoson, & M. Ulfendahl (Eds.), *Active Hearing* (pp. 221–238). New York: Elsevier Science.

Hudspeth, A. J., & Gillespie, P. G. (1994). Pulling springs to tune transduction: adaptation by hair cells. *Neuron, 12*, 1–9.

Iwasa, K. H. (2010). Electromotility of outer hair cells. In P. A. Fuchs (Ed.), *The Oxford Handbook of Auditory Science: The Ear* (pp. 179–212). Oxford: Oxford University Press.

Julien, N., Loiseau, A., Sterkers, O., Amiel, C., & Ferrary, E. (1994). Antidiuretic hormone restores the endolymphatic longitudinal K^+ gradient in the Brattleboro rat cochlea. *Pflügers Arch, 426*, 446–452.

Kakehata, S., Akaike, N., & Takasaka, T. (1993). Substance P decreases the non-selective cation channel conductance in dissociated outer hair cells of guinea pig cochlea. *Ann NY Acad Sci, 707*, 476–479.

Kemp, D. T. (2010). Otoacoustic emissions and evoked potentials. In P. A. Fuchs (Ed.), *The Oxford Handbook of Auditory Science: The Ear* (pp. 93–137). Oxford: Oxford University Press.

Kikuchi, T., Kimura, R. S., Paul, D. L., Takasaka, T., & Adams, J. C. (2000). Gap junction systems in the mammalian cochlea. *Brain Res Brain Res Rev, 32*, 163–166.

Kim, S. H., & Marcus, D. C. (2011). Regulation of sodium transport in the inner ear. *Hear Res, 280*, 21–29.

Kim, S. H., Kim, K. X., Raveendran, N. N., Wu, T., Pondugula, S. R., & Marcus, D. C. (2009). Regulation of ENaC-mediated sodium transport by glucocorticoids in Reissner's membrane epithelium. *Am J Physiol Cell Physiol, 296*, C544–C557.

Konishi, T., Hamrick, P. E., & Walsh, P. J. (1978). Ion transport in guinea pig cochlea. I. Potassium and sodium transport. *Acta Otolaryngol, 86*, 22–34.

Kros, C. J. (1996). Physiology of mammalian cochlear hair cells. In P. Dallos, A. N. Popper, & R. R. Fay (Eds.), *The Cochlea* (pp. 318–385). New York: Springer-Verlag.

Kros, C. J., Ruppersberg, J. P., & Rusch, A. (1998). Expression of a potassium current in inner hair cells during development of hearing in mice. *Nature, 394*, 281–284.

Lee, J. H., & Marcus, D. C. (2001). Estrogen acutely inhibits ion transport by isolated stria vascularis. *Hear Res, 158*, 123–130.
Lee, J. H., & Marcus, D. C. (2002). Nongenomic effects of corticosteroids on ion transport by stria vascularis. *Audiol Neurootol, 7*, 100–106.
Lee, J. H., & Marcus, D. C. (2008). Purinergic signaling in the inner ear. *Hear Res, 235*, 1–7.
Ma, Y. L., Gerhardt, K. J., Curtis, L. M., Rybak, L. P., Whitworth, C., & Rarey, K. E. (1995). Combined effects of adrenalectomy and noise exposure on compound action potentials, endocochlear potentials and endolymphatic potassium concentrations. *Hear Res, 91*, 79–86.
Marcus, D. C., & Shen, Z. (1994). Slowly activating, voltage-dependent K^+ conductance is apical pathway for K^+ secretion in vestibular dark cells. *Am J Physiol, 267*, C857–C864.
Marcus, D. C., & Wangemann, P. (2009). Cochlear and vestibular function and dysfunction. In F. J. Alvarez-Leefmans, & E. Delpire (Eds.), *Physiology and Pathology of Chloride Transporters and Channels in the Nervous System – From Molecules to Diseases* (pp. 425–437). New York: Elsevier.
Marcus, D. C., & Wangemann, P. (2010). Inner ear fluid homeostasis. In P. A. Fuchs (Ed.), *The Oxford Handbook of Auditory Science: The Ear* (pp. 213–230). Oxford: Oxford University Press.
Marcus, D. C., Raveendran, N. N., & Wu, T. (2011). Reissner's membrane, mouse. *GEO* GSE6196.
Meyer, A. C., & Moser, T. (2010). Structure and function of cochlear afferent innervation. *Curr Opin Otolaryngol Head Neck Surg, 18*, 441–446.
Mori, N., Shugyo, A., & Asai, H. (1989). The effect of arginine-vasopressin and its analogues upon the endocochlear potential in the guinea pig. *Acta Otolaryngol, 107*, 80–84.
Morton, C. C., & Giersch, A. B. (2010). Genetics of hearing loss. In P. A. Fuchs (Ed.), *The Oxford Handbook of Auditory Science: The Ear* (pp. 377–408). Oxford: Oxford University Press.
Nance, W. E. (2003). The genetics of deafness. *Ment Retard Dev Disabil Res Rev, 9*, 109–119.
Neuweiler, G., & Schmidt, S. (1993). Audition in echolocating bats. *Curr Opin Neurobiol, 3*, 563–569.
Ogawa, K., & Schacht, J. (1995). P2y purinergic receptors coupled to phosphoinositide hydrolysis in tissues of the cochlear lateral wall. *Neuroreport, 6*, 1538–1540.
Parsons, T. D., Lenzi, D., Almers, W., & Roberts, W. M. (1994). Calcium-triggered exocytosis and endocytosis in an isolated presynaptic cell: capacitance measurements in saccular hair cells. *Neuron, 13*, 875–883.
Patuzzi, R. (1996). Cochlear micromechanics and macromechanics. In P. Dallos, A. N. Popper, & R. R. Fay (Eds.), *The Cochlea* (pp. 186–257). New York: Springer-Verlag.
Ricci, A. J., & Fettiplace, R. (1998). Calcium permeation of the turtle hair cell mechanotransducer channel and its relation to the composition of endolymph. *J Physiol (Lond.), 506*, 159–173.
Roberts, W. M. (1994). Localization of calcium signals by a mobile calcium buffer in frog saccular hair cells. *J Neurosci, 14*, 3246–3262.
Russell, I. J., & Koessl, M. (1995). Measurements of the basilar membrane resonance in the cochlea of the mustached bat. In A. Flock, D. Ottoson, & M. Ulfendahl (Eds.), *Active Hearing* (pp. 295–306). New York: Elsevier Science.
Salt, A. N., & Hullar, T. E. (2010). Responses of the ear to low frequency sounds, infrasound and wind turbines. *Hear Res, 268*, 12–21.
Salt, A. N., Melichar, I., & Thalmann, R. (1987). Mechanisms of endocochlear potential generation by stria vascularis. *Laryngoscope, 97*, 984–991.
Shah, D. M., Freeman, D. M., & Weiss, T. F. (1995). The osmotic response of the isolated, unfixed mouse tectorial membrane to isosmotic solutions: effect of Na^+, K^+, and Ca^{2+} concentration. *Hear Res, 87*, 187–207.
Shen, Z., Marcus, D. C., Sunose, H., Chiba, T., & Wangemann, P. (1997). I_{sK} channel in strial marginal cells: voltage-dependence, ion-selectivity, inhibition by 293B and sensitivity to clofilium. *Auditory Neurosci, 3*, 215–230.
Shigemoto, T., & Ohmori, H. (1990). Muscarinic agonists and ATP increase the intracellular Ca^{2+} concentration in chick cochlear hair cells. *J Physiol (Lond.), 420*, 127–148.
Simmons, J. A. (1993). Evidence for perception of fine echo delay and phase by the FM bat, Eptesicus fuscus. *J Comp Physiol A, 172*, 533–547.
Simmons, J. A., Dear, S. P., Ferragamo, M. J., Haresign, T., & Fritz, J. (1996). Representation of perceptual dimensions of insect prey during terminal pursuit by echolocating bats. *Biol Bull, 191*, 109–121.
Simmons, J. A., Ferragamo, M., Moss, C. F., Stevenson, S. B., & Altes, R. A. (1990). Discrimination of jittered sonar echoes by the echolocating bat, Eptesicus fuscus: the shape of target images in echolocation. *J Comp Physiol A, 167*, 589–616.
Sterkers, O., Saumon, G., Tran Ba, H. P., & Amiel, C. (1982). K, Cl, and H_2O entry in endolymph, perilymph, and cerebrospinal fluid of the rat. *Am J Physiol, 243*, F173–F180.
Sugasawa, M., Erostegui, C., Blanchet, C., & Dulon, D. (1996). ATP activates non-selective cation channels and calcium release in inner hair cells of the guinea-pig cochlea. *J Physiol (Lond.), 491*, 707–718.
Sziklai, I., He, D. Z., & Dallos, P. (1996). Effect of acetylcholine and GABA on the transfer function of electromotility in isolated outer hair cells. *Hear Res, 95*, 87–99.
Takeuchi, S., & Ando, M. (1998). Dye-coupling of melanocytes with endothelial cells and pericytes in the cochlea of gerbils. *Cell Tissue Res, 293*, 271–275.
ten Cate, W. J., Curtis, L. M., & Rarey, K. E. (1994). Effects of low-sodium, high-potassium dietary intake on cochlear lateral wall Na^+, K^+-ATPase. *Eur Arch Otorhinolaryngol, 251*, 6–11.
ten Cate, W. J., Curtis, L. M., Small, G. M., & Rarey, K. E. (1993). Localization of glucocorticoid receptors and glucocorticoid receptor mRNAs in the rat cochlea. *Laryngoscope, 103*, 865–871.
Thiers, F. A., Nadol, J. B., Jr., & Liberman, M. C. (2008). Reciprocal synapses between outer hair cells and their afferent terminals: evidence for a local neural network in the mammalian cochlea. *J Assoc Res Otolaryngol, 9*, 477–489.
Vetter, D. E., Mann, J. R., Wangemann, P., et al. (1996). Inner ear defects induced by null mutation of the isk gene. *Neuron, 17*, 1251–1264.
Wangemann, P. (1996). Ca^{2+}-dependent release of ATP from the organ of Corti measured with a luciferin-luciferase bioluminescence assay. *Auditory Neurosci, 2*, 187–192.
Wangemann, P. (2002). Adrenergic and muscarinic control of cochlear endolymph production. *Adv Otorhinolaryngol, 59*, 42–50.
Wangemann, P., Itza, E. M., Albrecht, B., et al. (2004). Loss of KCNJ10 protein expression abolishes endocochlear potential and causes deafness in Pendred syndrome mouse model. *BMC Med, 2*, 30.
Wangemann, P., Liu, J., & Marcus, D. C. (1995). Ion transport mechanisms responsible for K^+ secretion and the transepithelial voltage across marginal cells of stria vascularis in vitro. *Hear Res, 84*, 19–29.

Wangemann, P., Nakaya, K., Wu, T., et al. (2007). Loss of cochlear HCO_3^- secretion causes deafness via endolymphatic acidification and inhibition of Ca^{2+} reabsorption in a Pendred syndrome mouse model. *Am J Physiol Renal Physiol, 292*, F1345–F1353.

Wangemann, P., Shen, Z., & Liu, J. (1996). K(+)-induced stimulation of K^+ secretion involves activation of the IsK channel in vestibular dark cells. *Hear Res, 100*, 201–210.

Wood, J. D., Muchinsky, S. J., Filoteo, A. G., Penniston, J. T., & Tempel, B. L. (2004). Low endolymph calcium concentrations in deafwaddler2J mice suggest that PMCA2 contributes to endolymph calcium maintenance. *J Assoc Res Otolaryngol, 5*, 99–110.

Yamauchi, D., Nakaya, K., Raveendran, N. N., et al. (2010). Expression of epithelial calcium transport system in rat cochlea and vestibular labyrinth. *BMC Physiol, 10*, 1.

Yamoah, E. N., Lumpkin, E. A., Dumont, R. A., Smith, P. J., Hudspeth, A. J., & Gillespie, P. G. (1998). Plasma membrane Ca^{2+}-ATPase extrudes Ca^{2+} from hair cell stereocilia. *J Neurosci, 18*, 610–624.

Yao, X. F., & Rarey, K. E. (1996). Localization of the mineralocorticoid receptor in rat cochlear tissue. *Acta Otolaryngol (Stockh), 116*, 493–496.

Zhao, H. B., Yu, N., & Fleming, C. R. (2005). Gap junctional hemichannel-mediated ATP release and hearing controls in the inner ear. *Proc Natl Acad Sci USA, 102*, 18724–18729.

Chapter 38

Visual Transduction

Anita L. Zimmerman

Chapter Outline

I. SUMMARY

The process of vertebrate vision begins with photon capture and visual transduction in the rods and cones. The rods are outstanding single photon detectors that are used in dim light, whereas the cones provide excellent visual acuity, movement detection and color vision in bright light. The first step in the response to light is the absorption of a photon by the chromophore, retinal, within a visual pigment molecule. This triggers activation of a G-protein cascade, causing hydrolysis of cyclic guanosine monophosphate (cGMP) and thereby closure of cyclic nucleotide-gated (CNG) cation channels. These channels are normally held open in the dark by cGMP, conducting the inward "dark current". Closure of the channels hyperpolarizes the cell, decreasing neurotransmitter release onto other retinal neurons. There are elaborate mechanisms for shutting off the cascade and for light and dark adaptation. Although many of the fundamental molecular steps in visual transduction have been determined, numerous mysteries still remain.

II. INTRODUCTION

The miracle of vision begins when our photoreceptors absorb light that is reflected by our surroundings. However, the photoreceptor's duty does not end with photon capture. In addition, the photoreceptor must convert the energy of the absorbed photon into an electrochemical signal to be relayed to the visual cortex of the brain. This process of visual transduction involves a G-protein-mediated second messenger system that ultimately controls membrane potential and neurotransmitter release.

This chapter gives an overview of vertebrate visual transduction. Further information can be obtained from many excellent reviews on the subject (e.g. Burns and Baylor, 2001; Fu and Yau, 2007; Kawamura and Tachibanaki, 2008; Gross and Wensel, 2011; Lamb, 2011; MacLeish and Makino, 2011). Details of the cyclic nucleotide-gated ion channels that mediate the light response are covered in Chapter 35. Invertebrate visual transduction is not discussed here, but thorough descriptions and comparisons are available elsewhere, along with discussions of evolutionary links between invertebrate and vertebrate visual transduction (e.g. Katz and Minke, 2009; Lamb, 2009; Yau and Hardie, 2009; Fain et al., 2010). Interestingly, invertebrate photoreceptors use a different light-activated enzyme cascade than that found in rods and cones and their membranes hyperpolarize in response to light, whereas rods and cones depolarize. Finally, this chapter will deal only with image-forming vision. The retina also contains a very interesting pathway for light detection without image formation that is involved in circadian rhythms. This pathway was recently discovered to involve the photopigment melanopsin and a third class of photoreceptors in the retina: intrinsically photosensitive retinal ganglion cells, ipRGCs (reviewed in Do and Yau, 2010; Wong and Berson, 2011).

III. PHOTORECEPTOR CELLS

The two kinds of vertebrate photoreceptors – rods and cones – are specialized for use under different conditions. The rods are employed for vision in dim light, whereas the cones are used in moderate to bright light. Thus, while a rod

Cell Physiology Sourcebook. DOI: 10.1016/B978-0-12-387738-3.00038-X

can reliably detect a single photon in a darkened room, its sensing mechanism shuts down completely when normal room lights are switched on. Cones, on the other hand, are not sensitive enough to detect single photons, but give us color vision and high spatial and temporal resolution when light levels are sufficiently high.

Rods and cones also occupy different parts of the retina. Cones are concentrated in the center of the retina, the fovea, which receives light from the center of our visual field. The rods, however, are almost entirely excluded from the fovea and instead dominate the peripheral retina. However, a few cones are scattered throughout the peripheral retina and a few rods exist at the edge of the fovea. Thus, in daylight, our peripheral vision has much lower spatial resolution than our central vision because of the sparse distribution of peripheral cones. At night, our ability to locate a dim star is enhanced by looking "out of the corners of our eyes", using the abundant rods in the peripheral retina.

As shown in Fig. 38.1, the vertebrate photoreceptor can be divided into three regions: the outer segment, the inner segment and the synaptic terminal. The outer segment is the region of the cell dedicated to photon capture and visual transduction. The inner segment, located closer to the front of the eye, contains the nucleus, abundant mitochondria and other general cell machinery. The synaptic terminal contains vesicles of the neurotransmitter glutamate for release onto the second-order retinal neurons (the bipolar cells).

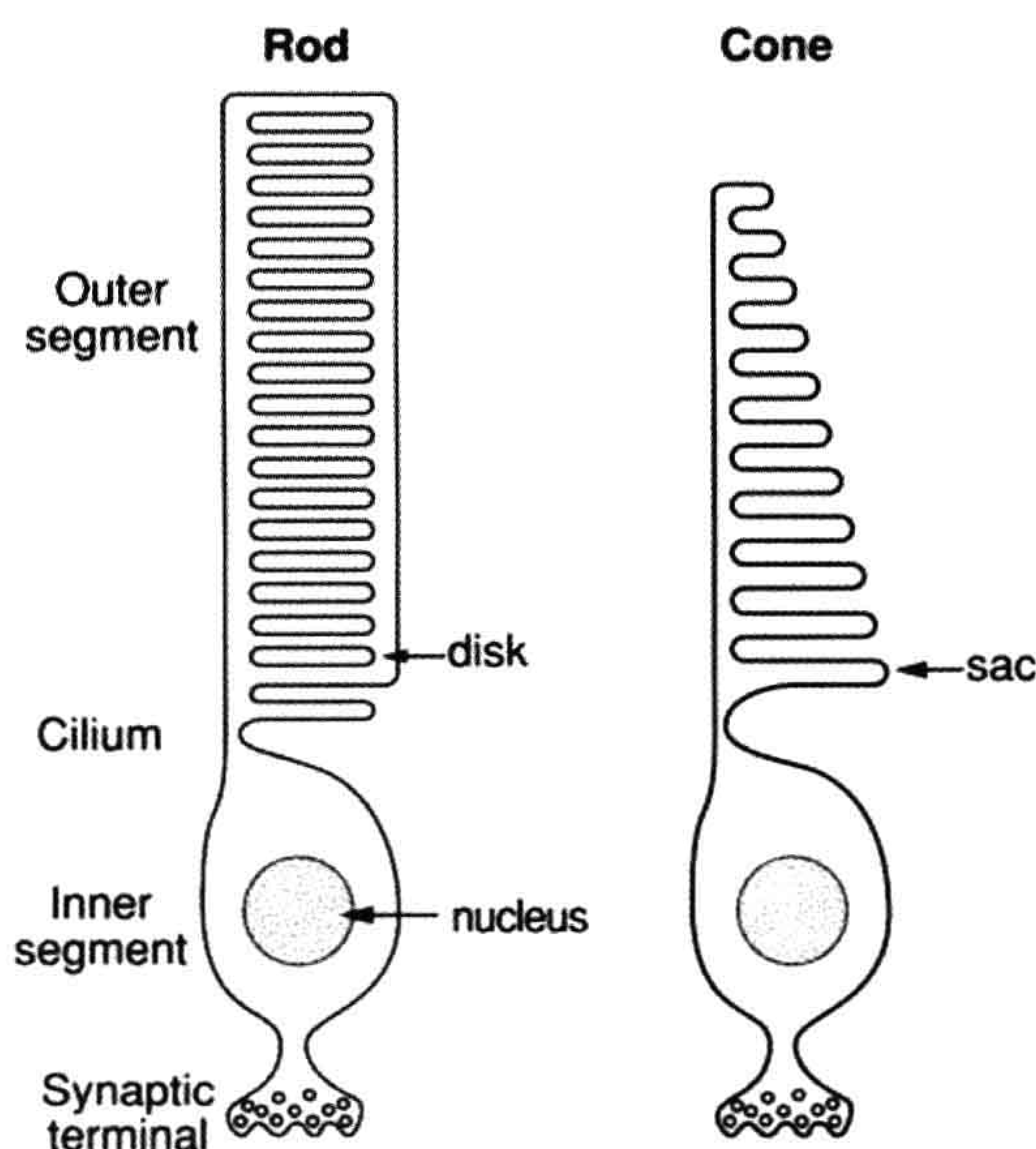


FIGURE 38.1 A simplified view of rod and cone structure. The outer segment is specialized for visual transduction. Cone photopigment molecules are located on infoldings of the plasma membrane, called sacs, rather than in the membranes of intracellular disks as in rods.

The anatomy of rods and cones is very similar, except that cones have a more conical shape and contain infoldings of the plasma membrane, called *sacs* (see Fig. 38.1), rather than the intracellular *disks* found in rods. The membranes of the disks and sacs contain photopigment molecules and various other proteins used in visual transduction. The disks or sacs are packed very tightly together: usually about 1000–2000 in a typical outer segment whose length is about 30–60 μm. This parallel array of membranes serves to align the photopigment molecules in the correct orientation for optimal absorption of light, which normally travels the length of the cell from the synaptic terminal toward the tip of the outer segment. The disks and sacs also serve to concentrate the photopigment molecules (e.g. about a hundred million in a typical rod) and to position the photopigment in close proximity to other important molecules in the visual transduction cascade.

In both rods and cones, the outer and inner segments are connected by a narrow region called the *cilium*. In some way that is not completely understood, the cilium segregates the inner and outer segment membrane proteins. For example, whereas the inner segment plasma membrane contains many types of ion channels (Bader et al., 1982; Barnes and Hille, 1989; reviewed in MacLeish and Makino, 2011), the outer segment plasma membrane contains essentially a pure population of light-regulated cyclic nucleotide-gated (CNG) ion channels (Baylor and Nunn, 1986). It is in the ciliary region that new disks or sacs are inserted during the outer segment regeneration process that occurs constantly. Recent evidence suggests that the formation of disks is accomplished by the repeated fusion of membrane vesicles containing the photopigment rhodopsin (reviewed in Sung and Chuang, 2010). Old disks or sacs are removed from the tip of the outer segment by phagocytosis by the retinal pigment epithelial (RPE) cells. These very opaque cells sit behind the retina, with finger-like cellular processes that hug the photoreceptor outer segments, reducing light scatter, as well as providing some of the molecules essential for visual transduction. Because the cilium is such a narrow structure, outer and inner segments often break apart (and their membranes reseal) during cell isolation from the retina. Thus, many studies of visual transduction are conducted on isolated outer segments, which are somewhat simpler preparations than whole cells.

IV. PHYSIOLOGY OF VISUAL TRANSDUCTION

The physiological trademark of the vertebrate photoreceptor is its light-regulated "dark current" (Fig. 38.2) (reviewed in Burns and Baylor, 2001; Fu and Yau, 2007; MacLeish and Makino, 2011). This current circulates between the outer and inner segments in the dark and is reduced upon light absorption. The dark current is carried

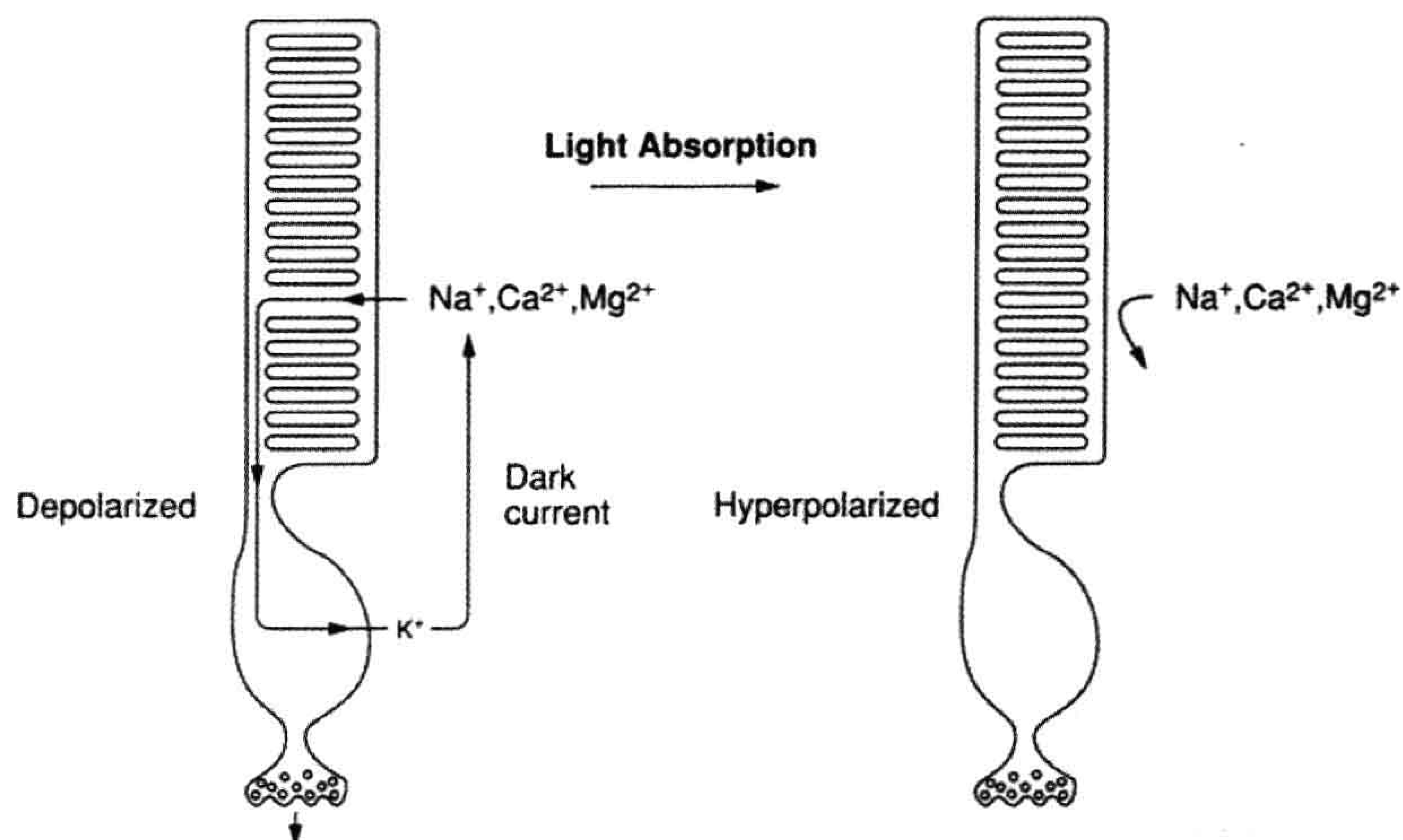


FIGURE 38.2 The absorption of light shuts down the dark current that circulates between the outer and inner segments of the photoreceptor. This reduction in current hyperpolarizes the cell, reducing the release of neurotransmitter.

into the outer segment mainly by Na^+ ions flowing through cyclic nucleotide-gated (CNG), non-selective cation channels (see Chapter 35) and out of the inner segment by K^+ ions flowing through voltage-gated K^+ channels. Because the CNG channels are non-selective cation channels, they allow the entry not only of Na^+, but also of Ca^{2+} and Mg^{2+}. These divalent cations have important consequences for visual transduction. First, Ca^{2+} regulates the light-dependent enzyme cascade (discussed below). Second, both Ca^{2+} and Mg^{2+} pass through CNG channels extremely slowly, reducing the effective single-channel conductance and thereby making the current–voltage relation for the dark current relatively flat in the physiological range of membrane voltages. Thus, under physiological conditions, the divalent cations make the dark current almost independent of voltage and, therefore, a faithful reporter of the light level, rather than of voltage changes induced by channel activity in the inner segment (Zimmerman and Baylor, 1992).

Since the cell has a relatively high Na^+ permeability in the dark, its resting potential is somewhat more positive than that for most cells (about -40 mV, instead of -70 mV). This resting depolarization tends to open voltage-gated Ca^{2+} channels in the synaptic terminal, allowing Ca^{2+} entry and vesicular release of neurotransmitter in the dark. When a photon is absorbed by a rhodopsin molecule in a disk membrane, a series of reactions leads to a reduction in the concentration of guanosine 3′, 5′-cyclic monophosphate (cGMP), which normally binds to, and opens, the outer segment CNG channels in the dark. Since there is less cGMP available to open the channels in the light, they close, decreasing the dark current (i.e. decreasing the Na^+ permeability), causing a membrane hyperpolarization which, in turn, causes closure of the voltage-gated K^+ and Ca^{2+} channels in the inner segment and synaptic terminal and, finally, a decrease in neurotransmitter release. The process is similar in cones.

The dark current and light response can be measured in a variety of ways, including a voltage-clamp method using intracellular microelectrodes, the whole-cell patch-clamp method and the suction electrode method. The relatively non-invasive suction electrode method (Fig. 38.3) works particularly well with mammalian photoreceptors, which are usually quite small and fragile. This method is much gentler than the other techniques, yet is able to measure the dark current without interference from inner segment currents.

Families of light responses recorded with a suction electrode from a monkey rod and cone are shown in Fig. 38.4. Light response amplitudes increase in a graded manner with light intensity until they reach a limiting value obtained with a "saturating light" that shuts off all the inward dark current (i.e. that closes all the CNG channels in the outer segment plasma membrane). Supersaturating light intensities cannot give larger responses, but instead give longer lasting ones. Cones are less sensitive than rods, requiring about a hundred times as many photons to shut down half the dark current; this seems to result at least in

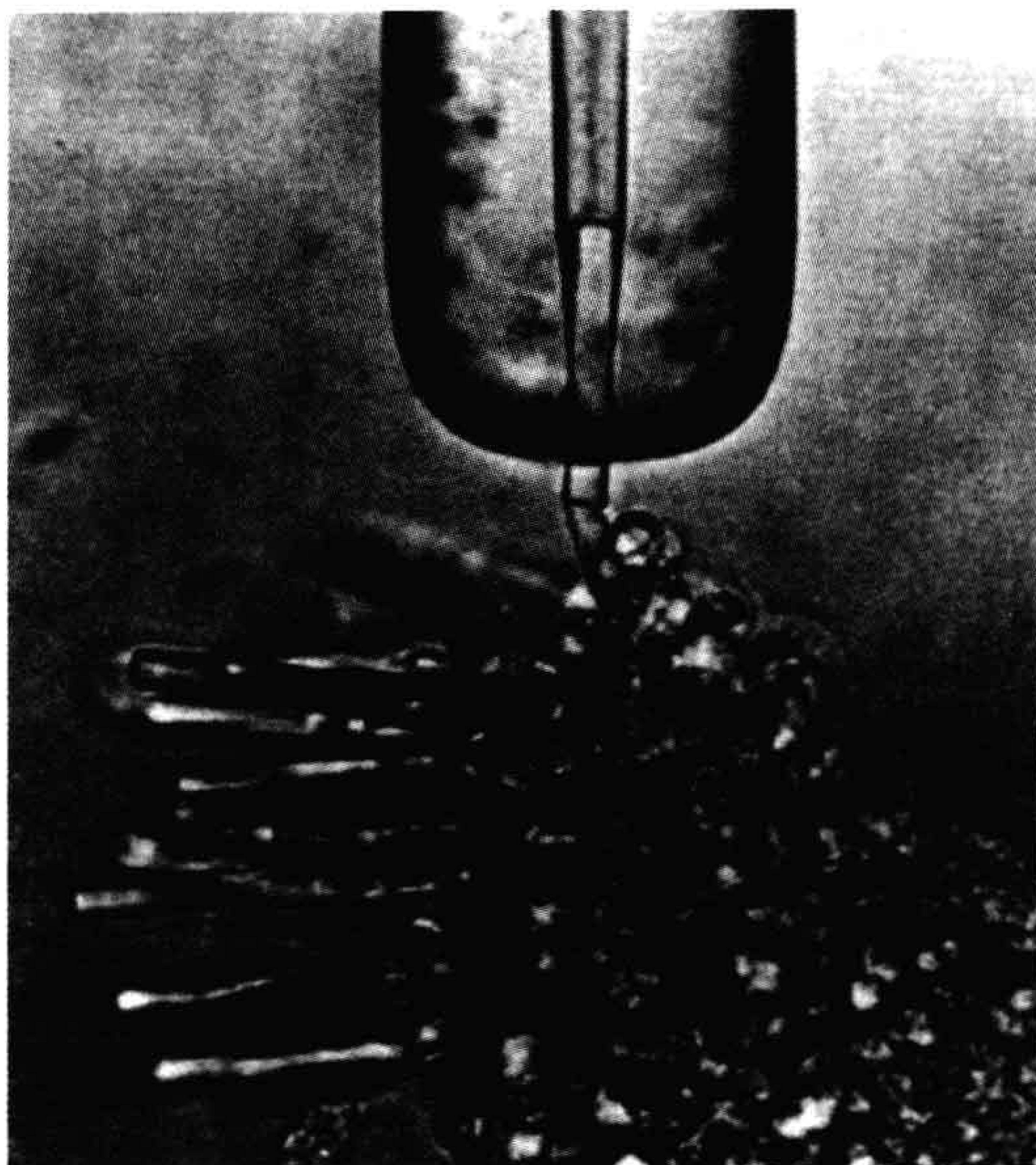


FIGURE 38.3 The use of a suction electrode to record the dark current flowing into the outer segment of a rod attached to a piece of toad retina. The horizontal line just below the suction electrode is the junction between the outer and inner segments. The electrode is filled with a physiological salt solution and connected to a sensitive amplifier. *(Reproduced with permission from Baylor et al., 1979.)*

part from a lower amplification in the G-protein-mediated enzyme cascade described below (reviewed in Gross and Wensel, 2011). However, the cone responses are several times faster than those of rods, as evidenced by the shorter time to peak and faster recovery, and this gives them an advantage over rods in the detection of movement and rapid changes in illumination. The undershoots seen in the cone responses (but not in normal rod responses) are not yet fully understood, but appear to make the cone especially sensitive to changes in illumination (Schnapf et al., 1990).

Although single photon responses are too small to be measured in cones, they are about 1.0 pA in rods, and therefore have been studied in some detail there. Single photon responses are very reliable: they occur at least 80% of the time after absorption of a photon by a rhodopsin molecule and they almost never occur in the absence of photon absorption (reviewed in Baylor, 1987). A single absorbed photon gives a highly amplified response, shutting down 3–5% of the total dark current by closing a few hundred CNG channels in a narrow band (one to a few micrometers in width) of outer segment plasma membrane near the site of absorption. Like the dim flash responses in Fig. 38.4 (bottom traces of each set), the single photon response has a stereotypical waveform, with a slow, S-shaped rise and a very slow decay. These complex, slow kinetics reflect the complex enzyme cascade underlying the response.

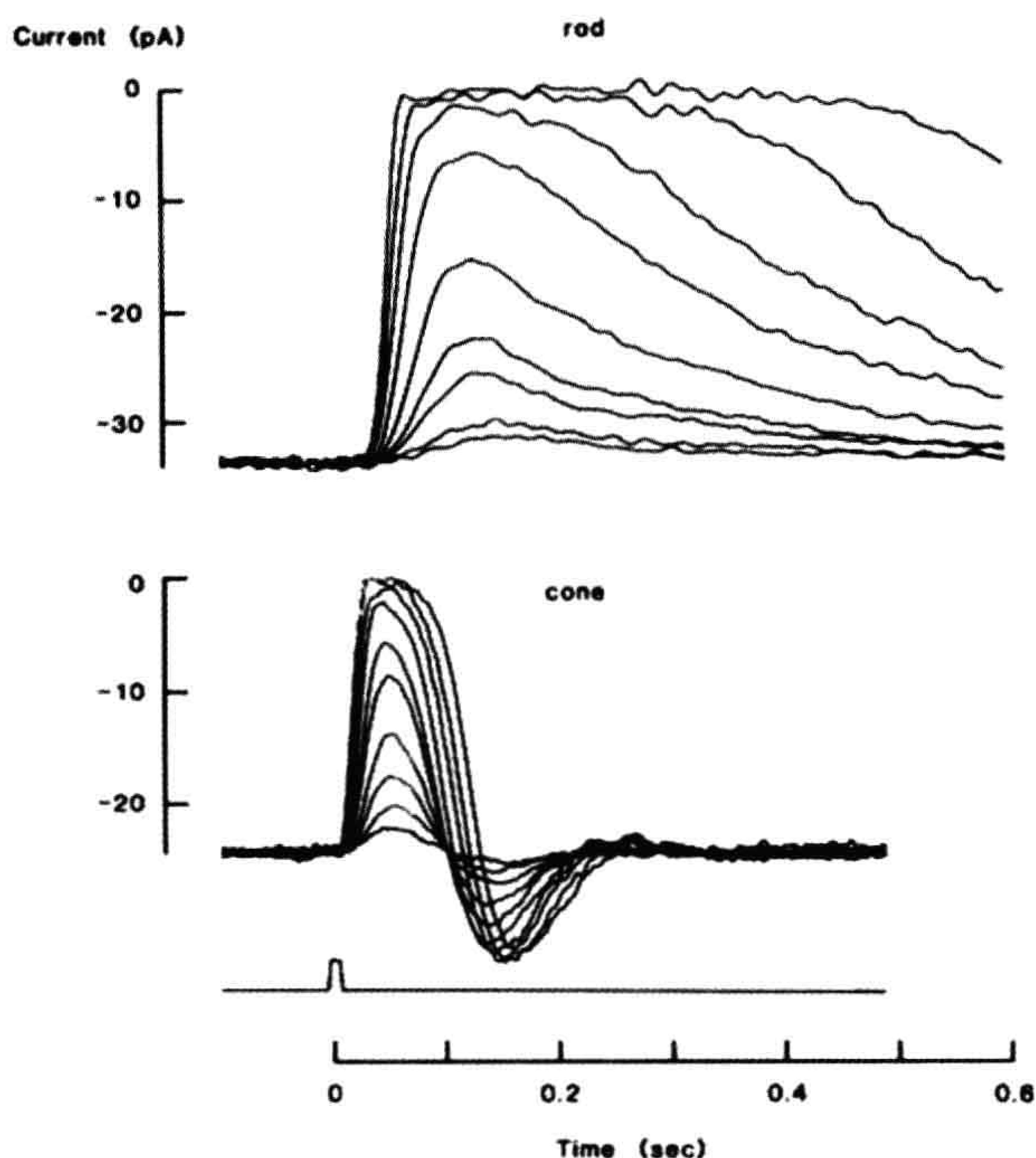


FIGURE 38.4 Families of photocurrents recorded by suction electrode from a rod and a cone of the monkey, *Macaca fascicularis*. Brief light flashes were given at time zero (rectangular pulse below the current recordings). Upward deflections indicate reductions in the inward dark current. From the bottom to the top of each family, flash strengths were increased by factors of 2. Expected numbers of photoisomerizations ranged from 2.9 to 860 for the rod and from 190 to 36 000 for the cone. Saturation of the responses (top traces in each family) occurred when all dark current was shut off. *(Reproduced with permission from Baylor, 1987.)*

When membrane voltage is recorded instead of outer segment current, the waveform resembles an inverted version of the current for dim lights but not for light levels near or beyond saturation. When many photons are absorbed, the voltage recordings (Fig. 38.5) show a characteristic "nose" and "plateau". These features result from a shaping of the response by ion channels in the inner segment. Several types of channels contribute to the waveform (reviewed in MacLeish and Makino, 2011), but the dominant channel giving rise to this more complicated shape appears to be an inner segment, non-selective cation channel that is opened by hyperpolarization (the HCN1 channel). Thus, the closure of outer segment CNG channels gives the initial hyperpolarization (beginning of the nose). This hyperpolarization opens the inner segment HCN1 non-selective cation channels which, in turn, depolarize the membrane, giving the transition from nose to plateau.

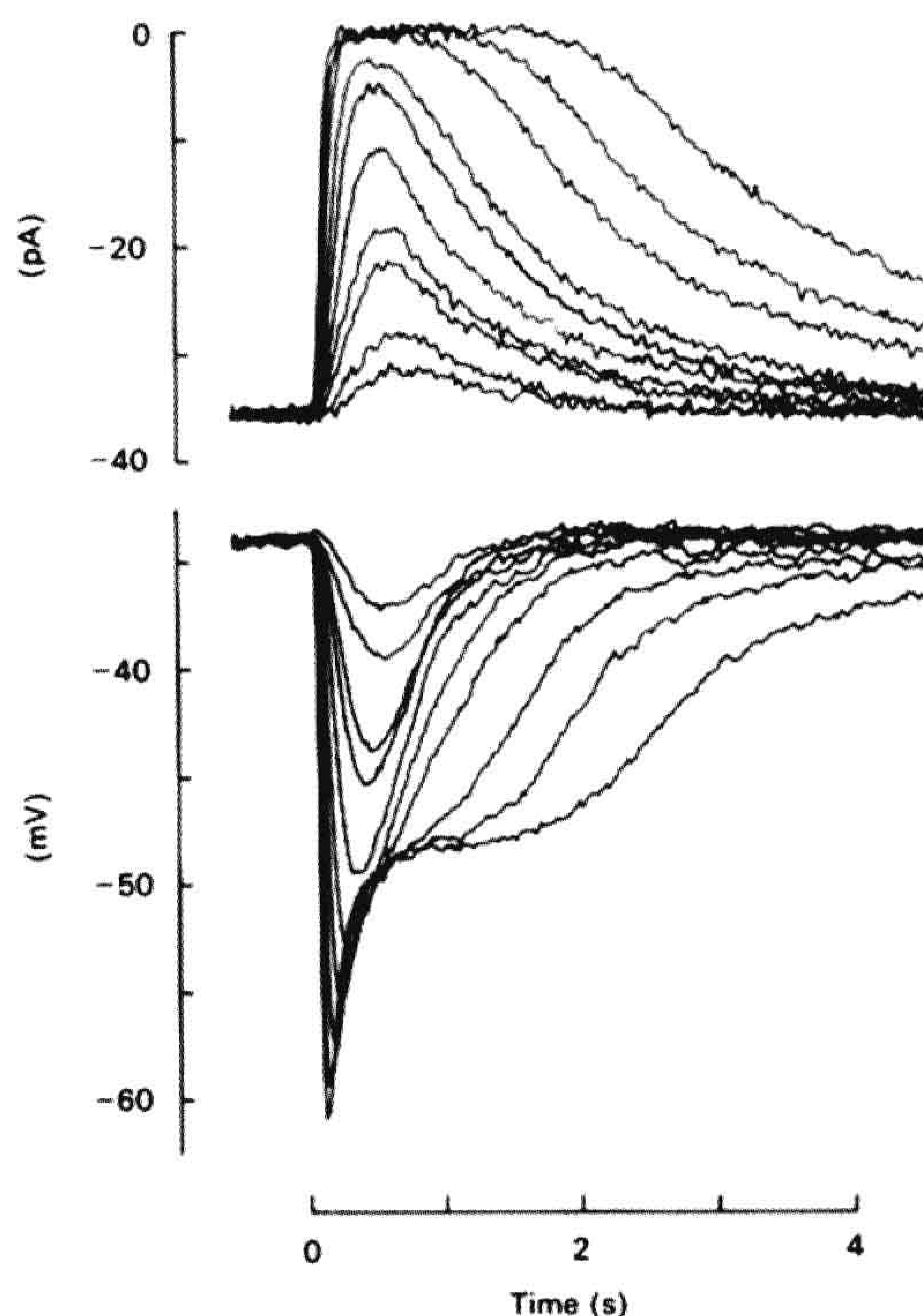


FIGURE 38.5 Comparison of light-evoked changes in outer segment current with those in membrane potential for a salamander rod. The currents were measured by a suction electrode, while the membrane potential was monitored by an intracellular microelectrode. The current and voltage responses to dim flashes have similar form, but a prominent "nose" and "plateau" are seen in the voltage responses to bright flashes. 500-nm, 11-ms flashes were given at $t = 0$ and photon densities increased by factors of about 2 between 1.5 and 430 photons μm^{-2}. *(Reproduced with permission from Baylor and Nunn, 1986.)*

Eventually, these channels close because of the depolarization while, at the same time, the outer segment CNG channels reopen during recovery from the light response and the membrane potential returns to its initial, relatively depolarized, dark value.

Aside from the ion channels described earlier, two other types of ion transport protein are of obvious importance to the vertebrate photoreceptor. First, Na^+-K^+ pumps in the inner segment are responsible for expelling the Na^+ that enters through the CNG channels in the outer segment. Second, Na^+:Ca^{2+},K^+ exchange carriers (NCKX; reviewed in Bauer, 2002; Schnetkamp, 2004) in the outer segment expel the Ca^{2+} that enters through the CNG channels and regulates the enzyme cascade. The Na^+:Ca^{2+},K^+ carriers are particularly important in light adaptation, where intracellular Ca^{2+} plays a large regulatory role.

The ability of the visual system to detect light depends partly on its degree of adaptation to background illumination. Although much of light and dark adaptation involves pupillary responses and processes occurring in the brain and non-photoreceptor layers of the retina, some aspects of adaptation clearly occur in the rods and cones themselves. In continuous light, there is a partial recovery of the dark current after its initial suppression when the light is switched on. This sag in the photoresponse is accompanied by a decrease in light sensitivity and an acceleration of response kinetics (although this acceleration is negligible in monkey cones; Schnapf et al., 1990). Thus, the response to a light flash during continuous background light is smaller and generally briefer than that to an equally bright flash occurring in the dark. To make the amplitude of the flash response equal to that obtained in the dark, one must increase the flash intensity (Fig. 38.6). This light adaptation allows the photoreceptor to respond over a much larger range of light intensities than it otherwise could. In effect, the photoreceptor uses a non-linear gain adjustment partially to overcome the response saturation that occurs as a result of having a finite number of CNG channels to close in the light. Cones light-adapt so well that it is essentially impossible to obtain saturation of their dark current in steady bright light. Saturation is only possible transiently when bright light is applied while the cone is in a very dark-adapted state (reviewed in Lamb, 2011).

Photoreceptor dark adaptation is a rather complicated set of processes that has been most thoroughly studied in rods (reviewed in Lamb and Pugh, 2004). After exposure to a light that is bright enough to bleach all the photopigment, a rod ultimately cannot return to its dark state until non-excited photopigment molecules have been regenerated (including reinsertion of the chromophore, see following). However, when a rod has been exposed to only moderately bright light, which leaves some photopigment unbleached, it is able to respond to light again after a briefer period of adaptation. This period is characterized by a lingering

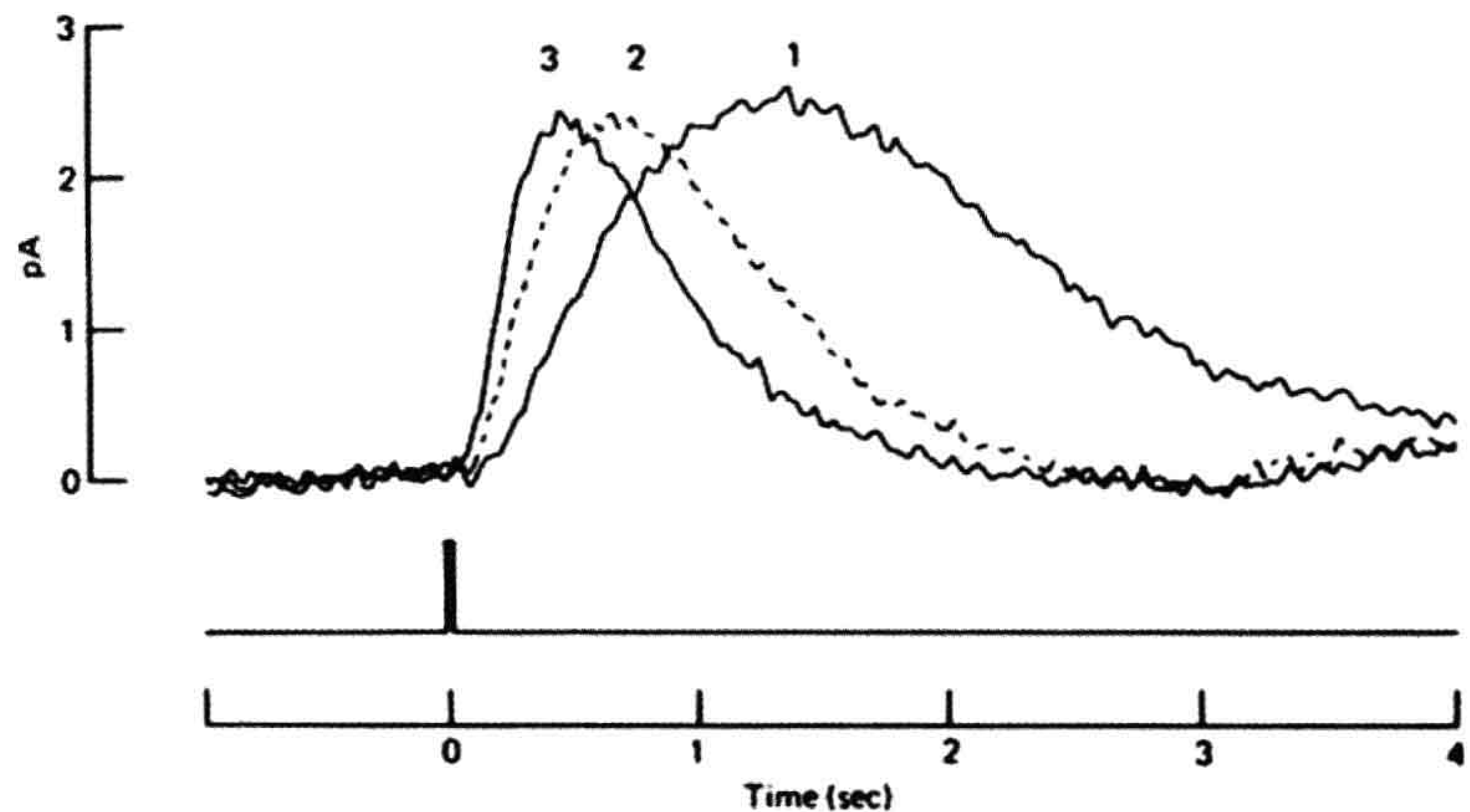


FIGURE 38.6 Decreased sensitivity and accelerated flash response kinetics characteristic of adaptation to background light in a rod. These outer segment currents were obtained by suction electrode recording from a toad rod that was given a test light flash in darkness (curve 1), with a dim background light (curve 2) and with a brighter background light (curve 3). In the presence of background light, the test flash intensity had to be increased to obtain responses of approximately the same amplitude. For example, the flash intensity used to obtain curve 2 was approximately five times the intensity used to obtain curve 1. *(Reproduced with permission from Baylor et al., 1979.)*

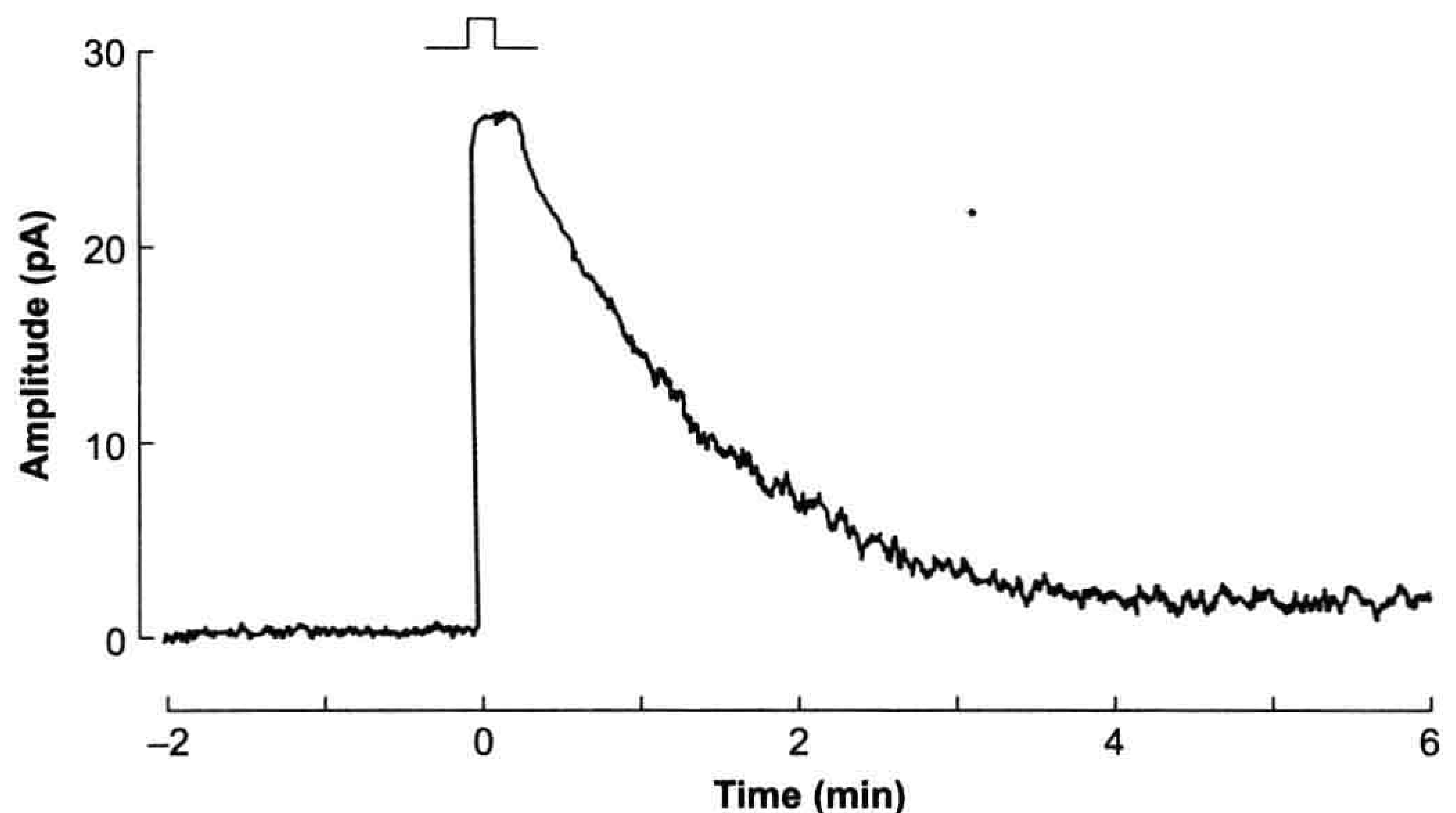


FIGURE 38.7 Prolonged dark current suppression and increased noise following a strong bleach. The rectangular pulse above the response indicates when the dark-adapted rod was given a bright flash of light that bleached about 0.7% of its rhodopsin (72×10^5 photons μm^{-2}, calculated to isomerize 1.8×10^7 rhodopsins). Closer examination of the lingering noise revealed a strong resemblance to that produced by the absorption of single photons. *(Reprinted with permission from Nature, Lamb, 1980. Copyright 1980 Macmillan Magazines Limited.)*

suppression of the dark current for many minutes after the light is switched off, a decrease in light sensitivity similar to that found in the presence of background light and an increase in outer segment current noise (Fig. 38.7). These features limit visual detection and appear to derive from incomplete shutoff of the photopigment after loss of its chromophore. Ultimately, the speed with which the rod recovers from a bright light is limited by the rate at which 11-*cis*-retinal is delivered to opsin. Cones recover from a bright light so rapidly that it has been hypothesized that the shut-off reactions in their transduction enzyme cascade must be extremely fast (reviewed in Lamb, 2011).

V. MOLECULAR MECHANISMS

VA. Photopigment Activation and Shut-off

Visual pigments are integral membrane proteins called *opsins* that consist of *apo-opsin* and a ubiquitous light-absorbing chromophore, *retinal* (Fig. 38.8). Retinal is in a class of molecules called *retinoids* that also includes vitamin A (all-*trans*-retinol). There are many excellent reviews of visual pigments and rhodopsin in particular (e.g. Palczewski, 2006; Nickle and Robinson, 2007; Hofmann et al., 2009; Smith, 2010). Retinal is derived from vitamin A and comes in two forms in vertebrates: $retinal_1$ and dehydroretinal, or $retinal_2$ (reviewed in Nickle and Robinson, 2007). Human photoreceptors use $retinal_1$. Interactions with different opsins change the spectral tuning characteristics of retinal. Thus, each type of photoreceptor has its own type of opsin, which results in a characteristic photopigment absorption spectrum and therefore a characteristic color sensitivity of the cell. Rods contain rhodopsin (Rh) and are therefore most sensitive to blue-green light (peak wavelength around 490 nm), whereas primate cones are of three types, with characteristic peak absorbances in the short-wavelength (peak about 430 nm), middle-wavelength (peak about 530 nm)

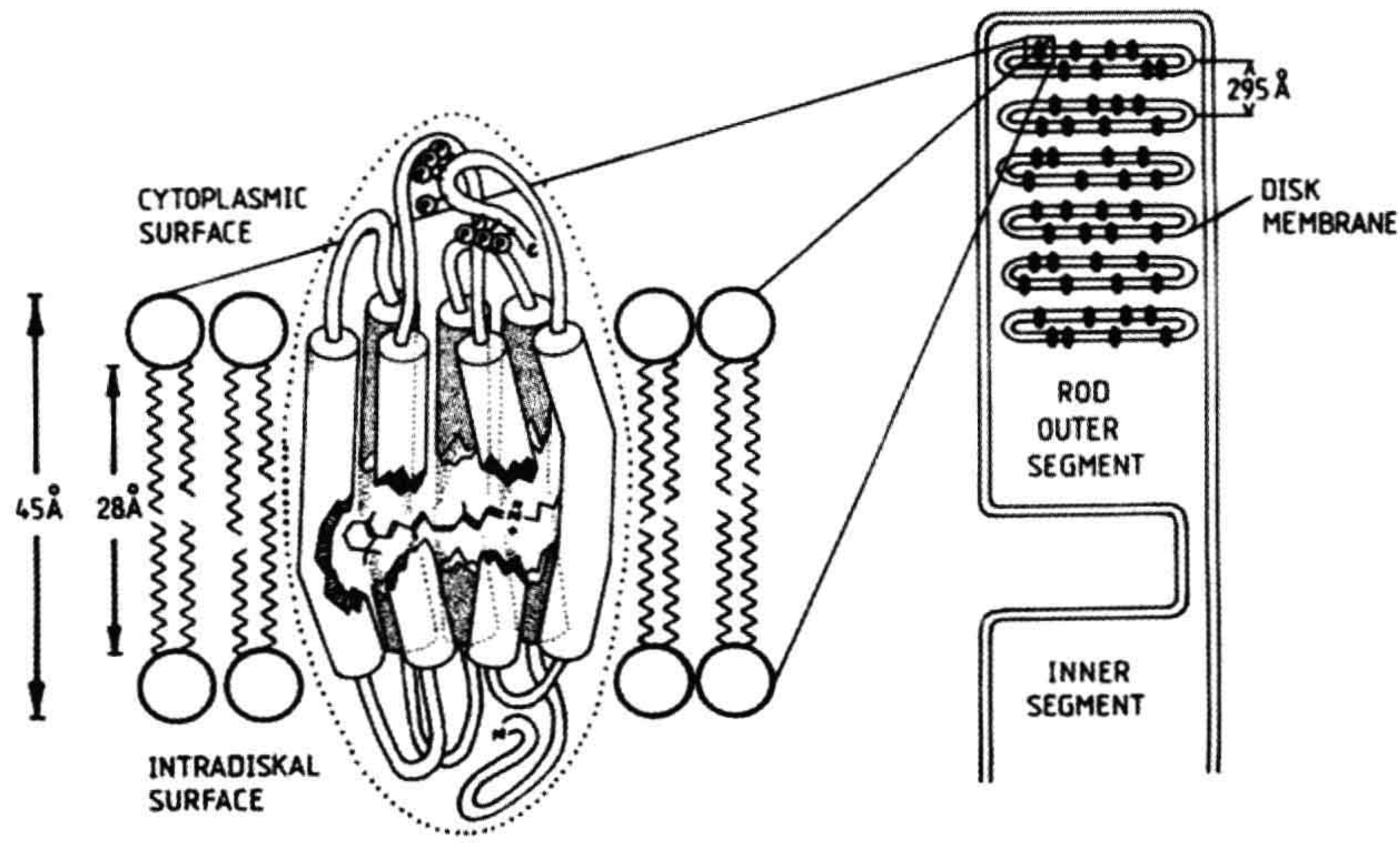


FIGURE 38.8 A model for the structure of rhodopsin in the disk membrane of a rod. The light-absorbing chromophore, retinal, sits in a binding pocket near the middle of the integral membrane protein, opsin. *(Reproduced with permission from Dratz and Hargrave, 1983.)*

and long-wavelength (peak about 560 nm) regions of the visible spectrum (Fig. 38.9). These three types of cone are sometimes referred to as blue-, green- and red-sensitive cones, respectively, although 560 nm actually corresponds to yellow, rather than red, light. The characteristic absorption spectra determine only the probability that a photon will be absorbed by the cell's photopigment. The photoreceptor responds in exactly the same way to any absorbed photon, independent of its wavelength.

Absorption of a photon causes isomerization of retinal from the 11-*cis* to the all-*trans* form (Fig. 38.10), breaking its covalent bond to the protein and destabilizing its position. Eventually all-*trans*-retinal hops out of its binding pocket within opsin, but a chain of conformational intermediates is generated before this dissociation occurs. For the best-studied pigment, rhodopsin, these intermediates are (in the order that follows photon absorption) photorhodopsin, bathorhodopsin, BSI (blue-shifted intermediate), lumirhodopsin, metarhodopsin I, metarhodopsin II and metarhodopsin III (reviewed in Palczewski, 2006; Smith, 2010). Similar transitions are thought to occur in other visual pigments. The metarhodopsin II (meta II) conformational state activates the G protein, transducin, which begins the cellular response to light. As all-*trans*-retinal leaves its binding pocket in opsin, it is released into the interior of the disk. It must then be transferred to the cytosolic side of the disk, apparently via diffusion through the plasma membrane and transport with phosphatidylethanolamine by the ABCA4 lipid carrier (reviewed in Molday and Zhang, 2010). On the cytosolic side, the aldehyde, all-*trans*-retin*al*, is converted by an enzyme (a retinol

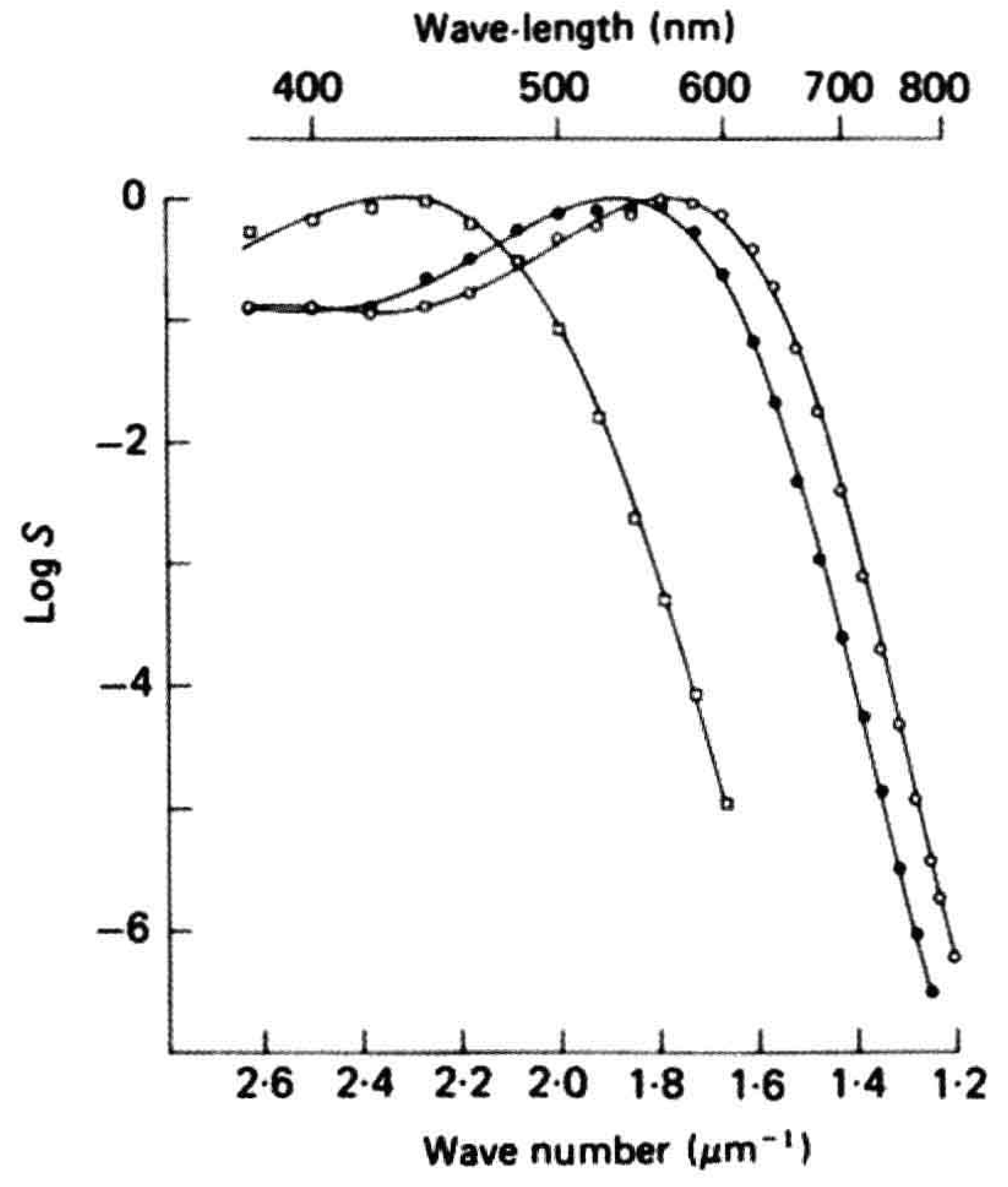


FIGURE 38.9 Cone spectral sensitivities, as measured by the suction electrode method. These spectra were obtained from blue-, green- and red-sensitive monkey cones (squares, filled circles, and open circles, respectively). The spectral sensitivity, S, was derived from the cone's response to flashes of different color and it reflects the probability of absorption of a photon of that color (or wavelength). *(Reproduced with permission from Baylor et al., 1987.)*

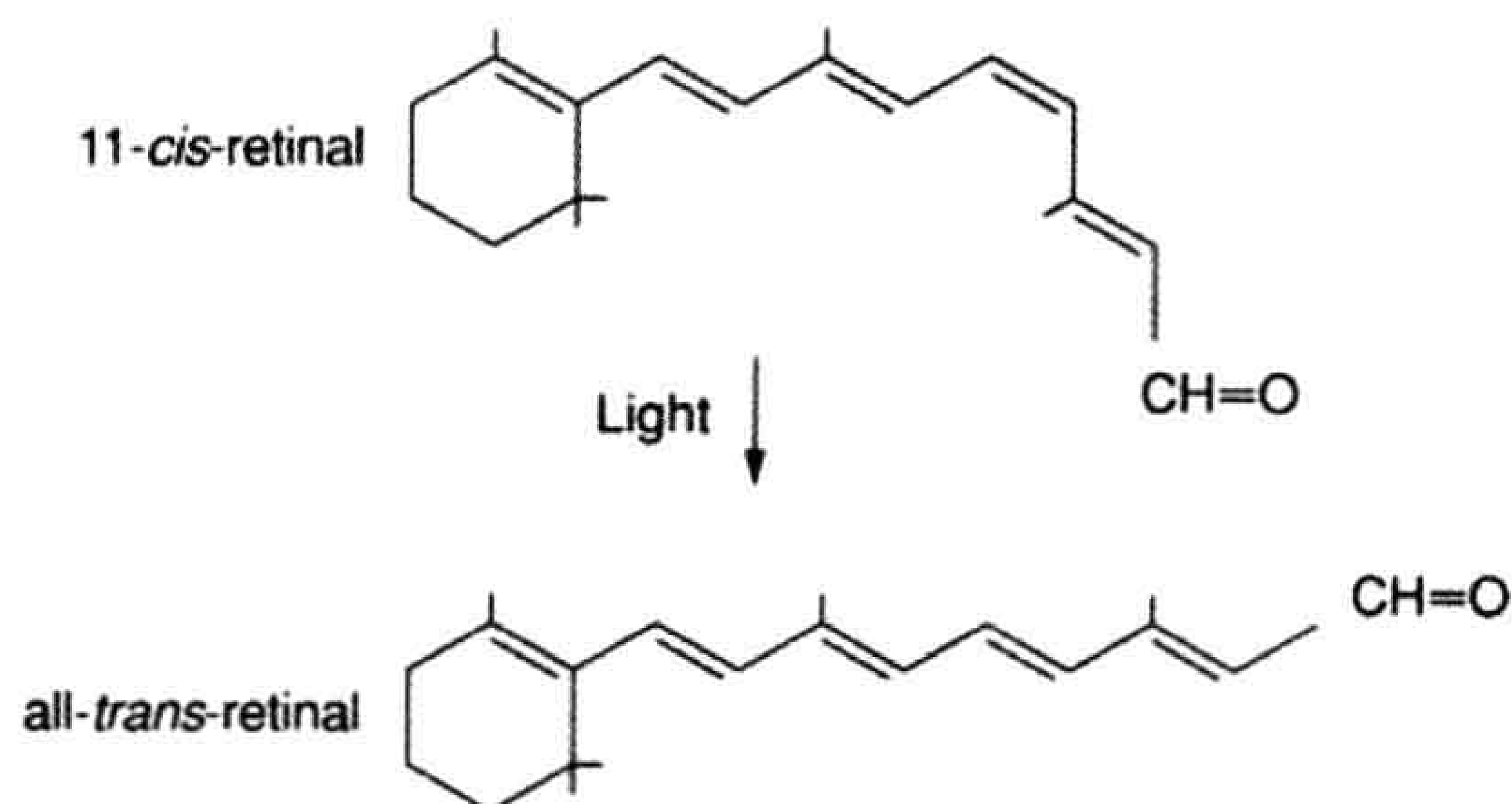


FIGURE 38.10 The light-induced isomerization of retinal$_1$ from the 11-*cis* to the all-*trans* form. This is the first step in vertebrate visual transduction and the only one that is a direct action of light.

dehydrogenase) to the alcohol form, all-*trans*-retin*ol*, which then travels through the plasma membrane into the extracellular space, where it is shuttled via retinoid binding proteins to the RPE and Müller cells. The process by which all-*trans*-retinal is transported and converted back into 11-*cis*-retinal for reloading into opsin is called the *visual cycle* (reviewed in Travis et al., 2007; Wang and Kefalov, 2011).

For the photoreceptor to reset to its dark condition after a light is switched off, the molecular players in the light response also must be switched off. Most of what we know about photopigment shut-off comes from work on rhodopsin (depicted in the top right loop of Fig. 38.11). The shut-off of rhodopsin's ability to activate transducin begins even before all-*trans*-retinal has left the protein. Rhodopsin kinase phosphorylates photoexcited rhodopsin at multiple serine and threonine residues near the C-terminal. A 48-kDa protein called *arrestin* then binds phosphorylated rhodopsin, reducing its interaction with transducin. There are recent hints for still other players in the shut-off process (e.g. RGS9), but all the details have not yet been resolved (reviewed in Gross and Wensel, 2011). Once all-*trans*-retinal has separated from opsin, the photopigment cannot be reset to its photon-receptive dark state until 11-*cis*-retinal has been reinserted, arrestin has been released and a phosphatase (serine/threonine phosphatase type 2A) has removed the phosphates from the C-terminal residues. This process takes several minutes. The new 11-*cis*-retinal that is inserted into opsin is made in the RPE cells and transported into the rods. However, cones obtain new 11-*cis*-retinal by a different mechanism: the surrounding Müller cells make the alcohol form, 11-*cis*-retin*ol*, which is transferred to the cones, where it is converted to the aldehyde, 11-*cis*-retin*al* (Mata et al., 2002; reviewed in Travis et al., 2007; Wang and Kefalov, 2011). Interestingly, in cones, there is much greater activity of the kinase that phosphorylates their pigments and this may partly explain why cones recover from a light response much more quickly than do rods (reviewed in Gross and Wensel, 2011). Furthermore, in cones there is a less stable interaction between 11-*cis*-retinal and the visual pigment, leading to a greater concentration of apo-opsin, which itself stimulates transducin (reviewed in Kawamura and Tachibanaki, 2008).

VB. Cyclic Nucleotide Cascade

A cyclic nucleotide enzyme cascade is used to translate the message of photon absorption into the language of the brain – electrical and chemical signals. The key second

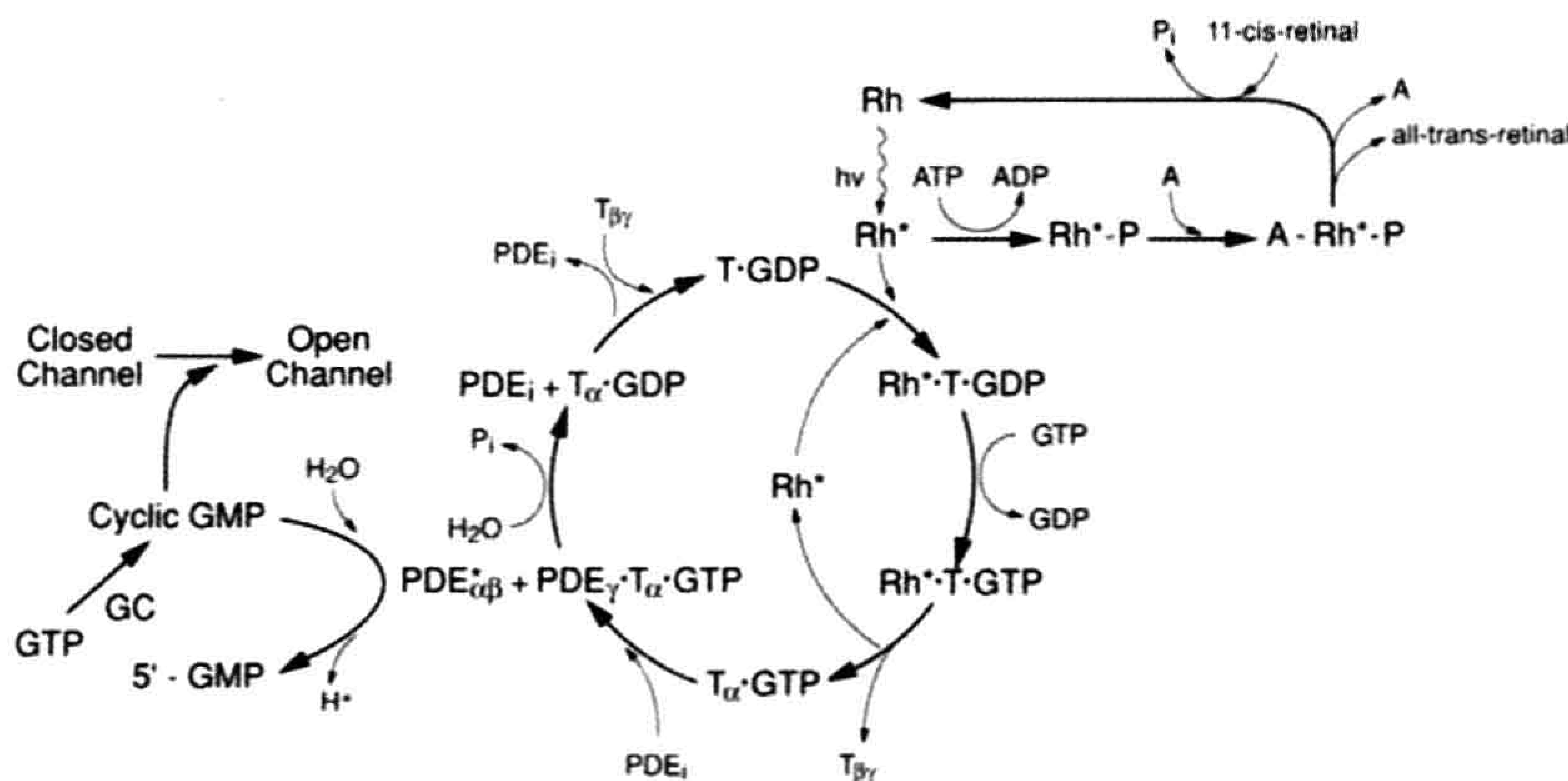


FIGURE 38.11 The enzyme cascade controlling visual transduction in rods. Abbreviations: A: arrestin; channel: cyclic nucleotide-gated (CNG) outer-segment ion channel; GC: guanylate cyclase; PDE: cGMP-specific phosphodiesterase (*, active form); Rh: rhodopsin (*, photoexcited, active form); T: the G protein, transducin. There is increasing evidence that, in spite of its complexity, this diagram is quite incomplete. *(Modified with permission from Stryer, 1991 and drawing on information from Palczewski, 2006; Nickle and Robinson, 2007; Hofmann et al., 2009; Smith, 2010.)*

messenger is cGMP, with another second messenger, Ca^{2+}, involved in more subtle aspects of visual transduction. Most of our information on the molecular mechanism of visual transduction derives from studies on rods, but the process appears to be similar in cones. A large body of biochemical and physiological evidence suggests that absorption of a single photon by rhodopsin initiates the following chain of events (diagrammed in Fig. 38.11):

1. Photoexcited rhodopsin (Rh*) catalyzes the replacement of GDP by GTP on the G protein, transducin (T). Both Rh* and the peripheral membrane protein, T, are able to diffuse laterally in the disk membrane, where they find each other and interact. Before Rh* is shut off, it activates about 500 Ts, representing the first amplification step in the transduction process.
2. The α subunit of T, now with GTP bound, dissociates from the rest of T (the $\beta\gamma$ subunit complex) and binds to and removes the γ inhibitory subunit of another peripheral disk membrane protein, cGMP-specific phosphodiesterase (PDE). Each $T\alpha$ can activate only one PDE since the catalytic portion of PDE, $PDE\alpha\beta$, is only free to work when $PDE\gamma$ is bound to $T\alpha$ (and therefore unable to reassociate with $PDE\alpha\beta$).
3. Once disinhibited, one PDE molecule ($PDE\alpha\beta$) hydrolyzes about a million cGMP molecules, leading to the closure of hundreds of CNG ion channels and thereby halting entry of over a million Na^+ ions during the time course of the single photon response.

The recovery of the dark current after photon absorption is accomplished by many processes, including these:

1. Shut-off of rhodopsin, as discussed above.
2. Inherent GTPase activity of $T\alpha$, converting $T\alpha$ back to the GDP-bound, inactive form that reassociates with $T\beta\gamma$.
3. Reassociation of $PDE\gamma$ with $PDE\alpha\beta$, returning PDE to its more inhibited, dark state.
4. Synthesis of new cGMP from GTP by guanylate cyclase (GC).
5. Reopening of CNG ion channels, as more cGMP becomes available.

Although these processes are the most established ones, there is recent evidence that other processes and factors may be involved in regulating the cGMP cascade, mostly through feedback mechanisms. Some of the factors that may play a role are: regulatory cGMP-binding sites on PDE; auxiliary retinoid binding sites on opsin (Heck et al., 2003; Makino et al., 2010); calcium-binding proteins and other regulatory proteins that affect guanylate cyclase, PDE, rhodopsin, transducin and/or the CNG channel (e.g. guanylate cyclase activating protein, or GCAP; reviewed in Gross and Wensel, 2011); members of the inositol phosphate system whose function has not yet been established; and various kinases and phosphatases whose functions are also not yet clear. The field of regulation of the photoreceptor cGMP cascade is currently very unsettled and very intriguing.

An interesting set of molecular interactions that seems to regulate visual transduction, and even rod outer segment morphogenesis, occurs at the interface between the rod disks and the plasma membrane. The rod CNG channel is a heterotetramer consisting of three α (CNGA1) subunits and one β (CNGB1) subunit (see Chapter 35). But this channel does not stand alone. Instead, its α subunits are linked to Na^+:Ca^{2+}, K^+ exchange carriers in the plasma membrane and these carriers expel the calcium ions that enter the cell through the CNG channel. Furthermore, the β subunit of the CNG channel is physically linked, via its cytosolic GARP (glutamic acid rich protein) region, to a molecular complex in the disk rim. This disk rim complex consists of an oligomer of Peripherin-2 and Rom-1, which also interacts with other GARPs that associate with the cytosolic side of the disks (reviewed in Sung and Chuang, 2010). Interestingly, a genetic knockout of the CNG channel's β subunit and the GARPs disrupts the orderly array of disks in the rod outer segment, produces shorter outer segments and reduces the light sensitivity of the rod (Zhang et al., 2009). Thus, these molecular complexes are vital to both visual transduction and rod morphogenesis.

One aspect of visual transduction that is controlled by feedback regulation is light adaptation (reviewed in Lamb, 2011) and a large body of evidence supports involvement of Ca^{2+} in this process. Coupled with calcium-binding proteins, Ca^{2+} has been found to inhibit guanylate cyclase (GC), to stimulate PDE via inhibition of Rh phosphorylation and to inhibit the CNG channels (see Chapter 35). All three types of Ca^{2+} feedback appear to occur in both rods and cones, but with different molecular details and rates. For example, inhibition of the CNG channels by Ca^{2+} is much greater in cones than in rods (Rebrik and Korenbrot, 2004). Calcium feedback in rods and cones is thought to involve the following steps. In the dark, when the cGMP concentration is relatively high, Ca^{2+} enters the cell through the CNG channels, raising the intracellular concentration of Ca^{2+} ($[Ca^{2+}]_i$). When the channels close following photon absorption, $[Ca^{2+}]_i$ decreases, because its influx through the channels is decreased while its extrusion by Na^+:Ca^{2+}, K^+ exchangers continues. The decreased $[Ca^{2+}]_i$ would be expected to stimulate guanylate cyclase and to inhibit PDE, leading to a subsequent partial recovery of the cGMP level and a reopening of some of the channels. The feedback mechanisms involving Ca^{2+} are mediated by several calcium binding proteins (reviewed in Gross and Wensel, 2011), but the most significant Ca^{2+} feedback effect on visual transduction appears to be that mediated by guanylate cyclase activating proteins, or GCAPs

(e.g. Burns et al., 2002; reviewed in Gross and Wensel, 2011). GCAPs are Ca^{2+} binding proteins that bind to guanylate cyclase. The GCAPs stimulate guanylate cyclase to make more cGMP but, when Ca^{2+} binds to a GCAP, the GCAP is less stimulatory, so guanylate cyclase makes less cGMP, resulting in closure of CNG channels and thereby reducing Ca^{2+} entry. This same negative feedback system works in reverse in the light: fewer CNG channels are open, so less Ca^{2+} enters; then lower intracellular $[Ca^{2+}]$ produces stimulation of guanylate cyclase by GCAPs, resulting in higher [cGMP], more channel opening and therefore more Ca^{2+} entry. The accumulated knowledge of these feedback processes and the associated enzyme cascade has made vertebrate visual transduction a model system for understanding G-protein-mediated signal transduction in general.

BIBLIOGRAPHY

Bader, C. R., Bertrand, D., & Schwartz, E. A. (1982). Voltage-activated and calcium-activated currents studied in solitary rod inner segments from the salamander retina. *J Physiol, 331*, 253–284.

Barnes, S., & Hille, B. (1989). Ionic channels of the inner segment of tiger salamander cone photoreceptors. *J Gen Physiol, 94*, 718–743.

Bauer, P. J. (2002). Binding of the retinal rod $Na^+/Ca^{2+}-K^+$ exchanger to the cGMP-gated channel indicates local Ca^{2+}-signaling in vertebrate photoreceptors. *Ann NY Acad Sci, 476*, 325–334.

Baylor, D. A. (1987). Photoreceptor signals and vision. *Invest Ophthalmol Visual Sci, 28*, 34–49.

Baylor, D. A., & Nunn, B. J. (1986). Electrical properties of the light-sensitive conductance of rods of the salamander *Ambystoma tigrinum*. *J Physiol London, 371*, 115–145.

Baylor, D. A., Lamb, T. D., & Yau, K.-W. (1979). The membrane current of single rod outer segments. *J Physiol London, 288*, 589–611.

Baylor, D. A., Nunn, B. J., & Schnapf, J. L. (1987). Spectral sensitivity of cones of the monkey *Macaca fascicularis*. *J Physiol London, 390*, 145–160.

Burns, M. E., & Baylor, D. A. (2001). Activation, deactivation, and adaptation in vertebrate photoreceptor cells. *Annu Rev Neurosci, 24*, 779–805.

Burns, M. E., Mendez, A., Chen, J., & Baylor, D. A. (2002). Dynamics of cyclic GMP synthesis in retinal rods. *Neuron, 36*, 81–91.

Do, M. T. H., & Yau, K.-W. (2010). Intrinsically photosensitive retinal ganglion cells. *Physiol Rev, 90*, 1547–1581.

Dratz, E. A., & Hargrave, P. A. (1983). The structure of rhodopsin and the rod outer segment disk membrane. *Trends Biochem Sci, 8*, 128–131.

Fain, G. L., Hardie, R., & Laughlin, S. B. (2010). Phototransduction and the evolution of photoreceptors. *Curr Biol, 20*, R114–R124.

Fu, Y., & Yau, K.-W. (2007). Phototransduction in mouse rods and cones. *Pflügers Arch, 454*, 805–819.

Gross, A. K., & Wensel, T. G. (2011). Biochemical cascade of phototransduction. In P. L. Kaufman, A. Alm, L. L. Levin, S. F. E. Nilsson, J. N. Ver Hoeve, & S. M. Wu (Eds.), *Adler's Physiology of the Eye* (11th ed.). (pp. 394–410). Elsevier.

Heck, M., Schädel, S. A., Maretzki, D., & Hofmann, K. P. (2003). Secondary binding sites of retinoids in opsin: characterization and role in regeneration. *Vis Res, 43*, 3003–3010.

Hofmann, K. P., Scheerer, P., Hildebrand, P. W., et al. (2009). A G protein-coupled receptor at work: the rhodopsin model. *Trends Biochem Sci, 34*, 540–552.

Katz, B., & Minke, B. (2009). Drosophila photoreceptors and signaling mechanisms. *Front Cell Neurosci, 3*, 1–18.

Kawamura, S., & Tachibanaki, S. (2008). Rod and cone photoreceptors: molecular basis of the difference in their physiology. *Comp Biochem Physiol Part A, 150*, 369–377.

Lamb, T. D. (1980). Spontaneous quantal events induced in toad rods by pigment bleaching. *Nature, 287*, 349–351.

Lamb, T. D. (2009). Evolution of vertebrate retinal photoreception. *Phil Trans R Soc B, 364*, 2911–2924.

Lamb, T. D. (2011). Light adaptation in photoreceptors. In P. L. Kaufman, A. Alm, L. L. Levin, S. F. E. Nilsson, J. N. Ver Hoeve, & S. M. Wu (Eds.), *Adler's Physiology of the Eye* (11th ed.). (pp. 429–442) Elsevier.

Lamb, T. D., & Pugh, E. N., Jr. (2004). Dark adaptation and the retinoid cycle of vision. *Prog Ret Eye Res, 23*, 307–380.

MacLeish, P. R., & Makino, C. L. (2011). Photoresponses of rods and cones. In P. L. Kaufman, A. Alm, L. L. Levin, S. F. E. Nilsson, J. N. Ver Hoeve, & S. M. Wu (Eds.), *Adler's Physiology of the Eye* (11th ed.). (pp. 411–428) Elsevier.

Makino, C. L., Riley, C. K., Looney, J., Crouch, R. K., & Okada, T. (2010). Binding of more than one retinoid to visual opsins. *Biophys J, 99*, 2366–2373.

Mata, N. L., Radu, R. A., Clemmons, R. S., & Travis, G. H. (2002). Isomerization and oxidation of Vitamin A in cone-dominant retinas: a novel pathway for visual-pigment regeneration in daylight. *Neuron, 36*, 69–80.

Molday, R. S., & Zhang, K. (2010). Defective lipid transport and biosynthesis in recessive and dominant Stargardt macular degeneration. *Prog Lipid Res, 49*, 476–492.

Nickle, B., & Robinson, P. R. (2007). The opsins of the vertebrate retina: insights from structural, biochemical, and evolutionary studies. *Cell Molec Life Sci, 64*, 2917–2932.

Palczewski, K. (2006). G protein-coupled receptor rhodopsin. *Annu Rev Biochem, 75*, 743–767.

Rebrik, T. I., & Korenbrot, J. I. (2004). In intact mammalian photoreceptors, Ca^{2+}-dependent modulation of cGMP-gated ion channels is detectable in cones but not in rods. *J Gen Physiol, 123*, 63–75.

Schnapf, J. L., Nunn, B. J., Meister, M., & Baylor, D. A. (1990). Visual transduction in cones of the monkey *Macaca fascicularis*. *J Physiol London, 427*, 681–713.

Schnetkamp, P. P. M. (2004). The SLC24 $Na^+/Ca^{2+}-K^+$ exchanger family: vision and beyond. *Pflügers Arch Eur J Physiol, 447*, 683–688.

Smith, S. O. (2010). Structure and activation of the visual pigment rhodopsin. *Annu Rev Biochem, 39*, 309–328.

Stryer, L. (1991). Visual excitation and recovery. *J Biol Chem, 266*, 10711–10714.

Sung, C.-H., & Chuang, J.-Z. (2010). The cell biology of vision. *J Cell Biol, 190*, 953–963.

Travis, G. H., Golczak, M., Moise, A. R., & Palczewski, K. (2007). Diseases caused by defects in the visual cycle: retinoids as potential therapeutic agents. *Annu Rev Pharm Toxicol, 47*, 469–512.

Wang, J.-S., & Kefalov, V. J. (2011). The cone-specific visual cycle. *Prog Ret Eye Res, 30*, 115–128.

Wong, K. Y., & Berson, D. M. (2011). Ganglion-cell photoreceptors and non-image-forming vision. In P. L. Kaufman, A. Alm, L. L. Levin, S. F. E. Nilsson, J. N. Ver Hoeve, & S. M. Wu (Eds.), *Adler's Physiology of the Eye* (11th ed.). (pp. 526–544) Elsevier.

Yau, K.-W., & Hardie, R. C. (2009). Phototransduction motifs and variations. *Cell, 139*, 246–264.

Zhang, Y., Molday, L. L., Molday, R. S., et al. (2009). Knock out of GARPs and the β-subunit of the rod cGMP-gated channel disrupts disk morphogenesis and rod outer segment structural integrity. *J Cell Sci, 122*, 1192–1200.

Zimmerman, A. L., & Baylor, D. A. (1992). Cation interactions within the cyclic GMP-activated channel of retinal rods from the tiger salamander. *J Physiol London, 449*, 759–783.

Chapter 39

Gustatory and Olfactory Sensory Transduction

Stephen D. Roper

Chapter Outline

I. SUMMARY

Taste and olfaction share certain common features. Receptor cells for both senses are epithelial cells and part of a renewing population. Olfactory and taste sensory cells alike lie at the interface between two strikingly different environments – an external environment of volatile odors or water-borne tastants, respectively, versus a relatively constant milieu of interstitial fluid. Moreover, transduction mechanisms in both these chemical senses involves G-protein-coupled receptors, although transduction mechanisms in gustation also include ion channels through which certain taste stimuli pass. Transduction channels and integral membrane receptors appear to be concentrated on the exposed apical tips of both types of chemosensory receptor cells, although the basolateral membranes of taste cells may be additional sites for chemosensory transduction. In some regards, sensory transduction in olfaction is similar to that in photoreception. Photoreceptors and olfactory receptor neurons alike possess cyclic nucleotide-gated ion channels. Nonetheless there are key differences between olfaction and taste. Olfactory receptor neurons are optimized for low concentrations of chemical stimuli; gustatory sensory cells require much higher concentrations of stimuli to become activated. Current topics of intensive research in the peripheral transduction mechanisms for taste and olfaction include, among others, discovering structural details of, and ligand-binding pockets for, the receptor proteins, learning how an olfactory receptor neuron determines which one odorant receptor gene it will express from the several hundred in its genome; identifying transmitters and determining synaptic mechanisms that transmit signals between cells in the taste bud; and understanding how the output signals from the peripheral sensory organs of olfaction and gustation are encoded as patterns of nerve impulses (the sensory code) that are transmitted to the brain and produce odor and taste perceptions.

II. INTRODUCTION

Peripheral sensory cells in olfaction, taste, hearing and vision are modified epithelial cells and share certain properties common to epithelial tissues. These properties

Cell Physiology Sourcebook. DOI: 10.1016/B978-0-12-387738-3.00039-1

include (1) an ongoing renewal of the cell population[1] and (2) cellular polarity, manifest in epithelial cells as two distinctive membrane regions — *apical* versus *basolateral surfaces*, with a barrier of tight junctions to separate the superficial (apical) environment from the tissue spaces surrounding the rest of the cell. Apical and basolateral cell surfaces in epithelial cells and many sensory receptor cells are exposed to two vastly different ionic milieus. This is especially true in *gustatory* and *olfactory* receptor cells. The apical membrane tips in these sensory cells confront external chemical environments in the oral and nasal cavities, respectively, that can change profoundly during stimulation and that can often be quite harsh. In contrast, the cell bodies of gustatory and olfactory sensory cells are bathed in a protected, relatively unchanging medium — interstitial fluid.

Chemical stimuli are initially *transduced* into intracellular electrical signals at the exposed apical tips of taste and olfactory sensory cells. Tight junctions confine most chemical stimuli to the specialized apical membrane and prevent the stimuli from penetrating deeper into the sensory epithelium (although there may be exceptions in gustatory sensory cells, see Section III). This has two implications for gustation and olfaction. First, molecular receptors for signal transduction must reside in the apical membrane of the sensory cells where chemical stimuli contact the cells. Second, because chemosensory stimulation is usually associated with a *receptor* (or *generator*) *current* (flux of ions) across the apical chemosensitive membrane, the ionic environment at the exposed apical region can have a significant impact on transduction. For example, olfactory sensory cells possess a Cl^- conductance that exploits the low external and high intracellular Cl^- concentrations at the apical membrane of these cells to generate an *inward current* during odor stimulation (discussed in detail below). This Cl^- current amplifies the sensory signal.

Olfactory receptor neurons possess axons and transmit their signals directly to the brain and, specifically, the olfactory bulb (Fig. 39.1). Odor signals are decoded and processed in the olfactory bulb and in higher brain centers. In sharp contrast, taste receptor cells transmit their signals via synapses onto primary sensory fibers innervating taste buds. The primary sensory fibers then communicate with the brain. Moreover, cells within a taste bud interact via *chemical* and *electrical synapses* to process gustatory signals via excitatory and inhibitory cell—cell interactions (Roper, 1992; Chaudhari and Roper, 2010). Thus, some degree of cross-talk and information processing occurs in the end organs of taste. The details and significance of these cell—cell interactions are only now emerging.

This chapter describes events taking place in mammalian taste and olfactory sensory cells. Reference to other vertebrate species will occasionally be made, but chemosensory transduction in mammals will be the focus. Distinctly different molecules and mechanisms for taste and olfaction occur in invertebrates and these will not be described.

III. TASTE RECEPTOR CELLS

IIIA. General Comments

Peripheral sensory organs for taste consist of clusters of receptor cells, the taste buds, found throughout the oral cavity. There are 2000—10 000 taste buds in humans. This number varies considerably from individual to individual. Each taste bud consists of 50—100 cells. Taste buds are embedded in the lingual epithelium in specialized protuberances, or papillae (*fungiform*, *foliate* and *circumvallate papillae*). Taste buds are also found on the soft palate, uvula, epiglottis, pharynx, larynx and have even been reported in the upper esophagus. Interestingly, certain cells in the walls of the stomach and intestine express proteins that previously were associated only with taste buds, indicating that chemosensing most likely occurs throughout the length of the digestive tract. However, cells in the stomach and intestines that have taste bud-like proteins are not gustatory sensory cells. They are not organized into collections resembling taste buds; they are not innervated by cranial gustatory nerves; and they are not known to generate taste perceptions.

Taste buds respond to a number of basic taste qualities, including sweet, sour, salty, bitter, *umami* (discussed later) and perhaps others such as fat. Early investigators tested whether particular regions of the tongue were specialized for these different qualities (Hänig, 1901). They found a somewhat greater sensitivity to bitter in the posterior tongue and to sweet at the tip (Fig. 39.2). However, these original findings were overinterpreted in the intervening years, leading to the popular misconception that there is a discrete and well-delineated "taste map" on the tongue. The truth is that all parts of the tongue sense the basic qualities, as shown in Fig. 39.2, and individual taste buds have been shown to respond to several different taste qualities.

Most of the cells in a taste bud are narrow elongate cells, extending nearly the full thickness of the lingual epithelium. The basal processes of taste bud cells reach to the basement membrane below the lingual epithelium and the apical processes extend up into a tiny cavity in the lingual surface at the top of the taste bud, the *taste pore*.

[1] This epithelial property is not shared, however, with inner ear hair cells (auditory and vestibular) or, strictly speaking, with retinal photoreceptors. These sensory cells do not renew and are not replaced if damaged. Admittedly, retinal photoreceptors undergo continuous recycling of their photoreceptive components (opsin-containing disk membranes are shed and renewed), but the somata remain stable.

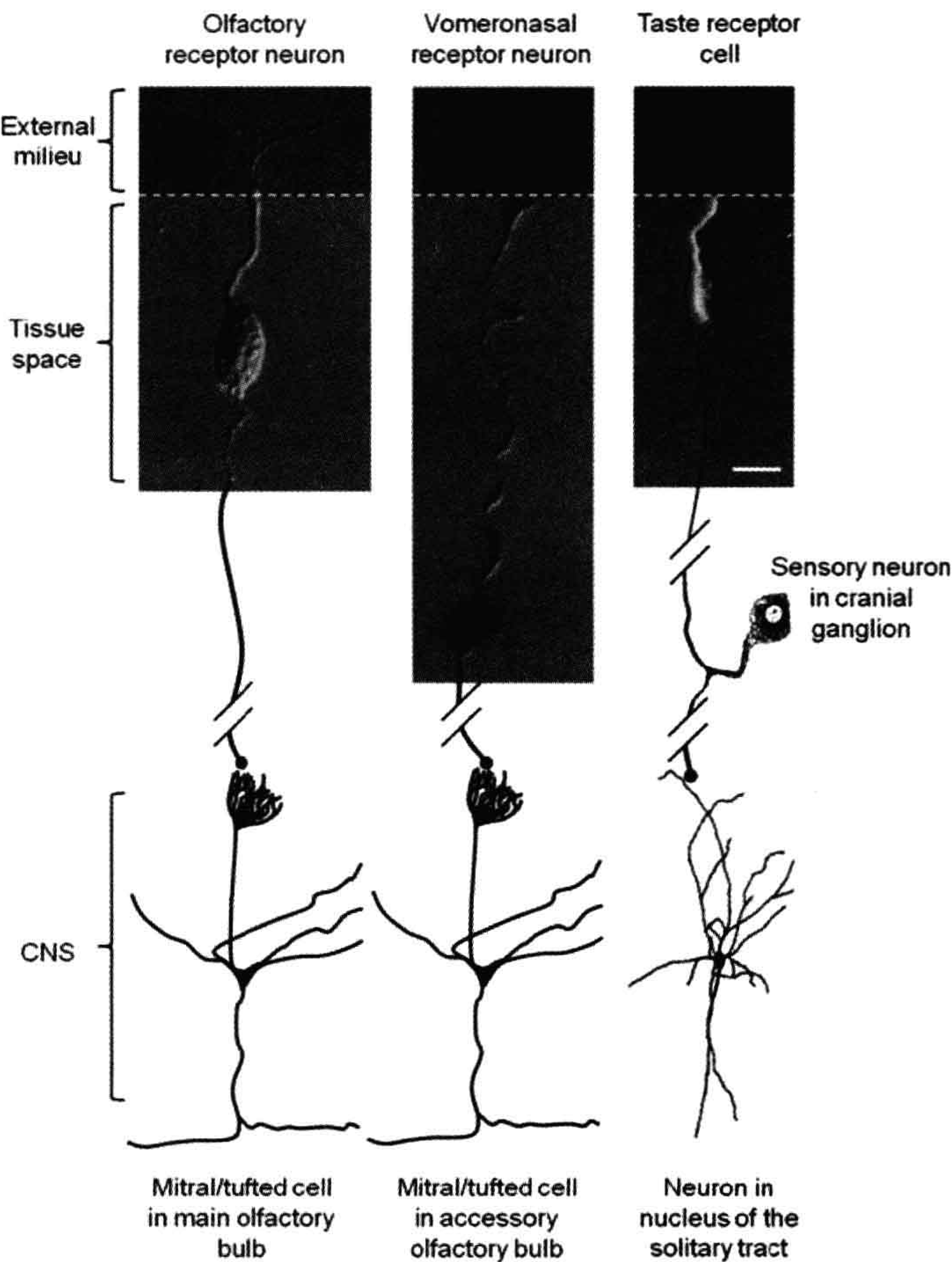


FIGURE 39.1 Schematic drawing comparing sensory cells experimentally isolated from olfactory epithelium, vomeronasal organs and taste buds. The apical tips of these cells are exposed to the external environment (dark shaded) where the initial events in chemosensory transduction occur. The basolateral membrane of the cells lies below the apical junctional complex (white dashed line) and is surrounded by interstitial fluid. Olfactory receptor neurons and vomeronasal sensory cells have axons (drawn in here) that project into the central nervous system (CNS) where they form synapses with mitral/tufted cells in the olfactory bulb. In contrast gustatory receptor cells form synapses in the taste bud with primary sensory fibers from cranial sensory ganglion neurons. Calibrations = 10 μm. *(Olfactory receptor neuron modified from Kleene and Gesteland, 1981; vomeronasal receptor neuron modified from Ghiaroni et al., 2003; taste receptor neuron modified from Bigiani et al., 2002.)*

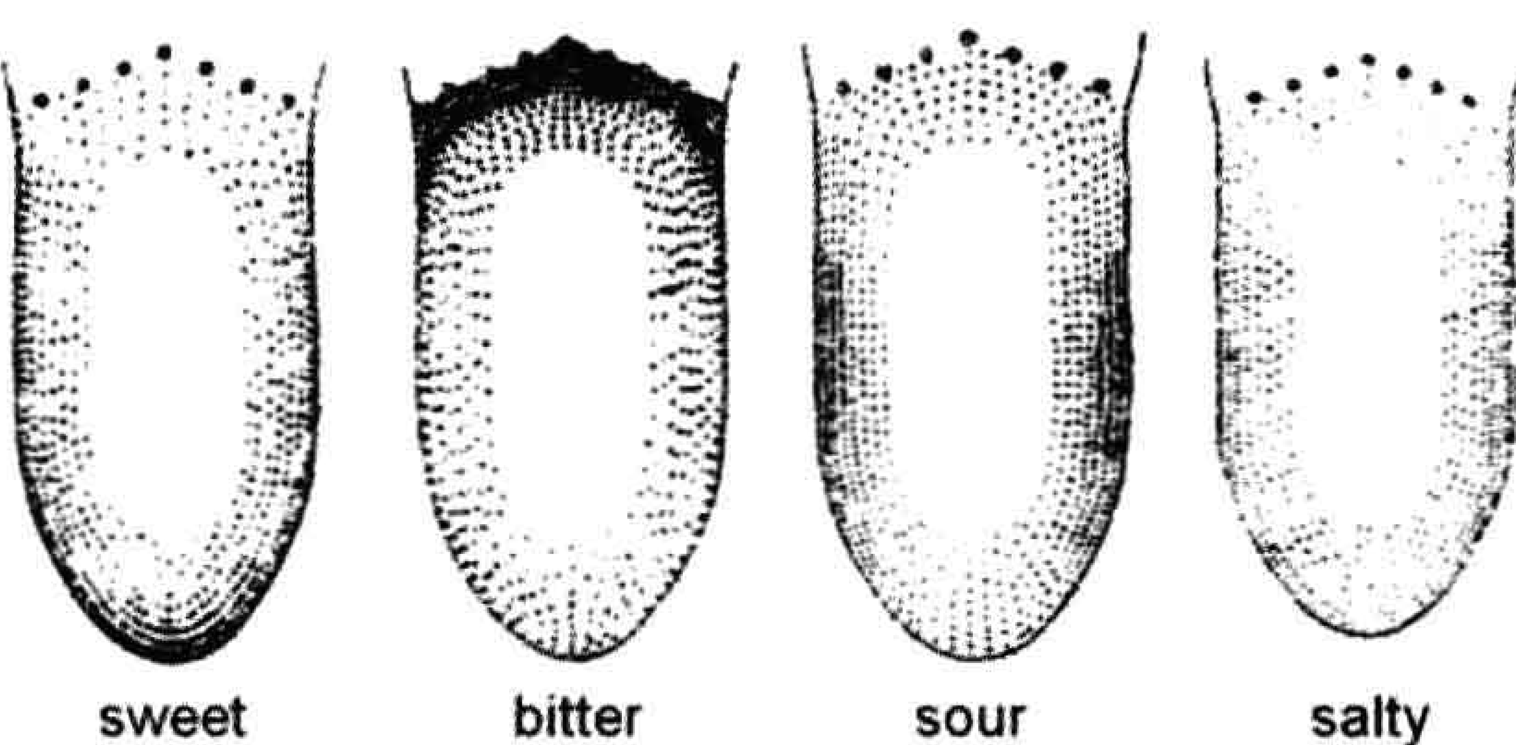


FIGURE 39.2 Regional distribution of sweet, bitter, sour and salty taste on the human tongue, as originally determined by D.P. Hänig (1901). The sensitivity for a particular taste quality is represented by the density of stippling. There is a slight tendency for the anterior tip of the tongue to be more sensitive to sweet, the lateral regions to be more sensitive to sour and the posterior to bitter. However, there is complete overlap for all these taste qualities. Also, see discussion in Lindemann, (1999).

The elongate, columnar morphology of gustatory sensory cells sets taste buds apart from the surrounding laminated ("stratified") epithelium. That is, taste buds form tiny islands of simple columnar epithelium within the larger sheet of stratified squamous lingual epithelium. Such an arrangement positions taste cells directly across the electric field generated by lingual transepithelial ion transport currents. This may have implications for taste transduction.

There are three or more different types of cells in mammalian taste buds. Based on cytological features, histologists categorized taste cells as dark cells and light cells. Later, electron microscopists delineated *types I, II* and *III cells* based on ultrastructural features, including that only one of the cell types (type III) possesses synaptic connections. These morphological classifications have

recently been tremendously clarified by combining molecular profiling with functional analyses on isolated taste cells. It is now recognized that type I cells are *glial-like*; type II cells express *G-protein-coupled receptors* for and respond to sweet, bitter and umami tastes; and type III cells express synaptic proteins associated with *vesicular release*, possess synaptic specializations and respond to sour (acid) taste (reviewed in Chaudhari and Roper, 2010). The taste cells responsible for salt (NaCl) taste have not yet been identified unambiguously, though there are suggestions that type I and III cells participate. In recognition of the functional roles of the cells comprising taste buds, type II cells have also been termed receptor cells and type III cells named presynaptic cells.

Taste cells, like the adjacent non-taste stratified epithelium, represent a *renewing population*. Taste bud cells have an estimated average life span of approximately 10 days in the mammal, longer than the surrounding non-sensory epithelium (3–4 days). There are early indications that the type I, II (receptor) and III (presynaptic) taste cells may have different longevities, but the data are only preliminary. Taste cells may be born from stem cells at the base of the taste bud. They may also originate from adjacent epithelial cells immediately surrounding taste buds. The precise origin of taste bud cells and whether the different cell types have a common lineage during development and in the adult are questions currently under investigation.

Recent investigations indicate that there are important cell–cell synaptic interactions in the taste bud, including feed forward and feedback signaling (reviewed in Roper, 2007; Herness and Zhao, 2009; Chaudhari and Roper, 2010). These interactions appear to shape the signals generated within the taste bud during taste excitation and may be critical in establishing a taste code that is transmitted to the brain for further processing. A discussion of signal processing in taste buds and how gustatory information is decoded in the central nervous system are topics beyond the scope of this chapter.

IIB. Nature of Taste Stimuli

Many, if not most water-soluble chemicals probably elicit a taste. Chemical stimuli have been grouped into five primary taste qualities: sweet, sour, salty, bitter and umami. There is ongoing debate whether there are additional taste qualities such as fatty and astringent, though these categories are blurred by somatosensory contributions (tactile, texture, etc). The existence of primary taste qualities argues there are distinct transduction mechanisms and signaling pathways for each of the basic tastes and this notion has guided taste research.

Chemicals that elicit taste usually do so only at high concentrations (millimolar to molar). However, certain bitter-tasting substances (such as quinine, caffeine, strychnine) and artificial sweeteners are relatively potent stimuli and elicit taste responses at μM concentrations. Nonetheless, it is clear that taste cells are relatively insensitive when compared with the exquisite responsiveness of photoreceptors (i.e. single photons) or olfactory and pheromone chemoreceptors (i.e. picomolar stimulus concentrations, possibly even single molecules). Primary functions of taste organs include regulating the intake of important nutrients and protecting against the ingestion of spoiled food and other harmful substances. Therefore, the generally low sensitivity of gustatory sensory cells to nutrients (carbohydrates, *sweet*; amino acids/protein, *umami*; Na^+, *salty*) and high sensitivity to potentially detrimental compounds (toxins and rancid food, bitter) may represent an optimization for tastant concentrations that are physiologically relevant. That is, low taste sensitivity prevents receptors from becoming saturated and unresponsive to tastants that are required in abundance (nutrients); high bitter sensitivity assures that dangerous compounds will be detected and avoided even at low concentrations. (Many bitter-tasting chemicals are toxic and, conversely, many toxic chemicals elicit bitter taste.) In this light, the biological significance of sour taste (acids) is somewhat enigmatic. Sourness is an aversive taste to non-human animals and human infants but can be an acquired taste in adults. Further, rancid or spoiled food is often acidic.

Taste stimuli are dissolved in saliva to bathe the chemosensitive (apical) surface of gustatory sensory cells. Most chemical stimuli are prevented from gaining access to the basolateral regions of the taste bud by the *tight junctions* of the junctional complex at the taste pore. Notable exceptions are organic acids, such as acetic acid (vinegar) and citric acid, which elicit sour taste, and which rapidly breach the epithelial barrier. In their fully protonated form (i.e. neutral molecules), these acids penetrate into and throughout the epithelium, including into the cellular interior. Inside cells, the protonated molecules dissociate to release H^+. This penetration of organic ("weak") acids into the cytosol is believed to be an important contribution to sour taste stimulation (see below). Also, tight junctions between taste bud cells are somewhat leaky to certain ions, such as Na^+, K^+ and Cl^- (Ye et al., 1993). These ions pass from the lingual surface into the intercellular spaces within the taste bud. It is possible that chemotransduction mechanisms for NaCl, KCl and possibly other stimuli exist on the basolateral membranes of taste receptor cells as well as on their exposed apical tips. Basolateral transduction mechanisms may explain intravascular taste, where blood-borne chemicals elicit gustatory sensations (Bradley, 1973). The bitter taste of some drugs injected intravenously and the sweet taste of intravenously-injected saccharin, once used

to monitor blood circulation, are examples of intravascular taste.

IIIC. Initiation of Taste Receptor Potentials

Taste cells are excitable and generate action potentials when depolarized sufficiently. This was first demonstrated with intracellular recordings from the large taste bud cells found in the amphibian, *Necturus maculosus* (Roper, 1983), but has subsequently been verified with patch-clamp recordings from mammalian taste cells (Fig. 39.3A, B). Specifically, taste bud cells (types II and III) possess inward, voltage-dependent, tetrodotoxin-sensitive Na^+ currents and outward, TEA-sensitive K^+ currents (Fig. 39.3C, D), typical of many neurons. Type III cells, but not type II cells, also have inward, voltage-dependent Ca^{2+} currents.

Gustatory stimuli generate *receptor potentials* and *transient increases of [Ca^{2+}]* inside taste bud cells (Fig. 39.3E–H). The conversion of a gustatory chemical signal into an intracellular receptor potential or Ca^{2+} transient is termed *taste transduction*. The endpoint of taste transduction is the release of neurotransmitter(s) from the sensory cell.

Unlike signal transduction in most other sensory cells, there is no single unifying mechanism underlying taste transduction. The necessity of taste organs to sense a wide

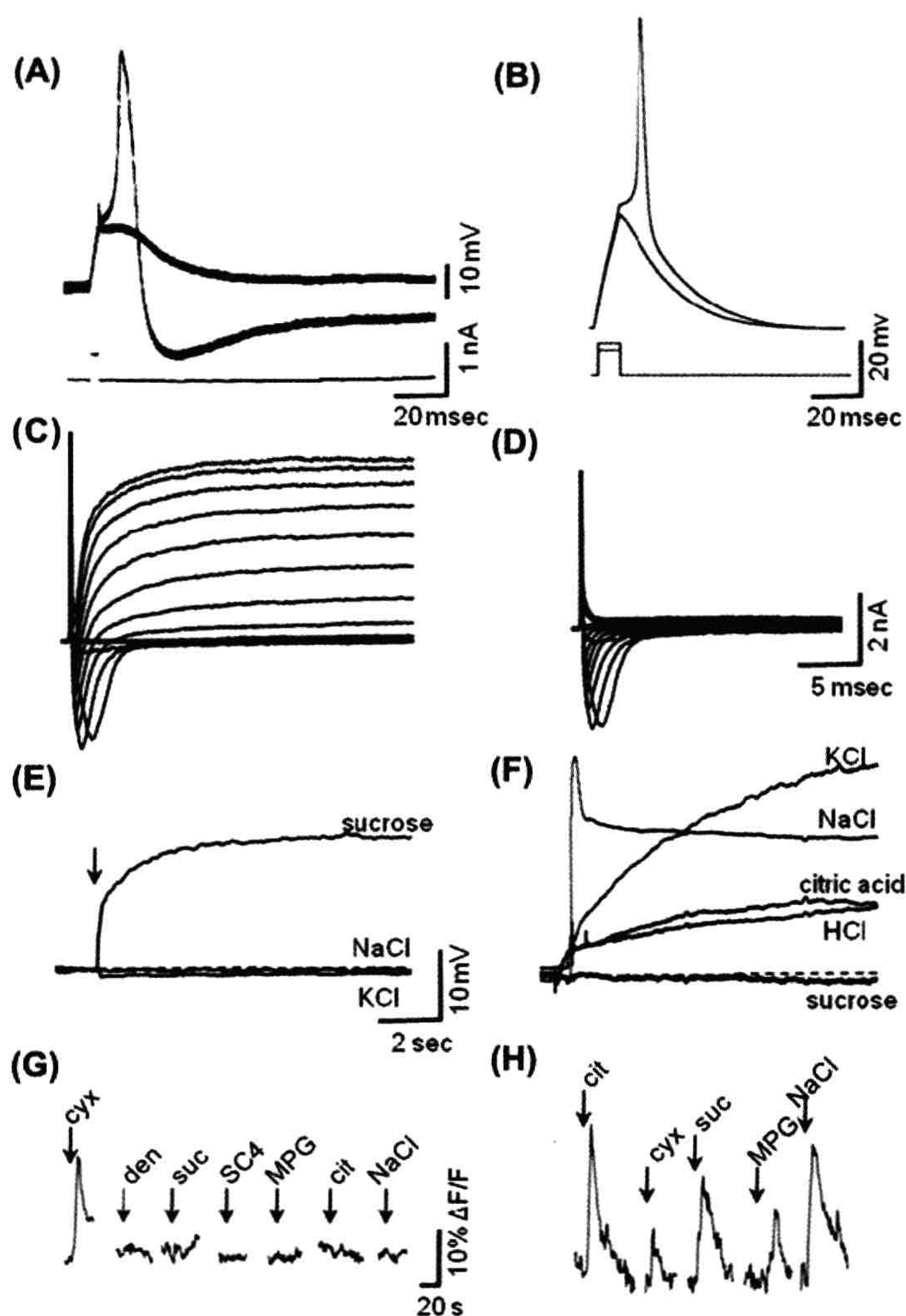


FIGURE 39.3 Taste receptor cells are excitable and respond to taste stimulation with depolarizing generator potentials and intracellular Ca^{2+} increases. (A) Intracellular recording from amphibian taste receptor cell showing responses to threshold current pulses passed through the recording electrode. (B) Patch electrode recording from mouse taste receptor cell, current clamp mode, showing responses to depolarizing current pulses at threshold. (C) Patch-clamp recording from mouse taste receptor cell showing inward and outward currents produced by current steps. (D) As in (C), but in presence of TEA to block outward K current. (E) Patch electrode recording of rat taste receptor cell, current clamp mode, showing a depolarizing response to sucrose applied to the apical, chemosensitive tip, but no responses to similarly applied solutions of NaCl or KCl. (F) As in (E), but showing another taste cell that was broadly sensitive to KCl, NaCl, citric acid and HCl, but not sucrose. (G) Mouse type II taste cell showing Ca^{2+} responses evoked by a series of different chemical stimuli applied to the apical chemosensitive tip. This cell responded only to one stimulus, a bitter taste (cycloheximide, cyx). (H) A mouse type III taste cell showing Ca^{2+} responses to several different stimuli, including sour (citric acid), bitter (cycloheximide, cyx), sweet (sucrose, suc), umami (monopotassium glutamate, MPG) and salty (NaCl). (G, H) were taken from calcium imaging experiments showing changes in fluorescence (ΔF) of an intracellular Ca^{2+}-sensitive dye. *((A) Modified from Roper, 1983, (B, C, D) modified from Bigiani et al., 2002, (E, F) modified from Gilbertson et al., 2001, (G, H) modified from Tomchik et al., 2007.)*

range of chemical substances, from simple ions to complex proteins, has led to the evolution of *multiple taste transduction mechanisms* (reviewed by Smith and Margolskee, 2001; Sugita, 2006; Roper, 2007; Chaudhari and Roper, 2010). Different taste bud cells possess distinct transduction mechanisms and respond to different taste stimuli. For instance, receptor (type II) taste cells respond specifically to sweet, bitter or umami taste compounds. Presynaptic (type III) taste cells respond to sour taste. Moreover, due to excitatory interactions between receptor and presynaptic cells, presynaptic cells also respond (indirectly) to sweet, bitter and umami (Tomchik et al., 2007). Presynaptic cells also are excited by salty stimuli, though whether this is due to direct stimulation or to indirect activation via intercellular communication from other taste bud cells remains unsolved.

Taste transduction can be divided into two primary mechanisms:

1. *Ion permeation through specific channels*. Certain taste stimuli, most notably Na^+, enter taste cells through ion channels in the membrane, thereby generating transmembrane *receptor currents* and receptor potentials. Protons may also pass through ion channels and elicit sour taste responses.
2. *Receptor-ligand binding*. Interactions occur between chemical stimuli (ligands) and specific membrane bound receptors (in particular, G-protein-coupled receptors, GPCRs) that ultimately lead to receptor currents or the release of intracellular Ca^{2+}, or both.

Parenthetically, some researchers believe that amphipathic stimuli, such as saccharin and quinine, may bypass ion channels and receptors and penetrate through the lipid plasma membrane to act directly on intracellular signaling cascades. Whether this occurs at physiologically relevant concentrations of the taste compounds, however, remains to be established.

IIIC1. Ion Permeation Through Specific Channels

ENaC Channels and Salt Taste

Sodium salts ("salty taste") are believed to be transduced in a subset of taste cells by the direct permeation of Na^+ through passive Na^+-selective channels (as opposed to TTX-sensitive, voltage-dependent Na^+ channels that underlie action potentials). Most of salt taste is transduced by a mechanism that is sensitive to the diuretic, amiloride. The most likely candidate Na taste transducer to date is the *amiloride-sensitive epithelial Na^+ channel* (ENaC) found in renal tubules and elsewhere (Heck et al., 1984). Indeed, mRNA isolated from lingual epithelium and immunostaining of taste buds shows that all three ENaC subunits (α, β and γ) are expressed in taste cells (Kretz et al., 1999; Lin et al., 1999). Where it has been measured (in frog taste cells), taste Na^+ channels have small unitary conductance (1–2 pS) and are blocked by low concentrations of amiloride (K_i = 0.2–1 μM), consistent with ENaC channels. Recent findings from mouse taste buds show that certain taste cells manifest ENaC-like ion currents (Vandenbeuch et al., 2008) and taste cells expressing ENaC respond to NaCl stimulation (Chandrashekar et al., 2010).

ENaC channels are open at rest and allow an ongoing influx of Na^+, driven by this cation's electrochemical gradient. The concentration of Na^+ in human saliva varies from about 3 to 63 mM, depending on the rate of salivary secretion. This results in an equilibrium potential for Na^+ (E_{Na}) of about −30 to +50 mV (assuming $[Na^+]_i$ is 10 mM) across the apical membrane of salt-sensitive taste cells. Thus, with a resting potential estimated to be −60 to −80 mV, there is likely to be a small steady-state influx of salivary Na^+. During stimulation with NaCl when $[Na^+]$ in the oral cavity can reach concentrations up to a fraction of a mole (a typical soup, for instance, contains ≈0.25 M NaCl), the electrochemical gradient driving Na^+ into the cells increases and Na^+ influx depolarizes the cell. This current exits across the base of the cell forming a complete current loop via an extracellular (paracellular) pathway that includes the junctional complex near the taste pore. Consequently, any factors that affect the basolateral membrane conductance or the paracellular resistance, especially at the tight junctions near the taste pore, will also affect the magnitude of the receptor currents.

As mentioned previously, Na^+ on the tongue surface may also partly penetrate the apical junctional complex of taste buds and raise $[Na^+]_o$ in the interstitial spaces surrounding taste cells. If Na^+ transduction channels are expressed on the basolateral as well as apical membrane of salt-sensitive taste cells, penetration of Na^+ into the interior of the taste bud would provide another avenue for Na^+ taste stimulation. Immunostaining for ENaC channels has suggested their presence on the basolateral membrane (Lindemann et al., 1998), but Na^+ responses in mouse fungiform taste cells were unaffected when their basolateral surface was exposed to the ENaC antagonist amiloride (Yoshida et al., 2009a). This suggests that if basolateral Na^+ transduction occurs, it is unlikely to be via ENaC channels.

Although the evidence is good in experimental animals, particularly rodents, a role for ENaC channels in human salt taste has been questioned. Amiloride appears to affect only the sourness, not saltiness, of NaCl solutions in psychophysical studies (Ossebaard and Smith, 1996). Furthermore, even in non-human species, not all salt taste can be explained by ENaC channels. A component of salt taste in experimental animals is unaffected by amiloride, especially in the posterior tongue. Mechanisms other

than amiloride-sensitive (presumably ENaC) channels must exist.

Proton (H^+) Channels and Sour Taste

How acids (sour taste) are transduced may differ from species to species and our understanding of sour transduction remains incomplete. In the amphibian, *Necturus*, protons block apical K^+ channels and depolarize the cell. Additionally, protons themselves permeate the apical membrane, providing a depolarizing inward receptor current. Interestingly, protons permeate hamster taste cells via amiloride-sensitive Na^+ channels, believed to be ENaC (Fig. 39.4A). Protons bind to the ion selectivity site in the ENaC channel more strongly than do Na^+ ions. Consequently, H^+ conductance of ENaC is less than that of Na^+. This also means that protons interfere with the flux of Na^+ through the channel. In contrast, protons permeate mouse taste cells via proton-gated channels that are unaffected by amiloride and thus are unlikely to be related to ENaC (Fig. 39.4B). In humans, psychophysical studies implicate a role for amiloride-sensitive Na^+ channels in sour taste (Ossebaard and Smith, 1996). (The interference between Na^+ and H^+ permeation of amiloride-sensitive Na^+ channels may help explain the culinary wisdom that acidifying food, for example by adding vinegar or lemon juice, reduces its salty taste.) In short, our understanding of roles for ion channels and proton influx in sour taste is fragmentary.

However, a major component of sour taste may be unrelated to the influx of protons and generation of a depolarizing H^+ current. Namely, organic acids such as acetic acid (vinegar), citric acid (fruit) and tartaric acid (wine) are potent sour stimuli. In fact, at equal pH values, organic ("weak") acids are more sour than mineral ("strong") acids such as HCl. This cannot easily be explained by H^+ influx through proton channels. At equal pH, the H^+ concentration of an organic and a mineral acid

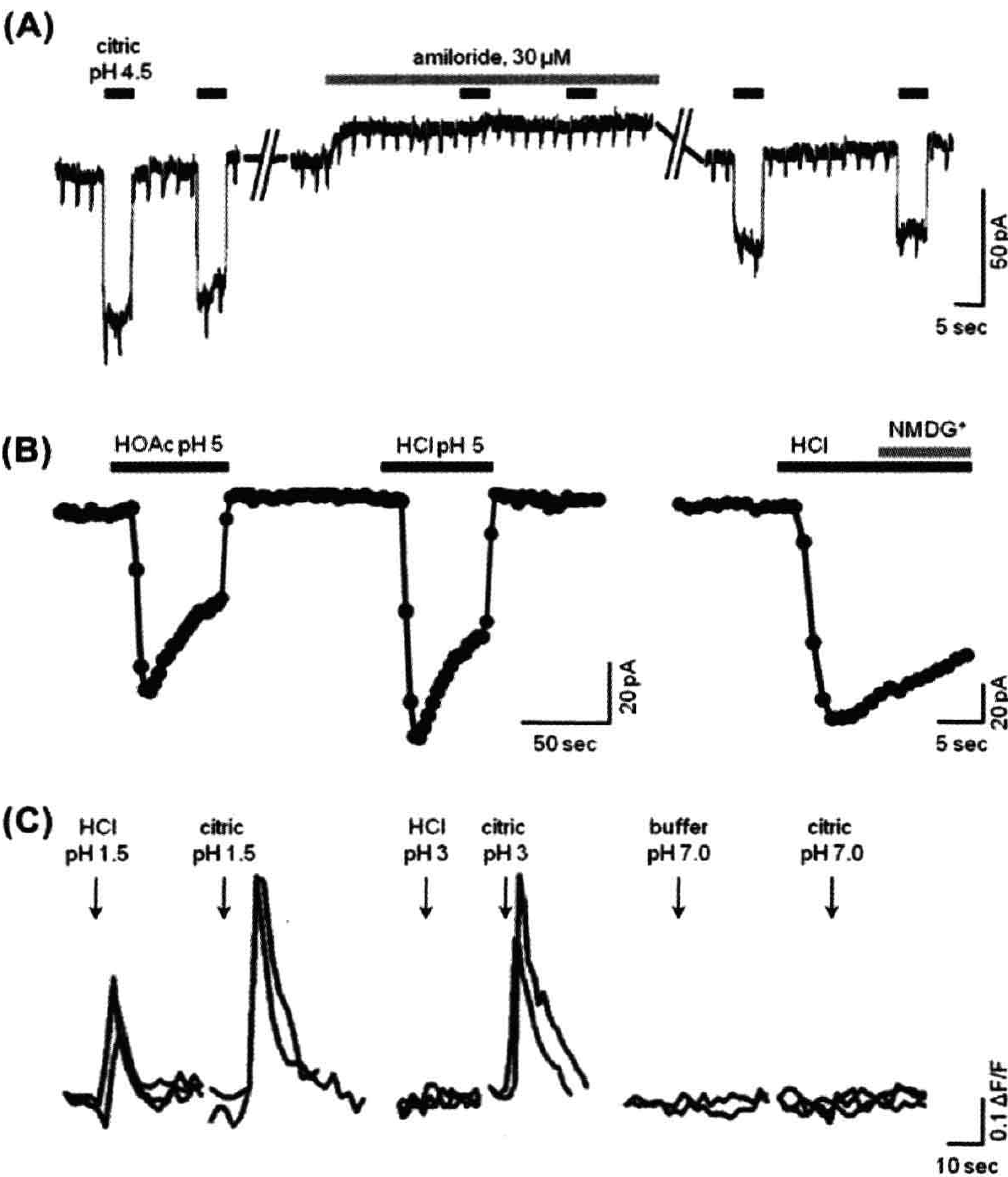


FIGURE 39.4 Sour taste transduction. (A) In hamsters, sour taste stimulation triggers an inward proton flux through amiloride-sensitive (presumably ENaC) channels. These traces are patch-clamp recordings of an isolated fungiform taste cell showing inward current responses evoked by 2.5 mM citric acid (pH 4.5) and their block by 30 μM amiloride (modified from Gilbertson et al., 1993). (B) In sour-sensitive taste cells from mice, acid stimulation also evokes inward proton currents. Unlike those in hamsters (A), these currents are not affected by amiloride (data not shown). Traces show patch-clamp recordings from an isolated mouse fungiform taste cell showing inward current responses evoked by 2 mM acetic acid (HOAc, pH 5) and 10 mM HCl (pH 5). Replacing Na^+ with $NMDG^+$ had no effect on the HCl-evoked response (final trace), consistent with the current being carried by protons, not Na^+ *(modified from Chang et al., 2010)*. (C) Sour stimuli also elicit Ca^{2+} transients in taste cells, recorded with functional imaging. The traces show Ca^{2+} influx in sour-sensitive circumvallate taste cells from a mouse. The responses were triggered by brief applications of acid stimuli applied focally to the taste pore in a lingual slice preparation. Citric acid was much more effective than HCl at equivalent pH values, *(modified from Richter et al., 2003)*.

stimulus, and hence the inward driving force for protons across the taste cell membrane, would be identical. Organic and mineral acids at the same pH would be expected to be equally sour, which is not the case. Psychophysical measurements of sourness, taste nerve responses to acid stimuli and responses of sour-sensitive taste cells consistently indicate that organic acids are more effective than mineral acids at a given pH (e.g. see Fig. 39.4C) (Richter et al., 2003; Huang et al., 2008). The explanation is that the protonated organic acid molecules readily pass through cell membranes and penetrate into the taste cell interior where they dissociate into proton(s) and anion(s) (see Roper, 2007). Permeation of organic acid molecules into the cell results in cytosolic acidification, which is believed to contribute markedly to sour taste transduction. That is, intracellular protons, not extracellular H^+, appear to be a proximate stimulus for sour taste (Lyall et al., 2001). Accordingly, a cytosolic protein or the intracellular face of a membrane transducer likely binds protons and initiates the events leading to a signaling cascade for sour taste. One such candidate that has been shown to transduce acid-evoked nociception and that involves cytosolic acidification is the cation channel TRPA1 (Wang et al., 2011). However, to date, there is no strong evidence for the expression of TRPA1 in taste buds or TRPA1-mediated sour taste transduction. Other candidate intracellular targets that have been hypothesized include 2-pore domain K^+ channels that are blocked by cytosolic acidification (Richter et al., 2004).

In all likelihood, sour taste transduction may eventually be explained by a combination of events – proton-gated channels triggered by extracellular H^+ and cytosolic acidification leading to modification of intracellular proteins. The end result of sour taste transduction is depolarization of the acid-sensitive (presynaptic or type III) taste cells, influx of Ca^{2+} through voltage-gated Ca channels and release of transmitter(s), including serotonin (Huang et al., 2008).

IIIC2. G-Protein-Coupled Receptors for Taste

G-protein-coupled receptors (GPCRs) have been identified for three of the primary tastes – sweet, bitter and umami. These are the *T1Rs* (sweet, umami) and *T2Rs* (bitter) and their corresponding genes, *Tas1Rs* and *Tas2Rs* (Chandrashekar et al., 2000, 2006; Nelson et al., 2001, 2002; Max et al., 2001; Sainz et al., 2001). In humans and many other mammals, there are three members of the small family of T1R GPCRs – T1R*1*, T1R*2* and T1R*3*. These GPCRs form heterodimers to create either a sweet (T1R2+T1R3) or an umami (T1R1+T1R3) receptor. (Interestingly, in frogs, there are no T1Rs, implying that these amphibia do not sense sweet or umami tastes, at least not transduced by T1Rs). The dimeric sweet receptor (T1R2+T1R3) responds to a variety of different sugars (sucrose, fructose, glucose, etc.) as well as to artificial sweeteners (e.g. saccharin, aspartame, acesulfame potassium, cyclamate) and sweet-tasting proteins (monellin, thaumatin, brazzein)[2]. The binding pockets on the dimeric T1R2+T1R3 differ for the different sweet ligands. For example, glucose, sucrose and aspartame bind to the extensive amino termini ("venus fly trap" domain) of T1R2 and T1R3; other artificial sweeteners, such as cyclamate, to a pocket in the transmembrane region of T1R3; and sweet proteins to a cysteine-rich domain that links the large extracellular amino terminus of T1R3 to its seven transmembrane domains. Nonetheless, ligand interactions with T1R2+T1R3, whether at one or more of these different binding sites, activate a common downstream effector pathway, described below.

Taste receptors responding to amino acids, particularly sodium glutamate (monosodium glutamate, MSG) and that elicit "umami" are constructed from the combination of T1R1+T1R3. Thus, T1R3 is common to sweet and umami taste receptors. Glutamate most likely binds to the large amino terminal, *venus fly trap domain*. Other binding sites have not been extensively explored to date. Taste receptors other than T1R1+T1R3 are believed to exist for umami, based on findings that mutant mice lacking T1R3 still detect, albeit less robustly, solutions of umami compounds. Additional candidate umami receptors include variants of G-protein-coupled synaptic glutamate receptors, mGluR4 and mGluR1.

Bitter taste is transduced by the T2R class of receptors. In contrast to the small number of T1Rs, T2R genes (Tas2R) comprise a larger family. The number of T2R genes varies from species to species. In humans, there are 25 functional T2R receptors; in frogs, 47; in zebrafish, 4. It is unclear whether T2Rs exist as monomers or oligomers. T2Rs lack the extensive N termini that characterize T1Rs. Bitter compounds are believed to bind in a single transmembrane pocket of a given T2R, with certain T2Rs being more selective and others more broadly responsive to multiple, related ligands.

Taste GPCRs (i.e. T1Rs and T2Rs) are expressed by the type II (receptor) taste cells. In general, a given receptor (type II) cell expresses only one type of taste receptor – either sweet, umami, or bitter receptors. Consistent with this finding, in physiological studies, receptor cells have been shown mainly to respond (i.e. are "tuned") to single taste qualities, sweet, bitter or umami (Tomchik et al., 2007; Yoshida et al., 2009b). Receptor taste cells that respond to bitter compounds express small, overlapping subsets of four to 11 T2Rs of the full repertoire of 25 human T2Rs (Behrens et al., 2007). Thus, it is understandable that

[2] The human T1R2+T1R3 dimer responds to monellin and thaumatin, but the equivalent rodent sweet receptor dimer does not. This is explained by sequence differences between human and rodent sweet taste receptors.

bitter-sensitive taste receptor cells, each expressing a subset of T2Rs, respond to multiple bitter compounds.

IIIC3. Downstream Effectors

Activating either T1Rs or T2Rs on receptor cells by sweet, umami or bitter compounds initiates a common signaling cascade, consisting of liberating $G_{\beta\gamma}$ proteins (specifically $G_{\beta3}/G_{\gamma13}$) bound to the taste GPCR, triggering a taste-specific phospholipase C (PLCβ2), generating IP_3 and consequently stimulating IP_3 receptors on intracellular Ca^{2+} stores (specifically, IP_3R3), thereby releasing Ca^{2+} into the cytosol (reviewed by Chaudhari and Roper, 2010). Thus, the net effect of taste stimulation is to mobilize intracellular Ca^{2+} (see Fig. 39.3G, H). The increased $[Ca^{2+}]_i$ has a dual effect. Intracellular Ca^{2+} opens taste-specific cation channels in the basolateral membrane of receptor cells, TRPM5, allowing Na^+ influx and thereby producing a depolarizing current. Ca^{2+} also acts on pannexin 1 gap junction hemichannels embedded in the plasma membrane. Pannexin 1 hemichannels are triggered open by the combined action of TRPM5-mediated depolarization and IP3-mediated Ca^{2+} increases. Opening pannexin 1 channels allows the efflux of taste transmitter, ATP, from receptor cells (Huang et al., 2007; Romanov et al., 2007), the end result of taste stimulation for these cells (Fig. 39.5A).

In addition to $G_{\beta\gamma}$ proteins released during taste GPCR activation, a taste-specific G_α protein, G_α gustducin (McLaughlin et al., 1992) is liberated from the receptor. Unlike the $G_{\beta\gamma}$ pathway, G_α signaling in taste transduction is not as well characterized. Gene-knockout mice lacking G_α gustducin show deficits in their ability to sense bitter, sweet and umami tastes, but whether this taste-specific G_α protein is directly intercalated in the taste transduction pathway is disputed. Evidence suggests that G_α gustducin plays an indirect role. G_α gustducin is a type of G_i protein, related to transducin in photoreceptors. By stimulating a phosphodiesterase present in taste cells, G_α gustducin acts to lower cytosolic cAMP. Because cAMP inhibits PLCβ2/ IP_3/Ca^{2+} signaling, lowering cytosolic cAMP enhances the receptor cell's sensitivity to taste compounds (Clapp et al., 2008). In mutant mice lacking G_α gustducin, cAMP accumulates in receptor cells and depresses sensitivity to sweet, umami and bitter taste stimuli.

Figure 39.5 summarizes the several transduction pathways for taste stimulation.

IIID. Termination of Taste Signals

Termination of chemostimulation in taste cells is probably due to two factors: diffusion of the stimulus away from the apical chemosensitive tips and receptor cell adaptation.

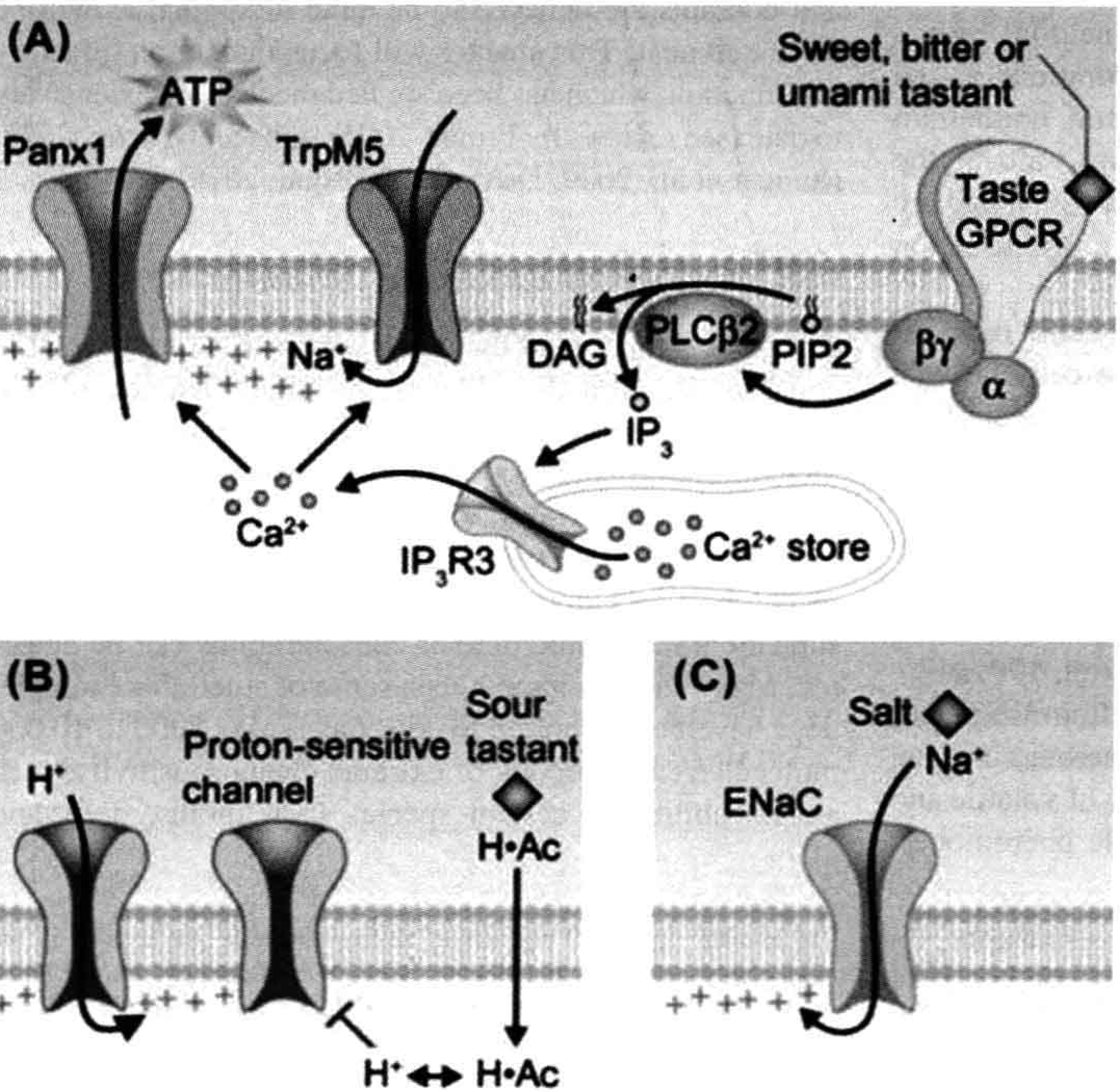


FIGURE 39.5 Taste transduction mechanisms for sweet, bitter, umami, sour and salty. (A) Sweet, bitter and umami compounds bind to G-protein-coupled taste receptors (shown at far right) on taste receptor (type II) cells and initiate a downstream cascade of $G_{\beta\gamma}$ proteins, phospholipase C and intracellular Ca^{2+} release. (G-protein-coupled receptors for sweet and umami exist as heterodimers, not depicted in this cartoon.) Intracellular Ca^{2+} activates a cation channel, TrpM5, and a plasma membrane gap junction hemichannel, pannexin 1 (Panx1). When Panx1 opens, the taste neurotransmitter ATP is released into the interstitial spaces (Huang et al., 2007; Romanov et al., 2007). (B) Sour taste may involve proton influx through channels (left) and penetration of the sour tastant (shown here, acetic acid, H · Ac) across the plasma membrane to acidify the cytosol. Cytosolic acidification may block proton-sensitive K^+ channels, as yet unidentified. (C) Salty taste can be evoked by Na^+ influx through ENaC channels. This mechanism has been demonstrated in rodents but its generalization to humans has been questioned and remains to be established, *(modified from Chaudhari and Roper, 2010).*

Little is known about adaptation in gustatory sensory cells. It is plausible that the Ca^{2+}-dependent Cl^- conductance that exists in taste bud cells contributes to sensory adaptation in taste (Taylor and Roper, 1994; Herness and Sun, 1999). Ca^{2+} mobilization in receptor cells during taste transduction would be expected to activate a basolateral Ca^{2+}-dependent Cl^--conductance, triggering an influx of Cl^- from the interstitial fluid surrounding taste cells and generating an outward, repolarizing current.

IV. OLFACTORY RECEPTOR CELLS

IVA. General Comments

Receptor cells for odorants are distributed in specialized patches of olfactory sensory epithelium embedded within the nasal respiratory epithelium. These patches comprise about 1 cm^2 of surface in each nostril in the human, or approximately 0.5−1% of the total nasal epithelium. The area of olfactory epithelium decreases with age, perhaps contributing to the decline of the sense of smell in the elderly.

Olfactory receptor cells are specialized neurons and are often termed olfactory receptor neurons (ORNs). Olfactory receptor neurons are elongate cells that extend from the base of the epithelium to the surface. Receptor neurons stand side by side with columnar supporting cells in the olfactory epithelium. The apical tips of ORNs consist of a tiny knob from which extend six to 12 long cilia (see Fig. 39.1). At their base, olfactory receptor neurons extend an axon that travels upward through perforations in the region of the cranium that overlies the olfactory epithelium (the cribriform plate) to reach the olfactory bulb of the CNS. Consequently, olfactory receptor neurons bypass any synaptic intervention in the periphery and transmit action potentials directly into the brain[3].

Stem cells (horizontal and globose basal cells) reside at the base of the olfactory epithelium. These cells provide a reservoir of progenitors for the continuous renewal of the olfactory epithelium. Basal stem cells divide and differentiate into olfactory receptor neurons and supporting cells. The lifespan of olfactory receptor neurons was originally thought to be approximately 30 days (Graziadei and Monti Graziadei, 1978), but later findings indicate that ORNs may live for many months (Mackay-Sim and Kittel, 1991a,b).

Closely related to nasal olfactory epithelium is another peripheral chemosensory structure, the vomeronasal organ (VNO). The VNO detects a special category of volatile and non-volatile chemical stimuli which include pheromones. This sensory end organ is an invagination of the nasal epithelium in mammals[4] or, in reptiles such as snakes, an opening in the oral cavity. Pheromones are chemical signals produced by one member of a species to communicate with other members of that same species (conspecific). Pheromones play a key role in endocrine responses and in shaping social and sexual interactions (e.g. territoriality, mating) among conspecifics, at least in non-human animals, and perhaps even in humans (Gelstein et al., 2011). Pheromone stimuli for VNO sensory neurons include airborne molecules (such as dihydro-exo-brevicomin, a volatile constituent of male mouse urine) and non-volatile molecules (such as aphrodisin, a component of vaginal secretions in hamsters). Animals also use their VNO to detect chemical stimuli such as predator odors from different species (heterospecific), as well as to identify food odors. Lastly, VNO sensory neurons may signal the health status of a conspecific (Riviere et al., 2009).

Receptor neurons in the VNO, as in the olfactory epithelium, possess axons that travel to and innervate portions of the olfactory bulb. However, unlike ORNs, sensory neurons of the VNO possess apical microvilli, not cilia. The initial events of transduction are believed to occur on the microvilli. Moreover, VNO sensory neurons send their axons to a separate portion of the olfactory bulb (the accessory olfactory bulb) reserved for processing pheromone stimuli. Sensory mechanisms for transducing pheromones and odorants are believed to be quite dissimilar, as will be discussed next. This chapter will focus mainly on olfactory transduction, which has been studied much more extensively to date (see reviews by Frings, 2001; Ache and Young, 2005; Munger et al., 2009; DeMaria and Ngai, 2010).

IVB. Nature of Olfactory Stimuli

Odorants for land-dwelling animals are volatile compounds, typically diluted in large volumes of air. Odorants are only poorly soluble in aqueous solutions, including the mucus layer overlaying the olfactory epithelium. ORNs and VNO sensory neurons are much more sensitive to chemical stimulation than are taste receptor cells. Odorants and pheromones in the range of subnanomolar to micromolar concentrations can be detected. Many animals have a keen sense of smell; for example, dogs have been reported to detect as few as 5000 to 10 000 molecules/cm^3. Reports of extreme chemosensitivity, such as the ability of certain species (e.g. moths, dogs and

[3] This raises the intriguing possibility that certain agents, such as drugs or toxins, can be taken up by ORNs and transported along their axons directly into the brain. That is, the olfactory epithelium represents a "window" into the brain that might be exploited for pharmaceutical therapies or may be at the root of certain central nervous system disorders that are linked to environmental contaminants.

[4] In humans, the VNO consists of shallow bilateral pits located in the nasal cavity, anterior to the olfactory epithelium. Arguably, the VNO may only be a vestigial structure in humans. If humans sense pheromones, these stimuli may be transduced by sensory cells lying in the olfactory epithelium. Meredith (2001) summarizes evidence for and against the existence of human vomeronasal organs.

sharks) to detect single molecules of pheromones or odorants may be overestimates based on theoretical calculations that assume uniform spread of the odors in air or water. The actual dispersion of odorant and pheromone molecules is more often in the form of irregular plumes rather than uniform diffusion. Within the plume, concentrations are much higher than predicted by simple diffusion. Nonetheless, olfactory and pheromone receptors are notoriously responsive to chemical stimuli. The acute sensitivity of these receptor neurons might be an optimization of the sensory neuron to the low concentrations of biologically important chemical signals that must be detected.

Volatile odoriferous compounds partition into the mucus layer covering the olfactory epithelial surface. A specialized carrier or transport protein has been identified in the mucus layer-odorant binding protein (OBP). It has been hypothesized that OBP facilitates the partitioning of odorants into the mucus. According to this hypothesis, odorants bound to OBP are carried and presented to the chemoreceptive surface on the cilia that protrude up into the mucus layer.

The low concentration of odorants imposes certain constraints on the possible receptor mechanisms for olfaction (pheromone transduction in VNO sensory neurons will be discussed later). Namely, amplifying second messenger cascades are involved in transduction. Additionally, ORNs have a substantial input resistance (up to 30 GΩ). Consequently, tiny receptor currents – some investigators believe even those generated by stimulation by a single odorant molecule – can produce measureable voltage changes in an olfactory receptor neuron. If sufficiently large, these currents depolarize an ORN to threshold and generate action potentials. Intracellular second messenger cascades and a high input resistance combine to increase the sensitivity of olfactory receptor neurons.

IVC. Initiation of Olfactory Receptor Potentials

Olfactory transduction involves ligand (odorant) binding to specific receptors localized in the ciliary membrane of olfactory receptor neurons.

IVC1. Odorant Receptors (ORs)

The transduction pathways that have been characterized for olfaction to date involve GPCRs that are integral proteins of the ciliary membrane. When stimulated by an odor, odorant receptors (ORs) activate an olfactory-specific G_α protein, G_{olf}, and increase cAMP inside the cilia (see below). Volatile compounds, being lipophilic, may also partition into the membrane. However, this is not believed to contribute prominently to olfactory transduction.

GPCRs for odorants have been cloned and sequenced (Buck and Axel, 1991; Reed, 1992; Raming et al., 1993). ORs are members of a huge GPCR superfamily. In rodents there are ≈ 1400 OR genes located in clusters throughout the genome, ≈ 1000 of which are functional (Zhang et al., 2004). In humans, there are perhaps 855 OR genes but only ≈ 400 are functional, the rest being pseudogenes (Hasin-Brumshtein et al., 2009). The total number of OR genes represents a sizeable fraction of the genome (the human genome having ≈ 30 000 genes). From the large number of possible OR genes, a given olfactory receptor neuron expresses but a single OR throughout its lifespan. How a receptor neuron selects which OR to express is a topic of intense research.

IVC2. G Proteins in Olfactory Receptor Neurons

Odorant binding to receptors triggers second messenger pathways, beginning with activation of G proteins. The canonical odorant transduction pathway involves G_{olf}, a type of G_s protein that is enriched in olfactory epithelium. Ligand binding to ORs liberates G_{olf}, which then activates type III adenylyl cyclase, also expressed selectively in olfactory epithelium, resulting in the formation of cAMP (Pace et al., 1985; Bakalyar & Reed, 1990). It has long been known that exposing isolated olfactory cilia to low concentrations of certain fruity, floral or herbaceous odors results in an increase in intracellular cAMP. These observations were key in establishing adenylyl cyclase in the intracellular pathway for signal transduction in olfaction, especially for what are considered pleasant odors. A less well-established G-protein pathway, believed by some to act as an intermediary for signaling in putrid and unpleasant odors, is discussed later.

IVC3. Cyclic AMP and Cyclic Nucleotide-Gated Channels in Olfactory Receptor Neurons

The ion channels that ultimately are activated by odorant binding and that produce a depolarizing flow of current into olfactory receptor neurons are triggered open by cAMP. Intracellular cAMP binds to and rapidly opens these non-selective cation (Na^+, K^+, Ca^{2+}) channels, named cyclic nucleotide-gated (CNG) channels. CNG channels are distributed along the ciliary membrane of the olfactory receptor neurons. CNG channels were first demonstrated by applying cAMP and cGMP to isolated patches of membrane removed from olfactory cilia (Nakamura and Gold, 1987) or to isolated olfactory receptor neurons (Firestein et al., 1991). CNG channels have little or no voltage dependence and, under physiological conditions (i.e. in the presence of extracellular Ca^{2+} and Mg^{2+}), have a small conductance, ≈ 100 fS. Inward depolarizing current (Fig. 39.6A) is carried principally by Ca^{2+} and Na^+.

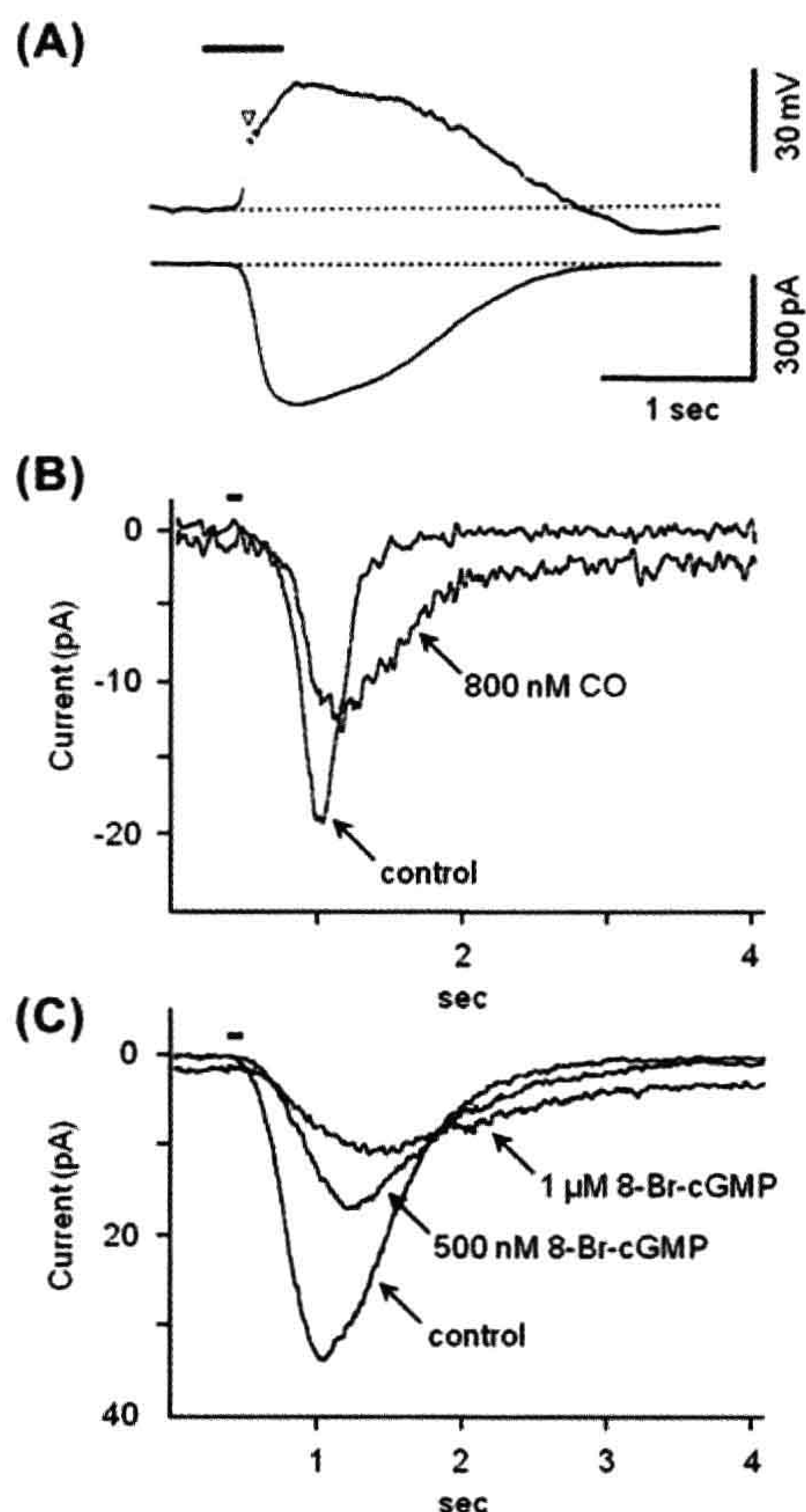


FIGURE 39.6 Patch-clamp recordings from olfactory receptor neurons. (A) Traces show the depolarizing receptor potential (top) and receptor current (bottom) elicited by applying an odorant (10 mM n-amyl acetate) to the olfactory cilia of isolated newt olfactory receptor neurons (bar above trace). Traces are from two different cells *(modified from Kurahashi, 1989)*. (B) Inhibitory effects of carbon monoxide, CO and (C) of 8-Br-cGMP on receptor currents in salamander olfactory receptor neurons after brief applications of an odorant (100 pM cineole, bar above traces). CO stimulates the formation of cGMP during odorant stimulation, which ultimately decreases odor responses and may underlie long-lasting olfactory adaptation, *(modified from Leinders-Zufall et al., 1996)*.

CNG channels from olfactory receptor neurons have been cloned and sequenced (Dhallan et al., 1990). Olfactory CNG channels are quite similar to CNG channels found in photoreceptors, though they differ in their sensitivity to cyclic nucleotides. CNG channels in olfactory receptor neurons respond to cAMP and cGMP alike, with cGMP being somewhat more potent. In contrast, cAMP is far less effective than cGMP in gating open photoreceptor CNG channels. It is an enigma that olfactory CNG channels are more sensitive to cGMP than cAMP because odorant stimulation is believed principally to elevate cAMP. A possible role for an indirect elevation of cGMP in olfactory adaptation (discussed later) may resolve this puzzle. Details of CNG channels are given in Chapter 35.

Calcium ion influx is a key component of the odorant-evoked current through olfactory CNG channels. The influx of Ca^{2+} has several important consequences in addition to supplying inward (depolarizing) current. First, Ca^{2+} influx activates a Ca^{2+}-dependent Cl^- conductance in the olfactory cilia[5]. This results in an outflow of Cl^-, thereby producing an inward (depolarizing) current[6]. Inward current through the Ca^{2+}-activated Cl^- channels (i.e. efflux of Cl^-) amplifies the ongoing inward current (Na^+ and Ca^{2+} influx) through CNG channels. Indeed, in mouse olfactory receptor neurons, the Ca^{2+}-activated Cl^- current is even greater than the initial Na^+ and Ca^{2+} current through CNG channels and can constitute up to 90% of the total inward current generated during odorant stimulation (Boccaccio and Menini, 2007). The combined action of the cAMP-gated cation channels and Ca^{2+}-dependent Cl^--channels may exist to ensure a depolarizing receptor current even in the face of fluctuating extracellular (mucosal) cation concentrations[7]. Figure 39.7 summarizes this olfactory transduction pathway.

Ca^{2+} influx through CNG channels during odorant stimulation also exerts negative feedback onto the CNG channel itself, acting as a brake to retard further activity. Lastly, Ca^{2+} regulates the activity of a number of the enzymes involved in the second messenger cascades in olfactory signal transduction. These actions of Ca^{2+} are particularly important for signal adaptation (discussed later).

---

[5] Initially, this conductance was believed to be generated by the bestrophin-2 (Best2) channels that are present in olfactory cilia. However, olfactory sensory neurons from mutant mice lacking Best2 channels show normal Ca^{2+}-activated Cl^- current (Pifferi et al., 2009), dispelling the notion that Best2 channels underlie this amplifying inward current.

[6] Olfactory cilia are suspended in a mucus that has a Cl^- concentration of about 55 mM. Cl^- concentration inside the apical tips of olfactory receptor neurons appears to be maintained at a remarkably high level ($\approx$50 mM, Kaneko et al., 2004). This ratio of $[Cl]_o/[Cl]_i$ yields an $\approx$0 mV Cl^--equilibrium potential across the apical tips and explains why opening Cl^- channels produces a Cl^- efflux (i.e. inward, depolarizing current).

[7] Activating the Ca^{2+}-dependent anion conductance in gustatory sensory cells results in the opposite effect than at the cilia of olfactory receptor neurons. Namely, in taste bud cells this conductance produces an influx of Cl^- (i.e. a repolarizing, outward current). This is because the basolateral membrane of taste cells – where the Cl^- conductance channels are situated – is exposed to interstitial fluid. Furthermore, $[Cl^-]_i$ in taste cells is believed to be low. Consequently, in taste cells, the equilibrium potential for Cl^- is likely to be near the resting potential. Opening Cl^- channels when the cell is depolarized will allow Cl^- to enter the taste cell and repolarize the membrane.

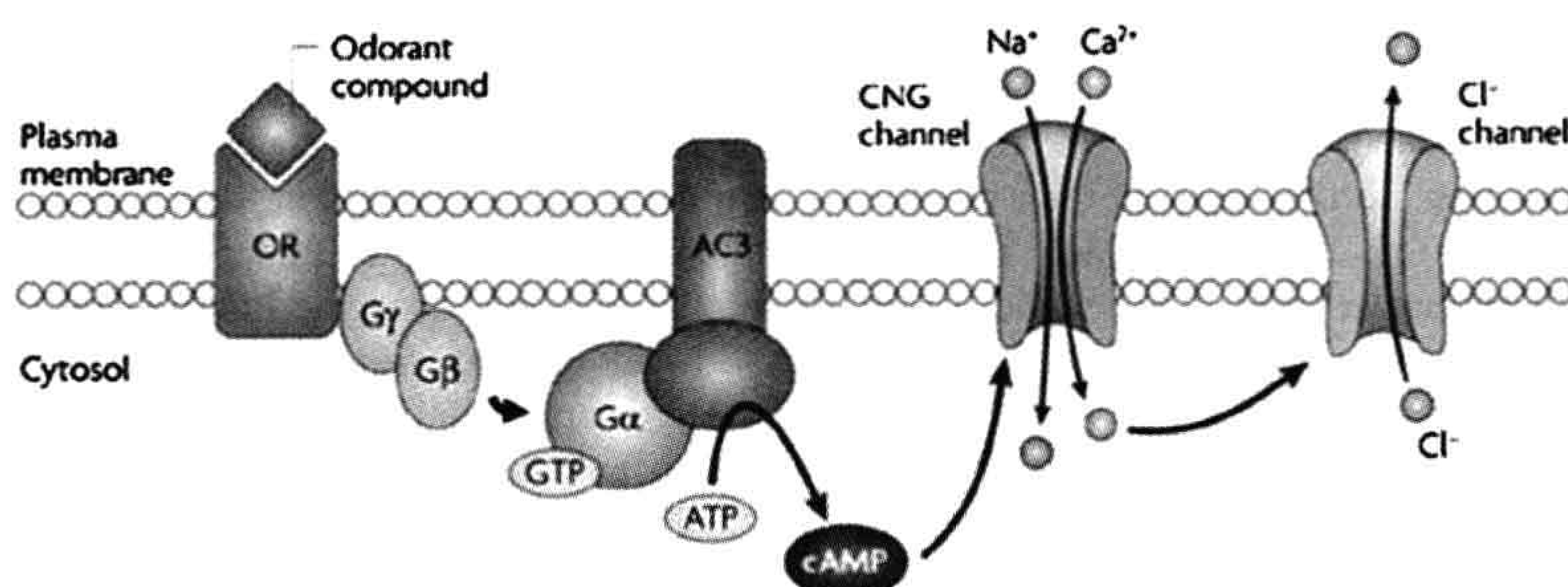


FIGURE 39.7 The canonical odorant transduction pathway. Binding of odorant compounds to an odorant receptor (OR far left) initiates a transduction cascade involving a G protein and activation of adenylate cyclase 3 (AC3) which, in turn, generates the second messenger cyclic AMP. cAMP binds to a cyclic nucleotide-gated (CNG) channel and results in the influx of cations (Na^+ and Ca^{2+}) which depolarize the cell membrane. Ca^{2+} also activates a Ca^{2+}-dependent Cl^- channel. Olfactory sensory neurons (OSNs) maintain a high intracellular Cl^- concentration, such that this channel supports an efflux of negatively charged Cl^-, producing a further depolarization of the cell membrane, *(modified from Zou et al., 2009).*

IVC4. TAAR Receptors

Another class of receptors found in olfactory sensory neurons and distinct from the OR superfamily was discovered in 2006 – trace amine-associated receptors (TAARs) (Liberles and Buck, 2006). These GPCRs are found in a small population of olfactory epithelial receptor neurons that do not express ORs. TAAR receptors comprise a much smaller family of GPCRs than ORs. Of the 15 TAAR receptor genes (mouse), at least 14 are expressed in ORNs (Liberles, 2009). In humans, there are six TAAR receptor genes (Fleischer et al., 2009). Ligands for TAARs are still being identified. In rodents, where they have been studied best, TAARs are stimulated by volatile amines, many of which are found in urine. This origin for TAAR ligands suggests that TAARs may function to detect social cues, akin to pheromones. Transduction mechanisms for olfactory TAARs are not known, though in rodent olfactory receptor neurons TAARs are co-expressed with G_{olf} and in heterologous expression systems, stimulating TAARs increases cAMP. These data suggest a downstream pathway for TAARs similar to that for ORs.

IVC5. IP_3 in Olfactory Receptor Neurons

There is suggestive evidence that a second messenger cascade other than the canonical pathway discussed above is activated in olfactory epithelial cells (reviewed in Ache, 2010). Albeit existence of this alternative pathway is controversial in mammals, there is little doubt that it exists in invertebrates. This alternative pathway may be triggered by a different set of odorants than those that are transduced by the canonical pathway involving G_{olf}, adenylyl cyclase and cAMP. The main impetus to search for alternative signal transduction pathways stems from observations that certain odorants stimulate the rapid generation of inositol trisphosphate (IP_3) in olfactory epithelium. According to this hypothesis, odorant receptors couple to $G_{\alpha q}/G_{\alpha 11}$-like proteins, quite different from G_{olf}. These G proteins are believed to activate membrane-bound enzyme phospholipase C (PLC). PLC hydrolyzes a phospholipid, phosphatidyl inositol 4,5-bisphosphate, in the plasma membrane. The resultant by-products, IP_3 and diacylglycerol (DAG), are powerful bioactive compounds. IP_3 in particular activates specific IP_3 receptors on internal Ca^{2+} stores and triggers Ca^{2+} release into the cytoplasm. Recently, IP_3 receptors have been localized only to a small population of microvillar cells within the olfactory epithelium (Hegg et al., 2010). These cells lack olfactory cilia and axons. They appear to be innervated and may represent a second, parallel chemosensory cell alongside olfactory receptor neurons. Little is currently understood about their function and the significance of an IP_3 pathway in mammalian olfaction remains unresolved.

IVC6. Transduction in the Vomeronasal Organ (VNO)

Transduction pathways in VNO sensory neurons for pheromones and other chemical stimuli are presently under investigation. It appears that VNO sensory neurons utilize distinctive GPCRs, a different set of G proteins and different downstream effectors than ORNs. For example, VNO sensory neurons express two different families of GPCRs, V1Rs and V2Rs, that are unrelated to odorant receptors (Dulac and Axel, 1995). In the mouse, there are ≈240 functional V1R and 60 functional V2R genes; in humans there are only three to five functional V1R genes and no functional V2R genes (Rodriguez and Mombaerts, 2002; Shi and Zhang, 2007; Young et al., 2010). Parenthetically, because there is only a vestigial, if any, vomeronasal organ in adults, V1R in humans must be expressed elsewhere, such as in the olfactory epithelium. In non-human mammals, the two families of VNO receptors are expressed in anatomically separate regions of the VNO sensory epithelium and they send their axons to different regions of the olfactory bulb. Furthermore, V1Rs versus V2Rs respond to different types of stimuli and may mediate different behavioral responses. For instance, V1Rs are found in the more superficial (apical) layer of VNO sensory cells and respond to volatile compounds. In contrast, V2Rs are expressed in the more

basal layer of the VNO epithelium and bind small water-soluble peptides. The behavioral consequences of activating V1Rs and V2Rs are still being scrutinized. To date, roles for V1Rs and V2Rs in gender discrimination, territoriality, aggression, social dominance and male/female sexual interactions have been implicated in non-human animals and perhaps in humans as well (Gelstein et al., 2011).

V1Rs and V2Rs initiate a downstream signaling pathway that markedly differs from that triggered by ORs in the olfactory epithelium. Instead of cAMP/CNG (or IP_3/Ca^{2+} pathways), V1Rs and V2Rs activate a Ca-permeable ion channel, TRPC2 (*c*anonical *t*ransient *r*eceptor *p*otential channel 2, formerly called TRP2) that is highly expressed in vomeronasal sensory neurons[8] (Liman et al., 1999). The complete signaling pathway for V1Rs/V2Rs and TRPC2 awaits elucidation. Indications to date are that activation of the vomeronasal V1 and V2 GPCRs leads to the formation of diacylglycerol (DAG) which stimulates TRPC2 and allows Ca^{2+} influx, thereby depolarizing the sensory cells and initiating action potentials.

In addition to the V1Rs and V2Rs, another small family of GPCRs was recently identified in vomeronasal sensory neurons – formyl peptide receptors (FPRs) (Riviere et al., 2009; Liberles et al., 2009). Five members of this family of receptors were identified. Interestingly, FPRs are also expressed on immune cells where they bind formyl peptides and lipids from microorganisms and signal the presence of pathogens. Expression of these FPR-like receptors in the vomeronasal organ may explain the ability of animals, especially rodents, to detect stimuli in urine and bodily secretions and recognize diseased conspecifics.

IVD. Termination of Olfactory Signals

Olfactory receptor neuron excitation is terminated by a number of mechanisms. An obvious one is the unbinding and disappearance of the odorant from the chemoreceptive surface of the cilia, perhaps aided by odorant binding protein (OBP). The removal of odorants is complicated by the lipophilic nature of most odoriferous compounds; they will tend to partition into the plasma membrane and thus may linger in the vicinity of the receptors. Although the details are only now unfolding, one proposed mechanism for ridding the chemosensitive surfaces of odorants is the enzymatic modification of odorants by broad-spectrum biotransformation enzymes found in the mucus. These enzymes are similar to the detoxification enzymes found in the liver. Olfactory epithelial supporting cells adjacent to receptor neurons contain high concentrations of the detoxifying enzymes glutathione transferase, cytochrome P-450 and UDP gluconosyl transferase (Lazard et al., 1991). Indeed, the lipophilic nature of many odorants and their absorption into the sensory epithelium may necessitate the existence of such degradative mechanisms. Enzymatic biotransformation of volatiles in the mucosal layer occurs very quickly. In addition to terminating the actions of inhaled odorants, enzymatic biotransformation can yield olfactory stimuli that differ chemically and produce smells distinct from what had initially been present.

Besides disappearance of the odorant, sensory adaptation is also key in terminating olfactory signals. Adaptation in olfactory receptor neurons is explained by multiple mechanisms, many of which involve Ca^{2+}. First, short-term adaptive mechanisms are believed to be set in motion by the Ca^{2+} that enters through CNG channels during odorant stimulation. Ca^{2+}, acting via calmodulin inhibits CNG channels themselves (Chen & Yau, 1994; Kurahashi and Menini, 1997), a direct negative feedback on the olfactory signal. That is, an increase in Ca^{2+} in the ciliary cytosol will depress odorant responses by shutting down effector (CNG) channels.

Second, heightened intracellular Ca^{2+} also depresses the cascade of enzymes that are triggered during olfactory transduction. At high (μM) concentrations, Ca^{2+} inhibits adenylyl cyclase, thereby reducing the continued generation of cAMP during maintained stimulation. In olfactory receptor neurons, this inhibition appears to be mediated by Ca^{2+}-calmodulin-induced phosphorylation via the enzyme Ca^{2+}-calmodulin-dependent protein kinase II (CaMKII). However, at nM to pM concentrations, Ca^{2+} has the opposite effect, namely, it stimulates adenylyl cyclase. Consequently, the net effect of Ca^{2+} influx on adenylyl cyclase activity during odor stimulation is concentration dependent.

Additionally, Ca^{2+} influx stimulates phosphodiesterase (PDE), thereby accelerating the degradation of cAMP and reducing the odorant response.

Finally, Ca^{2+} influx activates Ca^{2+}-dependent K^+ channels that initiate an outward, repolarizing current. Counterbalancing this, Ca^{2+} also activates a Cl^- conductance in the olfactory cilia that produces an inward depolarizing current, as described previously.

Thus, the actions of Ca^{2+} are complex. The net effect of Ca^{2+} entry through CNG channels during olfactory stimulation appears to be to reduce the responsiveness of olfactory receptor neurons perhaps as much as 20-fold, moving the stimulus–response relationship to a higher range of odorant concentrations. Longer-lasting adaption to a maintained odor stimulus involves another mechanism. A prolonged adaptation in olfactory receptor neurons, involving an intriguing role for the novel gaseous neurotransmitter carbon monoxide (CO), has been proposed (Leinders-Zufall et al., 1996) (see Fig. 39.6 B,C). CO, like the related neurotransmitter nitric oxide (NO), is a highly-diffusible substance and is generated during olfactory

[8] In humans, TRPC2 is a pseudogene and thus no functional channels are expressed. This fact, combined with the severely limited number of V1Rs and absence of V2Rs in humans, underscores the lack of definitive evidence for human pheromones (but see Gelstein et al., 2011).

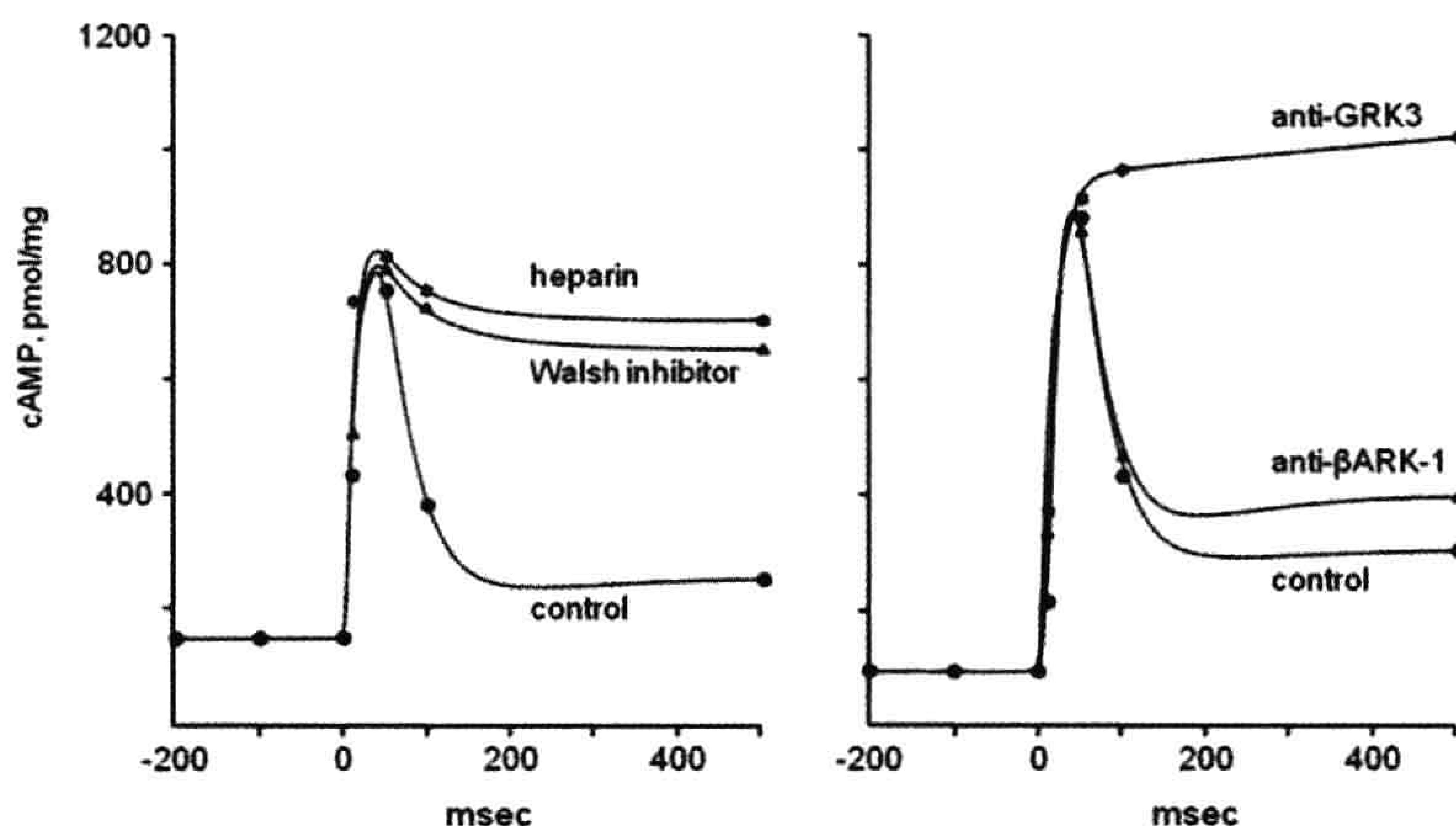


FIGURE 39.8 Desensitization of odorant receptors during prolonged stimulation. Olfactory second messenger signaling is quenched by phosphorylation cascades. Left, inhibiting protein kinase activity with Walsh inhibitor or heparin markedly prolongs increases in olfactory cAMP induced by odorant stimulation in cilia preparations from the rat. (●) odorant alone (1 μM citralva); (▲) odorant stimulation of cilia pretreated with Walsh inhibitor (3.8 μM); (*) odorant stimulation of cilia pretreated with heparin (1 μM). Right, pretreating the cilia preparation with antibodies to GRK3 specifically prevents desensitization of odorant receptors and prolongs their activation (measured here as an increase in cAMP). (●) odorant alone (1 μM citralva); (▲) odorant stimulation of cilia pretreated with anti-βARK-1 antibodies (diluted 1:5000); (*) odorant stimulation of cilia pretreated with anti-GRK3 antibodies (diluted 1:5000); abscissae, time in ms, *(modified from Schleicher et al., 1993).*

transduction via a mechanism that is not yet well characterized. CO, in turn, activates soluble guanylyl cyclase (sGC) and leads to the production of cGMP in the stimulated olfactory receptor neuron as well as in surrounding cells. As discussed previously, cGMP is a very effective ligand for olfactory CNG channels. At first glance, generating cGMP might seem contrary to adaptation and represent positive feedback during odorant stimulation. However, activation of olfactory CNG channels via the CO pathway produces only a low-level, subthreshold inward current. This maintains a persistent trickle of Ca^{2+} into the olfactory receptor neurons, chronically reducing CNG channel activity. The rapid transient influx of Ca^{2+} through CNG channels (the immediate effect of odorant stimulation), combined with a sustained low-level influx via cGMP activation of these channels (the CO pathway), overall leads to a long-lasting (minutes) reduction of the sensitivity of olfactory receptor neurons after the initial excitation.[9]

In addition to these sensory adaptation mechanisms, direct desensitization of ORs following odorant stimulation also plays a key role in terminating odorant responses (Schleicher et al., 1993). cAMP produced by odor stimulation opens CNG cation channels and secondarily activates protein kinase A (PKA). PKA and a specialized G-protein-coupled receptor kinase, GRK3[10], phosphorylate odorant-bond receptors (Fig. 39.8). These protein kinases, together with regulatory proteins, such as arrestin, render the odorant receptor inactive and quench the subsequent transduction cascade. Receptors are resensitized by the action of phosphatases. Thus, a cycle of phosphorylation/dephosphorylation controls the active state of odorant receptors and, ultimately, the responsiveness of olfactory receptor neurons.

Collectively, short-term adaptation, long-term adaptation and receptor desensitization act to shape and terminate olfactory responses to prolonged odor stimulation. Sensory adaptation in many sensory systems, including olfaction, serves a dual purpose. First, over time, a steady stimulus ceases to excite responses, i.e. the sensory organ adapts to the stimulus. In this sense, adaptation tends to accentuate signals from stimuli that fluctuate and emphasizes the dynamic aspects of sensory stimuli. Second, adaptation reduces responsivity to increasingly intense stimuli. This prevents the output from the sensory organs from becoming saturated by only moderately intense stimulus intensities while, at the same time, preserving the ability of the organ to respond well to very weak stimuli. That is, adaptation greatly extends the dynamic range of stimulus intensities over which a sensory organ can respond.

[9] Previously, it was believed that NO played this role in olfactory adaptation. However, data utilizing blockers of CO synthesis now implicate CO, not NO, as the diffusible intra- and intercellular controller of CNG channel activity in olfactory receptor neurons.

[10] GRK3 was formerly named β-adrenergic receptor kinase 2, or βARK-2.

BIBLIOGRAPHY

Ache, B. W. (2010). Odorant-specific modes of signaling in mammalian olfaction. *Chem Senses, 35*, 533–539.

Ache, B. W., & Young, J. M. (2005). Olfaction: diverse species, conserved principles. *Neuron, 48*, 417–430.

Bakalyar, H., & Reed, R. R. (1990). Identification of a specialized adenylyl cyclase that may mediate odorant detection. *Science, 250*, 1403–1406.

Behrens, M., Foerster, S., Staehler, F., Raguse, J. D., & Meyerhof, W. (2007). Gustatory expression pattern of the human TAS2R bitter

receptor gene family reveals a heterogenous population of bitter responsive taste receptor cells. *J Neurosci, 27*, 12630–12640.

Bigiani, A., Cristiani, R., Fieni, F., Ghiaroni, V., Bagnoli, P., & Pietra, P. (2002). Postnatal development of membrane excitability in taste cells of the mouse vallate papilla. *J Neurosci, 22*, 493–504.

Boccaccio, A., & Menini, A. (2007). Temporal development of cyclic nucleotide-gated and Ca^{2+} -activated Cl^{-} currents in isolated mouse olfactory sensory neurons. *J Neurophysiol, 98*, 153–160.

Bradley, R. M. (1973). Electrophysiological investigations of intravascular taste using perfused rat tongue. *Am J Physiol, 224*, 300–304.

Buck, L., & Axel, R. (1991). A novel multigene family may encode odorant receptors: a molecular basis for odor recognition. *Cell, 65*, 175–187.

Chandrashekar, J., Hoon, M. A., Ryba, N. J., & Zuker, C. S. (2006). The receptors and cells for mammalian taste. *Nature, 444*, 288–294.

Chandrashekar, J., Kuhn, C., Oka, Y., et al. (2010). The cells and peripheral representation of sodium taste in mice. *Nature, 464*, 297–301.

Chandrashekar, J., Mueller, K. L., Hoon, M. A., et al. (2000). T2Rs function as bitter taste receptors. *Cell, 100*, 703–711.

Chang, R. B., Waters, H., & Liman, E. R. (2010). A proton current drives action potentials in genetically identified sour taste cells. *Proc Natl Acad Sci USA, 107*, 22320–22325.

Chaudhari, N., & Roper, S. D. (2010). The cell biology of taste. *J Cell Biol, 190*, 285–296.

Chen, T. Y., & Yau, K. W. (1994). Direct modulation by Ca^{2+}-calmodulin of cyclic nucleotide-activated channel of rat olfactory receptor neurons. *Nature, 368*, 545–548.

Clapp, T. R., Trubey, K. R., Vandenbeuch, A., et al. (2008). Tonic activity of Galpha-gustducin regulates taste cell responsivity. *FEBS Lett, 582*, 3783–3787.

DeMaria, S., & Ngai, J. (2010). The cell biology of smell. *J Cell Biol, 191*, 443–452.

Dhallan, R. S., Yau, K. W., Schrader, K. A., & Reed, R. R. (1990). Primary structure and functional expression of a cyclic nucleotide-activated channel from olfactory neurons. *Nature, 347*, 184–187.

Dulac, C., & Axel, R. (1995). A novel family of genes encoding putative pheromone receptors in mammals. *Cell, 83*, 195–206.

Firestein, S., Darrow, B., & Shepherd, G. M. (1991). Activation of the sensory current in salamander olfactory receptor neurons depends on a G protein-mediated cAMP second messenger system. *Neuron, 6*, 825–835.

Fleischer, J., Breer, H., & Strotmann, J. (2009). Mammalian olfactory receptors. *Front Cell Neurosci, 3*, 9.

Frings, S. (2001). Chemoelectrical signal transduction in olfactory sensory neurons of air-breathing vertebrates. *Cell Mol Life Sci, 58*, 510–519.

Gelstein., S., Yeshurun, Y., Rozenkrantz, L., et al. (2011). Human tears contain a chemosignal. *Science, 331*, 226–230.

Ghiaroni, V., Fieni, F., Tirindelli, R., Pietra, P., & Bigiani, A. (2003). Ion conductances in supporting cells isolated from the mouse vomeronasal organ. *J Neurophysiol, 89*, 118–127.

Gilbertson, T. A., Boughter, J. D., Jr., Zhang, H., & Smith, D. V. (2001). Distribution of gustatory sensitivities in rat taste cells: whole-cell responses to apical chemical stimulation. *J Neurosci, 21*, 4931–4941.

Gilbertson, T. A., Roper, S. D., & Kinnamon, S. C. (1993). Proton currents through amiloride-sensitive Na+ channels in isolated hamster taste cells: enhancement by vasopressin and cAMP. *Neuron, 10*, 931–942.

Graziadei, P. P. C., & Monti Graziadei, G. A. (1978). Continuous nerve cell renewal in the olfactory system. In M. Jacobson (Ed.), *Handbook of Sensory Physiology* (pp. 55–82). New York: Springer-Verlag.

Hänig, D. P. (1901). Zur Psychophysik des Geschmackssinnes. *Philosophische Studien, 17*, 576–623.

Hasin-Brumshtein, Y., Lancet, D., & Olender, T. (2009). Human olfaction: from genomic variation to phenotypic diversity. *Trends Genet, 25*, 178–184.

Heck, G. L., Mierson, S., & DeSimone, J. A. (1984). Salt taste transduction occurs through an amiloride-sensitive sodium transport pathway. *Science, 223*, 403–405.

Hegg, C. C., Jia, C., Chick, W. S., Restrepo, D., & Hansen, A. (2010). Microvillous cells expressing IP3 receptor type 3 in the olfactory epithelium of mice. *Eur J Neurosci, 32*, 1632–1645.

Herness, M. S., & Sun, X. D. (1999). Characterization of chloride currents and their noradrenergic modulation in rat taste receptor cells. *J Neurophysiol, 82*, 260–271.

Herness, S., & Zhao, F. L. (2009). The neuropeptides CCK and NPY and the changing view of cell-to-cell communication in the taste bud. *Physiol Behav, 97*, 581–591.

Huang, Y. A., Maruyama, Y., Stimac, R., & Roper, S. D. (2008). Presynaptic (Type III) cells in mouse taste buds sense sour (acid) taste. *J Physiol, 586*, 2903–2912.

Huang, Y. J., Maruyama, Y., Dvoryanchikov, G., Pereira, E., Chaudhari, N., & Roper, S. D. (2007). The role of pannexin 1 hemichannels in ATP release and cell-cell communication in mouse taste buds. *Proc Natl Acad Sci USA, 104*, 6436–6441.

Kaneko, H., Putzier, I., Frings, S., Kaupp, U. B., & Gensch, T. (2004). Chloride accumulation in mammalian olfactory sensory neurons. *J Neurosci, 24*, 7931–7938.

Kleene, S. J., & Gesteland, R. C. (1981). Dissociation of frog olfactory epithelium with N-ethylmaleimide. *Brain Res, 229*, 536–540.

Kretz, O., Barbry, P., Bock, R., & Lindemann, B. (1999). Differential expression of RNA and protein of the three pore-forming subunits of the amiloride-sensitive epithelial sodium channel in taste buds of the rat. *J Histochem Cytochem, 47*, 51–64.

Kurahashi, T. (1989). Activation by odorants of cation-selective conductance in the olfactory receptor cell isolated from the newt. *J Physiol, 419*, 177–192.

Kurahashi, T., & Menini, A. (1997). Mechanism of odorant adaptation in the olfactory receptor cell. *Nature, 385*, 725–729.

Lazard, D., Zupko, K., Poria, Y., et al. (1991). Odorant signal termination by olfactory UDP glucuronosyl transferase. *Nature, 349*, 790–793.

Leinders-Zufall, T., Shepherd, G. M., & Zufall, F. (1996). Modulation by cyclic GMP of the odour sensitivity of vertebrate olfactory receptor cells. *Proc Biol Sci, 263*, 803–811.

Liberles, S. D. (2009). Trace amine-associated receptors are olfactory receptors in vertebrates. *Ann NY Acad Sci, 1170*, 168–172.

Liberles, S. D., & Buck, L. B. (2006). A second class of chemosensory receptors in the olfactory epithelium. *Nature, 442*, 645–650.

Liberles, S. D., Horowitz, L. F., Kuang, D., et al. (2009). Formyl peptide receptors are candidate chemosensory receptors in the vomeronasal organ. *Proc Natl Acad Sci USA, 106*, 9842–9847.

Liman, E. R., Corey, D. P., & Dulac, C. (1999). TRP2: a candidate transduction channel for mammalian pheromone sensory signaling. *Proc Natl Acad Sci USA, 96*, 5791–5796.

Lin, W., Finger, T. E., Rossier, B. C., & Kinnamon, S. C. (1999). Epithelial Na+ channel subunits in rat taste cells: localization and regulation by aldosterone. *J Comp Neurol, 405*, 406–420.

Lindemann, B. (1999). Receptor seeks ligand: on the way to cloning the molecular receptors for sweet and bitter taste. *Nat Med, 5*, 381–382.

Lindemann, B., Barbry, P., Kretz, O., & Bock, R. (1998). Occurrence of ENaC subunit mRNA and immunocytochemistry of the channel subunits in taste buds of the rat vallate papilla. *Ann NY Acad Sci, 855*, 116–127.

Lyall, V., Alam, R. I., Phan, D. Q., et al. (2001). Decrease in rat taste receptor cell intracellular pH is the proximate stimulus in sour taste transduction. *Am J Physiol Cell Physiol, 281*, C1005–C1013.

Mackay-Sim, A., & Kittel, P. (1991a). Cell dynamics in the adult mouse olfactory epithelium: a quantitative autoradiographic study. *J Neurosci, 11*, 979–984.

Mackay-Sim, A., & Kittel, P. W. (1991b). On the life span of olfactory receptor neurons. *Eur J Neurosci, 3*, 209–215.

Max, M., Shanker, Y. G., Huang, L., et al. (2001). Tas1r3, encoding a new candidate taste receptor, is allelic to the sweet responsiveness locus Sac. *Nat Genet, 28*, 58–63.

McLaughlin, S. K., McKinnon, P. J., & Margolskee, R. F. (1992). Gustducin is a taste-cell-specific G protein closely related to the transducins. *Nature, 357*, 563–569.

Meredith, M. (2001). Human vomeronasal organ function: a critical review of best and worst cases. *Chem Senses, 26*, 433–445.

Munger, S. D., Leinders-Zufall, T., & Zufall, F. (2009). Subsystem organization of the mammalian sense of smell. *Annu Rev Physiol, 71*, 115–140.

Nakamura, T., & Gold, G. H. (1987). A cyclic nucleotide-gated conductance in olfactory receptor cilia. *Nature, 325*, 442–444.

Nelson, G., Chandrashekar, J., Hoon, M. A., et al. (2002). An amino-acid taste receptor. *Nature, 416*, 199–202.

Nelson, G., Hoon, M. A., Chandrashekar, J., Zhang, Y., Ryba, N. J., & Zuker, C. S. (2001). Mammalian sweet taste receptors. *Cell, 106*, 381–390.

Ossebaard, C. A., & Smith, D. V. (1996). Amiloride suppresses the sourness of NaCl and LiCl. *Physiol Behav, 60*, 1317–1322.

Pace, U., Hanski, E., Salomon, Y., & Lancet, D. (1985). Odorant-sensitive adenylate cyclase may mediate olfactory reception. *Nature, 316*, 255–258.

Pifferi, S., Dibattista, M., Sagheddu, C., et al. (2009). Calcium-activated chloride currents in olfactory sensory neurons from mice lacking bestrophin-2. *J Physiol, 587*, 4265–4279.

Raming, K., Krieger, J., Strotmann, J., et al. (1993). Cloning and expression of odorant receptors. *Nature, 361*, 353–356.

Reed, R. R. (1992). Signaling pathways in odorant detection. *Neuron, 8*, 205–209.

Richter, T. A., Caicedo, A., & Roper, S. D. (2003). Sour taste stimuli evoke Ca2+ and pH responses in mouse taste cells. *J Physiol, 547*, 475–483.

Richter, T. A., Dvoryanchikov, G. A., Chaudhari, N., & Roper, S. D. (2004). Acid-sensitive two-pore domain potassium (K2P) channels in mouse taste buds. *J Neurophysiol, 92*, 1928–1936.

Riviere, S., Challet, L., Fluegge, D., Spehr, M., & Rodriguez, I. (2009). Formyl peptide receptor-like proteins are a novel family of vomeronasal chemosensors. *Nature, 459*, 574–577.

Rodriguez, I., & Mombaerts, P. (2002). Novel human vomeronasal receptor-like genes reveal species-specific families. *Curr Biol, 12*, R409–R411.

Romanov, R. A., Rogachevskaja, O. A., Bystrova, M. F., Jiang, P., Margolskee, R. F., & Kolesnikov, S. S. (2007). Afferent neurotransmission mediated by hemichannels in mammalian taste cells. *EMBO J, 26*, 657–667.

Roper, S. (1983). Regenerative impulses in taste cells. *Science, 220*, 1311–1312.

Roper, S. D. (1992). The microphysiology of peripheral taste organs. *J Neurosci, 12*, 1127–1134.

Roper, S. D. (2007). Signal transduction and information processing in mammalian taste buds. *Pflügers Arch, 454*, 759–776.

Sainz, E., Korley, J. N., Battey, J. F., & Sullivan, S. L. (2001). Identification of a novel member of the T1R family of putative taste receptors. *J Neurochem, 77*, 896–903.

Schleicher, S., Boekhoff, I., Arriza, J., Lefkowitz, R. J., & Breer, H. (1993). A beta-adrenergic receptor kinase-like enzyme is involved in olfactory signal termination. *Proc Natl Acad Sci USA, 90*, 1420–1424.

Shi, P., & Zhang, J. (2007). Comparative genomic analysis identifies an evolutionary shift of vomeronasal receptor gene repertoires in the vertebrate transition from water to land. *Genome Res, 17*, 166–174.

Smith, D. V., & Margolskee, R. F. (2001). Making sense of taste. *Sci Am, 284*, 32–39.

Sugita, M. (2006). Taste perception and coding in the periphery. *Cell Mol Life Sci, 63*, 2000–2015.

Taylor, R., & Roper, S. (1994). Ca(2+)-dependent Cl conductance in taste cells from Necturus. *J Neurophysiol, 72*, 475–478.

Tomchik, S. M., Berg, S., Kim, J. W., Chaudhari, N., & Roper, S. D. (2007). Breadth of tuning and taste coding in mammalian taste buds. *J Neurosci, 27*, 10840–10848.

Vandenbeuch, A., Clapp, T. R., & Kinnamon, S. C. (2008). Amiloride-sensitive channels in type I fungiform taste cells in mouse. *BMC Neurosci, 9*, 1.

Wang, Y. Y., Chang, R. B., Allgood, S. D., Silver, W. L., & Liman, E. R. (2011). A TRPA1-dependent mechanism for the pungent sensation of weak acids. *J Gen Physiol, 137*, 493–505.

Ye, Q., Heck, G. L., & DeSimone, J. A. (1993). Voltage dependence of the rat chorda tympani response to Na+ salts: implications for the functional organization of taste receptor cells. *J Neurophysiol, 70*, 167–178.

Yoshida, R., Horio, N., Murata, Y., Yasumatsu, K., Shigemura, N., & Ninomiya, Y. (2009a). NaCl responsive taste cells in the mouse fungiform taste buds. *Neuroscience, 159*, 795–803.

Yoshida, R., Miyauchi, A., Yasuo, T., et al. (2009b). Discrimination of taste qualities among mouse fungiform taste bud cells. *J Physiol, 587*, 4425–4439.

Young, J. M., Massa, H. F., Hsu, L., & Trask, B. J. (2010). Extreme variability among mammalian V1R gene families. *Genome Res, 20*, 10–18.

Zhang, X., Rodriguez, I., Mombaerts, P., & Firestein, S. (2004). Odorant and vomeronasal receptor genes in two mouse genome assemblies. *Genomics, 83*, 802–811.

Zou, D. J., Chesler, A., & Firestein, S. (2009). How the olfactory bulb got its glomeruli: a just so story? *Nat Rev Neurosci, 10*, 611–618.

Infrared Sensory Organs

Stephen D. Roper and Michael S. Grace

Chapter Outline

I. SUMMARY

Certain snakes, such as pythons and rattlesnakes, utilize infrared radiation as well as visible light to detect prey. Infrared radiation emitted from warm objects is captured mainly by specialized sensory structures in the snake head called pit organs. The anatomy of pit organs is such that a crude image of the infrared-emitting object is cast upon a thin membrane within the organ. This infrared image locally warms the thin tissue which is innervated by heat-sensitive axon terminals of trigeminal sensory ganglion cells. Molecular profiling of snake trigeminal ganglion neurons indicates that a unique variant of the heat-sensitive *t*ransient *r*eceptor *p*otential cation channel, TRPA1, is the heat-transducing protein found in infrared sensory neurons.

II. INTRODUCTION

Infrared radiation is an important and ubiquitous component of the diverse physical environments in which animals live. All warm objects radiate infrared energy. Naturally-occurring infrared sources include terrestrial, atmospheric and astronomical bodies. Animals, especially ectothermic species, use radiant infrared energy to assist in maintaining their body temperature and must avoid excess infrared radiation to avoid overheating. In a few species, infrared radiation is also used in a novel manner – to form spatial images of the environment and to hunt prey. These animals possess specialized infrared-receptive sensory organs, the topic of this chapter.

Infrared-receptive organs occur in both vertebrate and invertebrate animals. Buprestid beetles, including the European fire beetle *Melanophila acuminata*, have specialized infrared receptive organs on the ventral surfaces of their abdomens (Evans, 1964). *Melanophila* and similar beetles congregate in large numbers at forest fire sites to deposit eggs in recently burned wood. They likely use chemoreceptors and mechanoreceptors (to detect wind direction) to guide them to sites of fires, and their infrared detectors to identify potential egg-laying sites of appropriate temperature. The deep-sea shrimp *Rimicaris exoculata* also possesses an elaborate organ capable of detecting 350°C "black smoker" thermal vents in the deep Atlantic Ocean (Pelli and Chamberlain, 1989). Their infrared sensory detection system may help the shrimp maintain close proximity to life-sustaining thermal vents in the deep sea without directly contacting the steep thermocline (350°C to 2°C over a 2–3 cm lateral distance) adjacent to the thermal vent. The common vampire bat (*Desmodus rotundus*) may possess infrared radiation detectors, but its infrared sensory system has been little investigated. Behavioral experiments show that vampire bats can detect infrared radiation as low as 50 $\mu W/cm^2$ and thus should be able to detect mammalian prey at distances of up to 16 cm (also see Campbell et al., 2002). Vampire bats may use their infrared detection system to locate suitable prey.

However, by far the best-studied infrared sensory detectors are those of snakes. As stated previously, ectothermic animals, such as snakes, rely on infrared radiation to regulate their body temperature. In some snakes (Boidae, which include boa constrictors and pythons, and Crotalinae, which include rattlesnakes and water moccasins), infrared radiation is also used for accurate and precise targeting of prey. These

Cell Physiology Sourcebook. DOI: 10.1016/B978-0-12-387738-3.00040-8

snakes preferentially feed on endothermic (warm-blooded) prey. In addition to mediating predatory behavior, the infrared imaging system also mediates defensive behavior (Van Dyke and Grace, 2010). Unlike other infrared-sensing animals, boid and crotaline snakes are the only animals known to form spatial images of their environments using extremely sensitive infrared-receptive organs.

Boid and crotaline snakes are efficient predators. While vision may be useful for some aspects of their predatory behaviors, infrared imaging alone can allow accurate prey targeting. Snakes experimentally blinded by occluding both eyes and snakes born without eyes are capable of accurately placing strikes at mammalian prey (Kardong and Mackessey, 1991). Infrared-imaging snakes can target based upon vision alone but when one eye is occluded, strike-targeting performance is indistinguishable from that of normally sighted snakes (Grace and Woodward, 2001). Moreover, snakes readily strike their prey regardless of visual contrast (black *versus* white mice against a black background) (Grace et al., 2001) and they preferentially target the warm aspect of thermal differentials (Van Dyke and Grace, 2010). Thus, vision and infrared imaging appear to be redundant targeting systems and the infrared imaging system can compensate for loss of visual information.

III. NATURE OF THE STIMULUS: WHAT IS INFRARED (IR) RADIATION?

Radiant infrared energy is a region of the spectrum of electromagnetic radiation that lies between visible light (wavelengths of 400–750 nm) and microwaves (wavelengths of ≈ 1 mm to 1 cm). The English astronomer Sir William Herschel discovered infrared radiation at the beginning of the 19th century. Herschel was exploring the ability of light passing through a prism to heat a thermometer that he positioned at different points in the color spectrum. Herschel noticed that visible light was capable of heating the thermometer to some extent but that this effect was much more pronounced when the thermometer was placed beyond the red end of the spectrum. Electromagnetic radiation in the infrared region is absorbed as the radiation passes through objects in its pathway. Most of this absorbed infrared energy is dissipated by the resulting increase in molecular collisions (i.e. heat). Infrared radiation penetrates body tissues deeper than does visible light, and thus IR generators produce the so-called deep heat used in physical therapy. Any object above absolute zero radiates electromagnetic waves in the infrared, the more so as it is warmed. With increasing heat, an object radiates increasingly shorter wavelengths. Objects at room temperature radiate entirely in the IR and not at all in the visible light spectrum. At 500°C, objects begin to radiate also in the visible spectrum and they appear dull red. Endothermic (warm-blooded) animals, such as rats and mice, radiate maximally in the infrared region at a wavelength of approximately 10 μm. IR radiation can thus be used to detect objects in the absence of visible light (i.e. in the dark) with an object's detection being enhanced by having a temperature that contrasts with its background temperature.

Water vapor and carbon dioxide in the atmosphere absorb and severely attenuate the transmission of certain wavelengths of the IR spectrum and allow other wavelengths to pass. That is, there are windows for IR transmission in the atmosphere. One of these windows is in a region where certain IR-sensitive photographic emulsions absorb well, thereby allowing IR images of landscapes and cityscapes to be collected by satellite cameras. Another atmospheric transmission window includes the region around 10 μm, i.e. the region of the IR spectrum in which endothermic animals maximally radiate. IR sensory organs in snakes are believed to have a maximum sensitivity in this region (Grace et al., 1999) and thus are well suited to detect endothermic prey.

IV. INFRARED-SENSITIVE PIT ORGANS IN SNAKES

Infrared sensory organs in snakes consist of pit organs. Pit organs are invaginations within or between scales in the head. These invaginations are up to 3–4 mm wide and 3–4 mm deep. In boid snakes (e.g. pythons), the pit organs are arrayed in rows within labial scales of both the upper and lower jaws.[1] In crotaline snakes (e.g. rattlesnakes), there is a single facial pit organ on each side of the face between the nostril and eye (Fig. 40.1). There may be additional infrared-sensitive receptor terminals in the oral cavity (especially the palate) that may be important for guiding the predatory strike when the snake's mouth is open and fangs extended (Dickman et al., 1987) (Fig. 40.2).

A dense plexus of infrared-receptive primary sensory afferent nerve terminals is present in pit organs. In boid snakes, these terminals lie in the epidermis just under the surface of the pit organ. Immediately below the layer of infrared-receptive neuronal terminals is a thick capillary network. In crotaline snakes, a thin (15 μm) membrane stretches across the cavity of the pit (see Fig. 40.1B). Infrared-receptive nerve terminals are embedded within this membrane, also over a thick capillary bed. Infrared receptor terminals and the dense capillary plexus are mainly confined to the pit organs.[2]

The anatomical configuration of the pit organ, namely that the receptive tissue is stretched across the bottom of a cavity that has a narrowed opening to the outside environment, provides the snake with a means to direct its pit

[1] Boid snakes that do not have obvious pit organs possess clusters of infrared-receptive neuronal terminals in these same labial areas.

[2] The oral cavity of rattlesnakes is also sensitive to infrared and possesses dense ramifications of infrared-receptive sensory nerve terminals, similar to those in pit organs (Dickman et al., 1987).

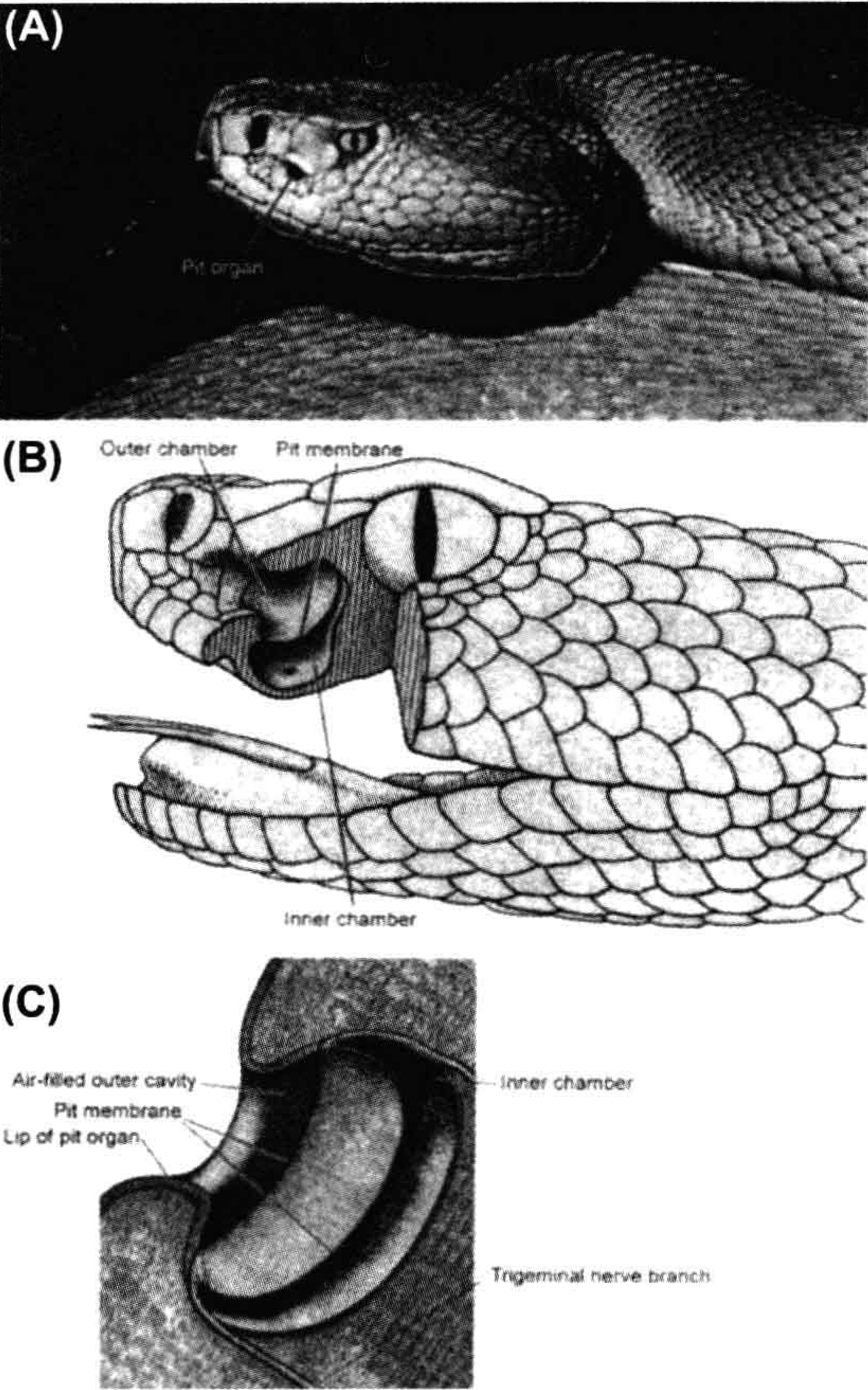


FIGURE 40.1 Infrared pit organ in the rattlesnake. (A) Photograph of the head of a rattlesnake (*Crotalus viridis*) showing the distinctive pit organ between the nostrils and the eye. *(Photograph by Bill Love from The World's Most Spectacular Reptiles and Amphibians, 1997. World Publications, Tampa, FL.)* (B) Schematic drawing of the internal structure of the infrared sensory organ in rattlesnake (*Crotalus viridis*). *(Reproduced from Gamow and Harris, 1973.)* (C) Higher magnification schematic view of the rattlesnake pit organ. *(Reproduced from Newman and Hartline, 1982.)*



FIGURE 40.2 Photograph of a rattlesnake striking at prey, demonstrating how infrared sensing receptors in the oral cavity may play a role in guiding the strike. *(Photograph by Pete Carmichael from Florida's Fabulous Reptiles and Amphibians, 1991. World Publications, Tampa, FL.)*

organs towards prey. Thus, the pit organs can provide information about the location of an infrared-emitting source in front of the snake. A distinct image, per se, such as a pin-hole camera might afford, is not formed in the pit organ, but the shadows cast by the infrared radiation passing through the narrowed opening into the pit project a crude approximation of the infrared source onto the sensory terminals. This "image" is conveyed to the snake's brain, much like visual information, to establish a spatiotopic map on the optic tectum (see Section IVA).

Infrared receptor terminals are embedded within the thin membrane that is stretched across the bottom of the pit organ. These terminals form large, highly-branched, entwined clusters surrounding an aggregate of Schwann cells. Collectively, this structure is called a terminal nerve mass ($\approx$30–100 μm diameter) (Fig. 40.3). Each terminal branch is densely packed with mitochondria. Clusters of electron-lucent vesicles are present just beneath the plasma membrane. These specialized endings are the sites where infrared transduction takes place (see Section IVB). A complex and extensive bed of capillary loops embraces the terminal nerve masses. This capillary bed is believed to have a dual function: (1) to provide a robust oxygen supply for the mitochondria in the receptor terminals; and (2) to act as a thermal exchanger to carry away excess heat and prevent the epithelial tissues from retaining temperature increases produced by infrared radiation (Amemiya et al., 1999). The thermal exchange function of the capillary bed, combined with the low heat capacity of the thin epithelial tissues in the pit organs, may ensure that the sensory receptors are capable of responding to the small transient temperature changes that are expected to occur when an infrared source (e.g. prey) passes in front of the pit organ (discussed in Section IVB).

IVA. Innervation and Central Nervous System Pathways of Pit Organs

Pit organs are innervated by branches of the trigeminal nerve (reviewed by Molenaar, 1992). These same nerve branches also subserve mechanoreception, nociception and thermoreception in the facial region of reptiles, mammals and other vertebrates. Cell bodies for the infrared-sensitive nerve terminals are located in sensory ganglia of the trigeminal nerve.

In infrared-sensitive snakes, sensory neurons in the trigeminal ganglia synapse with neurons in two distinct nuclei located in the hindbrain – the nucleus of the solitary

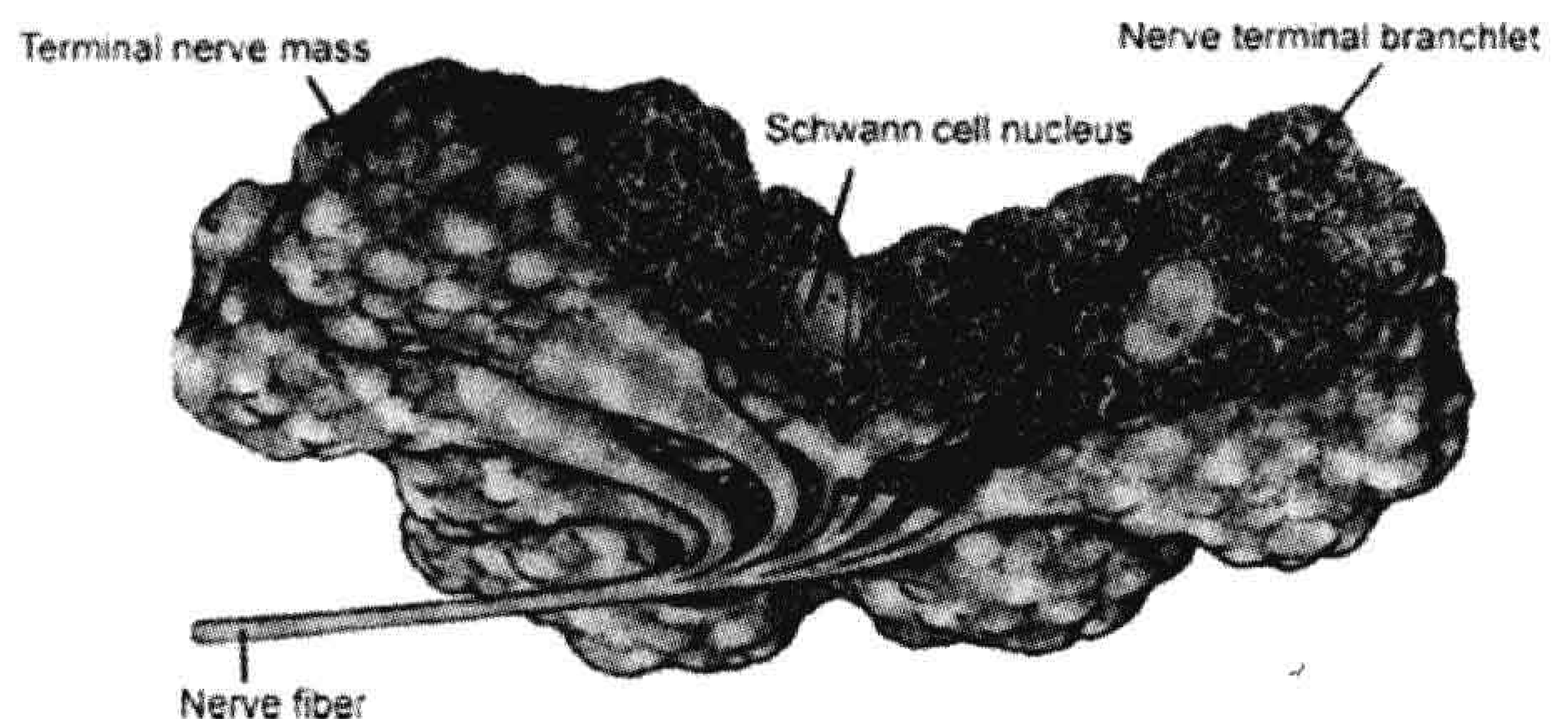


FIGURE 40.3 Reconstruction of the nerve terminals for infrared sensing trigeminal sensory axons. The branches form nerve terminal masses that include Schwann cells and receptor terminals. The nerve terminals are filled with numerous mitochondria. *(Reproduced from Terashima et al., 1970.)*

tract (NST) and a unique group of cells termed the nucleus of the lateral descending trigeminal tract (nLTTD) (see Molenaar, 1992). Neurons in the NST subserve such functions as mechanoreception, thermoreception and nociception, as in other vertebrates. However, the nLTTD is found only in infrared-sensing snakes and is responsible for processing information specifically from the pit organs (Stanford et al., 1981). This nucleus is present in all infrared-sensitive snakes studied thus far, and is absent from animals that are not infrared-sensitive.

Ultimately, infrared information from the nLTTD reaches the optic tectum. Spatial relationships among the axons and synapses of the infrared receptor pathway are preserved such that a systematic topographical map of the receptive membrane in the pit organ is projected onto the tectum, much like the orderly retinotopic mapping of visual information that also occurs in the optic tectum. Indeed, the infrared sensory map overlies and is aligned with the retinotopic map. Individual neurons in the optic tectum may be excited by visual and infrared stimuli arising from approximately the same point in space[3] (Hartline et al., 1978). Thus, snakes possessing infrared-sensitive pit organs view their environments simultaneously using two distinct regions of the electromagnetic spectrum.

IVB. Infrared Sensory Transduction

Infrared-detecting pit organs in snakes are exquisitely sensitive and selective (Bullock and Diecke, 1956; Gamow and Harris, 1973; de Cock Buning et al., 1981a,b; Newman and Hartline, 1982; Hartline, 1999). The adequate stimulus is a sharp thermal gradient, or contrast, in the surrounding environment, such as an endothermic animal (e.g. a mouse) against thermoneutral vegetation, or cool prey (e.g. a frog) against a cooler background (e.g. a pond). The temperature of the snake's body itself is not a significant factor, nor is the average temperature of the surroundings. Air temperature is irrelevant; the pit organ responds only to radiant energy in the infrared, not conductive energy transferred by warm air. Thus, a snake is an effective hunter in the heat of midday as well as in the cool of the night. The sensitivity of pit organs is such that a pit viper can use its infrared detector to orient to and accurately strike a rat at a distance of about 0.5 m. At this distance, a rat with a surface temperature 10°C above background emits infrared radiation ($\approx$10 μm wavelength) that would be expected to warm the pit organ tissues by only 0.001°C (Bullock and Diecke, 1956). This low threshold for temperature detection was also observed experimentally. Researchers infused water of different temperatures into pit organs and measured threshold nerve responses to temperature changes as small as 0.003°C in 0.06 s (Bullock and Diecke, 1956). Rapid temperature increases as small as 0.1°C in the pit organ elicit robust responses (i.e. well above threshold detection) in the receptors (de Cock Buning et al., 1981a,b).[4]

Recent studies at the molecular level have tremendously illuminated how infrared radiation can be transduced into neuronal excitation. Gracheva et al. (2010) reported that rattlesnake trigeminal sensory ganglia express a unique variant of the heat-activated cation channel, TRPA1 (Fig. 40.4). When expressed in heterologous systems, rattlesnake TRPA1 channels are exceptionally sensitive to heat and begin conducting at or above 28°C. In contrast, TRPA1 channels from snakes lacking pit organs are not activated until temperatures reach 37°C.

[3] The two maps – visual and infrared – do not appear to overlap well in the peripheral fields of view. The overlap is more precise in the central field, i.e. directly in front of the snake.

[4] Bullock and Diecke (1956) and de Cock Buning et al. (1981a,b) alike point out that when factors such as the relative thickness of the overlying tissues, the low heat capacity of the thin pit organ membrane and the density of innervation are taken into account, the threshold for snake pit organs is similar to that of other warm receptors, including human cutaneous thermoreceptors. One reason for the apparent higher sensitivity to small temperature increases in snakes is that the density of innervation in pit organs is very high and the epithelial tissue overlying the sensory nerve terminals is extremely thin. Thus, infrared radiation can readily and rapidly increase the temperature around a dense plexus of sensory nerve terminals.

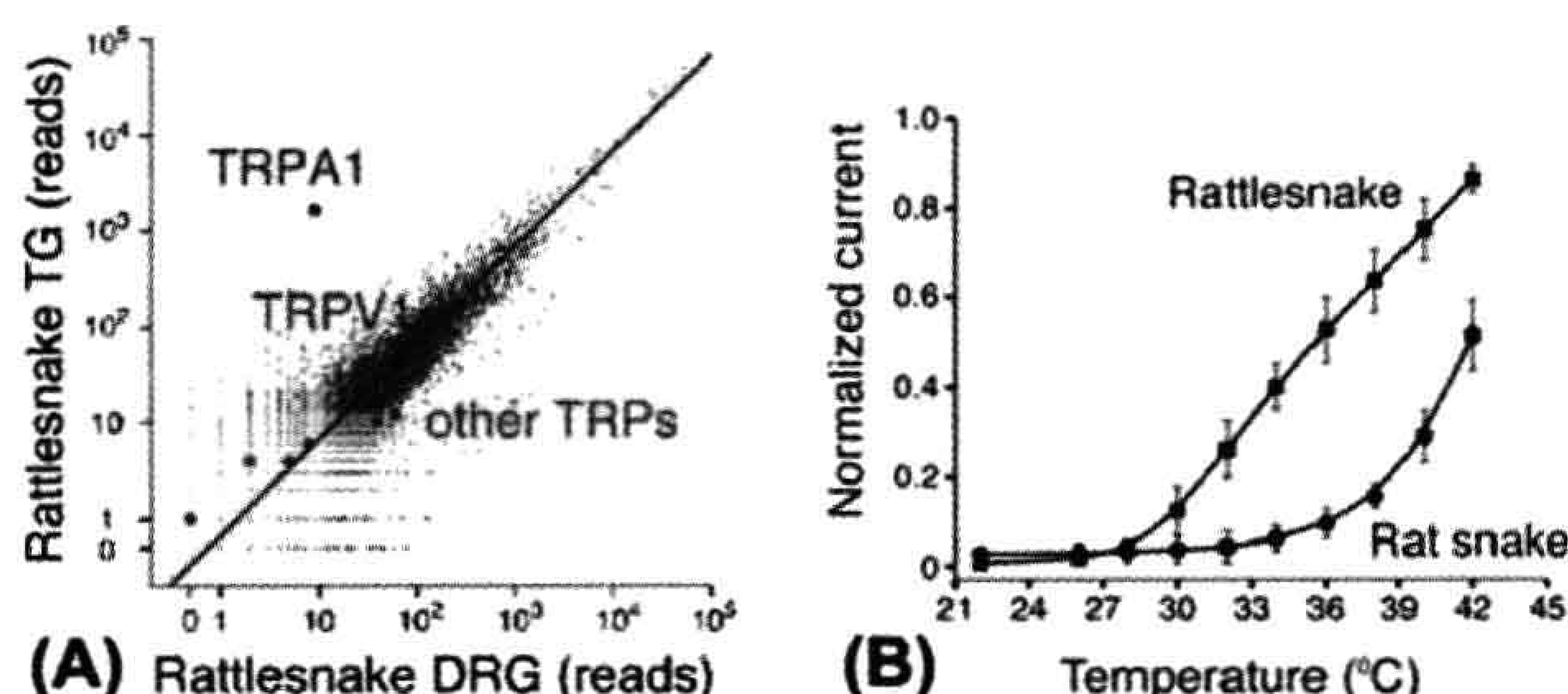


FIGURE 40.4 Rattlesnake TRPA1 channels are highly expressed in sensory neurons innervating the pit organ and are activated by temperatures above 28°C. (A) Quantification of genes expressed in rattlesnake ganglia that innervate the pit organ (trigeminal, TG) relative to rattlesnake dorsal root ganglia (i.e. non-pit organ sensory neurons). Axes show number of mRNA-Seq reads from snake ganglia that align to the chicken proteome. TRPA1 and another heat-sensitive channel, TRPV1, are highlighted, as are other TRP channels. Blue line indicates similar expression levels in the two samples. (B) Functional analysis of snake TRPA1 channels. The graph shows the relative heat response profiles of infrared-sensitive rattlesnake and infrared-sensitive rat snake channels expressed in oocytes (response at each temperature was normalized to maximal response at 45°C). *(Modified from Gracheva et al., 2010.)*

Gracheva et al. (2010) concluded that rattlesnake TRPA1 is the pit organ receptor activated by heat that is generated in the pit membrane during absorption of infrared radiation.[5]

Interestingly, the pit organs in pythons are exquisitely sensitive to gentle touch in addition to infrared radiation (de Cock Buning et al., 1981b). This observation may be explained by the expression of TRPA1 in trigeminal ganglion cells innervating the pit organ. TRPA1 has been identified with mechanotransduction in other species, including mice (Vilceanu and Stucky, 2010).

BIBLIOGRAPHY

Amemiya, E., Nakano, M., Goris, R. C., et al. (1999). Microvasculature of crotaline snake pit organs: possible function as a heat exchange mechanism. *Anat Rec, 254*, 107–115.

Bullock, T. H., & Diecke, E. P. J. (1956). Properties of an infra-red receptor. *J Physiol, 134*, 47–87.

Campbell, A. L., Naik, R. R., Sowards, L., & Stone, M. O. (2002). Biological infrared imaging and sensing. *Micron, 33*, 211–225.

[5] Despite these impressive findings, the identification of rattlesnake TRPA1 as the infrared sensor is not entirely without question. There is a discrepancy between the operating range for rattlesnake TRPA1 channels and the temperature response of the pit organ. Rattlesnake TRPA1 channels expressed in HEK293 cells or *Xenopus* oocytes show a monotonic increase in activity with a threshold ≈28° and continuing to respond ≥42°, roughly comparable to the temperature sensitivity of trigeminal ganglion cells isolated from rattlesnakes (Gracheva et al., 2010). In marked contrast, the effective temperature range for the pit organ membrane, measured by the impulse activity of axons innervating the pit organ, is an inverted "U" shape with a threshold of ≈14°C, a peak at ≈25°C and a return to inactivity at ≈33°C (de Cock Buning et al., 1981a). This discrepancy may be explained by technical differences such as properties of TRPA1 in native versus heterologous expression systems, or species differences, or it may indicate that additional molecular mechanisms are involved in infrared detection. In this light, it may be pertinent that a light-sensitive G protein-coupled receptor, rhodopsin, was recently shown to be co-expressed with TRPA1 in temperature-sensitive neurons of *Drosophila* larvae (Shen et al., 2011). Remarkably, the two proteins appear to function in tandem as a temperature sensor, in the vicinity of 18°C.

de Cock Buning, T., Terashima, S., & Goris, R. C. (1981a). Crotaline pit organs analyzed as warm receptors. *Cell Mol Neurobiol, 1*, 69–85.

de Cock Buning, T., Terashima, S., & Goris, R. (1981b). Python pit organs analyzed as warm receptors. *Cell Mol Neurobiol, 1*, 271–278.

Dickman, J. D., Colton, J. S., Chiszar, D., & Colton, C. A. (1987). Trigeminal responses to thermal stimulation of the oral cavity in rattlesnakes (*Crotalus viridis*) before and after bilateral anesthetization of the facial pit organs. *Brain Res, 400*, 365–370.

Evans, W. G. (1964). Infra-red receptors in *Melanophila acuminata* DeGeer. *Nature, 202*, 211.

Gamow, R. I., & Harris, J. S. (1973). The infrared receptors of snakes. *Sci Am, 228*, 94–100.

Grace, M. S., Church, D. R., Kelley, C., & Cooper, T. M. (1999a). The python pit organ: immunocytochemical and imaging analysis of a sensitive natural infrared detector. *Biosens Bioelectron, 14*, 53–59.

Grace, M. S., & Woodward, O. M. (2001). Altered visual experience and acute visual deprivation affect predatory targeting by infrared-imaging Boid snakes. *Brain Research, 919*, 250–258.

Grace, M. S., Woodward, O. M., Church, D. R., & Calisch, G. (2001). Prey targeting by the infrared-imaging snake python: effects of experimental and congenital visual deprivation. *Behav Brain Res, 119*, 23–31.

Gracheva, E. O., Ingolia, N. T., Kelly, Y. M., et al. (2010). Molecular basis of infrared detection by snakes. *Nature, 464*, 1006–1011.

Hartline, P. H. (1999). Infrared sense. In G. Adelman, & B. H. Smith (Eds.), *Encyclopedia of Neuroscience* (pp. 957–959). New York: Elsevier.

Hartline, P. H., Kass, L., & Loop, M. S. (1978). Merging of modalities in the optic tectum: infrared and visual integration in rattlesnakes. *Science, 199*, 1225–1229.

Kardong, K., & Mackessey, G. (1991). The strike behavior of a congenitally blind rattlesnake. *J Herpetol, 25*, 208–211.

Molenaar, G. J. (1992). Anatomy and physiology of infrared sensitivity of snakes. In C. Gans, & E. S. Ulinski (Eds.), *Biology of the Reptilia* (pp. 367–453). Chicago: University of Chicago Press.

Newman, E. A., & Hartline, E. H. (1982). The infrared "vision" of snakes. *Sci. Am, 246*, 116–127.

Pelli, D. G., & Chamberlain., S. C. (1989). The visibility of 350°C blackbody radiation by the shrimp *Rimicaris exoculata* and man. *Nature, 337*, 460–461.

Shen, W. L., Kwon, Y., Adegbola, A. A., Luo, J., Chess, A., & Montell, C. (2011). Function of rhodopsin in temperature discrimination in Drosophila. *Science, 331*, 1333–1336.

Stanford, L. R., Schroeder, D. M., & Hartline, E. H. (1981). The ascending projection of the nucleus of the lateral descending trigeminal tract: a nucleus in the infrared system of the rattlesnake (*Crotalus viridis*). *J Comp Neurol, 201*, 161–174.

Terashima, S., Goris, R. C., & Katsuki, Y. (1970). Structure of warm fiber terminals in the pit membrane of vipers. *J Ultrastruct Res, 31*, 494–506.

Van Dyke, J. U., & Grace, M. S. (2010). The role of thermal contrast in infrared-based predatory targeting behavior by the copperhead, *Agkistrodon contortrix*. *Anim Behav, 79*, 993–999.

Vilceanu, D., & Stucky, C. L. (2010). TRPA1 mediates mechanical currents in the plasma membrane of mouse sensory neurons. *PLoS One, 5*, e12177.

Chapter 41

Electroreceptors and Magnetoreceptors

Timothy C. Tricas and Bruce A. Carlson

Chapter Outline

I. SUMMARY

Many animals have the ability to detect electric and magnetic fields. Although many species respond and orient to magnetic stimuli, only recently were putative vertebrate receptor systems identified. All organisms generate weak electric fields in water, due to an uneven distribution of ions between the interior of the organism and the external aqueous environment. Ampullary electroreceptors are an ancestral vertebrate trait that allows for the passive detection of these electric fields, which is useful for detecting prey, predators and mates. Although ampullary electroreceptors were lost during vertebrate evolution, they subsequently re-evolved several times independently. In two groups of teleost fishes, both ampullary and tuberous electroreceptors evolved, the latter specialized for the detection of actively generated electric organ discharges, or EODs. These fish generate EODs to communicate in the electrosensory domain, as well as actively to sense their environment by detecting distortions in the self-generated EOD. Many physiological mechanisms involved in electrosensory processing are unique.

II. INTRODUCTION

The production of potent shocks by the electric catfishes (*Malapterurus*), eel (*Electrophorus*) and rays (*Torpedo*) to capture prey were reported in antiquity but it was much later that the shock from these animals, and the imperceptible discharges of others, were found to be electrical in nature (Moller, 1995). Further, the production of weak electrical discharges in the millivolt range indicated that weak electrical signals serve functions other than attack or defense (Lissman, 1958; Lissman and Machin, 1958). Because these weak electrical discharges offered a possible system for sensing the environment and communication among conspecifics, scientists sought the identity of the sensory receptors that detected them. Thus, the study of electroreception arose and has since produced much information on electroreceptors, electrogenic organs and their physiology.

Electroreception is an ancient vertebrate sense that occurred in the predecessors of jawless and jawed vertebrates (Bullock et al., 1983). The electrosense is retained in numerous extant taxa (Fig. 41.1) including lampreys, chondrichthyan fishes, bichirs, sturgeon and paddlefishes, lung-fishes, coelacanths and non-anuran amphibians (salamanders and caecilians). Phylogenetic analysis of character traits indicates that the electrosenses of these animals are homologous, reflecting their common phylogenetic origin (Bullock et al., 1983; Bullock and Heiligenberg, 1986). Electroreception, however, was lost in the vast majority of teleosts, the lineage to which most modern bony fishes belong. Most teleosts, together with their sister groups of gars and bowfin, which collectively comprise the Neopterygii, lack an electrosense. Remarkably, only two distantly related lineages of teleost fishes do possess electroreceptors and it is apparent from character analysis that

Cell Physiology Sourcebook. DOI: 10.1016/B978-0-12-387738-3.00041-X

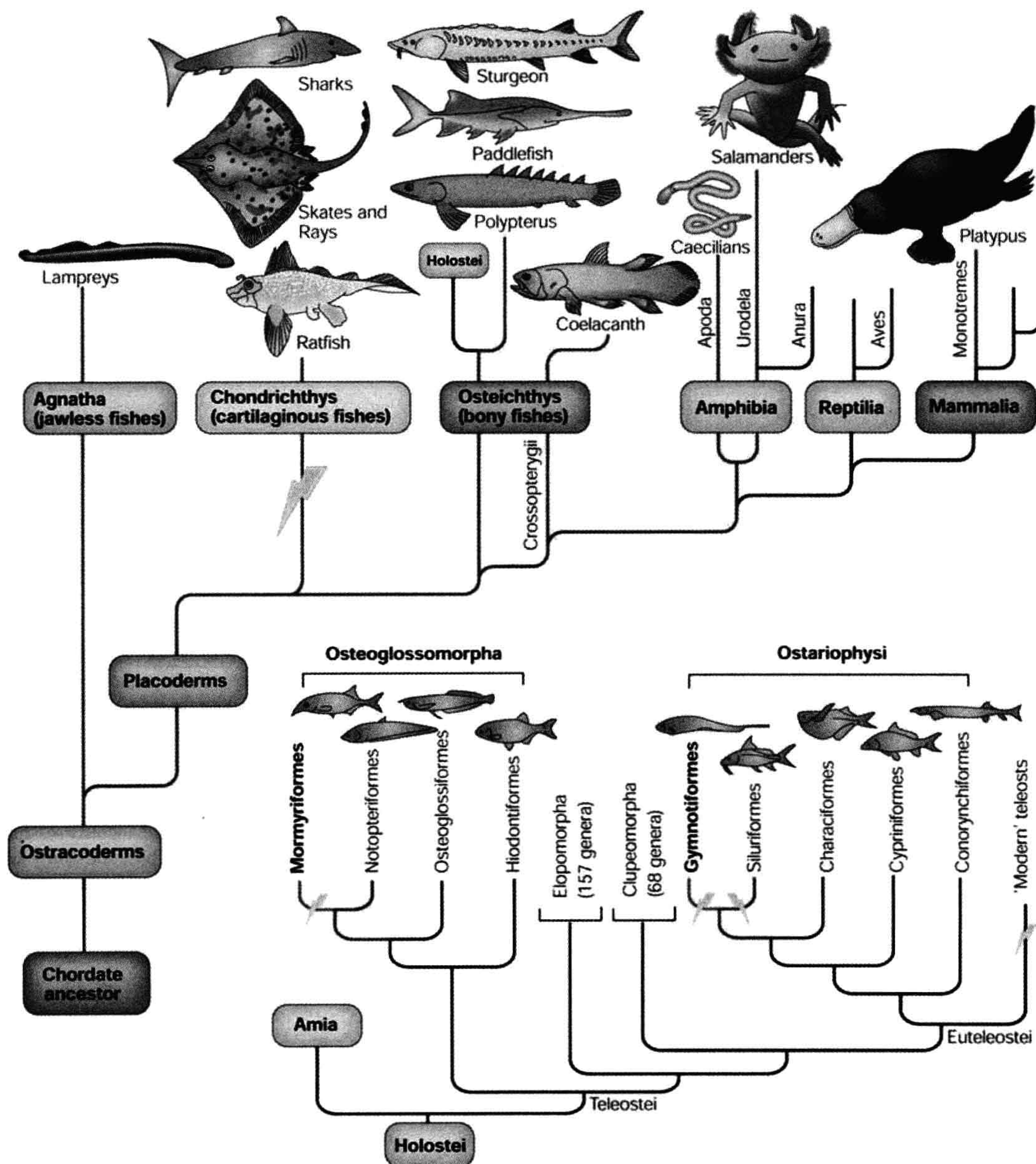


FIGURE 41.1 Cladogram showing the phylogenetic distribution of electroreception and electric organs. Clades with ampullary electroreceptors are indicated by magenta lines, clades with both ampullary and tuberous electroreceptors are indicated by cyan lines (and bold lettering), and clades with electric organs are indicated by lightning bolts. *(Modified from Rose, 2004).*

these have evolved independently (Fig. 41.1). In addition, two species of monotreme mammal, the semiaquatic platypus and the truly terrestrial echidnas, are electroreceptive (Fig. 41.1). Because electrosenses are not present in most other tetrapod lineages, this clearly represents yet another "reinvention" of electroreception.

Electroreceptors of most aquatic vertebrates are classified as either ampullary or tuberous (see Zakon, 1986,

1988). *Ampullary receptors* respond to low-frequency stimuli with best sensitivity to varying electric frequencies between 0.1 and 20 Hz. This range of frequencies includes the detection of standing (DC) bioelectric fields produced by other aquatic organisms that are experienced by a swimming electrosensitive animal as well as those produced by non-living physicochemical sources in aquatic environments. Detection of these extrinsic sources by ampullary receptors is often referred to as electroreception in the *passive mode* (Kalmijn, 1974, 1988). *Tuberous electroreceptors* are tuned to much higher frequencies, with best frequencies in the 0.1–10 kHz range. Tuberous organs are found in fishes possessing weak electric organs of the sort initially described by Lissman (1958) and these receptors have best frequencies that correspond closely to the peak spectral frequency of the discharge of the animal's electric organ. The tuberous organs detect changes in the intensity and temporal pattern of the electric field produced across the body by the electric organ discharge (EOD), whether by the presence of items in the field of objects with different conductances than the water, or by the addition of the electric organ discharges of another individual. Such forms of electrodetection that respond to alterations of the self-generated EOD and the detection of induced electric fields caused by swimming through the Earth's magnetic field are referred to as electroreception in the *active mode* (Kalmijn, 1988). In this chapter, we consider current information on the morphology and physiology of ampullary and tuberous electroreceptors. Space limitations preclude a discussion of the central processing of electrosensory information, which remains one of the most captivating stories in modern neuroethology. The reader is referred to several excellent recent reviews on this topic (Bullock and Heiligenberg, 1986; Bell and Maler, 2005; Kawasaki, 2005).

The ability directly to detect geomagnetic fields is known as *magnetoreception* and the ability to sense and respond to magnetic stimuli is known for a number of animal groups and bacteria (for reviews see Tenforde, 1989; Wiltschko and Wiltschko, 1995). These studies are primarily behavioral, with incomplete information on magnetoreceptor organs and receptors in most taxa. The direct identification of a magnetoreceptor cell has many technical challenges because direct magnetoreception is believed to be associated with localized deposits of magnetite crystals (Fe_3O_4) which are extremely small, easily contaminated, degrade easily in preserved tissues and are difficult to verify. Localized magnetite domains are described in tissues of bees, salmon, tuna, turtles, pigeons, dolphins, humans and many other species (Wiltschko and Wiltschko, 1995). In several birds and one species of fish, candidate magnetoreceptor cells were identified in close association with small rostral branches of the trigeminal nerve. In the homing pigeon, superparamagnetic crystals occur along the surface of afferent nerve terminals of the somatosensory branch that innervates the upper beak (Fleissner et al., 2003) and this arrangement is similar in other migratory and non-migratory species (Falkenberg et al., 2010). Neurophysiology experiments show that fast adapting trigeminal neurons in bobolinks respond to changes in applied magnetic fields as low as 30–50 nT, whereas slow adapting units respond as amplitude detectors (Beason and Semm, 1987; Semm and Beason, 1990). Potential receptor cells that contain single-domain magnetite exist in the lamina propria of the rainbow trout olfactory rosette and are in close association with endings of a rostral branch of the trigeminal nerve that penetrates the olfactory epithelium (Walker et al., 1997; Diebel et al., 2000). Single cell neurophysiology bench experiments show that units respond to rapid changes in applied magnetic fields (Walker et al., 1997). Indirect magnetoreception is also possible in some electroreceptive taxa via the detection of electric fields induced by an animal's movement through a geomagnetic field or drifting in an oceanic current (see discussion later). Evidence for chemical magnetoreception that involves magnetic actions on correlated spin states of radical ions is also proposed for the bird visual system (Ritz et al., 2000) but is not covered here. For recent reviews of the waning magnetoreception controversy, readers are referred to Johnsen and Lohmann (2005) and Walker et al. (2007).

III. AMPULLARY ELECTRORECEPTORS

The wide phylogenetic distribution of ampullary electroreceptors among extant vertebrate taxa indicates that this class of electroreceptor has served important biological functions for hundreds of millions of years and has subsequently "re-evolved" several times (see Fig. 41.1). With the exception of weakly-electric fishes that also possess tuberous electroreceptors, most species with ampullary electroreceptors lack electric organs. Thus, behaviorally relevant ampullary stimuli are thought to originate primarily from extrinsic sources. Ampullary electroreceptors are known to be important for the detection of prey (Kalmijn, 1971; Tricas, 1982; Wilkens et al., 2001), mates (Tricas et al., 1995), potential predators (Sisneros et al., 1998) and orientation to local inanimate electric fields (Kalmijn, 1982; Pals et al., 1982). In addition, the ampullary electroreceptor system is theoretically capable of mediating navigation by detecting electric fields induced by movement of the animal through the Earth's magnetic field (Kalmijn, 1974, 1988; Paulin, 1995), which would represent a form of electroreception in the *active mode*.

IIIA. Development and Morphology

Information on the ontogeny and development of electroreceptors is based largely on descriptive studies and we

refer readers to the excellent recent discussion provided by Northcutt (2005). Ampullary electroreceptor cells in non-teleost aquatic vertebrates develop from ampullary primordia that are derived from the neural crest in the shark (Freitas et al., 2006), associated with the lateral line placodes and sensory ridges (Northcutt et al., 1994, Gibbs and Northcutt, 2004) and possess either a kinocilium, microvilli or both. In teleosts, it remains to be experimentally demonstrated whether tuberous electroreceptors arise from induction in the general ectoderm (Vischer, 1995) or from lateral line placodes (Northcutt, 2003). In contrast, the electrosense of monotreme mammals evolved as a specialization of the trigeminal nerve associated with dermal mucus glands of the snout (Gregory et al., 1989; Pettigrew, 1999).

The lampreys possess an electroreceptor known as an *end bud* that differs considerably in morphology from the ampullary electroreceptors of other fishes (Ronan and Bodznick, 1986). Each end bud consists of numerous support cells and three to 25 sensory cells in the epidermis that are in direct contact with the surrounding water. Individual receptor cells have numerous small microvilli on the apical surface but lack a kinocilium. Small groups or lines of end buds are distributed over the head and body surface with multiple buds being innervated by a single sensory lateral line nerve fiber (Bodznick and Preston, 1983; Ronan, 1986). The excitation of end bud electroreceptors by cathodal (−) stimuli indicates a possibly similar transduction mechanism as the ampullary receptors of more derived non-teleosts (see discussion below). However, it is not known whether end buds represent the ancestral electroreceptor state or whether they are a derived condition unique to the lampreys.

Elasmobranch fishes (rays, skates and sharks) and rat fishes (Fields et al., 1993) possess ampullary electroreceptor organs of a similar morphology. In elasmobranch fishes, the electroreceptive unit is a highly specialized structure known as an *ampulla of Lorenzini* (Fig. 41.2). The ampulla proper in the marine skate is composed of multiple *alveolar sacs* or diverticulae which share a common lumen (Waltman, 1966). The apex of each ampulla chamber is connected by a highly insulated *marginal zone* to a single subdermal *canal*, which is approximately 1 mm in diameter and terminates as a small epidermal pore. The canal wall is 1−2 μm thick and composed of two layers of flattened epithelial cells, which are separated by a basement membrane to which the lumenal layer is also united by tight junctions. Both the canal lumen and the ampullary chambers are filled with a K^+-enriched, mucopolysaccharide, jelly-like matrix that is secreted by the superficial layer. While the resistivity of the gel (25 ohm cm) is similar to that of sea water and has similar responses as seawater to standing DC fields, recent work shows that the electrical properties of the gel exhibit reduced electrical admittance to varying electric stimuli. In combination with long canals

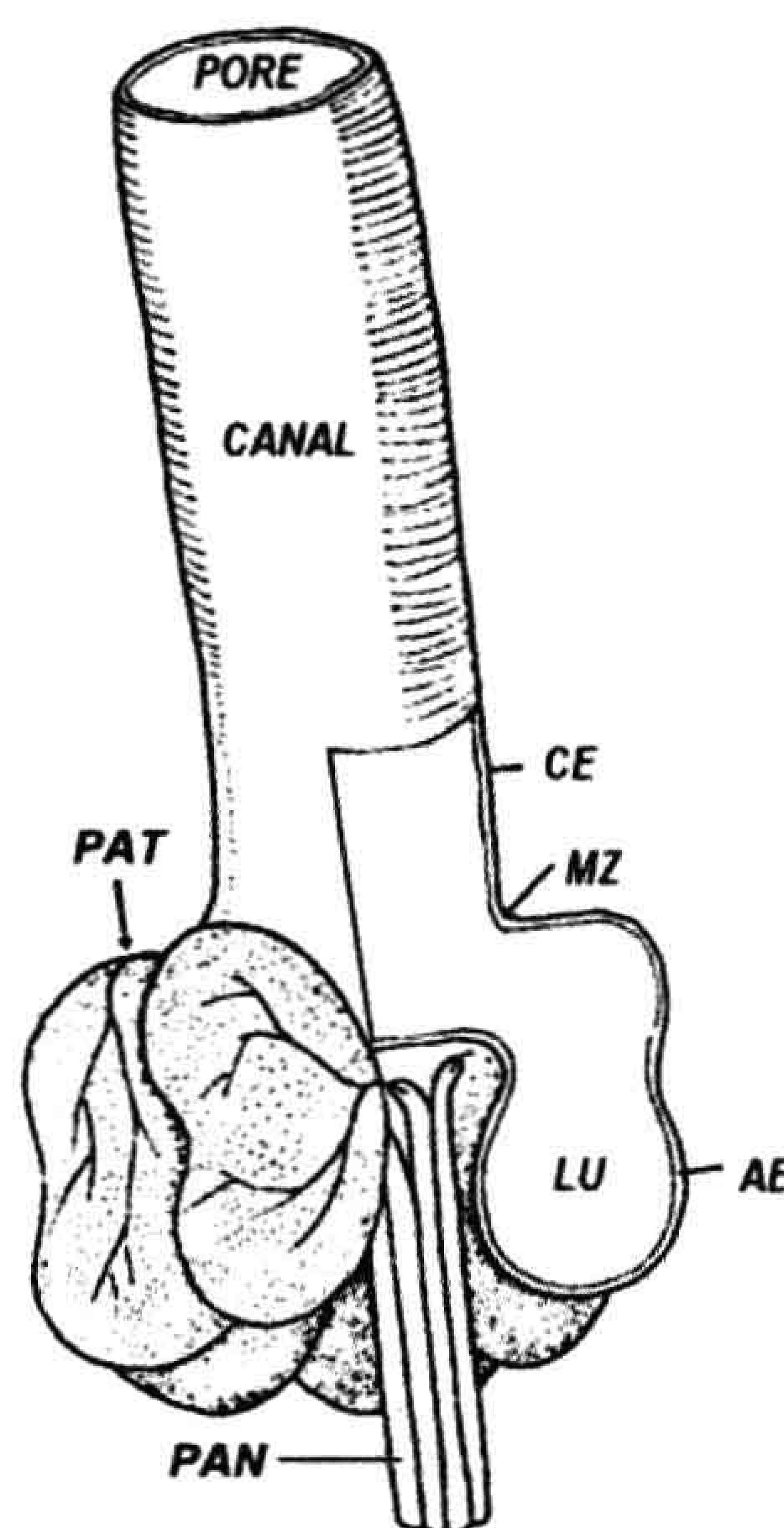


FIGURE 41.2 Ampulla of Lorenzini from the marine skate, *Raja*. The ampulla proper consists of multiple alveoli formed by the alveolar epithelium (AE). A high-resistance marginal zone (MZ) connects the sensory walls of the ampulla to the high-resistance canal epithelium (CE), which projects to the surface of the skin and terminates as a small pore confluent with the surrounding water. The ampulla lumen (LU) and canal are filled with a gel that provides electric conductivity along the length of the canal. Myelinated primary afferent neurons (PANs) innervate the base of the ampullae and their unmyelinated primary afferent terminals (PATs) receive chemical excitation from the basal region of the sensory cells in the epithelial layer. *(Modified from Waltmann, 1966, with permission).*

of narrow 1 mm diameter, the high resistance ampulla−gel−canal complex promotes detection of differences along the length of the canal rather than direct isopotential contact between the ampullary electroreceptors and seawater at the location of the surface pore (Brown et al., 2002, 2005). The sensory epithelium within the alveolus is composed of two cell types, which form a monolayer that is approximately 15 μm thick (Fig. 41.3). The vast majority of the alveolar surface is formed by accessory cells that are highly resistive to transmembrane currents and are bound together by tight junctions that prevent ionic leakage across the lumenal and basal surfaces of the epithelium. Interspersed among the accessory cells are flask-shaped receptor cells (thought to be modified hair cells), which possess a single kinocilium on the apical surface and lack microvilli. This physical arrangement results in only a small fraction of the receptor cell surface being exposed to the ampullary chamber.

The basal membrane surface of the receptor cell forms a ridge seated in a postsynaptic invagination that is separated by a distance of 100−200 Å (Waltmann, 1966).

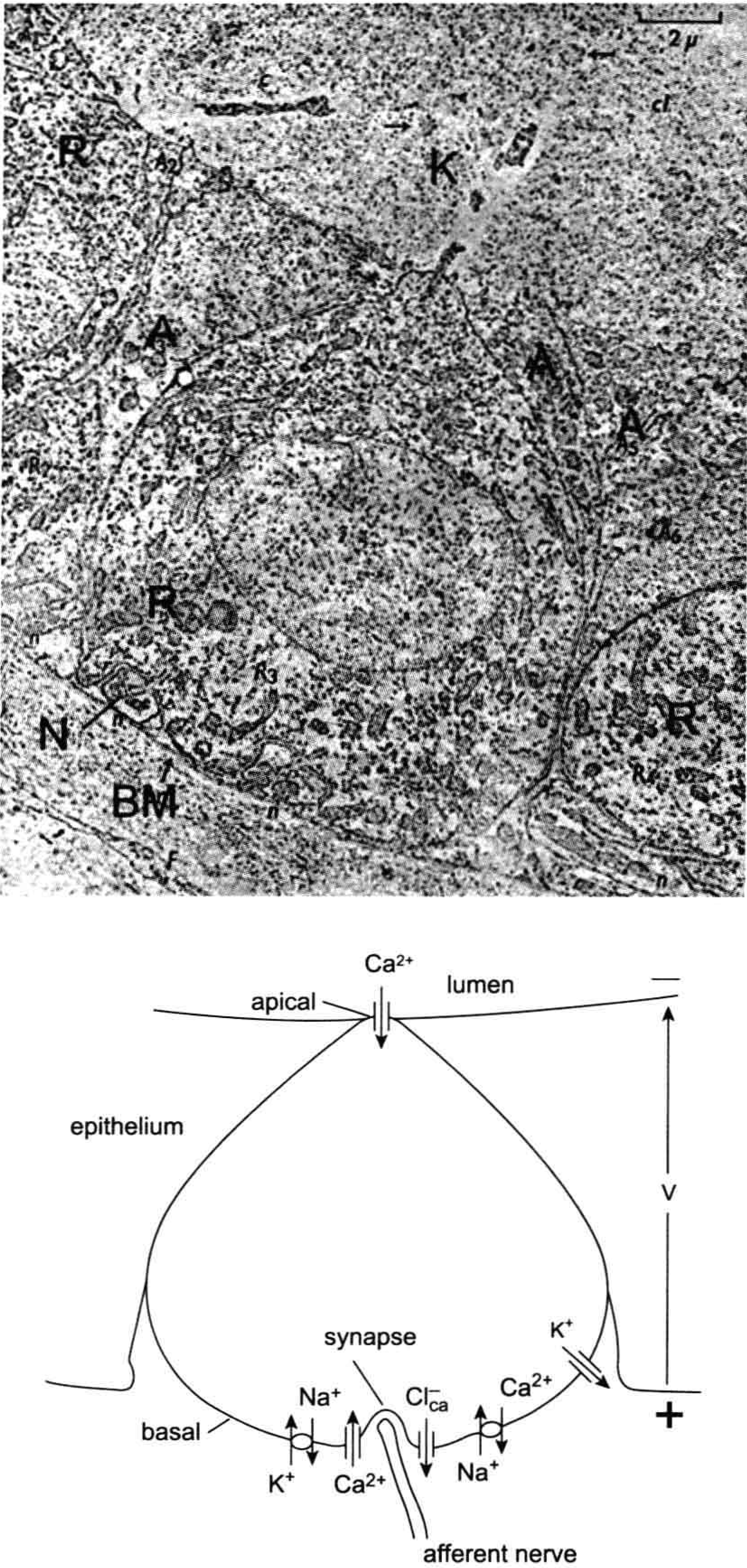


FIGURE 41.3 Receptor cell of the ampulla of Lorenzini in the skate, *Raja*. Top figure is photomicrograph of flask-shaped receptor cells (R) and adjacent accessory cells (A) that are united by tight junctions to form the alveolar epithelium. A single kinocilium (K) projects from each receptor cell into the lumen and, together with a small portion of the apical surface, is exposed to electric stimuli. Primary afferent neurons (N) innervate the basal portion of the receptors. The basement membrane (BM) is located beneath the sensory epithelium (*modified from Waltmann, 1966.*). Bottom figure shows ion channels and transporters involved in steady state conductance and sensory transduction. The excitable region of the cell is the apical membrane that has a partially activated inward bias current. The apical conductance is thought to work with oscillations created by exchangers and channels in the basal membrane that produce regular afferent discharges at the postsynaptic neuron. A weak electric stimulus in the ampulla that is more negative than the potential at the outside basal surface results in excitation of the cell and increased discharge potential in the afferent nerve. *(Top figure from Waltmann, 1966 with permission from Wiley Press and bottom figure modified from Lu and Fishman, 1994 with permission from Elsevier Limited, Kidlington, Oxford.)*

A *synaptic ribbon* about 250 Å wide and 2 μm in length is located within the presynaptic ridge. A single layer of synaptic vesicles covers the ribbon and exocytotic release of chemical neurotransmitter contained within these vesicles depolarizes the postsynaptic membrane of the innervating fibers of the anterior lateral line nerves. Unlike the hair cell receptors of the mechanosensory lateral line and octaval systems, all ampullary electroreceptors, both primitive and derived, lack efferent innervation.

Chondrichthyan fishes typically possess hundreds (or thousands) of ampullae that are associated in specific *ampullary clusters* associated with specific branches of the anterior lateral line nerve and are often closely bound by a dense matrix of connective tissue (Fig. 41.4A). From these clusters the subdermal canals radiate omnidirectionally and terminate in surface pores on the head and on the enlarged pectoral disk of batoids (Rivera-Vicente et al., 2011). The multiple orientations of the receptor canals and the copious distribution of the ampullary pores over the cephalic surface provide an extensive array of receptors with a high degree of spatial resolution. The morphology of the ampullary electroreceptors in freshwater elasmobranchs is thought to reflect sensory adaptations to their highly resistive environment (Kalmijn, 1974; Raschi and Mackanos, 1989). The freshwater rays, *Potamotrygon* and *Dasyatis garouaensis*, have a hypertrophied, thick epidermis that functions to increase transcutaneous electrical resistance. The ampullary electroreceptors are greatly reduced in size and are referred to as *miniampullae* or *microampullae*, which are distributed individually across the skin rather than in clusters and which have very short canals (about 0.3–2.1 mm long) that traverse the integument.

The anatomy and organization of ampullary electroreceptor organs in other non-teleost fishes and amphibians are generally similar to those of elasmobranch fishes, with which they are believed to be homologous. Ampullary electroreceptors in chondrostean (sturgeon and paddlefishes), cladistian (bichirs) and dipnoan fishes (lungfishes) share in most respects a similar morphology among alveoli, canals and ampullary pores. However, the ampullary organs in these freshwater fishes are most commonly arranged as single units or small groups (as opposed to large clusters) and have very short (generally <0.25 mm) and small diameter (generally <0.14 mm) canals. The abundance of receptors are distributed in the head region, with the exception of the lungfishes, in which there are single ampullary electroreceptors on the head and small groups consisting of three to five ampullae scattered widely over the body (Pfeiffer, 1968). Ampullary electroreceptors of the head are innervated by a ramus of the anterior lateral line cranial nerve, while those on the body are innervated by

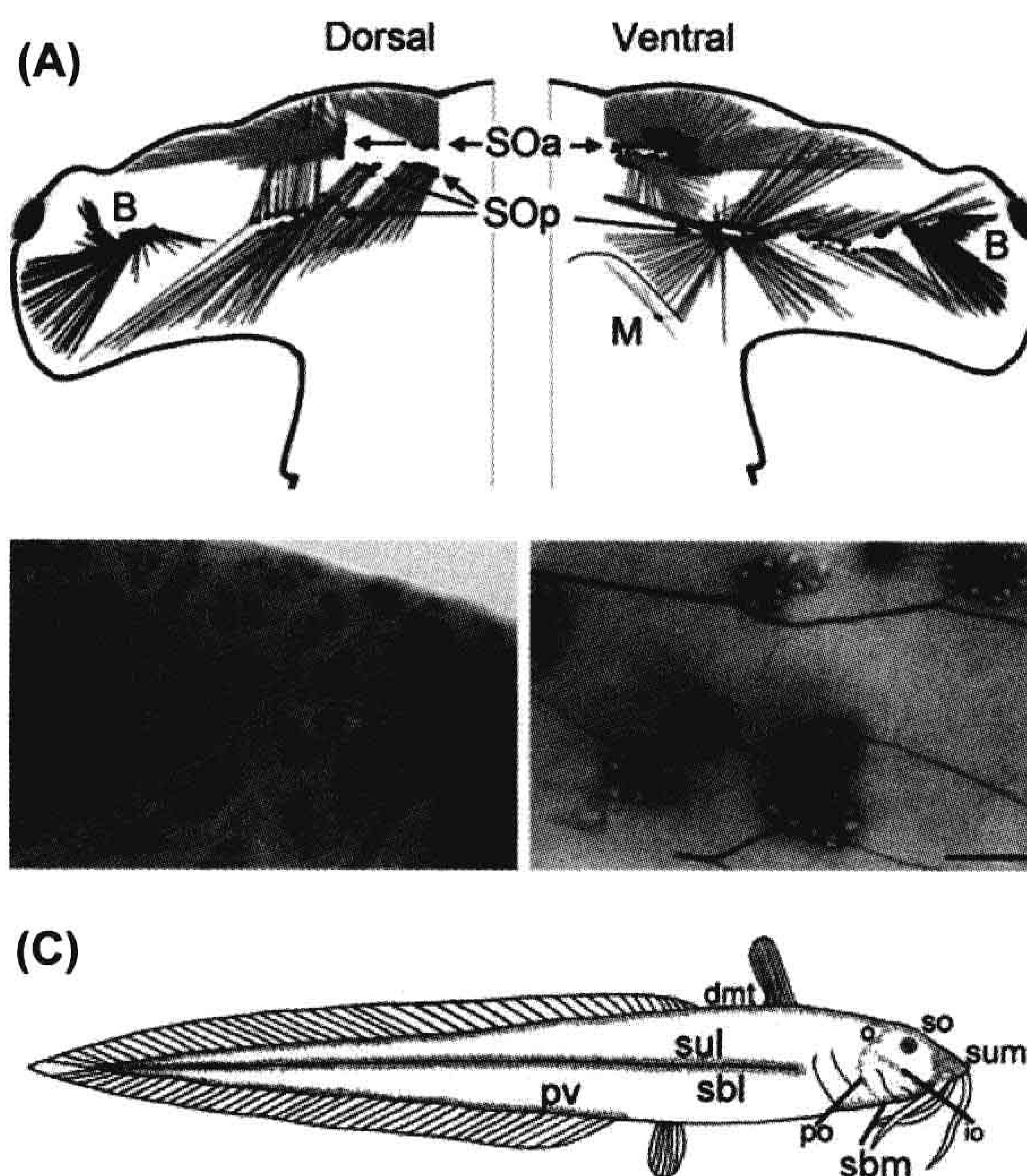


FIGURE 41.4 Distribution of ampullary electroreceptor canal pores in fishes. (A) The scalloped hammerhead shark, *Sphyrna lewini*, has more than 2800 ampullary pores on the dorsal and ventral surfaces of head many of which have long canals that project to the sensory ampullae. Ampullae (small black dots) are grouped into clusters that are associated with branches of the anterior lateral line nerve. Canals and associated clusters are B = buccal (blue), SOa = superficial ophthalmic anterior (green), SOp = superficial ophthalmic posterior (red), M = mandibular nerve (light blue). *(From Rivera-Vicente et al., 2011, with permission from PLoS One.)* (B) Ampullae in the paddlefish, *Polyodon spathula*, have transdermal pores that occur in small clusters. Left photo shows arrangement of pores across the ventral surface of the rostrum. Scale bar = 2 mm. Right photo is a cleared and stained preparation that shows innervation of primary afferent fibers. Scale bar = 1 mm. *(From Wilkens et al., 2002 with permission from Elsevier Limited, Kidlington, Oxford.)* (C) Ampullary pore distributions in the estuarine catfish, *Euristhmus lepturus* (Plotosidae). Each spot represents a single ampullary pore or cluster. Pore distributions are associated with nerve branches: dmt = dorsal midtrunkline, io = infraorbital, o = otic, po = preopercular, pv = posterior ventral, sbl = sublateralis, sbm = submandibular, so = supraorbital, sul = supralateralis and sum = supramandibular. *(From Whitehead et al., 2009, Copyright Springer-Verlag, Inc. Reprinted with permission.)*

a recurrent branch of the anterior lateral line nerve complex. In the bichir, *Polypterus* (Cladistia), there are about 1000 ampullae on the head region (Northcutt, 1986). In sturgeon, the electroreceptor organs are arranged in about 1300 clusters of about 20 ampullae each whereas, in the related paddlefish, *Polyodon*, there are 50 000 to 75 000 ampullae on the elongate rostral "paddle" (see Fig. 41.4B) which are also arranged in small clusters (Wilkens et al., 2001; Jørgensen, 2005). In the marine coelacanth, *Latimeria*, the "rostral organ" located between the eye and olfactory organ represents a complex of three principal canals that end centrally in small sensory crypts (Millot and Anthony, 1956) and is thought to be a homologous structure to the elasmobranch ampullae of Lorenzini (Bemis and Heatherington, 1982).

There is significant variability also in ampullary receptor cell morphology, particularly at the level of the apical membrane (Jørgensen, 2005). Ampullary receptor cells in bichirs and reedfish possess both a single kinocilium and 8–10 microvilli, whereas those of chondrostean sturgeons and paddlefish possess only a kinocilium as in the elasmobranchs. The receptor cells in lungfishes lack a kinocilium, but possess microvilli as in the jawless lampreys. The receptor cells of the urodele amphibians (salamanders) are highly variable in morphology, whereas the tropical subterranean gymnophion have only microvilli. The ancestral condition for non-teleost electroreceptors is generally thought to be one possessing both kinocilium and microvilli (like other hair cells), but the reason for the loss of either kinocilium or microvilli in the various taxa and possible physiological ramifications is not known. These receptors also possess synaptic ribbons in the basal cell region, although some variation in synaptic morphology occurs.

Ampullary canals of marine teleost species are often long as in marine elasmobranchs, although morphological differences associated with habitat may occur within species (Whitehead et al., 2000). Ampullary pores are concentrated on the head and may also occur across the body (see Fig. 41.4C). The fine structure of ampullary electroreceptors in freshwater teleost fishes closely resembles that of the freshwater elasmobranchs (Szabo, 1974) (Fig. 41.5). These receptors, however, are not homologous to non-teleost receptors rather they represent a case of parallel homoplasy, presumably the result of developmental and functional constraints necessary for the detection of extrinsic electric fields and their derivation from the hair cell receptors of the lateral line. The organs are located at the level of the basement membrane of the epidermis with a very short canal (usually about 200 μm)

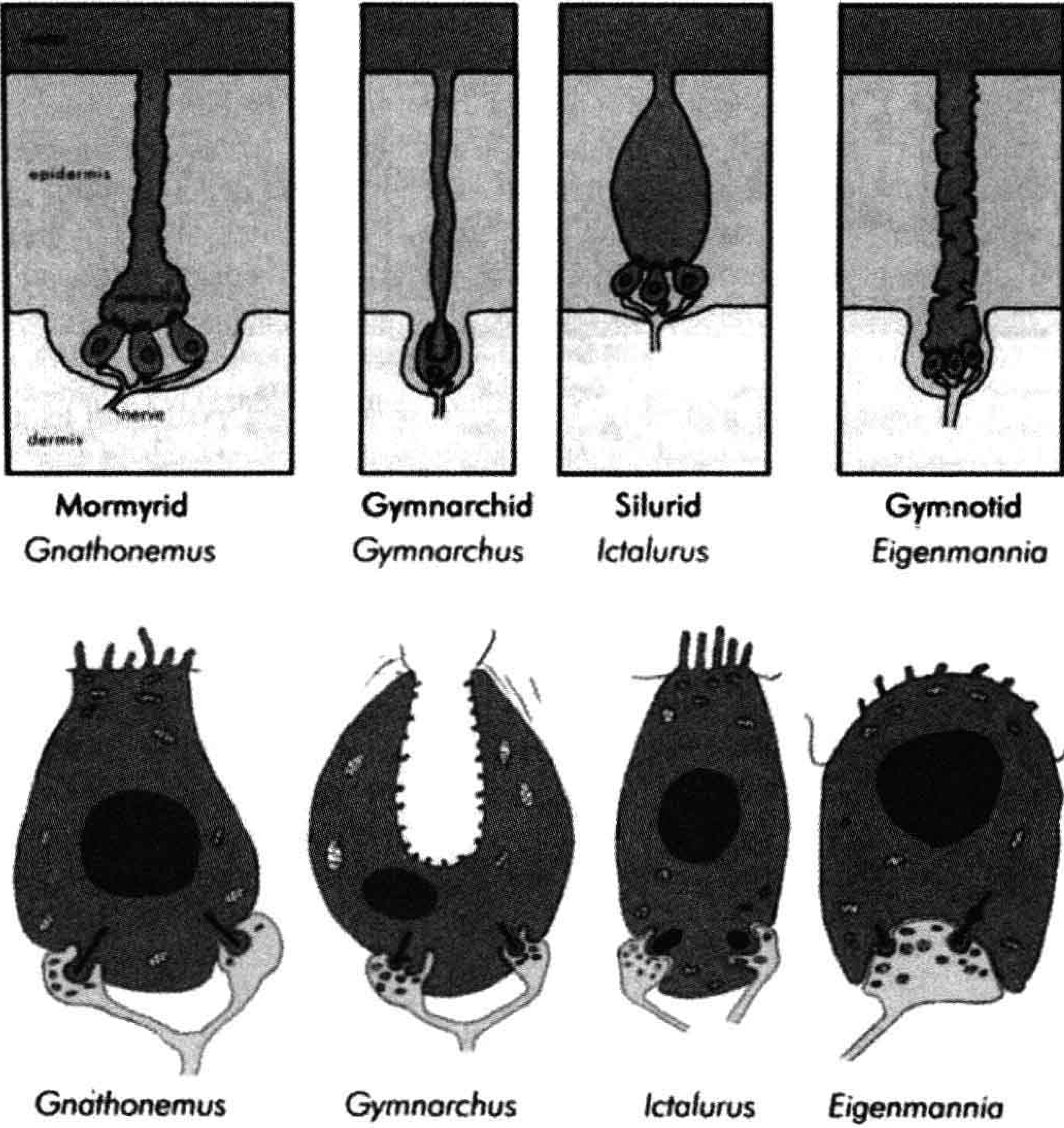


FIGURE 41.5 Diagrammatic representation of ampullary receptor organs in four families of freshwater teleosts. Top row shows cross-section of ampulla pores in contact with water, short canals and the receptor epithelium in the epidermis. Bottom row shows representative differences in receptor morphology and innervation. *(Modified from Jørgensen, 2005.)*

connected to a pore on the skin surface. The cells of the inner walls of the ampulla and canal consist of three to five layers of flattened epithelial cells connected by tight junctions preventing current leakage across the canal wall and the canal is filled with a conductive jelly that provides a low-resistance pathway through the lumen (Pfeiffer, 1968). The parallelism of ampullary electroreceptors among both ancient and derived groups is further demonstrated in the few existing species of electroreceptive marine teleosts. In the marine catfish, *Plotosus*, the ampullary canals are elongated, forming long subdermal tubules terminating centrally in alveolar clusters strikingly similar to the ampullae of Lorenzini in marine elasmobranchs (Obara, 1976). These teleosts can detect electric field stimuli at 80 μV/cm (Kalmijn, 1988), which is much more sensitive than the ampullary system of freshwater species.

The ampullary receptor cells of teleosts are located in the base of the alveolus and are connected to the supporting cells via tight junctions, with only a small portion of their apical face exposed to the lumen. Teleost electroreceptor cells generally possess only microvilli with the exception of the African knifefish *Xenomystus* (Notopteridae) that shows a single short cilium on the electroreceptor (Jørgensen, 2005). The synaptic structure of receptors in more recently derived fishes is similar to those of the more primitive species, in which synaptic ribbons and presynaptic membrane evaginations are surrounded by a prominent postsynaptic "cup" (Szabo, 1974). Unlike most non-teleost ampullary electroreceptor cells, ampullary receptors in teleosts may be innervated by either anterior or posterior lateral line nerves, depending upon location on the body surface. Like most other non-teleost fishes, the ampullae are distributed widely over the head, but differ in that they are usually distributed across the trunk in distinct patterns that are species-specific.

IIIB. Physiology

For marine elasmobranches, such as the thornback ray, *Platyrhinoides*, the resistance of the skin is moderately higher than that of the body tissues (Kalmijn, 1974). When the body encounters a weak external dipole source, such as that produced by small prey, penetration of the electric field into the body is limited and makes the voltage drop across the skin in the region of the pore the effective stimulus. In contrast, external uniform fields, such as those produced by geomagnetic induction in streaming ocean currents, invade the body along the length of the canal and detection may be enhanced by long canal length under these conditions. In freshwater elasmobranches, such as *Potamotrygon*, the resistance of the skin is relatively high compared to marine species and the resistance of the internal tissues is relatively low, presumably as a result of osmoregulatory constraints. In these fishes, the internal environment is essentially at a common reference potential. Individual ampullae detect the transepidermal voltage drop between an applied external field and the internal tissue reference. Hence, most strictly freshwater elasmobranchs, as well as most other ampullary-bearing taxa, have short ampullary canals that cross only the dermis.

Technical challenges make it very difficult to obtain detailed intracellular single-cell recordings from ampullary electroreceptor cells. The membrane biophysics of ampullary receptor excitation for non-teleosts is best described for the skate, *Raja*, in which the voltage stimulus could be clamped or controlled near the sensory epithelium of the ampulla (see Obara and Bennett, 1972; Bennett and Clusin, 1978; Lu and Fishman, 1994, 1995a,b). The excitability of the electroreceptor cell results from voltage-gated Ca^{2+} channels located in the apical membrane (see Fig. 41.4). In unstimulated electroreceptors, there exists a steady-state inward current by L-type Ca^{2+}-channels. The basal membrane has a net outward current that involves K^+ and Ca^{2+}-dependent Cl^- channels that produce an oscillation thought to drive presynaptic neurotransmitter release. In addition, intracellular Ca^{2+} concentrations and the basal membrane voltage are tightly regulated and maintained by Na^+-K^+ and Na^+-Ca^{2+} ion transporters (Lu and Fishman, 1995b). Electric stimuli applied to the ampulla lumen that are more negative than those at the basal outside surface will depolarize the apical membrane and promote additional inward Ca^{2+} conductance. This results in a net outward current across the basal surface of the cell, an influx of Ca^{2+} that promotes presynaptic neurotransmitter release and subsequent depolarization of the postsynaptic afferent fiber. Weak anodal stimuli applied to the lumen decrease apical Ca^{2+} conductance and neurotransmitter release. This model is supported by electric models and empirical measurements (Fig. 41.6A). Voltage clamp experiments provide data on complex admittance (the reciprocal of impedance) at different frequencies and indicate the real part of the admittance at low frequencies is negative and is consistent with inward current at the apical membrane (Lu and Fishman, 1994).

The membrane biophysics of the teleost ampullary electroreceptor also involves several ion channels that also include voltage-sensitive Ca^{2+} channels, but the excitable membrane is at the basal surface of the receptor cell. In the marine catfish (*Plotosus*) and likely in other teleosts, the electroreceptors are excited by anodal potentials in the ampulla chamber near the low resistance and passive apical membrane. Voltage and current clamp experiments on isolated ampullae reveal the existence of an electrogenic Na^+-K^+ pump in the basal receptor membrane (Sugawara, 1989a). This provides a steady outward bias current that activates a sustained non-inactivating inward Ca^{2+} L-type

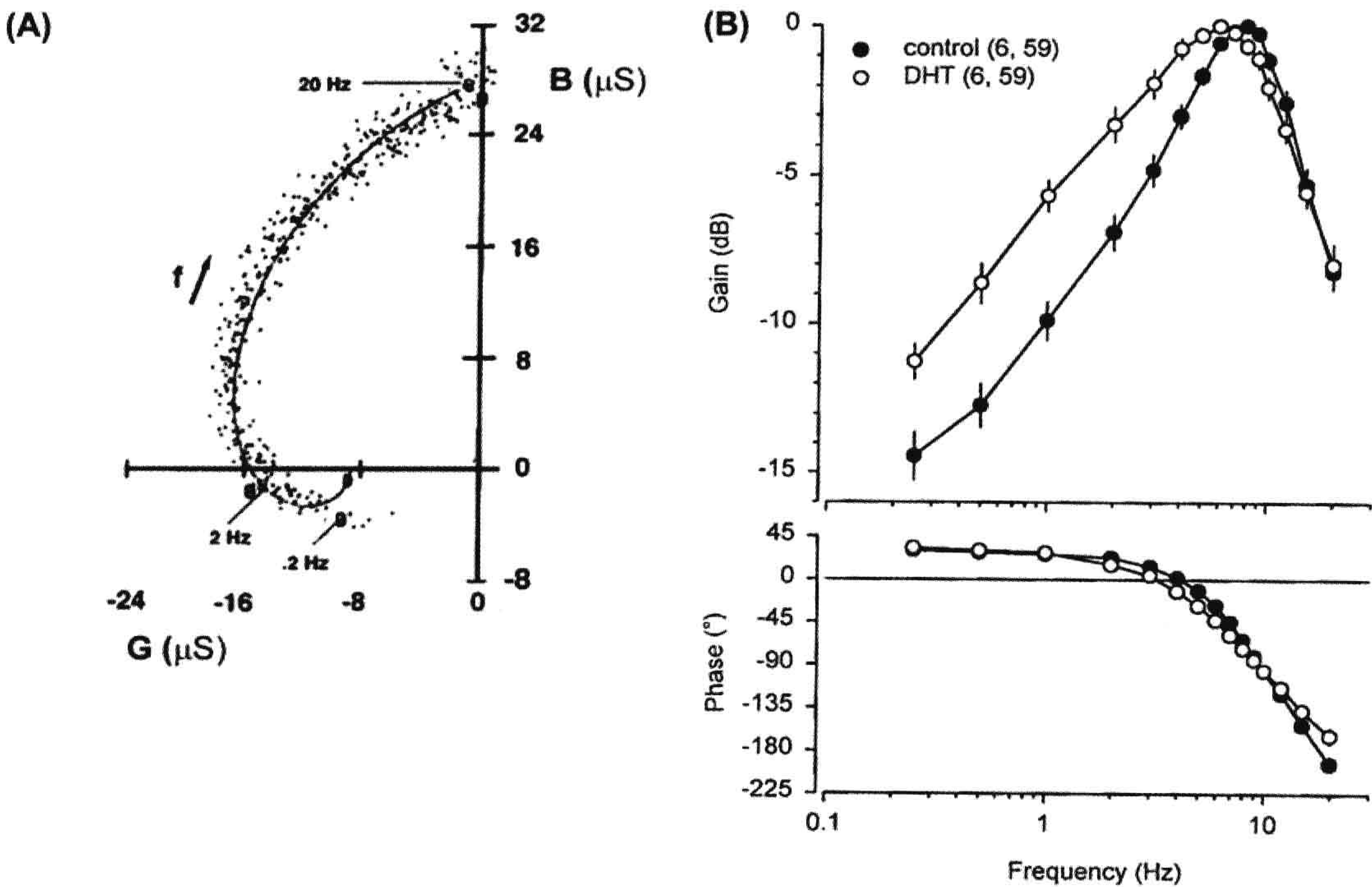


FIGURE 41.6 Frequency response of ampullary receptors and primary afferent neurons in elasmobranch fishes. (A) Locus of the admittance function of complex frequency as determined by voltage clamp experiments on an ampullary organ of the skate, *Raja*. The locus of 400 data point at low frequencies from 0.05 to 20 Hz are plotted in the complex plane [*B(f)* vs *G(f)*] and fall in the left half plane. This describes a negative conductance in this low frequency range. Also, note that the locus plot intercepts the real axis (B(uS) = 0) at 2.1 Hz which indicates solely negative (inward) conductance. *(Reproduced from Lu and Fishman, 1994 with permission from Elsevier Limited, Kidlington, Oxford.)* (B) Bode plot and phase diagram for frequency response of electrosensory primary afferent neurons recorded from adult male Atlantic stingrays, *D. sabina*, after DHT implants. Peak frequency sensitivity decreased from 7–8 Hz to 5–6 Hz for DHT-treated fish and also the low frequency response. The numbers of animals and electrosensory primary afferent neurons tested are indicated in parentheses. Data are plotted as mean and SE. *(Modified from Sisneros and Tricas, 2000.)*

current that maintains the tonic release of neurotransmitter and the regular resting discharge firing rate of afferent neurons (Sugawara, 1989b). This Ca^{2+} conductance is enhanced by an anodal (positive) stimulus in the ampulla to create a superimposed fast Ca^{2+} N-type current that initiates an outward transient Ca^{2+}-gated K current. The conductances are inhibited by phasic cathodal stimuli in the ampullary lumen (Bennett, 1971a; Bennett and Obara, 1986). Primary afferents that innervate ampullary electroreceptors in freshwater fish show regular resting discharges that are excited by anodal stimuli at the lumen and have a dynamic range of ± 1 mV in *Gymnotus* (Bennett, 1968) with thresholds that can range from tens to hundreds of microvolts (see Zakon, 1986). The low frequency response of primary afferents in the paddle fish are efficient detectors of bioelectric stimuli from single plankton (Wilkens, 2004) and have proved an intriguing model for detection of signals in noisy environments and sensory oscillators (Neiman and Russell, 2004; Neiman et al., 2007).

The high sensitivity of electrosensory primary afferent neurons was first established for the elasmobranch at a voltage gradient of about 1 μV/cm (Murray, 1962) and has recently been extended to near 20 nV/cm applied to ampullae with long canals by Tricas and New (1998). The neural response to a prolonged, constant current field is sustained for a duration of a few seconds before it begins to adapt back to the resting discharge rate. Prolonged, constant stimulation results in a return to resting levels and accommodation of the receptor, resulting in no change in the overall sensitivity of the receptor (Bodznick et al., 1993). Work on a variety of species with both non-teleost and derived ampullary electrosenses shows a maximum response to sinusoidal electric fields at frequencies of 1–10 Hz (Andrianov et al., 1984; Montgomery, 1984b; Peters and Evers, 1985; New, 1990; Tricas and New, 1998). Sensitivities of primary afferent fibers innervating ampullary electroreceptors to a sinusoidal uniform field are 0.9 spikes per second per μV/cm for the little skate, *Raja*

erinacea (Montgomery and Bodznick, 1993), four spikes per second per μV/cm for the thornback guitarfish, *Platyrhinoidis triserata* (Montgomery, 1984a) and 24 spikes per second per μV/cm average for the round stingray, *Urolophus halleri* (Tricas and New, 1998). The frequency response of primary afferents neurons were shown in the stingray *Dasyatis sabina* to vary across the reproductive season in association with natural surges in serum androgens (Sisneros and Tricas, 2000). In wild males, there was an increased sensitivity to low frequency stimuli from 0.01 to 4 Hz. Experimental implants of dihydrotestosterone induced a similar increased sensitivity in the band of 0.5–2 Hz. These androgen dependent shifts in sensitivity may serve to enhance the detection of potential female mates or other reproductive-related behaviors.

Recordings from the lateral line nerve in behaving elasmobranchs and bench preps show that the regular discharge of primary afferent neurons is modulated in rhythmic bursts that are in phase with the ventilatory movements of the fish. This reafferent neuromodulation is explained by the standing (DC) bioelectric field that arises from the differential distribution of ionic charges in the animal which, in the skate, is a result of both diffusion potentials and osmoregulatory ion pumping at the gills (Bodznick et al., 1992). The modulation of this standing field occurs as the animal opens and closes the mouth, gills or spiracles during the ventilatory cycle, which changes the resistance pathway between the animal's internal tissues and surrounding seawater. The resultant transcutaneous potential is the source of electrosensory self-stimulation or *ventilatory reafference* (Montgomery, 1984b), by which a change in the internal potential of the animal (and basal regions of the ampullary receptor cells) proportionately modulates the regular discharge of all primary afferent neurons. Thus, electrosensory receptors and primary afferents exhibit common mode noise and also a central adaptive filter in the hindbrain circuit, which has important implications for noise rejection and central processing of electrosensory information (see Bodznick and Montgomery, 2005).

IV. TUBEROUS ELECTRORECEPTORS

Tuberous electroreceptors have only been found in teleost fish, though they have evolved multiple times independently (Bullock et al., 1983). They are found only in fish that also have ampullary electroreceptors and the phylogenetic distribution of ampullary and tuberous organs suggest that tuberous organs are evolutionarily derived from ampullary organs (see Fig. 41.1). Within the Osteoglossomorpha, both ampullary and tuberous organs are found within the African Mormyriformes (Zakon, 1986). However, within the closely related Notopteridae, the African subfamily Xenomystinae has only ampullary organs, whereas the Asian subfamily Notopterinae lacks electroreceptors altogether (Braford, 1986). Within the Ostariophysi, the South American Gymnotiformes (knifefishes) possess both ampullary and tuberous organs (Zakon, 1986). The closely related Siluriformes (catfish) generally possess only ampullary organs, although tuberous organs have been described in one species. Despite the independent origins of tuberous electrosensory systems, there are many remarkable similarities in receptor morphology and physiology (Zakon, 1986; Jørgensen, 2005), as well as in the anatomy and physiology of the central sensory systems (Finger et al., 1986).

In general, tuberous electroreceptors are found in fish that have specialized electric organs for actively generating electric fields (see Fig. 41.1), underscoring their functional role in the detection of these fields. However, there is one exceptional case, the blind catfish *Pseudocetopsis* spp., which does not appear actively to generate electric fields and yet has both ampullary and tuberous electroreceptors (Andres et al., 1988). In all other cases, tuberous electroreceptors are tuned to the power spectrum of the species-specific electric organ discharge, or EOD (Carlson, 2006). EODs can be categorized as "wave-type" or "pulse-type": for wave-type EODs, the duration of each pulse is equal to the interval between pulses, resulting in a quasi-sinusoidal, continuous electric field; for pulse-type EODs, the duration of each pulse is much shorter than the intervals between pulses, resulting in discrete pulses of electricity. Both pulse- and wave-type species are found within the African Mormyriformes and South American Gymnotiformes (Fig. 41.7). EODs serve two functions (Fig. 41.8): communication, which is based on detecting the EODs of other individuals (Hopkins, 1986, 2005; Carlson, 2006) and active electrolocation, which is navigation and orientation based on detecting distortions in the self-generated electric field (von der Emde, 1999; Nelson, 2005). Both groups of fish are nocturnal and typically live in tropical rivers, streams and creeks. The electric sense thereby provides an effective sensory modality in conditions under which vision is of limited use. Studies on the neurobiology and behavior of these fish have generated many fundamental insights into neural structure and function (Moller, 1995; Rose, 2004).

IVA. Electric Organs

Strongly electric fish that use electricity as a weapon have electric organs capable of generating hundreds of volts. Weakly electric fish, those that use the EOD for active electrolocation and communication, generate much weaker electric fields (millivolts to a few volts). Electric organs have evolved independently at least six different times (see Fig. 41.1): once in the African Mormyriformes, once in the South American Gymnotiformes, once in the "modern" teleost order Perciformes (the stargazer *Astroscopus*), twice

in cartilaginous fishes (once in the torpedinoids or electric rays and once in the rajoids or skates) and at least once in the Siluriformes (catfish).

In nearly all cases, electric organs are of myogenic origin, i.e. they are derived from muscle (Bass, 1986). The excitable cells, termed electrocytes, are packed densely into the electric organ. They are driven to fire in synchrony by spinal electromotor neurons that receive input from a hindbrain command circuit, such that their individual action potentials (AP) summate to generate an external electric field (Caputi et al., 2005; Carlson, 2006). In wave-type species with a myogenic electric organ, the EOD frequency varies from about 100 to 500 Hz. Pulse-type species typically discharge at a lower rate (<100 Hz). In pulse-type mormyriforms, the EOD rate is highly variable, whereas in pulse-type gymnotiforms, EOD rates are quite regular. In general, the maximum energy in the power

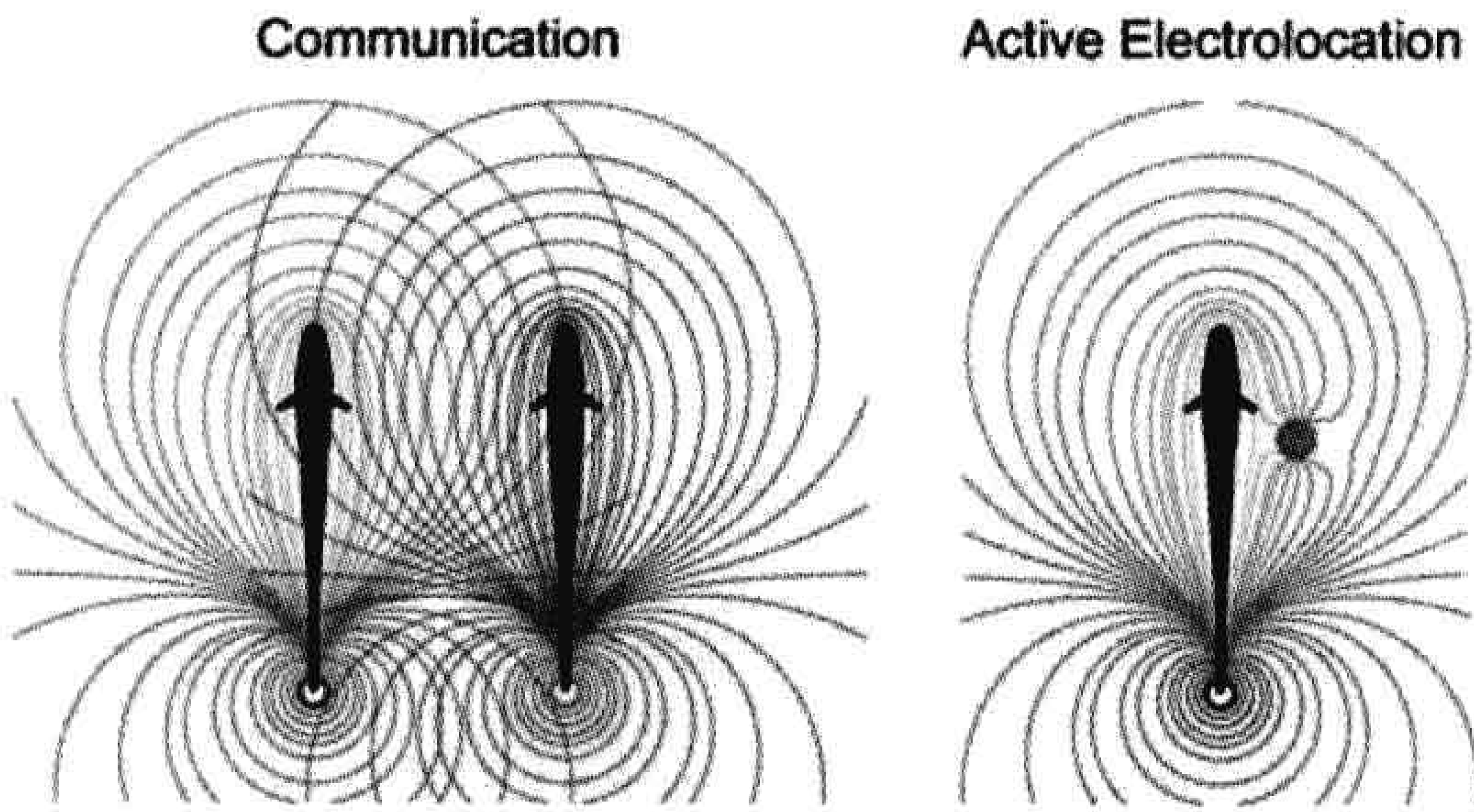


FIGURE 41.8 Electric organ discharges (EODs) serve two distinct functions: electric communication and active electrolocation. The EOD results in an electric field surrounding the fish, shown as isopotential field lines. Electric communication occurs when a fish enters the electric field of a neighboring fish. Active electrolocation occurs when nearby objects cause distortions in the self-generated electric field. The fish can detect these distortions and use them for orientation and navigation purposes. *(From Krahe and Gabbiani, 2004, with permission from Nature Publishing Group.)*

FIGURE 41.7 Electric organ discharges (EODs) and corresponding power spectra produced by several wave-type (left column) and pulse-type (right column) electric fish from the orders Gymnotiformes and Mormyriformes. *(Modified from Heiligenberg, 1991.)*

spectra of pulse-type EODs occurs in the range of about 100 to 10 000 Hz (see Fig. 41.7). Within the Gymnotiformes, one family, the Apteronotidae, possess a neurogenic electric organ that is composed of the axons of spinal electromotor neurons rather than derived from muscle (Bass, 1986). This may represent an adaptation to generating especially high EOD frequencies: the Apteronotidae generate wave-type EODs at frequencies ranging from about 650 to 1500 Hz (see Fig. 41.7). Detailed reviews of electric organ morphology, physiology and central control were published elsewhere (Bennett, 1971b; Bass, 1986; Caputi et al., 2005; Carlson, 2006).

IVB. Tuberous Electroreceptor Anatomy

In general, tuberous electroreceptor organs are distributed across the body surface (Szabo, 1974; Zakon, 1986; Jørgensen, 2005), although the distribution is not always uniform. High densities of tuberous receptors associated with improved electrosensory acuity have been described as electrical fovea, analogous to the visual fovea of the retina (Pusch et al., 2008). In addition, some tuberous organs in some species are organized into discrete clusters, or rosettes, that are localized to specific parts of the body surface (Zakon, 1986; Carlson et al., 2011). The organs themselves consist of a roughly spherical chamber located in the epidermis (Fig. 41.9). This chamber is connected to the external environment by a short canal that perforates the epidermis. Unlike ampullary organs, which have a mucous-filled duct that connects the receptor cells to the surface of the skin, the canals of tuberous organs are composed of a plug of loosely packed epithelial cells. This epithelial plug creates a capacitance in series with the receptor cells, which acts to filter out low stimulus frequencies (Bennett, 1965). Further, the walls of the canal and chamber consist of numerous layers of epithelial cells. These many

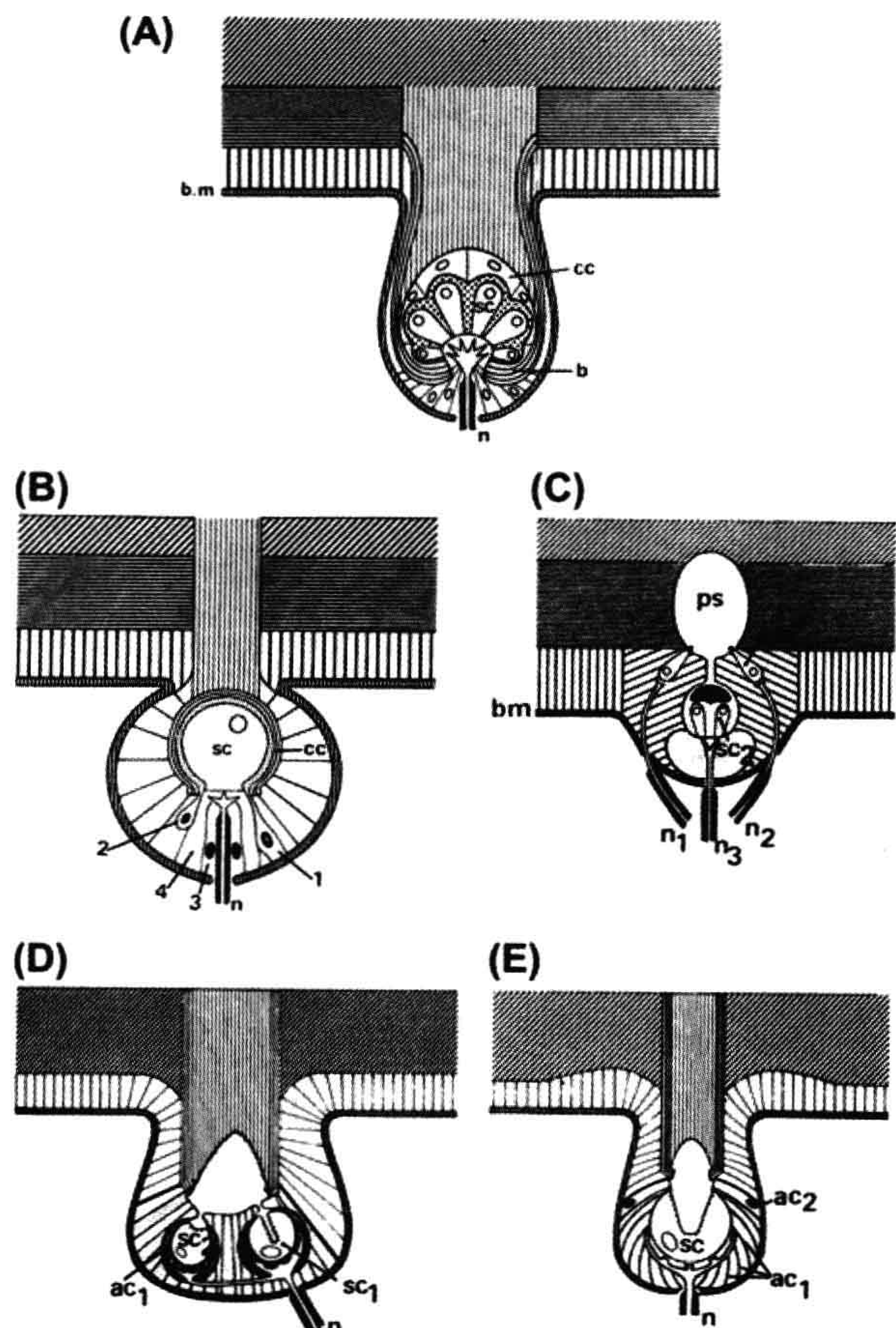


FIGURE 41.9 Schematics illustrating the anatomy of tuberous electroreceptor organs in (A) gymnotiform, (B, C) mormyrid and (D, E) gymnarchid weakly electric fishes. Abbreviations: ac1, ac2: accessory cells; b: capsule wall; bm: basement membrane; cc: covering cells; n#: afferent nerve fibers; ps: perisensory space; sc#: sensory cells. Numbers indicate different cell types within a given organ. *(From Szabo, 1974, with permission from Springer-Verlag, Berlin.)*

epithelial layers cause the wall to have relatively low capacitance, so that there is reduced shunting of high frequencies (Bennett, 1971a). These two distinguishing morphological features partly account for the tuning of tuberous receptors to much higher frequencies than ampullary receptors (Fig. 41.10). Indeed, EOD frequency correlates with the number of epithelial layers in the canal wall: species with low frequency EODs have fewer layers than those with high frequency EODs (Zakon, 1986).

At the base of the canal, the tuberous organ swells into a capsule within the corium. The sensory receptor cells themselves are located on the basal surface of this capsule, with their apical faces exposed to a mucopolysaccharide-filled receptor lumen. These apical faces contain either numerous microvilli or membrane foldings, both of which act to increase surface area, thereby increasing series capacitance while decreasing series resistance (Bennett, 1967, 1971b; Zakon, 1986). The number of receptor cells per organ varies from one to as many as 100, depending on the species and the type of tuberous organ. In all cases, the receptor cells are innervated by branches of the lateral line nerves, with primary afferent fibers that terminate within hindbrain electrosensory regions. In most cases, synaptic vesicles are found near the basal membrane of receptor cells and these mediate chemical synaptic transmission with primary afferent fibers. In one case, however, there may be an electronic junction between receptor cells and

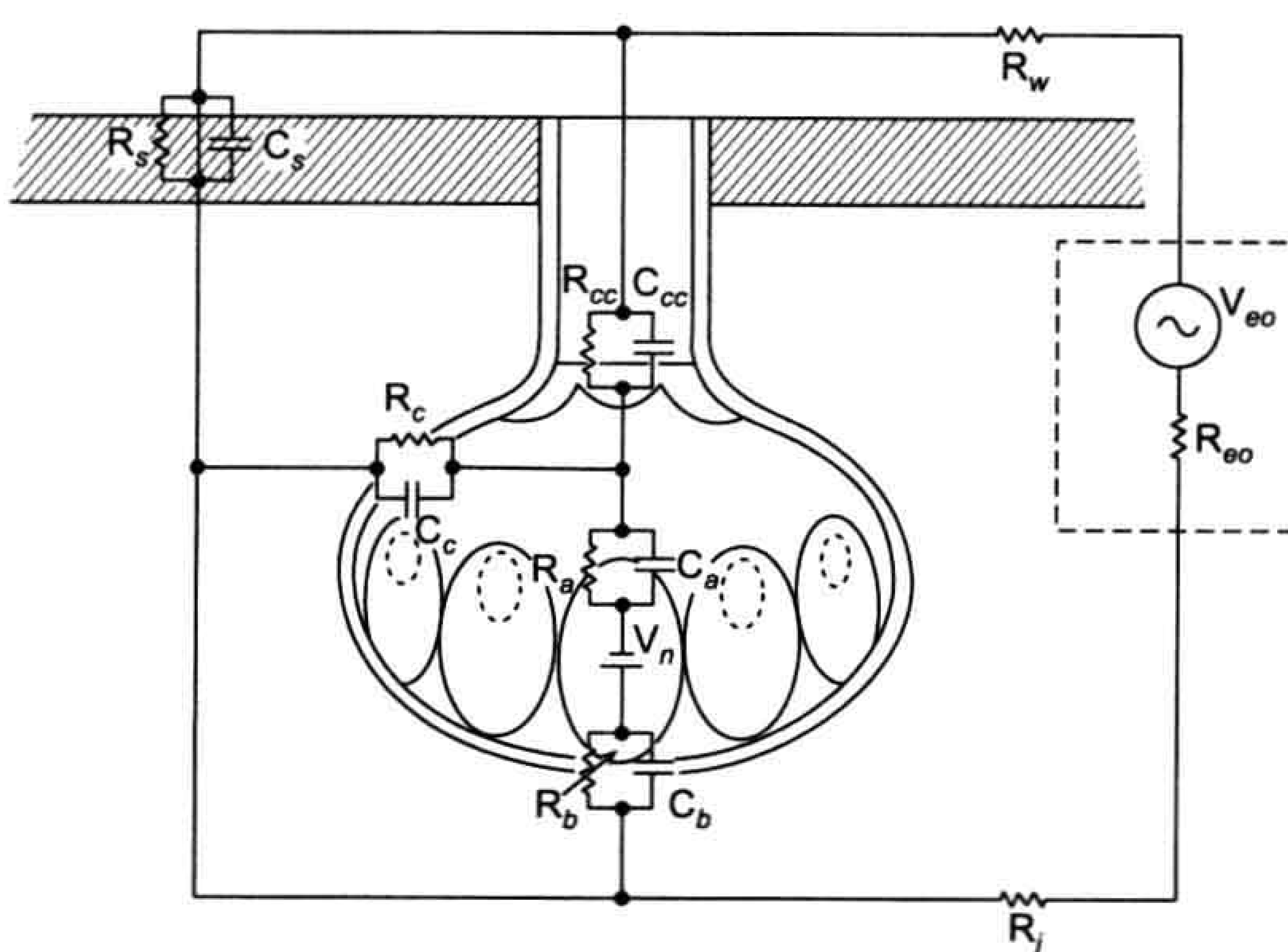


FIGURE 41.10 Electrical equivalent circuits of tuberous electroreceptors. Abbreviations: C_a: capacitance of the receptor cell apical membrane; C_b: capacitance of the receptor cell basal membrane; C_c: capacitance of the canal and capsule wall; C_{cc}: capacitance of the covering cells; C_s: capacitance of the skin; R_a: resistance of the receptor cell apical membrane; R_b: resistance of the receptor cell basal membrane; R_c: resistance of the canal and capsule wall; R_{cc}: resistance of the covering cells; R_{eo}: internal resistance of the electric organ; R_i: internal resistance of the fish; R_s: resistance of the skin; R_w: resistance of the water; V_{eo}: internal voltage of the electric organ; V_n: resting potential of receptor cells. Resistances and capacitances of supporting cells are not indicated and are believed to be passive. The resistance of the receptor cell basal membrane is thought to be voltage-gated. *(Modified from Bennett, 1967.)*

primary afferent fibers (see below). Details on the anatomy and physiology of central tuberous electrosensory pathways were reviewed elsewhere (Bell and Maler, 2005; Kawasaki, 2005).

IVC. Tuberous Electroreceptor Physiology

Intracellular recordings from individual tuberous receptor cells have yet to be obtained; therefore, we know little about the underlying transduction mechanisms and much of what we do know about tuberous receptor physiology comes from recordings from their primary afferent fibers. While the apical membrane of receptor cells appears to act solely as a series capacitance that contributes to high-pass filtering, the basal membrane appears to be electrically excitable, generating graded potentials or, in some cases, even spikes (Bennett, 1971a). The receptor cells respond to inward current that creates a voltage drop across the basal membrane of the receptor cell (see Fig. 41.10). Thus, they effectively measure the difference in voltage between the interior of the receptor cell and the internal "reference" potential of the animal (Bennett, 1971a). Tuberous receptors are sensitive to much higher frequencies than ampullary receptors as they are generally tuned to the power spectrum of the species-specific EOD. In wave-type species, this tuning is typically quite sharp, whereas the tuberous receptors of pulse-type species are more broadly-tuned. Although some of this tuning relates to passive electrical filtering due to the morphology of tuberous organs and the apical face of the receptor cells (see above), active mechanisms also contribute substantially to frequency tuning (see Fig. 41.10). Tuberous receptors typically respond to stimulation with potentials that oscillate at a frequency equal to the best frequency of the receptor (Bennett, 1971a) and, in some species at least, this appears to be based on both inward Ca^{2+} and outward K^+ currents (Zakon, 1986). Across taxa, tuberous receptors can be divided into two broad classes based on their responses to electrosensory stimuli: "amplitude-coding" and "time-coding" receptors (Fig. 41.11). As their names suggest, amplitude-coding receptors function primarily in encoding EOD amplitude, whereas time-coding receptors function primarily in encoding the timing of EOD pulses or cycles (Zakon, 1986). Time-coding receptors may generally be distinguished from amplitude-coding receptors as having lower thresholds, greater response probabilities, reduced timing jitter and shorter response latencies.

IVD. Tuberous Electroreceptors in Gymnotiformes

There are currently five recognized families with the order Gymnotiformes, two of which have wave-type EODs (Sternopygidae and Apteronotidae) and three of which

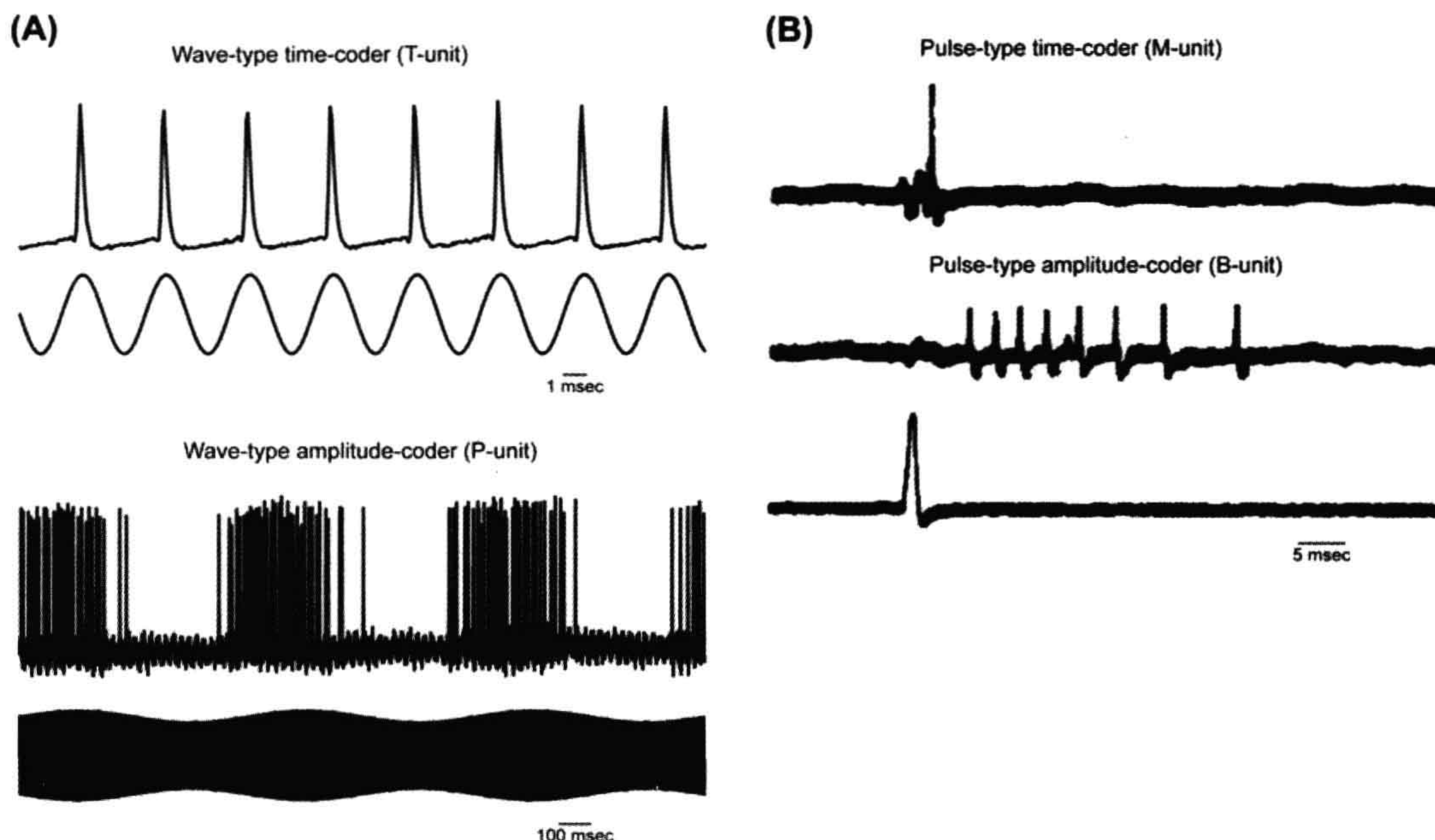


FIGURE 41.11 The primary afferent fibers of tuberous electroreceptors can be classified as either amplitude-coding or time-coding depending on which stimulus feature they respond most strongly to. (A) In the wave-type gymnotiform *Eigenmannia*, T-units fire a single, time-locked action potential (AP) in response to every cycle of an EOD (or a substitute sine wave as shown here), providing a precise marker of EOD timing. P-units do not fire an AP in response to every cycle; instead, their firing probability varies as a function of stimulus amplitude, as can be seen when a stimulus is modulated in amplitude over longer timescales. (*Unpublished recordings from Carlson, 2008a.*) (B) In the pulse-type gymnotiform *Hypopomus*, M-units fire a single, time-locked AP in response to each EOD pulse, whereas B-units fire a burst of spikes in response to each EOD pulse. The number of spikes in a B-unit burst varies as a function of stimulus amplitude. *(From Bastian, 1976.)*

have pulse-type EODs (Gymnotidae, Hypopomidae, and Rhamphichthyidae). The morphology of gymnotiform tuberous organs is essentially similar across all species studied (see Fig. 41.9A) (Szabo, 1974; Zakon, 1986; Jørgensen, 2005). Directly beneath the epithelial plug and above the sensory receptor cells, there is a layer of covering cells that extends across the capsule. These cells are joined to each other and to the walls of the capsule by tight junctions. The layer of covering cells maintains a constant ionic environment within the receptor lumen and also adds an additional series capacitance to the receptor organ.

The number of sensory receptor cells per organ typically varies from 20 to 30, but some tuberous organs can have as many as 100 receptors (Szabo, 1974; Zakon, 1986). The receptor cells are about 20–30 μm long. The apical region of the receptor cell has numerous microvilli exposed to the lumen and large numbers of mitochondria (Szabo, 1974). The receptors are attached to the base of the chamber via tight junctions only at the basal-most portion of the receptor cell's membrane. Thus, 95% of the membrane surface is exposed to the surrounding lumen. The remaining basal portion of the cell membrane is electrically isolated from the lumen via tight junctions with supporting cells (Szabo, 1974; Zakon, 1986). All of the receptor cells within a tuberous organ are innervated by a single afferent fiber, though one fiber may innervate either one or several organs. When an afferent fiber innervates several tuberous organs, those organs form a distinct cluster called a rosette, resulting from the division of a single organ with growth. The receptive field of each primary afferent fiber is centered on the pore of a single tuberous organ (Bennett, 1967; Zakon, 1986).

Two distinct physiological classes of primary afferent fibers have been described in wave-type gymnotiforms: T-units (for *Time-coder*) and P-units (for *Probability-coder*). Within the natural range of stimulus intensities, T-units fire one phase-locked spike per EOD cycle with less than 100 μs of timing jitter (see Fig. 41.11A), thus providing a precise marker of the timing of positive transitions in the EOD (Zakon, 1986; Heiligenberg, 1991; Carlson, 2006, 2008a,b). By contrast, P-units do not fire a spike during each EOD cycle and they have timing jitter greater than 500 μs (Zakon, 1986; Heiligenberg, 1991; Carlson, 2006, 2008a). The probability of P-unit firing

varies with amplitude; thus, the firing rate of P-units codes for EOD amplitude (see Fig. 41.11A). There are a number of additional distinguishing features between the two types of receptors (Zakon, 1986): T-units are more sharply frequency tuned and they are typically tuned to higher frequencies than P-units; P-units readily adapt to changes in steady-state amplitude, whereas T-units do not; although both types of units have dynamic ranges of about 20 dB, the threshold stimulus intensity for T-units is about 15–20 dB lower than that of P-units. Although it remains unclear, P- and T-units may correspond to two distinct anatomical classes of tuberous organs, one which is characterized by one to two receptor organs per axon with thick axon branches and a second which is characterized by four or more receptor organs per axon with thin axon branches (Zakon, 1986).

P- and T-units both play important roles in electrosensory-mediated behaviors (Heiligenberg, 1991). Interference between the EODs of neighboring fish results in modulations in both the amplitude and timing (i.e. phase) of the resulting electric field (Fig. 41.12). Information about the temporal relationship between amplitude and phase modulation is used to determine the EOD frequency of a neighboring fish, a determination that is important for both communication behavior and avoidance of electrosensory jamming (Heiligenberg, 1991; Carlson, 2006, 2008a). Further, wave-type gymnotiforms are able to distinguish purely resistive objects from capacitive objects having complex impedances by comparing the activities of P- and T-units (von der Emde, 1999). Although the two classes of units are clearly specialized for separately encoding the amplitude and timing of stimuli, the distinction is not complete: the spike times of T-units are affected by stimulus amplitude and the firing rate of P-units can be affected by stimulus timing, and this "cross-talk" can ultimately influence electrosensory perception (Carlson, 2008a).

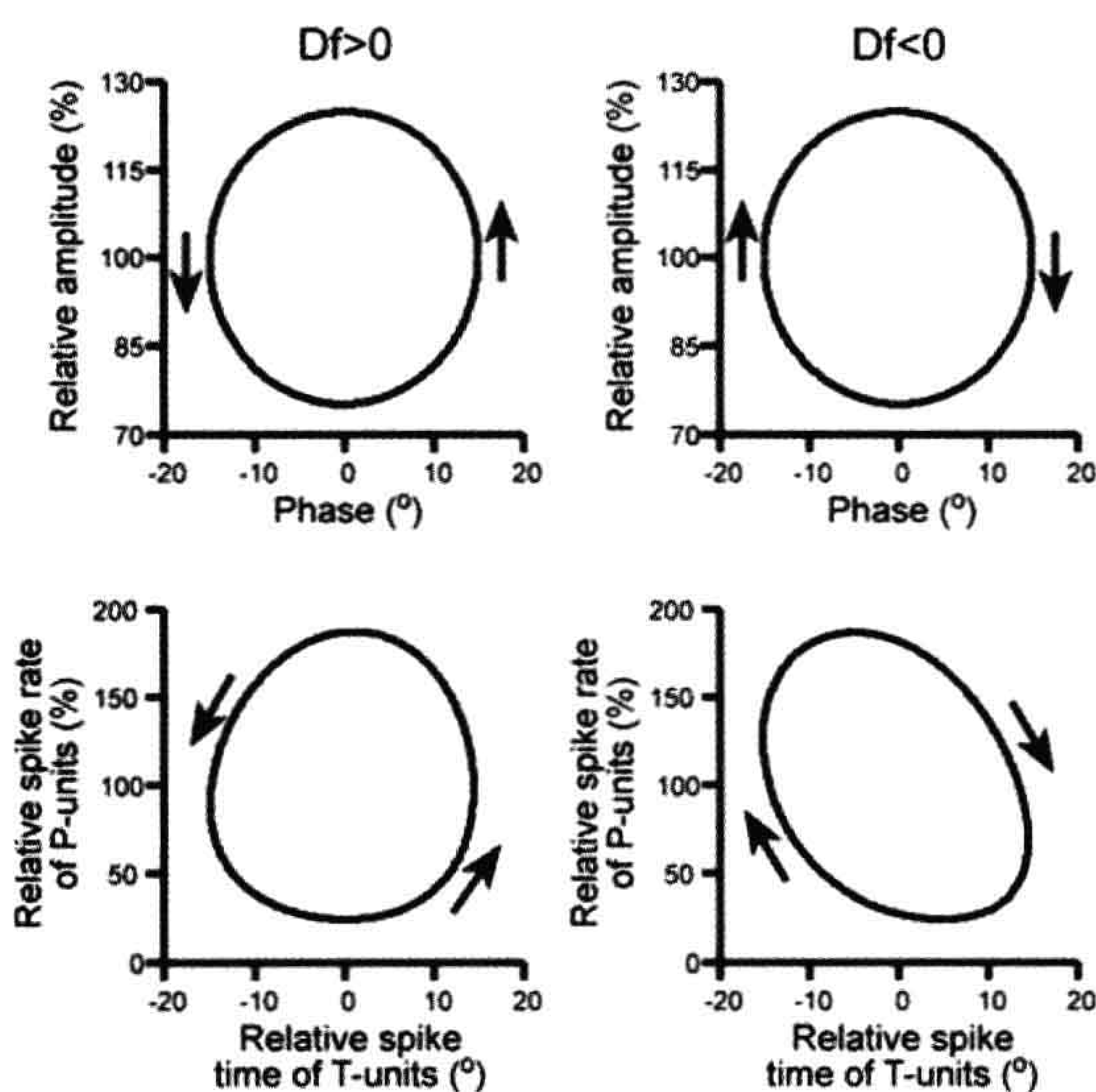


FIGURE 41.12 Neural representations of sinusoidal stimulus modulations caused by interference from a neighboring fish's EOD in the wave-type gymnotiform *Eigenmannia*. The top row shows Lissajous plots that illustrate the temporal relationship between amplitude modulation and phase modulation, with the sense of rotation indicating how these two variables change over time: when the neighboring fish has a higher EOD rate than the focal fish (Df > 0, left), the resulting plot has a counterclockwise sense of rotation. When the neighboring fish has a lower EOD rate than the focal fish (Df < 0, right), the resulting plot has a clockwise sense of rotation. The bottom row shows similar Lissajous plots, except that the average spike rate of P-units is plotted against the average spike time of T-units. Notice how the neural representations of the two different conditions exhibit the same sense of rotation as the stimuli themselves. *(Modified from Carlson, 2008a.)*

Pulse-type gymnotiforms also have two distinct physiological classes of primary afferents (see Fig. 41.11B): M-units (for *pulse Marker*) and B-units (for *Burst duration-coder*). Similar to T-units, M-units fire a single, short latency spike in response to each EOD pulse with little timing jitter; by contrast, B-units respond to each EOD pulse with a longer-latency burst of spikes (Bastian, 1976; Zakon, 1986). The duration of the burst increases with increasing EOD amplitude: at near threshold intensities, B-units may respond to an EOD with a single spike, whereas they respond with 20–40 spikes at higher intensities. Both units are sensitive to the direction of current flow, with greatest responses to stimuli at the best azimuth for transepidermal current flow (Hopkins, 2005).

The physiological distinction between M- and B-units is clearly linked to anatomical differences in the associated receptor organs (Szabo, 1974; Zakon, 1986). M-units have large-diameter axons with large myelinated terminal enlargements within the receptor capsule that give rise to boutons that innervate the receptor cells. By contrast, B-units have smaller-diameter axons that lose their myelination upon entering the capsule and give rise to several thin, unmyelinated terminal branches that innervate the receptor cells.

IVE. Tuberous Electroreceptors in Mormyriformes

The Mormyriformes consist of two distinct sister families, the Mormyridae and the monotypic Gymnarchidae, *Gymnarchus niloticus*. All of the mormyrids have pulse-type EODs, while *Gymnarchus* has a wave-type EOD (see Fig. 41.7). Two distinct physiological classes of receptors have been described in *Gymnarchus*: S- and O-units, which are remarkably similar to the T- and P-units of wave-type gymnotiforms, respectively (Kawasaki, 1997; Carlson, 2008a). S-units have lower thresholds, higher firing probabilities, reduced jitter and less adaptation to steady-state

changes in intensity than O-units. Thus, within the natural range of stimulus intensities, S-units fire 1:1 with each cycle of the EOD and provide a precise marker of the timing of positive transitions, whereas the firing rate of O-units codes for stimulus amplitude. As in the wave-type gymnotiforms, both units provide critical information for determining the EOD frequency of neighboring fish (Kawasaki, 1997). Further, S-units do respond to changes in stimulus amplitude and O-units can respond to changes in stimulus timing, similar to the effects seen in T- and P-units (Carlson, 2008a).

Anatomically, the tuberous organs of *Gymnarchus* are referred to as Gymnarchomasts (Szabo, 1974; Zakon, 1986; Jørgensen, 2005). Type I gymnarchomasts contain two distinct sensory receptor cell types; the organ may contain one or many pairs of these two cell types (see Fig. 41.9D). The larger of the two receptor cell types has a deep invagination filled with numerous microvilli. The microvilli located at the base of the depression are especially long and project upwards into the apical cavity. The smaller receptor cell type has only a slight depression at its apical surface, although it too has densely-packed microvilli. Both sensory cells are surrounded by numerous support cells and only a small portion of receptor cell membrane surface is exposed to the surrounding lumen. All of the receptor cells in an organ are innervated by a single afferent nerve fiber. Physiologically, type I gymnarchomasts have been linked to S-unit primary afferent fibers (Bennett, 1971a; Zakon, 1986). Type II gymnarchomasts consist of several (12–13) sensory receptor cells that are innervated by a single primary afferent fiber. Each individual receptor cell is separated from the surrounding receptor cells by a ring of accessory cells. Thus, the type II organ can be thought of as composed of multiple sensory "units", each with a single receptor cell and multiple accessory cells (see Fig. 41.9E). The receptor cells are similar in morphology to the larger receptor cell of the type I gymnarchomast in having a deeply invaginated apical surface filled with microvilli that project upwards. Type II gymnarchomasts are thought to correspond to O-unit primary afferent fibers (Bennett, 1971a; Zakon, 1986).

The pulse-type mormyrids also have two distinct classes of tuberous receptor organs, amplitude-coding mormyromasts and time-coding knollenorgans (Bennett, 1965, 1971a; Szabo, 1974; Zakon, 1986). Knollenorgans typically have one to 10 sensory receptor cells, although some species have especially large knollenorgans with as many as 60 receptor cells. The receptor cells are large (40–50 μm in diameter) and each is enclosed in its own cavity within the receptor capsule (Szabo, 1974; Zakon, 1986; Jørgensen, 2005). Only the basal-most portion of the receptor cell's membrane is attached to the base of the chamber, similar to the tuberous receptors of gymnotiforms (see Fig. 41.9B). The apical cell membrane is densely packed with microvilli, below which is a dense band of mitochondria. Knollenorgans are unique among tuberous receptors in that the receptor itself generates APs rather than only graded receptor potentials. Further, physiological evidence suggests an electrotonic synapse between the receptor cell and primary afferent fiber (Bennett, 1971a), a conclusion supported by the small numbers of synaptic vesicles and close apposition of pre- and postsynaptic membranes (Zakon, 1986). However, gap junctions have never actually been observed. All of the receptor cells within a knollenorgan are innervated by a single primary afferent fiber that divides to form several terminal boutons onto each individual receptor cell.

Like the pulse marker primary afferents (M-units) of pulse-type gymnotiforms, knollenorgans have a relatively low threshold and fire a single AP in response to an EOD (Bennett, 1965, 1967; Bell, 1990; Carlson, 2008b). The primary afferents of knollenorgans terminate in the hindbrain, where an inhibitory input arising from the electromotor pathway blocks ascending knollenorgan responses whenever the fish generates its own EOD (Carlson, 2008c). Thus, the downstream knollenorgan pathway never "hears" the fish's own EOD, strongly suggesting that knollenorgans function solely in communication behavior (Carlson, 2006). The timing of the knollenorgan AP is tightly phase-locked to the timing of outside-positive positive transitions in the stimulus waveform (Bennett, 1965; Hopkins and Bass, 1981). In response to natural stimuli, different knollenorgans receive EODs with different polarities, resulting in small differences in spike timing across the population of knollenorgans (Fig. 41.13). Behavioral, anatomical and physiological evidence suggests that these spike timing differences mediate the detection of species-specific EOD waveforms (Hopkins and Bass, 1981; Xu-Friedman and Hopkins, 1999; Carlson, 2006), although certain clades of mormyrids appear to lack this ability (Carlson et al., 2011).

Mormyromasts have a distinctive morphology (Jørgensen, 2005). Although the pore and epithelial plug are similar to other tuberous organs, the organ itself consists of two separate chambers, one superficial and one deep, connected to each other by a short duct (see Fig. 41.9C). The two chambers each have their own distinct type of sensory receptor cell: the sensory cells in the upper chamber are referred to as A-type receptor cells, whereas those in the lower chamber are referred to as B-type receptor cells. The number of receptor cells in the two chambers is nearly always equal, varying from two each in the smaller mormyromasts to more than 12 in the larger ones (Jørgensen, 2005). The A-type cells lack microvilli and have only a small portion of their apical surface exposed to the receptor lumen. By contrast, the B-type cells have microvilli and, like knollenorgan receptors, nearly the entire receptor surface area is exposed to the surrounding lumen. The A-cells are contacted by two to three primary

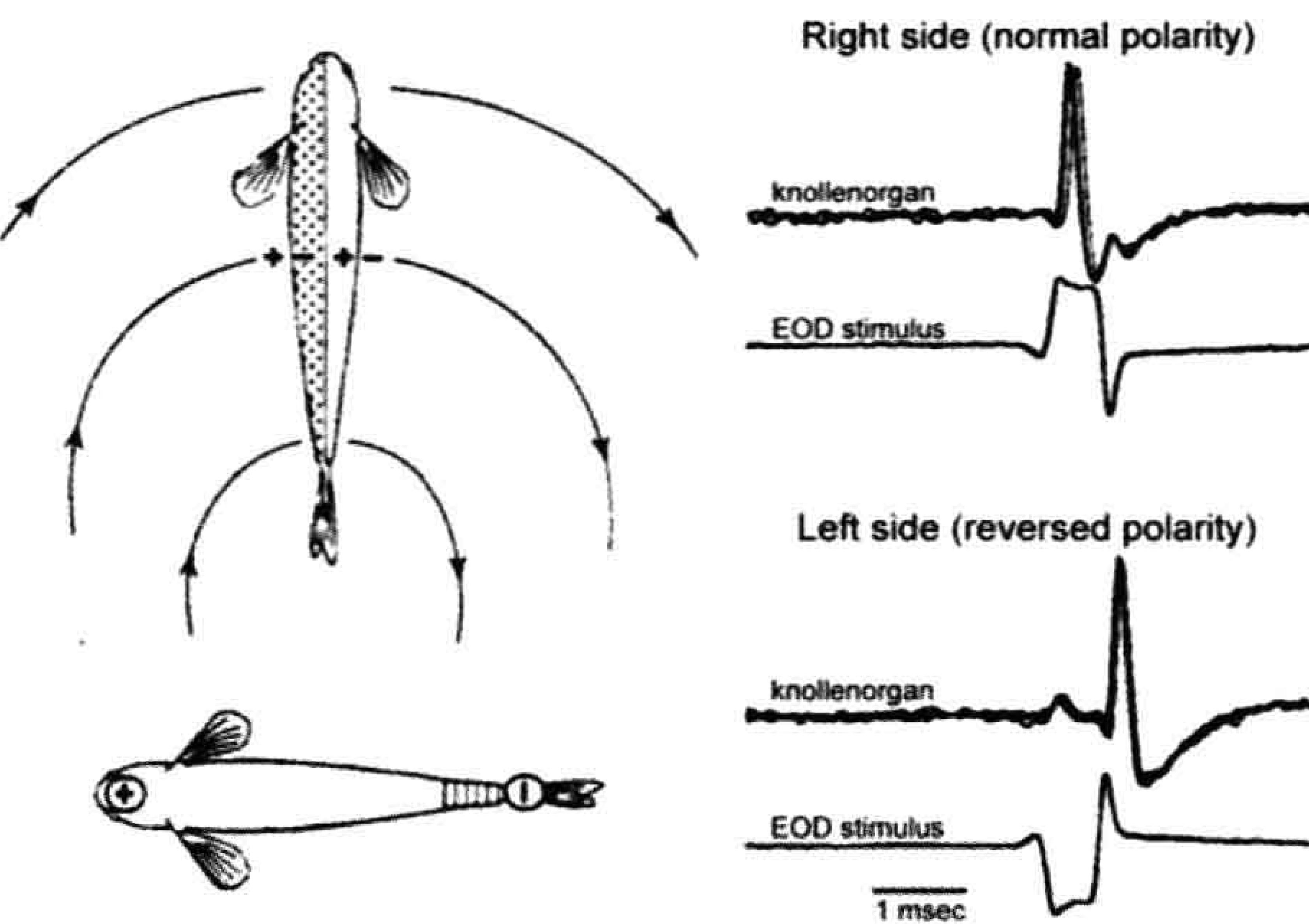


FIGURE 41.13 Knollenorgan electroreceptors in mormyrids mediate species recognition during electric communication. On the left, a signaling fish and receiving fish are viewed from below. The signaling fish is modeled as a simple dipole with "+" and "−" poles at the head and tail, respectively. This causes current to flow into the right side of the receiving fish and out the left side. *(Modified from Hopkins, 1986.)* On the right, the responses of a single knollenorgan to opposite polarity EOD stimuli are shown. Knollenorgans respond to outside-positive changes in voltage. As a result, knollenorgans respond to the start of a normal polarity EOD (simulating the response of a knollenorgan on the right side of the body), but they respond to the end of a reversed polarity EOD (simulating the response of a knollenorgan on the left side of the body). The resulting difference in response latency is used to determine EOD duration. *(Modified from Hopkins and Bass 1981.)*

afferent fibers, whereas all of the B-cells are always contacted by a single primary afferent fiber. The A- and B-cell primary afferents terminate in separate portions of the hindbrain electrosensory lateral line lobe, forming two distinct maps of the body surface (Bell and Maler, 2005). Interestingly, in one genus of mormyrid, *Stomatorhinus*, both the A- and B-cells are present, but only the A-cells receive innervation from primary afferent fibers and this is associated with a complete loss of the associated electrosensory lateral line map (McNamara et al., 2005). This may be related to the extremely short duration (≈250 μs) and high peak power spectral frequencies (≈14−26 kHz) of the EODs in these species, which may preclude the detection of complex impedances based on waveform distortions (see below).

Both A- and B-cell afferents may be classified as amplitude-coding. Like the burst duration coders of pulse-type gymnotiforms, they respond to suprathreshold stimuli by generating a burst of spikes (Bennett, 1965; Bell, 1990). Increases in stimulus amplitude cause both a decrease in first-spike latency, as well as an increase in the number of spikes (Fig. 41.14) (Bennett, 1965; Bell, 1990), although behavioral and physiological evidence suggests that first-spike latency appears to be the critical feature for stimulus coding. In contrast to the knollenorgan sensory pathway, mormyromast input to the hindbrain is gated by an excitatory input arising from the electromotor pathway, rather than inhibited (Carlson, 2008c). As a result, the downstream mormyromast pathway is selectively responsive to the fish's own EOD, indicating that mormyromasts function solely in active electrolocation behavior (von der Emde, 1999).

Compared to knollenorgans, mormyromast primary afferent fibers have higher thresholds and they tend to be

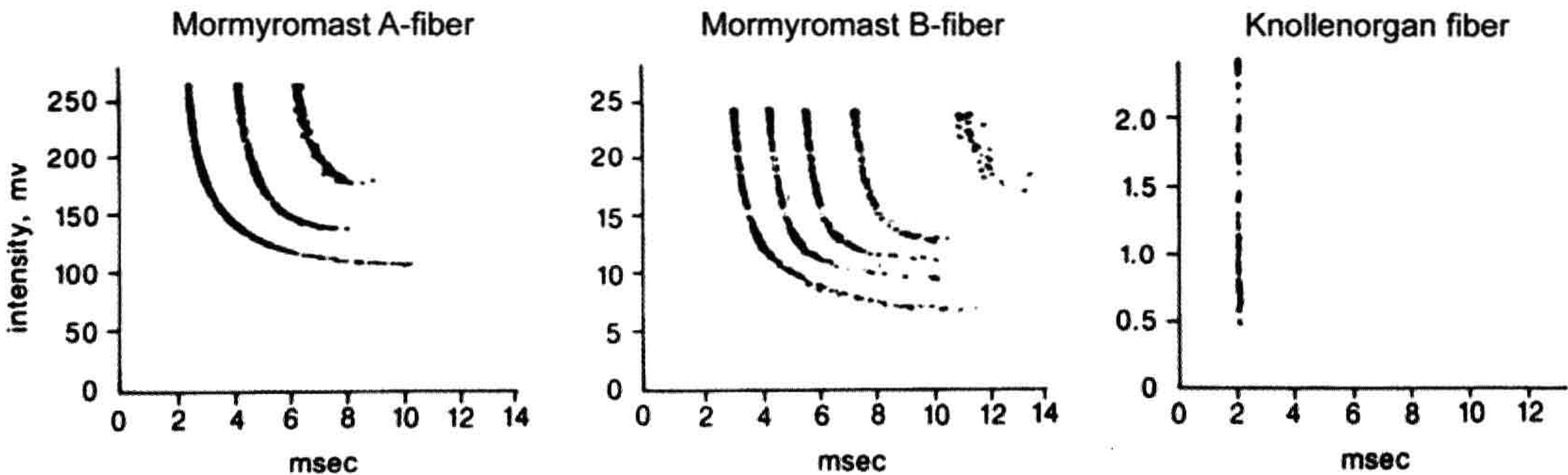


FIGURE 41.14 Differences in the coding of electrosensory stimuli among tuberous electrosensory primary afferent fibers in mormyrids. Stimulus intensity is plotted against the latency of action potentials (Aps) relative to the stimulus. The minimum stimulus intensity required to elicit a response (i.e. threshold) is indicated by the lowest intensity at which any APs occurred. Mormyromast fibers have a much higher threshold than knollenorgan fibers. Further, increases in stimulus intensity cause a decrease in the latency to the first spike, as well as an increase in the number of spikes in mormyromasts, whereas knollenorgans fire only a single spike at a relatively fixed latency. Mormyromast B-fibers tend to have a lower threshold and greater number of spikes per burst compared to A-fibers. *(Modified from Bell, 1990.)*

tuned to frequencies below the peak power frequency of the species-specific EOD (see Fig. 41.14) (Bell, 1990). B-cell afferents tend to have a lower threshold, smaller dynamic range and greater maximum burst number than A-cell afferents. Further, A-cells tend to be tuned to higher frequencies and show more variation in frequency tuning than B-cells. Most importantly, B-cell afferents respond to subtle changes in EOD waveform caused by complex impedances, whereas A-cell afferents do not (von der Emde, 1999). Thus, comparing the responses of the two types of primary afferents may be the mechanism by which mormyrids distinguish simple from complex impedances during active electrolocation (von der Emde, 1999).

IVF. Tuberous Electroreceptors in Siluriformes

Compared to the mormyriforms and gymnotiforms, we know very little about the tuberous receptors found in siluriforms (catfishes). Tuberous organ morphology has been described only in the blind catfish *Pseudocetopsis* spp. (Andres et al., 1988). Compared to tuberous organs in other taxa, this tuberous organ, referred to as a siluromast, is located superficially within the epidermis (Jørgensen, 2005). Each organ has a single sensory receptor cell with a diameter of ≈25 μm and an apical surface covered with microvilli. A single primary afferent fiber loses its myelin sheath within the supporting cell layer and then synapses onto the receptor cell with a flattened terminal face. The function of this tuberous organ is unclear, as these fish are not known actively to generate EODs. One intriguing possibility is that these tuberous organs serve a predatory function by allowing the blind catfish passively to electrolocate sympatric gymnotiforms by detecting their EODs (Andres et al., 1988).

BIBLIOGRAPHY

Andres, K. H., von Düring, M., & Petrasch, E. (1988). The fine structure of ampullary and tuberous electroreceptors in the South American blind catfish *Pseudocetopsis* spec. *Anat Embryol, 177*, 523–535.

Andrianov, G. N., Broun, G. R., & Ilyinsky, O. B. (1984). Frequency characteristic of skate electroreceptive central neurons responding to electrical and magnetic stimulation. *Neurophysiology, 16*, 365–376.

Bass, A. H. (1986). Electric organs revisited: evolution of a vertebrate communication and orientation organ. In T. H. Bullock, & W. Heiligenberg (Eds.), *Electroreception* (pp. 13–70). New York: John Wiley and Sons.

Bastian, J. (1976). Frequency-response characteristics of electroreceptors in weakly electric fish (Gymnotoidei) with a pulse discharge. *J Comp Physiol, 112*, 165–180.

Beason, R. C., & Semm, P. (1987). Magnetic responses of the trigeminal nerve system of the Bobolink (*Dolichonyx oryzivorus*). *Neurosci Lett, 80*, 229–234.

Bell, C. C. (1990). Mormyromast electroreceptor organs and their afferent fibers in mormyrid fish. III. Physiological differences between two morphological types of fibers. *J Neurophysiol, 63*, 319–332.

Bell, C., & Maler, L. (2005). Central neuroanatomy of electrosensory systems in fish. In T. H. Bullock, C. D. Hopkins, A. N. Popper, & R. R. Fay (Eds.), *Springer Handbook of Auditory Research: Vol. 21, Electroreception* (pp. 68–111). New York: Springer.

Bemis, W. E., & Hetherington, T. E. (1982). The rostral organ of Latimeria chalumnae: morphological evidence of an electroreceptive function. *Copeia, 1982*, 467–471.

Bennett, M. V. L. (1965). Electroreceptors in mormyrids. *Cold Spring Harbor Symp Quant Biol, 30*, 245–262.

Bennett, M. V. L. (1967). Mechanisms of electroreception. In P. Cahn (Ed.), *Lateral Line Detectors* (pp. 313–393). Bloomington: Indiana University Press.

Bennett, M. V. L. (1968). Similarities between chemically and electrically mediated transmission. In F. D. Carlson (Ed.), *Physiological and Biochemical Aspects of Nervous Integration* (pp. 73–128). Englewood Cliffs: Prentice-Hall.

Bennett, M. V. L. (1971a). Electroreception. In W. S. Hoar, & D. S. Randall (Eds.), *Fish Physiology, Vol. 5* (pp. 493–574). New York: Academic Press.

Bennett, M. V. L. (1971b). Electric organs. In W. S. Hoar, & D. J. Randall (Eds.), *Fish Physiology, Vol. 5* (pp. 347–491). New York: Academic Press.

Bennett, M. V. L., & Clusin, W. T. (1978). Physiology of the ampulla of Lorenzini, the electroreceptor of elasmobranchs. In E. S. Hodgson, & R. F. Mathewson (Eds.), *Sensory Biology of Sharks, Skates, and Rays* (pp. 483–505). Arlington: Office of Naval Research.

Bennett, M. V. L., & Obara, S. (1986). Ionic mechanisms and pharmacology of electroreceptors. In T. H. Bullock, & W. Heiligenberg (Eds.), *Electroreception* (pp. 157–181). New York: John Wiley and Sons.

Bodznick, D., & Montgomery, J. C. (2005). The physiology of low-frequency electrosensory systems. In T. H. Bullock, C. D. Hopkins, A. N. Popper, & R. R. Fay (Eds.), *Springer Handbook of Auditory Research, Vol. 21. Electroreception* (pp. 132–153). New York: Springer.

Bodznick, D., & Preston, D. G. (1983). Physiological characterization of electroreceptors in the lampreys, *Ichthyomyzon unicuspis* and *Petromyzon marinus*. *J Comp Physiol A, 152*, 209–217.

Bodznick, D., Hjelmstad, G., & Bennett, M. V. L. (1993). Accommodation to maintained stimuli in the ampullae of Lorenzini: how an electroreceptive fish achieves sensitivity in a noisy world. *Jap J Physiol, 43*(Suppl. 1), S231–S237.

Bodznick, D., Montgomery, J. C., & Bradley, D. J. (1992). Suppression of common-mode signals within the electrosensory system of the little skate, *Raja erinacea*. *J Exp Biol, 171*, 107–125.

Braford, M. R. (1986). African knifefishes: the Xenomystines. In T. H. Bullock, & W. Heiligenberg (Eds.), *Electroreception* (pp. 453–464). New York: John Wiley and Sons.

Brown, B. R., Hughes, M. E., & Russo, C. (2005). Infrastructure in the electric sense: admittance data from shark hydrogels. *J Comp Physiol A, 191*, 115–123.

Brown, B. R., Hutchison, J. C., Hughes, M. E., Kellogg, D. R., & Murray, R. W. (2002). Electrical characterization of gel collected from shark electrosensors. *Phys Rev E, 65*, 061903.

Bullock, T. H., & Heiligenberg, W. (1986). *Electroreception*. New York: John Wiley and Sons.

Bullock, T. H., Bodznick, D. A., & Northcutt, R. G. (1983). The phylogenetic distribution of electroreception: evidence for convergent evolution of a primitive vertebrate sense modality. *Brain Res Rev, 6*, 25–46.

Caputi, A. A., Carlson, B. A., & Macadar, O. (2005). Electric organs and their control. In T. H. Bullock, C. D. Hopkins, A. N. Popper, & R. R. Fay (Eds.), *Springer Handbook of Auditory Research, Vol. 21, Electroreception* (pp. 410–451). New York: Springer.

Carlson, B. A. (2006). A neuroethology of electrocommunication: senders, receivers, and everything in between. In F. Ladich, S. P. Collin, P. Moller, & B. G. Kapoor (Eds.), *Communication in Fishes, Vol. 2* (pp. 805–848). Enfield: Science Publishers.

Carlson, B. A. (2008a). Phantoms in the brain: ambiguous representations of stimulus amplitude and timing in weakly electric fish. *J Physiol Paris, 102*, 209–222.

Carlson, B. A. (2008b). Temporal coding in electroreception. In M. D. Binder, N. Hirokawa, U. Windhorst, & M. C. Hirsch (Eds.), *Encyclopedia of Neuroscience* (pp. 4039–4044). New York: Springer.

Carlson, B. A. (2008c). Reafferent control in electric communication. In M. D. Binder, N. Hirokawa, U. Windhorst, & M. C. Hirsch (Eds.), *Encyclopedia of Neuroscience* (pp. 3368–3373). New York: Springer.

Carlson, B. A., Hasan, S. M., Hollmann, M., Miller, D. B., Harmon, L. J., & Arnegard, M. E. (2011). Brain evolution triggers increased diversification of electric fishes. *Science, 332*, 583–586.

Diebel, C. E., Proksch, R., Green, C. R., Neilson, P., & Walker, M. M. (2000). Magnetite defines a vertebrate magnetoreceptor. *Nature, 406*, 299–302.

Falkenberg, G., Fleissner, G., Schuchardt, K., et al. (2010). Avian magnetoreception: elaborate iron mineral containing dendrites in the upper beak seem to be a common feature of birds. *PloS one, 5*, e9231.

Fields, R. D., Bullock, T. H., & Lange, O. D. (1993). Ampullary sense organs, peripheral, central and behavioral electroreception in chimeras (Hydrolagus, Holocephali, Chondrichthyes). *Brain Behav Evol, 41*, 269–289.

Finger, T. E., Bell, C. C., & Carr, C. E. (1986). Comparisons among electroreceptive teleosts: why are electrosensory systems so similar? In T. H. Bullock, & W. Heiligenberg (Eds.), *Electroreception* (pp. 465–481) New York: John Wiley and Sons.

Fleissner, G., Holtkamp-Rotzler, E., Hanzlik, M., Winklhofer, M., Petersen, N., & Wiltschko, W. (2003). Ultrastructural analysis of a putative magnetoreceptor in the beak of homing pigeons. *J Comp Neurol, 458*, 350–360.

Freitas, R., Zhang, G., Albert, J. S., Evans, D. H., & Cohn, M. J. (2006). Developmental origin of shark electrosensory organs. *Evol Devel, 8*, 74–80.

Gibbs, M. A., & Northcutt, R. G. (2004). Development of the lateral line system in the shovelnose sturgeon. *Brain Behav Evol, 64*, 70–84.

Gregory, J. E., Iggo, A., McIntyre, A. K., & Proske, U. (1989). Responses of electroreceptors in the snout of the echidna. *J Physiol (London), 414*, 521–538.

Heiligenberg, W. (1991). *Neural Nets in Electric Fish*. Cambridge: MIT Press.

Hopkins, C. D., & Bass, A. H. (1981). Temporal coding of species recognition signals in an electric fish. *Science, 212*, 85–87.

Hopkins, C. D. (1986). Behavior of mormyridae. In T. H. Bullock, & W. Heiligenberg (Eds.), *Electroreception* (pp. 527–576). New York: John Wiley and Sons.

Hopkins, C. D. (2005). Passive electrolocation and the sensory guidance of oriented behavior. In T. H. Bullock, C. D. Hopkins, A. N. Popper, & R. R. Fay (Eds.), *Springer Handbook of Auditory Research, Vol. 21, Electroreception* (pp. 264–289). New York: Springer.

Johnsen, S., & Lohmann, K. J. (2005). The physics and neurobiology of magnetoreception. *Nat Rev Neurosci, 6*, 703–712.

Jørgensen, J. M. (2005). Morphology of electroreceptive sensory organs. In T. H. Bullock, C. D. Hopkins, A. N. Popper, & R. R. Fay (Eds.), *Springer Handbook of Auditory Research, Vol. 21, Electroreception* (pp. 47–67). New York: Springer.

Kalmijn, A. J. (1971). The electric sense of sharks and rays. *J Exp Biol, 55*, 371–383.

Kalmijn, A. J. (1974). The detection of electric fields from inanimate and animate sources other than electric organs. In A. Fessard (Ed.), *Handbook of Sensory Physiology, Vol. III/3* (pp. 147–200). New York: Springer-Verlag.

Kalmijn, A. J. (1982). Electric and magnetic field detection in elasmobranch fishes. *Science, 218*, 915–918.

Kalmijn, A. J. (1988). Detection of weak electric fields. In J. Atema, R. R. Fay, A. N. Popper, & W. N. Tavogla (Eds.), *Sensory Biology of Aquatic Animals* (pp. 151–186). New York: Springer-Verlag.

Kawasaki, M. (1997). Sensory hyperacuity in the jamming avoidance response of weakly electric fish. *Curr Opin Neurobiol, 7*, 473–479.

Kawasaki, M. (2005). Physiology of tuberous electrosensory systems. In T. H. Bullock, C. D. Hopkins, A. N. Popper, & R. R. Fay (Eds.), *Springer Handbook of Auditory Research, Vol. 21, Electroreception* (pp. 154–194). New York: Springer.

Krahe, R., & Gabbiani, F. (2004). Burst firing in sensory systems. *Nat Rev Neurosci, 5*, 13–23.

Lissman, H. W. (1958). On the function and evolution of electric organs in fish. *J Exp Biol, 35*, 156–191.

Lissman, H. W., & Machin, K. E. (1958). The mechanisms of object location in *Gymnarchus niloticus* and similar fish. *J Exp Biol, 35*, 451–486.

Lu, J., & Fishman, H. M. (1994). Interaction of apical and basal membrane ion channels underlies electroreception in ampullary epithelia of skates. *Biophys J, 67*, 1525–1533.

Lu, J., & Fishman, H. M. (1995a). Localization and function of the electrical oscillation in electroreceptive ampullary epithelium from skates. *Biophys J, 69*, 2458–2466.

Lu, J., & Fishman, H. M. (1995b). Ion channels and transporters in the electroreceptive ampullary epithelium from skates. *Biophys J, 69*, 2467–2475.

McNamara, A. M., Denizot, J.-P., & Hopkins, C. D. (2005). Comparative anatomy of the electrosensory lateral line lobe of mormyrids: the mystery of the missing map in the genus Stomatorhinus (Family: Mormyridae). *Brain Behav Evol, 65*, 188–201.

Millot, J., & Anthony, J. (1956). L'organe rostral de Latimeria (Crossoptérygien Coelacanthidé). *Ann Sci Nat Zool 11 Sér, 18*, 381–387.

Moller, P. (1995). Electric fishes: history and behavior. In *Fish and Fisheries Series, 17, pp. xxiv, 584*. London: Chapman & Hall.

Montgomery, J. C. (1984a). Noise cancellation in the electrosensory system of the thornback ray; common mode refection of input produced by the animal's own ventilatory movement. *J Comp Physiol A, 155*, 103–111.

Montgomery, J. C. (1984b). Frequency response characteristics of primary and secondary neurons in the electrosensory system of the thornback ray. *Comp Biochem Physiol, 79A*, 189–195.

Montgomery, J. C., & Bodznick, D. (1993). Hindbrain circuitry mediating common-mode suppression of ventilatory reafference in the electrosensory system of the little skate. *Raja erinacea, J. Exp. Biol., 183*, 203–315.

Murray, R. W. (1962). The response of the ampullae of Lorenzini of elasmobranches to electrical stimulation. *J Exp Biol, 39*, 119–128.

Nelson, M. E. (2005). Target detection, image analysis, and modeling. In T. H. Bullock, C. D. Hopkins, A. N. Popper, & R. R. Fay (Eds.), *Springer Handbook of Auditory Research, Vol. 21, Electroreception* (pp. 290–317). New York: Springer.

New, J. G. (1990). Medullary electrosensory processing in the little skate. I. Response characteristics of neurons in the dorsal octavolateralis nucleus. *J Comp Physiol A, 167*, 285–294.

Neiman, A. B., & Russell, D. F. (2004). Two distinct types of noisy oscillators in electroreceptors of paddlefish. *J Neurophysiol, 92*, 492–509.

Neiman, A. B., Yakusheva, T. A., & Russell, D. F. (2007). Noise-induced transition to bursting in responses of paddlefish electroreceptor afferents. *J Neurophysiol, 98*, 2795–2806.

Northcutt, R. G. (1986). Electroreception in nonteleost bony fishes. In T. H. Bullock, & W. Heiligenberg (Eds.), *Electroreception* (pp. 257–285). New York: John Wiley and Sons.

Northcutt, R. G. (2003). Development of the lateral line system in the channel catfish. In H. I. Browman, & A. B. Skiftesvick (Eds.), *The Big Fish Bang. Proceedings of the 26th Annual Larval Fish Conference* (pp. 137–159). Bergen, Norway: Institute of Marine Research.

Northcutt, R. G. (2005). Ontogeny of electroreceptors and their neural circuitry. In T. H. Bullock, C. D. Hopkins, A. N. Popper, & R. R. Fay (Eds.), *Electroreception* (pp. 112–131). New York: Springer.

Northcutt, R. G., Catania, K. C., & Criley, B. B. (1994). Development of lateral line organs in the axolotl. *J Comp Neurol, 340*, 480–514.

Obara, S. (1976). Mechanisms of electroreception in ampullae of Lorenzini of the marine catfish *Plotosus*. In J. P. Reuben, D. P. Purpura, M. V. L. Bennett, & E. R. Kandel (Eds.), *Electrobiology of Nerve, Synapse and Muscle* (pp. 128–147). New York: Raven Press.

Obara, S., & Bennett, M. V. L. (1972). Mode of operation of ampullae of Lorenzini of the skate, *Raja*. *J Gen Physiol, 60*, 534–557.

Pals, N., Valentijn, P., & Verwey, D. (1982). Orientation reactions of the dogfish, *Scyliorhinus canicula*, to local electric fields. *Netherlands J Zool, 32*, 495–512.

Paulin, M. G. (1995). Electroreception and the compass sense of sharks. *J Theoret Biol, 174*, 325–339.

Peters, R. C., & Evers, H. P. (1985). Frequency selectivity in the ampullary system of an elasmobranch fish (*Scyliorhinus canicula*). *J Expl Biol, 118*, 99–109.

Pettigrew, J. D. (1999). Electroreception in monotremes. *J Exp Biol, 202*, 1447–1454.

Pfeiffer, W. (1968). Die Fahrenholzschen Organe der Dipnoi und Brachiopterygii. *Z Zellforsch, 90*, 127–147.

Pusch, R., von der Emde, G., Hollmann, M., et al. (2008). Active sensing in a mormyrid fish – electric images and peripheral modifications of the signal carrier give evidence of dual foveation. *J Exp Biol, 211*, 921–934.

Raschi, W., & Mackanos, L. A. (1989). The structure of the ampullae of Lorenzini in *Dasyatis garouaensis* and its implications on the evolution of freshwater electroreceptive systems. *J Exp Zool, 2*, 101–111.

Ritz, T., et al. (2000). A model for vision-based magnetoreception in birds. *Biophys J, 78*, 707–718.

Rivera-Vicente, A. C., Sewell, J., & Tricas, T. C. (2011). Electrosensitive spatial vectors in elasmobranch fishes: implications for source localization. *Pub Lib Sci One, 6*, e16008, 1-15.

Ronan, M. C. (1986). Electroreception in cyclostomes. In T. H. Bullock, & W. Heiligenberg (Eds.), *Electroreception* (pp. 209–224). New York: John Wiley and Sons.

Ronan, M. C., & Bodznick, D. (1986). End buds: non-ampullary electroreceptors in adult lampreys. *J Comp Physiol A, 158*, 9–16.

Rose, G. J. (2004). Insights into neural mechanisms and evolution of behaviour from electric fish. *Nat Rev Neurosci, 5*, 943–951.

Semm, P., & Beason, R. C. (1990). Responses to small magnetic variations by the trigeminal system of the bobolink. *Brain Res Bull, 25*, 735–740.

Sisneros, J. A., & Tricas, T. C. (2000). Androgen-induced changes in the response dynamics of ampullary electrosensory primary afferent neurons. *J Neurosci, 20*, 8586–8595.

Sisneros, J. A., Tricas, T. C., & Luer, C. A. (1998). Response properties and biological function of the skate electrosensory system during ontogeny. *J Comp Physiol A, 183*(1), 87–99.

Sugawara, Y. (1989a). Electrogenic NA-K pump at the basal face of the sensory epithelium in the *Plotosus* electroreceptor. *J Comp Physiol A, 164*, 589–596.

Sugawara, Y. (1989b). Two Ca^{++} current components of the receptor current in the electroreceptors of the marine catfish *Plotosus*. *J Gen Physiol, 93*, 365–380.

Szabo, T. (1974). Anatomy of the specialized lateral line organs of electroreception. In A. Fessard (Ed.), *Handbook of Sensory Physiology, Vol. III/3* (pp. 13–58). Berlin: Springer-Verlag.

Tenforde, T. S. (1989). Electroreception and magnetoreception in simple and complex organisms. *Biomagnetics, 10*, 215–221.

Tricas, T. C. (1982). Bioelectric-mediated predation by swell sharks, *Cephaloscyllium ventriosum*. *Copeia, 1982*, 948–952.

Tricas, T. C., & New, J. G. (1998). Sensitivity and response dynamics of elasmobranch electrosensory primary afferent neurons to near threshold fields. *J Comp Physiol A, 182*, 89–101.

Tricas, T. C., Michael, S. W., & Sisneros, J. A. (1995). Electrosensory optimization to conspecific phasic signals for mating. *Neurosci Lett, 202*, 129–132.

Vischer, H. A. (1995). Electroreceptor development in the weakly electric fish *Eigenmannia*: a histological and ultrastructural study. *J Comp Neurol, 360*, 81–100.

Von der Emde, G. (1999). Active electrolocation of objects in weakly electric fish. *J. Exp. Biol., 202*, 1205–1215.

Walker, M. M., Diebel, C. E., Haugh, C. V., Pankhurst, P. M., Montgomery, J. C., & Green, C. R. (1997). Structure and function of the vertebrate magnetic sense. *Nature, 390*, 371–376.

Walker, M. M., Diebel, C. E., & Kirschvink, J. L. (2007). Magnetoreception. In J. H. Toshiaki, & S. Z. Barbara (Eds.), *Fish Physiology, Vol. 25* (pp. 337–376). San Diego: Academic Press.

Waltmann, B. (1966). Electrical properties and fine structure of the ampullary canals of Lorenzini. *Acta Physiol Scand, 66*(Suppl. 264), 1–60.

Whitehead, D., Kwik, J., & Tibbetts, I. (2009). Distribution and morphology of the ampullary organs of the estuarine long-tailed catfish, *Euristhmus lepturus* (Plotosidae, Siluriformes). *Zoomorphology, 128*, 111–117.

Whitehead, D. L., Tibbetts, I. R., & Daddow, L. Y. M. (2000). Ampullary organ morphology of freshwater salmontail catfish, *Arius graeffei*. *J Morphol, 246*, 142–149.

Wilkens, L. A. (2004). Adaptation of the rostral ampullary electrosense for plankton feeding by the paddlefish. In G. von der Emde, J. Mogdans, & B. G. Kapoor (Eds.), *The Senses of Fishes: Adaptations for the Reception of Natural Stimuli* (pp. 288–307). New Dehli: Narosa Publishing House.

Wilkens, L. A., Wettring, B., Wagner, E., Wojtenek, W., & Russell, D. (2001). Prey detection in selective plankton feeding by the paddlefish: is the electric sense sufficient? *J Exp Biol, 204*, 1381–1389.

Wiltschko, R., & Wiltschko, W. (1995). *Magnetic Orientation in Animals*. Berlin: Springer.

Xu-Friedman, M. A., & Hopkins, C. D. (1999). Central mechanisms of temporal analysis in the knollenorgan pathway of mormyrid electric fish. *J Exp Biol, 202*, 1311–1318.

Zakon, H. H. (1986). The electroreceptive periphery. In T. H. Bullock, & W. Heiligenberg (Eds.), *Electroreception* (pp. 103–156). New York: John Wiley and Sons.

Zakon, H. H. (1988). The electroreceptors: diversity in structure and function. In J. Atema, R. R. Fay, A. N. Popper, & W. N. Tavolga (Eds.), *Sensory Biology of Aquatic Animals* (pp. 813–850). New York: Springer.

Section VI

Muscle and Other Contractile Systems

Chapter 42

Skeletal Muscle Excitability

Nicholas Sperelakis, Judith Heiny and Hugo Gonzalez-Serratos

Chapter Outline

I. SUMMARY

The resting potential (RP) of skeletal muscle twitch fibers is about −80 mV (mammalian) or −90 mV (amphibian) and the action potential (AP) overshoots to about +40 mV. The maximal rate of rise of the AP is very fast, being about 500−700 V/s and is due to a large inward *fast* Na^+ *current* (I_{Na}) which brings E_m up close to E_{Na}. The duration of the AP (at 50% repolarization or APD_{50}) is brief, being about 1−3 ms and the falling phase of the AP is produced by several repolarizing factors: (1) increase in the delayed rectifier K^+ conductance; (2) Na^+ channel inactivation and deactivation (due to some repolarization); and (3) Cl^- influx (outward I_{Cl}).

The skeletal muscle fibers are long, being formed by the *fusion of myoblast cells* and thereby producing a multinucleated long myotube or fiber. The fast-rising AP propagates at a velocity of about 5 m/s. Each skeletal muscle twitch fiber is normally closely controlled by the motor innervation, there being one or two *motor end-plates* (neuromuscular junctions) located near the midregion of each fiber. Excitation spreads in both directions from the neuromuscular junction.

The twitch fibers undergo *developmental changes* similar to those in cardiac muscle and neurons. In early development, there are few or no fast Na^+ channels and the AP upstroke is slow and produced by an inward current through slow Ca^{2+} channels. The AP duration is also long because the delayed rectifier K^+ conductance is not fully developed. During subsequent development, fast Na^+ channels are gained, the RP increases (becomes more negative) and the AP shortens to a brief spike.

The skeletal muscle AP spike is immediately followed by a large and prominent early depolarizing afterpotential that slowly decays over 10−20 ms. This *early afterpotential* is caused in part by the persistence and slow decay of the delayed rectifier K^+ conductance (that was turned on by the Na^+ influx-caused depolarization), which has a Na^+:K^+ selectivity or P_{Na}/P_K ratio higher (e.g. 1/30) than that of the resting membrane (e.g. 1/100). This delayed rectifier K^+ conductance holds E_m for a time more depolarized than the normal RP.

After (and during) a tetanic burst (train) of AP spikes, a large prominent *late depolarizing afterpotential* is

Cell Physiology Sourcebook. DOI: 10.1016/B978-0-12-387738-3.00042-1

produced. This late afterpotential is caused by K^+ accumulation in the T-tubules that acts to depolarize them due to the decrease in E_K. Thereby, the surface sarcolemma is depolarized passively. In addition, a slow component of the delayed rectifier K^+ conductance (less selective for K^+ than the resting conductance) may persist during the train.

The *AP invades into the T-tubules* and propagates inward at a slower velocity of about 7–10 cm/s (Gonzalez-Serratos et al., 1978). At this velocity, it would take about 1.0–1.5 ms to propagate to the center of a myofiber having a radius of 30–40 μm. This serves to bring excitation deep into the fiber interior quickly. The depolarization of the T-tubules activates slow (L-type) Ca^{2+} channels located in them and this serves as a critical step in excitation–contraction (EC) coupling. The chapter on EC coupling provides a detailed discussion of a mechanism that involves the Ca^{2+} channels acting as voltage sensors that are coupled to and open the Ca^{2+} release channels in the TC-SR (surface facing the T-tubule).

Some skeletal muscles also contain a fraction of fibers that are non-twitch *slow muscle fibers*, which normally do not fire APs. They are multiply innervated by the motor neuron, with numerous motor end-plates spaced about 1 mm apart along the entire length of the fiber. Graded contraction of each fiber is produced by varying the frequency of axon APs that increase the amplitude of the end-plate potentials (EPPs) by temporal summation. The membrane potential change produced by the summed EPPs is carried passively into the T-tubules to bring about contraction.

II. INTRODUCTION

The normal contraction of vertebrate *twitch-type skeletal muscle fibers* is always preceded by an AP. The AP depolarizes the sarcolemma beyond the membrane potential (E_m) level at which contraction is triggered, i.e. the *mechanical threshold* (see the subsequent chapter on E-C coupling). This is the first step in the chain of events triggered by the initial excitatory process in the sarcolemma, linking it to the final mechanical response. This chain of events is known as *excitation–contraction (E-C) coupling*. In this chapter, we will study the sarcolemmal electrophysiological properties that are the basis of the AP generation. AP generation and excitability in neurons were covered in an earlier chapter. Most of the general electrophysiological principles discussed there also apply to skeletal muscle fibers and so are only briefly reviewed and summarized in this chapter. In most respects, the electrogenesis of the APs in nerve axons and skeletal muscle fibers is quite similar. Both are long fibers and have very brief and fast-rising APs whose inward current is carried by Na^+ ions through fast Na^+ channels. Skeletal muscle fibers, however, have the added complexity of an extensive internal transverse (T) tubular system formed by a periodic invagination of the surface cell membrane (Fig. 42.1), forming an orderly three-dimensional array of tubules that propagate excitation from the cell surface into the deep interior of the fiber for purposes of E-C coupling. In addition, electrogenesis in skeletal muscle fibers differs from nerve fibers in that (1) different types of afterpotentials are produced, (2) propagation is continuous (i.e. saltatory propagation does not occur) and (3) the membrane has a high Cl^- conductance.

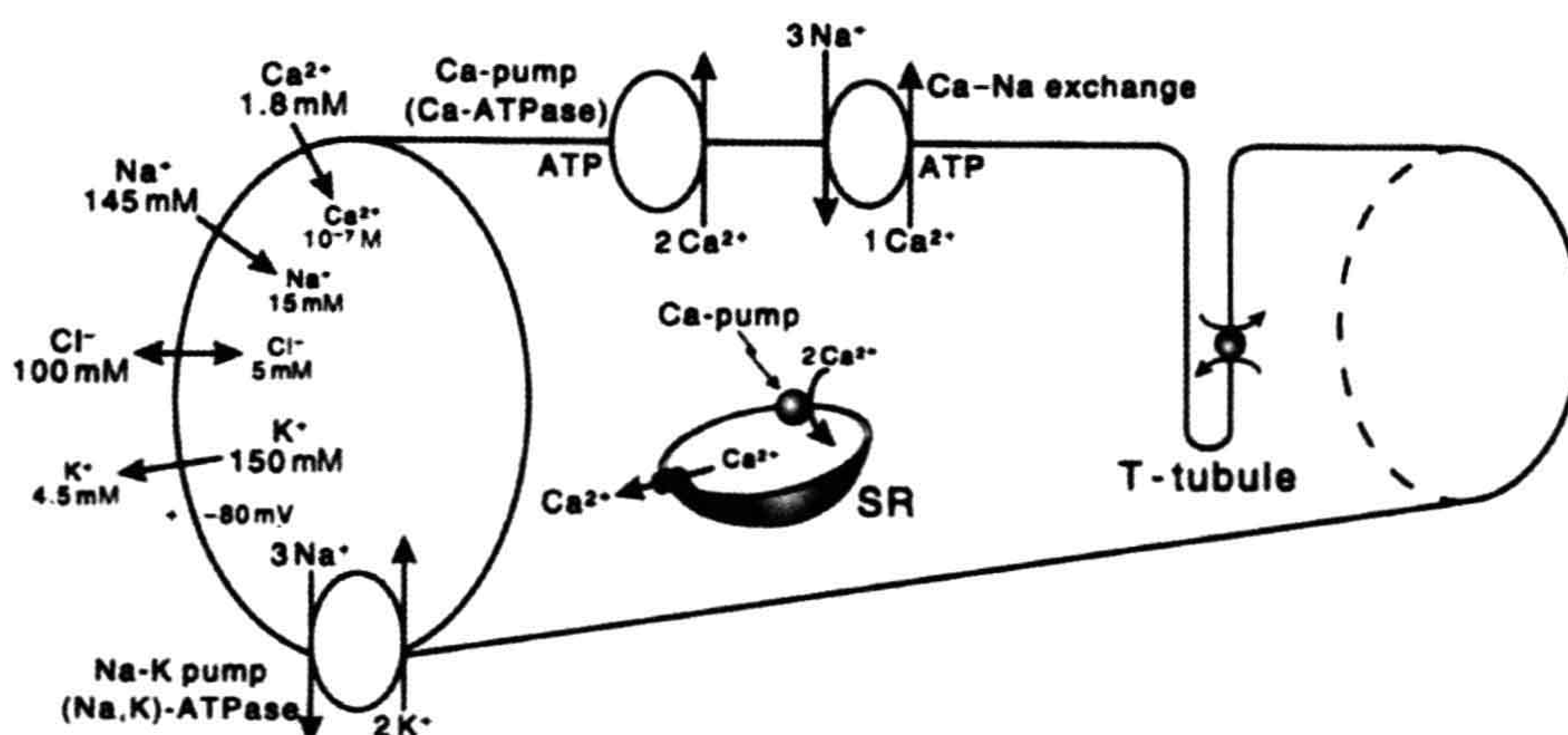


FIGURE 42.1 Intracellular and extracellular ion distributions in vertebrate skeletal muscle fibers. Also shown are the polarity and magnitude of the resting potential (RP). Arrows indicate direction of the net electrochemical gradient. The Na^+-K^+ pump and Ca^{2+}-Na^+ exchange carrier are located in the cell surface and in the T-tubule membranes. A calmodulin-dependent Ca^{2+}-ATPase and Ca^{2+} pump, similar to that in the sarcoplasmic reticulum (SR), is located in the cell surface and T-tubule membranes.

The skeletal muscle AP is considerably different from the AP of *cardiac muscle cells* which have a very long duration with a pronounced plateau and a substantially lower rate of rise and propagation velocity. The myocardial cells are short and there is a slight delay in propagation at each cell-to-cell junction. Like skeletal muscle fibers, myocardial cells have a fast I_{Na} responsible for the rapid upstroke of the AP, but the delayed rectifier K^+ conductance is turned on slowly and there is a substantial inward I_{Ca} during the entire plateau.

The APs of *smooth muscle cells* (SMCs) also are markedly different from those of skeletal muscle fibers, in that the RP (takeoff potential) is lower (more depolarized), the rate of rise of the AP is much slower, the AP overshoot is much less and the AP duration (APD) is considerably longer. Propagation velocity is much slower and the SMCs are short and small in diameter. The inward current for the APs in SMCs is primarily a slow Ca^{2+} current carried through L-type Ca^{2+} channels, but some cells do possess some functioning fast Na^+ channels.

III. GENERAL OVERVIEW OF ELECTROGENESIS OF THE ACTION POTENTIAL

The ion distributions and ion pumps and exchangers found in skeletal muscle fibers are similar to those of other types of cells, as described in the chapters on the RP and nerve APs (see Fig. 42.1). The APs in vertebrate skeletal muscle twitch fibers consist of a *spike* followed by a *depolarizing* (*"negative"*) *afterpotential* (Figs. 42.2 and 42.3). A large fast inward Na^+ current, passing through voltage-dependent fast Na^+ channels, is responsible for electrogenesis of the spike depolarization, which rises rapidly (500–700 V/s). Subsequently, a small slow inward Ca^{2+} current, passing through kinetically slow channels, may be involved in E-C coupling. Outward currents passing through K^+ channels and Cl^- channels are responsible for repolarization of the AP.

The skeletal muscle cell membrane has at least two types of voltage-dependent K^+ channels (Fig. 42.4). One type allows K^+ ions to pass more readily inward than outward, the so-called *inward-going rectifier.* This channel is responsible for *anomalous rectification* (i.e. *decrease* in g_K with depolarization). There is a quick decrease in K^+ conductance on depolarization and increase in K^+ conductance with repolarization. The second type of K^+ channel is similar to the usual K^+ channel found in nerve membrane (e.g. squid giant axon), the so-called *delayed rectifier.* Its conductance turns on more slowly than g_{Na} on depolarization. This channel allows K^+ to pass readily outward down the electrochemical gradient for K^+. The activation of this channel produces the large increase in total g_K that helps to terminate the AP (see Fig. 42.3).

The AP amplitude is about 120 mV, from an RP of −80 mV in mammalian myofibers (−90 mV in amphibian)

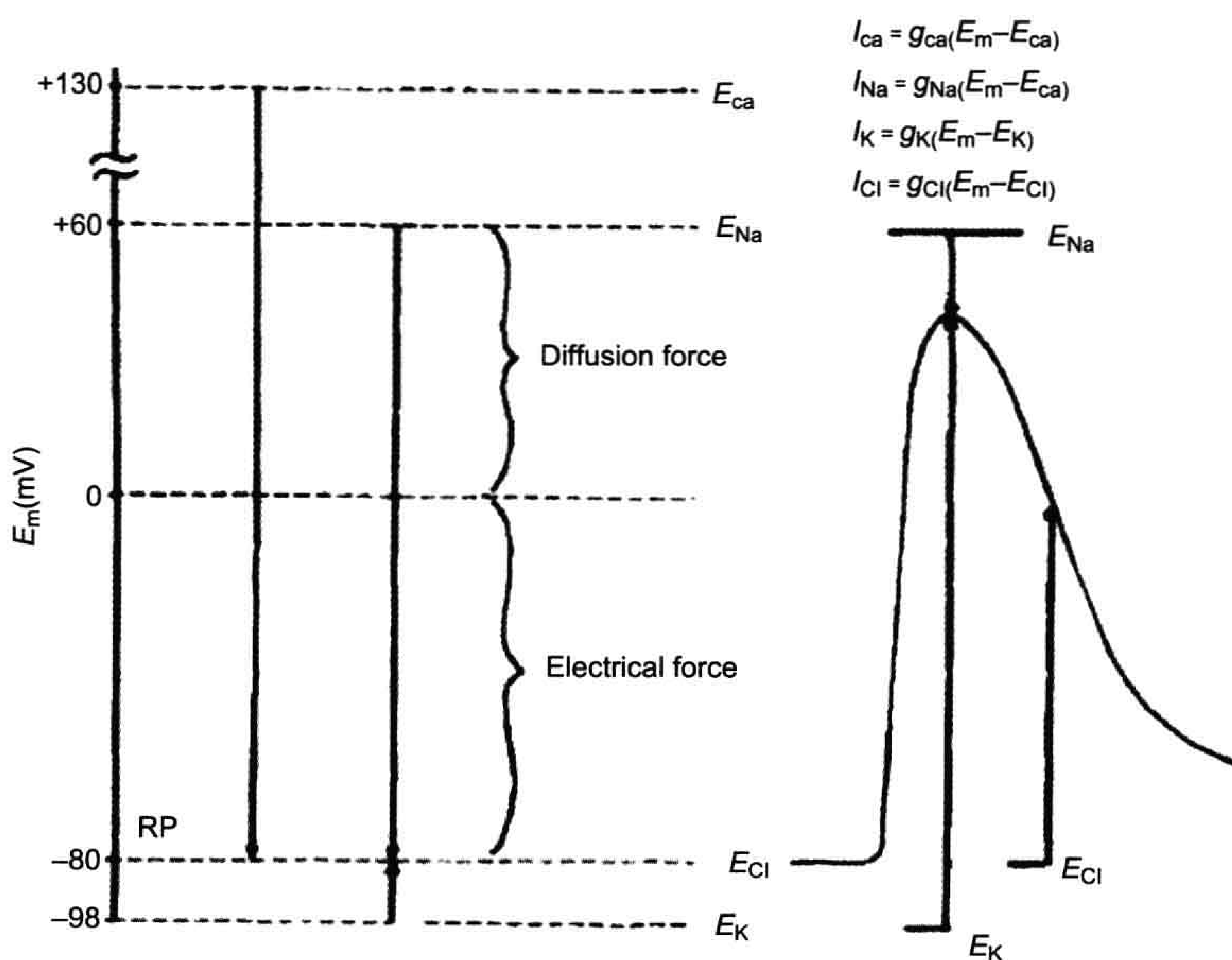


FIGURE 42.2 Representation of the electrochemical driving forces for Na^+, Ca^{2+}, K^+ and Cl^- at rest (left diagram) and during the AP in a skeletal muscle fiber (right diagram). Equilibrium potentials for each ion (e.g. E_{Na}) are positioned vertically according to their magnitude and sign; they were calculated from the Nernst equation for a given set of extracellular and intracellular ion concentrations. Measured RP is assumed to be −80 mV. Electrochemical driving force for an ion is the difference between its equilibrium potential (E_i) and the membrane potential (E_m), i.e. ($E_m - E_i$). Thus, at rest, the driving force for Na^+ is the difference between E_{Na} and the resting E_m; if E_{Na} is +60 mV and resting E_m is −80 mV, the driving force is 140 mV. The driving force is then the algebraic sum of the diffusion force and the electrical force and is represented by the length of the arrows in the diagram. Driving force for Ca^{2+} (about 210 mV) is even greater than that for Na^+, whereas that for K^+ is much less (about 18 mV). Direction of the arrows indicates the direction of the net electrochemical driving force, namely, the direction for K^+ is outward, whereas that for Na^+ and Ca^{2+} is inward. If Cl^- is passively distributed, then for a cell sitting a long time at rest, $E_{Cl} = E_m$ and there is no net driving force. The driving forces change during the AP, as depicted. The equations for the different ionic currents are given in the upper right-hand portion of the figure. *(Adapted from Sperelakis, 1979.)*

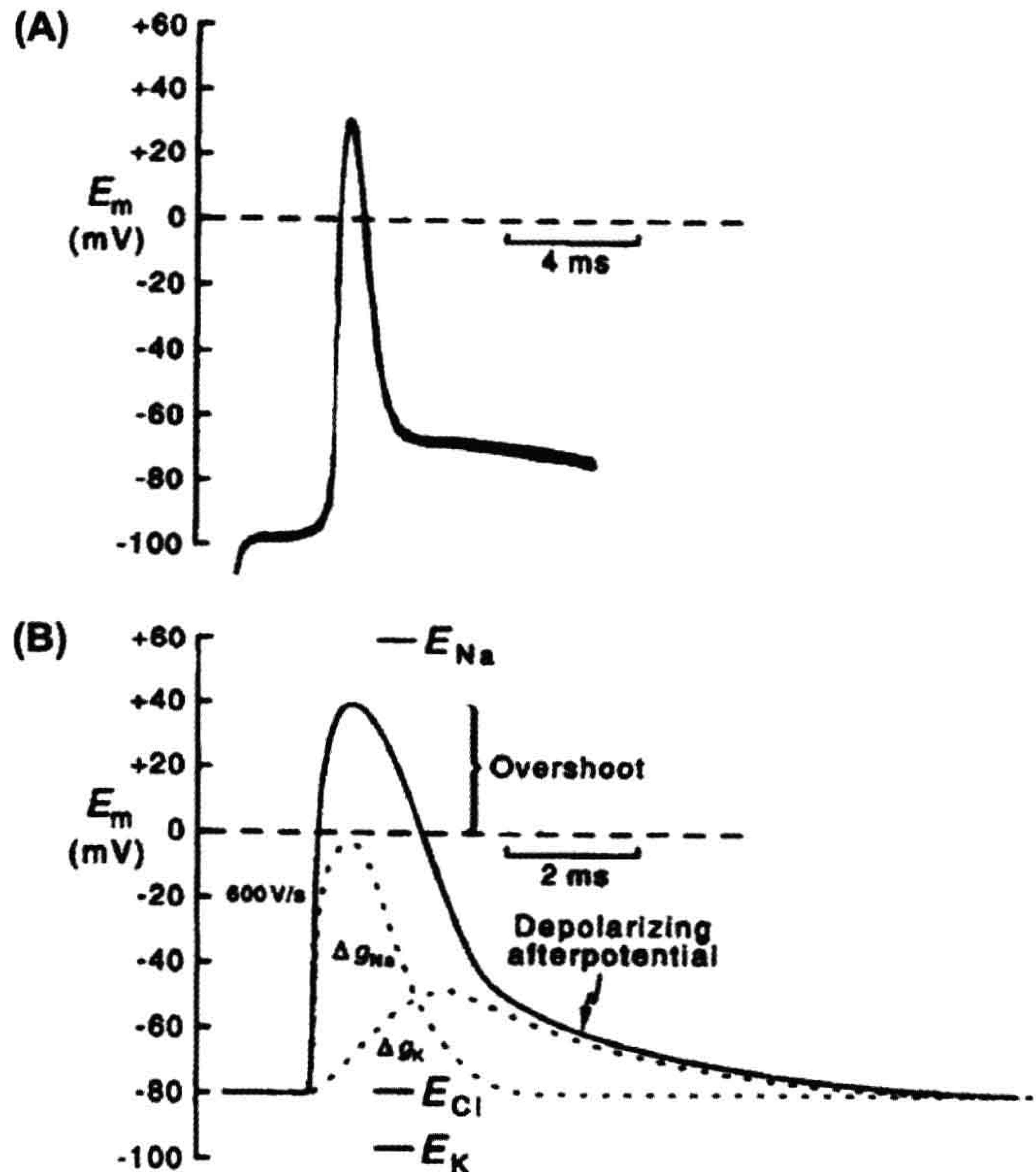


FIGURE 42.3 (A) Action potential (AP) recorded with an intracellular microelectrode in a skeletal muscle fiber of frog semitendinosus muscle bathed in normal frog Ringer's solution. Note the prominent depolarizing afterpotential. Shock artifact is at left of spike. (*Modified from Sperelakis et al., 1973.*) (B) Diagrammatic representation of the relative conductance changes for Na^+ and K^+ during an AP. The rising phase of the AP is caused by an increase in g_{Na}, which brings the E_m toward E_{Na}. The falling phase of the AP is due to the rise in g_K, the decrease in g_{Na}, and to an outward Cl^- current. The depolarizing afterpotential is explained in part by the fact that the delayed rectifier K^+ channel is less selective for K^+ (30:1 over Na^+) than is the resting channel (100:1) and, in part, by the contribution of the AP traveling down the T-tubular network.

to a peak overshoot potential of about +40 mV (see Figs. 42.2 and 42.3). The duration of the AP (at 50% repolarization, or APD_{50}) ranges between 3 and 6 ms, depending on the species and temperature. The *threshold potential* (V_{th}) for triggering of the fast Na^+ channel conductance is about −65 to −55 mV; thus, a *critical depolarization* of about 25 mV is required to reach V_{th}. The turn-on of the fast g_{Na} (fast I_{Na}) is very rapid (within 0.2 ms) and E_m is brought rapidly toward E_{Na} (see Figs. 42.2 and 42.3). There is an explosive (positive exponential initially) increase in g_{Na}, caused by a *positive feedback* relationship between g_{Na} and E_m.

From the current versus voltage (I/V) curves, the maximum inward fast Na^+ current occurs at an E_m of about −20 mV. The current decreases at more depolarized E_m levels because of the diminution in electrochemical driving force as the membrane is further depolarized, even though the conductance remains high. At the reversal potential (E_{rev}) for the current, the current goes to zero; I_{Na} then reverses direction with greater depolarization.

As E_m depolarizes, it crosses V_{th} for slow Ca^{2+} channels (also called *L-type Ca^{2+} channels* or *dihydropyridine receptors*), which is about −35 mV. These Ca^{2+} channels are primarily located in the transverse tubules. Turn-on of the Ca^{2+} conductance (g_{Ca}) and I_{Ca} is relatively slow and the peak I_{Ca} is considerably smaller than the peak I_{Na}. *This Ca^{2+} influx is involved in E-C coupling.*

The molecular rearrangements involved in activation of the slow Ca^{2+} channels are directly coupled to opening of *Ca^{2+}-release channels* (or *ryanodine receptors*) in the sarcoplasmic reticulum (SR) membrane. However, the open probability of these channels is very low. Therefore, the resulting increase in Ca^{2+} conductance (g_{Ca}) and the peak I_{Ca} is relatively slow and considerably smaller than the peak I_{Na}. This Ca^{2+} influx is small during a single AP, but can contribute to E-C coupling during repetitive AP firing.

IV. ION CHANNEL ACTIVATION AND INACTIVATION

As discussed in the chapter on nerve excitability (see Chapter 19), the fast Na^+ channels (and the slow Ca^{2+} channels) have a double gating mechanism; one gate is the *activation gate* (A-gate) and the second gate is the *inactivation gate* (I-gate). For a channel to be conducting, both the A-gate and I-gate must be open; if either one is closed, the channel is non-conducting. The A-gate is closed at the

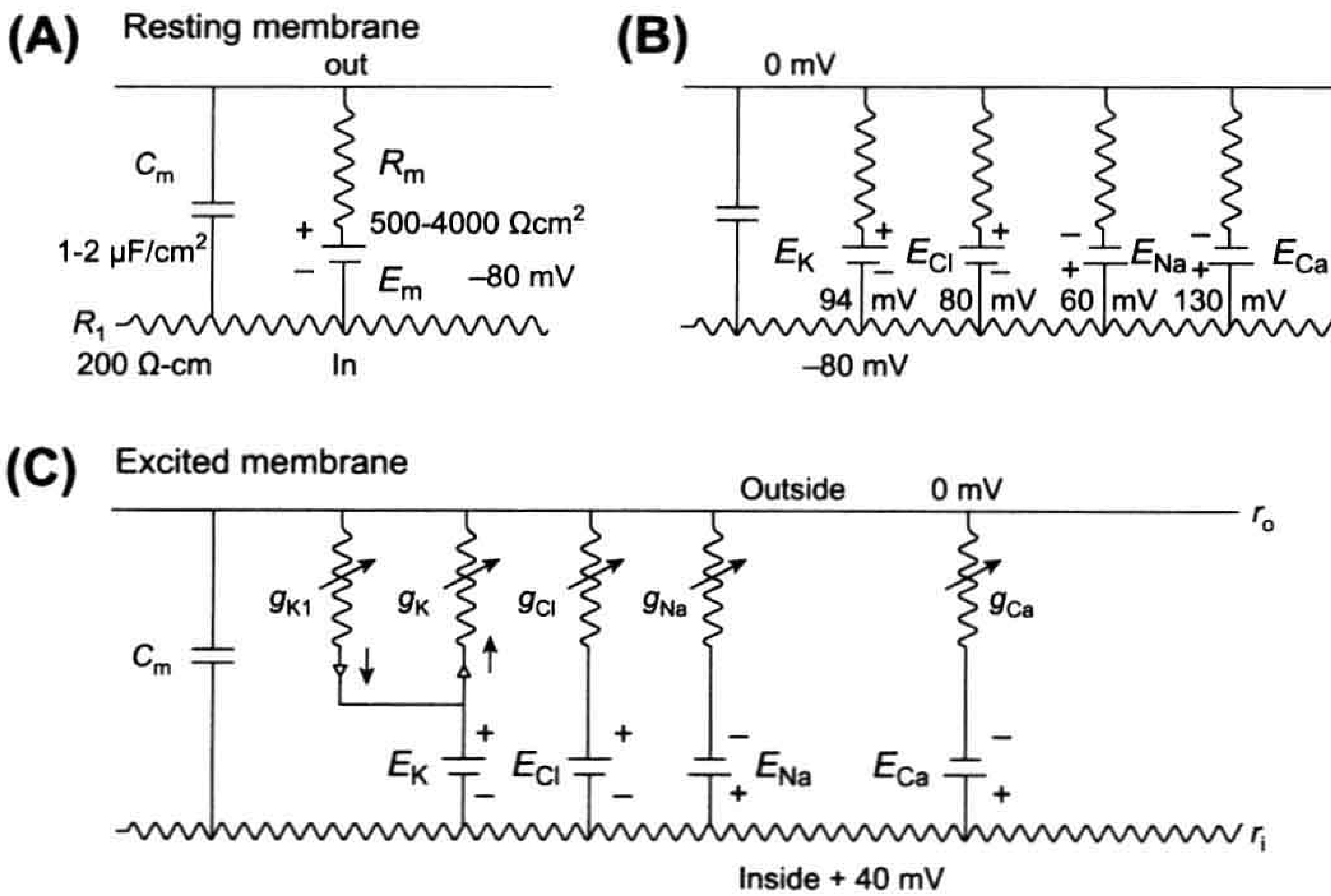


FIGURE 42.4 Electrical equivalent circuits for a skeletal muscle fiber cell membrane at rest (A and B) and during excitation (C). (A) Membrane as a parallel resistance-capacitance circuit, the membrane resistance (R_m) being in parallel with the membrane capacitance (C_m). RP (E_m) is represented by an 80 mV battery in series with the membrane resistance, the negative pole facing inward. (B) Membrane resistance is divided into four component parts, one for each of the four major ions of importance: K^+, Cl^-, Na^+ and Ca^{2+}. Resistances for these ions (R_K, R_{Cl}, R_{Na} and R_{Ca}) are parallel to one another and represent totally separate and independent pathways for permeation of each ion through the resting membrane. These ion resistances are depicted as their reciprocals, namely, ion conductances (g_K, g_{Cl}, g_{Na} and g_{Ca}). Equilibrium potential for each ion (e.g. E_K), determined solely by the ion distribution in the steady-state and calculated from the Nernst equation, is shown in series with the conductance path for that ion. RP of −80 mV is determined by the equilibrium potentials and by the relative conductances. (C) Equivalent circuit is further expanded to illustrate that, for the voltage-dependent conductances, there are at least two separate K^+-conductance pathways (labeled here g_{K1} and g_K). In series with the K^+ conductances are rectifiers pointing in the direction of least resistance to current flow. There is one Na^+ conductance pathway, the kinetically fast Na^+ conductance (g_{Na}). In addition, there is a kinetically slow pathway that allows Ca^{2+} to pass through. Arrows drawn through the resistors indicate that the conductances are variable, depending on membrane potential and time. *(Adapted from Sperelakis, 1979.)*

resting E_m and opens rapidly on depolarization, whereas the I-gate is open at the resting E_m and closes slowly on depolarization. In the Hodgkin–Huxley (1952) analysis, the opening of the A-gate requires simultaneous occupation of three negatively-charged sites by three positively-charged m^+ particles. Therefore:

$$g_{Na} = \bar{g}_{Na} m^3 h \qquad (42.1)$$

where m is the activation variable, h is the inactivation variable and $\bar{g}_{Na}$ is the maximum conductance. A small gating current (I_g) has been measured that corresponds to the movement of the charged m particles (or rotation of an equivalent dipole). The outward I_g leads into the inward I_{Na}.

The fast I_{Na} lasts only for 1–2 ms because of the spontaneous voltage inactivation of the fast Na^+ channels, i.e. they inactivate quickly, even when the membrane remains depolarized. Inactivation is produced by the voltage-dependent closing of the I-gate. The voltage dependence of inactivation is given by the h_∞ versus E_m curve. The Na^+ conductance (g_{Na}) at any time is equal to the maximal value ($\bar{g}_{Na}$) times m^3h. Therefore, when $h = 0$, $g_{Na} = 0$, and when $h = 1.0$, $g_{Na} = \bar{g}_{Na}$ (if $m = 1.0$). At the normal RP, h_∞ is nearly 1.0 and diminishes with depolarization, becoming nearly zero at about −30 mV. The maximal rate of rise of the AP (max dV/dt) is directly proportional to the net inward current or I_{Na}, which is directly proportional to g_{Na} and can be expressed as:

$$\max dV/dt \propto \frac{I_{Na}}{C_m} = \frac{\bar{g}_{Na}\, m^3 h\, (E_m - E_{Na})}{C_m} \qquad (42.2)$$

Therefore, a decrease in h_∞ causes decrease in max dV/dt. Thus, depolarization by any means (e.g. elevated $[K+]_o$ or applied current pulses) decreases max dV/dt, and excitability disappears at about −50 mV.

The slow Ca^{2+} channels behave much the same way as the fast Na^+ channels with respect to activation and inactivation, with one main difference being the voltage range over which the slow channels activate and inactivate. Slow channels inactivate between −45 mV and −10 mV, compared to −70 and −30 mV for the fast Na^+ channels. Another major difference is that the slow Ca^{2+} conductance inactivates much more slowly than the fast Na^+ conductance; i.e. they have a long inactivation time constant (τ_{inact}). (The h variable for the slow channel is sometimes referred to as the f variable and the m variable as the d variable.) Because slow Ca^{2+} channels are located in the T-tubular system, their function is affected by tubular Ca^{2+} depletion caused by the Ca^{2+} ions that flow into the myoplasm. The recovery process for the slow Ca^{2+} channels is slow compared to 1–2 ms for fast Na^+ channels.

The K^+ channel (*delayed rectifier*) may have only an activation gate, because it does not inactivate quickly. In the Hodgkin–Huxley analysis of squid giant axon, the A-gate opens when four positively-charged n^+ particles simultaneously occupy four favorable positions (negatively-charged sites). If n is the probability that one site is occupied, then n^4 is the probability that all four sites are occupied. Therefore,

$$g_K = \bar{g}_K n^4 \qquad (42.3)$$

The fourth power to which n must be raised causes a delay (sigmoidal foot) in turn-on of the K^+ conductance.

V. SLOW DELAYED RECTIFIER K^+ CURRENT

Two types of K^+ delayed rectifier currents occur in skeletal muscle. A slow I_K was first described by Adrian and coworkers (1970a,b) in voltage-clamped frog sartorius fibers. The *slow component* of outward I_K reached a maximum in about 3 s and declined with a time constant of about 0.5 s. In voltage-clamped frog toe muscle, Lynch (1978) observed that most fibers had both a slow component and a *fast component* of the outward I_K (threshold of −55 mV). The voltage dependences of both K^+ currents were shifted equally in the depolarizing direction by elevated $[Ca^{2+}]_o$ or $[H^+]_o$, presumably due to altering the net negative outer surface charge of the membrane, thereby hyperpolarizing. Acidosis also increased the rate of turn-on of the slow delayed rectifier. The fast delayed current was relatively selectively blocked by TEA or by a sulfhydryl reagent, whereas the slow delayed current was selectively depressed by a histidine reagent. It was estimated that about 25% of the delayed rectifier channels are in the T-tubular membrane. The functional significance of the slow I_K is unknown, although it may be partly responsible for the late depolarizing afterpotential (see Section VIII).

VI. MECHANISMS OF REPOLARIZATION

The skeletal muscle AP is terminated by three processes: turn-on of g_K, turn-off of g_{Na} and influx of Cl^- ions. The turn-on of the V-dependent K^+ conductance (g_K) (the *delayed rectifier*) (see Fig. 42.3) acts to bring E_m towards E_K (about −98 mV), since the membrane potential at any time is determined primarily by the ratio of g_{Na}/g_K. This type of g_K channel is activated by depolarization and turned off by repolarization. Therefore, this g_K channel is *self-limiting*, in that it turns itself off as the membrane is repolarized by its action.

In addition to the g_K turn-on, turn-off of g_{Na} occurs (see Fig. 42.3) (contributing to repolarization) for two reasons: (1) spontaneous *inactivation* of fast Na^+ channels that had been activated, i.e. closing of their I-gate (inactivation τ of 1−3 ms) and (2) reversible shifting of activated channels directly back to the resting state (*deactivation*), because of the rapid repolarization that is occurring due to the g_K increase (Fig. 42.5). Theoretically, it would be possible to have an AP that would repolarize (but more slowly) even if there were no g_K mechanism, because the g_{Na} channels would spontaneously inactivate and so the g_{Na}/g_K ratio and E_m would be more slowly restored to their original resting values.

In addition, there is an important third factor involved in repolarization of the AP in skeletal muscle: the *Cl^- current* (see Fig. 42.2). The Cl^- permeability (P_{Cl}) and conductance (g_{Cl}) are very high in skeletal muscle (and are not strongly V-dependent). In fact, P_{Cl} of the surface membrane is much higher than P_K, the P_{Cl}/P_K ratio being about 3−7. As discussed in the chapter on RP (see Chapter 9), the Cl^- ion is passively distributed, or nearly so, and thus cannot determine the RP. However, net Cl^- movements inwards (hyperpolarizing) or outward (depolarizing) do affect E_m transiently until re-equilibration occurs and there is no further net movement. At the RP, there is no net Cl^- current (I_{Cl}), since there is no electrochemical driving force for Cl^- (since $E_m = E_{Cl}$). However, during the AP depolarization, there is a larger and larger driving force for outward I_{Cl} (i.e. Cl^- influx), since $I_{Cl} = g_{Cl}\,(E_m - E_{Cl})$. In other words, the large electric field that was keeping Cl^- out (i.e. $[Cl^-]_i << [Cl^-]_o$) diminishes during the AP and so Cl^- ion enters the fiber. This Cl^- entry is hyperpolarizing and so tends to repolarize the membrane more quickly than would otherwise occur. That is, AP repolarization is sharpened by the Cl^- mechanism. (Note that influx of the negatively-charged Cl^- ion is an outward Cl^- current, which is repolarizing.)

To illustrate further some of the preceding points on the role of Cl^-, when skeletal muscle fibers are placed into Cl^--free Ringer solution (e.g. methanesulfonate substitution), depolarization and spontaneous APs and twitches occur for a few minutes until most or all of the $[Cl^-]_i$ is washed out. After equilibration, the resting E_m returns to the original value ca. −90 mV for frog skeletal muscle and −80 mV for mammalian, clearly indicating that Cl^- does not determine the RP and that net Cl^- efflux produces depolarization. Re-addition of Cl^- to the bath produces a rapid large hyperpolarization, e.g. to −120 mV, due to net Cl^- influx; the E_m then slowly returns to the original value (e.g. −90 mV) as Cl^- re-equilibrates, i.e. redistributes itself passively. These same effects occur in cardiac muscle, smooth muscle and nerve, but to a lesser extent, because in these tissues P_{Cl} is much lower (e.g. P_{Cl}/P_K ratio is only about 0.5 in vascular smooth muscle).

The importance of the Cl^- current in repolarization in skeletal muscle fibers is illustrated by one type of *myotonia* in which an abnormally low P_{Cl} causes repetitive APs to occur. Because g_{Cl} is abnormally low, total membrane conductance G_m is also low. From the relationship between membrane current (I_m) and G_m ($I_m/G_m = E_m$), it can be deduced that only a smaller outward depolarizing membrane current I_m is necessary to reach threshold E_{th} for an AP. Since g_{Cl} is abnormally low, the membrane resistance R_m will be abnormally high, making the space constant λ larger than normal. Because g_{Cl} is abnormally low, the Cl^- influx during AP repolarization is much less than normal and so the repolarization process is slowed, thus increasing the duration of the AP. As a consequence of the above, when depolarization occurs, the AP threshold is easily and quickly reached and the generated APs spread easily along the sarcolemma. These factors make the whole

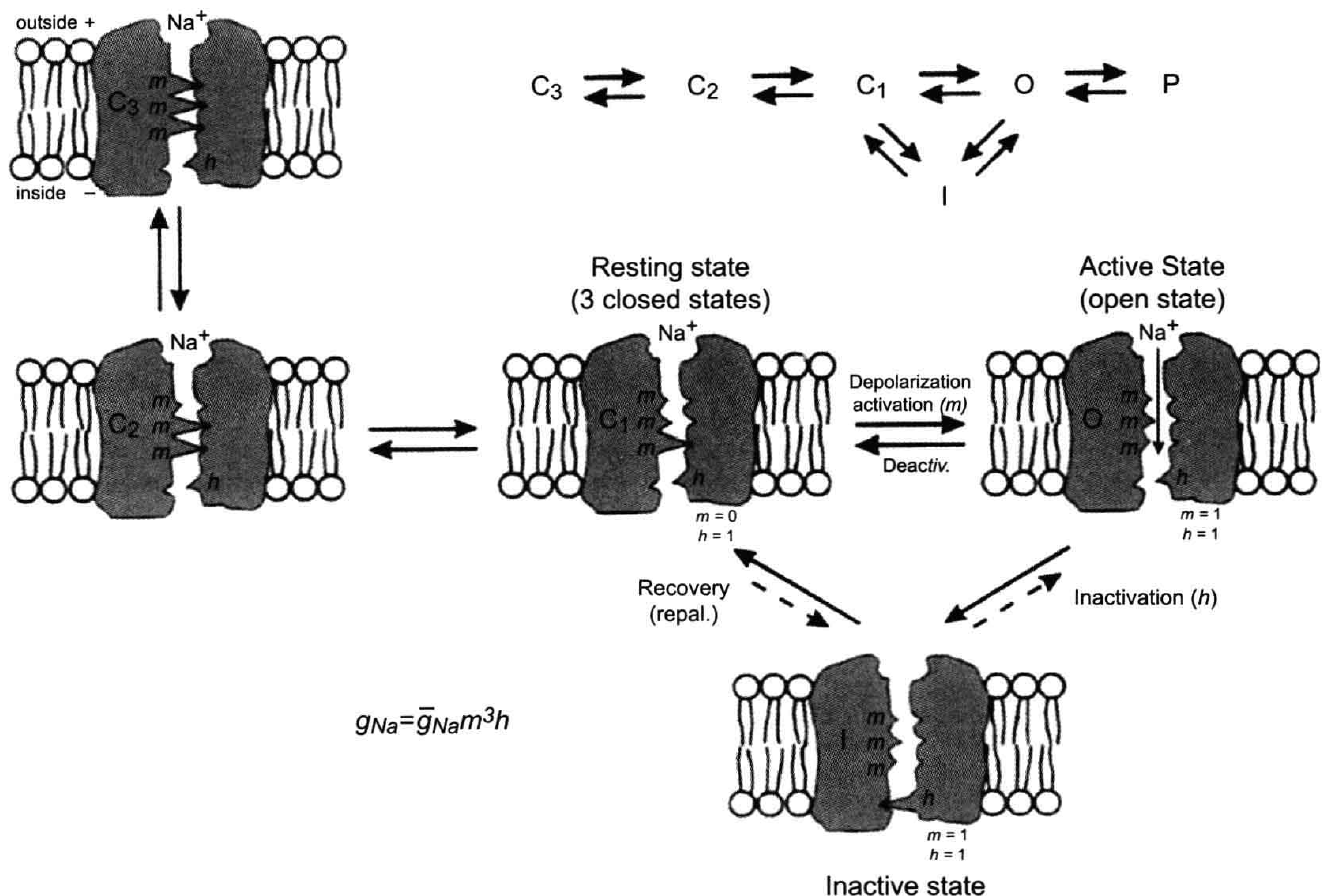


FIGURE 42.5 Illustration of the hypothetical states of the fast Na^+ channel. The three states patterned after the Hodgkin–Huxley view were modified to reflect the fact that there is evidence for three closed states. As depicted, in the most closed state (C_3), all three *m* gates (or particles) are in the closed configuration. In the mid-closed state (C_2), two *m* gates are closed and one is open. In the least closed state (C_1), one gate is closed and two are open. In the resting state, the activation gate (A) is closed and the inactivation gate (I) is open: $m = 0, h = 1$. Depolarization to the threshold activates the channel to the active state, the A-gate opening rapidly and the I-gate still being open: $m = 1, h = 1$. The activated channel spontaneously inactivates to the inactive state due to closure of the I-gate: $m = I, h = 0$. The recovery process on repolarization returns the channel from the inactive state back to the resting state, thus making the channel again available for reactivation. Na^+ ion is depicted as being bound to the outer mouth of the channel and poised for entry down its electrochemical gradient when both gates are open. The reaction between the resting state and the active state is readily reversible and there is some reversibility of the other reactions. The fast Na^+ channel is blocked by tetrotodoxin (TTX) binding to the outer mouth and plugging it.

system unstable and oscillations trigger *repetitive discharge* of APs. That is, the muscle fibers lose their tight control by the motor neurons and so contraction becomes partly involuntary. For example, persons with myotonia find it difficult to release a handshake or to remove their hand from a drinking glass. There are several causes of myotonia, including genetic abnormalities in ion channels, as well as drug-induced conditions. Any agent that greatly lowers P_{Cl} or g_{Cl} will have the same effect. It has been shown that simply decreasing g_{Cl} causes repetitive firing in equivalent circuit models of skeletal muscle fibers. In addition, K^+ ions tend to accumulate in the lumen of the T-tubules under normal conditions (see Section VIII). This accumulation is exaggerated with the prolonged APs and so tends partially to depolarize the fibers and increase their excitability. Some forms of myotonia are produced by *abnormal fast Na^+ channels*; namely, a small fraction of these channels do not inactivate as quickly as usual (i.e. their I-gates do not close normally) and so causes a prolonged small depolarization after the AP and, consequently, a repetitive discharge.

In myotonia, AP repolarization is slowed and the duration of the AP is increased. As AP duration increases, more Na^+ channels have time to return to the resting conformation by deactivation or recovery from inactivation (a process which has a time constant of 2–3 ms). This creates a window of instability during AP repolarization. The membrane potential remains depolarized above threshold, allowing some Na^+ channels to reopen and trigger another AP. The skeletal muscles have a large safety factor with respect to the number of Na^+ channels in the membrane and as few as 3–5% in the open state can trigger an AP. This instability in membrane repolarization is further enhanced by the high membrane resistance. Without

the normal large g_{Cl}, only a smaller than normal outward depolarizing current is required to reach threshold. Because of the high membrane resistance R_m, the space constant λ is longer than normal. Consequently, the APs propagate at a faster velocity. These factors act synergistically to make the whole system unstable. Consequently, when depolarization occurs, the AP threshold is easily and quickly reached, the generated APs spread fast along the sarcolemma and the membrane is more excitable and susceptible to repetitive discharge of APs.

The high g_{Cl} *in skeletal muscle fibers* is due to a large number of voltage-dependent gated Cl^- channels, which are outwardly rectifying. The major Cl^- channel of skeletal muscle is the ClC-1 channel (Steinmeyer et al., 1991), a member of the ClC family of Cl^- channels and Cl^-/H^+ antiporters (Zifarellli and Pusch, 2007). These Cl^- channels are located both on the surface sarcolemma and T-rubule membrane in frogs and mammals. Denervation of mammalian fibers causes g_{Cl} to decrease almost to zero.

VII. ATP-DEPENDENT K^+ CHANNELS

K_{ATP} channels are among the most abundantly expressed K^+ channels in the skeletal muscle sarcolemma, reaching densities of 10 channels per μm^2 of surface membrane (Spruce et al., 1987), comparable to that of K^+ delayed rectifier channels (Standen et al., 1985). K_{ATP} channel currents can be recorded from both surface (Spruce et al., 1985) and transverse tubular membranes (Heiny et al., 1983). However, their physiological role in skeletal muscle is not well understood (reviewed in Flagg et al., 2010). The functional K_{ATP} channel is an octomeric protein composed of four pore-forming Kir subunits (Kir 6.1 and Kir 6.2) and four regulatory SUR (sulfonylurea receptor) subunits assembled in a 4:4 stoichiometry. Functioning of the K_{ATP} channel requires the proper coupling between Kir and SUR subunits. More details on the subunits is given in the Appendix to this chapter.

ATP-dependent K^+ (K_{ATP}) channels are characterized by the inhibition of channel openings by ATP (Yokoshiki et al., 1998). In addition to being ligand sensitive, these K_{ATP} channels are voltage-dependent; the open state probability increases with depolarization. Most studies of K_{ATP} channels have been performed using patch-clamp of isolated inside-out patches of skeletal muscle (Spruce et al., 1987). The unitary conductance of this channel varies with $[K^+]_o$, ranging from 15 pS in 2.5 mM $[K^+]_o$ to 42 pS in 60 mM. K_{ATP} channels are closed when the ATP concentration in the intracellular myoplasm is in the range of 1.0 mM or higher, which is the normal physiological concentration. A decrease in ATP concentration or depolarization activates the channel. The half-maximum inhibition of this channel opening by ATP, measured at a constant $[K^+]_o/[K^+]_i$, is 0.135 mM at pH 7.2 (Fig. 42.6).

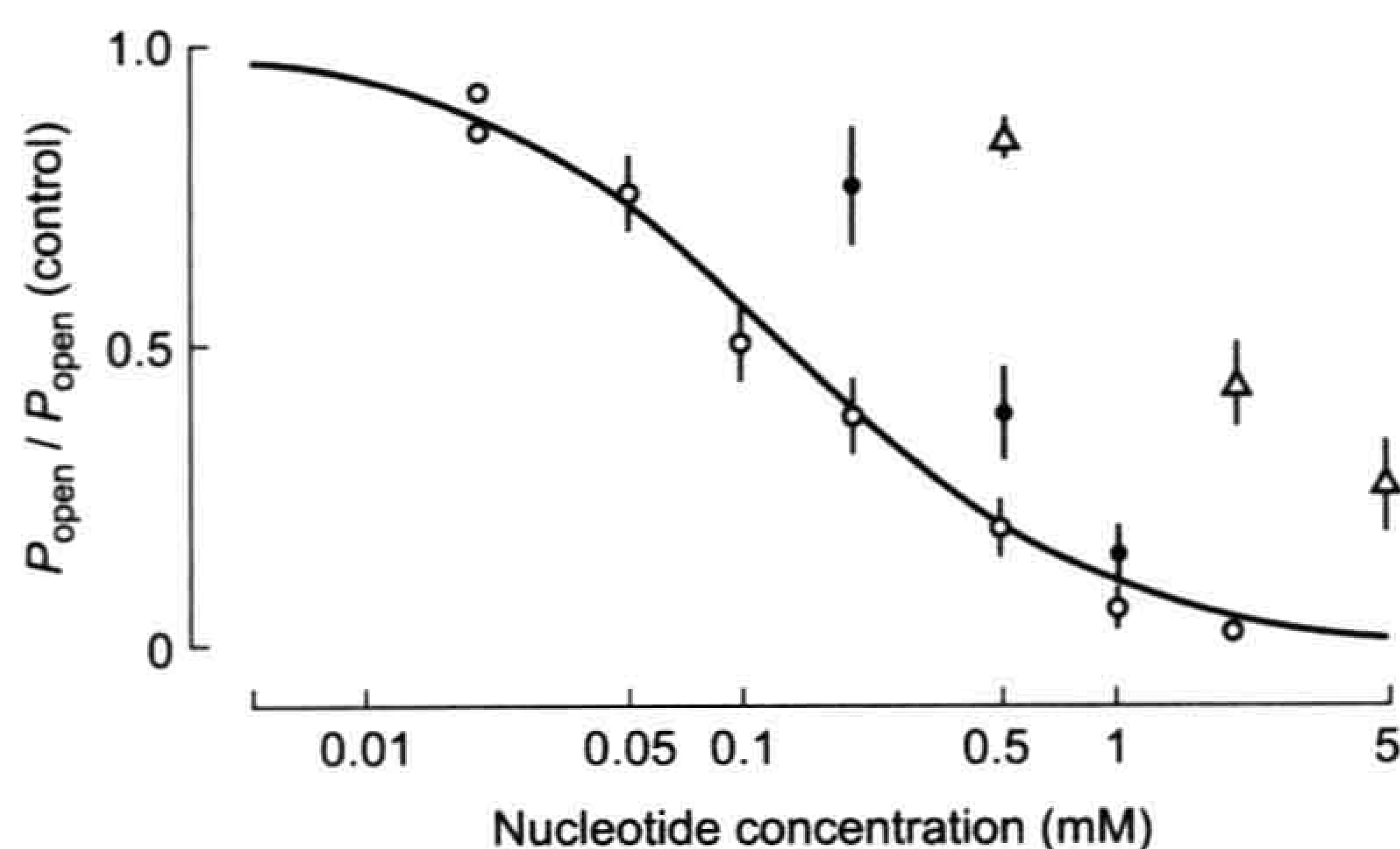


FIGURE 42.6 Effect of ATP (open circles), ADP (filled circles) and AMP (open triangles) on closing the ATP-regulated K^+ channels. Ordinate: open-state probability (P_o) of the channel relative to its value in nucleotide-free solution (P_{open} control). *(Reproduced with permission from Spruce et al., 1987.)*

Hydrolysis of ATP (into ADP + P_i) is not required for ATP to close K_{ATP} channels.

Although ATP is the most specific ligand to close K_{ATP} channels, there are other ligands that modulate these channels. The metabolites produced during contraction, like ADP, Mg^{2+} and H^+ also modulate the channels. The two adenine nucleotides, ADP and AMP (in the absence of ATP), also can block K_{ATP} channels in a dose-dependent manner. However, they are less effective than ATP (see Fig. 42.6). ATP analogs like GTP, ITP, XTP, CTP and UTP also have reduced effectiveness (about tenfold) in closing these channels. ADP shifts the ATP dose—response curve, raising the half-inhibition concentration, consistent with competition between ATP and ADP for the nucleotide binding site on the channel (Spruce et al., 1987; Vivaudou et al., 1991).

A decrease in pH at the cytoplasmic surface (pH_i) reduces the degree of K_{ATP} channel inhibition caused by ATP. The ATP concentration for half-inhibition is 2.5 times and 15 times greater at pH_i 6.8 and 6.3, respectively, as compared to that at pH_i 7.2. Thus, during acidosis, a smaller decrease in ATP concentration will lead to a larger opening of K_{ATP} channels. It was proposed that proton binding to the channel prevents ATP binding (Davies et al., 1992). Mg^{2+} has a similar effect as protons. An increase of cytosolic Mg^{2+} reduces the ability of ATP to close K_{ATP} channels (Vivaudou et al., 1991). Mg^{2+} may bind to the channels and plug them (Woll et al., 1989). In addition, the inhibitory effect may be partly due to the ability of Mg^{2+} to bind to ATP.

K_{ATP} channels have been studied in excised patches of surface membrane blebs from muscles of frogs and mammals. These channels are, therefore, likely to be present in the sarcolemma. It is not known whether they are present in the T-tubular system. As stated earlier, the K_{ATP} channel density has been estimated to be as high as 10 channels per μm^2 of surface membrane (Spruce et al., 1985), a density comparable to that for K^+ delayed rectifier channels.

The physiological role played by K_{ATP} channels in skeletal muscle is not clear. Under physiological conditions, the intracellular ATP concentration is about 5 mM at rest. Therefore, at the resting ATP level, almost all of the K_{ATP} channels should be inactive (Spruce et al., 1987; Davies et al., 1992). Even during repetitive contractions that lead to muscle fatigue, the ATP concentration is maintained at near normal levels by the action of creatine kinase and creatine phosphate (Carlson and Siger, 1960; Nassar-Gentina et al., 1978).

It has been proposed that K_{ATP} channels may be associated with the decrease in force development underlying muscle fatigue. A drug (SR44866) that opens K_{ATP} channels (in frog skeletal muscles) also reduces the AP duration, the early afterpotential and the peak twitch force (without affecting the RP) in intact muscles (Sauviat et al., 1991). The high K^+ permeability found in muscle fibers that have undergone a permanent contracture (rigor) produced by repetitive stimulation when poisoned with cyanide and iodocetate (Fink and Lüttgau, 1976), may be caused by the decreased ATP concentration opening K_{ATP} channels. In metabolically-exhausted frog semitendinosus muscle fibers, the addition of tolbutamide and glyburide, two K_{ATP} channel antagonists, significantly reduces the K^+ efflux rate (Castle and Haylett, 1987). Fatigued muscle fibers can contract when Ca^{2+} is released directly from the intracellular SR stores (Gonzalez-Serratos et al., 1978; Garcia et al., 1991). In intact animals, some of the skeletal muscle fatigue results from synaptic fatigue, including at the neuromuscular junction.

As stated previously, a decrease in pH_i (e.g. from lactic acid production) reduces the inhibitory effect of ATP on K_{ATP} channels. During exercise, with fatigue development, pH_i may decrease by about one unit (Renaud, 1989). A small decrease in ATP concentration is accompanied by an increase in ADP, H^+ and Mg^{2+} concentrations and the overall combination of these chemical changes may then lead to the activation of K_{ATP} channels. As K_{ATP} channels open, they contribute to the increased K^+ efflux found during repetitive muscle contraction. Because of the restricted diffusion out of the T-tubular system and the closeness of the intercellular fiber spacing, extracellular K^+ concentration increases, especially inside the tubular system. This may cause a decrease in cell excitability, which may be reflected as decreased force development. This mechanism may protect skeletal muscle cells from large ATP depletions that would have deleterious effects.

VIII. ELECTROGENESIS OF DEPOLARIZING AFTERPOTENTIALS

As mentioned previously, the AP spike in skeletal muscle fibers is followed by a prominent *depolarizing afterpotential* (also called a *negative afterpotential* based on the old terminology from external recording) (see Fig. 42.3). In addition to this *early depolarizing afterpotential* (i.e. emerging from the spike downstroke), there is a *late depolarizing afterpotential* that follows a tetanic train of spikes (e.g. 10 spikes). The electrogenesis of the early and late afterpotentials is different. The early afterpotential is due to a membrane conductance change, whereas the late afterpotential is due primarily to K^+ accumulation in the T-tubules.

The early depolarizing afterpotential of frog skeletal fibers is about 25 mV in amplitude immediately after the spike component and gradually decays to the RP in 10–20 ms. This afterpotential results from the fact that the delayed rectifier K^+ channel that opens during depolarization to terminate the spike is less selective for K^+ (ca. 30:1, K^+:Na^+) than is the K^+ channel in the resting membrane (ca. 100:1) (Adrian et al.,1970a). Therefore, the constant-field equation predicts that the membrane should be partly depolarized when E_M is dominated by this K^+ conductance that is turned on during the AP. Thus, the early depolarizing afterpotential is partly due to the persistence and slow decay of this less-selective K^+ conductance. Adrian and Peachey (1973) were able to reconstruct the time course of the AP and the early depolarizating afterpotential by giving values to the access resistance of the T-tubular system, presence of Na^+ and K^+ tubular membrane currents and velocity of the tubular AP. The early depolarizing afterpotential reflects, in part, the tubular AP, as evidenced by the disappearance of the early depolarizing afterpotential in muscles in which the T-tubular system has been disrupted and disconnected from the surface membrane by the glycerol osmotic shock method[1] (Eisenberg and Gage, 1969).

The late depolarizing afterpotential of frog skeletal fibers may result from accumulation of K^+ ions in the T-tubules (Adrian and Freygang, 1962). During the AP depolarization and turn-on of g_K (delayed rectifier), there is a large driving force for K^+ efflux from the myoplasm coupled with a large K^+ conductance, resulting in a large outward K^+ current [$I_K = g_K (E_m - E_K)$] across all surfaces of the fiber, namely across the surface sarcolemma and T-tubule walls. The K^+ efflux at the fiber surface membrane can rapidly diffuse away and mix with the relatively large interstitial fluid (ISF) volume, whereas the K^+ efflux into the T-tubules (TT) is trapped in this restricted diffusion space. The resulting high $[K^+]_{TT}$ decreases E_K across the T-tubule membrane and thereby depolarizes this membrane. Because of cable properties, part of this

[1] To produce glycerol osmotic shock, about 300 mOsm glycerol is added to Ringer's solution (Eisenberg and Gage, 1969). The glycerol rapidly permeates into the fiber interior (so the fiber shrinks transiently) and equilibrates. But when the glycerol is washed out, there is a great hypotonic shock produced that disrupts the T-tubules.

depolarization is transmitted to the surface sarcolemma and is recorded by an intracellular microelectrode. The K^+ accumulation in the T-tubules can only be dissipated relatively slowly by diffusion out of the mouth of the T-tubules and by active pumping back into the myoplasm (across the T-tubule wall) by the Na^+-K^+ pump sites located in the T-tubular membrane. Thus, the decay of the late depolarizing afterpotential will be a function of these two processes.

The amplitude and duration of the late depolarizing afterpotential is a function of the number of spikes in the train and their frequency. That is, the greater the spike activity, the greater its amplitude and duration. If the train consists of 20 spikes at a frequency of 50/s, a typical value for the amplitude of the late depolarizing afterpotential in frog fibers is about 20 mV. When the diameter of the T-tubules is increased by placing the fibers in hypertonic solutions[2], the amplitude of the late afterpotential decreases as expected because of the greater dilution of the K^+ ions accumulating in the T-tubule lumen. When the T-tubular system is disrupted and disconnected from the surface membrane by the glycerol osmotic shock method, the late afterpotentials disappear together with the early afterpotentials.

An alternative explanation for the late depolarizing afterpotential is that it may be due to the slow delayed rectifier g_K change described above (Adrian et al., 1970b). The equilibrium potential for the slow I_K is -83 mV and the sign (direction) of the late afterpotential reverses when the fiber is depolarized beyond -80 mV (e.g. to -70 mV). Hence, the late afterpotential could arise from the slow relaxation of a component of the K^+ conductance increase, which is less selective for K^+ than the K^+ channels open in resting membrane. In this view, the electrogenesis of the late afterpotential would be similar to that for the early afterpotential.

All depolarizing afterpotentials, regardless of whether early or late, have physiological importance because they alter excitability and the propagation velocity of the fiber. A depolarizing afterpotential should enhance excitability (lower threshold) to a subsequent AP. This is because the *critical depolarization* required to reach the *threshold potential* would be decreased. A large late depolarizing afterpotential, such as that due to K^+ *accumulation* in the T-tubules, can, under certain pathological conditions, trigger repetitive APs. The effect of depolarizing afterpotentials on velocity of propagation involves two opposing factors: (1) the decrease in critical depolarization required; and (2) the decrease in maximal rate of rise of the AP (max dV/dt), which is a function of the takeoff potential (h_∞ versus E_m curve). Therefore, what factor dominates will depend on the degree of depolarization and the shape of the h_∞ curve. When frog skeletal fibers are depolarized slightly by elevating $[K^+]_o$, only a decrease in propagation velocity is observed (Sperelakis et al., 1970).

[2] In hypertonic solutions, skeletal muscle fibers shrink (fiber diameter decreases) like a perfect osmometer (but with an osmotically-inactive volume of about 32%), but their T-tubules swell.

IX. Ca^{2+}-DEPENDENT SLOW ACTION POTENTIALS

Slow APs are recorded under conditions in which the fast Na^+ current is blocked by Na^+-deficient solution, tetrodotoxin (TTX) or voltage inactivation of the fast Na^+ channels in elevated $[K^+]_o$. Under these conditions, the only carrier of inward current available to produce an AP is Ca^{2+} ion. Spontaneously-occurring slow APs were first observed in frog sartorius fibers equilibrated in Cl^--free solution containing TTX (Sperelakis et al., 1967). Upon addition of Ba^{2+} ion (e.g. 0.5 mM), which is a potent blocker of K^+ channels and P_K, the fibers partially depolarize and spontaneously discharge slowly-rising (e.g. 1–10 V/s), overshooting APs of long duration (e.g. several seconds), having a prominent plateau component (resembling a cardiac AP in shape). An abrupt repolarization terminates the slow AP. Ba^{2+} depolarizes rapidly in Cl^--free solution, because the voltage-clamping effect of the Cl^- distribution (E_{Cl}), due to the large P_{Cl}, is circumvented. Cl^--free solution raises the resistance of the cell membrane about sevenfold.

In a frog skeletal muscle fiber, using two intracellular microelectrodes, one for applying current intracellularly and the other for recording voltage a short distance away in the same fiber ($[K^+]_o$ of 25 mM to depolarize the fiber to about -45 mV and thereby inactivate the fast Na^+ channels and $[Na^+]_o$ reduced to zero so that there could be no inward Na^+ current), application of small hyperpolarizing current pulses during the slow AP indicated that membrane resistance increases progressively during the plateau (Kerr and Sperelakis, 1982). The rate of rise, overshoot and duration of the slow APs are a function of $[Ca^{2+}]_o$ (Beaty and Stefani, 1976; Vogel et al., 1978; Kerr and Sperelakis, 1982). For example, the AP duration at 50% amplitude (APD_{50}) was generally 2–8 s. The amplitude of the slow AP plotted against log $[Ca^{2+}]_o$ gave a straight line with a slope of 28 mV/decade, which is close to the theoretical 29 mV/decade (at 21°C) from the Nernst relationship for a situation in which only Ca^{2+} ion carried the inward current. The slow APs were depressed and blocked by the Ca^{2+}-antagonistic and slow-channel-blocking drugs, verapamil and bepridil, with an ED_{50} of about 5×10^{-8} M. The slow AP arises from the T-tubular system of the fiber (Vogel et al., 1978; Kerr and Sperelakis, 1982), based on their disappearance when the T-tubules were disrupted and disconnected from the surface membrane by the glycerol osmotic shock method. The normal fast APs are not affected by the glycerol treatment. These results indicate

that the slow Ca^{2+} channels giving rise to the slow APs are located primarily in the tubular system.

Isotope flux measurements have shown that there is a net Ca^{2+} influx during contractions of phasic skeletal muscle fibers, suggesting that an influx from the extracellular space may initiate the contraction (Bianchi and Shanes 1959). Additionally, voltage-clamped muscle fibers have slow inward Ca^{2+} currents (I_{Ca}) (Stanfield, 1977; Sanchez and Stefani, 1978). Elevation of $[Ca^{2+}]_o$ increased I_{Ca}, and I_{Ca} was depressed by the slow Ca^{2+} channel blockers D-600, nifedipine and Ni^{2+} (Stanfield, 1977; Sanchez and Stefani, 1978; Almers et al., 1981). Detubulation by the glycerol osmotic shock method abolishes I_{Ca} (Nicola-Siri et al., 1980; Potreau and Raymond, 1980). These results support the conclusion that I_{Ca} produces the slow APs. The various conformational states that the Ca^{2+} slow channels undergo during excitation are depicted in Fig. 42.7. These states are similar to those of the fast Na^+ channels (see Fig. 42.5), except there are only two closed states.

Do slow inward calcium currents (I_{CaS}), play a role in E-C coupling? A substantial contraction, of between 20 and 50% of the normal twitch tension, accompanies the slow APs (Vogel et al., 1978), suggesting that the Ca^{2+} channels in the tubular system may play a role during E-C coupling. However, skeletal muscle fibers contract for several minutes after $[Ca^{2+}]_o$ is lowered to 10^{-8} M (Armstrong et al., 1972) and the Ca^{2+}-channel blocker diltiazem did not depress twitch or tetanic force development (Gonzalez-Serratos et al., 1982). These results suggest that I_{Ca} may play no role in E-C coupling in normal amphibian muscles. Nevertheless, in dysgenic mice, in which contraction of skeletal muscles is weak, the Ca^{2+} channels in the T-tubules are few or absent.

Ca^{2+} influx during the slow AP could trigger the release of more Ca^{2+} from the nearby TC-SR via the Ca^{2+}-trigger Ca^{2+}-release mechanism (Fabiato, 1982). Because the time course of the slow AP is much longer than that of a twitch contraction, it was suggested that the inward Ca^{2+} current may play a role in K^+ contracture, in tetanic contraction, or in long-term regulation of contraction, perhaps by increasing the Ca^{2+} concentration in the SR and thereby increasing the amount of internal Ca^{2+} available for release

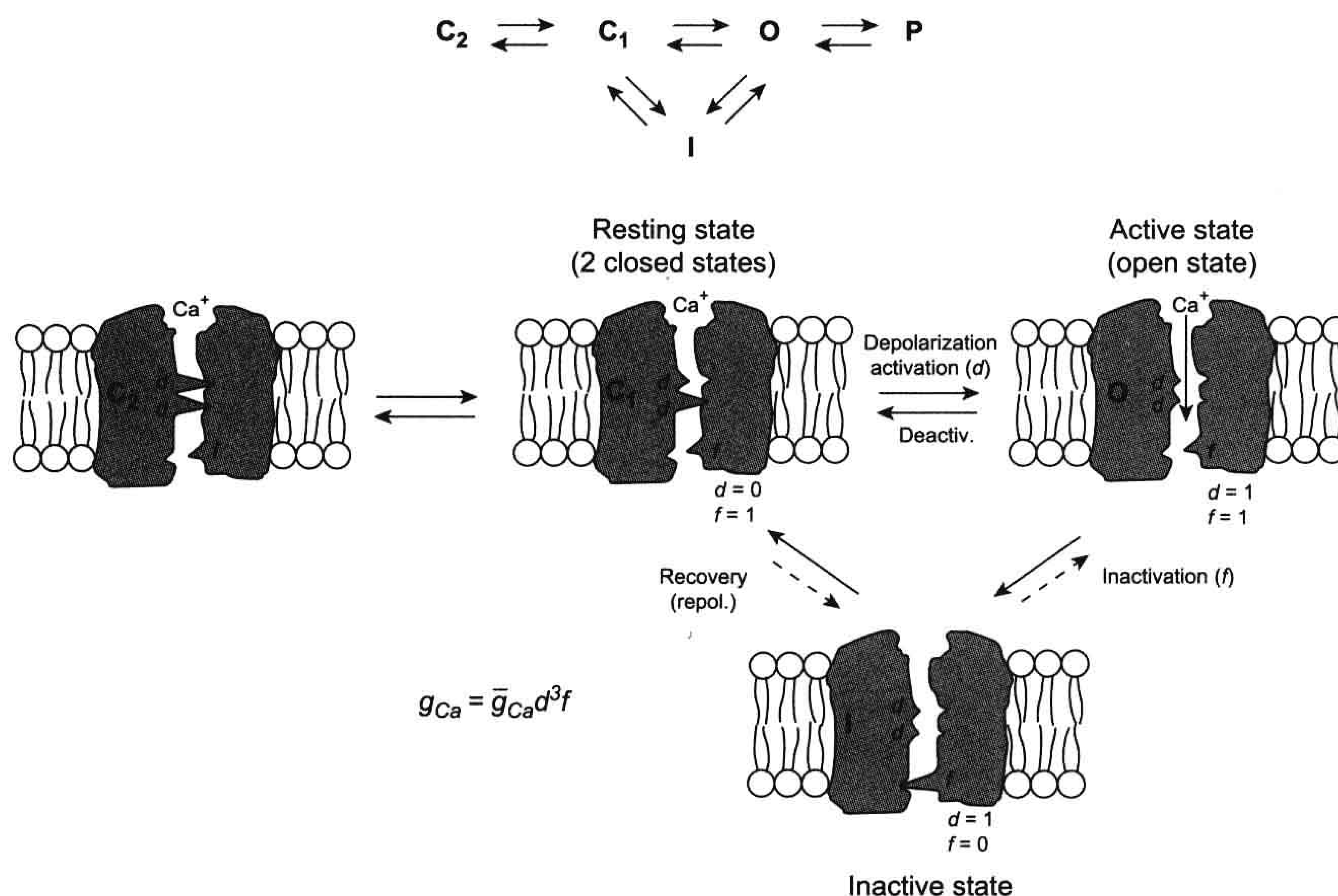


FIGURE 42.7 Illustration of the four hypothetical states of the slow Ca^{2+} channel. There is evidence for two closed states. As depicted, in the most closed state (C_2), both *d* gates (or particles) are in the closed configuration. In the least closed state (C_1), one gate is closed and one is open. In the resting membrane, the activation gate (A) is closed and the inactivation gate (I) is open: $d = 0, f = 1$. Depolarization to the threshold activates the channel to the active state, the A-gate opening rapidly and the I-gate still being open: $d = 1, f = 1$. The activated channel spontaneously inactivates to the inactive state due to closure of the I-gate: $d = 1, f = 0$. The recovery process on repolarization returns the channel from the inactive state back to the resting state, thus making the channel again available for reactivation. Ca^{2+} ion is depicted as being bound to the outer mouth of the channel and poised for entry down its electrochemical gradient when both gates are open. The reaction between the resting state and the active state is readily reversible and there is some reversibility in the other reactions. The slow channels behave similarly to the fast channels, except that their gates appear to move more slowly on a population basis; i.e. the slow channels activate and recover more slowly. (Although the gates of any individual slow channel may move quickly, the stochastic behavior of the population of channels is such that their summed conductance changes slowly.) The slow channel gates operate over a different voltage range than the fast channels (i.e. less negative, more depolarized). TTX does not block the slow channels, but drugs such as nifedipine do block by binding to the channel.

on subsequent activation (Nicola-Siri et al., 1980). $[Ca^{2+}]_{SR}$ does increase following tetanic stimulation (Gonzalez-Serratos et al., 1982).

Slow APs were also recorded from mouse skeletal muscle fibers equilibrated in a solution that was Cl^--free, low Na^+ (10 mM) and high K^+ (20 mM) (Kerr and Sperelakis, 1982). As with frog muscle, the slow APs were abolished after detubulation and blocked by verapamil, bepridil, Mn^{2+} and La^{3+}. Their rate of rise, amplitude and duration increased as a function of $[Ca^{2+}]_o$, with max dV/dt being about 0.5 V/s in 8 mM.

During the first 5 days in culture, embryonic skeletal muscle cells from *Xenopus laevis* need extracellular Ca^{2+} to contract when stimulated (in contrast to adult muscles). Thus, an inflow of Ca^{2+} from the extracellular space may be required in embryonic cells as the means to produce contraction. In whole-cell voltage-clamp studies, I_{Ca} currents have been observed in embryonic and neonatal skeletal muscle cells in culture (Moody-Corbett et al., 1989; Cognard et al., 1992; Gonzalez-Serratos et al., 1996; Cordoba-Rodriguez et al., 1997). The current density increased from 1.7 to 3.3 and to 7.9 pA/pF at 1, 5 and 15 days in culture, respectively. These results indicate that the T-tubules and SR are poorly developed or not functional in early stages of muscle development and that, in early development, I_{Ca} may be an important mechanism to trigger contraction.

X. DEVELOPMENTAL CHANGES IN MEMBRANE PROPERTIES

The cell membranes of most excitable cells apparently pass through similar stages of differentiation during development. For example, young (2- to 3-day-old) embryonic chick hearts (tubular) have few or no functional fast Na^+ channels, but have a high density of slow channels (both Na^+ and Ca^{2+}) and fire slowly-rising TTX-insensitive APs. Fast Na^+ channels then appear and progressively increase in number, reaching the maximal (adult) level at late embryonic development (e.g. day 20). The P_{Na}/P_K ratio is high in young hearts, due to a low P_K, and accounts for the low RP and automaticity in nearly all the cells.

Skeletal muscle fibers and neurons also undergo developmental changes in membrane electrical properties (e.g. Spector and Prives, 1977; Spitzer, 1979) (see Chapter 25). In general, fast Na^+ channels are absent in the young, less differentiated cells, but they do possess excitability because of a large number of slow channels. The AP is TTX-insensitive, slowly rising and of long duration (resembling a slow AP in cardiac muscle). Later during development, fast Na^+ channels make their first appearance and the fast Na^+ channels and slow channels coexist. During that period, TTX does not abolish the APs, but reduces max dV/dt (i.e. slow APs remain). At a later stage, the slow channels in the sarcolemma are lost (or greatly reduced in number) and the fast Na^+ channels progressively increase in density. The APs become fast rising and of short duration and are completely abolished by TTX. As discussed previously, some functional slow Ca^{2+} channels remain in the T-tubular system.

XI. ELECTROGENIC Na^+-K^+ PUMP STIMULATION

The Na^+,K^+-ATPase pump is *electrogenic* in skeletal muscle fibers (both mammalian and amphibian). The pump produces a net outward current, because three Na^+ ions are pumped out to every two K^+ ions pumped in. The *electrogenic pump potential* contribution to the RP (see Chapter 11 to 9) is very large, about 12–16 mV, in rat skeletal muscle fibers (Sellin and Sperelakis, 1978). The *net pump current* can be stimulated by increasing the number of pump sites per unit area of cell membrane or by increasing the turnover rate of each pump site. β-Adrenergic agonists (e.g. isoproterenol) rapidly hyperpolarize skeletal muscle fibers by 7–9 mV within 5 min. Insulin has a similar effect, but hyperpolarizes more slowly (e.g. peak reached by 10 min) and to a smaller degree (e.g. 5–7 mV) (Iannaccone et al., 1989). Since cAMP also hyperpolarizes, the action of *β*-agonists is believed to be mediated by elevation of cAMP and phosphorylation of the Na^+-K^+ pump (or an associated regulatory protein) by protein kinase A (PKA). The action of insulin is thought to be mediated by the incorporation of spare membrane from an internal pool, which contains Na^+-K^+ pumps, into the cell membrane.

The pump current (I_p) can be directly measured in single fibers (cultured skeletal myotubes rounded by use of colchicine, a microtubule disrupter) by doing whole-cell voltage clamp under conditions in which all the ionic conductances are blocked. When this is done, the pump current can be measured at different voltages and normalized for unit membrane capacitance (hence membrane area). Values of about 1 pA/pF or 1.0 $\mu A/cm^2$ were obtained, with a *reversal potential* (or zero current) of about −140 mV (Li and Sperelakis, 1994).

When $[K^+]_o$ is lowered below the normal physiological level, e.g. from 4.5 mM to about 0.1 mM, a large depolarization occurs in mammalian skeletal muscle fibers (Fig. 42.8). This depolarization is caused, in part, by inhibition of the Na^+-K^+ pump current. The K_m value for $[K^+]_o$ for the Na^+, K^+-ATPase is about 2 mM and the relationship between Na^+, K^+-ATPase activity and $[K^+]_o$ is very steep. Therefore, inhibition of the Na^+-K^+ pump occurs.

XII. SLOW FIBERS

One type of skeletal muscle fibers, known as *slow fibers*, subserves tonic functions, including posture. Slow fibers should not be confused with "*slow twitch fibers*". The true

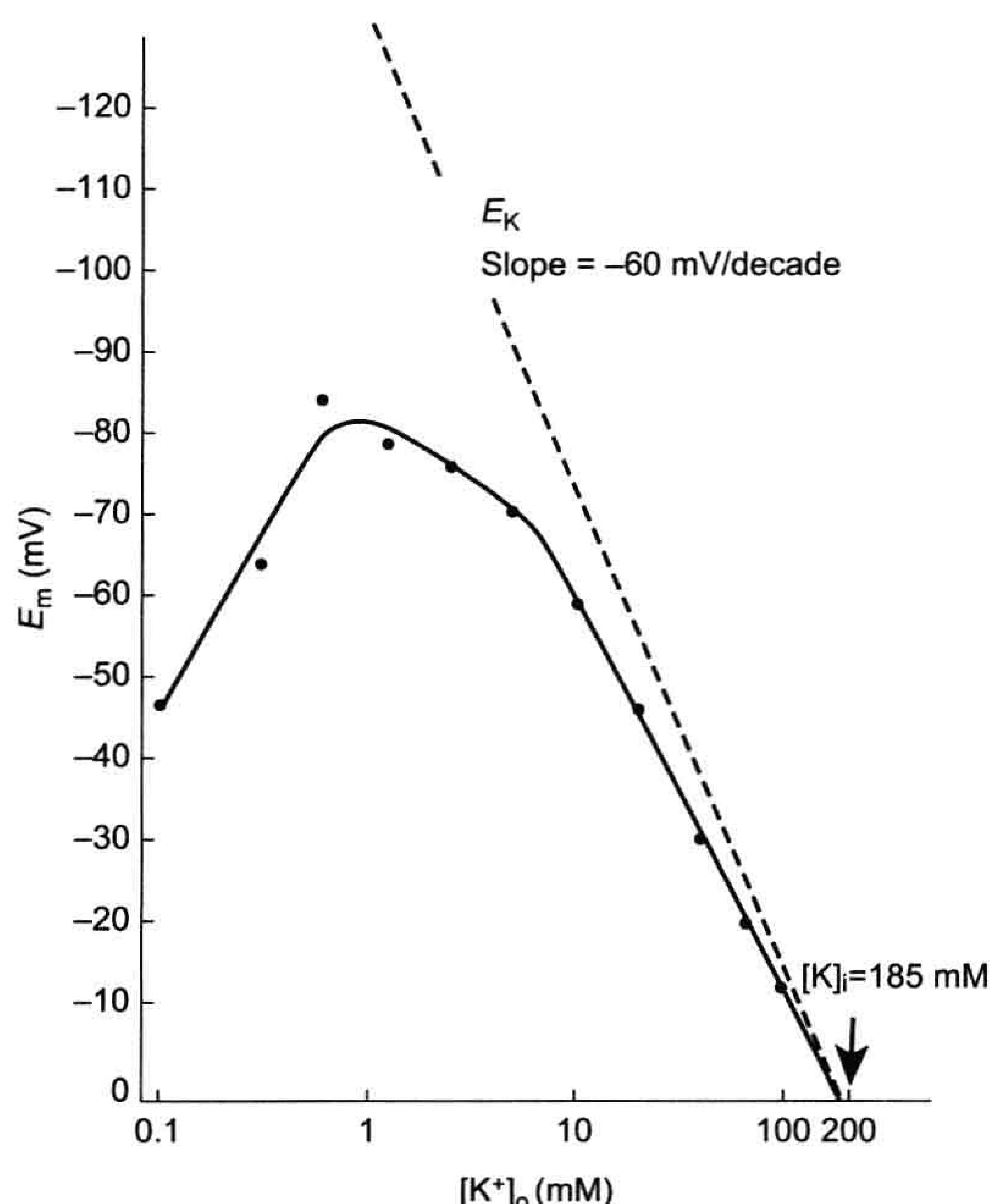


FIGURE 42.8 The mean resting membrane potential (E_m) of normal mouse skeletal muscle plotted as a function of the extracellular K^+ concentration ($[K^+]_o$) on a logarithmic scale. The straight line drawn through the data points for 20 mM $[K^+]_o$ and above has a slope of 50 mV/decade. Extrapolation of this line to zero potential gives the intracellular K^+ concentration ($[K^+]_i$) of 185 mM. The dashed line gives the calculated E_K values (slope of 61 mV/decade). Note the "fold-over" of the E_m curve at $[K^+]_o$, levels below 1 mM, presumably due to inhibition of the electrogenic pump potential (V_p) and to a decrease in P_K and g_K at low $[K^+]_o$ levels. *(Reproduced from Sellin and Sperelakis, 1978.)*

slow fibers do not fire APs, whereas all types of twitch fibers do. The slow fibers are usually smaller in diameter than twitch fibers and they exhibit a less distinct myofibrillar arrangement (so-called *"felden" structure*). Slow fibers have been found in a number of vertebrate muscles, e.g. in the frog rectus abdominus muscle, frog ileofibularis muscle and mammalian extraocular muscles. It is probable that careful searching will reveal some slow fibers in other mammalian muscles as well.

The slow fibers have *multiple innervation* by a *series of motor end-plates* (spaced about 1 mm apart), all from a single motor neuron. As with twitch fibers, acetylcholine (ACh) is the synaptic transmitter. The force of contraction of the slow fibers is controlled by graded *end-plate potentials* (EPPs). That is, an increase in frequency of impulses in the motoneuron produces a larger EPP (by *temporal summation*) and this, in turn, produces a greater contraction in the vicinity of the end-plate. Since the end-plates are spaced closely together — at a distance of about one length constant — the entire fiber becomes nearly uniformly depolarized, even though there are no propagated APs. Therefore, the entire length of the slow fiber contracts almost uniformly.

The slow fibers do possess T-tubules which abut at the triadic junctions with the terminal cisternae of the SR (TC-SR). Therefore, the T-tubules may act as *passive conduits* in the slow fibers to bring the depolarization (produced in the surface membrane by the EPP) deep into the fiber interior. Thus, depolarization of the T-tubule occurs by their cable properties. This depolarization, in turn, could bring about the influx of Ca^{2+} by activation of voltage-dependent slow Ca^{2+} channels located in the T-tubules.

APs normally cannot be induced to occur in vertebrate slow fibers under a variety of experimental conditions. However, denervation of frog slow fibers does allow an AP-generating mechanism to appear (Miledi et al., 1971). APs can be induced in slow fibers of invertebrates (e.g. crustacean skeletal muscles) (Fatt and Ginsborg, 1958). Similarly, in the neurogenic horseshoe crab (*Limulus*) heart, which normally is activated by summating excitatory postsynaptic potentials, propagating (ca. 5 cm/s) and overshooting spontaneous APs can be rapidly induced by Ba^{2+} (0.1−10 mM) (Rulon et al., 1971). These slowly-rising (ca. 1.0 V/s) APs are resistant to TTX and these voltage-dependent slow channels can pass Ba^{2+}, Sr^{2+} and Ca^{2+}.

XIII. CONDUCTION OF THE ACTION POTENTIAL

When the EPP, generated at the neuromuscular junction, reaches threshold for eliciting an AP in the vertebrate twitch skeletal muscle fiber, an AP is propagated down the muscle fiber in both directions from the end-plate. (In some muscle fibers, there is a second end-plate innervated by a motoneuron exiting the spinal cord at another level.) The AP is overshooting (to about +40 mV) and propagates at a constant velocity of about 5 m/s over the surface sarcolemma. Propagation occurs by means of the *local-circuit currents* that accompany the impulse, as discussed in Chapter 19. The reader is referred to that chapter for details on the *radial (transmembrane) currents* and the *longitudinal (axial) currents*. The external longitudinal currents can use the entire ISF space (since current takes the path of least resistance), allowing the electromyogram (EMG) to be recorded from the skin overlying an activated skeletal muscle. The amplitude of the EMG potentials becomes larger when more fibers within the muscle are activated (*fiber summation*), because of summation of the IR voltage drops produced by each fiber activated simultaneously. The frequency of the EMG potentials reflects the frequency and asynchrony of activation of the muscle.

The skeletal muscle fibers are formed by *myoblast cells* that have fused end to end to become long multinucleated myotubes and then cylindrical fibers later in development.

They behave as semi-infinite cables. That is, an AP can propagate from one end of the fiber to the other, uniformly and unimpeded. The space constant or *length constant* (λ) of the fiber cable is about 1.5 mm for frog sartorius fibers (Sperelakis et al., 1967) and about 0.76 mm for the rat EDL muscle (Sellin and Sperelakis, 1978). The length constant is the distance over which a voltage applied at one region would decay to 1/e (1/2.717 = 0.368) or 36.8% of the initial value. That is, in a passive cable, voltage decays exponentially with a certain length constant as given by:

$$V_x = V_o\, e^{-x/\lambda} \qquad (42.4)$$

where V_x is the voltage at the distance x and V_o is the voltage at the origin ($x = 0$). λ is given by:

$$\lambda = \sqrt{\frac{r_m}{r_i + r_o}} \qquad (42.5)$$

$$\text{cm} = \sqrt{\frac{\Omega.\text{cm}}{\frac{\Omega}{\text{cm}} + \frac{\Omega}{\text{cm}}}} = \sqrt{\text{cm}^2}$$

Assuming that r_o (the outside longitudinal resistance) is negligibly small compared to r_i (this would be true for a superficial fiber in a bundle immersed in a large bath):

$$\lambda = \sqrt{\frac{r_m}{r_i}} = \sqrt{\frac{R_m}{R_i}\frac{a}{2}} \qquad (42.6)$$

$$\text{cm} = \sqrt{\frac{\Omega.\text{cm}}{\Omega/\text{cm}}} = \sqrt{\frac{\Omega.\text{cm}^2}{\Omega.\text{cm}}\frac{\text{cm}}{}} = \sqrt{\text{cm}^2}$$

where r_m ($\Omega\cdot$cm) and r_i (Ω/cm) are the membrane resistance and the internal longitudinal resistance normalized for unit length of fiber, R_m ($\Omega\cdot\text{cm}^2$) is the membrane resistance normalized for both fiber radius and length, R_i ($\Omega\cdot$cm) is the resistivity of the myoplasm (normalized for length and cross-sectional area), and a (cm) is the fiber radius. R_m is often loosely called membrane resistivity, but this is not accurate because for true membrane resistivity (ρ_m) there must be correction for membrane thickness δ:

$$\rho_m = \frac{R_m}{\delta} \qquad (42.7)$$

$$\Omega.\text{cm} = \frac{\Omega.\text{cm}^2}{\text{cm}}$$

The factors that determine active velocity of propagation (θ_α) include the intensity of the local-circuit current, threshold potential and the passive cable properties, λ and τ_m. As discussed previously, the greater the rate of rise of the AP, the greater the intensity of the local-circuit current, hence the greater the θ_α. In addition to its dependence on the density of the fast Na^+ channels (determinant of the maximum Na^+ conductance, $\bar{g}_{Na}$), the kinetic properties of the channel gating and the threshold potential (V_{th}), max *dV/dt* is determined also by the RP (or takeoff potential) (related to the h_∞ versus E_m curve), as discussed previously (Fig. 42.9). In addition, because cooling decreases Na channel activation ($Q_{10} \simeq 3$), max *dV/dt* and θ_α are slowed accordingly. R_m is increased by cooling, the Q_{10} for R_K in frog sartorius fibers being about 2.8 (ion diffusion in free solution has a Q_{10} of about 1.2) (Sperelakis, 1969). For a description of passive conduction, see Appendix III to this chapter.

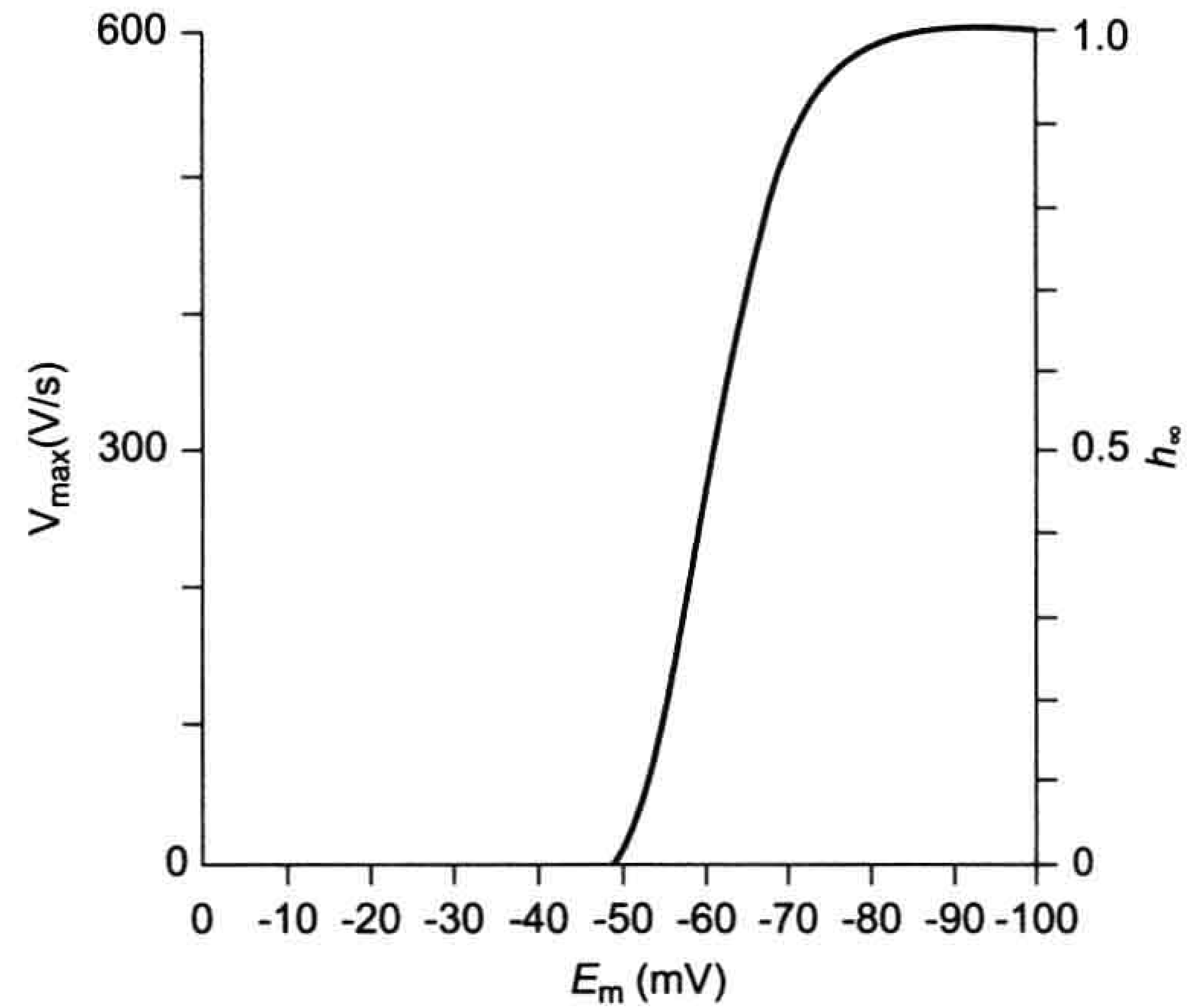


FIGURE 42.9 Graphic representation of the maximal rate of rise of the API (max *dV/dt*) as a function of resting E_m or takeoff potential. Max *dv/dt* is a measure of the inward current intensity (membrane capacitance being constant), which is dependent on the number of channels available for activation; h is the inactivation factor of Hodgkin–Huxley as $g_{Na} = \bar{g}_{Na} m^3 h$, where g_{Na} is the Na^+ conductance, $\bar{g}_{Na}$ is the maximal conductance and m and h are variables; h_∞ represents h at $t = \infty$ or steady state (practically, after 20 ms). The fast Na^+ channels begin to inactivate at about −75 mV and nearly complete inactivation occurs at about −30 mV (h_∞ low). Therefore, max *dV/dt* decreases because h_∞ decreases.

XIV. EXCITATION DELIVERY TO FIBER INTERIOR BY CONDUCTION INTO THE T-TUBULAR SYSTEM

The experiments of Huxley and Taylor (1958) were the first to provide evidence that there was some structure, located at the level of the Z-lines in frog skeletal muscle fibers, which is involved in E-C coupling. This structure allows relatively fast conduction of the excitatory process (AP) from the surface membrane to the center of the muscle cells. These investigators applied current pulses at different points along the length of the sarcomeres in isolated fibers and found that when the microelectrode tip was opposite the Z-line, graded contractions of the two half-sarcomeres occurred. The greater the current, the greater was the inward spread of the contraction. In

addition, they discovered that there were sensitive spots located around the perimeter of the fiber at the Z-line level; i.e. the membrane was not uniformly sensitive. At about the same time, it was discovered by electron microscopy that transverse (T-) tubules were located at the level of the Z-lines in amphibian skeletal muscle (and at the level of the A-I junctions of the sarcomere in mammalian skeletal muscle). Thus, the T-tubules probably represent the morphological conduit for the findings of Huxley and Taylor. The morphological arrangements of the sarcotubular system of skeletal muscle fibers are illustrated in Fig. 42.10.

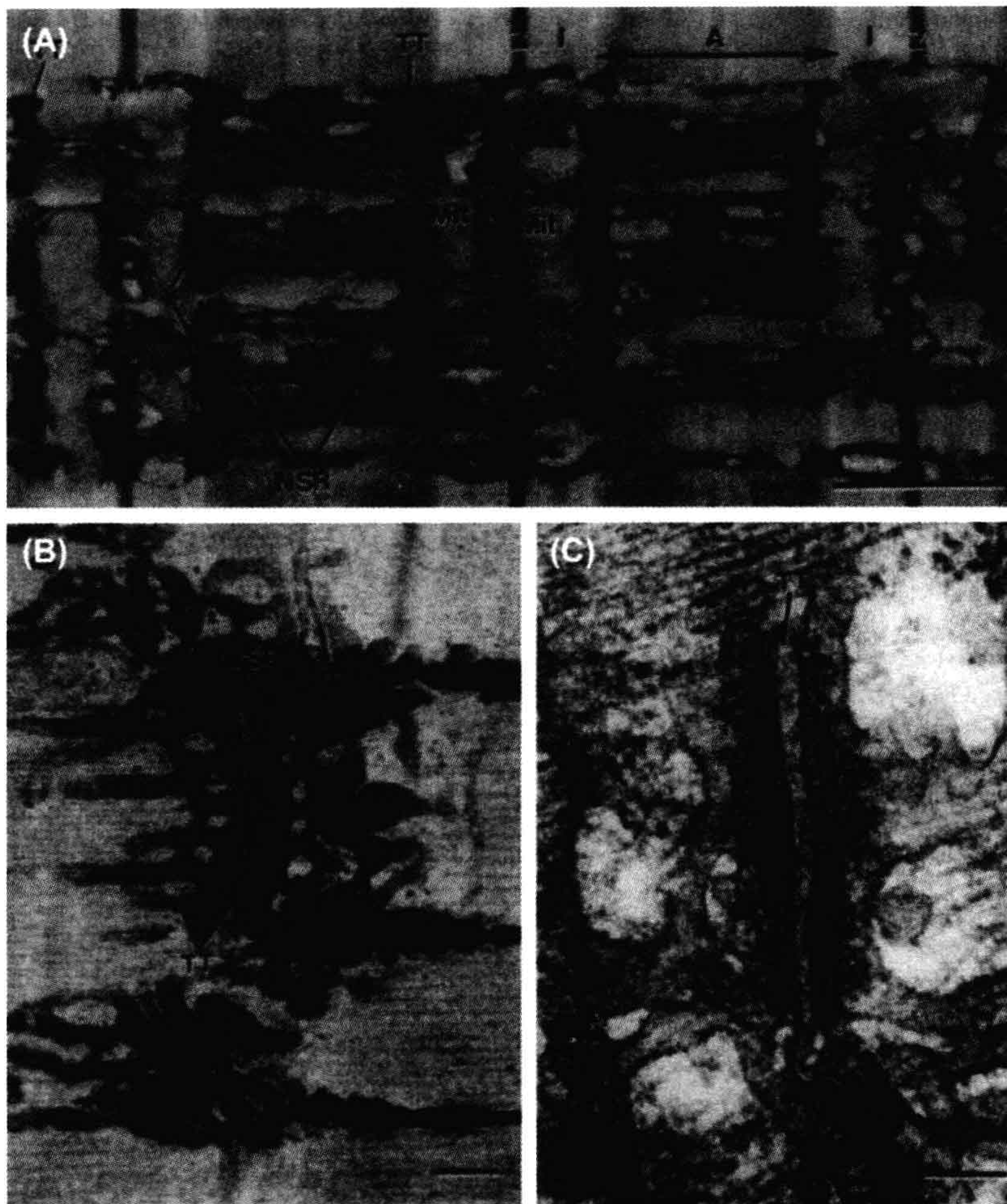


FIGURE 42.10 Sarcotubular system of skeletal muscle fibers from tibialis anterior muscle of mouse (A,C) and iliotibialis muscle of lizard (B). (A) Longitudinal section showing the sarcomere structure of several myofibrils: A-band, I-band, Z-line. The network sarcoplasmic reticulum (N-SR), also known as the longitudinal SR, appears as a torn sleeve surrounding the surface of each myofibril. The N-SR is continuous with the junctional SR (J-SR) that abuts close to the transverse tubules (TT). The TT membranes are invaginations of the cell surface membrane at the level of the A-I junctions in mammalians (or at the level of the Z-line in lizards and amphibians). The J-SR and TT form the complex coupling known as a triad (*). The N-SR is continuous across the I-band, but this is obscured in this section by the presence of paired mitochondria (Mit) over the I-bands. The TT and SR are both selectively filled with osmium tetroxide precipitate, causing their profiles to be more electron opaque than the other structures. Scale bar at lower right represents 1.0 μm. (B) Higher magnification of a triad to show more detail. As shown, the triad consists of a single T-tubule sandwiched between two cisternae of the J-SR. Scale bar = 0.1 μm. (C) High magnification of a triadic junction to illustrate the array of regularly-spaced junctional processes or SR foot processes (several indicated by arrowheads) that project between the TT membrane and the J-SR membrane. There are dense granules within the lumen of the J-SR cisternae (*). Scale bar = 0.1 μm. *(Electron micrographs provided courtesy of Dr Mike Forbes, University of Virginia.)*

Diffusion of some substance from the surface membrane into the skeletal muscle fiber interior is much too slow to account for the relatively short latent period of about 1–3 ms between the beginning of the AP and the beginning of contraction. That is, the diameter of the fibers (mean value of about 70 μm in frog sartorius fibers) is much too large for a diffusion mechanism from the fiber surface to be involved. Diffusion time (for 95% equilibration) increases by the square of the distance and would require about 2.5 s for a small molecule freely diffusing across a cell radius of 50 μm; estimates for Ca^{2+} diffusion time are considerably longer than this (Podolsky and Costantin, 1964). Therefore, the T-tubular system serves as an electrical conduit to bring excitation deep into the fiber interior rapidly and thereby reduces the required diffusion distance to an average value of about 0.7 μm (Sperelakis and Rubio, 1971). It was reported that disruption of the T-tubule system (by a glycerol osmotic-shock method) uncouples contraction from excitation (Eisenberg and Gage, 1969).

Estimates of the length constant of the T-tubules (λ_{TT}), assuming the T-tubule membrane has about the same resistivity (R_m) as the surface membrane $\lambda_{TT} = \sqrt{R_m/R_i}\sqrt{a/2}$ give values of about 50 μm. Because the resistivity of the T-tubule membrane of frog muscle is probably higher than that of the surface sarcolemma because of lower g_{Cl} (Hodgkin and Horowicz, 1959; Adrian and Freygang, 1962; Sperelakis and Schneider, 1968), this would give a longer value. Therefore, it is theoretically possible for the T-tubules to serve as *passive conduits* to bring the depolarization from the surface membrane (during its AP) into the fiber interior. (This mechanism does operate when small depolarizing voltage changes [below the AP threshold] occur on the surface sarcolemma, and conversely any voltage change originating in the T-tubules can be conducted passively to the surface sarcolemma.)

However, direct microscopic observations of the degree of myofibril activation across the width of the fiber caused by raised $[K^+]_o$ depolarization suggested otherwise (Gonzales-Serratos, 1975). Also, during the foot of the AP, only a small outer ring of the tubular network depolarizes beyond the mechanical threshold (Hodgkin and Nakajima, 1972). These results imply that in order for all the myofibrils in the cross-section of a fiber to be activated, which had been demonstrated previously (Gonzalez-Serratos, 1971), there must be a T-tubular AP (TT-AP).

There is evidence that the T-tubules actually do fire APs, i.e. they *actively propagate impulses* inward and so bring large depolarization deep into the fiber interior. The evidence for this includes the observation of a threshold for sudden initiation of localized contraction (Costantin and Podolsky, 1967; Costantin and Taylor, 1973). The TT-AP is sensitive to TTX and is Na^+ dependent and, therefore, is apparently similar in nature to the surface membrane AP. By use of high-speed cinemicrography to measure sequential activation of the myofibrils in a radial direction, Gonzalez-Serratos (1971) estimated the propagation velocity of the TT-AP (θ_{TT}) to be about 10 cm/s, with a Q_{10} of 2.2 (which is similar to the Q_{10} of the surface membrane for AP conduction). This velocity is sufficient to account for the short latent period before contraction begins.

Early evidence for the existence of *active propagation* in the T-tubules came from a number of indirect measurements (reviewed in Caputo, 1978). The speed and Q_{10} (2.2) of the spread of mechanical activation were greater than expected for passive conduction (Gonzalez-serratos 1971). Moreover, twitch tension was reduced by TTX or a Na^+-deficient medium (Costantin, 1970). Depolarization by elevated $[K^+]_o$, which inactivates Na^+ channels, fails to activate contraction in deeper myofibrils (Gonzales-Serratos, 1975). These results suggested that in order for all the myofibrils in the cross-section of a fiber to be activated, there must be fast Na^+ channels in the T-tubules and a T-tubular AP (TT-AP). Subsequently, tubular Na^+ currents have been measured directly (Hille and Campbell, 1976) and direct experimental confirmation of propagating APs in the T-tubules have been demonstrated in amphibian (Nakajima and Gilai, 1980) and mammalian muscle fibers (DiFranco et al., 2005). These direct recordings of the propagating AP in the T-tubules were achieved using potential-sensitive dyes, since the T-tubule membranes are not accessible to conventional microelectrode methods.

In muscles placed in low $[Na^+]_o$ and stimulated briefly at high frequency, the normal tetanic tension rapidly falls, simultaneous with the central myofibrils becoming inactive. These results are due to Na^+ depletion in the T-tubule network, particularly in the deeper parts far from the orifice at the fiber surface (Bezanilla et al., 1972). It is thought that the Na^+ influx (the inward fast Na^+ current) with each AP in the T-tubule produces a progressive decline in $[Na^+]_{TT}$, which slows propagation velocity down the T-tubules and eventually leads to loss of excitability when $[Na]_{TT}$ drops below some critical level (e.g. 30 mM). Na^+ depletion should occur more rapidly deep in the T-tubule network because there would be less diffusion of Na^+ in from the mouth of the T-tubule to replenish the Na^+ loss. Active Na^+-K^+ pumping in the T-tubules may not occur fast enough to keep up with the Na^+ loss into the fiber myoplasm.

There are also voltage-dependent slow Ca^{2+} channels in the T-tubule membrane and slow APs that arise from the T-tubule can be recorded under appropriate conditions (Sperelakis et al., 1967; Vogel et al., 1978). The evidence for the existence of this type of channel and some of its properties was discussed above. The Ca^{2+} influx into the myoplasm through these Ca^{2+} channels could play a role in E-C coupling. For a discussion of the relationship between the T-tubules and the terminal cisternae of the SR, see Appendix IV.

APPENDIX

AI. MORE INFORMATION ON Cl^- CHANNELS

In frog, there are several subtypes of Cl^- channels that have single-channel conductances ranging between 40 and 70 pS and each channel may exhibit several subconductance states. But there is usually a main gate that opens or closes the entire channel. In fetal mammalian fibers, Cl^- channels with conductances of about 40, 60 and 300 pS have been observed. Myoballs cultured from muscle biopsies of patients having one form of myotonia had a reduced (ca. 50%) single-channel conductance for the Cl^- channel, which would contribute to the myotonia (Fahlke et al., 1993). In primary cultures of rat skeletal muscle, the fast Cl^- channel showed a behavior consistent with six closed states and two open states (Weiss and Magleby, 1992). The Cl^- channel in myoblasts and myotubes of the L6 cell line derived from rat skeletal muscle had a high conductance of about 330 pS (Hurnak and Zachar, 1992). Voltage-gated Cl^- channels have also been found in the SR membrane of skeletal muscle.

Some Cl^- channels described for other tissues include: (1) Ca^{2+}-dependent Cl^- channels; (2) stretch-activated Cl^- channels; and (3) cyclic AMP-stimulated Cl^- channels. The receptor-operated Cl^- channels apparently have a G-protein (e.g. G_s or G_i) as intermediate for coupling.

The voltage-dependent Cl^- channels can be blocked relatively selectively by several methods, including acidosis and use of compounds such as the stilbene derivatives (DIDS and SITS) and 9-anthracene carboxylic (9-AC) acid. The Cl^- channels in frog skeletal muscle are relatively insensitive to 9-AC acid, whereas those in adult mammalian muscle are highly sensitive. The anion selectivity sequence for some voltage-dependent Cl^- channels is $I^- > Br^- > Cl^- > F^-$.

AII. MORE INFORMATION ON K_{ATP} CHANNELS

It has been proposed that K_{ATP} channels may be associated with the decrease in force development underlying muscle fatigue. A drug (SR44866) that opens K_{ATP} channels (in sarcolemmal membrane patches from frog skeletal muscles) also reduces the AP duration, the early afterpotential and the peak twitch force (without affecting the RP) in intact frog muscles (Sauviat et al., 1991). The high K^+ permeability found in muscle fibers that have undergone a permanent contracture (rigor) produced by repetitive stimulation while metabolically-poisoned with cyanide and iodocetate (Fink and Lüttgau, 1976), may be caused by the decreased ATP concentration opening K_{ATP} channels. In metabolically-exhausted frog semitendinosus muscle fibers, the addition of tolbutamide and glyburide, two K_{ATP} channel antagonists, significantly reduce the K^+ efflux rate (Castle and Haylett, 1987). As said previously, even under fatigue induced by prolonged repetitive stimulation, the decrease in intracellular ATP is small (Nassar-Gentina et al., 1978) and fatigued muscle fibers can contract when Ca^{2+} is released directly from the intracellular SR stores (Gonzalez-Serratos et al., 1978; Garcia et al., 1991). In intact animals, some of the skeletal muscle fatigue results from synaptic fatigue, including fatigue at the neuromuscular junction.

The Kir6.x channel is a typical inward-rectifier type K^+ channel protein. It has two transmembrane helices that form the pore and K^+ selectivity filter. The cytoplasmic NH_2 and COOH termini interact to form an ATP binding site. A key property of Kir channels is inhibition of channel opening by ATP (Spruce et al., 1987). Each Kir subunit can bind one molecule of ATP. Inhibition by ATP is not a consequence of phosphorylation or ATP hydrolysis, but of direct binding to intracellular domains on the Kir channel (Kakei et al., 1985). That is, ATP is not consumed in this action.

SUR is a regulatory protein that is linked to the C-terminus of Kir. SUR is an ATP-binding cassette (ABC) protein, which itself (unlike other ABC proteins) has no intrinsic transport function, but associates with Kir6.x K^+ channels to form the functional K_{ATP} channel. SUR serves as a regulatory subunit which fine-tunes the activity of Kir6.x in response to changes in cell metabolism. Each SUR subunit contains two nucleotide-binding folds which contain binding sites for Mg^{2+}-adenosine nucleotides. Cytosolic free Mg^{2+} is high in resting skeletal muscles (ca 1 mM). In the absence of Mg^{2+}, nucleotides (such as ADP) act on SUR to inhibit K_{ATP} activity. Therefore, nucleotides can regulate K_{ATP} channels through interactions with both Kir and SUR.

As with other members of the Kir family, the K_{ATP} channel exhibits inward rectification (ir). That is, the open channels pass inward current with increasing hyperpolarization, but outward K^+ current does not flow when the membrane is depolarized by more than about 10 mV above the E_K potential. This property of inward rectification is caused by cytoplasmic ions such as Mg^{2+} and polyamines plugging the pore pathway upon depolarization and thereby obstructing the outward flow of K^+ (Woll et al., 1989).

The half-maximum inhibition of opening of K_{ATP} channels by ATP in skeletal muscle (measured at a constant $[K^+]_o/[K^+]_i$) is 0.135 mM at pH 7.2 (see Fig. 42.6). Intracellular [ATP] is about 5 mM in resting muscle (Dawson et al., 1978, 1980) and it is maintained at near basal levels even during repetitive contractions that lead to muscle fatigue (Carlson and Siger, 1960; Nassar-Gentina et al., 1978). Therefore, the K_{ATP} channels are

largely inactive (or masked) under normal physiological conditions.

In searching for a possible role of the K_{ATP} channel under other conditions, a modest role was demonstrated in maintaining membrane polarization under sustained muscle use and fatigue. Although ATP is the controller of K_{ATP} opening, K_{ATP} activity can be modulated by a number of metabolites through interactions with Kir, SUR or both. These include: K^+, H^+ and phospholipids (such as PIP_2), all of which are known to increase during muscle contraction.

Extracellular K^+ concentration ($[K]_o$) rises dramatically in the muscle extracellular space during repetitive AP activity and can reach 15–50 mM in the transverse tubules (Almers, 1980; Clausen, 2008). The unitary conductance of the K_{ATP} channel increases with $[K^+]_o$, from 15 pS in 2.5 mM to 42 pS in 60 mM. Therefore, at higher $[K_o]$, K_{ATP} channels are more conductive at the same ATP concentration.

Kir channels are also regulated by pH at the cytoplasmic surface (pH_i) (reviewed in Jiang et al., 2002; Qu et al., 2000). Intracellular pH may drop by up to one unit during intense muscle use (Renaud, 1989). A decrease in pH_i reduces the inhibitory effect of ATP on K_{ATP} channels, leading to an increase in the probability of K_{ATP} channel opening (Davies et al., 1992). The ATP concentration required for half-inhibition increases by 2.5 times and 15 times, respectively, at pH_i 6.8 and 6.3, compared to that at pH_i 7.2. That is, a decrease in pH_i increases the ATP concentration required for half-inhibition of channel activity. During acidosis, a small decrease in ATP concentration leads to a greater opening of K_{ATP} channels.

The decrease in pH_i during contraction is matched by an increase in cytosolic free Mg^{2+}. A rise in cytosolic Mg^{2+} reduces the ability of ATP to close K_{ATP} channels (Vivaudou et al., 1991). This is most likely related to the ability of Mg^{2+} to bind to ATP and to the stimulatation of K_{ATP} channels via the SUR regulatory subunit. Although the increases in $[K]_o$, pH_i and $[Mg^{2+}]_i$ may act collectively and synergistically to activate K_{ATP} channels during repetitive muscle contraction, this effect is modest at normal muscle $[ATP]_i$.

On the other hand, K_{ATP} channels may become activated when the muscle is stressed or metabolically compromised (Hussain et al., 1994). Adenosine, which is released from metabolically-compromised muscle, stimulates K_{ATP} (Bartlett-Jolley and Davies, 1997) and, as said previously, intracellular acidosis is a potent activator of K_{ATP} channels. Although the skeletal muscles of genetically-altered mice which lack Kir (Kir6.2 knockout mice) develop fatigue more rapidly than control muscles (Cifelli et al., 2007), the more rapid onset of fatigue is not associated with K_{ATP} channel activation (Boudreault et al., 2010). These findings indicate that K_{ATP} channels are not essential for maintaining force during fatigue.

The activation of K_{ATP} channels after fatigue has developed helps preserve a polarized membrane potential, keeping it near E_K. This function prevents voltage-dependent Ca^{2+} entry that can occur following fatigue and cause fiber injury. Consistent with this idea, both Kir6.2 knockout mice and SUR knockout mice show extensive muscle fiber damage when subjected to exercise training (Thabet et al., 2005; Stoller et al., 2007). Therefore, K_{ATP} channels in muscle serve a myoprotective role to prevent fiber damage following intense fatigue or during metabolic exhaustion. In this respect, the role of K_{ATP} channels in skeletal muscles is similar to that in other cell types, i.e. K_{ATP} channels serve as molecular sensors of cellular metabolism, linking metabolism to membrane excitability.

AIII. FURTHER EVIDENCE THAT THE T-TUBULES FIRE Na^+-DEPENDENT APs

Further evidence of a Na^+-dependent TT-AP came from observations in which muscles placed in low $[Na^+]_o$ and stimulated briefly at high frequency, initially develop normal tetanic tension that rapidly falls and steadily decreases to a lower sustained tension; simultaneously the central myofibrils becoming inactive. These results are due to Na^+ depletion in the T-tubule network, particularly in the deeper parts far from the orifice at the fiber surface. Na^+ depletion occurs because g_{Na} increases during the TT-AP generation, causing an inward Na^+ flow into the myoplasm (Bezanilla et al., 1972). The fatigue occurs more rapidly in fibers pre-equilibrated in low $[Na^+]_o$ (e.g. 60 mM). There is a progressive decline in $[Na^+]_{TT}$, which slows propagation velocity down the T-tubules and eventually leads to loss of excitability when $[Na]_{TT}$ drops below some critical level (e.g. 30 mM). Na^+ depletion should occur more rapidly deep in the T-tubule network because there would be less diffusion of Na^+ in from the mouth of the T-tubule to replenish the Na^+ loss. Active Na^+-K^+ pumping in the T-tubules may not occur fast enough to keep up with the Na^+ loss into the fiber myoplasm.

There is evidence that the T-tubules actually do fire APs, i.e. they actively propagate impulses inward and so bring large depolarization deep into the fiber interior. The evidence for this includes the observation of a threshold for sudden initiation of localized contraction (Costantin and Podolsky, 1967; Costantin and Taylor, 1973). The TT-AP is sensitive to TTX and is Na^+ dependent and, therefore, is apparently similar in nature to the surface membrane AP. By use of high-speed cinemicrography to measure sequential activation of the myofibrils in a radial direction, Gonzalez-Serratos (1971) estimated the propagation velocity of the TT-AP (θ_{TT}) to be about 10 cm/s. The Q_{10} of 2.2 is similar to that of the surface membrane AP. Although this velocity is about 16 times slower than propagation

down the fiber longitudinally (about 1.6 m/s), it is sufficient to account for the short latent period before contraction begins. Additional data supporting the presence of APs in the T-tubules has been obtained more recently using V-sensitive dyes.

AIV. PROPAGATION VELOCITY IN A PASSIVE CABLE

In a passive cable, such as in a resting skeletal muscle fiber, the *passive propagation velocity* (θ_p) is directly proportional to the length constant and inversely proportional to the time constant:

$$\theta_p = \frac{\lambda}{\tau_m} \qquad \frac{\text{cm}}{\text{s}} = \frac{\text{cm}}{\text{s}} \tag{42A.1}$$

$$\theta_p = \frac{\sqrt{\frac{R_m}{R_i}\frac{a}{2}}}{R_m C_m} \qquad \frac{\text{cm}}{\text{s}} = \frac{\sqrt{\frac{\Omega.\text{cm}^2}{\Omega.\text{cm}}\frac{\text{cm}}{}}}{\Omega.\text{cm}^2 \frac{\text{F}}{\text{cm}^2}} = \frac{\sqrt{\text{cm}^2}}{\text{s}} \tag{42A.2a}$$

$$\theta_p = \frac{\sqrt{a}}{\sqrt{R_m R_i 2 C_m}}$$

$$\frac{\text{cm}}{\text{s}} = \frac{\sqrt{\text{cm}}}{\sqrt{\Omega.\text{cm}^2}\sqrt{\Omega.\text{cm}}\frac{\text{F}}{\text{cm}^2}} = \frac{\sqrt{\text{cm}}}{\text{cm}\sqrt{\text{cm}}\frac{\text{s}}{\text{cm}^2}} = \frac{\text{cm}}{\text{s}} \tag{42A.2b}$$

Therefore, propagation velocity is directly proportional to the square root of the fiber radius (a) and inversely proportional to membrane capacitance (C_m) and to the square root of R_i and the square root of R_m. For example, propagation velocity is greater in large-diameter muscle fibers. The length constant for sinusoidally-varying applied currents (λ_{ac}) is shorter than λ_{dc}, depending on the ac frequency.

The relationship between propagation velocity and membrane current density (I_m) is given by:

$$I_m = \frac{a}{2}\frac{1}{R_i}\frac{1}{\theta^2}\frac{d^2V}{dt^2}$$

$$\frac{\text{amp}}{\text{cm}^2} = (\text{cm})\left(\frac{1}{\Omega.\text{cm}}\right)\left(\frac{1}{\text{cm}^2/\text{s}^2}\right)\left(\frac{\text{V}}{\text{s}^2}\right) = \frac{\text{amp}}{\text{cm}^2} \tag{42A.3}$$

where d^2V/dt^2 is the second time derivative of the AP. As indicated, membrane current is proportional to d^2V/dt^2, whereas the longitudinal current (I_l) or the capacitative current (I_c) is proportional to dV/dt:

$$I_c = C_m \frac{dV}{dt} \tag{42A.4}$$

AV. EVIDENCE FOR T-TUBULE COMMUNICATION WITH THE SR ACROSS THE TRIADIC JUNCTION UNDER SOME CONDITIONS

This Appendix section is included to let the student know that there are data that do not fit with currently accepted hypotheses.

Ca^{2+} for contraction in skeletal muscle is primarily released from the TC-SR (Winegrad, 1968) and there is an internal cycling of Ca^{2+} ion. Changes in $[Ca^{2+}]_o$ of the bathing solution take a relatively long time (e.g. 30 min) before exerting a large effect on the force of contraction. In contrast, in cardiac muscle, the effect of lowered $[Ca^{2+}]_o$ is significant within a few seconds, indicating that the primary determinant of the force of contraction is the Ca^{2+} influx across the sarcolemma through the slow Ca^{2+} channels. Therefore, in skeletal muscle, excitation propagates actively down the T-tubules and Ca^{2+} is released from the TC-SR, but it is controversial as to how the signal is transferred from the T-tubule to the TC-SR across the triadic junction.

Electron-opaque tracer molecules, like horseradish peroxidase (HRP) (ca. 60 Å diameter), enter into the T-tubules and from there can enter into some of the TC-SR of frog skeletal muscle (Rubio and Sperelakis, 1972; Kulczycky and Mainwood, 1972) (Fig. 42A.1A,B). Exposure of the fibers to hypertonic solutions facilitates the entry of HRP into the TC-SR, so that nearly 100% of the TC-SR become filled (Fig. 42.A.1C,D). Thus, there may be a functional connection between the SR and the extracellular space (Sperelakis et al., 1973). If so, there may be lumen-to-lumen continuity between the T-tubules and TC-SR during excitation, allowing the AP in the T-tubules to invade directly into the TC-SR to depolarize and bring about the release of Ca^{2+}. The depolarization of the TC-SR could activate voltage-dependent Ca^{2+} channels, allowing Ca^{2+} influx into the myoplasm down an electrochemical gradient.

If the longitudinal SR (L-SR) were electrically isolated from the TC-SR by a substantial resistance (e.g. *zippering* between the two SR compartments, described later), this would account for the fiber capacitance measured being relatively low (Mathias et al., 1980). The effect of this would be to remove the very large membrane surface area of the L-SR and hence greatly reduce the capacitance that would be measured.

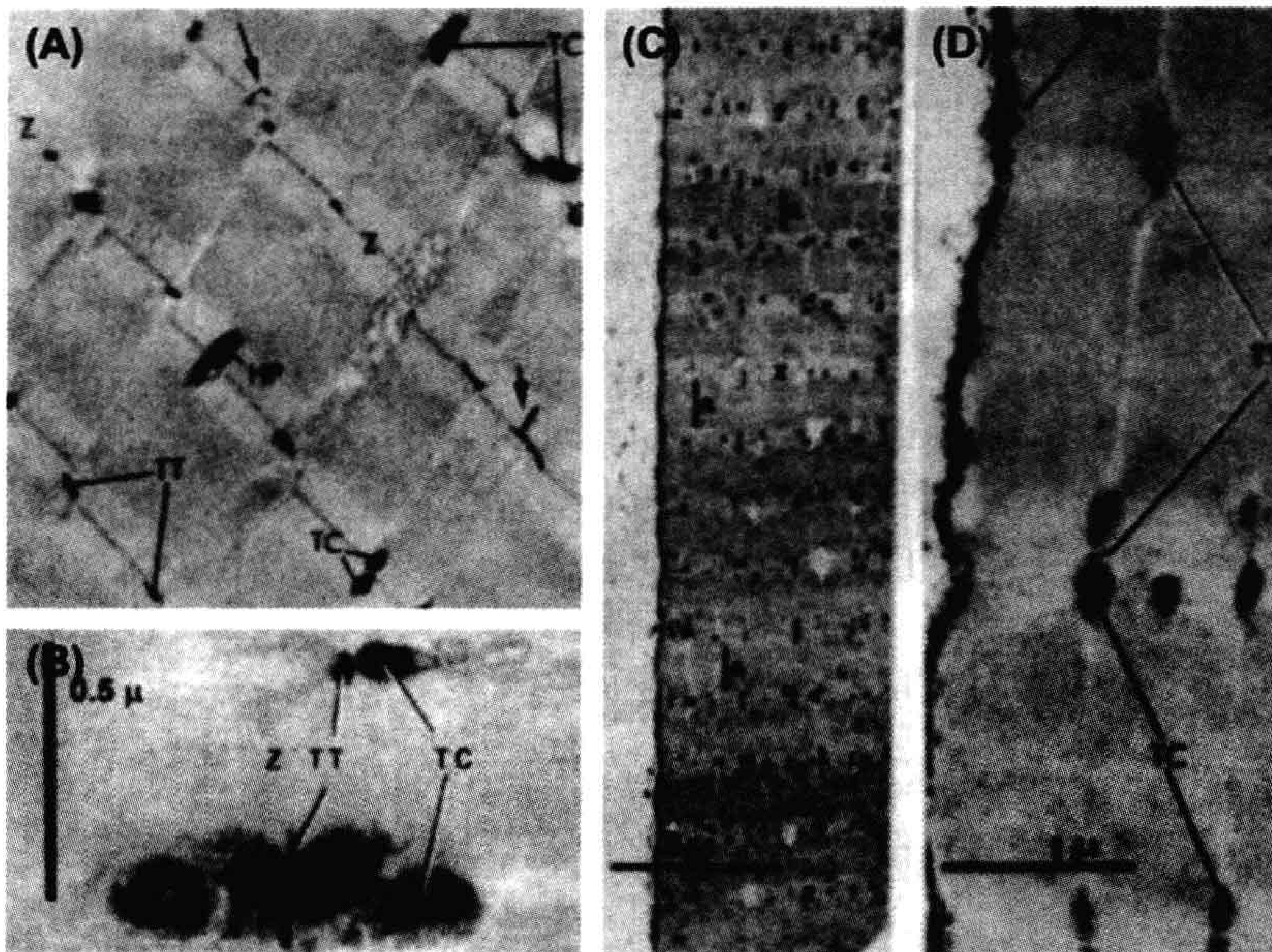


FIGURE 42A.1 Evidence that large molecules of horseradish peroxidase (HP) can enter into the terminal cisternae (TC) of the SR via the transverse tubules (TT) of frog sartorius fibers. Electron micrographs of longitudinal sections. (A,B) Fiber was exposed to HP under isosmotic conditions. (A) Section through several myofibrils showing presence of HP activity (as a dense electron-opaque material) in the TT and in some of the TC at triadic junctions. In amphibian muscle, the TT occur at the level of the Z-lines (Z) of the sarcomeres. Arrows point to two branches of the TT running longitudinally. (B) Higher magnification of two triads, one with both cisternae filled with HP and the other with only one cisterna filled. (C,D) Fiber was exposed to HP under hypertonic condition (3 X isotonic, using NaCl), showing that almost all cisternae were filled with peroxidase. (C) Section at low magnification. (D) Portion of same section as in Part C shown at higher magnification. The surface vesicles (Ves) also became filled with HP. *(Modified from Figs. 2 and 4 of Rubio, R. and Sperelakis, N. (1972). Z. Zellforsch. 124, 57–72.)*

It has been suggested that the SR is depolarized during the release of Ca^{2+} in E-C coupling. For example, optical signals (e.g. birefringence and fluorescence changes) can be recorded from the SR membranes during contraction (e.g. Baylor and Oetliker, 1975; Bezanilla and Horowicz, 1975). In addition, Natori (1965) demonstrated that propagation of contraction (1–3 cm/s) triggered by electrical stimulation can occur in muscle fiber regions that had been denuded (skinned) of their sarcolemma, the propagation of excitation presumably occurring by means of the SR membranes.

It was demonstrated that E-C uncoupling could be produced by exposing frog skeletal muscle fibers to Mn^{2+} (1 mM) or La^{3+} (1 mM) while in hypertonic solution (to facilitate entry of the blockers into the TC-SR) (Sperelakis et al., 1973). After the fibers were returned to normal Ringer solution, normal fast APs could be elicited, but there were no contractions accompanying them; i.e. a "permanent" E-C uncoupling was produced. These results were interpreted as suggesting that Mn^{2+} and La^{3+} entered into the lumen of the TC-SR and blocked the Ca^{2+} channels. A similar exposure of frog sartorius fibers to Mn^{2+}, La^{3+} or to Ca^{2+}-free solution blocked the caffeine-induced contracture as well (Rubio and Sperelakis, 1972). Thus, from these physiological and ultrastructural studies, it was suggested that the lumen of the SR is continuous with that of the T-tubule under conditions of hypertonicity and that substances can enter into the TC-SR to exert an effect on Ca^{2+} release into the myoplasm.

Compartmental analysis of skeletal muscle has also suggested that the SR is open to the ISF. (In contrast, in cardiac muscle, there is no evidence that the SR is open to the ISF [Rubio and Sperelakis, 1972].) For example, Conway (1957), Harris (1963) and Keynes and Steinhardt (1968) concluded that Na^+ inside frog skeletal muscle fibers is distributed in two separate compartments. Harris (1963) suggested that the Na^+, K^+ and Cl^- concentrations in one compartment (presumably the SR) were about equal to those of the ISF. Rogus and Zierler (1973) concluded that the Na^+ concentration in the SR of rat skeletal muscle approximates that of the ISF. The volume of the SR compartment was 14.3% of fiber volume and, in hypertonic solution, the SR volume increased and the washout of the SR compartment was faster. Tasker et al. (1959) also had reported a large sucrose space of 26.5% for frog sartorius fibers.

Other researchers (Birks and Davey, 1969) have demonstrated that the volume changes of the SR of skeletal muscle in hypertonic (sucrose) and hypotonic solutions were always opposite of those occurring within the myoplasmic compartment. They concluded that sucrose must enter into the SR, pulling in water osmotically from the myoplasm, to produce the marked swelling of the SR that occurred in hypertonic solutions. Vinogradova (1968) concluded from the distribution of non-penetrating sugars in frog sartorius muscle that the SR compartment is continuous with the ISF; the inulin space was 19.0% and increased in hypertonic solution and decreased in hypotonic solution and in glycerol-treated fibers (for disruption of the T-tubules).

The total [3H]-sucrose space of frog sartorius muscles was found to be 18.0% in isotonic solution and 22.6% in twofold hypertonic solution (Sperelakis et al., 1978). The relative SR volume (including the small T-tubule volume) was 12.4% and 17.0% of fiber volume, respectively. This value for SR volume of frog skeletal muscle is close to that measured by ultrastructural techniques (Peachey, 1965; Mobley and Eisenberg, 1975). Evidence that the TC-SR and L-SR may not be freely connected to one another under resting conditions comes from the observations that: (1) the L-SR did not fill with HRP, whereas the TC-SR did (Rubio and Sperelakis, 1972); and (2) there is a zippering of the membranes connecting these two components of the SR in mouse and frog skeletal muscle (Howell, 1974; Wallace and Sommer, 1975; Forbes and Sperelakis, 1979).

In ^{45}Ca washout experiments on frog muscles, Kirby et al. (1975) found three compartments, similar to the three sucrose compartments described previously, except the half-times were about two- to threefold shorter. They suggested that the first compartment was the ISF space, the second was the T-tubule plus the TC-SR and the third was the L-SR. Bianchi and Bolton (1974) also found a transient increase in ^{45}Ca efflux and a marked loss of muscle Ca^{2+} from frog sartorius muscles exposed to hypertonic solutions (twice isotonicity) and suggested that hypertonicity produces transient communication between the TC-SR and the T-tubules, thus allowing their Ca^{2+} to be lost to the ISF. In addition, it has been reported in a human muscle disease, polymyositis, that the T-tubules are spatially continuous with the SR, as visualized with lanthanum tracer, and that enzymes leak from the TC-SR into the T-tubules and ISF (Chou et al., 1980).

Frog skeletal muscle fibers have an osmotically inactive volume of about 32% when placed into Ringer solution made hypertonic with sucrose or other non-penetrating solutes; i.e. fiber diameter does not shrink to the theoretical value expected if it were a perfect osmometer (Sperelakis and Schneider, 1968; Sperelakis et al., 1970). For example, in twofold hypertonic solution, there should be a decrease in fiber volume to one-half and fiber radius to 0.707 ($1/\sqrt{2}$) of the original value. The observed change is to only 0.81 of the original diameter. Because the SR volume increases in hypertonic solution (Huxley et al., 1963; Sperelakis and Schneider, 1968; Birks and Davey, 1969), it is likely that the osmotic inactive volume is due to the SR. The swollen SR would prevent the fiber volume from decreasing to one-half in twofold hypertonic solution, even if the volume of the myoplasm proper were to decrease to one-half.

In cardiac muscle, an osmotically-inactive volume is not present (Sperelakis and Rubio, 1971), electron-opaque tracers do not enter the SR (Sperelakis et al., 1974) and the SR volume does not increase with hypertonicity (Sperelakis and Rubio, 1971).

AVI. INVERTEBRATE STRIATED MUSCLE FIBERS

This Appendix was prepared by Hugo Gonzalez-Serratos and Hector Rasgado-Flores and was edited by Nicholas Sperelakis.

Introduction

In 1902, Overton observed that frog skeletal muscle cells lost their excitability when the extracellular Na^+ concentration ($[Na^+]_o$) was decreased below 10% of normal. This was the first indication that excitability of vertebrate skeletal muscle fibers was Na^+-dependent. Using intracellular microelectrodes, Nastuck and Hodgkin demonstrated, in 1950, that skeletal muscle fibers of the frog have a clear relationship between the amplitude of the AP and $[Na^+]_o$. They concluded that vertebrate striated skeletal muscle APs are generated by mechanisms similar to those in squid giant nerve axons. In an attempt to test this Na^+ hypothesis in striated muscle fibers of the crustacean, Fatt and Katz (1953) bathed crayfish muscles with different external Na^+ concentrations. However, against their prediction, they found that there was no effect on the amplitude of the APs. That is, striated invertebrate crayfish muscles were excitable and capable of developing full APs in the absence of external Na^+ ions. Thus, they concluded that invertebrate striated muscle fibers did not have an Na-dependent excitability. Instead, the APs were generated by currents using other ions. The APs of invertebrate striated muscle fibers, compared to vertebrates, are longer in duration and some of them even have a plateau (similar to cardiac muscle) (Fig. 42A.2).

Calcium Hypothesis

What are the ionic currents that generate the APs in invertebrate striated muscle fibers? With zero extracellular Na^+, the invertebrate muscles were capable of generating APs as long as there were Ca^{2+} ions in the bathing solution.

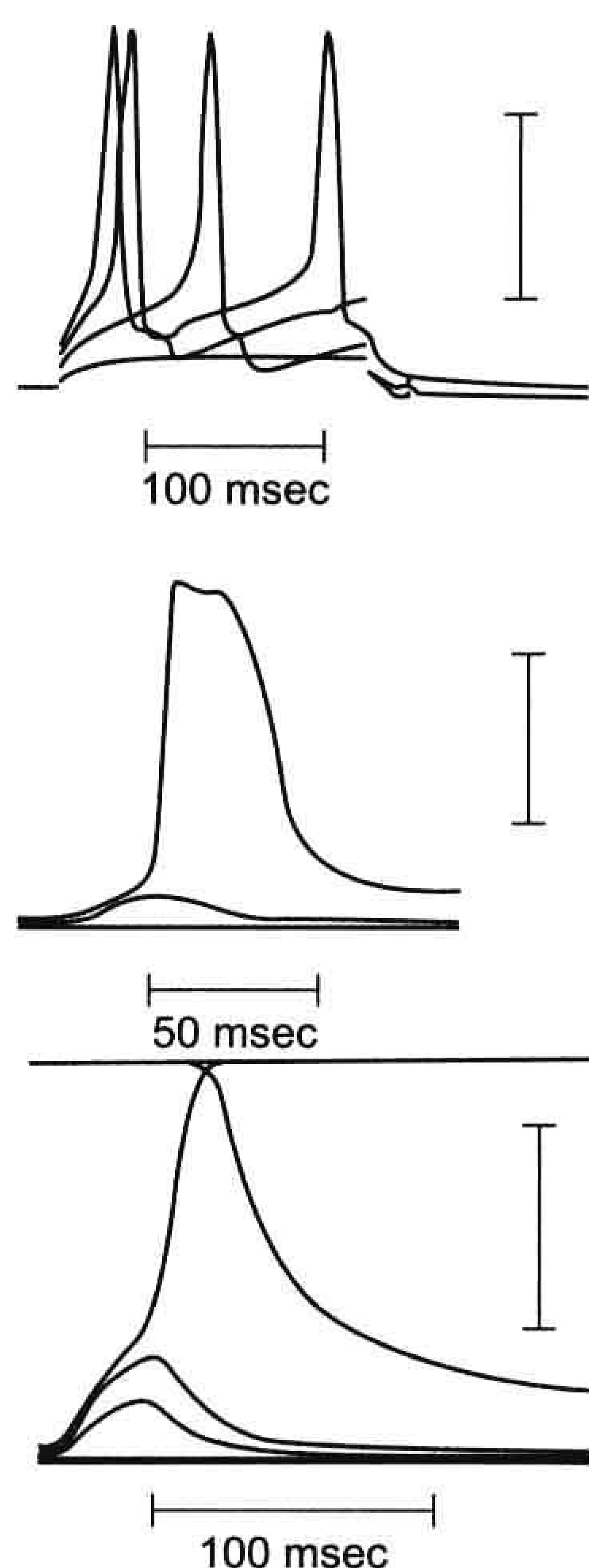


FIGURE 42A.2 Different action potentials in invertebrate striated muscle fibers of different crab species. (A) *Portunus (from Atwood, 1965).* (B) *Carcinus maenas (from Fatt and Katz, 1953).* (C) *Portunus deporatus (from Fatt and Katz, 1953).* Voltage calibration bars:40 mV.

It was concluded that these fibers produced Ca^{2+}-dependent APs (Fatt and Ginsborg, 1958). These APs persisted when Sr^{2+} or Ba^{2+} (which have some physicochemical properties similar to Ca^{2+}) replaced the Ca^{2+}. This led to the *calcium hypothesis*. Hagiwara and Naka (1964) induced APs in the giant barnacle striated muscles fibers (*Balanus nubilus*) in which they changed the intracellular Ca^{2+} concentration by injecting the fibers with Ca^{2+}chelating substances. As the internal free Ca^{2+} concentration was decreased progressively, the AP amplitude increased progressively. At an internal Ca^{2+} concentration of 8×10^{-8} M, the AP became all-or-none (Hagiwara and Nakajima, 1966). Thus, they confirmed the generation of Ca^{2+} APs in invertebrate striated muscle fibers.

Three types of experiments have proven the Ca^{2+} hypothesis for invertebrate striated muscle cells: (1) the Ca^{2+}-dependence of the AP amplitude; (2) the lack of APs in zero Ca^{2+} bathing solution; and (3) the entry of Ca^{2+} ions during the APs.

Ca^{2+} dependence of the APs. Fatt and Ginsborg in 1958 and Pilgrim and Wiersma in 1963 demonstrated that the striated myofibers of the crayfish (*Orconectes virilis*) and lobster (*Homarus americanus*) were capable of generating propagated all-or-none APs. These APs did not disappear when the muscles were immersed in bathing solutions without Na^+, K^+ or Mg^{2+}. However, the amplitude of the APs depended on the extracellular Ca^{2+} concentration $[Ca^{2+}]_o$. The AP amplitude increased with a slope of 25 mV per decade of $[Ca^{2+}]_o$. These results strongly supported the proposal that the APs of invertebrate striated skeletal muscle fibers are generated by inward Ca^{2+} currents. In the crayfish (*Astacus fluvilis*), the potentiating effect of $[Ca^{2+}]_o$ was strongly enhanced in the presence of quaternary ammonium ions like tetraethylammonium (TEA, an inhibitor of outward I_K) (Fig. 42A.3). The maximum rate of depolarization of the APs increased from 8 V/s to 15 V/s when $[Ca^{2+}]_o$ was changed from 4 to 16 mM. In the giant muscle fibers from the barnacle (*Balanus nubilus*), Hoyle and Smith (1963) and Hagiwara and Naka (1964) found that the usual graded responses were converted to all-or-none responses when the gradient between extracellular and intracellular $[Ca^{2+}]$ increased by injecting the cells with Ca^{2+}-chelating substances like EDTA and K_2SO_4. The amplitudes of the APs were a function of the extracellular and intracellular $[Ca^{2+}]$ ratios.

Calcium influx. Hagiwara and Naka (1964) found that, during prolonged stimulations that produced repetitive APs, there was a substantial amount of radioactive Ca^{2+} influx into barnacle giant muscle. They estimated that the intracellular Ca^{2+} concentration increased by an average of 75 pmole/cm^2/impulse and calculated that, during each AP, there was an influx of 6 pmoles of Ca^{2+}/cm^2. This is a very high Ca^{2+} influx compared with the values reported for vertebrate skeletal muscle fibers (Bianchi and Schanes, 1959).

Prolonged depolarization (elicited with high concentrations of extracellular K^+) above the mechanical threshold leads to sustained mechanical activation (contractures). When K^+-contractures were elicited in a bathing solution without Ca^{2+} ions, the K^+-contractures disappeared after a short time, even though the membrane remained depolarized. This indicates that, during prolonged depolarization of invertebrate striated muscles, there is a substantial inflow of Ca^{2+} that brings about the mechanical activation.

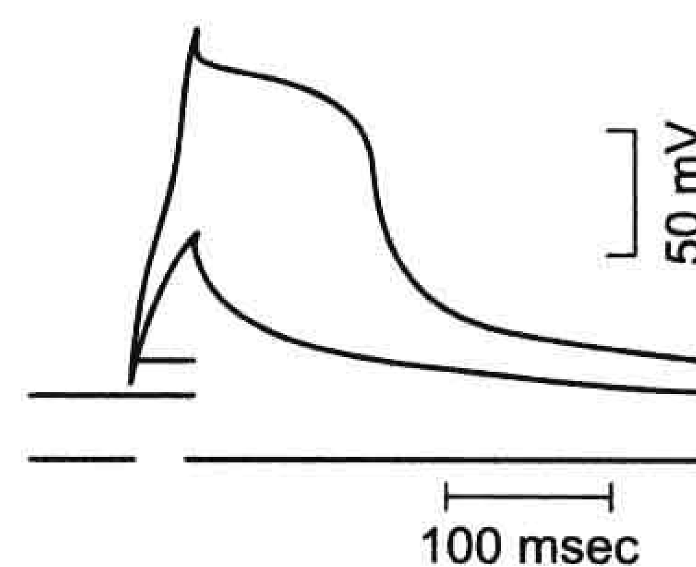


FIGURE 42A.3 Potentiation of invertebrate striated muscle of the crayfish (*Astacus fluvialitis*) with TEA. Upper trace: action potential. Lower trace: applied current. *(From Fatt and Ginsborg, 1958.)*

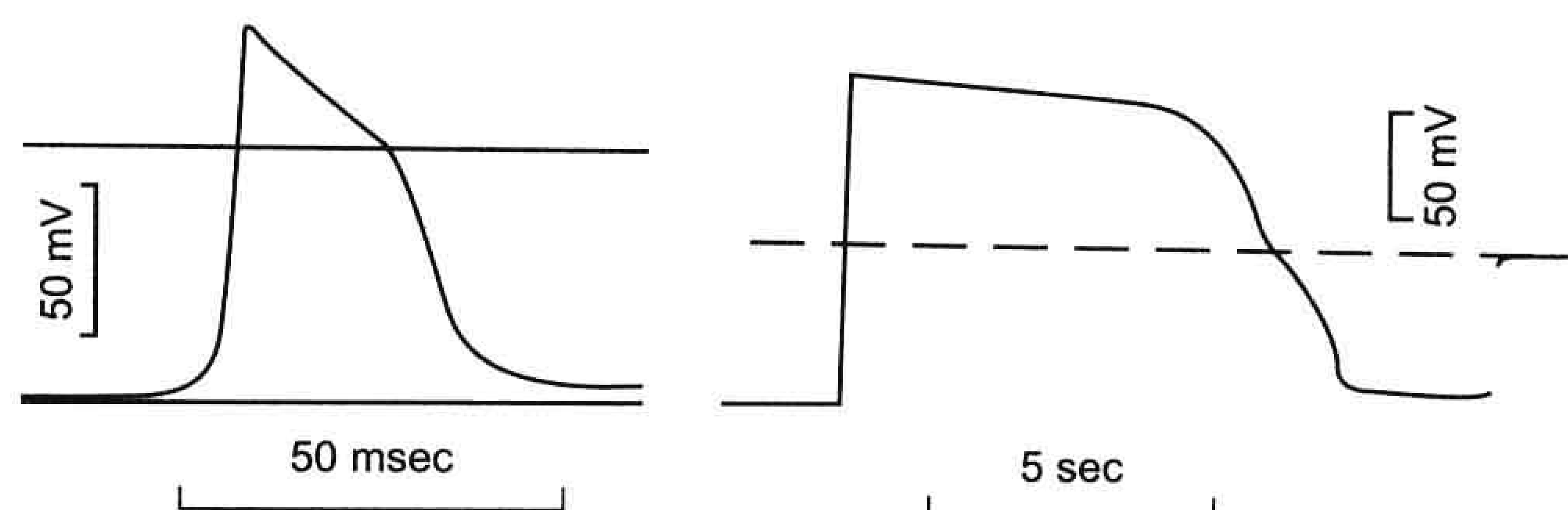


FIGURE 42A.4 Crayfish striated muscles fibers. Action potentials of fibers bathed with strontium (left panel) and barium (right panel). *(From Fatt and Ginsborg, 1958.)*

Potentiation of APs. Fatt and Ginsborg (1958) observed that when all the extracellular Ca^{2+} was removed and substituted with equimolar concentrations of $SrCl_2$ or $BaCl_2$, the crayfish striated muscles not only produced all-or-none APs, but they were of higher amplitude and longer duration (Fig. 42A.4). The RPs were unaffected. These results were confirmed by Werman and Grundfest (1961) in lobster muscle fibers and by Werman et al. (1961) in the muscle of the grasshopper (*Romalea microptera*). Thus, inward $Sr^{2+}$and Ba^{2+} currents are also capable, like Ca^{2+} ions, of generating APs. The increased AP durations were the result of increased durations of the plateau. The control muscle fibers had an average duration of only 3–6 ms. The duration of the Ba^{2+} APs was 15–100 ms, compared with 400–12 000 ms for the Sr^{2+} APs (Fig. 42A.4). The AP overshoot was about 20 mV larger with Ba^{2+} compared with Sr^{2+} in striated muscles from crayfish (*Astacus fluvialis*) and lobster (*Homarus americanus*) (Fatt and Ginsburg, 1958; Werman and Grundfest, 1961). The RP of −90 mV did not change with Sr or Ba ions.

Ionic currents. Hagiwara and Naka (1964), by using a voltage-clamp method, showed that the currents developed during the AP were composed of early inward Ca^{2+} currents, since they varied in amplitude with extracellular Ca^{2+} concentration and were not affected by TTX. It was concluded that, in invertebrate striated muscle fibers, the propagated AP was the consequence of inward Ca^{2+} current. Henĉek et al. (1969) measured Sr^{2+} current in the crayfish (*Astacus fluviaitilis*) using a sucrose-gap voltage-clamp. They found that the currents consisted of early inward current followed by outward current. The Ca^{2+} currents were smaller than the Ba^{2+} currents (Fig. 42A.5). The late outward current was decreased by the K^{+}-current blocker TEA (Fig. 42A.6).

The AP in invertebrate striated muscles, like in vertebrate striated muscles, fulfills two main roles. One role is to propagate a depolarization wave all along the length of the entire muscle fiber. Another role is to increase the myoplasmic Ca^{2+} to levels that induce the binding of myosin with actin to bring about activation of the contractile proteins (Fig. 42A.7). The mechanical activation develops either shortening, force, or both (producing muscle work).

Regulation of Intracellular Ca^{2+}

Vertebrate skeletal muscle fibers bathed in Ringer's solution containing 1 mM [Ca^{2+}] had an average Ca^{2+} influx at rest of 0.26 pmoles/cm^2/s and, during stimulation, the Ca^{2+} influx increased to 0.73 pmoles/cm^2/impulse (Curtis,1966). Blocking the inward Ca^{2+} current has no effect on the contraction or E-C coupling mechanism (Gonzalez-Serratos et al., 1982). Thus, the main role of inward Ca^{2+} current in vertebrate skeletal muscles fibers is to maintain long-term adequate amounts of intracellular Ca^{2+} (mainly in the SR^{2+}).

In contrast, invertebrate striated muscle fibers have an average Ca^{2+} influx of 75 pmoles/cm^2/impulse (Hagiwara and Naka, 1964). Since the SR is sparse, there must be

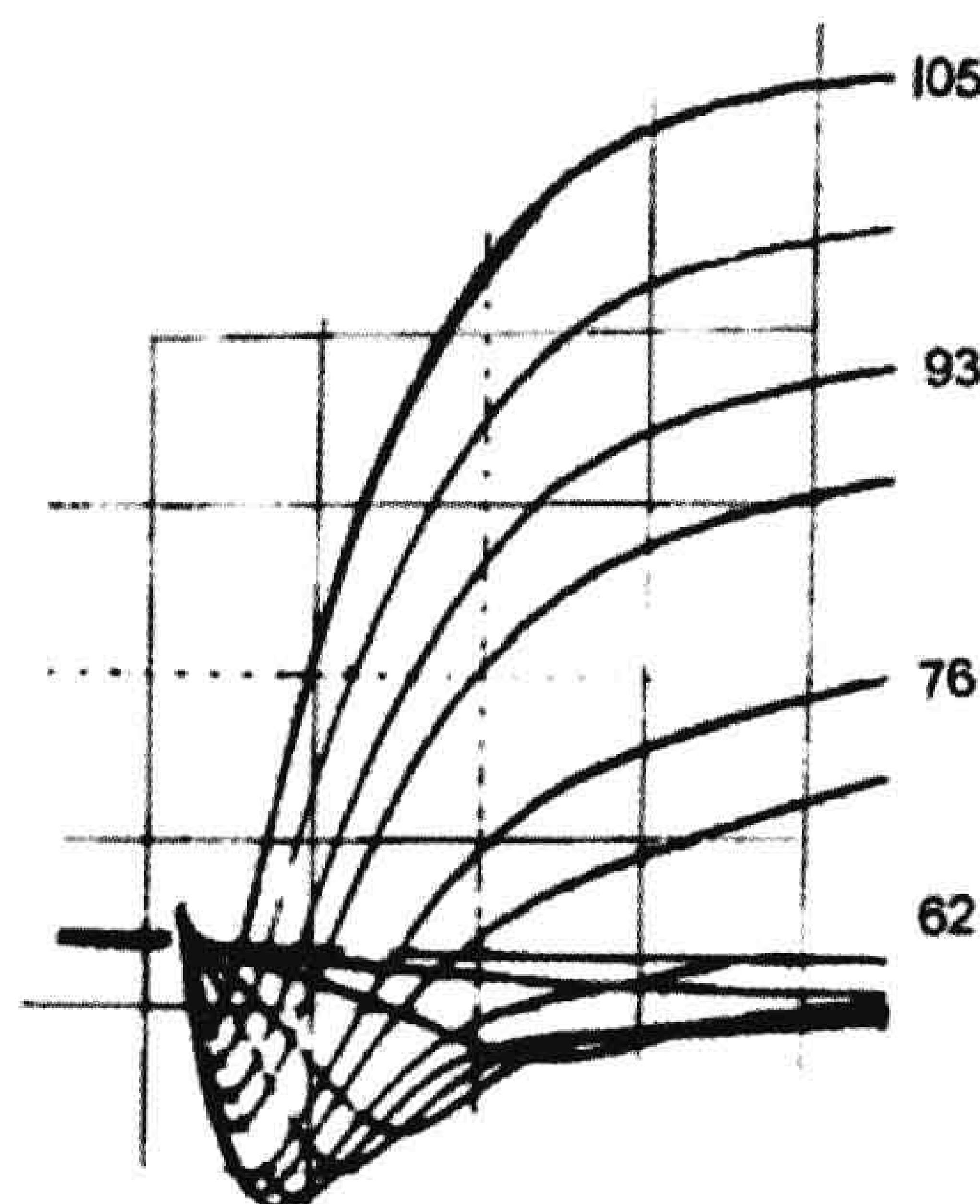


FIGURE 42A.5 Membrane currents under voltage clamp from crayfish striated muscle (*Astacus Fluviatilis*) bathed with extracellular strontium chloride isotonic solution. The clamped membrane potentials are shown in mV. Records below the zero line are inward currents, above are outward currents.

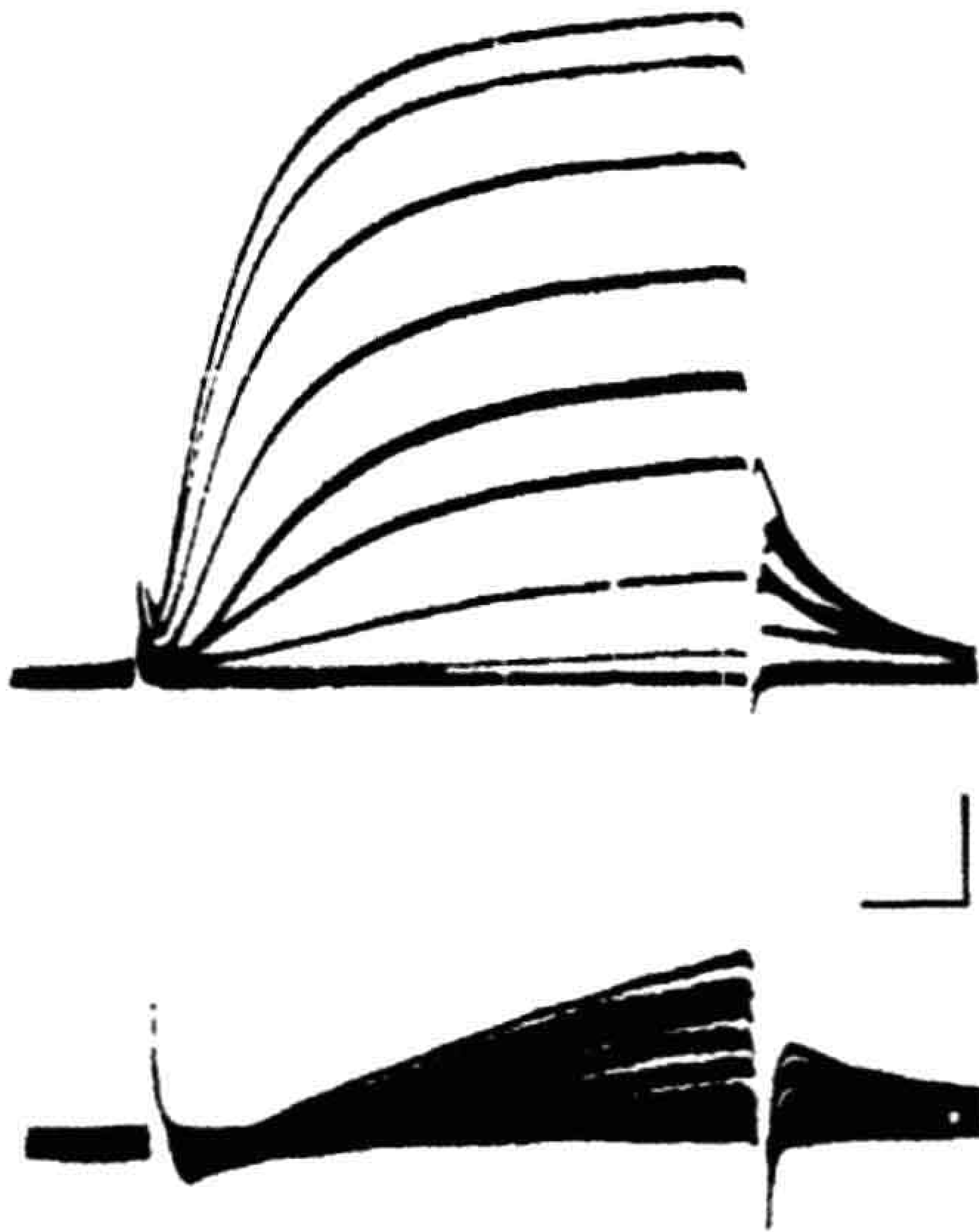


FIGURE 42A.6 Effect of TEA on membrane currents from the crayfish striated muscle (*Astacus Fluviatilis*) under voltage clamp. Top records, bathed with normal extracellular solution. Bottom records, after addition of 50 mM of TEA to the bathing solution. Calibrations: 0.15 mA/cm^2 and 5 ms. *(From Henĉek et al., 1969.)*

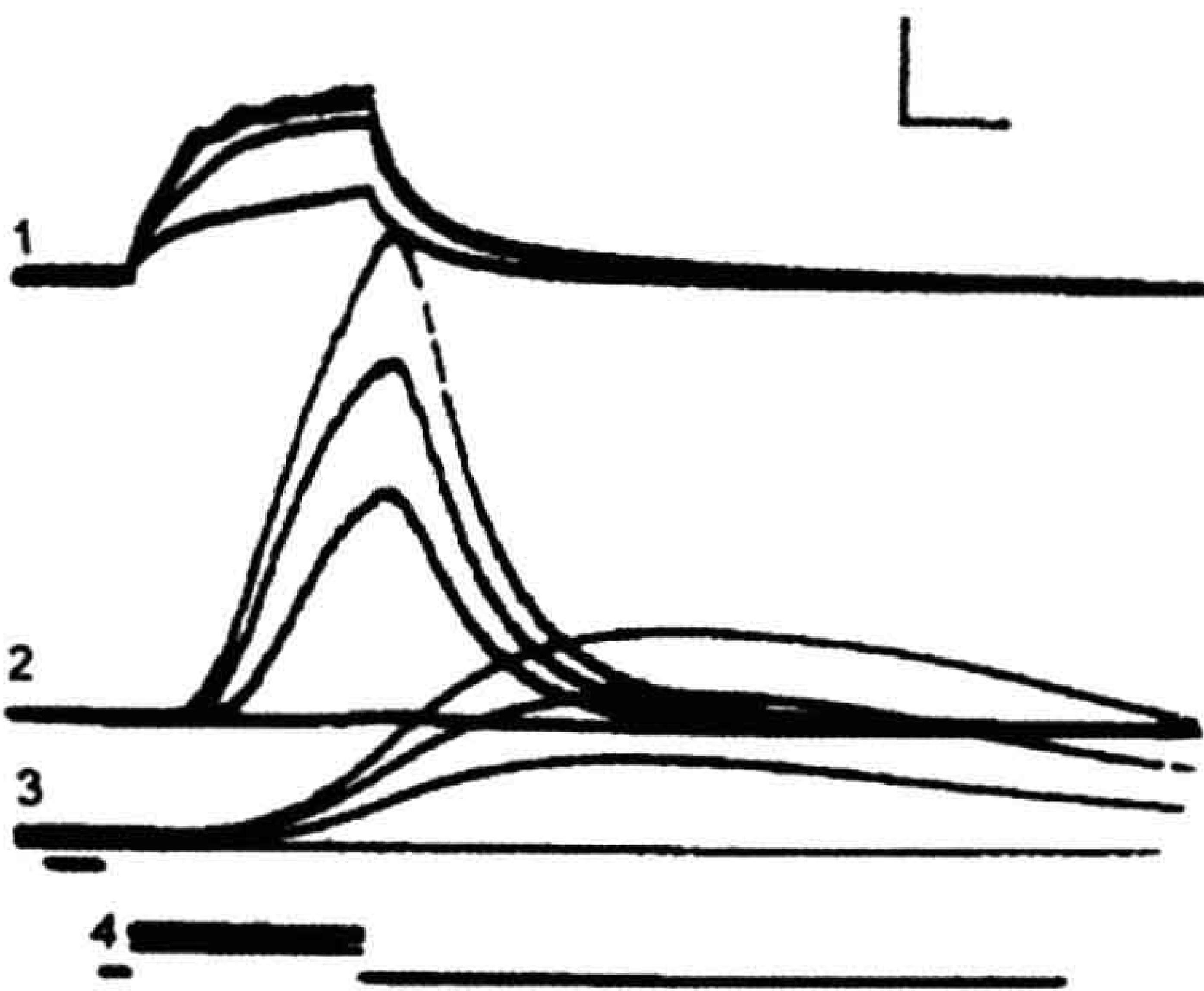


FIGURE 42A.7 Myoplasmic calcium transients recorded with the luminescent ptotein aequorin during stimulations of barnacle (*Balanus nubilis*) striated muscle. Traces: 1: membrane potentials; 2: light output, myoplasma calcium transients; 3: isometric forces; 4: stimulating electrical pulses. On each set of recording traces, the recordings from top to bottom correspond to each other. Vertical calibrations: 20 mV, 3.8×10^{-9} lumens, 5 g. Horizontal calibration: 100 ms. *(From Ashley and Ridgway, 1968.)*

another mechanism to decrease the free myoplasmic Ca^{2+} after activation. Otherwise, these muscles would develop permanent and powerful contractures and suffer deleterious effects. The mechanism by which invertebrate striated muscles decrease and regulate the free intracellular Ca^{2+} concentration is via the sarcolemmal Ca^{2+}/H^{+} exchanger mediated by Ca^{2+}-ATPase (DeSantiago et al., 2007) and the Na^{+}/Ca^{2+} exchanger (Rasgado-Flores et al., 1991). The Na^{+}/Ca^{2+} exchanger mediates the coupling of the movement of external Na^{+} ions down their electrochemical gradient, with the movement of internal Ca^{2+} ions (in the opposite direction) across the sarcolemma. In giant striated muscle of the barnacle (*Balanus nubile*) (like most excitable cells), the Na^{+}/Ca^{2+} exchanger has a stoichiometry of three Na^{+} ions exchanged per each Ca^{2+} ion (Rasgado-Flores et al., 1989).

Innervation of Invertebrate Muscle Fibers

One important characteristic of the innervation of non-vertebrate striated muscle fibers is that the nerve terminals on the muscle fibers form terminal buttons spread all along the muscle fiber. This is in contrast with vertebrate muscle where a motor nerve ends in one button localized near the middle of the fiber. The branching of invertebrate motor nerves leads to multiple nerve terminals that are distributed along the length and around the perimeter of the muscle fibers. There are some differences as a consequence of the differences in the topological distribution of the nerve terminals. The excitatory responses to motor nerve APs can trigger in the muscle fiber either local APs or full-size APs all along the muscle fiber. The transmission of the excitatory process leads to multiple postsynaptic potentials. The regulation of force development during contractions of vertebrate muscles is under central nervous system control. In contrast, in invertebrate muscles, the regulation of the degree of contractions is done peripherally and depends on the number of either excitatory or inhibitory nerve terminals that are activated.

Another feature of invertebrate neuromuscular junctions is that they are structurally simpler than vertebrate motor end-plates. The motor nerves of the crustaceans have short nerve terminals that have periodical swellings in series. The swellings make contact with the surface membrane of the muscle fiber. The nerve terminals are very close together. The response of the invertebrate neuromuscular junction to a nerve AP is called the *junctional potential* (JP). Evoked JPs are due to a large and synchronized release of neurotransmitters triggered by the nerve terminal AP. The JPs of invertebrates are either *excitatory* (EJPs) or *inhibitory* (IJPs). The excitatory neurotransmitter is *glutamate*. The inhibitory neurotransmitter is *GABA* (γ-aminobutyric acid). The release of these transmitters will lead either to excitation and mechanical activation of the muscle fiber or inhibition of the excitation and thus producing relaxation. The RP can be hyperpolarized due to the IJPs. Therefore, the amount of current necessary to

reach the mechanical threshold voltage (for E-C coupling) can also increase as a consequence of the IJPs hyperpolarizing the membrane.

The electrical responses (*postsynaptic potentials*) at the neuromuscular junctions are, in most cases, small and graded. But when the small responses are summated, the muscle membrane reaches threshold that generates a full AP that propagates along the muscle fiber. Another important feature of invertebrate muscle innervations is that a single myofiber can be innervated by more than one motor neuron, i.e. *polyneural innervation*. The polyneural innervation leads to complex electrical and mechanical responses. The topological distribution of nerve junctions and the graded activation permit the existence of fast and slow contractions, as well as excitation and inhibition (often within a single myofiber).

When an EJP reaches the mechanical threshold, a local contraction is produced. When several EJPs are elicited in synchrony, they generate a graded contraction that can show summation. This summation causes a large contraction. IJPs cause hyperpolarization, moving the membrane potential away from the mechanical threshold, thereby causing relaxation. The multiple innervations characteristics of invertebrate muscles cause one muscle fiber to produce EJPs while its neighbor may produce IJPs. The same muscle fiber can show an excitatory response that develops force and an inhibitory response that reduces the force developed (Dudel and Kuffler, 1961). From one to nine excitatory nerves may innervate a single muscle fiber, while the number of inhibitory nerves can be up to three (Kennedy et al., 1966). The size of EJPs (initially of low magnitude) increases progressively during repetitive stimulation and this is called *facilitation* (Hoyle and Wiersma, 1958). In contrast, the large EJPs decrease in size during the repetitive activation due to transmitter depletion or fatigue, a process known as *fatigue* or *anti-facilitation* (Hoyle and Burrows, 1973). Another feature of invertebrate muscle fibers is that the faster fibers display higher E-C thresholds. Therefore, they require EJPs of larger magnitude to reach the E-C threshold. They also develop stronger twitches.

There is relevant information about crayfish muscle stretch receptors given in a previous chapter.

BIBLIOGRAPHY

Adrian, R. H., & Freygang, W. H. (1962). The potassium and chloride conductance of frog muscle membrane. *J Physiol (London), 163*, 61–103.

Adrian, R. H., & Peachey, L. D. (1973). Reconstruction of the action potential of frog sartorius muscle. *J Physiol (London), 235*, 103–131.

Adrian, R. H., Chandler, W. K., & Hodgkin, A. L. (1970a). Voltage clamp experiments in striated muscle fibers. *J Physiol (London), 208*, 607–644.

Adrian, R. H., Chandler, W. K., & Hodgkin, A. L. (1970b). Slow changes in potassium permeability in skeletal muscle. *J Physiol (London), 208*, 645–668.

Almers, W., Fink, R., & Palade, P. T. (1981). Calcium depletion in frog muscle tubules: the decline of calcium depletion in frog muscle tubules: the decline of calcium current under maintained depolarization. *J Physiol (London), 312*, 177–207.

Armstrong, C. M., Bezanilla, F. M., & Horowicz, P. (1972). Twitches in the presence of ethylene glycol bis(β-aminoethyl ether)-N, N'tetraacetic acid. *Biochem Biophys Acta, 267*, 605–608.

Ashley, C. C., & Ridgway, E. B. (1968). Simultaneous recording of membrane potential, calcium transient and tension in single muscle fibers. *Nature, 219*, 1168–1169.

Atwood, H. L. (1965). Characteristics of fibres in the extensor muscle of a crab. *Comp Biochem Physiol, 14*, 205–207.

Baylor, S. M., & Oetliker, H. (1975). Birefingence experiments on isolated skeletal muscle fibres suggest a possible signal from the sarcoplasmic reticulum. *Nature, 253*, 97–101.

Beaty, G. N., & Stefani, I. (1976). Calcium dependent electrical activity in twitch muscle fibers of the frog. *Proc R Soc London (Biol), 194*, 141–150.

Bezanilla, F., & Horowicz, P. (1975). Fluorescence intensity changes associated with contractile activation in frog muscle stained with Nile Blue A. *J Physiol (London), 246*, 709–735.

Bezanilla, F., Caputo, C., Gonzalez-Serratos, H., & Venosa, R. A. (1972). Sodium dependence of the inward spread of activation in isolated twitch muscle fibres of the frog. *J Physiol (London), 223*, 507–523.

Bianchi, C. P., & Bolton, T. C. (1974). Effect of hypertonic solutions and glycerol treatment on calcium and magnesium movements of frog skeletal muscle. *J Pharmacol Exp Ther, 188*, 536–522.

Bianchi, C. P., & Shanes, A. M. (1959). Calcium influx in skeletal muscle at rest, during activity, and during potassium contracture. *J Gen Physiol, 42*, 803–815.

Birks, R. I., & Davey, D. F. (1969). Osmotic responses demonstrating the extracellular character of sarcoplasmic reticulum. *J Physiol (London), 21*, 171–188.

Boudreault, L., Cifelli, C., Bourassa, F., Scott, K., & Renaud, J. M. (2010). Fatigue preconditioning increases fatigue resistance in mouse flexor digitorum brevis muscle with non-functioning K(ATP) channels. *J. Physiol., 588*, 4549–4562.

Caputo, C. (1978). Excitation and contraction processes in muscle. *Annu. Rev. Biophys. Bioeng., 7*, 63–83.

Carlson, E. D., & Siger, A. (1960). The mechanochemistry of muscular contraction. I. The isometric twitch. *J Gen Physiol, 44*, 33–60.

Castle, N. A., & Haylett, D. G. (1987). Effect of channel blockers on potassium efflux from metabolically exhausted frog skeletal muscle. *J Physiol, 383*, 31–43.

Chou, S. M., Nonaka, I., & Voice, G. F. (1980). Anastomoses of transverse tubules with terminal cisternae in polymyositis. *Arch Neurol, 37*, 257–266.

Cifelli, C., Bourassa, F., Gariepy, L., Banas, K., Benkhalti, M., & Renaud, J. M. (2007). KAPT channel deficiency in mouse flexor digitorum brevis causes fiber damage and impairs Ca^{2+} release and force development during fatigue in vitro. *J. Physiol., 582*, 843–857.

Clausen, T. (2008). Clearance of extracellular K^{+} during muscle contraction–roles of membrane transport and diffusion. *J. Gen. Physiol., 131*, 473–481.

Cognard, C., Rivet-Bastide, M., Constantin, B., & Raymond, G. (1992). Progressive predominance of 'skeletal' versus 'cardiac' types of excitation-contraction coupling during in vitro skeletal myogenesis. *Pflügers Arch, 422*, 207–209.

Conway, E. J. (1957). Nature and significance of concentration relations of potassium and sodium ions in skeletal muscle. *Physiol Rev, 37*, 84–132.

Cordoba-Rodriguez, R., Gonzalez-Serratos, H., Matteson, D. R., & Rozycka, M. (1997). Ica is important in E-C coupling in developing cultured embryonic amphibian skeletal muscle cells. *Biophys J, 72*, A119, H5.

Cordoba-Rodriguez, R., Matteson, D. R., & Gonzalez-Serratos, H. (1996). Embryonic E-C coupling in cultured skeletal muscle cells. *Biophys J, 70*, A390.

Costantin, L. L. (1970). The role of sodium current in the radial spread of contraction in frog muscle fibers. *J Gen Physiol, 55*, 703–715.

Costantin, L. L., & Podolsky, R. J. (1967). Depolarization of the internal membrane system in the activation of frog skeletal muscle. *J Gen Physiol, 50*, 1101–1124.

Costantin, L. L., & Taylor, S. R. (1973). Graded activation in frog muscle fibers. *J Gen Physiol, 61*, 424–443.

Curtis, R. A. (1966). Ca fluxes in single twitch muscle fibers. *J Gen Physiol, 50*, 225–267.

Davies, N. W., Standen, N. B., & Stanfield, P. R. (1992). The effect of intracellular pH on ATP-dependent potassium channels of frog skeletal muscle. *J Physiol, 445*, 549–568.

Dawson, M. J., Gadian, D. G., & Wilkie, D. R. (1978). Muscular fatigue investigated by phosphorus nuclear magnetic resonance. *Nature, 274*, 861–866.

Dawson, M. J., Gadian, D. G., & Wilkie, D. R. (1980). Mechanical relaxation rate and metabolism studied in fatiguing muscle by phosphorus nuclear magnetic resonance. *J Physiol, 299*, 465–484.

DeSantiago, J., Batlle, D., Khilnani, M., et al. (2007). Ca^{2+}/H^{+} exchange via the plasma membrane Ca^{2+} ATPase in skeletal muscle. *Front Biosci, 12*, 4641–4660.

DiFranco, M., Capote, J., & Vergara, J. L. (2005). Optical imaging and functional characterization of the transverse tubular system of mammalian muscle fibers using the potentiometric indicator di-8-ANEPPS. *J Memb Biol, 208*, 141–153.

Dudel, J., & Kuffler, S. W. (1961). Presynaptic inhibition at the crayfish neuromuscular junction. *J Physiol, 155*, 543–562.

Eisenberg, R. S., & Gage, P. W. (1969). Ionic conductances of the surface and transverse tubular membranes of frog sartorius fibers. *J Gen Physiol, 53*, 279–297.

Fabiato, A. (1982). Mechanism of calcium-induced release of calcium from the sarcoplasmic reticulum of skinned cardiac cells studied with potential-sensitive dyes. In S. T. Ohnishi, & M. Endo (Eds.), *The Mechanism of Gated Calcium Transport Across Biological Membranes* (pp. 237–255). New York: Academic Press.

Fahlke, C., Zachar, E., & Rudel, R. (1993). Chloride channels with reduced single-channel conductance in recessive myotonia congenita. *Neuron, 10*, 225–232.

Fatt, P., & Ginsborg, B. L. (1958). The ionic requirements for the production of action potentials in crustacean muscle fibers. *J Physiol (London), 142*, 156–543.

Fatt, P., & Katz, B. (1953). The electrical properties of crustacean muscle. *J Physiol, 120*, 171–204.

Fink, R., & Lüttgau, H. C. (1976). An evaluation of the membrance constants and the potassium conductance in metabolically exhausted muscle fibers. *J Physiol, 263*, 215–238.

Flagg, T. P., Enkvetchakul, D., Koster, J. C., & Nichols, C. G. (2010). Muscle KATP channels: Recent insights to energy sensing and myoprotection. *Physiol. Rev., 90*, 799–829.

Flucher, B. E., Takekura, H., & Franzini-Armstrong, C. (1993). Development of the excitation-contraction coupling apparatus in skeletal muscle: association of sarcoplasmic reticulum and transverse tubules with myofibrils. *Dev Biol, 160*, 135–147.

Forbes, M. S., & Sperelakis, N. (1979). Ruthenium red staining of skeletal and cardiac muscles. *Z Zellforsch Cell Tissue Res, 200*, 367–382.

Garcia, M.del C., Gonzalez-Serratos, H., Morgan, J. P., Perreault, C. L., & Rozycka, M. (1991). Differential activation of myofibrils during fatigue in phasic skeletal muscle cells. *J Musc Res Cell Motil, 12*, 412–424.

Gonzalez-Serratos, H. (1971). Inward spread of activation in vertebrate muscle fibers. *J Physiol (London), 212*, 777–799.

Gonzalez-Serratos, H. (1975). Graded activation of myofibrils and the effect of diameter on tension development during contractures in isolated skeletal muscle fibers. *J Physiol (London), 253*, 321–339.

Gonzalez-Serratos, H., Cordoba-Rodriguez, R., Matteson, D. R., & Rozycka, M. (1996). Role of calcium currents in excitation-contraction coupling in developing cultured embryonic amphibian skeletal muscle cells. *J Physiol*, 494P.

Gonzalez-Serratos, H., Somlyo, A. V., McClellan, G., Shuman, H., Borrero, L. M., & Somlyo, A. P. (1978). Composition of vacuoles and sarcoplasmic reticulum in fatigued muscle: electron probe analysis. *Proc Natl Acad Sci USA, 75*, 1329–1333.

Gonzalez-Serratos, H., Valle-Aguilera, R., Lathrop, D. A., & Garcia, M.del (1982). Slow inward calcium currents have no obvious role in muscle excitation-contraction coupling. *Nature, 298*, 292–294.

Hagiwara, S., & Naka, K. (1964). The initiation of spike potential in barnacle-muscle fibers under low intracellular Ca^{++}. *J Gen Physiol, 48*, 141–162.

Hagiwara, S., & Nakajima, S. (1966). Difference in Na and Ca spikes as examined by application of tetrodotoxin, procaine, and manganese ions. *J Gen Physiol, 49*, 793–806.

Hagiwara, S., Chichibu, S., & Naka, K. (1964). The effect of various ions on resting and spike potentials of barnacle muscle fibers. *J Gen Physiol, 43*, 163–179.

Harris, E. J. (1963). Distribution and movement of muscle chloride. *J Physiol (London), 166*, 87–109.

Heiny, J. A., Ashcroft, F. M., & Vergara, J. (1983). T-system optical signals associated with inward rectification in skeletal muscle. *Nature, 301*, 164–166.

Henček, M., Nonner, W., & Stämpfli, R. (1969). Voltage clamp of a small muscle membrane area by means of a circular sucrose gap arrangement. *Pflügers Arch, 313*, 71–79.

Hille, B., & Campbell, D. T. (1976). An improved vaseline gap voltage clamp for skeletal muscle fibers. *J Gen Physiol, 67*, 265–293.

Hodgkin, A. L., & Horowicz, P. (1959). The influence of potassium and chloride ions on the membrane potential of single muscle fibers. *J Physiol (London), 148*, 127–160.

Hodgkin, A. L., & Huxley, A. F. (1952). Currents carried by sodium and potassium ions through the membrane of the giant axon of *Loligo*. *J Physiol (London), 116*, 449–472.

Hodgkin, A. L., & Nakajima, S. (1972). Analysis of the membrance capacity in frog muscle. *J Physiol (London), 221*, 121–136.

Howell, J. N. (1974). Intracellular binding of ruthenium red in frog skeletal muscle. *J Cell Biol, 62*, 242–247.

Hoyle, G., & Burrows, M. (1973). Correlated physiological and ultrastructural studies on specialized muscles. 3. neuromuscular physiology of the power-stroke muscle of the swimming leg of portunus sanguinolentus. *J. Exp. Zool., 185*, 83–95.

Hoyle, G., & Smith, T. (1963). Neuromuscular physiology of giant muscle fibres of a barnacle, *Balanus nubilus* Darwin. *Comp Biochem Physiol, 10*, 219–314.

Hoyle, G., & Wiersma, C. A. G. (1958). Excitation at neuromuscular junctions in Crustacea. *J Physiol, 143*, 493–425.

Hurnak, O., & Zachar, J. (1992). Maxi chloride channels in L6 myoblasts. *Gen Physiol Biophys, 11*, 389–400.

Hussain, M., Wareham, A. C., & Head, S. I. (1994). Mechanism of action of a K^+ channel activator BRL 38227 on ATP-sensitive K^+ channels in mouse skeletal muscle fibres. *J. Physiol., 478 Pt 3*, 523–532.

Huxley, A. F., & Taylor, R. E. (1958). Local activation of striated muscle fibres. *J Physiol (London), 144*, 426–441.

Huxley, H. E., Page, S., & Wilkie, D. R. (1963). Appendix. An electron microscopic study of muscle in hypertonic solutions. *J Physiol (London), 169*, 312–329.

Iannaccone, S. T., Li, K.-X., Sperelakis, N., & Lathrop, D. A. (1989). Insulin-induced hyperpolarization in mammalian skeletal muscle. *Am J Physiol, 256*, C368–C374.

Jiang, C., Qu, Z., & Xu, H. (2002). Gating of inward rectifier K(+) channels by proton-mediated interactions of intracellular protein domains. *Trends Cardiovasc. Med., 12*, 5–13.

Kakei, M., Noma, A., & Shibasaki, T. (1985). Properties of adenosine-triphosphate-regulated potassium channels in guinea-pig ventricular cells. *J. Physiol., 363*, 441–462.

Kennedy, D., Evoy, W. H., & Fields., H. L. (1966). The unit bases of some crustacean reflexes. *Symp Soc Exp Biol, 20*, 75–109.

Kerr, L. M., & Sperelakis, N. (1982). Effects of the calcium antagonists verapamil and bepridil (CERM-1978) on Ca^{2+}-dependent slow action potentials in frog skeletal muscle. *J Pharmacol Exp Ther, 222*, 80–86.

Keynes, R. D., & Steinhardt, R. A. (1968). The components of the sodium efflux in frog muscle. *J Physiol (London), 198*, 581–599.

Khan, A. R. (1981). Influence of ethanol and acetaldehyde on electromechanical coupling of skeletal muscle fibres. *Acta Physiol Scand, 111*, 425–430.

Kirby, A. C., Lindley, B. D., & Picken, J. R. (1975). Calcium content and exchange in frog skeletal muscle. *J Physiol (London), 253*, 37–52.

Kulczycky, S., & Mainwood, G. W. (1972). Evidence for a functional connection between the sarcoplasmic reticulum and the extracellular space in frog sartorius muscle. *Can J Physiol Pharmacol, 50*, 87–98.

Li, K.-X., & Sperelakis, N. (1994). Electrogenic Na-K pump current in rat skeletal myoballs. *J Cell Physiol, 159*, 181–186.

Lueck, J. D., Rossi, A. E., Thornton, C. A., Campbell, K. P., & Dirksen, R. T. (2010). Sarcolemmal-restricted localization of functional ClC-1 channels in mouse skeletal muscle. *J Gen Physiol, 136*, 597–613.

Lynch, C., III (1978). *Kinetic and biochemical separation of potassium currents in frog striated muscle. PhD. thesis*. New York: University of Rochester.

Mathias, R. T., Levis, R. A., & Eisenberg, R. S. (1980). Electrical models of excitation-contraction coupling and charge movement in skeletal muscle. *J Gen Physiol, 76*, 1–31.

Miledi, R., Parker, R. I., & Schalow, G. (1977). Measurement of calcium transients in frog muscle by the use of arseno III. *Proc R Soc London (Biol), 198*, 201–210.

Miledi, R., Stefani, E., & Steinbach, A. B. (1971). Induction of the action potential mechanism in slow muscle fibres of the frog. *J Physiol (London), 217*, 737–754.

Mobley, B. A., & Eisenberg, B. R. (1975). Sizes of components in frog skeletal muscle measured by methods of stereology. *J Gen Physiol, 66*, 31–45.

Moody-Corbett, F., Gilbert, R., Akbarali, H., & Hall, J. (1989). Calcium current in embryonic Xenopus muscle cells in culture. *Can J Physiol Pharmacol, 67*, 1259–1264.

Nakajima, S., & Gilai, A. (1980). Action potentials of isolated single muscle fibers recorded by potential-sensitive dyes. *J Gen Physiol, 76*, 729–750.

Nassar-Gentina, V., Passonneau, J. V., Vergara, J. L., & Rapoport, S. I. (1978). Metabolic correlates of fatigue and of recovery from fatigue in single frog muscle fibers. *Gen Physiol, 72*, 593–606.

Nastuk, W. L., & Hodgkin, A. L. (1950). The electrical activity of single muscle fibres. *J Cell Comp Physiol, 35*, 39–74.

Natori, R. (1965). Propagated contractions in isolated sarcolemma-free bundle of myofibrils. *Jikeidai Med J, 12*, 214–221.

Nicola-Siri, L., Sanchez, J. A., & Stefani, E. (1980). Effect of glycerol treatment on calcium current of frog skeletal muscle. *J Physiol (London), 305*, 87–96.

Ortega, A., Gonzalez-Serratos, H., & Lepock, J. (1997). Effect of organic calcium channel blocker D-600 on sarcoplasmic reticulum calcium uptake in skeletal muscle. *Am J Physiol, 272*, C310–C317.

Overton, E. (1902). Beitrage zur allgemeinen muskel- und nervenphysiologie I. Abh. I Ueber die osmotischen figenschatten der muskeln. *Pflugers Arch, 92*, 115–280.

Peachey, L. D. (1965). The sarcoplasmic reticulum and transverse tubules of the frog's sartorius. *J Cell Biol, 25*, 209–231.

Peachey, L. D., & Huxley, A. F. (1964). Transverse tubules in crab muscles. *J Cell Biol, 23*, 70A.

Pilgrim, R. I. C., & Wiersma, C. A. G. (1963). Observations on the skeletal and somatic musculature of the abdomen and thorax of *Procambaru clarkii* (Girard) with notes on the thorax of *Panulirus interruptus* and *Astacus*. *J Morphol, 113*, 453–487.

Podolsky, R. J., & Costantin, L. L. (1964). Regulation by calcium of the contraction and relaxation of muscle fibers. *Fed Proc, 23*, 933–939.

Potreau, D., & Raymond, G. (1980). Calcium-dependent electrical activity and contraction of voltage-clamped frog single muscle fibers. *J Physiol (London), 307*, 9–22.

Qu, Z., Yang, Z., Cui, N., Zhu, G., Liu, C., Xu, H., Chanchevalap, S., Shen, W., Wu, J., Li, Y., & Jiang, C. (2000). Gating of inward rectifier K+ channels by proton-mediated interactions of N- and C-terminal domains. *J. Biol. Chem., 275*, 31573–31580.

Rasgado-Flores, H., DeSantiago, J., & Espinosa-Tanguma, R. (1991). Stoichiometry and regulation of the Na-Ca exchanger in barnacle muscle cells. *Ann NY Acad Sci, 639*, 22–33.

Rasgado-Flores, H., Santiago, E. M., & Blaustein, M. P. (1989). Kinetics and stoichiometry of coupled Na efflux and Ca influx (Na/Ca exchange) in barnacle muscle cells. *J Gen Physiol, 93*, 1219–1241.

Renaud, J. M. (1989). The effect of lactate on intracellular pH and force recovery of fatigued sartorius muscles of frog, *Rana pipiens*. *J Physiol, 416*, 31–47.

Rogus, E., & Zierler, K. L. (1973). Sodium and water contents of sarcoplasm and sarcoplasmic reticulum in rat skeletal muscle: Effects

of anisotonic media, ouabain, and external sodium. *J Physiol (London), 233*, 227–270.

Rubio, R., & Sperelakis, N. (1972). Penetration of horseradish peroxidase into the terminal cisternae of frog skeletal muscle fibers and blockade of caffeine contracture by Ca^{++} depletion. *Z Zellforsch, 124*, 57–71.

Rulon, R., Hermsmeyer, K., & Sperelakis, N. (1971). Regenerative action potentials induced in the neurogenic heart of *Limulus polyphemus*. *Comp Biochem Physiol, 39A*, 333–335.

Sanchez, J. A., & Stefani, E. (1978). Inward calcium current in twitch muscle fibers of the frog. *J Physiol (London), 283*, 197–209.

Sauviat, M.-P., Ecault, E., Faivre, J.-F., & Finlay, I. (1991). Activation of ATP-sensitive K channels by a K channel opener (SR 44866) and the effect upon electrical and mechanical activity of frog skeletal muscle. *Pflügers Arch, 418*, 261–265.

Sellin, L. C., & Sperelakis, N. (1978). Decreased potassium permeability in dystrophic mouse skeletal muscle. *Exp Neurol, 62*, 609–617.

Spector, I., & Prives, J. M. (1977). Development of electrophysiological and biochemical membrane properties during differentiation of embryonic skeletal muscle in culture. *Proc Natl Acad Sci USA, 74*, 5166–5170.

Sperelakis, N. (1969). Changes in conductance of frog sartorius fibers produced by CO_2, ReO_4, and temperature. *Am J Physiol, 217*, 1069–1075.

Sperelakis, N. (1979). Origin of the cardiac resting potential. In R. Berne, & N. Sperelakis (Eds.), *Handbook of Physiology, the Cardiovascular System, Vol. 1: the Heart* (pp. 187–267). Bethesda: American Physiological Society.

Sperelakis, N., & Gonzalez-Serratos, H. (2001). Skeletal muscle action potentials. In N. Sperelakis (Ed.), *Cell Physiology Sourcebook* (3rd ed.). (pp. 865–886). San Diego: Academic Press.

Sperelakis, N., Mayer, G., & Macdonald, R. (1970). Velocity of propagation in vertebrate cardiac muscles as functions of tonicity and [K+]. *Am. J. Physiol., 219*, 952–963.

Sperelakis, N., & Rubio, R. (1971). Ultrastructural changes produced by hypertonicity in cat cardiac muscle. *J Mol Cell Cardiol, 3*, 139–156.

Sperelakis, N., & Schneider, M. F. (1968). Membrane ion conductances of frog sartorius fibers as a function of tonicity. *Am J Physiol, 215*, 723–729.

Sperelakis, N., Forbes, M. S., & Rubio, R. (1974). The tubular systems of myocardial cells: ultrastructure and possible function. In N. S. Dhalla, & G. Rona (Eds.), *Recent Advances in Studies on Cardiac Structure and Metabolism, Myocardial Biology, Vol. 4* (pp. 163–194). Baltimore: University Park Press.

Sperelakis, N., Schneider, M. F., & Harris, E. J. (1967). Decreased K^+ conductance produced by Ba^{++} in frog sartorius fibers. *J Gen Physiol, 50*, 1565–1583.

Sperelakis, N., Shigenobu, K., & Rubio, R. (1978). ^{3}H-Sucrose compartments in frog skeletal muscle relative to sarcoplasmic reticulum. *Am J Physiol, 234*, C181–C190.

Sperelakis, N., Valle, R., Orozco, C., Martinez-Palomo, A., & Rubio, R. (1973). Electromechanical uncoupling of frog skeletal muscle by possible change in sarcoplasmic reticular content. *Am J Physiol, 225*, 793–800.

Spitzer, N. C. (1979). Ion channels in development. *Annu Rev Neurosci, 2*, 363–397.

Spruce, A. E., Standen, N. B., & Stanfield, P. R. (1985). Voltage-dependent ATP-sensitive potassium channels of skeletal muscle membrane. *Nature, 316*, 736–738.

Spruce, A. E., Standen, N. B., & Standfield, P. R. (1987). Studies of the unitary properties of adenosine-5′-triphospate-regulated potassium channels of frog skeletal muscle. *J Physiol, 382*, 213–236.

Standen, N. B., Stanfield, P. R., & Ward, T. A. (1985). Properties of single potassium channels in vesicles formed from the sarcolemma of frog skeletal muscle. *J Physiol, 364*, 339–358.

Stanfield, P. R. (1977). A calcium-dependent inward current in frog skeletal muscle fibers. *Pflügers Arch, 368*, 267–270.

Stephenson, E. W. (1981). Activation of fast skeletal muscle: contributions of studies on skinned fibers. *Am J Physiol, 240*, C1–19.

Steinmeyer, K., Ortland, C., & Jentsch, T. J. (1991). Primary structure and functional expression of a developmentally regulated skeletal muscle chloride channel. *Nature, 354*, 301–304.

Stoller, D., Kakkar, R., Smelley, M., Chalupsky, K., Earley, J. U., Shi, N. Q., Makielski, J. C., & McNally, E. M. (2007). Mice lacking sulfonylurea receptor 2 (SUR2) ATP-sensitive potassium channels are resistant to acute cardiovascular stress. *J. Mol. Cell. Cardiol, 43*, 445–454.

Tasker, P., Simon, S. E., Johnstons, B. M., Shankly, K. H., & Shaw, F. H. (1959). The dimensions of the extracellular space in sartorius muscle. *J Gen Physiol, 43*, 39–53.

Thabet, M., Miki, T., Seino, S., & Renaud, J. M. (2005). Treadmill running causes significant fiber damage in skeletal muscle of KATP channel-deficient mice. *Physiol. Genomics, 22*, 204–212.

Vinogradova, N. A. (1968). Distribution of nonpenetrating sugars in the frog's sartorius muscle under hypo- and hypertonic conditions. *Tsitologiya, 10*, 831–838.

Vivaudou, M. B., Arnoult, C., & Villaz, M. (1991). Skeletal muscle ATP-sensitive K^+ channels recorded from sarcolemmal blebs of split fibers: ATP inhibition is reduced by magnesium and ADP. *J Membr Biol, 122*, 165–175.

Vogel, S., Harder, D., & Sperelakis, N. (1978). Ca^{++} dependent electrical and mechanical activities in skeletal muscle. *Fed Proc, 37*, 517.

Wallace, N., & Sommer, J. R. (1975). Fusion of sarcoplasmic reticulum with ruthenium red. *Proc Electron Microsc Soc A, 33*, 500–501.

Weiss, D. S., & Magleby, K. L. (1992). Voltage-dependent gating mechanism for single fast chloride channels from rat skeletal muscle. *J Physiol (London), 453*, 279–306.

Werman, R., & Grundfest, H. (1961). Graded and all-or-none electrogenesis in arthropod muscle. II. The effects of alkali-earth and strontium ions on lobster muscle fibers. *J Gen Physiol, 44*, 997–1027.

Werman, R., McCann, F. V., & Grundfest, H. (1961). Graded and all-or-none electrogenesis in arthropod muscle. I. The effects of alkali-earth cations on the neuromuscular system of *Romalea microptera*. *J Gen Physiol, 44*, 979–995.

Winegrad, S. (1968). Intracellular calcium movements of frog skeletal muscle during recovery from tetanus. *J Gen Physiol, 51*, 65–83.

Woll, K. H., Lonnendonker, U., & Neumcke, B. (1989). ATP-sensitive potassium channels in adult mouse skeletal muscle: different modes of blockage by internal cations, ATP, and tolbutamide. *Pflügers Arch, 414*, 622–628.

Yokoshiki, H., Sunagawa, M., Seki, T., & Sperelakis, N. (1998). ATP-sensitive K^+ channels in pancreatic, cardiac, and vascular smooth muscle cells. Invited Review. *Am J Physiol, 274*, C25–C37.

Zifarelli, G., & Pusch, M. (2007). CLC chloride channels and transporters: A biophysical and physiological perspective. *Rev. Physiol. Biochem. Pharmacol., 158*, 23–76.

Chapter 43

Cardiac Action Potentials

Gordon M. Wahler

Chapter Outline

I. SUMMARY

Action potentials (APs) in the heart are generated by the complex time-dependent interplay of several currents carried primarily by Na^+, K^+ and Ca^{2+} ions. Ventricular APs have very long duration compared to nerve and skeletal muscle APs, due to a plateau phase during which there is an approximate balance between depolarizing and repolarizing currents. Some cardiac cells display automaticity, due to the presence of a cyclical spontaneous depolarization. The cells of the sinoatrial node normally exhibit the fastest spontaneous depolarization of automatic cells in the heart and are therefore the normal pacemaker cells. Automaticity in nodal cells is initiated by several currents, including a hyperpolarization-activated cation current (the "funny current"), a small background Na^+ current, the delayed rectifier K^+ current and Ca^{2+} currents. The sympathetic and parasympathetic nerves play important (and opposite) roles in regulating the force of myocardial contraction and heart rate via their effects on several currents. Mutations in a number of ion channels can lead to arrhythmias.

II. INTRODUCTION

The electrophysiological behavior of heart cells subserves the function of the heart; namely to pump blood to the body. Heart cells are similar to other cell types in that their internal ionic composition is quite different from the extracellular ionic environment. For example, measurement of the intracellular versus extracellular ionic composition shows that the intracellular ionic composition is low in sodium ions (Na^+) and high in potassium ions (K^+), while the reverse is true of the extracellular ionic composition. These concentration differences, together with the selective permeability characteristics of the cell membrane, generate a potential difference of between 80 and 90 mV across the cell membrane of the resting cardiac cell, with the inside being negative with respect to the outside. Additionally, heart cells are excitable cells. That is, they are capable of generating all-or-none electrical responses known as action potentials (APs). The cardiac AP is caused by the complex interaction of a number of different ionic currents. This chapter reviews the characteristics of the cardiac AP, with emphasis on the major

Cell Physiology Sourcebook. DOI: 10.1016/B978-0-12-387738-3.00043-3

currents responsible for the various components or phases of the ventricular APs, as well as the regional differences in cardiac APs. The electrical activity of cardiac cells has been studied for several decades by impaling the cells with high-resistance microelectrodes. The development of methods to isolate viable single adult cardiac cells, together with the development of the patch-clamp technique for recording single-channel (microscopic) currents and whole-cell (macroscopic) currents from single cells, led to an explosion of information on the currents responsible for generation of the cardiac AP. The use of molecular biology techniques to clone and express channel subunits is further revolutionizing our understanding of the precise nature of various currents.

While most of the information on cardiac ion currents has been necessarily obtained from cardiac cells isolated from experimental animals, studies on human cardiac myocytes (e.g. Coraboeuf and Nargeot, 1993) suggest that the currents in the human heart are generally similar to those observed in other animals.

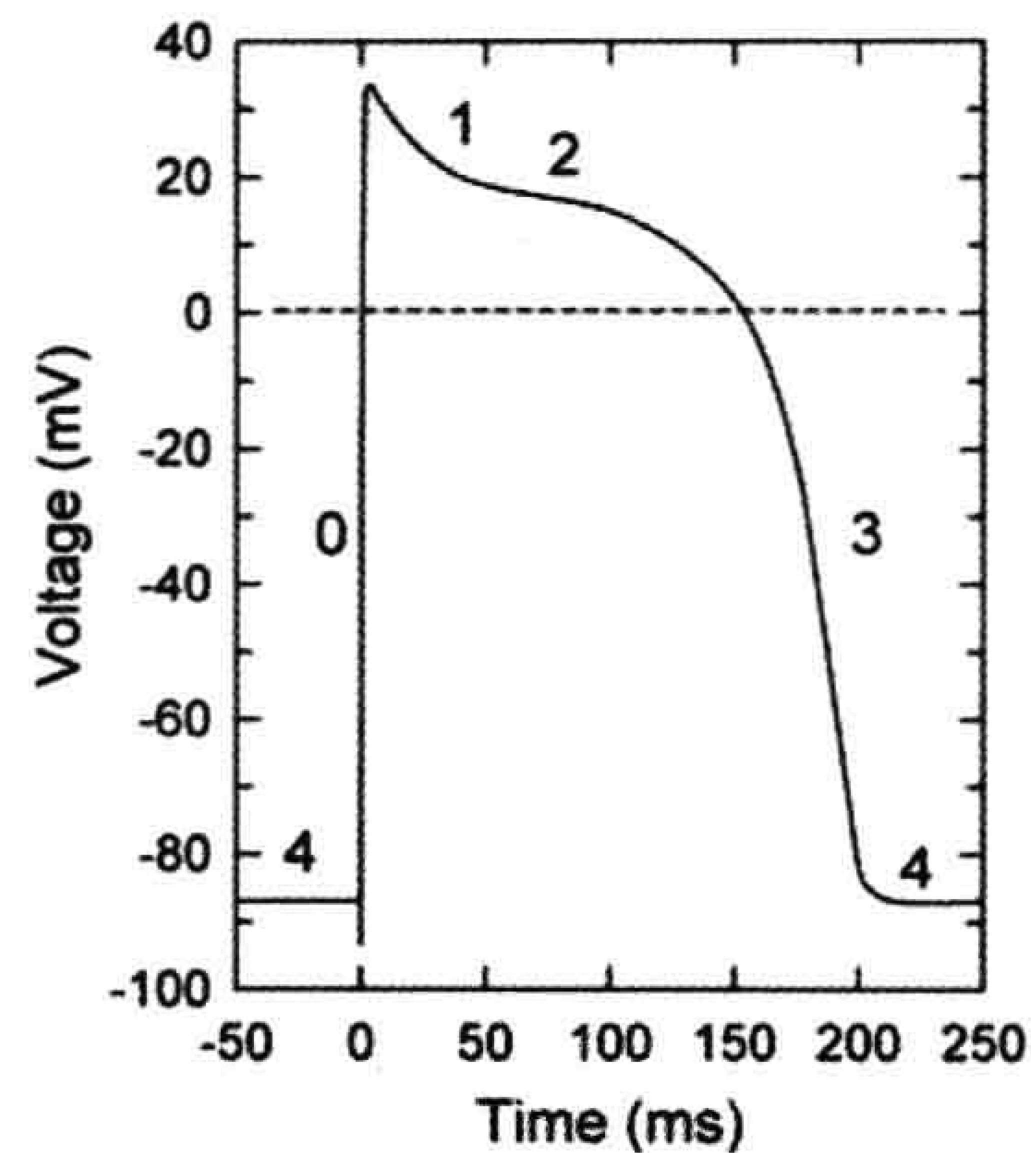


FIGURE 43.1 Ventricular action potential. This is a diagrammatic representation of a typical adult mammalian ventricular AP. The five phases of the ventricular AP are labeled (0–4).

III. RESTING MEMBRANE POTENTIAL

Details on the origin of the resting potential (RP) have been given in a previous chapter. In brief, the cardiac cell membrane is quite permeable to K^+ and relatively impermeable to Na^+ and other ions when at rest. Thus, K^+ flows out of the cell down its concentration gradient, resulting in rapid build up of a negative potential inside the cell. As the electric potential build up increases in magnitude, it becomes sufficient to counterbalance the chemical driving force generated by the concentration gradient. At this potential, called the equilibrium potential, the net ion flux is zero. Note that this does not mean there is no flux of the ion, only that the inward and outward fluxes of the ion are equal and opposite. The Nernst equation describes the relationship between the intracellular and extracellular concentrations of a single ion and its equilibrium potential. The equilibrium potential for ion X (E_X) is calculated by the Nernst equation:

$$E_x = \frac{RT}{ZF} \ln \frac{[X]_i}{[X]_o}$$

where T is the absolute temperature (in degrees Kelvin), z is the valence (or charge) of the ion (for K^+ it is +1, for Ca^{2+} it is +2, etc.), R is the universal gas constant, F is the Faraday constant, $[X]_i$ is the ion concentration inside the cell, $[X]_o$ is the ion concentration outside the cell and ln is the natural logarithm.

The intracellular and extracellular concentrations of K^+ are such that the equilibrium potential for K^+ (E_K) is approximately −90 mV at 37°C. Since the ventricular cell at rest (i.e. between APs) is very permeable to K^+ and not very permeable to other ions, the RP should be close to the calculated E_K. Indeed, this is the case. For example, in Fig. 43.1, the resting membrane potential is approximately −87 mV. The RP does not quite reach E_K because at rest there is a small, but finite, permeability to Na^+ ions. In addition, there are other ion transport systems (primarily the electrogenic Na^+-K^+-ATPase) which contribute slightly to the RP.

IV. CURRENTS DURING THE ACTION POTENTIAL PHASES

IVA. Overview

Cardiac cells have certain properties in common with other excitable cells, such as nerve and skeletal muscle cells. However, the behavior of cardiac cells also differs from the behavior of nerve and skeletal muscle cells in some important respects. The nerve and skeletal muscle APs are relatively brief, consisting primarily of a rapid depolarization phase (when the inside of the cell becomes more positive) followed immediately by a rapid repolarization phase (when the inside of the cell returns to a more negative potential). The depolarization phase of nerve and skeletal muscle cells is caused by the rapid influx of positive sodium ions into the cell, down the electrochemical gradient for Na^+, which makes the cell interior more positive. The subsequent repolarization is caused by the effiux of positive potassium ions from the cell, down the electrochemical gradient for K^+, which returns the cell interior to its original more negative resting membrane potential. The entire process of the nerve or skeletal muscle APs is largely complete within a few milliseconds. In cardiac cells, the APs are more complex and generally much longer in duration. Thus, for example, a typical cardiac ventricular

AP may be 200 ms or more in duration (see Fig. 43.1). Additionally, unlike for nerve and skeletal muscle cells, APs from different regions of the heart vary substantially in shape.

There are two primary types of cardiac cells. One cell type is found in the working (contractile) cells of the atria and ventricles and also in the specialized conduction cells of the His–Purkinje network. These cells have a high resting K^+ permeability between APs. The APs in these cells are generated by a fast Na^+ current and are known as fast APs. The prolonged duration of the AP in ventricular cells and Purkinje fibers is caused by an approximate balance of inward depolarizing currents (primarily a Ca^{2+} current) and outward repolarizing K^+ currents, which results in a prominent plateau phase. Atrial cells have a less prominent plateau.

The second type of cardiac cell is found in the sinoatrial and atrioventricular nodes. These nodal cells have a low K^+ permeability between APs and are automatic (i.e. they fire APs spontaneously). The upstroke of these nodal APs is generated by a Ca^{2+} current, which is smaller and slower than the fast Na^+ current. Because of this, and the comparatively low density of Ca^{2+} channels when compared to the density of Na^+ channels in fast cells, conduction in nodal cells is much slower than conduction in regions having Na^+-dependent APs. These nodal APs are known as slow APs. Slow APs (a.k.a. slow responses) may sometimes also occur in cells that normally have fast APs when fast Na^+ current (I_{Na}) is blocked pharmacologically or pathophysiologically by tetrodotoxin or voltage inactivation by depolarization with high extracellular K^+.

The shape of the fast cardiac AP is generally divided into phases. The spike and slow wave (plateau) phases were described for isolated cardiac muscle (Hoshiko and Sperelakis, 1962). The following description details all of the five phases found in ventricular cells (phases 0 through 4) and indicates the current or currents that are primarily responsible for each phase. The phases of the ventricle and primary currents responsible are summarized in Table 43.1. Phase 0 is the upstroke of the AP, phase 1 is the early repolarization phase, phase 2 is the plateau phase, phase 3 is the primary repolarization phase and phase 4 is the resting membrane potential phase of the ventricular AP. Additional information about regional differences in the AP phases and currents will be also presented. It should be noted that an isolated single myocardial cell in cell culture exhibits a cardiac AP almost identical to that of a myocardial cell in the intact heart (Sperelakis and Lehmkuhl, 1964).

TABLE 43.1 Phases of the Ventricular Action Potential and Primary Currents Responsible

Phase	Current	Channel Protein
Phase 0	I_{Na}	$Na_v1.5$
Phase 1	I_{to} [I_{to1} ($I_{to,f}$ & $I_{to,s}$)]	$K_v4.2/4.3$ [$I_{to,f}$], $K_v1.4$ [$I_{to,s}$]
Phase 2	$I_{Ca(L)}$ I_{to} I_K I_{Na} "window current"	$Ca_v1.2$ (as in phase 1) (as in phase 3) $Na_v1.5$
Phase 3	I_K [I_{Ks}, I_{Kr}, I_{Kur}] I_{K1}	$K_v7.1$ (a.k.a. K_vLQT1) [I_{Ks}] $K_v11.1$ (a.k.a. HERG1 or ERG1) [I_{Kr}] $K_v1.5$ [I_{Kur}] (as in phase 4)
Phase 4	I_{K1}	Kir2.1/2.2

IVB. Phase 0

Phase 0 is the rapid upstroke of the AP in ventricular cells, as well as in the cells of the atria and His–Purkinje network. This upstroke is dependent on a fast Na^+ current (I_{Na}) quite similar to the current responsible for the upstroke of the nerve or skeletal muscle APs. However, the cardiac channel has a much lower sensitivity to the neurotoxin tetrodotoxin (e.g. Yu and Catterall, 2003). The voltage-gated channel protein ($Na_v1.5$) responsible for this current in cardiac myocytes is encoded by the gene SCN5A. As expected, the $Na_v1.5$ channels are expressed in atrial and ventricular myocytes and the His–Purkinje conduction cells, but not in nodal cells that do not fire fast APs (Nerbonne and Kass, 2005).

This current is designated as fast because it exhibits very rapid activation and inactivation kinetics in comparison to other currents. Thus, in the vast majority of openings, the channel is open for less than 1 ms. Because of the fast upstroke and fast conduction of the ventricular APs, the APs of these cells (and those of atrial and Purkinje fiber cells) are referred to as fast APs, as noted earlier. Figure 43.2 illustrates the kinetics and voltage-dependence of I_{Na}. Following a large depolarization, I_{Na} reaches a peak in less than 1 ms, even at room temperature. Following this peak activation of I_{Na} the amplitude of this current spontaneously decreases. This decay of I_{Na} is due to inactivation of the fast Na^+ channels; thus, I_{Na} is nearly zero after only a few milliseconds. The fast activation and large magnitude of I_{Na} often causes difficulties in accurately recording this current in voltage-clamped cardiac cells. Thus, I_{Na} can generally only be recorded in adult cardiac cells at reduced $[Na^+]_o$ levels and/or at low temperatures. Alternatively, I_{Na} can be studied in very small cells, such as the embryonic chick ventricular cell (e.g. Fig. 43.2) in which I_{Na} (and other currents) are at least an order of magnitude smaller

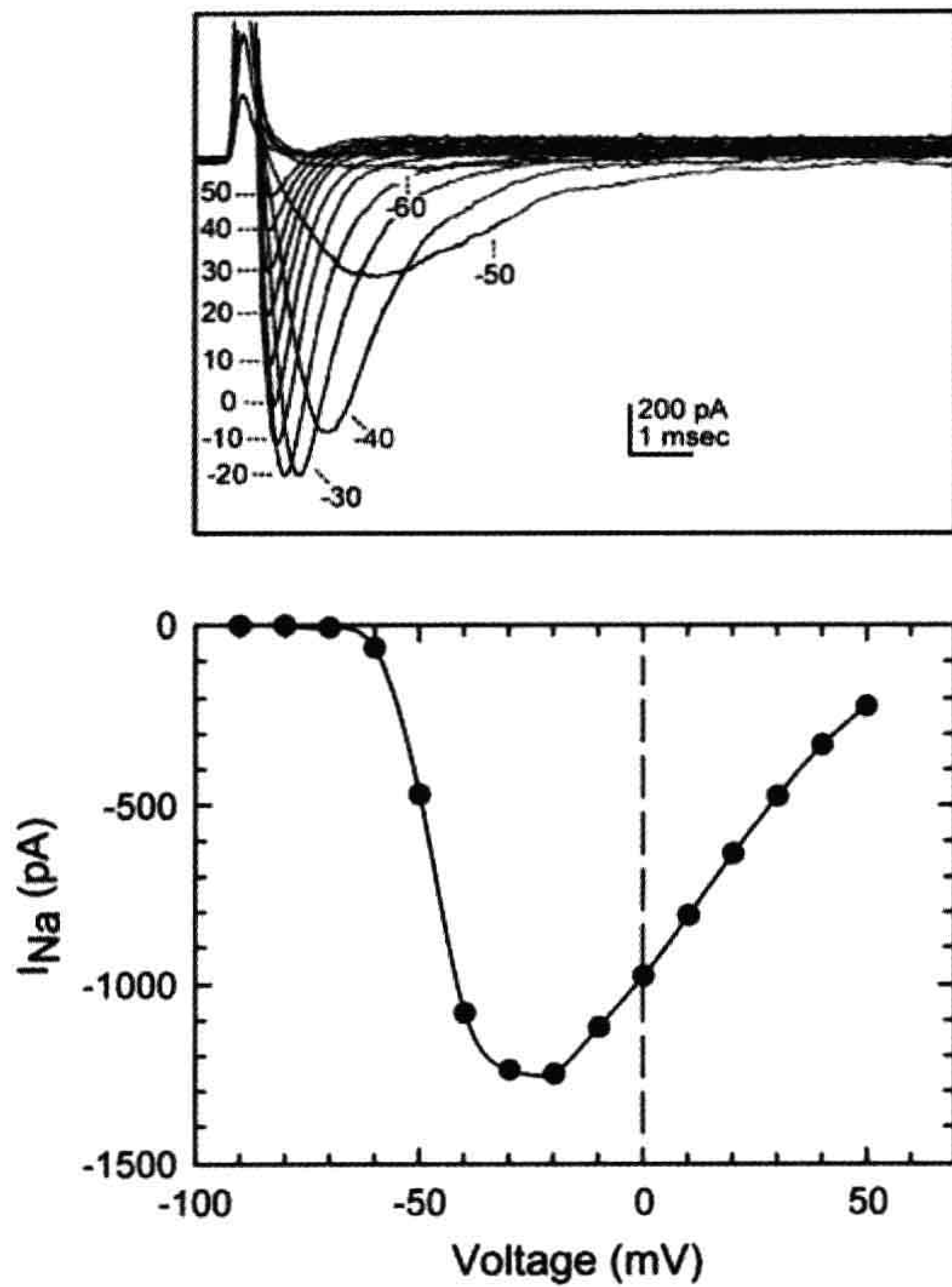


FIGURE 43.2 Sodium current (I_{Na}) recorded from a small embryonic chick ventricular cell. I_{Na} in these cells is much smaller than in adult cells, due to the very small size of these cells. Additionally, the small spherical shape of these cells and lack of t-tubules also contribute to better voltage control. Upper panel: shown are the original I_{Na} currents obtained upon stepwise depolarization from -100 mV to the indicated voltages. The current peaks in less than 1 ms at very depolarized potentials and then rapidly inactivates. Lower panel: the current–voltage curve of the peak current at each voltage. Note that the threshold for I_{Na} is approximately -70 mV and the current peaks at approximately -25 mV.

than in adult cells. For the rapid upstroke of phase 0 to occur, the cell needs to be depolarized to the voltage necessary to open some of the fast Na^+ channels. When the Na^+ channels begin to open, Na^+ flows down its electrochemical gradient into the cell. This causes the cell to depolarize further (i.e. the inside becomes more positive), which opens additional Na^+ channels. Therefore, once sufficient Na^+ channels open, the process becomes self-perpetuating (i.e. a positive-feedback loop), resulting in rapid depolarization (i.e. the membrane potential rapidly moves toward the equilibrium potential for Na^+). The voltage at which a sufficient number of Na^+ channels open to initiate the AP is the threshold for firing of the fast AP (approximately -55 mV). As the cell begins to depolarize further beyond the threshold, I_{Na} increases as more Na^+ channels are activated. Eventually, with even greater depolarization, I_{Na} begins to decline as the membrane potential approaches E_{Na}. Thus, the peak I_{Na} occurs between -30 and -20 mV. The membrane potential never reaches E_{Na} for several reasons: (1) as the membrane potential gets closer to E_{Na}, the driving force for Na^+ influx is diminished; (2) the Na^+ channels close (inactivate) shortly after opening (beginning after about 1 ms), thus, some Na^+ channels are already closing during the latter part of the upstroke; (3) repolarizing currents are beginning to activate during the latter portion of the upstroke. Nevertheless, the upstroke causes a substantial voltage change (110–120 mV) within 1–2 ms in ventricular myocytes and other fast cardiac cells.

IVC. Phase 1

Phase 1 of the cardiac AP is the transient and relatively small repolarization phase which immediately follows the upstroke of the AP. The size of phase 1 repolarization varies greatly between species and also between different regions of the heart within a given species. Thus, APs recorded from the outer (epicardial) layer of ventricular cells display a more prominent phase 1, whereas APs recorded from the inner (endocardial) layer of ventricular cells, display a small phase 1 repolarization (e.g. Antzelevitch and Dumaine, 2002). Phase 1 is also very large in Purkinje fibers and in atrial cells, but is largely absent in nodal cells.

Phase 1 repolarization is primarily due to a transient outward current (I_{to}). I_{to} turns on rapidly with depolarization (i.e. beginning during the final portion of the AP upstroke) and is only active at very depolarized potentials; the threshold for activation is approximately -30 mV (Fig. 43.3). I_{to} has a characteristic transient shape because the rapid activation of this current is followed by inactivation during the AP plateau. I_{to} is actually composed of separate currents (I_{to1} and I_{to2}) which are carried through three physically distinct channels (Tseng and Hoffman, 1989). One of the currents (I_{to1}) is a K^+ current that is independent of the internal Ca^{2+} concentration ($[Ca^{2+}]_i$) and is sensitive to the K^+ channel blocker 4-aminopyridine (4-AP) (Fig. 43.3). This component of I_{to} is very similar to the I_A current recorded in nerve fibers. In cardiac myocytes, I_{to1} consists of fast and slow components ($I_{to,f}$ and $I_{to,s}$) (Xu et al., 1999) which are pharmacologically separable due to the sensitivity of $I_{to,f}$ to Heteropoda spider toxins (Sanguinetti et al., 1997). A heteromultimer made up of channel proteins $K_v4.2$ and $K_v4.3$, and encoded by genes KCND2 and KCND3, corresponds to $I_{to,f}$. $K_v1.4$ is the channel protein for $I_{to,s}$ (for review, see Grunnet, 2010).

In addition to I_{to1}, another component of I_{to} (I_{to2}) is sometimes observed. I_{to2} is a Ca^{2+}-dependent Cl^- current (Zygmunt and Gibbons, 1992) that is less sensitive to 4-AP, but is more sensitive to another K^+ channel blocker,

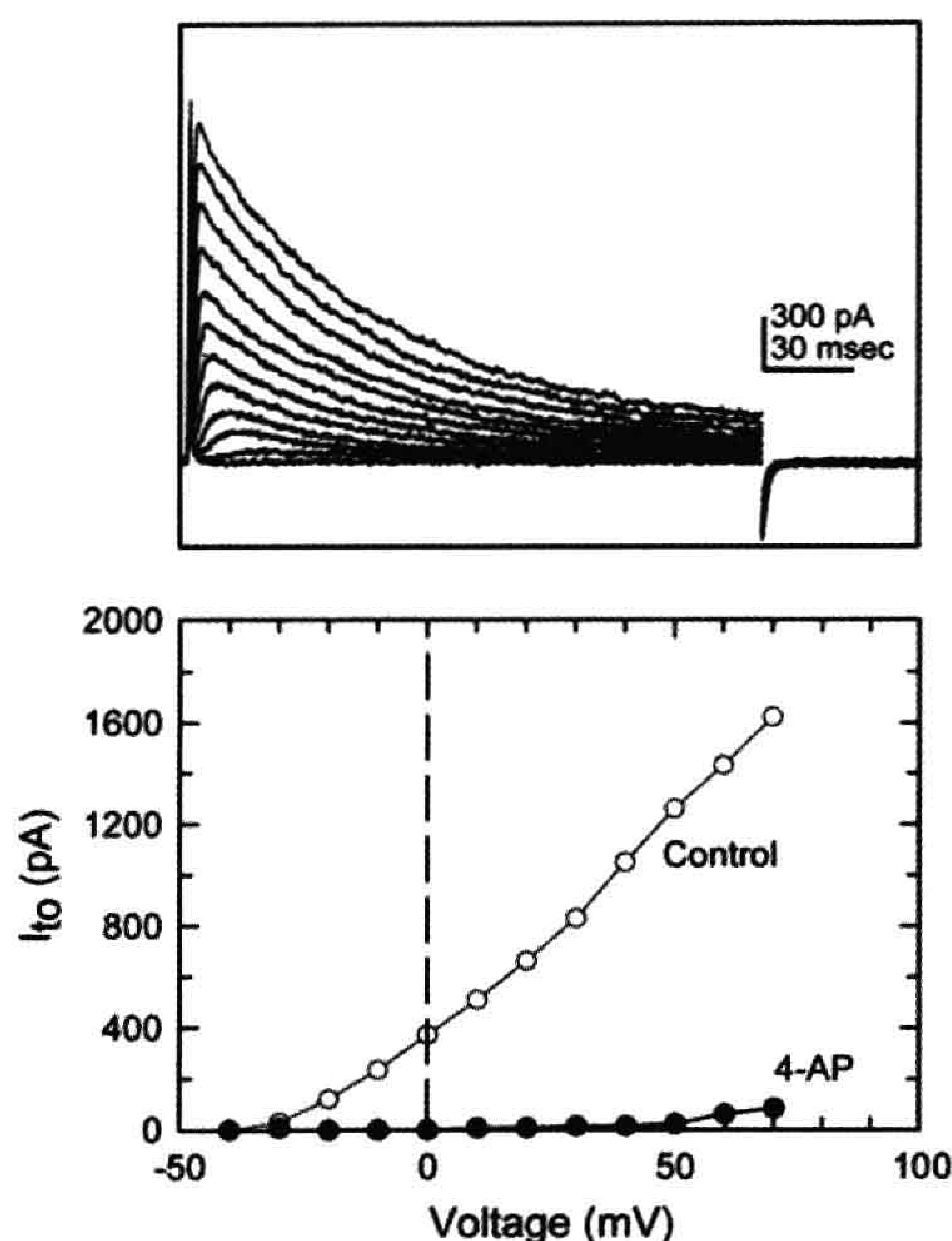


FIGURE 43.3 Transient outward current (I_{to}) recorded from a 21-day-old rat ventricular cell. Upper panel: shown are the original currents obtained upon stepwise depolarization from −80 mV. I_{to} activates rapidly and then inactivates. Currents were recorded in the presence of tetrodotoxin to eliminate I_{Na} and cadmium to eliminate overlapping I_{Ca}. Lower panel: the current-voltage curve shows increasing activation of this current at voltages above approximately −30 mV (indicated by open circles). This current is the Ca^{2+}-independent, 4-aminopyridine-sensitive component of I_{to} (i.e. I_{to1}) and is therefore readily blocked by 4-aminopyridine (4-AP, indicated by closed circles).

tetraethylammonium ion (TEA^+). Under physiological conditions, I_{to1} is much larger than I_{to2}. Thus, efflux of K^+ through the I_{to1} channels is normally responsible for the vast majority of phase 1 repolarization. The second component (I_{to2}) may become more important when intracellular levels of Ca^{2+} become too high. That is, under Ca^{2+}-overload conditions, I_{to2} would be activated and shorten the AP duration, thereby indirectly abbreviating the duration of Ca^{2+} current, resulting in a reduced Ca^{2+} influx. Thus, activation of I_{to2} by intracellular Ca^{2+} likely acts as a protective negative feedback mechanism that reduces calcium overload.

IVD. Phase 2

Phase 2 is commonly called the plateau phase. It follows the early repolarization phase (phase 1) and is a period of time during which the membrane potential remains relatively constant (see Fig. 43.1). The presence of this prominent plateau phase is responsible for the long AP duration in cardiac cells, which is the major difference between cardiac cells and nerve or skeletal muscle fibers. The plateau is caused by an approximate balance of positive inward (depolarizing) and positive outward (repolarizing) currents. The primary inward current during this phase is a Ca^{2+} current. The primary outward current during the plateau phase of ventricular cells, particularly during the latter part of the plateau, is the slowly activating K^+ current known as the delayed rectifier, which is described in greater detail under phase 3 repolarization. The transient outward K^+ current, I_{to}, also contributes to the early plateau phase in those cells that have a substantial I_{to}. As a result of its voltage dependence and time course (see Fig. 43.3), I_{to} significantly overlaps (and opposes) the inward L-type Ca^{2+} current (which is the primary depolarizing current during the plateau phase).

In addition to the Ca^{2+} and K^+ currents, there is a small contribution of the voltage-gated Na^+ current (I_{Na}) to the plateau. Thus, while I_{Na} largely inactivates within a few milliseconds after depolarization, a very small fraction (approximately 1%) of the I_{Na} inactivates slowly (see Fig. 43.2), causing a late Na^+ current known as the sodium window current, which is sufficient to affect the plateau of the AP and, hence, AP duration (Attwell et al., 1979).

The inward Ca^{2+} current (I_{Ca}) exhibits activation and inactivation much like I_{Na} but on a slower time scale (Fig. 43.4). This second inward current peaks within a few ms, but requires a few hundred ms to inactivate completely. I_{Ca} is at least one order of magnitude smaller than I_{Na} in a given cell. The threshold for activation of I_{Ca} is approximately −40 mV, the current is maximal near 0 mV and the E_{Ca} is around +100 mV. Thus, I_{Ca} is active over a more positive (depolarized) potential range than I_{Na}. This classical Ca^{2+} current is commonly referred to as the L-type (for "*L*ong-lasting" or "*L*arge") calcium current ($I_{Ca(L)}$) to distinguish it from the T-type (for "*T*ransient" or "*T*iny") Ca^{2+} current ($I_{Ca(T)}$) described later. The L-type channel is $Ca_v1.2$ encoded by CACNA1C (Catterall, 2000). These channels are located throughout the heart, i.e. they are expressed in the contractile cells of the atria and ventricles, the conduction cells of the His–Purkinje system and the nodal cells (Boyett et al., 2000).

The L-type Ca^{2+} current is central to many aspects of cardiac function. For example, it is the primary link in excitation–contraction coupling in heart muscle. Thus, the influx of Ca^{2+} ions during the plateau of the AP is what links the electrical events of the AP to the mechanical event, namely contraction. Ca^{2+} influx via $I_{Ca(L)}$ stimulates Ca^{2+} release from internal (sarcoplasmic reticular) stores, replenishes the internal Ca^{2+} stores available for subsequent release and also directly activates the contractile proteins. $I_{Ca(L)}$ is also very important in automaticity and conduction, due to the Ca^{2+} dependence of the nodal APs.

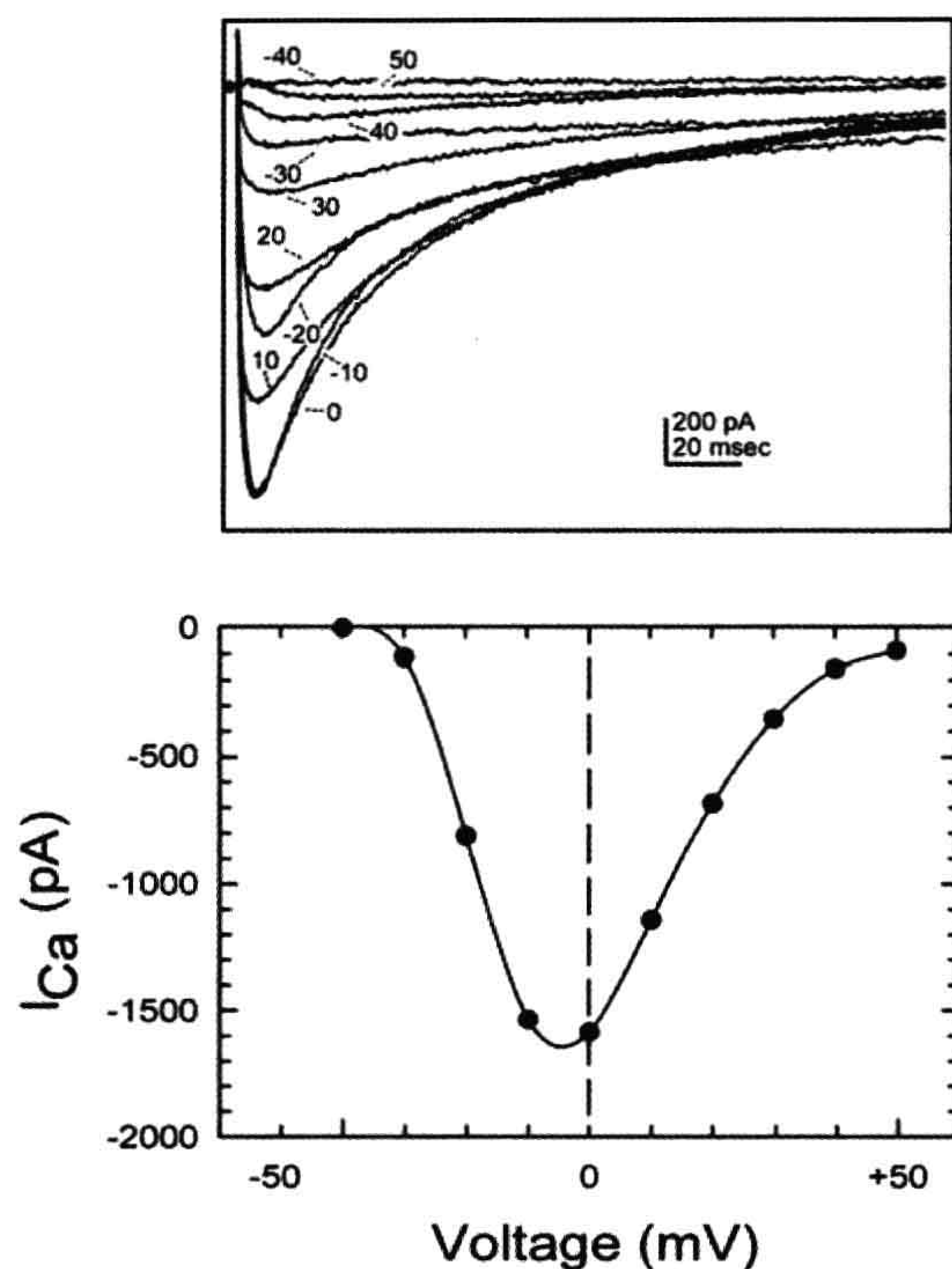


FIGURE 43.4 L-type calcium current ($I_{Ca(L)}$) recorded from an adult guinea pig ventricular cell. Upper panel: shown are the original currents obtained upon stepwise depolarization from −80 mV to the indicated voltages. I_{Na} was inactivated by briefly pulsing to −40 mV prior to applying the indicated test pulse. The Ca^{2+} currents show the same general shape as the Na^+ currents (see Fig. 43.2.), i.e. they activate upon depolarizing steps and inactivate during the voltage pulse. However, both activation and inactivation are much slower than for I_{Na} (note difference in time scale). Lower panel: the current−voltage curve shows a similar shape to the I_{Na} current−voltage relationship; however, both the threshold voltage and peak voltage are shifted approximately 30 mV in the depolarizing direction. $I_{Ca(L)}$ is roughly the same size as the I_{Na} example shown in Fig. 43.2 only because this cell is so much larger than the embryonic chick cell used in Fig. 43.2, I_{Na} in this guinea pig cell would be approximately 20 nA or more and could not be voltage-clamped under these conditions.

The L-type Ca^{2+} channel is also a major regulatory site in control of cardiac electrical activity and contraction by neurotransmitters, hormones, intracellular ions, etc. Perhaps the most important regulator of $I_{Ca(L)}$ in the heart is the autonomic nervous system. Thus, release of norepinephrine from cardiac sympathetic nerves or release of epinephrine from the adrenal gland stimulates the β-adrenergic receptors of the cardiac myocyte. The net result of β-adrenergic stimulation is that $I_{Ca(L)}$, and thereby force of contraction, is augmented. For a detailed review of this process, see Chapter 23. The parasympathetic neurotransmitter, acetylcholine (ACh) has a smaller, inhibitory (anti-adrenergic) effect on $I_{Ca(L)}$. For information about the Ca^{2+} channels in developing hearts, the reader is referred to Chapter 25.

IVE. Phase 3

Phase 3 is the late or final repolarization phase following the AP plateau. It is similar to the repolarization observed in nerve and skeletal muscle cells. Phase 3 repolarization is primarily caused by the unbalance of the currents that were relatively balanced during phase 2. $I_{Ca(L)}$ decreases with time (due to inactivation) and the delayed rectifier current (I_K) increases (due to slow activation). This gradually leads to the outward current, the delayed rectifier (I_K), overwhelming the inward current ($I_{Ca(L)}$). I_K is the primary repolarizing current in most ventricular preparations. The classical delayed rectifier activates slowly, compared to most other currents and does not inactivate significantly with time. Thus, I_K increases gradually during sustained depolarization at voltages around the plateau level. This current is similar to the delayed rectifier in nerve cells, although slower. I_K can be clearly distinguished from I_{to} by slow activation, lack of inactivation and different pharmacology.

The classical delayed rectifier current is divided into a very slowly activating component (I_{Ks}) and a more rapidly activating component (I_{Kr}) (see Grunnet, 2010). The I_{Ks} channel is $K_v7.1$ encoded by KCNQ1 (a.k.a. KVLQT1). The β-adrenergic-cAMP cascade can stimulate I_{Ks}, similar to its ability to stimulate $I_{Ca(L)}$ (e.g. Walsh and Kass, 1988; Sanguinetti and Jurkiewicz, 1990), which would tend to shorten the AP. Thus, β-adrenergic stimulation tends to lengthen the AP duration by enhancing $I_{Ca(L)}$ and, at the same time, tends to shorten AP duration by enhancing I_K. The overall effect of β-adrenergic stimulation on AP duration is thus determined by the relative contribution of the changes in these two currents (and perhaps also a contribution of I_{Cl}, see later discussion). Some ventricular preparations also exhibit a Ca^{2+}-dependent I_K (Tohse, 1990). This component may also help to shorten the AP duration. The other, so-called rapid component of the traditional delayed rectifier (I_{Kr}) opens during phase 3 because the deactivation process is much slower than the rapid recovery from inactivation (following a very transient early opening). This I_{Kr} channel is Kv11.1 (a.k.a. HERG1 or ERG1) encoded by KCNH2 (Grunnet, 2010).

An ultrarapid-activating delayed rectifier K^+ current (I_{Kur}) also contributes to phase 3 repolarization in many preparations. I_{Kur} has slow deactivation and different pharmacology than I_{Ks} and I_{Kf}. It is made up of $K_v1.5/3.1$ encoded by KCNA5 and KCNA1, respectively (Grant, 2009). As the repolarization nears the RP, the inwardly rectifying K^+ current (I_{K1}, which is the primary determinant of the RP; see below) also begins to contribute to phase 3 repolarization. Thus, a number of K^+ currents contribute to phase 3 repolarization of the AP.

IVF. Phase 4

In ventricular cells, and most other cardiac cells, phase 4 is the RP. The RP is defined as the stable negative potential that occurs between APs in non-spontaneous cells. The resulting negative membrane potential is maintained by the Na^+-K^+ pump. The RP is very near E_K due to a relatively high permeability of the resting ventricular cell membrane to K^+ and a very low permeability to other ions (e.g. Na^+). Thus, the RP of non-automatic cardiac cells is similar to the RP in skeletal muscle cells. The RP is largely set by a K^+, current known as the inward rectifier, I_{K1}, made up of Kir2.1/2.2 encoded by KCNJ2/J12 (Grant, 2009). Inward rectification means that, instead of a linear "ohmic" relationship between voltage and current, this channel passes current more readily in the inward direction than in the outward direction. This characteristic is evident in Fig. 43.5. Of course, the outward K^+ current is the only one occurring physiologically, since the membrane potential does not normally hyperpolarize beyond E_K. In most preparations, I_{K1} actually demonstrates a negative slope region in the outward direction. That is, as the cell is depolarized from near its resting membrane potential to progressively more depolarized potentials, the outward current first increases and then decreases with further depolarization, with the outward current dropping to very low levels at voltages positive to -40 mV (Fig. 43.5). Thus, the contribution of I_{K1} to repolarization tends to be less at potentials near the plateau and greater as the membrane potential approaches the resting membrane potential (from approximately -40 mV to the resting membrane potential), at the same time that I_K is declining. Therefore, I_{K1} contributes significantly to late phase 3 repolarization. The inward rectification of the I_{K1} channel current is thought to be due to blockade of the channels by intracellular Mg^{2+} (Matsuda et al., 1987) and polyamines (Lopatin et al., 1994), which is removed late in phase 3 as the interior of the cell becomes quite negative (Lopatin and Nichols, 2001). The large expression of I_{K1} channels in ventricular cells reduces the possibility of ventricular automaticity.

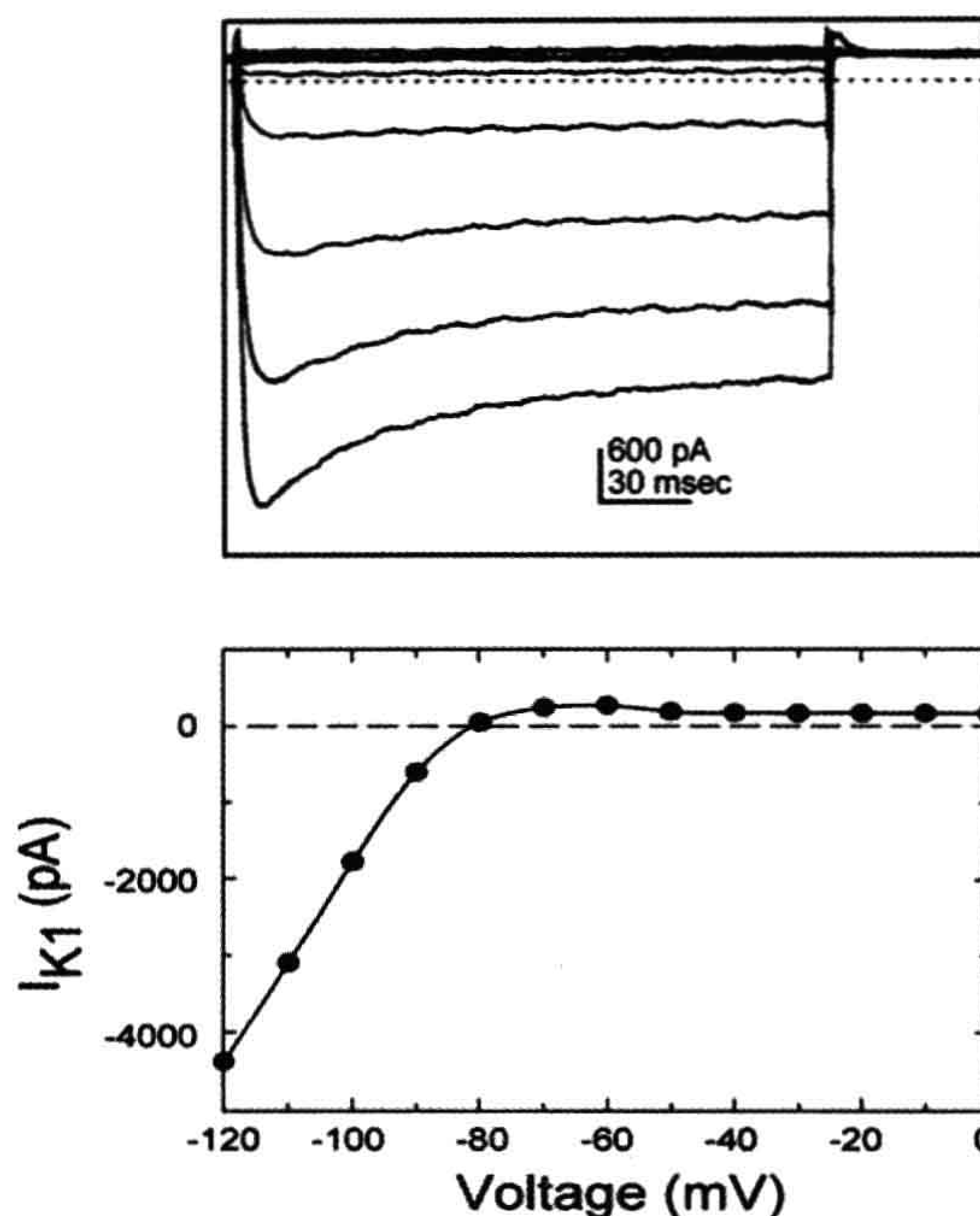


FIGURE 43.5 Inwardly-rectifying K^+ current (I_{K1}) recorded from an adult guinea pig ventricular cell. Upper panel: shown are the original barium-subtracted currents obtained upon stepwise hyperpolarization and depolarization from a holding potential of -40 mV. The current displays the typical inward rectification. That is, the current is smaller in the outward (physiological) direction than the inward direction. Lower panel: the current–voltage curve for I_{K1}. The current also displays a negative slope region between approximately -60 mV and -30 mV. Thus, larger depolarizations actually result in a decrease in outward K^+ flux during this voltage range, such that the current at -30 mV is less than half as large as at -60 mV. The net result is that during repolarization (phase 3) the K^+ current increases as the membrane potential approaches the resting membrane potential.

V. ADDITIONAL CURRENTS CONTRIBUTING TO THE ACTION POTENTIAL

VA. Pump Current

The Na^+,K^+-ATPase, or pump, is the primary transport system that maintains the normal ionic imbalance between the cell exterior and interior. Each pump cycle extrudes three Na^+ ions out of the cell and transports two K^+ ions into the cell, thus building up $[K^+]_i$ and reducing $[Na^+]_i$. Because of the exchange of three positive ions for two positive ions, each pump cycle generates a net loss of one positive charge, which generates a small pump current (I_p). At the RP, I_p is an outward current which may hyperpolarize the membrane potential slightly. In addition, I_p can cause considerable shortening of the AP when $[Na^+]_i$ increases pathologically (Gadsby, 1984). Additionally, blockade of the pump with toxic concentrations of digitalis may lead to a significant increase in intracellular $[Na^+]_i$, which may in turn activate a Na^+-dependent K^+ current ($I_{K(Na)}$) (Luk and Carmeliet, 1990). However, the primary role of the Na^+,K^+-ATPase is to set up and maintain the ionic gradients that generate the electrochemical driving forces for the currents responsible for the AP.

VB. Na^+-Ca^{2+} Exchange Current

An Na^+-Ca^{2+} exchanger (NCX) also exists in the cardiac sarcolemma. Working in the "normal mode" NCX

exchanges intracellular Ca^{2+} for extracellular Na^+; thus, the exchanger is an important mechanism whereby Ca^{2+} is removed from the cytoplasm. The exchanger may also work in the "reverse" mode, exchanging intracellular Na^+ for extracellular Ca^{2+}. Under these conditions, during the initial part of phase 2, NCX contributes a small Ca^{2+} influx for excitation–contraction coupling. The exchanger transports three Na^+ for each Ca^{2+} under most conditions, leading to the net movement of one positive charge. Thus, NCX generates a current which can also contribute to the action potential. The equilibrium potential for this Na^+-Ca^{2+} exchange current (I_{NCX}) is generally slightly negative to 0 mV; therefore, near the resting membrane potential, the exchanger works in the normal mode and I_{NCX} is an inward current. During the initial portion of the plateau, the Na^+-Ca^{2+} exchanger transiently works in the reverse mode and briefly generates an outward current prior to returning to the normal mode. Thus, I_{NCX} may contribute to the shape of the AP (for review, see Janvier and Boyett, 1996).

VC. Chloride Current

Under basal conditions, the Cl^- current (I_{Cl}) in the heart is relatively small and probably does not contribute a great deal to the configuration of the AP. However, when cAMP levels are stimulated (as with sympathetic nerve stimulation), a significant time-independent Cl^- current develops that is separate from the Cl^- current responsible for I_{to2}. Activation of this current by β-adrenergic stimulation can cause a small depolarization of the resting membrane potential and significant shortening of the action potential (Harvey, 1996).

VD. ATP-Sensitive Potassium Current

Many details of this current have been given in the preceding chapter. When the oxygen supply declines, as occurs during ischemia, AP duration shortens. The shortening of the AP duration accelerates inactivation of I_{Ca} thereby reducing contractility. The reduced contractility greatly decreases the energy demands of the cell, thereby sparing ATP. This mechanism contributes to the survival of the myocardial cell during temporary ischemia. However, in addition to this beneficial effect, regional shortening of the AP can also lead to arrhythmias, due to the dispersion of refractory periods.

The shortening of the AP during ischemia is largely caused by activation of a unique outward K^+ current, which is inhibited by intracellular ATP. The decreased oxygen supply reduces ATP levels in the cell and I_{K1} is inhibited. At the same time, the fall in ATP disinhibits the ATP-sensitive K^+ current ($I_{K(ATP)}$) (Noma, 1983), since the current is inhibited by physiological levels of intracellular ATP (Fig. 43.6) and thus appears to contribute little to the AP configuration under conditions of adequate oxygenation. However, during inadequate oxygenation, the AP is shortened as $I_{K(ATP)}$ replaces I_{K1}. This is in large part because $I_{K(ATP)}$ displays less inward rectification than I_{K1} and, thus, has a greater effect on repolarization. This shortening of the AP leads to a shortened phase 2.

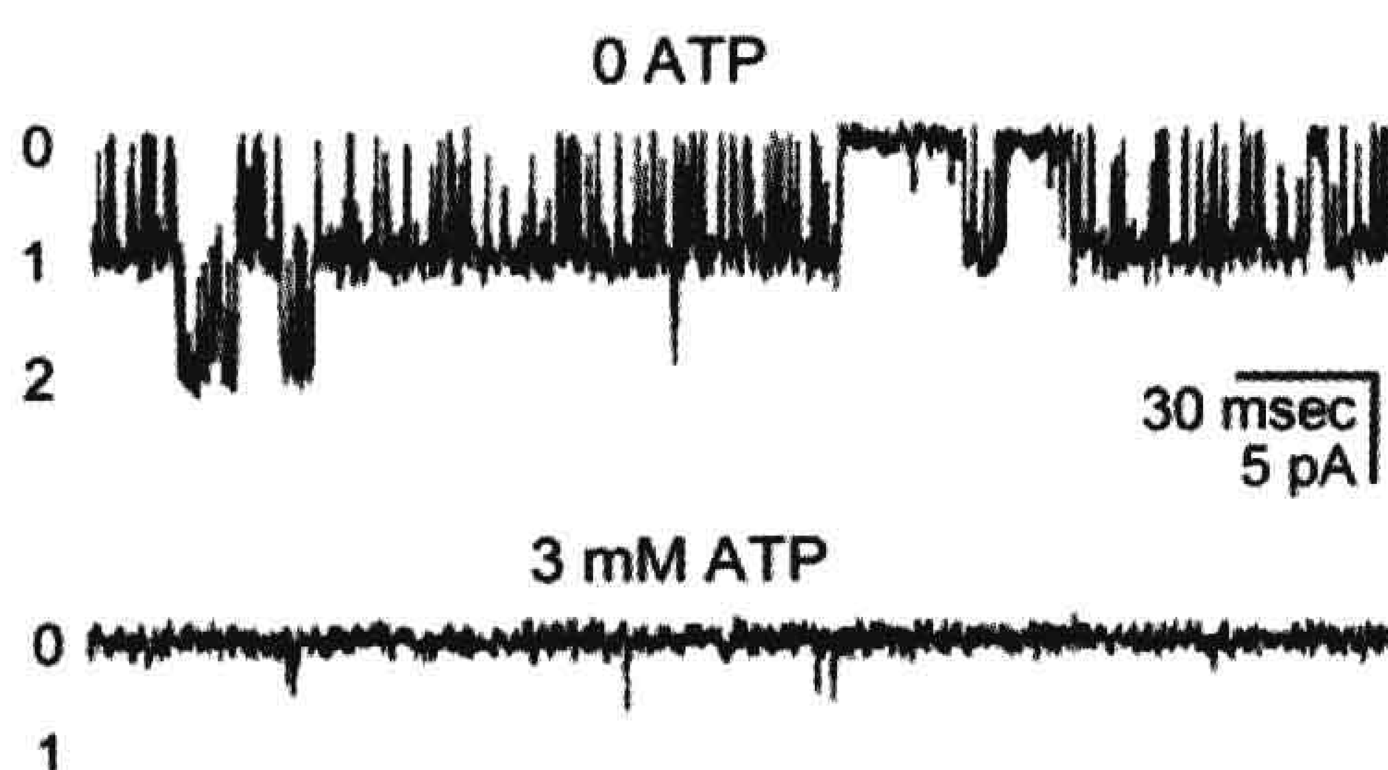


FIGURE 43.6 ATP-sensitive K^+ current $I_{K(ATP)}$ recorded from an inside-out patch from an adult rat ventricular cell. Single-channel currents shown were recorded in the absence of ATP (upper traces) and in the presence of physiological levels of ATP (3 mM, lower traces). Channel openings are downward. In the absence of ATP, channel activity is high. Thus, up to two channels are open simultaneously (number of open channel levels are indicated at the side). In the presence of 3 mM ATP, the channels are rarely open. In the presence of ATP, the openings are extremely brief, such that they do not appear to reach the normal open level (1).

The intracellular ATP levels reached during acute ischemia are generally not sufficiently low to open a substantial number of $I_{K(ATP)}$ channels on its own. However, the decreasing intracellular pH and increasing lactate accumulation that accompany ischemia also enhance $I_{K(ATP)}$ channel opening (Fan and Makielski, 1993) in addition to a fall in intracellular ATP levels. Furthermore, opening of only a small fraction of the large number of $I_{K(ATP)}$ channels may be sufficient to shorten substantially the AP (Faivre and Findlay, 1990).

The physical characteristics of the $I_{K(ATP)}$ channel (e.g. ATP sensitivity and/or degree of rectification) are altered in some pathophysiological states, such as hypertrophy (Cameron et al., 1988) or diabetic cardiomyopathy (Smith and Wahler, 1996; Shimoni et al., 1998). This may be an important factor in the abnormal responses to ischemia in these conditions.

Other channels may also be activated by ischemia, in addition to $I_{K(ATP)}$ channels; e.g. lysophosphatidylcholine and long-chain acylcamitine resulting from membrane phospholipid metabolism rapidly accumulate in early ischemia and may activate the arachidonic acid-activated K^+ channel ($I_{K(AA)}$) and the phosphatidylcholine-activated K^+ channel ($I_{K(PC)}$) (Montsuez, 1997).

VI. REGIONAL DIFFERENCES IN ACTION POTENTIALS

VIA. Overview

The normal pathway for electrical activation of the heart is the following: sinoatrial (SA) node, atria, atrioventricular

(AV) node, bundle of His, Purkinje fibers, ventricles. The APs differ from region to region, reflecting the different roles played by the different cell types. The following description characterizes the APs for each region and indicates how each differs from the ventricular AP.

VIB. Sinoatrial Node

The SA node contains specialized cells that generate APs that are quite different from the ventricular APs described above (Fig. 43.7). Unlike ventricular APs, these cells do not have a true resting membrane potential; i.e. the membrane potential between APs is not stable but rather exhibits a slow spontaneous depolarization known as phase 4 depolarization, or the pacemaker potential. Since there is no resting membrane potential in these cells, the most negative potential the cell reaches between APs is called the maximum diastolic potential. This potential is less negative than the resting membrane potential of ventricular cells, due to a lower K^+ permeability (caused by a lack of I_{K1} in these cells). The maximum diastolic potential ranges from approximately −55 mV for true primary pacemaker cells, to approximately −70 mV for transitional cells on the border between the SA node and atria. The pacemaker potential takes the nodal cell from the maximum diastolic potential to the threshold for generating an AP in these cells (approximately −40 mV). Thus, these cells are spontaneously active and the slope of the phase 4 depolarization is an important determinant of the rate of AP generation and, thereby, heart rate.

VIC. Atria

Atrial cells have APs that are similar in many aspects to the ventricular APs described above. Thus, the resting membrane potential (phase 4) is approximately −85 mV and there is a fast upstroke (phase 0) generated by I_{Na}. The most distinguishing feature of the atrial AP is that it has a more triangular appearance than the ventricular AP. That is, atrial cells do not always have a distinct plateau. This is likely due to the relatively large I_{to} in atrial cells.

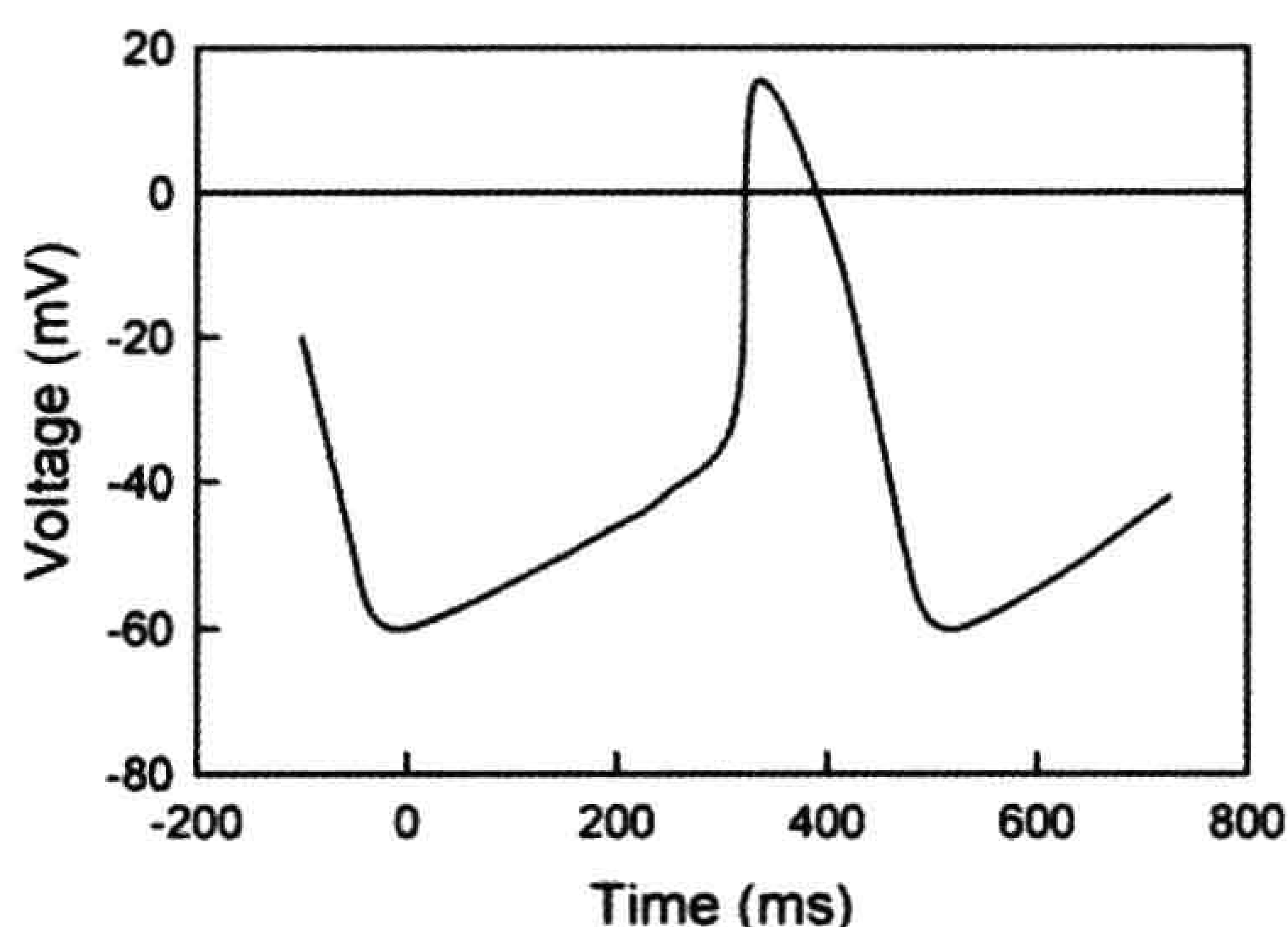


FIGURE 43.7 Sinoatrial node action potential. This is a diagrammatic representation of a typical sinoatrial node AP in the mammalian heart. Note the pacemaker potential and the absence of a resting membrane potential and the slower upstroke compared to the fast AP of the ventricular cell (see Fig. 43.1).

VID. Atrioventricular Node

The cells of the AV node generate APs that are quite similar to the APs of the SA node. Thus, these cells fire Ca^{2+}-dependent APs and also display spontaneous phase 4 depolarization (i.e. automaticity). However, the rate of the phase 4 depolarization in AV nodal cells is much slower than the rate of phase 4 depolarization in SA nodal cells. Thus, the SA node cells fire APs before the AV node cells fire, which is why the SA node cells are the normal pacemaker cells of the heart.

VIE. Purkinje Fibers

Purkinje APs are in most respects similar to the ventricular APs. Thus, these cells have a negative resting membrane potential between APs (phase 4) and a very rapid upstroke (phase 0) generated by I_{Na}. Purkinje fibers do differ from ventricular cells in that they have a more prominent phase 1 repolarization and a longer plateau (phase 2). The plateau is followed by a phase 3 repolarization that is virtually identical to phase 3 in ventricular cells. Cells in the bundle of His appear to have APs similar to those in the Purkinje fibers; however, in general, bundle of His cells have not been studied in detail.

Additionally, Purkinje cells may exhibit automaticity, especially when the extracellular K^+ concentration is low. Thus, under some conditions, they exhibit phase 4 depolarization. Purkinje cells have all the currents found in ventricular cells, described above. However, Purkinje cells also have some additional currents, which are absent or very small in ventricular cells, that are related to the latent pacemaker function of these cells. These additional currents are described in the following section on automaticity.

VII. AUTOMATICITY

VIIA. Overview

Automaticity refers to the ability of some cardiac cells to depolarize and fire repetitive APs spontaneously. Thus, as noted above, automatic cells (e.g. in the SA node) do not have a stable resting membrane potential between APs, but rather have a maximum diastolic potential followed by a spontaneous phase 4 depolarization, known as the pacemaker potential. The spontaneous depolarization to threshold generates the AP in that cell type. Following repolarization of

the AP, the spontaneous phase 4 depolarization occurs again. The slope of the pacemaker potential (i.e. rate of spontaneous phase 4 depolarization) largely determines the rate of AP firing. Because the rate of firing of APs is normally fastest in the primary pacemaker cells of the SA node, this region acts as the normal pacemaker of the heart. Once this region fires an AP, the wave of depolarization is propagated to other regions of the heart, ultimately leading to contraction of the heart. Automatic cells in other regions of the heart (e.g. AV node) normally do not have the opportunity to fire spontaneously before the wave of depolarization arising from the SA node drives them to threshold.

VIIB. Mechanisms of Automaticity

Automaticity is a property of several cell types in the heart under physiological conditions (for review, see Mangoni and Nargeot, 2008). Under pathophysiological conditions, even normally non-spontaneous cells (e.g. ventricular cells) may exhibit automaticity. Physiologically, the most important pacemaker potential is that of the normal pacemaker cells in the SA node. However, technical difficulties have limited our understanding of the pacemaker process in nodal cells and more is known about automaticity in other automatic cell types (e.g. Purkinje fibers).

VIIB1. Automaticity in Purkinje Fibers

Under physiological conditions, Purkinje fibers can have an extremely slow phase 4 pacemaker potential. In contrast to SA node cells, the mechanisms for automaticity in Purkinje cells are fairly well understood. As noted above, the Purkinje cells have all the currents that ventricular cells have, plus some additional currents not found to any significant degree in adult ventricular cells. The large I_{K1} current in Purkinje cells tends to clamp the membrane potential near E_K and, therefore, a large depolarizing current is needed to overcome this clamping effect. The primary current responsible for the pacemaker potential in Purkinje cells has some unusual properties, earning it the designation as the "funny current" (I_f).

I_f is a slowly activating inward depolarizing current which is present in automatic cells. It is a mixed cation current carrying both Na^+ and K^+ ions. In Purkinje cells, I_f is responsible for most of the depolarizing current which generates the pacemaker potential. The molecular basis of I_f will be described in detail below (see Section VIIB2).

In addition to $I_{Ca(L)}$, pacemaker cells have an additional Ca^{2+} current which is activated at more negative potentials and exhibits a much more rapid activation and inactivation than $I_{Ca(L)}$ (Hagiwara et al., 1988). This second Ca^{2+} current (carried by $Ca_v3.1$ and $Ca_v3.2$) has been named the transient T-type Ca^{2+} current ($I_{Ca(T)}$) in contrast to the classical, slowly inactivating long-lasting L-type Ca^{2+} current ($I_{Ca(L)}$). The T-type Ca^{2+} current is small to non-existent in adult ventricular cells, but is present in Purkinje cells. There may be a small contribution of the T-type Ca^{2+} current to the latter stages of the pacemaker potential in Purkinje cells. During pacemaker activity, a small amount of Na^+ through I_{Na} channels may also contribute to the final phase of the pacemaker potential in Purkinje cells, as the membrane potential approaches the threshold for AP generation. Then, as sufficient voltage-gated Na^+ channels are opened, the Purkinje fiber will fire an AP which is generated by essentially the same mechanisms as previously described for ventricular cells.

VIIB2. Automaticity in Nodal Cells

Several factors contribute to the pacemaker potential in nodal cells. Because of the very low density of I_{K1} channels in nodal cells, the resting K^+ permeability is much lower in nodal cells than in ventricular cells. The large resting K^+ permeability in ventricular cells generated by I_{K1} tends to keep the interior of the cells negative, opposing depolarization of the cell toward threshold by "clamping" the membrane potential near E_K. A much smaller current is sufficient to depolarize the nodal cells due to the much lower resting K^+ permeability, leading to a very high input resistance. Thus, currents which may be too small to measure accurately using present electrophysiological techniques (small background currents or currents produced by various electrogenic transport mechanisms) could produce sufficient current to affect the pacemaker potential. Because of this limitation, the analysis of the relative contribution of various currents to the pacemaker potential in nodal cells is much less clear than for Purkinje cells, leading to considerable controversy regarding the precise mechanism of automaticity in SA node cells.

The major depolarizing current during the pacemaker potential of Purkinje cells, I_f, is also present in nodal cells. The hyperpolarization-activated cyclic nucleotide-gated (HCN) channels responsible for I_f are encoded by four gene isoforms (HCN1−4) (for review, see Baruscotti et al., 2010). HCN2 and HCN4 are expressed in the heart, with HCN4 being the predominant isoform in the SA node. As noted earlier, I_f is an unusual depolarizing current in that it is activated by hyperpolarization (DiFrancesco, 1993). As a result, I_f is thought to contribute significantly to the early part of the pacemaker potential in SA node cells.

There is a low density of HCN channels found in ventricular myocytes (see Baruscotti et al., 2010). In contrast to the situation in nodal cells, HCN are normally non-functional in ventricular myocytes because the voltage-dependence of the channels is quite different from HCN channels in nodal cells. That is, the channels can only be activated at unphysiologically negative voltages in ventricular cells (Yu et al., 1993). However, in certain

pathological conditions (e.g. heart failure), the voltage-dependence of the I_f channels in ventricular myocytes shifts to a more positive level (Mangoni and Nargeot, 2008), suggesting that I_f may contribute to ventricular arrhythmias under such conditions.

Other small currents, e.g. the sodium-potassium ATPase pump current (I_p) and the Na^+-Ca^{2+} exchange current (I_{NCX}), also likely contribute to and/or modulate the pacemaker potential in nodal cells. For example, in SA node cells, I_p may help set the maximum diastolic potential (Noma and Irisawa, 1975). A novel involvement of SR calcium release in contributing to the pacemaker potential has also been proposed (see Mangoni and Nargeot, 2008). In this mechanism, local Ca^{2+}-induced-Ca^{2+} release near the sarcolemma leads to a depolarizing current that contributes to the pacemaker potential due to the electrogenic (swapping three Na^+ for one Ca^{2+}) nature of the exchanger.

As noted earlier, the upstroke (phase 0) of nodal cells is generated by an L-type Ca^{2+} current ($I_{Ca(L)}$) rather than a voltage-gated Na^+ current (I_{Na}). The channel responsible appears identical to the classic L-type Ca^{2+} channel ($Ca_v1.2$) for the plateau in ventricular cells. Interestingly, in nodal cells, another $I_{Ca(L)}$ channel isoform ($Ca_v1.3$) has been reported that has a slightly more negative threshold (approximately -50 mV). This component of $I_{Ca(L)}$ is thought to contribute to the late phase of the pacemaker potential and effectively lower the threshold for $I_{Ca(L)}$ (for review, see Mangoni et al., 2003).

The complex interaction of so many different currents leads to the following hypothesis of the generation of the pacemaker potential by sequential activation of several different currents: (1) activation of I_f in late phase 3 repolarization is largely responsible for generating the early part of the pacemaker potential; (2) this early diastolic depolarization depolarizes the cells to the threshold for opening of T-type Ca^{2+} channels, leading to further depolarization; (3) the next threshold to be reached is the threshold for opening of $Ca_v1.3$ channels, causing further depolarization; (4) ultimately, at the very end of the pacemaker potential, $Ca_v1.3$ channels are opened; (5) opening of sufficient number of L-type channels leads to the upstroke of the Ca^{2+}-dependent action potential. Thus, opening of each channel in the sequence depolarizes the cell to the threshold for the opening of the next channel.

An alternative proposal to the sequential activation of I_f and various I_{Ca} components hypothesizes that the interaction between a depolarizing voltage- and time-independent background current (I_b) and the decay of the delayed rectifier (I_K) develops the pacemaker potential in nodal cells. This small, constant depolarizing current (I_b) in nodal cells is a cation current carried primarily by Na^+ ions (Hagiwara et al., 1992). Due to the small size of this current, relatively little is known about its magnitude and characteristics in mammalian SA node cells; however, indirect evidence suggests that it may be a very important component in determining automaticity (Campbell et al., 1992; Dokos et al., 1996). The role of a constant I_b in generating a variable pacemaker potential results from the interaction of I_b with I_K. I_K is the primary current responsible for repolarization in nodal cells, as in other cardiac cells. Similar to ventricular cells, I_K has also been shown to consist of at least two components (I_{Ks} and I_{Kr}) (Dokos et al., 1996). I_K displays essentially no inactivation during a prolonged depolarizing pulse, but displays a slow decay upon repolarization toward E_K. The time course of the I_K decay is very slow at membrane potentials in the voltage range of the pacemaker potential in nodal cells. The depolarizing action of I_b is opposed by I_K. Thus, the depolarization due to a constant background current I_b effectively increases progressively over time due to a gradual loss of opposing repolarizing current (I_K), thereby leading to diastolic depolarization in nodal cells. Since the relative contribution of the various currents to the pacemaker potential in nodal cells cannot be accurately determined experimentally, there has been considerable controversy over which depolarizing current (I_f or I_b) plays the greater role in generating the pacemaker potential in these cells. It is likely that both play a significant role in contributing to automaticity in nodal cells.

VIIC. Modulation of Automaticity by the Autonomic Nervous System

The pacemaker cells of the SA node are richly innervated by sympathetic and parasympathetic nerves. These actions of norepinephrine (NE) and acetylcholine (ACh) on several currents in SA node cells are the basis of the stimulating and inhibiting effect on heart rate of sympathetic or parasympathetic nerve stimulation.

I_f and $I_{Ca(L)}$ are both enhanced by the sympathetic neurotransmitter, norepinephrine and inhibited by the parasympathetic neurotransmitter, acetylcholine. Thus, NE increases the slope of the pacemaker potential, the threshold is reached sooner and heart rate increases. In contrast, ACh decreases the slope of the pacemaker potential. The I_f channel is directly activated by cAMP (DiFrancesco and Mangoni, 1994). Thus, the effects of NE and ACh are mediated by raising and lowering the intracellular cAMP concentration, respectively.

In addition to the cAMP-mediated effects on I_f and $I_{Ca(L)}$, ACh activates a G-protein-coupled inwardly-rectifying K^+ current ($I_{K(ACh)}$) whose structure is similar to I_{K1}. Cardiac $I_{K(ACh)}$ channels are tetramers made up of Kir3.1 and Kir3.4 subunits expressed by KCNJ3 and KCNJ5 and are highly expressed in the SA and AV nodes and atria, but not ventricles (Wickman et al., 1999). Binding of ACh to muscarinic M-2 receptors causes the

release of G-protein $G_{\alpha i}$ and $G_{\beta\gamma}$ subunits. The $G_{\beta\gamma}$ subunit then activates the $I_{K(ACh)}$ channel, causing hyperpolarization (which drives the maximum diastolic potential further from threshold) and a reduction of the slope of the pacemaker potential (for review, see Mangoni and Nargeot, 2008). The end result of activation of $I_{K(ACh)}$ is that it takes SA node cells a longer time to reach threshold and the heart rate is decreased.

VIII. CHANNELOPATHIES

Mutations in the genes encoding I_{Kr}, I_{Ks} and I_{Na} have been reported to be responsible for long QT syndrome, a familial disorder characterized by slowed repolarization, recurrent syncope, increased incidence of torsades de pointes arrhythmias and an increased risk for sudden death (Veldkamp, 1998; Vizgirda, 1999). Interestingly, APs are normally longer in adult females than males, resulting in a greater QT interval. This suggests that the repolarizing currents may be smaller in females than males, which may explain the greater incidence of torsades de pointes arrhythmias in females (Vizgirda, 1999). Gain-of-function mutations in the genes that cause long QT syndrome can cause the opposite effect, namely more rapid repolarization, leading to short QT syndrome (Priori and Cerrone, 2005).

Other mutations in the genes for these ion channels are responsible for a number of other familial arrhythmogenic conditions, such as Brugada syndrome and catecholaminergic polymorphic ventricular tachycardia (Clancy and Kass, 2005; Tester and Ackerman, 2009). It is certain that more electrophysiological abnormalities will be found to have their origins in mutations of genes encoding numerous channel proteins and associated regulatory proteins.

BIBLIOGRAPHY

Antzelevitch, C., & Dumaine, R. (2011). Electrical heterogeneity in the heart: physiological, pharmacological and clinical implications. *Comprehensive Physiology* 654–692.

Attwell, D., Cohen, I., Eisner, D., Ohba, M., & Ojeda, C. (1979). The steady-state TTX-sensitive ("window") sodium current in cardiac Purkinje fibers. *Pflügers Arch, 379*, 137–142.

Baruscotti, M., Bottelli, G., Milanesi, R., DiFrancesco, J. C., & DiFrancesco, D. (2010). HCN-related channelopathies. *Pflügers Arch, 460*, 405–415.

Boyett, M. R., Honjo, H., & Kodama, I. (2000). The sinoatrial node, a heterogenous pacemaker structure. *Cardiovasc Res, 47*, 658–687.

Cameron, J. S., Kimura, S., Jackson-Bums, D. A., Smith, D. B., & Bassett, A. L. (1988). ATP-sensitive K^+ channels are altered in hypertrophied ventricular myocytes. *Am J Physiol, 255*, H1254–H1258.

Campbell, D. L., Rasmussen, R. L., & Strauss, H. C. (1992). Ionic current mechanisms generating vertebrate primary cardiac pacemaker activity at the single cell level: an integrative view. *Annu Rev Physiol, 54*, 279–302.

Catterall, W. A. (2000). Structure and regulation of voltage-gated Ca^{2+} channels. *Annu Rev Cel Dev Biol, 16*, 521–555.

Clancy, C. E., & Kass, R. S. (2005). Inherited and acquired vulnerability to ventricular arrhythmias: cardiac Na^+ and K^+ channels. *Physiol Rev, 85*, 33–47.

Coraboeuf, E., & Nargeot, J. (1993). Electrophysiology of human cardiac cells. *Cardiovasc Res, 27*, 1713–1725.

DiFrancesco, D. (1993). Pacemaker mechanisms in cardiac tissue. *Annu Rev Physiol, 55*, 455–472.

DiFrancesco, D., & Mangoni, M. (1994). Modulation of single hyperpolarization-activated channels [I_f] by cAMP in rabbit sino-atrial node. *J Physiol, 474*, 473–478.

Dokos, S., Celler, B., & Lovell, N. (1996). Ion currents underlying sinoatrial node pacemaker activity: a new single cell mathematical model. *J Theor Biol, 181*, 245–272.

Faivre, J.-E., & Findlay, I. (1990). Action potential duration and activation of ATP-sensitive potassium current in isolated guinea-pig ventricular myocytes. *Biochim Biophys Acta, 1029*, 167–172.

Fan, Z., & Makielski, J. C. (1993). Intracellular H^+ and Ca^{++} modulation of trypsin modified ATP sensitive K^+ channels in rabbit ventricular myocytes. *Circ Res, 72*, 715–722.

Gadsby, D. C. (1984). The Na^+/K^+ pump of cardiac cells. *Annu Rev Biophys Bioeng, 13*, 373–378.

Grant, A. O. (2009). Cardiac ion channels. *Circ Arrhythm Electrophysiol, 2*, 185–194.

Grunnet, M. (2010). Repolarization of the cardiac action potential. Does increase in repolarization capacity constitute a new anti-arrhythmic principle? *Acta Physiol, 198*(Suppl. 676), 1–48.

Hagiwara, N., Irisawa, H., & Kameyama, M. (1988). Contribution of two types of calcium currents to the pacemaker potential of rabbit sino-atrial node cells. *J Physiol, 395*, 233–254.

Hagiwara, N., Irisawa, H., Kasanuki, H., & Hosoda, S. (1992). Background current in sino-atrial node cells of the rabbit heart. *J Physiol, 448*, 53–72.

Harvey, R. D. (1996). Cardiac chloride currents. *NIPS, 11*, 175–181.

Hoshiko, T., & Sperelakis, N. (1962). Components of the cardiac action potential. *Am J Physiol, 203*, 258–260.

Janvier, N. C., & Boyett, M. R. (1996). The role of Na-Ca exchange current in the cardiac action potential. *Cardiovasc Res, 32*, 69–84.

Lopatin, A. N., & Nichols, C. G. (2001). Inward rectifiers in the heart: an update on I(K1). *J Mol Cell Cardiol, 33*, 625–638.

Lopatin, A. N., Makhina, E. N., & Nichols, C. G. (1994). Potassium channel block by cytoplasmic polyamines as the mechanism of intrinsic rectification. *Nature, 372*, 368–369.

Luk, H. N., & Carmeliet, E. (1990). Na^+ activated K^+ current in cardiac cells: rectification, open probability block and role in digitalis toxicity. *Pflügers Arch, 416*, 766–768.

Mangoni, M. E., & Nargeot, J. (2008). Genesis and regulation of the heart automaticity. *Physiol Rev, 88*, 919–982.

Mangoni, M. E., Couette, B., Bourinet, E., Platzer, J., Reimer, D., & Streissnig, J. (2003). Functional role of L-type $Ca_v1.3$ Ca^{2+} channels in cardiac pacemaker activity. *Proc Natl Acad Sci USA, 100*, 5543–5548.

Matsuda, H., Saigusa, A., & Irasawa, H. (1987). Ohmic conductance through the inwardly rectifying K channel and blocking by the integral Mg^{++}. *Nature, 325*, 156–159.

Montsuez, J.-J. (1997). Cardiac potassium currents and channels. Part I: basic science aspects. *Internat J Cardiol, 61*, 209–219.

Nerbonne, J., & Kass, D. (2005). Molecular physiology of cardiac repolarization. *Physiol Rev, 85*, 1205–1253.

Noma, A., & Irisawa, H. (1975). Contribution of an electrogenic sodium pump to the membrane potential in rabbit sinoatrial node cells. *Pflügers Arch, 358*, 289–301.

Noma, A. (1983). ATP-regulated K^+ channels in cardiac muscle. *Nature, 305*, 147–148.

Priori, S. G., & Cerrone, M. (2005). Genetic arrhythmias. *Ital Heart J, 6*, 241–248.

Sanguinetti, M. C., & Jurkiewicz, N. K. (1990). Two components of cardiac delayed rectifier K^+ current. Differential sensitivity to block by class III antiarrhythmic agents. *J Gen Physiol, 96*, 195–215.

Sanguinetti, M. C., Johnson, J. H., Hammerland, L. G., et al. (1997). Heteropodotoxins: peptides isolated from spider venom that block $K_V4.2$ potassium channels. *Molec Pharmacol, 52*, 491–498.

Shimoni, Y., Light, E. E., & French, R. J. (1998). Altered ATP sensitivity of ATP-dependent K^+ channels in diabetic rat hearts. *Am J Physiol, 275*, E568–E576.

Smith, J. M., & Wahler, G. M. (1996). ATP-sensitive potassium channels are altered in ventricular myocytes from diabetic rats. *Mol Cell Biochem, 158*, 43–51.

Sperelakis, N., & Lehmkuhl, D. (1964). Effect of current on transmembrane potentials in cultured chick heart cells. *J Gen Physiol, 47*, 895–927.

Tester, D. J., & Ackerman, M. J. (2009). Cardiomyopathic and channelopathic causes of sudden unexplained death in infants and children. *Annu Rev Med, 60*, 69–84.

Tohse, N. (1990). Calcium-sensitive delayed rectifier potassium current in guinea pig ventricular cells. *Am J Physiol, 258*, H1200–H1207.

Tseng, G. N., & Hoffman, B. E. (1989). Two components of transient outward current in canine ventricular myocytes. *Circ Res, 64*, 633–647.

Veldkamp, M. W. (1998). Is the slowly activating component of the delayed rectifier, I_{Ks}, absent from undiseased human ventricular myocardium? *Cardiovasc Res, 40*, 433–435.

Vizgirda, V. M. (1999). The genetic basics for cardiac dysrhythmias and the long QT syndrome. *J Cardiovasc Nurs, 13*, 34–45.

Walsh, K. B., & Kass, R. S. (1988). Regulation of a heart potassium channel by protein kinase A and C. *Science, 242*, 67–69.

Wickman, K., Krapivinsky, G., Corey, S., et al. (1999). Structure, G protein activation, functional relevance of the cardiac G protein-gated K^+ channel, I_{KACh}. *Ann NY Acad Sci, 868*, 386–398.

Xu, H., Guo, W., & Nerbonne, J. M. (1999). Four kinetically distinct depolarization-activated K^+ currents in adult mouse ventricular myocytes. *J Gen Physiol, 113*, 661–678.

Yu, F. H., & Catterall, W. A. (2003). Overview of the voltage-gated sodium channel family. *Genome Biol, 4*, 207.

Yu, F. H., Chang, E., & Cohen, I. S. (1993). Pacemaker current exists in ventricular myocytes. *Circ Res, 72*, 232–236.

Zygmunt, A. C., & Gibbons, W. R. (1992). Properties of the calcium-activated chloride current in the heart. *Gen Physiol, 99*, 391–414.

Chapter 44

Smooth Muscle Excitability

Neil D. Detweiler, Anup K. Srivastava, Asif R. Pathan, Sujay V. Kharade and Nancy J. Rusch

Chapter Outline

I. INTRODUCTION

Smooth muscle cells[1] (SMCs) compose many tissues including blood vessels, airways, the gastrointestinal tract, bladder, uterus and vas deferens. These organs have very diverse functions and so, not surprisingly, their SMCs exhibit highly diverse patterns of electrical excitation that have evolved to support the unique physiological roles of the individual organs. For example, the SMCs in blood vessels generally lack spiking action potentials that would drive rhythmic contraction and relaxation of the vasculature and thereby cause profound changes in blood flow and blood pressure. Instead more stable resting membrane potentials (E_m) and slower depolarizing patterns are characteristic of vascular SMCs. This electrical profile enables steady-state Ca^{2+} influx through voltage-gated Ca^{2+} channels to regulate tightly and incrementally vessel diameter. Similarly, the resting SMCs of airways and bladder lack electrical spiking that could trigger rhythmic bronchial constriction or solicit phasic bladder contraction, respectively. In contrast, gastrointestinal (GI) smooth muscle shows spontaneous electrical activity that drives rhythmic contractions and relaxations to enable digestion and peristalsis. The SMCs in the lengthy GI tract that is composed of both circular and longitudinal muscle are further distinguished by their highly site-specific excitability patterns that are tailored to local function. Thus, SMC excitability is highly heterogeneous and characterized by site-specific differences in the resting E_m levels and patterns of excitability in organs with very diverse functions (Fig. 44.1; Table 44.1) (Steedman, 1966; Lee et al., 1990; Lombard et al., 1990; Berccczi et al., 1992; Brayden and Nelson, 1992; Kamei et al., 1994; Gokina and Bevan, 2000; Bramich, 2000; Sanders et al., 2006; Morin et al., 2007; Forrest et al., 2009). Further diversity in patterns of SMC excitation is generated by the wide array of physiological factors (i.e. neurotransmitters, autacoids, circulating factors, stretch) that can quickly modify SMC excitability.

At least several key differences exist between SMCs and the muscle cells that compose skeletal and cardiac tissues. By definition, SMCs lack striations (aligned dark and light bands at the light microscopic level) and, instead, have a less strictly organized arrangement of contractile fibers that mediate graded tone. Another important difference is the very small size of SMCs compared to skeletal or cardiac muscle cells, which requires their dependence on multicellular interactions to coordinate smooth muscle contraction and relaxation even at the local level. Some SMCs exhibit electrical or chemical coupling, whereby a change in the level of E_m or in the concentration of intracellular signaling molecules in individual cells can be propagated to adjacent cells to produce coordinated contraction or relaxation. Finally, SMCs appear to have a mechanism for sustaining contractions for long periods of

[1] Additional information on the basics of excitability of smooth muscles is presented in Appendix I.

Cell Physiology Sourcebook. DOI: 10.1016/B978-0-12-387738-3.00044-5

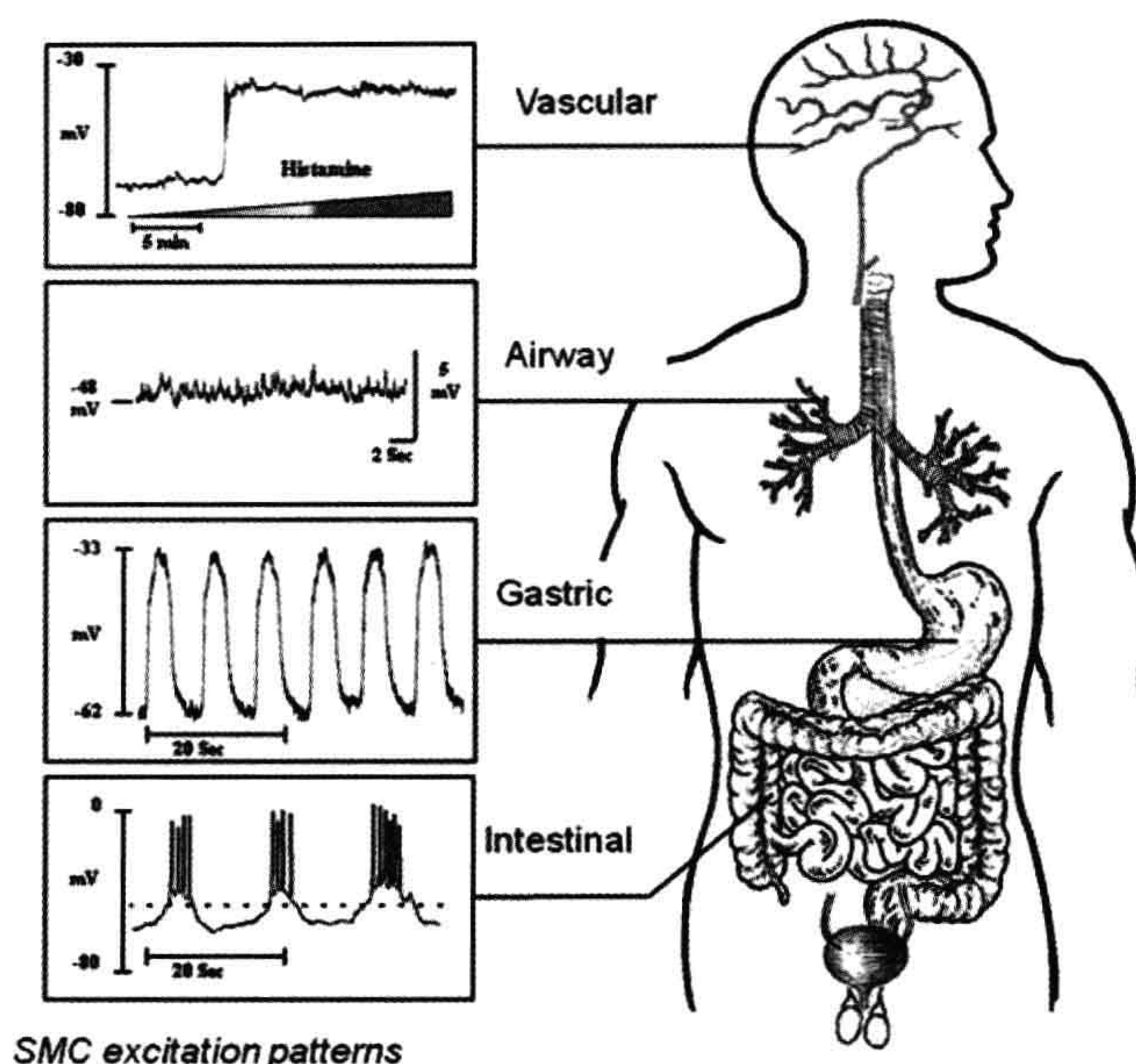


FIGURE 44.1 There are many organs which contain smooth muscle, including the vasculature, airways and gastrointestinal tract. The patterns of excitation are highly heterogeneous, to support the unique functions of each of the organs. *(Reproduced with permission from (A): Gokina et al., Am J Physiol. 2000; (B): Bramich, Am J Physiol. 2000; (C): Forrest et al., Am J Physiol. 2009; (D): Sanders et al., Annu Rev Physiol. 2006.)*

time with relatively low energy cost, a concept referred to as the "latch-state". Physiologically, this is manifested as the ability of SMCs to sustain cross-bridge attachments and contraction while intracellular Ca^{2+} concentration, cross-bridge phosphorylation and ATP consumption rates fall. The mechanisms that enable the "latch-state" are reviewed elsewhere (Hai and Murphy, 1990), but one key concept is that the graded excitation patterns in many types of SMCs combined with their unique ability to sustain contraction at low energy cost permits *smooth muscle tone*, a term that refers to graded, sustained levels of smooth muscle contraction.

II. DETERMINATION OF RESTING MEMBRANE POTENTIAL IN SMCs

The origin of the resting membrane potential (E_m) is detailed elsewhere in this book. However, a short discussion is warranted here, since some determinants of E_m are tissue-specific and unique to SMCs. First, SMCs do not densely express voltage-gated sodium (Na^+) channels in their plasma membrane, which are a hallmark feature of skeletal and cardiac muscle cells. In these striated muscle cells, Na^+ influx, enabled by the opening of voltage-gated Na^+ channels, mediates the rapid depolarization or "upstroke" of the action potential. However, action potentials (if present or induced) in SMCs are primarily mediated by Ca^{2+} influx through voltage-gated Ca^{2+} channels; the Na^+ channels are sparse or absent. Second, the resting E_m in SMCs is generally more positive (−60 mV to −40 mV) than the more negative E_m level (−90 mV to −60 mV) observed in skeletal and cardiac muscle cells. Importantly, the more positive resting E_m of the SMCs is near or even resides within the lower E_m range for opening of voltage-gated Ca^{2+} channels. Thus, even small depolarizations of the SMCs depolarization will result in the opening of voltage-gated Ca^{2+} channels, Ca^{2+} influx and SMC activation. Notably, smooth muscle can contract in either a phasic (short term/rhythmic) or a tonic (long term/sustained) pattern depending on the properties of the particular SMC and its input from external excitatory or inhibitory signals. When smooth muscle initiates phasic contraction, such as during peristalsis of the GI tract, the phasic contractions usually mirror and rely on phasic depolarizations that trigger the voltage-gated Ca^{2+} influx required for SMC activation. Other smooth muscle is characterized by tonic contraction, including the smooth muscle of sphincters, airways and the vasculature. In this case, the level of E_m also is relatively constant. For example, vascular smooth muscle responds to changing needs for oxygen by maintaining tonic states of contraction, which change as a function of arterial oxygen concentration (Fig. 44.2) (Welsh et al., 1998). Thus, the E_m of SMCs can be finely tuned to ensure that the intensity of contraction is placed precisely on the continuum between full relaxation and maximal contraction.

Notably, the control of E_m in all cells is accomplished by a complex system of ion channels, pumps and

TABLE 44.1 Representative Electrical Properties of Different Types of Smooth Muscle

	Smooth Muscle Type Species	Resting E_m (mV)	Slow Wave Amplitude (mV)	Slow Wave Frequency (waves/min)	Ref
Vascular					
Mesenteric artery	Rat	−39	n/a	n/a	Steedman, 1966
Cerebral artery	Rabbit	−37	n/a	n/a	Brayden & Nelson, 1992
Renal artery	Dog	−38	n/a	n/a	Lombard et al., 1990
Saphenous artery	Rat	−39	n/a	n/a	Berczi et al., 1992
Mesenteric artery	Guinea pig	−39	n/a	n/a	Steedman, 1966
Airway					
Trachea	Dog	−60	n/a	n/a	Kamei et al., 1994
Bronchus	Dog	−70	n/a	n/a	Kamei et al., 1994
Bronchus	Human	−52	n/a	n/a	Morin et al., 2007
Trachea	Ferret	−60	n/a	n/a	Lee et al., 1990
Bronchus	Ferret	−70	n/a	n/a	Lee et al., 1990
Gastrointestinal					
Gastric antrum	Mouse	−62	30	8	Forrest et al., 20093
Small intestine	Human	−55	15	8	Sanders et al., 2006
Colon	Human	−55	20	4	Sanders et al., 2006
Small intestine	Canine	−55	25	8	Sanders et al., 2006
Colon	Canine	−75	55	4	Sanders et al., 2006

These values illustrate the adaptation of smooth muscle to the specific needs of each organ. Gastrointestinal smooth muscle exhibits rhythmic and regular depolarizations known as slow waves, which mediate peristalsis. Depolarization in airway and vascular smooth muscle is variable in magnitude and duration. The more depolarized resting E_m in vascular smooth muscle closely couples small reductions in E_m to increases in Ca^{2+} influx.

exchangers, which regulate the movement of ions across the lipid bilayer of the plasma membrane. Active transport systems (ATP-driven ion pumps and exchangers) maintain non-equilibrium concentration gradients across the plasma membrane. There are multiple active transport systems in a single SMC, but the activity of ATP-driven ion pumps still contributes less to resting E_m in SMCs than ion channel flux. The most prominent ATP-driven pump in SMCs is the Na^+,K^+-ATPase enzyme, an electrogenic pump in the plasma membrane that generates a hyperpolarizing current to maintain resting E_m. Traditionally, it is thought that three Na^+ ions are pumped out of the cell in exchange for two K^+ ions that enter during a single pump cycle, which would result in a net intracellular charge of -1. The contribution of Na^+, K^+-ATPase to resting E_m varies between different types of SMCs, but its hyperpolarizing influence may contribute between 5 and 20% of the negative E_m level. Additionally, because the Na^+,K^+-ATPase molecules pump K^+ ions into the cell, they establish a high concentration of intracellular K^+ (135−145 mmol/L), whereas the extracellular K^+ concentration is relatively low (3.5−5 mmol/L). This steep transmembrane K^+ gradient, combined with a dense expression of K^+ channels on the SMC surface, results in basal K^+ efflux and this hyperpolarizing K^+ current is the main determinant of the negative resting E_m in SMCs. Thus, pharmacological block of K^+ channels in SMCs causes a profound depolarization and contraction. In contrast, resting ionic flux through other channels has less influence on resting E_m, but may critically contribute to SMC contraction. For example, voltage-gated, L-type Ca^{2+} channels and cation-permeable *t*ransient *r*eceptor *p*otential (TRP) channels provide activator Ca^{2+} for SMC contraction. Although chloride (Cl^-) channels are expressed in SMCs, their contribution to resting E_m is less clear and the reader is referred to Verkman and Galieta (2009) for

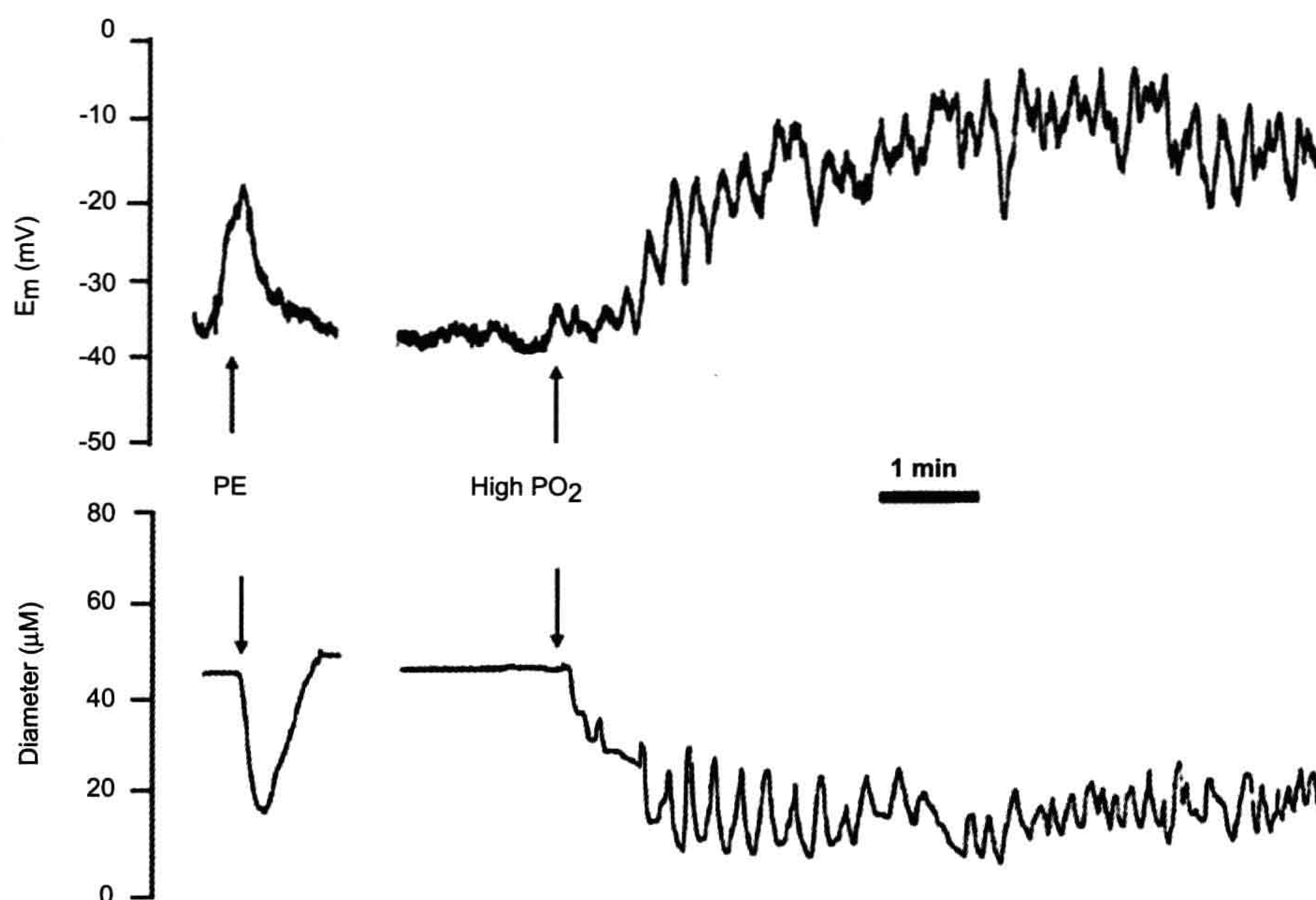


FIGURE 44.2 The vasoconstrictor response of a hamster cheek pouch arteriole to high PO_2 acts as a compensatory mechanism to normalize oxygen delivery to the distal tissues. Membrane potential (E_m) was recorded using an intracellular microelectrode in a vascular SMC (top trace) while recording the corresponding diameter response (lower trace). The arteriole was sequentially exposed to the α-adrenergic receptor agonist, phenylephrine (PE), and then after washout of PE, exposed to high ambient PO_2. High PO_2 elicited a sustained depolarization (top panel) with superimposed oscillations in E_m that was associated with a tonic, vacillating vasoconstriction (lower panel). *(Reproduced with permission from Welsh et al., Am J Physiol. 1998.)*

a review of this topic. For the sake of brevity, this chapter will only focus on the key K^+ and Ca^{2+} -permeable ion channels in SMCs using vascular SMCs as a model (Fig. 44.3). Two final sections will discuss key aspects of excitability in GI and airway smooth muscle.

III. POTASSIUM CHANNELS

The plasma membrane of SMCs expresses diverse populations of K^+ channels and the opening of K^+ channels promotes hyperpolarization and relaxation of SMCs. Distinct types of K^+ channels work in concert to optimize

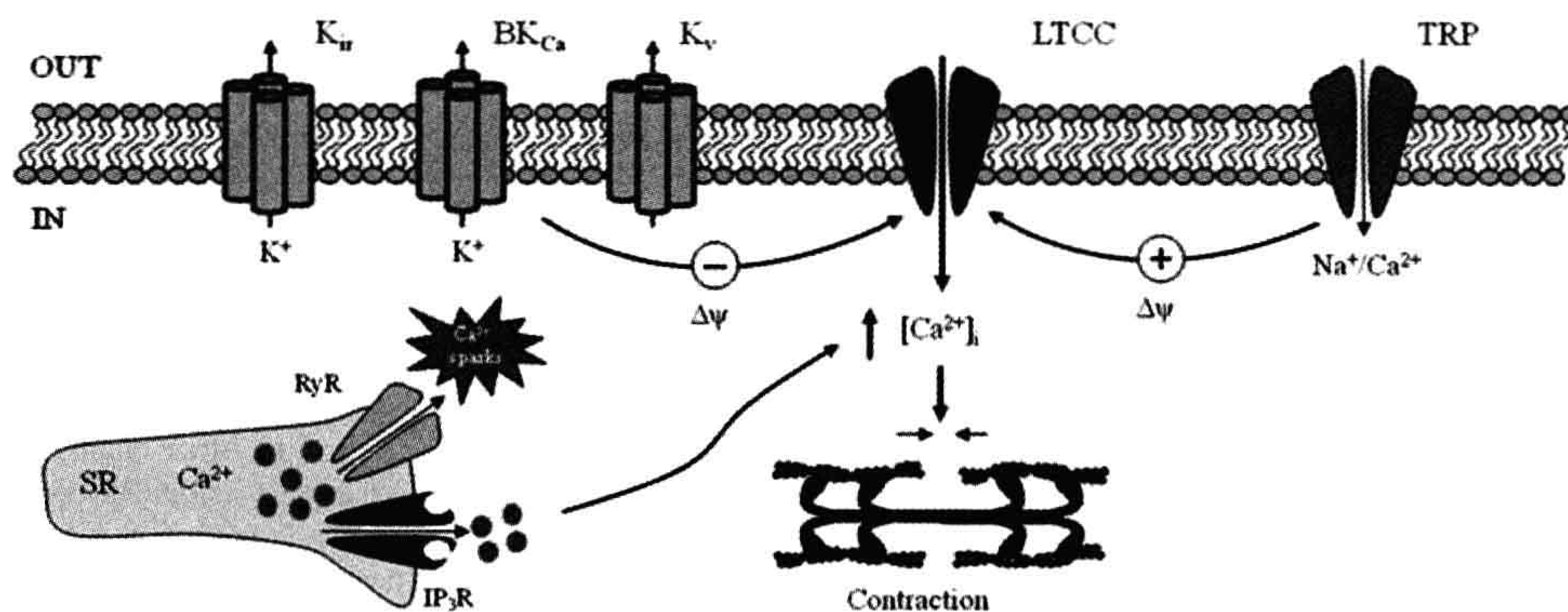


FIGURE 44.3 Some key families of ion channels in vascular SMCs. The K^+ channels include the inwardly rectifying (K_{ir}), voltage-gated (K_v) and high-conductance, Ca^{2+}-sensitive (BK_{Ca}) K^+ channels. The interplay between transient receptor potential (TRP) channels and L-type Ca^{2+} channels (LTCC) provides activator Ca^{2+} for SMC contraction. All of these channels interact with the ryanodine receptors (RyR) and inositol triphosphate receptors (IP_3R) to modulate SMC excitability.

SMC tone in different organs. This section will review three important K^+ channel families: (1) the voltage-gated K^+ (K_V) channels; (2) high-conductance Ca^{2+}-sensitive K^+ (BK_{Ca}) channels; and (3) inwardly rectifying K^+ (K_{ir}) channels. Information on other K^+ channels including the ATP-sensitive K^+ channels and the two pore domain K^+ channels is available elsewhere (Coetzee et al., 1999; Brayden, 2002; Gurney and Manoury, 2009).

IIIA. Voltage-Gated K^+ Channels

The voltage-gated K^+ (K_V) channels are a highly diverse superfamily of K^+ channels that share the common properties of potassium selectivity and voltage-dependent activation. The α subunits are composed of six hydrophobic transmembrane segments (S1−S6) flanked by hydrophilic amino- and carboxyl termini located in the cell interior (Fig. 44.4A) (Epperson et al., 1999). An intrinsic voltage sensor conferred by positively charged amino acids in transmembrane domain S4 is associated with channel gating, while the pore loop (P) confers K^+ selectivity. Four α subunits compose the pore-forming structure of the K_V channel and assemble in the endoplasmic reticulum with four regulatory β subunits that modulate channel expression and function. The K_V channels contribute to the resting E_m of some SMCs. For example, pharmacological block of "*Shaker*-type" K_V channels by correolide (COR) in vascular SMCs of isolated, perfused cerebral arteries (depicted in Fig. 44.4G) causes depolarization and constriction (Fig. 44.4D). Additionally, excitatory stimuli that depolarize and contract SMCs also simultaneously open the voltage-dependent K_V channels. The resulting hyperpolarizing K^+ current limits Ca^{2+} influx through voltage-dependent Ca^{2+} channels (VDCC) to buffer contraction. Thus, the K_V channels have an important role in counteracting SMC excitation (Chen et al., 2006; Albarwani et al., 2003).

IIIB. Large-Conductance, Ca^{2+}-Sensitive K^+ Channels

The large-conductance, Ca^{2+}-sensitive K^+ channels, referred to as "BK_{Ca}" or "maxi-K" channels because of their large single-channel currents, are densely expressed in many SMCs. The α subunit shows partial homology with the K_V channel in six (S1−S6) of its seven (S0−S6) transmembrane domains that include the S4 voltage sensor (see Fig. 44.4B) (Ledoux et al., 2006; Wu and Mark, 2010).

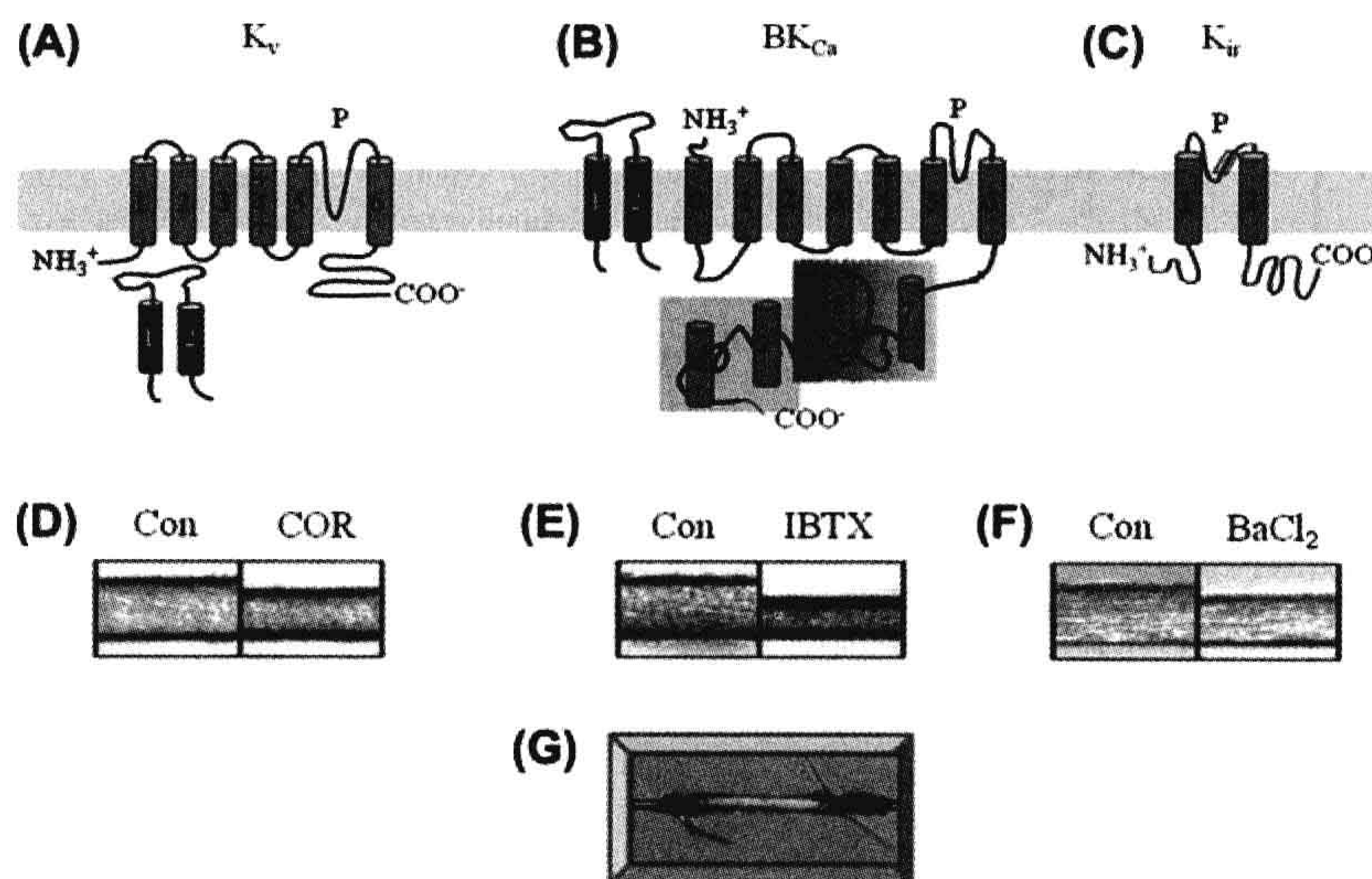


FIGURE 44.4 Proposed topology of K^+ channel α subunits in SMCs and their vasodilator role in cerebral arteries. Details are provided in the text. (A, B) The multiprotein K_V and BK_{Ca} channels are presumed to be composed of pore-forming α subunits and regulatory β subunits. The β subunit is assumed to be intracellular in K_V channels and membrane-delineated in BK_{Ca} channels. (C) The α subunit of the K_{ir} channel is composed of only two transmembrane domains spanning a pore loop. All three K^+ channel types are composed of four α subunits that co-assemble to form a functional tetramer. An additional four β subunits compose the K_V and BK_{Ca} channels. (D, E, F) All three types of K^+ channels contribute to the resting diameter of a rat middle cerebral artery. The artery was cannulated and perfused at an intraluminal pressure of 80 mmHg. In each case, the left panels show the control resting diameter. The right panels show the decrease in vessel diameter after addition of: 10 μmol/L correolide (COR) to block *Shaker*-like K_V channels (D), 100 nmol/L iberiotoxin (IBTX) to block BK_{Ca} channels (E) and 10 μmol/L $BaCl_2$ to block K_{ir} channels (F). Drugs were washed out and the artery returned to resting diameter between drug responses (not shown). (G) A photograph depicting a rat cerebral artery cannulated on glass micropipettes and perfused at 80 mmHg.

Although BK_{Ca} channels are only weakly opened by depolarization in the absence of intracellular calcium ($[Ca]_i$), the voltage-sensitivity of the BK_{Ca} channel increases markedly when $[Ca]_i$ rises. The "Ca^{2+}-sensitivity" of the α subunit is conferred by cytosolic domains S7–S10 and by its β subunit that interacts with the N-terminal S0 domain. Despite their low level of opening at the resting E_m of SMCs, the densely expressed BK_{Ca} channels can mediate a significant hyperpolarizing current. For example, iberiotoxin (IBTX) -induced block of BK_{Ca} channels in cerebral arterial SMCs results in a sustained depolarization (Fig. 44.5A) and elevation of $[Ca]_i$ mediated by Ca^{2+} influx through L-type Ca^{2+} channels (Fig. 44.5B) (Knot et al., 1998). The functional outcome is vasoconstriction (see Fig. 44.4E). Thus, during SMC excitation, the K_V channels and BK_{Ca} channels work in concert as a negative feedback mechanism to buffer excess depolarization and SMC contraction. Not surprisingly, a loss of these K^+ channels has been linked to diseases characterized by abnormal SMC tone.

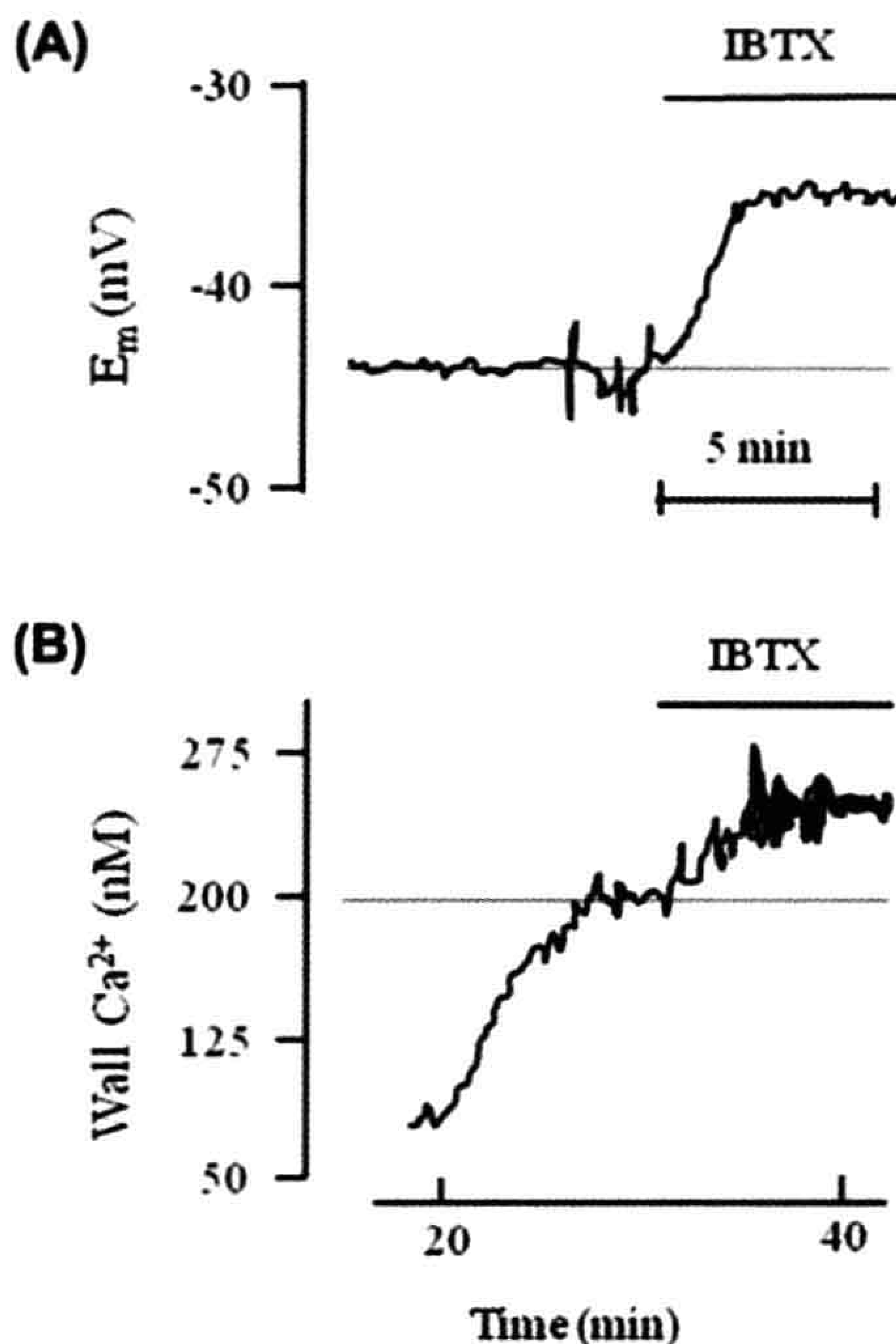


FIGURE 44.5 Measurement of membrane potential (E_m) and arterial wall calcium ($[Ca^{2+}]$) in a rat cerebral artery loaded with the Ca^{2+} indicator, fura-2. Block of BK_{Ca} channels by iberiotoxin (IBTX) resulted in depolarization of the arterial SMCs (A) and a rise in arterial wall $[Ca^{2+}]$ (B). The level of E_m and arterial wall $[Ca^{2+}]$ in the absence of drugs is indicated by the horizontal dotted line. *(Reproduced with permission from Knot et al., J Physiol. 1998.)*

IIIC. Inwardly Rectifying K^+ Channels

Inwardly rectifying K^+ (K_{ir}) channels exhibit the property of "inward rectification", indicating that they readily conduct K^+ into cells at E_m below the K^+ equilibrium potential but show only a limited ability to mediate K^+ efflux at more positive membrane potentials. The property of inward rectification is at least partially conferred by voltage-dependent block of the channel pore by Mg^{2+} and polyamines at the cytoplasmic side (Quayle et al., 1997; Hibino et al., 2010). Similar to the K_v and BK_{Ca} channels, the K_{ir} channels are tetrameric structures composed of four α subunits but no corresponding β subunit has been identified (see Fig. 44.4C). Since the K_{ir} channels are not voltage-dependent they are thought to open readily at negative voltages and contribute to the resting E_m of many cell types including SMCs. Thus, block of K_{ir} channels by barium chloride ($BaCl_2$) results in a loss of hyperpolarizing K^+ current, depolarization and Ca^{2+}-dependent vasoconstriction (see Fig. 44.4F). In contrast, the K_{ir} channels that conduct K^+ poorly at more depolarized potentials may be silenced by vascular activation.

IV. VOLTAGE-DEPENDENT CALCIUM CHANNELS

Calcium influx through voltage-dependent Ca^{2+} channels (VDCCs) is required for normal excitation–contraction coupling in SMCs and at least two gene families of voltage-gated Ca^{2+} channels are expressed. Transient ("T-type") Ca^{2+} channels activate at very negative E_m and then rapidly inactivate to provide a short "burst" of Ca^{2+} influx. The T-type Ca^{2+} channels have been identified in a small subset of SMCs as reviewed by Cribbs (2006). However, T-type Ca^{2+} channels cannot be the prominent Ca^{2+} channel type in most types of SMCs, including those composing blood vessels, airway and bladder, since these tissues require sustained Ca^{2+} influx to maintain tonic contraction and avoid sudden fluctuations of $[Ca^{2+}]_i$ in the SMCs.

In contrast, the long-lasting ("L-type") Ca^{2+} channels open in response to membrane depolarization within the range of resting E_m found in SMCs. The L-type Ca^{2+} channels are thought critically to supply the activator Ca^{2+} that drives contraction in most types of smooth muscle. These channels are multisubunit complexes composed of a large α_{1C} subunit that forms the channel pore and confers most functional properties to the channel including voltage sensing and Ca^{2+} permeability (Dophin, 2009). Smaller regulatory subunits (β, $\alpha_2\delta$) may finely tune Ca^{2+} channel function and promote its expression at the cell surface (Fig. 44.6A).

Voltage-dependent Ca^{2+} channels are the critical link between membrane potential and contraction (electromechanical coupling) in SMCs (Nelson et al., 1990). More

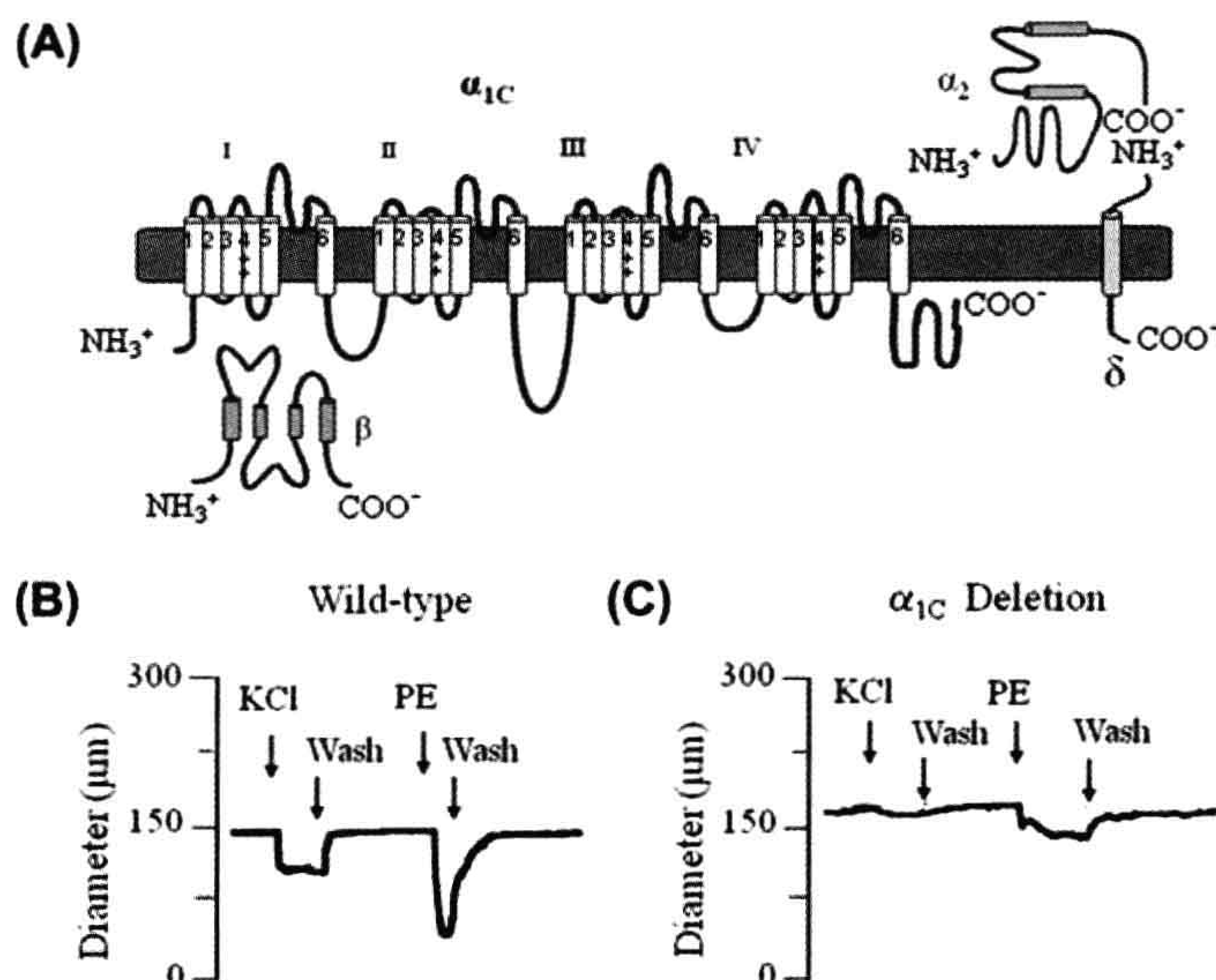


FIGURE 44.6 The α_{1C} subunit (A) is critical for mediating the response to many vasoconstrictor stimuli. Diameter tracings show the different responses of tibialis arteries from wild-type mice (B) and mice lacking the α_{1C} subunit (C). *(Reproduced with permission from Moosmang et al., EMBO J. 2003.)*

positive E_m levels cause more frequent Ca^{2+} channel openings, more Ca^{2+} influx and greater Ca^{2+}-dependent activation of the contractile proteins. Furthermore, since the L-type Ca^{2+} channels inactivate slowly during sustained depolarization, the Ca^{2+} influx permitted by a small fraction of these channels may be sufficient to mediate tonic contraction. For example, direct depolarization of vascular SMCs by high concentrations of potassium chloride (KCl) or activation of excitatory α-adrenergic receptors by phenylephrine (PE) contract small tibialis arteries of normal, wild-type mice (see Fig. 44.6B) (Moosmang et al., 2003). However, similar arteries of genetically modified mice, in which the pore-forming α_{1C} subunit of the L-type Ca^{2+} channel is deleted, only weakly contract to the same stimuli (see Fig. 44.6C). Thus, the L-type Ca^{2+} channel permits many tissues composed of SMCs to perform properly their contractile functions that may involve regulating blood flow (vascular SMCs) or air flow (airway SMCs) or enabling peristalsis and digestion (intestinal SMCs). The SMC tone also provides an excitatory template upon which endogenous substances may act to further modify organ function.

V. TRANSIENT RECEPTOR POTENTIAL (TRP) CHANNELS

Nearly 28 mammalian transient receptor potential (TRP) channels have been identified to date and at least 11 of them are expressed in SMCs (Guibert et al., 2011). Unlike L-type Ca^{2+} channels, TRP channels are non-voltage gated and they are permeable to more than one ion species. The TRP channels conduct cations including Na^+ and Ca^{2+} ions; the preference for a single ion species depends on the channel subtype. The TRP channels are classified into six related protein families on the basis of amino acid sequence homology (Montell, 2005). The "classical" or "canonical" TRP channels have drawn the most attention in SMCs. Notably, whereas the α subunit of the L-type Ca^{2+} channel is composed of a single large polypeptide, TRP channels are formed by the assembly of four smaller polypeptide subunits as homo- or heterotetramers giving rise to variable channel properties. Each α subunit has six transmembrane spanning domains (S1–6), a pore-forming loop between S5 and S6 and intracellularly located NH_2 and COOH termini (Fig. 44.7A). The S4 segment lacks the positively charged residues necessary for voltage sensing (Gaudet, 2008). Based on their mechanism of activation, TRP channels can be grouped as receptor-operated, store-operated or stretch-activated channels. As examples, store- and receptor-operated TRP channels are activated by muscarinic (M2 and M3) receptor stimulation in visceral SMCs and by α_1-adrenergic receptors in vascular SMCs (Dietrich et al., 2006). Other excitatory native stimuli also can open TRP channels through G-protein coupled receptors in the plasma membrane. A number of signaling molecules generated by receptor occupation can regulate the activity of TRP channels in SMCs (Beech et al., 2004; Albert and Large, 2006).

The functional significance of specific TRP channel subtypes is largely unexplored. Knockout mice with specific TRP channel deletions have been generated

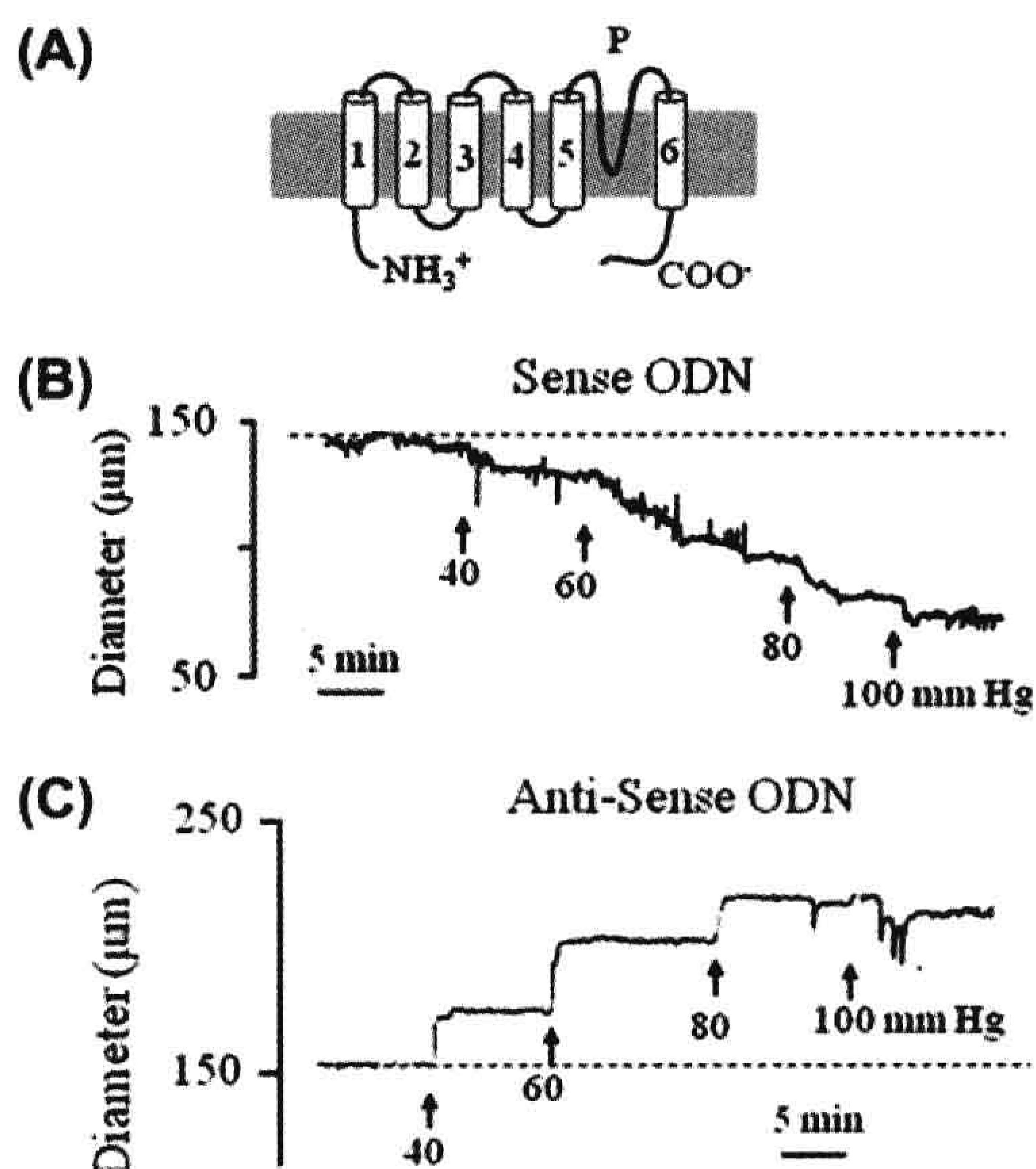


FIGURE 44.7 Structure and function of TRP channels. (A) The α subunit contains six transmembrane spanning domains (S1–S6) with the pore (P) formed between S5 and S6. The S4 domain lacks the positive residues that confer voltage sensitivity. (B) In control vessels treated with sense oligonucleotides (ODNs), step elevations of intraluminal pressure in isolated rat cerebral arteries result in pressure-induced constriction. (C) Arteries treated with TRPC6 antisense ODNs fail to show pressure-induced constriction. The horizontal dotted line represents the arterial diameter before intraluminal pressure was increased. *(Reproduced with permission from Welsh et al., Circ Res. 2002.)*

recently. However, the impact of TRP gene deletion on SMC function often is not straightforward, possibly due to the redundancy generated by this large channel superfamily. This potential dilemma has led to the design of double or triple TRP knockout mice including TRPC4/6 gene-deficient animals. In the intestinal SMCs of these animals, the dual deletion of TRPC4 and TRPC6 impairs muscarinic receptor-induced cationic current and contraction, suggesting the potential importance of the TRP channels in SMC excitability (Tsvilovskyy et al., 2009). Notably, different TRP channel subtypes show highly variable Ca^{2+} permeability and it is unclear if Ca^{2+} influx through TRP channels directly contributes to SMC contraction. However, the combined Na^{+} and Ca^{2+} influx corresponding to the inward cationic current through TRP channels is thought to depolarize SMCs leading to the opening of L-type Ca^{2+} channels, Ca^{2+} influx and contractile protein activation. Thus, it appears that one important function of TRP channels is to serve as a triggering mechanism for the activation of L-type Ca^{2+} channels (Gudermann et al., 2004; Dietrich et al., 2006).

Stretch is another important stimulus that regulates visceral and vascular SMC tone. Historically, the existence of stretch-activated cationic channels was recognized. These channels were observed to respond to mechanical stimuli including osmotic stress, membrane stretch and shear force. Now, several TRP channel families are considered to contain member subtypes that are mechanosensitive, but their role in regulating the contractile responses to mechanical stimuli is controversial and not well defined to date (Dietrich and Gudermann, 2011). For example, isolated, perfused rat cerebral arteries respond to step elevations of intraluminal pressure (40, 60, 80 and 100 mmHg) by vasoconstriction (see Fig. 44.7B) (Welsh et al., 2002). However, knockdown of TRPC6 channels using antisense oligonucleotides eliminates the pressure-induced constrictor response in the cerebral arteries, which instead show passive dilation as intraluminal pressure is elevated (see Fig. 44.7C) (Welsh et al., 2002). In contrast to these results, however, another study failed to confirm the mechanosensitivity of TRPC6 channels in arteries of TRPC6 knockout mice (Dietrich et al., 2005). The stimuli that activate TRP channels and the role of specific TRPC subtypes in regulating SMC excitability is an exciting area of discovery that is being intensely investigated.

VI. EXCITATION OF GASTROINTESTINAL SMCs

The excitation patterns of SMCs in the gastrointestinal (GI) tract are designed to provide the contractions required for mixing the ingested food with the digestive enzymes and propulsion of the resulting gastric contents. These two functions are accomplished by highly coordinated movements of circular and longitudinal smooth muscles, which are aligned perpendicular to each other in the wall of the GI tract. Additionally, different organs within the GI tract are required to perform different functions. For example, the stomach and small intestine enable digestion and absorption, whereas the large intestine enables the drying and compaction of waste. Clearly, a complex scheme of excitation is needed to integrate the different functions of the GI tract and electrical mechanisms provide an important source of modulation to regulate organ function. For example, the resting E_m in SMCs varies between −85 mV and −40 mV along the GI tract. The SMCs in the small intestine are more depolarized (≈ −55 mV) than those in stomach or colon (≈ −75 mV) (Sanders et al., 2006). This electrical heterogeneity is partially achieved by expression of a diverse population of ion channels. The main classes of ion channels expressed in GI smooth muscle mirror those in vascular SMCs and include similar K^{+} channel families that set the resting E_m and buffer contraction and the voltage-gated Ca^{2+} channels and cationic TRPC channels that mediate SMC contraction. The tight regulation of resting E_m is vital

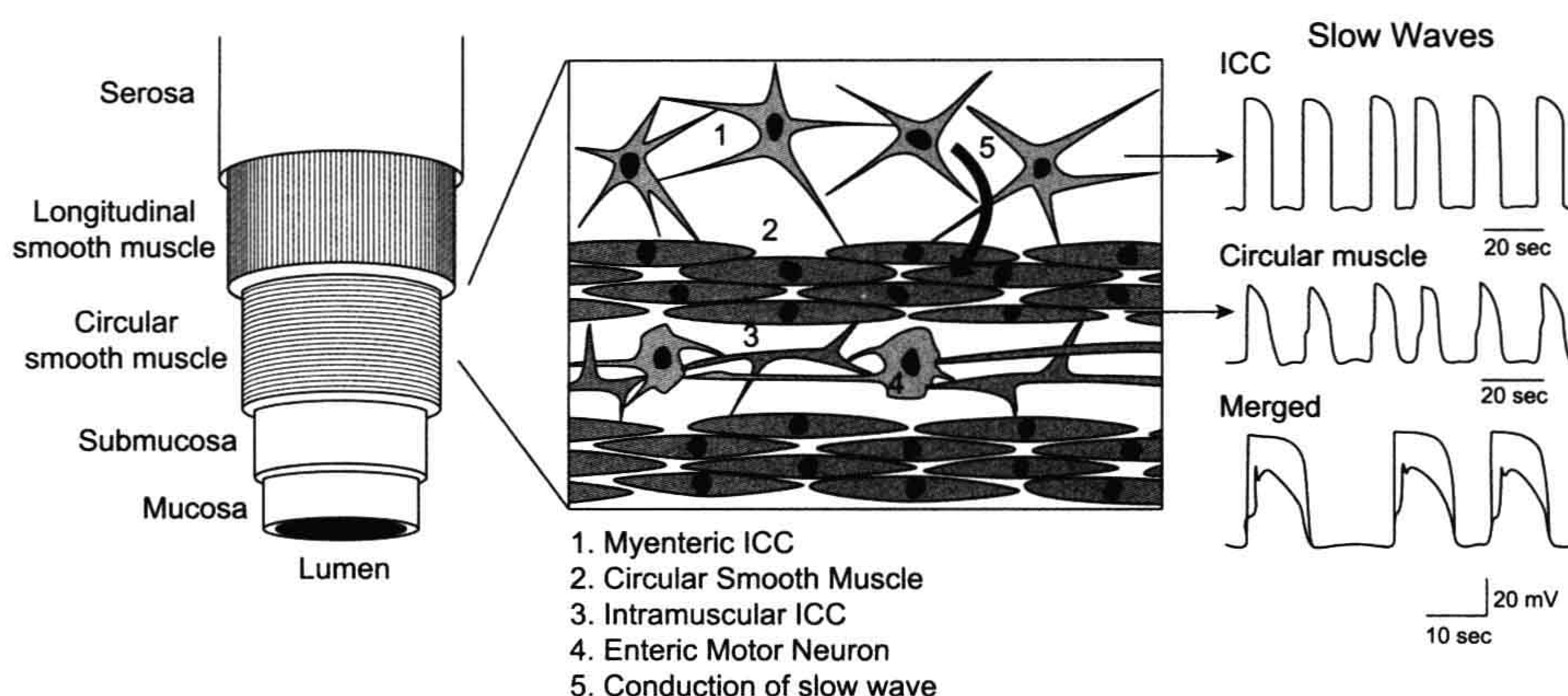


FIGURE 44.8 A cutaway view showing the different layers of the intestinal tract (left). A magnified view of the smooth muscle layers and surrounding layers of ICC (center). Membrane potential recordings of ICC and circular smooth muscle showing the propagation of slow waves from the myenteric ICC to the circular smooth muscle (right). *(Reproduced with permission from Hirst et al., J Physiol. 2001 and Horowitz et al., Annu Rev Physiol. 1999.)*

because it determines if the SMCs can respond to depolarizing stimuli from the interstitial cells of Cajal (explained later) and receptor agonists (Sanders, 2008).

Calcium influx through voltage-gated L-type Ca^{2+} channels is indispensable for GI motility. Slow waves depolarize the SMC membrane to open L-type Ca^{2+} channels and, thus, pharmacological block of L-type Ca^{2+} channels attenuates contraction in GI SMCs (Lyford and Ferrugia, 2003). Additionally, members of the TRPC family are gaining attention for their role in SMC excitability. As mentioned in the previous section, intestinal SMCs of TRPC4/6 knockout mice show defective muscarinic receptor-mediated cationic current and depolarization (Tsvilovskyy et al., 2009).

Although the SMCs ultimately execute force development, a type of interstitial cell in the GI tract called the interstitial cells of Cajal (ICC) plays a vital role in coordinating SMC contraction. The ICC are classified based on morphology: stellate-shaped ICC are found mainly between the muscle layers of the stomach; spindle-shaped ICC largely reside between the smooth muscle fibers of the intestine (Fig. 44.8) (Horowitz et al., 1999; Hirst and Edwards, 2001). They are electrically coupled to each other, the enteric nervous system (ENS) and the SMCs of the GI tract through gap junctions. Networks of ICC generate pacemaker activity and propagate "slow waves" across and down the GI tract. GI motility relies on these rhythmic depolarizations that spread through the GI SMCs at a low frequency (<5/min) and activate voltage-dependent Ca^{2+} channels to cause Ca^{2+}-dependent electrical spiking (Fig. 44.8) and SMC contraction (Sanders, 2008). A key feature of the slow waves is that they propagate faster circumferentially (depolarizing circular SMCs) but slow as they pass down the GI tract (depolarizing longitudinal SMCs) to allow enough time for digestion.

Although the SMCs of the vasculature and GI tract share many ion channels, there are some mechanistic differences in their electrical profiles. Vascular SMCs generally show a stable resting E_m and a tonic level of contraction under resting conditions, whereas the SMCs of the GI tract exhibit tonic and phasic patterns of contractions that reflect stable or fluctuating E_m levels, respectively. The spontaneous excitability of the SMCs in the GI tract emanates from the unique influence of the ICC, which also receive signals from the enteric nervous system (ENS) and paracrine substances. Similarly, the vascular SMCs also are subjected to unique stimuli not found in the GI tract. For example, the intraluminal pressure inside blood vessels can be a powerful force for depolarization and contraction of arterial SMCs (see Fig. 44.7) and this stimulus for cell excitation is unique to the vascular system. In addition to voltage-dependent Ca^{2+} influx mediated by L-type Ca^{2+} channels, the influx of cations through TRP channels may contribute to pressure-induced constriction. Other factors that influence vascular SMC excitability not discussed in this short chapter include neurotransmitters, circulating factors and the release of vasoactive substances from the endothelial cells that line the blood vessel lumen.

VII. AIRWAY SMOOTH MUSCLE

The airway SMCs express a diverse assortment of K^+ channels, voltage-dependent Ca^{2+} channels and TRP channels similar to vascular and GI SMCs. The resting E_m of airway SMCs ranges between −70 mV and −30 mV

(Hirota et al., 2007). It varies slightly between the tracheal and bronchial SMCs with the former value more negative by 10 mV than the latter (Honda and Tomita, 1987; Oonuma et al., 2000). Human airways possess inherent tone which is largely the result of contractile 5-lipoxygenase products (Watson et al., 1997). Although the source of contractile leukotrienes is unclear, airway SMCs or bronchial epithelium and inflammatory cells associated with the SMCs are potential candidates. These electrical characteristics of airway smooth muscle support the function of the respiratory system. The more positive resting E_m in the bronchial compared to tracheal SMCs may reflect the fact that the bronchi play a far more important role in determining resistance to airflow, and the more positive resting E_m may lend susceptibility to excitatory stimuli. Notably, the bronchi also are the locus of inflammation and other functional/structural changes associated with asthma and other conditions of airway hyperexcitability.

The similarities of ion channels and excitation mechanisms between airway smooth muscle and other types of SMCs will not be reiterated here; instead differences will be emphasized. First, the SMCs of airways are uniquely exposed to a broad spectrum of environmental factors that can regulate airway diameter and they also are exposed to autacoids released by mast cell activation. The excitatory ligands may bind to surface receptors on airway SMCs to initiate Ca^{2+} influx through Ca^{2+}-permeable ion channels and/or release Ca^{2+} from the sarcoplasmic reticulum (SR) to elevate $[Ca]_i$. In contrast to the central importance of voltage-dependent Ca^{2+} influx in activation of vascular SMCs, the main trigger for bronchoconstriction may be the release of Ca^{2+} sequestered within the SR. Thus, the two major Ca^{2+} release channels in the SR, the inositol-1, 4, 5-trisphosphate receptor (IP_3R) and the ryanodine receptor (RyR), appear to be prominent features of airway SMCs. The properties of the IP_3R and RyR channels are reviewed elsewhere (Bai and Sanderson, 2006; Tazzeo et al., 2008). Second, agonist activation of SMCs in airways often evokes recurring $[Ca^{2+}]_i$ transients that distinguish airway SMCs from other cell types. This pattern of excitation is characterized by intracellular Ca^{2+} oscillations, whose frequency is inversely dependent on agonist concentration. For example, activation of excitatory cholinergic receptors by methacholine (MCh) on a bronchial SMC triggers Ca^{2+} oscillations in the cell cytosol (Fig. 44.9A) (Bai and Sanderson, 2006). These Ca^{2+} oscillations are associated with SMC contraction (Fig. 44.9B) and a reduction of airway area (Fig. 44.9C). The subsequent addition of isoproterenol (ISO), a β-adrenergic receptor agonist with bronchodilator properties, transiently increases the frequency of Ca^{2+} oscillations, an event that is coupled to a temporary loss of contractile force and increased airway area.

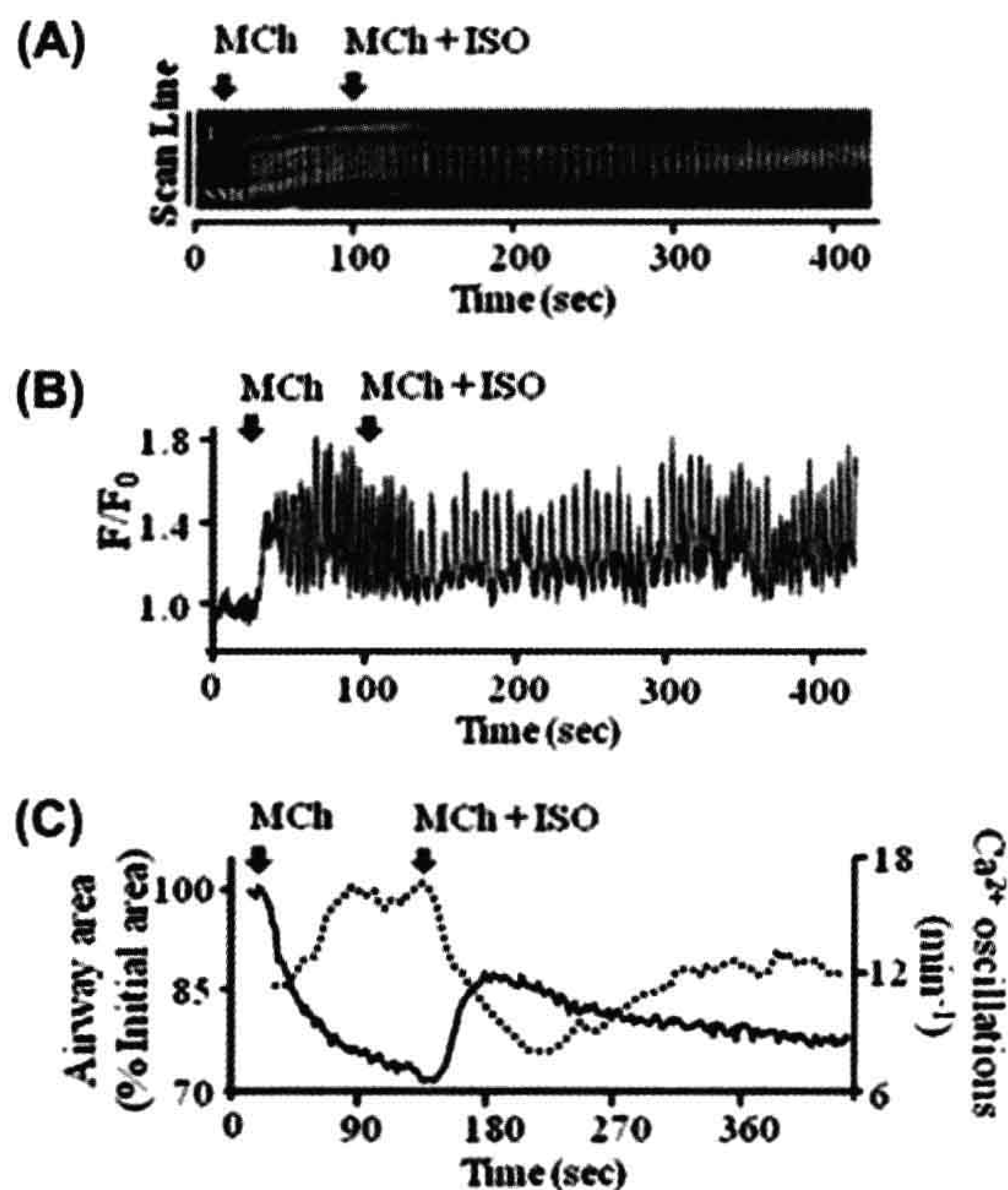


FIGURE 44.9 The effect of methacholine (MCh) and isoproterenol (ISO) on Ca^{2+} signaling of airway SMCs. (A) Line-scan plot constructed from a fluorescent image of an airway SMC loaded with Oregon Green 488 BAPTA-1 AM. Images were obtained by a two-photon microscope and the sequence of recorded images of Ca^{2+} fluorescence in response to MCh (200 nM) and ISO (1 μM) are depicted. (B) Corresponding changes in force generated by the same concentrations of MCh and ISO. (C) The correlation of the Ca^{2+} oscillation frequency (dotted line) and airway area (solid line) in a single cell during contraction induced by MCh (200 nM) and relaxation induced by ISO (10 μM). The frequency of the Ca^{2+} oscillations was inversely coupled to the contraction of the airway. *(Reproduced with permission from Bai et al., Resp Res., 2006.)*

VIII. CONCLUDING REMARKS

This chapter has provided a succinct overview of the basis for SMC excitability with an emphasis on vascular, gastrointestinal and airway smooth muscle. It has outlined the structure and function of key ion channels, including three types of K^+ channels that contribute to the resting E_m of SMCs and counteract cell excitability by mediating a hyperpolarizing K^+ current. Additional sections have reviewed the structure and function of the L-type Ca^{2+} channels and TRP channels, which mediate the influx of Ca^{2+} for excitation–contraction coupling. The cationic TRP channels lack voltage-dependent opening and are activated by receptor-mediated signaling molecules and physical stimuli that include stretch. The ensuing influx of depolarizing cations through the TRP channels is proposed to open the voltage-gated L-type Ca^{2+} channels resulting

in Ca^{2+} influx. Other depolarizing stimuli also open the L-type Ca^{2+} channels that often are vital to SMC contraction. These and other gene families of ion channels and exchangers constitute a large and highly diverse population of proteins that act in concert to regulate the levels of contraction and relaxation in the SMCs of the vasculature, GI tract, airways and other SMC-containing physiological systems. Scrutiny of different types of SMCs has revealed organ and site-specific patterns of cell excitability that are finely tuned to provide unique and localized electrical responses that collectively enable the entire organism to flourish.

ACKNOWLEDGMENTS

The authors were supported by a stipend award from National Center for Research Resources grant UL1RR029884 (N.D.D.), an American Heart Association –South Central Affiliate predoctoral fellowship grant 09PRE2250224 (S.V.K.) and grants R01 HL64806-10 and R01 HL0932526-02 from the National Heart, Lung and Blood Institute of the NIH (N.J.R.).

BIBLIOGRAPHY

Albarwani, S., Nemetz, L. T., Madden, J. A., et al. (2003). Voltage-gated K^+ channels in small rat cerebral arteries: molecular identity of the functional channels. *J Physiol, 551*, 751–763.

Albert, A. P., & Large, W. A. (2006). Signal transduction pathways and gating mechanisms of native TRP-like cation channels in vascular myocytes. *J Physiol, 570*, 45–51.

Bai, Y., & Sanderson, M. J. (2006). Airway smooth muscle relaxation results from a reduction in the frequency of Ca^{2+} oscillations induced by a cAMP-mediated inhibition of the IP_3 receptor. *Resp Res, 7*, 34–53.

Beech, D. J., Muraki, K., & Flemming, R. (2004). Non-selective cationic channels of smooth muscle and the mammalian homologues of Drosophila TRP. *J Physiol, 1559*, 685–706.

Berczi, V., Stekiel, W. J., Contney, S. J., & Rusch, N. J. (1992). Pressure-induced activation of membrane K+ current in rat saphenous artery. *Hypertension, 19*, 725–729.

Bramich, N. J. (2000). Electrical behavior of guinea pig tracheal smooth muscle. *Am J Physiol, 278*, L320–L328.

Brayden, J. E. (2002). Functional roles of K_{ATP} channels in vascular smooth muscle. *Clin Exp Pharmacol Physiol, 29*, 312–316.

Brayden, J. E., & Nelson, M. T. (1992). Regulation of arterial tone by activation of calcium-dependent potassium channels. *Science, 256*, 532–535.

Chen, T. T., Luykenaar, K. D., Walsh, E. J., Walsh, M. P., & Cole, W. C. (2006). Key role of Kv1 channels in vasoregulation. *Circ Res, 99*, 53–60.

Coetzee, W. A., Amarillo, Y., Chiu, J., et al. (1999). Molecular diversity of K^+ channels. *Ann NY Acad Sci, 868*, 233–285.

Cribbs, L. L. (2006). T-type Ca^{2+} channels in vascular smooth muscle: multiple functions. *Cell Calcium, 40*, 221–230.

Dietrich, A., & Gudermann, T. (2011). TRP channels in the cardiopulmonary vasculature. *Adv Exp Med Biol, 704*, 781–810.

Dietrich, A., Chubanov, V., Kalwa, H., Rost, B. R., & Gudermann, T. (2006). Cation channels of the transient receptor potential superfamily: their role in physiological and pathophysiological processes of smooth muscle cells. *Pharmacol Ther, 112*, 744–760.

Dietrich, A., Mederos y Schnitzler, M., Gollasch, M., et al. (2005). Increased vascular smooth muscle contractility in TRPC6$^{-/-}$ mice. *Mol Cell Biol, 25*, 6980–6989.

Dophin, A. C. (2009). Calcium channel diversity: multiple roles of calcium channel subunits. *Curr Opin Neurobiol, 19*, 237–244.

Epperson, A., Bonner, H. P., Ward, S. M., et al. (1999). Molecular diversity of Kv α- and β-subunit expression in canine gastrointestinal smooth muscles. *Am J Physiol, 277*, G127–G136.

Forrest, A. S., Hennig, G. W., Jokela-Willis, S., Park, C. D., & Sanders, K. M. (2009). Prostaglandin regulation of gastric slow waves and peristalsis. *Am J Physiol, 296*, G1180–G1190.

Gaudet, R. (2008). TRP channels entering the structural era. *J Physiol, 586*, 3565–3575.

Gokina, N. I., & Bevan, J. A. (2000). Histamine-induced depolarization: ionic mechanisms and role in sustained contraction of rabbit cerebral arteries. *Am J Physiol, 278*, H2094–H2104.

Gudermann, T., Mederos y Schnitzler, M., & Dietrich, A. (2004). Receptor-operated cation entry–more than esoteric terminology? *Sci Signal, 243*, pe35.

Guibert, C., Ducret, T., & Savineau, J. P. (2011). Expression and physiological roles of TRP channels in smooth muscle cells. *Adv Exp Med Biol, 704*, 687–706.

Gurney, A., & Manoury, B. (2009). Two-pore potassium channels in the cardiovascular system. *Eur Biophys J, 38*, 305–318.

Hai, C. M., & Murphy, R. A. (1990). Crossbridge phosphorylation and regulation of vascular smooth muscle contraction. *Am J Hypertens, 3*, 235–237.

Hibino, H., Inanobe, A., Furutani, K., Murakami, S., Findlay, I., & Kurachi, Y. (2010). Inwardly rectifying potassium channels: their structure, function, and physiological roles. *Physiol Rev, 90*, 291–366.

Hirota, S., Helli, P., & Janssen, L. J. (2007). Ionic mechanisms and Ca^{2+} handling in airway smooth muscle. *Eur Resp J, 30*, 114–133.

Hirst, G. D., & Edwards, F. R. (2001). Generation of slow waves in the antral region of guinea-pig stomach–a stochastic process. *J Physiol, 535*, 165–180.

Honda, K., & Tomita, T. (1987). Electrical activity in isolated human tracheal muscle. *Jap J Physiol, 37*, 333–336.

Horowitz, B., Ward, S. M., & Sanders, K. M. (1999). Cellular and molecular basis for electrical rhythmicity in gastrointestinal muscles. *Annu Rev Physiol, 61*, 19–43.

Kamei, K., Yoshida, S., Imagawa, J., Nabata, H., & Kuriyama, H. (1994). Regional and species differences in glyburide-sensitive K+ channels in airway smooth muscles as estimated from actions of KC 128 and levcromakalim. *Br J Pharmacol, 113*, 889–897.

Knot, H. J., Standen, N. B., & Nelson, M. T. (1998). Ryanodine receptors regulate arterial diameter and wall $[Ca^{2+}]$ in cerebral arteries of rat via Ca^{2+}-dependent K^+ channels. *J Physiol, 508*, 211–221.

Ledoux, J., Werner, M. E., Brayden, J. E., & Nelson, M. T. (2006). Calcium-activated potassium channels and the regulation of vascular tone. *Physiology, 21*, 69–78.

Lee, H. K., Leikauf, G. D., & Sperelakis, N. (1990). Electromechanical effects of endothelin on ferret bronchial and tracheal smooth muscle. *J Appl Physiol, 68*, 417–420.

Lombard, J. H., Eskinder, H., Kauser, K., Osborn, J. L., & Harder, D. R. (1990). Enhanced norepinephrine sensitivity in renal arteries at elevated transmural pressure. *Am J Physiol, 259*, H29–H33.

Lyford, G. L., & Farrugia, G. (2003). Ion channels in gastrointestinal smooth muscle and interstitial cells of Cajal. *Curr Opin Pharmacol, 3*, 583–587.

Montell, C. (2005). The TRP superfamily of cation channels. *Sci Signal, 272*, re3.

Moosmang, S., Schulla, V., Welling, A., et al. (2003). Dominant role of smooth muscle L-type calcium channel Cav1.2 for blood pressure regulation. *EMBO J, 22*, 6027–6034.

Morin, C., Sirois, M., Echave, V., Gomes, M. M., & Rousseau, E. (2007). Functional effects of 20-HETE on human bronchi: hyperpolarization and relaxation due to BK_{Ca} channel activation. *Am J Physiol, 293*, L1037–L1044.

Nelson, M. T., Patlak, J. B., Worley, J. F., & Standen, N. B. (1990). Calcium channels, potassium channels, and voltage dependence of arterial smooth muscle tone. *Am J Physiol, 259*, C3–C18.

Oonuma, H., Nakajima, T., Nagata, T., et al. (2000). Endothelin-1 is a potent activator of non-selective cation currents in human bronchial smooth muscle cells. *Am J Respir Cell Mol Biol, 23*, 213–221.

Quayle, J. M., Nelson, M. T., & Standen, N. B. (1997). ATP-sensitive and inwardly rectifying potassium channels in smooth muscle. *Physiol Rev, 77*, 1165–1232.

Sanders, K. M. (2008). Regulation of smooth muscle excitation and contraction. *Neurogastroenterol Motil, 20*(Suppl. 1), 39–53.

Sanders, K. M., Koh, S. D., & Ward, S. M. (2006). Interstitial cells of cajal as pacemakers in the gastrointestinal tract. *Annu Rev Physiol, 68*, 307–343.

Steedman, W. M. (1966). Micro-electrode studies on mammalian vascular muscle. *J Physiol, 186*, 382–400.

Tazzeo, T., Zhang, Y., Keshavjee, S., & Janssen, L. J. (2008). Ryanodine receptors decant internal Ca^{2+} store in human and bovine airway smooth muscle. *Eur Resp J, 32*, 275–284.

Tsvilovskyy, V. V., Zholos, A. V., Aberle, T., et al. (2009). Deletion of TRPC4 and TRPC6 in mice impairs smooth muscle contraction and intestinal motility in vivo. *Gastroenterology, 137*, 1415–1424.

Verkman, A. S., & Galietta, L. J. (2009). Chloride channels as drug targets. *Nat Rev Drug Discov, 8*, 153–171.

Watson, N., Magnussen, H., & Rabe, K. F. (1997). Inherent tone of human bronchus: role of eicosanoids and the epithelium. *Br J Pharmacol, 121*, 1099–1104.

Welsh, D. G., Jackson, W. F., & Segal, S. S. (1998). Oxygen induces electromechanical coupling in arteriolar smooth muscle cells: a role for L-type Ca^{2+} channels. *Am J Physiol, 274*, H2018–H2024.

Welsh, D. G., Morielli, A. D., Nelson, M. T., & Brayden, J. E. (2002). Transient receptor potential channels regulate myogenic tone of resistance arteries. *Circ Res, 90*, 248–250.

Wu, R. S., & Marx, S. O. (2010). The BK potassium channel in the vascular smooth muscle and kidney: α- and β–subunits. *Kidney Int, 78*, 963–974.

Chapter 45

Excitation–Contraction Coupling in Skeletal Muscle

Judith A. Heiny and Gerhard Meissner

Chapter Outline

I. SUMMARY

Excitation–contraction coupling in skeletal muscle is a fast signal transduction process by which depolarization of the sarcolemmal membranes is coupled to the opening of Ca^{2+} release channels on the sarcoplasmic reticulum (SR). This transduction occurs at specialized triad junctions and is mediated by two key proteins – the t-tubule dihydropyridine receptor (DHPR)/Ca^{2+} channel and the SR ryanodine receptor (RyR) channel. The DHPR and RyR1 associate with other junctional proteins to form a macromolecular complex which spans the triad junction and interacts to control RyR opening. This interaction produces a fast transient rise in $[Ca^{2+}]_i$ which activates the contractile proteins and results in muscle contraction.

II. INTRODUCTION

Skeletal muscle is activated to contract by a sequence of fast, electrically driven events that are collectively termed *excitation–contraction coupling* (EC coupling). EC coupling is a highly organized process of signal transduction that utilizes specialized membranes, membrane junctions and ion channels on both the exterior and interior of the cell. This chapter describes the cellular and molecular processes that mediate electrical excitation of the outer plasma membrane and transduces it into a signal for Ca^{2+} release from the intracellular sarcoplasmic reticulum (SR). The focus is on vertebrate fast-twitch skeletal muscle which is the best characterized.

Skeletal muscle is the fastest contracting of the three major muscle types and is related to cardiac and smooth muscle types evolutionarily and embryonically. The same two key proteins – a voltage-dependent calcium channel on the surface membrane (*dihydropyridine receptor* Ca^{2+} channel, DHPRs) and a Ca^{2+}-release channel (ryanodine receptor, RyR) in the sarcoplasmic reticulum – mediate excitation–contraction in cardiac, smooth and skeletal muscle. These two proteins share a high degree of homology but the different muscle types express different isoforms and combinations of these proteins. Importantly, each muscle type has evolved highly differentiated mechanisms of using these proteins to serve its specialized functions. Cardiac and smooth muscle primarily mediate enteric contractile processes that are under autonomic and humoral control,

Cell Physiology Sourcebook. DOI: 10.1016/B978-0-12-387738-3.00045-7

while skeletal muscle primarily mediates rapid, willed bodily movements that are under the control of the central nervous system. Consequently, the defining features of skeletal muscle activation are speed and voluntary control, as needed for fine control of body movement.

III. OVERVIEW OF EC COUPLING

The sequence of EC coupling in a vertebrate fast-twitch skeletal muscle fiber is shown in Fig. 45.1. Activation begins when an action potential from a *motor neuron* arrives at the *neuromuscular junction* and causes the neurotransmitter *acetylcholine* (ACh) to be released into the postsynaptic clefts (see chapter on synaptic transmission). The opening of AChRs produces a local depolarization, termed the *end-plate potential*, which brings the postsynaptic membrane to threshold potential for exciting an action potential (see chapter on synaptic transmission). The action potential rapidly propagates the depolarization along the outer sarcolemma and into the fiber interior via a specialized system of transversely oriented tubular membranes (*transverse-tubules* or *t-tubules*). The transverse tubules are continuous with and invaginate transversely from the sarcolemma at periodic intervals to form a planar network. The t-tubules provide the conduit for the action potential to reach the fiber interior and also bring the outer membranes into close proximity with the internal *sarcoplasmic reticulum* (SR) at specialized intracellular junctions called *triads*. The triad junctions serve as a platform for assembling sarcolemmal calcium channels (DHPRs), SR Ca^{2+}-release channels (ryanodine receptors) and additional proteins into a macromolecular complex which spans the junctional gap and controls Ca^{2+} release from the SR. The DHPRs serve as the voltage-sensors in this process. DHPRs contain charged, intramembrane domains which move in response to the action potential depolarization; these molecular rearrangements, termed *charge movement*, in turn, drive a conformational change on the RyR1 which causes it to open. These concerted molecular interactions occur between cytoplasmic regions

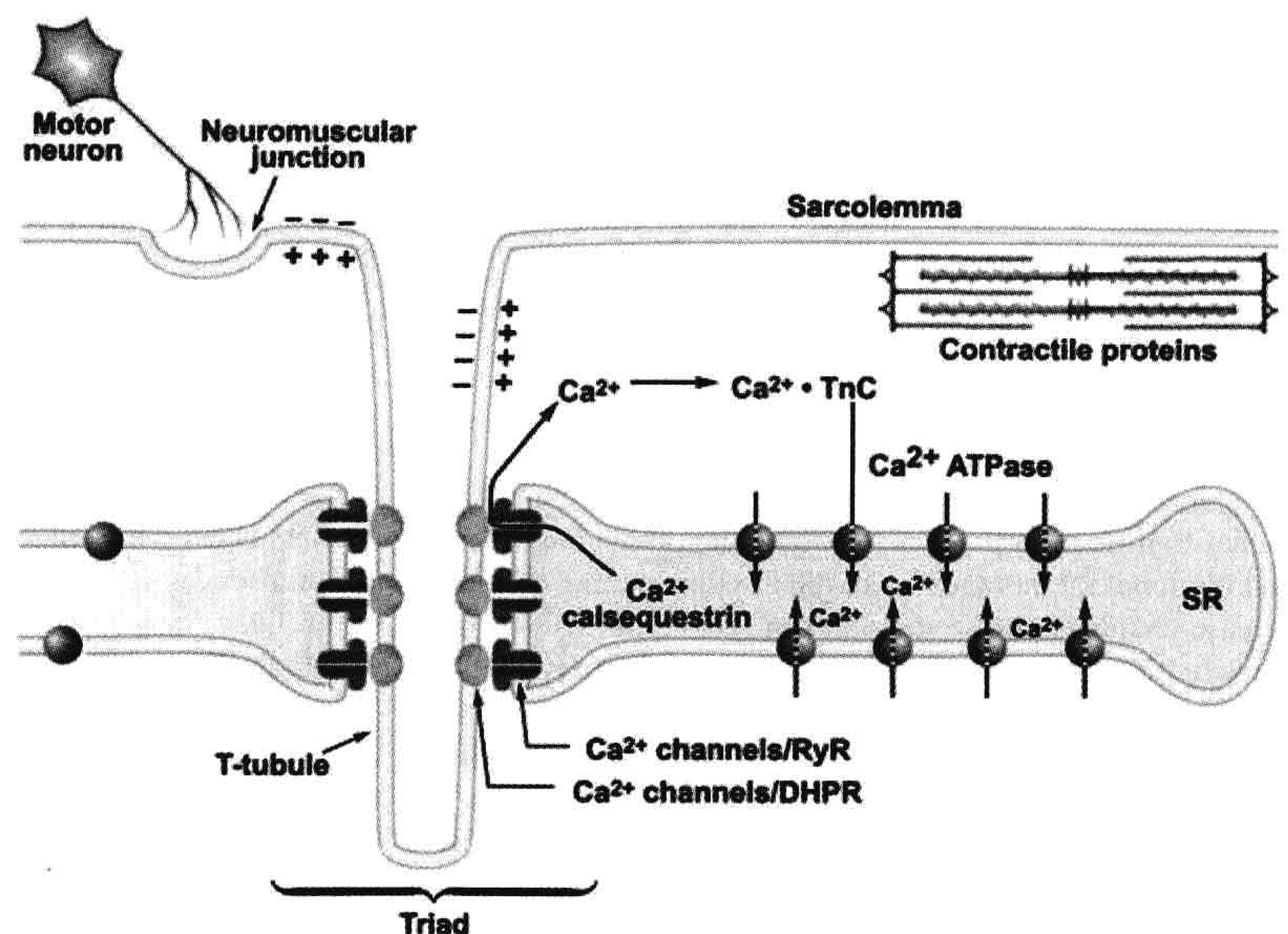


FIGURE 45.1 Sequence of excitation–contraction coupling in skeletal muscle.

of the DHPR and cytoplasmic domains of the RyR1 which face each other at the triad junction. In this way, the opening of an integral SR membrane calcium channel is gated by conformational transitions of a sarcolemmal, voltage-dependent calcium channel. Consequently, Ca^{2+} release in skeletal muscle remains under tight control of the plasma membrane potential.

The SR is a subcellular membrane compartment that is related evolutionarily to the endoplasmic reticulum. In skeletal muscle, it is a highly specialized for controlling cytosolic Ca^{2+}, $[Ca^{2+}]_i$. The SR actively sequesters Ca^{2+} in resting muscle via an ATP-dependent Ca^{2+} pump (SERCA), to maintain the intracellular Ca^{2+} concentration, $[Ca^{2+}]_i$, at submicromolar levels (typically $\approx 0.1\ \mu M$). Ca^{2+} is stored in bound form within the SR, complexed to the Ca^{2+}-binding protein *calsequestrin*. When a muscle is excited to contract, RyRs open and release this Ca^{2+} into the cytosol at rates approaching 100 μM/ms. This rapid Ca^{2+} release transiently raises cytosolic $[Ca^{2+}]_i$ to micromolar levels (typically 1–10 μM). The released Ca^{2+} ions diffuse and bind to *troponin-C* (TnC), the regulatory subunit of troponin, thereby removing troponin's inhibitory effect on the *contractile proteins*, actin and myosin, which shorten to generate force (see Chapter 46). Force output in skeletal muscle is directly proportional to cytosolic Ca^{2+} concentration (Fig. 45.2). Ca^{2+} release from the SR is brief and terminates quickly. As the t-tubule membrane repolarizes, DHPRs return to their inactive conformation and the RyR is itself inactivated by a Ca^{2+}-dependent mechanism. Multiple mechanisms return cytosolic Ca^{2+} to resting levels. The *Ca^{2+}-ATPase* of the SR membrane (SERCA) is stimulated rapidly to pump Ca^{2+} back into the SR. Cytosolic Ca^{2+}-binding proteins with rapid kinetics buffer Ca^{2+} transiently while the SERCA pumps return it to the SR.

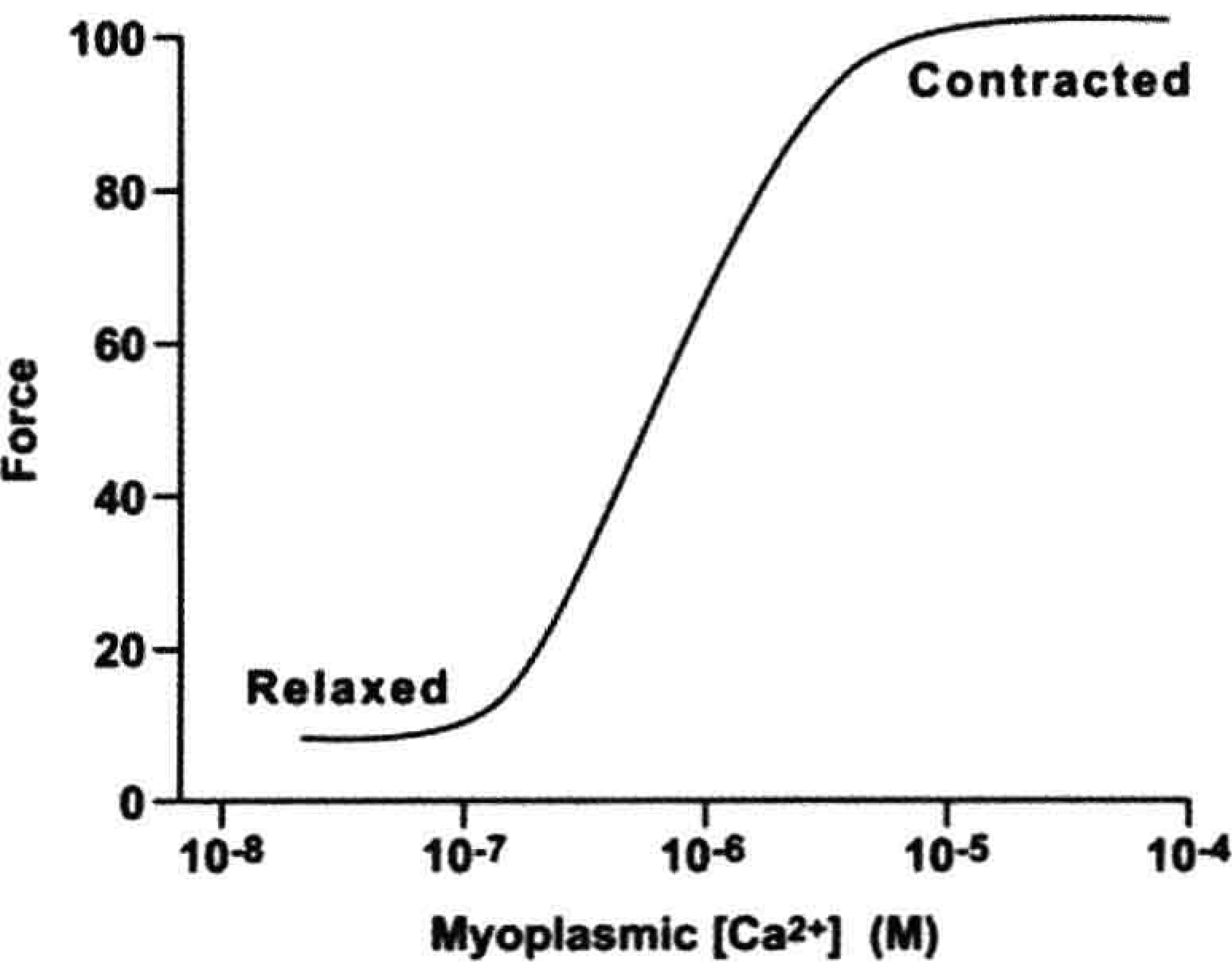


FIGURE 45.2 Relationship between force and myoplasmic Ca^{2+} concentration.

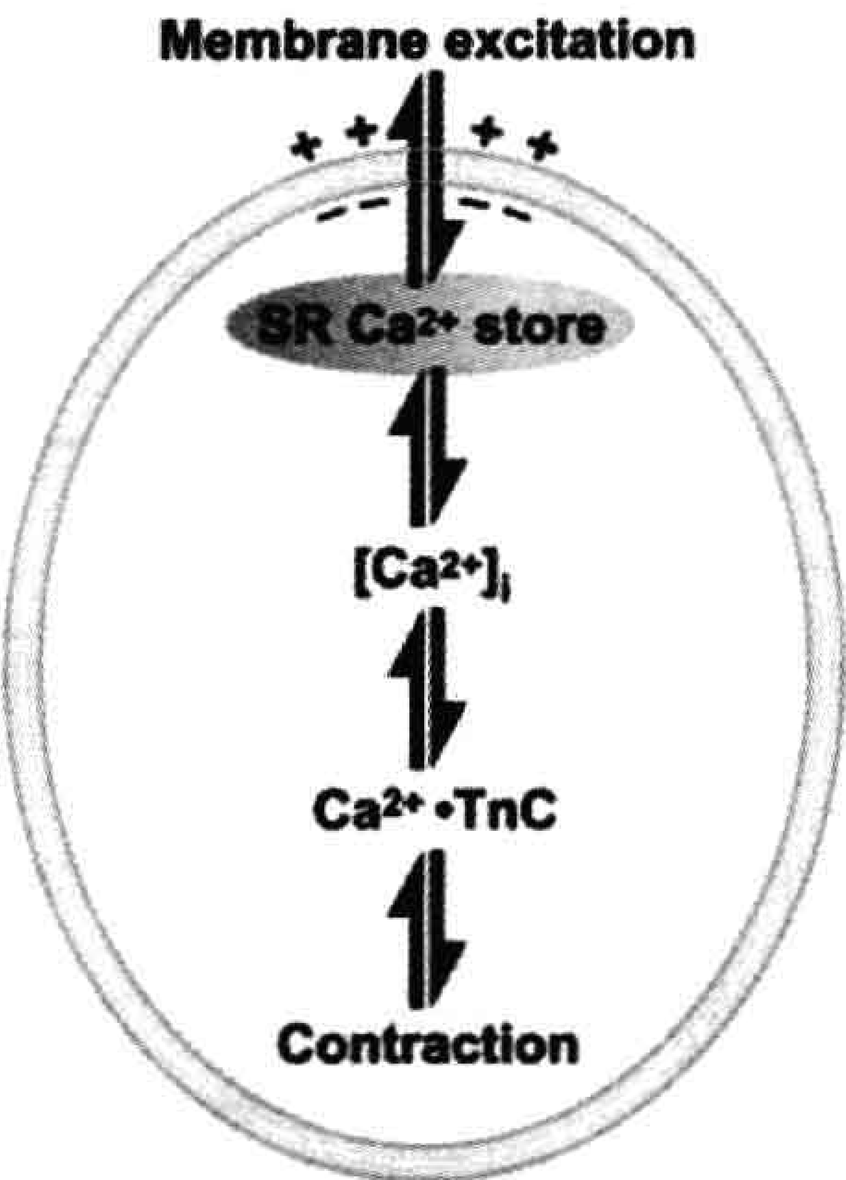


FIGURE 45.3 A rise in cytosolic $[Ca^{2+}]$ links membrane excitation to activation of contractile proteins.

Some Ca^{2+} is also extruded extracellularly by active Ca^{2+} transporters and Ca^{2+} exchangers on the plasma membrane. Force terminates when cytosolic Ca^{2+} returns to resting levels. Thus, cytosolic $[Ca^{2+}]_i$ is the central link between membrane excitation and activation of the contractile proteins (Fig. 45.3). Contraction is inhibited at low resting Ca^{2+} levels, and proceeds when Ca^{2+} is elevated transiently in response to membrane excitation.

IV. SPEED OF SKELETAL MUSCLE ACTIVATION

Activation of skeletal muscle is extremely rapid, occurring in milliseconds. This speed is remarkable given that skeletal muscle fibers are among the largest of mammalian cells. Skeletal muscle fibers are multinucleated cells that form during embryogenesis by fusion of myoblasts. They have a cylindrical shape with diameters from 30 to 150 μM and lengths from millimeters to centimeters. To produce effective mechanical force, the contractile proteins in all regions of a muscle fiber must shorten simultaneously. This synchronous activation is achieved by the propagating action potential which spreads the depolarization along the sarcolemma and into the transverse tubules within milliseconds, and by the anatomical configuration of the triad junctions which directly connect voltage-sensing DHPRs to the RyR Ca^{2+} release channels. Figure 45.4 and Table 45.1 show the relative timing and durations of key events in excitation contraction coupling for amphibian and mammalian muscle. The entire process, from membrane excitation to RyR1 opening, is complete within milliseconds. Overall, it operates largely as an on/off switch, insuring that Ca^{2+} release occurs rapidly and synchronously in response to each excitatory input from the motor nerve.

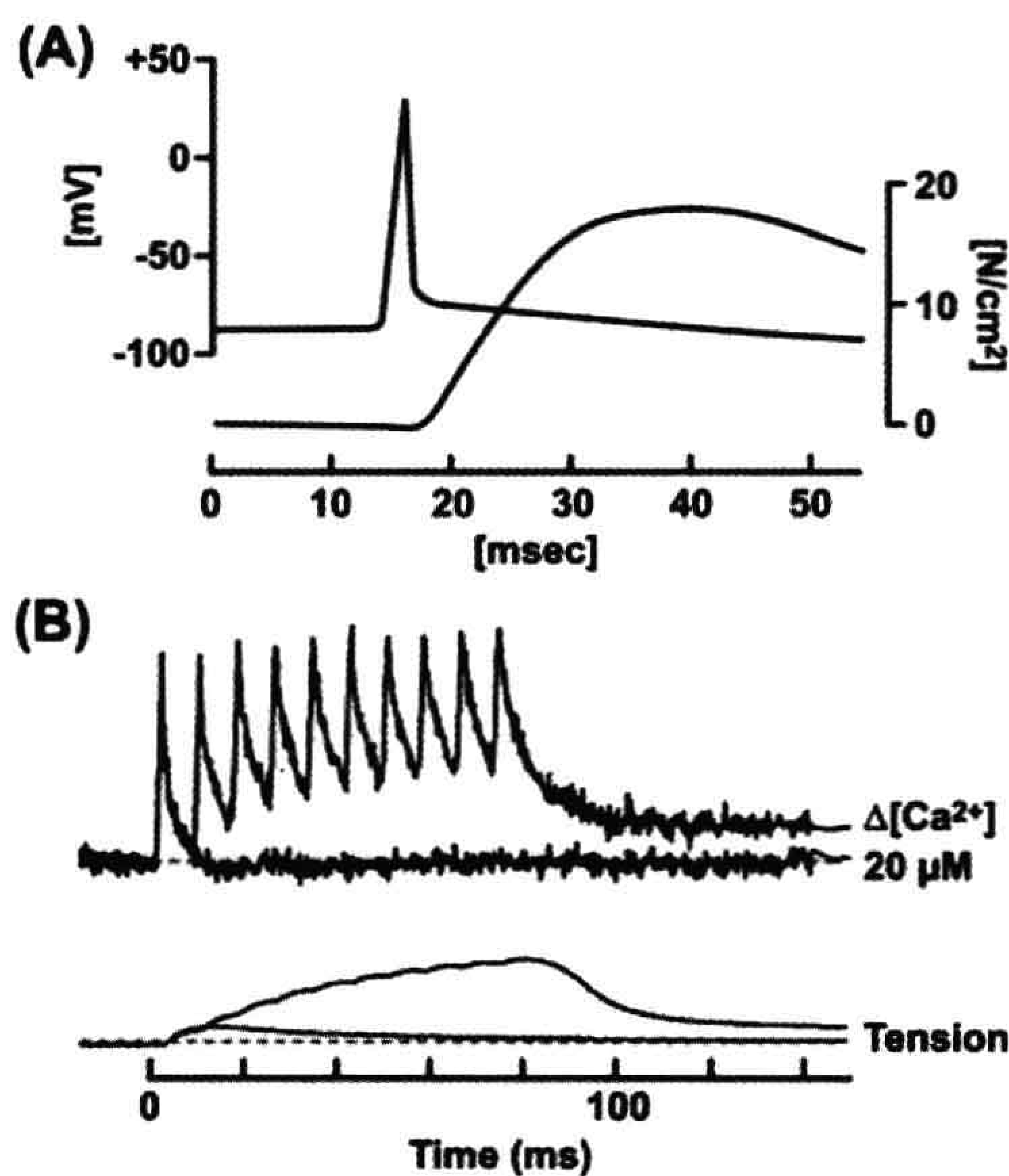


FIGURE 45.4 Speed of EC coupling in amphibian and mammalian skeletal muscles. (A) Time course of the action potential (top trace) and tension development (lower trace) in a fast-twitch frog skeletal muscle fiber at 18°C. *(Modified from Hodgkin and Horowicz, 1957.)* (B) Time course of EC coupling in a mouse skeletal muscle fiber at 37°C. The top traces record the cytosolic $[Ca^{2+}]_i$ change measured with a Ca^{2+} indicator dye. The lower trace shows tension. The fiber was stimulated at time zero with a single action potential and with repetitive action potentials at high frequency, to simulate a muscle tetanus. *(Reproduced from The Journal of General Physiology, 1996, 108, 455–469 by copyright permission of The Rockefeller University Press.)*

V. MEMBRANE ARCHITECTURE OF EC COUPLING

As noted, the outer and intracellular membranes of skeletal muscle are highly organized to achieve rapid communication between the extracellular sarcolemma and the interior SR membrane (Franzini-Armstrong and Jorgensen, 1994; Franzini-Armstrong and Protasi, 1997). Figure 45.5 illustrates the three-dimensional architecture of the sarcolemma, t-tubules, triad junctions and SR membranes of a fast-twitch frog skeletal muscle fiber and their physical relationship to the contractile proteins. The t-tubules comprise the majority of the sarcolemma membrane, representing 50–80% of the plasma membrane area (Peachey, 1965). They invaginate from the sarcolemma in a transverse plane approximately twice every 1–2 μM (or, at two planes per sarcomere in mammalian muscle). Within this plane they branch extensively to form a planar network that covers the entire cross-section of the muscle fiber (Fig. 45.6). This geometry insures that the Ca^{2+} binding sites on TnC are less than a few tenths of a micron diffusion distance from the Ca^{2+} release channels. Up to 80% of the tubular membrane area forms triad junctions with the SR (Peachey, 1965, Dulhunty, 1984). In mammalian skeletal muscles, two planes of transverse tubules form in each sarcomere, at the A-I bands.

The specific positioning of skeletal-type DHPRs in relation to RyR molecules at the triad junction allows the two channels to interact during excitation–contraction coupling (Fig. 45.7). The t-tubule and SR membranes flatten and face each other across a narrow gap of about 15 nm. RyR1s assemble on the junctional surface of the terminal cisternae in an ordered array of two rows with a center-to-center spacing of about 30 nm. Each RyR1 is a tetramer composed of four identical subunits. The RyRs are extremely large molecules (≈5000 amino acids and ≈560 kDa) of approximately 29 × 29 × 12 nm size. An intramembrane region of RyR1 inserts into the SR membrane and a large cytosolic domain extends across the junctional gap and associates with cytosolic domains of the DHPR. Viewed from above, the cytosolic domains of RyR1 roughly resemble a double row of quatrefoil-shaped proteins which interlock with each other in a precisely ordered array. In side view, the RyR1 tetramer assumes

TABLE 45.1 Duration of Key Steps in the Activation of Fast-Twitch Skeletal Muscle

EC Coupling Steps	Duration[a] (ms)
Action potential propagation along sarcolemma	5–10
Action potential propagation to center of fiber along t-tubules	≈0.7
Signal transduction at triad junction, from t-tubule depolarization to activation of RyR on SR	≈0.5
Peak rate of Ca^{2+} release to peak Ca^{2+} binding to TnC (start of tension)	2–3
Peak myoplasmic Ca^{2+} change to peak tension	15–25

[a]*Durations were calculated for a hypothetical frog fiber of 50 μm diameter and 5 cm length, having a central end-plate. Literature values for conduction velocity and duration of intermediate steps (Gonzales-Serratos, 1971; Vergara and Delay, 1986; Jong et al., 1996) were adjusted to 18°C.*

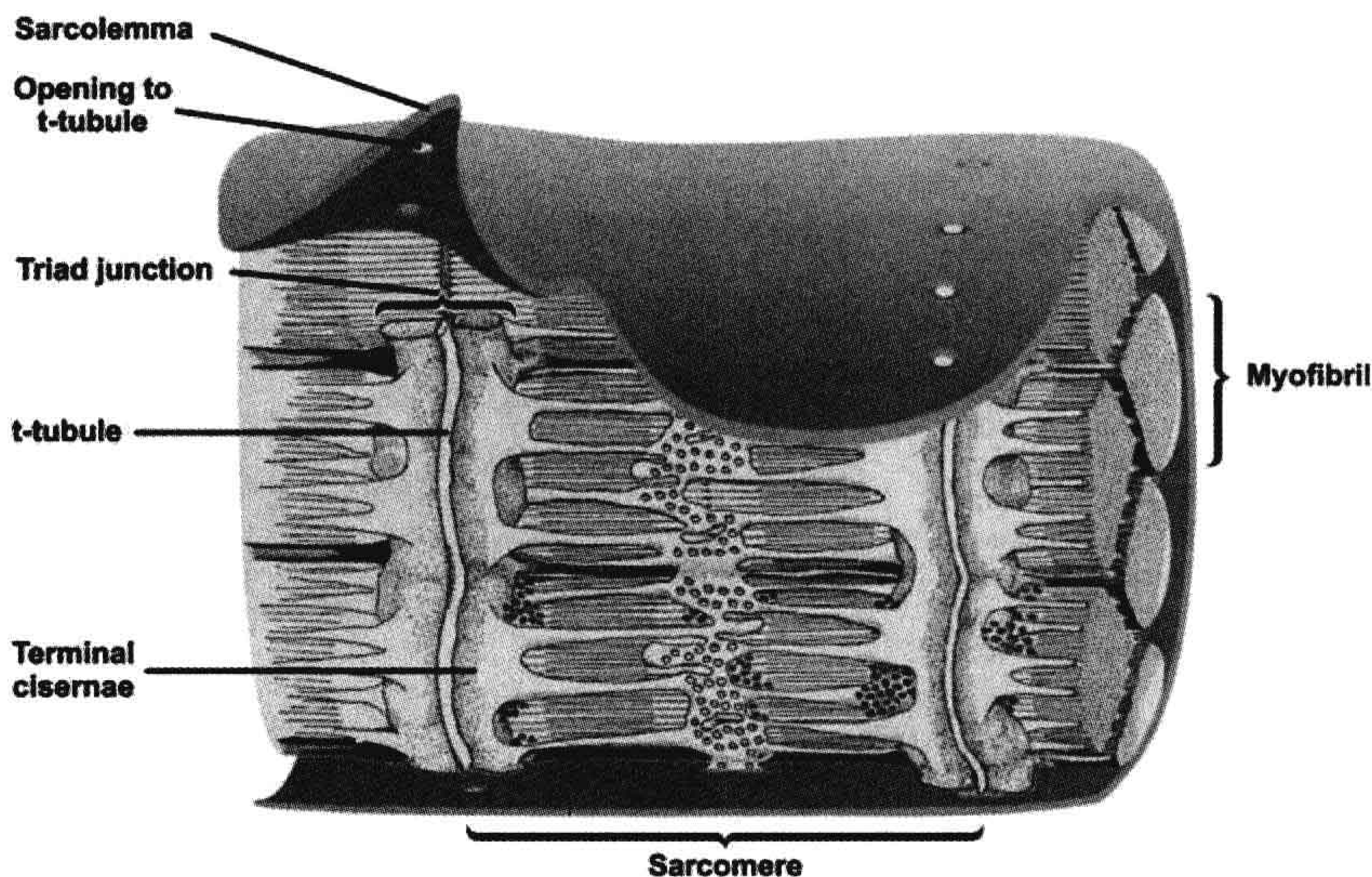


FIGURE 45.5 Three-dimensional reconstruction of a longitudinal section of a skeletal muscle fiber from the frog. The sarcolemma surrounds bundles of contractile proteins called myofibrils. Transverse tubules (t-tubules) invaginate from the sarcolemma in a plane at periodic intervals. The t-tubules form triad junctions with the SR along most of their length. At the triad junctions, the longitudinally oriented SR membranes widen into sacs called terminal cisternae, which closely oppose the t-tubules and contain the Ca^{2+} release channels/RyRs. The terminal cisternae are positioned near the activating Ca^{2+} sites on TnC. The functional unit of force generation is the sarcomere, consisting of overlapping actin and myosin filaments anchored at each end. The longitudinally oriented tubular regions of SR contain the Ca^{2+}-ATPase which takes up released Ca^{2+} all along the sarcomere. *(Reproduced from The Journal of Cell Biology, 1965, 25, 209–232 by copyright permission of The Rockefeller University Press.)*

a mushroom shape with a large extracellular domain and a smaller transmembrane domain that contains the Ca^{2+}-conducting pore (see Section VII below). Every alternate RyR1 associates with a cluster of four DHPRs, termed a *tetrad* (shown here as small blue spheres), i.e. each DHPR in a tetrad interacts with one of the four subunits of RyR1 and every other RyR1 is not directly associated with a tetrad of DHPRs. The DHPR tetrads are arranged in a pattern approximately corresponding to the four outer corners of the cytosolic spheres of the RyR. The outline of the DHPR tetrad is larger than the outline of the RyR1 tetramer and this may explain why tetrads associate only with alternate RyR1s. In non-mammalian muscle, a second ryanodine receptor isoform, RyR3 is present on peripheral regions of the SR junctional membrane. RyR3s do not associate with DHPRs.

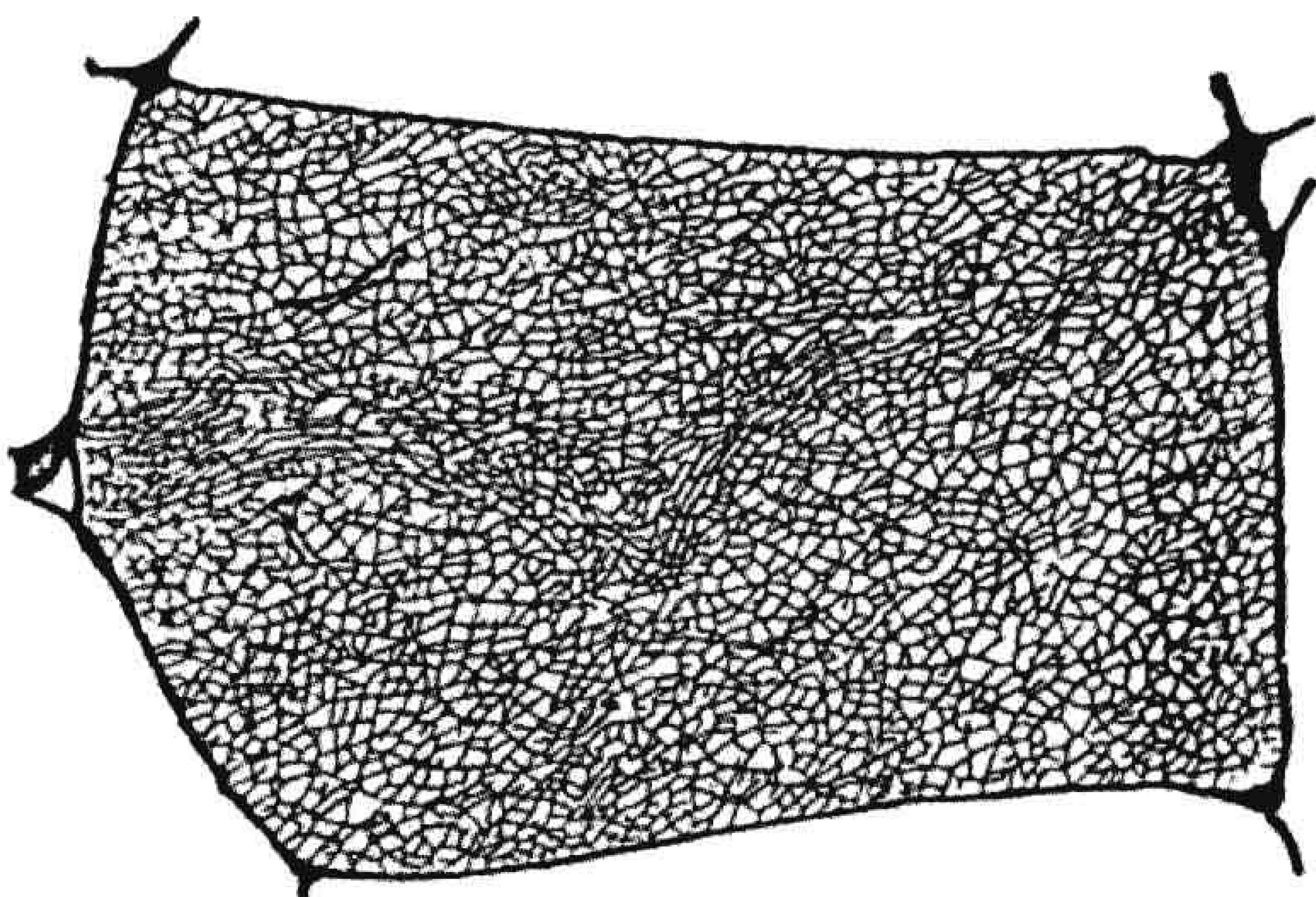


FIGURE 45.6 Reconstruction of the t-tubule network in one cross-sectional plane through a single frog twitch muscle fiber. The reconstruction was made from electron micrographs of transverse serial slices of a muscle fiber perfused with the electron-dense and membrane-impermeant molecule peroxidase, which diffused into the t-tubules. *(From Peachey and Eisenberg, 1978.)*

Figure 45.7 is based on a fish skeletal muscle fiber. A similar arrangement of tetrads is suggested in triads and peripheral couplings of other skeletal muscles from the frog, rat, chicken, mouse and human (Franzini-Armstrong and Jorgensen, 1994). Variations on this structure can occur in different species. These include *dyads*, in which a junctional region of terminal cisterna is opposed to a single short segment of t-tubule, and *peripheral couplings*, in which a junctional region of terminal cisterna is opposed to an approximately circular invagination of the surface membrane. Triads, dyads and peripheral couplings are structurally and functionally equivalent. Each is the intracellular site at which DHPRs and RyR1s interact to control Ca^{2+} release from the SR.

The triad junction has a strong structural integrity. Early studies demonstrated that purified fractions of t-tubule membrane could form junctions with SR membranes and that triad fractions could be isolated intact, despite stringent

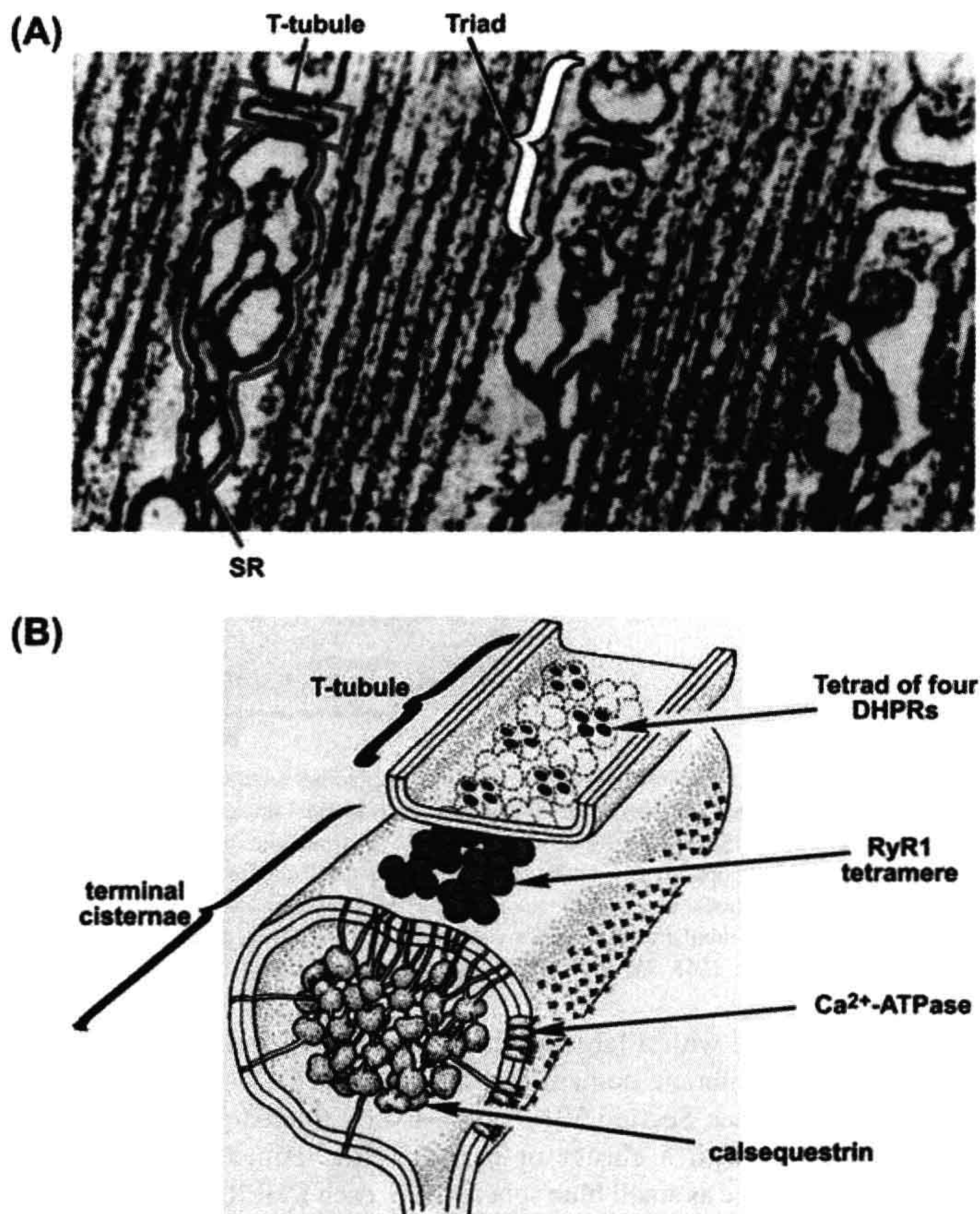


FIGURE 45.7 (A) Electron micrograph showing triad junctions in a longitudinal section through a fish skeletal muscle. Each t-tubule (outlined in red) is flanked on both sides by terminal cisternae of the SR (outlined in green). Contractile proteins are oriented longitudinally. The RyR1s appear as dense electron opaque material between the gap and were initially named "foot proteins" because of this appearance *(From Franzini-Armstrong and Peachey, 1981.)* (B) Three-dimensional reconstruction of a triad showing the spatial organization of the junctional membranes, DHPRs and RyRs. The t-tubule (TT) flattens and apposes a region of SR across a gap of 12–15 nm. RyR1 Ca^{2+} release channels (red) in the SR align in a double row with a skewed spacing such that each RyR1 makes multiple contact points with adjacent RyR1s. A tetrad of four DHPRs (blue) in the TT couples to every *other* RyR1. Non-mammals, such as frog and fish, have a second, RyR3 (green), isoform which is localized at the periphery of the SR membrane at the triad junction. RyR3 isoforms are not associated with TT tetrads (red). *(Reproduced with permission from Felder and Franzini-Armstrong, 2002.)*

fractionation procedures (Caswell et al., 1979). Such strong protein–protein associations at the triad junction are required to preserve the structural integrity of the triad junction as it sustains the strong forces of contraction.

VI. THE DHPR PROTEIN

The skeletal muscle DHPR is a voltage-gated Ca^{2+} channel ($Ca_V1.1$) belonging to the voltage-dependent superfamily of Ca^{2+} channels which share common structural and functional motifs (Yu et al., 2005; see also chapter on structure and mechanisms of voltage-gated ion channels). All Ca_V channels are multisubunit complexes composed of at least three subunits associated in an equimolar ratio: $\alpha 1$, $\alpha 2$-δ and β. The skeletal muscle channel has a fourth γ subunit. Multiple isoforms of the subunits exist and are distributed in a tissue-specific manner. The complete skeletal muscle calcium channel is a heteromultimeric complex consisting of $\alpha 1_s$ (212 kDa), $\alpha 2$-δ_1 (125 kDa), β_{1a} and γ_1 subunits (Fig. 45.8A). The individual subunits have been purified, sequenced, cloned and studied in expression systems. The $\alpha 1_s$ alone can reconstitute a functional Ca^{2+} ion current. However, all four subunits are required to form a functional skeletal muscle DHPR with properties of the native channel (Suh-Kim et al., 1996).

The primary $\alpha 1_s$ subunit contains the major functional domains of the channel. It is an integral membrane protein (212 kDa) that contains the pore-forming and voltage-sensing regions as well as the binding site for dihydropyridines and other calcium channel blockers. It is composed of four hydrophobic repeat domains – I, II, III and IV (see Fig. 45.8B) – which share a high degree of homology. Domains I–IV assemble to form a transmembrane protein with a central pore. Each domain consists of six transmembrane alpha-helical segments, denoted S1–S6, plus two smaller helices between S5 and S6 (pore helices) which fold into the membrane to line the pore. The S4 transmembrane helix within each domain forms the voltage sensor that moves in response to the action potential

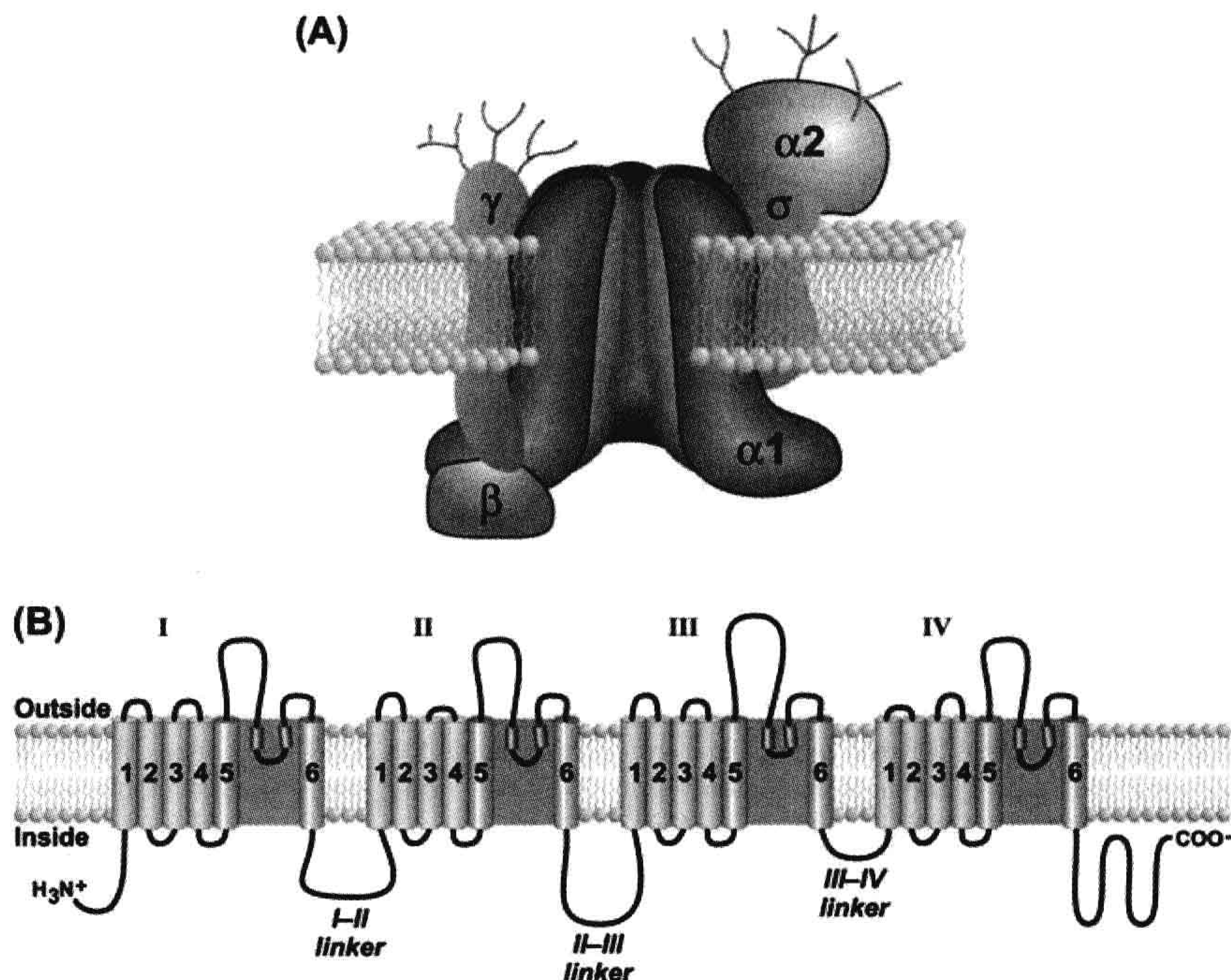


FIGURE 45.8 The skeletal muscle DHPR protein. (A) The skeletal muscle DHPR is composed of four subunits (α_{1s}, α_2-δ, β_{1a}, and γ). The α_{1s} subunit contains the key functional domains of the channel, including the voltage-sensing helices (S4) and the pore (S5–S6 extracellular domains). (B) The primary amino acid sequence of α_{1s} contains four homologous transmembrane domains (I–IV) connected together by cytosolic linker sequences (I–II, II–III and III–IV linkers). Each of the four domains is composed of six transmembrane helices (drawn schematically as cylinders) plus two shorter intramembrane helices that fold into the bilayer (S5–S6 pore helices) to form the ion conducting pore. The cytosolic linker between domains II–III is a key interaction domain with the RyR and is required for skeletal-type EC coupling. The β_{1a} subunit interacts with the I–II linker and with RyR1 and is also required for skeletal muscle type EC coupling.

depolarization. The S4 alpha helix is highly charged, containing a positively-charged residue on every third amino acid. Upon depolarization, all four S4 helices move in a cooperative fashion to activate the DHPR and, in turn, allosterically activate a coupled RyR1. Movement of the intramembrane S4 helices generates the macroscopic charge movement currents that are detected electrically during EC coupling (Schneider and Chandler, 1973). Domains I–IV are connected at the cytosolic face by segments of more hydrophilic amino acids (denoted I–II, II–III and III–IV linkers). The cytosolic region between domains II and III (II–III linker) plays a critical role in interactions with RyR1. The I–II linker also plays an essential role in EC coupling because it is the site for interaction with the β_{1a} subunit which is required for EC coupling (see Section VIIIC; below). The $\beta 1_a$ subunit is a smaller cytoplasmic protein (58 kDa) that associates specifically with the skeletal alpha isoform at an interaction domain on the I–II cytoplasmic linker. The $\alpha 2$-δ_1 subunit (125 kDa) may participate in membrane targeting and anchoring, The γ_1 subunit is a small glycosylated membrane protein (25 kDa) that associates with the skeletal $\alpha 1_s$ isoform but not with heart or brain alpha subunits and may play a regulatory role.

The skeletal muscle Ca^{2+} channel is capable of functioning both as a voltage sensor for EC coupling and as a Ca^{2+} ion channel. However, as a Ca^{2+} channel it has a low probability of opening and is characterized by high-voltage activation, brief openings and small single-channel currents. These features result in a very small, slow Ca^{2+} current through skeletal muscle DHPRs compared to the cardiac isoform (α_{1c}). Therefore, in skeletal muscle, movement of the S4 gating domains may be followed by slower, less steeply voltage-dependent conformational changes that open the pore. It is thought that the early rapid movement of S4 domains, and not the Ca^{2+} current that follows after a delay of several hundred milliseconds, has been exploited evolutionarily by skeletal muscle to control RyR1 activation. This small, slow Ca^{2+} influx through skeletal muscle DHPRs is not significant during a single

action potential. However, it may accumulate to measurable levels during a tetanus, when a skeletal muscle is activated repetitively at rates of 50–100 Hz to elicit a sustained contraction. In this case, Ca^{2+} entry may add to and perhaps modulate intracellular Ca^{2+} release from the SR (Dirksen, 2009).

VII. THE RYANODINE RECEPTOR

VIIA. Distribution, Structure and Isolation of RyRs

The release of Ca^{2+} ions from the endo/sarcoplasmic reticulum via *Ca^{2+}-release channels* is a key step in a wide variety of biological functions. The endo/sarcoplasmic reticulum Ca^{2+}-release channels are commonly referred to as *ryanodine receptors* (RyRs) to distinguish them from other intracellular Ca^{2+} channels. RyRs have been identified in non-vertebrate and vertebrates including flies, crustaceans, birds and amphibians. In mammals, there are three RyR isoforms. RyR1 is the dominant isoform in skeletal muscle. RyR2 is found in high levels in cardiac muscle. RyR3 was initially identified in brain but is expressed in many tissues including diaphragm, smooth muscle and brain.

The RyR/Ca^{2+}-release channels have been extensively studied with rabbit skeletal muscle as the source for RyRs. Fragmentation of the sarcoplasmic reticulum during homogenization and subsequent fractionation by differential and density-gradient centrifugation yields a *heavy SR* vesicle fraction which is enriched in Ca^{2+}-release channels and [^{3}H]ryanodine-binding activity and corresponds to the junctional region of the SR (*junctional SR*) (Meissner, 1984). Another important advance has been the isolation of triads, membrane fractions composed of a t-tubule segment sandwiched between two junctional SR vesicles (Fleischer and Inui, 1989). Microsomal membrane fractions enriched in ryanodine-sensitive Ca^{2+}-release channels have been also isolated from other excitable tissues, including cardiac muscle, smooth muscle and brain. In these cases, however, the membrane fractions are typically of a lower purity than those from skeletal muscle.

The RyRs are 2200 kDa multiprotein complexes that typically span the narrow gap where the SR and t-tubule (and plasmalemma) are within ≈15 nm of each other (Franzini-Armstrong and Protasi, 1997). The mammalian RyRs share ≈70% sequence homology, with the greatest homology in the carboxyl-terminal region. In all isoforms, the C-terminal portion of the protein contains the transmembrane domain. More recent studies suggest that six membrane spanning segments per RyR subunit are sufficient to form a channel. The remaining RyR amino acids form the large catalytic cytoplasmic *"foot"* structure. Experimental information on the structure of the RyRs has been mainly obtained by cryoelectron microscopy. Three-dimensional reconstruction of electron micrographs of frozen-hydrated RyR specimen shows dimensions of 29 × 29 × 12 nm for the large cytoplasmic assembly with a 7 nm length and 8 nm diameter for the transmembrane domain (Fig. 45.9).

The isolation of the RyRs has been greatly facilitated by the identification of ryanodine as a channel-specific ligand. Ryanodine is a neutral plant alkaloid that is obtained from the stems of the South American shrub, *Ryania speciosa*, and is composed of two major compounds: ryanodine and 9,21-didehydroryanodine (Fig. 45.10). Ryanodine is a highly toxic compound. Its pharmacological effects have been most clearly shown in muscle where, depending on muscle type and activity, it can cause either contracture or a decline in contractile force (Sutko and Airey, 1996). Ryanodine activates the channel at low (nanomolar) concentrations, but inhibits the channel at high (micromolar) concentrations (Fig. 45.11). Because the drug binds with high specificity and dissociates slowly from the

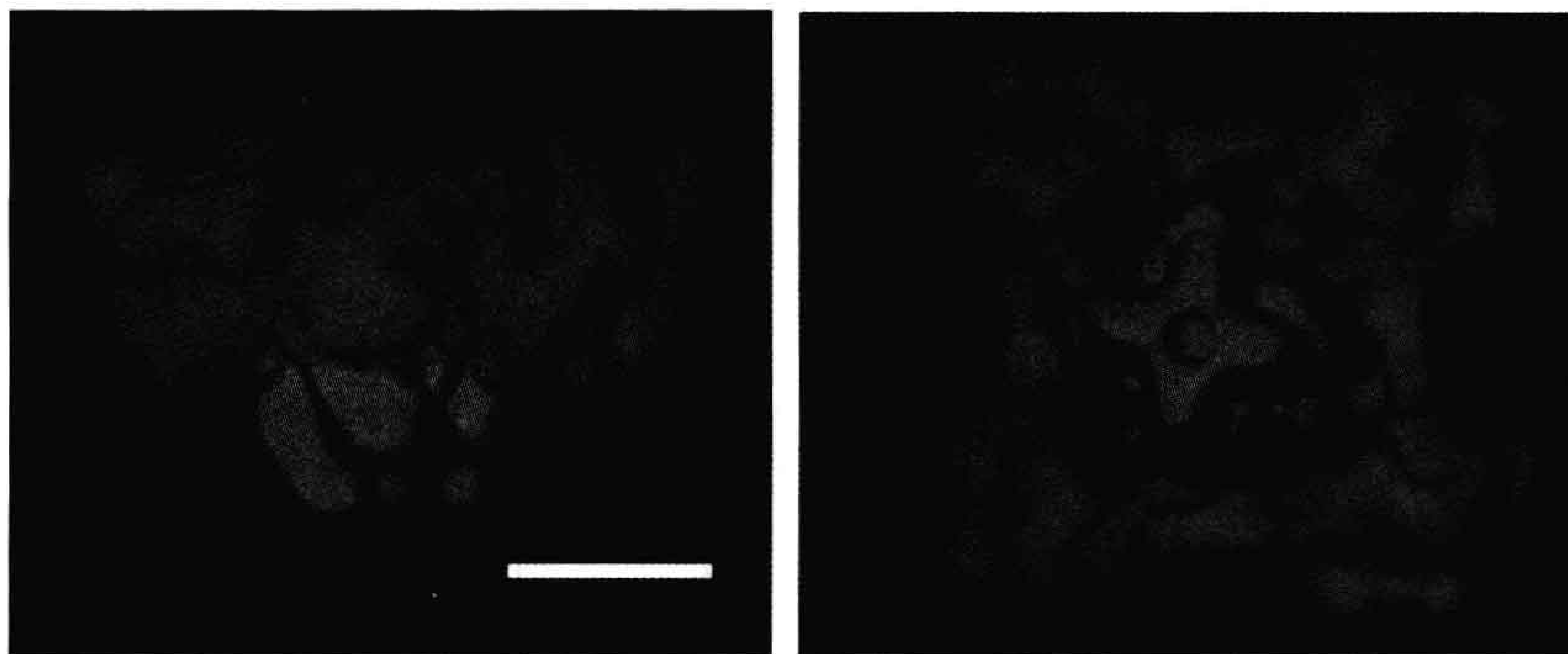


FIGURE 45.9 Dimensional reconstruction of RyR1. The cytoplasmic (green) and transmembrane (pink) domains are shown. Scale bar, 10 nm. *(With permission from M. Samso and T. Wagenknecht (1998) J Struct Biol. 121,172–180.)*

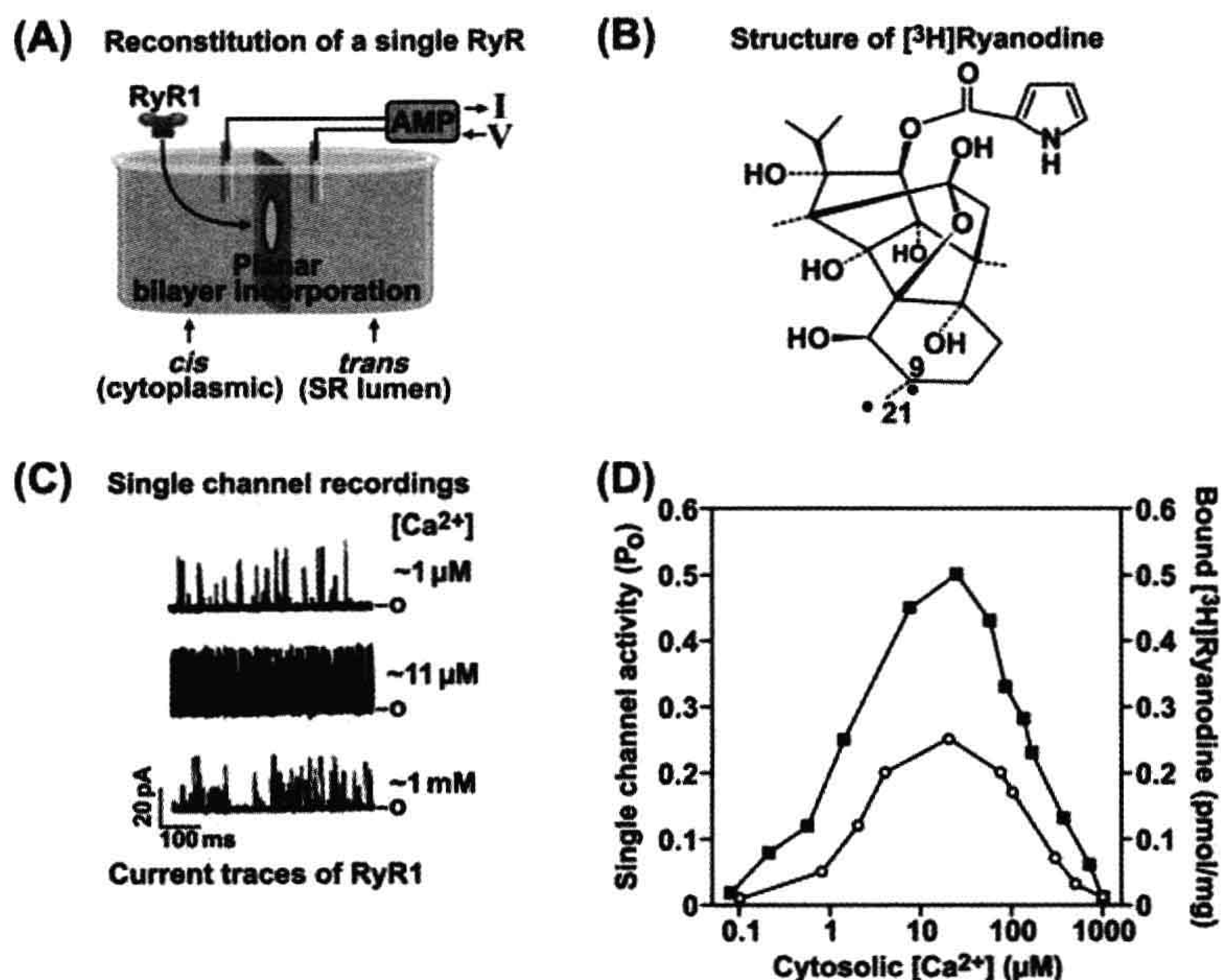


FIGURE 45.10 Measurement of RyR1 activity. (A) Planar lipid bilayer setup. (C) Three current traces of a single RyR1 ion channel recorded in symmetric 250 mM K^+ medium. Bars on right represent the closed (c) channel. The effects of three different *cis* (cytoplasmic) $[Ca^{2+}]$ on channel activity are shown. In the upper trace, the channel is minimally activated by 1 μM Ca^{2+}. Short, often poorly resolved events are seen. Channel activity is increased by increasing cytoplasmic Ca^{2+} from 1 to 11 μM and decreased when further increasing cytoplasmic Ca^{2+} to 1 mM. (D) Bimodal Ca^{2+} dependence of channel activity suggests the presence of high-affinity activating and low-affinity inhibitory Ca^{2+} binding sites. (B) Structure of $[^3H]$ryanodine. (D) $[^3H]$ryanodine binding measurements yield a Ca^{2+} dependence in good agreement with single channel measurements.

high-affinity site of the receptor (either membrane-bound or detergent-solubilized), $[^3H]$ryanodine has been found to be an ideal probe in the isolation of the RyRs from a variety of tissues and species.

The RyR was first isolated from striated muscle because its role in regulating free cytoplasmic Ca^{2+} levels was originally recognized in muscle and relatively large amounts of membranes enriched in $[^3H]$ryanodine-binding activity can be obtained from skeletal muscle and cardiac muscle. The membrane-bound Ca^{2+} release channels were solubilized in the presence of $[^3H]$ryanodine, using the zwitterionic detergent Chaps and high ionic strength (1.0 M NaCl); they can then be purified in essentially one step by density gradient centrifugation through a linear sucrose gradient. Fig. 45.12A shows the $[^3H]$ryanodine pattern on the sucrose gradients and sedimentation profile of the proteins associated with junctional SR vesicles isolated from rabbit skeletal muscle. A single peak of bound radioactivity, co-migrating with a small protein peak possessing an apparent sedimentation coefficient of 30 S, is observed in the lower half of the gradients. Binding to the small protein peak is specific since no radioactivity is present in the lower half of the gradients when the membranes are incubated with an excess of cold ryanodine. A sedimentation coefficient of 30 S revealed that the RyR is a very large protein complex.

The sucrose gradient centrifugation procedure is relatively simple and straightforward. The procedure results in efficient separation of the large 30 S RyR complex from the other solubilized smaller SR proteins because of its faster sedimentation rate. This method has been used to isolate a functional 30 S RyRs from several species and tissues including skeletal muscle, cardiac muscle, smooth muscle and brain.

SDS polyacrylamide gel electrophoresis shows that the 30 S protein complexes of mammalian skeletal and cardiac muscles are composed of a single major high molecular weight RyR polypeptide and isoform-specific low molecular weight immunophilin (FK506 binding protein) which migrate with apparent $M_r > 340\,000$ (see Fig. 45.12B) and $M_r \approx 12\,000$ (not visible on the gels in Fig. 45.12B), respectively. Cloning and sequencing of the complementary DNA of the mammalian skeletal and cardiac muscle RyR isoforms have revealed an open reading frame of about 15 kb and encoding RyR polypeptides of $M_r \approx 560\,000$. In contrast, the presence of two immunologically distinct high molecular weight RyR protein bands (corresponding to the mammalian RyR1 and RyR3) has been described for the main skeletal muscles of chicken, frog and fish (Sutko and Airey, 1996). The two RyR isoforms are present as discrete homo-oligomers in amphibian and avian skeletal muscles. The appearance of the RyR1 isoform alone in some very fast-contracting muscle of fish suggests that this isoform is selectively expressed when rapid contraction is required in non-mammalian vertebrate muscles (O'Brien et al., 1993).

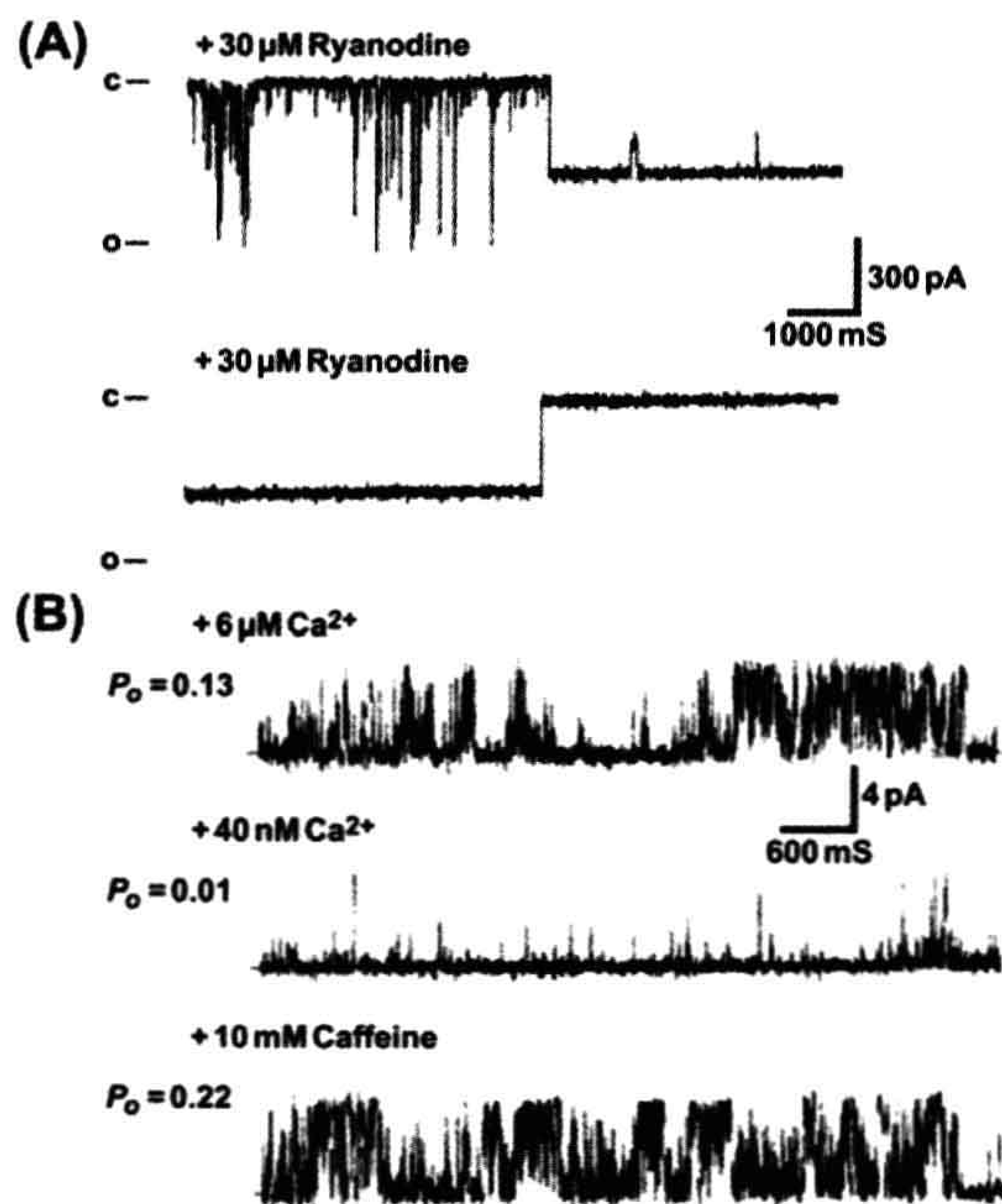


FIGURE 45.11 Effects of ryanodine and caffeine on single skeletal muscle RyRs. 30S purified channel complexes are reconstituted into planar lipid bilayers. (A) Upper trace shows appearance of subconducting channel state with open probability (P_o) of ≈ 1, following several minutes after the addition of 30 μM *cis* ryanodine. An additional, infrequent substate is also observed. Lower trace illustrates the sudden transition from the subconductance state to a fully closed state 1 min after addition of 2 mM *cis* (cytoplasmic) ryanodine *(from Lai et al., 1989 J Biol Chem. 264, 16776-16785)*. Note, relatively high ryanodine concentrations were used to shorten the time of binding to RyR1. (B) Single channel activity is with 6 μM free cytoplasmic Ca^{2+} (upper trace). Upper free Ca^{2+} is decreased to 40 nM by the addition of a Ca^{2+} buffer (EGTA) (middle trace). After the addition of 10 mM caffeine to the 40 nM free cytoplasmic Ca^{2+} medium (bottom trace). In contrast to ryanodine, caffeine activates the channel without changing its conductance. Bars on left represent the closed (c) channel. Po, channel open probability. *(From Rousseau et al., Arch Biochem Biophys. 267, 75–86, 1988).*

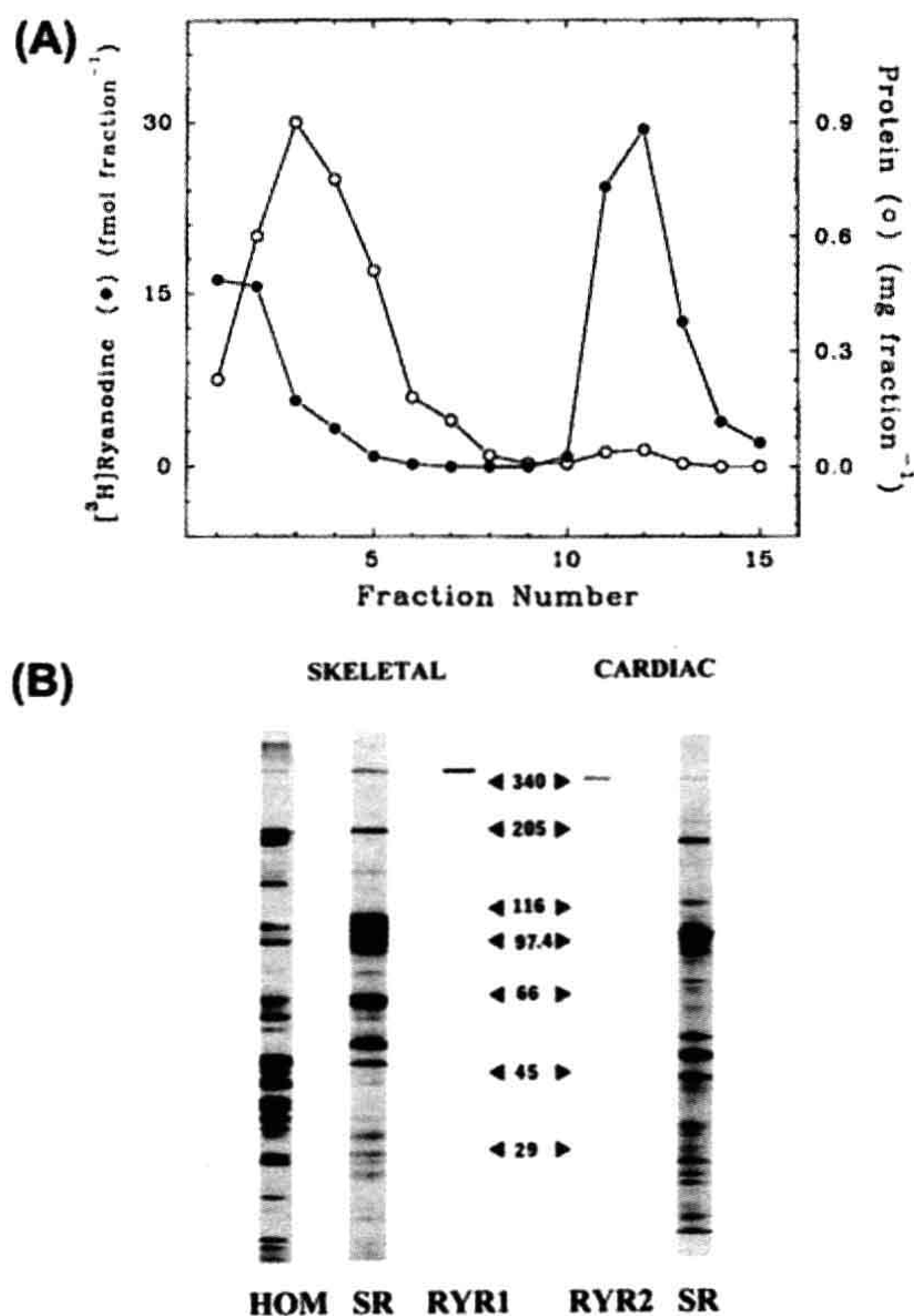


FIGURE 45.12 Sedimentation profile of RyR1 and SDS gel electrophoresis of rabbit skeletal muscle and canine cardiac RyRs. (A) Junctional skeletal muscle SR vesicles were solubilized in Chaps, centrifuged through a linear sucrose gradient and fractionated. Fractions were analyzed for protein and ^{3}H-radioactivity. Unbound [^{3}H]ryanodine and the majority of the solubilized proteins sedimented near the top of the gradient (fractions 1–6), whereas the [^{3}H]ryanodine-labeled RyR comigrated with a small protein peak to the bottom of the gradient (fractions 11–13) *(in modified form from Lai et al., Nature. 331, 315–319, 1988)*. (B) Silver stained SDS-polyacrylamide gel of whole rabbit skeletal muscle homogenate (HOM) and rabbit skeletal and canine cardiac muscle heavy SR membranes (SR) and purified RyRs (RYR1 and RYR2). Sizes of molecular weight standards are shown ($\times 10^{-3}$). *(From Meissner et al., 1989 Mol. Cell Biochem. 82, 59–65.)*

VIIB. RyR1 Pore Structure

RyRs have large conductances for both monovalent (≈ 750 pS with 250 mM K^+) and divalent (≈ 150 pS with 50 mM Ca^{2+}) cations, while maintaining divalent vs monovalent selectivity (P_{Ca}/P_K ≈ 7). Sequence comparison, cryoelectron microscopy and extensive mutagenesis and single channel studies indicate that the RyRs have a pore structure similar to that of K^+ channels whose structure is known (Fig. 45.13). In the RyRs, the residues between the two C-terminal membrane-spanning segments are luminally located and have a *pore helix* and an *amino acid motif* (GGGIG) that is similar to the *selectivity filter motif* (TV/IGYG) of K^+ channels whose structure is known. Mutagenesis shows that rings of negative charges in the luminal and cytosolic vestibules maintain the high rates of RyR1 ion fluxes (Xu et al., 2006). Several models of RyR ion permeation based on Eyring rate theory (Tinker et al., 1992), Poisson Nernst Planck-Density Functional Theory (Gillespie et al., 2005) and the solution structure of K^+ channels (Fig. 45.13) have been described.

VIIC. Regulation by Ca^{2+} and Endogenous Effectors

The in vitro function of RyR ion channels has been studied by measurement of *single channels* incorporated in planar

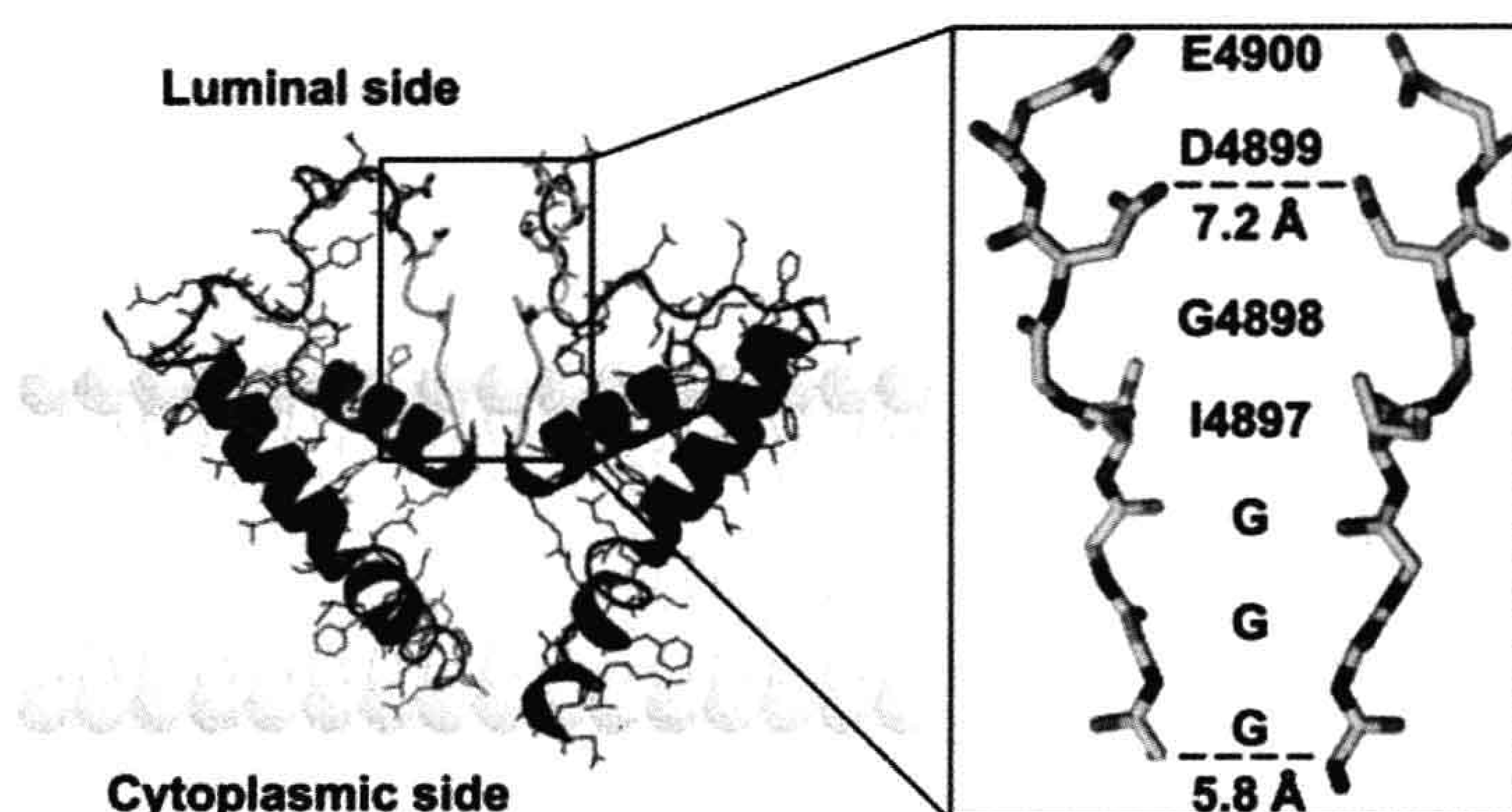


FIGURE 45.13 Pore model of RyR1. (Left panel) Two opposing RyR1 monomers (shown is only one of the six membrane spanning segments per monomer) in cartoon representation. The selectivity filter (4894GGGIGDE) is shown in yellow. (Right panel) Selectivity filter region of two opposing RyR1 monomers in stick representation. The sequence is shown along the path of the ions. *(From Ramachandran et al. PLoS Comput Biol. 5, e1000367, 2009.)*

lipid bilayers and *[^{3}H]ryanodine binding*. These studies have shown that RyRs are *Ca^{2+}-gated channels* that are activated by micromolar Ca^{2+} concentrations and inhibited by millimolar Ca^{2+} concentrations (see Fig. 45.10) (Lanner et al., 2010). Mg^{2+} inhibits RyRs by binding to high-affinity and low-affinity Ca^{2+} binding sites. ATP complexed with Mg^{2+} modifies regulation of RyRs by Ca^{2+} indicating that it is an allosteric modulator of Ca^{2+}-gated RyR activity. In addition to cytosolic Ca^{2+}, SR luminal Ca^{2+} regulates RyRs at several channel sites. Ca^{2+} binds to luminal channel sites and, by passing through the channel, accesses cytosolic Ca^{2+}-activation and inactivation sites.

VIID. RyR-Associated Proteins

A large number of junctional SR membrane proteins and cytosolic and SR luminal proteins have been reported to form a macromolecular complex with the RyRs.

Kinases and phosphatases that are part of the RyR1 and RyR2 multiprotein complexes include protein kinase A (PKA), Ca^{2+}/calmodulin-dependent protein kinase II (CaMKII) and protein phosphatase 1 and protein phosphatase 2A (Zalk et al., 2007). RyR1 has been reported to be phosphorylated at Ser2843. RyR2 is phosphorylated at Ser-2030 by PKA, at Ser-2809 by PKA and CaMKII (corresponding to Ser2843 in RyR1) and at Ser-2815 by CaMKII. Phosphorylation of RyRs by protein kinases has been suggested to result in leaky SR Ca^{2+} channels (see below).

Calmodulin (CaM) is a small, cytoplasmic Ca^{2+}-binding protein that regulates cellular activities including protein kinases and ion channels. RyRs interact with CaM in the absence and presence of Ca^{2+} (Balshaw et al., 2002). The Ca^{2+}-free and Ca^{2+}-bound forms of CaM bind to a highly conserved CaM-binding domain of RyRs. CaM inhibits the three mammalian RyR isoforms at micromolar Ca^{2+} concentrations. At submicromolar Ca^{2+} concentrations, RyR2 is also inhibited by CaM, but RyR1 and RyR3 are activated to different extents by CaM. Mutagenesis, peptide studies and cryoelectron microscopy suggest that Ca^{2+}-free and Ca^{2+}-bound forms of CaM bind to an overlapping region distal to the effector site (ion pore) (Lanner et al., 2010). This suggests that CaM exerts its effects allosterically over relatively long distances within the RyRs. To determine the physiological importance of CaM regulation of RyR2, a mutant mouse was generated with three amino acid substitutions in the CaM-binding site (Yamaguchi et al., 2007). Mice expressing only the mutant form of RyR2 have cardiac hypertrophy as early as 1 day after birth and die around 2 weeks after birth, which suggests that CaM inhibition of RyR2 is required for normal cardiac function in mice.

Other RyR associated proteins include S100A1, triadin, junctin, JP-45, junctate, juncophilin, homer, sorcin, selenoprotein 1 and calseqestrin.

VIIE. Pharmacology of RyRs

A large number of pharmacological reagents modulate the activity of the RyRs. Exogenous effectors found to affect RyR function include ryanodine (see Fig. 45.11A) and other ryanoids, caffeine (see Fig. 45.11B) and other xanthines, toxins, anthraquinones, phenol derivatives, dantrolene, local anesthetics and polycationic and sulfhyryl reacting reagents.

VIIF. RyRs and Muscle Disorders

Mutations in RyR1 give rise to muscle diseases, *malignant hyperthermia* (MH), *central core disease* (CCD) and *multiminicore disease* (MmD) (Lanner et al., 2010). MH is an inherited disease that causes a rapid rise in body temperature and muscle contraction when the affected person receives general anesthesia. MH-linked mutations were

initially mapped to the NH_2 and central domains; however, more recently identified MH mutations appear to be distributed throughout the entire RyR1 coding sequence. CCD is an autosomal dominant congenital myopathy leading to the formation of cores void of mitochondria and oxidative enzymes. In many cases, dominant RyR1 mutations linked to CCD localize to the COOH-terminal domain of the channel. Single channel measurements indicate that CCD mutants lose the ability to conduct Ca^{2+}. MmD is an autosomal recessive congenital myopathy leading to formation of multiple small areas of disorganized sarcomeres. MmD is a genetically heterogeneous disease that is linked to recessive mutations in RyR1 and selenoprotein 1, an RyR1-associated protein that is thought to maintain the receptors normal response to redox active molecules.

RyR2 mutations are associated with catecholaminergic polymorphic ventricular tachycardia and arrhythmogenic right ventricular cardiomyopathy (Lanner et al., 2010). A deficiency in SR lumenal cardiac calsequestrin and missense mutation D307H also result in imbalances of Ca^{2+} handling and catecholaminergic polymorphic ventricular tachycardia. Overexpression of CSQ2 results in severe cardiac hypertrophy in mice. Abnormal Ca^{2+} handling is also observed in mice that lack or overexpress RyR-associated proteins including triadin (Eltit et al., 2010) and junctin (Pritchard and Kranias, 2009).

Loss of the small 12 and 12.6 kDa FK506-binding proteins from RyR1 and RyR2 has been suggested to result in leaky Ca^{2+} channels (Zalk et al., 2007; Kushnir et al., 2010; Lanner et al., 2010). In failing hearts, PKA hyperphosphorylation of RyR2 has been reported to lead to removal of the FKBP12.6 subunit and increased channel activity. In skeletal muscle of animal models with heart failure and patients with heart diseases, exercise is linked to hyperphosphorylation, FKBP12 depletion of the skeletal muscle RyR1, increased RyR1 channel activity and decreased exercise capacity. However, other laboratories have failed to confirm this. In addition to PKA-mediated phosphorylation, mechanisms implicated in generation of "leaky" release channels include increased S-nitrosylation, oxidation and loss of protein phosphatases 1 and 2A and phosphodiesterase 4D from the RyR macromolecular complexes. A 1,4-benzothiazepine derivative, JTV519 (also known as K201), and the more specific derivative S107, have been reported to improve muscle function by stabilizing the RyR—FKBP complexes.

VIII. PHYSIOLOGICAL INTERACTIONS BETWEEN THE DHPR AND RyR1

At the triad junction, a unique intracellular signal transduction occurs whereby a voltage-gated Ca^{2+} channel on an extracellular membrane controls the opening of a separate Ca^{2+} channel on an intracellular membrane. The unique structure of the RyR1, with a Ca^{2+} channel domain embedded in the SR and a large cytosolic domain facing cytosolic regions of the DHPR, suggests that opening and closing of RyR1 could be remotely controlled by the DHPR. The essential steps in this coupling are: detection of the action potential depolarization by voltage-sensing DHPRs in the t-tubules, interactions between the DHPR and RyR1 leading to RyR1 channel opening and Ca^{2+} efflux from the SR.

VIIIA. Voltage Sensing

It was recognized early that EC coupling in fast skeletal muscles of higher vertebrates is directly controlled by membrane potential, without a requirement for extracellular Ca^{2+}. This contrasts with EC coupling in the skeletal muscles of some lower invertebrates and cardiac muscle, in which Ca^{2+} influx through sarcolemmal Ca^{2+} channels is absolutely required for contraction. In cardiac muscle, the Ca^{2+} that enters through the cardiac-specific DHPR ($\alpha 1_c$) functions as a second messenger to activate the cardiac ryanodine receptor isoform, RyR2. This process in cardiac muscle is termed *calcium-induced calcium release*. In a classic experiment, it was demonstrated that a frog skeletal muscle stimulated by action potentials is able to twitch continuously in the complete absence of extracellular Ca^{2+} (Armstrong et al., 1972). Similarly, voltage-clamp experiments demonstrated that a skeletal muscle fiber can develop tension provided only that the membrane is depolarized to a minimum potential and duration, termed the *mechanical threshold*. That is, when the Na^+, K^+ and Cl^- ion channels which mediate the action potential are blocked and/or their permeant ions are removed, all that is required to activate contraction in skeletal muscle is a suprathreshold change in membrane potential. A precise relationship between tension and membrane potential exists in skeletal muscle (Fig. 45.14); development of tension is steeply voltage-dependent in the range from −60 to −40 mV.

Subsequently, Schneider and Chandler (1973) discovered the presence in skeletal muscle membranes of mobile intramembrane charges whose movement could be detected electrically as a voltage-dependent dielectric current, termed *charge movement* (Fig. 45.15). This charge movement was steeply voltage-dependent in the same range of potentials as mechanical activation. Based on the similar kinetics and voltage dependence of charge movement and mechanical activation, they proposed that these gating currents reflected the movement of charged intramembrane domains of a molecule in the t-tubules that functioned as the *voltage sensor* for EC coupling. These measurements suggested that positively-charged regions of the DHPR undergo a net outward movement upon depolarization, away from RyR1. Therefore, they suggested that the voltage sensor might interact directly with a hypothetical Ca^{2+}-release channel on the SR to cause its opening. This mechanical or

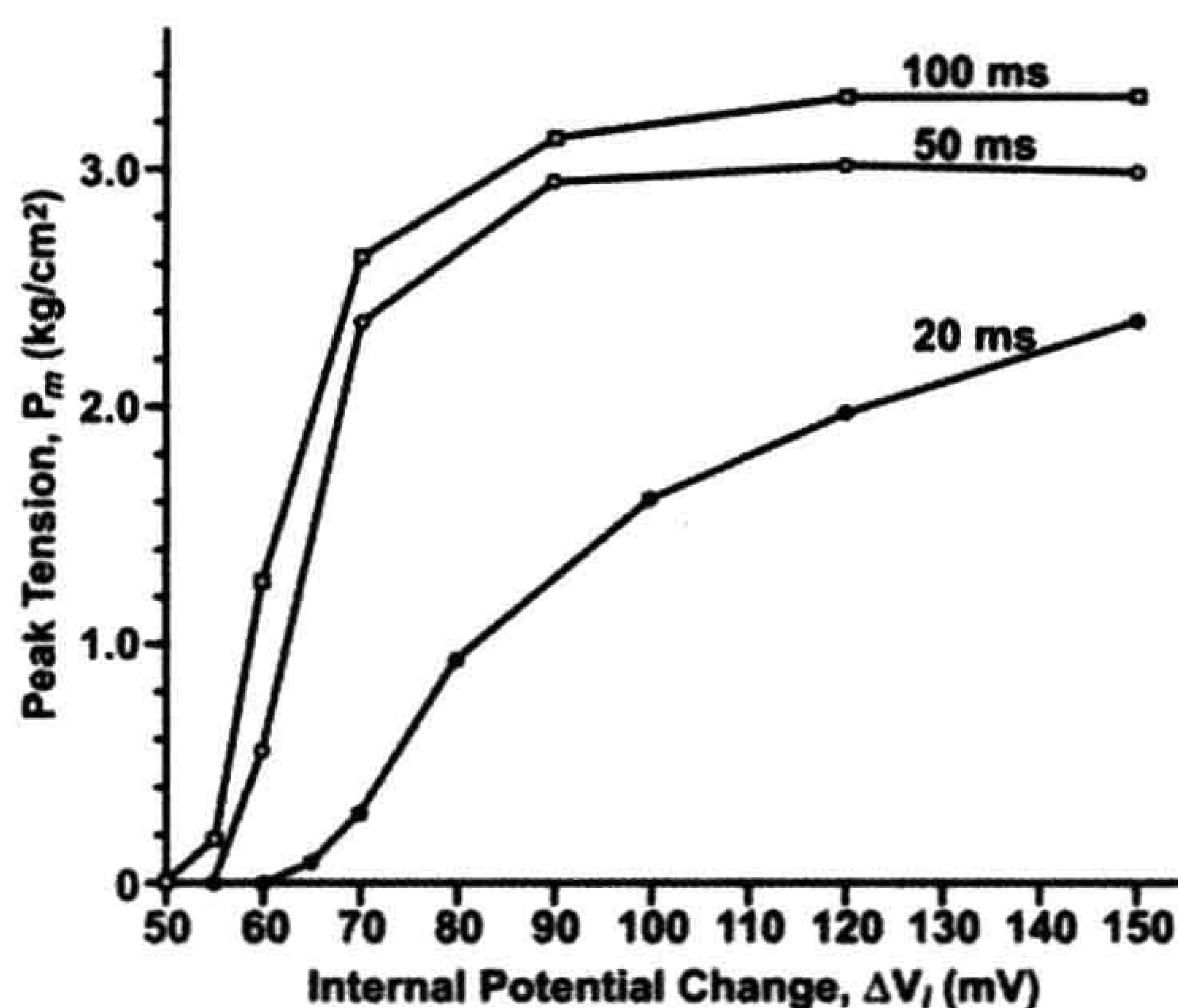


FIGURE 45.14 Voltage-dependence of tension in the absence of an action potential. The fibers were depolarized by holding the membrane potential constant for 20–100 ms with a voltage-clamp. Tension was measured simultaneously with a transducer attached to one tendon. *(Reproduced from The Journal of General Physiology, 1984, 84,133–154, by copyright permission of The Rockefeller University Press.)*

allosteric model of EC coupling, formulated before the proteins of the triad junction had been identified, has formed the framework for subsequent investigations into the nature of the coupling mechanism.

Several lines of evidence led to the identification of the voltage sensor as the DHPR/t-tubule Ca^{2+} channel (Rios and Pizarro, 1991, Schneider, 1994, Melzer et al., 1995). A definitive identification came following the cloning of the skeletal muscle Ca^{2+} channel (Tanabe et al., 1987) and its use in experiments on dysgenic mice (Adams and Beam,

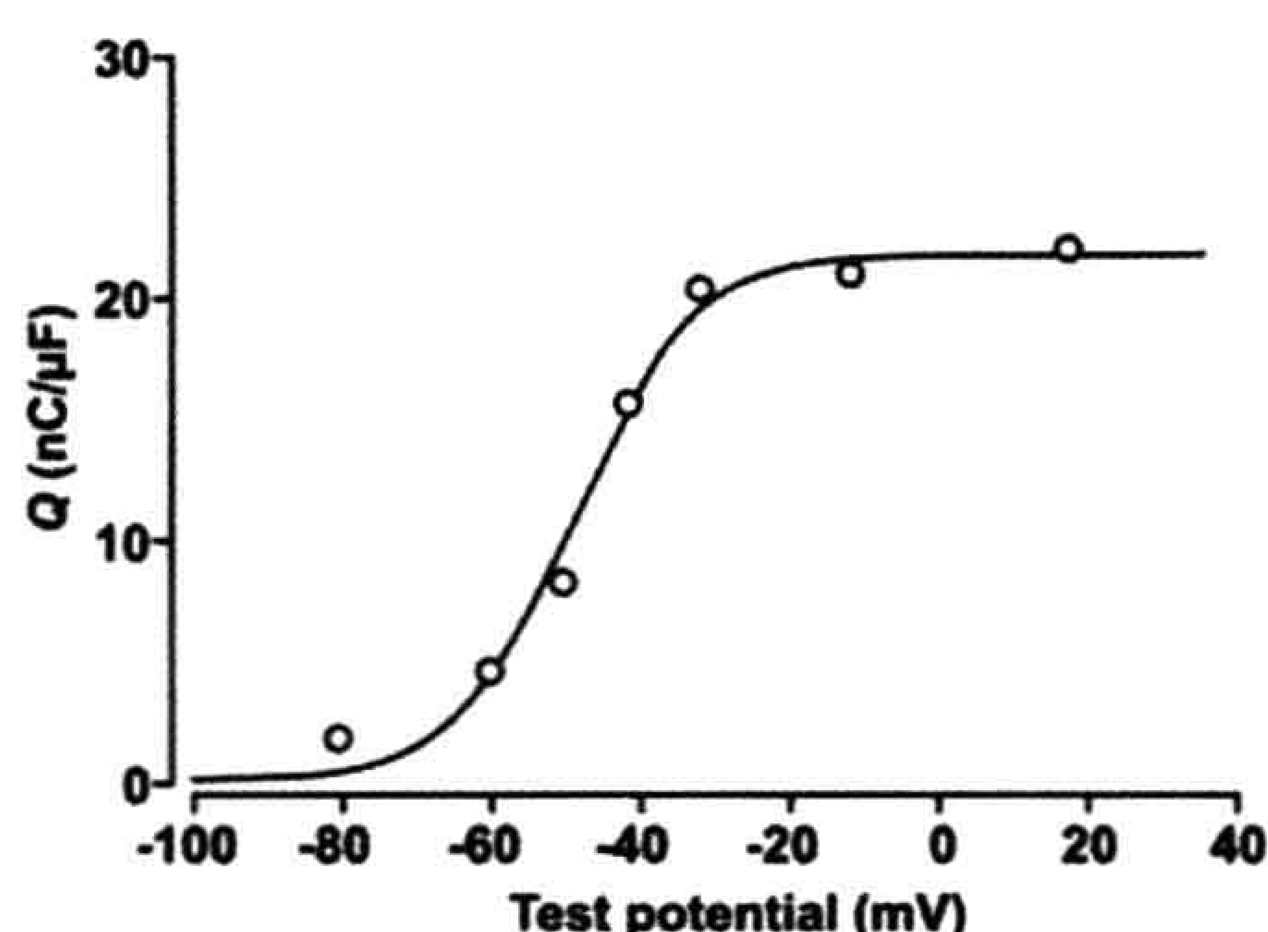


FIGURE 45.15 Voltage-dependence of charge movement (nC/µF vs membrane potential, mV). Charge moved at each potential was obtained by integrating the voltage-dependent capacity current, normalized to the fiber linear capacitance near the resting potential. Symbols represent the mean values of charge moved at the "on" and "off" of the pulse. The continuous curve is a fit of the data to a two-state Boltzmann function, with parameters: $V_{mid} = -47.7$ mV, $k = 8$ mV and $Q_{max} = 21.5$ nC/µF. *(From Chandler et al., 1976.)*

1990). Muscular dysgenesis is a lethal disorder arising from a single point mutation in the gene for the DHPR $\alpha 1_S$; it results in loss of DHPR protein, the absence of slow Ca^{2+} currents and charge movement and failure of EC coupling. Tanabe and colleagues (Tanabe et al., 1988) demonstrated that Ca^{2+} currents, charge movement and EC coupling could be restored in dysgenic muscle fibers by transfecting the cDNA for the $\alpha 1_s$ subunit of the DHPR. This demonstration established the DHPR Ca^{2+} channel as the essential voltage-sensing molecule in EC coupling.

VIIIB. The Myoplasmic Ca^{2+} Release Transient and SR Ca^{2+} Release Flux

In studies using intact skeletal muscle cells, SR Ca^{2+} release is detected by monitoring myoplasmic Ca^{2+} transients using Ca^{2+} indicator dyes introduced into the myoplasm (as shown in Fig. 45.4B). These measurements record the global Ca^{2+} change occurring throughout the myoplasm. Much useful information on the kinetics and voltage-dependence of SR Ca^{2+} release under physiological conditions has come from these studies (Rios and Pizarro, 1991, Melzer et al., 1995). These studies confirmed that a strict relationship exists between the voltage-dependence of Ca^{2+} release and voltage-dependent charge movement, as expected for a coupling mechanism which is controlled by the t-tubule membrane potential. Importantly, it was shown that SR Ca^{2+} release can both be turned on by membrane depolarization and turned off by membrane repolarization. Other studies have also demonstrated that considerable cross-talk exists between t-tubule Ca^{2+} channel functions and SR Ca^{2+} release (Sheridan et al., 2006; Dirksen, 2009). For example, the RyR1 release channel, through its interaction with calsequestrin, is able to respond to surface depolarization in a manner that depends on the Ca^{2+} load within the SR. Changes in SR Ca^{2+} load are reflected in the kinetics of charge movement and the rate of Ca^{2+} release. In addition, although Ca^{2+} entry is not required for skeletal muscle type EC coupling, manipulations that alter the RyR1 or the Ca^{2+} release transient also modify the slow Ca^{2+} current through DHPRs. Such bidirectional cross-talk between the DHPR and RyR, involving both forward and retrograde interactions, is expected for a mechanism that involves protein–protein interactions within a macromolecular complex.

The global myoplasmic Ca^{2+} change (see Fig. 45.4) arises from the summation of thousands of individual Ca^{2+} release events. Discrete, local Ca^{2+} signals, termed Ca^{2+} *sparks*, have been detected in skeletal and cardiac muscle (Fig. 45.16) (Cheng and Lederer, 2008). These discrete Ca^{2+} changes are limited in time and space and can occur spontaneously or in response to membrane depolarization. The Ca^{2+} spark does not reflect the unitary opening of a single RyR1 channel, but is proposed to report an elementary unit of SR Ca^{2+} release arising from

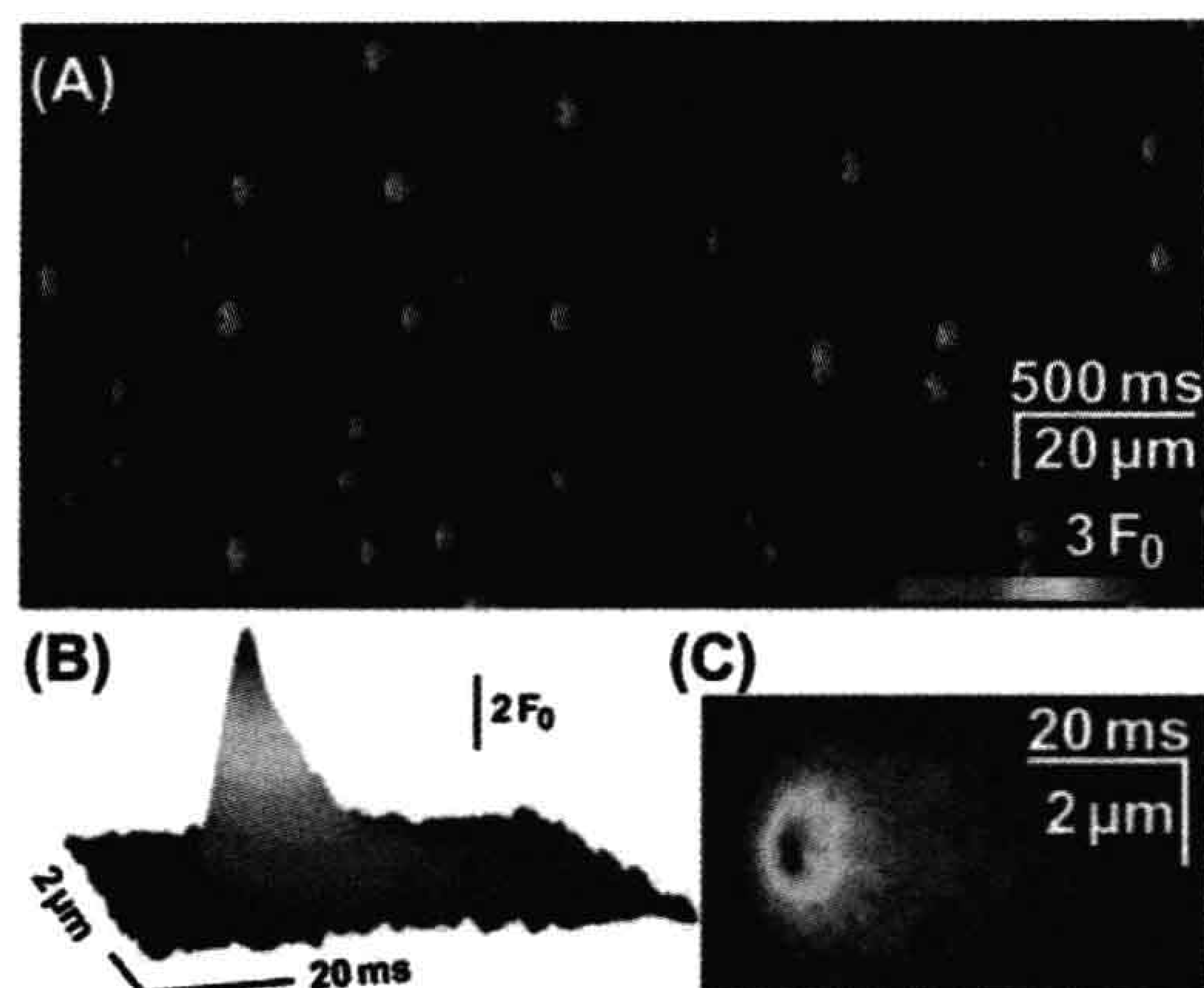


FIGURE 45.16 Spontaneous elementary calcium release events in an amphibian skeletal muscle. (A) A typical line scan image from a permeabilized frog skeletal muscle fiber immersed into a glutamate-based internal solution containing 50 μM fluo-4 as the calcium-sensitive fluorescence indicator. The sparks occur with high frequency and appear relatively homogenous. Time course (B) and spatial distribution (C) of the average spark in amphibian skeletal muscle. *(Reproduced with permission from Csernoch et al., 2004.)*

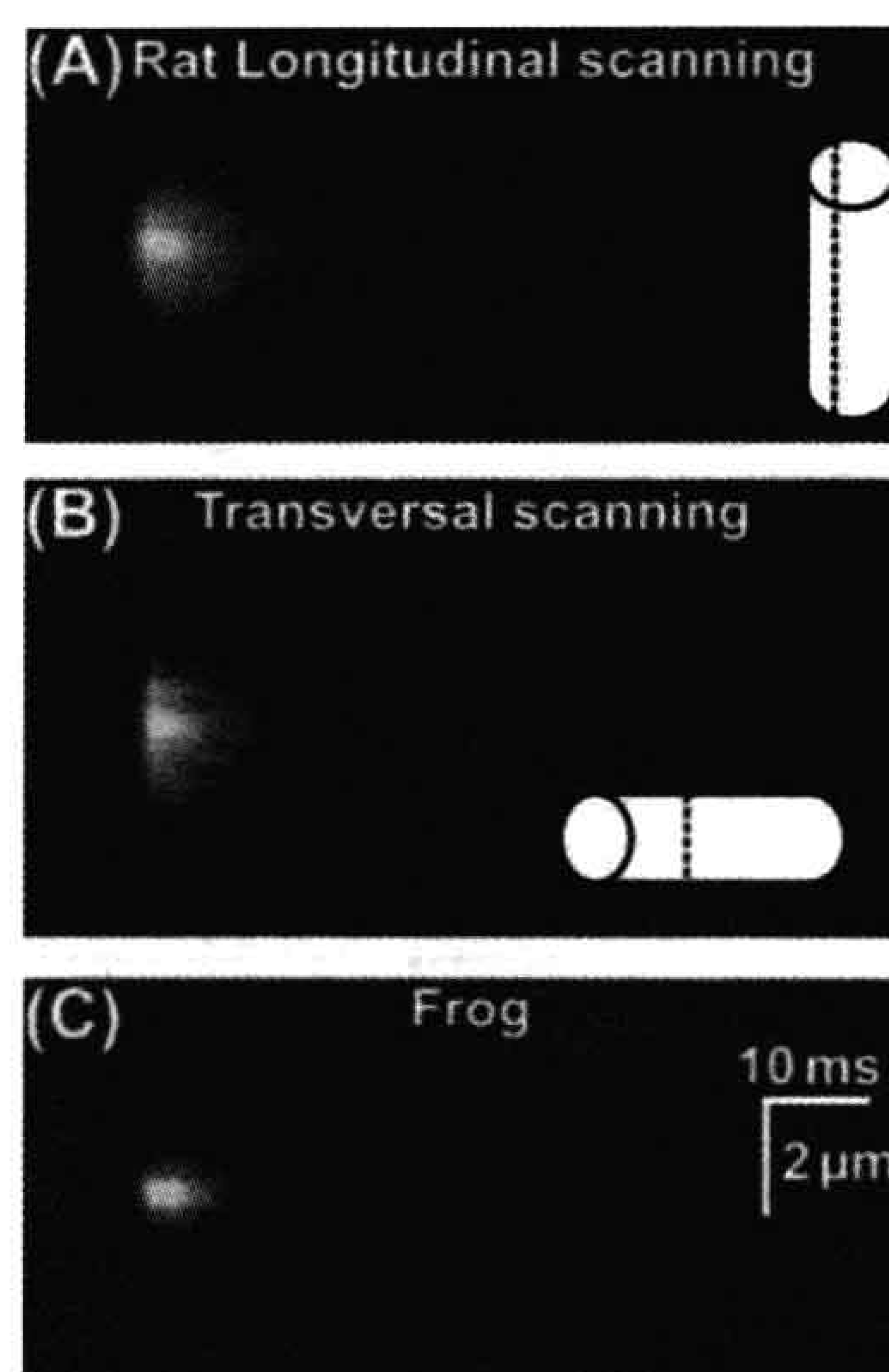


FIGURE 45.17 Elementary Ca^{2+} release events, termed "embers", in a mammalian skeletal muscle of the rat (A, B) compared to frog (C). Averages detected in line scans parallel (A) or perpendicular (B) to the fiber axis. Mammalian embers are wider and longer than the frog sparks. *(Reproduced with permission from Zhou et al., 2003.)*

a Ca^{2+}-release unit. Calcium-release units consist of a cluster of DHPRs, RyR1s and possibly other proteins acting together as a functional unit (see below). Thus, the global depolarization-triggered Ca^{2+} transient represents a summation of discrete unitary events. This mechanism may allow a more graded control of Ca^{2+} release. Some important differences in sparks exist between vertebrate amphibian and mammalian skeletal muscles. Mammalian muscles do not readily show spark activity. Rather, discrete Ca^{2+} release events, termed embers, with longer duration and constant amplitude are observed (Fig. 45.17) (Zhou et al., 2003, Csernoch et al., 2004; Klein and Schneider, 2006). The voltage dependence of embers is manifested in the duration and latency, but not in the amplitude of the individual events. It is possible that these differences in the elementary Ca^{2+} release events may reflect the different protein composition of the unitary Ca^{2+}-release units of amphibian and mammalian muscle. Although both species share the same two key proteins – a skeletal DHPR and RYR1 – amphibian muscle has an addition RyR3 isoform that is positioned peripheral to the double rows of RyR1 which oppose the DHPR tetrads. These parajunctional RyR3 channels in amphibian muscle do not associate with DHPR tetrads and may participate in a secondary Ca^{2+}-induced Ca^{2+} release, to generate sparks with properties similar to those in cardiac muscle. As described above, additional junctional proteins associate with the RyR1 and the molecular composition of the complete, elementary Ca^{2+}-release complex in amphibian and mammalian muscles is not yet defined.

VIIIC. Molecular Interactions Between the DHPR and RyR

The molecular mechanisms by which the pore of RyR1 opens under control of the t-tubule DHPR/Ca^{2+} channel has been the subject of intense research and is still not entirely resolved. Studies using dysgenic and transgenic mice have provided powerful experimental models for identifying the key proteins that are absolutely required for skeletal type EC coupling (Beam and Bannister, 2010). These are the $\alpha 1_s$ and β_{1a} subunits of the DHPR and RyR1. Mice null for either the $\alpha 1_s$ or β_{1a} subunit or the DHPR, or mice lacking the RYR1 protein, show an EC coupling dead phenotype and die perinatally. On the other hand, ablation of the $\alpha 2\text{-}\delta_1$ *or* γ_1 subunits of DHPR has little effect on EC coupling (Obermair et al., 2008).

The muscular dysgenesis mouse (lacking $\alpha 1_s$) has been used to identify further regions of DHPR $\alpha 1_s$ that are critical for interactions with RyR1. The α subunits of the skeletal ($\alpha 1_s$) and cardiac ($\alpha 1_c$) DHPR share a high degree of homology, but only the $\alpha 1_s$ can restore a skeletal-type EC coupling. When the skeletal muscle $\alpha 1_s$ subunit was expressed in dysgenic myotubes, Ca^{2+} release could be elicited in response to electrical depolarization and did not require Ca^{2+} entry; whereas, Ca^{2+} entry was required to elicit Ca^{2+} release when the cardiac $\alpha 1_c$ subunit was expressed. The main sequence differences between $\alpha 1_s$ and $\alpha 1_c$ reside in the large cytosolic regions at the N- and C-termini and the

linker sequences I–II, II–III and III–IV. By constructing chimeric DHPRs with various mixes of cardiac and skeletal sequences, Beam and collaborators (Tanabe et al., 1990) demonstrated that the 138-amino-acid cytoplasmic sequence between domains II and III is a critical determinant of skeletal-type EC coupling. A chimeric DHPR having the cardiac protein backbone but the not critical skeletal II–III linker could elicit skeletal-type EC coupling when expressed in dysgenic myotubes. Further experiments demonstrated that the cytosolic I–II linker, which binds the cytosolic β_{1a} subunit, is also essential for skeletal-type EC coupling. EC coupling is lost in myotubes of transgenic mice when the β subunit gene is knocked out, but is rescued when β_{1a} (but not the cardiac β_{2b}) is expressed. Thus, the interaction of β_{1a} with the I–II linker of the skeletal α_{1s} is also required for skeletal-muscle-type EC coupling.

Other cytosolic regions on the $\alpha 1_s$ subunit have been implicated in interactions with RyR1. A mutation in the III–IV cytosolic linker of the human DHPR (A1086H) is associated with susceptibility to one form of malignant hyperthermia (MH), a hereditary skeletal muscle disorder that is characterized by an uncontrolled, sustained Ca^{2+} release (Monnier et al. 1997). Studies using more complex chimeras between $\alpha 1_s$ and $\alpha 1_c$ have identified specific sites within the II–III linker which interact with RyR1. Biochemical studies have also demonstrated binding of specific fragments of the II–III sequence to RyR1. However, these studies have not yet yielded a consistent picture of the specific sequences which form interaction sites between DHPR and RyR1.

Similarly, regions of RyR1 critical for skeletal-type EC coupling have been studied using mice having a disrupted RyR1 gene (dyspedic mice). Dyspedic mice lack EC coupling, as expected and, in addition, have a 30-fold lower density of calcium channel current (Nakai et al., 1996). Thus, the absence of RyR also alters DHPR function, as expected if the DHPR and RYR1 associate in a macromolecular complex. Expression of the cDNA for RyR1 in dyspedic myotubes restores EC coupling and enhances the DHPR calcium current. This suggests that RyR1, in addition to receiving the EC coupling signal from the DHPR, also transmits a retrograde signal that enhances the function of skeletal DHPRs as calcium channels. These interactions require the skeletal muscle RyR1 isoform and indicate that the identity of the ryanodine receptor isoform also determines the mode of EC coupling. Expression of the predominant cardiac isoform, RyR2, did not restore skeletal-type EC coupling or enhance DHPR calcium channel activity (Nakai et al., 1997). Other studies combining freeze-fracture and pharmacology demonstrate that the spatial orientation of DHPRs and the conformational state of RyR1 are intimately related, further supporting the idea that the DHPR and RyR1 are capable of bidirectional interactions. The average distance between centers of each adjacent DHPR within a tetrad ($\approx 19.5 \approx$ nm) is decreased by ≈ 2 nm upon application of ryanodine at a concentration (500 μM) which locks RyR1 in a subconductance state (Paolini et al., 2004). Thus, the functional state of RyR1 is able to alter the spatial orientation of DHPRs within a tetrad, a phenomenon that could only be a result of physical coupling between RyR1 and the DHPR.

Biochemical studies of isolated triad membranes and proteins in vitro have also provided compelling evidence for protein–protein interactions between the skeletal DHPR and RyR1 (Meissner and Lu, 1995; Leong and MacLennan, 1998) and confirmed that the skeletal muscle isoforms of both DHPR and RyR1 are essential for skeletal type EC coupling. Peptides composed of either the skeletal or cardiac II–III linker sequence can activate isolated RyR1s (Lu et al., 1995), but do not activate the cardiac RyR2 isoform. Binding assays have also been used to identify regions on RyR1 that interact specifically with the skeletal DHPR. However, these studies have not yet led to a consensus on the specific interaction sites. Taken together, the body of biochemical evidence and results of studies using transgenic mice indicate that a minimal complex containing the skeletal muscle DHPR α_{1s} and β_{1a} subunits plus RyR1 is required to initiate Ca^{2+} release by the physiologically relevant (independent of Ca^{2+} entry) mode in fast twitch skeletal muscle. Moreover, the data suggest that the bidirectional interaction between DHPR and RyR1 may involve multiple contact points on both proteins and possibly low affinity interactions (Sheridan et al., 2006; Beam and Bannister, 2010). A more specific identification of the interaction sites will likely become available when detailed structural information becomes available from crystallographic studies.

VIIID. Overall Control and Integration of Ca^{2+}-Release Events

There is general agreement that the initial event leading to calcium release in vertebrate skeletal muscle is a depolarization-driven interaction between a DHPR tetrad and at least one RyR1 tetramer. However, the mechanism by which this signal is communicated to adjacent RyRs which do not underlie a DHPR tetrad is less well understood. The alternate disposition of DHPR tetrads opposite every other RyR1 suggests a dual control of RyR1 activation. One RyR1 may be opened by allosteric movements of the associated DHPR tetrad (a coupled RyR1), while a neighboring RyR1 (non-coupled to a tetrad) may be opened by a different mechanism. One early proposal was that the local Ca^{2+} released through coupled RyR1s binds to and activates adjacent, non-coupled RyR1s (Fig. 45.18), acting as a ligand-gated channel. However, all of the functional evidence indicates that there is little Ca^{2+}-induced-Ca^{2+} release in the mammal. An alternate proposal is that the

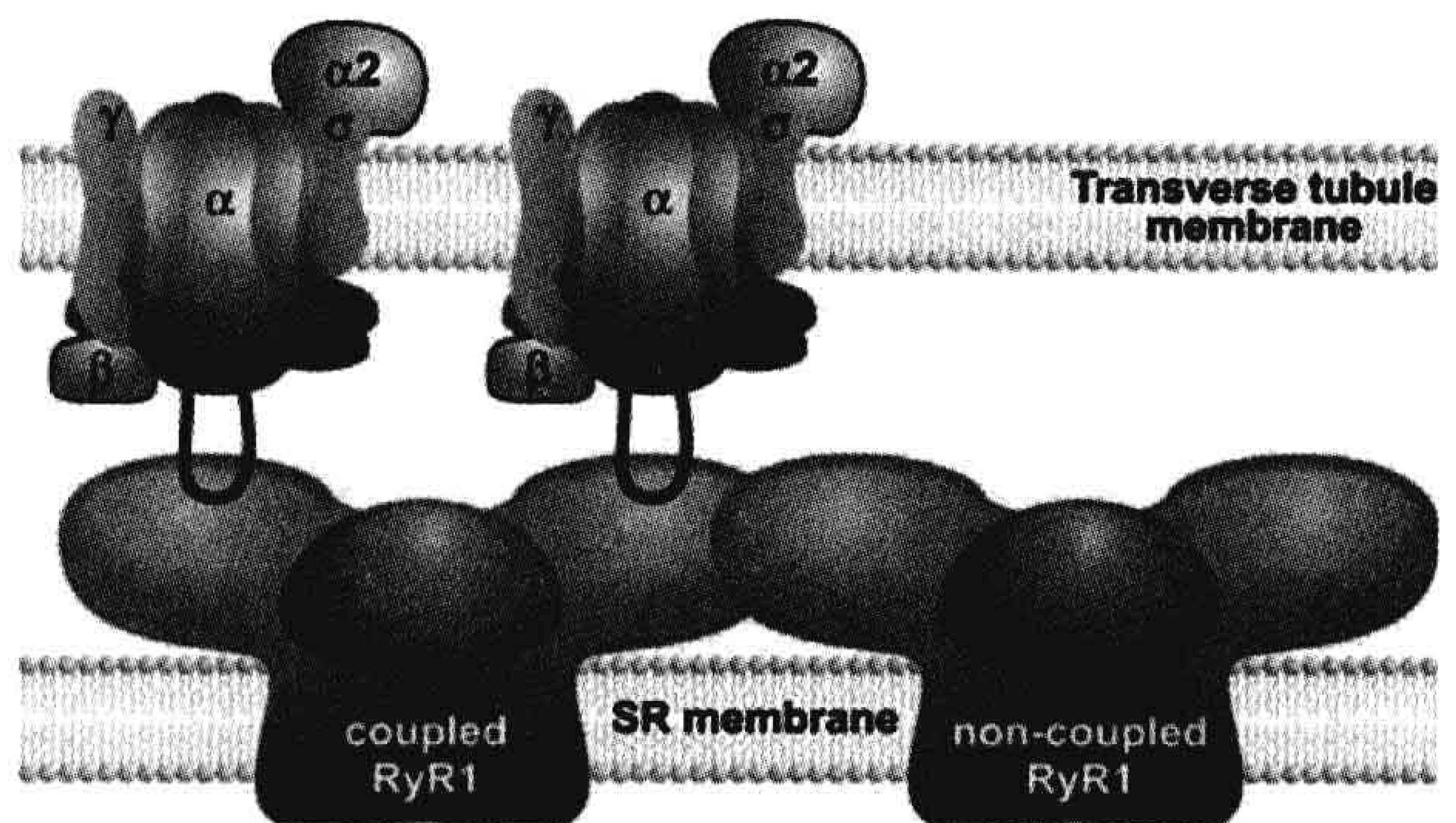


FIGURE 45.18 Integration of Ca^{2+} release from coupled and non-coupled RyR1s. RyR1s associate with each other on the SR surface of the triad junction in an ordered array. Every alternate RyR1 is coupled to a tetrad of four DHPRs in the transverse tubule membrane. This schematic depicts a cross-sectional plane through two subunits of a RyR1 (left) interacting with two DHPRs. Voltage-driven movements of the DHPR initiate molecular interactions between cytosolic regions of the DHPR (II–III loop) and a coupled RyR1, leading to RyR1 channel opening. This initiating event activates non-coupled RyR1s, possibly via coordinated interactions between adjacent RyR1s, to effect a rapid and synchronous efflux of Ca^{2+}.

conformational changes initiated between a coupled RyR1 and a DHPR tetrad is communicated to non-coupled RyR1s through coordinated interactions between physically linked RyR1s. In this model, both populations of RyR1s are activated by depolarization without requiring Ca^{2+} as a ligand. This model is suggested by the tight packing of RyR1s in an ordered, interlocking array. In this model, clusters of RyR1s open simultaneously as a functional Ca^{2+} release unit. Opening of one RyR1 by its coupled DHPR tetrad results in simultaneous opening of all contiguous RyRs in the cluster. The minimal number of RyR1s which constitute an elementary Ca^{2+}-release unit (generating an "ember") is not yet resolved. Such clusters of RyRs operating as a functional unit is expected to generate fast local Ca^{2+} release events and a more synchronous global change in myoplasmic Ca^{2+}. An additional mechanism may operate in amphibian muscle where parajunctional RyR3 channels are also present. The RyR3 channels may be opened by a Ca^{2+}-induced-Ca^{2+}-release mechanism, similar to the cardiac RyR2 channel, and generate the more cardiac-like sparks recorded from frog muscle.

VIIIE. Modulation of EC Coupling

EC coupling can be modulated in response to different demands of muscle use. Potential regulatory sites on both the DHPR and RyR1 have been identified. The DHPR α_{1S} subunit contains consensus phosphorylation sites including a serine residue, Ser 687, within the critical II–III loop that is rapidly phosphorylated by a cAMP-dependent kinase. Phosphorylation of this residue is required for binding of the II–III loop to RyR1 (but not RyR2), but only the dephosphorylated II–III loop can activate the RyR (Lu et al., 1995). Moreover, Ca^{2+} release can be both inhibited and activated by Ca^{2+} acting at specific sites on the RyR1 or α_{1S} (El-Hayek et al., 1995; Meissner, 2004). As noted (see Section VI), RyR1 has both Ca^{2+}-activating and Ca^{2+}-inactivation sites as well as a CaM binding site which can bind either CaM or the soluble protein S100 to modulate Ca^{2+} release. The complete RyR1 complex includes other associated proteins which contribute to EC coupling and to the structural integrity of the triad junction. Finally, long-term regulation of EC coupling may occur at the level of gene expression. It is known that the expression of α_{1S} can be altered during adaptation to physiological demands, including altered patterns of nerve activity, exercise, changes in the load-bearing state and metabolic or endocrine status.

ACKNOWLEDGMENT

Support by National Institutes of Health grants AR018697 and HL073501 and the Physiology Research Fund of the University of Cincinnati is gratefully acknowledged.

BIBLIOGRAPHY

Adams, B. A., & Beam, K. G. (1990). Muscular dysgenesis in mice: a model system for studying excitation-contraction coupling. [Review]. *FASEB J, 4*, 2809–2816.

Armstrong, C. M., Bezanilla, F. M., & Horowicz, P. (1972). Twitches in the presence of ethylene glycol bis(-aminoethyl ether) -N, N'-tetracetic acid. *Biochim Biophys Acta, 267*, 608.

Balshaw, D. M., Yamaguchi, N., & Meissner, G. (2002). Modulation of intracellular calcium-release channels by calmodulin. *J Membr Biol, 185*, 1–8.

Beam, K. G., & Bannister, R. A. (2010). Looking for answers to EC coupling's persistent questions. *J Gen Physiol, 136*, 7–12.

Caswell, A. H., Lau, Y. H., Garcia, M., & Brunschwig, J. P. (1979). Recognition and junction formation by isolated transverse tubules and terminal cisternae of skeletal muscle. *J Biol Chem, 254*, 202–208.

Cheng, H., & Lederer, W. J. (2008). Calcium sparks. *Physiol Rev, 88*, 1491–1545.

Csernoch, L., Zhou., J., Stern, M. D., Brum, G., & Rios, E. (2004). The elementary events of Ca^{2+} release elicited by membrane depolarization in mammalian muscle. *J Physiol, 557*, 43–58.

Dirksen, R. T. (2009). Checking your SOCCs and feet: the molecular mechanisms of Ca^{2+} entry in skeletal muscle. *J Physiol, 587*, 3139–3147.

Dulhunty, A. F. (1984). Heterogeneity of t-tubule geometry in vertebrate skeletal muscle fibres. *J Muscle Res Cell Motil, 5*, 333–347.

El-Hayek, R., Antoniu, B., Wang, J., Hamilton, S. L., & Ikemoto, N. (1995). Identification of calcium release-triggering and blocking regions of the II-III loop of the skeletal muscle dihydropyridine receptor. *J Biol Chem, 270*, 22116–22118.

Eltit, J. M., Feng, W., Lopez, J. R., et al. (2010). Ablation of skeletal muscle triadin impairs FKBP12/RyR1 channel interactions essential for maintaining resting cytoplasmic Ca^{2+}. *J Biol Chem, 285*, 38453–38462.

Felder, E., & Franzini-Armstrong, C. (2002). Type 3 ryanodine receptors of skeletal muscle are segregated in a parajunctional position. *Proc Natl Sci USA, 99*, 1695–1700.

Fleischer, S., & Inui, M. (1989). Biochemistry and biophysics of excitation-contraction coupling. *Annu Rev Biophys Biophys Chem, 18*, 333–364.

Franzini-Armstrong, C., & Jorgensen, A. O. (1994). Structure and development of E-C coupling units in skeletal muscle. *Annu Rev Physiol, 56*, 509–534.

Franzini-Armstrong, C., & Peachey, L. D. (1981). Striated muscle-contractile and control mechanisms. *J Cell Biol, 91*, 166s–186s.

Franzini-Armstrong, C., & Protasi, F. (1997). Ryanodine receptors of striated muscles: a complex channel capable of multiple interactions. *Physiol Rev, 77*, 699–729.

Gillespie, D., Xu, L., Wang, Y., & Meissner, G. (2005). (De)constructing the ryanodine receptor: modeling ion permeation and selectivity of the calcium release channel. *J Phys Chem B, 109*, 15598–15610.

González-Serratos, H. (1971). Inward spread of activation in vertebrate muscle fibres. *J Physiol, 212*, 777–799.

Hodgkin, A. L., & Horowicz, P. (1957). Effects of K and Cl on the membrane potential of isolated muscle fibres. *J Physiol, 137*, 30P.

Jong, D. S., Pape, P. C., Geibel, J., & Chandler, W. K. (1996). Sarcoplasmic reticulum calcium release in frog cut muscle fibres in the presence of a large concentration of EGTA. *Soc Gen Physiol Ser, 51*, 255–268.

Klein, M. G., & Schneider, M. F. (2006). Ca^{2+} sparks in skeletal muscle. *Prog Biophys Mol Biol, 92*, 308–332.

Kushnir, A., Betzenhauser, M. J., & Marks, A. R. (2010). Ryanodine receptor studies using genetically engineered mice. *FEBS Lett, 584*, 1956–1965.

Lanner, J. T., Georgiou, D. K., Joshi, A. D., & Hamilton, S. L. (2010). Ryanodine receptors: structure, expression, molecular details, and function in calcium release. *Cold Spring Harb Perspect Biol*, 2.

Leong, P., & MacLennan, D. H. (1998). Complex interactions between skeletal muscle ryanodine receptor and dihydropyridine receptor proteins. *Biochem Cell Biol, 76*, 681–694.

Lu, X., Xu, L., & Meissner, G. (1995). Phosphorylation of dihydropyridine receptor II-III loop peptide regulates skeletal muscle calcium release channel function. Evidence for an essential role of the beta-OH group of Ser687. *J Biol Chem, 270*, 18459–18464.

Meissner, G. (2004). Molecular regulation of cardiac ryanodine receptor ion channel. *Cell Calcium, 35*, 621–628.

Meissner, G. (1984). Adenine nucleotide stimulation of Ca2+-induced Ca2+ release in sarcoplasmic reticulum. *J Biol Chem, 259*, 2365–2374.

Meissner, G., & Lu, X. (1995). Dihydropyridine receptor-ryanodine receptor interactions in skeletal muscle excitation-contraction coupling. *Biosci Rep, 15*, 399–408.

Melzer, W., Herrmann-Frank, A., & Luttgau, H. C. (1995). The role of Ca2+ ions in excitation-contraction coupling of skeletal muscle fibres. *Biochim Biophys Acta, 1241*, 59–116.

Monnier, N., Procaccio, V., Stieglitz, P., & Lunardi, J. (1997). Malignant-hyperthermia susceptibility is associated with a mutation of the alpha 1-subunit of the human dihydropyridine-sensitive L-type voltage-dependent calcium-channel receptor in skeletal muscle. *Am J Hum Genet, 60*, 1316–1325.

Nakai, J., Dirksen, R. T., Nguyen, H. T., Pessah, I. N., Beam, K. G., & Allen, P. D. (1996). Enhanced dihydropyridine receptor channel activity in the presence of ryanodine receptor. *Nature, 380*, 72–75.

Nakai, J., Ogura, T., Protasi, F., Franzini-Armstrong, C., Allen, P. D., & Beam, K. G. (1997). Functional nonequality of the cardiac and skeletal ryanodine receptors. *Proc Natl Acad Sci USA, 94*, 1019–1022.

Obermair, G. J., Tuluc, P., & Flucher, B. E. (2008). Auxiliary Ca(2+) channel subunits: lessons learned from muscle. *Curr Opin Pharmacol, 8*, 311–318.

O'Brien, J., Meissner, G., & Block, B. A. (1993). The fastest contracting muscles of nonmammalian vertebrates express only one isoform of the ryanodine receptor. *Biophys J, 65*, 2418–2427.

Paolini, C., Fessenden, J. D., Pessah, I. N., & Franzini-Armstrong, C. (2004). Evidence for conformational coupling between two calcium channels. *Proc Natl Acad Sci USA, 101*, 12748–12752.

Peachey, L. D. (1965). The sarcoplasmic reticulum and transverse tubules of the frog's sartorius. *J Cell Biol, 25*(Suppl), 209–231.

Peachey, L. D., & Eisenberg, B. R. (1978). Helicoids in the T system and striations of frog skeletal muscle fibers seen by high voltage electron microscopy. *Biophys J, 22*, 145–154.

Pritchard, T. J., & Kranias, E. G. (2009). Junctin and the histidine-rich Ca2+ binding protein: potential roles in heart failure and arrhythmogenesis. *J Physiol, 587*, 3125–3133.

Rios, E., & Pizarro, G. (1991). Voltage sensor of excitation-contraction coupling in skeletal muscle. *Physiol Rev, 71*, 849–908.

Samsó, M., & Wagenknecht, T. (1998). Contributions of electron microscopy and single-particle techniques to the determination of the ryanodine receptor three-dimensional structure. *J Struct Biol, 121*, 172–180.

Schneider, M. F. (1994). Control of calcium release in functioning skeletal muscle fibers. [Review]. *Annu Rev Physiol, 56*, 463–484.

Schneider, M. F., & Chandler, W. K. (1973). Voltage dependent charge movement of skeletal muscle: a possible step in excitation-contraction coupling. *Nature, 242*, 244–246.

Sheridan, D. C., Takekura, H., Franzini-Armstrong, C., Beam, K. G., Allen, P. D., & Perez, C. F. (2006). Bidirectional signaling between calcium channels of skeletal muscle requires multiple direct and indirect interactions. *Proc Natl Acad Sci USA, 103*, 19760–19765.

Suh-Kim, H., Wei, X., Klos, A., et al. (1996). Reconstitution of the skeletal muscle dihydropyridine receptor. Functional interaction among alpha 1, beta, gamma and alpha 2 delta subunits. *Receptors Channels, 4*, 217–225.

Sutko, J. L., & Airey, J. A. (1996). Ryanodine receptor Ca2+ release channels: does diversity in form equal diversity in function? *Physiol Rev, 76*, 1027–1071.

Tanabe, T., Beam, K. G., Adams, B., Niidome, T., & Numa, S. (1990). Regions of the skeletal muscle dihydropyridine receptor critical for excitation-contraction coupling. *Nature, 346*, 567–569.

Tanabe, T., Beam, K. G., Powell, J., & Numa, S. (1988). Restoration of excitation-contraction coupling and slow calcium current in dysgenic muscle by dihydropyridine receptor complementary DNA. *Nature, 336*, 134–139.

Tanabe, T., Takeshima, H., Mikami, A., et al. (1987). Primary structure of the receptor for calcium channel blockers from skeletal muscle. *Nature, 328*, 313–318.

Tinker, A., Lindsay, A. R., & Williams, A. J. (1992). A model for ionic conduction in the ryanodine receptor channel of sheep cardiac muscle sarcoplasmic reticulum. *J Gen Physiol, 100*, 495–517.

Xu, L., Wang, Y., Gillespie, D., & Meissner, G. (2006). Two rings of negative charges in the cytosolic vestibule of type-1 ryanodine receptor modulate ion fluxes. *Biophys J, 90*, 443–453.

Yamaguchi, N., Takahashi, N., Xu, L., Smithies, O., & Meissner, G. (2007). Early cardiac hypertrophy in mice with impaired calmodulin regulation of cardiac muscle Ca release channel. *J Clin Invest, 117*, 1344–1353.

Yu, F. H., Yarov-Yarovoy, V., Gutman, G. A., & Catterall, W. A. (2005). Overview of molecular relationships in the voltage-gated ion channel superfamily. *Pharmacol Rev, 57*, 387–395.

Vergara, J., & Delay, M. (1986). A transmission delay and the effect of temperature at the triadic junction of skeletal muscle. *Proc R Soc Lond B Biol Sci, 229*, 97–110.

Zalk, R., Lehnart, S. E., & Marks, A. R. (2007). Modulation of the ryanodine receptor and intracellular calcium. *Annu Rev Biochem, 76*, 367–385.

Zhou, J., Brum, G., Gonzalez, A., Launikonis, B. S., Stern, M. D., & Rios, E. (2003). Ca^{2+} sparks and embers of mammalian muscle. Properties of the sources. *J Gen Physiol, 122*, 95–114.

Chapter 46

Contraction of Muscles: Mechanochemistry

Richard J. Paul

Chapter Outline

I. SUMMARY

This chapter focuses largely on muscle structure in relation to muscle mechanics and energetics and relevance to different muscle types. Striated muscle structure is first developed as a paradigm in conjunction with mechanics, leading to the formulation of the sliding-filament theory. Muscle contractility continues with further characterization of the relationships among force, velocity, work and adenosine triphosphate (ATP) utilization. The mechanism at the molecular level, i.e. the cross-bridge cycle, is similarly developed, matching structural and biochemical knowledge with transient mechanical studies. An investigation of the energy requirements in terms of ATP hydrolysis of the cross-bridge cycle is then followed by a discussion of muscle metabolism and the route for synthesis of the ATP necessary for contractile activity. The chapter then shifts from considerations of muscle in general to comparative muscle physiology and behavior of different fiber types. In particular, smooth muscle is treated in detail and its regulation, mechanical properties and energetics are considered and contrasted to those of striated muscle.

II. INTRODUCTION

The generation of force and movement by muscle is an area of physiology and biophysics that has fascinated scientist and layman alike since the dawn of scientific inquiry and reverberates strongly in today's nanomachine quest (Huang and Juluri, 2008). The history of the study of muscle is elegantly chronicled by Dorothy Needham in *Machina Carnis* (1971). Because of its highly organized and repeating structure, skeletal muscle has proven more amenable to structural analysis (such as x-ray diffraction) than most biological tissues. Thus, it has served as a paradigm for unraveling relationships between function and structure. This has become particularly exciting in conjunction with the techniques of molecular biology, which offer the potential for altering particular amino acids and molecular measurements with manipulators, such as laser tweezers. These tools offer the potential for directly testing the links between structure at nanometer resolution and function. The focus of this chapter is on the nature of the muscle mechanics and mechanochemical energy conversion. Muscle is one of the most efficient energy

Cell Physiology Sourcebook. DOI: 10.1016/B978-0-12-387738-3.00046-9

converters known and studies in this area couple classical enzyme kinetics, muscle mechanics and cross-bridge theories (Barclay et al., 2010).

The major focus of this chapter is on the molecular and cellular levels which form the basis understanding muscle contraction for organ and whole organism function, such as sports medicine and kinestheology. Muscle mechanochemistry at the cellular level also has major consequences at the organ and whole-animal levels. Skeletal muscle constitutes approximately 40% of human body mass. If we include cardiac and smooth muscle, the total muscle mass reaches the 50% level. One consequence of this is that approximately 30% of basal metabolism is related to muscle and as much as 90% of a person's total metabolism during strenuous exercise can be related to meeting the energy requirements of muscle. This chemical activity can in turn produce a significant heat load for the organism. Other functions that are associated with the large muscle mass are the storage and mobilization of metabolites (primarily glucose and amino acids). Also, there are significant consequences to alterations in muscle electrolyte metabolism, since it is a major storage site for ions such as H^+, Cl^- and Mg^{2+}. Some of these ramifications are presented as related to molecular processes in muscle.

Our study of the muscle contraction first involves investigation of mechanisms underlying the generation of macroscopic force and shortening. We first consider how force is developed and how the mechanical behavior of muscle is quantitated, a field known collectively as *muscle mechanics*. This is then integrated with the current picture of muscle structure as a first step in constructing theories of muscle function. Next, we consider *muscle energetics*, governed by thermodynamic rules for energy conversion and the constraints they place on models proposed for muscle contraction. We relate energetics and mechanics to the kinetics of the myosin ATPase as a basis for cross-bridge cycling mechanisms. *Muscle metabolism* and the matching of ATP demand with ATP synthesis will complete the picture of mechanochemical energy conversion.

The second major area involves study of the mechanisms underlying the regulation of muscle contraction. The control of intracellular Ca^{2+} concentration, a key intracellular messenger, forms an area of study known as *excitation–contraction coupling*. The intracellular receptors transducing the Ca^{2+} signal reflect the great diversity of types of muscle that have evolved in response to a wide variety of functional needs. These muscles also have much in common. All muscle contains the proteins actin and myosin, which are the locus of the mechanochemical energy conversion. Chemical energy in the form of ATP hydrolysis is the immediate driving reaction for all muscle energy transduction. Another feature common to all muscle types is that calcium ions, at micromolar concentrations, are the primary second messenger in the regulatory mechanisms. We first focus on these common aspects, using a generalized striated muscle as the model. Then with an understanding of these common mechanisms, we consider the different muscle types.

III. THE MECHANISMS OF FORCE PRODUCTION AND SHORTENING: MUSCLE MECHANICS

Studies of the mechanical behavior of muscle have played a central role in our understanding of muscle and have also formed an integral part of the language of muscle physiology (Hill, 1965). These studies before the late 1950s were primarily phenomenological, though they were also important in characterization of muscle performance. Such studies remain important in characterization of muscle myopathies and in current mechanistic studies, e.g. in describing the functional consequences of changing muscle protein isoforms in transgenic animals.

There are two arbitrary but natural divisions in studies of muscle mechanics. The first division involves steady-state relationships in which force and velocity are constant in time. This information was crucial to the development of the three-component model of muscle contraction (see below), a model still valid for whole muscle behavior (Jewell and Wilkie, 1958). Such studies also provided one pillar supporting the sliding-filament theory and were extensively investigated in the 1960s (Gordon et al., 1966).

Studies of mechanical transients form a second division. They assumed a more central importance during the early 1970s (Huxley and Simmons, 1971) with the growing realization that information at the level of individual cross-bridges could be gained from mechanical studies on single fibers. These studies of muscle responses to rapid changes in mechanical constraints are even more valuable to unraveling cross-bridge behavior when coupled with recently improved temporal resolution of x-ray diffraction of muscle (Huxley, 2004; Squire and Knupp, 2005).

IIIA. Steady-State Relations Between Force and Length and the Sliding-Filament Theory

A first step in muscle mechanics involves a description of muscle behavior in terms of relationships between the mechanical variables of force and length. Apparatus for transduction and recording of these variables has evolved considerably over this century, but the historical apparatus is still responsible for much of the language of muscle physiology. Since it was easier to control force than length, by hanging a fixed weight on the muscle, terms such as

preload and afterload entered the vocabulary (see later section on force—velocity relationships). However, in view of what is now known about structure, it is conceptually easier to use length as the independent variable.

Figure 46.1 shows a schematic of an experimental apparatus for measurement of muscle force—length relationships. In this setup, length is the controlled variable and the steady-state force at various lengths is measured. In developing these relationships, we consider the performance of an isolated muscle, or single muscle cell known as a muscle fiber. After mounting in the apparatus, muscle length is adjusted to a specific length then set isometric (fixed total length) and the steady-state force is measured. The relationship between the unstimulated force (often designated as passive force) and muscle length is designated the passive length—tension relationship. This relationship can be characterized as an exponential spring, $F = A_1 + A_2 \exp(A_3X)$, whose behavior is similar to that of

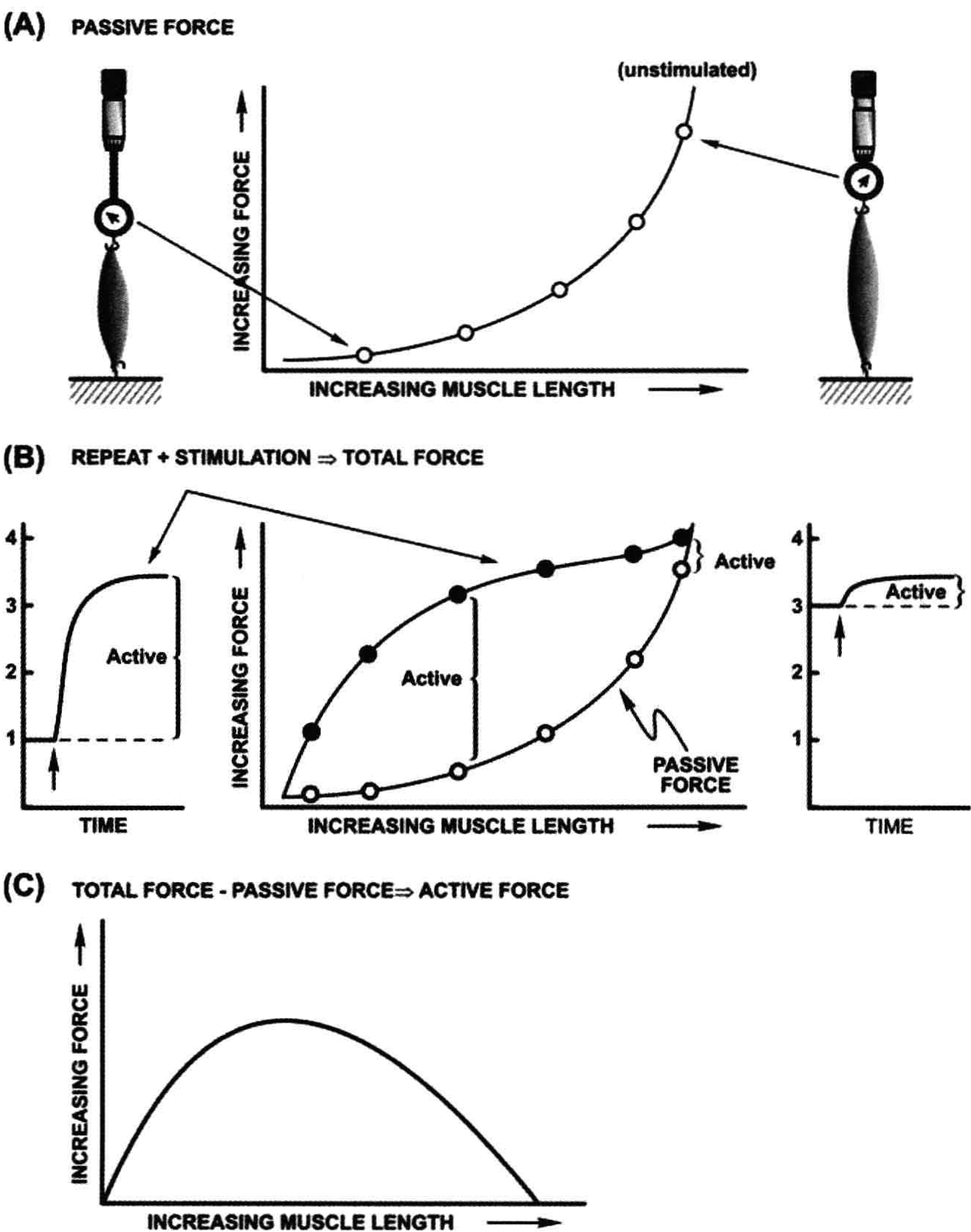


FIGURE 46.1 Measurement and operational definitions of muscle force—length relationships. (A) Relation between isometric force under unstimulated conditions, passive force and muscle length. (B) Relation between isometric force and length under stimulated conditions, total force. (C) Active force operationally defined as the difference between total force and passive force is shown as a function of muscle length.

a rubber band with its stiffness increasing with length. This relationship can also show a dependence on the direction of the imposed length changes, known as hysteresis, but deviations are small in a true steady state. Some form of passive force is common to all muscles, but an exact anatomical assignment of the structures underlying passive force is dependent on both the type of muscle and the preparation studied.

The next stage of this analysis involves a similar protocol but includes stimulation of the muscle to characterize the parameters associated with activated muscle. With active muscle, the language that evolved reflected the state of understanding and the experimental apparatus. The response to a single electrical shock is known as a *twitch* contraction. At one time, this was believed to be some form of elemental or quantal behavior of muscle, hence its historical importance. Increasing the frequency of stimulation leads to a summation in time of the individual twitch responses, known as temporal summation. Beyond a certain frequency (depending on muscle type and temperature), the force response becomes a smooth, fused curve, called an *isometric tetanus*. These responses to stimulation are ultimately related to the Ca^{2+} handling underlying activation of the contractile proteins. For our present purposes, we consider only isometric tetani, so that the mechanical behavior of the fully activated contractile apparatus can be considered, without complications arising from behavior attributable to non-steady-state Ca^{2+} signaling.

Tetanic stimulation adds an additional increment of force to the passive force present at a given length. The passive force plus active (stimulated) force measured as a function of muscle length is shown in Fig. 46.1. This relationship is known as the total force—length curve. The total force—length relationship varies considerably from muscle to muscle, though the component passive and active force—length relationships for skeletal muscles are qualitatively similar. The differences are largely ascribable to the relative amount of passive force developed at the length at which active force is optimal.

For a structure—function mechanism, the relationship between the additional active force generated when a muscle is stimulated and muscle length is paramount. The active force—length relationship is calculated by subtracting the passive force relation from that for *total force*. The active force—length curve is unusual in that it decreases to zero at both long and short muscle lengths. For most materials, including polymers like rubber, force increases as length is increased. This typical behavior is also seen for the passive force as shown in Fig. 46.1. The observation that active force decreased at long muscle lengths was critical to eliminating theories that involved folding of continuous muscle filaments as the basis for the generation of force upon activation. To understand the relationship between active force and muscle length, it is necessary to consider muscle structure.

IIIB. The Structure of Muscle: Interdigitating Filament Systems

Muscle cells are composed of a filament system underlying their mechanical properties and internal membrane systems related to control of contraction. The filament structure repeats on both the transverse and longitudinal directions as shown in Fig. 46.2. A muscle fiber is composed of myofibrils whose fundamental longitudinal repeating unit is the sarcomere. The sarcomere consists of two interdigitating filament systems, thick (14 nm) myosin-containing filaments and thin (7 nm) actin-containing filaments which underlie the banding pattern seen under optical microscopy and the moniker, striated or striped muscle. The optical properties of the sarcomere due to the overlapping filaments gave rise to the nomenclature for the banding regions. The I-band contains only thin filaments and is optically isotropic, whereas the A-band contains both filament types and is anisotropic. The constancy of A-band dimensions, independent of total muscle length (Huxley amd Niedergerke, 1954), was a key experimental finding, leading to the concept that filament length was constant. Constant filament lengths and interdigitating filaments are best observed at the electron microscope level (Fig. 46.3), where interpretation of the changing banding pattern with muscle length was first elucidated (Huxley, 1953).

IIIC. Sliding-Filament Theory

Based on this structure, the sliding-filament theory explains the active—force relationship in terms of active force being proportional to the overlap between thick and thin filaments of constant length, which are free to interdigitate and slide past one another. This mechanical correlate of the proposed sliding-filament structure was tested in the classic work of Gordon et al. (1966) and is summarized in Fig. 46.4. The clearest correlation between the level of active isometric force and extent of filament overlap is in the region of decreasing force between sarcomere lengths of 2.2 and 3.6 μm, i.e. the descending limb of the active force—length curve. The interpretation of the ascending limb of the force—length relation (e.g. 1.2—2.2 μm) is not as straightforward. This is of particular interest for cardiac muscle which normally operates in the ascending limb. Changes in activation, Ca^{2+}-sensitivity and cooperatively of myosin—actin interaction at short lengths have been proposed to explain the ascending limb in cardiac muscle. The loss of force at these lengths can also be attributed to double filament

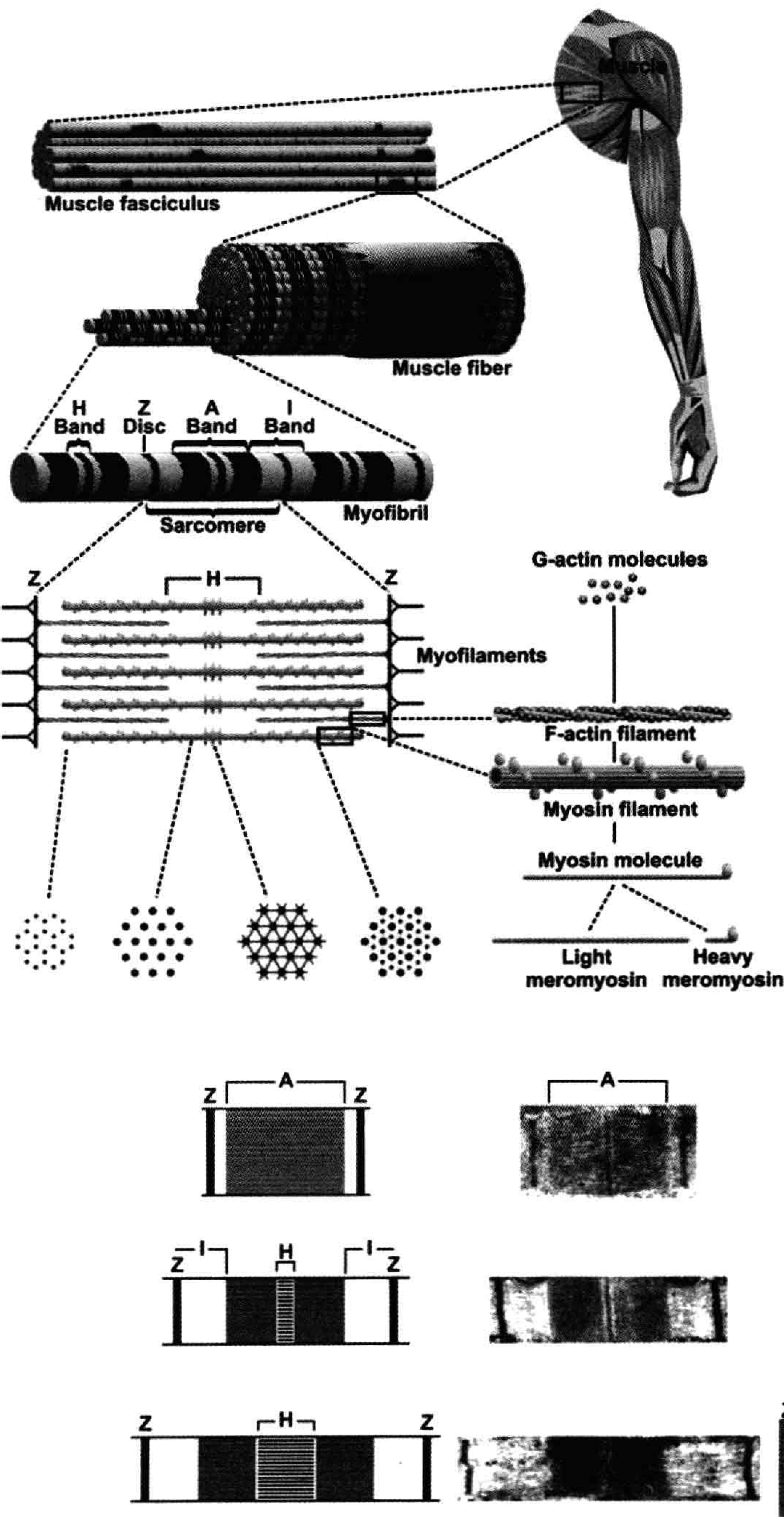


FIGURE 46.2 Skeletal muscle structure. The whole muscle is constructed of fundamental repeating units. A muscle cell or fiber is composed of myofibrils whose fundamental repeating unit is the sarcomere. All views are longitudinal except the cross-sections of the sarcomere (G, H, I).

FIGURE 46.3 Electron micrographs and diagrams of sarcomeres at various muscle lengths. The sliding-filament theory is based on the constant length of the thick and thin filaments. Under light microscopy, this leads to the constancy of A-bands (containing both thick and thin filaments, anisotropic, A), while I-bands (containing only thin filaments, isotropic, I). Other designations from light microscopy are the Z-band (Z) and H-zone (H).

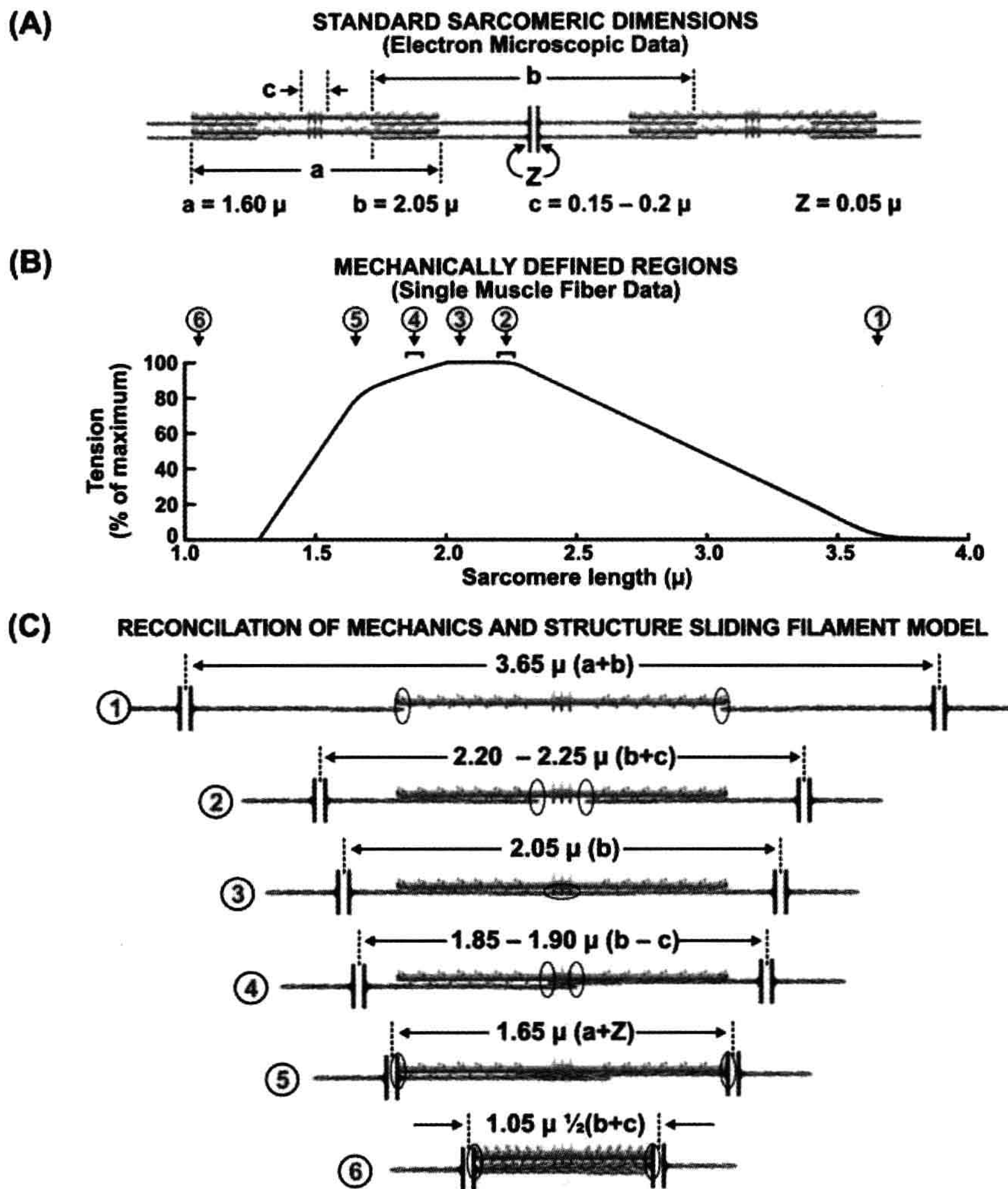


FIGURE 46.4 Structural basis for the active isometric force-length relationship. *(Modified from Gordon et al., 1966.)*

overlap and compression of the contractile elements while interdigitating. Recent interest in structure–function analysis involves the sarcomeric giant protein nebulin (MW 700–900 kDa). Experiments with knockout mice indicate that nebulin plays a critical role in setting the length of the thin filament. One consequence is the length–tension is shifted leftward and maximum force is reduced. This appears to be an important contributor to muscle weakness in patients with nemaline myopathy (Ottenheeeijm and Granzier, 2010). The sliding-filament theory is widely accepted, but the basis of force generation remains an active area of research (see Section IIIE on cross-bridge theory).

IIID. Relationships among Force, Velocity, Work and Energy Utilization

Together with the relationship between force and length, the relationship between force and shortening velocity and the derived work and power are fundamental to characterizing muscle performance. With current technology, one would mechanically impose a constant velocity or force and measure the other as a function of time. Measurements would be carried out under tetanic conditions to eliminate transients during activation and are limited to the plateau region of the force–length relation to avoid any length dependence.

It is of more than just historical interests to consider the apparatus used more than 70 years ago, as the nomenclature prevalent in muscle physiology today, particularly in the language of cardiac physiology, reflects these early measurement protocols.

Figure 46.5A depicts the experimental apparatus used for measurement of force–velocity relations. Using the lever system, a *preload* is placed on the unstimulated muscle. Because the muscle is unconstrained, it stretches to the length at which the preload matches the force on the passive force–length relation. Then a mechanical stop is placed so that no further increases in length can occur. The importance of the preload is that it determines the initial length of the muscle and, consequently, the maximum force possible, in keeping with the active force–length relation. Then a mechanical stop is placed so that no further increases in length can occur. Additional loads now can be placed on the apparatus without changing muscle length. The total load is known as the *afterload*. The name "afterload" derives from the fact that the muscle does not "see" this load, as it is borne by the stop, until "after" it is stimulated. The muscle is then stimulated and when the muscle generates an isometric force just greater than the afterload, the muscle shortens, as indicated in tracing on the drum and shown on the unrolled drum paper in the right panel of Fig. 46.5. During the initial moments after shortening begins, there is a steady rate of shortening (often extrapolated), which subsequently declines and stops as the muscle reaches its final shortened length. This length will correspond to that point in the active force–length curve corresponding to the afterload. Another way of visualizing "why shortening stops" can be seen in Fig. 46.5, in which the route of contraction can be shown against the force–length relation. As the muscle shortens, the afterload becomes isometric at a shorter length where, according to its force–length relation, the muscle can only generate force equal to that of the afterload. This is where shortening stops. Both the distance shortened and the velocity can be seen to be dependent on the afterload. In Fig. 46.5C, the relation between shortening velocity and afterload is plotted. The interesting feature is that this relationship is hyperbolic with the velocity decreases rapidly as the afterload is increased. Several equations have been proposed to fit these data, however, the one most widely used is an equation attributed to A.V. Hill, which is expressed as:

$$(F + a) \times (V + b) = a \times (V_{max} + b) = b \times (F_o + a) \quad (46.1)$$

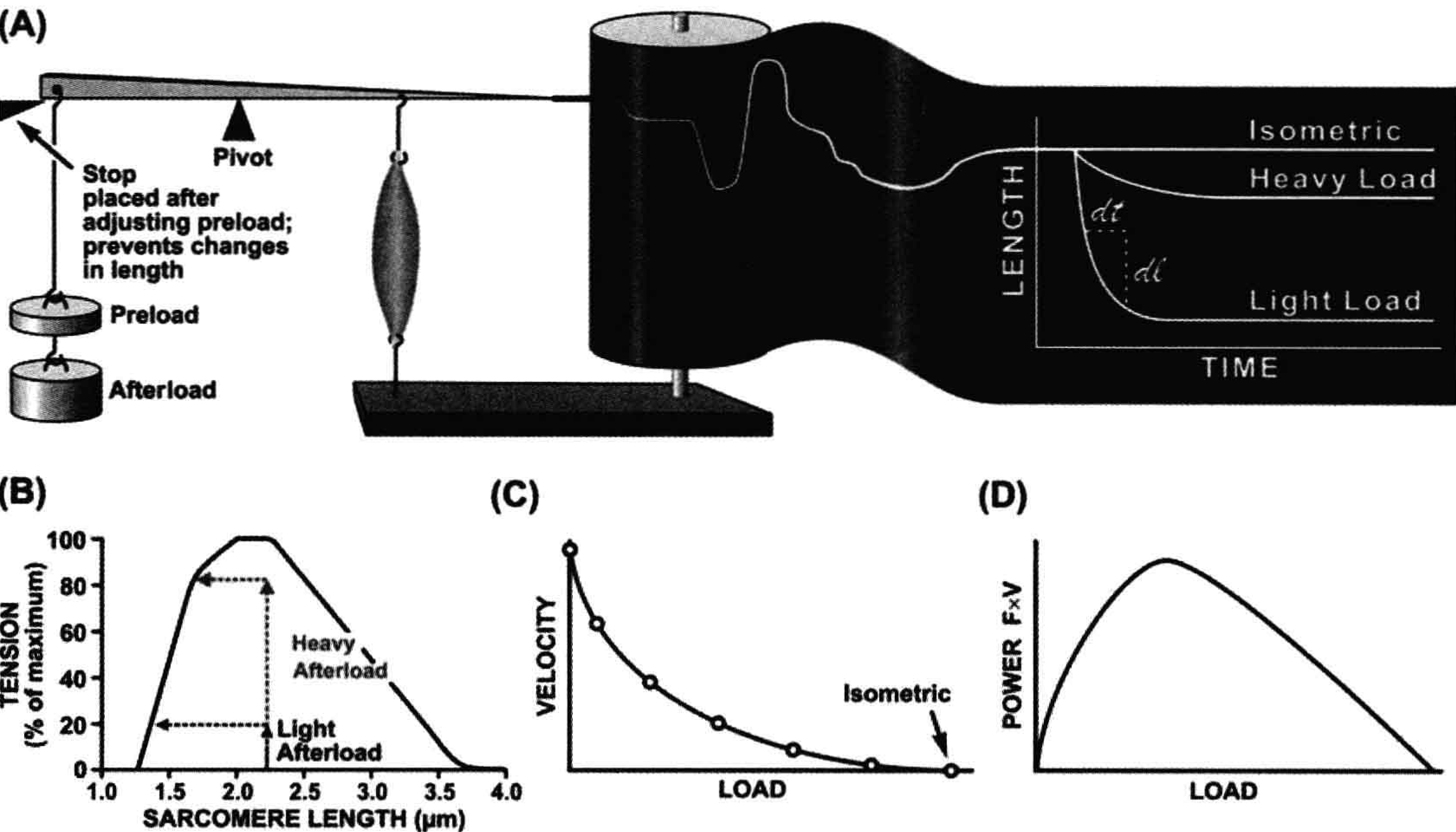


FIGURE 46.5 Relations between afterload and velocity, extent of shortening, and power generated by muscle. (A) Historical "Afterload Contraction" apparatus (left panel) and length tracing vs time (right panel). (B) Afterload contraction trajectory plotted on a length–tension plot. Muscle force–length relation is superimposed, showing its limitation on the extent of muscle shortening. (C) Velocity vs afterload relation. (D) Power (= load×velocity) vs Afterload relation.

where a and b are constants, Fo is the isometric force and Vmax is the unloaded shortening velocity. a/Fo = b· Vmax are dimensionless constants that determine the curvilinearity of the Hill equation and are equal to ≈0.3 for skeletal muscle. The mechanistic origin of this parameter is controversial. Although low values are often associated with efficient muscle performance, a generally accepted theoretical basis remains to be found. The parameter a was initially proposed by Hill to be related to a heat measurement, called the shortening heat, tying energetics to mechanics, but this was shown not to be constant. Although many other equations have been proposed, the scientific stature and an apparent link between heat and mechanical measurements led to the dominance of the Hill equation in the literature.

The power output of muscle, which is the product of afterload times velocity, can be calculated from the relation between afterload and velocity. A consequence of the hyperbolic nature of the Hill equation is that the power output of muscle shows a relatively broad range around a maximum. An advantage of the Hill formulation over others is that it is symmetrical. This can be seen best in its normalized form:

$$(\chi + \theta) \times (\vartheta + \theta) = \theta \times (\theta + 1) \qquad (46.2)$$

where χ is the normalized force (F/Fo), ϑ is normalized velocity (V/Vmax)s and θ = a/Fo = b/Vmax. As power is given by the product of force times velocity, Equation 46.1 or 46.2 can be readily used to derive a relationship between power and load or velocity. The optimal load or velocity for maximum power output can also be derived from these equations and is equal to $\sqrt{\theta^2 + \theta} - \theta$; for skeletal muscle this equals about 0.3 times the maximum load or velocity. These equations are useful in the design of ergonometric devices to optimize performance. The molecular basis for the force–velocity relation is not clear and many hypotheses have been put forth. The widely known of these models is the kinetic scheme of A.F. Huxley (1957). In this model, rate constants for cross-bridge formation/breakage are functions of position. This model (Fig. 46.6) can explain the relationship between force and velocity, but it is not adequate for the transient behavior as those seen (see Fig. 46.10) when rapid step changes are imposed (see Section IIIF on tension transients). While it is relatively easy to envision the "geometric limits" imposed by the sliding-filament model which underlie the force–length relation, especially at long sarcomere lengths (see Fig. 46.4), it is not as easy to visualize the "kinetic constraints" which underlie the force–velocity relation. Simplistically, one possible view is that the probability of making a force generating attachment of a myosin head to an actin is lower when the thick and thin filaments are moving relative to one another.

IIIE. Cross-Bridge Theory

The most prevalent theory for force generation involves the concept of cyclic interactions between the heads of myosin molecules (cross-bridges) projecting from the thick filaments and the actin molecules comprising the thin filaments. Evidence from electron micrographs indicates that these cross-bridges, in various conformations, bridge the gap between thick and thin filaments. Based on both micrographs and x-ray diffraction data, these projections occur at intervals of 14.3 nm. The best evidence (from mass comparisons) is that three myosin molecules are located at each site, with an identical repeat at about 43 nm. The structure of the thick filament is shown in Fig. 46.7.

The evidence for cyclic interaction is partly based on structural considerations. Striated muscle can generate force and shorten over a range of about 50–150% of its rest

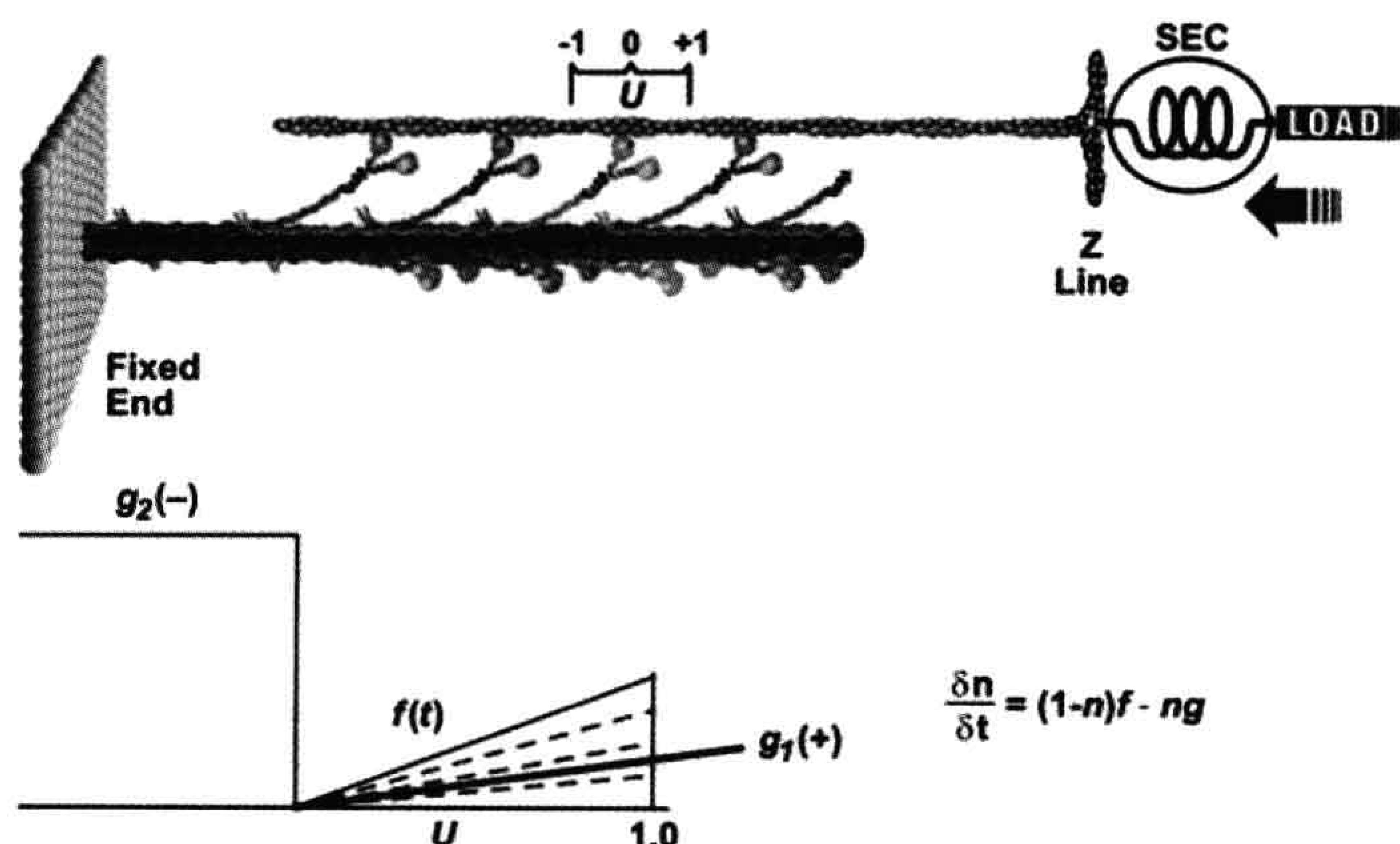


FIGURE 46.6 Schematic representing a two-element model of muscle and Huxley's (1957) mathematical model. Top: Half-sarcomere containing a myosin thick filament and actin-containing thin filament, which constitutes a contractile component, coupled in series with an elastic component (SEC). Bottom left: functional form of rate constants for cross-bridge attachment (f) and detachment (g_1 and g_2) as a function of U, the cross-bridge position coordinate shown at top. Bottom, right: differential equation describing the change in number of cross-bridges. Force generated in this model is equal to the number of attached cross-bridges, n, times the force of an individual cross-bridge.

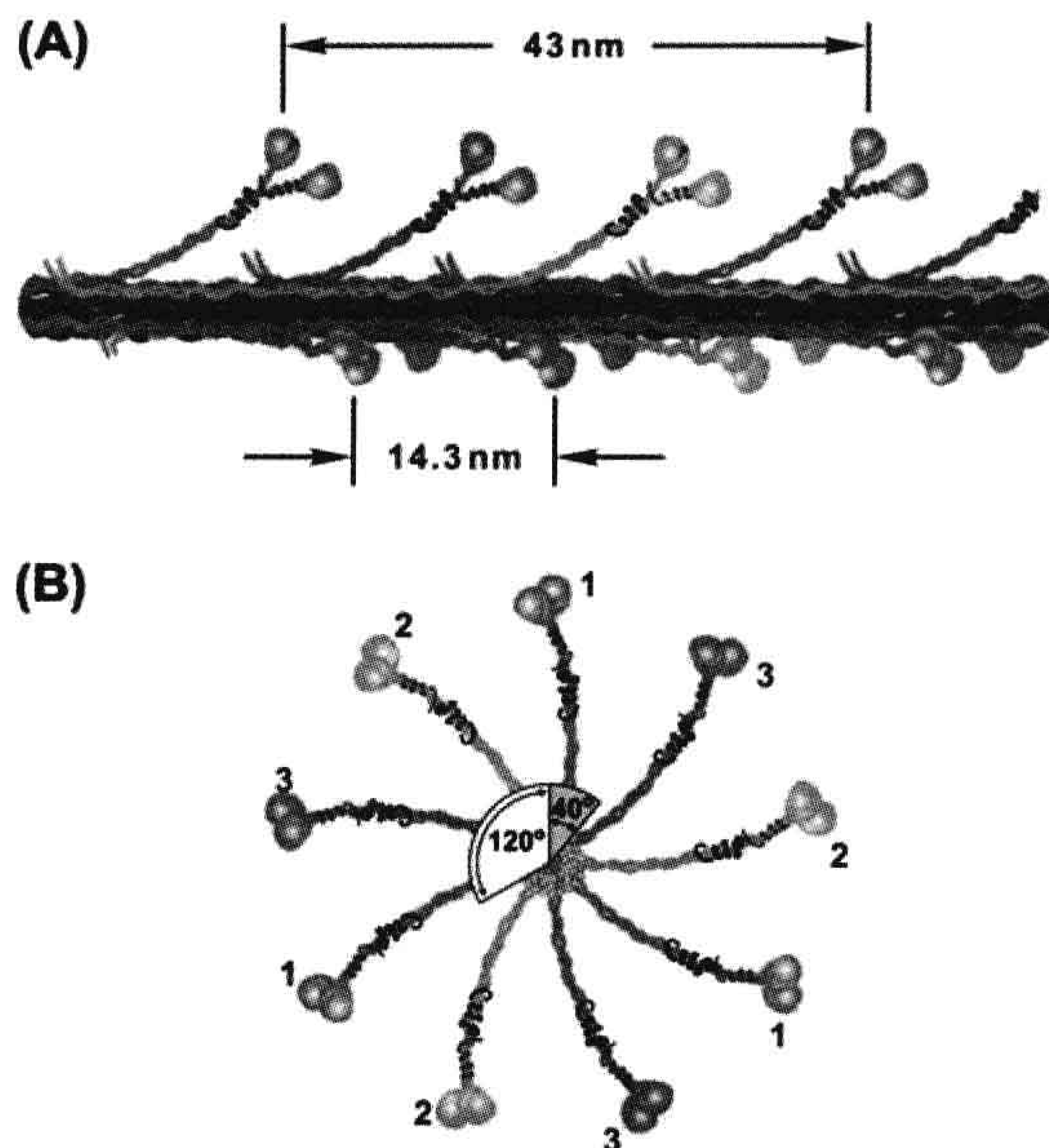


FIGURE 46.7 Rendition of the myosin thick-filament structure based on current evidence. (A) Longitudinal view showing three myosin molecules per site rotated from one another by 120°. Cross-bridge sites occur every 14.3 nm, but are rotated by 40° with respect to the previous site, so that an identical repeat occurs every 43 nm. (B) End view of the filament showing three superimposed color-coded sites.

length. Since a muscle is composed of identical sarcomeres, each sarcomere operates over the same range. For a sarcomere of 2.2 μm, this operating range would be about 1.1−3.3 μm. Since the thin filaments of each half of the sarcomere move toward the center, a sarcomere shortening from 3.3 to 1.1 μm (Δ of 2.2 μm) would require a movement of thin filaments on each side of the sarcomere of one half that distance or 1.1 μm relative to the thick filament. This distance is considerably longer than the cross-bridge spacing (0.014 μm) and is, in fact, longer than a single myosin molecule (0.150 μm). So, it is not possible for a myosin cross-bridge to remain attached to actin in a structure with interdigitating filaments of constant length and relative sliding of more than 1 μm. Hence some form of cyclic interactions between myosin cross-bridges and actin is required to permit the observed relative filament movement. For example, if a cross-bridge can attach over a working range of 10 nm, than 100 repeated cycles of attachment/detachment would be required for a relative filament movement of 1 μm.

A second basis for the cross-bridge theory arises from biochemical studies on isolated muscle proteins. The myosin molecule consists of a long rod-like region important for assembly into thick filaments and a globular head region, which contains the ATPase activity. The globular head, or S1 region (see Fig. 46.7), has dimensions consistent with the projections identified as cross-bridges in electron micrographs. Studies of the kinetics of ATP hydrolysis by myosin, involving stopped-flow apparatus and other techniques for the measurement of rapid time courses, have provided a framework for cyclic interaction of the S1 myosin head with actin. The kinetic scheme is shown in Fig. 46.8. The physiological ATPase activity (known as Mg^{2+}-ATPase activity) of purified myosin is relatively low, but, importantly, it is activated 200-fold by actin, the principal protein of the thin filament. In the absence of ATP, purified actin and myosin bind strongly. In intact muscle, this is the cause for the stiffness of muscle in the absence of nucleotide associated with "rigor". Addition of ATP to a "rigor complex" of actin and myosin dissociates the complex by producing a weak binding state, because the binding of ATP to myosin weakens the binding to actin (see Fig. 46.8, steps 3 to 4). ATP hydrolysis by myosin alters the binding characteristics and cross-bridge orientation (step 4 to 1), leading to a strong binding state (step 1 to 2). The biochemical cycle is completed as the products of ATP hydrolysis, first inorganic phosphate (Pi) and then ADP, dissociate from the myosin head. One ATP molecule is hydrolyzed per cross-bridge cycle. The structural details of this cycle have recently been significantly upgraded due to the high resolution x-ray diffraction data of the myosin head (Rayment et al., 1996) and of single muscle fibers (Lombardi et al., 2004). As shown in the insets in Fig. 46.8, these data suggest that binding of ATP to myosin alters the conformation of the myosin head and consequently its binding to actin. Correlating this cross-bridge cycle based on biochemical data with mechanical steps in force generation is a major focus of muscle

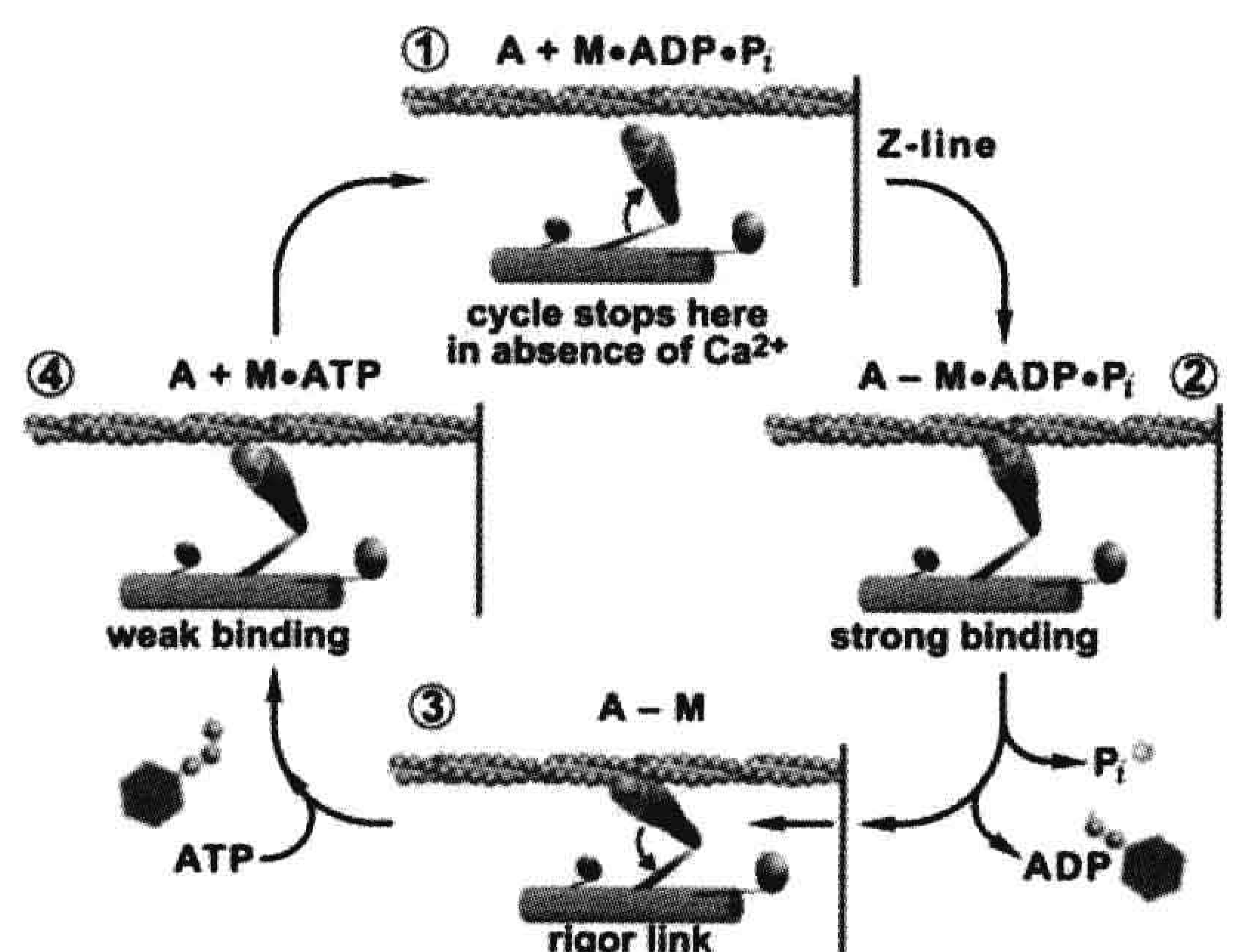


FIGURE 46.8 The cross-bridge cycle. Schematic of the combination of information from muscle mechanics and biochemical kinetics of the actin activated myosin ATPase (see text for details).

physiology. One approach involves the study of rapid mechanical transients.

IIIF. Transient Mechanical Behavior and the Cross-Bridge Cycle

Analysis of the mechanical properties of any material generally involves the imposition of known mechanical perturbations (e.g. step or sinusoidal changes in length or force; called strain) while recording the force (stress) response of the system. When modeling the time course of the response, combination of two types of components (spring-like and viscous elements) can account for the behavior of most materials. The behavior of spring-like material is characterized by an instantaneous relationship between force and length, whereas for a viscous element, a resistive force is proportional to the rate of imposed length change. Combination of these elements can approximate the behavior of many materials (Fig. 46.9).

Using this type of analysis, the steady-state behavior of muscle has long been adequately described by two parallel elements: a spring-like element, representing the passive force—length characteristics and a contractile element representing the characteristics an activated muscle (Hill, 1938). For our generalized skeletal muscle at L_0, a length of optimal filament overlap, little parallel passive force exists. Thus, the behavior we are describing is that of the contractile component alone. Imposition of a rapid step shortening leads to a rapid drop in active force, followed by a redevelopment of tension. This suggests that muscle behavior can be modeled by two elements linked in series (see Fig. 46.9). This model consists of a series elastic spring, which instantaneously responds to the imposed length change and a contractile component, whose behavior is described by the Hill equation, a non-linear, viscous like relationship between force and velocity. For this model, step changes in force yield a rapid, in-phase shortening, attributable to the series elastic spring followed by a slower shortening phase, attributable to the contractile component. This model can explain some aspects of transient mechanical behavior and was the first to be used to associate anatomical elements with model elements. The anatomical site associated with the series elastic component (SEC) has evolved and has considerably altered our view of muscle mechanics.

The SEC can be characterized in terms of the extent of shortening required to discharge the maximal isometric force (F_o). Studies on intact, whole muscle suggested that a change in the length of muscle of 2—3% L_o was sufficient transiently to reduce active force to zero (Jewell and Wilkie, 1958). This elasticity can be attributed to connective elements, such as tendons and similar passive structures, as well as any elasticity in the apparatus used to measure force. A 2—3% change in L_o can be translated to

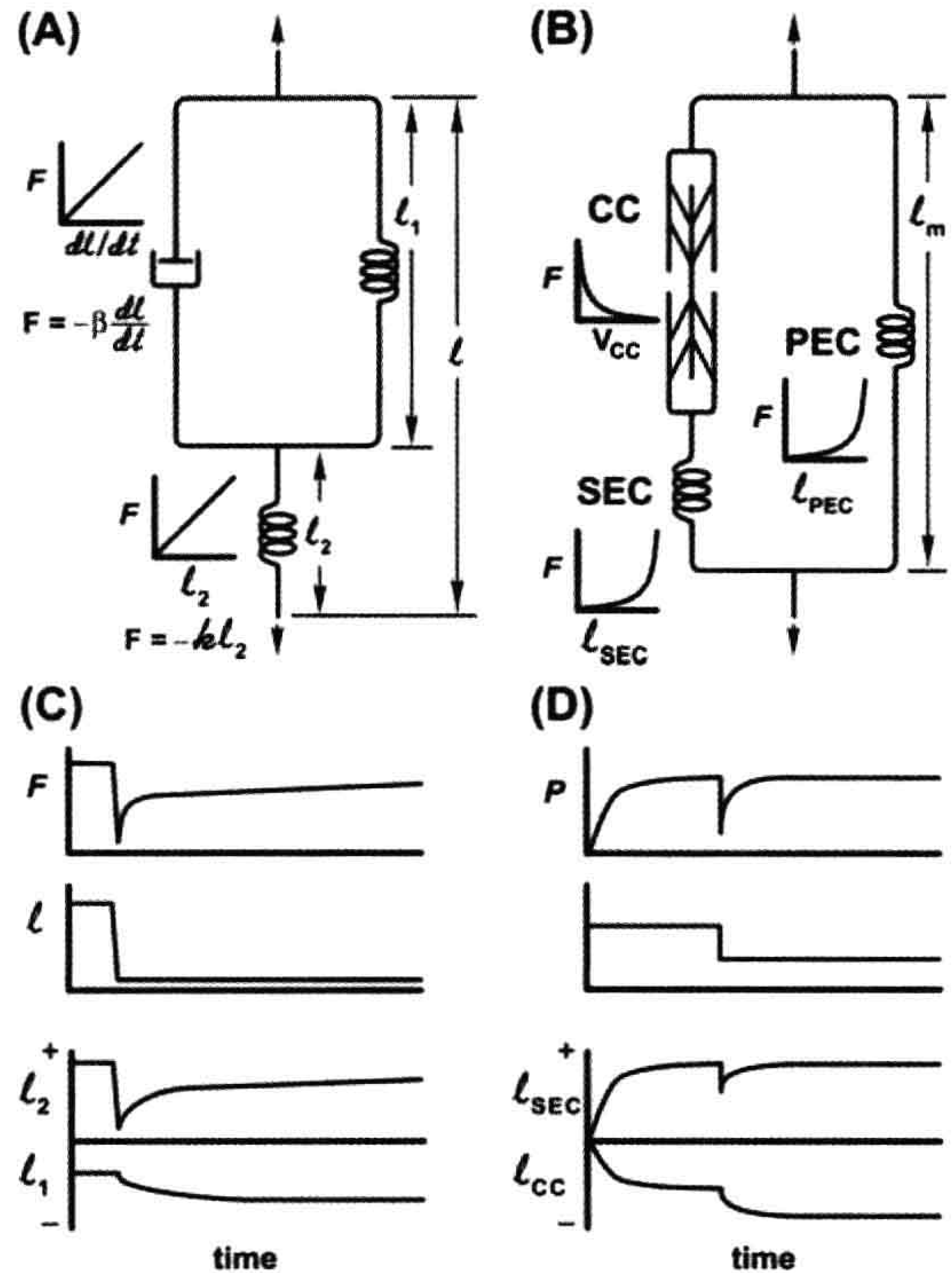


FIGURE 46.9 Models forming the basis of classic analysis of muscle mechanics. (A) Three-element Voight model containing two linear spring elements (l_l and l_2) combined with a "dashpot", a linear viscous element. (B) Three-element model of muscle containing a contractile component (CC), a parallel elastic component (PEC) and a series elastic component (SEC). Graphs indicate the behavior of each element. (C) Time course of the response of the Voight model and its individual components to imposition of a rapid step change in length. (D) Similar responses of the muscle model to a rapid step change (note that the initial muscle length here is chosen such that the PEC does not play a role in this response).

a relative filament motion of 20—30 nm, i.e. 40—60 nm for a 2.2 μm sarcomere. This is significantly larger than the cross-bridge spacing (14.3 nm), reinforcing the concept that such behavior is external to the contractile component and in series with cross-bridges. The two-component model is phenomenologically useful and it can predict behavior of many whole tissues, particularly those with large intrinsic SEC, such as some smooth muscle. However, as improvements in the temporal resolution of mechanical measurements advanced, this model was found to be inadequate for the behavior of single skeletal muscle fibers.

In the 1970s, techniques for imposition of step changes greatly improved as devices to impose length changes, transducers and recording apparatus achieved millisecond resolution. At the same time, techniques for working with single muscle fibers and "spot follower" devices for control of sarcomere length, rather than overall muscle length,

were developed. These new measurements indicated that the true SEC extent was much smaller than that previously measured in whole muscle. (Previous measurements apparently also included an artifact of the slow response time of the recording system.) Current estimates of the SEC for striated muscle are less than 0.5% L_o, approximately 6 nm per half-sarcomere, clearly in a range to be potentially associated with cross-bridges themselves. Moreover, the time courses of responses (Fig. 46.10) were not consistent with an instantaneous spring connected in series with a contractile element, which also was characterized by an instantaneous force–velocity relationship.

Huxley and Simmons (1971) provided the first evidence that an instantaneous spring-like behavior could be attributed to the cross-bridges themselves. They exploited the fact that the number of cross-bridges could be varied by taking advantage of the force–length relationship. As shown in Fig. 46.10, if the SEC is intrinsic to the cross-bridge, then the magnitude of the shortening step required to discharge the instantaneous elasticity is also intrinsic to the cross-bridge. Thus, the change in length to discharge force would be independent of the number of cross-bridges and, consequently, independent of force. Alternatively, if the instantaneous elasticity were external to the cross-bridges, it would be governed by its own relationship between force and extension. Reduction of force (and number of cross-bridges) by changing the initial muscle length in this case would reduce the step shortening required. They showed that altering active force by changing the initial muscle length did not alter the size of the step shortening required to discharge the maximum isometric force at any initial length. These results supported the concept that the instantaneous spring-like behavior is an intrinsic cross-bridge property and the cross-bridges act as independent force generators. An important corollary of these studies is that the instantaneous stiffness can be used as an index of the number of attached cross-bridges at any moment. This corollary has been used in numerous studies to assess the effects of various interventions on attached cross-bridge number. There is evidence, however, both mechanical (Higuchi et al., 1995) and x-ray

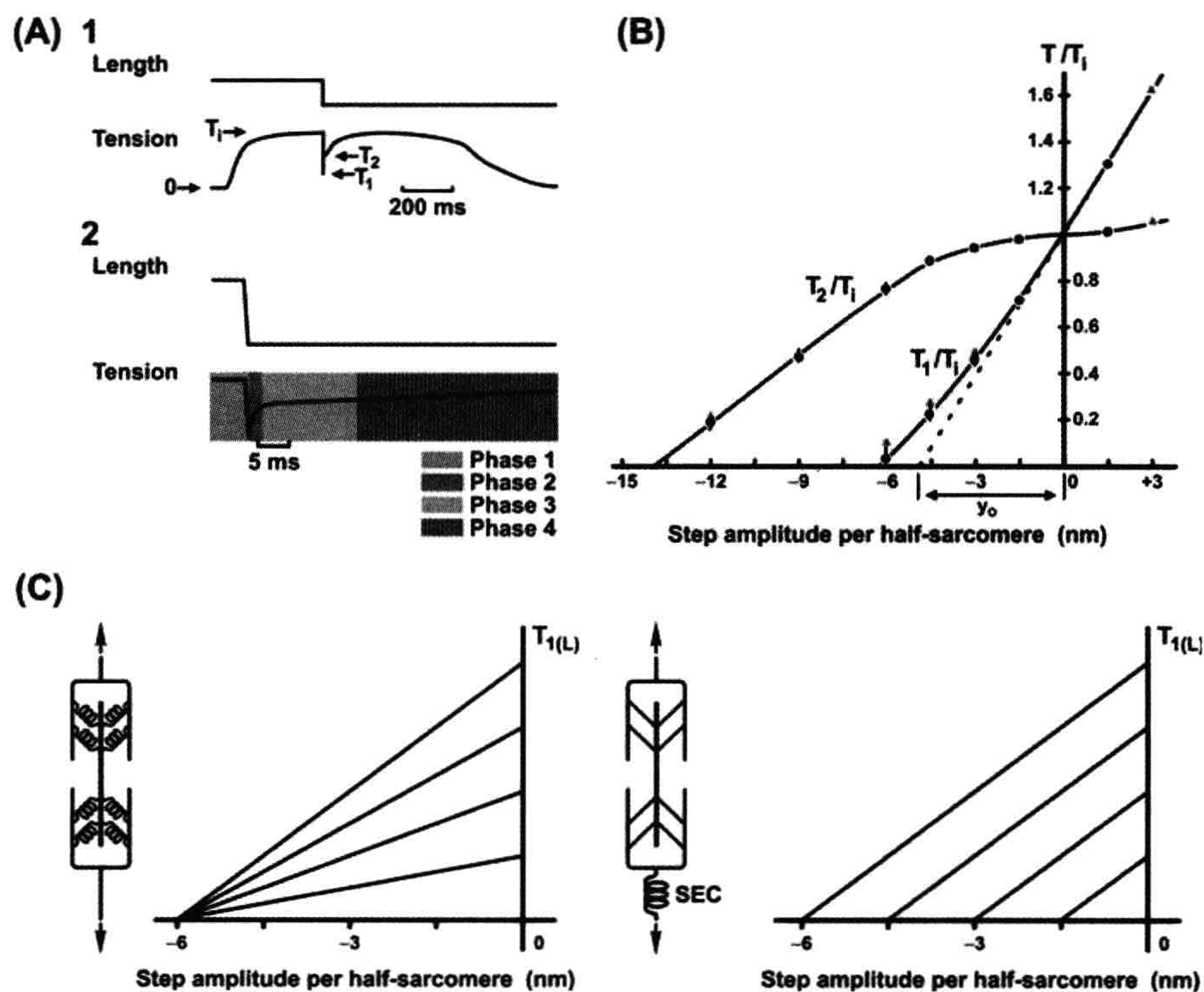


FIGURE 46.10 Huxley–Simmons (1971) experiments. (A) Transient force responses to very rapid (<1 ms) step changes in length, which led to revision of classical muscle mechanics. (B) Dependence of phase 1 and phase 2 force amplitudes on muscle length. (C) Dependence of T_1 if the series elasticity resided within the cross-bridge itself (left) and if the series elasticity was located in a classic SEC (right). Huxley and Simmons data support in the model shown in the left panel of panel of (C).

diffraction (Huxley, 1996), which suggests that a significant fraction of the instantaneous stiffness is attributable to the thin filaments. Thus, one should exercise some caution in the interpretation of stiffness measurements in terms of the number of attached cross-bridges.

To summarize a current consensus understanding of muscle contraction, force generation is due to cyclic interaction of myosin heads projecting from the thick filament with actin of the thin filament. These cross-bridges act as independent sites for force generation. Total active force is proportional to the number of activated cross-bridges whose number is geometrically constrained by the extent of filament overlap. The mechanism of cross-bridge force generation is still the subject of considerable investigation. A current model based on biochemical kinetics and cross-bridge mechanics studies is shown in Fig. 46.8. A shift in orientation of the cross-bridge in the strong binding states (steps 3–4) is associated with the force generating step in this model. Of course, any consensus is just an approximation, likely to be refined in the future. Some of the areas of interest to the understanding cross-bridge mechanisms for the next iteration include (Huxley, 2000, Offer and Ranatunga, 2010): significance, location and accurate measurement of cross-bridge compliance; significance of filament compliance, dependence of rate constants on compliance and the independence of cross-bridges.

IV. MUSCLE ENERGETICS

Studies of muscle energetics parallel those of mechanical and biochemical kinetics and have the same ultimate goal understanding the mechanism of mechanochemical transduction at the cross-bridge level (Barclay et al., 2010). Historically, muscle energetics has been associated with the measurement of muscle heat production. A rise in temperature, the first indication of chemical reactions in muscle, can be measured with a temporal resolution which far exceeds that of direct chemical determinations. Moreover, heat measurements were made long before the chemical reactions driving muscle contraction were known (Hill, 1912). In fact, heat measurements and thermodynamic analysis were essential to ultimately identifying the chemical reactions underlying muscle activity. The essential principle comes from application of the first law of thermodynamics which, under constant pressure, states that the change in enthalpy (ΔH) is equal to the sum of heat (Q) production plus work done (W) by the muscle. The change in enthalpy, in turn, can be related to the sum of the changes in number of moles of each species (Δn_i) multiplied by its specific enthalpy (h_i):

$$\Delta H = \sum (\Delta n_i \times h_i) = Q + W \qquad (46.3)$$

Thus, by measuring muscle heat and work restrictions can be placed on potential underlying chemical reactions. For example, one can test whether the enthalpy change in predicted reaction x sufficient to explain the heat plus work produced during contraction.

One of the first application based on of this type of analysis was carried out by Wallace Fenn (1923), who tested a theory known as the viscoelastic model of muscle contraction:

> *Thus the view came to be accepted that on stimulation a muscle developed a given amount of heat and a given amount of elastic potential energy, both varying with the length of the fibres of the muscle. The amount of elastic potential energy which could be recovered as work depended merely upon the art of the experimenter in arranging his levers and had no relation to the total energy liberated.*

In other words, stimulation elicited a fixed or quantal extent of some unknown reaction(s), whose energy was transduced to a fixed amount of heat plus work. A muscle shortening under a load would produce work and, according to this theory, less heat would be produced than a muscle under isometric conditions not producing work. Fenn's studies showed that the $Q + W$ in a work-producing contraction exceeded the heat produced in an isometric contraction (in which work is minimal). This "Fenn effect" ruled out the viscoelastic model and was important in that theories of muscle energy conversion had to be configured in terms of chemical reactions that were closely coupled to mechanical events. Since that time all models of muscle contraction must pass this stringent energetics test.

The studies of the nature of the chemical reactions coupled to muscle activity, both those immediately coupled mechanical events and those involved in the subsequent recovery by intermediary metabolism, have been closely associated with muscle energetics. The history of the search for the identity of the reactions immediately coupled to muscle mechanical output parallels the history of biochemistry itself. Because of increased understanding of the biochemistry of fermentation and association of lactate with muscle contraction, it was first believed to be a driving reaction, "lactate acid theory". However, Lundsgaard (1938) showed that muscle treated with iodoacetate (which blocks glycolysis via inhibition of G3P dehydrogenase and thus lactate production) could still contract. Fiske and SubbaRow (1927) showed that inorganic phosphate (P_i) is liberated during contraction, arising not from a glycolytic intermediate, but from a new "phosphagen", phosphocreatine (PCr). Myosin was known to be an ATPase, but there was little change in ATP concomitant with contractile activity. The connection was made by Lohmann (1934), who

discovered an enzyme (creatine kinase) which catalyzes the reversible phosphorylation:



$$PCr + ADP \longleftrightarrow ATP + Cr \quad (46.4)$$

From these observations grew the energetic schema that ATP is the immediate energy source for contraction directly coupled to the myosin ATPase. In intact muscle, PCr rapidly rephosphorylates ADP via the Lohmann reaction (or creatine kinase reaction) and only breakdown of PCr to Cr and P_i can be measured. Tests of whether this was sufficient to account for the change in enthalpy or to account for the free energy change required for the work produced awaited the development of rapid-freezing technology and microchemical analysis of muscle extracts which occurred during the late 1960s. These "energy balance" studies, reviewed in Woledge et al. (1985), tested the validity of Equation 46.3. Under conditions in which metabolic resynthesis was minimized, the measured breakdown of PCr multiplied by its partial molar enthalpy (34 kJ/mol) should be equal to $Q + W$, if this was the only chemical reaction occurring. As shown in Fig. 46.11, this equality was not valid; $Q + W$ was significantly greater than that accounted for by PCr breakdown (Gilbert et al., 1971). The implication was that there was a "missing" reaction associated with an "unexplained" enthalpy production occurring during contraction and, if valid, would overturn the reigning energetic dogma. Moreover, if heat records could not be interpreted in terms of ATP breakdown (coupled to PCr breakdown), then most kinetic models, starting with the classic Huxley (1957) formulation would need to be revised. Thus, energetics studies were focused on identification of the nature of the unexplained enthalpy

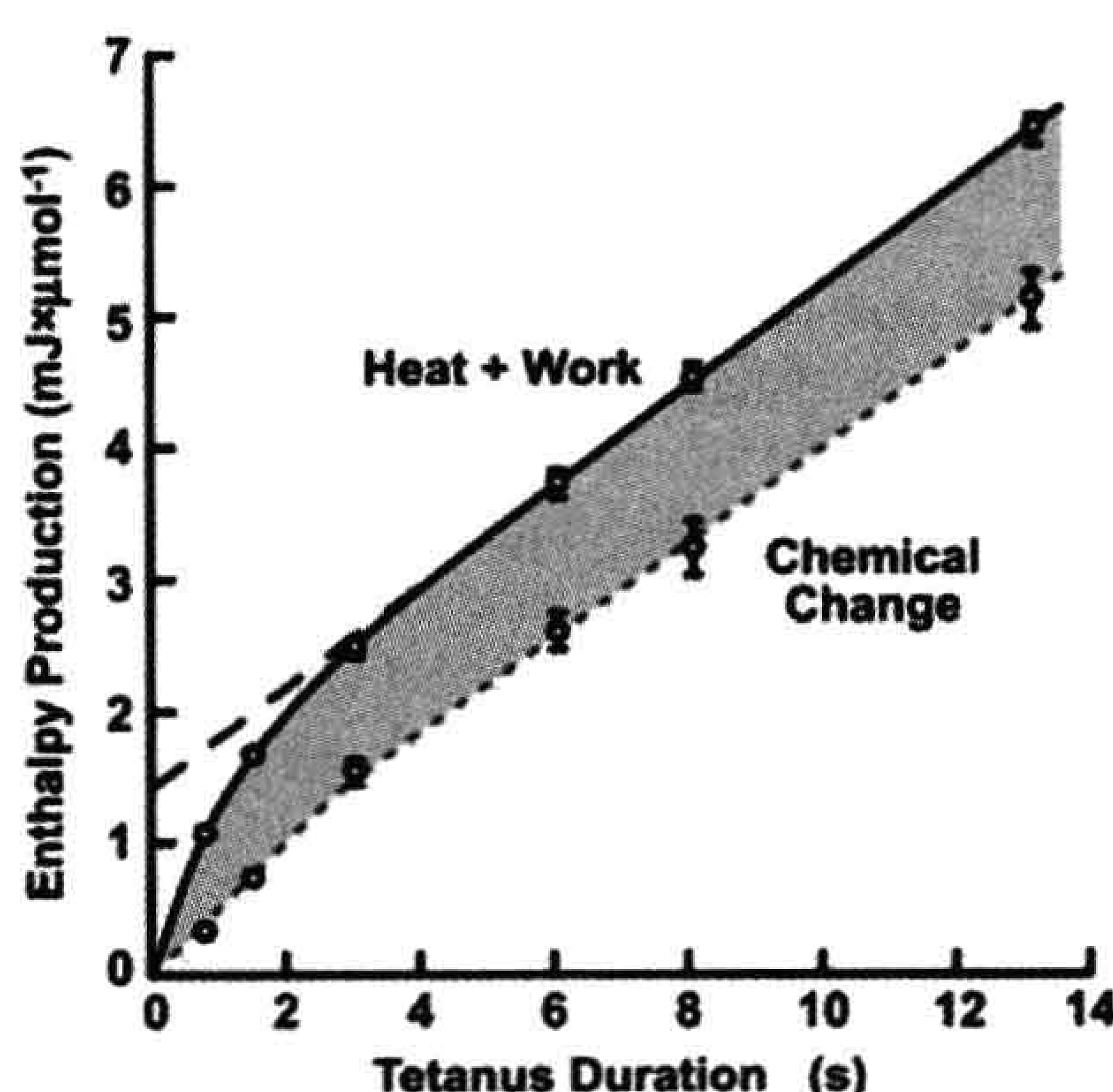


FIGURE 46.11 Skeletal muscle "energy balance". Enthalpy (heat+work) production as a function of tetanus duration is given as the solid line. The expected enthalpy (chemical change times the enthalpy of PCr breakdown, 34 KJ/mol) is plotted as the dotted line. Shaded area represents the unexplained enthalpy. *(Adapted from Woledge et al., 1985.)*

and a potential missing reaction associated with contraction.

In a parallel fashion, "biochemical" balance studies (Kushmerick, 1983) were also directed at the question of a missing reaction, but with chemical rather than physical techniques. The rationale is that if ATP hydrolysis and its rephosphorylation by PCr are the only reactions occurring during contraction, then the extent of this reaction should be equal to the ATP synthesized during recovery. If resynthesis is governed by theoretical biochemical stoichiometry, then the amount of oxygen consumed during recovery would have been equal to 1/6.5 times the PCr broken down during contraction. The experimental test of this hypothesis is shown in Fig. 46.12. Again an imbalance was observed; the extent of recovery metabolism associated with resynthesis of ATP exceeded that which could be accounted for by PCr breakdown during contraction. Paul (1983), using both physical and biochemical "energy balance" techniques, showed that oxidation of glucose was the only net reaction occurring during a complete contraction/relaxation cycle. Not surprising in today's worldview, this ruled out a number of theories of the time based on a continuous degradation of muscle for each contraction. The combinations of techniques yield data that indicated that the initial chemical imbalance, i.e. less ATP breakdown than predicted during contraction, is accompanied by additional breakdown of ATP after contraction.

A resolution of the "missing" reaction question apparently resided in the discovery of the protein parvalbumin in amphibian muscle and its role as a Ca^{2+}-binding site (Gillis et al., 1982). Parvalbumin binds a significant amount of the Ca^{2+} released by the sarcoplasmic reticulum (SR) during contraction. This binding is associated with a substantial evolution of heat. There is also evidence that Ca^{2+} is returned to the SR after the contraction ceases, which would require activity of the Ca^{2+} pump and concomitant hydrolysis of ATP. This explanation is perhaps the most widely held, but it is not a universal explanation. For example, the biochemical balance studies would suggest that the post-contractile ATP breakdown is proportional to the duration of stimulus, whereas the enthalpy balances apparently indicate that the unexplained enthalpy attains a plateau value. Moreover, some unexplained enthalpy is associated with mammalian striated muscle, which does not contain parvalbumin. Nevertheless, the schema involving ATP as the immediate driving reaction, with PCr as the source of chemical energy for rapid resynthesis in intact muscle appears valid. This is further supported by (1) thermodynamic data indicating that the free energy provided by ATP during contraction is sufficient to account for the work produced (reviewed in Woledge et al., 1985) and (2) many studies using permeabilized muscle indicating that ATP is the only chemical energy source required for contraction.

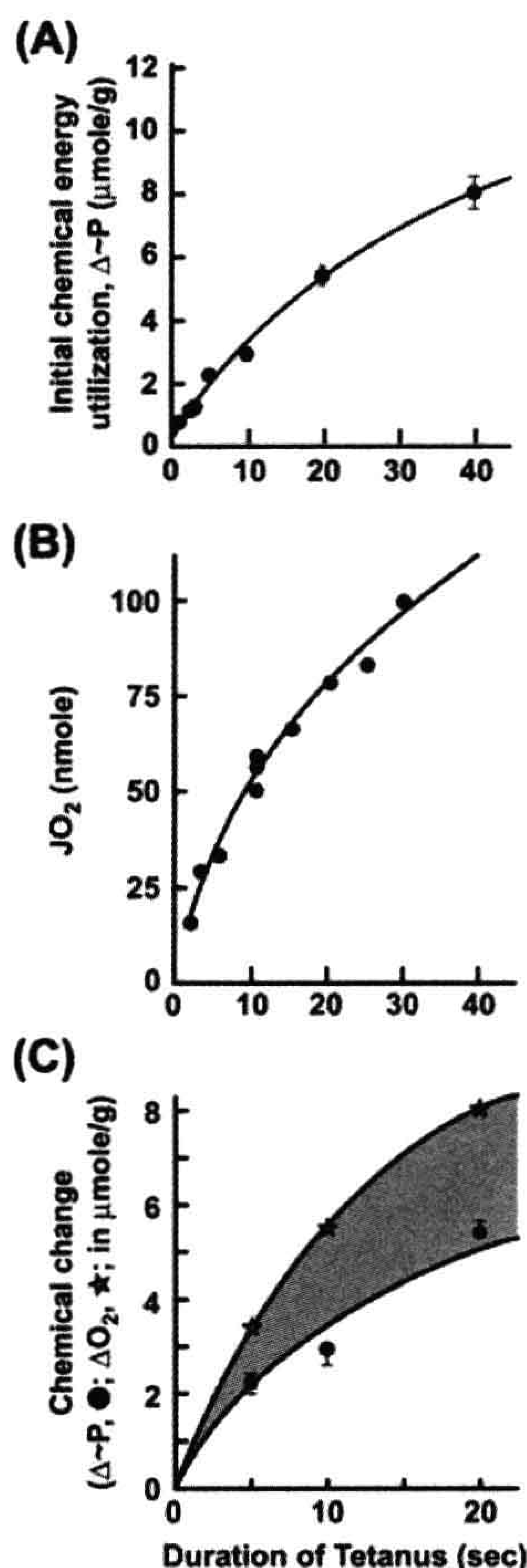


FIGURE 46.12 Skeletal muscle "biochemical energy balance". (A) The initial high-energy phosphagen (PCr + ATP) breakdown during contraction as a function of tetanus duration. (B) Total recovery oxygen consumption elicited by the contraction durations plotted on the ordinate. (C) The total phosphagen resynthesized based on theoretical stoichiometry and the measured O_2 consumption (open stars) and the measured phosphagen breakdown during contraction (filled circles). The shaded area represents the excess of ATP synthesis over the phosphagen breakdown measured during contraction. *(Adapted from Kushmerick, 1983.)*

V. MUSCLE METABOLISM

Mechanochemical energy transformation and the breakdown of high-energy phosphagens under various conditions form one branch of study known as muscle energetics. Energy metabolism and intermediary metabolism are two terms often used to describe the other major branch of energetics, that of the study of the metabolic provision of phosphagen in support of muscle activity and the mechanisms of coordination of metabolism with contractility. Muscle mechanical activity is supported by ATP provided by both oxidative phosphorylation and glycolysis. Historically, the biochemistry of these pathways often mirrors our understanding of muscle, as this tissue was often the major model for biochemical studies. For the historical aspects with respect to muscle contraction, the treatise of Needham is highly recommended (Needham, 1971).

Perhaps of most recent interest in this field is the re-examination of the theories whereby contractile ATP use is coordinated with metabolic resynthesis of ATP. For skeletal muscle, most prevalent theory is that of acceptor- or ADP-limited respiration. In the case of isolated mitochondria in the presence of substrate, their rate of oxidative phosphorylation, state III is limited by the availability of ADP as the substrate for rephosphorylation. Because the hydrolysis of ATP concomitant with contractile activity is increased, one might anticipate that an increase in ADP could naturally couple the increased usage with synthesis. The creatine kinase reaction, coupled with the amount of PCr in striated muscle, buffers the ATP concentration. Under the assumption that this reaction is in equilibrium, the level of free (i.e. not bound) ADP can be calculated to be in the region of 10 μM. This is also in the range for the K_m for ADP for ADP control of mitochondrial oxidative phosphorylation. This mechanism can reasonably well predict PCr breakdown and its resynthesis for a contraction/relaxation cycle in human muscle (Kushmerick, 2005). On the other hand, significant increases in cardiac (Balaban, 2009) and smooth muscle (Hardin et al., 2000) oxidative metabolism occur in the absence of changes in PCr or ATP, indicating that increases in energy metabolism can match the contractile ATP utilization in the absence of changes in ADP. There are a number of hypotheses in this area. The most prominent ones propose regulation of oxidative metabolism by $[Ca^{2+}]_i$ (Liu and O'Rourke, 2009) and mechanisms involving a substrate level "push," e.g. by mobilization of substrate, leading to increased NADH levels.

A second area of growing interest on the metabolism side of muscle energetics is the effect of micro-compartmentation of metabolism and its subserved function. Instead of being distributed in a random fashion in solution in the cytosol, many enzymes important in energy metabolism are apparently localized within the cell, often in close apposition to energy-dependent processes. Perhaps the most widely studied system is that of creatine kinase (Ishida et al., 1994) which is localized at the m-line of striated muscle as well as in membrane structures and mitochondria. In permeabilized muscle, endogenous phosphocreatine alone can support contractile activity, suggesting a close relationship between the myosin ATPase and creatine kinase. Similarly, phosphocreatine has been shown to support Ca^{2+} uptake by sarcoplasmic reticulum isolated from skeletal muscle. The enzymes involved with

glycolysis are also localized primarily on the thin filaments and associated with the plasmalemma and sarcoplasmic reticulum. There are increasing numbers of studies for skeletal (James et al., 1996; Levy et al., 2008), cardiac (Weiss and Lamp, 1987) and smooth muscle (Hardin et al., 2000), indicating that ATP provided by glycolysis supports functions different from those dependent on oxidative metabolism. This is particularly striking in smooth muscle, in which the oxidative and glycolytic components of metabolism can be of similar magnitude (Paul et al., 1979). ATP-dependent processes associated with the plasma membrane, such as the Na^+-pump and ATP-dependent potassium channels, are apparently particularly dependent on ATP generated by aerobic glycolysis, whereas the ATP requirements for the force generating actin–myosin ATPase interaction are apparently more strongly correlated with oxidative metabolism. The bases and consequences of this cellular organization are not fully understood, but have been suggested to be related to either greater energy transduction efficiency or the need for independent regulation of different cellular functions.

VI. COMPARATIVE MECHANOCHEMICAL FUNCTION

VIA. Striated Muscle

The general features just described are common to all muscle function, however, there is a great variety of muscle types adapted to specialized conditions. Among skeletal muscle, perhaps the most familiar adaptation is the difference between red and white muscle. The nomenclature has a long history and many different schemes exist. Histologically and functionally three major classifications predominate, termed fast glycolytic (FG), slow oxidative (SO) and fast oxidative–glycolytic (FOG), reflecting their gross properties. Most whole muscle contains various mixtures of these three basic muscle fibers and appears pale compared to red muscle, which is composed primarily of SO fibers. The red color is due to the presence of myoglobin, a protein that facilitates the diffusion of oxygen.

These fiber types are adapted for different power requirements. The FG fibers provide large forces that can be rapidly activated and relaxed, but are susceptible to fatigue. Their metabolism depends heavily on glycolytic production of ATP, which can respond rapidly to large changes in energy requirements associated with muscle contraction but has relatively limited capacity. For low level but continuous muscular activity, such as that required by postural muscles, the SO fibers are adapted with a high oxidative metabolic capacity. A lower actin-activated myosin ATPase of the SO fibers relative to FG fibers facilitates a more economical maintenance of force, however, this is accompanied by a slower velocity of shortening.

In primates, FOG fibers are relatively rare and highly specialized muscles (some ocular muscles appear to be composed primarily of this fiber type). Their twitch duration and shortening speed are intermediate between those of SO and FG fibers and are characterized by high levels of both glycolytic and oxidative metabolism. These differences in adaptation also extend to speed of activation, which is approximately three times faster in FG than SO fibers. Cardiac muscle has its own special adaptations and, in many ways, shares similarities with SO skeletal muscle fibers. A third muscle type, smooth muscle, is significantly different from striated muscle and is discussed in detail in the following section.

These gross differences in muscle fiber type have long been studied. Applying advanced molecular biology techniques, we now know that most muscle proteins exist as isoforms. Thus, recent interest has focused on the isoform–function relationships as well as the regulation of the expression of these various isoforms. What is of particular interest is that the number of expressed isoforms – and the theoretical possible variants – far exceed the three gross skeletal fiber types. Detailed information on isoforms is beyond the scope of this text and is available in specialized treatises (Pette and Staron, 2001; Westerblad et al., 2010).

VIB. Smooth Muscle

Historically, smooth muscle has been of interest because of its specialized function. It lines the hollow organs, such as blood vessels and the gastrointestinal (GI) tract. Its structure is less organized than that of striated muscle and thus somewhat less amenable to biophysical experimentation. For many years, its properties have been simply extrapolated from striated muscle. However, it is now clear that while many similarities exist, there are also significant differences. Studies of smooth muscle have significantly increased over the past decade. This can be attributed largely to its clinical relevance in terms of the diseases of industrialized society such as hypertension, asthma and GI motility disorders. However, much of the current interest has arisen from the discovery that the regulatory mechanisms at the contractile filament level are radically different from those of striated muscle.

Smooth muscle can develop isometric forces per cross-sectional area that are equal to or greater than those generated by striated muscle. This is all the more surprising in that the myosin content of smooth muscle is considerably less (about one-fifth) than that of striated muscle. These large forces can be maintained with a rate of ATP utilization that is 100-to 500-fold lower than the corresponding rate in skeletal muscle. The trade-off for high forces and economy of force maintenance is apparently shortening

velocity, which is much slower (up to 1000-fold) than that in striated muscle. The efficiency, in terms of work per ATP, is also somewhat lower (approximately one-fifth that of skeletal muscle), however, the data here are less extensive. The key question then is how does smooth muscle accomplish these specialized functions given that its contractile apparatus uses basically similar actin and myosin components?

VIB1. Smooth Muscle Structure and Its Relationship to Function

The structure of smooth muscle is shown in Fig. 46.13. Smooth muscle cells are smaller than skeletal muscle, with maximum diameters of the spindle-shaped cells in the range 10–20 μm. Filament structure is less organized, with no distinct sarcomeric or banding structure, hence the name "smooth". There are no Z-bands, but actin filaments are organized through attachment to specialized cytoskeletal regions called dense bodies or patches. These areas contain α-actinin, a Z-band protein, which further strengthens this analogy. It is also likely that these structures mediate transmission of force between cells. The ratio of thin to thick filaments is much higher in smooth muscle (≈15:1) than in striated muscle (2:1).

This latter observation raises the question of whether structural factors could account for these functional differences. The answer clearly depends on the mechanism of contraction in smooth muscle. It is assumed, by analogy to striated muscle, that a sliding-filament mechanism is involved in smooth muscle contraction. There is much less direct evidence than skeletal muscle, but the available data are consistent with this theory. Primarily, the evidence in intact tissue is largely limited to the dependence of active force on length, which is qualitatively similar to that of striated muscle. Smooth muscle appears to shorten to a greater extent, 0.2–0.4 of the optimal length for force generation (Herlihy and Murphy, 1973; Paul and Peterson, 1975), compared to 0.6 for skeletal muscle. On the descending limb of the active force–length curve, the decline may be more rapid, but the large passive forces in this region preclude precise measurements. There is also an element of plasticity in these force–length relations which show a hysteresis, dependent on how the measurements are made (Peterson and Paul, 1974; Seow and Pare, 2007). The loose organization of myofilaments is not readily amenable to direct structural measurements which precludes conclusive evidence based on comparison of the extent of thin–thick filament overlap to force–length behavior. From "motility assays," in which actin filaments are observed to move on a myosin-coated surface, or myosin-coated beads move on actin filament networks (Harris and Warshaw, 1993), one can infer that folding of filaments is not essential to motion, consistent with a sliding-filament model. The only difference between striated and smooth

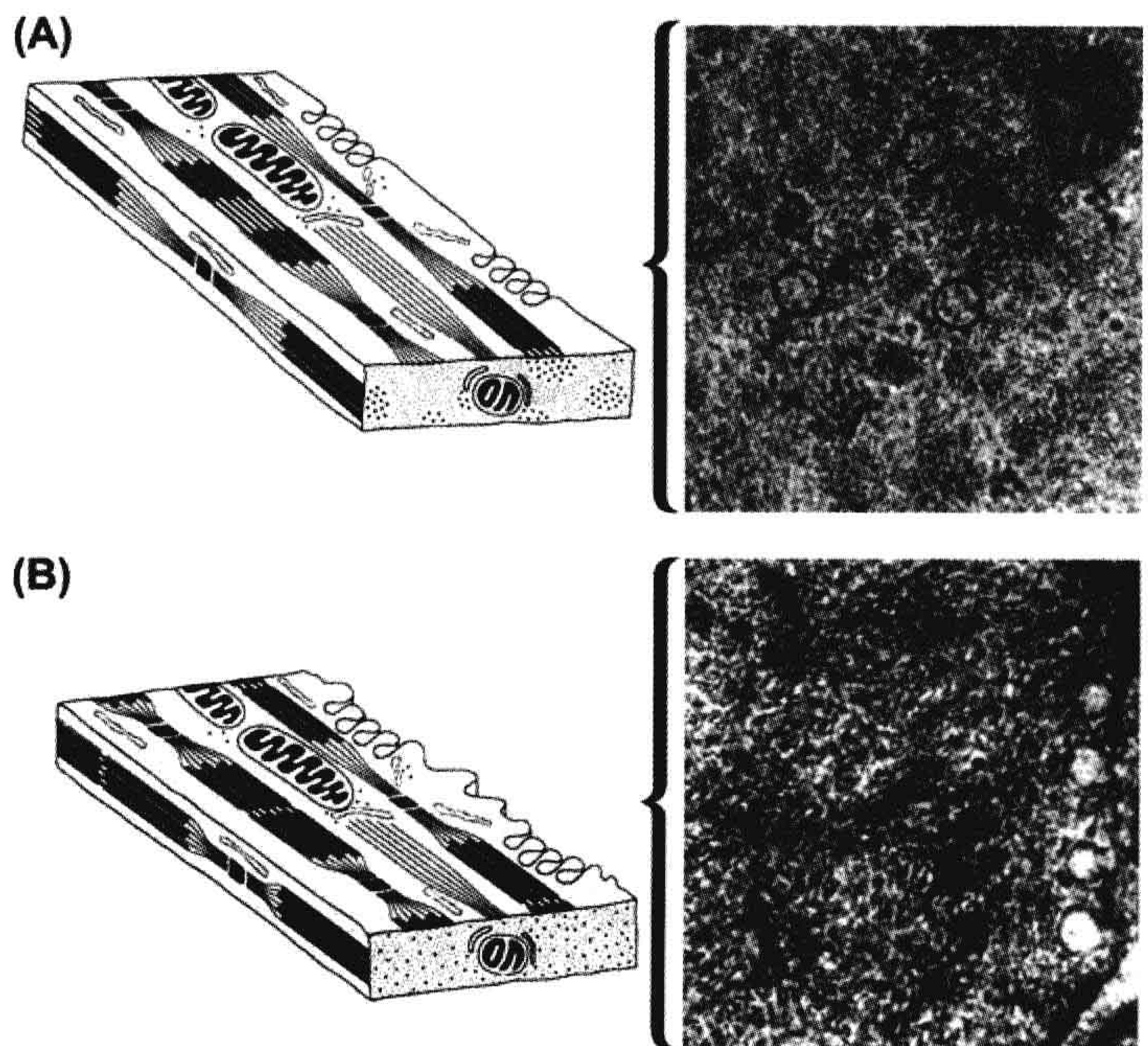


FIGURE 46.13 Morphology of relaxed and contracted smooth muscle. (A) This diagram represents a portion of a relaxed smooth muscle cell, highlighting the arrangement of the actin-containing thin filaments and the myosin-containing thick filaments. This rendering is greatly simplified from the actual arrangement. From the longitudinal orientation, thin filaments arise at dense bodies and project to interact with thick filaments, forming the contractile apparatus. In the cross-section, the filaments are distributed in a non-uniform manner, with thick filaments forming clusters surrounded by groups of thin filaments. This arrangement is shown in the electron micrograph (circled), which is a cross-section of a relaxed visceral smooth muscle cell. (B) A contracted smooth muscle cell. The notable differences from the relaxed cell shown in part (A) are that, in the longitudinal views, the thin filaments overlap considerably more of the thick filaments, drawing the dense bodies closer together and shortening the cell. In cross-section, the thin and thick filaments are randomly distributed to form a uniform pattern. The electron micrograph is a cross-section of a contracted visceral smooth muscle cell which shows more uniform distribution of the thin and thick filaments. *(Diagrams are modified from Heumann, 1973.)*

muscle myosin in these experiments is a slower velocity observed with smooth muscle myosin.

Assuming that an analogous sliding-filament mechanism operates in smooth muscle, what types of structure could account for the differences in function? Force is proportional to the number of cross-bridges in parallel, whereas shortening velocity and the maximal shortened length are related to the number of fundamental units in series. Models of arrangement of cells or sarcomeres yielding an increase in force and holding economy while reducing velocity are shown in Fig. 46.14. While increasing the number of cells in parallel (Fig. 46.14A) works in the appropriate direction (large force, low tension cost), it falls short of true smooth muscle behavior in that the amount of total tissue shortening in this model is very limited. Smooth muscle can shorten to relatively short lengths; some 20–30% of initial tissue length is not uncommon. In the model of Fig. 46.14A, the absolute length change would be that attributable to shortening of only one cell and would not account for the shortening of any macrosize tissue.

In Fig. 46.14B, different mechanical properties are associated with the assembly of the sarcomere. Longer myosin filaments and, consequently, longer sarcomeres are associated with more parallel cross-bridges and higher forces. However, for a given myosin content, this arrangement has fewer sarcomeres in series and hence a slower overall velocity. Moreover, if the individual myosin cross-bridge ATPase is not altered, one would have a similar ATP use for both models and thus the longer sarcomere version would have a greater economy (force maintained per rate of ATP hydrolysis) or a lower tension cost (reciprocal of economy). These changes are in the direction that distinguishes smooth muscle from skeletal

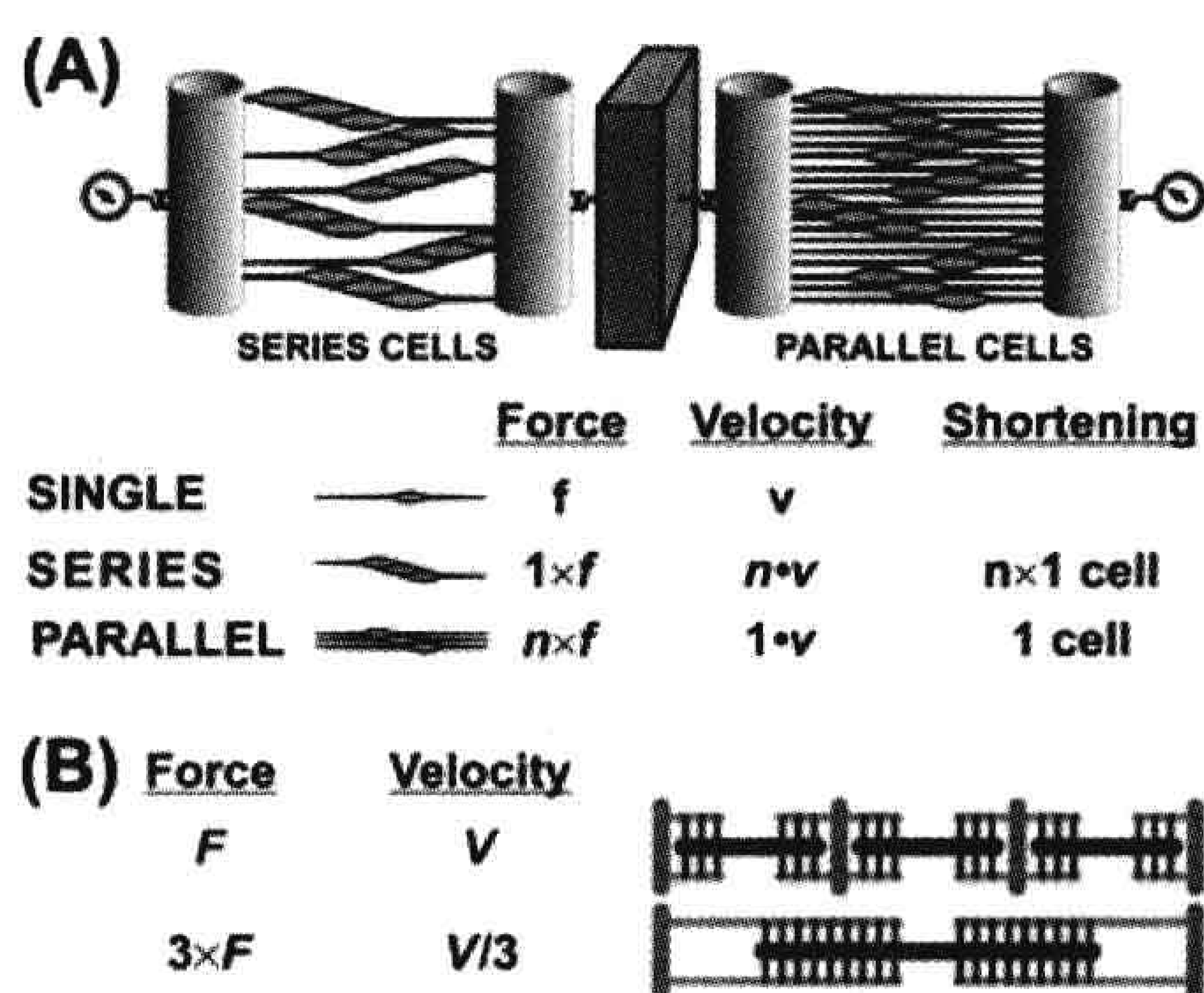


FIGURE 46.14 (A) Parallel and series models of force transmission in a smooth muscle-containing tissue. Parallel arrangement increases total force, but with a decrease in velocity and total shortening compared with cells coupled in series. (B) Parallel and series model at the level of the sarcomere. Both sliding filament models have the same myosin content, but it is arranged in short (top) and long sarcomeres (bottom).

muscle. The question then is how much of the difference between skeletal and smooth muscle can be related to simply the "mechanical advantage" of longer sarcomeres? Although no obvious sarcomeric structure exists for smooth muscle, the length of the myosin filament of smooth muscle relative to striated answers this question. There is evidence that some smooth muscles, particularly in invertebrates, such as the scallop or mussel, whose sarcomere lengths may be up to 10-fold greater than mammalian skeletal muscle, make use of this mechanical advantage. However, for mammalian tissues, myosin filament length has been estimated at approximately 2.2 μm (Somlyo, 1980), a figure not significantly different from that of striated muscle (1.6 μm). The differences in contractile properties between smooth and. skeletal muscles would thus appear to reside largely in the nature of the smooth muscle myosin molecule and its intrinsically lower ATPase.

VIB2. Regulation of Smooth Muscle Contractility

Regulation of contractility can be divided into (1) mechanisms for control of $[Ca^{2+}]_i$ and (2) mechanisms for transduction of the Ca^{2+} signal to activation of the contractile apparatus. Regulation of $[Ca^{2+}]_i$ is considered elsewhere and the focus here is on transduction mechanisms.

Up to the mid-1970s, regulation of mammalian smooth muscle contractility was based largely by analogy to striated muscle and considered to be a "thin-filament" regulated system; i.e. one in which troponin is the Ca^{2+} receptor and tropomyosin is the transducing element. It was quite a surprise when this canonical theory was shown not to be valid for mammalian smooth muscle. Several lines of evidence led to the current, widely accepted view that phosphorylation of the 20 kDa regulatory light chain of myosin (MRLC-P_i) is the primary transduction site for the Ca^{2+} signal (Hartshorne and Siemenkowski, 1981; Kamm and Stull, 1985; Hartshorne, 1987; de Lanerolle and Paul, 1991). Although tropomyosin is known to be a major smooth muscle protein, the Ca^{2+} transducer, troponin, is not present in smooth muscle. Proving that a protein is absent is difficult and that proof came slowly. Smooth muscle actomyosin also proved considerably different from that of striated muscle. One aspect was that as its purity increased, its ATPase activity decreased, the opposite of striated actomyosin. This suggested that purified smooth muscle actomyosin requires activation; in contrast to striated muscle actomyosin which is constitutively active, and requires de-inhibition of the associated troponin–tropomyosin inhibitory proteins. This was rigorously tested by "competition" experiments. In these experiments, the Ca^{2+} sensitivity of the actin-activated, Mg^{2+}-ATPase of myosin was measured using "unregulated" thin filaments (i.e., purified actin without troponin and tropomyosin). Striated muscle myosin showed little Ca^{2+}

sensitivity, whereas mammalian smooth muscle myosin retained Ca^{2+} sensitivity, indicating that the site of its regulation was on the myosin itself. The regulatory site was identified when it was discovered that the ATPase activity of smooth muscle myosin was dependent on phosphorylation of the 20-kDa regulatory light chain (MRLC) of the myosin hexamer. This phosphorylation involves Ca^{2+} binding to calmodulin, the ubiquitous Ca^{2+} binding protein, which in turn binds and thereby activates myosin light chain kinase (MLCK). This kinase is rather remarkable in that MRLC is its only substrate, rare among most kinases which often have multiple targets.

Several lines of evidence supported this thick filament regulatory mechanism. One strategy was to alter MRLC-P_i independent of $[Ca^{2+}]_i$ through manipulation of the kinase or phosphatase. Inhibition of MLCK led to relaxation and dephosphorylation in the presence of Ca^{2+}. Another path involved the proteolysis of MLCK to obtain a constitutively active fragment which, added to permeabilized smooth muscle, generated a contraction in the absence of Ca^{2+} which was indistinguishable from that induced by Ca^{2+}. Another line involved targeting the phosphatase; addition of myosin phosphatase enriched fractions relaxed contracted smooth muscle (Rüegg et al., 1982). Inhibition of myosin phosphatase also leads to smooth muscle contraction. Taken in total, these results suggest that myosin light chain phosphorylation is the major regulatory site and is necessary for activation.

In the past 10 years, the biggest surprise in the regulation of smooth muscle is the importance played by modulation of phosphatase activity (Somlyo and Somlyo, 2000). Myosin phosphatase activity is regulated by it targeting subunit (MYPT1) or myosin binding subunit. MYPT1 binds to the catalytic subunit of type 1 phosphatase and also acts as an interactive platform for many other proteins, in particular, myosin filaments. Phosphorylation of MYPT1 weakens the binding to myosin and, consequently, decreases its apparent phosphatase activity. There are several phosphorylation sites: S696 and S854 are PKA/PKG sites; T697 and T855 are the inhibitory/regulatory sites phosphorylated by several kinases most notably Rho-kinase (ROK) (Matsumura and Hartshorne, 2008).

Activation of smooth muscle contraction by MRLC phosphorylation/dephosphorylation provides multiple points for modulation. Phosphorylation of MLCK by cAMP dependent kinase weakens its binding to calmodulin and leads to Ca^{2+} desensitization of contraction; i.e. less force generated for a given $[Ca^{2+}]_i$ than control. On the other hand, there are two major paths currently known to decrease phosphatase activity, thus leading to an increase in Ca^{2+} sensitivity. In addition to Rho-Kinase, C-kinase phosphorylation of a small inhibitory protein, CPI-17, forms a complex that retards dephosphorylation of MYPT1 decreasing myosin phosphatase activity (Eto et al., 2004). In some smooth muscles, myosin phosphatase can clearly dominate MLCK phosphorylation, such as inhibition of the phosphatase by Rho kinase, a major player in activation. For example, inhibition of Rho kinase can lead to the complete relaxation of receptor-mediated stimulation (Nobe and Paul, 2001). A schematic for the regulation of MRLC phosphorylation/dephosphorylation is shown in Fig. 46.15.

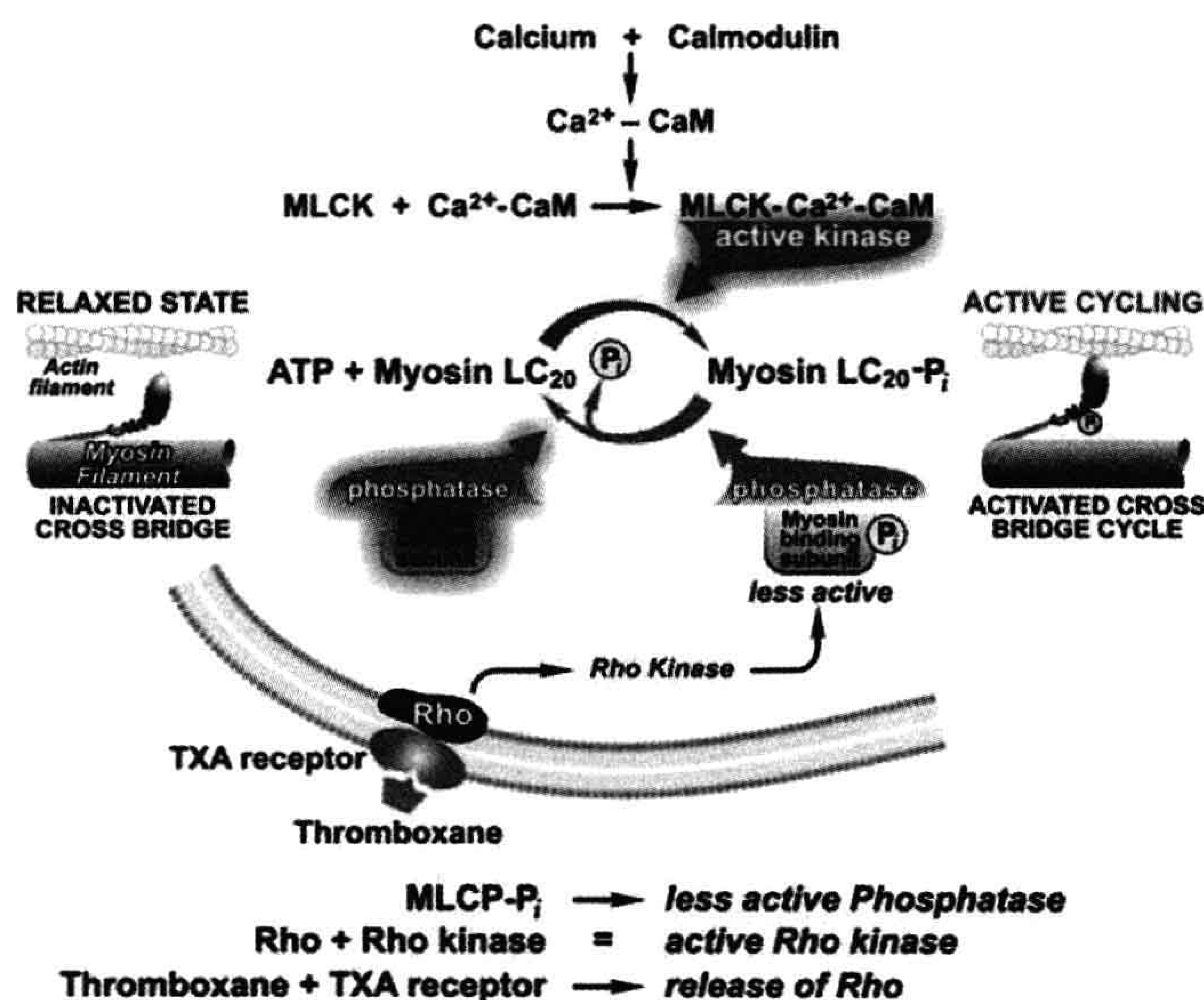


FIGURE 46.15 Schematic showing the mechanisms for phosphorylation/dephosphorylation of myosin regulation light chains and contractile state of smooth muscle.

Whether myosin light chain phosphorylation is sufficient as a regulatory mechanism or indeed has roles in addition to actomyosin activation is open to question. A number of experimental observations suggest that smooth muscle regulation may be more complex than initially envisioned. Figure 46.16 summarizes the time courses of several parameters after stimulation. Isometric force increases monotonically and then maintains a plateau value, whereas MRLC-P_i rapidly increases to a maximum achieved early in the contraction and then decreases. The extent of the decline in the MRLC-P_i is controversial and this is likely attributable to different smooth muscle types, dependence on the nature of the stimulus and measurement technique. Since force is usually assumed to reflect the number of activated cross-bridges, the decline in MRLC-P_i with maintained or increasing force suggests that this is not a simple on-off switch and/or other regulatory factors may play a role. Moreover, near maximal forces are attained with MRLC-P_i levels considerably lower than 100%, often reported to be in the 15–40% range, which further questions its role as a simple switch. The decline in MRLC-P_i also parallels that of $[Ca^{2+}]_i$ and, interestingly, to the decline in shortening velocity and ATPase activity. In view of these observations, Murphy and colleagues (Hai and Murphy, 1988, 1989a) suggested that MRLC-P_i might be a regulator of contractile velocity. They coined the expression "latch" for the state of maintained force with reduced MRLC-P_i and slower contraction speeds. Latch bridges, or cross-bridges, in this state were initially postulated to be non- or slowly cycling and thus they reduced the overall tissue velocity by acting as a type of internal load on the more rapidly cycling bridges. As force retained its dependence on Ca^{2+} in the latch state, it was postulated that latch bridges may be regulated by a system different from MRLC-P_i.

Currently, there are two major classes of theories for latch behavior, which are not necessarily mutually exclusive. Thin-filament regulatory mechanisms based on several actin-binding proteins, namely, leiotonin, caldesmon and calponin, have been suggested. A common feature is that they are all proposed to be inhibitory and, for the latter two, the interaction with actin is sensitive to Ca^{2+}calmodulin. Although all are promising in terms of the ability to inhibit myosin ATPase activity in the test tube, the relevance to intact smooth muscle has yet to be unequivocally demonstrated. As smooth muscle myosin requires activation, these systems could only be ancillary. Based on the ability of MRLC-P_i to activate smooth muscle in the absence of Ca^{2+}, it is difficult to postulate that these systems can be inhibitory in the sense that they regulate activation on an "on-off" basis. However, these systems could regulate cross-bridge cycling and thus velocity (Kim et al., 2008), but more evidence of this is needed.

An alternative hypothesis suggested by Murphy and Rembold (2005) does not require regulatory components beyond myosin light chain phosphorylation–dephosphorylation. A version of their model is shown in Fig. 46.17. They postulate that if a phosphorylated cross-bridge were dephosphorylated while attached, its detachment rate would be significantly slower than if it were to remain phosphorylated. The kinetic scheme of Fig. 46.17 is sufficient to fit the available data on the time courses of force and MRLC-P_i. It can also predict the time course of ATP utilization, which also decreases similarly to velocity, with stimulation duration. This scheme also predicts that the "futile" cycle of myosin light chain phosphorylation–dephosphorylation is the dominant (≈85%) source of ATP utilization, which was challenged based on the

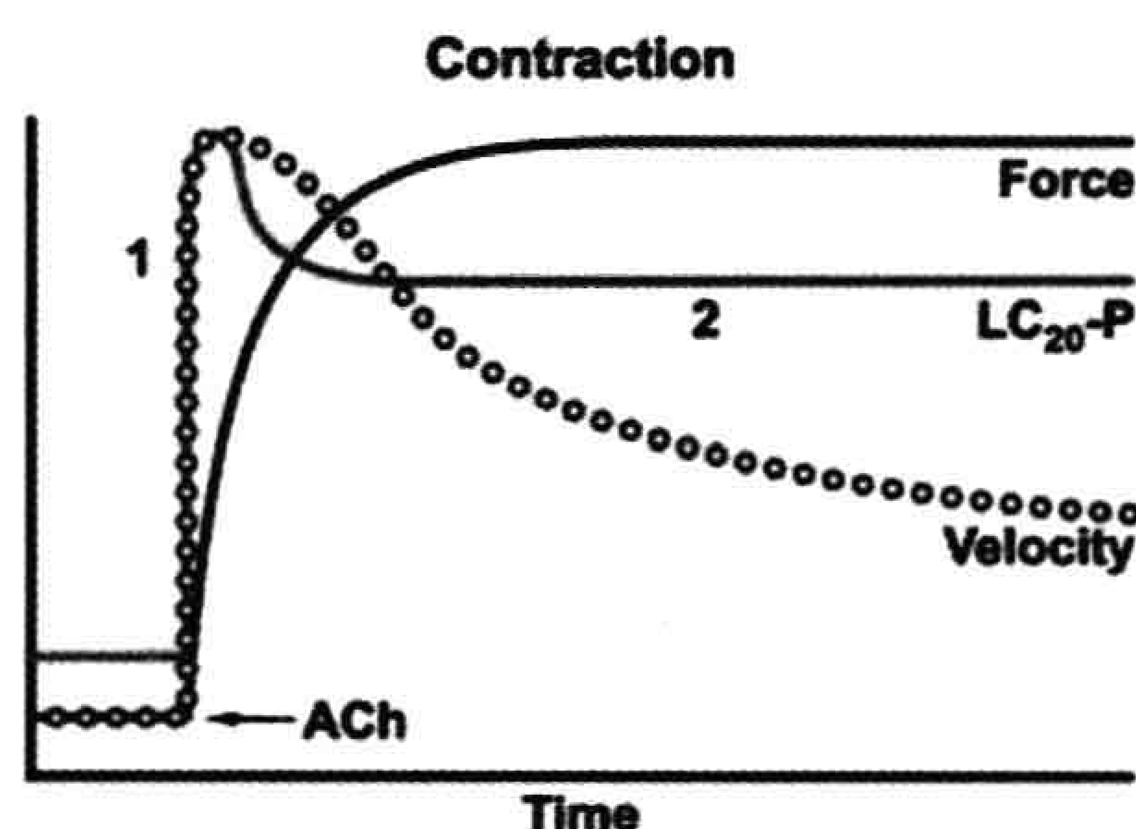


FIGURE 46.16 Relations between isometric force, maximum shortening velocity and myosin regulatory light chain phosphorylation (LC_{20}-P) and the duration of stimulation. Data are for tracheal smooth muscle *(adapted from de Lanerolle and Paul, 1991)*. The decrease in velocity at times when force is maintained is the basis for the latch bridge theories.

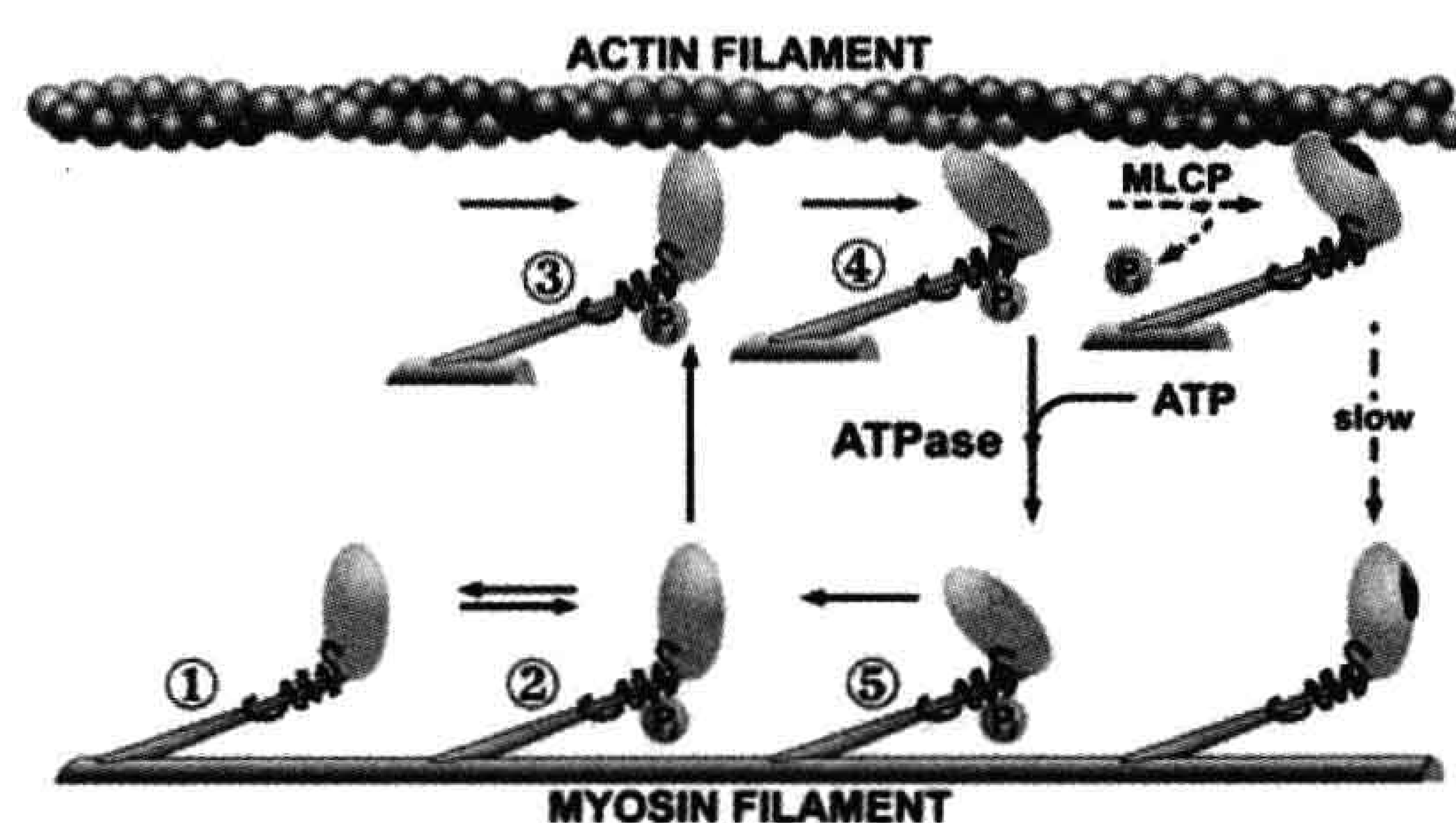


FIGURE 46.17 A schematic model of the interaction of smooth muscle myosin cross-bridges with actin filaments. The transition from state 1 to state 2 represents the Ca^{2+}-calmodulin dependent phosphorylation/dephosphorylation activation mechanism proposed for smooth muscle regulation. The cycle of interaction (states 2–5) hydrolyzes 1 ATP molecule and generates 1 quantum of tension with each pass. Only the angulated attached myosin cross-bridge (state 4) generates isometric force. The inherent speed of the cycle is much slower in smooth muscle than in striated, with the ATP-dependent dissociation step (state 4–5) apparently being slower. The dashed arrows indicate formation of a proposed dephosphorylated actomyosin cross-bridge (Hai and Murphy, 1989b), which dissociates only very slowly and may be responsible for the latch state of vascular smooth muscle.

available smooth muscle energetics data (Paul, 1990). This discrepancy was resolved when it was shown (Wingard et al., 1997) that myosin phosphorylation–dephosphorylation can be an appreciable source of ATP utilization during the initial force development when levels of MRLC-P_i are high, but rapidly drops paralleling Ca^{2+}, MRLC-P_i and velocity. Thus, the high economy of tension maintenance in smooth muscle or lower tension cost in smooth than striated muscle includes a low intrinsic actomyosin ATPase ($\approx$100-fold), longer sarcomeres ($\approx$1.5-fold) and decreasing the cross-bridge cycle rate at constant force ($\approx$3-fold). The role of latch bridges or thin filament proteins in the latter is yet to be fully resolved and universally accepted.

BIBLIOGRAPHY

Balaban, R. S. (2009). Domestication of the cardiac mitochondrion for energy conversion. *J Mol Cell Cardiol, 46*, 832–841.

Barclay, C. J., Woledge, R. C., & Curtin, N. A. (2010). Inferring cross-bridge properties from skeletal muscle energetics. *Prog Biophys Mol Biol, 102*, 53–71.

de Lanerolle, P., & Paul, R. J. (1991). Myosin phosphorylation/dephosphorylation and regulation of airway smooth muscle contractility. *Am J Physiol, 261*, L1–14.

Eto, M., Kitazawa, T., & Brautigan, D. L. (2004). Phosphoprotein inhibitor CPI-17 specificity depends on allosteric regulation of protein phosphatase-1 by regulatory subunits. *Proc Natl Acad Sci USA, 101*, 8888–8893.

Fenn, W. O. (1923). A quantitative comparison between the energy liberated and the work performed by the isolated sartorius muscle of the frog. *J Physiol, 58*, 175–203.

Fiske, C. H., & SubbaRow, Y. (1927). The nature of the "inorganic phosphate" in voluntary muscle. *Science, 65*, 401–403.

Gilbert, C., Kretzschmar, K. M., Wilkie, D. R., & Woledge, R. C. (1971). Chemical change and energy output during muscular contraction. *J Physiol, 218*, 163–193.

Gillis, J. M., Thomason, D., Lefevre, J., & Kretsinger, R. H. (1982). Parvalbumins and muscle relaxation: a computer simulation study. *J Muscle Res Cell Motil, 3*, 377–398.

Gordon, A. M., Huxley, A. F., & Julian, F. J. (1966). The variation in isometric tension with sarcomere length in vertebrate muscle fibres. *J Physiol (Lond), 184*, 170–192.

Hai, C., & Murphy, R. (1989a). Crossbridge phosphorylation and the energetics of contraction in swine carotid media. In R. Paul, G. Elzinga, & K. Yamade (Eds.), *Muscle Energetics* (pp. 253–264). New York: A.R. Liss Publisher.

Hai, C. M., & Murphy, R. A. (1988). Regulation of shortening velocity by cross-bridge phosphorylation in smooth muscle. *Am J Physiol, 255*, C86–C94.

Hai, C. M., & Murphy, R. A. (1989b). Ca2+, crossbridge phosphorylation, and contraction. *Annu Rev Physiol, 51*, 285–298.

Hardin, C. D., Allen, T. J., & Paul, R. J. (Eds.). (2000). *Metabolism and energetics of vascular smooth muscle*. San Diego: Academic Press.

Harris, D. E., & Warshaw, D. M. (1993). Smooth and skeletal muscle actin are mechanically indistinguishable in the in vitro motility assay. *Circ Res, 72*, 219–224.

Hartshorne, D. (1987). Biochemistry of the contractile process in smooth muscle. In L. Johnson (Ed.), *Physiology of the Gastrointestinal Tract* (pp. 423–482). New York: Raven Press.

Hartshorne, D. J., & Siemankowski, R. F. (1981). Regulation of smooth muscle actomyosin. *Annu Rev Physiol, 43*, 519–530.

Herlihy, J. T., & Murphy, R. A. (1973). Length-tension relationship of smooth muscle of the hog carotid artery. *Circ Res, 33*, 275–283.

Heumann, H. G. (1973). Smooth muscle: contraction hypothesis based on the arrangement of actin and myosin filaments in different states of contraction. *Philos Trans R Soc Lond B Biol Sci, 265*, 213–217.

Higuchi, H., Yanagida, T., & Goldman, Y. E. (1995). Compliance of thin filaments in skinned fibers of rabbit skeletal muscle. *Biophys J, 69*, 1000–1010.

Hill, A. V. (1912). The heat-producton of surviving amphibian muscles, during rest, activity, and rigor. *J Physiol, 44*, 466–513.

Hill, A. V. (1938). The heat of shortening and the dynamic constants of muscle. *Proc R Soc Lond B, 126*, 136–195.

Hill, A. V. (1965). *Trails and Trials in Physiology*. London: Arnold.

Huang, T. J., & Juluri, B. K. (2008). Biological and biomimetic molecular machines. *Nanomedicine (Lond), 3*, 107–124.

Huxley, A. F. (1957). Muscle structure and theories of contraction. *Prog Biophys Biophys Chem, 7*, 255–318.

Huxley, A. F. (2000). Mechanics and models of the myosin motor. *Philos Trans R Soc Lond B Biol Sci, 355*, 433–440.

Huxley, A. F., & Niedergerke, R. (1954). Structural changes in muscle during contraction; interference microscopy of living muscle fibres. *Nature, 173*, 971–973.

Huxley, A. F., & Simmons, R. M. (1971). Proposed mechanism of force generation in striated muscle. *Nature, 233*, 533–538.

Huxley, H. E. (1953). Electron microscope studies of the organisation of the filaments in striated muscle. *Biochim Biophys Acta, 12*, 387–394.

Huxley, H. E. (1996). A personal view of muscle and motility mechanisms. *Annu Rev Physiol, 58*, 1–19.

Huxley, H. E. (2004). Recent X-ray diffraction studies of muscle contraction and their implications. *Philos Trans R Soc Lond B Biol Sci, 359*, 1879–1882.

Ishida, Y., Riesinger, I., Wallimann, T., & Paul, R. J. (1994). Compartmentation of ATP synthesis and utilization in smooth muscle: roles of aerobic glycolysis and creatine kinase. *Mol Cell Biochem, 133-134*, 39–50.

James, J. H., Fang, C. H., Schrantz, S. J., Hasselgren, P. O., Paul, R. J., & Fischer, J. E. (1996). Linkage of aerobic glycolysis to sodium-potassium transport in rat skeletal muscle. Implications for increased muscle lactate production in sepsis. *J Clin Invest, 98*, 2388–2397.

Jewell, B. R., & Wilkie, D. R. (1958). An analysis of the mechanical components in frog's striated muscle. *J Physiol, 143*, 515–540.

Kamm, K. E., & Stull, J. T. (1985). The function of myosin and myosin light chain kinase phosphorylation in smooth muscle. *Annu Rev Pharmacol Toxicol, 25*, 593–620.

Kim, H. R., Appel, S., Vetterkind, S., Gangopadhyay, S. S., & Morgan, K. G. (2008). Smooth muscle signalling pathways in health and disease. *J Cell Mol Med, 12*, 2165–2180.

Kushmerick, M. (1983). Energetics of muscle contraction. In L. Peachey (Ed.), *Handbook of Physiology* (pp. 189–236). Bethesda: American Physiological Society.

Kushmerick, M. J. (2005). From crossbridges to metabolism: system biology for energetics. *Adv Exp Med Biol, 565*, 171–180, discussion 180-172, 379-195.

Levy, B., Desebbe, O., Montemont, C., & Gibot, S. (2008). Increased aerobic glycolysis through beta2 stimulation is a common mechanism involved in lactate formation during shock states. *Shock, 30*, 417–421.

Liu, T., & O'Rourke, B. (2009). Regulation of mitochondrial Ca2+ and its effects on energetics and redox balance in normal and failing heart. *J Bioenerg Biomembr, 41*, 127–132.

Lohmann, K. (1934). Ueber die enzymatische Aufspaltung der Kreatinephosphorsauere zugleich ein Beitrag zum Chemismus der Muskelcontraktion. *Biochem Z, 271*, 264–277.

Lombardi, V., Piazzesi, G., Reconditi, M., et al. (2004). X-ray diffraction studies of the contractile mechanism in single muscle fibres. *Philos Trans R Soc Lond B Biol Sci, 359*, 1883–1893.

Lundsgaard, E. (1938). The biochemistry of muscle. *Ann Rev Biochem, 7*, 377–398.

Matsumura, F., & Hartshorne, D. J. (2008). Myosin phosphatase target subunit: many roles in cell function. *Biochem Biophys Res Commun, 369*, 149–156.

Murphy, R. A., & Rembold, C. M. (2005). The latch-bridge hypothesis of smooth muscle contraction. *Can J Physiol Pharmacol, 83*, 857–864.

Needham, D. M. (1971). *Machina carnis*. Cambridge: University Press.

Nobe, K., & Paul, R. J. (2001). Distinct pathways of Ca(2+) sensitization in porcine coronary artery: effects of Rho-related kinase and protein kinase C inhibition on force and intracellular Ca(2+). *Circ Res, 88*, 1283–1290.

Offer, G., & Ranatunga, K. W. (2010). Crossbridge and filament compliance in muscle: implications for tension generation and lever arm swing. *J Muscle Res Cell Motil, 31*, 245–265.

Ottenheijm, C. A., & Granzier, H. (2010). Lifting the nebula: novel insights into skeletal muscle contractility. *Physiology (Bethesda), 25*, 304–310.

Paul, R. J. (1983). Physical and biochemical energy balance during an isometric tetanus and steady state recovery in frog sartorius at 0 degree C. *J Gen Physiol, 81*, 337–354.

Paul, R. J. (1990). Smooth muscle energetics and theories of cross-bridge regulation. *Am J Physiol, 258*, C369–C375.

Paul, R. J., & Peterson, J. W. (1975). Relation between length, isometric force, and O2 consumption rate in vascular smooth muscle. *Am J Physiol, 228*, 915–922.

Paul, R. J., Bauer, M., & Pease, W. (1979). Vascular smooth muscle: aerobic glycolysis linked to sodium and potassium transport processes. *Science, 206*, 1414–1416.

Peterson, J. W., & Paul, R. J. (1974). Effects of initial length and active shortening on vascular smooth muscle contractility. *Am J Physiol, 227*, 1019–1024.

Pette, D., & Staron, R. S. (2001). Transitions of muscle fiber phenotypic profiles. *Histochem Cell Biol, 115*, 359–372.

Rayment, I., Smith, C., & Yount, R. G. (1996). The active site of myosin. *Annu Rev Physiol, 58*, 671–702.

Ruegg, J. C., DiSalvo, J., & Paul, R. J. (1982). Soluble relaxation factor from vascular smooth muscle: a myosin light chain phosphatase? *Biochem Biophys Res Commun, 106*, 1126–1133.

Seow, C. Y., & Pare, P. D. (2007). Ultrastructural basis of airway smooth muscle contraction. *Can J Physiol Pharmacol, 85*, 659–665.

Somlyo, A. P., & Somlyo, A. V. (2000). Signal transduction by G-proteins, rho-kinase and protein phosphatase to smooth muscle and non-muscle myosin II. *J Physiol (Lond), 522* Pt 2, 177–185.

Somlyo, A. V. (1980). Ultrastructure of vascular smooth muscle. In *Handbook of Physiology (Section 2) – The Cardiovascular System (Vol. II) Vascular Smooth Muscle* (pp. 33–67). Bethesda: American Physiological Society.

Squire, J. M., & Knupp, C. (2005). X-ray diffraction studies of muscle and the crossbridge cycle. *Adv Protein Chem, 71*, 195–255.

Weiss, J. N., & Lamp, S. T. (1987). Glycolysis preferentially inhibits ATP-sensitive K+ channels in isolated guinea pig cardiac myocytes. *Science, 238*, 67–69.

Westerblad, H., Bruton, J. D., & Katz, A. (2010). Skeletal muscle: energy metabolism, fiber types, fatigue and adaptability. *Exp Cell Res, 316*, 3093–3099.

Wingard, C. J., Paul, R. J., & Murphy, R. A. (1997). Energetic cost of activation processes during contraction of swine arterial smooth muscle. *J Physiol, 501*(Pt 1), 213–223.

Woledge, R. C., Curtin, N. A., & Homsher, E. (1985). Energetic aspects of muscle contraction. *Monogr Physiol Soc, 41*, 1–357.

Chapter 47

Flagella, Cilia, Actin- and Centrin-based Movement

Kenneth W. Foster

Chapter Outline

I. INTRODUCTION

To place emphasis on understanding integrated structure and mechanism, I use these pages to discuss just a few examples chosen from a vast literature. A much broader survey of the field with emphasis on the earlier literature is available (Kaneshiro, 2001; Kaneshiro et al., 2001).

Physiology is about the way life works, dynamically. Learning the mechanisms of how something works has

Cell Physiology Sourcebook. DOI: 10.1016/B978-0-12-387738-3.00047-0

often proven to be the most intractable problems in biology. We illustrate this reality with a number of intensely interesting and studied, but incompletely solved problems in the cell physiology of non-muscle motion systems.

Several mechanisms for the generation of force have evolved, including motors driven by ion gradients or ATP, the use of molecular springs driven by calcium regulated conformation change and use of turgor pressure to fire projectiles.

To maintain an easy distinction, bacterial and archaeal flagella are called *flagella* and the completely unrelated eukaryotic flagella and cilia are exclusively called *cilia*. Bacterial and archaeal flagella are quite different structures of separate evolutionary origin but with very similar function as they are both very slender rotating cylinders that enable a cell to move.

IA. Conversion of Free Energy into Work

Basic to movement is the conversion of free energy (the energy in a system that is available to do work) into work. Biology has employed motors with several characteristics atypical compared to most man-made motors. First, the motors are very small with individual force limits of the order of 8 pN. Second, when they are off they keep their position and hence do not require continued energy input unlike electromagnetic continuous and stepping motors. The reason for both characteristics of biomotors is to minimize energy requirements. Recently, with interest in making devices more portable, humans have designed motors with similar characteristics.

It is important to understand how free energy is converted to work and, as a consequence, why making the motors small maximizes their efficiency. While a much more complete discussion is available (Nelson, 2008), let me repeat here the portion of the argument as to why motors need to be small. He considers an analogous system that extracts mechanical work.

Consider the process of lifting a weight with a cylinder of gas with a piston of area A at one end, held down by weights w_1 and w_2 (Fig. 47.1A).

To determine the relationship between free energy and work, let us compare the change in free energy of the gas (equivalently the loss of available energy) that is driving the work with the mechanical work done. Removing w_2 will reduce the weight on the gas causing w_1 to rise. Specifically, removing w_2 will result in $L_{initial}$ increasing by ΔL to L_{final}.

Hence, the work done will be $W = w_1(L_f - L_i)$. From the ideal gas law $p_f L_f A = N k_B T$, where k_B is Boltzmann's constant, p_f is the final pressure, L_f is the final length, A is the cross-section of the gas cylinder, N is the number of molecules and T is the absolute temperature. Since $p_f = w_1/A$, then $w_1 = N k_B T/L_f$ and hence the work $W = N k_B T (L_f - L_i)/L_f$ or $W = N k_B T (\Delta L/L_f)$.

The change in free energy will be due to the change in entropy times the absolute temperature, T. The change in entropy is just $N k_B$ times the logarithm of the ratio of the final to initial volumes. Hence, the change in free energy: $\Delta F = N k_B T \ln(L_f/L_i)$.

Comparing work and free energy:

$$\Delta L/L_f(\text{the work}) < \ln(1/(1-\Delta L/L_f))$$

$$(\text{the change in free energy}) =$$

$$\begin{aligned} -\ln(1-\Delta L/L_f) &\approx -\{-\Delta L/L_f - 1/2\cdot(\Delta L/L_f)^2 \\ &\quad -1/3\cdot(\Delta L/L_f)^3 - \ldots\} \\ &= \Delta L/L_f + 1/2\cdot(\Delta L/L_f)^2 \\ &\quad +1/3\cdot(\Delta L/L_f)^3 + \ldots.. \end{aligned} \tag{47.1}$$

By inspection, the first term on the right hand side of the less-than symbol is equal to the term on the left hand side and all other terms on the right are positive. So in general, work is always less than the available free energy to drive it. However, inspection of the positive terms on the right leads one to recognize that they are all small if ΔL is small, so if the steps are sufficiently small almost all the free energy can be converted to work.

Bottom line is that small steps make the most efficient use of available free energy. Of course, chemical energy can be used as the source of free energy.

A few parameters to remember: thermal energy at room temperature is $k_B T = 25$ meV $= 4.1$ pN nm, a typical membrane potential is ≈ 70 mV, motor forces are a few pN and the energy of ATP hydrolysis is $\approx 25 k_B T$. These parameters apply to all biological motors.

IB. Reynolds Number

Critical to understanding motors and application of molecular devices is appreciating the low Reynolds number regime. Reynolds number is the ratio of inertial forces relative to viscous forces,

$$R = \frac{vL\rho_m}{\eta} \tag{47.2}$$

where v is the velocity, L is the characteristic dimension (length) of the object, typically the diameter for a sphere, ρ_m is the density of the object, and η is the viscosity. When R is small, friction dominates, stirring produces laminar flow and, if an external force stops, fluid flow stops almost immediately. For example, if a swimming cell stops its thrust it comes exponentially to a stop. The time constant of the exponential for coasting is

$$\tau \sim \frac{L^2\rho_m}{18\eta} \tag{47.3}$$

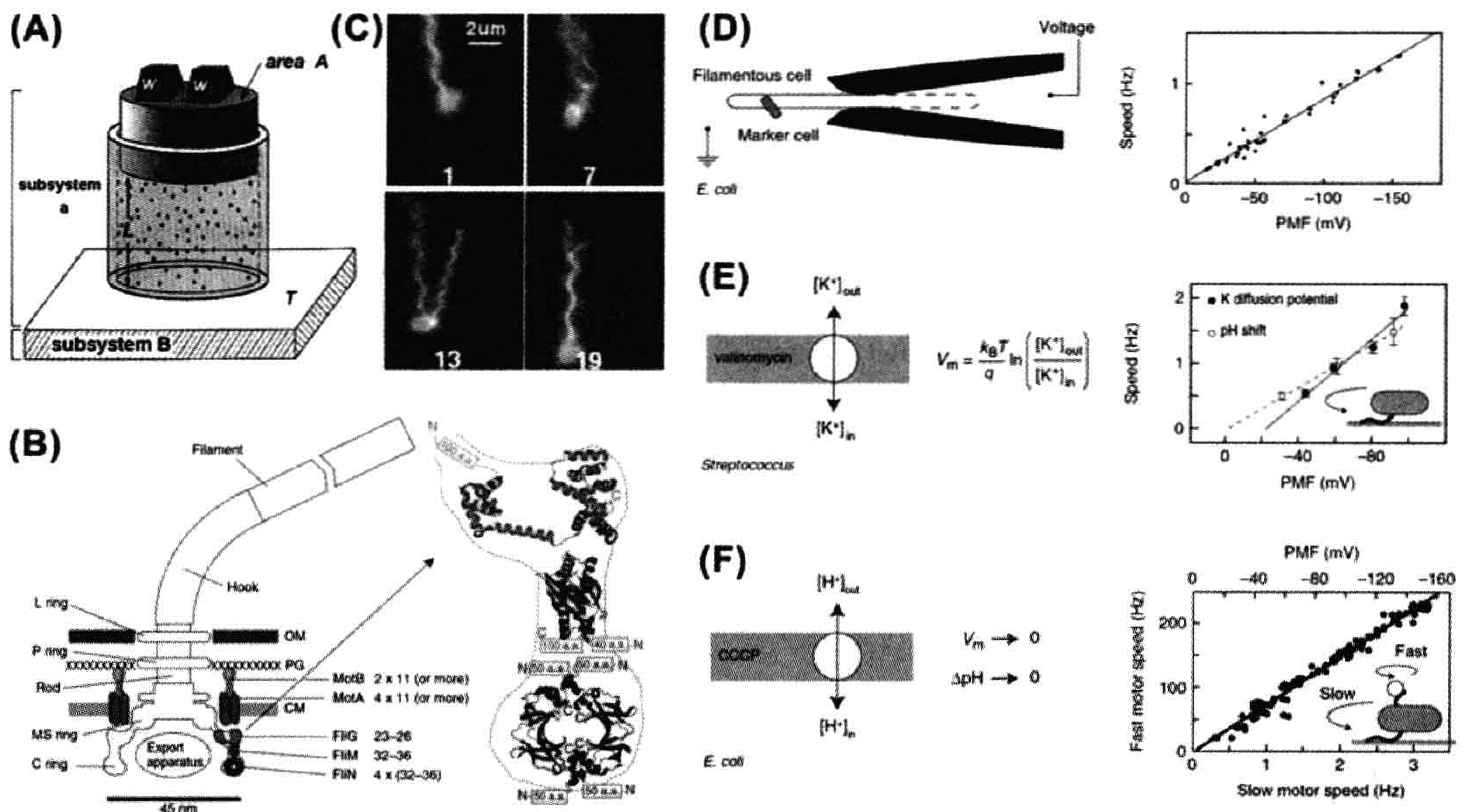


FIGURE 47.1 (A) Obtaining work from available free energy may be illustrated by the mechanical work of lifting a weight extracted by removing a second weight from a gas compressed by this second weight. *(Modified from Nelson, 2008, p. 215, Fig. 6.5.)* (B) Left: Schematic view of an H^+-driven flagellar motor with the proposed locations of proteins involved in torque generation. MotA and MotB form stator complexes with stoichiometry A_4B_2 and FliN forms a tetramer with a 1:1 stoichiometry with FliM. The motor spans the outer membrane (OM), peptidoglycan cell wall (PG) and cytoplasmic membrane (CM). Right: The proposed location and orientation of rotor proteins. X-ray crystal structures of truncated rotor proteins, FliG (cyan), FliM (magenta) and FliN (blue), are shown docked into the rotor structure. N- and C-termini and missing amino acids are indicated (Sowa and Berry, 2008). (C) Stroboscopic images of a fluorescently labeled swimming *E. coli* cell. The numbers are frame numbers, at 1/60 s intervals. Between frames 7 and 13, a single filament leaves the bundle and undergoes polymorphic transitions that cause a change in swimming direction known as a "tumble" (Turner et al., 2000). (D) Torque versus IMF. Left: Schematic of a voltage-clamp method using *E. coli* cells held in micropipettes. The part of the membrane inside the pipette (indicated by the dashed line) is made permeable using the ionophore gramicidin S. Motor speed from observation of a dead cell attached to the motor. Right: Motor speed found proportional to membrane voltage (=PMF) between 0 and −150 mV (Sowa and Berry, 2008). (E) Left: Membrane voltages in *Streptococcus* controlled by a K^+ diffusion potential in the presence of valinomycin. Right: The speed of tethered *Streptococcus* cells found proportional to PMF, and membrane voltage found equivalent to pH gradient (Sowa and Berry, 2008). (F) Left: PMF varied from −150 mV down to 0 by adding small concentrations of carbonyl cyanide, m-chlorophenylhydrazone (CCCP) or sodium azide. Right: Using the result of (D), the speed of a tethered *E. coli* motor (x-lower axis) was used as a proxy for PMF (x-upper axis, absolute value shown). The speed of a second motor on the same cell, attached to a submicron bead, was found proportional to PMF (Sowa and Berry, 2008).

A 2 μm long bacterium, whose motors we will discuss below, swims about 30 μm/s (v_0) with an R of 3×10^{-5} and τ of 0.2 μs and would coast a distance ($\tau \cdot v_0$) of $d_{coast} \approx 6$ pm if its motors were to stop (of course it will move much more by Brownian motion). Even a much larger (10 μm) eukaryotic swimming cell (140 μm/s) like *Chlamydomonas* has an R of 1.4×10^{-4}, a τ of 20 μs and a $d_{coast} = 2.8$ nm, still very short. The border line between low and modest Reynolds numbers comes with organisms like *Volvox* (1 mm length, 1 mm/s velocity) with an R of ≈ 1 and a τ of 200 ms and a $d_{coast} = 0.2$ mm. This border can also be crossed slightly by somewhat smaller organisms under special circumstances. *Paramecium* (typically 0.2 mm, 1 mm/s) has an R of ≈ 0.2, but it can transiently go as fast as 10 mm/s with an R of ≈ 2 and a d_{coast} of ≈ 20 μm (Hamel et al., 2011). It might jump most of its length in this burst of motion, but coasting is still a minimal part of it. The low Reynolds number regime is characterized by the uselessness of reciprocal motions as there is nothing to be gained by inertia and hence propulsive systems involve crawling, rotating appendages and wave propagation down appendages (Nelson, 2008).

Study of non-muscle contraction and motility is a work in progress. Substantial changes in understanding of mechanisms are anticipated in the near term with further opportunities for more detailed study likely. Consequently, what is attempted here is emphasis on some basic principles, a coarse description and some suggestions for how to approach future research. If the challenge of researching problems in this area excites you, please appreciate that significant further reading will be necessary.

II. BACTERIAL FLAGELLA

IIA. Introduction

Flagellated bacteria, such as *Escherichia coli*, swim by rotating thin helical filaments; each driven at their base by a reversible 45-nm-diameter rotary motor powered by ion flux (see Fig. 47.1B). The motor develops maximum torque at stall, but can rotate at several hundred Hertz. Its rotation direction is controlled by a sensory system that makes it possible for cells to accumulate in favored regions. A great deal is known about motor structure, genetics, assembly and function, but not precisely how it works (Berg, 2003).

The following sections on the structure, energy supplies and mechanism of motion primarily follows the review by Sowa and Berry (2008), however, it is also further informed by the review of Berg (2003). A brief discussion of the associated behavior follows and the study of fluctuation follows that.

IIB. The Structure

The flagellum is a $\approx$23-nm-thin, $\approx$10 000-nm-long helical filament with a rotary motor at its base that turns it like a propeller. The flagellar motor, by bacterial standards, is a large molecular machine made from $\approx$13 different proteins and a further $\approx$25 proteins are required for its expression and assembly. The best studied motors are those of the peritrichously flagellated bacterium *Escherichia coli* and the related *Salmonella enterica* Sv *typhimurium* (*S. typhimurium*). These motors switch between rotating counterclockwise (CCW, viewed from the outside) with formation of a bundle of flagella that produces smooth swimming and rotating clockwise (CW) that causes tumbles or rapid rotational diffusion.

The power of bacterial flagella may be estimated from the input and outputs that can be calculated. The input power may be estimated from the measured 1200 protons/revolution at 10 Hz rotation speed with a protonmotive force of -170 mV. Since the proton is a single charge, this corresponds to 2040 eV/s (3.3×10^5 pN nm/s). The output power under the same conditions can be estimated by the torque times the angular velocity, namely 4600 pN nm $\times$ 2 $\pi \times$ 10 Hz $= 2.9 \times 10^5$ pN nm/s (1800 eV/s), essentially the same as the input. There are other flagellated bacteria that swim differently. That bacterial flagella rotate was first observed by the rotation of the cell body tethered to a surface by its flagella. These tethered cells rotated up to $\approx$20 Hz. They spin faster with lower loads with the maximum recorded speed so far being 1700 Hz in the Na^+-driven motor of *Vibrio alginolyticus* at 37°C.

To measure flagellar rotation, the currently preferred method is to attach submicron polystyrene beads to truncated flagellar filaments of immobilized cells and to record their rotation with either back-focal-plane interferometry or high-speed fluorescence microscopy. The viscous drag coefficient of a 0.5 μm diameter bead on a truncated filament is similar to that of a flagellar filament. The smaller the bead the lower is the load and the higher the speeds that can be recorded.

Single particle image reconstruction from cyroelectron microscopy (EM) has determined the structure of the flagellar motor and their components have been identified by genetic and biochemical studies. Like any rotary motor, the bacterial flagellar motor consists of a rotor, the moving part, and a stator, the stationary part. The rotor spins relative to the cell and is attached to the helical filament by a universal joint called the hook, whereas the stator is anchored to the cell wall. Figure 47.1B shows a schematic diagram of the bacterial flagellum of a Gram-negative bacterium, based on an EM reconstruction of the rotor from *S. typhimurium*. The core of the motor is called the basal body and consists of a set of rings up to $\approx$45 nm in diameter that spans three layers of the cell envelope. The L and P rings are thought to be embedded in the outer lipopolysaccharide membrane and peptidoglycan cell wall, respectively, and act as a bushing between the rotor and the outer parts of the cell envelope. The rod connects the hook to the MS ring located at the cytoplasmic membrane. The MS ring consists of $\approx$26 copies of a single protein, FliF. After the MS ring is assembled, the rest of the motor is built from it. The cytoplasmic face of the MS ring is attached to the C ring, which contains the rotor proteins FliG, FliM and FliN and is the site of torque generation. The stators are a complex of two proteins: MotA and MotB in H^+-driven flagellar motors such as those of *E. coli*. The filament grows from its distal end supplied by a channel down its center. To do this an export apparatus inside the C ring pumps down the center of the proteins needed to make the hook and extend the filament.

IIC. Propeller and Universal Joint

The hollow hook and filament are single-protein thin tubular polymers consisting of 11 helical protofilaments. Monomer incorporation is regulated by pentameric cap complexes. Each polymer has a long and short form which creates the helical structures of the hook and filament. During steady rotation, the filament is a rigid propeller. Motor switching in *E. coli* causes a torsionally induced transformation between the alternative filament forms changing the handedness of the filament helix. The transformed filament breaks up the bundle of filaments currently propelling the cell and thus leads to cell reorientation (see Fig. 47.1C). To see this, flagellar filaments have been fluorescent labeled and swimming cells have been recorded with stroboscopic laser illumination and high-speed video microscopy. Response to external forces has been studied with optical tweezers. The hook is much more flexible than

the filament and works as a universal joint to allow several filaments from motors all over the cell to rotate together in a bundle in peritrichiously flagellated species. A great simulation of the assembly process is available at http://www.fbs.osaka-u.ac.jp/labs/namba/npn/index.html.

IID. Energy Transduction

Molecular motors convert chemical or electrical energy to mechanical work and operate close to the level of thermal energy, k_BT. In the bacterial flagellar motor, the free energy input from a single ion passing through the cytoplasmic membrane is a single electric charge times the ion-motive force (IMF; either proton-motive force [PMF] or sodium-motive force [SMF]). The electrochemical potential, IMF $= V_m + k_BT/q \ln (C_i/C_o)$, where V_m is the transmembrane voltage (inside minus outside) and q, C_i and C_o are the charge, inside and outside concentrations of the coupling ion, respectively. With a typical IMF of around -150 mV, the free energy of a single ion transit is $\approx 6\,k_BT$. Torque is defined as the product of force and the perpendicular distance to an axis of rotation and therefore has dimensions of Newton-meters or energy. Because Reynolds number for a spinning flagellar motor is $<<1$, inertia is negligible and torque can be calculated as $M = f\,\omega$, where f is the rotational drag coefficient and ω is the angular velocity.

IIE. Ion Selectivity

Bacterial flagellar motors are driven by ions and not ATP hydrolysis like muscle motors. These can be the driven by the membrane potential and/or by the hydronium or Na^+ gradients.

IIF. Motor Dependence upon IMF

The IMFs drive bacterial flagellar motors oriented in the membrane and ions travel through the motor in a particular direction. Ion drives permit the high stator turnover speeds and high power output. The free energy of $\approx 6\,k_BT$, corresponding to one ion crossing the membrane, is smaller than the free energy of hydrolysis of ATP ($\approx 20\,k_BT$). In addition, the enthalpic contribution is proportional to the continuously variable and reversible membrane voltage. The estimated flux is around 1200 H^+ ions per revolution per motor over a speed range of 20–60 Hz.

By voltage clamping the membrane voltage at the flagellar motor and monitoring motor motion by video microscopy of dead cells attached to the motors, it has been found that their rotation speed is proportional to the applied voltage up to -150 mV (see Fig. 47.1D). By varying the concentration of driving ions and diffusion potential it has also been shown that the electrical and chemical components of the IMF are equivalent at high load in H^+-driven flagellar motors (see Fig. 47.1E). Subsequently, it was found that at low load the faster speed of the motor is also proportional to IMF (see Fig. 47.1F).

IIG. Torque Versus Speed

The torque–speed relationship of the flagellar motor has been measured to clarify the mechanochemical cycle. The speed can be measured over a wide range of viscous load or externally applied torque. With the latter method, the torque of the motor can be measured when forced to rotate backwards or forwards faster than its zero-load speed. The electrorotation method was particularly effective; a rotating electric field (megaHertz) polarizes the cell body and torque is exerted on the cell due to a phase lag between the field and induced dipole moment. Figure 47.2A summarizes the data from spinning the cell body in both directions at speeds up to ≈ 1 kHz. There is a plateau of nearly constant torque up from backwards speeds of about ≈ 100 Hz to a "knee" forward speed of several 100 Hz, then the torque falls linearly towards the zero-torque speed at ≈ 400 Hz (Fig. 47.2A, circles, triangles), at which point the motor resists rotation with a torque of similar magnitude to the plateau torque (Fig. 47.2A, large gray circles). The absolute magnitude of torque generated by the *E. coli* motor was determined to be 1260 ± 190 pN nm using measurements with polystyrene beads of 1 μm diameter. In the torque plateau region, since the output power is proportional to the torque times the angular velocity, the output power increases linearly with speed. Also because the number of protons through the motor per revolution is constant, the input power also increases linearly with the angular velocity, so that a constant efficiency is maintained.

At the torque plateau, transitions linked to ion flux are not rate limiting so speed is only mechanically limited by the load on the motor and depends only on the IMF, a thermodynamic quantity. The continuity of torque on either side of stall indicates that there is no irreversible step in the mechanochemical cycle. Faster than the "knee" transitions in the motor are rate limiting, possibly due to a requirement that ions must be gated across the structure. In this case, motor speed depends on absolute temperature, the hydrogen isotope and which component of the SMF is dominant. High rotation speed decreases the efficiency of ion going across the ion gate through the motor.

IIH. Mechanism of Torque Generation

IIH1. Interactions Between Rotor and Stator

The C ring (containing FliG, FliM and FliN) of the rotor is the key component for torque generation and switching direction from CCW to CW. FliG interacts with MotA to generate torque. Stator complexes anchor to the peptidoglycan cell wall and span the cytoplasmic membrane,

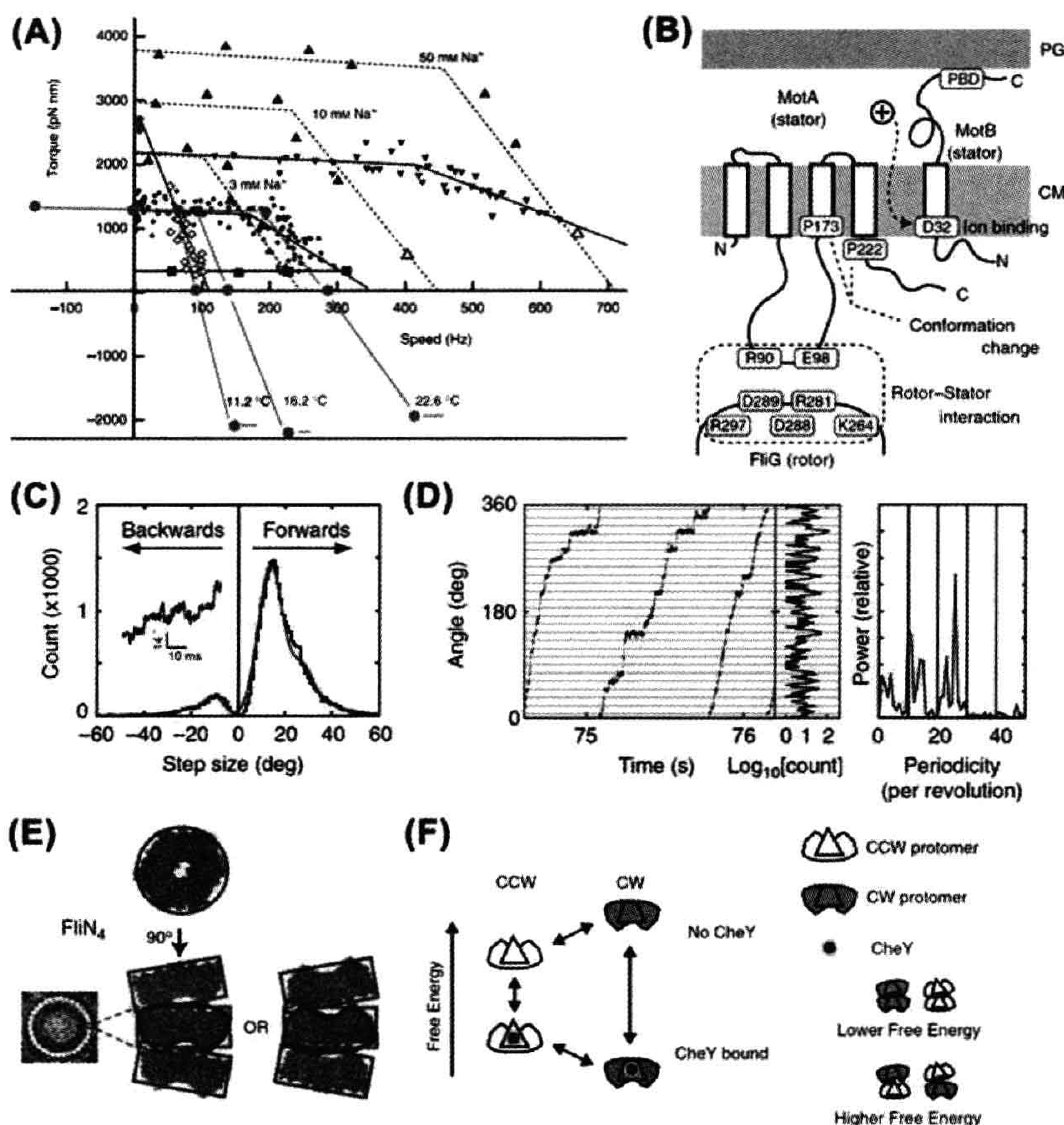


FIGURE 47.2 (A) Torque—speed relationships for flagellar motors of diverse species measured using various methods. All measurements were made at room temperature except where indicated. The *E. coli* experiments using electrorotation (gray circles) and beads (black circles) did not report absolute torques, so these curves are scaled to a stall torque of 1260 pN nm (Sowa and Berry, 2008, where more details may be sought). (B) Stator topology and interaction between rotor and stator in *E. coli*. MotA has four transmembrane α-helices and a cytoplasmic domain between the 2nd and 3rd transmembrane regions. Charged residues of this cytoplasmic domain contains interact with charged residues of FliG. MotB has a periplasmic domain containing a peptidoglycan-binding domain (PBD). PG, peptidoglycan cell wall; CM, cytoplasmic membrane (Sowa and Berry, 2008). (C) Step size distribution (black) with multiple Gaussian fit (red). The peak of forward steps is 13.7°, indicating 26 steps per revolution. An example of steps identified by a step-finding algorithm is shown (inset) (Sowa and Berry, 2008). (D) Plot of angle versus time during three revolutions, a histogram of the corresponding dwell angles and its corresponding power spectrum. The peak at 26 per revolution corresponds to a step size of 13.8° and shows that the motor stops at the same angles on successive revolutions (Sowa and Berry, 2008). (E) X-ray crystal structure of the FliN tetramer showing the puckered ring structure and proposed equivalent stacking configurations of tetramers in the C ring (EM structure of C ring, left) (Sowa and Berry, 2008). (F) Conformational spread model of flagellar switching. Protomers consisting of a FliN tetramer and one molecule of FliM with or without bound CheY can be in either the CW or CCW configurations. CheY binding lowers the free energy of the CW configuration relative to CCW, increasing the probability of CW rotation. Adjacent protomers have a lower free energy of interaction when both are in the same state, which leads to cooperative switching of the whole ring (Sowa and Berry, 2008).

forming ion channels. The cytoplasmic domain of MotA contains two charged residues that interact with five charged residues in the C-terminal domain of FliG to generate torque. An electrostatic interaction at the interface between the two proteins is suggested since no single mutation in these residues completely abolishes torque generation and charge-reversing mutations in both proteins can compensate. The stoichiometry of the stator complexes (of MotA and MotB) appears to be A_4B_2 with the membrane-spanning helices of MotA subunits surrounding a suspected proton-binding site at residue Asp32 (in *E. coli*) of MotB (see Fig. 47.2B).

This charged residue is essential for function. Each stator contains two ion channels with one MotB-Asp32 each. There is evidence that the protonation of Asp32 causes a conformational change in MotA. Proline residues are particularly important as they make possible bends in a helix. This makes particularly interesting that mutations in the conserved proline residues P173 and P222 in *E. coli* MotA severely impair motor function. Thus, a putative mechanism for the motor is that the proton flux coordinates conformational changes in MotA via MotB-Asp32 and that these conformational changes involve motions about the MotA proline residues that lead to a cyclic interaction with FliG that generates torque.

IIH2. Independent Torque Generating Units

When functional Mot proteins are introduced into a mot minus mutant strain, motor speed increases in discrete increments implying independent stator units provide the torque. Up to 11 or 12 speed increments were seen, consistent with the EM images and similarly for the Na^+-driven chimera in *E. coli.* There are also transient speed changes in normally expressed motors, indicating that stators are not permanent, but in constant turnover.

An average of 22 GFP-MotB molecules per cell have been counted consistent with 11 stator complexes each with the A_4B_2 stoichiometry predicted biochemically. Furthermore, a mobile pool of $\approx$200 GFP-MotB molecules was seen in the cell membrane exchanging with GFP-MotB in the motor on a timescale of minutes, confirming that stator units are in dynamic flux.

III. Stepping Rotation

The hook twists when an external torque is applied so that even a single stator generating $\approx$150 pN-nm twists the hook 0.35 radians. In a subsequent step, the motion of an attached bead will be damped with a relaxation time equal to the viscous drag coefficient divided by the spring constant of the hook. To detect steps, the time between steps must be greater than this relaxation time. To overcome these problems, stators were expressed at low levels and the SMF was reduced by lowering external sodium concentration. This achieved $\leq$10 Hz rotation combined with a fast bead response. Rotation was detected by tracking either 0.5-μm beads using back-focal plane interferometry or 0.2-μm fluorescent beads using a high-speed EMCCD camera. The distribution of step sizes was fitted by multiple Gaussians to deal with the possibility that the step-finding algorithm combined two adjacent steps into a double-size step (see Fig. 47.2C). The most probable step size was 13.7° corresponding to 26 steps per revolution (360°/13.7°= 26.3). Histograms of the dwelling angle of beads during several revolutions showed a 26-fold periodicity (see Fig. 47.2D), confirming the step size and showing that the 26 stopping angles are the same in successive revolutions.

Twenty-six steps per revolution is consistent with the periodicity of the ring of FliG, the track on the rotor where rotational torque is believed to be generated.

IIJ. Models of the Mechanism

Most models can be divided into ion turbines, ion turnstiles or binding with conformational change. In an ion turbine model, the path of ions across the membrane is formed by elements in the stator and in the rotor and these elements are arranged in lines that are tilted with respect to each other. The "elements" can be half-binding sites on the rotor and stator that need to be aligned to bind a permeant ion or ion channels in the stator that interact with tilted lines of charge on the rotor by long-range electrostatic interactions. The charged residues on the surface of FliG that are involved in torque generation could, in principle, be arranged in such a way as to provide the electrostatic interactions that are proposed. In a turnstile model, ions are deposited onto the rotor from outside the cell by one type of stator channel and can only complete a transit if the rotor rotates, carrying them to a second type of stator channel that connects to the cell interior as suggested for the F_0-ATPase. In that case, an essential conserved residue on the C subunit provides a probable binding site for ions halfway across the membrane, however, such a binding site is missing in the flagellar motor. In a conformational change model, ion transiting through a stator is proposed to be coupled to a cycle of conformational changes of the stator, which exerts torque on the rotor, either by long-range electrostatic or short-range steric interactions. This type of mechanism is proposed for the ATP-driven molecular motors actin–myosin and F_1-ATPase. Conformational changes in MotA linked to the proposed ion-binding site in MotB provide indirect evidence for this type of model. This model assumes a soft elastic linkage between the motor and the viscous load, tight coupling of motor rotation and ion transport as in the F_0 motor, the power stroke is a conformational transition in the stator triggered by the protons hoping onto and off the stator and the ion channel through the stator is gated by the motor on the rotor.

IIK. Reversibility and Switching

The flagellar motors of *E. coli* are reversible in two ways. Under natural conditions, with an IMF of around −150 mV, motors spontaneously switch direction stochastically about every second. Also, non-switching mutants rotate in the opposite direction when the PMF is reversed. This was achieved using a K^+ diffusion potential in *Streptococcus* and a voltage clamp in *E. coli*. In both cases, only a fraction of motors rotated when the PMF was reversed. In the *E. coli*

experiment, removal of the normal PMF appeared to cause the detachment of stators after a few revolutions. These results indicate that the mechanochemical cycle of the flagellar motor is essentially reversible. As discussed further below, chemotactic switching is induced by binding of the active phosphorylated form of the response regulator CheY (CheY-P) to FliM on the rotor. [CheY-P] is controlled by the chemotactic signaling system with a very steep dependence of motor bias (probability of CW rotation) upon [CheY-P], with a Hill coefficient of ≈ 10.

Currently, the best candidate to explain the switch mechanism is the conformational spread model (see Fig. 47.2E,F) in which the rotor contains ≈ 34 bi-stable protomers (in proportions of 4 of FliN to 1 of FliM to ≈ 1 of FliG). The steep dependence and lack of cooperative binding are predicted if there is a free-energy penalty for adjacent protomers to be in different states, so that the rotor is most stable with all protomers in either the CW or CCW states. A recent atomic structure of the FliN tetramer (lacking 50 amino acids at the C terminal) shows a puckered ring (see Fig. 47.2E) that fits well into the bottom of the C ring from EM reconstructions (see Fig. 47.1B). The pucker breaks the symmetry of the tetramer so they could stack in two equivalent ways, pointing either way around the C ring. Thus, the FliN tetramer is thought to be the bi-stable element in the conformational spread model, with the free-energy penalty coming from adjacent tetramers being puckered in opposite directions.

Sowa and Berry (2008) suggest that the flagellar motor is the first ion-driven molecular machine that can be studied at this level of mechanical detail. The ability to measure the enthalpic (membrane voltage) and entropic (ion concentration gradient) components of the SMF of the chimeric sodium-driven motor in *E. coli* will make it possible to study how molecular motors convert these components of free energy into mechanical work.

IIL. Chemotaxis

These motors enable a cell to swim with an orientation relaxation time constant of about 1 s due to the bacterium's rotational diffusion (Fig. 47.3A). Given they are a very elaborate piece of optimized engineering and must be quite costly to produce, there must be an advantage to swimming. Perhaps then it is not a surprise that their control for chemotaxis is also highly optimized often in surprising ways (Hazelbauer et al., 2007) (Fig. 47.3D,E). From a physiological point of view, understanding how the system works is perhaps best described from a simple linear prospective as represented by a Bode plot and then adding on the additional non-linear modifications that have given it enormously increased dynamic range from what you might anticipate, temperature robustness (Oleksiuk et al., 2011) and extraordinary sensitivity.

The gain-frequency Bode plot (see Fig. 47.3B) (Segall et al., 1986) and temporal plot (see Fig. 47.3C) (Segall et al., 1986) show that, functionally, the linear description is, in no particular order, a differentiator of the input signal (usually most associated with comparison of receptor occupancy and methylation level) and two quadratic-lag second-order low pass filters (≈ 0.2 and ≈ 1.6 Hz). It is left to the reader to assign components and the reactions that are likely responsible. Further optimization is obtained by a so-called trimers-of-dimers-architecture cheA-cheW complex. It would appear that for every receptor molecule activated, 36 kinases are activated, a considerable amplification.

Fluctuation analysis. One might anticipate that, since a responding system cannot distinguish between noise input and signal, then it must respond at low levels of signaling molecules to noise input in the same way as small real signals. The response network is tuned to maximize simultaneously both the random spread of cells in the absence of attractants and the cellular response to gradients of attractant. This advanced topic may be pursued profitably by further reading Emonet and Cluuuzel (2008).

More complex systems. Comparison of the other bacterial chemotactic systems to that of *E. coli*, has shown that most other systems are more complex, even involving cascaded feedback loops which bring greater stability to response. This advanced topic is worth further reading (Hamadeh et al., 2011).

III. CILIA

IIIA. Introduction

Eukaryotic flagella and cilia are alternative names for the slender cylindrical protrusions exclusively of eukaryotic cells that propel a cell or move fluid. Cilia are extraordinarily successful complex organelles found throughout the eukaryotes and perform many tasks in animals. They play a direct or developmental role in the sensors of fluid flow, light, sound, gravity, smells, touch, temperature and taste in mammals. The failure of cilia can lead to hydrocephalus, infertility and blindness. However, in spite of their large role in human function and pathology in terms of their physiology, there is as yet no consensus on how cilia beat or in detail how they are controlled to perform their many functions. Examples of function include moving fluids in brain ventricles and lungs and propelling and steering sperm, larvae and many microorganisms. Hence, there remains a significant opportunity for further research.

Here we are concerned with their role in motility (Foster, 2009). Typically, they are very slender (240 nm to 1200 nm in diameter, but not the 23 nm flagellar thin) and can be quite short (5 μm), most typically 12–50 μm or even amazingly long (>10 000 μm). They can propagate waves

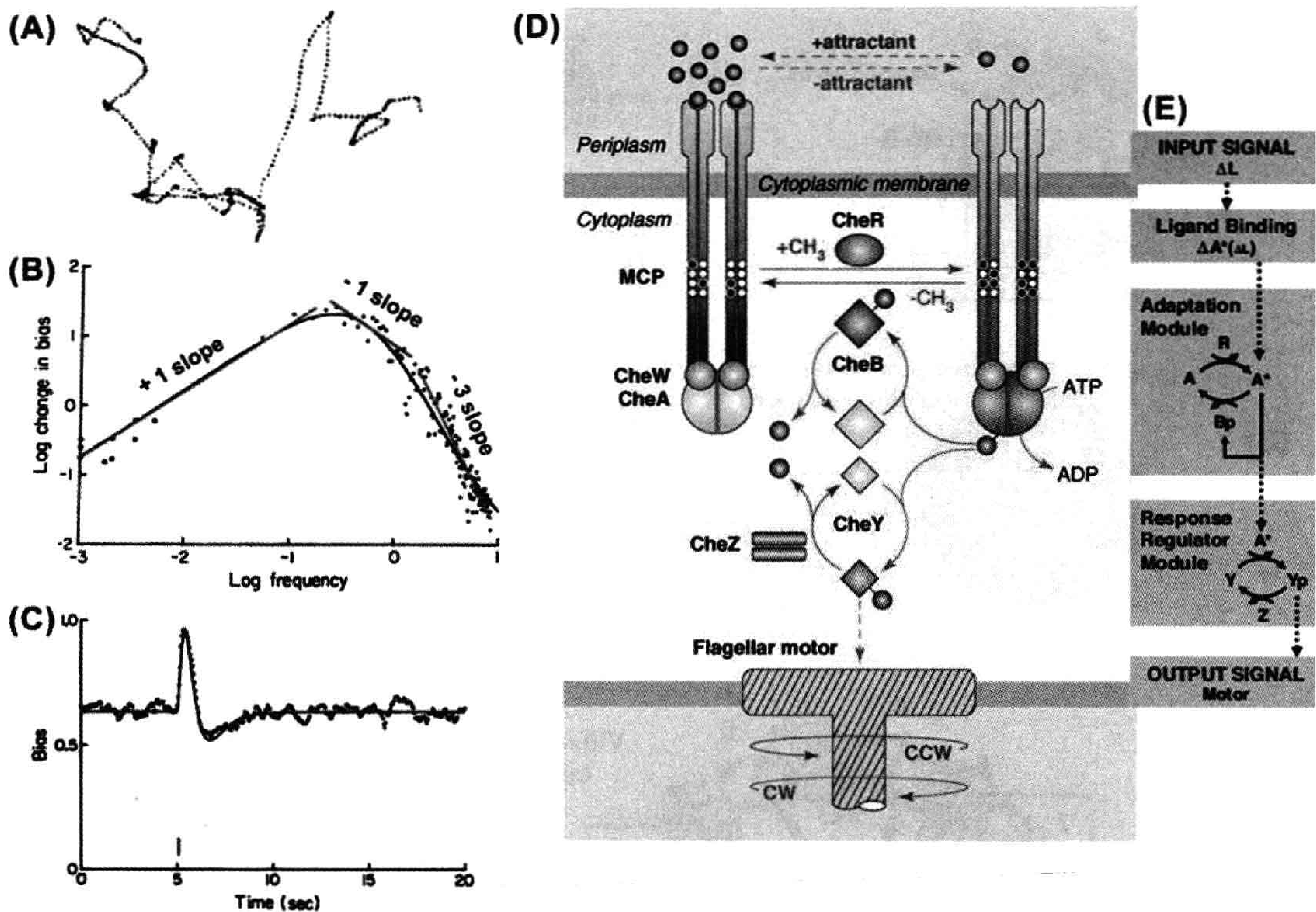
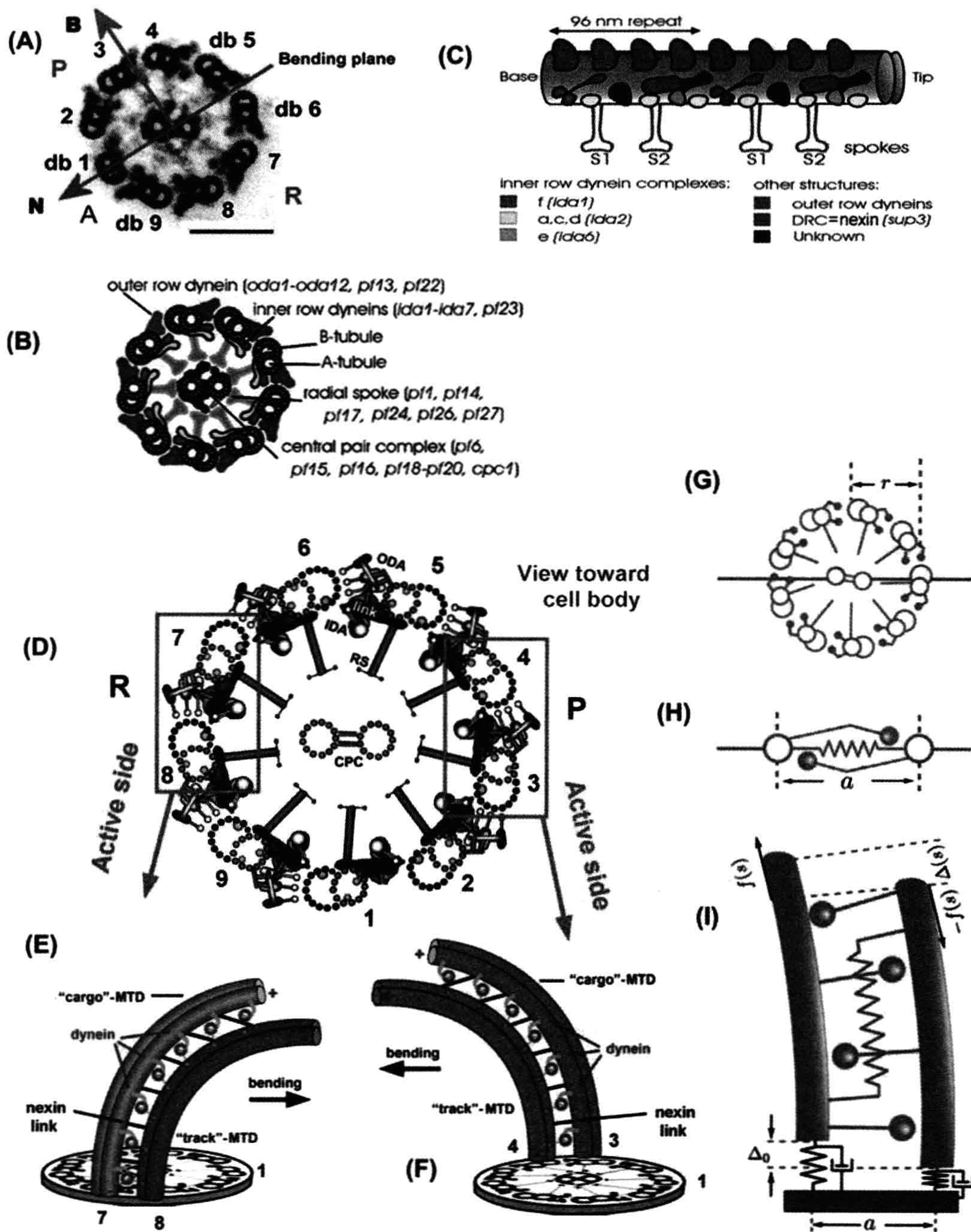


FIGURE 47.3 (A) Swimming track of *E. coli* (Berg and Brown, 1972). (B) Amplitude frequency domain Bode plot of the change in the CW–CCW bias in flagellar rotation of *E. coli* resulting from modulation of attractant, plotted as log (change in bias) versus log (frequency) of temporal modulation of the concentration of α-methylaspartate. The low-frequency data set comes from exponentiated sine-wave stimuli, while the high-frequency data comes from Fourier transforming the impulse response. The red curves show the probable dependences associated with the biochemical pathways (modified from Foster, 2009 and Segall et al., 1986). (C) Impulse response to attractant in wild-type cells. The dotted curve is the probability determined from repetitive stimulation that tethered cells of strain AW405 spin CCW when exposed to pulses of L-aspartate or α-methyl-DL-aspartate beginning at 5.06 s (vertical bar). The smooth curve is a fit to a sum of exponentials. The curve was constructed from 378 records comprising 7566 reversals of 17 cells. Points were determined every 0.05 s (Segall et al., 1986). (D) The chemoreceptor signaling pathway in *E. coli*. Components and reactions in red promote counter clockwise (CCW) flagellar rotation; those in green promote clockwise (CW) flagellar rotation. Components in gray represent inactive forms. Solid lines represent enzymatic reactions; broken lines indicate binding interactions. CheA-derived phosphoryl groups are shown as blue spheres. Receptor modification sites are shown as white (unmethylated) and black (methylated) circles (Hazelbauer et al., 2007). (E) Summary of essentials of chemotaxis pathway. Transmembrane receptors bind the ligand (L) and control the activity of histidine kinases CheA. The kinase CheA phosphorylates the response regulator CheY (Y) into the active form CheY-P (Yp). CheY-P diffuses throughout the cell and interacts with the flagellar motors to induce clockwise rotation (tumble). The phosphatase CheZ (Z) dephosphorylates CheY-P. A sudden increase of ligands L causes the kinase activity to decrease by A*. The chemotaxis system has an adaptation module in which two antagonistic enzymes regulate the activity of the kinase-receptor complexes. Note this is unlike most electronic circuits; here there is a feedback circuit to increase a variable and one to decrease the same variable. The methyltransferase CheR (R) catalyzes the autophosphorylation of CheA by methylating the receptors. The active kinase A* phosphorylates the methylesterase CheB in CheB-P (Bp). CheB-P removes methyl groups from active receptor complexes, which catalyzes kinase deactivation (Emonet amd Cluzel, 2008).

from the base or the tip or, in a few cases, even switch from one to the other. They can have two distinct modes, so-called flagellar or symmetric beating which is whip like and is typically like a sperm, or ciliary or asymmetric beating which is breast-stroke like (see Fig. 47.5C). It is not unusual to be able to switch between the two modes of beating. On a surface, including an air–water interface, they may also crawl.

IIIB. History

It is thought that cilia evolved from a protruding structure with sensory capabilities. Later, some motors invaded the structure from the cytoplasm enabling crawling on a surface much like the cilium of *Peranema* that pulls itself along an air–water interface or harder substrate at 50 μm/s. Later, more motors were inserted and, spontaneously, the


(A)
B
P
N
A
R
db 5
db 6
db 1
db 9
Bending plane
(C)
96 nm repeat
Base
Tip
S1
S2
spokes
inner row dynein complexes:
f (ida1)
a,c,d (ida2)
e (ida6)
other structures:
outer row dyneins
DRC=nexin (sup3)
Unknown
(B)
outer row dynein (oda1-oda12, pf13, pf22)
inner row dyneins (ida1-ida7, pf23)
B-tubule
A-tubule
radial spoke (pf1, pf14, pf17, pf24, pf26, pf27)
central pair complex (pf6, pf15, pf16, pf18-pf20, cpc1)
(D)
View toward cell body
ODA
IDA
RS
CPC
Active side
Active side
(E)
"cargo"-MTD
dynein
nexin link
bending
"track"-MTD
(F)
"cargo"-MTD
dynein
bending
"track"-MTD
nexin link
(G)
(H)
(I)

device started to beat in some uncontrolled twirling or nutating fashion with waves propagating from the base toward the tip and the attached cell moved. Later, tip to base waves became possible and, in some species, the ability to do either and hence regulate their direction. Subsequently, the more efficient planar beat was achieved in many species and further optimizations crept into the cilia of different species. One example is that ATP can be supplied consistently at one point in the beating cycle in *Chlamydomonas*. Subsequently, its specializations into sensing and motion established cilia as one of the most useful devices in nature, with most human cells being ciliated at some time in their development. These machines are very complex requiring in humans about 650 genes (representing about 3% of human genome) devoted to their synthesis and control. Consequently, defective cilium has led to ciliary pathologies which has made the study of cilia medically important (Marshall, 2008a).

IIIC. Structure and Beating Cycle

It is very hard to appreciate a cilium without understanding its complex structure.

IIIC1. Basics of Ciliary Geometry and the Beating Cycle

Considerable effort has been aimed at understanding the cilium structure (Foster, 2009). The core structure of each cilium is known as the axoneme (cross-section shown in Fig. 47.4A,B). It consists of nine doublet microtubules (db) arranged around the central pair doublet (the dynein "arms" point to the next higher numbered doublet, if numbers increase clockwise you are looking toward the tip, if counterclockwise you are looking toward the base). Fig. 47.4C shows one of the doublets with its dynein motors, which drive the sliding between the doublets and spokes that connect the doublets to the central pair. The observed bending implies that the motor activity periodically varies from being higher on one side of the axoneme to being higher on the other side. During a P (principal) bend, walking on doublets 1–4 dominates (by attaching/ detaching) on the adjacent higher numbered doublet toward the base of the cilium making the cilium bend with doublets 5 and 6 on the inside of the curve (negative curvature according to convention) (Fig. 47.4D,F). Similarly, during an R (recovery) bend, walking on doublets 6–9 dominates on the adjacent higher numbered doublet toward the base making the cilium bend in the opposite direction (positive curvature) (Fig. 47.4D,E). Since the cilium is thin and the distance between the doublets is short, even a short walk can produce a significant bend in the cilium (e.g. 100 nm relative sliding of a doublet may induce a bend as large as 50°). The full sliding of doublets at the end of a cilium measured by in-vitro experiments is no more than ±200 nm. A simplified way of thinking about it is to consider the axoneme as two elastic filaments that slide relative to each other resulting in the bending (Fig. 47.4 G,H,I). The dynein motors provide the shear forces to produce the relative sliding.

The dynein motors are in some ways similar to piezoelectric motors used to focus lenses in cameras and cell phones. As shown in Fig. 47.4C, there are several motors periodically arranged in rows along a doublet. The upper row motors are referred to as the outer dyneins and the lower ones are referred to as the inner dyneins. Fig. 47.5A shows the force–velocity relationship in a limited range for one of the inner dynein motors at two different concentrations of ATP. The force exerted by the motor decreases with the increases in sliding velocity of the driven doublet microtubule and the velocity is approximately linear with ATP concentration.

In addition to causing shear between neighboring doublets, dyneins bind, to variable degrees, the doublet microtubules that together make up the axoneme (interior structure) of a cilium. These doublet attachments remarkably

FIGURE 47.4 (A) EM micrograph through a demembranated ciliary axoneme of *Chlamydomonas* (scale bar = 100 nm). Note the P-side consisting of microtubules doublets (MTD)1–4,which facilitate the principal bend, and the R-side consisting of MTD 6–9,which facilitate the recovery bend *(modified from Foster, 2009).* (B) Structural components of the axoneme and assembly mutations. Viewed from the cell body looking outward *(modified from Foster, 2009).* (C) One doublet showing dyneins and related structures along a tubule *(modified from Foster, 2009).* (D) Simplified cross-sectional view from the ciliary tip of an axoneme with nine outer MTDs surrounding the central pair complex (CPC). Three structures connect neighboring MTDs, the ODAs and IDAs and the nexin link (also called the dynein regulatory complex). The blue and green boxes highlight the most important active doublets from opposite sides of the axoneme. Binding is twelve times higher in the boxed regions *(modified from Heuser et al., 2009).* (E) and (F) Interdoublet sliding model for ciliary bend formation. Two pairs of MTDs from opposite sides of the axoneme, as highlighted in (D), are shown. The dynein arms are anchored on the cargo MTD in an ATP-independent manner and walk toward the minus end of the track MTD in an ATP-dependent manner, which causes sliding between neighboring MTDs. The links between MTDs are important for transforming MT sliding into bending. Note that the minus end-directed dynein motors (red) have to be active and produce MT sliding on alternate sides of the axoneme (switching between the blue and green side) to generate the principal and reverse bends (with opposite bending directions; black arrows) *(modified from Heuser et al., 2009).* (G) Cross-section of an axoneme with radius r as seen from the basal end. The microtubule doublets and the central pair are shown in red, the dynein motors in blue and the radial spokes in green. The horizontal gray line indicates the plane of the beat. With this beat plane, the largest sliding displacement occurs between adjacent microtubule doublets at the top and bottom (Riedel-Kruse et al., 2007). (H) Cross-section of a two-dimensional representation of the axoneme in which two flexible filaments slide relative to each other in the beating plane. The shear forces are generated by active elements acting antagonistically between the filaments. Passive elastic elements are represented in green. The separation of the two filaments is $a = 2r$ (Riedel-Kruse et al., 2007). (I) View of the beat plane of this 2D axoneme. Indicated are the local sliding displacement $\Delta(s)$ and the internal shear force density $f(s)$ due to the active elements (blue) and the passive cross-linkers (green). The basal connection has a finite stiffness and friction indicated by black springs and dashpots (Riedel-Kruse et al., 2007).

account for most of the bending or flexure rigidity of a cilium. The all dynein attached flexure rigidity, $\kappa = 11\,000$ pN μm^2, is at least 14 times stiffer than when the dyneins are unattached, estimated in the range $\kappa = 150-800$ pN μm^2.

Inspired by the motor characteristics of the similar piezoelectric linear motors, these are the hypothesized characteristics of the dynein–tubulin linear motors. The sliding and oscillating mechanism could exploit the dependence of motor characteristics with the distance between the motor and the binding sites as suggested by analogy with ultrasonic motors (see Fig. 47.5B).

IIIC2. Central Pair

The central pair of microtubules carries several complexes of known and unknown function. What is particularly

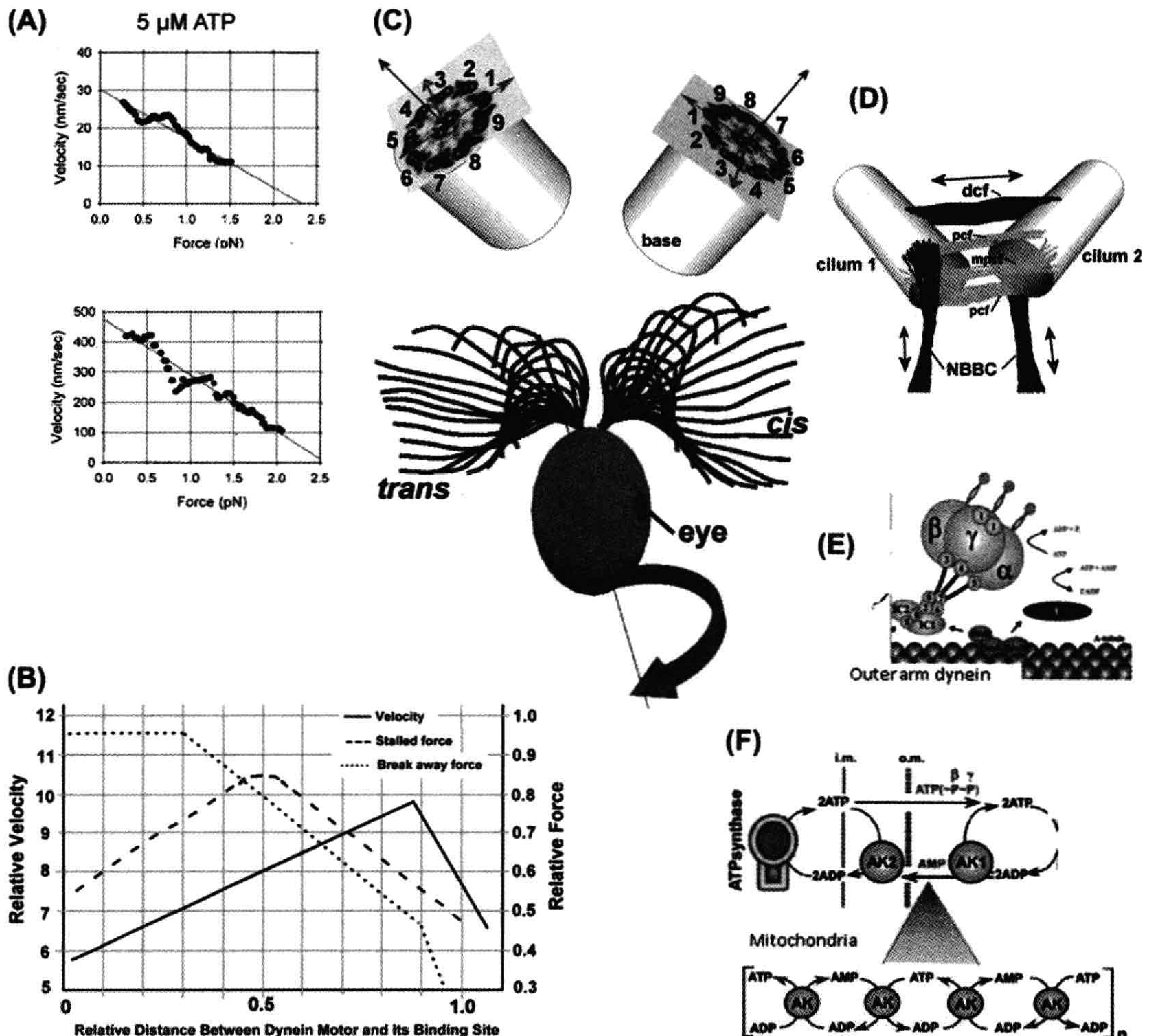


FIGURE 47.5 (A) Velocity-force curve for inner dynein c in the presence of 5 μM ATP and 100 μM ATP. The solid lines are linear fits to the data (Foster, 2009). (B) Inspired by the motor characteristics of the similar piezoelectric linear motors, these are hypothesized characteristics of the dynein–tubulin linear motors (Foster, 2009). (C) Shows attachment of the cilia to the cell body with C2 symmetry (from animation of JyothishVidyadharan and the axoneme cross-section image of Fig. 47.4A). Note the left-hand rotation of the cell, the ciliary beating patterns and the eye (Foster, 2009). (D) An angled view through the basal bodies and the base of the cilia of *C. reinhardtii*. dcf, distal connecting striated fiber joining the two basal bodies; pcf, proximal connecting fiber joining the two basal bodies; medial proximal connecting fibers joining the two basal bodies; NBBC, nucleus-basal body connectors. The NBBC and pcf are contractile. Note the offset of ends of the two cilia at the base (Foster, 2009). (D) Outer dynein arm site for use of ATP from Wirschell et al. (2004). (E) Shows the adenylate kinase (AK) shuttle that facilitates ATP transport from generation site (mitochondria) to utilization site such as outer arm dynein (Dzeja and Terzic, 2009).

noteworthy is that the central pair has chirality and it is not attached directly to any structure, so that for every bending wave that passes it rotates it once, so that the same side is always adjacent to the interior bend. This permits, for example, ATP synthesis to be maintained at the same phase with respect to the bending cycle. Potentially, many ciliary controls could also be positioned at a constant phase with respect to the bending.

IIC3. Attachment of the Cilia to the Cell Body

The cilia have a very specific orientation with respect to the cell body. Looking down from above near the base, the number-1 doublet microtubule faces the other cilium, in twofold-rotation or C2 symmetry (see Fig. 47.5C), which leads to consistent left-handed cell rotation. According to Riedel-Kruse et al. (2007 and references therein), with respect to bull sperm, the dynamics of the base connecting the cilium to the cell body plays a crucial role in determining the waveform of beating. Thus, cells may control their beating by changing the properties of their basal connection. In the case of *Chlamydomonas*, where much is known about the base, the two cilia (see Fig. 47.5D) are connected to each other through proximal fibers (pcf and mpcf) at the base plate and distal fibers (dcf) at about 250 nm from the base (see Fig. 47.5D). As a result, the dynamics of the two cilia are connected and the cell may use this connection to control or influence the beating pattern. In addition to the distal fibers, which link the dynamics of two cilia, there are other components, such as the nuclear-basal body connectors (NBBC), in the basal body region that may play a significant role in cellular control of the beating. The NBBC and dcf contain centrin (caltractin), which shows calcium-sensitive contractile or elastic behavior. It has been shown that centrin-based flagellar roots are contractile under conditions of elevated calcium in a variety of eukaryotes, including *Chlamydomonas* and *Tetraselmis*. There is also a fine filament that runs between the centers of the proximal ends of each basal body which would be very sensitive to the relative motion of either cilium. However, with very different compliance machinery in a similar organism, the cilia still beat with similar waveforms and the cell still shows phototaxis.

The distal striated fiber (dcf, see Fig. 47.5D) of nominal length 280 nm can contract to as much as 220 nm resulting in the decreased angle between the two cilia from about 65° to 55°. Contraction of the NBBC would also aid this movement and pull the base end inward so that the cilia can more easily exit the fixed holes in the cell wall. This change will induce a force in addition to the force due to sliding caused by dyneins. Now the sum of the forces due to base sliding and connection must be balanced by the component of the total hydrodynamic force parallel to the cilium at the base.

IIID. Energy Supplied to Cilia

A significant part (and in some cases such as mammals, all) of the ATP needed to supply the dynein ATPases (see Fig. 47.5E) is supplied from the base. Mitochondria are typically massed at the base of a cilium. In every case, the ATP has to be transported effectively along the cilium which can be very long. Any time you have long lengths like tens of microns, the idea of diffusion fulfilling requirements seems unlikely. Diffusion of ATP down a centimeter long cilium is utterly unrealistic (at a diffusion rate of 64 $\mu m^2/s$ it would take $\approx 10^6$ s to reach 1 cm or ≈ 9 days). Not surprisingly, there is an adenylate kinase (AK) shuttle (see Fig. 47.5F) that facilitates ATP transport from the ATP synthesis site (mitochondria) to the dynein motors (ATPases) along the cilium. It is reputed to achieve a constant velocity of transport.

In addition, an interior ATP synthesis system exists in some cilia, such as that of *Chlamydomonas*, which is associated with faster beating cilia. Further, it can be rotated with the beating so that it always supplied with the same phase relationship with the motor activity. In *Chlamydomonas*, 3-phosphoglycerate (3PG) (Mitchell et al., 2005), which is central in the glycolytic pathway and is a product of photosynthesis, is processed by the cilium with aid of an enzyme complex containing enolase situated on the C1b arm of the central pair. Since the central pair rotates so that C1 to C2 vector always points toward the inside of the bend, the C1b arm is always to the outside of a bend. However, at the forward traveling edge of a bending wave, the front receives increased ATP. How the 3PG is transported versus diffused or even if it is actively transported is not currently known.

IIIE. Known Effects on Beating and Refinements that Possibly Optimize the Beating Cycle

There are many known effects on ciliary beating. However, their role may not yet be fully appreciated (Woolley, 2010). The list includes, but is not limited to the following:

1. The concentration of ATP affects the beating frequency by changing the sliding velocity (see Fig. 47.5A)
2. Variations in temperature, pressure and the pH have effects consistent with the activity of dynein ATPases
3. External mechanical effects, such as viscosity, lower beating frequency, wavelength and wave velocity while increasing the bend angle
4. The beating behavior is particularly sensitive to the hydrodynamic differences associated with walls
5. Synchronization of beating between adjacent cilia occurs at a higher frequency than either alone, but only occurs where there is mechanical attachment between them

6. Typically, there is beat asymmetry, where the bend in one direction is consistently greater than in the other direction, already referred to as the principal and reverse bends. Even so-called symmetrical beating is not really all that symmetric. The degree of beat asymmetry is calcium concentration dependent
7. Short truncated cilia beat faster than longer ones
8. When the head of a sperm attaches to a surface, there is a decrease in the speed of wave propagation along the cilium.

All these and many other effects must be accounted for in the details of any model.

Refinements that may contribute to improved performance of beating include: (1) splitting the task of moving the cilia into multiple (8) types of dynein motors which can be potentially independently controlled; (2) intricate compliance devices at the attachment site to the cell body; (3) an interior ATP delivery system that rotates with the beating so that it always has the same phase relationship with the motor activity; and (4) geometric changes that accentuate motor activity on the inside of bends.

IIIF. Mechanism of Ciliary Beating

We use the Woolley (2010) review as our starting point.

Each of the many explanations of beating offers some insight into how cilia beat. Woolley optimistically says that what is occurring in molecular terms "has presented an intractable level of difficulty". When the sliding velocity is maximum, the amount of sliding is minimum and vice versa. It is known (most, but not all agree on this) that the dyneins walk unidirectionally and are going in their forward direction when they are progressing toward the base. There is the observed active mode in which the dyneins move forward toward the base. Due to the geometry of the cilia motors, on the opposite side, dyneins must move in the opposite direction, namely backwards. For some authors, this suggests that the dynein motors operate in two modes, active and passive, of motor activity (Brokaw, 2009). Whether there is a controller that switches the motor activity is a basic point which lacks consensus, however, since there is no concrete evidence in its favor, we will assume it does not exist and account for the observations another way. This uncertainty has come about because the action of the relevant dynein motors which are going backwards is not known and, critically, the level of dynein binding on the two sides is not known dynamically.

Many, including this author, believe that ciliary beating is a self-organized beating (SOB) process and that the basic oscillation is not being controlled at the level of every beat, rather the inherent properties of the components is sufficient to get the basic ciliary oscillation. The oscillation is indicated by its phase plot at a particular position along the cilium, rate of sliding versus the amount of sliding (Fig. 47.6A). Potentially confusing researchers are a number of refinements added during evolution that modify the phase and amplitude of beating. If this author is correct there is no per se regulation or switch of the mode of activity of the dynein motors, for example, by some threshold curvature or threshold transverse force or some switch point or basal elastic recoil or by the central pair. However, the forces and sliding these ideas represent may indeed be playing a role in the inherent activity of the dyneins and central pair may (likely) be playing a role in the control of behavior as discussed later. One should note here that the inherent properties of the components will be strongly affected by the degree of sliding, the rate of sliding and the direction of sliding and the forces at that local location.

IIIG. How to Find Out What is Happening

A good start can be made by forming a model and then by analysis of data to determine the relevant parameters (Foster, 2009).

IIIG1. Motor Forces and Sliding

The hydrodynamic force $F_j(s, t)$, together with the cilium position $r_j(s, t)$, s being the distance along the cilium measured from its base, and t the time, may be used to determine the motor forces along the cilium. Since the inertial effects are negligible, the hydrodynamic force is balanced by the elastic forces arising from the bending of the doublets and the internal forces consisting of active forces due to motor activity and passive restraining forces due to nexins (the dynein regulatory complex). The nexins connecting adjacent doublets provide an elastic resistance to longitudinal sliding with a complex non-linear dependence on stretch (estimated to be 16–100 pN/μm (see Fig. 47.6B) (Lindemann et al., 2005). It is assumed that each doublet is inextensible, but flexible since a single microtubule has been measured to be anisotropic with a shear modulus of ≈1.4 MPa and a Young's modulus of ≈100 MPa. The sum of the internal forces at any cross-section of an axoneme must vanish even though some doublets are under tension and others under compression.

For planar beats, it has been shown that the 9 + 2 structure of the axoneme can be equivalently replaced by two elastic filaments (groups of doublets) separated by distance a and bending rigidity κ, both of which can be estimated from the known geometry and mechanical properties of the axoneme ($\kappa \approx 1700$ pN μm^2 for bull sperm) (Riedel-Kruse et al., 2007). Let f be the internal shear force acting along the filament on the inner side of the bend and $-f$ the shear

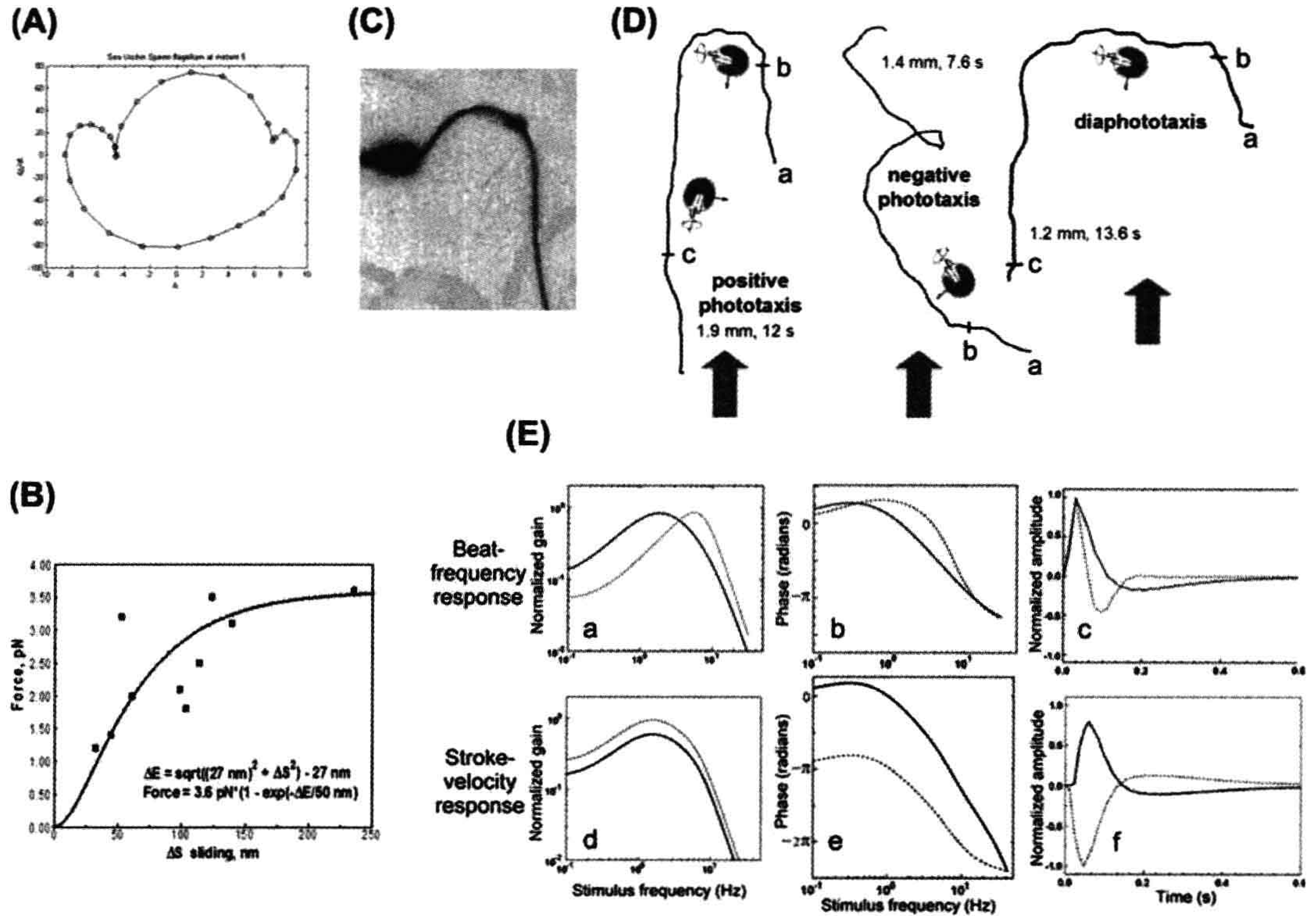


FIGURE 47.6 (A) Shows the dynamic phase plot at a local spot on a sea urchin cilium through one beating cycle. (B) The nexin (dynein regulatory complex) force–extension curve *(data from Lindemann et al., 2005)*. (C) Shows relative sliding of two beads attached to a naked cilium on different microtubules, from which one can estimate the sliding at the base (Brokaw, 1991). (D) Three of the seven types of phototaxis: helical positive, superhelical negative and diaphototaxis *(modified from Foster, 2009)*. (E) Typical ciliary beating frequency (CBF) of the negatively phototactic strain 806 in response to green light (543 nm) modulated by a pseudorandom Gaussian-white-noise (GWN) stimulus. The *cis*- and *trans*-CBF for each record were separately cross-correlated with log10 (stimulus intensities) to produce respective impulse responses (C). The *cis* and *trans* responses were then separately averaged (solid lines for *cis* and dotted lines for *trans*). The Fourier transform of the averaged impulse responses yielded the gains (A) and phases (B). Typical ciliary stroke-velocity response to green light modulated by a GWN stimulus. Stroke velocities for the *cis* and *trans* cilia for each record were independently cross-correlated with log10 (stimulus intensities) to produce impulse responses (F) that were then separately averaged in for *cis* cilium (solid line) and *trans* cilium (dotted line). The Fourier transform of the averaged impulse responses yielded the gains (D) and phases (E). *(Modified from Foster, 2009.)*

force on the outer one. From balancing the forces on a pair of inextensible elastic elements leads to:

$$af(s,t) = \kappa(s,t)\partial_s C(s,t) + n_j(s,t)\int_s^L F_j(s',t)ds' \quad (47.4)$$

where C is the curvature, n_j is the unit normal to the filament in the plane of the beating, δ_s represents the derivative with arc length s, L is the cilium length, and F_j is the hydrodynamic force per unit length. Since all the quantities on the right-hand side of the above equation can be determined from imaging and hydrodynamic analysis, f can be determined along the cilium length.

It is possible that the local bending rigidity or flexure is under control and alterable by internal viscosity, mechanical feedback or cell command. In addition to causing shear between neighboring doublets, dyneins bind, to variable degrees, the doublet microtubules that together make up the axoneme (interior structure) of a cilium. These doublet attachments remarkably account for most of the bending or flexure rigidity of a cilium. The all dynein attached flexure rigidity, $\kappa \approx 11\,000$ pN μm^2, is 14 times stiffer than when the dyneins are unattached, $\kappa \approx 800$ pN μm^2. In our formulation we use the dynein-unattached flexure rigidity, which we find to be about 150 pN μm^2.

All SOB models assume that the motor force is a function of doublet sliding. The relative sliding of the filaments is given by:

$$\Delta(s,t) = \Delta_0(t) + \Delta^c(s,t) \quad (47.5)$$

where

$$\Delta^c(s,t) = \int_0^s aC(s',t)ds' = a(\psi(s) - \psi(0))$$

and $\Delta_0(t)$ is the relative sliding of the two filaments at the base ($s = 0$). Note that since $\Delta^c(s,t)$ can be determined from the ciliary images, the total sliding along the cilium can be determined to within a single parameter $\Delta_0(t)$. This parameter has been assumed to be zero by a number of investigators in the past, an assumption that may not be valid.

IIIG2. Modeling of Basal Connection

According to Riedel-Kruse et al. (2007) and, as previously suggested, $\Delta_0(t)$ the dynamics of the base connecting the cilium to the cell body likely plays a crucial role in determining the waveform of beating in bull sperm. Thus, cells may control their beating by changing the properties of the basal connection. In the case of *Chlamydomonas*, the two cilia (see Fig. 47.5C) are connected to each other through proximal and distal fibers. As a result, the dynamics of the two cilia are connected and the cell may use this connection to control the beating pattern.

In addition to the distal fibers which link the dynamics of two cilia, there are other components in the basal body region that may play significant role in cellular control of the beating. Some of these components contain centrin which shows calcium-sensitive contractile or elastic behavior. It has been shown that centrin-based flagellar roots are contractile under conditions of elevated calcium in a variety of algae, including *Chlamydomonas* and *Tetraselmis*. The contraction of centrin is responsible for changing the base angle in a ciliary to flagellar beating transition in *Chlamydomonas*. The average angle between the cilia decreases with light intensity, the expected result for a calcium dependent contraction. Riedel-Kruse et al. (2007) modeled the component of the base force parallel to the cilium at base as given by:

$$F_B = \gamma_s(d\Delta_0/dt) + k_s\Delta_0 \qquad (47.6)$$

where γ_s and k_s are, respectively, basal friction and stiffness. In the case of bull sperm with a single cilium, the force F_B can be determined by equating it to the component of the total hydrodynamic force parallel to the cilium at the base, thus providing sufficient information for determining γ_s and k_s. In the case of sea urchin sperm experiments (Brokaw, 1991), two beads were attached to the cilium and the relative sliding determined (see Fig. 47.6C). This in principle should give sufficient information to determine the $\Delta_0(t)$ and compared to $F_B(t)$ determine γ_s and k_s.

The base structure in *Chlamydomonas* is different than in bull sperm. The axoneme of each cilium extends to the attached basal bodies connected by a distal striated fiber, which can contract. Any change in the angle θ between the two cilia will therefore induce a force in addition to the force F_B due to sliding. We may assume that this additional connection force is given by $F_C = b\,[\cos(\theta/2 - \cos(\theta_0/2)] \approx -b'(\theta-\theta_0)$ where the (complex) stiffness b is related to the strength of distal fiber and $b' = b\sin(\theta_0/2)/2$. Now, the sum of the forces due to base sliding and connection must be balanced by the component of the total hydrodynamic force parallel to the cilium at the base. We note here that, since these cilia are mechanically linked, it is not surprising they can maintain synchrony.

IIIG3. Hydrodynamic Calculations

The procedure is clear. From rapid images of ciliary motion, one has the local velocities along their length which, with hydrodynamic calculations, can lead to the net forces along their length.

Since the Reynolds number based on the length of the cilium and its stroke velocity is O (10^{-3}; of the order of) or smaller, the flow induced by the cilia beating can be described by the simple Stokes equations of motion. Furthermore, since the diameter of a cilium ($\approx 0.24\ \mu m$) is much smaller than its length ($12-14\ \mu m$), slender body theory may be used to determine the force exerted by the fluid along the cilia. The theory is fairly well established and a number of studies show in detail how it may be used to determine the force distribution. The velocity at a point in the fluid is expressed as a line integral (along the cilium) of the force distribution times the velocity induced by the force (Green's function for Stokes equations, also known as the Stokeslet). The Green's function derivative is chosen so that the no-slip boundary condition on the surface of the cell body (approximated as a sphere of diameter about $8\ \mu m$) is automatically satisfied. In addition to the Stokeslet distribution along the centerline of the cilium, a source dipole distribution is added that improves the accuracy without significantly increasing the computational effort. Since cells may be held by a micropipette at the posterior end where the flow induced by the cilia is minimal, interference due to the presence of the micropipette may be minimized. All the other boundaries are at least a few millimeters away from the cell so that their effect can be made negligible.

Approximating the velocity by means of a line distribution of Stokeslet is valid in the outer region, away from the surface of the cilium. In the inner region, close to the surface of the cilium, one must construct another approximation that satisfies the no-slip boundary condition at the cilium surface taking into account its cross-section shape. The requirement of matching the inner and outer region

approximations in the overlap region (at large distances from the surface compared to the cilium diameter, but small compared with its length) gives rise to an integral equation for determining the force distribution along the cilium length.

IIIG4. In the Final Analysis

One obtains the net (sum of both sides of the cilium) relationship between the motor forces and doublet sliding along the ciliary length with time in the beating in cycle. In isolation it is likely that the motor force-sliding-velocity curve looks as depicted in Fig. 47.5A, except extended on the right steeply downward at negative velocities and extended to negative forces (the motor is being pushed) at slightly increased velocities. In addition, one must be concerned with the differences in the probability of binding depending on the load, the curvature, the ATP level, the direction of sliding, etc.

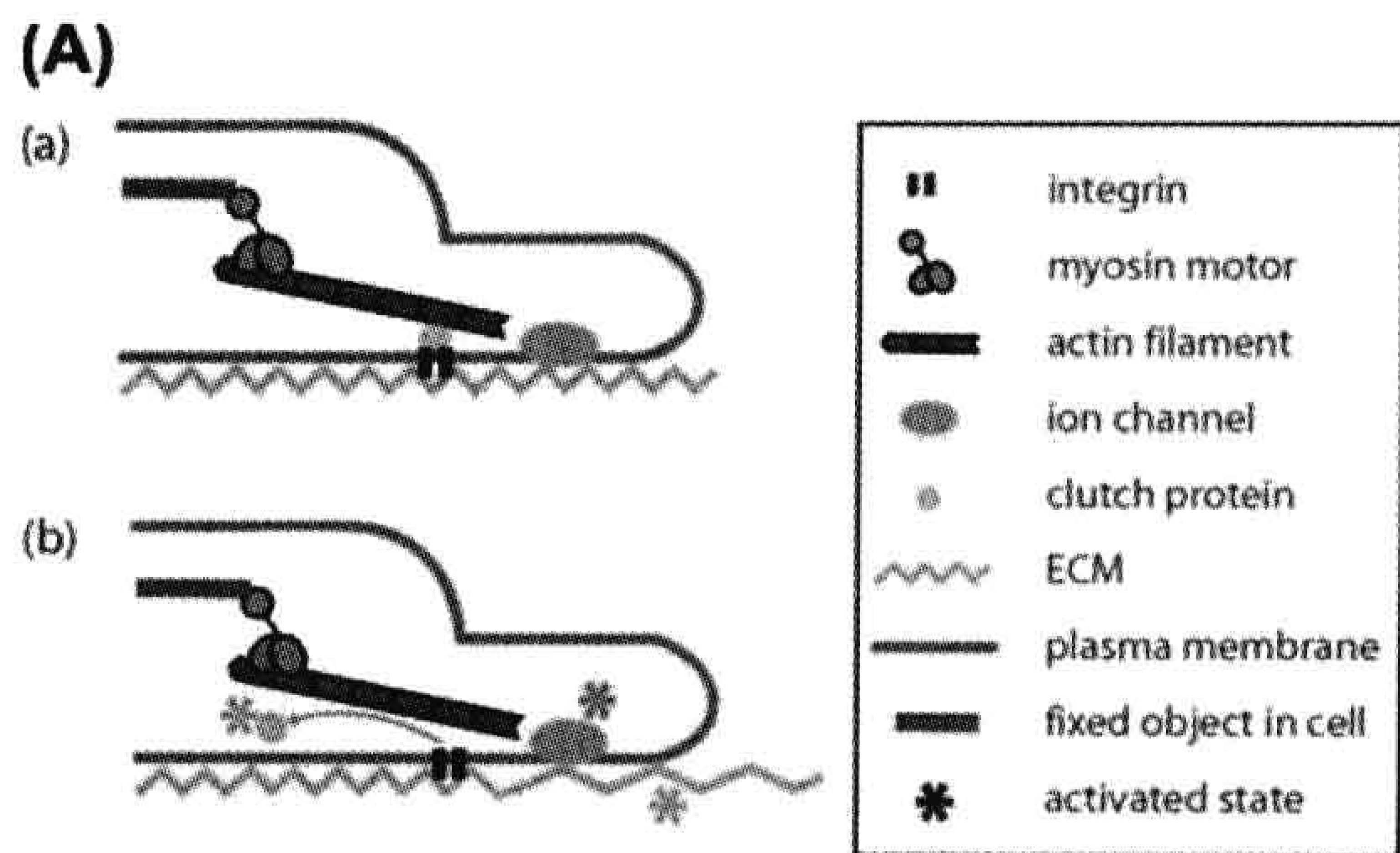
After considering Woolley's (2010) review, a tentative consensus maybe made uniting the switching-two-modes view of dynein activity and the SOB model as advocated here. He has suggested the direction of sliding is the primary controlling factor for flagellar oscillation. He adds that "dyneins actively generate force when sliding in one direction is detected and are inhibited from doing so by the detection of sliding in the other direction" (see Fig. 47.4E,F). This is stated in the two-mode view. However, the SOB one-mode view has some similar consequences. In the SOB view, dyneins move according to the force they are pushing against or the force that is pushing them. In other words, they have a single force–velocity curve with force and velocity both vectors relative to their substrate or, in effect, the magnitude and direction of sliding (see Fig. 47.5A and recall above discussion). Quite possibly, when being pushed backward they do not use ATP, as the backward force may be sufficient to disengage dynein motors from attachment sites. Of course, detaching motors causes drag, but it may be minimized if the geometry favors lower binding rates. There are many factors that can also influence the force and movement on each side of the planar beating cilium. These include ATP availability and, likely, calcium which probably influences attaching and detaching of the dyneins. If the opposed force is beyond their stall force they inevitably go backward. Due to the nexins and the passive restoring force associated with a bent cilium, dyneins may also be pushed forward.

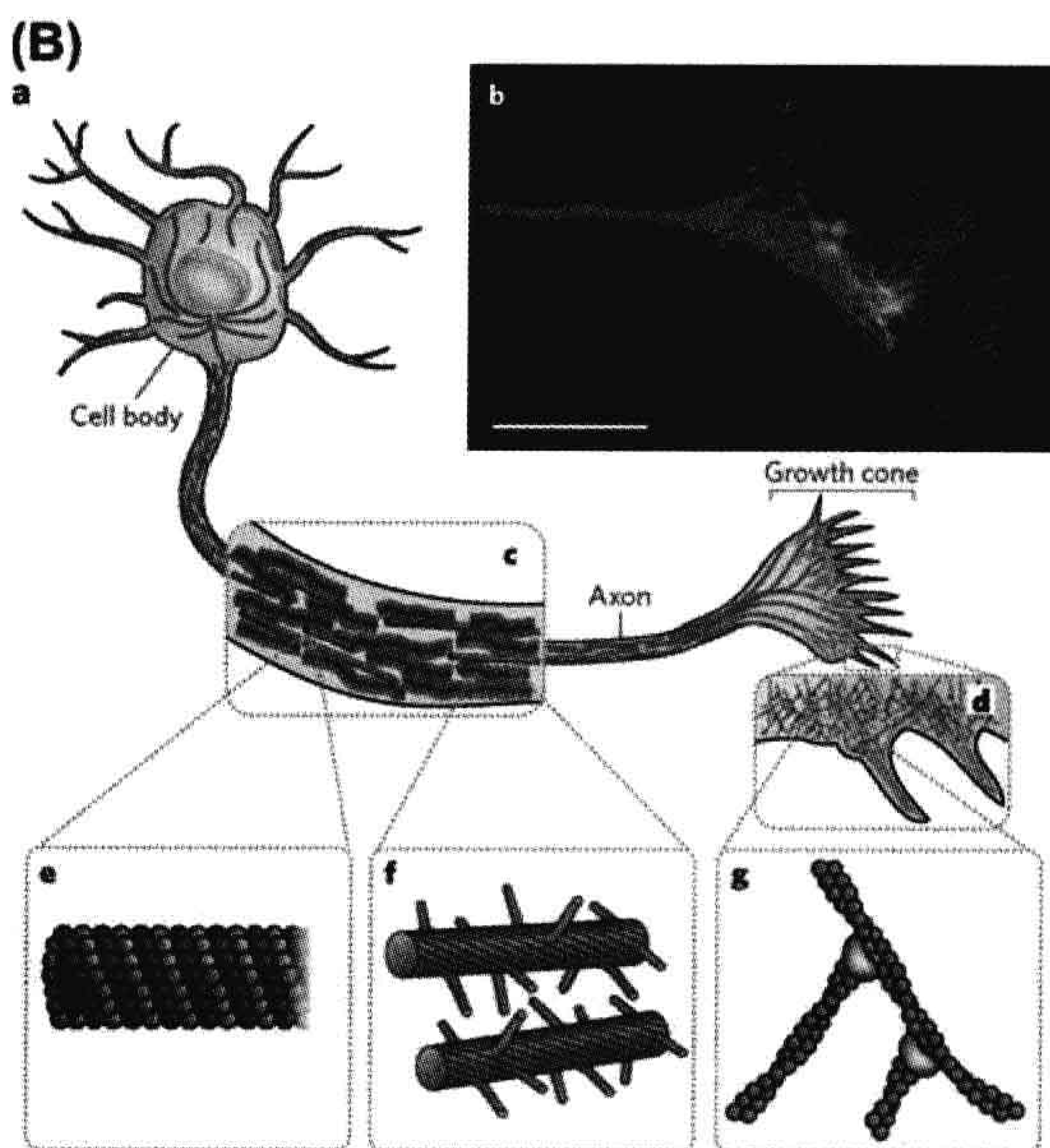
IIIH. Behavioral Controls

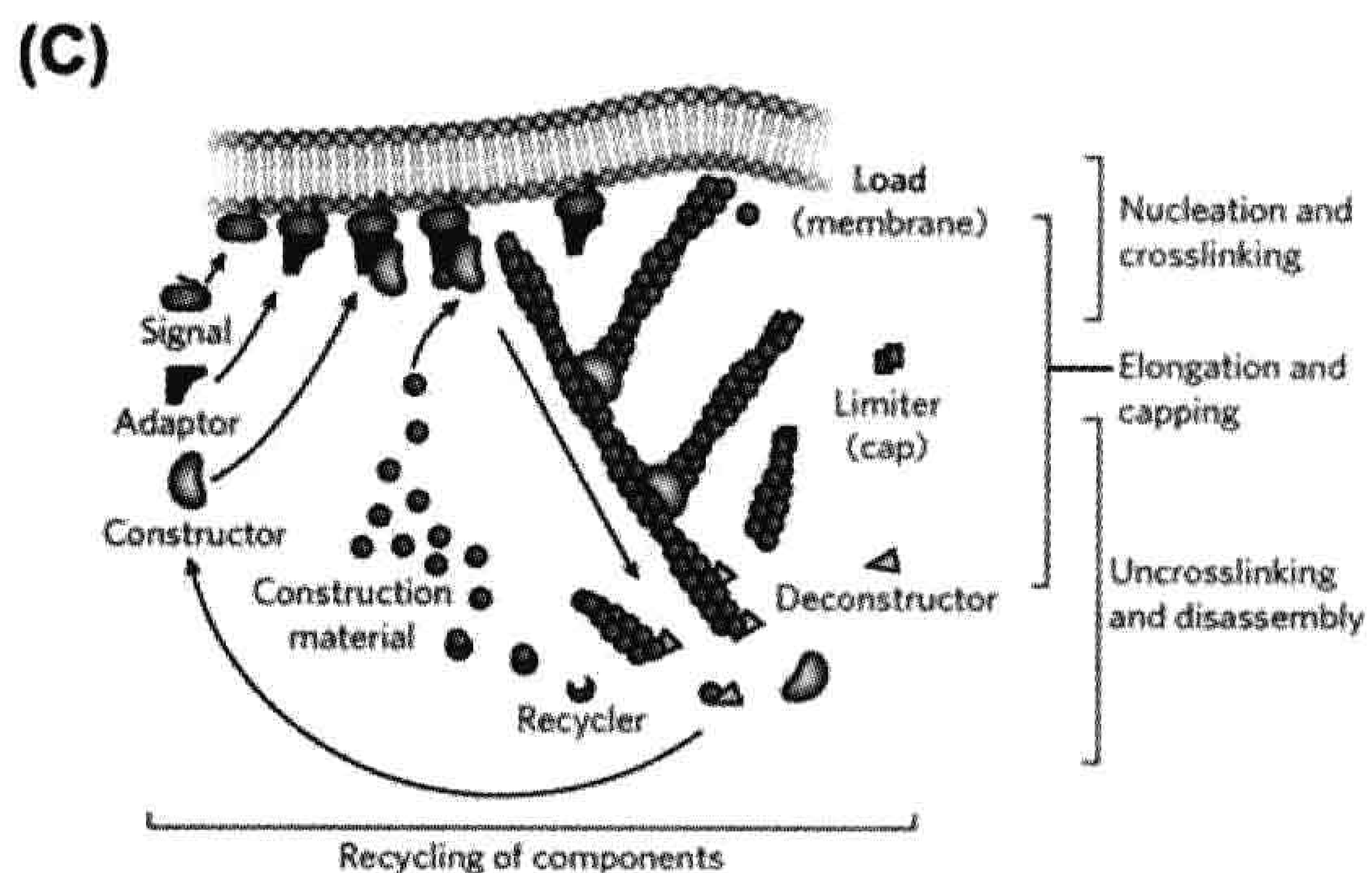
Overlaid on top of the self-organized beating and its optimizations are cellular controls to achieve a rich variety of functions. These include control of cell steering associated with phototaxis and chemotaxis (hypothesized to be at the S2 locus), the stopping of beating to facilitate mating (at the S1 locus, involving a cAMP signal), the temporary turning off of phototaxis when an obstacle is encountered (at the S1 locus, involving calmodulin/Ca^{2+} and not cAMP) and the optimum balance between ballistic and diffusive motion (at the S1 locus, involving cAMP and calmodulin/Ca^{2+}). S1 and S2 refer to the spokes (see Fig. 47.4C). Note that, in the short term, even though S1 and S2 sites are only 48 nm apart, there is enough separation for these controls to be relatively independent in the 18–20 ms of a beat cycle.

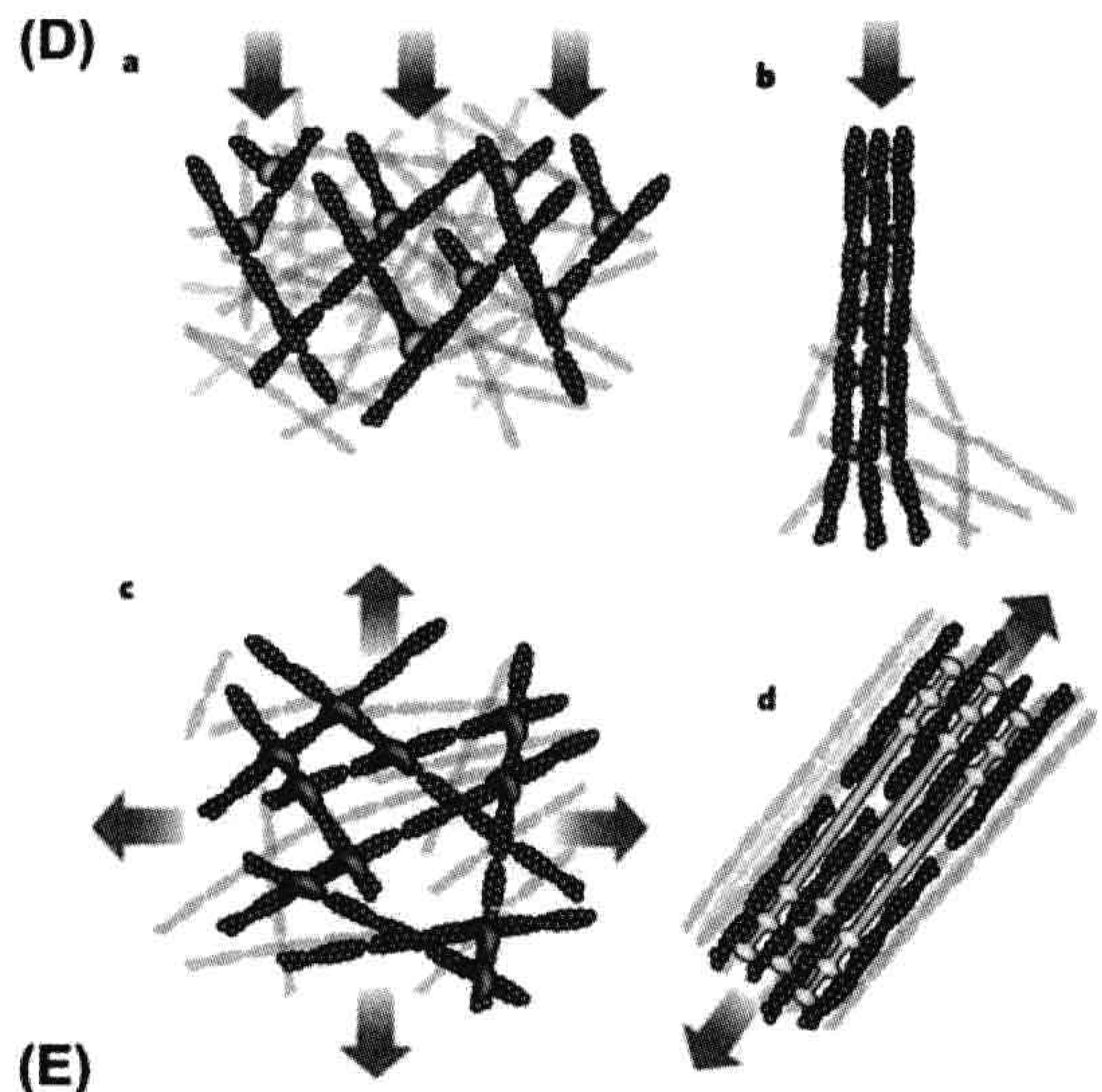
By way of an example, it is sufficient here to discuss some of the temporal characteristics of phototaxis control as measured in *Chlamydomonas* (Foster, 2009). The correlation of the ciliary responses with stimuli has been measured with a low spatial-resolution quad-photodiode ciliary monitor. Most classical analysis is done in the frequency domain because of the simplicity of its interpretation and its ability to distinguish simply between the beating cycle at 50–60 Hz and response control in the 2–6 Hz range. This approach is represented by Bode plots (see Fig. 47.6E a and b) showing the CBF and stroke-velocity responses (see Fig. 47.6E d and e). The output response was correlated with a 196-s long input light stimulus. The slopes of the gain plot and the phase changes provide directly the nature of the functional processes. For example, the slope at high frequency gives the number of processes involved in the cascade of the processing and the functional modeling is easy. The temporal response (see Fig. 47.6E c and f) is mathematically equivalent and with this representation it is easier to see how the cell would respond as it rotates, but functional modeling is less transparent. The *trans* and *cis* cilia are different. They have their own unique as well as common responses. For example, the CBF and stroke velocity (SV) SRF are quite different. On the other hand, response to changes in availability of ATP (not shown here) appear to be similar. Note, in particular, that the *trans* cilium has a much higher frequency response for CBF than the *cis*. Further, that the phase of the *trans* cilium is about π different from the *cis* and that the delay is markedly, actually reproducibly, longer than for the *trans* cilium.

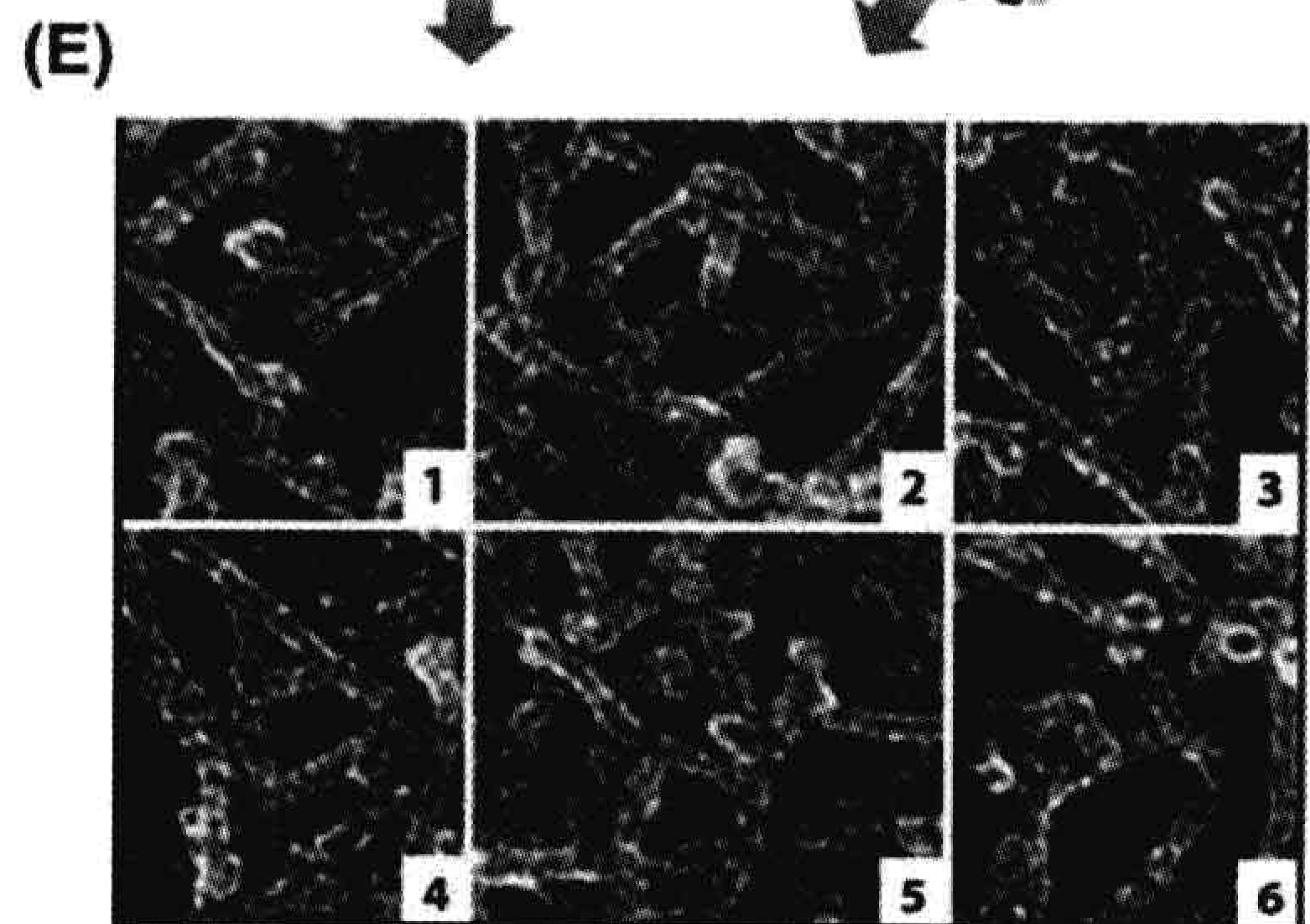
Such results provide insight into what the signal processing system does to optimize the cell's phototaxis. By averaging over 196 s, high temporal resolution is obtained in spite of the noisiness of individual ciliary responses. Note that the observed delays to response are short relative to a single beating cycle of $\approx$18 ms. Furthermore, these measured responses show significant *cis-trans* differences which contribute to how the cell steers. Note there is an initial delay of the *cis* cilium stroke velocity in Fig. 47.6E f and, further, the *cis* cilium has a slower CBF response than the *trans* in Fig. 47.6E c. The peak times for *cis* and *trans* CBF are approximately 40 and 30 ms, respectively, whereas the peak times for the stroke velocity are 80 and 50 ms. Why the system has *cis* slower than *trans* for both responses is not known. Figure 47.6E f also shows that

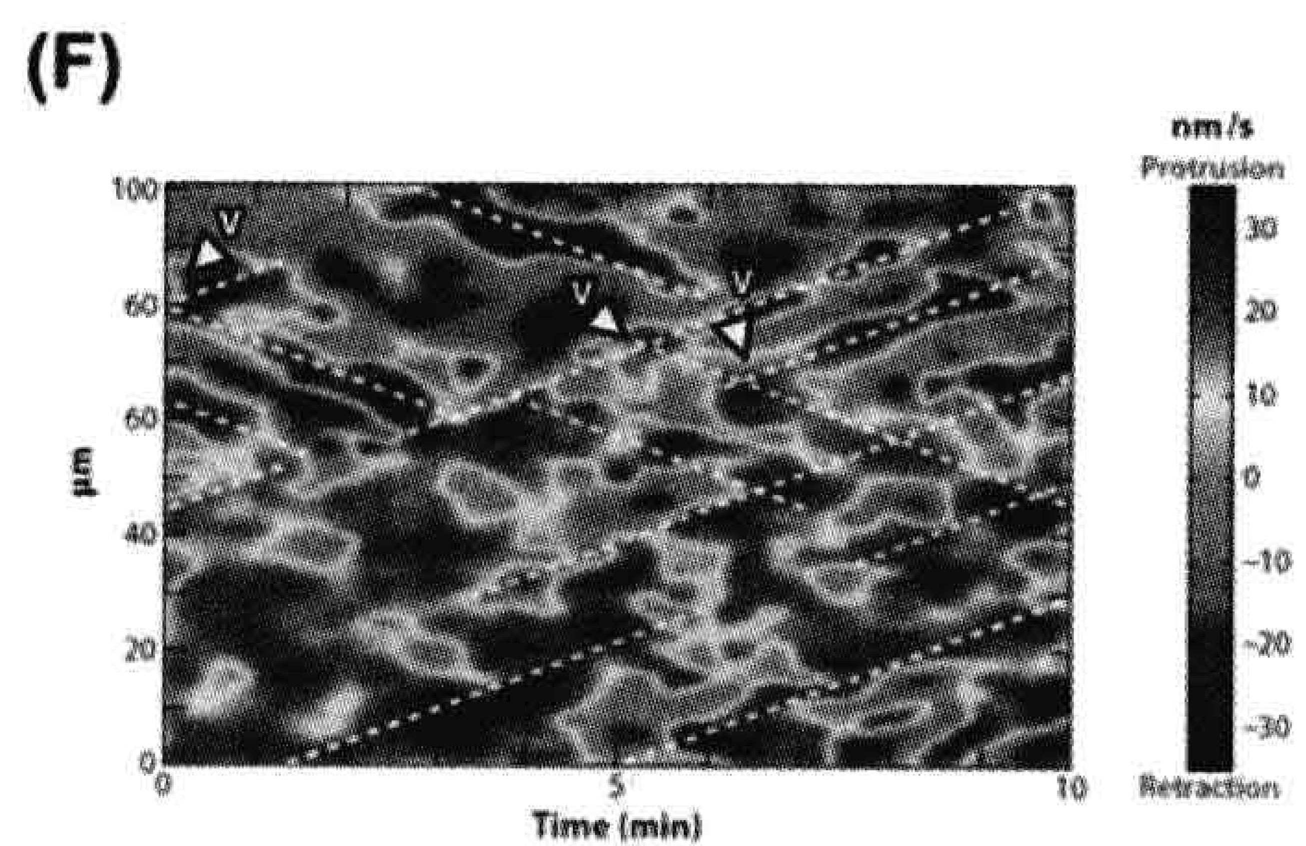

(A)
(a)
(b)
integrin
myosin motor
actin filament
ion channel
clutch protein
ECM
plasma membrane
fixed object in cell
activated state


(B)
a
b
Cell body
Growth cone
c
Axon
d
e
f
g


(C)
Load
(membrane)
Nucleation and
crosslinking
Signal
Adaptor
Constructor
Limiter
(cap)
Elongation and
capping
Construction
material
Deconstructor
Uncrosslinking
and disassembly
Recycler
Recycling of components


(D) a
b
c
d


(E)
1
2
3
4
5
6


(F)
nm/s
Protrusion
Retraction
μm
Time (min)

steering for phototaxis involves briefly altering the relative effectiveness of the stroke velocity of the *cis* relative to the *trans* cilium. The changes are as if the shape of the *trans* beat exclusively involves the outer dynein arms and the *cis* beat shape is exclusively determined by the inner arms, but with the frequency and power contributed by the outer arms. Eighty percent of the observed variance is captured by a simple linear model (Foster, 2009).

It is anticipated that in future work with the many mutants available, it will be possible to extend into molecular detail the processes involved both in ciliary beating and its behavioral controls.

IV. NON-MUSCLE ACTIN

IVA. Actin-Associated Sensing

IVA1. Mechanical Sensing

Cells appear to be sensitive to information about force, stiffness and adhesiveness. Different cell types respond uniquely to a wide range of forces and stiffness (Fig. 47.7A).

External forces applied to a cell and the resistances that extracellular matrices or surfaces exert on cell-derived forces generate signals that direct cell growth, survival, differentiation and function. Examples of the roles for external forces (Tee et al., 2009) are the promotion of axonal elongation by pN to nN forces to the tips of the neuronal growth cone, the effects of fluid flow on the morphology and signaling of vascular endothelial cells and the loss of bone or muscle mass when gravity or exercise is reduced. Further, mechanical properties of the environment modify a cell's behavior: sarcomeres only form in cultured myocytes when the surface has the approximate stiffness of a muscle and mesenchymal stem cells only differentiate into osteocytes when growing on the appropriately soft surfaces.

IVA2. Force Sensing

A cellular force sensor can passively respond to changes in forces as do the stereocilia of hair cells in the ear when transducing sound waves into neural impulses initiated by changes in membrane ion channel activity or be active as cilia that detect urine flow.

IVA3. Stiffness Sensing

To sense stiffness, a durosensor applies a stress and measures strain or vice versa and then derives the ratio of these variables. To perform this assay, the durosensor uses molecular motors to apply a force to its substrate and measures the resulting movement. From this information, the cell knows

FIGURE 47.7 (A) Cellular components involved in stiffness sensing. (a) A cell in its resting state. Molecular motors such as non-muscle myosin walk on actin filaments exerting forces through focal adhesion proteins, which are connected to transmembrane proteins such as integrins via slip or catch bonds. In this way, traction forces are transmitted to the external substrate via integrin–ligand interactions. Any protein in this pathway from molecular motor to actin to focal adhesion protein to integrin to ligand to extracellular matrix can be stretched and therefore could be activated. Further ligands such as fibronectin and laminin might also be activated. On the plasma membrane, integrins or focal adhesion proteins can also be activated by being stretched; the membrane may be deformed or sheared inducing protein clustering or recruitment. Internally, the tension on the actin filament might affect molecular motor affinity and hence transport of proteins; the nucleus might deform affecting transcription. (b) The response of a cell that applies a stress or a strain will depend on the rigidity of the substrate. In essence, the elasticity of their substrate strongly influences a cell's ability to stretch proteins, generate tension and deform membranes or nuclei (Tee et al., 2009). (B) The cytoskeleton of eukaryotic cells sets the structure and organization, resists and transmits stresses, and drives shape change and movement. (a) Neurons are specialized eukaryotic cells that extend long processes to form connections. Like other eukaryotic cells, neurons have a cytoskeleton that consists of three main polymers: microtubules (green), intermediate filaments (purple) and actin filaments (red). (b) The neuronal growth cone migrates in response to chemical cues during the development of the nervous system (fluorescence micrograph). Microtubules (green) emanate from the axon and actin-filament networks (red) form sheet-like structures and filopodial protrusions at the leading edge. Scale bar, 20 μm. (c) The neuronal axon is a long membrane-bounded extension, in which neurofilaments (a class of intermediate filaments in neurons) form a structural matrix that embeds microtubules, which transport materials from the cell body to the axon terminals at the synapse. (d) The growth cone contains dendritic actin-filament networks and parallel actin-filament filopodia. (e) Microtubules consist of 13 protofilaments of tubulin dimers arranged in a hollow tube. (f) Neurofilaments have flexible polymer arms that repel neighboring neurofilaments and determine the radius of the axon. (g) Actin filaments are arranged into networks. These networks can have various architectures, including branched structures formed by the Arp2/3 complex (blue). The diameters of microtubules, intermediate filaments and actin filaments are similar, but their relative flexibilities differ markedly, as indicated by their persistence lengths [microtubules (5000 μm), actin filaments (13.5 μm) and intermediate filaments (0.5 μm)] (Fletcher and Mullins, 2010). (C) Long-range order of the cytoskeleton network is created by simple rules for assembly and disassembly. The three basic steps in assembly of protrusive, branched actin-filament networks are filament elongation, nucleation and cross-linking of new filaments from filaments close to the membrane and capping of filaments. Disassembly uses a different set of proteins that severs the filaments and recycles the subunits (Fletcher and Mullins, 2010). (D) The cytoskeleton forms structures with a wide variety of architectures associated with different types of cellular force. Shown are four structures generated by actin filaments and the stresses typically encountered by these structures (red arrows, compression; green arrows, tension). (a) Branched actin-filament networks push against the plasma membrane and external barriers generating protrusions, facing an inward compressive force. (b) Filaments bundled into filopodia generate protrusive forces that extend from the cell body and face similar compressive forces. (c) Cortical networks form below the plasma membrane and carry tension loads in multiple directions. (d) Stress fibers form from bundled actin filaments, which are often associated with filaments of myosin, and generate tension against cell adhesions to the extracellular matrix (Fletcher and Mullins, 2010). (E) Branched network structure in keratocyte lamellipodium (Carlsson, 2010). #5 is 0. 17 μm wide. (F) Patterns of protrusion in a PtK1epithelial cell. Color (red for protrusion and blue for retraction) indicates velocity of membrane motion. The y-axis is the distance along the edge of the cell and the x-axis is time. Diagonal lines show the transverse motion of waves (Carlsson, 2010).

the elasticity. Myosin has been suggested as the active stress generator and that the stress is transmitted through actin filaments onto flexible proteins such as talin or filamin which bind transmembrane proteins like integrins.

IVB. Cytoskeleton

The three main functions of the cytoskeleton are spatially to organize the contents of the cell; connect the cell physically and biochemically to the external environment; and coordinate forces to enable the cell to move and change shape (Fletcher and Mullins, 2010). Researchers are motivated by the prospect of understanding the process of self-organization that generates dynamic, robust and elaborate structures that organize and make cells alive. There are three main types of cytoskeletal polymer: actin filaments with at least 150 associated proteins, microtubules and a group of polymers known as intermediate filaments. These polymers control the shape and mechanics of eukaryotic cells (see Fig. 47.7B). The many copies of key pieces fit together to form larger objects that assemble into structures with diverse properties depending on the assembly process, and which can be disassembled and reassembled as needed. The differences among the polymers that distinguish the architecture and function of the networks they form are their mechanical stiffness, the dynamics of their assembly, their polarity and the molecular motors with which they associate.

The stiffest of the three polymers are microtubules and have the most complex assembly and disassembly dynamics. The persistence length of microtubules ($\approx$5 mm), a measure of filament flexibility that increases with stiffness, is so large that single microtubules can form straight tracks that span the length of a typical animal cell. Microtubules have two states they switch between: stably growing and rapidly shrinking. This "dynamic instability" enables the microtubule cytoskeleton to reorganize rapidly.

Actin filaments are much less rigid than microtubules, but cross-linkers bind them to assemble organized, stiff structures, including isotropic networks, bundled networks and branched networks. Unlike microtubules, actin filaments do not switch between two discrete states; instead, they elongate steadily in the presence of nucleotide-bound monomers. This steady elongation produces the sustained forces that advance the leading edge of a migrating cell. Also unlike the microtubule cytoskeleton, which is characterized by one or two central organizing centers, the actin cytoskeleton is continually assembled and disassembled in response to signals it receives.

The subunits of both actin filaments and microtubules are structurally asymmetrical at the molecular level making them polarized polymers. Consequently, both polymers function as tracks for molecular motors that move preferentially in one direction. For microtubules, the motors are dyneins or kinesins whereas for actin filaments, they are myosin proteins.

The (de)polymerization of actin filaments and microtubules generates forces that drive changes in cell shape and guide intracellular organization with molecular motors that move along them. The structured networks are controlled by regulatory proteins: nucleation-promoting factors, which initiate filament formation; capping proteins, which terminate growth; polymerases, which promote faster or more sustained growth; depolymerizing factors and severing factors, which disassemble filaments; and cross-linkers and stabilizing proteins, which further organize the networks. External and internal mechanical forces can influence these regulatory factors and hence the network.

The least stiff of the three types of cytoskeletal polymers are the intermediate filaments that resist tensile forces much more effectively than compressive forces. They can be cross-linked to each other, as well as to actin filaments and microtubules, by proteins called plectins. Unlike microtubules and actin filaments, intermediate filaments are not polarized and cannot support directional movement of molecular motors.

One example of how long-range order of an actin-filament network can be created is the formation of branched actin networks (see Fig. 47.7C). Nucleation-promoting factors activate the Arp2/3 complex (including actin-related protein 2 (Arp2) and Arp3) to bind to actin and initiate new actin filaments (typically less than 1 μm, from the sides of pre-existing filaments, forming entangled "dendritic" networks.

In whole cells, the actin cytoskeleton has a wide variety of architectures that are associated with specific functional structures (see Fig.47.7D).

When reconstituted on the end of an atomic-force-microscope cantilever, dendritic networks grow at a constant velocity over a wide range of load forces, suggesting that the network regulates local filament density through a force-sensing element in the network. This same behavior is also observed in lamellipodial protrusions in crawling cells. The observation that growth velocity varies with the force suggests that actin-filament network growth depends on history. Given the cytoskeleton involvement mechanically and biochemically in cellular processes, long-lived cytoskeletal structures could guide variation towards certain phenotypes.

IVC. Actin Dynamics

Actin monomers (G-actin) assemble to form polarized filaments (F-actin) that have a fast-growing barbed end and a slower-growing pointed end (Carlsson, 2010). The actin subunits are arranged in a double helix with a length increment of $a = 2.7$ nm per added subunit. This

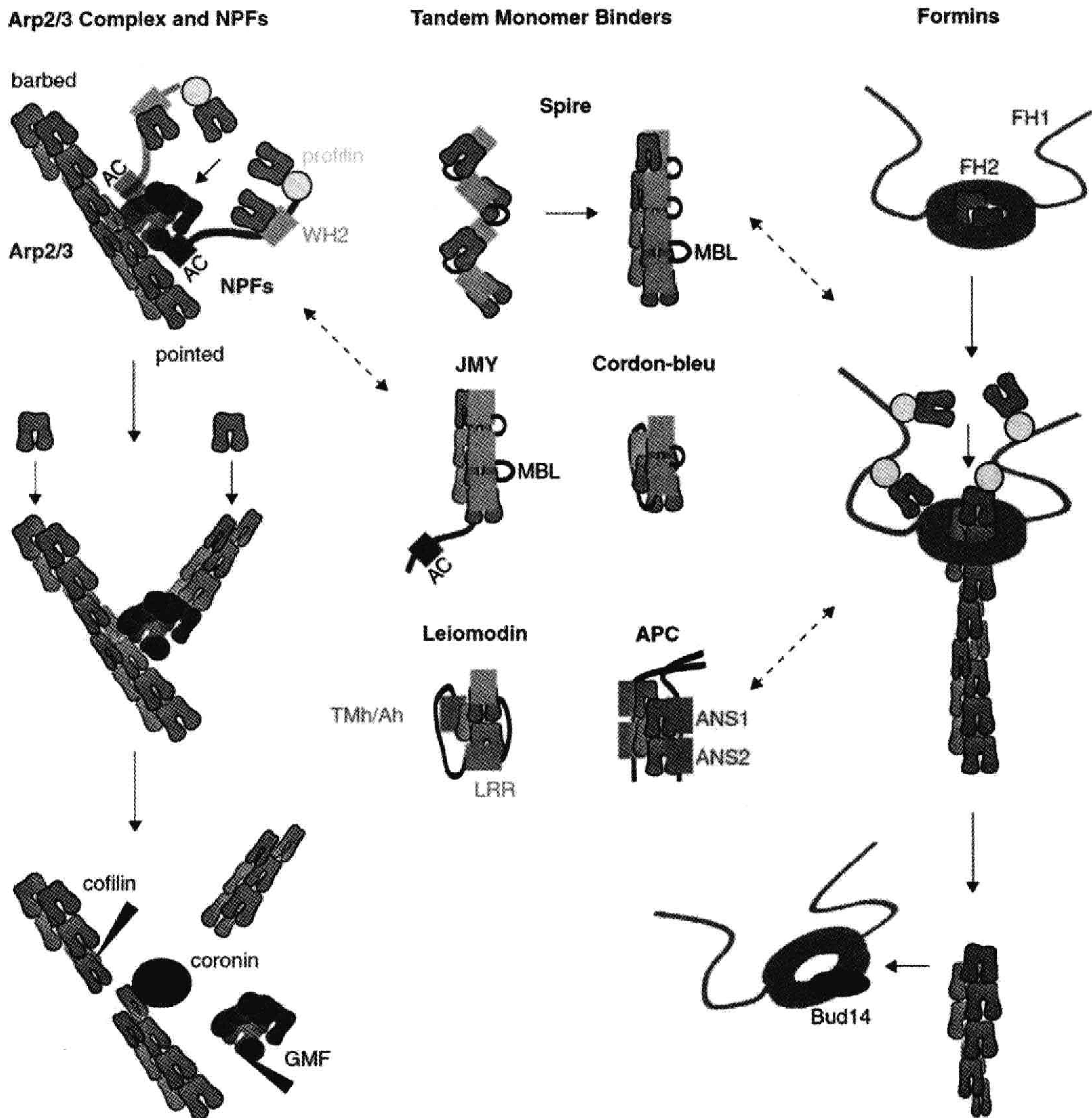
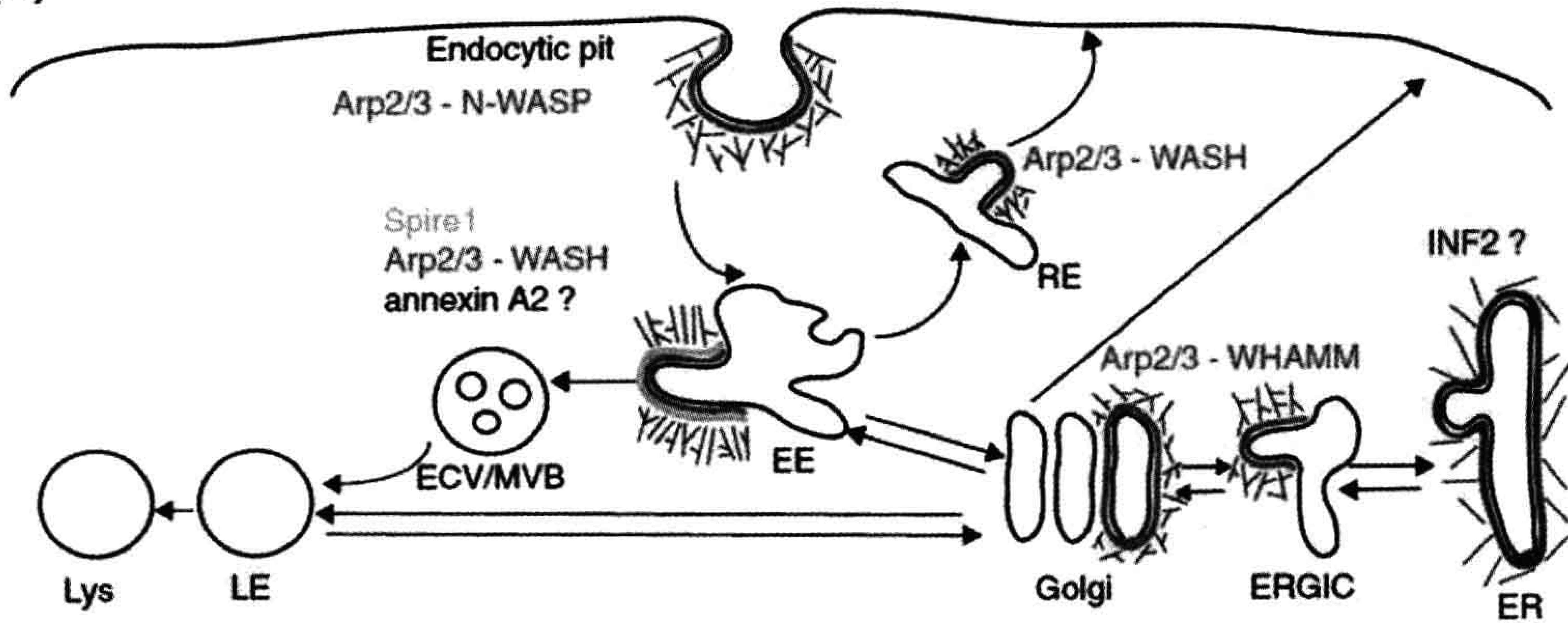
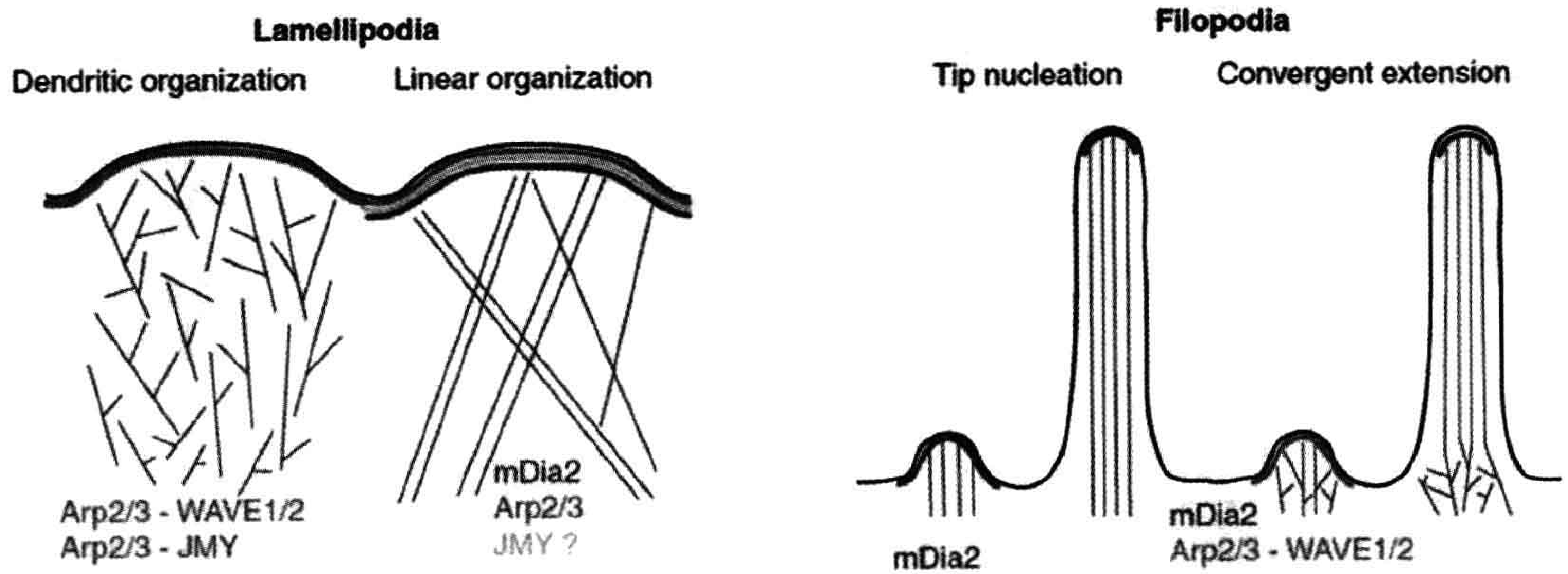
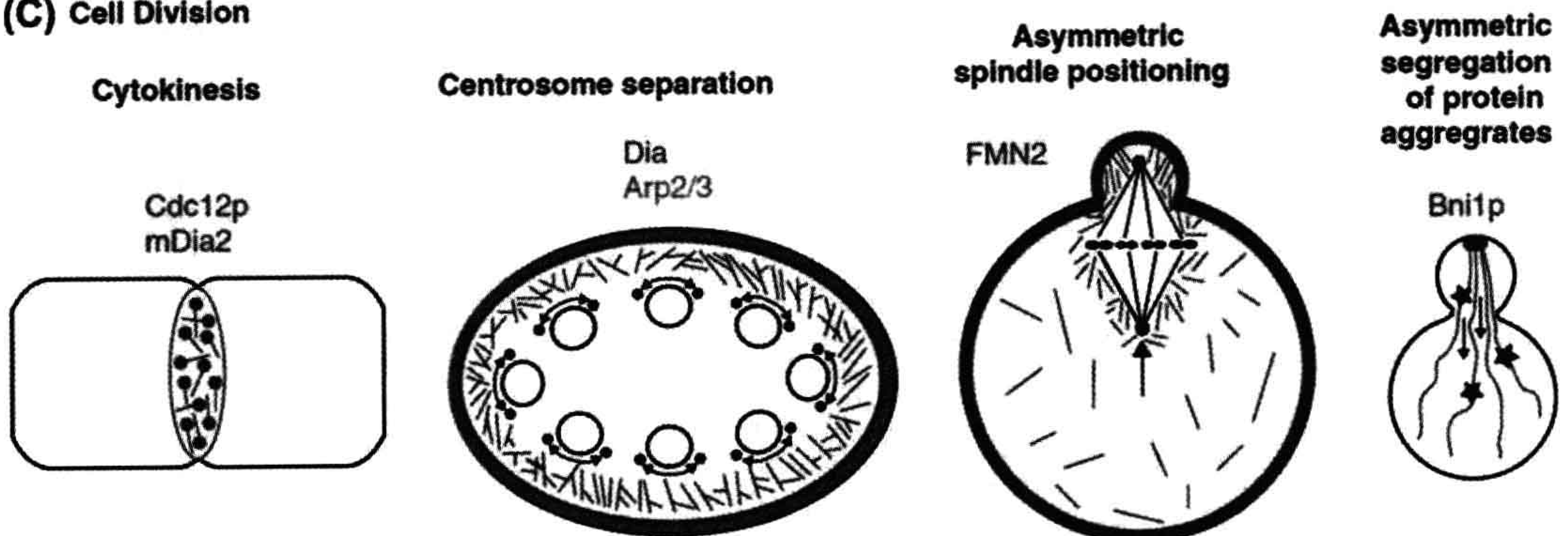


FIGURE 47.8 Models of actin nucleation. Left: Arp2/3 complex is activated by binding to the CA region of NPFs and to the side of actin filaments. In turn, NPFs bind actin monomers via their WH2 domains and profilin—actin monomers via their proline-rich regions and deliver these to a nucleating complex. NPF dimerization enhances their activity, suggesting that dimers may bind to two sites on the Arp2/3 complex. After branch formation, cofilin and GMF stimulate debranching by binding to F-actin and Arp2/3 complex, respectively. Coronin binds both to F-actin and Arp2/3 complex, replaces Arp2/3complex and synergizes with cofilin to promote debranching. Middle: Tandem-monomer-binding nucleators bring together actin monomers through their clustered actin-binding motifs to form a nucleus. Spire and JMY stabilize actin monomers aligned along the long-pitch helix with their WH2domains and monomer-binding linkers (MBL). Cordon-bleu, leiomodin and dimeric APC, with their combination of WH2 domains, leucine-rich repeats (LRR), tropomyosin and actin-binding helices (Tmh/Ah) and actin-nucleating sequences (ANS1-2), stabilize cross-filament interactions along the short pitch helix of an actin filament. Right: Formins generate actin polymerization nuclei by stabilizing actin dimers through their homodimeric FH2 domains. The FH2 dimer stays processively attached to the barbed end of an actin filament as the flanking FH1 domains deliver profilin—actin to the barbed end for continued elongation. In yeast, Bud14p interacts with the FH2 domain and displaces formins from growing barbed ends. Dotted arrows point to the cross-talk between different actin nucleators (Firat-Karalar and Welch, 2011, where additional details may be found).


(A) Membrane trafficking
Endocytic pit
Arp2/3 - N-WASP
Arp2/3 - WASH
RE
Spire1
Arp2/3 - WASH
annexin A2 ?
INF2 ?
Arp2/3 - WHAMM
EE
ECV/MVB
Lys
LE
Golgi
ERGIC
ER


(B) Leading edge protrusion during cell migration
Lamellipodia
Dendritic organization
Linear organization
Filopodia
Tip nucleation
Convergent extension
Arp2/3 - WAVE1/2
Arp2/3 - JMY
mDia2
Arp2/3
JMY ?
mDia2
mDia2
Arp2/3 - WAVE1/2


(C) Cell Division
Cytokinesis
Cdc12p
mDia2
Centrosome separation
Dia
Arp2/3
Asymmetric spindle positioning
FMN2
Asymmetric segregation of protein aggregrates
Bni1p

arrangement allows an incoming subunit to have connections to two subunits in the filament. This double connection means that binding of an incoming subunit can be strongly exothermic, even though a G-actin dimer is unstable. This renders spontaneous *nucleation of actin filaments slow* in comparison to polymerization of existing filaments. Spontaneous nucleation is further slowed by actin-binding proteins.

Because polymerization is exothermic, it can supply the energy to propel a cell through its environment. Actin in cells is dynamic and strongly out of equilibrium. Actin undergoes continuous changes in polymerization fueled by input of chemical energy (ATP) enabling the actin cytoskeleton to respond rapidly to changing external stimuli and to have spontaneous dynamic behaviors. The critical concentrations, the free-actin concentration at which polymerization precisely balances depolymerization, is AcB (barbed) $\approx 0.1\ \mu M$ and AcP (pointed ends) $\approx 0.6\ \mu M$. The difference of the critical concentrations means that the two ends are thermodynamically not equivalent. Actin binds a nucleotide, either ATP, ADP-P_i or ADP, where ADP-Pi is hydrolyzed ATP whose phosphate has not yet been released. In intracellular G-actin, ADP is rapidly exchanged to ATP. In F-actin, ATP spontaneously hydrolyzes to ADP-P_i actin and subsequently becomes ADP. ADP-actin polymerizes less strongly than ATP-actin, and this causes the difference between ABc and APc. Branched networks often occur in broad, thin protrusions extending at the front of a cell or lamellipodia, as shown in Fig. 47.7E. Barbed ends preferentially point toward the membrane. Because the rate of new branch formation is proportional to the number of existing branches, filament nucleation by branching is an autocatalytic process. Additional mechanical stability is provided by cross-linking. Polymerization occurs mainly near the membrane and depolymerization mainly away from the membrane. Their assembly is often signaled by upstream external agents such as growth factors. Disassembly occurs in the absence of active intervention. However, active intervention is a possibility.

Bundles are composed of tightly cross-linked filaments and occur in protrusions such as filopodia. Actin polymerizes near the cell edge and depolymerizes farther way. In response to a stimulus, actin polymerizes and then depolymerizes and actin waves are spatially segregated assembly/disassembly cycles (see Fig. 47.7F).

IVD. Actin Filament Nucleation

IVD1. Introduction

The first assembly step of actin filaments, a stable multimer of actin monomers, is nucleation (Firat-Karaler and Welch, 2011). While slow it is essential for function (Fig. 47.8). This is the rate-limiting step in polymerization due to the instability of actin dimer intermediates and actin monomer-sequestering proteins that suppress spontaneous nucleation in cells. To overcome the kinetic hurdle for nucleation, cells use a diverse set of actin-nucleating proteins, including the actin-related protein 2/3 (Arp2/3) complex, formins and tandem-monomer-binding nucleators.

As these proteins control nucleation they can manipulate the cell structure and its motion and hence nature has found it convenient to involve them in many essential cellular processes (Firat-Karaler and Welch, 2011). A variety of nucleation events is illustrated in Fig. 47.8.

IVD2. Cellular Functions of Actin Nucleators

Membrane Trafficking

Membrane trafficking events include endocytic internalization, endocytic transport and endoplasmic reticulum (ER)- to-Golgi transport (Fig. 47.9). Common to each of these processes is the dynamic shaping and remodeling of membranes. The responsible actin nucleators span all three classes and include the Arp2/3 complex and its NPFs, the

FIGURE 47.9 Models of the cellular localization and function of actin nucleators. (A) A depiction of the role of actin nucleators in membrane-trafficking events including endocytic internalization as well as various stages of endocytic and ER-to-Golgi trafficking. Abbreviations: EE, early endosomes; ECV/MVB, endosomal carrier vesicles/multivesicular bodies; LE, late endosomes; RE, recycling endosomes; Lys, lysosome; ER, Endoplasmic reticulum; ERGIC, endoplasmic reticulum-Golgi intermediate compartment. (B) Diagram of the role of actin nucleators in lamellipodia and filopodia. In the dendritic organization model of actin organization in lamellipodia, branched actin networks are nucleated by the Arp2/3 complex and the NPFsWAVE1/2 and JMY. In the linear organization model, filaments are nucleated by the Arp2/3 complex, but are unbranched, or are nucleated by mDia2 or perhaps JMY. In the tip nucleation model of filopodium formation, bundled arrays of actin filaments are nucleated by mDia2, whereas in the convergent elongation model, filaments are nucleated by the Arp2/3 complex and WAVE1/2, and are elongated by mDia2. (C) Cartoons depicting the role of actin nucleators in cell division. During cytokinesis, formins (Cdc12p in yeast, mDia2 in mammalian cells) nucleate actin filaments from multiple nodes at the division site that then coalesce into the contractile ring in the search, capture, pull and release model. During centrosome separation, dynamic actin reorganization by Dia and Arp2/3 drives centrosome separation in the early syncytial *Drosophila* embryo. For asymmetric spindle positioning in mouse oocytes, FMN2 nucleates a dynamic actin network that moves the spindle to the cell cortex. During the segregation of protein aggregates in *S. cerevisiae*, Bni1p generates actin cables extending from the polarisome that are required for transport of protein aggregates from the daughter to the mother cell. In (A)–(C) nucleators are color-coded as follows: Arp2/3 complex and NPFs (blue), formins (green), tandem-monomer-binding nucleators (yellow). Question marks indicate that the precise role of the nucleating protein is unclear (Firat-Karalar and Welch, 2011).

inverted formin 2 (INF2) and the tandem-monomer-binding nucleator Spire.

Modes of Cell Migration

In migrating cells, actin polymerization in lamellipodia and finger-like protrusions called filopodia provides the driving force for leading edge protrusion. Lamellipodia are proposed to be Y-branched filament networks nucleated by Arp2/3 complex while filopodia are proposed to be linear bundles nucleated by formins, however, the situation may be more complex.

Cell Division

Actin nucleation is also involved in several stages of cell division. The best-studied is the assembly of the contractile ring, essential for cytokinesis, but other proposed roles include centrosome separation and asymmetric positioning of the spindle and chromosomes in oocytes, as well as segregation of protein aggregates in yeast and involvement of cross-participation of diverse actin nucleators.

IVE. Cell Migration

Lämmerman and Sixt (2009) argue that shifting the balance between actin protrusion, actomyosin contraction and adhesion to the extracellular substrate can explain the diversity of amoeboid movement and that blebbing and gliding are just variants of one common migration strategy.

So what do they consider the principles of force generation and force transduction to be that lead to the observed distinct amoeboid phenotypes. Amoeboid migrating cells are heterogeneous and comprise different unicellular eukaryotes and several individually migrating metazoan cell types. Whatever their size, compactness and habitat, during locomotion they constantly change shape by rapidly protruding and retracting cellular extensions. However, different amoeboid cells employ different mechanical strategies like contraction-based blebbing or polymerization-driven gliding.

The different modes of amoeboid migration can be better appreciated by dissecting the components of force generation (protrusion and contraction) and force transduction (adhesiveness). Lämmerman and Sixt (2009) suggest that the relative role of these components creates the observed distinct modes of amoeboid movement (Fig. 47.10), which are driven by the forces of a polarized actomyosin cytoskeleton. Force is generated by network expansion (polymerization) and network shrinkage (contraction). While only contraction can retract the cell, both forces can protrude the plasma membrane: when expanding below the leading plasma membrane, they generate sufficient force to push out lamellipodia (flat, sheet-like) and filopodia (thin, needle-like). Actin-network contraction generates protrusions via hydrostatic pressure gradients. To contract type II myosins, actin filaments slide past one another to create tension in the actin networks. Consequently, there is a local rise in hydrostatic pressure which leads to ruptures in the cortical actin network or to local detachment of the plasma membrane from the cortical cytoskeleton. Along the pressure gradient, a flow of cytosol will protrude the plasma membrane and form a radially expanding membrane bleb. When the pressure equilibrates the bleb will cease to inflate. F-actin and actin binding proteins stabilize the bleb. Eventually myosin II may retract the bleb.

Migrating cells also need adhesion receptors to anchor them to 2D surfaces, consequently, the adhesions need to be disassembled at the trailing edge. Adhesion receptors like integrins can be locally switched off releasing the substrate at the rear of the cell. Myosin II-dependent contraction forces at the trailing edge are also needed mechanically to support de-adhesion and retraction. Imbalances between these forces do not stall protrusion, but result in blebbing or the polymerization driven phenotype.

While surface anchoring is required for 2D-substrates migration, this might not be true for cells in a 3D matrix. Tightly surrounded by fibrils or surfaces, a cell's confinement might sufficiently immobilize it such that anchoring might not be necessary (Fig. 47.10 IV–VI). Traction forces alone might be sufficient to move a cell.

IVF. Focal Adhesions (and Invadopodia and Podosomes)

Focal adhesions are the best-characterized adhesive structures (Fig. 47.11). They contain clusters of transmembrane integrin receptors tethered at one end to the extracellular matrix (ECM) and at the other to actin stress fibers, which are responsible for cell traction and ECM reorganization (Albiges-Rizo et al., 2009). Other adhesive structures are podosomes and invadopodia. Podosomes are found on the ventral side of a wide range of cells, including osteoclasts, macrophages and endothelial cells. In osteoclasts, podosomes are involved in the formation of a sealing zone that establishes an isolated compartment in which bone is degraded. Lymphocytes use podosomes to palpate the surface of, and ultimately form transcellular pores through, the vascular endothelium. Invasive cancer cells and Src-transformed cells have actin-rich membrane protrusions called invadopodia, which are primary sites of rapid actin polymerization and which represent the major sites of matrix degradation in these cells. Invadopodia of tumor cells appear as irregular dots in the vicinity of the nucleus and in proximity to the Golgi complex. Podosomes in osteoclasts and invadopodia in Src-transformed cells self-organize into a ring (the so-called rosette); in the case of osteoclasts, this can expand to a belt called the sealing zone. This self-organization is crucial for efficient matrix degradation and cell invasion.

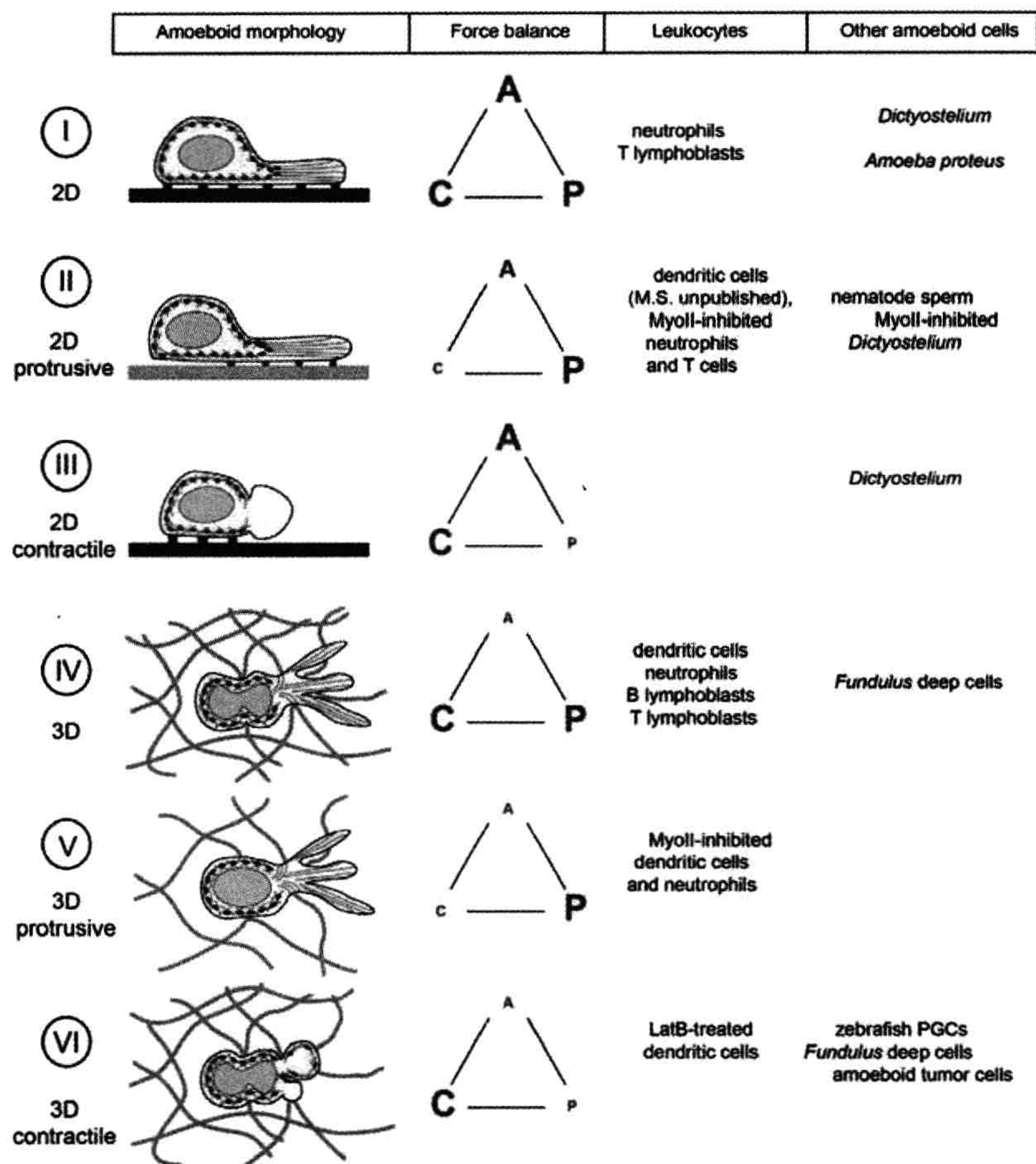


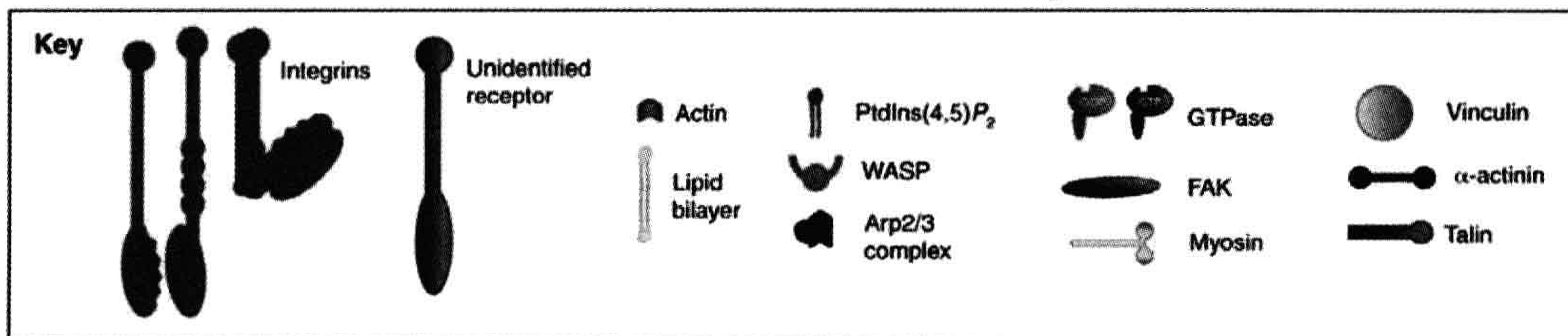
FIGURE 47.10 The force relationship between adhesion, contraction and polymer-network expansion determines the "amoeboid" phenotype. The three major forces in cell migration are adhesion (A), contraction (C) and polymer-network expansion (P). Cell forward locomotion results from their balanced interplay (indicated by the red-lettered triangles). (I—VI) "Amoeboid" crawling shows various migration modes differing in their primary driving forces, however, all are variants of the same scheme. The amoeboid morphology of a specific cell type is determined by its inherent adhesive, contractile and polymerizing equipment. Apart from that, individual cells (e.g. leukocytes) can switch between amoeboid modes after genetic or pharmacological interference with adhesion, contraction or polymer-network expansion. (I—III) Amoeboid cell movement on two-dimensional (2D) surfaces requires adhesion to transduce internal contractile forces onto the substratum. (I) A polymerizing network (green, in most cases actin) "pushes" the membrane forward. Myosin II (MyoII, red ellipses)-based contraction behind the leading edge produces traction underneath the adhesion points (blue). On high adhesive surfaces (black thick line), actomyosin contraction at the back is required to detach the cell from the substrate. Rear end contraction is not necessary when cells migrate on low adhesive substrates (gray thick line) (II). When the contractile function of myosin II is defective (black ellipses), actin polymerization alone can produce traction under adhesion points as has been shown in *Dictyostelium*. Migration without contraction suggests cell retraction can occur either by membrane tension or by polymer-network disassembly. (III) Myosin II-based contraction alone can generate internal hydrostatic pressure to bulge out the plasma membrane. The forming bleb is first cytoplasm-filled and devoid of actin, but fills with actin and myosin II during retraction. Even though blebs are observed during 2D migration, whether they can transduce traction on the surface is still unclear. (IV— VI) Three-dimensional (3D) and confined environments enable migrating cells to exert orthogonal forces between surfaces, which is not possible on 2D substrates. As 3D migration does not require adhesion-mediated traction, orthogonal forces might act as fixation points. (IV) Amoeboid movement in interstitial fibrillar networks (gray) requires contraction only when cells have to squeeze the nucleus (light blue) through narrow pores. (V) In less dense networks, this deforming contraction is not necessary. Here, amoeboid migration is solely driven by polymer-network expansion. Front-to-back gradients of internal stiffness (gel—sol gradients) might facilitate this movement. (VI) Contraction-based increase in internal hydrostatic pressure and directed bleb formation can protrude the leading edge as seen in the migration of zebrafish primordial germ cells (PGCs). How short-lived blebs (first actin-devoid, then actin-filled and myosin II-filled during retraction) generate traction on the environment is unclear. LatB: latrunculin B (actin-depolymerizing agent) (Lämmermann and Sixt, 2009 and references therein).

(A)

(B)

(C)

(D)


Key
Integrins
Unidentified receptor
Actin
Lipid bilayer
PtdIns(4,5)P_2
WASP
Arp2/3 complex
GTPase
FAK
Myosin
Vinculin
α-actinin
Talin

Invadopodia, podosomes and focal adhesions are all cell-matrix adhesion sites that connect the actin cytoskeleton within the cytosol to the extracellular matrix, but they differ in their architecture and dynamics despite sharing most of the same proteins (such as integrin, talin and paxillin).

IVG. The Model System of Melanophore Transport

The transport of pigment is dependent on an intact cytoskeleton and motor proteins associated with cytoskeletal components (Aspengren et al., 2007). The easily cultured melanophores have proven to be excellent models for organelle transport because the intracellular movements of pigment can be easily visualized and the granules move in response to chemical signals. The ease of morphological and functional transport studies is the advantage of the melanophore system. These studies have the responsible molecular motors, their adapters and transfer of vesicles to other cells. Cellular components are transported by actin and microtubule systems and hence are good models to study such transport in general. Tracking individual melanosomes optically has determined the speed and duration of melanosome movements as a result of different individual motor proteins.

Intracellular transport of melanosomes in fish and amphibian melanophores depends largely on microtubules (MT). Melanosome movements toward the MT plus end result in dispersion, whereas transport toward the minus end results in aggregation of pigment to a central pigment mass that dynein could be involved in aggregation of melanosomes, kinesin-II is the motor responsible for dispersion of melanosomes in *Xenopus* melanophores.

As demonstrated in fish melanophores, actin also plays a role for short-range pigment distribution and in frog melanophores for long-range pigment dispersion.

High levels of the second messenger cAMP are thought to induce dispersion, whereas low levels of cAMP induce aggregation of pigment in melanophores. The subsequent steps in the signaling cascade have been shown to involve protein kinases and phosphatases.

V. BIOLOGICAL SPRINGS

An extended spring may contract when it is triggered or a compressed spring may extend when triggered.

VA. Contractile Springs

The centrin-based family of springs typically contract, sometimes slowly, but sometimes dramatically. Spasmin belongs to this family and is used in the contractile spring spasmoneme.

Centrin molecular springs can be like those used to set and vary the angle between the pair of *Chlamydomonas* cilia (Foster, 2009). The distal fibers connecting the two cilia and the nuclear-basal body connectors respond in a continuous analog fashion to the internal calcium concentration. These fibers contain centrin (also called caltractin). They set the base impedance for the attachment of a cell's cilia to the cell body. Their contraction is much faster than their extension. While the exact purposes of the settings are not understood, this response does facilitate the angle changes needed for flagellar versus ciliary beating. On the other hand, spasmonemes (Marshall, 2008b) are an example of a molecular spring which is designed to release a large amount of stored energy almost all at once and then slowly recover. In this case, calcium triggers further release of calcium in positive feedback so that a dramatic action occurs.

In both cases, energy is required to switch the calcium concentration back and forth between the different levels. Multiple cycles of contraction and extension require multiple switches of calcium concentration. Contraction of isolated spasmonemes is driven by increasing the calcium concentration from 10^{-8} M to 10^{-6} M.

The spasmoneme is triggered when a *Vorticella* cell feels threatened; contracting its tail at a rate of 60–100 mm/s with a tensile force up to 500 nN (Fig. 47.12A,B,C) (Upadhyaya et al., 2008). The speed works out to about 200 lengths per second (L/s). This speed is faster than the fastest muscles, which contract at around 20 L/s. Since the spasmoneme winds helically inside the stalk, the contraction collapses the straight stalk into a helix. The reverse process (recovery) is powered by

FIGURE 47.11 Schematic view of signaling pathways that lead to organization of actin at focal adhesions. (A) In the initial stage of adhesion formation, integrins or other unidentified receptors bind to components of the ECM (gray), leading to clustering of receptors into PtdIns(4,5)P2-enriched areas of plasma membrane. (B) In early spreading adhesions at the cell periphery, the Arp2/3 complex and WASP are targeted to adhesions by FAK. Blue arrows represent the spatiotemporal sequence of structure assembly. Pink arrows indicate protein recruitment. (C) Autophosphorylation of FAK at Tyr397 destabilizes the Arp2/3-WASP-FAK complex. Talin is recruited to adhesions so that integrin-ECM linkages couple to actomyosin; this enables contraction of actomyosin to influence adhesion reinforcement and subsequent maturation. Actin filaments can be cross-linked by α-actinin. Myosin II incorporates into the α-actinin-cross-linked actin-filament bundles. (D) The actin-stress-fiber-mediated connection of focal adhesions describes their collective dynamics. These connections are seen at the front of the cell and with sliding trailing adhesions at the rear of the cell (Albiges-Rizo et al., 2009).

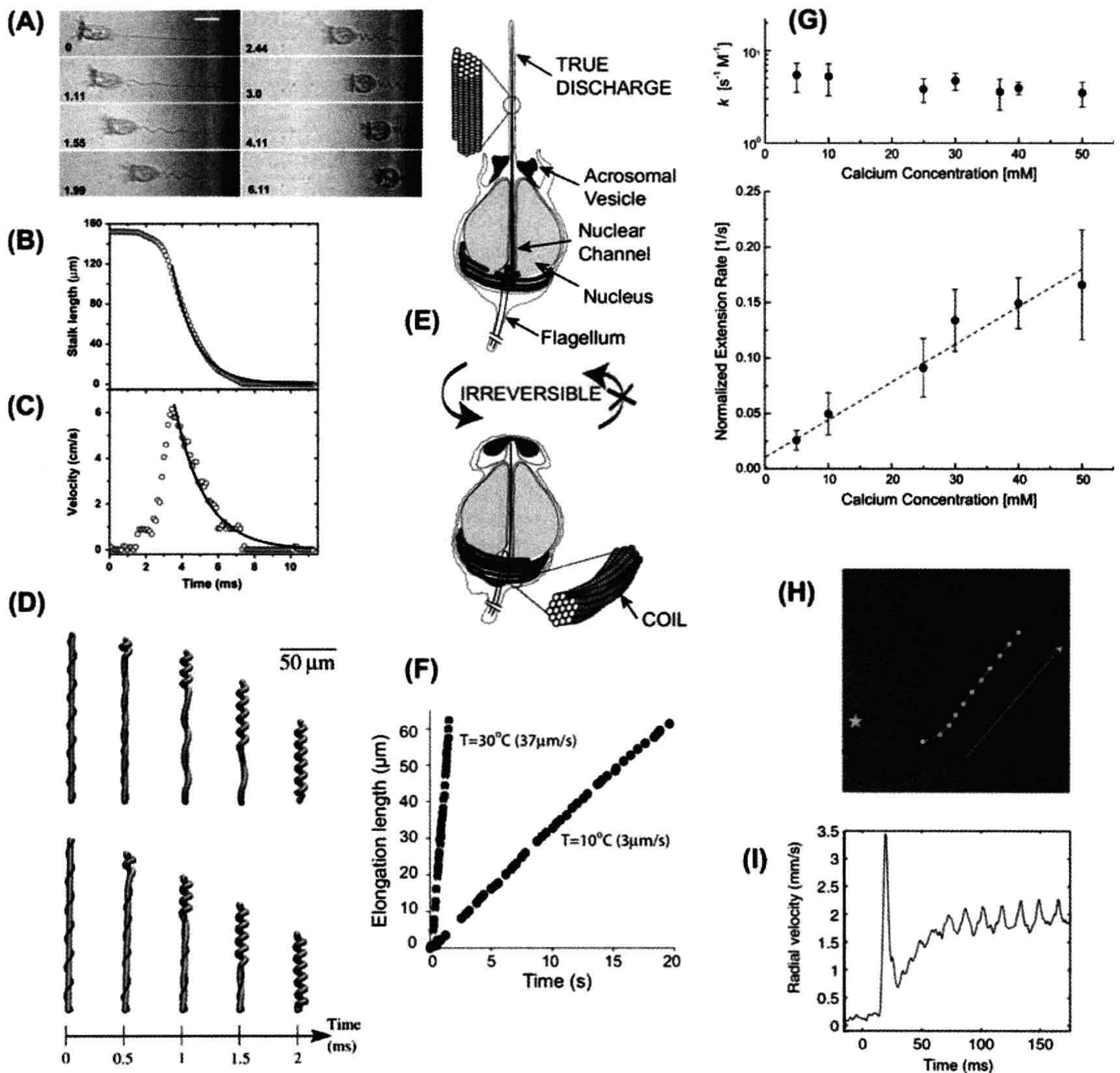


FIGURE 47.12 (A) Dynamics of *Vorticella* contraction. Time series of contraction (time shown in ms). The scale bar is 35 mm (Upadhyaya et al., 2008). (B) *Vorticella* stalk length as a function of time during a contraction. The solid curve is an exponential fit (Upadhyaya et al., 2008). (C) Instantaneous velocity of the cell body as a function of time. The solid curve is an exponential fit to the decaying part of the velocity (Upadhyaya et al., 2008). (D) Time-lapse images of the initial phase of *Vorticella* contraction driven by a propagating calcium signal (for clarity, the head is not shown). (Top) Young's modulus Y = 1 kPa. (Bottom) Y = 4 kPa (Misra et al., 2010). (E) Expansion of actin spring. The geometry and dynamics of the acrosomal reaction. Geometry shows that, in the presence of Ca^{2+}, the bundle switches irreversibly from coil (bottom) to true discharge (top) (Mahadevan et al., 2011). (F) Extrusion occurs at constant speed. The two traces correspond to extrusion at 10°C (3 mm/s) and 30°C (37 mm/s) (Mahadevan et al., 2011). (G) Top: Rate constant *k* calculated using a non-cooperative, constant rate CaM-Ca^{2+} binding mechanism. The slight dependence on [Ca^{2+}] suggests a deviation from the mechanism due to an overestimation of [CaM] participating in the reaction. Bottom: Normalized volume extension rates. Values were calculated from least-squares fitting of volumetric extension profiles as functions of time. The linear behavior (dashed line) suggests a rate mechanism involving calmodulin with one calcium binding site (Tam et al., 2009). (H) Images showing *Paramecium* at different times following a laser pulse in the close neighborhood (Hamel et al., 2011). (I) Radial velocity of the center of mass away from the laser position for the experiments shown above. Time t = 0 corresponds to the moment the laser is switched on (Hamel et al., 2011).

dissociation of Ca^{2+} ions from spasmin and active sequestration back into the calcium storage sites.

Of interest are what molecular mechanisms drive the contraction and how is the contraction coordinated along the length of the entire structure. Using high speed video microscopy, the rate of contraction has been measured as a function of the viscosity of the surrounding media (see Fig. 47.12D) (Misra et al., 2010). From the scaling relation between maximum speed and viscosity, one can conclude that the speed is limited by the power dissipated by dragging the top of the *Vorticella* through the surrounding viscous media. Given that the contraction only takes a few milliseconds, one wonders how the contraction-triggering signal can be transmitted over the whole length of the spasmoneme. The motion of beads stuck onto the *Vorticella* stalk have been tracked to show that contraction initiates near the body of the *Vorticella* and propagates like a wave down the stalk (see Fig. 47.12D). This suggests that the trigger comes from the body and travels down the stalk. Given that contraction is driven by calcium binding, the obvious suggestion would be a calcium wave mediated by calcium-triggered calcium release from the endoplasmic reticulum. In-vivo experiments show that a Ca^{2+} concentration as small as 10^{-7} M is sufficient to trigger the release of stored calcium. However, there is disagreement as to whether such a wave can be as fast as the observed 100 mm/s rate. Perhaps there is an electrical signal or a propagating wave of protein conformational change within the spasmoneme. Its main protein constituent spasmin (40–60% of the spasmoneme dry mass) is closely related to the centrin family of calcium-binding protein found associated with centrioles and basal bodies in many eukaryotes including humans. Centrin assembles into fibers that can contract when calcium is added and, in some organisms, the contraction of centrin fibers is used to steer cell motility by changing the angle at which cilia emerge from the cell surface (Foster, 2009). Presumably the spasmoneme evolved from such structures under selective pressure to contract at high speeds. This suggests that detailed molecular comparisons of centrin and spasmin, together with the behaviors of their corresponding fibers, may shed light on the adaptations that allow spasmin to contract so fast.

VB. Expanding Springs

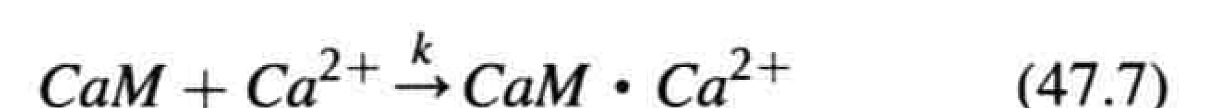
The acrosomal bundle (cross-linked actin fibers) of the horseshoe crab (*Limulus*) sperm cell is a molecular spring (see Fig. 47.12E) (Tam et al., 2009). The actin bundle is stored at the base of the sperm cell as a twisted coil. Calcium binding to the actin cross-linking protein, scruin, changes its conformation. With further calcium binding along the bundle along its length, the acrosome extends from the sperm cell in order to penetrate and fertilize the horseshoe crab egg. Provided external calcium is continuously available, the 60-μm long bundle extends in 15 s, fast relative to either polymerization or motor protein drive movements. This device illustrates how conformation energy in the form of a twisted bundle can be rapidly released by calcium binding to generate significant cellular movements.

During the acrosome reaction, a 60-μm long coiled and twisted bundle of actin filaments straightens and extends from a sperm cell, penetrating the vitelline layer surrounding the egg. A subtle over twist of 0.2/subunit underlies the mechanochemical basis for the extension of this actin spring. Upon calcium activation, this conformational strain energy is converted to mechanical work, generating the force required to extend the bundle through the vitelline layer. The calcium sequentially binds to calmodulin molecules decorating the actin filaments leading to a collective wave of untwisting of the actin filaments. About a million subunits of actin–scruin–calmodulin achieve a constant expansion of 10 μm/s (3 μm/s at 10°C, 37 μm/s at 30°C (see Fig. 47.12F) with a maximum of force of 1.9 nN and a puncturing pressure of 1.6 MPa (about 15 atmospheres). This force of extension is three times larger than that needed to puncture the vitelline layer.

Mahadevan and collaborators (2011) propose the following model for this mechanochemical engine: (1) Ca^{2+} binds to scruin; (2) the scruin–actin interactions subtly change; (3) a small region of the coil begins to untwist mediated by the scruin which decorates neighboring actin filaments; (4) driven by the potential energy difference between the coil and true states of the bundle, this untwisting deforms the bundle of actin without completely un-cross-linking it in the binding region; and (5) later Ca^{2+} binds to calmodulin releasing the twisted state, leading to the propagation of a front of untwisting that travels along the bundle converting the twisted state irreversibly to the extended state.

This helical arrangement of the bundle is tightly coupled to the conformation of individual actin filaments, each of which has a small overtwist of 0.23°/actin subunit (5 nm in size) relative to the natural chiral structure of an actin filament in the TD. The untwisting produces the extension.

The volumetric rate of expansion is constant at a given concentration of calcium and the volumetric extension rate is proportional to the continuously available calcium concentration (see Fig. 47.12G). These observations (Tam et al., 2009) make sense if the binding of Ca^{2+} to the scruin–CaM complex is according to simple reaction mechanism:



$$CaM + Ca^{2+} \xrightarrow{k} CaM \cdot Ca^{2+} \qquad (47.7)$$

where k is an effective rate constant with units of $[M^{-1}\,s^{-1}]$, which governs the binding of Ca^{2+} to the scruin–CaM complex associated with the twisted filaments.

How strain energy is built in, does not at present appear to be understood.

VI. CANNONS

Another means to achieve motion is to use accentuated turgor pressure Δp and the energy stored in stretched spore cases (Vogel, 2005). At the desired precise time and place (usually at the tip), a weakness is created that fires the spores and fluid out within the case at incredible velocities. The purpose of these "cannons" is to distribute seeds or, for example, spores from coprophilous fungi, like the zygomycete *Pilobolus* (range about 0.8 m, launch velocity 20 m/s), away from the dung they are living on out onto forage plants where they may more probably be eaten.

The energy in a spore case or ascus of the Ascomycetes that can be stored is proportional to the pressure squared and the radius cubed. Given that the biomaterial is basically the same in these organisms, the limit of wall tension is likely to be similar limiting the range of design. The wall tension is due to the pressure difference Δp (inside minus outside) times the radius, so this product is fairly constant among organisms to prevent premature blowout. This means that large asci will have a lower pressure. Hence, a large ascus might have a turgor pressure of 3 atmospheres while a small one up to 15 atmospheres. The energy stored in the stretching of the chamber, which starts out crinkled up, presumably is what leads to its rapid contraction maintaining the pressure during the emptying of the chamber resulting in a complete release of the contents.

The simple consideration that the work, ΔpV, where V is volume available due turgor pressure, should be equal to the consequent kinetic energy of the projectile, $\rho V \frac{v^2}{2}$ where p is the particle density and v is the launch velocity leads to:

$$\text{the launch velocity. } v = \sqrt{\frac{2\Delta p}{\rho}} \tag{47.8}$$

However, the energy storage capability in the larger chamber more than makes up for the lower pressure. The osmolytes include sugars but probably primarily come from ions pumped into the chamber.

Mechanisms for triggering the breaking of the tip, firing the cannon, do not seem to be described.

There is a helical orientation of wall fibers as is typical for pressurized systems in nature. Also note that the hoop stress is double the longitudinal stress. A further sort of amazing aspect is the incredibly large accelerations seen. This is of course possible due to the small mass of the projectiles, a = F/m (acceleration = force/mass). For example, *Gibberella zeae* exhibits an acceleration of 8.5×10^6 m/s^2 and *Pilobolus* with its relative large 200 μm diameter projectile only has an acceleration of 5×10^5 m/s^2.

Finally, these systems are interesting from the hydrodynamic point of view as they have a big aerodynamic drag problem. The *Pilobolus* sporangium loses 98% of its potential range due to drag (if it could fire into a vacuum it would be really amazing and maybe have a 40 m range). Perhaps not surprisingly spore shapes seem to be optimized to minimize their drag (Roper et al., 2008).

In the above, the cannons fire projectiles, however, for every action there is a reaction and sometimes the reaction is quite important, likely getting oneself out of the way of a predator. *Paramecium* fires trichocysts from its body enabling a transient speed of 10 mm/s, approximately ten times the speed it achieves with its synchronized waves of ciliary beating (see Fig. 47.12H,I) (Hamel et al., 2011).

VII. A FEW LESSONS LEARNED

1. In all instances described, apart from release of turgor pressure, motion is a result of conformation change. Whether it is flagellar motors or dynein, kinesin or myosin or centrin contraction, always it has been found that the key is protein conformation change. This is unlike the mechanical devices that humans have designed where the shape of stators and rotors do not change. The components simply move relative to each other under electromagnetic forces. There are of course biomimetic motors that do depend on repeated conformation change as, for example, ultrasonic motors. An advantage of ultrasonic motors and all the biological motors described here is that they do not have to be energized to hold their place, which is an enormous economy for portable devices.
2. All these motors are actually very efficient and significantly owe their efficiency to the very small steps each motor takes as discussed at the beginning of this chapter.
3. Note continuity of torque or force on each side of stall in each case implying the reversibility of actions, "there is no irreversible step in the mechanochemical cycle" (Sowa and Berry, 2008).

Final comment: with the enlargement of the Web, a search engine will place before you animations and real movies of much of what is described here. Sites have mostly not been given here because they are often transient, but finding them is not hard. Be aware that non-scientific sites exist about flagella and cilia that peddle nonsense.

BIBLIOGRAPHY

Albiges-Rizo, C., Destaing, O., Fourcade, B., Planus, E., & Block, M. R. (2009). Actin machinery and mechanosensitivity in invadopodia, podosomes and focal adhesions. *J Cell Sci, 122*, 3037–3049.

Aspengren, S., Hedberg, D., & Wallin, M. (2007). Melanophores: a model system for neuronal transport and exocytosis? *J Neurosci Res, 85*, 2591–2600.

Berg, H. C. (2003). The rotary motor of bacterial flagella. *Annu Rev Biochem, 7*, 19–54.

Berg, H. C., & Brown, D. A. (1972). Chemotaxis in *Escherichia coli* analyzed by three-dimensional tracking. *Nature, 239*, 500–504.

Brokaw, C. J. (1991). Microtubule sliding in swimming sperm flagella: direct and indirect measurements on sea urchin and tunicate spermatozoa. *J Cell Biol, 114*, 1201–1215, and. http://www.cco.caltech.edu/~brokawc/Demo1/BeadExpt.html.

Brokaw, C. J. (2009). Thinking about flagellar oscillation. *Cell Motil Cytoskeleton, 66*, 425–436.

Carlsson, A. E. (2010). Actin dynamics: from nanoscale to microscale. *Annu Rev Biophys, 39*, 91–110.

Dzeja, P. P., & Terzic, A. (2009). Adenylate kinase and AMP signaling networks: metabolic monitoring, signal communication and body energy sensing. *Int J Mol Sci, 10*, 1729–1772.

Emonet, T., & Cluzel, P. (2008). Relationship between cellular response and behavioral variability in bacterial chemotaxis. *Proc Natl Acad Sci USA, 105*, 3304–3309.

Firat-Karalar, E. N., & Welch, M. D. (2011). New mechanisms and functions of actin nucleation. *Curr Opin Cell Biol, 23*, 4–13.

Fletcher, D. A., & Mullins, R. D. (2010). Cell mechanics and the cytoskeleton. *Nature, 463*, 485–492.

Foster, K. W. (2009). Analysis of the ciliary/flagellar beating of *Chlamydomonas*. In S. M. King, & G. J. Pazour (Eds.), *Cilia: Structure and Motility. Methods in Cell Biology, vol. 91* (pp. 173–239). San Diego: Academic Press.

Hamadeh, A., Roberts, M. A. J., August, E., et al. (2011). Feedback control architecture and the bacterial chemotaxis network. *PloSComputBiol, 7*, e1001130, doi:10.1371/journal.pcbi.1001130.

Hamel, A., Fisch, C., Combettes, L., Dupuis-Williams, P., & Baroud, C. N. (2011). Transitions between three swimming gaits in *Paramecium* escape. *Proc Natl Acad Sci USA, 108*, 7290–7295.

Hazelbauer, G. L., Falke, J. J., & Parkinson, J. S. (2007). Bacterial chemoreceptors: high-performance signaling in networked arrays. *Trends Biochem Sci, 33*, 9–19.

Heuser, T., Raytchev, M., Krell, J., Porter, M. E., & Nicastro, D. (2009). The dynein regulatory complex is the nexin link and a major regulatory node in cilia and flagella. *J Cell Biol, 187*, 921–933.

Kaneshiro, E. S. (2001). Centrin-based contraction and bacterial flagella. In N. Sperelakis (Ed.), *Cell Physiology Source Book* (3rd ed.). (pp. 985–1002) San Diego: Academic Press.

Kaneshiro, E. S., Sanderson, M. J., & Witman, G. B. (2001). Amoeboid movement, cilia, and flagella in cell physiology. In N. Sperelakis (Ed.), *Cell Physiology Source Book* (3rd ed.). (pp. 959–984) San Diego: Academic Press.

Lämmermann, T., & Sixt, M. (2009). Mechanical modes of 'amoeboid' cell migration. *Curr Opin Cell Biol, 21*, 636–644.

Lindemann, C. B., Macauley, L. J., & Lesich, K. A. (2005). The counterbend phenomenon in dynein-disabled rat sperm flagella and what it reveals about the interdoublet elasticity. *Biophys J, 89*, 1165–1174.

Mahadevan, L., Riera, C. S., & Shin, J. H. (2011). Structural dynamics of an actin spring. *Biophys J, 100*, 839–844.

Marshall, W. F. (2008a). .The cell biological basis of ciliary disease. *J Cell Biol, 180*, 17–21.

Marshall, W. F. (2008b). Don't blink: observing the ultra-fast contraction of spasmonemes. *Biophys J, 94*, 4–5.

Misra, G., Dickinson, R. B., & Ladd, A. J. C. (2010). Mechanics of *Vorticella* contraction. *Biophys J, 98*, 2923–2932.

Mitchell, B. F., Pedersen, L. B., Feely, M., Rosenbaum, J. L., & Mitchell, D. R. (2005). ATP production in *Chlamydomonas reinhardtii* flagella by glycolytic enzymes. *Mol Biol Cell, 16*, 4509–4518.

Nelson, P. (2008). *Biological Physics: Energy, Information, Life*. New York: W.H. Freeman.

Oleksiuk, O., Jakovljevic, V., Vladimirov, N., et al. (2011). Thermal robustness of signaling in bacterial chemotaxis. *Cell, 145*, 312–321.

Riedel-Kruse, I. H., Hilfinger, A., Howard, J., & Julicher, F. (2007). How molecular motors shape the flagellar beat. *HFSP J, 1*, 192–208.

Roper, M., Squires, T. M., & Brenner, M. P. (2008). Symmetry unbreaking in the shapes of perfect projectiles. *Phys Fluids, 20*, 093606.

Segall, J. E., Block, S. M., & Berg, H. C. (1986). Temporal comparisons in bacterial chemotaxis. *Proc Natl Acad Sci USA, 83*, 8987–8991.

Sowa, Y., & Berry, R. M. (2008). Bacterial flagellarmotor. *Quart Rev Biophys, 41*, 103–132.

Tam, B. K., Shin, J. H., Pfeiffer, E., Matsudaira, P., & Mahadevan, L. (2009). Calcium regulation of an actin spring. *Biophys J, 97*, 1125–1129.

Tee, S.-Y., Bausch, A., & Janmey, P. A. (2009). The mechanical cell. *Curr Biol, 19*, R745–R748.

Turner, L., Ryu, W. S., & Berg, H. C. (2000). Real-time imaging of fluorescent flagellar filaments. *Journal of Bacteriology, 182*, 2793–2801.

Upadhyaya, A., Baraban, M., Wong, J., Matsudaira, P., van Oudenaarden, A., & Mahadevan, L. (2008). Power-limited contraction dynamics of *Vorticella convallaria*: an ultrafast biological spring. *Biophys J, 94*, 265–272.

Vogel, S. (2005). Living in a physical world II. The bio-ballistics of small projectiles. *J Biosci, 30*, 167–175.

Wirschell, M., Pazour, G., Yoda, A., Hirono, M., Kamiya, R., & Witman, G. B. (2004). Oda5p, a novel axonemal protein required for assembly of the outer dynein arm and an associated adenylate kinase. *Mol Biol Cell, 15*, 2729–2741.

Woolley, D. M. (2010). Flagellar oscillation: a commentary on proposed mechanisms. *Biol Rev Camb Philos Soc, 85*, 453–470.

Chapter 48

Electrocytes of Electric Fish

Anthony L. Gotter, Marcia A. Kaetzel and John R. Dedman

Chapter Outline

I. SUMMARY

Both the freshwater electric eel and the saltwater electric ray produce extraordinarily powerful electrical discharges with membrane ion channels, receptors and pumps common to other excitable cells. These fish have separately evolved a specialized anatomy and cellular morphology designed for this function. Because of their specialized membrane asymmetry, action potentials and end-plate potentials generated on the innervated membrane are not reproduced on the non-innervated membrane, thereby setting up an asymmetrical flow of current across the cell. The arrangement allows transcellular potentials to be generated, which is essentially the basis for the generation of bioelectricity within the electric organs of these fish. Connective tissue septa that delineate columns of electrocytes prevent transcellular potentials from being short-circuited around the outside of individual electrocytes and also channel the resulting current along the electric organ.

The membrane potentials used by electrocytes to produce transcellular potentials are remarkably similar to those of other excitable cells, such as myocytes and neurons. The electrophysiology, therefore, can be explained by currents conducted through ligand-gated receptors and channels having known characteristics. Currents that give rise to electrocyte membrane potentials can even be represented by equivalent circuits similar to those of other excitable cells. However, two major differences exist between electrocytes and other excitable cells: (1) electrocytes express exaggerated amounts of key excitable membrane proteins, such as the Na^+ channel of *Electrophorus* and the acetylcholine receptor (AChR) of *Torpedo*. These proteins that exist in high density tend to produce greater currents and peak potentials than what is customarily seen on other excitable cells. (2) Membrane proteins are polarized to particular sides of the cell to facilitate the production of transcellular potentials. In the past, however, researchers have taken advantage of these differences to utilize these fish as useful model systems.

Electrophorus electrocytes provide a general model system for excitable cells, such as neurons and myocytes, since they contain common membrane receptors, channels and ATPases. They are also large and easy to dissect in order to perform potential recording, voltage-clamp analysis and patch-clamp measurements. Since it expresses large quantities of proteins, such as the Na^+ channel, the Na^+,K^+-ATPase, AChR and calmodulin, eel electric tissue has been used as a source for the purification of these proteins for molecular and functional analysis.

Torpedo electrocytes, on the other hand, are richly innervated with ACh-releasing electromotor neurons and are electrically inexcitable. Therefore, they provide a very specialized model for the motor end-plate. Because of the

Cell Physiology Sourcebook. DOI: 10.1016/B978-0-12-387738-3.00048-2

exaggerated cholinergic nature of *Torpedo* electric tissue, it has been used as a rich protein and mRNA source for the AChR and AChE. The expression of Cl^- channels on the non-innervated membrane of these cells has led researchers to use this tissue as a source for ClC-0 protein and mRNA as well.

Investigations with electric tissue of both the electric eel and the electric ray have opened wide avenues of study in electrophysiology, protein biochemistry and clinical research. Electrophysiological techniques have been used, refined and, in some cases, developed while using electrocytes as model systems. Like the squid giant axon, these cells have been instrumental in defining and confirming the ionic currents responsible for excitable cell membrane potential changes. Biochemically, *Electrophorus* and *Torpedo* electric tissue has supplied abundant quantities of key excitable membrane proteins that exist in only trace amounts in mammalian tissues. Since electric tissue develops from skeletal muscle, the biochemical properties and three-dimensional structures of these proteins are similar, if not identical, to those of mammalian skeletal muscle and other excitable cells. These discoveries will continue to further our understanding of the mechanisms by which membrane potentials of excitable cells are generated and regulated, as well as the understanding and the treatment of disease.

II. INTRODUCTION

Electric fish such as the marine *electric ray* (genus *Torpedo*) and the freshwater *electric eel* (*Electrophorus electricus*) are capable of generating powerful electrical discharges that can be measured in the water surrounding these animals. These fish use the production of bioelectricity as an effective mechanism to stun prey and ward off predators. Electrical discharges are generated by electric cells, called *electroplax* or *electrocytes*, that produce end-plate potentials and action potentials (APs) that are remarkably similar to the membrane potentials of neurons and myocytes. In fact, the membrane receptors, ion channels and ATPases responsible for electric tissue electrophysiology are biochemically and functionally identical to those of mammalian muscle and nerve. For this reason, electrocytes have been used extensively as a specialized and appropriate model system for the study of excitable cell membrane electrophysiology and biochemistry. Due to the specialized nature of electric tissue, it has also been used as an enriched source of membrane proteins for biochemical studies. Previous chapters have described in detail the generation of acetylcholine (ACh)-mediated muscle end-plate potentials and the propagation of action potentials of nerve and muscle (see Chapters 18, 19, 32, and 42). This chapter examines the anatomy and cellular morphology that electric fish have evolved in order to produce powerful electrical discharges. An electrophysiological and biochemical comparison is made between the electrocytes of the freshwater electric eel and the marine electric ray. The major contributions that electric tissue has made to the understanding of the electrophysiology and biochemistry of excitable membranes are also reviewed.

The shocking sensations produced by electric fish were undoubtedly experienced by mankind long before the recording of scientific phenomena. Some of the first recorded reports of unusual effects produced by electrical discharges of electric fish were of the Nile river catfish, *Malapterus electricus*. Nile river fishermen reported unpleasant sensations when handling live *Malapterus*, or even the water-soaked nets containing the fish. Godigno, a seventeenth century Jesuit father, noted that dead fish could be induced to move when a live *Malapterus* was thrown among them (Grundfest, 1957). At the time when Ben Franklin and other investigators were experimenting with static electricity of the Leyden jar, the electric eel provided insight into the basic conductive properties of electricity. In 1775, John Walsh conducted numerous experiments, one of which involved 10 people holding hands in a circle where the first and last "subjects" touched the opposite ends of a moderate-sized eel. All 10 people received a severe shock. The relative conductivities of various materials, including glass, wood, silk, brass chains and iron rods, were then determined by holding these materials between two of the investigators and noting the severity of the electrical discharge. Although these experiments were likely to be very convincing to Walsh and his assistants, others doubted the electrical nature of the discharge from *Electrophorus* and *Torpedo*. The bioelectric nature of the discharge had not gained widespread acceptance until Du Bois-Raymond demonstrated that nerve and muscle were electrogenic (Grundfest, 1957). Since that time, the usefulness of *Electrophorus*, *Torpedo* and other electric fish as models for excitable membranes has been realized.

III. ANATOMY OF *ELECTROPHORUS* AND MECHANISM OF THE ELECTRICAL DISCHARGE

Powerful electric fish possess a specialized anatomy and cellular morphology devoted to the production of electrical discharges. The electric eel is an excellent example of this specialization. It has been well characterized on the cellular and biochemical level and is used here to describe the production of bioelectricity. Figure 48.1A depicts the location of the electric organs within *Electrophorus*. The viscera are crowded into the rostral 20% of the animal; the remaining 80% is comprised predominantly of electric tissue and swimming muscles. The electric organs are confined to the ventral portion of this caudal region,

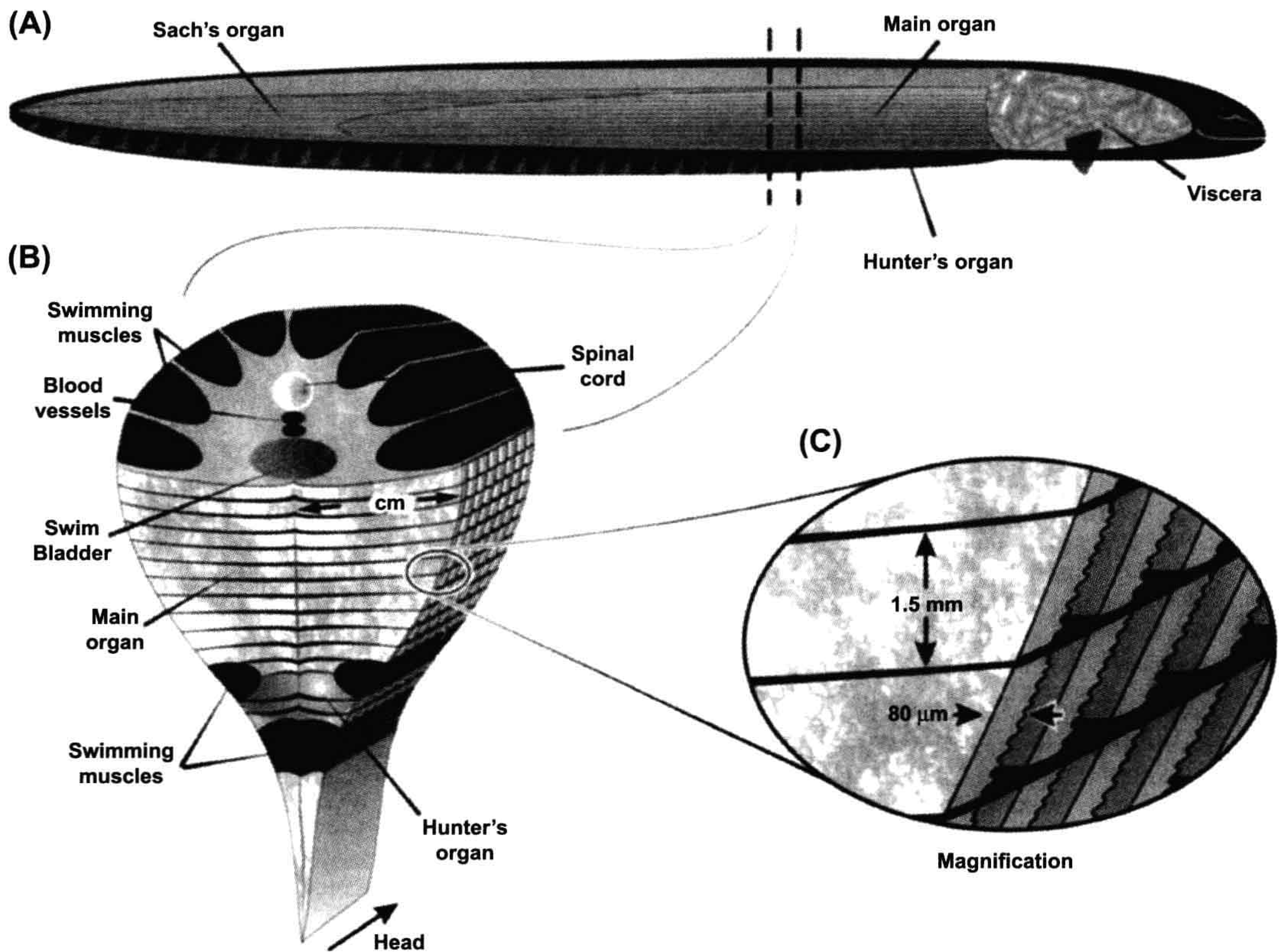


FIGURE 48.1 Anatomy of the electric eel. (A) Diagram illustrating the anatomical orientation of electric organs. (B) A section through the middle portion of the eel, drawn such that the anterior surface is nearest the reader. (C) Columns of electrocytes extend the length of the electric organ. In this panel, the flatter, caudal surface of each electrocyte would be innervated by numerous electromotor neurons (not shown).

whereas most of the swimming muscles, major blood vessels and spinal cord are situated in the dorsal one-third (Fig. 48.1B). The eel also possesses a tubular swim bladder that extends the length of the fish and is positioned dorsal to the main electric organ and ventral to the spinal cord. The central nervous system consists of a small brain typical of teleost fish and a spinal cord that extends down the length of the animal. The electrical discharge is coordinated in the central control nucleus in the medulla. Axons from these neurons of the brain project caudally and synapse on neurons of the electromotor nucleus of the spinal cord. *Electromotor neurons* radiate into the electric organ, innervating individual electrocytes (Bennett and Sandri, 1989). To generate the whole-animal electrical discharge, each electrocyte of the entire electric organ must be stimulated simultaneously. In other words, action potentials reaching proximal electrocytes of the electric organ must be delayed to varying degrees relative to more distal regions. Neurons innervating proximal electrocytes are smaller in diameter and conduct action potentials more slowly. Some of these neurons wind their way to these rostral electrocytes, thereby slowing stimulation of this part of the electric organ, aiding in synchronous activation (Bennett, 1971). The delay may also occur in the electromotor nucleus of the spinal cord where central neurons synapse on electromotor neurons. Presumably, synaptic transmission is slower to electromotor neurons innervating proximal portions of the electric organ, whereas faster signaling occurs between neurons that innervate electrocytes near the tail (Szabo, 1961).

As depicted in Fig. 48.1, *Electrophorus* has three well-defined electric organs. The main organ is the largest and is responsible for voluntarily generating powerful high-voltage discharges. The main organ extends from behind the peritoneal cavity of the viscera down the tail of the eel, where it eventually gives rise to Sach's organ. This organ, along with Hunter's organ, generates repetitive low-voltage discharges and is thought to be involved in electrolocation

of objects in the eel's environment. In the cross-sectional view of Fig. 48.1B, Hunter's organ is seen to be partially delineated from the main organ by two columns of skeletal muscles. Electric tissue develops from these columns of skeletal muscle tissue in immature eels and is thought to arise from embryonic myocyte precursor cells (Keynes, 1961). As shown later, the membranes of electrocytes are biochemically and functionally very similar to skeletal muscle sarcolemma.

Electrocytes of both the main electric organ and Sach's organ are large ribbon-shaped cells. Each electrocyte extends laterally from the midline of the electric organ to the skin, a distance of up to 4 cm. They have a width of up to 1.5 mm and thickness of 80 μm. As seen in Fig. 48.1C, electrocytes are positioned one after another along their flat axis to give rise to long rectangular columns of cells running along the longitudinal axis of the eel. These columns are delineated and electrically insulated from one another by *connective tissue septa*, which help to maintain the physical structure of the electric organ. This stacked arrangement is a common feature of electric organs in electric fish and enables greater voltages to be produced (see later). When viewed under light microscopy, electrocytes are seen as multinucleated syncytia, similar to the skeletal muscle myocytes from which they are derived. Electrocytes are seen in cross-section to have one relatively flat posterior membrane relative to the other more undulated anterior membrane. The flat caudal membrane is innervated by ACh-releasing electromotor neurons that form synapses that are morphologically similar to motor end plates of skeletal muscle cells (Chapter 32).

Immunofluorescent localization microscopy and electrophysiological experiments have led to the understanding of how the electrical discharge is generated at the cellular level. Electrocytes use membrane receptors and ion channels polarized to either the innervated or non-innervated membrane in order to produce *transcellular potentials* that give rise to the discharge of the electric organ (Fig. 48.2A). The caudal innervated membrane contains acetylcholine receptors (AChRs), inward and outward rectifying K^+ channels, a high density of voltage-gated Na^+ channels and only trace amounts of Na^+, K^+-ATPase. This membrane is both chemically and electrically excitable. That is, this surface of the electrocyte produces APs in response to artificial stimulation with AChR agonists or direct electrical stimulation. The non-innervated membrane, on the other hand, does not respond to these manipulations, since it has no AChRs or voltage-gated Na^+ channels. Instead, this membrane contains a high concentration of Na^+, K^+-ATPase and ion channels responsible for maintaining the *resting potential* of −70 to −85 mV. Evidence suggests that the resting current of *Electrophorus* electrocytes is carried predominantly by K^+ channels (Lester, 1978), but the contribution of a Cl^- conductance cannot be excluded (Nakamura et al., 1965). In *Torpedo,* the resting current has been shown to be carried at least partially by Cl^- (Miller and White, 1980). In skeletal muscle myocytes, 30–70% of the resting current is carried by this anion (Chapter 42). Since *Electrophorus* electric tissue is derived from skeletal muscle, it is possible that the resting current of these cells is also carried by Cl^-.

APs arriving at the nerve termini of electromotor neurons cause ACh to be released onto the innervated membrane of electrocytes (see Fig. 48.2A). *End-plate potentials* (EPPs) produced by AChRs surpass the threshold for Na^+ channel activation and trigger the production of APs that propagate very short distances between electromotor junctions and have overshoots of +40 to +65 mV. Meanwhile, the potential of the non-innervated membrane remains at the resting value of up to −85 mV, due to the abundance of resting current channels and the absence of voltage-gated Na^+ channels. When the AP peaks on the innervated membrane, a net *transcellular potential* of up to 150 mV results across the electrocyte (+65 mV of the innervated membrane minus −85 mV of the non-innervated membrane). This transcellular potential difference is accompanied by a net flow of positive current moving in the innervated membrane-to-non-innervated membrane direction (left to right as shown in Fig. 48.2). Insulating septa that form electrocyte columns effectively insulate the extracellular regions on either side of the electrocyte. These connective tissue structures prevent current from flowing around the outside of the electrocyte, which would short-circuit the transcellular potential difference (see Fig. 48.2B). This arrangement allows each electrocyte to act as a simple battery having an electrical potential of up to 150 mV. Since each electrocyte of a column is stimulated simultaneously, the potentials of each electrocyte battery within a column summate to generate a large voltage, as predicted by Ohm's law. In Fig. 48.2B, the potentials of three electrocytes summate to give a potential of 450 mV. In large eels, where the potentials of many thousands of electrocytes summate, the net electric discharge can reach 700 V.[1] Connective tissue septa channel the current down the longitudinal axis of the electric organ toward the head of the eel. The current leaves the eel through low-resistance regions of the skin and is conducted through the water, producing an electric field, the magnitude of which diminishes with the square of the distance from the animal. Objects, like other fish or the human hand, experience a potential difference in this electric field and currents

[1] A discharge of this magnitude requires that at least 4700 electrocytes be stimulated simultaneously. That is, 4700 electrocytes × 0.15 V per electrocyte = 705 V. This situation is analogous to a flashlight, where more batteries aligned in series produce a brighter light source.

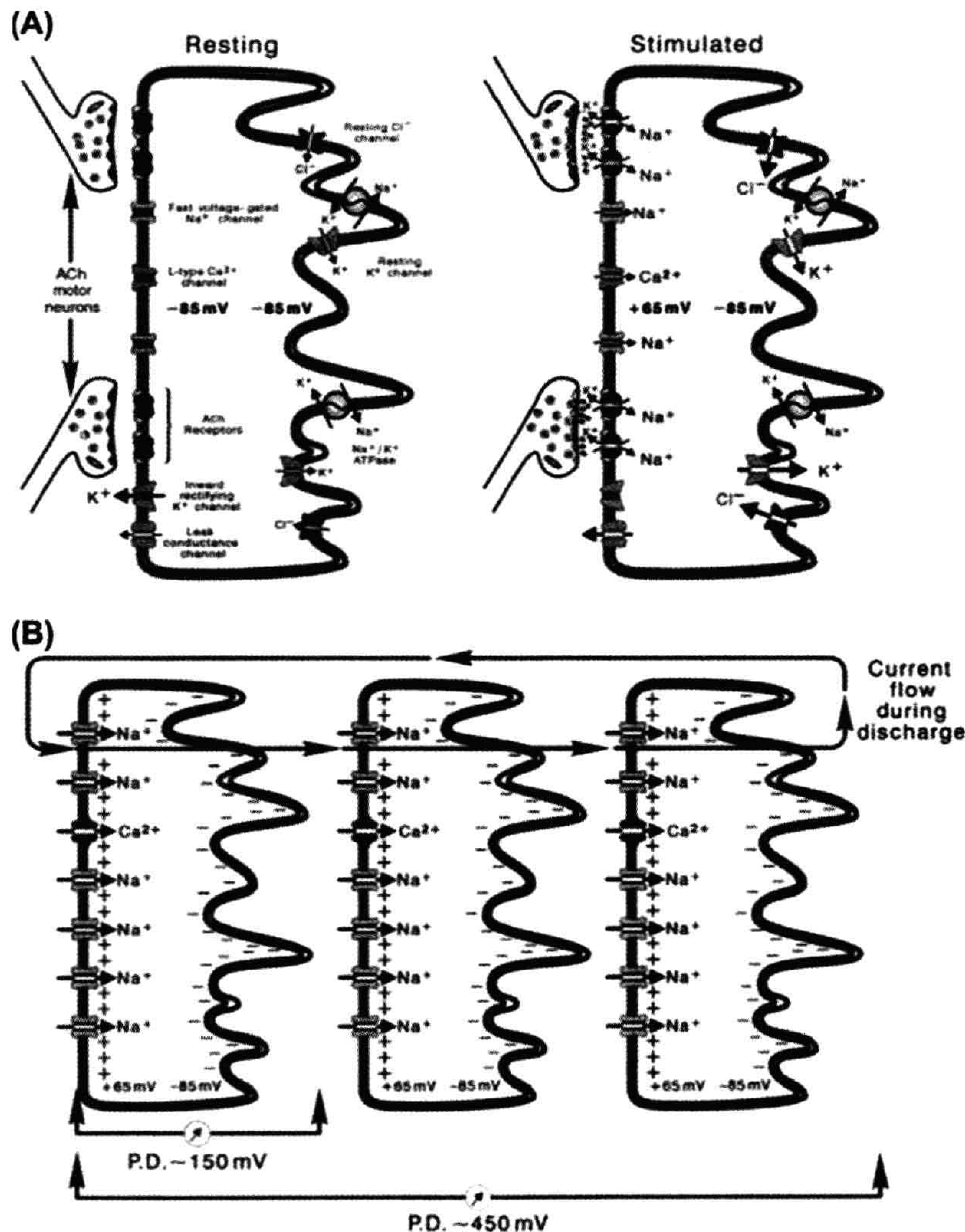


FIGURE 48.2 Diagrammatic representation of electrocytes. The left surface of each cell represents the posterior innervated membrane. (A) At rest, both the innervated and non-innervated membranes exhibit a potential of −85 mV. When stimulated, activated AChRs generate EPPs, triggering Na^+ channel-mediated APs peaking at +55 mV on the innervated membrane. The non-innervated membrane contains no voltage-gated Na^+ channels and maintains the −85-mV resting potential. The result is a transcellular potential difference of approximately 150 mV. (B) Because each cell is stimulated simultaneously, electrocyte transcellular potentials summate. The potentials of three electrocytes culminate to produce 450 mV. Currents generated by stimulated electrocytes flow down electrocyte columns in the posterior-to-anterior direction. The circuit is closed by current flowing out the head of the eel, through the water, and back into the tail region.

sufficient to excite muscles, nerves and sensory endings flow through them, producing a shocking sensation. The circuit of the discharge is closed by current flowing through the skin of the tail region of the eel back into electrocyte columns from which the electromotive force (EMF) originated (Bennett, 1971).

IV. ELECTROCYTE MEMBRANE ELECTROPHYSIOLOGY

IVA. Membrane and Extracellular Potentials

Electrocyte membranes contain many of the same protein elements found in myocytes and neurons. In fact, the

individual APs of the innervated membrane of *Electrophorus* electrocytes are quite similar to those of other excitable cells. However, electric cells are different in that potential changes are polarized to a particular membrane, resulting in the generation of transcellular potentials and an asymmetric flow of current. Also, to produce whole-animal electrical discharges having the maximum possible voltage or current output, electrocytes have evolved to express exaggerated amounts of key excitable membrane proteins.

In electric tissue preparations where the flat innervated electrically excitable surface of electrocytes is exposed, APs can be triggered with extracellular stimulating electrodes situated close to the membrane surface. Membrane potentials and transcellular potentials can then be measured through recording electrodes lowered across the innervated membrane or through the entire cell, respectively (Fig. 48.3). As the recording electrode approaches the innervated membrane and a stimulus is applied, a negative deflection is recorded (Fig. 48.3A). Because the recording electrode measures the potential difference between the region just outside the membrane compared to the reference electrode placed in the bath, the AP here is recorded as a negative deflection. After the electrode is advanced through the innervated membrane, an AP that has propagated from the site of stimulation to the recording electrode is detected. The characteristics of electrocyte membrane potentials vary considerably from cell to cell, but are typically similar to those measured on the myocyte sarcolemma or neuronal axolemma. As seen in Fig. 48.3B, a typical resting potential is about −75 mV and ranges from −65 to −85 mV. The electrocyte AP seen in Fig. 48.3B is typical in its 3.5-ms duration and +50-mV overshoot. Generally, the duration ranges from 2 to 4 ms and the overshoot between +35 and +65 mV. These values for the overshoot are considerably larger than that of other excitable cells and are due to an extraordinarily high density of voltage-gated Na^+ current and a relatively low level of outward rectifying K^+ current (see discussion later). When the recording electrode is lowered even further until it completely penetrates the electrocyte, transcellular APs are recorded. Because the recording electrode is once again in the extracellular space, the resting potential here is measured as 0 mV. However, the interstitium where the recording electrode is positioned is electrically insulated by connective tissue septa from the reference electrode located in the bath solution. When the electrocyte is stimulated, an AP is recorded that is identical to the intracellular AP, except that it initiates at 0 mV. It has a peak equal to the total amplitude of the intracellular AP, in this case about 125 mV. This transcellular AP arises because the non-innervated non-excitable membrane does not fire an AP that would cancel out the spike of the innervated membrane. Insulating connective tissue septa prevent the potential difference from being short-circuited around the outside of the electrocyte. If the stimulus is increased such that the electrocyte beneath the recording electrode is also stimulated, a negative deflection in the extracellular potential is recorded just behind the 125-mV transcellular AP (see Fig. 48.3C, right). This negative deflection corresponds to the resulting AP of the lower electrocyte, which is stimulated later than the electrocyte on the surface. In the intact electric organ, these electrocytes would be stimulated simultaneously by the eel's nervous system such that these APs would be occurring at the same time. In this way, the transcellular potentials summate to yield a powerful electrical discharge.

Ionic currents responsible for *Electrophorus* electrocyte resting potentials, as well as EPPs and APs are similar to other excitable cells and the reader is referred to previous chapters where their mechanisms have been described in detail. However, some differences between electrocyte membranes and those of neurons and myocytes are worthy of mention. The non-innervated membrane of electrocytes has a very low resistance of about 0.1 Ω/cm^2, which is one to two orders of magnitude less than that typically found for nerve or muscle (Nakamura et al., 1965). Physiologically, the eel needs this high K^+ and Cl^- current to clamp the non-innervated membrane at the resting potential in order to set up transcellular potentials like those observed in Fig. 48.3C. On the other hand, the innervated membrane at rest has a resistance of 3−6 Ω/cm^2 (Nakamura et al., 1965). On stimulation, this resistance decreases due to a large voltage-activated Na^+ current. In fact, Shenkel and Sigworth (1991) were able to measure macroscopic Na^+ currents in excised patches of the innervated membrane corresponding to a density of as much as 1300 channels/μm^2. This high density of Na^+ channels is accompanied by relatively few outwardly rectifying K^+ channels. Because of this distribution of channels in the innervated membrane, the electrocyte AP has a large overshoot that nearly reaches the Na^+ equilibrium potential, E_{Na}. The repolarization phase is therefore due primarily to the inactivation of Na^+ channels and secondarily to delayed rectifier K^+ channels and the resting current of the innervated membrane.

Skeletal muscle-like EPPs that trigger APs on the surface of electrocytes are generated by AChR-mediated currents. Basically, macroscopic and single-channel currents conducted by the eel AChR are very similar to those seen on skeletal muscle sarcolemma. The permeability of the eel receptor to both Na^+ and K^+ is nearly equal since the reversal potential is the midpoint between E_{Na} and E_K (Sheridan and Lester, 1977; Pasquale et al., 1986). In other words, the peak of the EPP moves toward a value of approximately −10 mV in order to activate Na^+ channels for an AP. Eel AChRs elicit single-channel opening events that are similar to the receptor from mammalian sources in that their mean open time is dependent on membrane potential, temperature and the

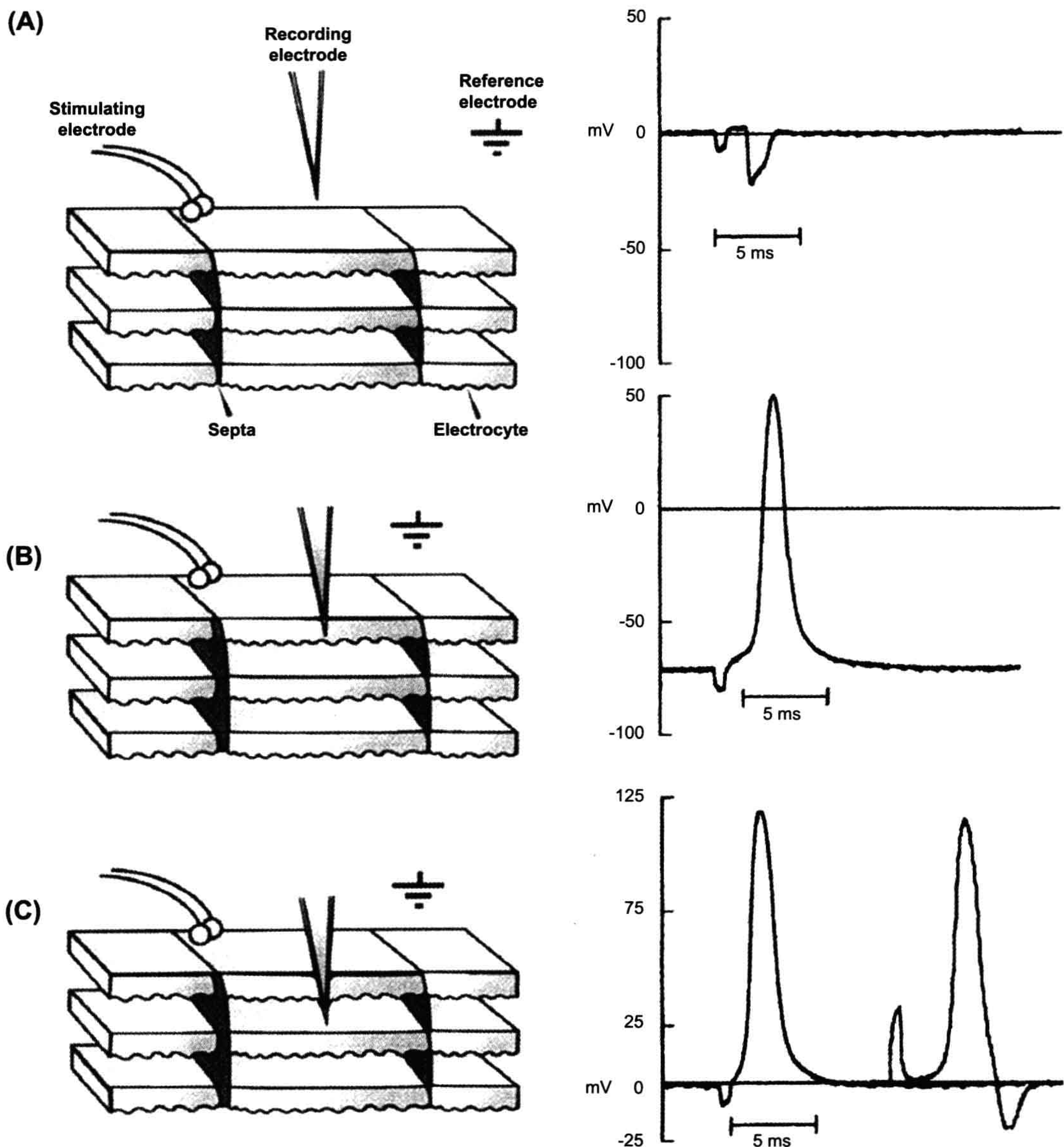


FIGURE 48.3 Extracellular potentials, APs and transcellular potentials of *Electrophorus* electrocytes in an electric tissue slice preparation. Diagrams to the left depict a slice of electric tissue in cross-section where electrocytes are oriented such that the innervated membrane is uppermost. Columns of electrocytes run in the vertical direction and are delineated by insulating connective tissue septa. Potentials recorded by the recording electrode in the indicated positions are shown on the right. (A) The recording electrode near the innervated membrane records a negative deflection in the extracellular potential. (B) The recording electrode penetrating the innervated membrane records an intracellular AP. (C) Transcellular potentials measured after the recording electrode has penetrated the entire electrocyte. The second potential recording on the right shows the negative deflection of the electrocyte beneath the recording electrode when a higher intensity stimulus is applied.

AChR agonist used. Single-channel conductances through individual receptors do not depend on the ligand used. However, these preparations of the eel AChR are different from other excitable cells in that single-channel open times can be fitted to a single exponential compared to the more complex distributions found for other sources of the receptor. This indicates that the eel expresses only one isoform of each of the receptor subunits, yielding a receptor with a single unique conductance.

IVB. Equivalent Circuits

From what is known of electrocyte electrophysiology, equivalent circuits can be derived that explain the production of transcellular potentials that arise during the AP. Because electrocytes are large flat cells comprised of essentially two parallel membranes having a uniform potential across their entire surfaces, whole-cell potentials can be described with two equivalent circuits, pertaining to the innervated and non-innervated membranes, connected by a resistor representing the resistance of the cytoplasm (R_t). At rest, the permeability of both membranes to K^+ and Cl^- is high, so that their equilibrium potentials are expressed more than that of Na^+, resulting in an E_m of about −85 mV (for a detailed description, see Chapter 9). The equivalent circuit for the electrocyte at rest can then be reduced to that seen in Fig. 48.4A (right), where both membranes have composite E_m values that drive an outward flow of positive current. Notice that the equivalent circuits for both membranes are mirror images of one another, both having a symmetrical outward movement of current that cancels to give a transcellular potential of 0 mV. At the peak of the AP, however, the permeability of the innervated membrane to Na^+ increases dramatically, such that the membrane potential is influenced primarily by E_{Na}. The composite E_m of the innervated membrane has now reversed its polarity, so that current across this membrane moves inward (Fig. 48.4B, right). Because the non-innervated membrane has no Na^+ conductance, the polarity of the potential here is the same as at rest and a net outward current continues to flow. Now, the total driving force for both membranes is in the same direction, so that current flows from the innervated membrane to and through the non-innervated membrane. If one considers that R_{cyt} and $R_{m(non)}$ are negligible compared to $R_{m(inn)}$, the equivalent circuit for the electrocyte can be reduced to a resistor and battery in series, where the resistance is equal to $R_{m(inn)}$ and the battery represents the composite potentials of $E_{m(inn)} + E_{m(non)}$. During stimulation, the potential across this unit, then, equals the transcellular potential and has a magnitude equal to that of the amplitude of the innervated membrane's AP, or approximately 150 mV.

In the electric organ of *Electrophorus*, electrocytes are stacked one after another in very long columns. Electrically, this arrangement is represented by many electrocyte resistor-battery units connected in series, as shown in Fig. 48.5A. Each unit contributes an additional 150 mV to the overall electrical discharge. However, Kirchhoff's first law dictates that the current measured at every point along an unbranching leg of a circuit, such as a series of batteries, is constant.[2] In other words, the value of the overall current output of a column of electrocytes does not depend on the number of cells in series, but on the electrocyte that has the greatest resistance to the flow of current. (For a comprehensive description of Ohm's law and Kirchoff's laws applied to biological equivalent circuits, see Sperelakis, 1979.) In order for an electric organ to increase the current of an electrical discharge, it must have additional electrocytes arranged in parallel. This amplification is accomplished in electric fish by having numerous electrocyte columns situated alongside one another. The electric eel, being a long slender animal, has fewer electrocyte columns arranged in parallel relative to some other electric fish. Because of this anatomical arrangement, the eel produces discharges of very high voltage with less current compared to other electric fish, such as *Torpedo*, the electric ray.

The electric ray is a marine elasmobranch with two large electric organs positioned laterally on either side of its flattened head (Fig. 48.6). Hexagonal-shaped columns of electrocytes run in the vertical direction and conduct current up away from the ocean floor, around the edge of the lateral fin and back into the bottom of the electric organ. *Torpedo* has a short but wide electric organ accommodating large numbers of electrocyte columns situated next to one another. As shown in Fig. 48.5B, Kirchoff's law predicts that electrocyte resistor-battery units in parallel will produce electrical discharges of low voltage and high current, proportional to the total number of electrocyte units in parallel. This is indeed the case with the electric ray, in which discharges of up to 16 A and 60 V, totaling up to 1 kW, have been measured (Grundfest, 1960).

V. COMPARATIVE PHYSIOLOGY OF *ELECTROPHORUS* AND *TORPEDO* – MODELS FOR MAMMALIAN EXCITABLE CELLS

VA. *Electrophorus*

VA1. Na^+ Channel

Because electric tissue is specialized for membrane excitability and carries out its function with membrane proteins common to mammalian tissues, electrocytes of electric fish

[2] Specifically, Kirchoff's first law states that the current entering a point along a circuit is equal to the sum of the currents of all the branches leaving that point. Therefore, if the circuit is unbranching, then the current at every point is constant.

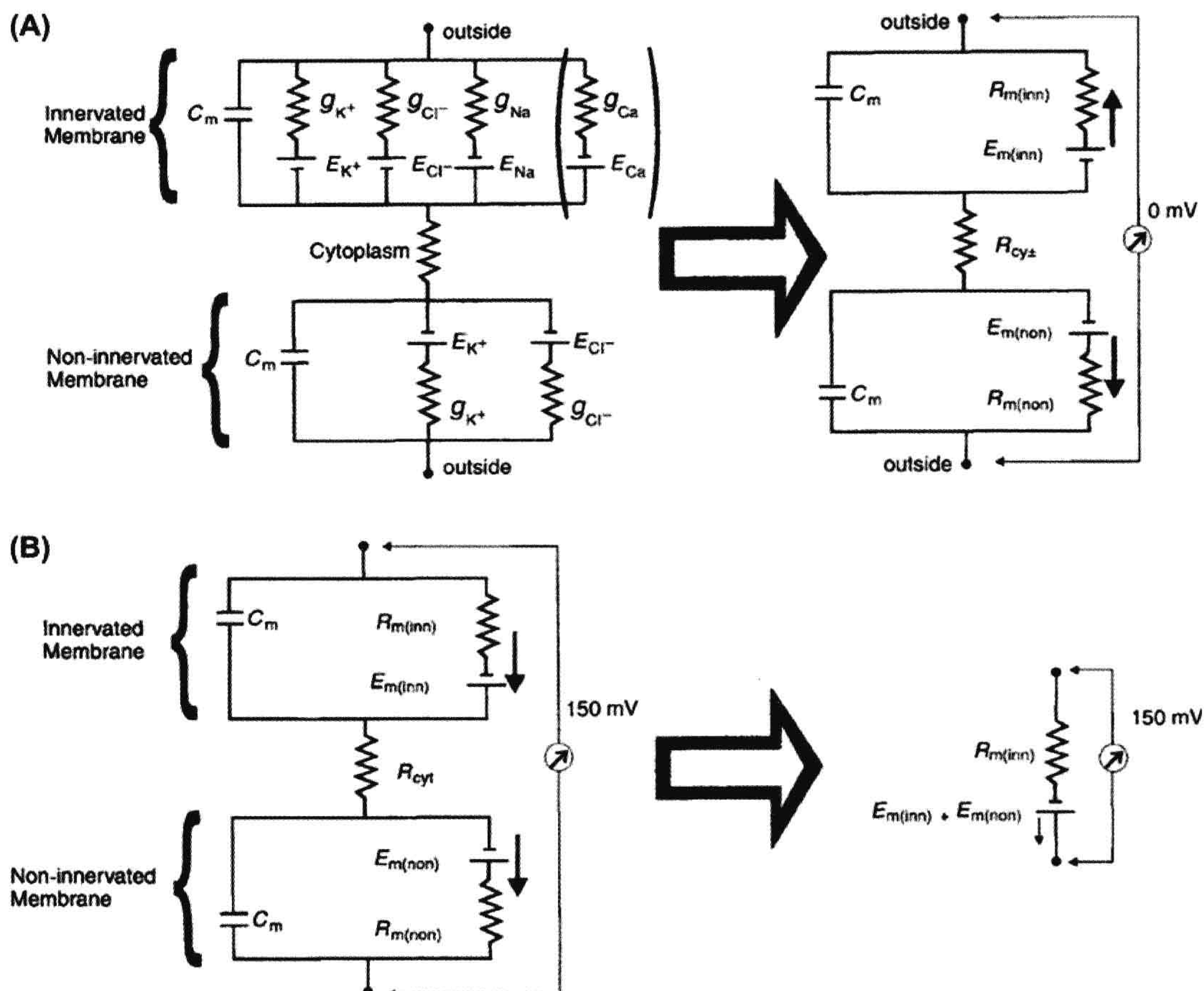


FIGURE 48.4 Electrical equivalent circuit diagrams for both the innervated and non-innervated membranes of an electrocyte. The innervated membrane is uppermost in both A and B. Both membranes are represented by parallel resistance–capacitance circuits and are connected by the cytoplasmic resistance, R_{cyt}. C_m is the membrane's capacitance. The conductances for K^+, Cl^-, Na^+ and Ca^{2+} across the membranes are represented by g_K, g_{Cl}, g_{Na} and g_{Ca}, respectively and are inversely proportional to the resistance of the membrane for these ions. Nernst potentials for each of these ions across the membranes are E_K, E_{Cl}, E_{Na} and E_{Ca}. The Ca^{2+} leg of the circuit is in brackets, since the existence of a selective Ca^{2+} conductance in the electrocyte has not yet been demonstrated. (A) At rest, the innervated membrane reduces to a circuit where $R_{m(inn)}$ represents the total membrane resistance of this face of the cell and is a composite of the resistances of the membrane to each of the ions listed to the left. The $E_{m(inn)}$ and $E_{m(non)}$ are the resting membrane potentials for the innervated membrane and non-innervated membrane, respectively. At rest, E_K and E_{Cl} are expressed the most, since the conductance of the membrane to both these ions is greatest. In this state, the circuit diagrams are mirror images of one another, no net current flows across the cell and the transcellular potential is 0 mV. (B) At the peak of the AP, the conductance of the membrane to Na^+ (and possibly Ca^{2+}) increases dramatically and E_{Na} and E_{Ca} is expressed more than E_K and E_{Cl}. The polarity of the $E_{m(inn)}$ battery is now reversed, such that there is a net flow of positive current in the direction of the non-innervated membrane and a transcellular 150-mV potential results. Given that R_{cyt} and $R_{m(non)}$ are negligible compared to $R_{m(inn)}$, the equivalent circuit can be reduced to the "electrocyte unit" on the right.

provide excellent models for mammalian excitable cell membranes. Compared to electrocytes of *Torpedo* and other electric fish, *Electrophorus* electrocytes express more of the membrane proteins common to mammalian excitable tissues and therefore provide a more general model for excitable membranes. For example, both voltage-gated Na^+ and AChR-mediated currents have been measured from the innervated membranes of these cells. Early preparations took advantage of the large size of these cells by sealing single electrocytes over windows in Lucite chambers (Schoffeniels, 1961). Because the resistance of the non-innervated membrane is negligible relative to the innervated membrane, electrocytes in this configuration are treated as a single membrane without having to thread

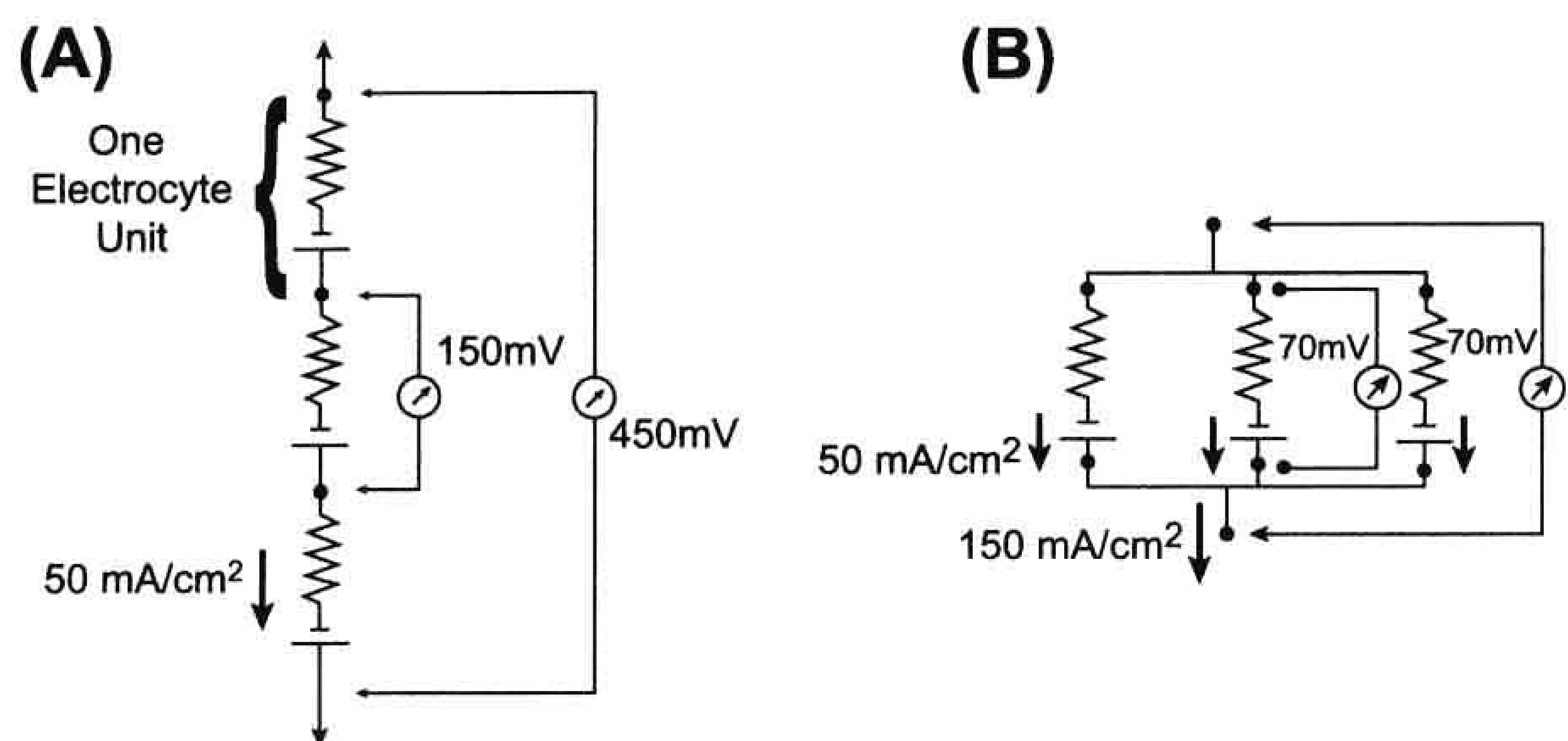


FIGURE 48.5 Electrocyte units in series and in parallel. (A) When connected in series, the potentials of each 150-mV electrocyte unit summate, while the current remains constant. In this case, three electrocyte units are shown to summate their potentials to yield a total of 450 mV. This tends to be the case in the electric organ of *Electrophorus*, where transcellular potentials of 150 mV and currents of 50 mA/cm^2 are measured. (B) The currents of electrocytes in parallel summate while the potential remains constant. Three electrocyte units, each having a current of 50 mA/cm^2, are shown to produce a 150 mA/cm^2 current when arranged in parallel. This is the case in *Torpedo*, where many electrocytes are situated next to one another in parallel. The transcellular potential produced by *Torpedo* electrocytes is 70 mV.

a space-clamping electrode down the middle of the cell. With this method, Nakamura et al. (1965) were able to measure Na^+ currents responsible for the rising phase of eel electrocyte APs and to construct a current–voltage (*I-V*) relation for the *Electrophorus* Na^+ channel. These researchers also described an abundant inward rectifying K^+ current that has an *I-V* relation similar to those seen in myocytes. However, since delayed K^+ currents are not seen in these preparations, the repolarization of the eel electrocyte AP is apparently due to Na^+ channel inactivation. Much of what is known about the electrogenesis of the AP of electrocytes and other excitable cells has come from studies such as this. The innervated membrane of *Electrophorus* electrocytes was also *patch-clamped* to examine macroscopic Na^+ currents in order to determine minute charge movements associated with channel opening, as well as to determine the permeability of the channel to K^+ relative to Na^+. Upon membrane depolarization, the Na^+

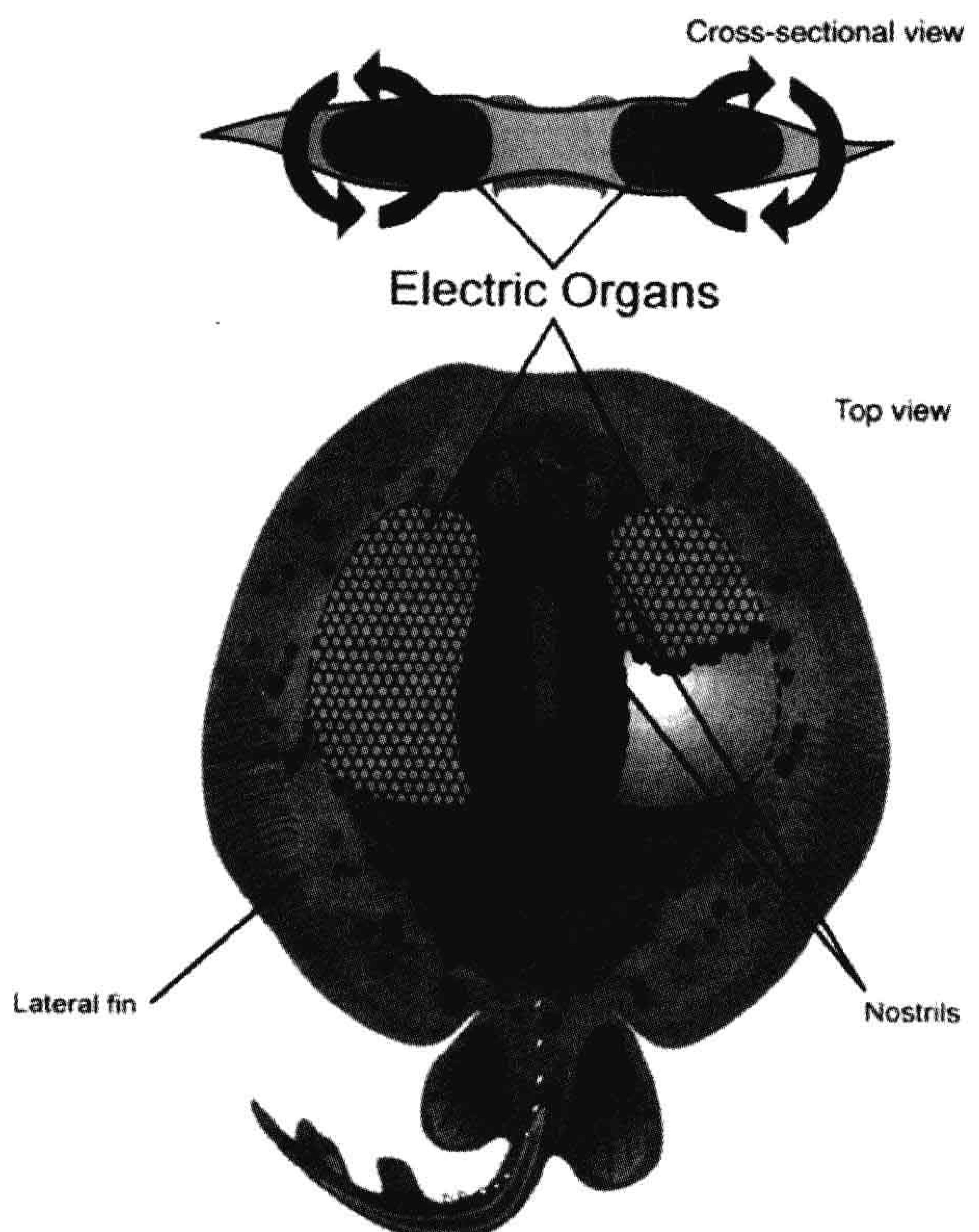


FIGURE 48.6 Drawing of an electric ray (genus *Torpedo*), depicting the location of its two lateral electric organs. The inset shows the direction of the flow of current around the fish while producing an electrical discharge.

channel undergoes a conformational change that is associated with the movement of positively charged amino acids within the protein. This movement of positive charge is thought to be a consequence of the opening of the channel gate and can be measured in a population of Na^+ channels as a small outward current. Opening of the eel Na^+ channel is associated with the movement of approximately 1.5 charges upon channel opening, a value similar to nerve and muscle preparations (Shenkel and Bezanilla, 1991; for a comprehensive description of gating mechanisms, see Hille, 1992). On examining the selective permeability of the eel Na^+ channel for this ion relative to K^+, Shenkel and Sigworth (1991) found P_{Na}/P_K ratios of 8 to 43. This range represents a substantial variation that was even seen in membrane patches taken from the same cell. Given that *Electrophorus* electrocytes are known to express just one isoform of the channel protein, these results suggested that this variability might arise from post-translational modifications such as glycosylation or even *phosphorylation*. This possibility was substantiated by experiments that showed the eel Na^+ channel to be modulated by exogenously applied protein kinase A (Emerick et al., 1993; also see Chapter 23 of this book). These studies contributed to our basic understanding of the electrophysiological function of the Na^+ channel protein.

The first Na^+ channel ever purified, and later sequenced, came from electric tissue of *Electrophorus*. The purified 260-kDa protein is heavily glycosylated and consists of a single functional α subunit (Agnew et al., 1978; Miller et al., 1983). Na^+ channels from mammalian brain and muscle express additional β subunits. Since it has been suggested that these auxiliary subunits may regulate channel gating, preparations of the eel Na^+ channel are advantageous in that they eliminate the possibly complicating influence of β subunits. An *Electrophorus* electric tissue cDNA library was used to clone and sequence the channel for the first time (Noda et al., 1984). Its structure includes four homologous repeats that each contain six membrane-spanning helices. The fourth transmembrane segment contains a cluster of positively charged amino acids thought to be involved in gating of the channel. Movement of these positive amino acids during opening of the channel is thought to be responsible for the minute currents measured in patch-clamp experiments such as those discussed earlier. Compared to sequences of Na^+ channels of mammalian muscle and brain, the eel Na^+ channel shows the greatest homology with the muscle protein, as expected since electrocytes develop ontogenetically from myocytes. Both of these channels, however, lack a 202-amino-acid segment located between the first and second homologous repeat domains of the brain Na^+ channel (for complete discussions of Na^+ channel purification, structure and diversity, see Chapter 21 in this book and Hille, 1992).

VA2. Acetylcholine Receptor

As mentioned in a previous section, the large size of eel electrocytes has facilitated their dissection in order to measure single-channel AChR conductances. Other excitable cells express numerous isoforms of the subunits that make up the receptor and produce single-channel recordings that show complex mean open-time distributions and variable conductance values. The eel AChR yields more homogeneous values owing to its simplified subunit composition (Pasquale et al., 1986). The simple mean open-time distributions for the eel AChR were found for both the main electric organ as well as for Sach's organ, suggesting that AChR diversity evolved in order to meet varying physiological needs of myocytes and neurons. The eel receptor also desensitizes to a lesser extent in the presence of sustained concentrations of agonists (Pallotta and Webb, 1980). Simple subunit composition and lack of agonist-induced desensitization make the eel AchR advantageous for electrophysiological and biochemical studies.

Recognizing the cholinergic nature and the specialization of *Electrophorus* electrocytes, biochemists utilized electric tissue as a source for some of the first purifications of AChRs. Using various separation techniques, including differential centrifugation to separate membrane fractions and affinity chromatography to purify selectively the AChR from other membrane proteins, a 260-kDa macromolecule was isolated (Olsen et al., 1972; Biesecker, 1973). Not knowing a priori that the receptor is a pentameric protein made up of α, β, γ and δ subunits (in a respective ratio of 2:1:1:1), the initial isolation and identification of the peptides that make up the whole receptor were arduous. After some debate, the 44-kDa α subunit was established as the ligand-binding portion of the protein. The 50- to 65-kDa β, γ and δ subunits, along with the α subunit, are arranged symmetrically around a central axis to make up the ion channel pore of the protein (Karlin and Cowburn, 1973; Chang, 1974).

VA3. Na^+, K^+-ATPase

As we have seen, electrocytes express massive quantities of membrane receptors and ion channels in order to carry out their specialized function. To maintain resting potentials in the face of currents associated with EPPs and APs that dissipate Na^+ and K^+ gradients, electrocytes need to express large amounts of *Na^+, K^+-ATPase*. For this reason, *Electrophorus* electric tissue has been used as a source for the purification of this enzyme for structure–function studies. The eel protein, like that from other tissues, consists of a 94-kDa α subunit and a glycosylated 47-kDa β subunit. During purification, the ATPase is solubilized from electrocyte membranes with various detergents. To analyze its functional characteristics, the protein was

reconstituted into liposomes where its ATP-driven translocation of radiolabeled Na^+ and K^+ has been found to be similar to preparations of native electrocyte membranes containing the ATPase (Yoda et al., 1984). These preparations of the eel protein have been invaluable in determining the reaction mechanisms of the ATPase involved in its function. Drugs that target and inhibit different partial reactions of the protein's translocation mechanism have also been investigated and used to examine the pump's function in cell physiology. Drugs, such as the cardiac glycoside digoxin, have also been used clinically specifically to inhibit Na^+, K^+-ATPase function in the heart. This treatment dissipates the membrane Na^+ gradient, which indirectly augments intracellular Ca^{2+} within cardiac myocytes. This results in an increase in the heart's force of contraction, which can alleviate some forms of heart disease (for literature review, see Lingrel and Kuntzweiler, 1994.)

VA4. Calmodulin

Electrophorus electric tissue also expresses large quantities of the calcium-binding protein *calmodulin*. (For a detailed discussion of Ca^{2+}-binding protein function, see Chapter 7.) In fact, calmodulin makes up roughly 2%, by weight, of electrocyte protein (Munjaal et al., 1986). Once again, electric tissue was used as a source for the purification of this 17-kDa soluble protein (Childers and Siegel, 1975). Unlike the membrane proteins discussed earlier, the function of calmodulin within electrocytes remains elusive, even though some of the functions of this Ca^{2+}-mediator protein in intracellular signaling mechanisms is well documented in other electrically excitable cells. Figure 48.7 shows the intracellular location of calmodulin within electrocytes. Calmodulin is present throughout the cytoplasm of electrocytes, but is particularly concentrated near both the innervated and non-innervated membranes. In light of this membrane localization, along with the fact that calmodulin is so abundant in this tissue specialized for membrane excitability, a role for this protein in membrane function is likely. Determining the role of calmodulin in electrocyte function will undoubtedly lend insight into the role of this protein in membrane function of other excitable cells.

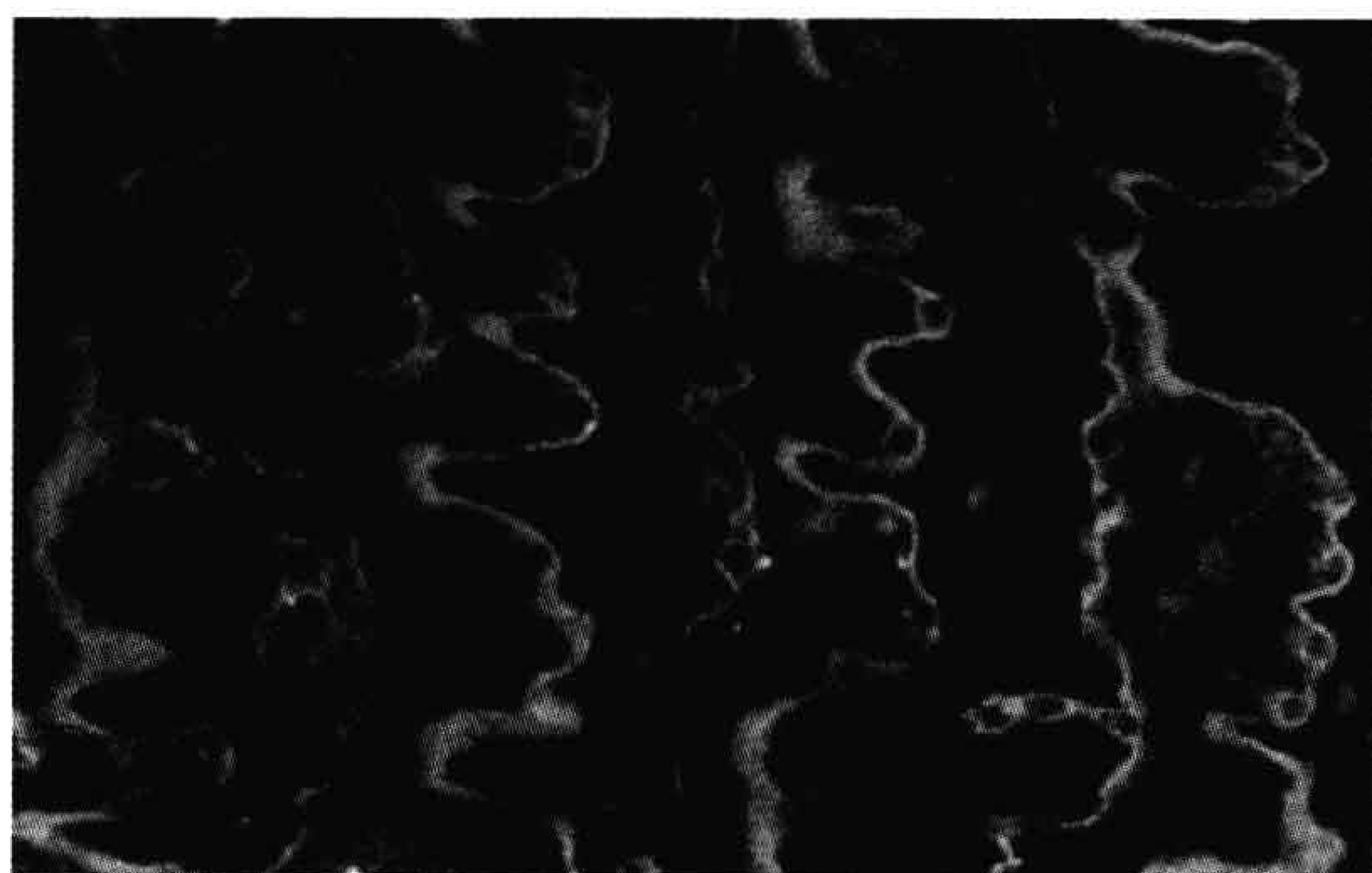


FIGURE 48.7 Immunofluorescent localization of calmodulin within main organ electrocytes. Paraffin-embedded 4-μm sections were probed with anti-calmodulin sheep antibodies. The location of primary antibodies was visualized with fluorescein-labeled rabbit anti-sheep secondary antibodies and photographed using epifluorescence microscopy.

VB. *Torpedo*

VB1. Comparative Electrophysiology

The marine electric ray (genus *Torpedo* and various species: *marmorata*, *californica*, *nobilianae*, *occidentalis*) can produce high-amperage electrical discharges by virtue of numerous electrocyte columns arranged in parallel, as discussed briefly earlier. In this way, it differs from *Electrophorus* which produces high-voltage discharges owing to numerous electrocytes arranged in series. The basic arrangement of *Torpedo* electrocytes within electric organ columns is remarkably similar to that of *Electrophorus*, considering that these two fish belong to different orders and the existence of electric tissue in both orders of fish represents convergent evolution. Although *Torpedo* electrocytes are smaller and pancake shaped (10–30 μm × 5 mm in diameter) relative to wafer-shaped *Electrophorus* electrocytes, they are still stacked one after another in columns delineated by electrically insulating connective tissue septa. *Torpedo* electrocytes also display membrane polarity similar to that depicted in the diagrams of Fig. 48.2.

Some basic differences in the membrane biochemistry and electrophysiology exist between electrocytes of these two fishes, however. Like the eel, *Torpedo* electrocytes can be stimulated to produce EPPs in response to nervous stimulation. That is, these electrocytes are chemically excitable. *Torpedo* electrocytes, however, do not fire APs in response to EPPs or artificially applied electrical stimuli and are therefore electrically non-excitable. This is due to a lack of voltage-dependent Na^+ channels on the innervated membrane that would generate and propagate APs. Instead, these cells are richly innervated by ACh-releasing electromotor neurons and have an abundance of postsynaptic AChRs. These ligand-gated channels conduct EPPs of 5-ms duration that peak just below 0 mV, halfway between E_{Na} and E_K. Like *Electrophorus* electrocytes, the non-innervated membrane of these cells has a large resting current, partially carried by Cl^-. Transcellular potentials measured across *Torpedo* electrocytes then, have an amplitude equal to that of the EPP, or 70 to 85 mV. The equivalent circuits diagrammed in Figs. 48.4A and B also apply to these electrocytes, except that the potential produced by each electrocyte unit equals 70 to 85 mV, instead of 150 mV for *Electrophorus* electrocytes.

VB2. Acetylcholine Receptor

Without voltage-gated Na^+ channels to propagate an AP, EPPs decay exponentially with the distance traveled from the *electromotor end-plate*. However, very little EPP decay is actually measured on the innervated membrane of *Torpedo* electrocytes, because the density of end-plates is so great. In fact, one might describe the innervated membrane of these cells as one large electromotor end-plate. These cells, therefore, provide a very specialized model for the motor end-plate. Like *Electrophorus* electric tissue, *Torpedo* electric tissue has been used for the purification of the AChR, which has supplied a wealth of knowledge about the biochemical properties of the receptor, as described in the previous section. The first sequences ever to be determined for each of the subunits of the receptor were obtained by screening *Torpedo* electric tissue cDNA libraries (Noda et al., 1982, 1983a,b; Claudio et al., 1983). The mRNAs encoding each of the receptor subunits were together injected into *Xenopus* oocytes in order for the functional protein to be expressed on the membrane of these cells. Interestingly, an increase in the ACh-induced conductance could be measured after microinjection (Mishina et al., 1984). By knowing the sequence of the receptor's subunits, a three-dimensional model of the receptor has been constructed and continually amended in light of ongoing biochemical research. (A model of the AChR appears in Chapter 32.) These studies established the basic protein structure of the nicotinic AChR, the findings of which have only been slightly modified to apply to the receptor of mammalian muscle and nerve.

VB3. Acetylcholinesterase

AChE is an important enzyme found in the postsynaptic membrane of cholinergic synapses of neurons, motor end-plates of myocytes and the electromotor end-plates of electrocytes. It catalyzes the hydrolysis of ACh to choline and acetate, thereby terminating ligand-gated activation of the AChR. Some pesticides and chemical warfare agents contain *anti-AChE agents* that cause acute and chronic alterations in central nervous system and neuromuscular function. Anti-AChE drugs have also been developed to alleviate symptoms of glaucoma, Alzheimer's dementia and myesthenia gravis – diseases marked by attenuated postsynaptic AChR density or compromised ACh release (for review, see Millard and Broomfield, 1995). Obviously, great care is needed when administering these drugs because overmedication can cause side effects similar to exposure to harmful anti-AChE agents.

Since the *Torpedo* electrocyte represents an exaggerated cholinergic system, it was used as a source for the purification and subsequent structural analysis of AChE. AChE is an 80-kDa protein that self-associates into tetramers, octamers and dodecamers and is anchored in the postsynaptic membrane through a phospholipid linkage (Parker et al., 1978; Ratman et al., 1986). *Torpedo* electric tissue provided massive enough quantities of AChE for the protein to be crystallized for subsequent x-ray diffraction studies. The resulting diffraction pattern obtained from x-rays shot through these crystals was analyzed to construct a three-dimensional structure of the protein, localizing atoms within the enzyme to within 2.8 Å (Sussman et al., 1991). These experiments with the *Torpedo* enzyme will continue to be invaluable to the development of new drugs aimed at the treatment of cholinergic diseases and for therapies for individuals exposed to toxic anti-AChE agents.

VB4. Cl^- Channel

Perhaps the most dramatic contribution that electric tissue has made to recent membrane biochemistry and physiology has been toward elucidating the structure and function of Cl^- channels. Recall that, in order for electrocytes to produce large transcellular potentials, the non-innervated membrane must have a tremendous resting current. This current clamps the non-innervated membrane potential at highly negative resting potentials even while the innervated membrane depolarizes dramatically. In *Torpedo* electrocytes, the resting current is carried at least partially by Cl^-. Electric tissue of the electric ray, therefore, has been used to isolate the channel protein for physiological studies and as a source for mRNA used in cloning and sequencing of the channel.

In the course of developing the planar lipid bilayer method for measuring ion channel conductances, Miller and White (1980) found that vesicles derived from the non-innervated membrane of *Torpedo* electrocytes contained Cl^- channels having novel *"double-barreled" gating kinetics*. With depolarization, individual Cl^- channel complexes acted as two channels with two separate but equal conductances. When one channel of the complex was open, the other was more likely to be subsequently activated as well. Single-channel recordings showed periods of inactivity until one channel of the complex was opened, after which a second equal conductance would superimpose on the first. Purification of the *Torpedo* Cl^- channel confirmed that the protein was a homodimer consisting of two 90-kDa polypeptides. When the purified protein was incorporated into planar lipid bilayers for single-channel recording, the same double-barreled gating kinetics were observed (Middleton et al., 1994).

The first Cl^- channel ever to be sequenced came from *Torpedo* electric tissue and has greatly expanded the field of Cl^- channel molecular biology. Using the expression cloning technique, the mRNA responsible for the *Torpedo* Cl^- conductance was identified and its corresponding cDNA sequenced. The encoded protein was predicted to

consist of 805 amino acids and to have a molecular weight similar to that of the purified protein (Jentsch et al., 1990). When mRNA for this channel, termed ClC-0, was injected into *Xenopus* oocytes, Cl^- conductances having double-barreled gating kinetics were expressed (Bauer et al., 1991). Recognizing that electric tissue is a model for skeletal muscle membranes, Steinmeyer et al. (1991b) screened a rat muscle cDNA library with oligonucleotide sequences derived from the *Torpedo* Cl^- channel. In this way, the sequence for the major Cl^- channel of mammalian skeletal muscle (called ClC-1) was obtained. It was later found that genetic aberrations in the mammalian ClC-1 gene result in symptoms of skeletal muscle myotonia (Steinmeyer et al., 1991a). These findings confirmed the results of Bryant and Morales-Aguilera (1971) that showed this disease to be associated with compromised Cl^- conductance. Once the sequences were known for both ClC-0 and ClC-1, investigators began screening libraries derived from virtually every mammalian tissue. Numerous Cl^- channel sequences have now been determined and have been implicated in various physiological functions from neuronal membrane excitability to epithelial solute transport (for a review, see Fong and Jentsch, 1995). More Cl^- channels having even greater diversity and function will undoubtedly be uncovered in the future.

BIBLIOGRAPHY

Agnew, W. S., Levinson, S. R., Brabson, J. S., & Raftery, M. A. (1978). Purification of the tetrodotoxin-binding component associated with the voltage-sensitive sodium channel from Electrophorus electricus electroplax membranes. *Proc Natl Acad Sci USA, 75*, 2606–2610.

Bauer, C. K., Steinmeyer, K., Schwartz, J. R., & Jentsch, T. J. (1991). Completely functional double-barreled chloride channel expressed from a single Torpedo cDNA. *Proc Natl Acad Sci USA, 88*, 11052–11056.

Bennett, M. V. L. (1971). Electric organs. In W. S. Hoar, & D. J. Randall (Eds.), *Fish Physiology* (pp. 347–491). New York: Academic Press.

Bennett, M. V. L., & Sandri, C. (1989). The electromotor system of the electric eel investigated with horseradish peroxidase as a retrograde tracer. *Brain Res, 488*, 22–30.

Biesecker, G. (1973). Molecular properties of the cholinergic receptor purified from *Electrophorus electricus*. *Biochemistry, 12*, 4403–4409.

Bryant, S. H., & Morales-Aguilera, A. (1971). Chloride conductance of normal and myotonic goat fibres and the action of monocarboxylic aromatic acids. *J Physiol (London), 219*, 367–382.

Chang, H. W. (1974). Purification and characterization of acetylcho-line receptor-I from *Electrophorus electricus*. *Proc Natl Acad Sci USA, 71*, 2113–2117.

Childers, S. R., & Siegel, F. L. (1975). Isolation and purification of a calcium-binding protein from electroplax of *Electrophorus electricus*. *Biochim Biophys Acta, 455*, 99–108.

Claudio, T., Ballivet, M., Patrick, J., & Heinemann, S. (1983). Nucleotide and deduced amino acid sequences of *Torpedo californica* acetylcholine receptor γ subunit. *Proc Natl Acad Sci USA, 80*, 1111–1115.

Emerick, M. C., Shenkel, S., & Agnew, W. S. (1993). Regulation of the eel electroplax Na channel and phosphorylation of residues on amino- and carboxyl-terminal domains by cAMP-dependent protein kinase. *Biochemistry, 32*, 9435–9444.

Fong, P., & Jentsch, T. J. (1995). Molecular basis of epithelial Cl channels. *J Memb Biol, 144*, 189–197.

Grundfest, H. (1957). The mechanisms of discharge of the electric organs in relation to general and comparative electrophysiology. *Prog Biophys, 7*, 3–74.

Grundfest, H. (1960). Electric organ. *McGraw-Hill Encycl Sci Technol, 8*, 427–433.

Hille, B. (Ed.). (1992). *Ionic Channels of Excitable Membranes*. Sunderland: Sinauer Associates.

Jentsch, T. J., Steinmeyer, K., & Schwarz, G. (1990). Primary structure of *Torpedo marmorata* chloride channel isolated by expression cloning in *Xenopus* oocytes. *Nature, 348*, 510–514.

Karlin, A., & Cowburn, D. (1973). The affinity-labeling of partially purified acetylcholine receptor from electric tissue of *Electrophorus*. *Proc Natl Acad Sci USA, 70*, 3636–3640.

Keynes, R. D. (1961). The development of the electric organ in Electrophorus electricus. In C. Chagas, & A. Paes De Carvalho (Eds.), *Bioelectrogenesis* (pp. 14–19). New York: Elsevier.

Lester, H. (1978). Analysis of sodium and potassium redistribution during sustained permeability increases at the innervated face of *Electrophorus* electroplaques. *J Gen Physiol, 72*, 847–862.

Lingrel, J. B., & Kuntzweiler, T. (1994). Na^+, K^+-ATPase. *J Biol Chem, 269*, 19659–19662.

Middleton, R. E., Pheasant, D. J., & Miller, C. (1994). Purification, reconstitution, and subunit composition of a voltage-gated chloride channel from *Torpedo* electroplax. *Biochemistry, 33*, 13189–13198.

Millard, C. B., & Broomfield, C. A. (1995). Anticholinesterases: medical applications of neurochemical principles. *J Neurochem, 64*, 1909–1918.

Miller, C., & White, M. M. (1980). A voltage-dependent chloride conductance channel from *Torpedo* electroplax membrane. *Ann NY Acad Sci, 80*, 534–551.

Miller, J. A., Agnew, W. S., & Levinson, S. R. (1983). Principal glycopeptide of the tetrodotoxin/saxitoxin binding protein from *Electrophorus electricus*: isolation and partial chemical and physical characterization. *Biochemistry, 22*, 462–470.

Mishina, M., Kurosaki, T., Tobimatsu, T., et al. (1984). Expression of functional acetylcholine receptor from cloned cDNAs. *Nature, 307*, 604–608.

Munjaal, R. P., Conner, C. G., Turner, R., & Dedman, J. R. (1986). Eel electric organ: hyperexpressing calmodulin system. *Molec Cell Biol, 6*, 950–954.

Nakamura, Y., Nakajima, S., & Grundfest, H. (1965). Analysis of spike electrogenesis and depolarizing K inactivation in electroplaques of *Electrophorus electricus*. *L. J Gen Physiol, 49*, 321–349.

Noda, M., Shimizu, S., Tanabe, T., et al. (1984). Primary structure of *Electrophorus electricus* sodium channel deduced from cDNA sequence. *Nature, 312*, 121–127.

Noda, M., Takahashi, H., Tanabe, T., et al. (1982). Primary structure of α-subunit precursor of *Torpedo californica* acetylcholine receptor deduced from cDNA sequence. *Nature, 299*, 793–797.

Noda, M., Takahashi, H., Tanabe, T., et al. (1983a). Structural homology of *Torpedo californica* acetylcholine receptor subunits. *Nature, 302*, 528–532.

Noda, M., Takahashi, H., Tanabe, T., et al. (1983b). Primary structures of β- and δ-subunit precursors of *Torpedo californica* acetylcholine receptor deduced from cDNA sequences. *Nature, 301*, 251–255.

Olsen, R. W., Meunier, J.-C., & Changeux, J.-P. (1972). Progress in the purification of the cholinergic receptor protein from *Electrophorus electricus* by affinity chromatography. *FEBS Lett, 28*, 96–100.

Pallotta, B. S., & Webb, G. D. (1980). The effects of external Ca^{++} and Mg^{++} on the voltage sensitivity of desensitization in *Electrophorus* electroplaques. *J Gen Physiol, 75*, 693–708.

Parker, K. K., Chan, S. L., & Trevor, A. J. (1978). Purification of native forms of eel acetylcholinesterase: active site determination. *Arch Biochem Biophys, 187*, 322–327.

Pasquale, E. B., Udgaonkar, J. B., & Hess, G. P. (1986). Single-channel current recording of acetylcholine receptors in electroplax isolated from the *Electrophorus electricus* main and Sachs' electric organs. *J Memb Biol, 93*, 195–204.

Ratman, M., Sargent, P. B., Sarin, V., et al. (1986). Location of antigenic determinants on primary sequences of subunits of nicotinic acetylcholine receptor by peptide mapping. *Biochemistry, 25*, 2621–2632.

Schoffeniels, E. (1961). The flux of cations in the single isolated electroplax of Electrophorus electricus (L.). In C. Chagas, & A. Paes De Carvalho (Eds.), *Bioelectrogenesis* (pp. 147–165). New York: Elsevier.

Shenkel, S., & Bezanilla, F. (1991). Patch recordings from the electrocytes of *Electrophorus*. Na channel gating currents. *J Gen Physiol, 98*, 465–478.

Shenkel, S., & Sigworth, F. J. (1991). Patch recordings from the electrocytes of *Electrophorus electricus*. Na currents and P_{Na}/P_K variability. *J Gen Physiol, 97*, 1013–1041.

Sheridan, R. E., & Lester, H. A. (1977). Rates and equilibria at the acetylcholine receptor of *Electrophorus* electroplaques. A study of neurally evoked postsynaptic currents and of voltage-jump relaxations. *J Gen Physiol, 70*, 187–219.

Sperelakis, N. (1979). Origin of the cardiac resting potential. In R. M. Berne, & N. Sperelakis (Eds.), *Handbook of Physiology, Vol. 1, The Cardiovascular System* (pp. 187–267). Bethesda: American Physiological Society.

Steinmeyer, K., Klocke, R., Ortland, C., et al. (1991a). Inactivation of muscle chloride channel by transposon insertion in myotonic mice. *Nature, 454*, 304–308.

Steinmeyer, K., Ortland, C., & Jentsch, T. J. (1991b). Primary structure and functional expression of a developmentally regulated skeletal muscle chloride channel. *Nature, 354*, 301–304.

Sussman., J. L., Harel, M., Frolow, F., et al. (1991). Atomic structure of acetylcholinesteras, from *Torpedo californica*: a prototypic acetylcholine-binding protein. *Science, 253*, 872–879.

Szabo, T. H. (1961). Anatomo-physiologie des centres nerveux specifiques de quelques organes electriques. In C. Chagas, & A. Paes De Carvalho (Eds.), *Bioelectrogenesis* (pp. 185–201). New York: Elsevier.

Walsh, J. (1775). Experiments and observations on the *Gymnotus electricus*, or electric eel. *Philos Trans, 65*, 94–101.

Yoda., A., Clark, A. W., & Yoda, S. (1984). Reconstitution of (Na^+ + K^+)-ATPase proteoliposomes having the same turnover rate as the membraneous enzyme. *Biochim Biophys Acta, 778*, 332–340.

Section VII

Protozoa and Bacteria

Chapter 49

Physiological Adaptations of Protists

Michael Levandowsky

Chapter Outline

I. INTRODUCTION: TERMINOLOGY AND PHYLOGENY

This chapter introduces the reader to the great diversity to be found in the physiology of the protists. These include many eukaryotic groups, some *autotrophic* or plant-like, some *phagotrophic* or *osmotrophic* and thus animal-like and many with a combination of these traits.

First, a word about terminology and classification. Traditionally, these organisms comprised the *algae* (plant-like) and the *protozoa* (animal-like). Early classifications of protozoa divided them into three groups based mainly on locomotion (*ciliates*, *flagellates*, *amoebae*) and a fourth, parasitic group (*sporozoa*). The algae were classified largely on the basis of pigments (*red algae*, *brown algae*, *golden-brown algae*, *green algae*) and certain distinctive structural features (*cryptophytes*, *dinoflagellates*). Many of the flagellated groups appeared in both classifications and were studied by both botanists and zoologists. All these characteristics are clearly important and the early classifications and terminology tend to persist in informal usage. However, subsequent work with the electron microscope, biochemical advances and, especially, molecular approaches, have

Cell Physiology Sourcebook. DOI: 10.1016/B978-0-12-387738-3.00049-4

changed many of our views on phylogenetic relationships. In this chapter, the term *Protista*, or simply *protists*, will be used to describe all of these groups. Essentially, the protists include all eukaryotic organisms except higher plants, fungi and animals. Most protists are single celled and microscopic, but some, like many of the red algae and the brown algae, are multicellular and macroscopic.

Since the last edition of this Sourcebook, our ideas about classification and phylogeny of the major groups of protists have undergone fundamental changes with the appearance of new molecular data. A decade and a half ago there was a strong general consensus that the earliest eukaryotic cells lacked mitochondria and that this early stage was still represented by certain anaerobic or microaerophilic "amitochondriate" protists, such as the parasites *Entamoeba, Trichomonas* and *Giardia*. Since then, however, it has been found that the "amitochondriate" groups retain some mitochondrial genes and the consensus now is that the earliest eukaryotes had mitochondria, derived from a bacterial endosymbiont, and that, in a number of anaerobic or microaerophilic lineages, the mitochondria have evolved to become hydrogenosomes or mitosomes, organelles with very different roles from the typical mirochondrion.

At present, a number of major groups or divisions of protists have been defined by various authors and, in 2005, an attempt at synthesis was made, bringing together a group of 28 experts to define the major groups of protists and other eukaryotes. The result of this was the definition of six major groups of eukaryotes, as follows (Adl et al., 2005):

1. *Amoebozoa*. Amoeboid cells. Includes many free-living and parasitic amoebas, as well as slime molds. Examples: *Acanthamoeba, Entamoeba, Dictyostelium*.
2. *Opisthokonta*. A large group that includes the fungi, the choanoflagellates and the metazoa.
3. *Rhizaria*. Most of these organisms are also amoeboid. Includes many ecologically important groups, such as the foraminifera and the radiolaria.
4. *Archaeoplastida*. These are photosynthetic, plastid-containing eukaryotes and include the red algae, the green algae and higher plants.
5. *Chromalveolata*. This is a composite group, certainly not monophyletic, and some experts would separate it into four distinct groups. The first of these would be the *alveolates*, which contains ciliates, such as *Paramecium* and *Tetrahymena*, the apicomplexa, such as the malaria parasite *Plasmodium* and the dinoflagellates, prominent in aquatic food chains and responsible for toxic "red tides" in the ocean. The second group would be the *stramenopiles*, which includes a wide variety of subgroups, many of them photosynthetic, such as the diatoms and the brown algae. The third and fourth groups would be the *haptophytes* and the *cryptophytes*, which also contain many photosynthetic species.
6. *Excavata*. This group is also composite, not monophyletic. It includes important parasites, such as the trypanosomes that cause African sleeping sickness, and also many free-living organisms, such as *Euglena*.

It is proposed that these groupings can be considered kingdoms. To explore this higher level classification in more detail on line, an interactive and dynamic Java applet is available (Wolf et al., 2006).

The six major categories give some idea of the great diversity of protists. They should be viewed as provisional, however, reflecting current data and analysis (Cavalier-Smith, 2004, 2009; Simpson and Patterson, 2006; Patterson et al., 2007; Keeling, 2009; Pawlowski and Burki, 2009). There are many protist species classified as *incertae sedis*, meaning that their phylogenetic affinities are unclear. Current studies of DNA extracts from field samples are finding evidence of many uncultured species and, in most cases, we have little or no idea about their morphology, physiology or ecology. Several groups comparable to the six above were proposed on the basis of environmental DNA samples alone (Dawson and Pace, 2003; Stoeck and Epstein, 2003), but these proposals were strongly criticized on technical grounds (Cavalier-Smith, 2004). More recently, an entire new group of uncultured plastid DNA-bearing protists, named the *Rappedomonads* and possibly comparable to the six groups above, has recently been identified solely on the basis of DNA extracts from field samples (*metagenomic data*) (Kim et al., 2011). We don't know what they look like but, since they have plastid DNA, they may be photosynthetic. A useful collection of articles on genomic approaches to the study of protistan evolution is found in a recent volume (Katz and Bhattacharya, 2006).

The phylogenetic diversity of the protists is mirrored by their ecological diversity. While, in general, they are typical eukaryotic cells and follow the principles described elsewhere in this book, a number of evolutionary solutions have appeared in protists that are not present in the cells of multicellular organisms. An example is the *light antenna* or "eyespot" (described below), present in many photoautotrophic flagellates. This structure, which has evolved independently in several protist groups, is not found in the multicellular animals and plants.

A feature of protists just starting to be appreciated is the apparent ease with which many cells "capture" and use physiological units of other cells. A prime example is the sequestration and use of *prey organelles*, such as *chloroplasts*, by phagotrophic protists. Indeed, the incorporation of symbionts is a pervasive feature of protistan physiology, occurring in most if not all groups. There are a variety of endosymbiotic phenomena, ranging from the temporary uptake, endocytosis and use of foreign cells or organelles, to established symbioses in which the endosymbiont has become a permanent, required part of the host cell.

A dramatic example of this was the appearance of an intracellular bacterial infection in a laboratory culture of *Amoeba*. The infecting bacterium, initially deleterious to the host cell, was transformed from an *endoparasite* to an obligate *endosymbiont* over the course of a few years' culture in the laboratory and the host and its endosymbiont are now mutually dependent (Jeon, 1987, 1995). This nearly universal tendency of protists to form temporary or permanent endosymbiotic complexes is a feature that physiologists have come to expect and a major theme of this chapter. Indeed, if one considers plastids and other organelles, it is clear that many of the groups listed above as separate are also linked by past endosymbiotic events. Thus, some (but not all) of the dinoflagellates are photosynthetic and it has become clear that their chloroplasts were obtained endosymbiotically from several other protistan sources. Euglenids, on the other hand, though distantly related to the dinoflagellates, apparently got their chloroplasts endosymbiotically from a different, green algal source. These and other complexities of protistan evolutionary relationships do not appear in simple branching "family tree" diagrams.

Also included in this chapter are descriptions of some striking protistan structures whose functions are not clear, such as the several types of *extrusomes*, microprojectiles that are found in many protistan groups. The functions of these are, in most cases, still a matter of speculation.

A comprehensive review of protistan physiology is not presented, because that would duplicate much of the treatment of basic cell physiology in other chapters. Rather, the focus is on unique or unusual features that have evolved in this group and are not found in the cells of multicellular organisms. These features are adaptations to the various free-living and parasitic niches filled by this very diverse group of organisms. In particular, emphasis is given here to understudied phenomena.

II. BIOPHYSICAL CONSTRAINTS OF SCALE: THE EXAMPLE OF FILTER-FEEDING

The dimensions of most protists and their appendages, the values of relative velocity in water and the viscosity of water all combine to yield *Reynolds numbers*[1] much smaller than one. Thus, inertial forces are generally completely excluded as a factor in protistan biophysics. As an illustration of the practical implications of this, *filter-feeding* in flagellates and ciliates is examined. This has been worked out theoretically and experimentally by Fenchel (1986a,b) for a number of species and his discussion is followed here. Filter-feeding at low Reynolds number has also been studied extensively experimentally and theoretically by Koehl and her colleagues, but mainly in the context of small metazoa, such as copepods (e.g. Cheer and Koehl, 1987; Childress et al., 1987).

Filter-feeding is widespread among protists that consume bacteria, other protists or other particles. Suspended food particles may be "captured" passively by diffusion, where the particle reaches the protist by chance, through Brownian motion or swimming, and sticks to an adhesive surface. This happens with many protistan cells with amoeboid tentacles (e.g. heliozoa). Particles may be caught raptorially by direct interception and ingestion during active swimming (many dinoflagellates, euglenids, ciliates). Finally, they may be obtained by filtering a current of water, which is often produced by the protist. This latter method is examined here.

Following Fenchel, let $U(x)$ be an *uptake function*, where x is the particle concentration. *Clearance*, F, is defined as the volume of water cleared per unit time. The relation between these two quantities is given by $F = U(x)/x$, where U is assumed to be nearly proportional to x at low particle concentrations, but becomes saturated at high concentrations. It is assumed that the rate of retention of particles by the filter is proportional to concentration and that ingestion of retained particles takes a finite time, t, during which no other particles are ingested. These assumptions lead to a hyperbolic equation:

$$U(x) = F_m x(1 - Ut) \tag{49.1}$$

Substituting variables and rearranging yields the equation:

$$U(x) = U_m x/(U_m/F_m + x) \tag{49.2}$$

where $U_m = 1/t$ (the maximum rate of ingestion as $x \rightarrow \infty$), F_m is the maximum clearance realized as $x \rightarrow 0$ and U_m/F_m is a constant (dimension L^{-3}). From Equation 49.2, we can see that the kinetics of filter-feeding is formally identical to the familiar Michaelis–Menten kinetics of enzymology, with the constant U_m/F_m corresponding to the half-saturation constant.

Equation 49.2 has been verified experimentally for protistan uptake of latex particles and of bacterial food and F_m varies greatly with the particle size (Fig. 49.1). When the size for which F_m is maximal is determined experimentally, that size is assumed to be retained with an efficiency approaching 100%; thus, that value of F_m can be taken as a direct measure of the rate of flow of water through the filter. This can then be compared for different flow fields of water and for different species' filter designs.

To understand the biological significance of clearance, it is useful to express it as volume-specific clearance, i.e.:

$$F_m/(\text{cellvolume})$$

[1] Reynolds number is defined as $R = dv/n$, where d is a spatial dimension, v is velocity, and n is the kinematic viscosity. Essentially, it can be thought of as the ratio of inertial to viscous forces acting on a body moving through a fluid. Thus, for a large, fast-moving organism in water, such as a fish, the ratio is much greater than one and inertial forces dominate. For microbes, on the other hand, the ratio is usually much less than one and they live in a world dominated by viscous forces.

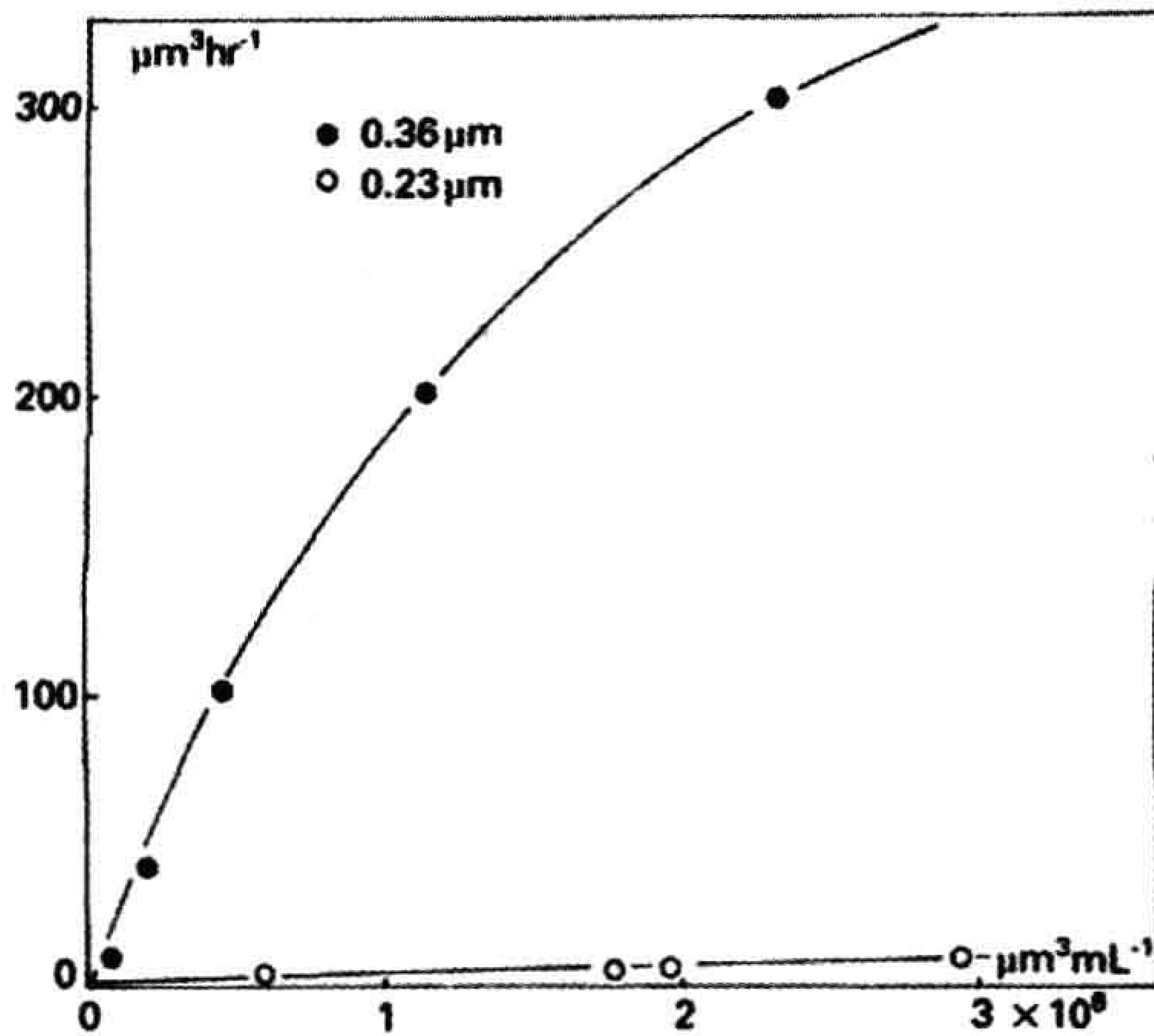


FIGURE 49.1 Volume uptake of two sizes of latex beads as functions of environmental concentration by *Cyclidium* and with the data fitted to Equation 49.2. *(Adapted with permission from Fenchel, 1986a,b.)*

As an example of the application of this theory, consider a situation in which the volume fraction of bacteria in a seawater sample is 10^{-6} (e.g. 2×10^6 cells/mL $\times$ 0.5 μm^3 cell volume). A typical heterotrophic flagellate with a specific clearance of 105/h (it filters 105 times its volume of water per hour) will need 10 h to ingest its own volume of bacteria. With a 50% growth efficiency, it would thus be able to divide every 20 h. Growth efficiency, or yield, of protists is nearly invariant over a large range of growth rates (Fenchel, 1986a, b). For balanced (i.e. log phase) growth:

$$u(x) = U(x)\ Y \tag{49.3}$$

where $u(x)$ is the instantaneous growth rate at a food concentration x and Y is a yield constant. Thus, and as verified experimentally, $u(x)$ and $U(x)$ have similar functional forms, so that growth data can be used to estimate clearance.

Fenchel (1986b) also investigated the flow field generated by various filter-feeding flagellates and ciliates both theoretically and empirically. It is here that the assumption of low Reynolds number is used in calculating the theoretical flow field produced in the medium relative to the cell by ciliary motion. An example is shown in Fig. 49.2, where the predicted theoretical flow field is compared to the observed paths of suspended particles through the filter

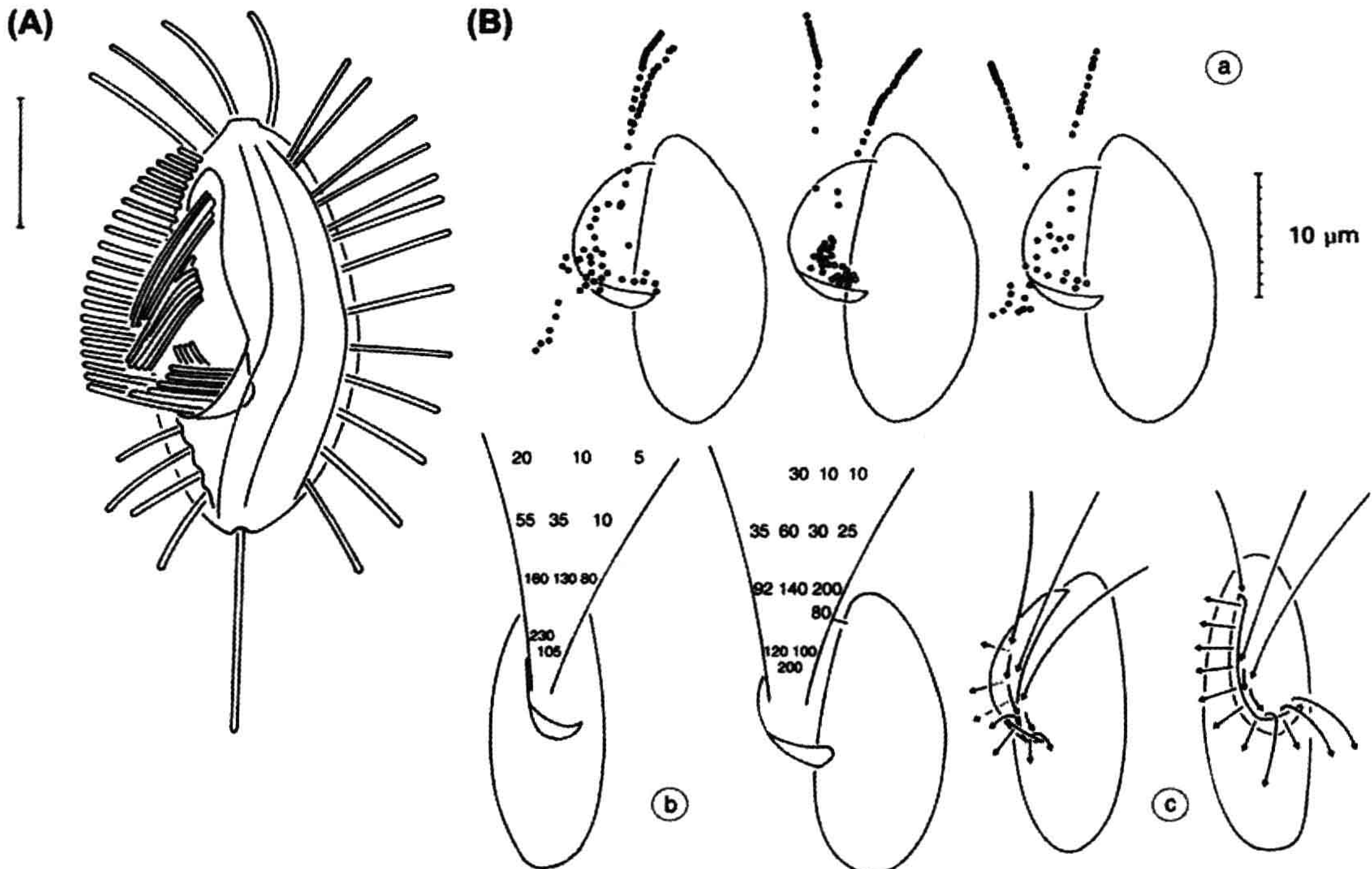


FIGURE 49.2 (A) Diagrammatic rendition of *Cyclidium*, showing filtration apparatus. Bar is 5 µm. (B) a. Position of 1.1-µm latex particles at 0.02-s intervals along six flow lines during fitration by *Cyclidium*. b. Schematic presentation of the critical flow lines and approximate velocities (µm/s). c. Schematic presentation of the flow lines. *(Reprinted with permission from Fenchel, 1986a.)*

apparatus of a ciliate. From these flow lines, one can see that a larger volume is sampled than might be expected simply from the area of the filter itself.

It should be noted that, as Cheer and Koehl (1987) noted in the case of filter feeding copepods and other metazoa, at very small Reynolds numbers the rows of cilia act more as paddles than as rakes. Thus, the picture of flow lines passing through a row of closely spaced cilia, as in Fenchel's picture, as well as the detailed mechanism of prey capture needs to be revisited and modified. Rather than straining the prey from the water, as we would do at high Reynolds number using, say a net, the low Reynolds number filter feeders may instead have to ingest a small blob of fluid that contains the prey.

III. NUTRITION AND EXCRETION

IIIA. Endocytosis, Digestion and Defecation

As with other cells, protists take in nutrients and other materials by a variety of passive and active mechanisms. Of particular interest here are specialized processes of phagocytosis and digestion not found elsewhere. Many ciliates and some flagellates have complex feeding structures. The best known case is *Paramecium*, the subject of many studies by Allen and Fok (Allen, 1984; Fok and Allen, 1990). This cell has a fixed cytopharynx (or buccal cavity), a tube-shaped cavity where food particles are taken in. At the end of this is the cytostome where the food vacuoles (FV) (also phagosomes, or digestive vacuoles) are formed. The cytostomal membrane, which pinches off to form the FV, is distinct from the cell membrane antigenically and in structure. During formation of the FV, it grows by fusion with disk-shaped vesicles, which are transported to it along microtubular ribbons. The movement is thought to be due to cytoplasmic dynein in a microtubule-based motor. The vesicles are essentially recycled membrane from earlier FVs, returning to the cytostome by a defined path.

After forming, the FV follows a defined path through the cytoplasm. As it progresses, vesicles called acidosomes also move along the cytopharyngeal microtubular ribbons and fuse with the vacuole just after it pinches off, lowering the pH of its interior. Whether the acidosomes are filled with acid or simply deliver proton pumps is not resolved yet. The low pH kills the prey and favors the activity of digestive enzymes. The release of the FV from the cytostome and its subsequent movement involve actin. As the acidosomes fuse with it, the original membrane of the FV pinches off to form small vesicles that recycle back to the cytostome, so that the FV is totally reconstituted. Next, lysosomes migrate from the Golgi apparatus and fuse synchronously with the FV, bringing acid hydrolases, including acid phosphatase. The membrane may be completely replaced again at this stage. Digestion takes about 20 m. At the end of this phase, vesicles form and are pinched off from the FV, probably to be used again in lysosomes. The remaining FV membrane binds to microtubules that guide it to the *cytoproct*, or *cytopyge*, where the FV membrane fuses with the cell membrane to form a pore. Its contents (undigested residue) are then egested (*defecation*) and the FV collapses. The cytoproct (cytopyge) is a specific location where the *plasmalemma*, a layer containing infraciliature and other structures, has a gap allowing the food vacuole to reach the cell membrane and fuse with it. After defecation, the membrane is recycled in discoidal vesicles to the cytostome, completing the cycle. This last step appears to involve an actin-based system that may be calcium regulated.

IIIB. The Contractile Vacuole

Protists without cell walls that live in hypotonic media (freshwater species) have *contractile vacuoles* (CV), which periodically excrete fluid. In the best-studied case, the ciliate *Paramecium*, this consists of a central vacuole, a surrounding complex of *ampullae* and a network, or *spongiome*, of tubules (Fig. 49.3). Certain tubules in this complex are decorated with peg-like elements that are vacuolar-type proton pumps. These are found in both the cellular slime mold *Dictyostelium* and the ciliate *Paramecium* (Heuser et al., 1993; Allen, 1997).

Excretion occurs through a cycle. During *diastole*, the vacuole forms and grows by the fusion of smooth-membrane vesicles. During this period, fluid travels from the spongiome to the CV. In *systole*, the vacuole membrane fuses with the cell membrane at one site to form a pore and

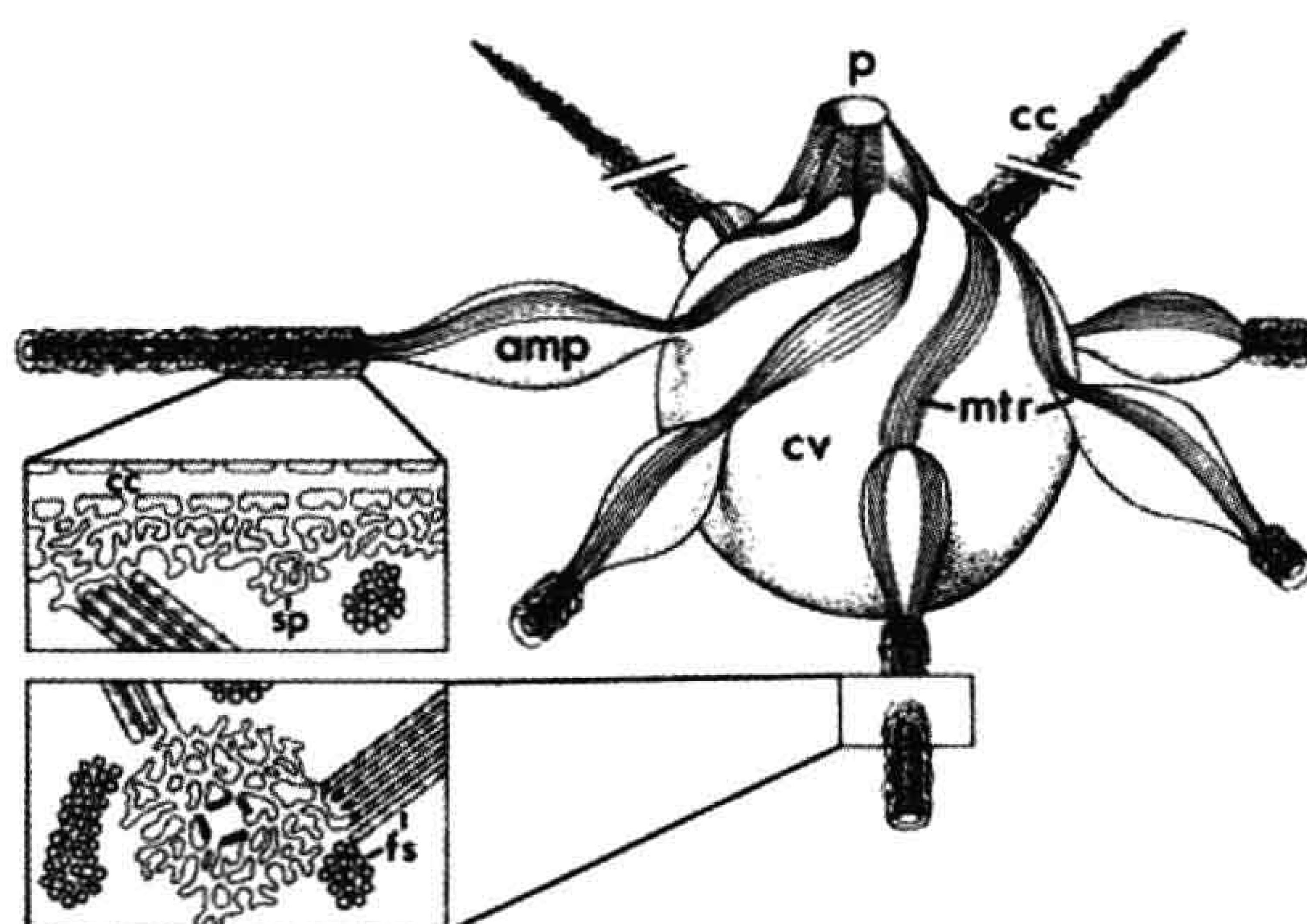


FIGURE 49.3 Contractile vacuole complex in *Paramecium*, showing ampullae (amp), collecting canal (cc), contractile vacuole (cv), pore (pv), spongiomal tubules (sp), fluid segregation organelles (fs) and microtubular ribbons (mtr). *(Adapted with permission from Hausmann and Hülsmann, 1996.)*

the fluid is excreted. As this happens, the vacuole contracts as its membrane fragments and forms vesicles again. Actin has not been detected near the CV and contraction is thought to be due to cellular pressure after the appearance of the pore opening to the exterior. At one time it was thought that the connections of the CV to the spongiome were interrupted during systole, preventing backflow. Recent work, however, indicates that the connections persist throughout the cycle. The narrowness of the tubular connections presents great resistance, so that considerable pressure would be required for a rapid backflow during systole.

A major function of the CV is clearly osmoregulation. The cycle ceases in cells placed in a hypertonic medium, resuming after a time when the cell adapts and increases internal tonicity. Fluid in the CV is high in K^+ and Na^+, relative to the cytoplasm, also suggesting a role in maintenance of ionic balance.

IV. ENERGETIC ADAPTATIONS: MITOCHONDRIA AND THEIR RELATIVES

As noted above in the introduction, evolutionary protistologists now consider the mitochondrion to have entered the eukaryotes at their origin as an endosymbiotic bacterium. Since a major function of the mitochondrion is oxidative metabolism, this suggests that the earliest eukaryotes were aerobes and would appear to have implications regarding conditions on the planet at that time. In any case, today, we find many parasitic and free-living protists inhabiting anaerobic and microaerophilic habitats, where oxidative metabolism is not useful. What appears to have happened, several times independently (convergently), is that the early mitochondrion has evolved into fermentative organelles, hydrogenosomes, which generate ATP anaerobically by metabolizing pyruvate to molecular hydrogen, carbon dioxide and acetate (Müller 1993). The mitosome, also a degenerate mitochondrion, occurs in some anaerobes, but its function is not yet clear (van der Giezen et al., 2005; Tachezy, 2008).

Another fermentative microbody, the glycosome, descended evolutionarily from the peroxisome, appears in trypanosomes and generates ATP by the glycolytic pathway under microaerophilic conditions (Parsons, 2004; Tachezy, 2008).

V. SENSORY ADAPTATIONS, MEMBRANE POTENTIALS AND ION CHANNELS

Like other cells, protists exhibit sensitivity and respond in various ways to environmental stimuli. The basic physiological and biochemical mechanisms, as far as they are known, are similar to those found in metazoan systems. *Paramecium,* for example, has been referred to informally as a "swimming neuron". In this section, several examples of photoreceptors and gravireceptors are examined and then the transduction mechanisms underlying the sensory responses are discussed.

VA. Photoreceptors

Ambient light can be a source of energy to autotrophic protists but, in addition, for motile species, it can serve as a directional signal. Many flagellates, and probably all the motile photosynthetic species, exhibit a positive phototaxis. For this purpose a directional receptor is needed. Directional receptors, or "eyespots", fall into two main categories: (1) receptors with opaque screens, which detect direction by the screen's shadow; and (2) receptors with *antennae* based on interference and diffraction to detect direction, essentially the same optical principle as that seen in a reflection hologram, or in structural color. In addition to these directional detectors, one group of predatory dinoflagellates has developed a system of *ocelloids* with intracellular lenses. In this section, we discuss the antennae and the ocelloids, two unique but understudied systems.

VA1. Receptors with Light Antennae

The interferometric *light antenna* is found in a phylogenetically diverse array of flagellates, including many genera of green algae, dinoflagellates and cryptophytes (Foster and Smyth, 1980; Melkonian and Robenek, 1984; Smyth et al., 1988). In the cases where experiments have been done, these antennae appear to be selective with regard to wavelength and light direction. The presence of essentially similar organelles in a wide array of groups considered on many other grounds, including molecular homology, to be phylogenetically diverse raises a question: are these all cases of convergent evolution? If not, have these organelles spread through endosymbiotic events?

The antennae operate through an interference mechanism similar to that which produces structural color in iridescent objects. The essential structure consists of a number of parallel reflective layers that act as partial mirrors. These are spaced evenly, separated by a distance of a quarter of the wavelength to be selected. Thus, incident light passes through a series of partially reflecting pigment layers spaced at quarter-wavelength intervals. Normally, incident light of the appropriate wavelength is reflected back at each partial mirror. These reflected light rays are in phase with each other and with the incoming radiation, leading to positive reinforcement of this light signal in front of the eyespot, where the receptor pigment is located. Light from other angles, and light of other wavelengths, also passes through this filter, but the reflections are out of phase with each other and the resultant interference minimizes their contribution. The basic principle is the same as that which produces structural color in iridescent feathers of

some birds and the wings of certain tropical butterflies and which is used in reflection (or Denisyuk) holograms.

The most intensive studies of light antennae were done with the green flagellate *Chlamydomonas* (Foster and Smyth, 1980), but the antennae are also found in dinoflagellates, chrysophytes and many other light-responsive flagellates.

VA2. Intracellular Lenses in Dinoflagellates

Perhaps the most complex and surprising photoreceptors are the ocelloids (ocelli), eyespots found in a family of non-photosynthetic dinoflagellates, the Warnowiaceae. A typical ocelloid consists of a lens, a retinoid and an opaque pigment cup (Fig. 49.4). The pigment cup, or *melanosome*, consists of a wall of pigment granules and it surrounds the paracrystalline *retinoid*. In front of this is the lens, or *hyalosome*, consisting of a peripheral corneal zone and a central crystalloid body. The entire organelle is approximately 24 μm long and 15 μm wide (Greuet, 1978, 1987).

Francis (1967) measured the refractive index of the lens in *Nematodinium* by three methods and found it to be approximately 1.52. He determined the focal plane by tracing rays parallel to the optic axis and found that light was focused in the retinoid layer. The field of view in these species was determined to be about 30° but may be wider in other species. From these observations, we conclude that the ocelloids could probably act as directional light receptors.

Given the presence of *nematocysts* (see Section VIC) in these same dinoflagellate species and the fact that they are predators rather than autotrophs, it has been suggested that the ocelloids might act as "range finders", leading to discharge of nematocysts when the contrast of the focused image on the retinoid is maximal. While certainly plausible, such behavior has not been reported yet. Unfortunately, these species have not been cultured and there appear to be no studies of ocelloid function, so that all we have at this time are speculations based on the structure.

VB. Gravity Receptors in Ciliates

Many single-celled organisms orient with respect to the earth's gravitational field while swimming. In some, such as the well-studied ciliate *Paramecium*, this is thought to be a purely hydrodynamic effect due to the shape and the distribution of mass in the cell: as the organism swims, the center of mass pulls the rear of the cell downward, orienting it so that it swims upward (Roberts, 1981). In this case, then, there seems to be no need for a gravity receptor. However, many protists can migrate either up or down, switching between a positive and a negative geotaxis in response to external signals or to a circadian or a tidal rhythm, suggesting a more complex type of response.

In particular, a group of ciliates containing the genera *Loxodes* and *Remanella* has a gravity response that depends

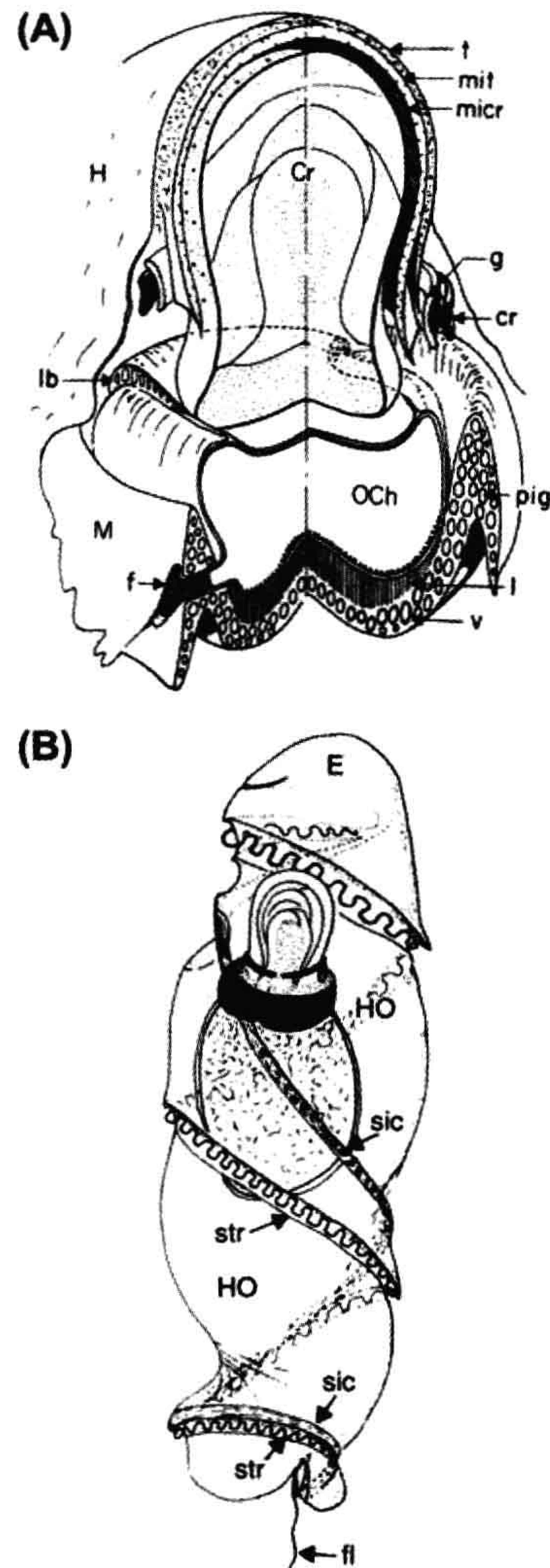


FIGURE 49.4 (A) Diagram of structure of *Nematodinium* ocellus, showing interior structure: crystalline body (Cr), ocelloid channel (f), constricting ring (cr), periocelloid gallery (g), hyalosome (H), lamellae of retinal body (1), microcrystalline layer (micr), mitochondrion (mit), ocelloid chamber (OCh), pigmentary ring (pig), basal plate (lb), micro-tubular layer (t), vesicular layer of the retinal body (v). Magnification: 3900×. (B) Position of ocellus in the *Nematodinium* cell, showing parts of the cell: episome (E), hyposome (HO), intercingular sulcus (sic), cingular sulcus with transverse flagellum (str), posterior flagellum (fl). *(From Greuet, 1978.)*

on the dissolved oxygen level. In nature, these ciliates collect at the interface between anaerobic and aerobic zones in the water column. In oxygen-containing water they swim downward, while in an anoxic environment they swim upward. They all contain a characteristic organelle, the

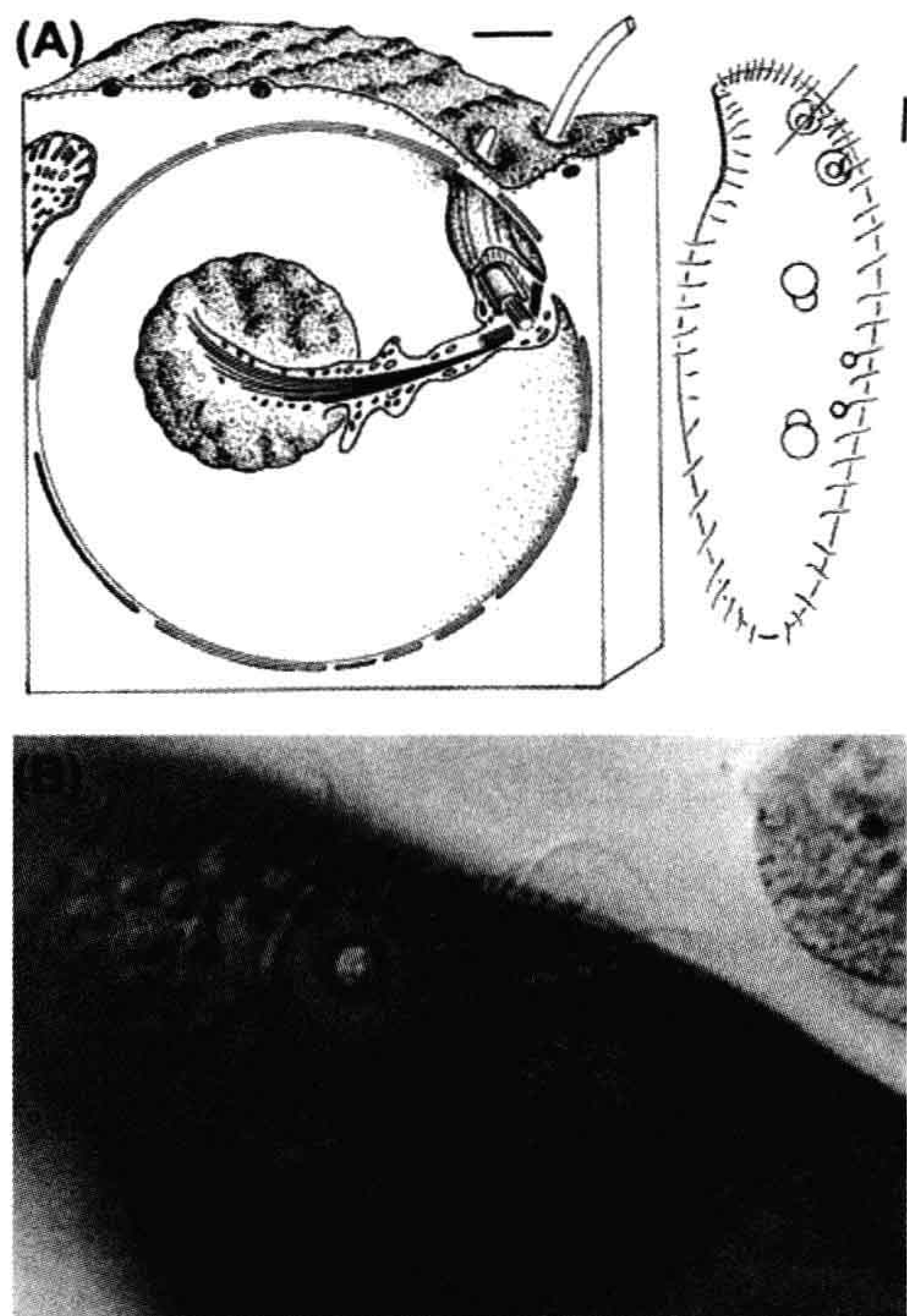


FIGURE 49.5 (A) Müller body, gravity receptor. Drawing showing position in *L. striatus* cell (scale bar: 10 μm) and a three-dimensional reconstruction from serial sections (scale bar: 1 μm). (B) Müller body in living cell of *L. striatus*. *(From Fenchel and Finlay, 1986.)*

Müller body, which acts as a gravity receptor. This is a fluid-filled vesicle in which a membrane-covered mineral body is suspended (Fig. 49.5). The mineral body, consisting of a strontium or barium salt, acts as a statolith, and its position on the interior surface of the vesicle appears to inform the cell of its orientation in the gravitational field (Fenchel and Finlay, 1986). The vesicle is anchored to the system of connected cilia of the cell and it is suggested, by analogy to other mechanoreceptors, that oriented mechanical stress on the cell membrane at this point of connection may lead to a depolarization which, in turn, would affect ciliary beating and determine the orientation of the swimming motion (Fenchel and Findlay, 1986) (see also Section VIII).

VC. Sensory Transduction: Membrane Potentials, Ion Channels and Intracellular Components

VC1. Membrane Potentials, Calcium and Behavior

As with many aspects of protistan physiology, membrane potentials are best known in the large ciliate *Paramecium*. A classic feature of ciliate behavior is the *avoidance reaction*, in which the cell stops, swims backward for a short time, then swims forward again, usually in a somewhat different direction. Early workers observed prolonged backward swimming in cells subjected to various stresses: high temperatures, sudden changes in pH or osmotic pressure, exposure to solvents and other deleterious chemicals. The common denominator in all these proved to be that the cell membrane became "leaky" or permeable to Ca^{2+} and other ions. Using the methods developed by Szent-Gyorgy and others for muscle tissues, *Paramecium* cells were exposed to detergents, such as Triton X-100, to render the cell membrane permeable. Such model extracted-cell preparations would swim forward if provided with ATP and Mg^{2+} in a medium containing $[Ca^{2+}] < 10^{-7}$ M. At higher Ca^{2+} concentrations, the cells swam backward (Naitoh and Kaneko, 1973).

Electrophysiological studies with intracellular electrodes in normal cells have given the following general picture: during forward swimming, a Ca^{2+}-dependent membrane potential is maintained. Appropriate mechanical, chemical or electrical stimuli cause an action potential in which calcium channels open in the membrane, causing depolarization and backward swimming. The membrane potential is restored by a calcium pump after a short time and forward swimming resumes. Cells are depolarized by repellents (stimuli that cause backward swimming) and hyperpolarized by attractants (stimuli that inhibit backward swimming).

VC2. Behavioral Mutants

Kung and his colleagues obtained a number of behavioral mutants in which swimming behavior could be correlated with abnormal electrophysiological properties of the *Paramecium* membrane. Examples include the following:

1. *Pawn* (several types), in which voltage-gated Ca^{2+} channels are affected, depolarization does not occur and the cell cannot swim backward.
2. *Pantophobiac*, where Ca^{2+}-dependent K^+ currents are affected and prolonged responses occur to all stimuli.
3. *Paranoiac* (several types), affecting Ca^{2+}-dependent Na^+ channels. Prolonged responses occur in Na^+ solutions.

Many other behavioral mutants are known (Saimi and Kung, 1987).

VC3. Ion Channel Types and Membrane Excitation

Electrophysiological and behavioral genetic studies have revealed eight distinct types of ion channels in *Paramecium* and at least three types of membrane excitation that govern

behavioral responses, as follows (Hinrichsen and Schultz, 1988):

1. Two mechanically induced currents: a depolarizing, Ca^{2+}-based current in the cell's anterior and a hyperpolarizing, K^+-based current in the posterior.
2. A rectifying K^+ current that can cause regenerating hyperpolarization during the action potential.
3. A second Ca^{2+}-dependent K^+ current, which may play a role in maintaining the resting potential.

VC4. Second Messengers and Transduction Pathways

Second messengers and internal biochemical events following mechanical or chemical stimuli have been the subject of study in various protists. In the case of the *Pantophobiac* mutants of *Paramecium*, for example, it was found that normal behavior could be restored by microinjection of wild-type calmodulin (CaM). This led to the discovery that these mutants were specific point mutations with amino acid substitutions at specific CaM sites. Further studies showed that the Ca^{2+}-CaM complex regulates calcium-dependent Na^+ channels by direct interaction and is also required for the functioning of K^+ channels. Work on responses to acetate and biotin in mutants with different defects in ion conductances, however, indicates that these two stimuli operate via different ion channels (Bell et al., 2007, Valentine et al., 2008).

Progress at this level has been greatest with the cellular slime mold *Dictyostelium discoideum*. In this organism, there appear to be several chemosensory transduction pathways, similar in general to those found in animal cells, such as leukocytes, but differing in some aspects (Van Haastert and Veltman, 2007). In both cases, the presence of multiple pathways introduces a complexity of potential response mechanisms and behavior (Iglesias and Devreotes, 2008).

VI. INCORPORATION OF PHYSIOLOGICAL UNITS FROM OTHER CELLS

Symbiotic relationships, including cellular endosymbiosis, are widespread in biology. In the protists, this tendency appears to be accentuated and many new physiological opportunities have been produced by endosymbiotic combinations. Thus, many protists have prokaryotic or eukaryotic endosymbionts. In some cases, these associations appear to be more or less permanent, as in the green ciliate *Paramecium bursaria*, which always has an algal *Chlorella* endosymbiont. Sometimes the association is more intimate and parts of another cell have been permanently incorporated into the host cell. There are also more transient associations, in which the host "cultures" and uses all or part of an ingested cell in its cytoplasm for a period of time. Examples of all of these possibilities are presented in this section.

VIA. Intracellular Capture and Culture of Foreign Organelles

Early reports of photosynthesis by certain natural populations of chlorophyll-containing ciliates suggested that these supposedly heterotrophic organisms might harbor algal symbionts. Electron microscopy, however, revealed that some ciliates contain isolated fragments of algal cells, which appear to be functional. The photosynthetic marine ciliate *Myrionecta rubrum* (formerly *Mesodinium rubrum*), which sometimes forms "red tides" (massive blooms that color the sea), contains endosymbiotic algal organelles in the form of chloroplast–mitochondrial complexes (Taylor et al., 1971). Other species of planktonic ciliates have been found to contain intact algal chloroplasts, pyrenoids and even eyespots. A significant proportion of the planktonic ciliates in marine habitats has been found to contain "captured" chloroplasts, which remain functional within the ciliate for extended periods, eventually being consumed by the host (Stoecker et al., 1987).

VIB. Xenosomes: Bacterial Endosymbionts

The term *xenosome* was used by Soldo (1987) to describe certain bodies in marine ciliates. These were later identified as endosymbiotic bacteria and Corliss (1985) suggested that the term be defined to include all DNA-containing, membrane-bound intracellular bodies or organisms. By this definition, mitochondria and chloroplasts would be included. In practice, however, the term has been used largely for bacterial endosymbionts of marine ciliates.

VIB1. Bacterial Endosymbionts in Ciliates

Some endosymbiotic bacteria, such as the *Kappa* and *Alpha* particles in *Paramecium* and the *Omicron* particles in Euplotes, are classical objects of study (Görtz 1996). More recently, there have been a number of studies by Soldo and colleagues of the xenosomes from marine ciliates (Soldo, 1987; Soldo et al., 1992). Originally found in the species *Parauronema acutum*, they are infective to 12 strains of this species and also to the phylogenetically distant species *Uronema marinum*, but not to strains from five other marine ciliate genera, or the freshwater genera *Paramecium* and *Tetrahymena*. They are toxic to some marine ciliates, such as *Uronema nigricans*, and the toxic effect is abolished by proteolytic enzymes.

These xenosomes contain DNA, RNA, proteins and lipids in amounts typical of small bacteria and are selectively destroyed by a number of antibiotics, including penicillin, ampicillin, tetracycline and chloramphenicol, but not neomycin or cycloheximide. They are small, Gram-negative

rods, present in numbers ranging from 100 to 200 per host cell and they divide in synchrony with the host. When released by gentle mechanical rupture of the host, they swim with darting motions or spin like propellers. They average two flagella per cell, inserted at random sites in the cell wall. Within the host cytoplasm, they have a fairly typical Gram-negative double outer membrane and single inner membrane, with a layer of peptidoglycan between these. They are not enclosed in vacuoles but contact the host cytoplasm directly.

Xenosome chromosomal DNA is multicopy, consisting of nine to 14 circularly permuted duplex molecules of about 515 kb (kilobase pairs). In addition, there are several plasmids. Analysis of restriction sites revealed that all the adenines of GATC sequences in the plasmids are methylated, whereas those in chromosomal sequences are not, suggesting that there are two replicons, one controlling chromosomal and the other plasmid replication.

Surprisingly, 30% of protein in xenosomes is from the host cell. This is, however, consistent with the relatively small genome. Assuming 1.3 kb of DNA is needed to encode a protein of average M_r 66 000, then the xenosome can encode fewer than 400 proteins, less than one-tenth the number for a typical free-living species such as *Escherichia coli*.

Xenosomes in vitro consume oxygen at a very low rate, comparable to that observed in Rickettsia and *Kappa* symbionts, and preferentially use succinate as an energy source. Symbiont-containing ciliates, on the other hand, consume oxygen at a rate 20–30% higher than symbiont-free ciliates and host glycogen is consumed at a significantly higher rate in the former than in the latter.

The affinities and origins of these organisms present an intriguing problem. Ribosomal RNA analysis of marine ciliate xenosomes indicates some homology to the μ and π xenosomes of *P. aurelia*, but little or no homology to known free-living species, suggesting that these endosymbionts may have a long history of association with ciliates (Soldo et al., 1992).

VIB2. Methanogenic Endosymbionts in Anaerobic Ciliates

Most of the free-living anaerobic ciliates examined have endosymbiotic and/or ectosymbiotic bacteria (Fenchel et al., 1977) and the role of some of the former have been studied in some detail. In particular, a number of species harbor methanogenic bacteria. In the cases where these have been investigated, the bacteria are intimately associated with a series of hydrogenosomes. The arrangement of bacteria and organelles has been compared to a stack of coins, with bacteria and hydrogenosomes alternating and the latter on the ends (Fig. 49.6). This complex is highly organized in some species and possibly a permanent feature of the host cell. In the ciliate *Plagiopyla frontata*, the bacteria divide synchronously with the host. The number of methanogens per host cell (about 3000) remains constant until a late stage in the host cell cycle, when it doubles. Thus, the ciliate apparently controls reproduction of the symbiont to maintain a stable population density.



FIGURE 49.6 Hydrogenosomes and methanogen symbionts in the ciliate *P. frontata*. The darker bodies are the hydrogenosomes and the lighter bodies are the symbionts. Magnification: 20 000×. *(From Fenchel and Finlay, 1991.)*

When the methanogen inhibitor 2-bromoethanesulfonic acid was used to inactivate the methanogenic symbionts of three ciliate species, *P. frontata*, *Metopus contortus* and *M. palaeoformus*, growth rate and yield were reduced in the first two species, but not in the last. It is suggested that the energetic advantage conferred by the symbiont in the first two species may be due to the secretion of organic material by the bacteria (Fenchel and Finlay, 1991). The advantage to the methanogens of consumption of H_2 and acetate from the adjacent hydrogenosomes seems clear. This could be a significant advantage, especially in marine or other sulfate-rich environments, where free-living methanogenic bacteria would compete with the more efficient sulfate-reducing bacteria for H_2.

VIB3. Bacterial Endosymbionts in Amoeba proteus

Many endosymbionts have been reported in large free-living amoebae, such as *Amoeba proteus* (Jeon, 1995). Particularly dramatic is the case of a bacterial endosymbiont that has been studied from its initial appearance as a contaminant in laboratory culture, through the co-evolution of host and endosymbiont, to a mutually dependent symbiotic

relationship (Jeon, 1987). The bacterium, which first appeared in the culture in 1966, is termed the *X-bacterium*. It infected a culture of the D strain of *A. proteus*, which already contained other symbiont-like particles of unknown origin. The X-bacterium is described as a Gram-negative rod, with an ultrastructure similar to *E. coli*, but is not otherwise identified taxonomically as yet. Initially, most of the infected amoebae died, but a few survived and the X-bacteria gradually lost virulence. The number of bacteria per amoeboid cell, originally greater than 100 000, stabilized at about 42 000. Within a few years, the host cell, now called the xD strain, became dependent on the presence of the endosymbiont. X-bacteria can be transferred into other D strain cells by microinjection or by induced phagocytosis. The bacteria are enclosed in host-generated vesicles, or *symbiosomes*, and when observed in freeze-fracture preparations are found to be embedded in a matrix of fibrous material. The symbiosomes do not fuse with lysosomes and, during infection, the X-bacteria seem to be somewhat resistant to lysozymes, since about 10% of them avoid digestion in the phagolysosomes. Two kinds of plasmids were found in X-bacteria and isolated X-bacteria treated with ethidium bromide or acridine orange for 3 h failed to infect amoebae.

Several molecules produced by the symbiont have been studied. One, the Xd29 protein, appears to be a peripheral membrane protein that is constantly shed into the host cytoplasm, passing readily through the symbiosome membrane. Symbiont-produced lipopolysaccharides (LPS) have also been identified and were shown by immunostaining to be present on the cytoplasmic side of the symbiosomes. Injected antibodies to the LPS abolished the fusion-avoiding properties of symbiosomes, causing them to fuse with lysosomes. A 96-kDa protein from the symbiont is also present on the symbiosome membrane and is suspected of playing a role in preventing lysosomal fusion. X-bacteria contain a large amount of 67-kDa heat-shock protein (HSP, GroEx) but, since there are no free-living X-bacteria cultures for comparison, it is not known whether this is an indication of stress. In other intracellular infective bacteria (e.g. *Legionella*), the GroEx protein in the intracellular bacteria is more than seven times greater than in free-living cells. The complete nucleotide sequence of the *GroEx* operon of the X-bacteria was determined and has a high degree of homology with those of other endoparasitic or symbiotic bacteria, such as *Legionella* and *Coxiella*, and further genomic study indicates that the organism should be considered a new species of *Legionella* (Park et al., 2004).

Some polypeptide bands detected by gel electrophoresis of the amoebae cytosol are no longer present after prolonged endosymbiosis. One protein that disappears after symbiosis is a SAMS (S-adenosyl-L-methionine synthetase). That is, the gene remains in the host genome but becomes inactive, while a gene in the symbiont replaces it and produces bacterial SAMS (Jeon and Jeon, 2003), which may be part of the explanation for the host cell's newly evolved dependance on the symbiont.

Clearly, the analysis of this evolving system is only beginning.

VII. STRUCTURES WITH UNKNOWN FUNCTIONS

Next, emphasizing the opportunities for future research, a number of more or less prominent structures are examined that are not understood at the basic level of function (though some have been the subject of interesting speculations).

VIIA. Rhoptries

A large group of medically important parasitic protists, the *Apicomplexa* (formerly the *Sporozoa*), is defined by a structure called the *apical complex*. This group includes such important parasites as *Plasmodium*, which causes malaria. All the apicomplexa are obligate intracellular parasites at some stage in their life cycle and the apical complex is thought to be an instrument of invasion. A prominent part of this complex are the *rhoptries*, secretory organelles containing lipids and proteins (Fig. 49.7) that

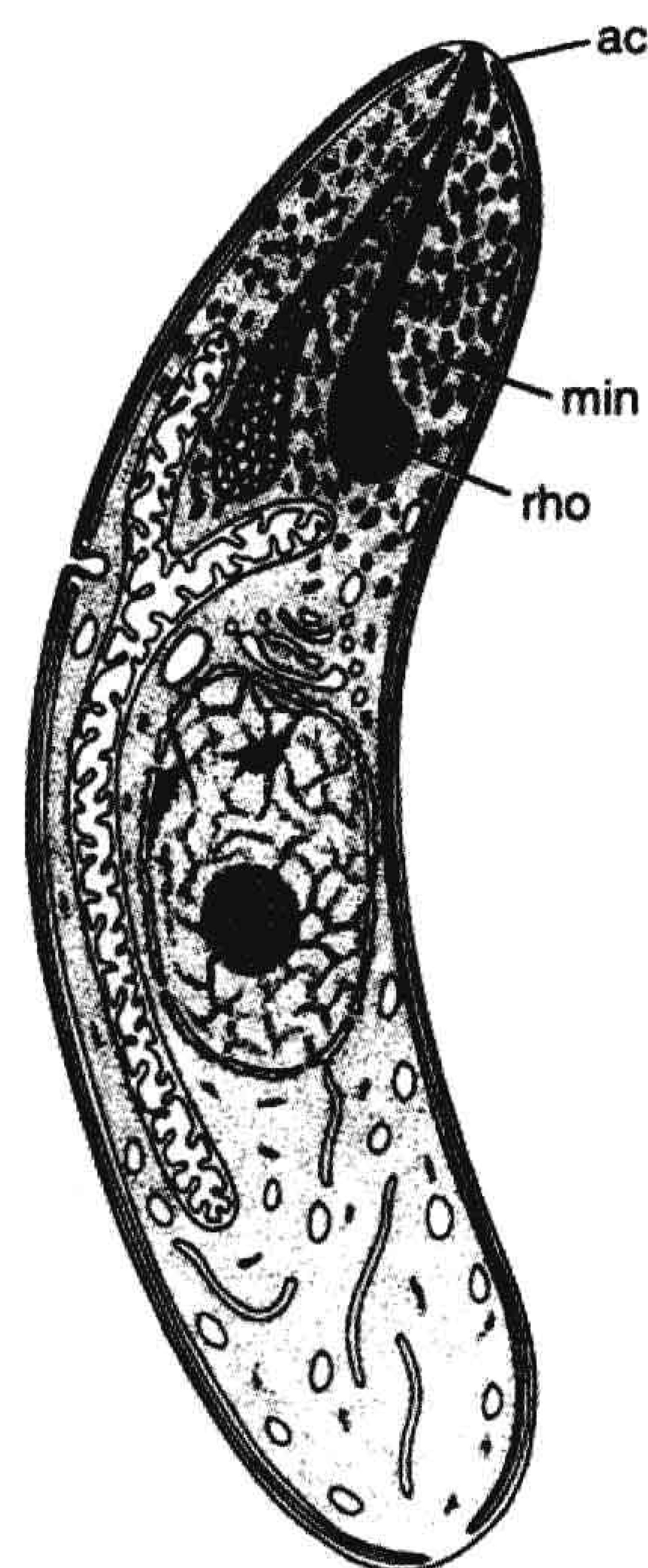


FIGURE 49.7 Diagram of apicomplexid cell, showing rhoptries (rho), micronemes (min), and apical complex (ac). *(Adapted from Chobotar and Scholtyseck, 1982.)*

originate in the *Golgi system*, filled with enzymes. For many years, the general assumption has been that rhoptry and microneme secretions must play a role in the invasion of the host cell, but it has proven difficult to identify actual function (Sam-Yellowe, 1996). In some apicomplexid species, the parasite is contained in a *parasitophorous vacuole* after invasion but, in others, the vacuole disappears and the parasite is in direct contact with the host cytoplasm. Rhoptries contain dense protein granules and epitopes corresponding to these have been identified in the host cell membrane, its cytoskeleton and also in the parasitophorous vacuole membrane, where present. Their role, however, is not clear.

VIIB. Apicoplastids

Plasmodium and other parasitic apicocomplexids have a structure that appears to be homologous to the chloroplast of green algae (Köhler et al., 1997). An organelle surrounded by four membranes contains a 35-kb circular fragment of DNA, which is shown by cluster analysis to be most closely related to DNA in green algal chloroplastids. Localization of the fragment was done by an in situ hybridization technique. The organelle divides by binary fission and is introduced into daughter cells early in replication. The genome is transcribed and transcription products have been identified. The presence of four membranes enclosing this organelle suggests that it originated endosymbiotically, following ingestion of an algal protist that contained a plastid (Dzierzinski et al., 1999).

The function of this organelle, which has been named the *apicoplastid*, is not known, but it clearly must have a function. The new organelle has been found in all apicocomplexids examined so far and has generated much excitement as a potential target in the design of new drugs for malaria and other apicocomplexid diseases. Preliminary results with several drugs that inhibit apicoplast replication or metabolism are most promising (Fichera and Roos, 1997; Jomaa et al., 1999).

VIIC. The Paraflagellar Rod

The *paraflagellar rod* (PFR) is found in parasitic kinetoplastids and also in the free-living euglenids and dinoflagellates. The PFR is a complex, lattice-like structure running parallel to the flagellum (Fig. 49.8). In both euglenids and kinetoplastids, there have been many ultrastructural, biochemical and molecular studies of this organelle (Hyams, 1982; Woodward et al., 1994).

Comparison of proteins from flagella of *Euglena* (with PFR) and *Chlamydomonas* (without PFR) indicated a pair of major proteins as PFR components. Subsequently,

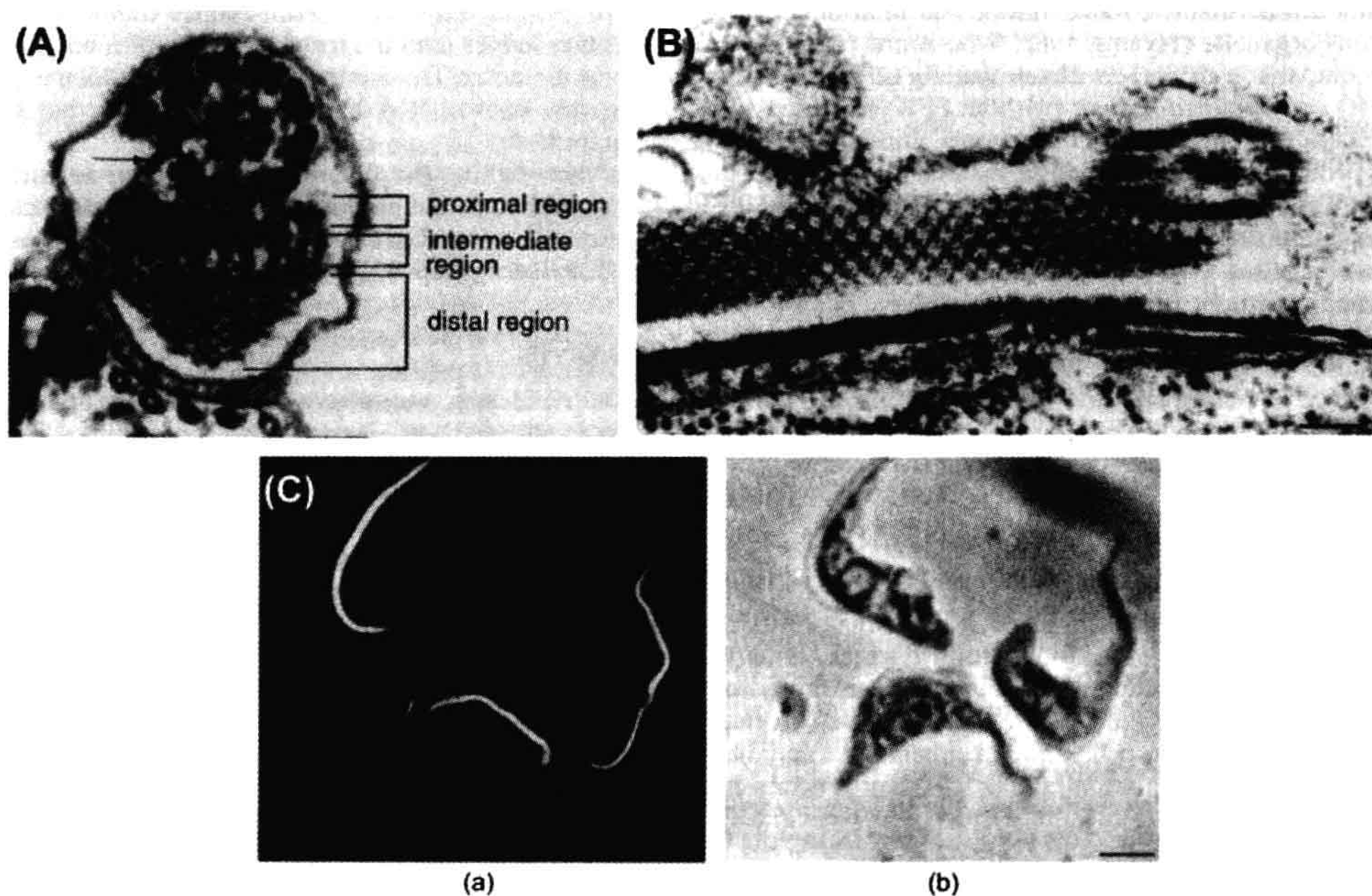


FIGURE 49.8 (A) Cross-section of the flagellum and paraflagellar rod of *Trypanosoma brucei* (scale bar: 74 nm). (B) Longitudinal section (scale bar: 256 nm). (C) Immunofluorescent staging of the PFR with monoclonal antibody ROD-1. Fluorescence picture (a) and phase image (b) (scale bar: 5.5 pm). *(From Sherwin, T. and Gull, K. (1989). Phil Trans Roy Soc Lond Ser B. 323: 575–588.)*

similar protein pairs were found in various kinetoplastid species. Cross-reactivity of kinetoplastid and euglenid PFR was established using antibodies to PFR of the kinetoplastid *Crithidia*. In addition to the two major proteins, a number of minor protein components have been found.

Regarding function, in the euglenids, the PFR is located adjacent to the eyespot and is thought to be the photoreceptor. In the parasitic kinetoplastids, current opinion favors a role in attachment to host cells during infection. Direct evidence for these rather different roles is lacking, however[2] (Bastin et al., 1996).

VIID. Extrusomes

A feature of many protists is the ability to extrude preformed structures. *Extrusomes* are vesicles that contain some organized substance or apparatus, which usually changes its form when released to the exterior in exocytosis. In some cases, these organelles are clearly related to the feeding activities of the cell, while in others, they may be a defensive adaptation but, in many cases, their function is as yet unknown. They are extruded in response to chemical, mechanical or electrical stimuli. While some metazoa eject structures, such as the *cnidocysts* (also called *nematocysts*) of *Hydra* and other coelenterates, such functions are usually performed by differentiated cells. In the unicellular protests, specialized organelles have evolved instead.

The terminology and organization of this section follows that of Hausmann and Hülsmann (1996). The classification is based largely on morphology and it is not clear whether, for example, *trichocysts* in ciliates and flagellates are homologous or represent parallel evolutionary developments. In the case of the *ejectosomes*, a truly remarkable question of homology arises: the *Kappa* particles in the ciliate *Paramecium* (bacterial endosymbionts, see earlier discussion) contain *R-bodies*, which are morphologically indistinguishable from the ejectosomes of certain flagellates (see later section) and these have even been observed to unroll and form tubes, as ejectosomes do. Did the ejectosome originate as part of a bacterial endosymbiont?

VIID1. Spindle Trichocysts

These are probably the best studied of the extrusomes. Spindle trichocysts of *Paramecium*, a favorite demonstration in introductory biology courses, are found in the cortex of the cell, just under the plasma membrane. In the resting state, the trichocyst is a spindle-shaped or rhomboid paracrystalline protein body. In response to various chemical and/or mechanical stimuli, this unfolds in a few milliseconds to form an expanded, thread-shaped filament, about eight times as long as the former resting form but having the same diameter. The driving force for this sudden expansion is not known. It is independent of ATP, but Ca^{2+} is required.

It is thought that the function of trichocysts is to repel predators, though the evidence for this is not very clear. Trichocysts are found in ciliates and in dinoflagellates and other flagellate groups (Hausmann and Hülsmann, 1996).

VIID2. Mucocysts

Like trichocysts, *mucocysts* are found just under the plasma membrane and consist of paracrystalline filamentous bodies. Expansion to the exterior takes place in three dimensions and lasts for several seconds. They are found in various ciliates, flagellates and the ameboid actinopods, where they may be responsible for the sticky surface used in capturing food organisms. Otherwise, they are thought to have a protective function. They resemble the cortical granules of sea urchin eggs, which are involved in the formation of the fertilization membrane.

VIID3. Discobolocysts

Discobolocysts are found in certain flagellates (*chrysophytes* and others). In the intracellular resting state they are almost spherical, with a disk in the part next to the plasma membrane. On ejection, the disk is unaltered, but the remainder is changed into long filamentous material. The function of these organelles is not known.

VIID4. Toxicysts

These are found in ciliates and some phagotrophic flagellates. They function in the capture of prey and perhaps in defense against predators. The toxicyst capsule contains a long tube which, during extrusion, is either telescoped or everted. This enters the prey and is used to inject a toxin, which kills or paralyzes the prey. In the suctorian ciliates, they discharge on contact and serve also to hold the prey until it can be taken in and consumed. The nature of the toxin(s) does not appear to have been investigated.

VIID5. Rhabdocysts

These are rod shaped and occur in one group of ciliates (the *karyorelictids*). As with toxicysts, they discharge telescopically – an event that has been compared to the discharge of an arrow from a blowpipe. Their function is unknown.

VIID6. Ejectosomes

These occur in certain flagellates (*cryptophytes* and *prasinophytes*). In the intracellular resting state, they are like tightly coiled ribbons. Extruded, they unroll and form very long tubes. This is said to be an escape reaction. The remarkable similarity of this organelle with the R-bodies in the *Kappa* particle endosymbionts of *Paramecium* was

[2] Interestingly, the only group of kinetoplastids that lacks a PFR is a group of monogenetic parasites that have bacterial endosymbionts of the genus *Bordetella*.

noted earlier and raises the possibility of an endosymbiotic origin for this organelle.

VIID7. Epixenosomes

Epixenosomes occur tightly bound to the outer surface of the plasma membrane in certain ciliates. They, like the ejectosomes, contain a tightly coiled band that unrolls and forms a tube. They contain DNA, however, and thus are epibionts, not organelles and, on the basis of several structural features, it has been suggested that they may represent a primitive type of organism somewhere between the prokaryotes and the eukaryotes. In any case, they are found in all specimens of different species of the genus *Euplotidinium* from different geographic regions. Thus, this appears to be a tight, ancient symbiotic relation.

VIID8. Nematocysts

These are found in certain dinoflagellates and are thought to function in predation, though this has not been observed. As with toxicysts, they strongly resemble the *cnidocysts* (also known as nematocysts) of multicellular coelenterates such as *Hydra*. They are capsules containing a coiled tube, which evaginates on extrusion.

VIIE. Crystalline Bodies

Many protists contain crystals, usually of calcium and phosphorus salts and with small amounts of magnesium, chloride or organic material, in some cases. Classically, these were considered simply waste products, since they seemed to be somewhat dependent on diet. More recently, it has been suggested that they may be reservoirs of ions needed in metabolism. They are often formed when the cells are grown in optimal conditions and when removed experimentally they tend to be replaced quickly.

VIII. COORDINATED PROTISTAN RESPONSES TO GRAVITY AND TO GRADIENTS OF OXYGEN AND LIGHT: AN EXAMPLE FROM PHYSIOLOGICAL ECOLOGY

In this section, an example is presented of the integration of protists in their environment, based on some of the physiological capacities discussed in earlier sections. The example is taken from a study of a nutrient-rich pond (Berninger et al., 1986). Figure 49.9 shows the distribution

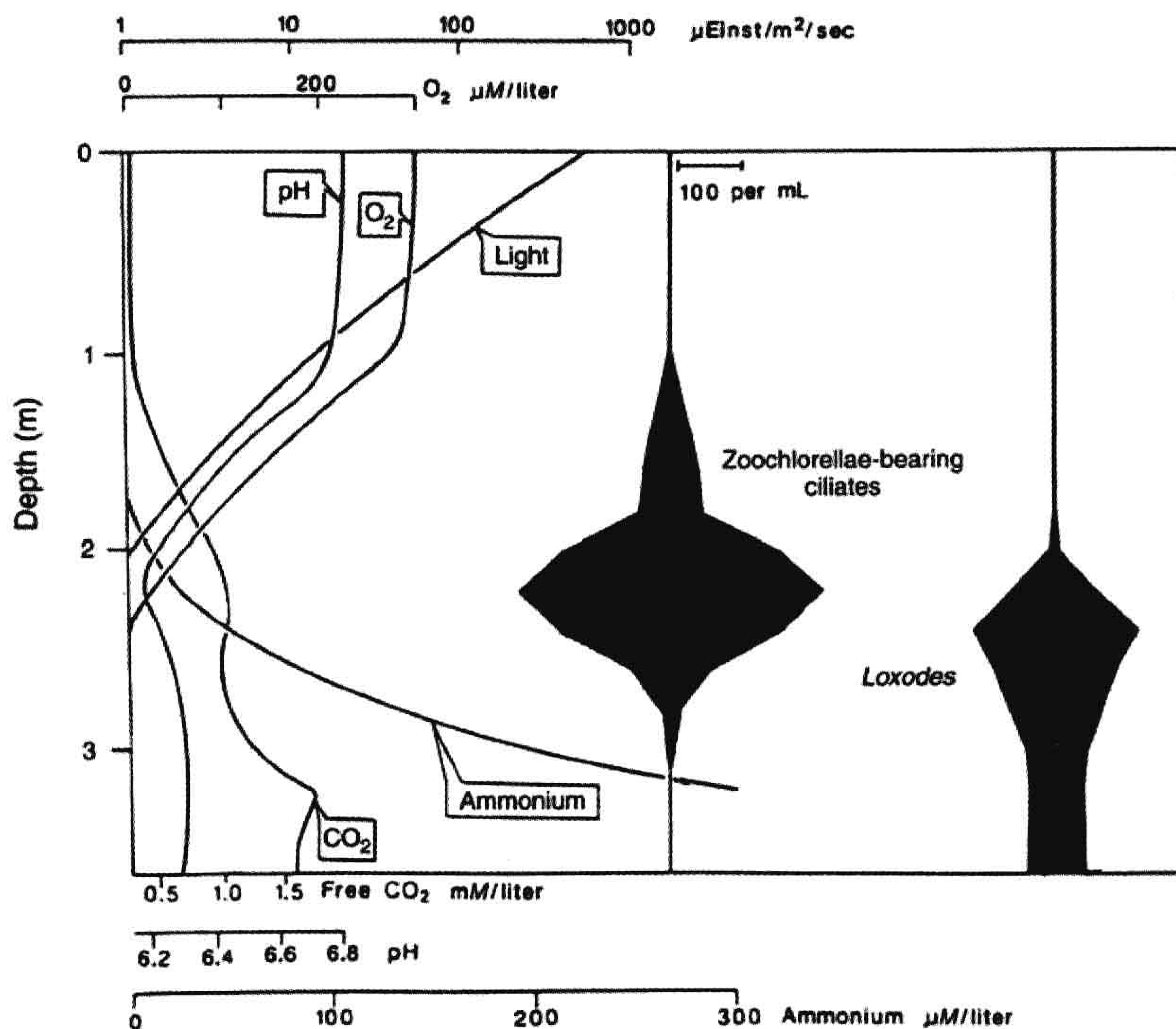


FIGURE 49.9 Vertical distribution of microaerophilic zoochlorellae (algal symbiont)-bearing ciliates and the ciliate *Loxodes* in a small productive pond, with profiles of some relevant physical and chemical factors. *(Adapted from Berninger et al., 1986 and Fenchel and Finlay, 1986.)*

of two kinds of ciliates in relation to several critical physicochemical factors. The situation depicted is typical of summer when temperatures are high and there is not much wind. In these circumstances, bacterial metabolism depletes oxygen in the lower part of the water column and, in the absence of mixing by wind, the pond becomes stratified. The depth profiles of two ciliate populations are shown. The first consists of three species of microaerophilic zoochlorellae-bearing ciliate. These remain in a low-oxygen zone, where major predators have difficulty following them. Their lower limit is set by the light requirement of their symbionts, which produce the oxygen that enables them to survive in this zone. The second group consists of a species of the ciliate *Loxodes*, mentioned earlier (Section VB) in connection with the gravity receptor, or Müller body.

Loxodes responds to three interacting factors: oxygen, blue light and the force of gravity. As noted earlier, in the dark, cells accumulate in regions of low oxygen tension (ca. 5% of saturation). If then exposed to light, they swim into the dark or into anaerobic water. When exposed to high O_2 and light simultaneously, after initial episodes of backward swimming (the *avoiding reaction*), they swim downward (a *positive geotaxis*). If placed in anaerobic water, especially in the dark, they respond by swimming upward (*negative geotaxis*). The end result of all this is that, in the pond, they accumulate by geotaxis in a zone in the *oxycline* (oxygen gradient) that is optimal. Typically this is in the dark, just below the ciliates with zoochlorellae symbionts. The cells are sensitive to very low light levels, so that levels as low as $10\,W\,m^{-2}$ will cause them to swim down into anaerobic water. *Loxodes* can use nitrate as a terminal electron acceptor, which is unusual in ciliates. Meanwhile, by swimming down into the anaerobic zone, the cells avoid most of their potential predators – zooplankters, planktonic larvae, juvenile fish – which are restricted to the aerobic zone.

Figure 49.10 summarizes what is known or suspected regarding the physiological basis for this adaptive behavior. Obviously, much remains to be done before the physiological basis for some of the arrows in the figure is understood. Photoreception remains to be worked out in detail, but it is clear that a blue light receptor is involved, possibly a flavin, and one product of its excitation in the presence of oxygen is superoxide radical (Finlay and Fenchel, 1986). However, *Loxodes* has only low levels of superoxide dismutase and catalase. Thus, superoxide, or a product of its dismutation, e.g. hydrogen peroxide, might be the internal signal for oxygen perception, binding to cytochrome oxidase or perhaps reducing another component of the electron transport system (ETS), such as cytochrome *c*. A drawback of this speculation is that the ETS is in the mitochondrion, while the pigment granules are in the cell membrane. Thus, a change in the ETS might influence the membrane potential of the mitochondrion, but it is not clear how this signal might be transmitted to the cell membrane to influence ciliary beating and change the swimming behavior (Finlay et al., 1986).

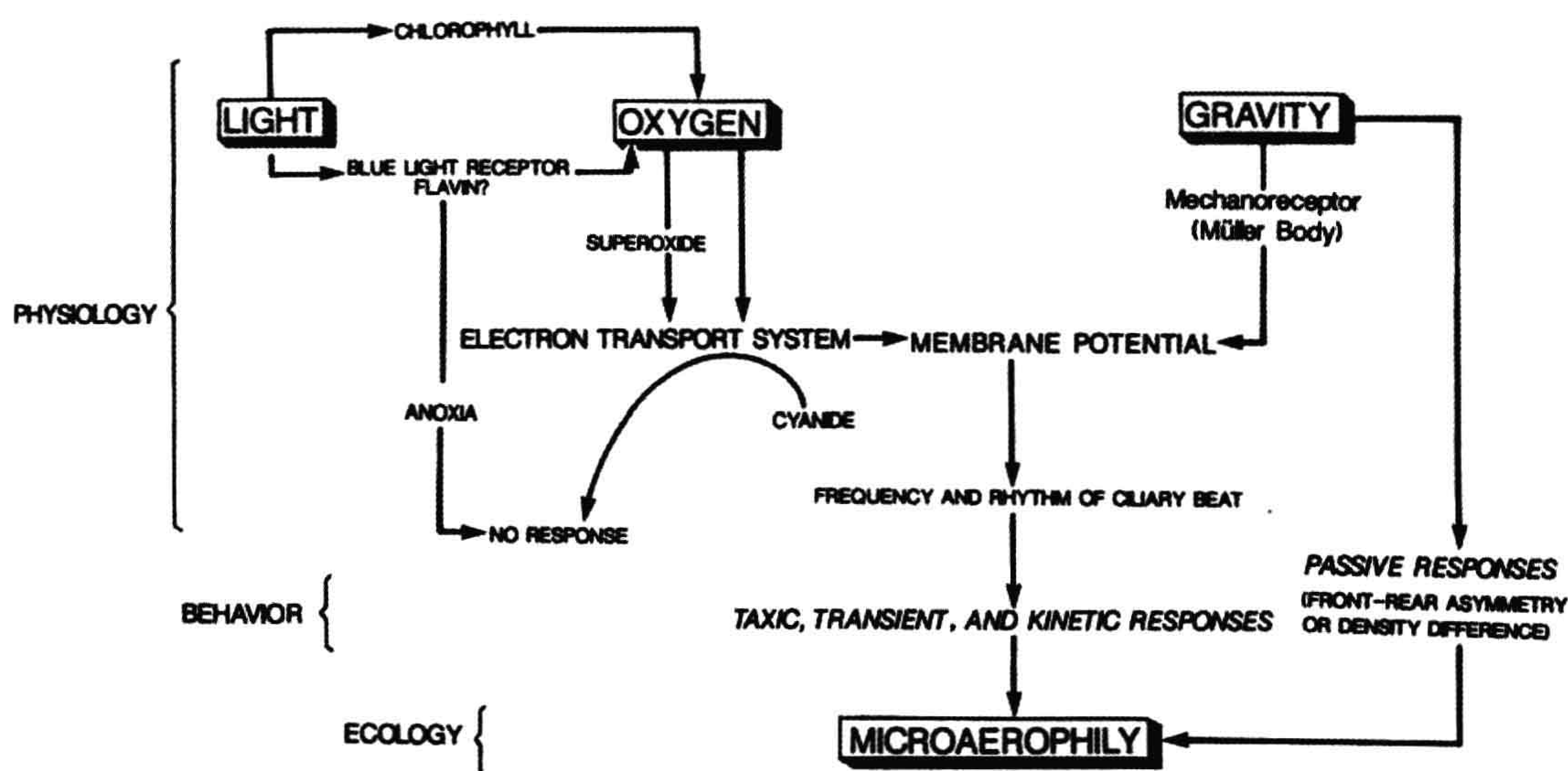


FIGURE 49.10 Model of the probable physiological and behavioral responses to the three cardinal factors (light, oxygen and gravity) controlling microaerophily in ciliated protozoa. *(Adapted with permission from Finlay, 1990.)*

In any case, the linked responses to light, oxygen tension and gravity seem very understandable given the ecology of this organism. What is attractive in this system is the possibility of linking the organism's physiology and its ecology.

IX. SUMMARY: PROTISTAN DIVERSITY

The theme of this chapter has been the physiological diversity that has evolved among the many protistan groups, as seen in some of the better-studied examples. However, even these examples are as yet only poorly understood and many groups remain unstudied or little studied. The diversity of known physiological systems and mechanisms is likely to increase enormously as these groups are explored. Let us consider this at several different levels of organization.

IXA. Molecular Diversity

There is great diversity at the level of molecular genetics, not treated in this chapter. Ciliates, for example, display a slight variation on the otherwise universal genetic code: the universal stop codons, TAA and TGA, instead code for glutamine in some (but not all) ciliates. (It has been suggested that this may serve as a barrier to viruses, which have not been detected in ciliates.) The presence of two nuclei in ciliates is also different: the *micronucleus* serves as the genetic archive, for storage and recombination of the genetic pattern, whereas the *macronucleus* is the regulator of cellular function. In trypanosomes and other kinetoplastids, the *kinetoplast* is a large network of DNA associated with a single giant mitochondrion. This kinetoplast DNA (kDNA) consists of a network of about 50 *maxicircles*, which carry the mitochondrial genes and about 10 000 *minicircles*. It was noticed that many genes in the maxicircles appeared non-functional, since they lacked conventional punctuation and contained frameshifts. However, mRNA with functional coding was produced. It turned out that the minicircle DNA was used to produce "guide RNA", which edited the pre-mRNA from the maxicircles. Since this discovery, similar RNA editing has been found in other organisms, including a mammalian nucleus.

Indeed, protists have been a fruitful source of discovery in fundamental biology. Early in the 20th century, it was noted that some ciliates could divide approximately 50 times asexually and then had to undergo sexual genetic recombination, anticipating Heyflick's epochal discovery of a similar mortality in mammalian cell lines by several decades. The mechanism involved here, change in length of the telomeres with each division, was first discovered in a ciliate, *Tetrahymena* (Blackburn, 1992; Blackburn and Greider, 1995). Studies with this ciliate also revealed for the first time that RNA could be an enzyme (Cech, 1987).

IXB. Organellar Diversity

As seen in this chapter, endosymbiotic events do occur often among protists. Protists are not necessarily prisoners of their phylogenetic past. If a useful invention appears in one evolutionary line, it can cross to another by a symbiotic transfer. Many dinoflagellates are photosynthetic, but ultrastructural evidence indicates that their chloroplasts originated in other evolutionary lines (the cryptophytes and the chrysophytes). The ciliates, distant relatives of the dinoflagellates, also lack chloroplasts but, as noted, planktonic species often "capture" and use chloroplasts from their algal prey and, in some cases, these symbioses appear to have become permanent.

In summary, many authors have constructed "trees" that reflect the phylogeny of sRNA and other nucleic acids in protistan and other eukaryotic cells but, in organellar organization, there has been a great deal of lateral transfer and one evolutionary line can borrow or take from another. At this level, a flowchart is probably more appropriate than a tree.

IXC. Cellular Diversity

Finally, protistan cells can vary in space and time. Some have complex life cycles or can form multicellular structures in which there is specialization and differentiation. Perhaps most well known here are the cellular slime molds. At one stage, these function as individual small amoebae. Under certain conditions, however, the individual cells send chemical signals to each other and come together to form multicellular "slugs". These move about for a time and then metamorphose into a more or less complex multicellular reproductive structure. Curiously, in one group of ciliates, essentially the same thing occurs – presumably a parallel evolution.

This chapter started with the description of filter-feeding by protists – an important ecological process that is illustrative of the problems faced by cells that are also free-living organisms. This was followed by a more detailed discussion of feeding: phagotrophy and digestion in the well-studied case of the ciliate *Paramecium*. Since mitochondria in the protists, though varying somewhat in structure, are essentially similar to those in other cells, their metabolism was not examined here. Instead, the unique glycosomes and hydrogenosomes of anaerobic and micro-aerophilic protists were discussed.

Returning to the view of protists as organisms, several sensory organelles unique to these cells were examined, followed by a consideration of their sensory transduction. Here, there are some exciting similarities and differences with vertebrate and invertebrate neurons and sensory cells. In particular, a calcium potential dominates in those cells that have been studied and calmodulin-based pathways are prominent aspects of transduction.

The widespread occurrence of endosymbiosis in protists was illustrated with well-documented examples. Next, to emphasize the opportunities for breaking new ground with protistan physiology, a number of striking organelles of unknown function were described. Finally, returning to the original emphasis on the cells as organisms, an example from the physiological ecology of a freshwater ciliate in a high-nutrient freshwater pond was described.

The record suggests that, by studying the diversity of protistan adaptations, cell physiologists can find new answers to old questions and also new questions.

ACKNOWLEDGMENTS

I thank Nigel Yarlett, Miklos Müller, Tom Fenchel, F.J.R. Taylor and Kenneth Foster for helpful discussions.

BIBLIOGRAPHY

Adl, S. M., Simpson, A. G. B., Farmer, M. A., et al. (2005). The next higher level classification of Eukaryotes with emphasis on the taxonomy of Protists. *J Eukaryot Microbiol, 52*, 309–451.

Allen, R. D. (1984). Paramecium phagosome membrane: from oral region to cytoproct and back again. *J Protozool, 31*, 1–6.

Allen, R. D. (1997). Membrane tubulation and proton pumps. New ideas in cell biology. *Protoplasma, 189*, 1–8.

Bastin, P., Matthews, K. R., & Gull, K. (1996). The paraflagellar rod of Kinetoplastida: solved and unsolved questions. *Parasit Today, 12*, 302–307.

Bell, W., Preston, R., Yano, J., & Van Houten, J. (2007). Genetic dissection of chemosensory conductances in Paramecium. *J Exp Biol, 210*, 357–365.

Berninger, U.-G., Finlay, B. J., & Canter, H. M. (1986). The spatial distribution and ecology of zoochlorellae-bearing ciliates in a productive pond. *J Protozool, 33*, 557–563.

Blackburn, E. H. (1992). Telomerases. *Annu Rev Biochem, 61*, 113–129.

Blackburn, E. H., & Greider, C. W. (Eds.). (1995). *Telomeres*. Cold Spring Harbor, New York: Cold Spring Harbor Laboratory Press.

Cavalier-Smith, T. (2004). Only six kingdoms of life. *Proc Roy Soc B, 271*, 1251–1262.

Cavalier-Smith, T. (2009). Megaphylogeny, cell body plans, adaptive zones: causes and timing of eukaryotic basal radiations. *J Eukaryot Microbiol, 56*, 26–33.

Cech, T. (1987). The chemistry of self-splicing RNA and RNA enzymes. *Science, 236*, 1532–1539.

Cheer, A. Y. L., & Koehl, M. (1987). Paddles and rakes. Fluid flow through bristled appendages of small organisms. *J Theoret Biol, 129*, 17–39.

Childress, W. S., Koehl, M., & Miksis, M. (1987). Scanning currents in Stokes flow and the efficient feeding of small organisms. *J Fluid Mech, 177*, 407–436.

Chobotar, W., & Scholtyseck, E. (1982). Ultrastructure. In D. M. Hammond, & P. L. Long (Eds.), *The Biology of the Coccidia* (pp. 10–37). Baltimore: University Park Press.

Corliss, J. O. (1985). Concept, definition, prevalence and host interactions of xenosomes (cytoplasmic and nuclear endosymbionts). *J Protozool, 32*, 373–376.

Dawson, S. C., & Pace, N. R. (2003). Novel kingdom-level eukaryotic diversity in anoxic environments. *Proc Natl Acad Sci USA, 99*, 8324–8329.

Dzierzinski, F., Popescu, O., Toursel, C., Slomianny, C., Yahiaoui, B., & Tomavo, S. (1999). The protozoan parasite *Toxoplasma gondii* expresses two functional plant-like glycolytic enzymes. Implications for evolutionary origin of apicomplexans. *J Biol Chem, 274*, 24888–24895.

Fenchel, T. (1986a). *Ecology of Protozoa*. New York: Springer-Verlag.

Fenchel, T. (1986b). Protozoan filter feeding. *Progr Protistol, 1*, 65–113.

Fenchel, T., & Finlay, B. J. (1986). The structure and function of Müller vesicles in loxodid ciliates. *J Protozool, 33*, 69–76.

Fenchel, T., & Finlay, B. J. (1991). Endosymbiotic methanogenic bacteria in anaerobic ciliates: significance for the growth efficiency of the host. *J Protozool, 38*, 18–22.

Fenchel, T., Perry, T., & Thane, A. (1977). Anaerobiosis and symbiosis with bacteria in free-living ciliates. *J Protozool, 24*, 154–163.

Fichera, M., & Roos, D. (1997). A plastid organelle as a drug target in apicocomplexid parasites. *Nature, 390*, 407–409.

Finlay, B. J. (1990). Ecology of free-living protozoa. *Adv Microb Ecol, 11*, 1–36.

Finlay, B. J., & Fenchel, T. (1986). Physiological ecology of the ciliated protozoon *Loxodes*. *Rep Freshwater Biol Ass, 54*, 73–96.

Finlay, B. J., Fenchel, T., & Gardner, S. (1986). Oxygen perception and O_2 toxicity in the freshwater ciliated protoozoon *Loxodes*. *J Protozool, 33*, 157–165.

Fok, A. K., & Allen, R. D. (1990). The phagosome–lysosome membrane system and its regulation in Paramecium. *Int Rev Cytol, 123*, 61–94.

Foster, K. W., & Smyth, R. D. (1980). Light antennas in phototactic algae. *Microbiol Rev, 44*, 572–630.

Francis, D. (1967). On the eyespot of the dinoflagellate, *Nematodinium*. *J Exp Biol, 47*, 495–501.

Görtz, H. D. (1996). Symbiosis in ciliates. In K. Hausmann, & P. Bradbury (Eds.), *Ciliates* (pp. 441–462). Stuttgart: Gustav Fischer.

Greuet, C. (1978). Organization ultrastructurale de l'ocelloide de Nematodinium. Aspect phylogenetique du photorecepteur de Peridiniens Warnowiidae Lindemann. *Cytobiologie, 17*, 114–136.

Greuet, C. (1987). Complex organelles. In F. J. R. Taylor (Ed.), *The Biology of Dinoflagellates* (pp. 119–142). Oxford: Blackwell.

Hausmann, K., & Hülsmann, N. (1996). *Protozoology*. Stuttgart: Georg Thieme Verlag.

Heuser, J., Zhu, Q., & Clarke, M. (1993). Proton pumps populate the contractile vacuoles of *Dictyostelium amoebae*. *J Cell Biol, 121*, 1311–1327.

Hinrichsen, R. D., & Schultz, J. (1988). Paramecium: a model system for the study of excitable cells. *Trends Neur Sci, 11*, 27–32.

Hyams, J. (1982). The Euglena paraflagellar rod: structure, relationship to other flagellar components and preliminary biochemical characterization. *J Cell Sci, 55*, 199–210.

Iglesias, P. A., & Devreotes, P. N. (2008). Navigating through models of chemotaxis. *Curr Opin Cell Biol, 20*, 35–40.

Jeon, K. W. (1987). Change of cellular pathogens into required cell components. *Ann NY Acad Sci, 503*, 359–371.

Jeon, K. W. (1995). The large, free-living amoebae: wonderful cells for biological studies. *J Eukaryot Microbiol, 42*, 1–7.

Jeon, T. J., & Jeon, K. W. (2003). Characterization of smas genes of *Amoeba proteus* and the endosymbiotic X-bacterium. *J Eukaryot Microbiol, 50*, 61–69.

Jomaa, H., Wiesner, J., Sanderbrand, S., et al. (1999). Inhibitors of the nonmevalonate pathway of isoprenoid biosynthesis as antimalarial drugs. *Science, 285*, 1573–1576.

Katz, L., & Bhattacharya, D. (2006). *Genomics and Evolution of Microbial Eukaryotes*. Oxford: Oxford University Press.

Keeling, P. (2009). Chromalveolates and the evolution of plastids by secondary endosymbiosis. *J Eukaryot Microbiol, 56*, 1–8.

Kim, E., Harrison, J. W., Sudek, S., et al. (2011). Newly identified plastid-bearing branch on the eukaryotic tree of life. *Proc Natl Acad Sci, 108*, 1496–1500.

Köhler, S., Delwiche, C. F., Denny, P., et al. (1997). A plastid of probable green algal origin in Apicomplexan parasites. *Science, 275*, 1485–1489.

Melkonian, M., & Robenek, H. (1984). The eyespot apparatus of flagellated green algae: a critical review. *Progr Phycol Res, 3*, 193–268.

Müller, M. (1993). The hydrogenosome. *J Gen Microbiol, 139*, 2879–2889.

Naitoh, Y., & Kaneko, H. (1973). Control of ciliary activities by adenosine triphosphate and divalent cations in Triton-extracted models of *Paramecium caudatum*. *J Exp Biol, 58*, 657–676.

Park, M., Yun, S. T., Kim, M. S., Chun, J., & Ahn, T. (2004). Legionella-like endosymbiotic X-bacterium in *Amoeba proteus*: a proposal for ' *Candidatus Legionella jeonii* sp. nov.' *Environ Microbiol, 6*, 1252–1263.

Parsons, M. (2004). Glycosomes: parasites and the divergence of peroxisomal purpose. *Mol Microbiol, 53*, 717–724.

Patterson, D. J., Bhattacharya, D., Cole, J., et al. (2006). Classifying protists. *Microbiol Today, Feb 07*, 44–45.

Pawlowski, J., & Burki, F. (2009). Untangling the phylogeny of amoeboid protists. *J Eukaryot Microbiol, 56*, 16–25.

Roberts, A. M. (1981). Hydrodynamics of protozoan swimming. In M. Levandowsky, & S. H. Hutner (Eds.) (2nd ed.). *Biochemistry and Physiology of Protozoa, Vol. 4* (pp. 5–66) New York: Academic Press.

Saimi, Y., & Kung, C. (1987). Behavioral genetics of *Paramecium*. *Annu Rev Genet, 21*, 47–65.

Sam-Yellowe, T. Y. (1996). Rhoptry organelles of the apicomplexa: their role in host cell invasion and intracellular survival. *Parasitol Today, 12*, 308–316.

Sherwin, T., & Gull, K. (1989). The cell cycle of *Trypanosoma brucei brucei*: Timing of event markers and cytoskeletal modifications. *Phil Trans Roy Soc ser B, 323*, 575–588.

Simpson, A. G. B., & Patterson, D. J. (2006). Current perspectives on high-level groupings of protists. In L. Katz, & D. Bhattacharya (Eds.), *Genomics and Evolution of Microbial Eukaryotes*. Oxford: Oxford University Press.

Smyth, R. D., Saranak, J., & Foster, K. W. (1988). Algal visual systems and their photoreceptor pigments. *Progr Phycol Res, 6*, 254–286.

Soldo, A. T. (1987). Parauronema and its xenosomes: a model system. *J Protozool, 34*, 447–451.

Soldo, A. T., Brickson, S. A., & Vazquez, D. (1992). The molecular biology of a bacterial endosymbiont. *J Protozool, 39*, 196–198.

Stoeck, T., & Epstein, S. (2003). Novel eukaryotic lineages inferred from small-subunit rRNA analysis of oxygen-deprived marine environments. *Appl Environ Microbiol, 69*, 2657–2663.

Stoecker, D. K., Michaels, A. E., & Davis, L. H. (1987). Large proportion of marine planktonic ciliates found to contain functional chloroplasts. *Nature, 326*, 790–792.

Tachezy, J. (2008). *Hydrogenosomes and Mitosomes: Mitochondria of Anaerobic Protozoa*. Heidelberg: Springer-Verlag.

Taylor, F. J. R., Blackbourne, D. J., & Blackbourne, J. (1971). The red-water ciliate *Mesodinium rubrum* and its "incomplete symbionts": a review including new ultrastructural observations. *J Fish Res Bd Can, 28*, 391–407.

Valentine, M., Yano, J., & Van Houten, J. (2008). Chemosensory transduction in *Paramecium*. *Jap J Protozool, 41*, 1–7.

Van der Giezen, M., Tovar, J., & Clark, C. G. (2005). Mitochondrion-derived organelles in Protists and fungi. *Int Rev Cytol, 244*, 173–225.

Van Haastert, P. J. M., & Veltman, D. M. (2007). Chemotaxis: navigating by multiple signaling pathways. *Sci STKE*, 40.

Wolf, M., Seibel, P. N., Dandekar, T., & Lynn, D. H. (2006). A java applet for exploring the new higher level classification of eukaryotes with emphasis on the taxonomy of protists. *J Eukaryot Microbiol, 53*, 315.

Woodward, R., Garden, M. J., & Gull, K. (1994). Molecular characterisation of a novel, repetitive protein of the paraflagellar rod in *Trypanosoma brucei*. *Mol Biochem Parasitol, 67*, 31–39.

Chapter 50

Physiology of Prokaryotic Cells

Dennis W. Grogan

Chapter Outline

I. THE DIVERSITY OF PROKARYOTIC ORGANISMS

Prokaryotic cells represent the smallest and simplest form of life that can metabolize, grow and reproduce. They are presumed to resemble the earliest forms of life and they reproduce much more quickly than multicellular organisms do. Taken together, these two properties imply that prokaryotic organisms have had more opportunity to evolve (by orders of magnitude) than plants or animals have had; accordingly, this predicts that prokaryotes should have the most functionally efficient, diverse and specialized of cells, despite their structural simplicity. The key to this paradox is the recognition that genetic variation and natural selection should allow a unicellular organism to improve its performance and acquire new functions without becoming structurally complex. Furthermore, as environments, survival strategies and ecological niches change over time, the criteria of optimal cellular function change which, in turn, sets the stage for new rounds of optimization in various directions. The resulting diversification and specialization can also be expected to make certain features superfluous in certain lineages, leading to cells that may be even simpler than their predecessor.

Functional specialization and optimization of a structurally simple cell seems to account for the observed diversity of modern prokaryotes. Molecular measures of divergence, such as small-subunit ribosomal RNA sequence, indicate that two prokaryotic lineages separated very early and that each encompasses more molecular diversity than multicellular organisms (Fig. 50.1). The two groups distinguished by this early split, *Bacteria* and *Archaea*, each have phylogenetic status equivalent to that of all eukaryotic organisms and the three resulting taxonomic units have been termed *Domains* (Woese et al., 1990). This extensive divergence is also evident in terms of cellular function. Certain bacteria and archaea have metabolic properties not represented among eukaryotes,

Cell Physiology Sourcebook. DOI: 10.1016/B978-0-12-387738-3.00050-0

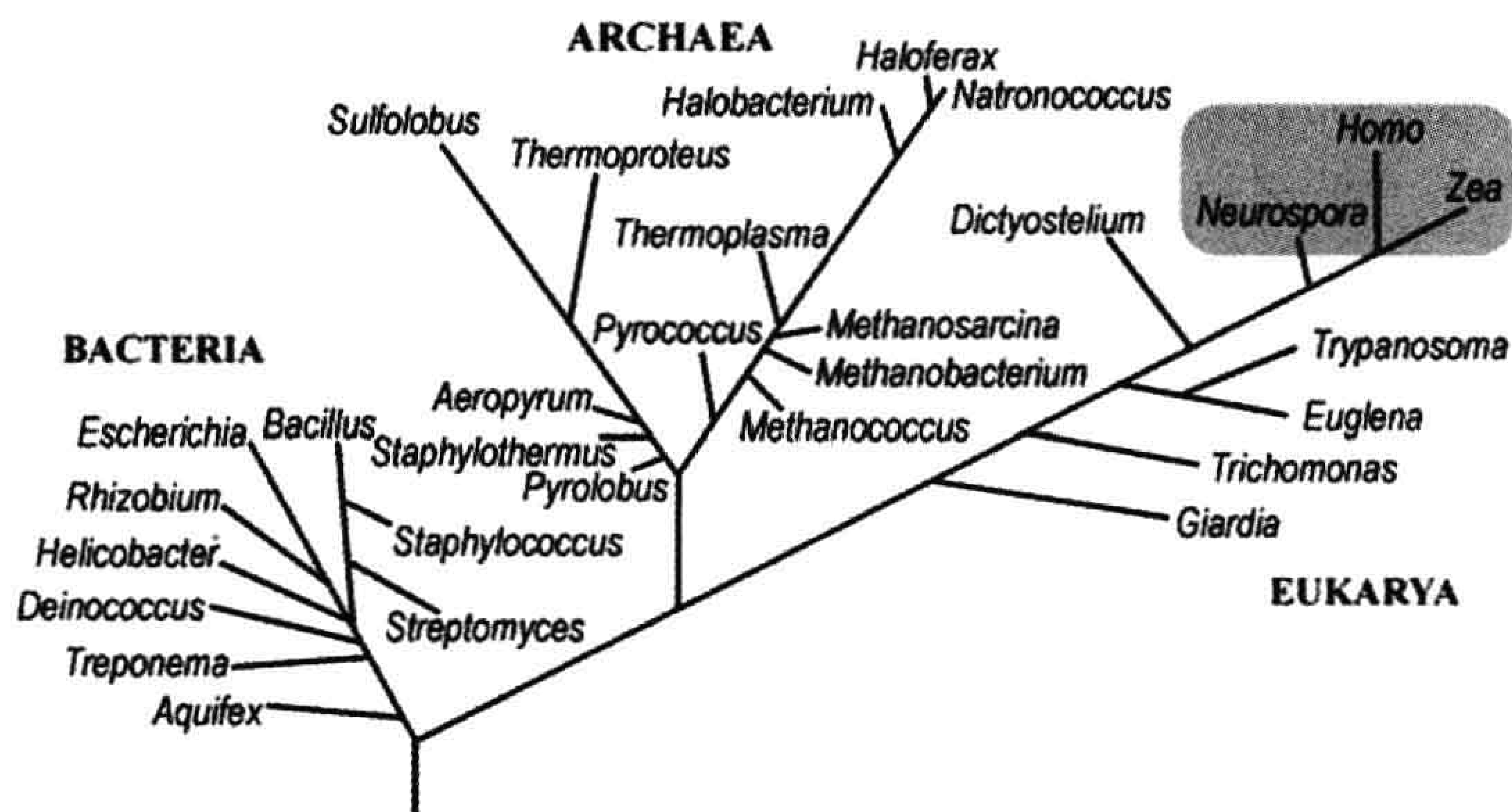


FIGURE 50.1 Phylogenetic relatedness of cellular organisms. Major groups of cellular organisms are indicated by genus names. The lengths of branches connecting two genera indicate the molecular divergence between them, as defined by the sequences of small-subunit ribosomal RNAs (16S rRNAs of bacteria and archaea, 18S rRNAs of eukarya [eukaryotes]). The gray box approximates the molecular diversity of multicellular organisms as measured by small-subunit rRNA.

including N_2 fixation, anoxic photosynthesis, additional routes of CO_2 assimilation and adaptation to extreme environmental conditions. Similarly, archaea (singular: archaeon, or less commonly, archaeum) have cellular features and metabolic pathways not found in bacteria. These uniquely archaeal features include isoprenoid membrane lipids (found in all archaea) and the ability to make methane (found in a number of genera).

One practical consequence of the deep diversity of the bacterial and archaeal lineages is that it precludes any one organism, such as the bacterium *Escherichia coli*, from modeling all aspects of prokaryotic physiology, even though this and several other species can be analyzed in great detail. It should also be noted that some components of eukaryotic cells have bacterial origins. In particular, at least two eukaryotic organelles, the *mitochondrion* and the *chloroplast*, resulted from endosymbiotic acquisitions of bacteria by progenitors of modern eukaryotic cells (Scwartz and Dayhoff, 1978). This relationship provides a context for understanding molecular structure and function of both the eukaryotic organelle and the bacterial cell.

II. PROKARYOTIC CYTOLOGY

IIA. Major Structural Types

Cells of bacteria and archaea generally measure about 1 μm in diameter and thus have about 0.1% or less of the volume and mass of a typical eukaryotic cell. This extremely small size limits the ability of light microscopy to visualize the structural features of these cells (Fig. 50.2). Prokaryotic cells generally have no obvious cytoskeleton, mitotic apparatus or intracellular organelles and span a limited range of structural complexity.

This range is illustrated in Fig. 50.3 as four structural types. Cells of the simplest structural type (Fig. 50.3, panel I) have only a *nucleoid*, a *cytoplasm* and a *cytoplasmic membrane*, each of which is described in more detail below. Examples of this truly minimal cell are relatively rare in nature and include members of the genera *Mycoplasma* and *Thermoplasma*. The former are bacteria, some of which are opportunistic pathogens, while the latter are archaea found in heated acidic soils (Kletzin, 2007). Both genera are osmotically fragile, due to an absence of cell walls (see below).

IIB. Nucleoid

Most prokaryotes have a single chromosome consisting of a single circular DNA of several million base-pairs which is neither confined within a nucleus nor evenly dispersed throughout the cytoplasm. The DNA instead occupies a convoluted region near the center of the cell, called the *nuclear region* or *nucleoid*, which bears a functional analogy to the eukaryotic nucleus (see Fig. 50.3, panel I).

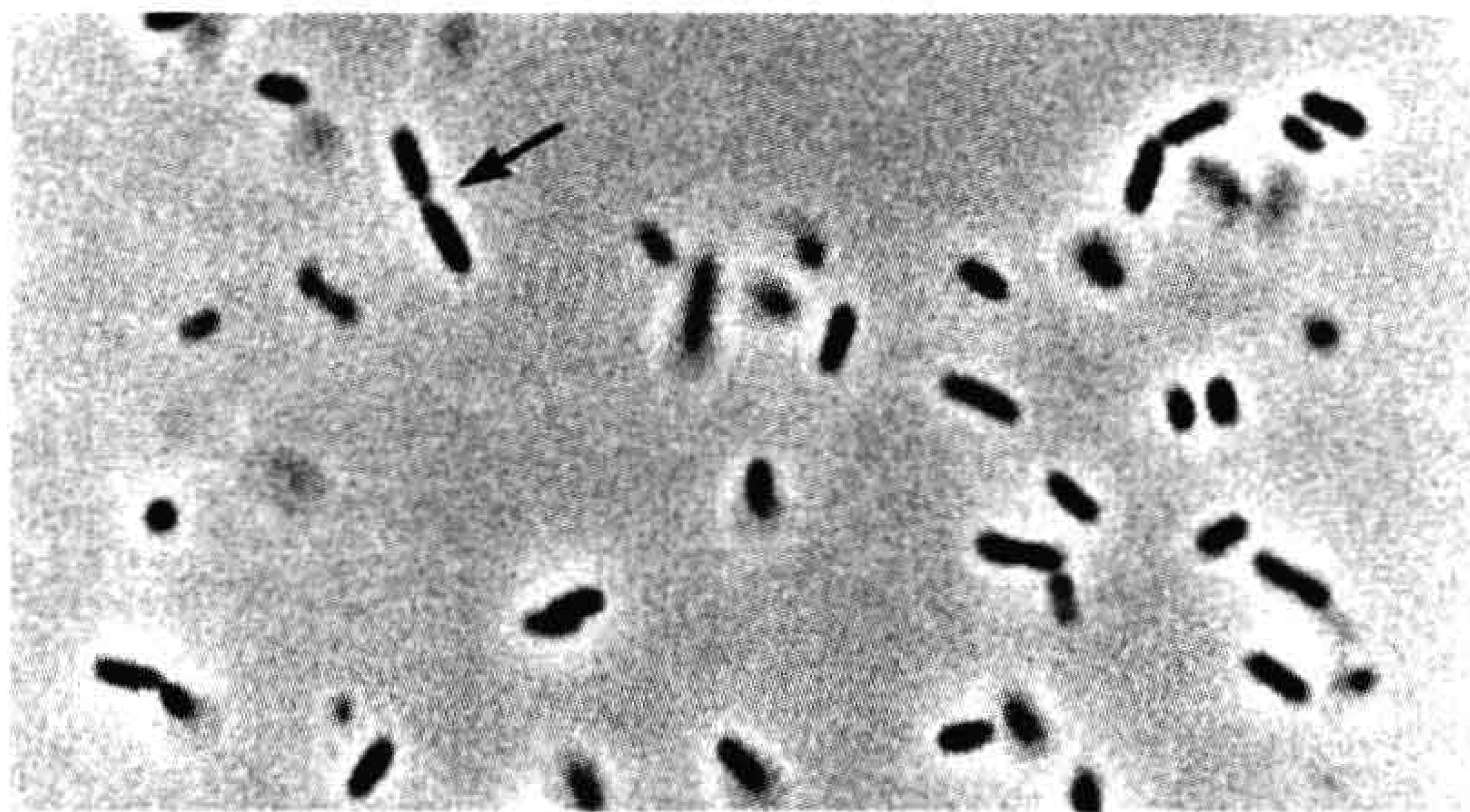


FIGURE 50.2 Live bacteria under the microscope. This is a light micrograph (phase contrast) of *Escherichia coli* cells suspended in growth medium. The average width of the cells is about 0.5 μm; arrowheads show site of constriction (septation) in a cell undergoing division. The micrograph illustrates the limited structural information obtainable by optical methods due to the small size of prokaryotic cells.

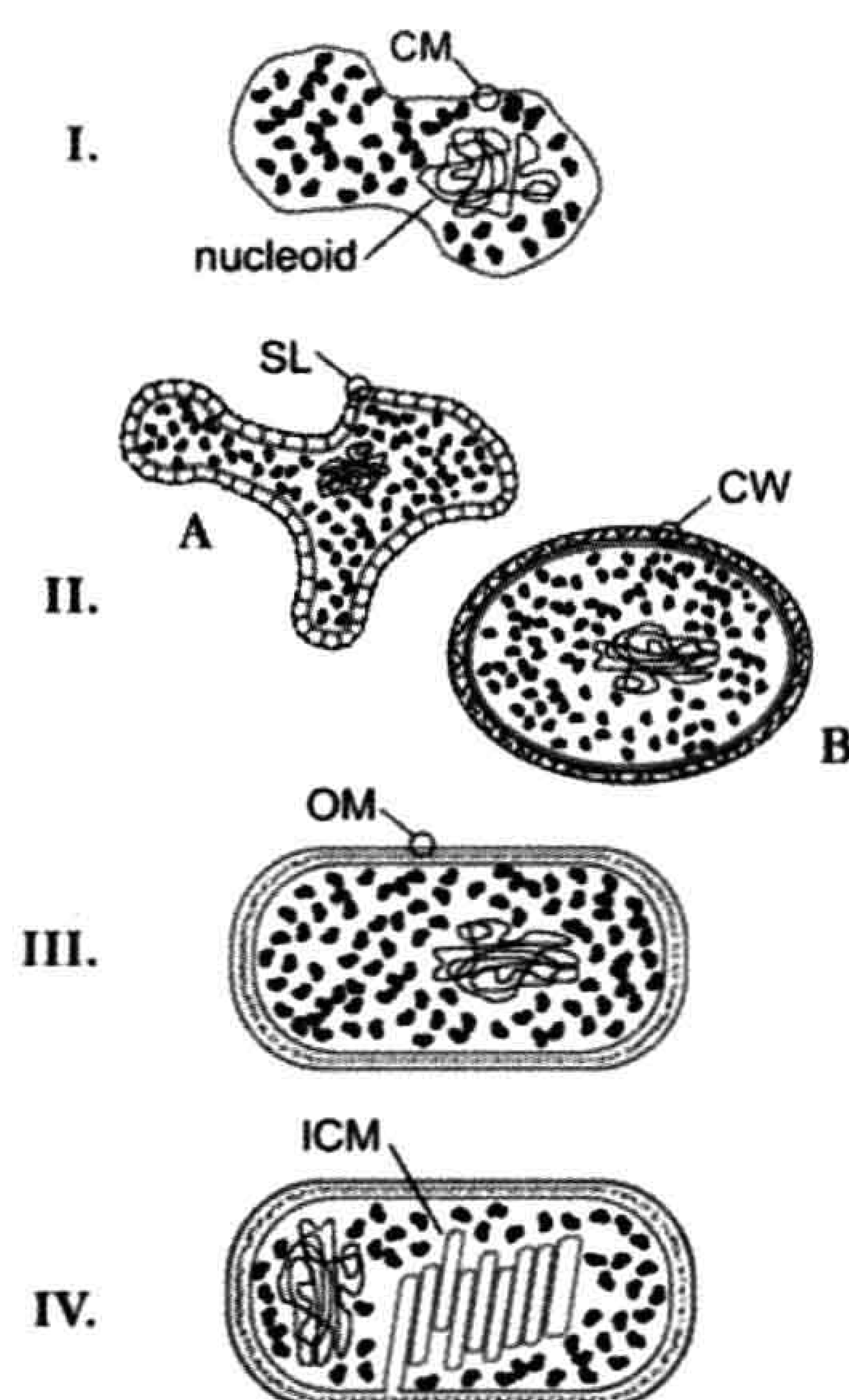


FIGURE 50.3 Examples of prokaryotic cellular structure. The limited range of cellular complexity found among prokaryotic cells has been represented in this diagram by four structural types. I: The minimal cell includes only a nucleoid, cytoplasm and cytyoplasmic membrane (CM). II. Most archaea (A) have an additional S-layer (SL), composed of glycoprotein subunits, providing external structural support for the cell membrane, whereas Gram-positive bacteria (B) have a thick cell wall (CW) composed of peptidoglycan. III. Gram-negative bacteria have a thin cell wall sandwiched between the CM and a second diffusional barrier, the outer membrane (OM). IV. Gram-negative photosynthetic bacteria produce a system of intracytoplasmic membranes (ICM). These contain specialized light-harvesting pigments and may be topologically continuous with each other and the CM.

The nucleoid replicates and partitions itself into daughter cells during growth and cell division and maintains its compacted form despite ongoing replication, transcription and repair. Cations, including Mg^{2+}, spermidine and other polyamines and small "histone-like" proteins contribute to this condensation. In *E. coli*, longer-range organization occurs in the form of 50 to 100 topologically constrained domains or "loops". Lysis of cells under appropriate conditions (non-ionic detergent and high salt concentration) releases nucleoids in a compact, relatively intact form and allows the loops to be visualized by electron microscopy (EM) (Pettijohn, 1996).

IIC. Cytoplasm

All other components of the cell interior are collectively termed the *cytoplasm* or *cytosol*. Although fluid, this mixture is very concentrated and probably reflects a complex and dynamic series of macromolecular associations. The cytosol of an *E. coli* cell adapted to growth in simple glucose medium at 37°C contains about 19 000 ribosomes which, together with transfer RNA and various translation factors, account for nearly half of the total cell mass. This large investment of cellular resources in the machinery of protein synthesis enables the *E. coli* cell to reproduce itself every 40 min under these conditions (Neidhardt et al., 1990). Enriching the simple glucose medium with other nutrients (such as peptides) increases the ribosome content and growth rate even more.

The lack of internal compartmentalization in most prokaryotic cells contributes to their ability to grow quickly and to respond quickly to environmental change. In general, prokaryotic cells have no diffusional barriers segregating the sources of energy, raw material or sequence information needed for DNA, RNA and protein synthesis; this lack of compartmentalization and the small dimensions of the cell ensure that molecular diffusion is extremely rapid throughout the cell interior. Transcription and translation are temporally and spatially coupled, so that ribosomes begin "reading" the mRNA before the mRNA itself has been completed and released from the transcription complex. This coupling not only supports rapid growth, but also provides uniquely prokaryotic modes of genetic regulation, as demonstrated by the phenomenon called *attenuation*. In this regulatory mechanism, adequate levels of particular amino acids lead to disruption of the normally tight coupling between ribosome and RNA polymerase as it begins to transcribe the corresponding amino acid biosynthetic genes. This transient uncoupling, in turn, causes RNA polymerase to terminate transcription before it reaches the biosynthetic genes, thereby avoiding wasteful overproduction of the corresponding enzymes (Yanofsky and Crawford, 1987).

IID. Cytoplasmic Membrane

The third component of the minimal prokaryotic cell structure (see Fig. 50.3 panel I) is a unit membrane called the *cytoplasmic (cell) membrane* (CM) which chemically separates the cytosol and nucleoid from the external environment. A bacterial CM generally conforms to the fluid mosaic model of biological membranes (see Chapter 3). Its matrix is a phospholipid bilayer impermeable to ionic or large polar molecules but intrinsically permeable to gases and water. The selective impermeability is essential for viability, because without it the cell cannot maintain ion potentials or retain metabolites (see below). However, cellular function also requires some chemical exchange with the surroundings, including nutrient uptake and environmental sensing. These functions are provided by a large number of different integral and peripheral proteins which breach the phospholipid bilayer with solute-specific pumps and gates. By means of these proteins, which comprise about 70% of the CM by weight, bacteria maintain

transmembrane gradients and controls transmembrane fluxes of critical solutes. Archaeal membranes appear to have analogous structure and function, although the polar lipids that provide the lamellar barrier differ radically from the phospholipids of other cells. Archaea contain only sn-(2,3 di-O-alkyl)-glycerol membrane lipids, in which the hydrocarbon chains are C_{20} or C_{40} saturated isoprenoids attached to the glycerol backbone via ether linkages (Boucher, 2007).

IIE. Cell Wall

Most archaea and bacteria have some form of *cell wall* immediately outside the cytoplasmic membrane (see Fig. 50.3, IIA, IIB). This structure solves a specific threat to the cell created by hypotonic environments, namely, that the CM cannot block the diffusion of water into the cell interior. Hypotonic environments thus promote cell swelling and rupture, i.e. *lysis*, of cells. Bacterial cell walls prevent lysis by enclosing the cell in a container that, like the cellulosic cell walls of plants, resists expansion. In contrast to plant cell walls, however, the bacterial cell wall is composed of a covalently cross-linked polymer, called *peptidoglycan* or *murein*. The repeating unit (two amino sugars linked via β-1,4 glycosidic bonds) is linked to form linear glycan chains, which are joined at frequent intervals by peptide bridges (Fig. 50.4). This results in one huge, bag-like macromolecule of high tensile strength that completely surrounds the cell membrane. This structural support allows the bacterial cell to maintain an osmotic (turgor) pressure (see Chapter 16), which can be as high as 20 atm. A morphological consequence of constitutive turgor pressure is that the bacterial cell wall determines cell shape and therefore plays a major role in cell division. This can be demonstrated in the effects on cell morphology of antibiotics that specifically disrupt the normal synthesis of peptidoglycan. In rod-shaped bacteria, low concentrations of β-lactam antibiotics, which block cell division but not cell growth, lead to elongated cells of normal diameter. At higher antibiotic concentrations, bulges (rather than constrictions) form at the normal site of bacterial cell division and, at very high antibiotic concentrations, the rod-like cells swell into spheres and lyse (Schwarz et al., 1969).

Some archaea synthesize a polymeric cell wall material similar to peptidoglycan, but most have only a layer of protein or glycoprotein that provides mechanical support for the CM. These archaeal *surface- (S-) layers* (Fig. 50.5) can be very strong structurally, despite the fact that they form by non-covalent association of individual subunits. For example, an experimental procedure used to purify bacterial cell walls as intact sacculi involves hot sodium dodecyl sulfate (SDS) extraction. Application of this method to *Sulfolobus* cells under mildly acidic conditions yields virtually intact S-layer sacculi. The non-covalent nature of the glycoprotein subunit interactions is seen, however, in the ease with which these structures dissociate into monomers at elevated pH (Grogan, 1996). Some archaeal S-layer cell walls appear to be relatively rigid and retain the cell shape, whereas others are flexible and thus not strictly equivalent to bacterial cell walls in all respects.

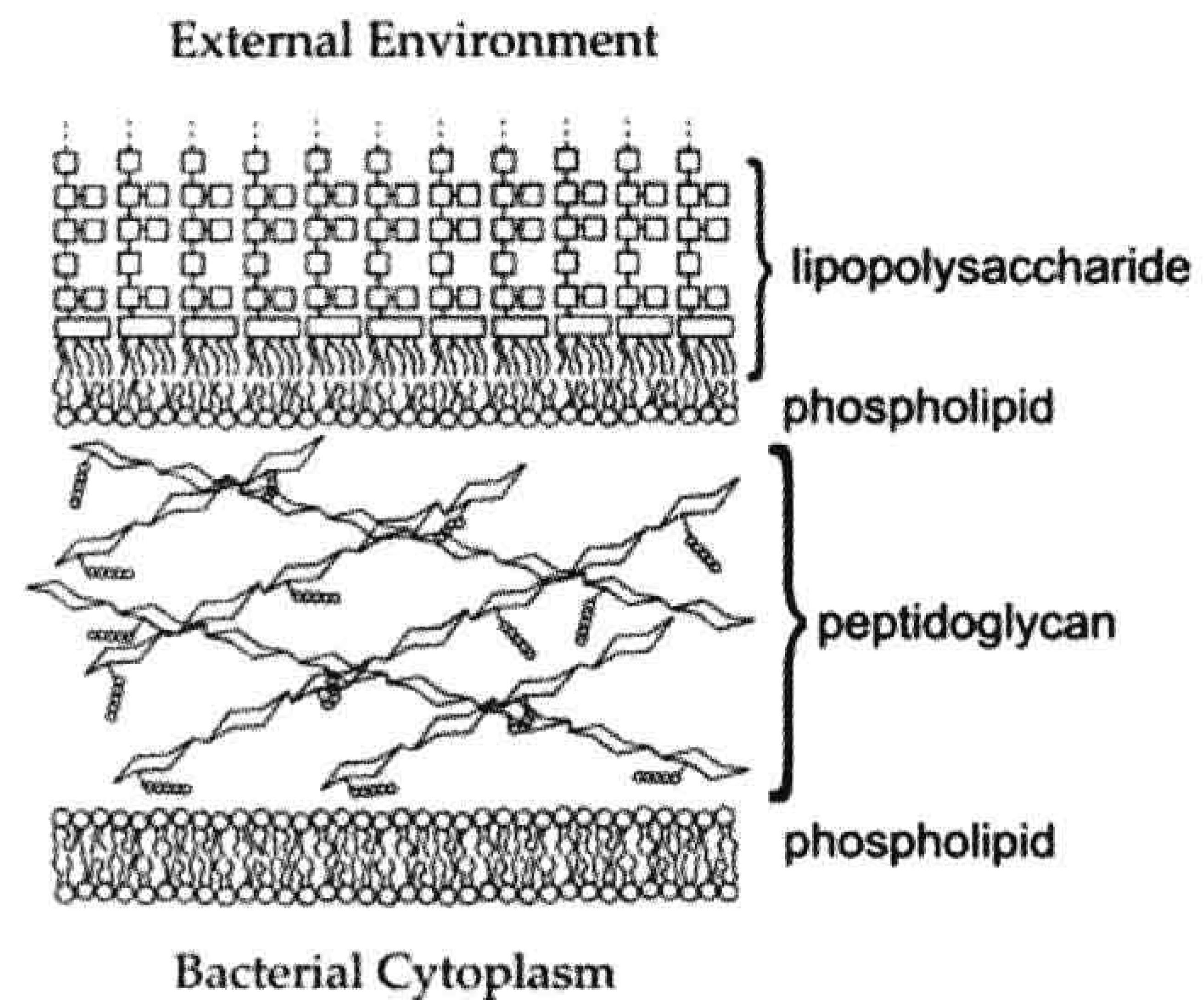


FIGURE 50.4 The cell envelope of Gram-negative bacteria. The bacterial cell wall (CW) is composed of peptidoglycan, whose repeating unit consists of a dimer of two modified amino sugars: N-acetyl muramic acid and N-acetyl glucosamine. Each repeating unit has a short peptide (circles) attached to the N-acetyl muramic acid; the peptides of adjacent glycan chains become joined by enzymes in the periplasm to form the periodic cross-links found in the mature peptidoglycan polymer. The outer membrane (OM) consists of one leaflet of lipopolysaccharide (LPS) and one of phospholipid. Each LPS molecule has a large polysaccharide chain (linked squares) whose precise structure depends on the bacterial species. The cytoplasmic membrane (CM) is composed of phospholipid. In addition to lipid, both the OM and CM contain protein species, which are not depicted in the figure.



FIGURE 50.5 Cells of *Sulfolobus acidocaldarius*, an archaeon from geothermal environments (Section VII). The ultrathin sections illustrate the irregular cell shape and extracellular location of the glycoprotein S-layer. The S-layer is held at a fixed distance from the cytoplasmic membrane by a spacer (Jaenicke and Böhm, 1998); this results in a "picket fence" appearance for the boundary around cells or cell ghosts at certain points. Bar = 100 nm.

IIF. Outer Membrane

A third, more complex cellular architecture seen in bacteria includes a second lipid bilayer, called the *outer membrane*, which surrounds the cell wall (see Fig. 50.3 panel III). This creates a protected compartment around the cell, bounded by the cytoplasmic and outer membranes, called the *periplasm* (Fig. 50.6). An important bacterial identification technique, the Gram stain, exploits the property of the peptidoglycan cell wall in these bacteria that it is relatively thin and does not retain a complex of crystal violet stain and iodine when rinsed with ethanol or acetone. This staining procedure therefore distinguishes bacteria which have the cell architecture shown in Fig. 50.3 panel IIB (Gram-positive), from those which have the more complex cell envelope illustrated in Fig. 50.3 panel III (Gram-negative). Table 50.1 summarizes the major differences between Gram-positive and Gram-negative bacteria.

The biochemical composition of the outer membrane (OM) differs from that of the bacterial CM with respect to both lipid and protein constituents. With respect to lipid, the OM is a hybrid membrane. Its inner leaflet, which faces the periplasm, incorporates the same phospholipids as the CM does. The outer leaflet, however, consists of much higher molecular weight class of lipid known as *lipopolysaccharide*, or *LPS* (see Fig. 50.4). With respect to protein, the OM has only a few protein species, but these are abundant (Nikaido and Vaara, 1985), which contrasts with the broad heterogeneity of CM proteins.

These two compositional features support the primary physiological function of the OM, which is shielding the Gram-negative cell from toxic, hydrophobic compounds in the environment. An intact LPS leaflet greatly impedes diffusion of soluble hydrophobic (i.e. lipophilic) molecules across the OM. This presumably reflects the permeability properties of the dense array of cooperatively interacting charged and polar sugar residues at the membrane surface, through which non-polar solutes must pass (Fig. 50.4). Experimental evidence of the importance of this screening function can be seen in the sensitivity of Gram-positive bacteria and LPS-depleted Gram-negative cells to toxic dyes, detergents and hydrophobic antibiotics. As in the case of the CM, the OM must nevertheless allow passage of nutrients, which is mediated by relatively non-specific solute channels, or *pores*. These structures form as trimers of corresponding proteins, called *porins*. In *E. coli*, OM pores exclude solutes with molecular weights of about 700 Da and above and tend further to discriminate against anionic solutes (Nikaido and Vaara, 1985).

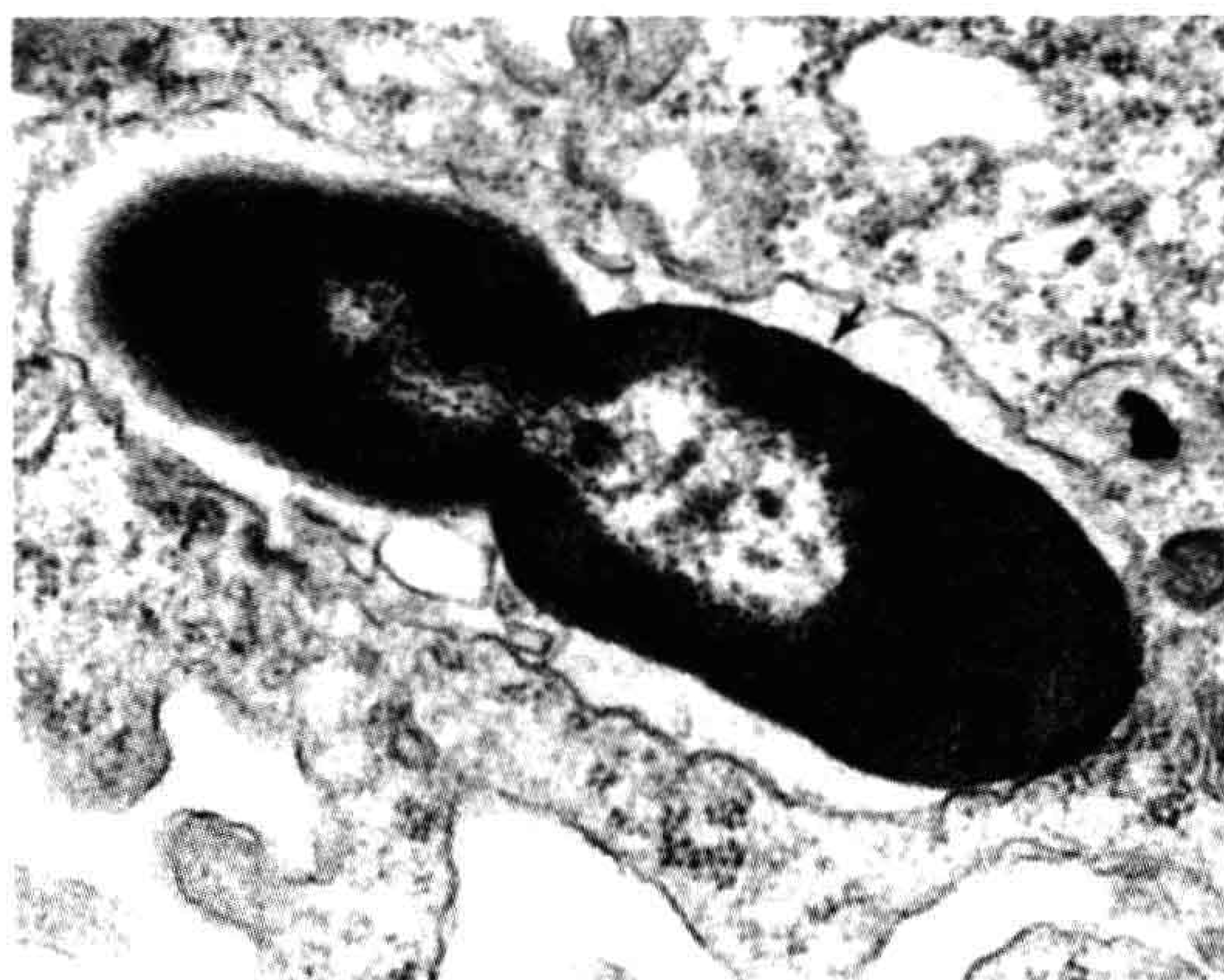


FIGURE 50.6 Electron micrograph (ultrathin section) of a Gram-negative bacterial cell. An *E. coli* cell is shown that has been engulfed by a macrophage and is in the late stages of cell division. The nucleoid is visible as a clear zone in each of the nascent daughter cells. The arrowhead indicates a region in which the three-layer structure of the Gram-negative cell envelope (CM-CW-OM) can be seen. *(Photograph courtesy of A. Mukkada).*

IIG. Intracellular Structures

Still greater complexity can be seen in a few bacterial cells which incorporate additional intracellular structures into the basic bacterial cell architecture described above. Examples of these specialized structures include photosynthetic membranes, internal cytoplasmic compartments and gas vesicles.

Although different groups of photosynthetic bacteria have biochemically diverse forms of photosynthesis, most involve specialized photosynthetic membranes located in the cytoplasm (see Fig. 50.3 panel IV). In the case of cyanobacteria, the intracellular photosynthetic membranes appear to be collapsed and lamellar in form and are called *thylakoids*, in conformity with the corresponding membranes of plant chloroplasts (see Chapter 51). For other types of photosynthetic bacteria, the membranes assume more rounded, vesicular shapes; these *intracytoplasmic membranes* (ICM) appear to be continuous with the CM (Dierstein et al., 1981).

Other membranes have been observed inside several genera of non-photosynthetic bacteria; most of the membranes have no confirmed metabolic function and they divide the cytoplasm into two or more compartments. These bacteria, collectively termed planctomycetes, all lack the peptidoglycan cell wall found in most bacteria and all have at least one large, internal membrane vesicle that divides the cytoplasm into two compartments of comparable volumes. One of these vesicles encloses the nucleoid, which tends to be highly condensed, forming a well-defined structure clearly visible in EM thin sections. In at least one species, a double-membrane structure surrounds the nucleoid, forming an analog of the eukaryotic nuclear membrane. Other species have multiple distinct membranes that create a nested series of cellular compartments (Fuerst, 2005).

TABLE 50.1 Cellular Properties of Gram-Positive and Gram-Negative Bacteria

Property	Gram-Positive Bacteria	Gram-Negative Bacteria
Cell wall		
Chemical constituents	Peptidoglycan	Peptidoglycan
	Teichoic, lipoteichoic and teichuronic acids	
Typical thickness	20–80 nm	2–3 nm
Outer membrane	(Absent)	Composed of LPS and phospholipid
Intrinsic resistance to detergents, dyes, and certain antibiotics	Low	High
Dessication resistance	High	Low
Examples	*Clostridium*	*Escherichia*
	Lactobacillus	*Thiobacillus*

Other bacteria and archaea produce small, regular vesicles in their cytoplasms which form from the self-assembly of protein subunits. The assembly process excludes water, so that the resulting vesicles contain only gas. The function of these *gas vesicles* (or gas vacuoles) appears to be to provide buoyancy, allowing the cell to migrate vertically in natural waters such as ponds. Consistent with this role, their synthesis is often regulated by environmental conditions, such a light intensity and oxygen concentration (Walsby, 1994).

IIH. Extracellular Structures

Bacteria and archaea have several structurally distinct types of external filaments which are anchored in the CM. *Flagella* are helical protein filaments that support rapid swimming motility. Depending on the bacterial species, they may be single or numerous, clustered or dispersed over the cell, or absent altogether. Each flagellum extends several cell lengths (2–20 μm) and is rotated by a protein complex at its base; as a result, it acts like a propeller to push the cell through its liquid medium. Thus, bacterial flagella have a cellular function (i.e. motility) analogous to that of eukaryotic cilia and flagella, but no structural, molecular or mechanistic homology to them (see Chapter 47).

Pili and *fimbriae* are structurally similar to each other and distinct from flagella. Both consist of straight protein fibers that protrude less than about 1 μm from the cell, giving it a bristled or hairy appearance in the electron microscope. Both types of appendages appear to mediate attachment of a bacterium to another cell. In many cases, pili attach a "donor" bacterium to a recipient cell for the subsequent transfer of DNA (conjugation), whereas fimbriae typically attach a pathogenic bacterium to specific cells of its host. In some bacteria, pili mediate a type of slow, surface-dependent motility (Strom and Lory, 1993).

Flagella, pili and fimbriae all form via self-assembly of small protein subunits. Bacterial flagella grow by adding protein subunits to the distal tip, which requires the subunits (monomers) to travel from the cytoplasm to the growing tip of the flagellum, several cell lengths away. This is accomplished by using the hollow core of the flagellum itself as a conduit. In contrast, pili and fimbriae appear to polymerize at the base of the fiber, where it attaches to the CM (Neidhardt et al., 1990).

In addition to these small, discrete structures, many bacteria secrete hydrophilic polymers (usually polysaccharides) that form a gelatinous matrix around the cell. If this matrix remains attached to the cell and forms a defined zone around it, it is called a *capsule*. Capsules inhibit the ingestion of bacteria by human phagocytes or by protozoa and may also help free-living bacteria survive temporary desiccation or starvation. Even if secreted polysaccharide does not form a defined capsule, it aids the non-specific adherence of bacteria to wetted solid surfaces, leading to the formation of "*biofilms*". Bacteria in biofilms tend to survive much higher concentrations of antibiotics than bacteria suspended in fluids and, accordingly, pose serious health risks if they form on surfaces of heart valves or implanted devices (Costerton et al., 1987).

III. ENERGETICS OF BACTERIAL CELLS

With a few notable exceptions, the endergonic cellular processes of bacteria are driven via enzymatic coupling to the hydrolysis of ATP and thus require the cell continuously

to re-supply this energy currency. An *E. coli* cell growing aerobically using glucose regenerates ATP by two fundamentally different strategies: *substrate-level phosphorylation* and *chemiosmotic coupling*. Other prokaryotes may use these two processes in ways that differ from *E. coli* and related bacteria, or may use only one of them.

IIIA. Substrate-Level Phosphorylation

As also occurs in the eukaryotic cytosol, soluble enzymes in the *E. coli* cytoplasm convert one mole of glucose to two moles of pyruvic acid via the Embden–Meyerhof–Parnas pathway ("glycolysis"); this process results in phosphorylation of 2 moles of ADP to form ATP and the reduction of 2 moles NAD^+ to NADH. If the cell has no exogenous electron acceptors available (see below), the two moles of ATP represents the cell's sole energy harvest and the reduced co-factor (NADH) represents unusable electrons. If the electrons are not transferred to some other molecule, the oxidized cofactor (NAD^+) will not be regenerated and additional glucose cannot be metabolized. Bacteria (and eukaryotic cells) solve the latter problem by transferring the electrons to pyruvate or its metabolites, thereby forming various organic compounds which the cell excretes; examples of these end-products include lactic, acetic, propionic or butyric acids and ethanol, butanol or acetone. This metabolic strategy of substrate-level phosphorylation, made possible by reduction of metabolites derived from the growth substrate, constitutes the biochemical definition of *fermentation*.

IIIB. Chemiosmotic Coupling

The general features of chemiosmotic coupling in bacteria and archaea resemble those of mitochondria and chloroplasts, which are described elsewhere in this volume (see Chapters 5 and 51). Also called *oxidative phosphorylation*, the process has two distinct stages, each of which involves vectoral enzymatic processes at the CM (Fig. 50.7). The first (oxidative) stage of chemiosmotic coupling transfers electrons taken from carbon compounds during glycolysis and the tricarboxylic acid cycle to some electron acceptor, such as O_2, via a series of enzymatically catalyzed, strongly exergonic, oxidation–reduction reactions. This respiratory electron transport is coupled at certain points to the extrusion of protons from the cytoplasm, creating a *proton potential* or *protonmotive force* (PMF) across the CM (Fig. 50.7). The second (phosphorylation) stage converts the PMF into ATP, using an F_1F_0 *proton-translocating ATPase* to couple the entry of three protons from outside the cell to phosphorylation of an ADP molecule (Harold and Maloney, 1996). The combination of these two stages yields many times more of ATP per glucose molecule than fermentation does.

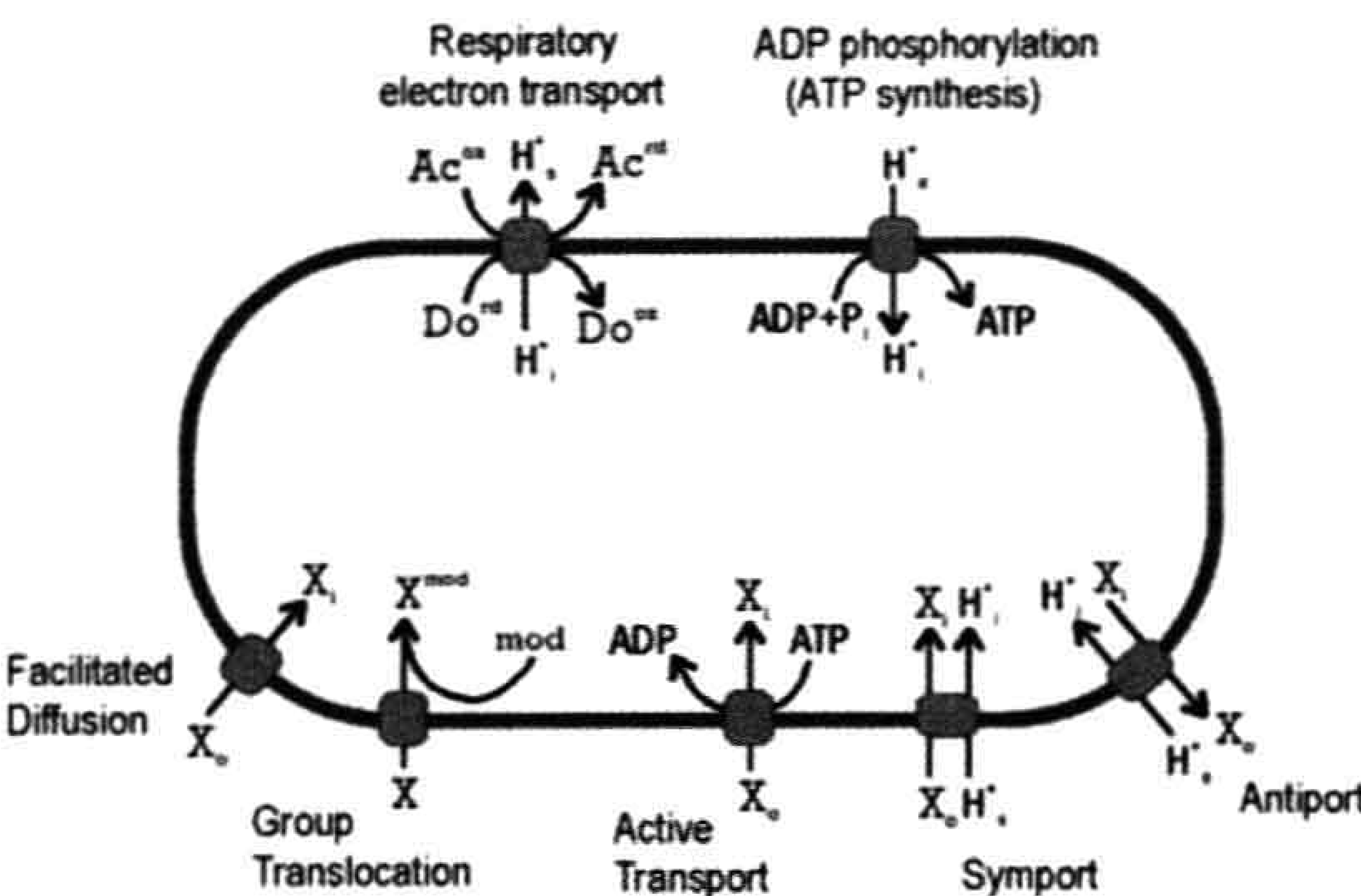


FIGURE 50.7 Energetics of solute transport across the CM. The diagram summarizes the salient features of major classes of energetic coupling to solute transport in prokaryotic cells. For example, the net result of respiratory electron transport is transfer of electrons from a donor (Do) to an acceptor (Ac) coupled to the extrusion of protons. Similarly, controlled entry of a proton through a membrane-bound ATPase drives the phosphorylation of ADP. The remaining processes are those which support growth by promoting the uptake of some necessary solute (X) from the environment. Cellular location is indicated by subscripts (o, outside; i, inside); "mod" indicates a chemical modification.

Oxygen represents only one of several terminal electron acceptors which prokaryotes can use to form a PMF. Accordingly, as summarized in Table 50.2, prokaryotes carry out various types of *anaerobic respiration*, but these may not be used under all conditions. *E. coli*, for example, can use four compounds in addition to oxygen as electron acceptors (Table 50.2), but it restricts the synthesis of the corresponding oxido-reductases according to a complex regulatory hierarchy. This hierarchy ensures that only the energetically most favorable electron acceptor is used, should more than one be available (Gunsalus, 1992).

TABLE 50.2 Respiratory Strategies of Prokaryotes

Electron Acceptor	Reduced Product	Organism
Oxygen	Water	*E. coli*, other aerobes
Nitrate	Nitrite	*E. coli*, other bacteria
Fumarate	Succinate	*E. coli*, other bacteria
Dimethyl sulfoxide	Dimethyl sulfide	*E. coli*, other bacteria
Trimethylamine oxide	Trimethylamine	*E. coli*, other bacteria
Sulfate	Hydrogen sulfide	*Desulfovibrio*, *Archaeoglobus**
Sulfur	Hydrogen sulfide	*Thermoproteus**
Carbon dioxide	Methane	*Methanobacterium**

*Denotes archaea; all others are bacteria.

The PMF of a respiring bacterium represents an energetic intermediate in the regeneration of ATP by the oxidation of carbon compounds, yet even bacterial cells that are not respiring, as well as those that cannot respire, maintain a PMF. The *lactic acid bacteria*, for example, have no electron-transport chain and generate ATP only by substrate-level phosphorylation. They nevertheless have an F_1F_0 ATPase and use it in the reverse sense of respiring bacteria, i.e. to maintain a PMF at the expense of ATP hydrolysis. This may reflect the fact that certain basic prokaryotic processes use the PMF directly as their energy source. *E. coli*, for example, uses direct coupling to H^+ influx, rather than ATP hydrolysis, to transport several nutrients (see below) and to drive flagellar rotation.

The PMF consists of two components: the electrical potential ($\Delta\psi$) and the chemical potential (ΔpH). Although the small size of prokaryotic cells precludes direct electrical measurement of these potentials, they can be estimated using chemical probes. The $\Delta\psi$ can be measured by the fluorescence yield of triphenylmethyl- or tetraphenylphosphonium ions, or by the equilibrium distribution of radioactive K^+ across the CM in the presence of valinomycin. The ΔpH can be estimated by the distribution of radioactive weak acids, such as acetic or benzoic acids, across the CM and the overall PMF can be independently estimated by the maximal accumulation of lactose by cells able to transport, but not metabolize, this sugar. According to these methods, which generally agree, a typical *E. coli* cell in medium at pH 6.5 has a $\Delta\psi$ of about 100 mV (inside negative) and a ΔpH that corresponds to an additional 100 mV (Harold and Maloney, 1996).

In those bacteria which live at pH values near 7, both components contribute significantly to the PMF. Extreme acidophiles, however, may maintain an electrical potential which is of opposite polarity as the normal $\Delta\psi$, i.e. inside positive. This helps counteract the very large ΔpH across the cytoplasmic membrane, which can be more than 4 pH units in these organisms. In contrast, extreme alkaliphiles, which grow at external pH values of 10–12, have a negative ΔpH across the CM and, accordingly, a very large $\Delta\psi$ (White, 2000). A number of these organisms, and certain neutrophiles from marine environments, use the more abundant Na^+ ion, rather than protons, to drive ATP synthesis via Na^+-coupled ATP synthases (Skulachev, 1994).

IV. SOLUTE TRANSPORT

While certain membrane proteins generate the ion potentials and ATP needed to drive metabolism, other proteins use related processes to transport a wide range of organic compounds and inorganic ions into the cell as raw material for metabolism and growth. These systems employ different mechanisms and they differ with respect to functional properties, including energetic cost, solute specificity and ability to concentrate the solute inside the cell. These functional properties, in turn, affect biological properties of the organism, including its ability to scavenge critical nutrients from its environment. Fig. 50.7 summarizes the basic transport strategies used by bacterial cells, and the energetic consequences of these processes, as described below.

IVA. Facilitated Diffusion

Although facilitated diffusion (see Fig. 50.7) is mechanistically simple and energetically cheap, it is rare among bacterial transport systems, presumably because it also relatively ineffective. One of the best-studied examples of a facilitated diffusion through a bacterial membrane is glycerol uptake in *E. coli*. In this case, extracellular glycerol diffuses passively through a polyol-specific membrane channel encoded by the *glpF* gene.

IVB. Group Translocation

In an elaboration of facilitated diffusion, the solute becomes chemically modified upon entering the cytoplasm. The chemical modification, or "group translocation" (typically phosphorylation or phosphoribosylation), converts an uncharged solute molecule into an ion that cannot diffuse out through the same membrane-bound carrier. In this way, the uncharged species actually transported by the channel can remain at a lower steady-state concentration inside the cell than outside and the modified solute can be concentrated in the cytoplasm, due to the investment of chemical energy. In most cases, however, the "trapping reaction" doubles as the first step in metabolizing the solute, so the modified form does not necessarily accumulate to high steady-state concentrations.

IVC. Active Transport

Active transport in bacteria is defined by the following features (Neidhardt et al., 1990):

1. specific steric recognition between the solute and a membrane-bound transport protein
2. release of the solute into the cytoplasm in its unmodified form
3. accumulation against a solute concentration gradient, and
4. expenditure of energy.

Two types of active transport are distinguished from each other by the immediate source of energy used (see Fig. 50.7). The first type requires the hydrolysis of ATP or an equivalent high-energy phosphoryl bond. In these

systems, the membrane-bound carriers typically consist of several subunits, one of which contains an ATP-binding site (Furlong, 1987). In Gram-negative bacteria, such a transporter often utilizes a non-membrane (i.e. soluble) protein located in the periplasm. Transport requires these periplasmic solute-binding proteins, as demonstrated by the fact that cold hypotonic shock treatment of bacterial cells, which releases only periplasmic proteins, also destroys transport capability. Studies of bacterial mutants and of cytoplasmic membrane vesicles confirm that the membrane-bound transporter interacts specifically not with external solute in its free form, but with the solute complexed to its cognate binding protein (Furlong, 1987).

The second type of active transport utilizes ionic potentials directly. In some cases, the solute enters via symport with a proton, in other cases, with an Na^+ ion. Alternatively, certain ions, such as Ca^{2+}, are pumped out of the cells by proton-coupled antiport systems (Harold and Maloney, 1996).

V. METABOLIC STRATEGIES

Prokaryotes are metabolically diverse and mediate many different conversions of compounds in their environments as a way to harvest energy and other metabolic resources. These conversions contribute to the global cycling of many ecologically essential elements and several are unique to archaea and bacteria.

VA. Autotrophy

A number of prokaryotes can derive all of their carbonaceous cell material from CO_2. This capability, termed *autotrophy*, requires environmental sources of energy and reducing equivalents (i.e. electrons). For several diverse families of bacteria (collectively called *photoautotrophs*), light provides the energy, whereas various inorganic and organic compounds in the environment provide electrons. Photoautotrophic bacteria exhibit great diversity with regard to the biochemistry of photosynthesis. Among them, only the *cyanobacteria* carry out *oxygenic photosynthesis* like that of plant chloroplasts, which reflects the ability to use water as the electron donor. Cyanobacteria contain *chlorophyll b* and have two connected *photosystems*: photosystem II (PS2) oxidizes water to supply electrons to photosystem I (PS1; see Chapter 51). This is the scheme also used by plant chloroplasts, to which cyanobacteria are evolutionarily related (Schwartz and Dayhoff, 1978).

The remaining groups of photoautotrophic bacteria perform *anaerobic (anoxygenic) photosynthesis*. They have only one photosystem, which can operate in a cyclic manner to produce a proton potential. In these cases, the electron equivalents for the reduction of CO_2 come from H_2S, H_2 or dissolved organic compounds, depending on the type of bacterium and the resources available to it. The photosynthetic pigments of the anoxygenic photoautotrophs, called *bacteriochlorophylls*, differ from cyanobacterial and plant chlorophylls in having intense absorbance maxima in the infra-red region of the spectrum. In many of these organisms, photoautotrophic growth represents only one among several metabolic options and production of photosynthetic pigments occurs only in the absence of oxygen.

Another form of autotrophy, *chemoautotrophy*, is unique to prokaryotes. Analogous to the harvesting of light energy by photoautotrophs, chemoautotrophs derive energy by mediating the oxidation and reduction of inorganic compounds in their environments. Aerobic chemoautotrophs include organisms that oxidize H_2, CO, NH_4^+, NO_2^-, elemental S, H_2S or Fe^{2+} using O_2. Anaerobic chemoautotrophs include organisms that derive energy from the reduction of CO_2 to CH_4, or of SO_4^{--} to H_2S.

Among both photo- and chemoautotrophs, at least three metabolic pathways have been identified by which CO_2 is "fixed" (i.e. reduced and incorporated into some common intermediary metabolite): (1) the *Calvin cycle*; (2) the *acetyl CoA pathway*; and (3) the *reductive tricarboxylic acid cycle* (Caldwell, 1995). Most photoautotrophic bacteria (and all green plants) use the Calvin–Benson cycle: carboxylation of ribulose bis-phosphate to yield two molecules of 3-phosphoglycerate, followed by a complex series of reactions to regenerate ribulose bis-phosphate (see Chapter 51). The acetyl-CoA pathway, used by methanogenic archaea and sulfate-reducing bacteria, involves the differential reduction of two CO_2 molecules. One is reduced to form a methyl group whereas another is reduced to form a carbonyl unit, which is condensed to the methyl group. The resulting acetyl unit is transferred to co-enzyme A for assimilation into cell material. The reductive tricarboxylic acid pathway begins with carboxylation of succinyl CoA to yield 2-oxo-glutarate, which is in turn carboxylated to yield isocitrate. The transformations of the TCA cycle then continue in reverse, leading to the cleavage of citrate by an ATP-dependent citrate lyase to yield acetyl CoA and oxaloacetate. Prokaryotes using this pathway include the "green" photosynthetic bacteria.

VB. Nitrogen Fixation

The only organisms that can fix nitrogen, i.e. convert N_2 into ammonia, are prokaryotes. This capability is relatively rare, however, and widely dispersed phylogenetically. It occurs in various aerobic, anaerobic, facultatively anaerobic bacteria (i.e. those able to grow either aerobically or anaerobically, including both heterotrophs and autotrophs) and in methanogenic archaea. N_2 reduction is carried out by a large enzyme complex, *nitrogenase*. It includes an iron-containing component and a molybdenum- and

iron-containing component and utilizes ATP plus a reduced low-potential ferredoxin or flavoprotein as the source of electrons. Nitrogenases are intrinsically O_2-sensitive and N_2-fixing prokaryotes use a variety of strategies to protect these enzymes from oxidative inactivation. For example, facultative anaerobes such as *Klebsiella* spp. express nitrogenase genes only under anaerobic conditions. Filamentous cyanobacteria, which generate O_2 during photosynthesis, sequester nitrogenase in specialized cells called *heterocysts*, in which the oxygenic photosystem II (PS2) does not operate. *Azotobacter* spp. are obligate aerobes that can fix nitrogen; they appear to scavenge intracellular O_2 by maintaining very high respiration rates.

VI. RESPONDING TO THE ENVIRONMENT

Prokaryotic cells cannot insulate themselves from the chemical and physical properties of their environments. As a result, they must routinely respond to stress and environmental change in order to optimize their growth or simply to survive. The molecular mechanisms underlying these responses are diverse, but all result in changes to the biochemical composition of the cell.

VIA. Osmotic Stress

Some cellular responses to environmental change are mediated directly by activation of existing proteins, as exemplified by the effects of osmotic stress on bacteria. A sharp increase in the extracellular solute concentration triggers a response in which the osmotic strength of the bacterial cytoplasm also increases (Neidhardt et al., 1990). In *E. coli*, the initial increase is primarily due to net K^+ uptake by transporters in the CM, which seem to sense cell turgor directly. At extremely high external ionic strength, however, K^+ accumulation alone does not appear to alleviate the deleterious effects of osmotic stress and the bacterial cells accumulate high concentrations of "*compatible solutes*" in the cytoplasm. Compatible solutes are charged organic molecules of which the two best studied examples are L-proline and glycine betaine. Typically, these compounds are scavenged from the environment and their accumulation in the cytoplasm permits growth at otherwise inhibitory external salt concentrations.

This osmotic stress response, which is typical of bacteria, indicates the physiological importance of water, solutes and turgor pressure for bacterial cells. In particular, the conservation, sophistication and energetic cost of this response suggest that turgor pressure per se is essential. This may reflect the fact that it provides the physical force that expands the bacterial cell, allowing its growth and subsequent division. Second, the importance of compatible solutes in physiological adaptation to high levels of osmotic stress suggests that these compounds perturb enzymatic and other cellular functions less than inorganic salts do, allowing them to accumulate to high intracellular concentrations with less impact on metabolism.

VIB. Acid Stress

Other responses to the environment involve changes in the pattern of gene expression which are often complex and lead to corresponding changes in the protein composition of the prokaryotic cell (Neidhardt et al., 1990). The response of enteric bacteria to pH stress provides an example of this strategy that involves changing the amount of enzymes and other proteins. When the pH of the growth medium decreases sharply, *E. coli* and *Salmonella enterica* increase the synthesis rate of about 50 proteins. These acid-induced proteins include catabolic (degradative) enzymes that decarboxylate basic amino acids (arginine, ornithine and lysine decarboxylases). The action of these enzymes on amino acids taken up from the environment generates CO_2 and diamines; the latter are exported from the cell and act to neutralize the acidic growth medium. Similarly, acid stress during anaerobic growth on a fermentable sugar increases lactate dehydrogenase and formate-hydrogen lyase; both of these enzymes divert the flow of intermediates through fermentative metabolism in ways that decrease the amount of acid produced (Slonczewski and Foster, 1996).

Many other prokaryotic responses to environmental change similarly involve changing the protein composition of the cell by modulating transcription of certain genes. This general strategy takes advantage of the relatively large biosynthetic capacity of the growing prokaryotic cell, its simple organization and a very short half-life of messenger RNA which, in *E. coli* (under standard conditions) averages 1.3 min. Studies of specific responses in bacteria have revealed an array of elegant and diverse molecular mechanisms for controlling gene expression, which lie outside the scope of this chapter. One example will be described, however, which involves transmembrane signaling and appears in many environmental responses in bacteria.

VIC. Phosphate Metabolism and "Two-Component" Regulatory Systems

When Gram-negative bacteria begin to starve for inorganic phosphate, they activate the transcription of several families of genes, whose products help the cell conserve phosphate and take up more of it from the environment (Wanner, 1993). The regulation process, which typifies a mechanism underlying many signal transduction systems in bacteria, involves the specific interaction and phosphorylation of two proteins, PhoR and PhoB, named after their respective genes in *E. coli*.

The phosphorylation state of the PhoB protein determines expression of the various genes of the

phosphate-starvation response. The phosphorylated form of PhoB (here designated "*PhoB") activates transcription of these genes, whereas the unphosphorylated form does not. The relative abundance of *PhoB is in turn determined by the conformational state of a CM protein, PhoR (Fig. 50.8). In its "activated" conformation ("*PhoR"), this protein acts as a PhoB kinase, whereas its "inactive" conformation ("PhoR") acts as a *PhoB phosphatase. Ultimately, the conformational state of PhoR is determined by the availability of inorganic phosphate in the external medium. By a mechanism which is not entirely clear, PhoR can sense the absence of phosphate-periplasmic binding protein complexes in the periplasm and assumes its active conformation under these conditions. The resulting *PhoR phosphorylates PhoB, forming *PhoB which, in turn, stimulates the transcription of *phoA* and other phosphate-scavenging genes (see Fig. 50.6). The result is a rapid increase in certain enzymatic activities which serve to alleviate a particular state of the cell, in this case, phosphate deficiency.

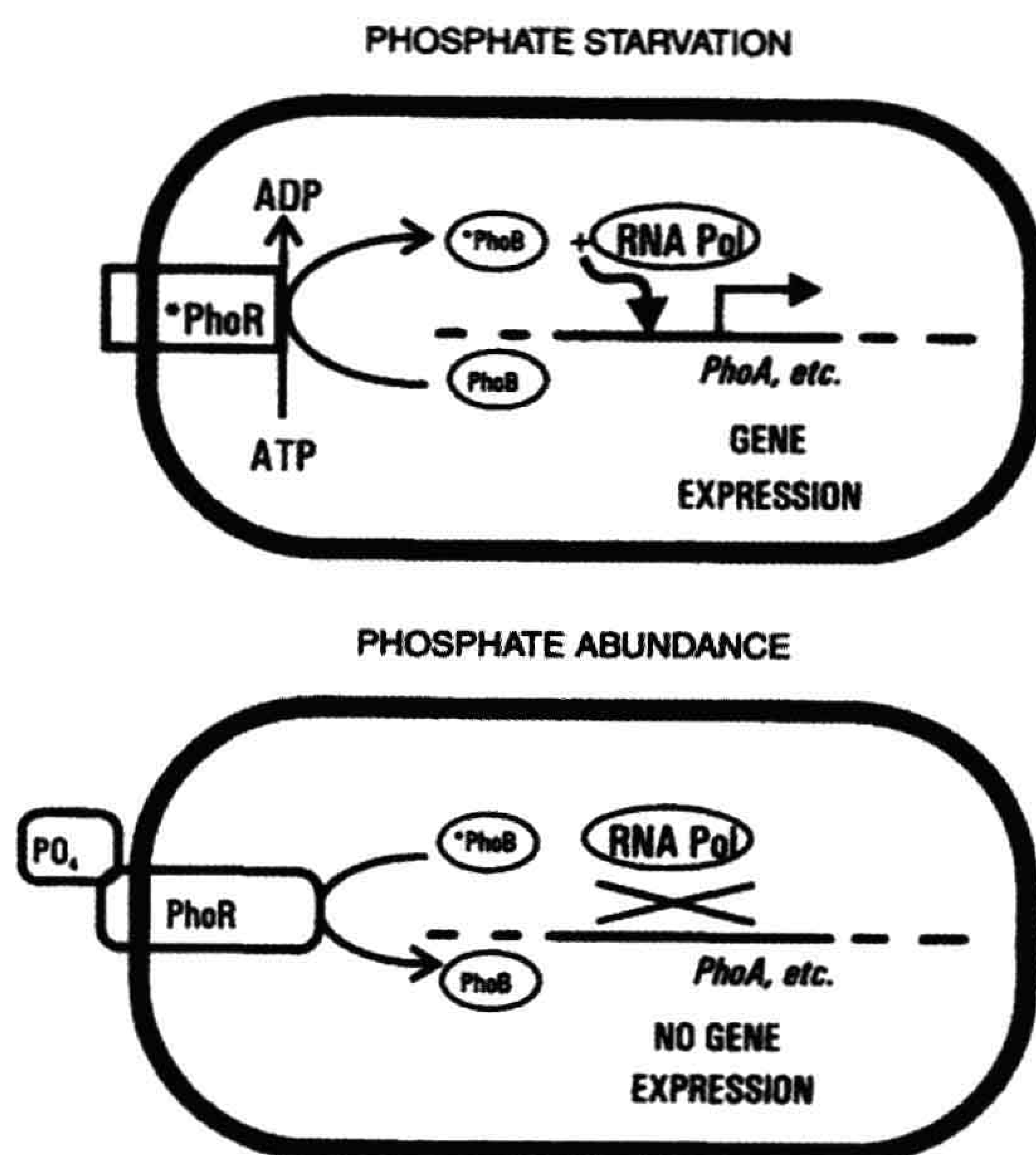


FIGURE 50.8 Essential features of two-component regulatory systems. A simplified version of phosphate-regulated gene expression is shown. The PhoR protein senses the extracellular availability of phosphate, either directly through an externally exposed domain, or indirectly via interaction with the high-affinity phosphate transporter (Neidhardt et al., 1990; Wanner, 1993). When the external phosphate concentration is low, PhoR becomes activated; this activated PhoR phosphorylates itself at the expense of intracellular ATP and then phosphorylates the PhoB protein. When the external phosphate concentration is high, PhoR becomes "de-activated"; in this form it removes phosphate groups from phosphorylated PhoB protein. PhoB is a soluble transcription factor for a specific set of genes, but stimulates transcription only when phosphorylated.

VID. Other Two-Component Regulatory Systems of Bacteria

Protein pairs resembling PhoR/PhoB mediate a wide variety of regulatory responses of bacteria to various types of environmental change (Table 50.3). The PhoR protein, a transmembrane signal transducer, typifies the *component I*, or *sensor-kinase*, of these systems. With a few exceptions, this is a protein of the cytoplasmic membrane that senses the status of some environmental parameter and accordingly adopts either of two conformations. In its "active" conformation, the component I has two characteristic phosphotransferase activities: (1) it phosphorylates one of its own histidine residues, using ATP; (2) it transfers the phosphate to an aspartyl residue on a cognate *component II* or *response regulator*. These two activities result in the net transfer of a phosphate group from ATP to the specific component II, which is usually a transcriptional regulator that activates transcription of a certain set of genes, but only in its phosphorylated form.

The similarities in interactions and biochemical properties of various components I and II (Table 50.4) are underscored by regions of sequence homology. Although they respond to diverse signals, all components I have two highly conserved sequence motifs at their carboxy termini. Similarly, all components II have sequence homology near their amino termini and various subfamilies may share regions of additional homology elsewhere in the amino acid sequence. The conserved regions of components I recognize and interact with the conserved regions of components II as an essential part of the signal-transmission process. The non-conserved regions among the components I and II presumably define their specificity for the external stimulus detected and for the particular cellular response, respectively.

VIE. Other Environmental Responses and their Mechanisms

VIE1. Iron Uptake

In oxidizing environments, iron occurs as the ferric ion and this form is extremely insoluble in neutral or basic solution. Bacteria have a characteristic strategy for scavenging ferric iron, which involves specialized iron chelators called *siderophores*, and transport systems specific for the iron–siderophore complexes (Earhart, 1996).

Nearly 100 distinct siderophores produced by microorganisms have been identified; all are relatively small molecules and they fall into two classes, i.e. those that use catecholate groups to complex the ferric ion vs those that use hydroxamate groups. Bacteria that have been examined intensively, such as *E. coli*, have been found to produce several siderophores of both classes, which they release into the environment under limiting-iron conditions. The siderophores complex ferric iron specifically and

TABLE 50.3 Examples of Two-Component Regulatory Systems

Mnemonic	Environmental Stimulus	Cellular Response	Component I	Component II
***Pho*sphate**	Low external [PO_4]	Induction of various PO_4-metabolizing enzymes	PhoR	PhoB
***N*itrogen *r*egulation**	Low external [NH_4^+]	Induction of glutamine synthetase	NR_I	NR_{II}
***O*uter *m*embrane *p*rotein**	External osmolarity	Regulation of alternate porin synthesis	EnvZ	OmpR
***A*erobic *r*espiratory *c*ontrol**	Oxygen concentration	Regulation of central metabolic enzymes	ArcB	ArcA
***N*itr*a*te *r*eductase**	External NO_3^- present, Oxygen absent	Induction of nitrate reductase	NarX	NarL
***Che*motaxis**	Temporal gradients of attractants and repellants	Change in swimming interval	CheA	CheY

with extremely high affinity (for ferric enterobactin, $K_d = 10^{-52}$ M) and bacteria use specialized, high-affinity transport systems to recover the resulting complexes. In the case of Gram-negative bacteria, transport is complicated by the fact that the complexes, though relatively small, are nevertheless too large to pass through the OM pores formed by porins. Gram-negative bacteria therefore have specialized OM receptors, which appear to function as gated pores that allow the complexes to enter the periplasm. This initial transport step involves a form of energetic coupling whose mechanism is still somewhat unclear, but requires a specific protein (TonB) that energizes transport of a few other solutes across the OM. Transport across the CM involves another siderophore-specific transporter (Earhart, 1996).

Once the iron–siderophore complex is inside the bacterial cytoplasm, the cell is faced with two additional challenges. First, the iron must be released from the siderophore; this is made difficult by the extreme affinity of the two components and appears to be solved by chemically modifying one or both of them. In some cases, the siderophore component of the complex appears to be destroyed enzymatically in the bacterial cytoplasm by hydrolases. The alternative strategy, reduction of the complexed ferric ion to ferrous ion, has also been detected, although some question remains as to whether reduction precedes release. Finally, it should be noted that excess (i.e. free) ferrous iron in the cytoplasm presents a serious threat, particularly to aerobic organisms, because it reacts with H_2O_2 to produce the extremely reactive hydroxyl radical. This problem is addressed by close regulation of the iron uptake systems and by synthesis of iron-storage proteins to sequester unused iron intracellularly (Earhart, 1996).

TABLE 50.4 General Features of Two-Component Regulators

Feature	Component I	Component II
Cellular location	Membrane	Cytoplasm
Cellular function	Sense and signal an external condition	Control gene expression
Biochemical activities	Autophosphorylation at histidine residue	Binding to regulatory regions of genes
	Phosphorylation of cognate component II	Stimulating transcription of specific genes
	may dephosphorylate cognate component II	May inhibit transcription of other specific genes
Sequence conservation	Two highly conserved regions near carboxyl end	One highly conserved region near amino end (subfamilies have additional regions of homology near carboxyl end)

VIE2. Magnetotaxis

Certain motile bacteria have been found that swim along the lines of an externally applied magnet field. Several species of these *magnetotactic bacteria* have been isolated and maintained as pure cultures in the laboratory, but most have resisted cultivation, although they can be observed in samples from natural environments. The difficulty of culturing magnetotactic bacteria stems, in part, from the fact that all known examples are *microaerophiles*, meaning that they require oxygen at low concentrations but are killed by it at atmospheric levels. Accordingly, these organisms typically occur at interfaces between oxic and anoxic layers of natural waters, as occur in marshes or swamps. In these settings, magnetotaxis along the

vertically inclined geomagnetic lines of force, perhaps combined with other environmental cues, may guide the cells to an appropriate position in a vertical oxygen gradient.

The dominant mechanism of magnetotaxis among these bacteria seems to be passive, in the sense that the cell aligns itself with the magnetic field while rotation of the helical flagellum drives it forward (Lefevre et al., 2009). This mechanism requires a strong magnetic dipole that is stably aligned (i.e. fixed) within the cell and parallel to the main axis of the flagellum. In magnetotactic bacteria, the dipole is provided by a short chain of single-domain magnetic crystals, called *magnetosomes*, each of which is enclosed in a phospholipid membrane. Other mechanistic details of magnetosome synthesis, including what determines the magnetic polarity of the chain and how the parallel orientation of internal magnet and flagellum is maintained, remain to be resolved (Jogler and Schüler, 2009).

VII. THE PHYSIOLOGY OF PATHOGENESIS

Bacteria capable of causing disease represent a tiny minority of known species. These *pathogens* are distinguished from the vast majority of bacteria by adaptations that allow them to invade their animal or plant host, elude multiple defense mechanisms (including the immune system), reproduce within host fluids and tissues, and damage host function in some way, thereby causing disease. The host defenses against the pathogens, as well as the mechanisms by which the pathogens damage the host, often involve specialized physiological functions of the host and bacterial cells, respectively.

One of the first host defenses encountered by a bacterium after invading the body is often a *phagocyte*, a specialized motile cell that circulates in the blood and engulfs bacteria. After a bacterial cell has been internalized (see Fig. 50.6), the resulting cytoplasmic vesicle fuses with a lysosome to form a phagolysosome. In addition to the low pH and digestive enzymes typical of lysosomes, phagolysosomes generate high concentrations of nitrous oxide, hypochlorous acid and reactive oxygen species, including hydrogen peroxide, singlet oxygen, superoxide and the hydroxyl radical. Synthesis of these strong oxidants is triggered when a phagocyte is activated and is accompanied by a sudden demand for oxygen, called the *respiratory burst*. The reactive compounds produced in this process, combined with the low pH inside the phagolysosome, normally kill the ingested bacterium.

However, certain pathogenic bacteria can survive in the phagolysosome, escape it and multiply in the cytoplasm of the phagocyte. In some cases, the strategy involves killing the phagocyte by secreting a toxin termed a *leukocidin*. Other bacterial countermeasures against phagocytosis include synthesis of cell-associated carotenoid pigments, which quench singlet oxygen, and synthesis of an external capsule (see Section II), which inhibits the initial engulfment of the bacterial cell.

Various pathogenic bacteria also secrete toxins at other stages of pathogenesis which target specific functions of host cells and tissues in causing disease. Several pathogens, for example, colonize the small intestine and produce an *enterotoxin* that induces diarrhea. *Vibrio cholerae*, which causes cholera, remains one of the most threatening of these bacteria globally, but pathogenic strains of *Bacillus cereus*, *E. coli* and *Salmonella enterica* also cause serious disease. Once established in the host, these bacteria produce enterotoxins that bind to specific gangliosides in the plasma membranes of intestinal epithelial cells. The cholera toxin covalently modifies and inactivates a GTP-binding protein that normally regulates an adenylate cyclase complex in the plasma membrane. Loss of this regulatory function causes overproduction of cAMP in the epithelial cell which, in turn, activates a number of cAMP-stimulated cellular functions, one of which is export of chloride ion. As large amounts of chloride are pumped into the lumen of the intestine, water follows by passive diffusion across the plasma membrane (O'Brien and Holmes, 1996). The massive secretion of salts and water into the lumen of the intestine results in a severe diarrhea, which may be lethal if water and salts are not replaced at an adequate rate.

Another class of damage-inducing proteins from pathogenic bacteria includes the *hemolysins*, named according to the fact that these proteins promote the lysis of erythrocytes (red blood cells). The most common technique for detecting hemolysin production involves incorporating whole blood into the agar plating medium used to grow bacterial colonies. If the bacterium produces a hemolysin, a clear zone, or halo, will form around the colony, caused by lysis of all the red blood cells within a short distance of the colony. Although they differ in some properties, hemolysins are generally small, secreted proteins which bind to the plasma membrane of the blood cells as individual subunits. The membrane-bound subunits then oligomerize to form a large pore in the plasma membrane, through which the cytoplasm escapes.

Bacterial toxins affecting yet a different host function, muscle contraction, are produced by two anaerobic, spore-forming pathogens: *Clostridium tetani* and *Clostridium botulinum*. Both species induce paralysis through disruption of the nervous system, but the two corresponding neurotoxins differ in the form of paralysis and the underlying mechanism. *Cl. tetani* infects host tissue, typically through deep puncture wounds, and produces *tetanus toxin*. This protein accumulates at the ends of inhibitory neurons where it blocks the inhibition of muscle contraction. The resulting uncontrolled contraction leads to a general spastic paralysis which can result in death by asphyxia. In contrast,

the neurotoxin of *Cl. botulinum* is normally produced during growth outside the host, but can be lethal if ingested, even in very small quantities. *Botulism toxin* binds to stimulatory motor neurons and prevents release of acetylcholine at the neuromuscular junction. This blocks muscle contraction, leading to a flaccid paralysis.

VIII. PROKARYOTES LIVING IN EXTREME ENVIRONMENTS

The physiological diversity and specialization of prokaryotes is illustrated dramatically by organisms which not merely tolerate chemical and physical extremes, but actually require them for normal cellular function. This heterogeneous group includes many species of archaea that have been discovered only in recent years as their natural habitats have been subjected to the appropriate sampling and cultivation methods.

Most *extreme halophiles*, organisms that thrive in concentrated brines, such as those that occur in natural salt lakes or artificial evaporation ponds, are archaea. Well-studied species include the rod-shaped *Halobacterium salinarum* (formerly *halobium*) and the irregularly shaped *Haloferax volcanii. H. salinarum* grows best in media containing 3–4 M NaCl and will not grow at salt concentrations less than 1.5 M. The cell maintains an internal K^+ concentration of upto 5 M and contains Cl^- as the major counterion. Accordingly, most *H. salinarum* enzymes function best in extremely high salt concentrations and denature at low salt concentrations (Kushner, 1985). The native structure of these halophilic enzymes tends to incorporate an unusually high number of acidic amino acid residues on the protein surface. Other notable features of the *H. salinarum* cell include gas vesicles in the cytoplasm and patches of a special retinal protein, *bacteriorhodopsin*, in the cytoplasmic membrane. The gas vesicles make the cells buoyant and thus help them maintain contact with two sources of energy: O_2 and light. Oxidation of organic compounds in the environment normally supports growth, but if oxygen becomes limiting, extra energy can be supplied by bacteriorhodopsin. This is a membrane-bound retinal protein that functions as a light-driven ion pump. When the cell is illuminated, it pumps protons from the cytoplasm; this contributes to the cell's PMF and thus, to the production of ATP, during O_2 deprivation (Kushner, 1985). Related proteins, collectively termed *proteorhodopsins* have more recently been identified in a number of archaea and also bacteria and some of these rhodopsins may have cellular functions distinct from ATP production (Fuhrman et al., 2008).

Extreme *acidophiles*, organisms which require low pH for optimal cell growth, include both bacteria and archaea. *Thiobacillus* spp. are Gram-negative bacteria that derive energy from the oxidation of reduced sulfur compounds. Since the oxidized end-product is usually H_2SO_4, these bacteria acidify their environment in the normal course of their metabolism. Some *Thiobacillus* cells grow optimally at about pH 2 but maintain a cytoplasmic pH near 6.5. At least one species, *Tb. ferrooxidans,* can also oxidize Fe^{2+}; this metabolic strategy is aided by the fact that autooxidation of Fe^{2+}, which would compete with the biologically mediated process, occurs very slowly at low pH values.

The most extreme acidophile known to date is a moderately thermophilic archaeon, *Picrophilus oshimae*. This organism, isolated from the soil of a Japanese geothermal field, grows optimally in dilute sulfuric acid at about pH 0.9. *P. oshimae* cells can grow at pH 0 but not at pH values above 3.5 and at pH values greater than 5, the cells lyse (Schleper et al., 1995).

Bacteria that require low temperatures are termed *psychrophiles* and typically occur in polar marine environments. Enzymes of these organisms may denature, and the cells may die, at room temperature. In several cases, the minimum temperature for growth has not been determined, but lies below about −10°C. The membrane phospholipids of these bacteria contain unusually high proportions of unsaturated and short-chain fatty acids (Morita, 1975).

At the other extreme, prokaryotes that grow optimally at 80°C or higher temperatures are termed *extreme thermophiles* or *hyperthermophiles* (Stetter et al., 1990). The cultivated species consist primarily of archaea isolated from geothermal habitats such as terrestrial hot springs or submarine thermal vents. Aerobic hyperthermophiles include *Sulfolobus* spp., which require acidic conditions as well as high temperatures. The combination of high temperature and low pH required for optimal growth (about 80°C and pH 3) is extremely effective at denaturing proteins. The *Sulfolobus* cell helps protect its cytoplasmic proteins, which appear to be generally heat-stable but not acid-stable (Grogan, 1996), by maintaining its cytoplasmic pH at about 6 (Schäfer et al., 1990). Physical properties of the unique lipids of *Sulfolobus* spp. probably help maintain the resulting ΔpH. The ether-linked phytanyl chains of these lipids span the entire membrane, forming a stable monolayer. Such membranes exhibit very low rates of proton leakage at high temperature, compared to ester-linked phospholipid bilayers (Van de Vossenberg et al., 1995) and this seems to represent an important prerequisite for efficient function of these cells.

The most thermophilic organisms known are anaerobic archaea isolated from submarine vents, where hydrostatic pressure permits liquid water to be superheated. *Pyrolobus fumarii*, the most thermophilic organism available in culture, grows optimally at about 106°C (Blöchl et al., 1997). The very existence of cells with such growth requirements raises fundamental questions regarding their need to stabilize nucleic acids, proteins and other

molecules necessary for all life. The thermostability of enzymes of most hyperthermophiles appears to be intrinsic, i.e. not due to counter-ions or other solutes. Biophysical analyses indicate that several classes of interactions of the amino acid residues contribute to this intrinsic structural stability (Jaenicke and Böhm, 1998).

IX. CONCLUSIONS

The smallest and simplest living cells are prokaryotic, consist of a nucleoid and cytoplasm enclosed in a cytoplasmic membrane. Most free-living prokaryotes also have a cell wall of some type and many bacteria have a second lipid membrane outside the cell wall, whereas a few have additional, internal structures. Though structurally simple, prokaryotic cells are evolutionarily diverse and include two distinct lineages, the Bacteria and the Archaea, each with a taxonomic status equal to all eukaryotic organisms. The cells of bacteria and archaea are functionally complex, mediating nutrient uptake, energy conversion and conservation, growth, secretion, genome replication, cell division and regulation of gene expression in response to environmental change. Prokaryotes encompass a wide range of metabolic strategies, including many not represented among eukaryotes. Several alternatives of CO_2 fixation and photosynthesis are represented among bacteria and archaea, of which only one, that of the cyanobacteria, has been adopted by green plants. Some prokaryotes grow chemoautotrophically, some can fix N_2 and some can "respire" anaerobically, using electron acceptors other than O_2 in their environments.

Bacteria depend on solute-specific transport proteins located in the CM to accumulate nutrients and to move inorganic ions into and out of the cell. Those proteins involved in active transport display a high affinity for the external solute and expend energy to accumulate it to high intracellular levels. A common type of active transport in Gram-negative bacteria utilizes soluble proteins which bind the solute in the periplasm and deliver it to the corresponding membrane-bound transporter. Some membrane transporters mediate homeostatic responses to environmental stress. Others communicate with "two-component" systems to regulate bacterial gene expression. In most cases, bacteria change their macromolecular compositions in response to changes in external conditions. This form of physiological adaptation can occur quickly, due to the high biosynthetic capacity of prokaryotic cells relative to cell mass.

A few bacteria are specialized to evade the defense systems of multicellular organisms and cause damage to their host. The host defenses of mammals include cells specialized for the destruction of bacteria via controlled generation of reactive chemicals, whereas the damage to the host caused by pathogenic bacteria is, in many cases, mediated by protein toxins which target specific proteins or cell types.

The specialization and functional diversity of prokaryotic cells becomes apparent in extreme environments. Certain bacteria require low external pH or low temperature to survive and grow. Certain archaea require extremely high salt concentration or extremely high temperature for normal cellular function. Because archaea differ radically from *E. coli* and other well-studied microorganisms, pinpointing the physiological and biochemical basis of their adaptation to harsh environments remains a challenging area of research.

BIBLIOGRAPHY

Blöchl, E., Rachel, R., Burggraf, S., Hafenbrandl, D., Jannasch, H., & Stetter, K. O. (1997). *Pyrolobus fumarii*, gen. and sp.nov., represents a novel group of archaea, extending the upper temperature limit for life to 113°C. *Extremophiles, 1*, 14–21.

Boucher, Y. (2007). Lipids: biosynthesis, function, and evolution. In R. Cavicchioli (Ed.), *Archaea: Molecular and Cellular Biology* (pp. 341–353). Washington, DC: American Society for Microbiology.

Caldwell, D. R. (1995). *Microbial Physiology and Metabolism*. Dubuque, IA: William C. Brown Publishers.

Costerton, J. W., Cheng, K.-J., Geesey, G. G., et al. (1987). Bacterial biofilms in nature and disease. *Ann Rev Microbiol, 41*, 435–464.

Dierstein, R., Schumacher, A., & Drews, G. (1981). On insertion of pigment-associated polypeptides during membrane biogenesis in *Rhodopseudomonas capsulata*. *Arch Microbiol, 128*, 376–383.

Earhart, C. F. (1996). Uptake and metabolism of iron and molybdenum. In F. C. Neidhardt (Ed.), *Escherichia coli* and *Salmonella:* Cellular and Molecular Biology (2nd ed.). (pp. 1079–1090) Washington, DC: American Society for Microbiology.

Fuerst, J. A. (2005). Intracellular compartmentation in planctomycetes. *Ann Rev Microbiol, 59*, 299–328.

Fuhrman, J. A., Schwalbach, M. S., & Stingl, U. (2008). Proteorhodopsins: an array of physiological roles? *Nat Rev Microbiol, 6*, 488–494.

Furlong, C. (1987). Osmotic-shock-sensitive transport systems. In F. C. Neidhardt (Ed.), *Escherichia coli* and *Salmonella:* Cellular and Molecular Biology (pp. 768–796). Washington, DC: American Society for Microbiology.

Grogan, D. W. (1996). Organization and interactions of cell envelope proteins of the extreme thermoacidophile *Sulfolobus acidocaldarius*. *Can J Microbiol, 42*, 1163–1171.

Gunsalus, R. P. (1992). Control of electron flow in *Escherichia coli*: coordinated transcription of respiratory pathway genes. *J Bacteriol, 174*, 7069–7074.

Harold, F. M., & Maloney, P. C. (1996). Energy transduction by ion currents. In F. C. Neidhardt (Ed.), *Escherichia coli* and *Salmonella:* Cellular and Molecular Biology (2nd ed.). (pp. 283–306) Washington, DC: American Society for Microbiology.

Jaenicke, R., & Böhm, G. (1998). The stability of proteins in extreme environments. *Curr Opin Struct Biol, 8*, 738–748.

Jogler, C., & Schüler, D. (2009). Genomics, genetics, and cell biology of magnetosome formation. *Annu Rev Microbiol, 63*, 501–521.

Kletzin, A. (2007). General characteristics and important model organisms. In R. Cavicchioli (Ed.), *Archaea: Molecular and Cellular Biology* (pp. 14–92). Washington, DC: American Society for Microbiology.

Kushner, D. J. (1985). The Halobactericeae. In J. R. Socatch, & L. N. Ornston (Eds.), *The Bacteria: vol. VIII Archaebacteria* (pp. 171–214). Orlando: Academic Press, Inc.

Lefevre, C. T., Song, T., Yonnet, J. P., & Wu, L. F. (2009). Characterization of bacterial magnetotactic behaviors by using a magnetospectrophotometry assay. *Appl Environ Microbiol, 75*, 3835–3841.

Morita, R. Y. (1975). Psychrophilic bacteria. *Bacteriol Rev, 89*, 144–167.

Neidhardt, F. C., Ingraham, J. L., & Schaechter, M. (1990). *Physiology of the Bacterial Cell.* Sunderland, MA: Sinauer Associates, Inc.

Nikaido, H., & Vaara, M. (1985). Molecular basis of bacterial outer membrane permeability. *Microbiol Rev, 49*, 1–32.

O'Brien, A. D., & Holmes, R. K. (1996). Protein toxins of *Escherichia coli* and *Salmonella*. In F. C. Neidhardt (Ed.), *Escherichia coli* and *Salmonella:* Cellular and Molecular Biology (2nd ed.). (pp. 2788–2802) Washington, DC: American Society for Microbiology.

Pettijohn, D. E. (1996). The nucleoid. In F. C. Neidhardt (Ed.), *Escherichia coli* and *Salmonella:* Cellular and Molecular Biology (2nd ed.). (pp. 158–166) Washington, DC: American Society for Microbiology.

Schäfer, G., Anemüller, S., Moll, R., Meyer, W., & Lübben, M. (1990). Electron transport and energy conservation in the archaebacterium *Sulfolobus acidocaldarius. FEMS Microbiol Rev, 75*, 335–348.

Schleper, C., Pühler, G., Holz, I., et al. (1995). *Picrophilus* gen. nov., fam. nov: a novel heterotrophic, thermoacidophilic genus and family comprising archaea capable of growth around pH 0. *J Bacteriol, 177*, 7050–7059.

Schwartz, R. M., & Dayhoff, M. O. (1978). Origin of prokaryotes, eukaryotes, mitochondria, and chloroplasts. *Science, 199*, 395–403.

Schwarz, U., Asmus, A., & Frank, H. (1969). Autolytic enzymes and cell division of *Escherichia coli. J Mol Biol, 41*, 419–429.

Skulachev, V. P. (1994). The latest news from the sodium world. *Biochim Biophys Acta, 1187*, 216–221.

Slonczewski, J. L., & Foster, J. W. (1996). pH-regulated genes and survival at extreme pH. In F. C. Neidhardt (Ed.), *Escherichia coli* and *Salmonella:* Cellular and Molecular Biology (2nd ed.). (pp. 283–306) Washington, DC: American Society for Microbiology.

Stetter, K. O., Fiala, G., Huber, G., Huber, R., & Segerer, A. (1990). Hyperthermophilic microorganisms. *FEMS Microbiol Rev, 75*, 117–124.

Strom, M., & Lory, S. (1993). Structure–function and biogenesis of the type IV pili. *Ann Rev Microbiol, 47*, 565–596.

Van De Vossenberg, J., Ubbink-Kok, T., Elferink, M., Driessen, A., & Konings, W. N. (1995). Ion permeability of the cytoplasmic membrane limits the maximum growth temperature of bacteria and archaea. *Molec Microbiol, 18*, 925–932.

Walsby, A. E. (1994). Gas vesicles. *Microbiol Rev, 58*, 94–144.

Wanner, B. L. (1993). Gene regulation by phosphate in enteric bacteria. *JCell Biochem, 51*, 47–54.

White, D. (2000). *The Physiology and Biochemistry of Prokaryotes* (2nd ed.). New York: Oxford University Press.

Woese, C. R., Kandler, O., & Wheelis, M. (1990). Towards a natural system of organisms: proposal for the domains Archaea, Bacteria, and Eucarya. *Proc Natl Acad Sci USA, 87*, 4576–4579.

Yanofsky, C., & Crawford, I. P. (1987). The tryptophan operon. In F. C. Neidhardt (Ed.), *Escherichia coli* and *Salmonella typhimurium:* Cellular and Molecular Biology (pp. 1453–1472). Washington, DC: American Society for Microbiology.

Section VIII

Specialized Processes: Photosynthesis and Bioluminescence

Chapter 51

Photosynthesis

Darrell Fleischman

Chapter Outline

I. SUMMARY

Plants, algae and photosynthetic bacteria capture the energy of sunlight and store it in molecules such as starch and sucrose. Light is absorbed by light-harvesting pigments such as chlorophyll. The energy is transferred to a special pair of chlorophyll molecules in the photosynthetic reaction center. The energy is converted to chemical energy as the special chlorophyll pair transfers an electron to an acceptor. The electron proceeds along an electron transport chain, ultimately reducing $NADP^+$ to NADPH or cycling back to the reaction center. The electron flow creates a proton concentration gradient across the membrane, which drives the formation of ATP. Plants contain chloroplasts. Chloroplasts have two photosystems, connected in series to form an electron transport system known as the Z scheme. In the System 2 reaction center, electrons are extracted from water, releasing O_2. The System 1 reaction center donates electrons to $NADP^+$. The ATP and NADPH are used for the synthesis of carbohydrates in a series of reactions known as the reductive pentose phosphate cycle.

II. INTRODUCTION

IIA. Historical Aspects

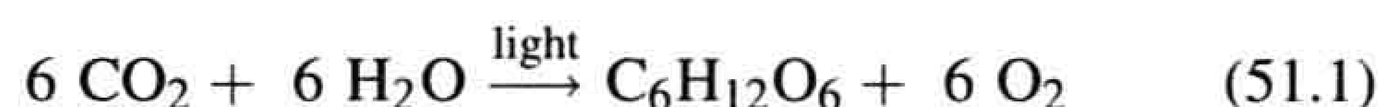
It must have been apparent from the earliest times that animals can survive only by eating plants or other animals, whereas plants seem to subsist on nothing but sunshine and a little water and earth. Julius Mayer, who introduced the concept of conservation of energy, suggested in 1845 that green plants can capture the energy of light and store it in a chemical form. His insight was correct. Almost all of the free energy used by living organisms is derived from energy of sunlight, which has been stored in photosynthetically produced molecules.

Clues about how plants might store free energy were obtained early (Loomis, 1960). In 1771, the English philosopher Joseph Priestly began a series of experiments that demonstrated that plants produce a gaseous substance, oxygen, which animals require for respiration. By the end of the 19th century, it was recognized that oxygen is produced only by the green parts of the plant and that its production requires light, carbon dioxide and water. The first visible products of

Cell Physiology Sourcebook. DOI: 10.1016/B978-0-12-387738-3.00051-2

photosynthesis were grains of starch, a polymer of glucose.

We now know that photons are captured by *chlorophyll*, the green pigment found in leaves, as well as by accessory pigments such as carotenoids (Fig. 51.1). Plants use the energy of the photons to extract electrons from water (leaving oxygen as a by-product) and use them to convert inorganic molecules such as carbon dioxide to organic molecules such as glucose:



$$6\ CO_2 + 6\ H_2O \xrightarrow{\text{light}} C_6H_{12}O_6 + 6\ O_2 \qquad (51.1)$$

The products of the above process contain more free energy per mole of glucose formed than do the reactants, that is:

$$\Delta G0 = 686\ \text{kcal/mol} \qquad (51.2)$$

Nitrogen and sulfur also can be fixed, i.e. converted from inorganic to organic form, by the photosynthetic system. Nitrogen and sulfur that are contributed by inorganic starting materials (including dinitrogen (N2), nitrate and sulfate) are incorporated into amino acids and other organic molecules. In this chapter, we discuss in detail only carbon fixation.

A comprehensive discussion of the history of photosynthesis research has been presented by Bacon Ke (2001). A timeline of photosynthesis research by Thomas Brennan (2008) is available on Photobiological Sciences Online. This site, sponsored by the American Society for Photobiology, includes a number of excellent review modules covering various aspects of photosynthesis.

IIB. Bacterial Reaction Centers

Higher plants are not the only organisms that perform photosynthesis. Algae also do, as do many bacteria. In all of them, the energy of light is converted to chemical energy in photosynthetic reaction centers. These are membrane-bound oligomeric protein complexes which contain a chlorophyll or bacteriochlorophyll dimer known as a special pair. The special pair donates an electron to an acceptor molecule following absorption of a photon. The reaction centers of plants, algae and photosynthetic bacteria resemble each other surprisingly closely. It has been suggested that they have evolved from a common ancestor. We will begin by describing bacterial reaction centers. Photosynthetic bacteria are described in more detail by Jones (2009) and Hunter et al. (2008) and reaction centers are discussed by Yocum (2008a).

It has been possible to isolate many of the oligomeric protein complexes involved in photosynthesis by dissolving the membranes in detergent and purifying the complexes through chromatography and other techniques. The reaction centers of purple photosynthetic bacteria are embedded in the cell membrane or in the membranes of

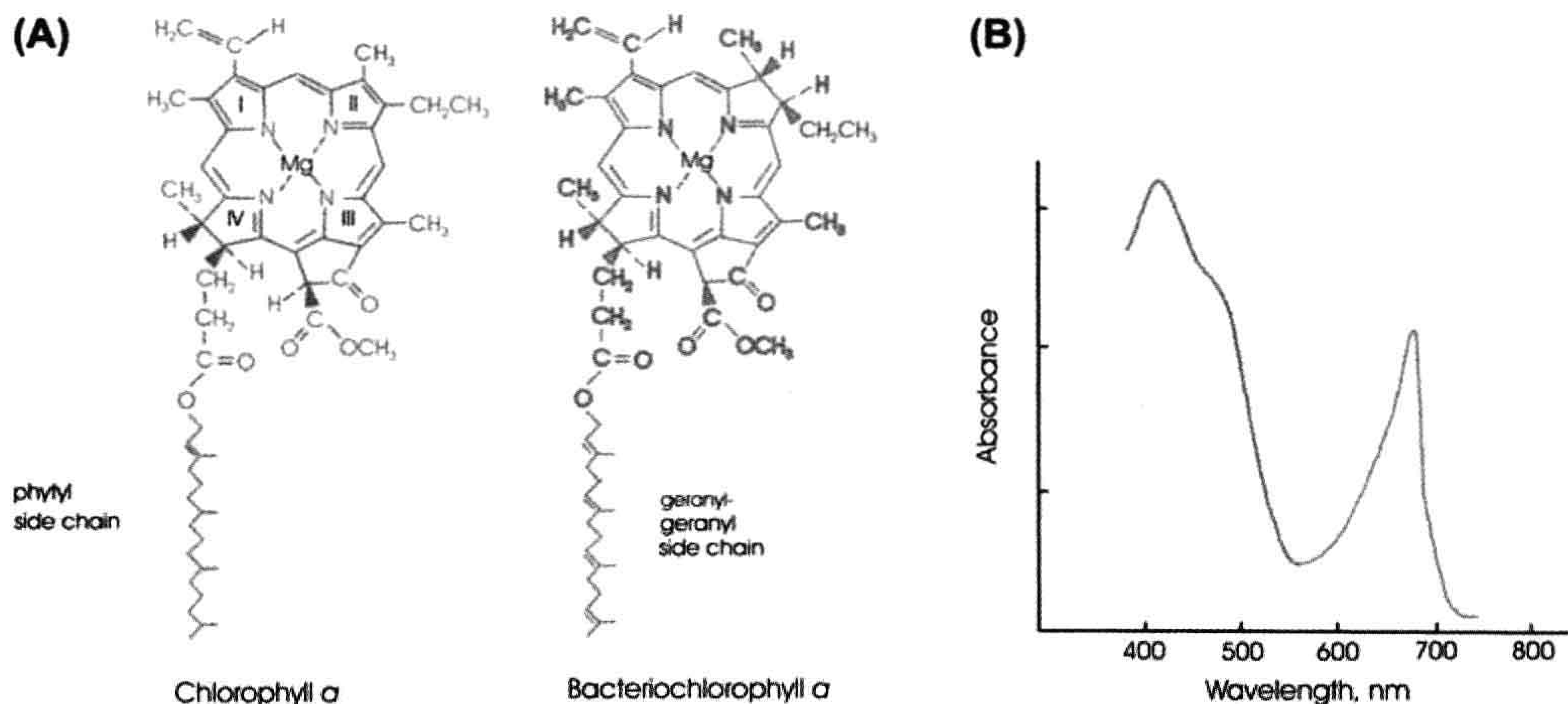


FIGURE 51.1 (A) The structures of chlorophyll *a* (Chl *a*) and bacteriochlorophyll *a* (BChl *a*). Differences between the structures of the various forms of chlorophyll contribute to differences between the absorption spectra of chlorophyll-containing proteins, allowing them to capture light in different regions of the spectrum. The conjugated system in BChl has one fewer double bond (in ring II) than that of Chl *a*. Single resonance forms of the conjugated systems of double bonds are shown. In Chl *b*,-HC=O replaces the red methyl substituent on ring II of Chl *a*. In BChl *b*, =CH-CH_3 replaces the red substituents on ring II of BChl *a*. In some bacteria, phytyl rather than geranylgeranyl serves as the side chain of bacteriochlorophyll *a* or bacteriochlorophyll *b*. Other forms of chlorophyll are found in some organisms. Pheophytins resemble the respective chlorophylls, but the Mg^{2+} is replaced by two protons. (B) Absorption spectrum of a typical plant chloroplast. Both Chl *a* and Chl *b* absorb light between 400 nm and 500 nm and between 600 nm and 700 nm. In addition, β-carotene absorbs light between 400 nm and 500 nm.

intracytoplasmic vesicles which are often called chromatophores. Hartmut Michel, Johann Deisenhofer and Robert Huber isolated reaction centers from the green-colored (!) purple bacterium *Blastochloris viridis* (formerly *Rhodopseudomonas viridis*), devised a way to crystallize them and determined their structure by x-ray diffraction (Diesenhofer and Michel, 1989). This was the first crystallization of a membrane protein and paved the way for determination of the structures of many prokaryotic and eukaryotic membrane proteins. In addition, the reaction center structure provided important insights into the general properties to be expected of integral membrane proteins. The *Blc. viridis* reaction center consists of four subunits. Subunits L and M have similar but not identical amino acid sequences. Each comprises five α-helices that cross the membrane. The co-factors that participate in electron transport are bound to the L and M subunits. Their arrangement is sketched in Fig. 51.2. The primary electron donor (known as P985 because a loss of optical density at 985 nm accompanies its photo-oxidation) is indeed a dimer, in this case of bacteriochlorophyll b. The reaction center also includes two additional molecules of bacteriochlorophyll b, two of bacteriopheophytin b, one molecule each of menaquinone, ubiquinone and carotenoid, and a non-heme ferrous iron ion. Bacteriopheophytin is similar to bacteriochlorophyll, but the Mg^{2+} is replaced by two protons.

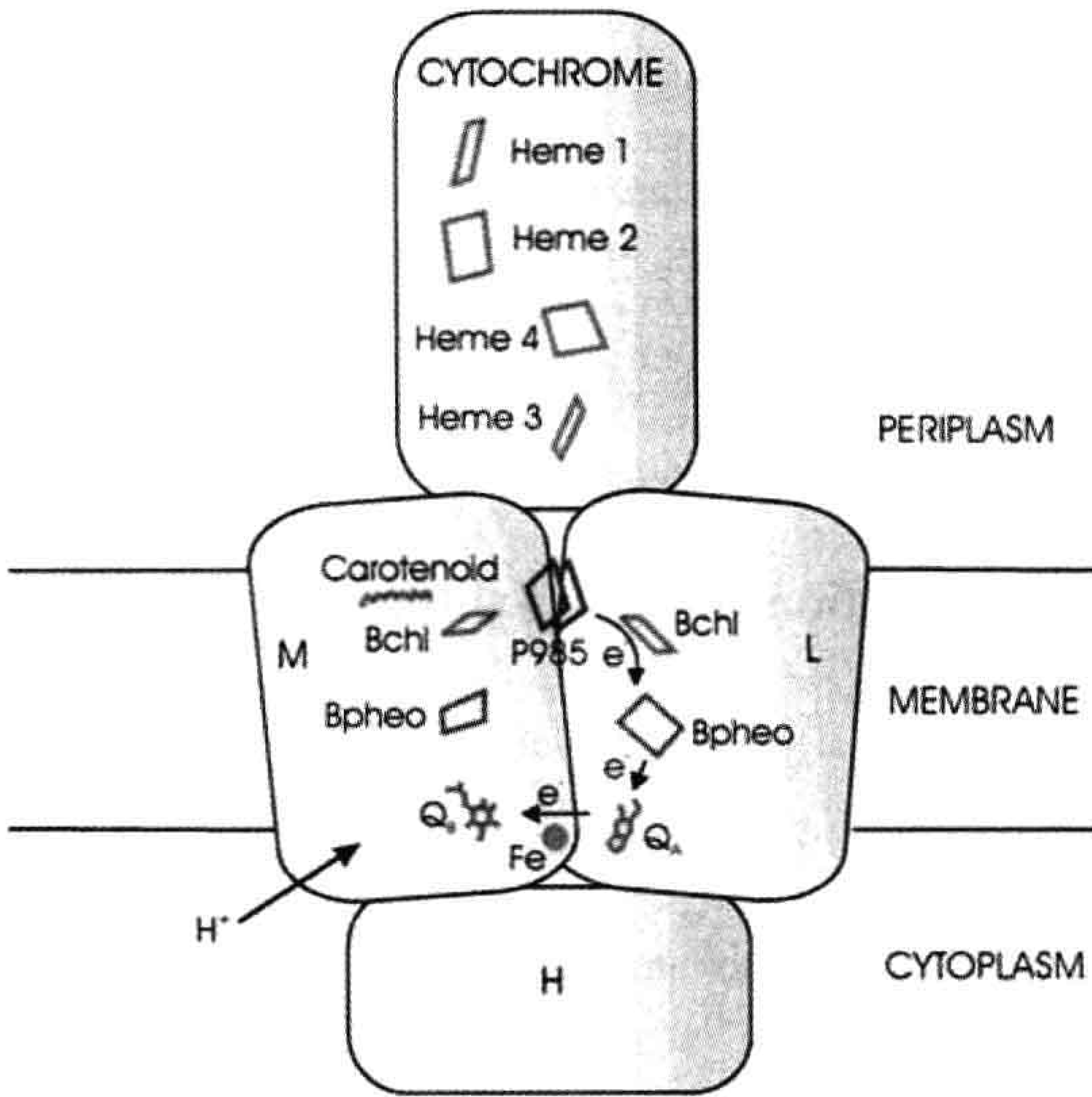


FIGURE 51.2 The arrangement of the co-factors in the *Blastochloris viridis* reaction center. The reaction center has approximate twofold (C_2) symmetry, but electrons move only along the path indicated. After Q_B accepts two electrons, two protons from the cytoplasmic side of the membrane are bound. P985, the photochemically active bacteriochlorophyll *b* dimer; Bchl, bacteriochlorophyll *b;* BPheo, bacteriopheophytin *b;* Q_A, menaquinone; Q_B, ubiquinone; Fe, ferrous iron.

Surprisingly, the reaction center has approximate twofold symmetry. The electrons leaving P985 move down only the L side of the reaction center. The first electron transfer, to the accessory bacteriochlorophyll b, occurs within a few picoseconds (10^{-12} s). The electrons move to the bacteriopheophytin b associated with subunit L, to QA (menaquinone) and, finally, to QB (ubiquinone). Upon receiving two electrons (after two photoacts), the ubiquinone binds two protons from the periplasm as it is reduced to ubihydroquinone. The ubihydroquinone dissociates into the membrane and diffuses to a cytochrome bc_1 complex, where it is re-oxidized. The reaction center also includes a cytochrome subunit containing four hemes, which is located on the periplasmic surface (facing the outside of the cell) of the membrane. The hemes donate electrons to oxidized P985. There is also an H subunit, which forms a sort of cap on the cytoplasmic side of the L and M subunits and is anchored to the membrane by a single membrane-spanning helix. Its function is not known. Purple bacterial reaction centers are embedded in the cytoplasmic membrane or in the membranes of intracellular vesicles which are often termed *chromatophores*.

Photosynthetic electron transport systems are capable of transporting electrons much more rapidly than photons of sunlight arrive at the special pairs. Therefore, reaction centers are accompanied by arrays of *light-harvesting* antenna pigments whose purpose is to capture photons and transfer the excitation energy to the special pairs. Purple bacterial reaction centers are surrounded by a "picket fence" of transmembrane dimers to which are bound bacteriochlorophyll and carotenoid molecules. The monomers, designated α and β, comprise the LH1 (light-harvesting 1) complex (Fig. 51.3). The carotenoids absorb photons in the middle of the visible spectrum and quickly pass the excitation to the bacteriochlorophyll. The bacteriochlorophyll absorbs photons in the blue, red and near-infrared regions of the spectrum. The excitations become delocalized within the circle of bacteriochlorophylls within femtoseconds (10^{-15} s) and are transferred to the special air in tens of picoseconds, faster than many can be lost as heat or fluorescence. Details of these processes are discussed by Blankenship (2002).

Other purple bacterial reaction centers have the same basic structure, but with variations. Most have bacteriochlorophyll α, bacteriopheophytin α and only ubiquinone. Many lack a bound cytochrome subunit. Observation of their topography by atomic force microscopy has revealed a variety of arrangements of LH1, including reaction centers multimers surrounded by continuous LH1 complexes (Sturgis and Niederman, 2008). Many have peripheral light-harvesting complexes, designated LH2, LH3, etc. Like LH1, they are composed of α and β subunits arranged in cylinders. They transfer absorbed excitations to LH1.

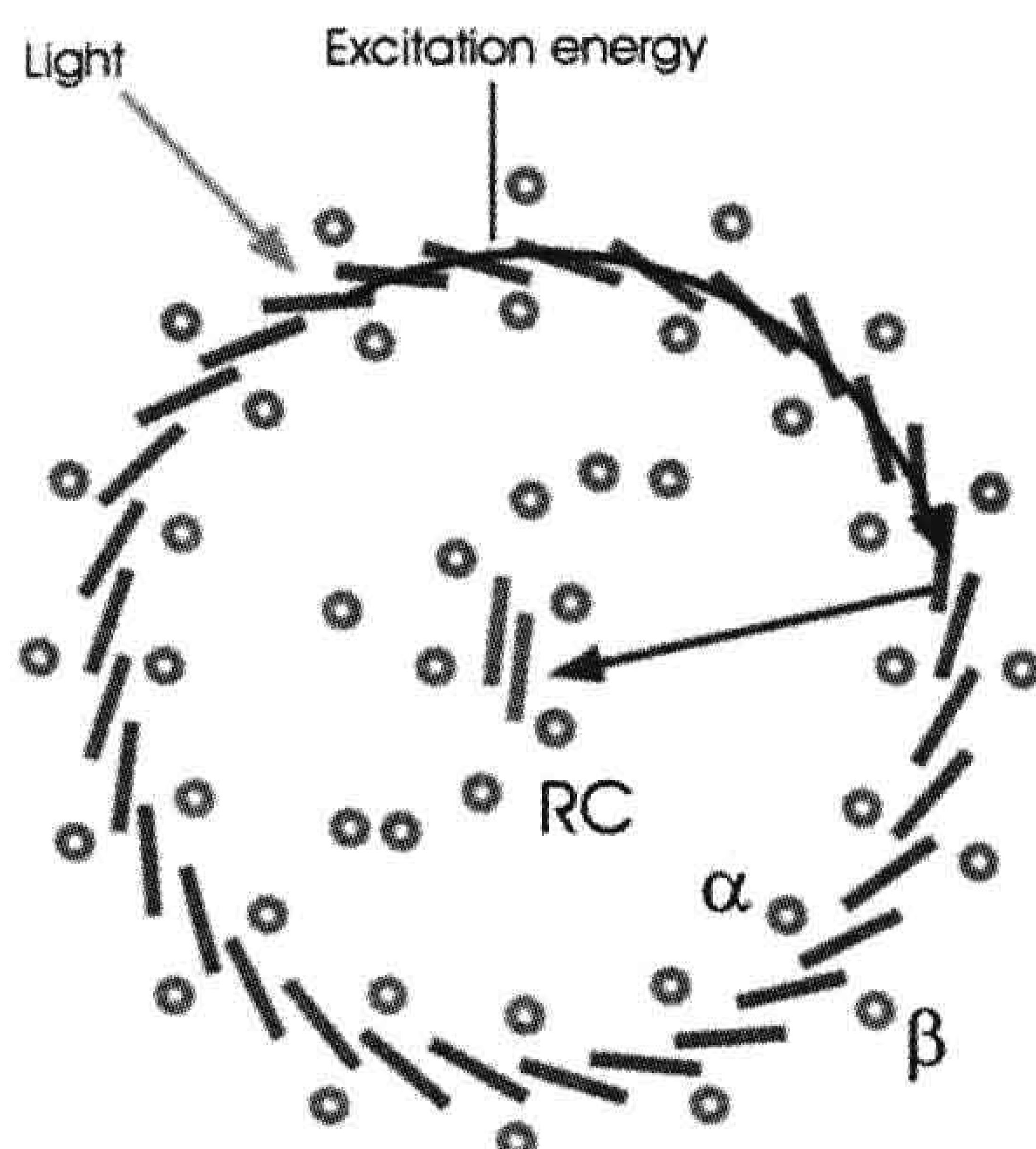


FIGURE 51.3 Light absorption and the transfer and capture of excitation energy. Protein dimers to which BChl and carotenoid molecules are bound form a ring around the reaction center. (Higher plant light harvesting pigments have a quite different structure.) Light is absorbed by any bacteriochlorophyll molecule (dark rectangles). The excitation energy is then delocalized among the bacteriochlorophyll molecules and finally captured by a special bacteriochlorophyll pair in the reaction center (RC). The figure is based on the structure of the bacterial light-harvesting complex reported by Cogdell et al. (1999).

IIC. Photosynthetic Bacteria

Photosynthetic bacteria play many important roles in the environment. As much as a third of the earth's photosynthesis is performed by microorganisms in the oceans. Six bacterial phyla include photosynthetic members (Blankenship, 2002; Jones, 2009; Golbeck, 2010; see Chapter 50). Five of them are termed *anoxygenic* because they are unable to oxidize water and evolve oxygen. Two of these possess *type II reaction centers*, which are basically similar to the *Blc. viridis* reaction center. Their terminal electron acceptors are quinones. Members of two phyla possess *type I reaction centers*. These have quinone acceptors, but rather than becoming doubly reduced and dissociating, the final quinone acceptor donates an electron to a bound iron-sulfur center (Fig. 51.4). Their core proteins are homodimers (identical monomers), rather than heterodimers like the L and M proteins of purple bacteria; they are flanked by two symmetrical light-harvesting domains. Members of the sixth phylum, the cyanobacteria, have both type I and type II reaction centers, connected in series. They are able to oxidize water and evolve oxygen and are termed *oxygenic*.

Purple bacteria belong to the Proteobacteria, along with such bacteria as *E. coli.* They are found in many terrestrial and aquatic environments, sometimes even in symbiotic associations with eukaryotes. Some are obligate anaerobes; others can grow photosynthetically in the absence of oxygen, heterotrophically (using organic compounds as carbon sources) in its presence, or by fermentation. One group, the aerobic anoxygenic phototrophs or aerobic photosynthetic bacteria, form the photosynthetic system only in the presence of oxygen. Most purple bacteria can fix nitrogen. One, related to *Rhodpseudomonas palustris*, may have been the ancestor of *Bradyrhizobum,* which includes the soybean symbiont. The Chloroflexi (green non-sulfur or green filamentous bacteria) have type II reaction centers, although their subunits and co-factors differ somewhat from those of the purple bacteria. They also possess a very large bacteriochlorophyll-containing light-harvesting structure known as a chlorosome (Blankenship, 2002), which allows them to grow in very dim light.

A special issue of *Photosynthesis Research* is devoted to bacteria having type I reaction centers (see Golbeck, 2010). The Chlorobi (green sulfur bacteria) are obligate anaerobes, use reduced sulfur compounds as electron sources and also contain chlorosomes. The Firmicutes (e.g. heliobacteria) are Gram-positive anaerobes that prefer high light environments, use light energy to fix nitrogen and grow on organic compounds. They are often found in rice fields. *Candidatus*, belonging to the Acidobacteria, is thought to be aerobic, contains chlorosomes and does not fix carbon or nitrogen. The Cyanobacteria are oxygenic – they can oxidize water and evolve oxygen and possess both type I and type II reaction centers. They have light-harvesting systems known as phycobilisomes whose chromophores (light-absorbing entities) are linear tetrapyrroles known as phycobilins. They are found in many environments, are active nitrogen fixers and are responsible for the toxic blooms that appear in eutrophic waters. The bacterium *Halobacterium halobium* performs photosynthesis in a quite different way. Rather than chlorophyll, it uses bacteriorhodopsin, a carotenoid-containing protein resembling the visual pigment rhodopsin, to capture the energy of light in a process that does not involve electron transfer (Subramaniam and Henderson, 2000).

IID. Evolution of Photosynthesis

It is believed that the earliest photosynthetic bacterium appeared as early as 3.4 billion years ago at a time when the earth's atmosphere contained almost no oxygen (Blankenship, 2002; Olson and Blankenship, 2004; Blankenship et al., 2007). Its ancestor was presumably a lithotrophic bacterium that used H_2 or sulfide as an electron donor and had an electron transport system that included cytochromes. The chlorophyll biosynthesis pathway probably evolved from the heme biosynhesis pathway; the early steps are identical. Substitution of magnesium for iron would have produced a pigment having a much longer-lived excited state, more able to transfer an electron before it decayed. Reductions of some of the double bonds, perhaps by reductases related to the already

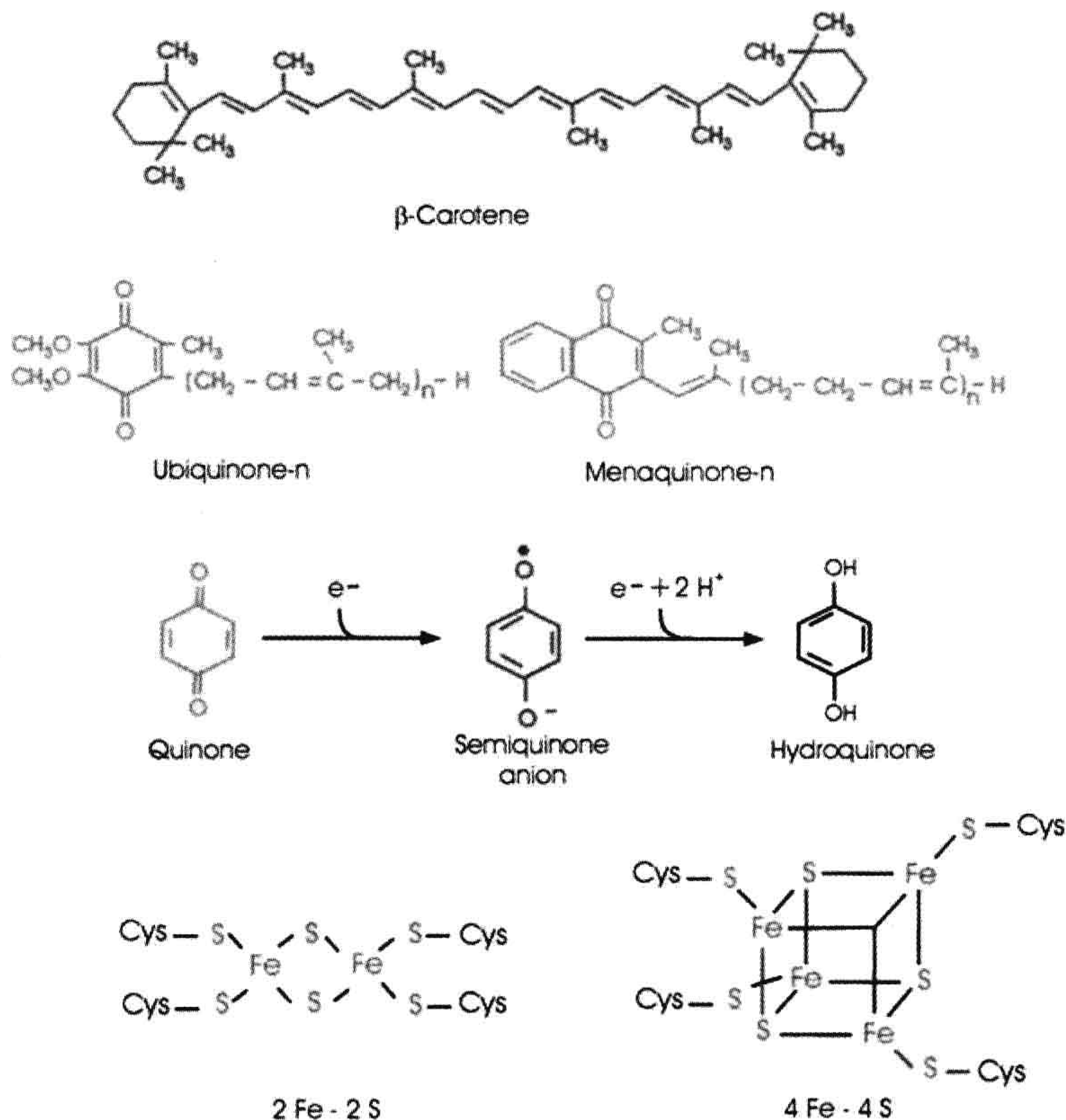


FIGURE 51.4 Structures of some of the molecules and co-factors involved in photosynthesis. Other carotenoids and quinones are found in many photosynthetic organisms. The quinone, semiquinone anion and hydroquinone forms of the quinone six-membered ring are shown.

present nitrogenase, created pigments able to absorb visible or near-infrared light. The first reaction center is thought to have been a monomer. Its structure may have resembled that of cytochrome *b*, which also binds tetrapyrroles and quinones. Gene duplication would have led to a bacterium having a homodimeric reaction center. Further duplications followed by evolutionary changes would have given rise to all of the contemporary reaction center types. Similarities in structure and amino acid sequence have led to the belief that they share a common ancestor. The evolutionary scenario is complicated by extensive lateral gene transfer.

Then, perhaps as early as 2.7 billion years ago, the cyanobacteria appeared. They possessed both type I and type II reaction centers, connected in series, and in the light could generate an oxidant strong enough to oxidize water. The new bacterium had access to a seemingly limitless source of electrons – water. The cyanobacteria may have arisen when genes for type I or type II reaction centers were transferred to a bacterium having the opposite type of reaction center. Alternatively, gene duplication and evolution may have created two reaction centers in the same bacterium. Loss of one or the other might have led to the appearance of each type of photosynthetic bacterium.

The cyanobactria formed oxygen as the byproduct of water oxidation. At first, the oxygen may have been consumed in chemical reactions with reductants such as Fe^{2+} but, by 2.3 billion years ago, it was accumulating in the atmosphere. The oxygen gave rise to the ozone layer and so permitted the development of higher organisms by shielding them from ultraviolet radiation.

Once oxygen was present, respiration and oxidative phosphorylation became possible. Using oxygen as an electron acceptor, bacteria could reoxidize photosynthetically synthesized molecules and regain some of the energy stored in them:



$$C_6H_{12}O_6 + 6\ O_2 \rightarrow O_2 + 6\ H_2O \quad (51.3)$$

$$\Delta G^0 = -686\ \text{kcal/mol} \quad (51.4)$$

Many of the proteins photosynthetic bacteria used for photosynthesis could also be used for oxidative

phosphorylation. Several lines of evidence suggest that purple photosynthetic bacteria might have been the ancestors of non-photosynthetic bacteria that perform oxidative phosphorylation and that the mitochondria of eukaryotic cells evolved from such bacteria which had formed symbiotic associations with primitive eukaryotic cells (Woese, 1987). Thus, it is no coincidence that the mechanisms of photosynthesis and respiration are similar in many respects. Much of our understanding of oxidative phosphorylation has come from studies of photosynthesis, which have exploited the experimental advantages of a system that can be driven by light.

In algae and higher plants, photosynthesis takes place in organelles known as *chloroplasts*. There is evidence that chloroplasts evolved from a cyanobacterium or *Prochloron*, which had formed a symbiotic association with a eukaryote about 1.5 million years ago. This eukaryote was the progenitor of the glycophyte, red and green algae (Margulis, 1970; Hackett et al., 2007). The green algae were the ancestors of the land plants. Secondary endosymbioses occurred when some of these algae were incorporated by other eukaryotes, leading to the appearance of still other types of algae.



FIGURE 51.5 Transmission electron micrograph of corn (*Zea mays*) chloroplasts. Upper left: chloroplast within mesophyll cell. Lower right: chloroplast within bundle sheath cell. Arrows indicate plasmodesmata through which metabolites are exchanged between the cells. The mesophyll cells lie near the leaf surface. The bundle sheath cells lie near the leaf vascular bundles. Note the grana in the mesophyll chloroplast. *(Micrograph courtesy of Iain M. Miller.)*

III. CHLOROPLASTS

In higher plants, most chloroplasts are found in the *mesophyll cells* of leaves (Fig. 51.5). The chloroplast contains a collection of flattened membranous vesicles called *thylakoids* which are enclosed in an *envelope* formed by a double membrane (Fig. 51.6). The outer membrane contains channels formed by the protein *porin* and is freely permeable to substances whose molecular mass is below about 10 kDa. The inner membrane is selectively permeable and contains a number of metabolite transporters which mediate the interaction between metabolism in the plant cytosol and within the chloroplast. The volume surrounding the thylakoids is known as the *stroma*. The thylakoid membranes contain the pigments that capture light and, like the cristae of mitochondria, they contain an electron transport system coupled to an adenosine triphosphate (ATP) synthase. The soluble enzymes responsible for carbon dioxide assimilation are found in the stroma. In many chloroplasts of land plants and green algae, the thylakoid membranes are stacked tightly together in some regions to form structures called *grana*, which look like green grains under the light microscope. The grana are connected by non-stacked thylakoid extensions, the *stroma lamellae*.

Chloroplasts still retain genes, which are located on a chromosome found in the stroma, for many of the proteins involved in photosynthesis and for transfer and ribosomal RNA. Proteins coded by chloroplast genes are synthesized on ribosomes located in the stroma. Genes for other chloroplast proteins are now located on nuclear chromosomes of the plant cell. Remarkably, many multisubunit proteins of the chloroplast thylakoid, including the ATP synthase, contain both subunits coded on nuclear genes and synthesized on cytosolic ribosomes and subunits coded on chloroplast genes and synthesized on stromal ribosomes. Blankenship (2002) summarizes the emerging understanding of how the plant coordinates the synthesis of these subunits. Regulation of the translation of chloroplast-coded mRNA by nucleus-coded proteins that are imported into the chloroplast and degradation of excess subunits that are not incorporated into complexes play major roles. Chloroplast proteins that are synthesized in the plant cytosol are initially formed with amino terminal extensions, termed *transit peptides*, which allow them to bind to receptors on the membranes and then enter the chloroplast. The process requires GTP, ATP and molecular chaperones. After the proteins have entered the chloroplast stroma, the transit peptides are removed by

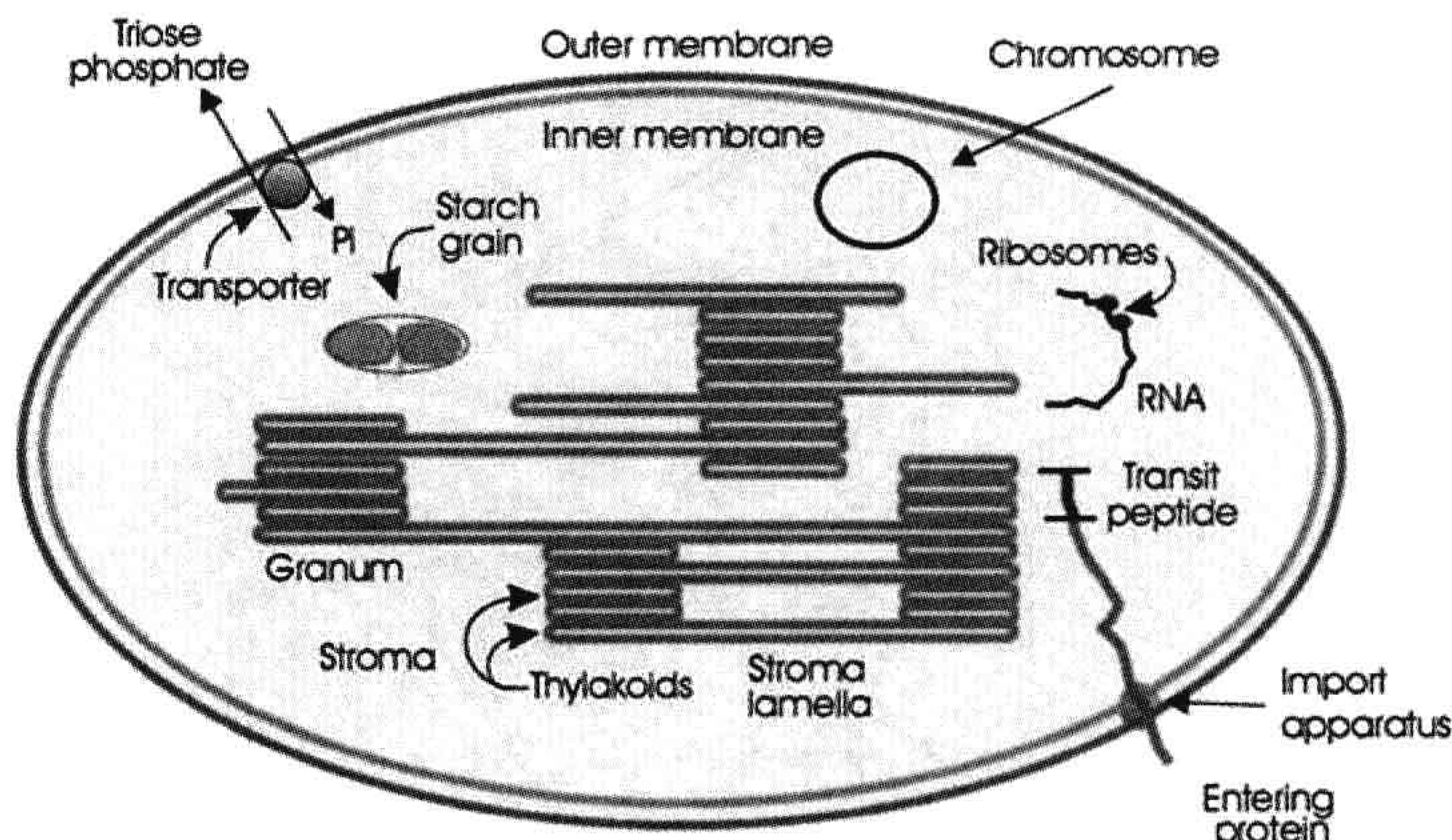


FIGURE 51.6 Diagram of a chloroplast.

a highly specific protease. Proteins destined for the membrane or lumen of the thylakoid are formed with an additional presequence, which is proteolytically cleaved after it has allowed the protein to enter the thylakoid membrane or lumen.

IV. BIOCHEMISTRY OF CARBON ASSIMILATION

IVA. The Reductive Pentose Phosphate Cycle

To determine the sequence of reactions involved in the conversion of carbon dioxide to sugars, in the early 1950s, Melvin Calvin and his associates exposed algae to $^{14}CO_2$ and light for different periods. After treatment with boiling alcohol, the carbon compounds that had been formed were separated by paper chromatography. The manner in which the distribution of ^{14}C among the carbon atoms of the various carbon compounds changed with time revealed the operation of a cyclic process, which has become known as the *reductive pentose phosphate cycle*, or *Calvin cycle* (Fig. 51.7).

In the first step, CO_2 combines with ribulose 1,5-bisphosphate to form two molecules of 3-phosphoglycerate. The reaction is catalyzed by ribulose 1,5-bisphosphate carboxylase/oxygenase, often referred to as *rubisco*. This enzyme has a rather low affinity for CO_2. To compensate, it is present in extremely high concentrations in the chloroplast and is probably the most abundant protein on earth. Next, the 3-phosphoglycerate is phosphorylated to form 1,3-bisphosphoglycerate which, in turn, is reduced to glyceraldehyde 3-phosphate by nicotinamide adenine dinucleotide phosphate (NADPH). In the remaining steps of the cycle, ribulose 1,5-bisphosphate is regenerated by a pathway that includes a complicated series of rearrangements catalyzed by transketolases and aldolases.

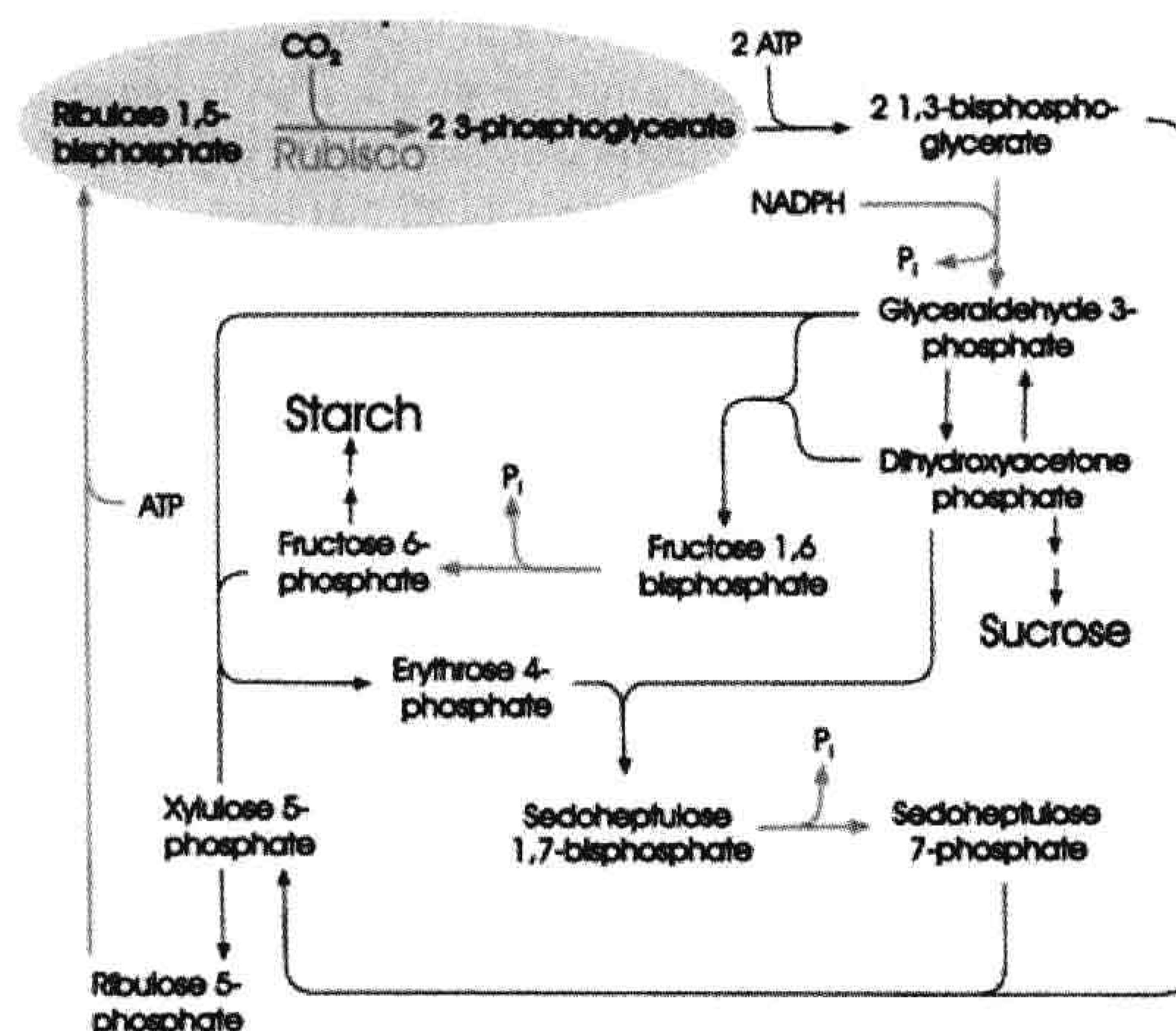


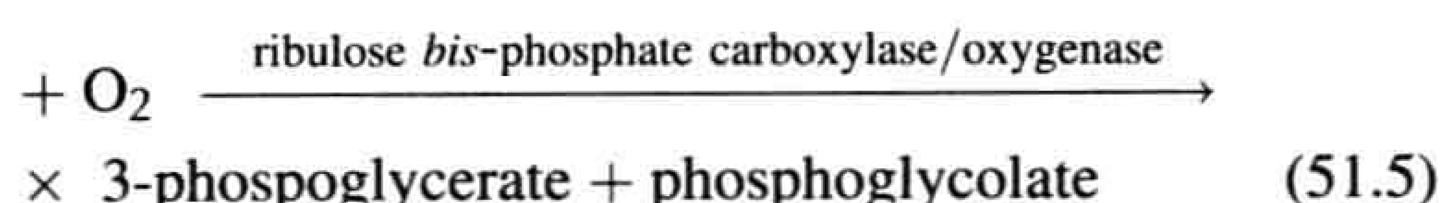
FIGURE 51.7 The reductive pentose phosphate or Calvin cycle. Stoichiometries are shown only for the first two steps. Erythrose, xylulose and sedoheptulose are sugars that contain 4, 5 and 7 carbons, respectively. Green arrows indicate steps catalyzed by light-regulated enzymes (Schurmann and Buchanan, 2008).

Intermediates in the cycle, including fructose 6-phosphate, glyceraldehyde 3-phosphate and dihydroxyacetone phosphate, serve as precursors for the starch, sucrose and amino acids that are the final products of photosynthesis.

ATP is required for the conversion of 3-phosphoglycerate to 1,3-bisphosphoglycerate and for the conversion of ribulose 5-phosphate to ribulose 1,5-bisphosphate. NADPH is required for the reduction of 1,3-bisphosphoglycerate to glyceraldehyde 3-phosphate. For each molecule of CO_2 fixed, three molecules of ATP and two molecules of NADPH are needed. It is the function of the light-driven reactions in the thylakoid membranes to furnish this ATP and NADPH.

IVB. Photorespiration and C_4 Plants

Not only does ribulose 1,5-bisphosphate carboxylase/oxygenase have a low affinity for CO_2, it also catalyzes a competing reaction in which O_2 rather than CO_2, is added to ribulose-1,5-bisphosphate. The products are 3-phosphoglycerate and phosphoglycolate.

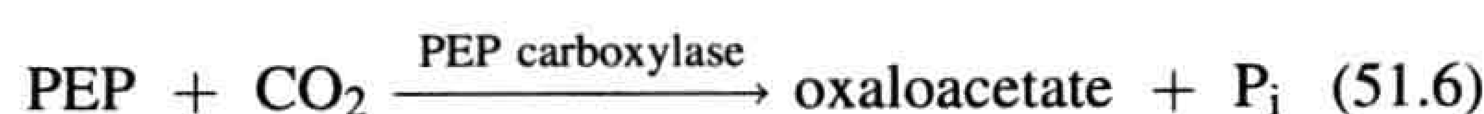


$$\text{Ribulose 1,5-bisphosphate} + O_2 \xrightarrow{\text{ribulose } bis\text{-phosphate carboxylase/oxygenase}} \times \text{ 3-phospoglycerate} + \text{phosphoglycolate} \quad (51.5)$$

This reaction seems to serve no useful purpose. Many plants grow much faster in a CO_2-enriched atmosphere in which the carboxylation reaction can compete more effectively with the oxygenation reaction. It appears that in the 2 billion years since plants began to fill the atmosphere with oxygen while removing CO_2 from it, they have been unable to modify the enzyme so that its affinity for CO_2 is increased or its affinity for O_2 is decreased significantly. Molecular biologists are now trying to accomplish that task.

Part of the carbon appearing in phosphoglycolate is rescued. In a series of reactions occurring in *peroxisomes* and in mitochondria, two molecules of phosphoglycolate are converted to one molecule of glycerate, which is returned to the chloroplast and re-phosphorylated. But one carbon atom is lost as CO_2 and ATP and O_2 are consumed. This process is known as *photorespiration*. It is not coupled to ATP formation and the net result is waste of ATP and fixed carbon.

A number of plants, including corn, sugarcane and crabgrass, partially avoid photorespiration by concentrating CO_2 in the cells that contain the Calvin cycle enzymes, so that carboxylation can compete more effectively with oxygenation. In these plants, the Calvin cycle enzymes are located in the chloroplasts of the *bundle sheath cells*, which surround the vascular bundles deep within the leaves (see Fig. 51.5). CO_2 is first captured in the mesophyll cells, which lie near the leaf surface, by carboxylation of phospho-enolpyruvate (PEP):



$$\text{PEP} + CO_2 \xrightarrow{\text{PEP carboxylase}} \text{oxaloacetate} + P_i \quad (51.6)$$

The carboxylation is catalyzed by PEP carboxylase, an enzyme that has a high affinity for CO_2 and does not catalyze an oxygenation reaction. Oxaloacetate is next reduced to malate (or transaminated to form aspartate in some plants). The malate or aspartate is transferred to the bundle sheath cells through fibers known as *plasmodesmata*. Some of these can be seen at the arrows in Fig. 51.5. Malate is oxidatively decarboxylated to pyruvate in the bundle sheath cells in a reaction that also generates NADPH. The CO_2 that is released enters the Calvin cycle in the bundle sheath cells (Fig. 51.8). Pyruvate returns to the mesophyll cells where it is again transformed to PEP. The net result is the transfer of CO_2 and NADPH to the bundle sheath cells.

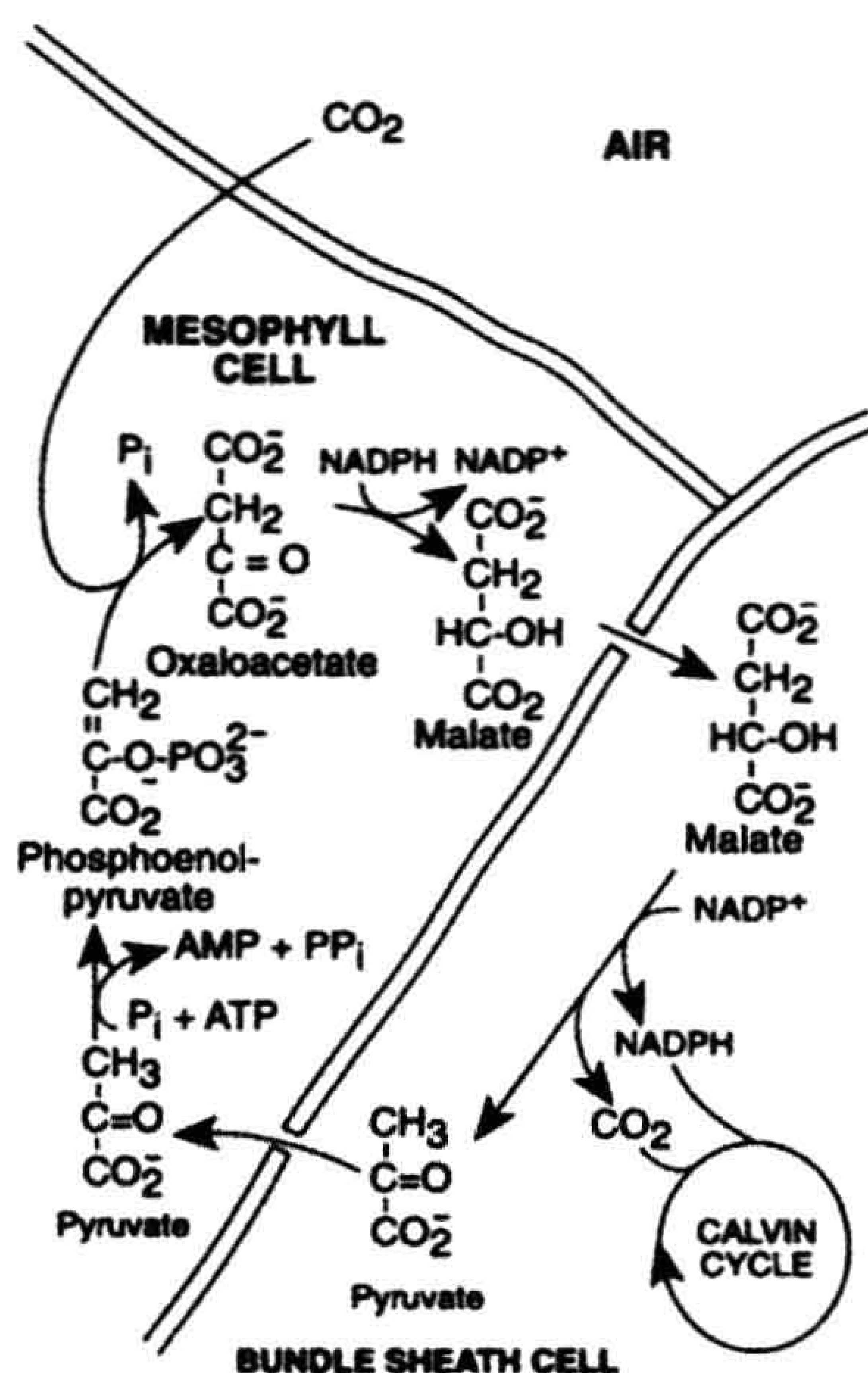


FIGURE 51.8 The mechanism used by C_4 plants to concentrate CO_2 and NADPH in bundle sheath cells. CO_2 is captured in the mesophyll cells by carboxylation of phosphoenolpyruvate. Malate is transferred to the bundle sheath cells where CO_2 is released and NADPH is formed to enter the Calvin cycle. Pyruvate returns to the mesophyll cells.

The CO_2-concentrating mechanism consumes energy, since ATP is converted to adenosine monophosphate (AMP) and phosphate. Nevertheless, plants that use it are often referred to as efficient plants because avoidance of photorespiration more than compensates for this expense. Such plants are usually known as C_4 plants because of the involvement of four-carbon acids. Many C_4 plants are native to tropical areas, where the C_4 pathway is especially advantageous since high temperatures and bright sunlight encourage photorespiration.

V. FORMATION OF ATP

VA. Light-Driven Electron Transport and ATP Synthesis

Carbon dioxide fixation requires ATP and NADPH. It seemed reasonable to suspect that the role of light is to provide the energy necessary for their formation. Photosynthetic membranes contain electron transport chains much like those of mitochondria, and light can drive electron transport along the chains (see Figs. 51.4 and 51.9). As in

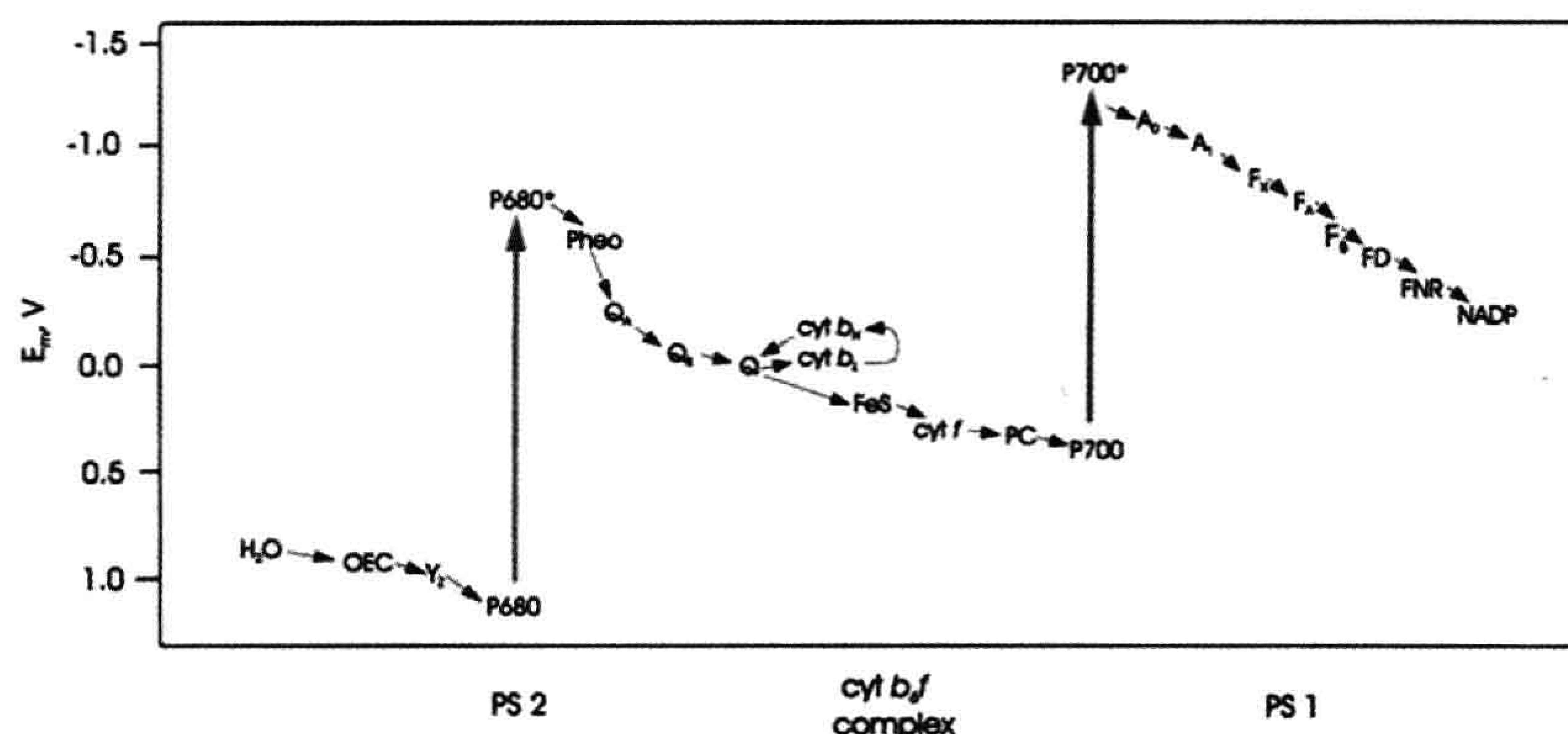


FIGURE 51.9 The electron transport system of higher plant chloroplasts. Midpoint redox potentials (E_m) of the components are indicated. P680 and P700 are chlorophyll *a* dimers which, when excited by light (large arrows), transfer an electron to the acceptors pheophytin *a* (Pheo) and chlorophyll *a* (A_0), respectively. Typical electron transfer times are shown for the electron transfer steps, which are indicated by arrows. ps: picoseconds; μs: microseconds; ms: milliseconds; OEC, a complex containing four manganese nuclei, a calcium ion and a chloride ion that accepts electrons from water; Y_Z, tyrosine; Q_A, Q_B and Q, plastoquinone; cyt b_H and cyt b_L, the high and low potential hemes, respectively, of cytochrome *b;* FeS, the 2Fe—2S center of the Rieske protein; cyt *f,* cytochrome *f;* PC, plastocyanin, a water-soluble copper-containing protein; A_1, phylloquinone; F_X, F_A, F_B, 4 Fe-4 S clusters; FD, ferredoxin, a water-soluble protein containing a 4 Fe—4 S cluster.

mitochondria, ATP formation is coupled to the electron transport.

How can electron flow through the electron carriers shown in Fig. 51.4 cause ATP formation? Mitchell (1979) suggested that electron transport and ATP formation are both coupled to the movement of protons across membranes. His *chemiosmotic hypothesis* helps us understand the reason for the arrangement of the electron carriers within photosynthetic membranes.

VB. The Chemiosmotic Hypothesis

It was known that electron transport in mitochondria and chloroplasts is accompanied by the movement of protons across the cristae or thylakoid membranes. Mitchell suggested that the transmembrane pH difference (often called a proton gradient) that is formed is an intermediate in phosphorylation. Electron transport would drive proton translocation and the proton gradient in turn would drive ATP synthesis.

Two experiments involving photosynthetic material played a critical role in convincing scientists that the chemiosmotic hypothesis must be taken seriously. Chloroplasts will synthesize ATP even if they are illuminated in the absence of ADP and P_i and then left in the dark for several minutes before these substrates are added. A relatively stable "high energy intermediate" has been formed in the light and can later drive ATP formation in the dark. Andre Jagendorf and Ernest Uribe (1966) learned that the illumination step was most efficient when the pH of the medium was about 4, while the ATP synthesis step was most efficient at pH 8. Therefore, they routinely illuminated the chloroplasts in medium buffered at pH 4 with succinate, then increased the pH to 8 before adding ADP and P_i. But ATP was formed by this procedure even if the chloroplasts were not illuminated! The quick increase in pH had created a proton gradient across the thylakoid membranes; the lumen pH had remained near 4 while the external pH had increased to 8. The simplest explanation was that the proton gradient had driven the ATP formation.

Halobacterium halobium is a red bacterium found in lakes that have a high salt content. It can form ATP in the light in a quite unusual way. The membrane of the bacterium contains purple domains in which molecules of the transmembrane protein bacteriorhodopsin are packed together in a hexagonal lattice. Each molecule of bacteriorhodopsin contains a molecule of all-*trans*-retinal attached as a Shiff base to a lysine residue. Upon absorbing light, the retinal is isomerized to the 13-*cis* isomer, initiating a cycle of events resulting in the translocation of a proton from the inside to the outside of the cell and regeneration of all-*trans*-retinal (Subramaniam and Henderson, 2000). The electrochemical proton gradient that is established is used to drive ATP formation.

ATP synthesis in mitochondria is catalyzed by a membrane-associated ATP synthase. Photosynthetic ATP formation is catalyzed by a similar protein. Ephraim Racker and Walter Stoeckenius (1974) incorporated purified bacteriorhodopsin into artificial phospholipid vesicles. When the vesicles were illuminated, protons were pumped into the vesicles. Protons were pumped

inward rather than outward because the bacteriorhodopsin is incorporated into the membranes in an orientation that was opposite to that in the bacterial membrane. When purified mitochondrial ATP synthase was also incorporated into the vesicles, light caused ATP to be formed from ADP and P_i. This experiment showed that the mitochondrial ATP synthase can catalyze ATP formation in the absence of any other mitochondrial protein, including those of the electron transport chain. Only an electrochemical proton gradient is required.

How might the pH gradient be established? Some electron carriers, such as cytochromes and iron–sulfur proteins, cannot cross membranes. Others, such as quinones, are soluble in membranes and, as illustrated in Fig. 51.4, may bind protons after they have accepted electrons.

Mitchell (1979) proposed that the electron carriers are arranged asymmetrically in the membrane. The principle is illustrated in the upper part of Fig. 51.10. Carriers that bind protons would alternate in the electron transport chain with those that do not. Electron transfers that result in H^+ binding (A → B) would occur on one side of the membrane (the stromal side in Fig. 51.10), while electron transfers that result in H^+ release (B → C) would occur on the opposite side (the luminal side). In one direction (from the stromal side to the luminal side), electrons and protons would always move together across the membrane. In Fig. 51.10, BH serves as the carrier of an electron and a proton. Electrons would always move alone across the membrane in the opposite direction (C → D). In this way, the net transfer of protons would accompany electron transport across the membrane. Such electron transport is sometimes described as *vectorial*, since it has a defined direction within the membrane, unlike electron transfer that occurs in solution. As we will see, proton translocation is coupled to electron transport in other ways as well.

Protons would flow back across the membrane through the *ATP synthase*. This proton flow would drive ATP formation. How it does so will be discussed in Section VD.

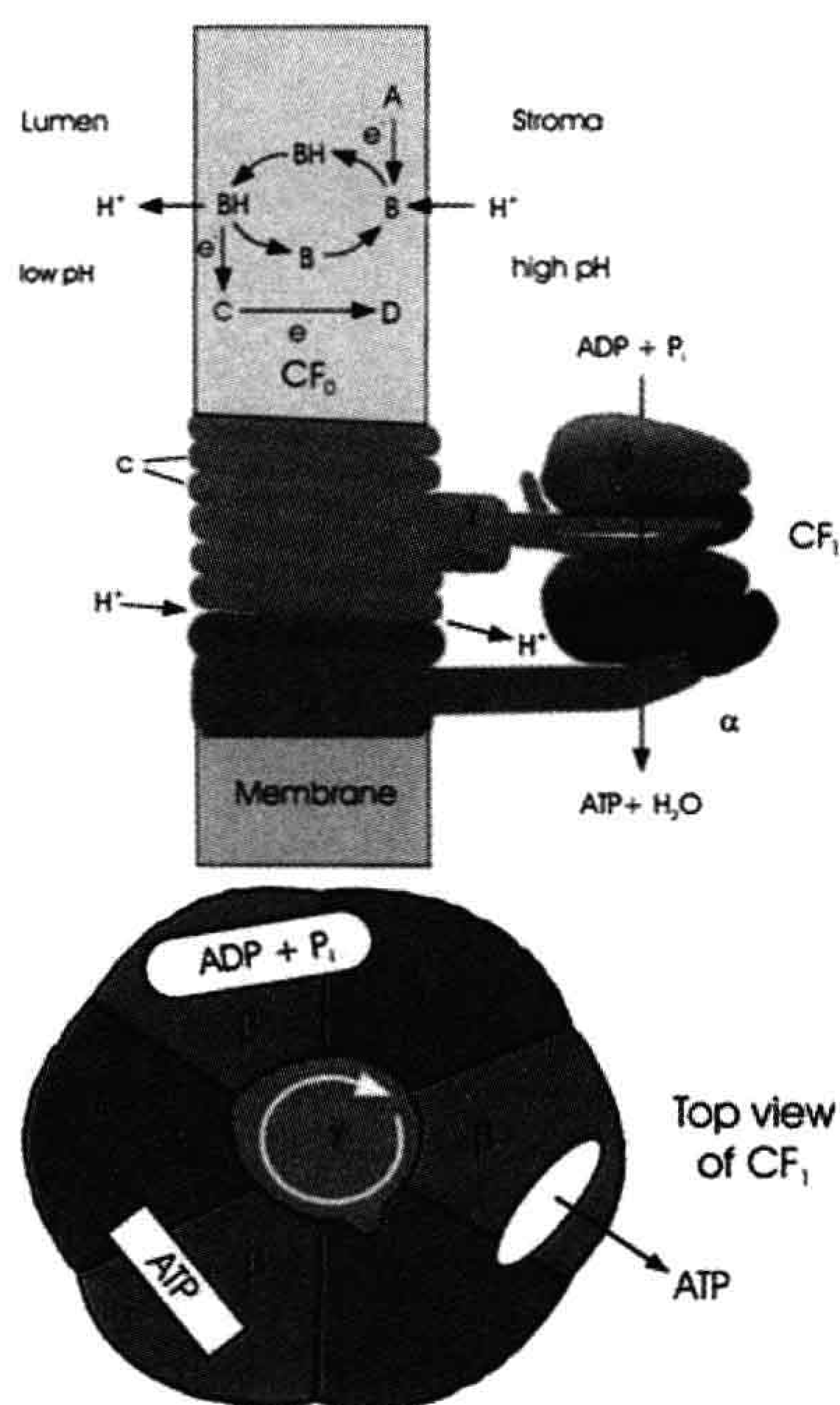


FIGURE 51.10 An illustration of how electron transport and ATP formation might be coupled. Top: Example of how electron and proton transport might be coupled. A, B, C and D are electron carriers that cannot move through the membrane. B is a molecule, such as a quinone, which becomes protonated when it accepts an electron, diffuses across the membrane and releases the proton when it is reoxidized. Center: The ATP synthase, illustrating current conceptions of how proton transport might be coupled to ATP formation. The α and β subunits of CF_1 are held fixed, while H^+ flow through CF_0 causes rotation of the c and γ subunits. As projections of γ contact each $\alpha\beta$ pair in succession, they cause conformational changes that allow binding of ADP and phosphate, ATP formation and ATP release. CF_1 is shown as a section through the γ subunit. Bottom: top view of CF_1, illustrating how rotation of the γ subunit may induce successive steps in ATP formation.

VC. Storage of Free Energy in an Electrochemical Gradient

When an uncharged molecule moves from a region where its concentration is C_1 to a region where its concentration is C_2 there is a free energy change:

$$\Delta G = RT \ln C_2/C_1 \tag{51.7}$$

per mole transferred. Since:

$$\Delta G = \Delta H - T\Delta S \tag{51.8}$$

this free energy change is due to the change in entropy, ΔS, that accompanies the change in distribution of the molecules. When a charged particle such as a proton moves between regions whose electrical potentials differ, there is an additional free energy change per mole transferred:

$$\Delta G = z\, F\, \Delta\psi \tag{51.9}$$

where z is the number of charges on the molecule, F is Faraday's constant (23 kcal/V mol) and $\Delta\psi$ is the electrical potential difference in volts. Such a difference in both concentration and electrical potential is often called an *electrochemical gradient*. There can be an electrochemical proton gradient between the chloroplast stroma and the thylakoid lumen. This gradient is created by the transfer of protons and electrons across the membrane

during electron transport. For the transfer of protons ($z = +1$) from the stroma to the lumen:

$$\Delta G = RT\ \text{In}([H^+]_{lumen}/[H^+]_{stroma}) + F\ (\psi_{lumen} - \psi_{stroma})$$

$$\Delta G = -2.30\ RT\ \Delta pH\ + F\Delta\psi \quad (51.10)$$

This free energy difference is sometimes known as *protonmotive force* and abbreviated Δp, $\Delta\mu_{H+}$, or pmf. Protons can be transported across the thylakoid membrane against their electrochemical gradient because the transfer is coupled to exergonic electron transfer. The proton translocation shown in Fig. 51.10 can occur if the sum of ΔG for proton translocation and ΔG of electron transfer from A to D is less than zero.

VD. ATP Synthase

The chloroplast ATP synthases are found in the stroma lamellae and in the unappressed membranes of the grana, but rarely in appressed granal membranes (see Fig. 51.6). The synthase has a structure similar to that of the mitochondrial ATP synthase (see Fig. 51.10). It consists of a transmembrane domain (CF_0) and a catalytic domain (CF_1) located on the stromal surface of the thylakoid membrane. Each includes several kinds of subunit.

Biochemical (Boyer, 1997) and crystallographic (Abrahams et al., 1994) studies of the ATP synthase have suggested that proton efflux through F_0 may be coupled to ATP formation in the following way. CF_1 includes three α and three β subunits, which form a ring of $\alpha\beta$ dimers (see Fig. 51.10, bottom). Each β subunit contains a catalytic site. At each of the three catalytic sites, the following steps occur. (1) ADP and phosphate bind loosely. (2) After a conformation change, the binding becomes tight and ATP is formed. (3) After a second conformation change, ATP is released. It is this step, rather than ATP formation, that requires the greatest energy input. (4) After a third conformational change, the site is ready to bind ADP and phosphate loosely again. The steps occur at each catalytic site in sequence and cooperatively, e.g. as one site is binding ADP and phosphate, another is converting them to ATP and the third is releasing ATP. What then causes the conformational changes? F_0 includes 9–15 copies of subunit c, a small transmembrane protein. The c subunits form a ring in the membrane. Each subunit may be able to bind a proton from the luminal side of the membrane; the proton may then be released on the stromal side, but only after the c-ring has rotated. Thus, rotation of the c-ring is coupled to proton flow much like rotation of a water wheel is coupled to water flow. The proton translocation is thought to occur at the interface of the c-ring and another transmembrane subunit, the a subunit. The c-ring is attached to the γ subunit, a rod-shaped protein that extends into the hole formed by the $\alpha\beta$ ring. Proton efflux through the c-ring would thus cause the γ subunit to δ subunit). As projections on the γ ring contact each $\alpha\beta$ dimer in turn, they would induce the conformational changes that lead to ATP formation. Translocation of 9–15 protons and formation of three ATPs would accompany each full rotation of the c–γ complex, consistent with the observation that translocation of three to four protons is required for each ATP formed (Feniouk and Junge, 2009). Thus, ATP formation is thermodynamically possible when μ_{H+} is more than one-third or one-fourth of ΔG of ATP formation.

The ATP synthase is intricately regulated, presumably to prevent the reversal of ATP synthesis in the dark. It is activated by the presence of a sufficiently large $\Delta\mu_{H+}$. Until it is activated, it will neither synthesize nor hydrolyze ATP. Reduction of a CF_1 disulfide bridge by reduced thioredoxin, which is formed when chloroplasts are illuminated, enhances the efficiency of the activated ATP synthase when $\Delta\mu_{H+}$ is small.

VI. PHOTOSYNTHETIC ELECTRON TRANSPORT

VIA. The Interaction of Light with Molecules

A light wave consists of an electric field and a magnetic field whose directions are perpendicular to each other. The wave moves through space at a velocity:

$$v = nc \quad (51.11)$$

where n is the refractive index of the medium through which the light is moving and c is the speed of light in a vacuum, 3.0×0^8 m/s. The wavelength of the light, λ, is the distance between the crests of the waves. Visible light has a wavelength between 400 and 700 nm. The frequency of the light, v, is the frequency with which crests of the waves pass a given point in space, and:

$$v = c/\lambda \quad (51.12)$$

According to the principles of quantum theory, light can be absorbed or emitted only in discrete units called *quanta*. The energy, E, of such a quantum depends upon the frequency of the light according to the equation:

$$E = hv \quad (51.13)$$

where h is Planck's constant, 2.86×10^{-37} kcal s.

Just as the electrons of atoms occupy atomic orbitals having discrete energies, the electrons in molecules occupy molecular orbitals having discrete energies. Molecular orbitals may extend over several nuclei. Each molecular orbital can contain two electrons of opposite spin. Absorption of light can promote (excite) an electron to an orbital of higher energy (Fig. 51.11) if the energy difference

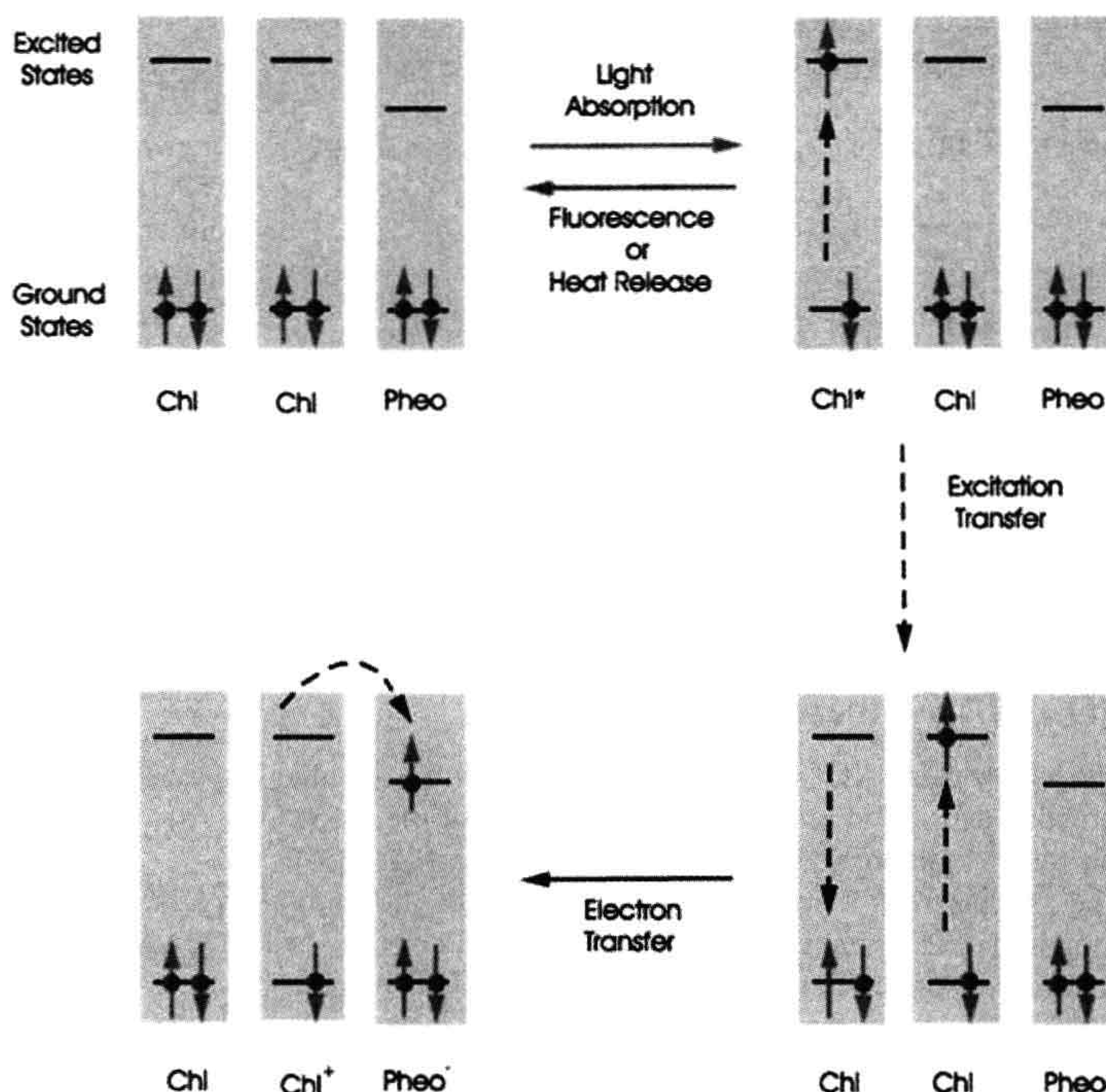


FIGURE 51.11 Light absorption and emission, excitation transfer and photochemical electron transfer. Chlorophyll (Chl) and pheophytin (Pheo) molecules are used as examples. Circles with upward and downward arrows represent electrons having opposite spins. Molecules have many ground and excited orbitals. Only one of each is shown. Chl*, electronically excited Chl; Chl^+, oxidized Chl; $Pheo^-$, reduced Pheo.

between the orbitals is equal to the energy of a quantum of the light. Several competing processes may occur after light is absorbed. The excited electron may drop back to its ground molecular orbital. As it does so, the excitation energy may be re-emitted as light (*fluorescence*), it may be lost as heat, or it may be transferred to a neighboring molecule, causing excitation of one of the neighbor's electrons to a higher orbital. Finally, the excited electron may be transferred to an empty orbital of a neighboring molecule. When this occurs, part of the energy of the absorbed light is conserved as chemical free energy of the electron donor—acceptor pair.

The tendency of a biological molecule to donate electrons is usually expressed as its midpoint redox potential at pH 7, E_{m7}. The *midpoint potential*, E_m, is the electrical potential difference that would exist between the standard hydrogen half cell and a solution in which the oxidized and reduced forms of the molecule are present in equal concentrations. In the standard hydrogen half-cell, the pH is 0 and the partial pressure of H_2 is 1 atm. The E_{m7} values for members of the chloroplast electron transport system are indicated in Fig. 51.9. A molecule in which an electron has been excited to a higher orbital has a more negative E_m than does the molecule in its ground state, by an amount about equal numerically to the energy difference between the ground and excited orbitals (in electron volts). Thus, it is a better electron donor. Note the difference between the E_ms of P680 and P680* (and between P700 and P700*) in Fig. 51.9.

The standard free energy change of an electron transfer is related to the difference between the E_m values of the electron donor and acceptor:

$$\Delta G^o = -n\ F\ \Delta E_m \qquad (51.14)$$

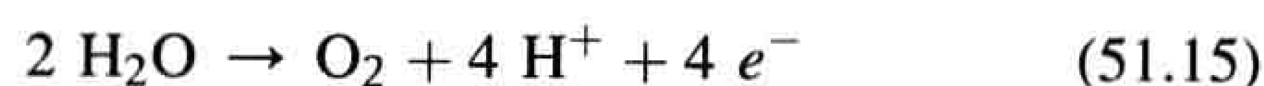
where n is the number of electron equivalents transferred per mole. Thus, excitation of a molecule lowers the free energy change accompanying the transfer of an electron to another molecule. This equation can be used to calculate the free energy changes accompanying the light-induced charge separations and the subsequent electron transfers shown in Fig. 51.9.

Especially lucid explanations of the photochemical processes involved in photosynthesis have been given by Clayton (1970, 1980).

VIB. The Presence of Two Photochemical Reactions in Chloroplasts

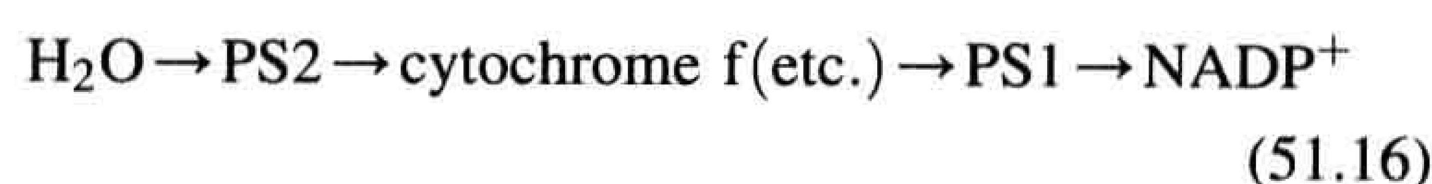
The most careful measurements of the *quantum yield* of oxygen evolution indicate that at least eight light quanta must be absorbed for each molecule of oxygen that is

evolved. Because the oxidation of two water molecules to form one O_2 molecule requires the removal of only four electrons,



$$2\,H_2O \rightarrow O_2 + 4\,H^+ + 4\,e^- \qquad (51.15)$$

it appeared that two quanta are necessary for the extraction of each electron from water. Robert Emerson illuminated the green alga *Chlorella* with light of different wavelengths and observed the rates of O_2 evolution. He found that when light of wavelength less than 680 nm and light of wavelength greater than 680 nm were given together, the rate of O_2 evolution was greater than the sum of the rates observed when the algae were illuminated with light of each wavelength separately; i.e. the two wavelengths acted synergistically (Emerson et al., 1957). This phenomenon, which has come to be known as *Emerson enhancement*, suggested that efficient O_2 evolution requires the cooperation of a system which absorbs long-wavelength light and a system which absorbs short-wavelength light. L.N.M. Duysens found that 680-nm light caused the oxidation of cytochrome *f*, whereas 562-nm light caused its re-reduction (Duysens et al., 1961). In 1960, R. Hill and F. Bendall (1960) suggested the *Z scheme*, in which a photosystem driven by short-wavelength light (*photosystem 2, PS 2*) and a photosystem driven by long-wavelength light (*photosystem 1, PS 1*) are connected in series. Light absorbed by PS 2 would cause the transfer of an electron from H_2O to a chain of electron carriers between the photosystems (cytochrome *f* is one of these). Light absorbed by PS 1 would cause the transfer of the electron from this chain to $NADP^+$ to form NADPH:



$$H_2O \rightarrow PS2 \rightarrow \text{cytochrome f(etc.)} \rightarrow PS1 \rightarrow NADP^+ \qquad (51.16)$$

Absorption of two quanta, one by each photosystem, would be required for the transfer of an electron all the way from H_2O to $NADP^+$. Cytochrome *f* would be reduced by PS 2 and oxidized by PS 1. The complete Z-scheme as it is now understood is presented in Fig. 51.9.

The light-absorbing pigments associated with PS 1 and PS 2 have somewhat different absorption spectra. The PS 2 pigments have very little absorption beyond about 680 nm, so light in this wavelength region drives PS 1 almost exclusively.

VIC. Primary Electron Donors and Light-Harvesting Pigments

The absorption spectrum of a typical chloroplast is shown in Fig. 51.1. Bessel Kok noticed that when chloroplasts are illuminated, there is a small decrease in their optical absorbance ("bleaching") at 700 nm. He suggested that the change was due to the light-induced oxidation of a chlorophyll molecule, resulting in the loss of its optical absorbance at that wavelength (Kok and Hoch, 1961). It was suggested that the primary light reaction is the transfer of an electron from a special chlorophyll molecule, named *P700*, to an electron acceptor (see Fig. 51.9). In bacteria, illumination caused cytochrome oxidation (detected as a change in optical absorbance at wavelengths where cytochrome absorbs light) as well as bacteriochlorophyll oxidation. To determine whether bacteriochlorophyll or cytochrome oxidation occurs first, William Parson illuminated bacteria with very short flashes from a Q-switched laser. Immediately after the flash, he observed oxidation of bacteriochlorophyll. The bacteriochlorophyll became reduced again in a few milliseconds and, as it did, the cytochrome became oxidized. The bacteriochlorophyll had been oxidized first; the cytochrome had then donated an electron to the oxidized bacteriochlorophyll (Straley et al., 1973).

The laser flash had been so brief that it ended before the electron lost by the bacteriochlorophyll had been replaced by an electron from the cytochrome, so the flash had caused the transfer of only a single electron from the bacteriochlorophyll. Such *single turnover flashes* have been a powerful tool for the study of photosynthetic electron transport. Lasers capable of producing flashes femtoseconds (10^{-15} s) in duration have made it possible to measure the rates of very early electron transfer steps, some of which occur in picoseconds (10^{-12} s).

P700 is the primary electron donor in PS 1. The primary donor of PS 2 absorbs at 680 nm and is known as *P680*. Oxidized chlorophyll contains an unpaired electron (see Fig. 51.11). Such molecules can be studied by the technique of *electron paramagnetic resonance spectroscopy*, in which the absorption of microwaves by the unpaired electrons is measured. Study of P680 and P700 by this technique, as well as other experiments, suggested that they are *dimers* of chlorophyll *a*. After they have lost an electron, the remaining unpaired electron is shared between the two chlorophyll molecules that comprise the dimers.

The details of many biophysical techniques, including optical spectroscopy and magnetic resonance, which are employed in photosynthesis research are described in Amesz and Hoff (1996).

Most of the chlorophyll in cells serves only to capture light and does not participate in photochemistry. Each photochemically active chlorophyll dimer (P680, P700) is associated with an aggregate of several hundred light-harvesting chlorophyll molecules, known as a *photosynthetic unit*. After any chlorophyll molecule in the unit absorbs a quantum of light, the excitation energy migrates among the chlorophyll molecules in the aggregate (see Fig. 51.11). When the excitation reaches the photochemically active dimer, electron transfer occurs. A typical photosynthetic unit contains about 300 chlorophylls molecules. *Beta-carotene* and other carotenoids also serve as light-harvesting pigments, as do tetrapyrrole pigments known as

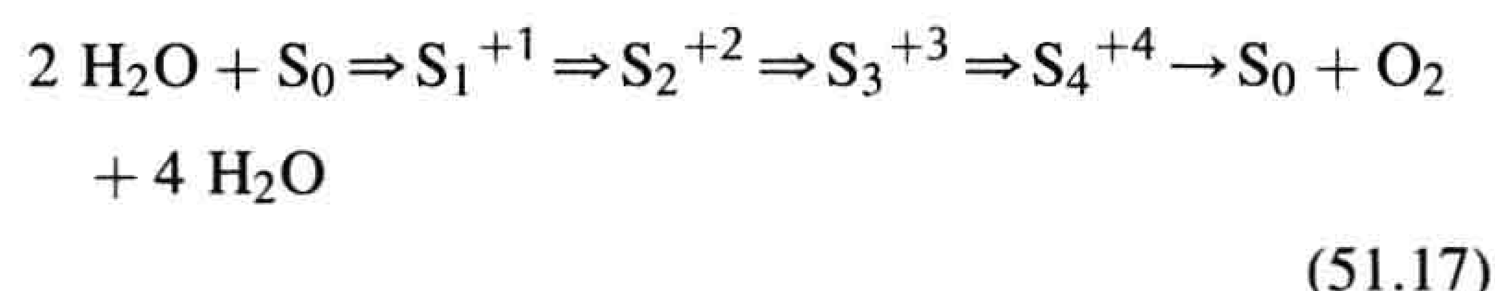
phycobilins in cyanobacteria and some algae. The pigments are attached to protein molecules. Such accessory pigments allow the capture of light in regions of the spectrum where chlorophyll does not absorb light strongly.

VID. The Structure and Function of the Chloroplast Electron Transport System

We can now summarize the way the chloroplast electron transport system is believed to operate (see Figs. 51.9 and 51.12). The components have redox potentials that allow electrons to move forward along the chain; they are arranged in the membrane and oriented in such a way that forward electron transfer is fast and electron flow results in translocation of protons across the membrane.

Photosystem 2 particles from a thermophilic cyanobacterium have been isolated and crystallized (Ferreira et al., 2004; Loll et al., 2005). The PS 2 reaction center contains two subunits, D1 and D2, whose amino acid sequences partially resemble those of purple bacterial reaction center subunits L and M. Like the L and M subunits, D1 and D2 bind the electron transport cofactors. PS 2 contains several additional proteins that are not discussed here.

Formation of one O_2 molecule requires the removal of four electrons from two molecules of H_2O. Kok suggested that each photochemical act removes one electron from an *oxygen-evolving complex (OEC)* (Kok et al., 1970). When four electrons have been removed, oxygen molecules are released. The OEC contains four manganese nuclei, a calcium ion and a chloride ion. Its structure and function have been reviewed by Yocum (2008b). The following sequence of events is now believed to occur (see Fig. 51.9). Upon excitation, P680 transfers an electron to a special pheophytin *a* molecule. An electron is then transferred to $P680^+$ from Y_Z, a tyrosine residue, which is part of D1. Next, Y_Z^+ receives an electron from the OEC, leaving a positive charge stored in the OEC. This sequence of events is repeated until four positive charges have been stored in the OEC and O_2 is released. During the process, four protons are released into the chloroplast lumen. The oxidation states of the manganese cluster are known as *S states*. Yocum (2008c) represents the series of events as follows:



$$2\ H_2O + S_0 \Rightarrow S_1{}^{+1} \Rightarrow S_2{}^{+2} \Rightarrow S_3{}^{+3} \Rightarrow S_4{}^{+4} \rightarrow S_0 + O_2 + 4\ H_2O \tag{51.17}$$

where the open arrows represent light-driven electron extractions. All of the S states relax to S_1 in the dark, so in practice O_2 is evolved after the third flash.

The first electron that had been transferred to pheophytin *a* moves to Q_A (plastoquinone) and then to Q_B (also plastoquinone) to form a plastosemiquinone anion. After a second photon is absorbed, a second electron moves down the chain to Q_B, reducing it to $Q_B^{2-} \cdot Q_B^{2-}$ then binds two protons from the stroma to form plastohydroquinone. The structures of quinone, semiquinone anion and hydroquinone are shown in Fig. 51.4. At this point, two protons have been taken up from the stroma and four protons have been released into the lumen.

The herbicides atrazine and diuron act by competing with plastoquinone for binding to the Q_B site on D1.

The plastohydroquinone is released from its binding site on PS 2 and diffuses within the membrane (as QH_2 in Fig. 51.12) until it reaches the cytochrome b_6f complex. Here it binds to a site (Qo) near the luminal surface of the membrane.

At this point, a series of reactions is initiated that will result in the transfer of additional protons across the membrane. A possible mechanism of the proton translocation, which was suggested by Mitchell, is known as a *Q cycle* (Crofts, 2004). The bound QH_2 donates an electron to a 2 Fe–2 S center known as the *Rieske Fe–S center*. The electron moves from there to cytochrome f. The

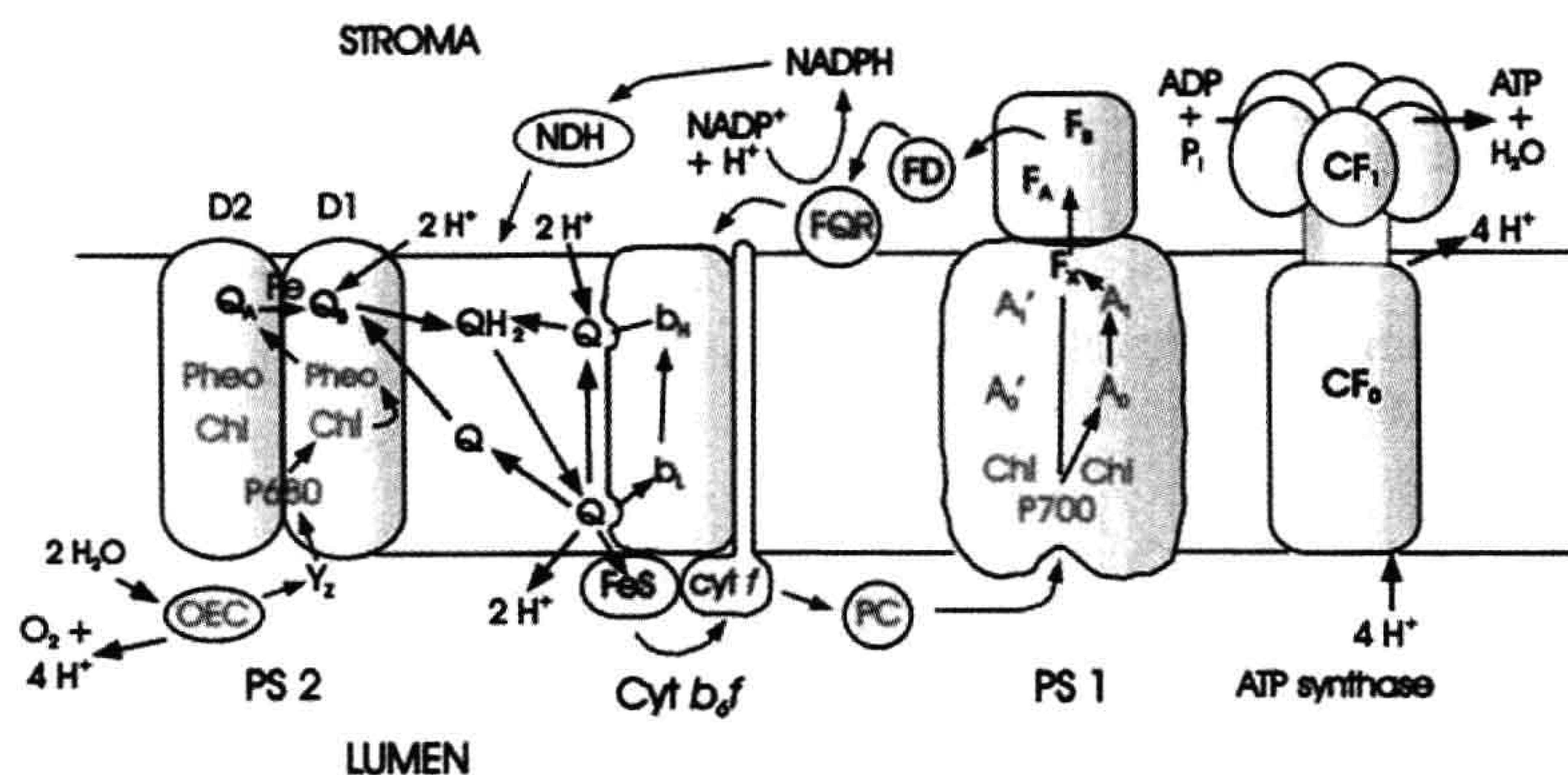


FIGURE 51.12 Electron and proton transport and ATP formation in chloroplasts. FNR, ferredoxin-NADP⁺ oxidoreductase; NDH, NADPH dehydrogenase; FQR, ferredoxin-plastoquinone oxidoreductase. Other symbols are defined in the legend of Fig. 51.9.

cytochrome b_6f complex also contains two cytochrome b-type hemes, b_H and b_L. QH_2 as a reductant is not strong enough to donate an electron to these hemes, but the plastosemiquinone that was formed when QH_2 transferred the electron to the Fe−S center is, and does so. In effect, the transfer of the first electron from QH_2 to the Fe−S center has driven the transfer of the second electron to b_L. QH_2 has been oxidized to Q, releasing two protons into the lumen. A second QH_2 molecule is oxidized by a similar mechanism and a second electron is donated to the hemes. The two heme electrons are then donated to a plastoquinone (Q) molecule, which is bound near the stromal surface. It then binds two protons from the stroma. In the net process occurring at the cytochrome b_6f complex, one QH_2 has been oxidized, two protons have been removed from the stroma and four protons have been released into the lumen.

The electrons that were transferred to cytochrome f move to *plastocyanin*, a soluble, copper-containing protein. The plastocyanin diffuses within the lumen until it reaches the PS 1 complex, where it transfers the electron to $P700^+$. P700 is a chlorophyll a dimer.

The x-ray structure of PS1 crystals has been determined (Ben-Shem et al., 2003; Nelson and Yocum, 2006). Along with several other proteins, PS 1 contains a protein dimer, the PsaA and PsaB proteins, to which electron transfer co-factors and a large number of light-harvesting chlorophylls are bound. The PsaA-PsaB dimer has approximate twofold rotational symmetry, as does the purple bacterial reaction center dimer. Excited P700 donates an electron to A_0, a chlorophyll a monomer (remember that the acceptor in PS 2 is pheophytin a. From A_0, the electron moves to A_1, which is phylloquinone, then through the [4Fe−4S] cluster F_X to the [4Fe−4S] clusters F_A and F_B and, finally, to *ferredoxin*, a soluble [4Fe−4S] protein. From ferredoxin the electron is transferred to ($NADP^+$) by way of the flavoprotein *ferredoxin-NADP oxidoreductase, FNR*. On reduction the NADP binds a proton in the stroma. Protons return from the lumen to the stroma through the ATP synthase and ATP is formed.

Some of the ferredoxin molecules may transfer their electrons back to oxidized quinone in the membrane to generate more ATP when cellular metabolism requires a higher ATP/NADH ratio than is provided by linear electron transport. This process is known as *cyclic photophosphorylation*. It may occur by an antimycin A-sensitive pathway from ferredoxin or, as shown in recent studies (Livingston et al., 2010), from NADPH in a process mediate by NADPH dehydrogenase.

VII. REGULATION OF PHOTOSYNTHESIS

Virtually every step in the photosynthetic process is tightly regulated. The precision of this regulation was illustrated in experiments with spinach (Servaites et al., 1989). During illumination of spinach leaves with light whose intensity was varied sinusoidally, the net rate of CO_2 fixation perfectly paralleled the light intensity except between hours 4 and 10, when it was saturated. As the light intensity changed, the rates of the reactions leading to CO_2 uptake changed in such a way that efficiency of the use of the light remained constant. The final output of photosynthesis, export of fixed carbon from the leaves, remained almost perfectly constant throughout the cycle.

If photosynthesis is to work efficiently, PS 1 and PS 2 must transfer electrons at the same rate. Chloroplasts regulate the rates of the photosystems by regulating the transfer of excitation energy to P680 and P700. Both PS 1 and PS 2 contain chlorophyll molecules bound to proteins that are a permanent part of the PS 1 and PS 2 complexes. CP 43 and CP 47 are part of PS 2 and LHC I is part of PS 1. Chlorophyll is also bound to the PsaA and PsaB proteins of PS 1. Such chlorophyll is known as *antenna chlorophyll*. In addition, chloroplasts thylakoids contain a protein, known as *LHC II* (for light-harvesting complex II), to which are typically attached eight molecules of chlorophyll a, seven of chlorophyll b and one or two of xanthophyll per peptide. Under some conditions, LHC II is tightly attached to PS 2 to which it transfers excitation energy. If PS 2 is working faster than PS 1, the quinone pool between PS 2 and PS 1 becomes overreduced. When this happens, a kinase is activated in response to plastohydroquinone binding to the Qo site of the cytochrome b_6f complex (Lemeille and Rochaix, 2010). The kinase catalyzes the phosphorylation of some of the LHC II. The phosphorylated molecules dissociate from PS 2. As a result, they no longer transfer excitation energy to PS 2 and so its rate slows. Some of the phosphorylated LHC II associates with PS 1, which is found predominantly in the stroma lamellae, and transfer excitation energy to it instead. Once the quinone pool between PS 2 and PS 1 are no longer overreduced, the kinase is inactivated and a phosphatase removes the phosphate from the LHC II. LHC II returns to the grana lamellae and reassociates with PS 2, most of which is located in the grana. These processes, known as *state transitions*, are accompanied by changes in the structures of the grana and stroma lamellae (Chuartzman et al., 2008).

A regulatory mechanism that deserves special mention involves the protein *thioredoxin*, which serves a signal that it is daytime. Thioredoxin contains a disulfide bridge which can be reduced by ferredoxin in a reaction catalyzed by ferredoxin−thioredoxin reductase. In the light, ferredoxin is reduced by PS 1 and, in turn, reduces thioredoxin. Thioredoxin then activates a number of Calvin cycle enzymes and increases the sensitivity of the ATP synthase to $\Delta\mu_{H+}$ by disulfide exchange. As a result, the Calvin cycle and the ATP synthase are active when there is enough light to drive electron transport (Schurmann and Buchanan, 2008).

BIBLIOGRAPHY

Abrahams, J. P., Leslie, A. G. W., Lutter, R., & Walker, J. E. (1994). Crystal structure at 2.8-angstrom resolution of F_1 ATPase from bovine heart mitochondria. *Nature, 370*, 621–628.

Amesz, J., & Hoff, A. J. (Eds.). (1996). *Biophysical Techniques in Photosynthesis*. Dordrecht: Kluwer Academic Publishers.

Ben-Shem., A., Frolow, F., & Nelson, N. (2003). The crystal structure of plant photosystem I. *Nature, 426*, 630–635.

Blankenship, R. E. (2002). *Molecular Mehanisms of Photosynthesis*. Oxford: Blackwell Science Ltd.

Blankenship, R. E., Sadekar, S., & Raymond, J. (2007). The evolutionary transition from anoxygenic to oxygenic photosynthesis. In P. G. Falkowski, & A. H. Knoll (Eds.), *Evolution of Primary Producers in the Sea* (pp. 21–35). San Diego: Elsevier.

Boyer, P. D. (1997). The ATP synthase: a splendid molecular machine. *Annu Rev Biochem, 66*, 717–749.

Brennan, T. (2008). Photosynthesis timelines. In K. C. Smith (Ed.), *Photobiological Sciences Online. American Society for Photobiology*. http://www.photobiology.info/.

Chuartzman, S. G., et al. (2008). Thylakoid membrane remodeling during state transptions in Arabidopsis. *Plant Cell, 20*, 1029–1039.

Clayton, R. K. (1970). *Light and Living Matter, Volume 1: the Physical Part*. New York: McGraw-Hill Book Company.

Clayton, R. K. (1980). *Photosynthesis: Physical Mechanisms and Chemical Patterns*. Cambridge: Cambridge University Press.

Cogdell, R. J., et al. (1999). How photosynthetic bacteria harvest solar energy. *J Bacteriol, 181*, 3869–3879.

Crofts, A. R. (2004). The cytochrome bc1 complex: function in the context of structure. *Ann Rev Physiol, 66*, 689–733.

Deisenhofer, J., & Michel, H. (1989). The photosynthetic reaction centre from the purple bacterium *Rhodopseudomonas viridis*. *EMBO J, 8*, 2149–2169.

Duysens, L. N. M., Amesz, J., & Kamp., B. M. (1961). Two photochemical systems in photosynthesis. *Nature, 190*, 510–511.

Emerson, R., Chalmers, R., & Cederstrand, C. (1957). Some factors influencing the long-wave limit of photosynthesis. *Proc Nat Acad Sci USA, 43*, 133–143.

Feniouk, B. A., & Junge, W. (2009). Proton translocatin and ATP synthesis by the F_0F_1-ATPase of purple bacteria. In C. N. Hunter, F. Daldal, M. C. Thurnauer, & J. T. Beatty (Eds.), *The Purple Photosynthetic Bacteria* (pp. 475–493). Springer Science Business Media BV.

Ferreira, K. N., Iverson, T. M., Maghlaoui, K., Barber, J., & Iwata, S. (2004). Architecture of the photosynthetic oxygen-evolving center. *Science, 303*, 1831–1838.

Golbeck, J. H. (2010). Editorial. *Photosynth Res, 104*, 101–102.

Hackett, J. D., Yoon, H. S., Butterfield, N. J., Anderson, M. J., & Bhattacharya, D. (2007). Plastid endosymbiosis: sources and timing of the major events. In P. G. Falkowski, & A. H. Knoll (Eds.), *Evolution of Primary Producers in the Sea* (pp. 109–132). San Diego: Elsevier.

Hill, R., & Bendall, F. (1960). Function of two cytochrome components in chloroplasts: A working hypothesis. *Nature, 1186*, 136–137.

Hunter, C. N., Daldal, F., Thurnauer, M. C., & Beatty, J. T. (Eds.). (2008). *The Purple Phototrophic Bacteria, Advances in Photosynthesis and Respiration, 28*. Dordrecht, The Netherlands: Springer.

Jagendorf, A. T., & Uribe, E. (1966). ATP formation caused by acid-base transition of spinach chloroplasts. *Proc. Nat. Acad. Sci. USA, 55*, 170–177.

Jones, M. (2009). Photosynthetic bacteria. In K. C. Smith (Ed.), *Photobiological Sciences Online. American Society for Photobiology*. http://www.photobiology.info/.

Ke, B. (2001). *Photosynthesis: Photobiochemistry, and Photobiophysics*. Dordrecht: Kluwer Academic Publishers.

Kok, B., & Hoch, G. (1961). Spectral changes in photosynthesis. In W. D. McElroy, & B. Glass (Eds.), *Light and Life* (pp. 397–416). Johns Hopkins Press.

Kok, B., Forbush, F., & McGloin, M. (1970). Cooperation of charges in photosynthetic O_2 evolution: A linear four step mechanism. *Photochem Photobiol, 11*, 457–475.

Lemeille, S., & Rochaix, J.-D. (2010). State transitions at the crossroad of thylakoid signalling pathways. *Photosynth Res, 106*, 33–46.

Livingston, A. K., Cruz, J. A., Kohzuma, K., Dhingra, A., & Kramer, D. M. (2010). An *Arabidopsis* mutant with high cyclic electron flow around photosystem I (*hcef*) involving the NADPH dehydrogenase complex. *Plant Cell, 22*, 221–233.

Loll, B., Kern, J., Saenger, W., Zouni, A., & Bies, J. (2005). Toward complete cofactor arrangement in the 3.0 A resolution structure of photosystem II. *Nature, 438*, 1040–1044.

Loomis, W. E. (1960). Historical introduction. In W. Ruhland (Ed.), *Encyclopedia of Plant Physiology, Vol. V* (pp. 85–114). Berlin: SpringerVerlag.

Margulis, L. (1970). *Origin of Eukaryotic Cells*. New Haven, Connecticut: Yale University Press.

Mitchell, P. (1979). Keilin's respiratory chain concept and its chemiosmotic consequences. *Science, 206*, 1148–1159.

Nelson, N., & Yocum, D. F. (2006). The structure and function of photosystems I and II. *Ann Rev Plant Biol, 57*, 521–565.

Olson, J. M., & Blankenship, R. E. (2004). Thinking about the evolution of photosynthesis. *Photosynth Res, 80*, 373–386.

Racker, E., & Stockenius, W. (1974). Reconstitution of purple membrane vesicles catalyzing light-driven proton uptake and adenosine triphosphate formation. *J Biol Chem, 249*, 662–663.

Schurmann, P., & Buchanan, B. B. (2008). The ferredoxin/thioredoxin system of oxygenic photosynthesis. *Antioxid Redox Signal, 10*, 1235–1274.

Servaites, J. C., Fondy, B. R., Li, B., & Geiger, D. R. (1989). Source of carbon for export from spinach leaves throughout the day. *Plant Physiol, 90*, 1168–1174.

Straley, S. C., Parson, W. W., Mauzerall, D. C., & Clayton, R. K. (1973). Pigment content and molar extinction coefficients of photosynthetic reaction centers from *Rhodopseudomonas sphaeroides*. *Biochem Biophys Act, 305*, 597–609.

Sturgis, J. N., & Niederman, R. A. (2008). Atomic force microscopy reveals multiple patterns of antenna organization in purple bacteria; implications for energy transduction mechanisms and membrane modeling. *Photosynth Res, 95*, 269–278.

Subramaniam, S., & Henderson, R. (2000). Molecular mechanisms of vectorial proton translocation by bacteriorhodopsin. *Nature, 406*, 653–657.

Woese, C. R. (1987). Bacterial evolution. *Microbiol Rev, 51*, 221–271.

Yocum, C. (2008a). Photosynthetic reaction centers. In K. C. Smith (Ed.), *Photobiological Sciences Online. American Society for Photobiology*. http://www.photobiology.info/.

Yocum, C. F. (2008b). The Ca^{2+} and Cl^- requirements of the O_2-evolving complex. *Coordination Chem Rev, 252*, 296–305.

Yocum, C. F. (2008c). Oxygen evolution. In K. C. Smith (Ed.), *Photobiological Sciences Online. American Society for Photobiology*. http://www.photobiology.info.

Chapter 52

Bioluminescence

J. Woodland Hastings

Chapter Outline

I. SUMMARY

Bioluminescence is an enzymatically-catalyzed chemiluminescence, a chemical reaction that emits light. Though relatively rare, it occurs in a phylogenetically-wide range of species, primarily marine, ranging from bacteria to vertebrates, and has many independent evolutionary origins. Thus, structures of the genes and proteins, as well as the physiological, biochemical and regulatory mechanisms involved, are very different. The principal biochemical components are referred to as luciferin and luciferase, terms that cannot stand alone, being different structurally in different groups. Luminescence provides a selective advantage mediated through its detection and responses by other organisms; its functions may be classed as defensive, offensive or for communication. Physiological control, biochemical mechanisms and functions in four of the major groups, and several less well-known ones, are described. Regulatory mechanisms include autoinduction (quorum sensing; bacteria), action potentials and voltage-gated membrane channels (dinoflagellates, protons; coelenterates, calcium), circadian control (dinoflagellates) and oxygen mobilization (beetles).

II. INTRODUCTION

Unlike most physiological processes, the mechanisms and biochemical components involved in bioluminescence are not the same in different phylogenetic groups, thus indicating that light emission originated many times independently in evolution. For example, fireflies and all beetles use ATP and their flash is triggered by a pulse of oxygen, while flashes of coelenterates are triggered by calcium and ATP is not involved, while bacteria utilize a flavin and dinoflagellates a tetrapyrrole as luciferins. But this is but the tip of the iceberg and, while knowledge of the chemistries and physiological mechanisms of a large fraction of such systems is still below the surface, those that have been elucidated provide important knowledge of physiological mechanisms.

In addition to contributing to fundamental knowledge, some systems have provided unique tools for investigating

Cell Physiology Sourcebook. DOI: 10.1016/B978-0-12-387738-3.00052-4

and understanding other basic physiological processes. Notable, to be sure, was the confirmation in 1976 of the theory that calcium triggers muscle contraction, demonstrated with single barnacle cells injected with the purified intermediate of the coelenterate bioluminescence system (aequorin); upon stimulation, the earliest event recorded was the onset of light emission. Even more familiar and now routinely used at the laboratory bench are genes of luciferases and green fluorescent protein (GFP; the light emitting protein in coelenterates) as reporters. Thereby, a wide variety of molecules and the time course of diverse processes can be visually localized at the cellular level.

Although bioluminescence is rather rare in nature, and in that sense a curiosity, it has several different and fascinating functions. Flashes may be used in several different ways, in fireflies to communicate in courtship or in fish to startle, either to escape predators or capture prey. Its use by many fish and other marine organisms to camouflage the silhouette by emitting a constant ventral glow (intensity adjustable) cries for a study of the physiological mechanism whereby the down-welling light intensity is detected and used to control the intensity of the bioluminescence.

The physiological mechanisms, biochemical systems and genes responsible are similarly very different, *not* evolutionarily conserved, and evidently originated and evolved independently. How many times this may have occurred is difficult to say, but it has been estimated that present day luminous organisms come from as many as thirty or forty different evolutionarily distinct origins (Hastings, 1983; Hastings and Morin, 1991; Haddock et al., 2010).

The four major systems to be described, as well as the lesser well-researched ones, exemplify differences in all aspects, highlighting their independent origins. The luciferases of each of the four have been cloned and sequenced and crystal structures determined. The luciferins and other biochemical components, as well as the identities of the emitting species, are different and known for all. The physiological mechanisms whereby light emission is controlled range from regulation of gene expression and membrane action potentials and channels to osmotically controlled triggering and shutter mechanisms.

III. WHAT IS BIOLUMINESCENCE? PHYSICAL AND CHEMICAL MECHANISMS

Bioluminescence displays, though sometimes obscured by the now-ubiquitous artificial illumination, are bright enough to be seen by other animals and do not include the very dim light emitted by some cells, which is detectable by sensitive instruments now available. This is a chemiluminescence, sometimes attributable to reactions of active oxygen species. And yes, bioluminescence is itself a chemiluminescence (McCapra in Herring, 1978; Wilson, 1985; Campbell, 1988), but distinct in that the reaction is catalyzed by enzymes (generically referred to as luciferases), as well as by the fact it can be seen by eye.

Bioluminescence does not come from or depend on light absorbed by the organism. It derives from a highly exergonic (energy yielding) chemical reaction in which excess energy is transformed into light energy instead of being all lost as heat (Wilson and Hastings, 1998). Thus, in the reaction of substance A with molecular oxygen, one of the reaction products is formed in an electronically *excited state* (B*), which then emits a photon (hν). In all known cases, the reactants remain bound to the luciferase throughout, so that the emission comes from a protein-bound fluorophore (B*, in this example).



$$A + O_2 \xrightarrow{\text{luciferase}} B^* + C$$



$$B^* \rightarrow B + h\nu$$

More generally, the term luminescence refers to any light emission in which energy is specifically channeled to a molecule so that an excited state is produced, not related or due to the temperature. Thus, in addition to chemiluminescence and bioluminescence, these include fluorescence and phosphorescence, in which the excited state is created by the prior absorption of light, as well as tribolum-inescence and piezoluminescence, involving crystal fracture and electric discharge, respectively. The color is a characteristic of the excited molecule, irrespective of how it was excited. But, as elaborated below, the color may be greatly affected by protein binding, as shown for some bioluminescent systems.

Luminescence is contrasted with incandescence, in which excited states are produced by virtue of the temperature, and the energy is thermal. An example is the light bulb, soon to be phased out for household use, in which a filament is heated, and the color of the light depends on the temperature ("red hot" reflecting a lower temperature than "white hot"). The phasing out is because of its relative inefficiency, due in part to the fact that, unlike luminescence, photons are emitted over a wide range of frequencies, most not in the visible range.

The energy (E) of the photon is related to the color or frequency of the light and is given by the equation $E = h\nu$, where h is Planck's constant and ν the frequency. In the visible-light range, E is quite large in relation to most biochemical reactions. Thus, in visible wavelengths the energy released by a mole of photons (6.02×10^{23}) is about 50 kcal, much more than the energy from the hydrolysis of a mole of ATP, about 7 kcal. In cells, chemical energy from the absorption of a visible photon can power photosynthesis, or it can do damage (mutation; photodynamic action, which can kill). Conversely, it takes a reaction yielding considerable energy to result in an excited state and visible photon.

A question of fundamental importance, then, is what kind of chemical process possesses enough energy, and evidently in a single step (an important point), to populate (create) an excited state? A clue is the fact that both chemi- and bioluminescence in solution require oxygen, which in its reaction with a substrate forms an organic peroxide. The energy from the reaction of such peroxides to form more stable products — which should generate up to 100 kcal per mole — is ample to account for a product in an electronically excited state. Thus, while all known bioluminescent reactions involve peroxide intermediates, their identities differ, because their luciferins (substrates) and also luciferases differ.

The terms luciferin and luciferase are not sufficient for their identification in a given organism. Dubois first showed in 1885 that bioluminescence in beetles could occur in cell-free extracts, with the emission continuing for minutes, or hours in some cases. He demonstrated that the reaction could be characterized as having two components, one heat stable (luciferin) and the other more labile to heat (luciferase). Luciferin was named from the Latin as the component responsible for the light emission (light bearing) and the luciferase as the enzyme. For half a century thereafter, in spite of clear evidence to the contrary, the fact that the luciferins and luciferases from different groups of organisms are different was ignored and the terms were used with abandonment for all species. Today, the persistence of the use of the terms in research publications without naming the organism can be confusing. Luciferin and luciferase are *generic* terms and, to be correct and specific, each must be identified with the organism, thus firefly luciferin or bacterial luciferase, for example.

While luciferases are single proteins, the luciferin fraction may contain more than one substrate, as well as co-factors (Table 52.1). For example, the firefly system involves both ATP and a unique luciferin (a benzothiazole), while the bacterial reaction involves the mixed function oxidation of two substances, reduced flavin mononucleotide and a long chain aliphatic aldehyde. In such cases, there has been some confusion as to which should be called the luciferin, since both contribute to the energy released in the reaction. Sticking to the etymology of the original definition, the benzothiazole and flavin, respectively, are the luciferins in those systems (Hastings, 2011).

IV. LUMINOUS ORGANISMS: ABUNDANCE, DIVERSITY AND DISTRIBUTION

While indeed rare in terms of the total number of luminous species, bioluminescence is phylogenetically diverse, being found in more than 13 phyla (Herring in Herring, 1978). These include bacteria, unicellular algae and fungi, as well as animals ranging from jellyfish, annelids and molluscs to shrimp, fireflies, echinoderms and fishes. Luminescence does not occur in higher plants or in vertebrates above the fishes (Cormier in Herring, 1978). It is also absent in several invertebrate phyla. In some phyla or taxa, a substantial proportion of the genera are luminous (e.g. ctenophores, ≈50%; cephalopods, >50%; echinoderms and annelids, ≈4%). In some cases, all members of a luminous genus emit light, but in others there are both luminous and non-luminous species.

Of the 30 or 40 groups that are believed to be evolutionarily independent, some are found even in different taxa within a phylum or class. Fewer than half of these have been studied in detail and some knowledge of their luciferins and luciferases is available for only about a dozen. Although luminescence is prevalent in the deep sea (Herring, 1985a,b), where there is no sunlight, it is not associated especially with organisms that live in total darkness. There are no known luminous species either in deep fresh water bodies, such as Lake Baikal, Russia, or in the total darkness of terrestrial caves. There are luminous dipteran larvae (*Arachnocampa*) that live near the mouths of caves in New Zealand and Australia, but they also occur in culverts and the undercut banks of streams, where there is considerable daytime illumination. Although insect displays are among the most spectacular, bioluminescence is relatively rare in the terrestrial environment (<0.2% of all genera). Some other terrestrial luminous forms are millipedes,

TABLE 52.1 The Different Luciferases and Luciferins

Luciferases: kDa and E.C.#			Structures of luciferins
Bacterial	~80 (α, 41; β, 39)	1.14.14.3	Reduced flavin mononucleotide long chain aldehyde
Dinoflagellate	~135	NA	Tetrapyrrole
Coelenterate	~35	1.13.12.5	Coelenterazine, Ca^{++}
Firefly	~60	1.13.12.7	Benzthiazole, ATP

centipedes, earthworms and snails, but in none of these is the display especially bright.

For reasons that are still not known, bioluminescence is most prevalent in the marine environment (Haddock et al., 2010), especially at mid-ocean depths (200–1200 m), where daytime illumination fluxes range between $\approx 10^{-1}$ and 10^{-12} $\mu W/cm^2$. In some such locations it may occur in over 95% of the individuals and 75% of the species in fish, and in shrimp and squid about 85% of the individuals and 80% of the species. The mid-water luminous fish *Cyclothone* is considered to be the most abundant vertebrate on the planet. Where high densities of luminous organisms occur, their emissions can exert a significant influence on the communities and may represent an important component in the ecology, behavior and physiology of these organisms. Above and below mid-ocean depths, luminescence decreases to $<10\%$ of all individuals and species. At abyssal depths it may be somewhat higher ($\approx 20\%$), while among coastal species, less than 2% are bioluminescent.

V. FUNCTIONS OF BIOLUMINESCENCE

Bioluminescence is unusual biologically because it is a clear and well-documented example of a function that is not metabolically essential but one that may confer an advantage on the individual. While bioluminescence has evidently arisen independently many times, it may also have been lost many times in different evolutionary lines, not being truly essential. No one can tell.

Bioluminescence may be thought of as a bag of tricks: the light can be used in different ways and for different functions. Most of the perceived functions of bioluminescence may be classed under three main rubrics: defense, offense and communication; a fourth less common one is to enhance propagation (Table 52.2).

Important defensive strategies are to frighten, to serve as a decoy, to provide camouflage, or aposematic, serving as a warning to would-be predators (e.g. the animal is distasteful) (Grober, 1988). Organisms may be frightened or diverted by flashes, which are typically bright and brief (0.1 s), too fast to allow a predator to locate motile prey; light is emitted in this way by many organisms, and experimental studies confirm that flashes can indeed frighten (Morin, 1983).

An organism can use a glow defensively by creating a luminous decoy to attract and divert a predator, while it slips off itself under the cover of darkness. This is done by several organisms, such as squid, which squirt luminescence instead of ink; ink would be useless in total darkness. Some organisms sacrifice more than light; in scaleworms and brittle stars, a part of the body may be automized (broken off) and left behind as a luminescent decoy to attract the predator. In these cases, the animal flashes while intact but the detached part glows.

A clever method for evading predation from below is to camouflage the silhouette by emitting light continuously matching the color and intensity of the downwelling background light. By analogy with countershading in reflected light, this is called counterillumination. Consider a plane in the sky during the day. If it could emit light from its belly matching the sky behind, it would be invisible from below. Actually, it is not necessary for the entire surface to emit light; emission by only a part would mean that the object would no longer look like a plane. This can be called disruptive illumination and many luminous marine organisms, including fish and the bobtail squid, use this to help escape detection. Many culture symbiotic

TABLE 52.2 Functions of Bioluminescence

Category	Function	How achieved
Deter, escape predators (defense)	Camouflage	Ventral emission, symbiosis
	Startle, frighten	Brief bright flashes
	Decoy, diversion	Luminous cloud, sacrificial lure
	Predators learn to avoid	Aposematism; danger signal
Aid in predation (offense)	Startle	Brief bright flashes
	Attract prey	Lure
	Aid in vision	See and capture prey
Communication	Courtship, mating	Flash signals
	Species recognition	Photophore patterns
Propagation	Bacterial light emission	Attract feeders, enhance growth

luminous bacteria for use as the light source (McFall-Ngai and Morin, 1991). Another novel defensive strategy has been dubbed the burglar alarm: dinoflagellates flash when grazed upon, which may reveal the grazers and enhance predation on them, thereby reducing grazing on the dinoflagellates (Abrahams and Townsend, 1993).

There are also several ways in which luminescence can aid in predation. Several of these, such as illuminating for vision, may be of value for both offense and defense; offensively, prey may be thereby seen and captured, as flashlight fish do (Fig. 52.1). And flashes, which are more typically used defensively, can be used offensively in order temporarily to startle or blind prey. A glow can also be used offensively: it can serve as a lure. The prey is attracted to the light but is then captured by the organism that produced the light. This is practiced by the deep-sea angler fishes; they also culture symbiotic luminous bacteria for the light source.

Communication involves information exchange between individual members of a species and luminescence is used for this in several groups, including annelids, crustaceans, insects, squid and fishes (Herring, 1990). The most common use of the light is for courtship and mating, as in fireflies (Lloyd, 1977, 1980; Buck, 1988). There are also numerous examples in the ocean (Herring, 1990). In the annelid (syllid) fireworm *Odontosyllis*, a truly extraordinary display occurs as the animals engage in mating, which occurs daily for only a few days after the full moon, timed to start a few minutes after sunset. Readily observed in many parts of the world (e.g. Bermuda), the females come to the surface and swim in a tight luminous circle. A luminous male streaks from below and joins the female; eggs and sperm are shed in the ocean. Another kind of behavior occurs over shallow reefs in the Caribbean: male ostracod crustaceans produce complex species-specific trains of secreted luminous material, ladders of light, which attract females (Fig. 52.2) (Morin and Cohen, 1991, 2010).

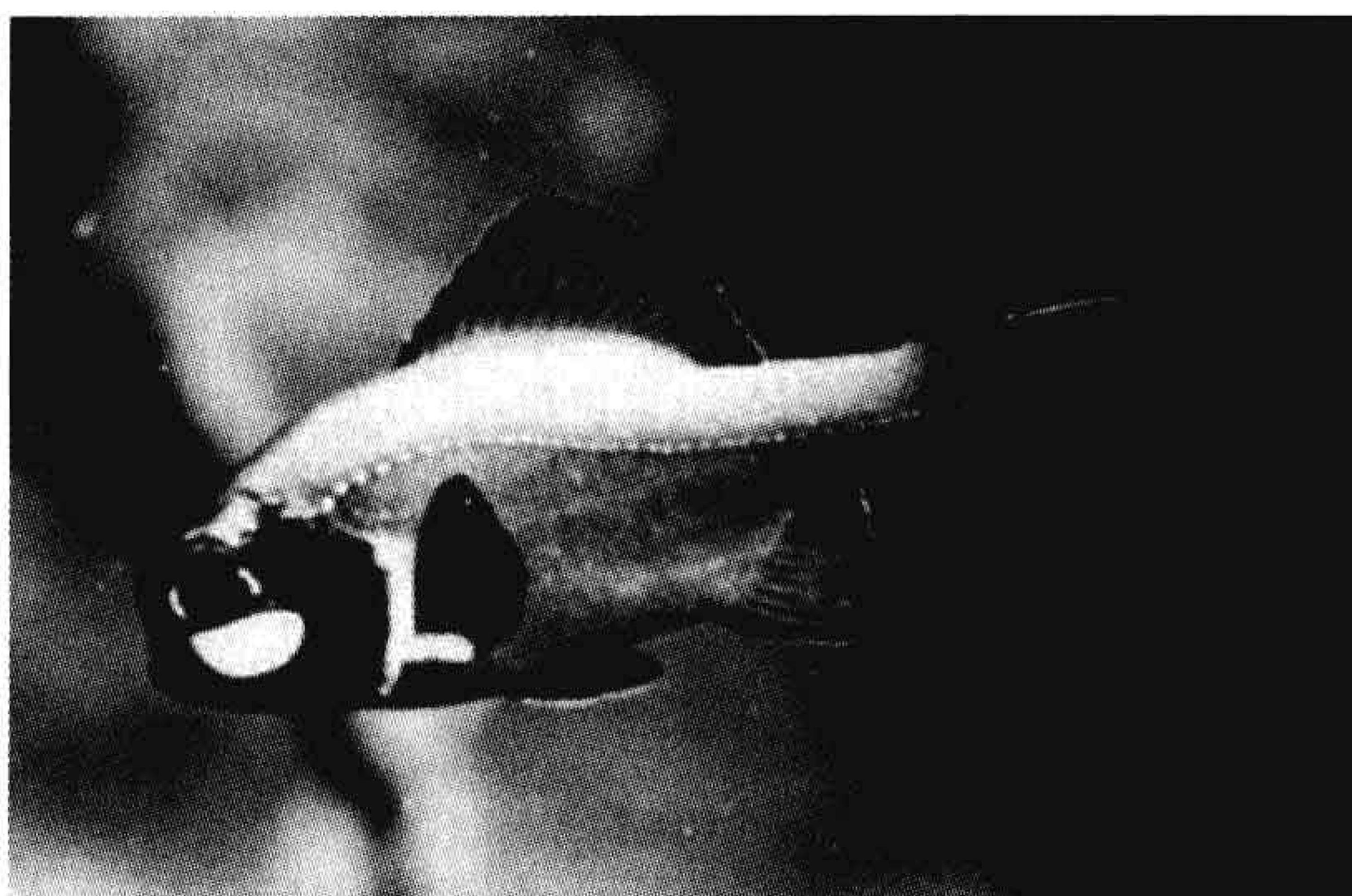


FIGURE 52.1 The flashlight fish (Photoblepharon) showing the light organ harboring luminous bacteria just below the eye. *(By permission J.G. Morin.)*



FIGURE 52.2 Video recording of pulses of light secreted sequentially by males of the ostracod crustacean *Vargula* about 1 cm apart in shallow water in the Caribbean as a display in courtship. The several different beads come from different animals active at the same time in the same area. *(By permission J.G. Morin and Martin Dohrn.)*

There remain some cases for which it is difficult to know what the function of the light emission may be. In some cases, it may be an aposematic signal, as coloration is in some animals, but not so recognized. But where the light is not seen, this would not explain it. For example, in the luminous fungi (Fig. 52.3) (Desjardin et al., 2008, 2010), which emit light continuously, the luminous cap is believed to attract insects, which would serve to disperse spores. But, in some, only the mycelium is luminous, and it is essentially never seen, living underground or inside a decaying tree. And no good explanation for luminescence in earthworms, where emission is also underground, has been advanced. The function of luminescence in these and some other cases remains to be understood.

VI. BACTERIAL LUMINESCENCE

VIA. Regulation by "Quorum Sensing" (Autoinduction) and by Shutters or Filters

Bacteria in general had long been regarded as cells that do their own thing, simply dividing and multiplying with no regard for other bacterial cells around them – no "communication". And light emission from luminous bacteria (Fig. 52.4) was well characterized as being continuous and its luminescence not typically subject to a rapid change. The discovery in luminous bacteria of "autoinduction" (Nealson et al., 1970), now referred to as "quorum sensing", revealed massive and environmentally significant regulation at the transcriptional level (Gambello and Iglewski, 1991; Fuqua and Greenberg, 2002).

The basic observation was that in newly inoculated cultures of a luminescent marine bacterium, *Vibrio fischeri*, the onset of exponential growth occurs without a lag but luminescence *does not* increase until mid-logarithmic

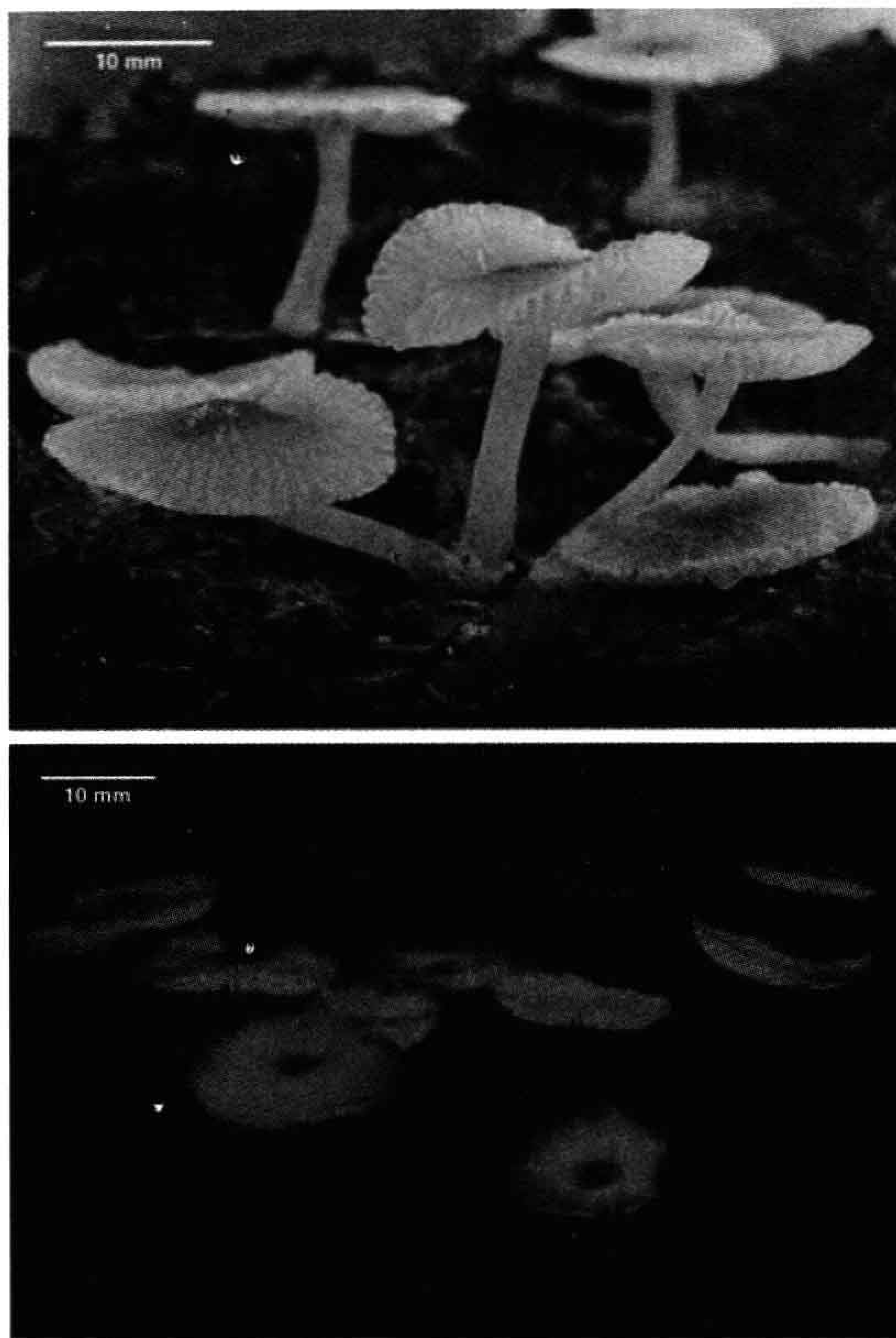


FIGURE 52.3 Photos taken in room light (above) and by their own light of the bioluminescent mushroom *Mycena chlorophos*. Caps but not stipes are luminous; in other species only stipes are luminous, in yet others both emit light, and in one only the underground mycelium emits. *(The specimens were grown and the photo was taken by Dr. Eiji Nagasawa, reproduced by permission).*

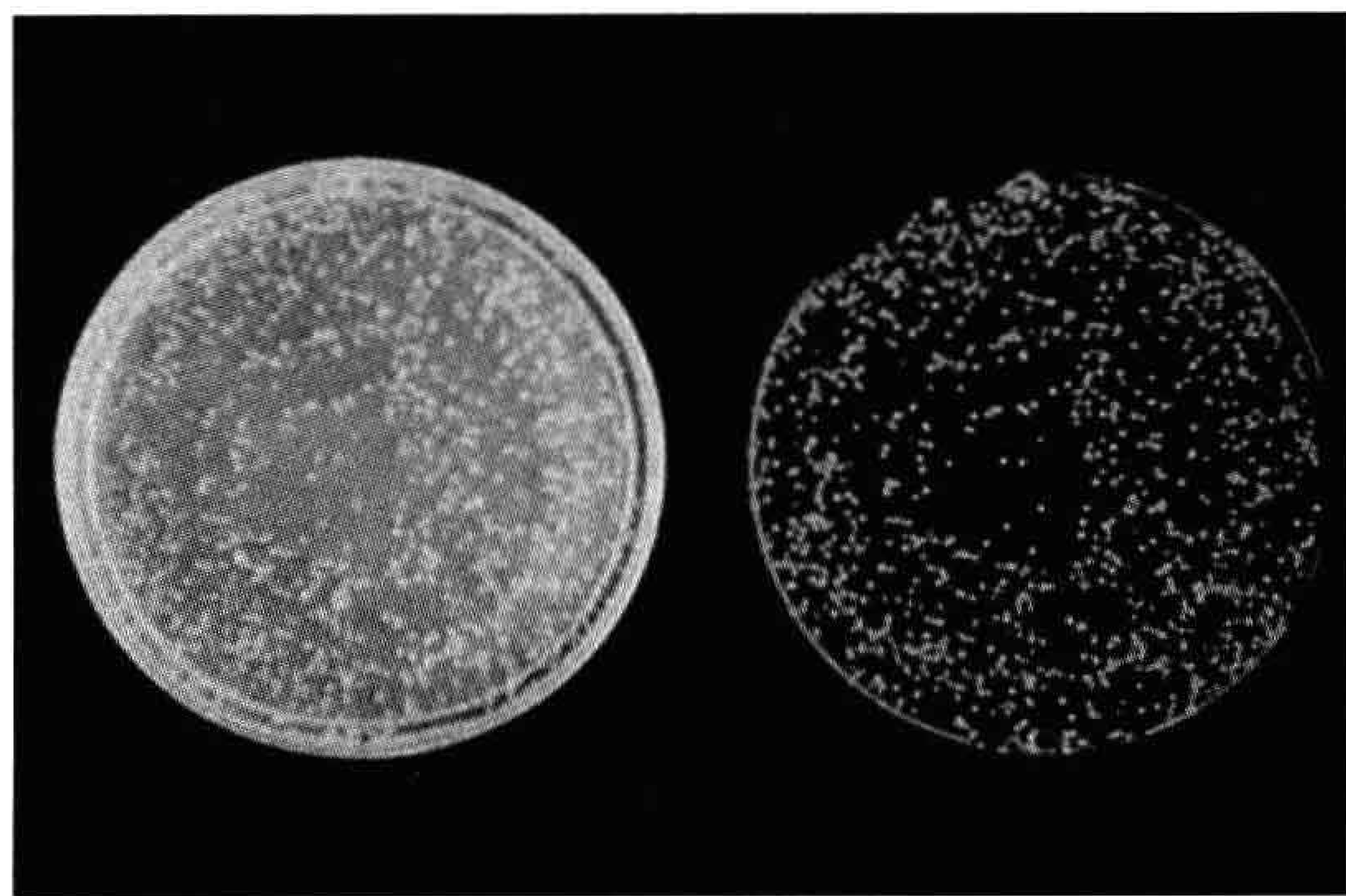


FIGURE 52.4 Petri plates inoculated with luminous bacteria, photographed in daylight (left) and by their own light (right) Note non-luminous colony among the cluster of four in the centre of the plate. *(Photograph by author.)*

phase, when transcription of the *lux* operon is triggered and light emission literally shoots up, doubling every four minutes or so (Fig. 52.5). This was shown to be due to an inducer of luciferase synthesis produced by the bacteria themselves, which was therefore dubbed the autoinducer. Its structure was found to be a homoserine lactone (Eberhard et al., 1981); other molecules serve the same role in other species and groups (Schaefer et al., 2008; Ng and Bassler, 2009).

The ecological implications are evident: in planktonic bacteria free-living in the ocean, autoinducer cannot accumulate, so no luciferase synthesis occurs. This makes sense; the open ocean is a habitat where the luminescence of a lone bacterium presumably has no value, whereas it evidently does in a light organ with a trillion others (Parsek and Greenberg, 2005). There, high autoinducer levels are readily reached, so the luminescence genes are transcribed. Many considered this as something special in luminous bacteria until the 1990s, when it was discovered that genes controlling autoinduction occur in many different bacteria, controlling specific genes having similarly evident functional importance (Gambello and Iglewski, 1991; Fuqua and Greenberg, 2002). For example, genes responsible for toxin production are not transcribed until the population is great enough to overwhelm the infected organism. This led to the adoption of the catchy term "quorum sensing" to refer to this mechanism, even though it does not strictly involve an enumeration mechanism as such.

There are a number of other control mechanisms that serve to regulate the transcription of the *lux* operon, including glucose (catabolic repression), nutrient levels, iron and oxygen. Each of these factors represents a different mechanism for the physiological control of gene expression

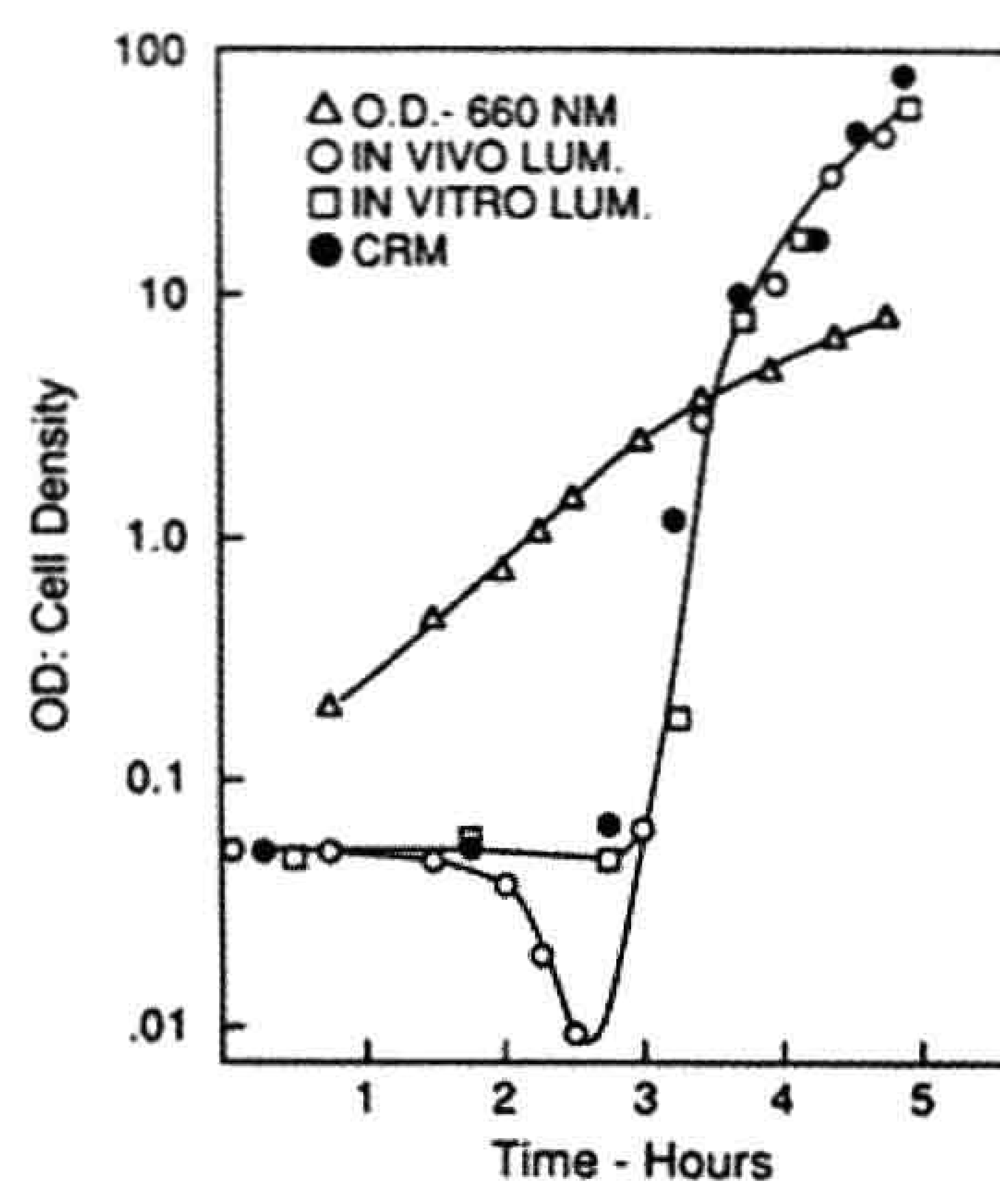


FIGURE 52.5 Autoinduction (quorum sensing) in luminous bacteria. Cells inoculated at a cell density of about 0.1 (660 nm) grow exponentially, but the luciferase remains constant for the first 3 hours, after which it rises steeply, attributable to the accumulation of autoinducer in the medium.

and each has implications concerning the ecology of luminous bacteria and the function of their luminescence. But there is also another control: in some species of bacteria, "dark" (very dim) strains arise spontaneously (see Fig. 52.4). In these, the transcription of the luminescent system scarcely occurs, irrespective of conditions, and this is heritable. However, the genes are evidently not lost, for revertants do occur. Thus, by selection for the dark strain, the organism can compete under conditions where luminescence is not advantageous, yet be able to select for luminous forms and populate the appropriate habitat when and where it is encountered. Indeed, the bacterial *lux* genes may thus occur in many bacterial strains but not be highly expressed. This means that there may be many more potentially luminous bacteria than would be deduced from colonies that are bright on plates.

The possibility that regulation of oxygen supply to bacterial light organs might control light emission has been considered, but there is no strong evidence in support of the idea. However, mechanical shutters, color filters and other optical devices are widespread and important (Morin and Cohen, 1991).

VIB. Occurrence and Functions

Planktonic luminous bacteria occur ubiquitously in the oceans and can be isolated from sea-water samples anywhere in the world, from the surface to depths of 100 m or more. A primary habitat where most species abound is in association with a higher organism or solid substrate, as commensals, parasites or symbionts, where growth and propagation occur. Planktonic forms are ubitquitous, but do not grow significantly, as sea water is a poor medium; their occurrence there is attributed to the overflow from primary habitats (Nealson and Hastings, 1991).

But there are displays in the ocean attributed to bacteria, the so-called "Milky Seas", which have been reported repeatedly over the centuries in logs of merchant ships and accurately described in Verne's "Twenty Thousand Leagues Under the Sea". The phenomenon was recently visualized by satellite imaging (Miller et al., 2005; Nealson and Hastings, 2006), recorded as a continuous night-time luminescence in the ocean off the Horn of Africa covering an area the size of the state of Connecticut, persisting for three nights (Fig. 52.6). It is believed that it is due to bacteria, indicated by the fact that the light is continuous. But this flies in the face of the fact that in all studied luminous bacteria, including "free-living" planktonic forms, regulation has been shown to involve quorum sensing, described above, and sea water should not have the requisite free-living bacterial concentration for autoinducer to accumulate. So, if bacteria are responsible, they may be growing on (possibly decomposing) microfilamentous algae, where autoinducer could accumulate. The isolation

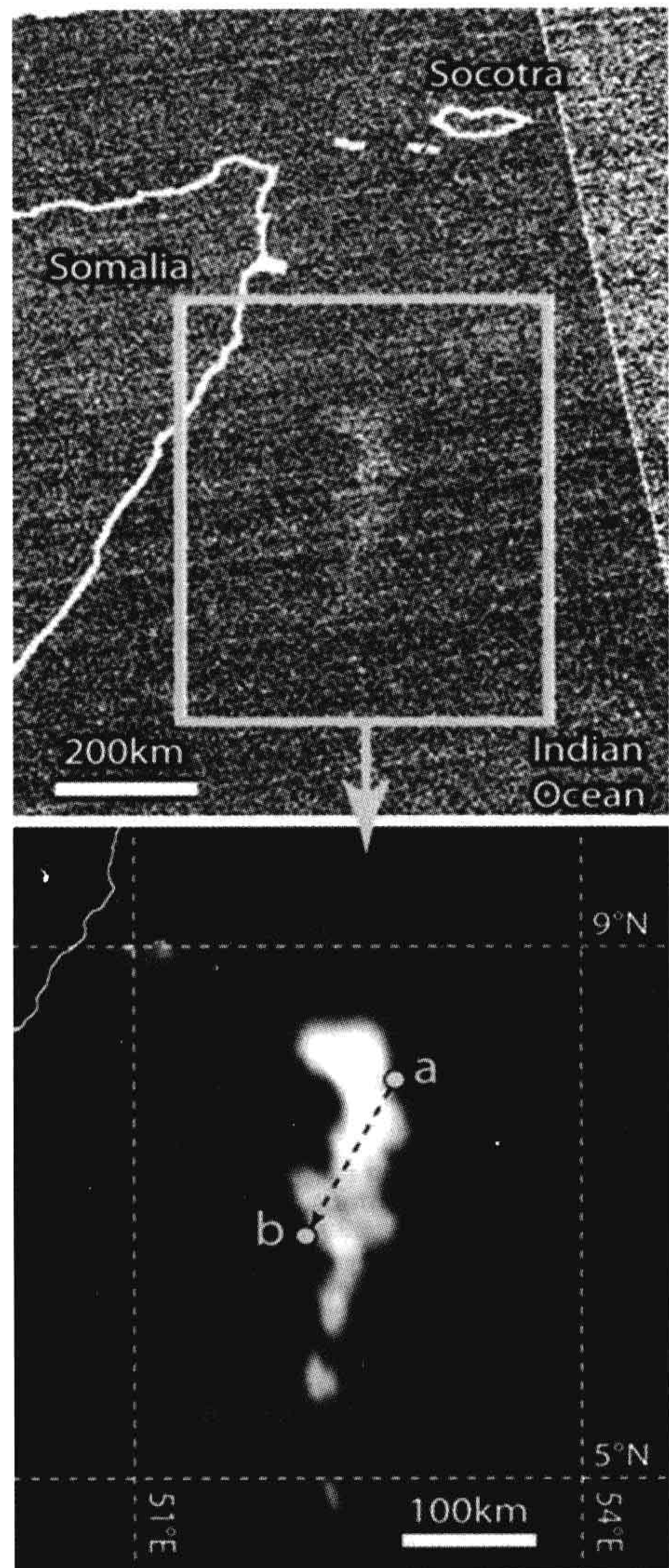


FIGURE 52.6 Raw (top) and digitally enhanced (bottom) images of a "milky sea" on January 25, 1995 detected by satellite-based camera. The land area at the left is the Horn of Africa in Somalia. The points of entry and exit of the ship from the luminous area, as reported in the log of the S.S. Lima, are points a and b in the enhanced image. Scale bars as shown. *(By permission, Steve Miller and Steve Haddock.)*

of the bacteria responsible and well-designed on-site studies of the phenomenon should be carried out.

The most exotic and specific habitats of luminous bacteria are specialized light organs (e.g. in fish and squid) in which a pure culture is maintained at a high density and at high light intensity, as in the flashlight fish. In teleosts,

some 11 different groups carrying such bacteria are known. In such associations, the bacteria receive a niche and nutrients, while the host receives the benefit of the light and may use it for one or more specific purposes, such as for concealing the silhouette. Many aspects of how such symbioses are achieved – the initial infection, exclusion of contaminants, nutrient supply, restriction of growth but bright light emission – are not fully understood (Hastings et al., 1987). But recent studies (Chun et al., 2008) in the bobtail squid have resulted in many new findings over the past decade, including the demonstration that rhodopsin is expressed in the light organ cells, suggesting the presence of extraretinal photoreceptors.

Intestinal bacteria in marine animals, notably fish, are often luminous, and heavy pigmentation of the gut tract is sometimes present, presumably to prevent the light from betraying the location of the fish to predators. Luminous bacteria growing on a substrate, be it a parasitized crustacean, the flesh of a dead fish, or a fecal pellet, can produce a light bright enough to attract other organisms to feed on the material. It has recently been shown by video recording that a fish will selectively feed in total darkness on prey baited with luminous bacteria but completely ignore non-baited prey (M. Zarubin and S. Belkin, personal communication).

The only known terrestrial luminous bacteria are those harbored as symbionts by nematodes, which are parasitic on insects such as caterpillars. The nematode carries the bacteria as symbionts and injects them into the host where they release fertilized eggs. The bacteria grow and the developing nematode larvae feed on them. The dead but now luminous caterpillar (Fig. 52.7) attracts scavengers, which disperse the nematode offspring, along with the bacteria.

VIC. Biochemistry

Luminous bacteria typically emit continuous light peaking at ≈ 490 nm. When strongly expressed, a single bacterium may emit $\approx 10^4 - 10^5$ photons/s. The system is biochemically unique and is diagnostic for a bacterial involvement in the luminescence of a higher organism; in some, but not all cases, they can be isolated and grown in the laboratory. (Some symbionts have not been cultured.) The biochemical pathway itself (Fig. 52.8) constitutes a shunt of cellular electron transport at the level of flavin and reduced flavin mononucleotide is the substrate (luciferin) that reacts with oxygen in the presence of bacterial luciferase to produce an intermediate peroxy flavin (Hastings et al., 1985; Baldwin and Ziegler, 1992).

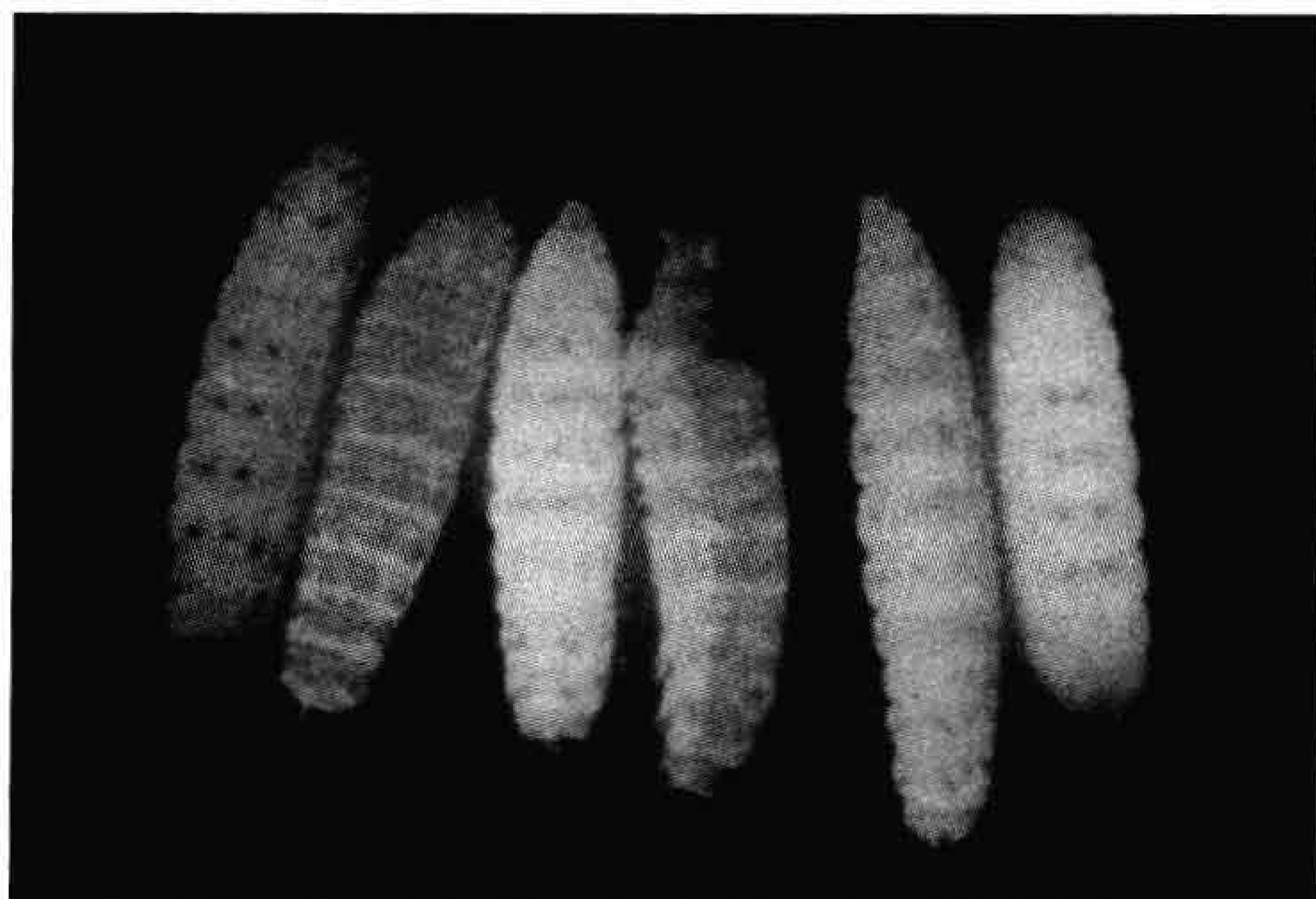


FIGURE 52.7 Caterpillar luminescence due to parasitic luminous bacteria.

This intermediate then reacts with myristic aldehyde to form the acid and the luciferase-bound hydroxy flavin in its excited state. Although there are two substrates in this case, the flavin can claim the name luciferin on etymological grounds, since it forms (bears) the emitter. The bioluminescence quantum yield has been estimated to be about 30%. There are enzyme systems that serve to maintain the supply of aldehyde, and genes coding for these enzymes are part of the lux operon, along with autoinducer and others (Meighen, 1991).

The luciferase and the mechanism of the bacterial reaction have been studied in great detail and its crystal structure is known (Fisher et al., 1996). The enzyme is an external flavin monoxygenase (EC #1.14.14.3), a heterodimeric (α-β) protein (≈ 80 kDa) in all species, with homology to long chain alkane monooxygenases (Li et al., 2008). Structurally, they appear to be relatively simple: no metals, disulfide bonds, prosthetic groups or non-amino acid residues are involved. The subunits are similar but possess only a single active center per dimer, located on the α subunit. A recent structure crystallized with FMN shows the site of its binding as well as insight concerning the way in the β subunit stabilizes the protein (Fig. 52.9) (Campbell et al., 2009). Curiously, none of other homologous enzymes of this type have been found to emit light, even at very low quantum yields.

An interesting feature of this luciferase reaction is its inherent slowness: at 20°C, the time required for a single catalytic cycle is about 20 s. The luciferase peroxy flavin itself has a long lifetime; at low temperatures (−20°C) it has been isolated, purified and characterized, but not crystallized. It can be further stabilized by aldehyde analogs such as long-chain alcohols and amines, which bind at the aldehyde site.

VII. DINOFLAGELLATE LUMINESCENCE

VIIA. Regulation by pH and a Circadian Clock

Dinoflagellate flashes are brief (≈ 100 ms), triggered by membrane action potentials, typically initiated mechanically, that sweep around the cell, as determined in the giant heterotrophic species, *Noctiluca* (Eckert, 1965). The active

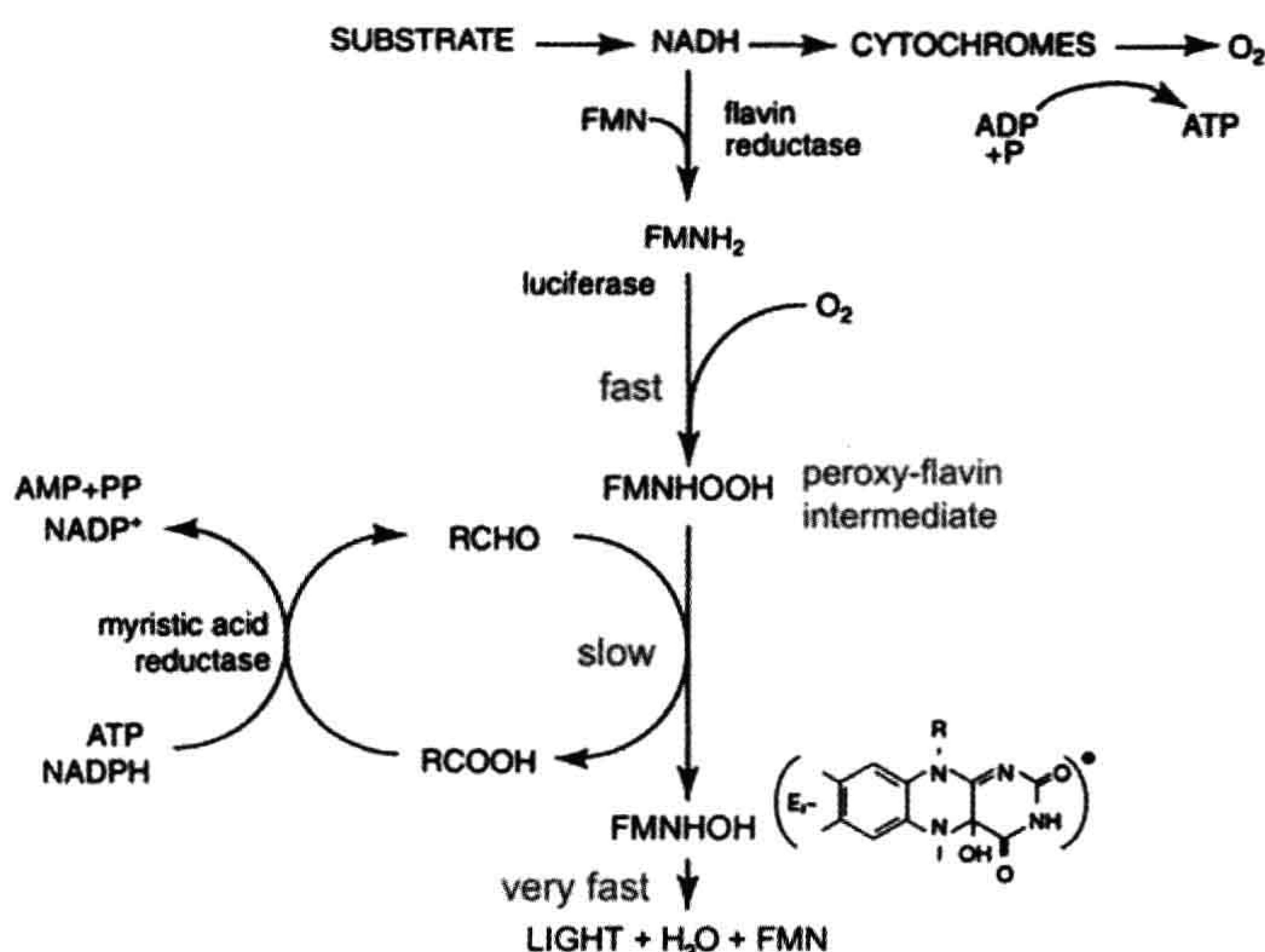


FIGURE 52.8 The luciferase reaction in bacteria. In the electron transport pathway, luciferase shunts electrons at the level of reduced flavin (FMNH2) directly to molecular oxygen. In the next step with long-chain aldehyde, hydroxy FMN is produced in its excited state (*) along with long-chain acid. The FMN product is reduced again and recycles; the aldehyde is also regenerated enzymatically.

membrane surrounding the cell vacuole is the tonoplast and, while the character of the action potential has not been definitely established, it was postulated some years ago (Fogel and Hastings, 1972) that voltage-gated proton channels allow protons from the vacuole to enter the many small membrane-enveloped luminous organelles, called scintillons (Fig. 52.10), initiating the highly pH dependent reaction. The presence of voltage-gated proton channels in a dinoflagellate has recently been demonstrated (Smith et al., 2011).

Neither quorum sensing nor the composition of the medium affect the development and expression of bioluminescence in dinoflagellates. But, on a far different time scale, luminescence in *L. polyedrum* and some other dinoflagellates is regulated by day—night light—dark cycles and an internal circadian biological clock mechanism (Morse et al., 1990; Hastings, 2007). Scintillons are numerous during the night phase but much less so by day (see Fig. 52.10) and both flashes and glow are greater then. The regulation is attributed to an endogenous mechanism; cultures maintained under constant conditions (light, temperature) continue to exhibit rhythmicity for many days, but with a period that is not exactly 24 hours: it is only about one day (=circa-diem).

The basic mechanism of circadian clocks appears to differ in different groups (Loras and Dunlap, 2001; Johnson et al., 2008; Mehra et al., 2009; Qin et al., 2010. Regulation of luminescence in the dinoflagellate *L. polyedrum* has been found to involve a daily de novo synthesis and

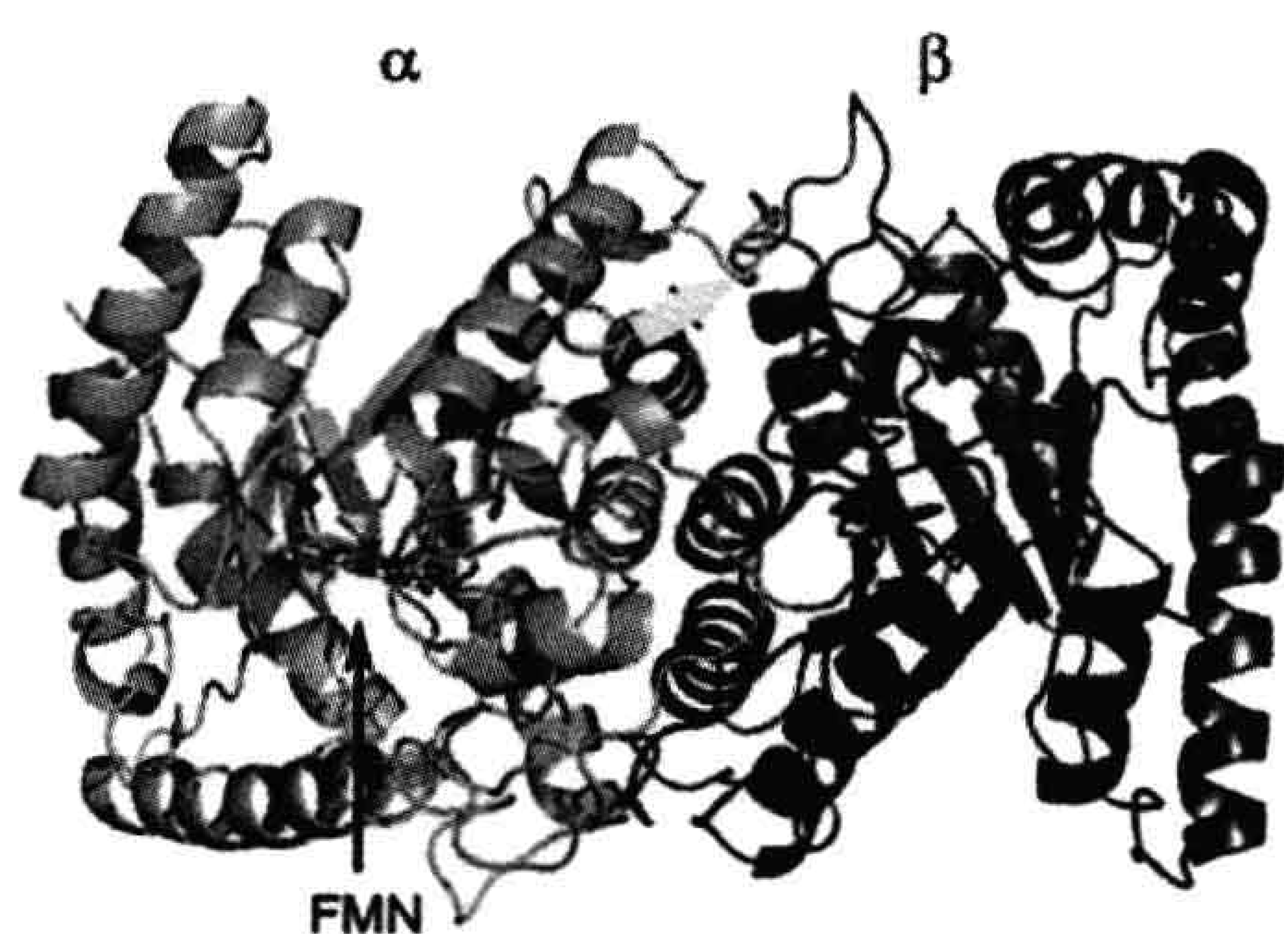


FIGURE 52.9 The crystal structure of FMN-bound bacterial luciferase, showing the α subunit (left, green) and β subunit (right, purple), as well as the site of the bound FMN. *(By permission of authors and publisher, Amer Chem Soc.)*

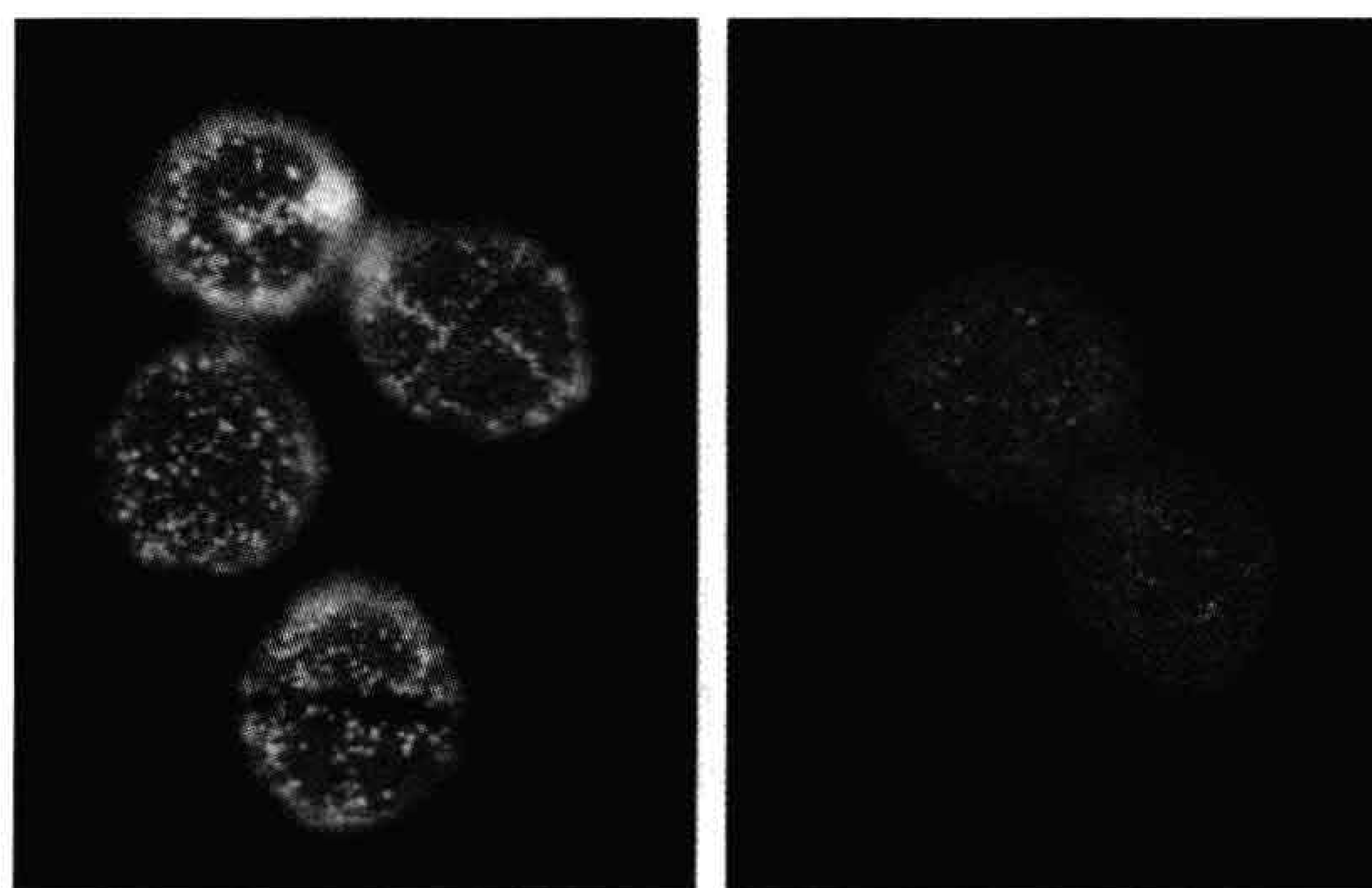


FIGURE 52.10 Fluorescence images of dinoflagellate cells (*Lingulodinium polyedrum*) at night (left) and during day phase (right), showing many luminous organelles (scintillons) at night and very few by day. The red background is fluorescence of the abundant chlorophyll.

destruction of specific proteins, translationally controlled by a still-unknown mechanism. This appears to differ from all other systems, both bacterial and animal, and remains an enigma. In humans and other higher animals, where it regulates the sleep–wake cycle and many other physiological processes, the mechanism involves the nervous system and transcriptional regulation.

VIIB. Occurrence and Function

Dinoflagellates occur ubiquitously in the oceans as planktonic forms and contribute substantially to the so-called "phosphorescence" commonly seen at night in summer when the water is disturbed. They occur abundantly in surface waters and most species are also photosynthetic; some produce neurotoxins (e.g. saxitoxin), which can accumulate in shellfish and constitute a health hazard. In the phosphorescent bays (e.g. in Puerto Rico and Jamaica), high densities of a single species (*Pyrodinium bahamense*) typically occur. The so-called red tides, which occur world-wide and may cause fish kills due to toxins or oxygen deprivation, are blooms of dinoflagellates, sometimes a luminous species. At night during such red tides, one can see waves breaking or the undulating luminescent pattern left behind by fish fleeing as the boat approaches. World War II aviators based on aircraft carriers in the South Pacific tell of the ease with which they relocated their base ship after a night mission – or equally well a target ship: a luminescent wake may extend for many kilometers behind a ship as the persistent turbulence stimulates the cells to emit light.

About 6% of all dinoflagellate genera contain luminous species, all marine. As a group, dinoflagellates are important as symbionts, notably for contributing photosynthesis and carbon fixation in animals but, unlike bacteria, no luminous dinoflagellates are known from symbiotic niches.

VIIC. Biochemistry and Cell Biology

As mentioned above, luminescence in dinoflagellates is emitted from scintillons, many small (≈0.5 μm), novel cortical organelles. They occur as outpocketings of the cytoplasm into the cell vacuole, like a balloon, with the neck remaining connected, as shown in electron micrographs labeled with antiluciferase-labeled gold particles (Fig. 52.11) (Nicolas et al., 1987), diagrammatically represented in Fig. 52.12. They can also be visualized by immunolabeling with fluorescent antibodies raised against the luminescence proteins (Fritz et al., 1990), in vivo by their bioluminescence (Johnson et al., 1985), as well as by the fluorescence of luciferin (see Fig. 52.10). Dinoflagellate luciferin is a novel tetrapyrrole related to chlorophyll (Nakamura et al., 1989). Lase and LBP are the only major proteins in scintillons, other cytoplasmic components being somehow excluded.

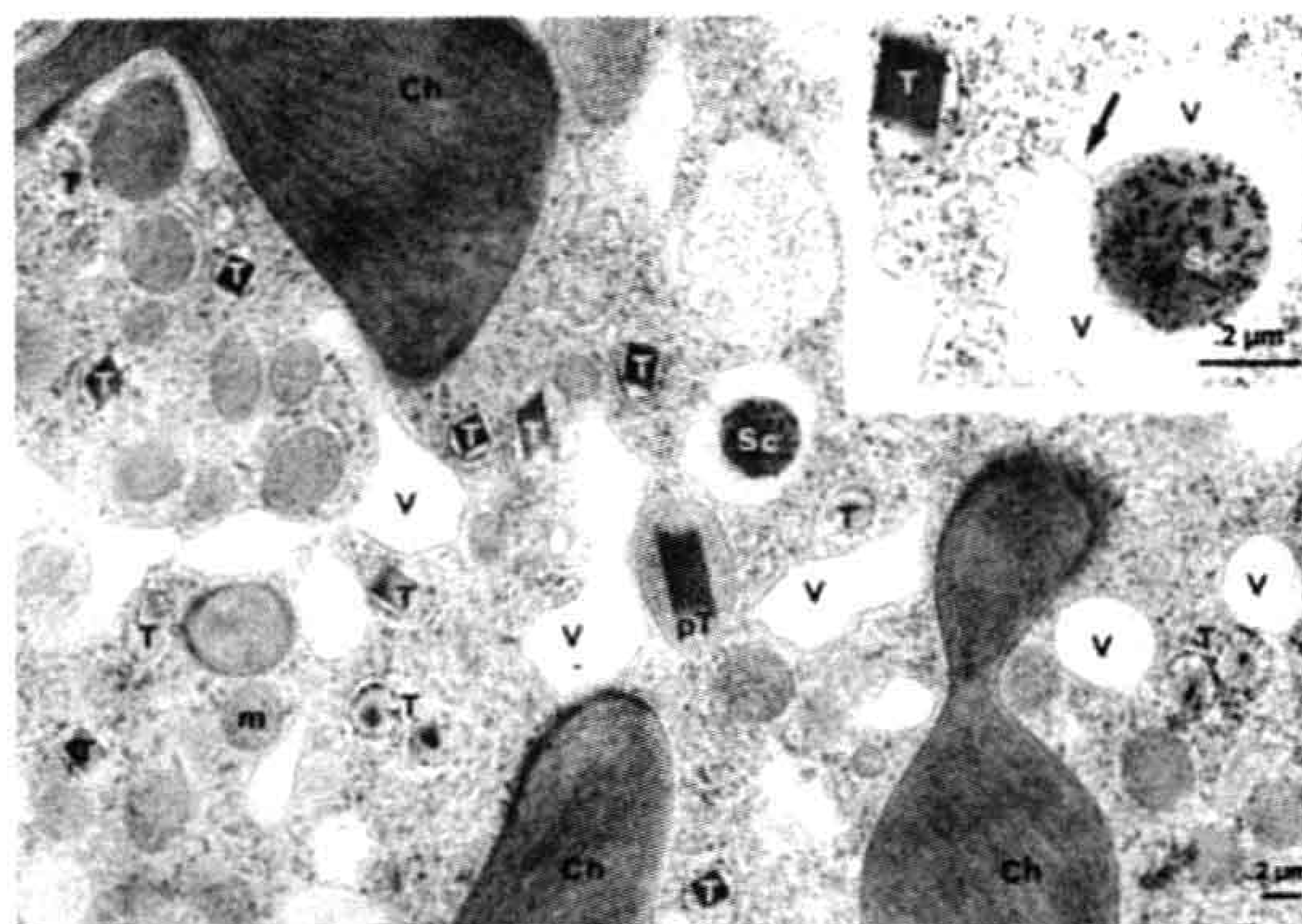


FIGURE 52.11 Immunoelectron microscopy of *Lingulodinium polyedrum*. Gold labeled anti-luciferase marks a scintillon (Sc) hanging in a vacuole (V). Ch, chloroplast; M, mitochondrion; T, trichocyst; pT, pre-trichocyst.

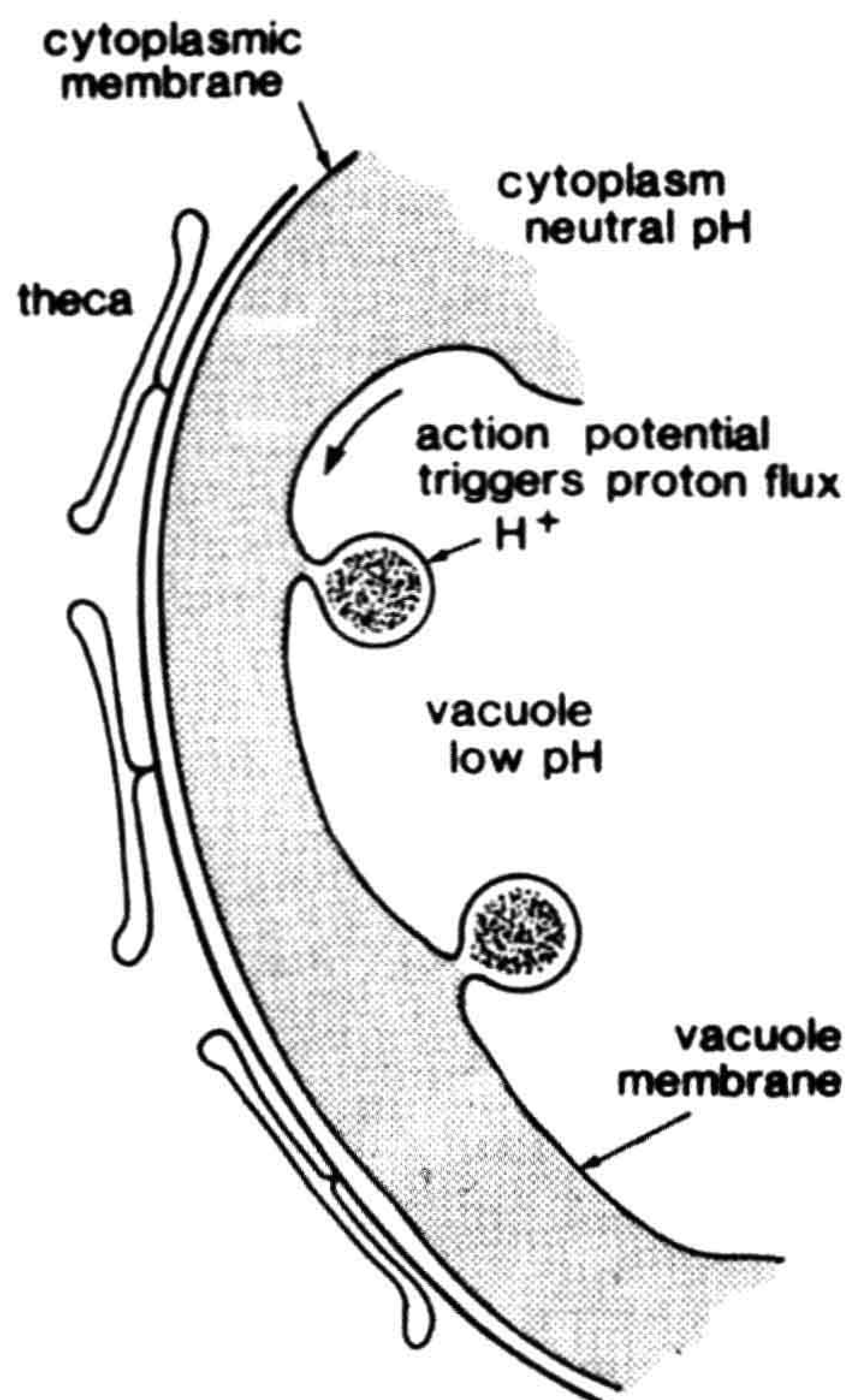


FIGURE 52.12 Scintillons of dinoflagellates represented as organelles formed as cytoplasmic outpocketings hanging in the vacuole.

Activity can be obtained in extracts made at pH 8 simply by shifting the pH from 8 to 6; it occurs in both soluble and particulate fractions; both activities peak at pH 6. The existence of activity in both soluble and particulate (scintillon) fractions indicates that during extraction some scintillons are lysed, while others seal off at the neck and form closed vesicles, which have been purified and characterized. The in vitro activity occurs as a flash (≈200 ms, 10°C), very similar to that of the living cell (Fig. 52.13) and the kinetics are independent of the dilution of the suspension. For the soluble fraction, the kinetics does depend on dilution, as enzyme concentration differs.

The Lase is unique in having three catalytic highly similar sequences, called domains, in a single molecule (Mr, ≈140 kDa). Each domain, when expressed and assayed individually, has activity and the sequences of the central 166 amino acid of the three (>95% identical) constitute the catalytic sites (Fig. 52.14) (Li et al., 1997). The luciferin is bound to LBP (Mr, ≈73 kDa), which also has domains, but four, and less well conserved. Both proteins occur in the genome in many tandem copies and the N-terminal 106 amino acids of the two are ≈50% identical, but the function of that region remain unknown.

In solution, both activities are pH dependent with pKs at 6.7; at pH 8, the LBP binds luciferin and Lase is inactive; at pH 6 luciferin is not bound and Lase is active. As shown by site directed mutagenesis, the pH dependence of Lase is due to four histidines located in the N-terminal region of each domain; if substituted by alanines, the luciferase is fully active at pH 8 (Li et al., 2001).

These Lase features can be visualized in the crystal structure of its domain 3 (Fig. 52.15) (Schultz et al., 2005).

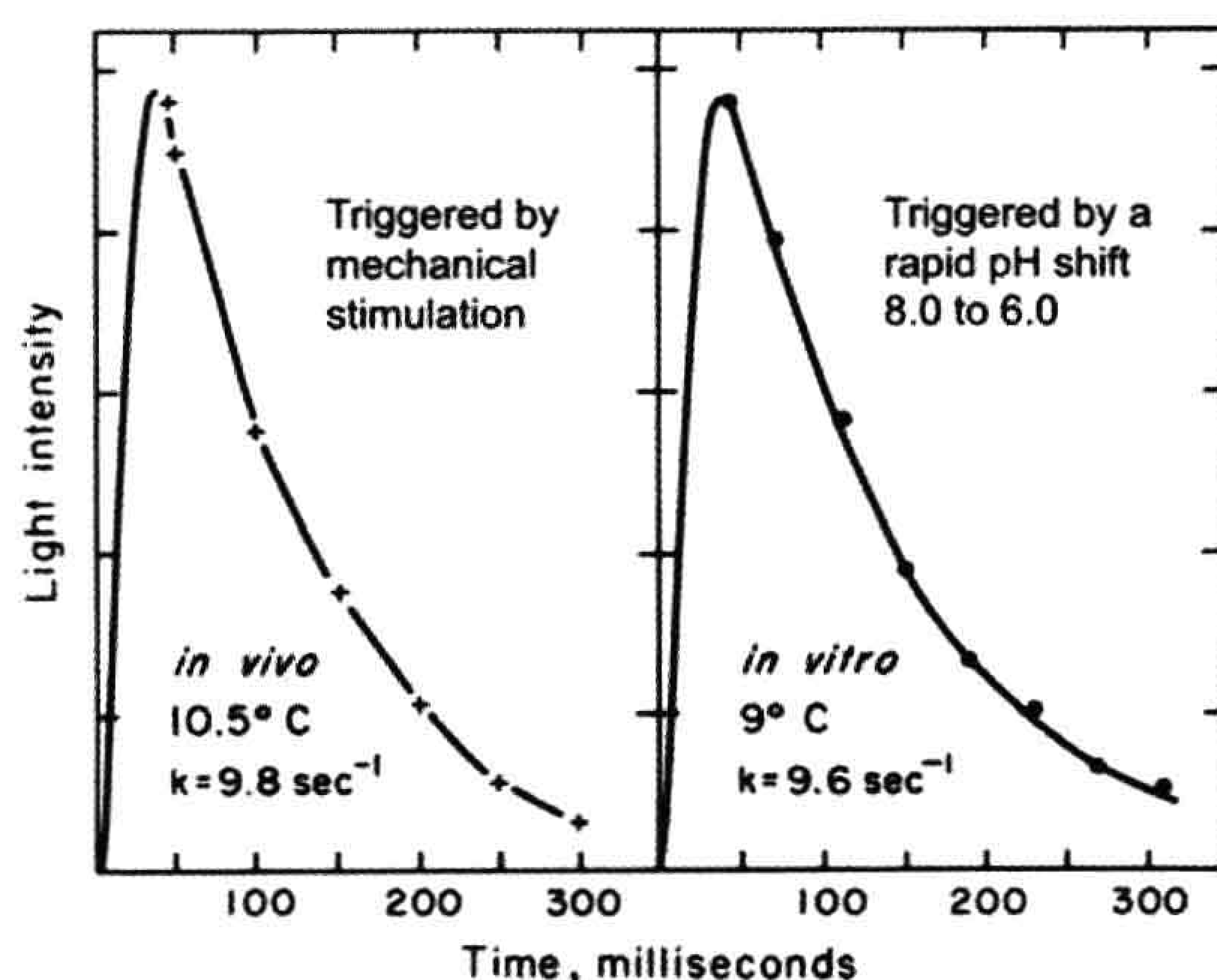


FIGURE 52.13 Kinetics of flashes of a living cell (left) and of isolated scintillons (right).

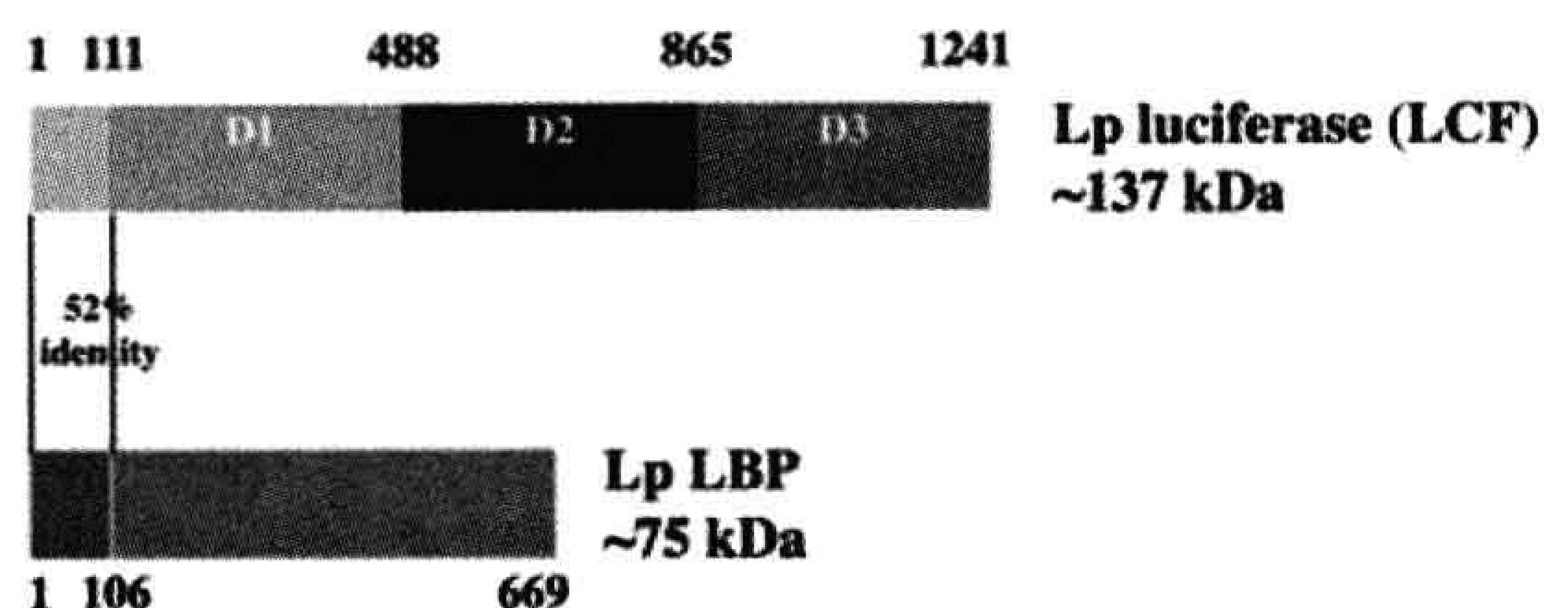


FIGURE 52.14 Organization of the two scintillon proteins in the bioluminescence of *Lingulodinium polyedrum*. The N-terminal regions of the two are similar, but its function is not known. The three domains of luciferase (LCF, upper) are similar and each has catalytic activity alone; the luciferin binding protein (LBP, lower) has four domains with significant but not great similarity.

A major part forms a barrel, inside of which is the luciferin binding site; three alpha helices form a channel but, at pH 8, it is too small for luciferin to enter. The four histidines responsible for the pH-dependent change are located in these sequences; molecular dynamics calculations indicate that when the histidines are protonated or substituted by alanines a conformation change would lead to an opened channel.

The presence of repeated conserved sequences in one enzyme molecule is not unprecedented but, to our knowledge, this is the only case in which each of the sequences has been shown to be separately active. A possible reason for the presence of three active sites on a single molecule is that it allows activity to be greater without an increase in the colloidal osmotic pressure of the scintillon.



FIGURE 52.15 A ribbon diagram of the crystal structure of *Lingulodinium* luciferase domain 3. The lower barrel structure, where the active site is located, is composed of 10 anti-parallel β-strands. The upper α-helices (green and blue) regulate the opening of a channel for the entry of luciferin.

VIII. COELENTERATES AND CTENOPHORES

VIIIA. Regulation by Ca^{2+}

Early attempts to isolate biochemically and identify active fractions of the luminous jellyfish *Aequorea* were frustrated, even though cell-free extracts exhibited strong light emission lasting an hour or longer. The clue, as once told by Shimomura (personal communication), came when he discarded a still-emitting extract in the sink and noticed that it became much brighter. Tracing this to calcium, he extracted the cells in the presence of EDTA to chelate calcium and discovered that the activity was retained in a single protein, which he named aequorin and dubbed a photoprotein (Shimomura et al., 1962). While at the time he considered photoprotein to be an altogether new type of bioluminescence system, it turned out that it is indeed a luciferin–luciferase type system and that aequorin is a reaction intermediate in which the luciferin bound to the luciferase (apoaequorin) has already reacted with oxygen to form a (very) stable peroxide, as confirmed by crystal structures. While aequorin is analogous in some respects to the bacterial flavin–peroxy intermediate, the latter is far less stable and has not been crystallized or its structure determined.

Aequorin is stored in photocytes; an action potential mobilizes Ca^{2+}, which reacts with aequorin and causes the reaction to go to completion, with the formation of luciferase-bound excited oxidized luciferin and then light emission.

VIIIB. Occurrence and Function

Luminescence is common and widely distributed in ctenophores and coelenterates (Cormier in Herring, 1978; Herring in Herring, 1978), but absent in sea anemones and corals. In the ctenophores (comb jellies), luminous forms comprise over half of all genera, whereas in the coelenterates (cnidaria), it is about 6%. Luminous hydroids, siphonophores, sea pens and jellyfish, among others, are well known. The organisms are mostly sessile or sedentary and, upon stimulation, emit light as flashes. In some groups the luminescence is secreted.

Hydroids occur as plant-like growths, typically adhering to rocks below low tide level in the ocean. Upon touching them there is a sparkling emission conducted along the colony; repetitive waves from the origin may occur. Luminous jellyfish (hydromedusae such as *Aequorea aequorea* and *Pelagia noctiluca*) are well known; the bright flashing comes from photocytes along the edge of the umbrella at the base of the tentacles. *Aequorea* occurs during the summer in the ocean off the northwest USA. The sea pansy, *Renilla*, which occurs near shore on sandy bottoms, has also figured importantly in the elucidation of the biochemistry of coelenterate luminescence (Cormier, 1981).

Photocytes occur as specialized cells located singly or in clusters in the endoderm. They are commonly controlled by epithelial conduction in hydropolyps and siphonophores and by a colonial nerve net in anthozoans. The light may be emitted as one or many flashes per stimulus. The putative neurotransmitter involved in neural control of luminescence in *Renilla* is adrenaline or a related catecholamine.

VIIIC. Biochemistry and Cell Biology

The luciferin of coelenterates, coelenterazine, is notable for its widespread phylogenetic distribution, speculated to serve in non-luminous organisms as an antioxidant. Actually, the jellyfish *Aequorea* obtains coelenterazine from its diet (Haddock et al., 2001), so it is analogous to a vitamin, except for the fact that light emission is not necessary for life. In some cases (e.g. *Renilla*), the sulfated form of luciferin may occur as a precursor or storage form and is convertible to active luciferin by sulfate removal with the co-factor 3′5′-diphosphadenosine. The active form may also be sequestered by a Ca^{2+} sensitive binding protein, analogous to the dinoflagellate binding protein. In this case Ca^{2+} triggers the release of luciferin and then flashing, thus different from the *Aequorea* mechanism.

As described above, in *Aequorea*, *Obelia* and other hydromedusae, the luciferin and luciferase (EC#1.13.12.5) react with oxygen to form a stable peroxide (aequorin or obelin); stored in photocytes, it remains poised for the completion of the reaction (Blinks et al., 1982; Charbonneau et al., 1985; Cormier et al., 1989; Shimomura, 2006). The crystal structure of this intermediate (Fig. 52.16) has been determined for both *Aequorea* and *Obelia* (Head et al., 2000; Liu et al., 2000). An action potential allows Ca^{2+} to enter and bind to the protein, shifting or breaking hydrogen bonds, thus changing its conformational state and allowing the reaction to continue, but without the need for free oxygen at this stage. An enzyme-bound cyclic peroxide, a dioxetanone, is a postulated intermediate; it breaks down with the formation of excited coelenteramide, the emitter, along with a molecule of CO_2. The enzyme itself, called apoaequorin, can react again with coelenterazine and oxygen to form aequorin anew; it is homologous with calmodulin (Lorenz et al., 1991).

It had been reported in the early literature that coelenterates could emit bioluminescence even if fully deprived of oxygen. The explanation is now evident: aequorin is an intermediate in which the substrate has already reacted with oxygen and the cells store it in a stable state; only calcium is needed to emit light.

Remarkably, in vitro, the light emitted from this isolated system is blue, with a broad spectrum peaking at $\approx$480 nm while, in vivo, the emission is green (λ_{max} = 508 nm) and its spectrum is narrow. This is due to a different protein with a second chromophore, green fluorescent protein

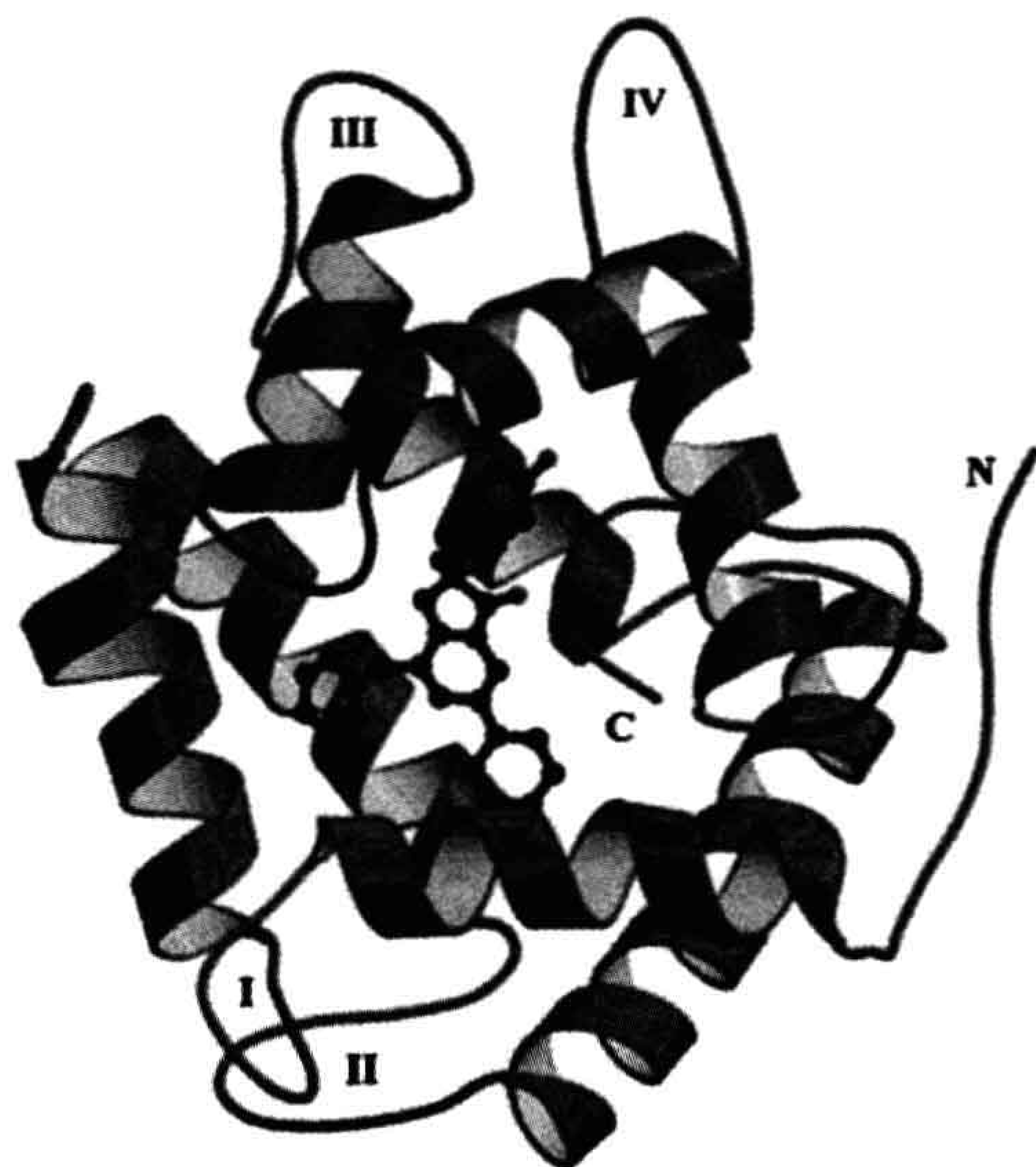


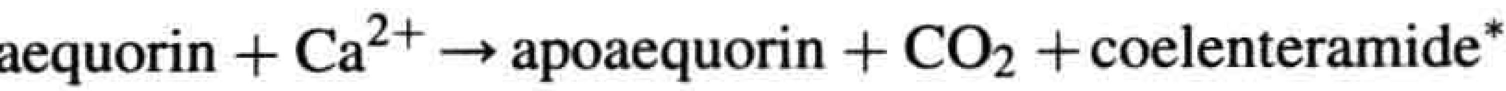
FIGURE 52.16 Structure of the calcium-regulated photoprotein obelin. The N-terminal α-helices are green (lower) and the C-terminal red (upper). The hydroperoxycoelenterazine substrate is the blue stick representation buried between green and red α-helices. *(By permission John Lee.)*

(GFP), which is the emitter. Some years earlier, it had been observed that the photocytes of *Aequorea* exhibited a green fluorescence, corresponding to the color of their bioluminescence. Johnson et al. (1962) observed the blue of the in vitro system along with a green fluorescence in extracts and suggested that it might be responsible by absorption and re-emission. Morin and Hastings (1971) observed that isolated photocytes triggered to emit by Ca^{2+} emitted green light whereas, if lysed before Ca^{2+} addition, the emission was blue, and proposed that this is due to radiationless (Foerster-type) energy transfer to the green fluorescent protein (GFP). This protein, whose chromophore is formed by the slow (≈1 hour, oxygen required) post-translational modification of three centrally located amino acids (Cody et al., 1993), thus covalently attached, is now widely used as a fluorescent marker or reporter gene (see Applications). Its crystal structure (Fig. 52.17) reveals a fascinating lantern-like structure (Ormö et al., 1996; Yang et al., 1996).

The overall reaction is thus:



$$\text{coelenterazine} + \text{apoaequorin} + O_2 \rightarrow \text{aequorin}$$



$$\text{aequorin} + Ca^{2+} \rightarrow \text{apoaequorin} + CO_2 + \text{coelenteramide}^*$$



$$\text{coelenteramide}^* + \text{GFP} \rightarrow \text{coelenteramide} + \text{GFP}^*$$



$$\text{GFP}^* \rightarrow \text{GFP} + hr$$



FIGURE 52.17 Crystal structure of GFP showing the chromophore in the center.

More recently, it was discovered that similar proteins occur in a variety of colors in other coelenterates, including corals, not associated with bioluminescence; their use as reporters has been evaluated (Baird et al., 2000) and color mutant GFPs have provided an array of colors that greatly expand the possible applications (Zhang et al., 2002).

Some strains of luminous bacteria also utilize an accessory protein, whereby the color may be either blue- or red-shifted, depending on the fluorophore which, however, is not covalently attached, so not suitable as a label. It has also been determined that the color shift is not attributable to Foerster-type energy transfer in this case; the protein participates in the luciferase reaction itself (Eckstein et al., 1990).

IX. FIREFLY LUMINESCENCE

IXA. Regulation by a Nerve Impulse and Oxygen

The firefly light organ comprises a series of photocytes arranged in a rosette, positioned radially around a central trachea, which supplies oxygen to the organ via tracheoles (Smith, 1963). The organ itself comprises a series of such rosettes, stacked side-by-side in many dorsoventral columns. Photocyte granules or organelles containing

luciferase have been identified with peroxisomes on the basis of immunochemical labeling.

The control of firefly flashing has long intrigued scientists and while there is agreement that it is ultimately controlled by regulating oxygen in the photocytes, the mechanism remains controversial. It is triggered in the first instance by a nerve impulse via the ventral nerve cord (Case and Strause in Herring, 1978); however, the nerves do not terminate on the photocyte, but on adjacent tracheal end cells, which surround the tracheoles entering the photocytes. The transmitter is octopamine and it takes some 50 ms or longer after the arrival of the nerve impulse for the onset of the flash to occur. Thus, the flash is not triggered directly by an action potential. Nor are any of the ions typically gated by membrane potential changes (Na^+, K^+ and Ca^{2+}) likely candidates for controlling luminescence chemistry.

All studies have concluded that the availability of oxygen regulates flashing; there is a strong positive relationship between the extent of the tracheal supply system in the adults of different species and their flashing ability. Also, all assume that photocytes are maintained anaerobic between flashes; the unusually large number of mitochondria buoys the belief. And all, except two recent ones (Trimmer et al., 2001; Ghiradell and Schmidt, 2004), concluded that the onset of the flash is regulated by the entry of oxygen to photocytes and the tracheolar cells were implicated in controlling it. Supporting evidence included the fact that the light organs of larval fireflies, which glow but do not flash, lack the end cells and are directly innervated. Also, firefly lantern tracheoles are reinforced against collapse. Some authors argued that a contractile action of end cells would force air into the photocytes; others proposed that fluid in the tracheoles normally blocks the entry of oxygen and a rapid but transient removal of the fluid, possibly by osmotic means, that allows oxygen to enter and initiate the flash (Timmins et al., 2001). Both were silent on the mechanism responsible for the termination of the flash, but removal of oxygen was tacitly assumed.

A quite different theory was put forward more recently, based on the finding that nitric oxide (NO) can affect the light emission in fireflies (Trimmer et al., 2001). Control of oxygen entry was assumed not to occur; instead it was proposed that oxygen enters continuously and that anaerobiosis is maintained by vigorous and continued mitochondrial respiration, whose inhibition by NO produced in tracheolar cells allows oxygen to enter and react with the luminous organelles. The decline is attributed to its reversal, principally photochemically by the light of the flash itself (Aprille et al., 2004). No follow up or repeats of the studies have appeared.

The second recent proposal is that the cells are indeed maintained anaerobic and that the flash is generated by the release of oxygen from H_2O_2 within the organelles that emit light, which are modified peroxisomes. No studies in support of the idea have appeared.

The rapid onset and decline characteristic of flashes with precision kinetics seem unlikely to be achieved by an inhibitory-type mechanism. Biochemical evidence suggests that the rate constants are determined by the reaction of oxygen with enzyme bound luciferyl adenylate, which accumulates in a slow reaction in the absence of oxygen (McElroy and Hastings, 1956), analogous to the reaction of aequorin with calcium. The firefly species-specific flash duration would be determined by rate constants, not by the enzyme concentration or the removal of oxygen or variable physiological factors. The formation of new luciferyl-adenylate is slow in relation to the flash, so emission terminates even though some oxygen may remain.

IXB. Occurrence, Function

There are only about 100 genera of insects classed as luminous out of a total number of approximately 70 000 (Lloyd in Herring, 1978). But where seen, their luminescence is impressive, most notably in the many species of beetles, the fireflies and their relatives. Fireflies themselves possess ventral light organs on posterior segments, but the South American railroad worm, *Phrixothrix*, has paired green light organs on the abdominal segments and red ones on the head (Fig. 52.18), while the click and fire beetles, Pyrophorini, have both running lights (dorsal) and landing lights (ventral).

The variety of different fireflies, with their different habitats and behaviors, is impressive. The major function of light emission in fireflies is for communication during courtship (Lloyd, 1977, 1980; Case, 1984) and the different flashing kinetics and patterns facilitate species identification. In North American species, a female on the grass or a leaf emits a query flash, while a male responds with a species-specific time delay. Flash flickering occurs in



FIGURE 52.18 The railroad worm, with green emitting photophores on each segment and red ones on the head.

some species, sometimes at frequencies higher than detectable by the human eye (≈40 Hz).

The signal mechanism in the synchronously flashing fireflies in Southeast Asia (*Pteroptyx* spp.) is not so well understood. These form congregations of many thousands in single trees, where the males produce an all-night-long display, with flashes every 1–4 s, dependent on species (Buck, 1988), which may serve to attract females to the tree.

The cave glow worm *Arachnocampa* (a fly) exudes beaded strings of slime from its ceiling perch (Fig. 52.19), which glisten in the reflected light from its caudal light organ and serve to entrap small flying prey that are attracted by the "fishing lines" (Fig. 52.20). While it is similar in some respects to its much less impressive American relative *Orfelia*, the two differ biochemically (Viviani et al., 2002).

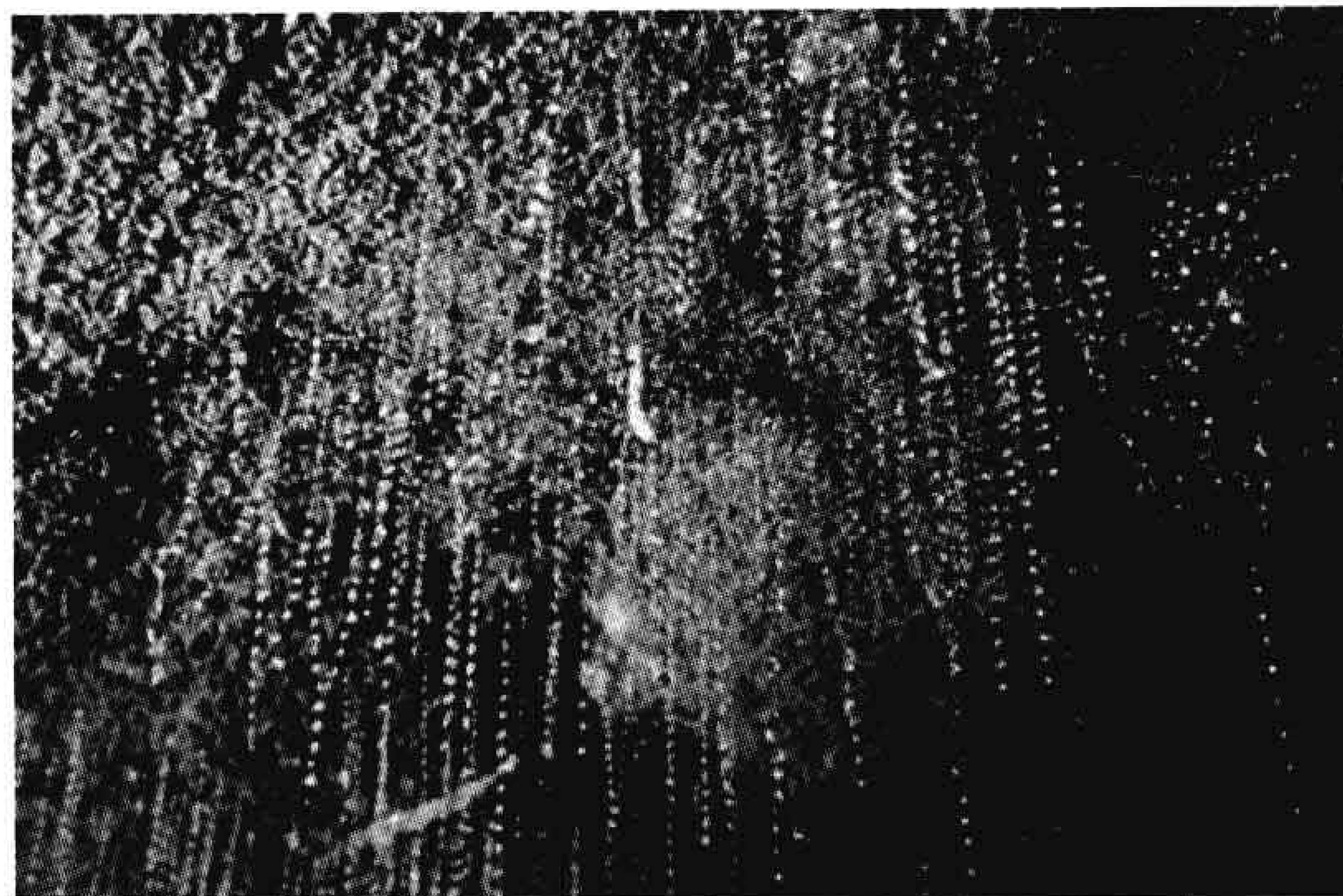


FIGURE 52.20 "Fishing lines" produced by *Arachnocampa* as traps for flying insects that wander into the cave.

IXC. Biochemistry and Cell Biology

The firefly system was the first in which the biochemistry was extensively studied. It had been known since before 1900 that cell-free extracts could continue to emit light for several hours or longer, and that after the complete decay of the light, emission could be restored by adding a second extract prepared with hot water (then cooled). The enzyme luciferase was assumed to be in the first, with all the luciferin substrate being used up during the emission, and luciferin in the second, since the enzyme was denatured by the hot-water extraction. This was named the luciferin–luciferase reaction by DuBois in 1885, and it was already known in the first part of the 20th century that luciferins and luciferases from the different major phyla would not cross react, indicative of their independent evolutionary origins (Harvey, 1952).



FIGURE 52.19 Luminous dipteran larvae (*Arachnocampa*) on the ceiling of a cave in New Zealand.

In 1947, it was discovered that the addition of adenosine triphosphate (ATP) alone to an "exhausted" cold water extract, resulted in an enormous bioluminescence response (McElroy, 1947). This response suggested that luciferin had not actually been used up in the cold water extract; but ATP could not be the emitter, since it does not have the appropriate fluorescence. For some time, ATP was thought to be providing the energy for light emission. But, as noted earlier, the energy available from ATP hydrolysis is only about 7 kcal per mole, whereas the energy of a visible photon is ≈50 kcal per mole. It was soon discovered that firefly luciferin, which was shown to be a unique benzothiazole, was still present in large amounts in the "exhausted" cold water extract, and that it was ATP that was used up (by ATPases in crude extracts), but available in the hot water extract. ATP was later shown to be required to form the luciferyl adenylate intermediate which, in a separate step, then reacts with oxygen to form a cyclic luciferyl peroxy species, which breaks down to yield CO_2 and an excited state of the carbonyl product (McElroy and DeLuca in Herring, 1978).

In in vitro reactions in which luminescence has decreased to a low level (emission may continue for days), it was found that emission is greatly increased by coenzyme A, but the reason for this was obscure. The recent discovery

that long-chain acyl-CoA synthetase (EC# 6.2.1.3) has homologies with firefly luciferase (EC# 1.13.12.7) both explains this observation (Fraga, 2008) and indicates the evolutionary origin of the gene.

Firefly luciferase catalyzes both the luciferin activation and the subsequent oxygen reaction leading to the excited product. The crystal structure (Fig. 52.21) revealed the structural basis for the two-step reaction and confirmed that the same protein is responsible for both (Conti et al., 1996). Luciferase has been cloned and expressed in other organisms, including *E. coli* and tobacco. For activity, luciferin must be added exogenously; tobacco "lights up" with the roots dipped in a luciferin solution (Ow et al., 1986). There are some beetles in which the light from different organs is a different color, shown to be due to the luciferase not the luciferin. The same ATP-dependent luciferase reaction with the same luciferin occurs in the different organs, but the luciferases are slightly different, coded by different (but homologous) genes (Wood et al., 1989; Viviani et al., 2006; Branchini et al., 2007; Viviani, 2009). They are presumed to differ with regard to the conformation of the site that binds the excited state, which thereby alters the emission wavelength.

X. OTHER ORGANISMS: OTHER CHEMISTRIES

The four systems described above are known best, but several others have been studied in some detail, revealing interesting differences in both physiological and biochemical aspects.



FIGURE 52.21 Ribbon diagram of the firefly luciferase (*Luc*) structure. The large N-terminal domain (amino acids 1–436) is connected to the smaller C-terminal domain (amino acids 440–550 shown in yellow) through a short hinge peptide. *(Reproduction permission from Nature Publishing Group.)*

XA. Molluscs

Snails (gastropods), clams (bivalves) and cephalopods (squid) all have bioluminescent members (Young and Bennett, 1988). The squid luminous systems are by far the most numerous, and also diverse, both in form and function, rivaling the fishes in these respects, and some produce brilliant displays (Fig. 52.22). As for fish, some squid utilize symbiotic luminous bacteria, but others are self-luminous, indicating that bioluminescence had more than one evolutionary origin within the classes.

Also like some fish, some squid possess photophores, which may be used in spawning and other interspecific displays (communication). Photophores are compound structures with associated optical elements, such as pigment screens, chromatophores, reflectors, lenses and light guides. They may emit different colors of light and are variously located near the eyeball, on tentacles, body integument or associated with the ink sac or other viscera. An octopus with luminescent suckers has been reported (Johnsen et al., 1999). In some species, luminescence intensity has shown to be regulated in response to changes in ambient light, indicative of a camouflage function.

Along the coasts of Europe, there is a clam, *Pholas dactylus*, which inhabits chambers that it makes by boring holes into the soft rock. When irritated, these animals produce a bright cellular luminous secretion, squirted out through the siphon as a blue cloud. This animal and its luminescence has been known since Roman times, and the system was used by DuBois in his discovery and description of the "luciferin–luciferase" reaction in the 1880s (see above). Well ensconced in its rocky enclosure, the animal presumably uses the luminescence somehow to thwart would-be predators.

The *Pholas* reaction has been studied extensively; the luciferin, now called pholasin, has a protein-bound chromophore; it is probably dehydrocoelenterazine. The



FIGURE 52.22 Firefly squid (*Watasenia*) in aquarium tank with onlookers.

luciferase is a copper-containing large (>300 kDa) glycoprotein (Hentry et al., 1975). It can serve as a peroxidase with several alternative substrates, suggesting the involvement of a peroxide in the light emitting pathway; the superoxide ion may be involved in the reaction.

There are luminous species in several families of gastropods; a New Zealand pulmonate limpet, *Latia neritoides*, is notable as the only known luminous organism that can be classed as a truly fresh-water species. It also secretes a bright luminous slime (green emission, λ_{max} = 535 nm), whose function may be to forewarn predators. Its luciferin is an enol formate of an aldehyde, but the emitter and products in the reaction are unknown; in addition to its luciferase (MW ≈ 170 kDa; EC#1.14.99.21), a "purple protein" (MW ≈40 KDa) is also required, but only in catalytic quantities, suggesting that it may be somehow involved as a recycling emitter.

XB. Annelids

The annelids also include numerous luminous species, both marine and terrestrial (Herring in Herring 1978). The marine polychaete *Chaetopterus* constructs and lives in buried U-shaped tubes with only the openings at the surface of the sea floor; they pump sea water through the tube and exude luminescence upon stimulation, but the chemistry of the reaction has completely eluded researchers. The function of its emission may be similar to that of *Pholas*. Other marine polychaetes include the Syllidae, such as the Bermuda fireworm, and the polynoid scale worms, which shed their luminous scales as decoys. Both have largely escaped biochemical elucidation, although extracts of the latter have been shown to emit light upon the addition of superoxide ion.

More but still limited knowledge is available concerning the biochemistry of the reaction in terrestrial earthworms, some of which are quite large, over 60 cm in length (Wampler, 1981). Upon stimulation they exude celomic fluid from the mouth, anus and body pores. This exudate contains cells that lyse to produce a luminous mucus, emitting in the blue-green region. In *Diplocardia longa*, the cells responsible for emission have been isolated; luminescence in extracts involves a copper-containing luciferase (MW ≈300 kDa) and the luciferin (N-isovaleryl-3 amino- 1 propanal). The in vitro reaction requires H_2O_2, not free O_2. The exudate from animals deprived of oxygen does not emit, but will do so after the admission of molecular oxygen to the free exudate.

XC. Crustaceans

Many crustaceans are luminescent (Herring, 1985b). The cypridinid ostracods, such as *Vargula* (formerly *Cypridina*) *hilgendorfii*, are small organisms that possess two glands with nozzles from which the luciferin and luciferase (EC#1.13.12.6) are squirted into the sea water, where they react and produce a spot of light that retains its integrity, useful either as a decoy or for communication.

Cypridinid luciferin and its reaction have differences and similarities to the coelenterazine system (Cormier in Herring, 1978). The luciferin in both is a substituted imidazopyrazine nucleus that reacts with oxygen to form an intermediate cyclic peroxide, which then breaks down to yield CO_2 and an excited carbonyl. However, the cypridinid luciferase gene has been cloned and appears to have no homologies with the gene for the corresponding coelenterate proteins and calcium is not involved in the cypridinid reaction. The two different luciferases reacting with similar luciferins have apparently had independent evolutionary origins, indicative of convergent evolution at the molecular level.

Euphausiid shrimp possess compound photophores with accessory optical structures and emit a blue ventrally-directed luminescence. The system is unusual because both luciferase and luciferin cross-react with the dinoflagellate system. This cross-taxon similarity indicates another possible exception to the rule that luminescence in distantly related groups had independent evolutionary origins, thus another case of convergent evolution. The shrimp might obtain luciferin nutritionally, but the explanation for the occurrence of functionally similar proteins is not evident. One possibility is lateral gene transfer; convergent evolution is another. The sequence of the shrimp luciferase has not been determined.

XD. Fishes

Bioluminescence in fishes is highly diverse and occurs in both teleost (bony) and elasmobranch (cartilaginous) fishes. Partly because the animals have not been so readily available, relatively little is known about their physiology and biochemistry, but many have been described from specimens (Herring, 1982).

As already noted, many fish obtain their light emitting ability by culturing luminous bacteria in special organs. Many coastal and deep-sea luminous fishes fall into this category, while others are self-luminous. Those include *Porichthys*, the midshipman fish, so-called because of the array of photophores distributed linearly along the lateral lines, like buttons on a military uniform. It has been the object of considerable study and more is known about the physiological control of luminescence in it than in any other fish. Its luciferin and luciferase cross-react with the ostracod (cypridinid) crustacean system described above. This cross-reactivity was an enigma until it was discovered that Puget Sound fish have photophores but are unable to luminesce, but can do so if the animals are injected with or fed cypridinid luciferin. This observation showed that

luciferin may be obtained nutritionally. Did the luciferase in this fish originate independently making use of the available substrate, or was the ability to synthesize luciferin lost secondarily? If the latter, this would be analogous to the loss of the ability to synthesize vitamins in mammals.

Open sea and mid-water species include sharks, some of which may have several thousand small photophores. The teleosts include the gonostomatids, such as *Cyclothone,* with simple photophores, and the hatchet fishes, having compound photophores with elaborate optical accessories; emission is directed exclusively downwards, indicative of a camouflage function of the light. A number of self-luminous fish eject luminous material; in the searsid fishes this is cellular in nature, but it is not bacterial and its biochemical nature is not known. Such animals may also possess photophores.

Fish often possess different kinds of photophores located on different parts of the body, especially ventrally and around the eyes, evidently with different functions. One interesting arrangement, known in both mid-water squid and myctophids, makes use of a special photophore positioned so as to shine on the eye or on a special photoreceptor. Its intensity parallels that of the other photophores, so it provides information to the animal concerning its own brightness, thus allowing it to match the intensity of its own counterillumination to that of the down-welling ambient light. Another clear case of functional use is in *Neoscopelus*; in addition to the many photophores on the skin, they also occur on the tongue, allowing it to attract prey to just the right location.

Sexual dimorphism is also frequent in luminescent fish. The appropriately named anglerfishes, with their dangling luminous lures, are the most extreme in this respect (Pietsch, 2009). But males and females of the myctophid, *Tarleltonbeania* are also very different and were originally thought to be different species. Only one (now known to be the male) has caudal luminous organs and the occurrence of those fish was only known from stomach contents of predator fishes; what turns out to be the female was captured in nets, but never in the company of the male. A proposed explanation is that when a predator attacks, the males dart off in all directions with their dorsal lights flashing, like a police car, leading the predators on a chase (and sometimes getting caught), leaving the females, who remain in place, safe from the predator in the cover of darkness, but easy to catch in a net.

XI. APPLICATIONS OF BIOLUMINESCENCE

In the recent past, the most frequently asked question about bioluminescence was "What is its function, its survival value for the organism?" Bioluminescence was thus viewed mostly as a fascinating feature of the living world, but the study of its physiological and biochemical basis had seemed a most unlikely area of research to contribute in any practical way. It was put in the category of basic research; knowledge for the sake of knowledge: curiosity driven studies, with no predictable applications. Such interests have not faded but, in more recent years, an equally frequent query has concerned the practical applications of research on bioluminescence, reflecting, to be sure, an awareness of the many ways in which science has enabled new advances over the past decades. Thus, speculative paragraphs in grant applications have turned into reality, largely based on advances in molecular biology. Practical applications, both achieved and in progress, have been mind-boggling, rivaling in that respect many other practical developments in biological sciences, ranging from vaccines and test tube babies to drugs, genetic engineering and stem cells.

Actually, analytical applications of bioluminescence have been in use for 50 years. With the discovery of the ATP requirement for light emission in fireflies and the fact that the amount of light is directly proportional to the amount of ATP, many uses emerged. Somewhat later, the isolation of aequorin opened the way for the detection of calcium. Those, and other such measurements of bioluminescence have at least three major advantages over others: (1) rapidity; only a few seconds or minutes are needed; (2) great sensitivity; amounts of substances a billion or more times less than conventional assays can be readily detected; and (3) proportionality over an enormous concentration range; many such assays can be made over a range of one million or more.

The use of firefly luciferase with luciferin added was quickly adopted for the measurement of the amount of ATP in cell and biochemical research. An application with a wider impact was its use in the slaughterhouse, where undetected fecal contamination of animal carcasses has led to sickness and even death from human consumption of the meat products. Detection of bacteria responsible (usually *E. coli*) was previously done by taking swabs and checking for growth on plates, which takes 24 hours or more; by that time, processing may be complete and the contaminated product on its way to consumers, expensive and hard to track and recall. While the firefly assay is ideal for rapid and sensitive detection of bacteria, such procedures may have a problem; in practice, not all carcasses are sampled so contaminated ones may readily get through, as is known from the fact that contaminated meat continues to be reported from time to time.

The same ATP test is now used for monitoring soft drink production, where mold contamination occurs rarely but unpredictably; all batches are tested, as may be readily done. If discovered only after bottling and distribution to outlets far and wide, it is not only difficult and costly to recall it, the brand may get a poor reputation.

For many years the firefly luciferase used in the ATP tests was purified from fireflies, usually collected by

children paid by the number. With the amounts now used this would be impractical or impossible, so recombinant luciferase is used. Today, the greatest demand may be for a new method for rapid determinations of nucleotide sequences of DNA called "pyro" sequencing (Metzker, 2005). The name is based on the fact that pyrophosphate is released in the nucleotide-determination step which, after being converted to ATP, produces a flash of light. With automation about 500 million base pairs can be determined per 10 hour run on a machine.

Concern with water contamination, especially from industry, led to the passage of the "Clean Rivers Act" and to the development of a test to determine the quality of water in rivers and streams. The problem is different from the earlier examples in that the typical contaminants are chemical substances, not living organisms, and different substances in different cases. The method first adopted was empirical; if a fish survived in the water in question for 5 days, the water was judged satisfactory. So a 5-day-long procedure for such an evaluation was developed, typically by sampling downstream from an industrial facility that discharged its waste water. Mobile laboratories, fully equipped with healthy fish in a tank and scientific personnel carried out the determination, traveled week after week from site to site. A team could check only about 50 sites in a year, and it was not cheap!

A curious scientist noted that the light emission from living luminous bacteria was decreased by many different foreign chemical substances and wondered if the light emission might be a proxy for fish survival. The results were positive and the test is now widely used for the determination of water quality both in the USA and many other countries. The success of the method is astonishing and still viewed with some caution; how can it be that the light emission of living bacteria is affected in the same way as a fish by what must be a wide diversity of (and unknown) chemical substances? But it does work!

As described, one of the features of different bioluminescent systems is that they are biochemically different. This means that many different substances can be determined with one luciferase or another, and many such assays have been established. One of the most significant and widely used in research is the jellyfish system, mentioned in the Introduction, where light emission from aequorin requires calcium ion, a substance of key importance in the physiology and regulation of many different processes in living cells, notably muscle and nerve. With the isolation of the jellyfish luciferase gene, the DNA can be inserted directly into individual cells which, with added coelenterazine, produce aequorin and emit light in the presence of calcium in the cytoplasm.

DNA that codes for a luciferase can be attached to the promoter of some target gene, thus serving as a reporter gene for one responsible for the production of some other substance, so when and where the latter is produced can be determined by light emission, all in a non-invasive way — one has only to observe. The expression of a specific gene can be tracked by time, whether it occurs during the day or the night phase, as in circadian control, or time during development. Similarly, the type of cell and location in the body where a specific gene is expressed can be established. Studies are now being carried out by many scientists to locate cancer cells in the body using such methods, with good preliminary results. Another feature: since different luciferase systems may emit light at different wavelengths, different genes can be tagged by different luciferases and their activities followed concurrently in the same cell.

Green fluorescent protein (GFP) is a remarkable and now widely used fluorescent protein discovered in the course of studies of bioluminescence (Chalfie et al., 2006; Zimmer, 2010); in addition to the fact that it is non-toxic (based on perhaps some 10 000 published studies), it has three other important features. First, like luciferases and some other genes, it can be used as a reporter by attaching the gene coding for its synthesis to a different promoter; second, the fluorophore is part of the primary sequence of the peptide chain, so does not dissociate even at very low concentrations; and mutant GFPs, in which the color of the fluorescence has been altered by virtue of protein conformation changes, have greatly expanded its applications (Baird et al., 2000; Zhang et al., 2002). A drawback is that, like all fluorescent markers, irradiation is required, which itself may have adverse effects on the cell and will always increase the background. But this has not interfered with its widespread use and is now perhaps the most important and widely used of all biological reagents in cell biology; its discovery and application were recognized by the award of a Nobel Prize in 2008 (Chalfie, 2009; Shimomura, 2009; Tsien, 2009).

XII. CONCLUDING REMARKS

Though relatively rare, the emission of visible light by living organisms occurs in a phylogenetically wide range of species, ranging from bacteria to vertebrates, and has many independent evolutionary origins. The structures of the genes and proteins, as well as the physiological, biochemical and regulatory mechanisms involved, are thus very different. Its functions are also many and diverse, and provide a selective advantage mediated by the detection and responses of other organisms to the light.

The functions of the light may be classed under three major headings: offense, defense and communication, and a fourth to enhance propagation. Light may be used defensively to startle or frighten (flashes), to divert predators, as a decoy or to provide camouflage. Offensively, light may be used as a lure to attract prey. Communication occurs in courtship and mating displays.

An unusual and unexplained fact is that bioluminescence is primarily a marine phenomenon. While there are terrestrial forms, it is virtually absent in fresh water; only one such species is known. It is also not confined to or especially prevalent in animals that live in complete darkness (caves, lakes and the deep ocean).

Bioluminescence is an enzymatically-catalyzed chemiluminescence, a chemical reaction that emits light. The enzymes involved are all referred to generically as luciferases, somewhat unfortunately, because they are many that are structurally different. The genes coding for several of the different luciferases have been cloned and sequenced, confirming that they possess no similar regions in common. The substrates, generically called luciferins, react with molecular oxygen to form intermediate luciferase-bound peroxides, which break down to give a product in an excited state, which subsequently emits light. Both terms should be coupled with the name of the organism or group where they occur, thus beetle luciferin or bacterial luciferase.

In the marine environment, luminous bacteria are ubiquitous as planktonic forms in sea water and they are also responsible for the light emission of many species of higher organisms by serving as symbionts. They are not common terrestrially, but do occur as symbionts in soil nematodes, as an agent in the nematode's parasitization of insects. All species utilize the same biochemical system, a shunt of the electron transport pathway, in which reduced flavin and aldehyde are oxidized by molecular oxygen to give a luciferase-bound flavin intermediate in an excited state. Luminous bacteria are versatile with respect to the alternate uses of light emission under different situations, the exploitation of alternate habitats and the capacity to turn the synthesis of the system on and off, regulated by quorum sensing and autoinducers.

Dinoflagellates are unicellular algae; in the ocean these organisms are largely responsible for the sometimes brilliant sparkling "phosphorescence" seen at night when the water is disturbed and also for "red tides". Their luminescent flashing originates from novel cellular organelles called scintillons, formed as spherical outpocketings of the cytoplasm into the vacuole. They contain dinoflagellate luciferase and luciferin (a novel reduced linear tetrapyrrole), the latter bound to a second protein. Flashing is triggered by an action potential in the vacuolar membrane that causes a transient pH change in the scintillon, activating the luciferase and releasing the luciferin from its binding protein. Luminescence in some dinoflagellates is controlled by a cellular circadian biological clock, which causes the synthesis and destruction of the components in some species to occur on a daily cycle.

There are many luminous coelenterates, such as comb jellies, hydroids, siphonophores, sea pens and jellyfish. Upon stimulation, many species emit brief bright flashes, or trains of flashes, triggered by conducted action potentials that facilitate Ca^{2+} entry to specialized photocytes. The reaction of coelenterate luciferase and luciferin (coelenterazine) with oxygen forms a stable enzyme peroxide intermediate called aequorin that requires Ca^{2+} for the completion of the reaction. In many species, an accessory protein, green fluorescent protein (GFP) is the light emitter. The luciferase is homologous with calmodulin.

Fireflies also emit light as flashes, which they use as species-specific signals for communication in courtship. The light organ is a complex structure with photocytes arranged in a rosette pattern, invested with tracheoles that transport the required molecular oxygen directly to the cells. Indeed, while oxygen triggers flashing, a nerve impulse initiates the process. The firefly reaction is unique in having a requirement for ATP, which serves to "activate" the luciferin (a benzothiazole). The luciferyl adenylate is thus the "true" substrate that reacts with oxygen, forming an intermediate luciferase-bound cyclic peroxide whose breakdown results in light emission. Firefly luciferase is homologous with long chain acyl-CoA synthetase.

Other major luminous groups include the molluscs (snails, clams, squid), annelid worms (both marine and terrestrial), crustacea (shrimp and ostracods), echinoderms (brittle stars, starfish, sea cucumbers) and fish, both cartilaginous (sharks) and teleost (bony fishes). Of all the groups, fish and squids have the greatest variety of luminous systems; some make use of symbiotic luminous bacteria as a source of light while others are self-luminous. Luminous organisms are most abundant at mid-water depths (500–1000 m) in the open ocean.

BIBLIOGRAPHY

Abrahams, M. V., & Townsend, L. D. (1993). Bioluminescence in dinoflagellates: a test of the burglar alarm hypothesis. *Ecology, 74*, 258–260.

Aprille, J. R., Lagace, C. J., Modica-Napolitano, J., & Trimmer, B. A. (2004). Role of nitric oxide and mitochondria in control of firefly flash. *Integr Comp Biol, 44*, 213–219.

Baird, G. S., Zacharias, D. A., & Tsien, R. Y. (2000). Biochemistry, mutagenesis, and oligomerization of DsRed, a red fluorescent protein from coral. *Proc Natl Acad Sci USA, 97*, 11984–11989.

Baldwin, T. O., & Ziegler, M. M. (1992). The biochemistry and molecular biology of bacterial luminescence. In F. Müller (Ed.), *Chemistry and Biochemistry of Flavoenzymes, Vol. 3* (pp. 467–530). Boca Raton: CRC Press.

Blinks, J. R., Wier, W. G., Hess, P., & Prendergast, F. G. (1982). Measurement of Ca^{2+} concentrations in living cells. *Prog Biophys Molec Biol, 40*, 1–114.

Branchini, B. R., Ablamsky, D. M., Rosenman, J. M., Uzasci, L., Southworth, T. L., & Zimmer, M. (2007). Synergistic mutations produce blue-shifted bioluminescence in firefly luciferase. *Biochemistry, 46*, 13847–13855.

Buck, J. (1988). Synchronous rhythmic flashing of fireflies II. *Quart Rev Biol, 63*, 265–289.

Campbell, A. K. (1988). *Chemiluminescence: Principles and Applications in Biology and Medicine*. VCH, Chichester and Weinheim.

Campbell, Z. T., Weichsel, A., Montfort, W. R., & Baldwin, T. O. (2009). Crystal structure of the bacterial luciferase/flavin complex provides insight into the function of the beta subunit. *Biochemistry, 48*, 6085–6094.

Case, J. (1984). Firefly behavior and vision. In T. Lewis (Ed.), *Insect Communication* (pp. 195–222). London: Harcourt, Brace, Jovanovich.

Chalfie, M. (2009). GFP: lighting up life (Nobel Lecture). *Angew Chem Int Ed, 48*, 5603–5611.

Chalfie, M., & Kain, S. R. (Eds.), (2006). *Green Fluorescent Protein: Properties, Applications, and Protocols*. Hoboken: Wiley-Interscience.

Charbonneau, H., Walsh, K. A., McCann, R. O., Prendergast, F. G., Cormier, M. J., & Vanaman, T. C. (1985). Amino-acid sequence of the calcium-dependent photoprotein Aequorin. *Biochemistry, 24*, 6762–6771.

Chun, C. K., Troll, J. V., Koroleva, I., et al. (2008). Effects of colonization, luminescence, and autoinducer on host transcription during development of the squid-vibrio association. *Proc Natl Acad Sci USA, 105*, 11323–11328.

Cody, C. W., Prasher, D. C., Westler, W. M., Prendergast, F. G., & Ward, W. W. (1993). Chemical structure of the hexapeptide chromophore of the *Aequorea* green-fluorescent protein. *Biochemistry, 32*, 1212–1218.

Conti, E., Franks, N. P., & Brick, P. (1996). Crystal structure of firefly luciferase throws light on a superfamily of adenylate-forming enzymes. *Structure, 4*, 287–298.

Cormier, M. J. (1981). *Renilla* and *Aequorea* bioluminescence. In M. DeLuca, & W. D. McElroy (Eds.), *Bioluminescence and Chemiluminescence* (pp. 225–233). New York: Academic Press.

Cormier, M. J., Prasher, D. C., Longiaru, M., & McCann, R. O. (1989). The enzymology and molecular biology of the Ca^{2+}-activated photoprotein, aequorin. *Photochem Photobiol, 49*, 509–512.

Desjardin, D. E., Oliveira, A. G., & Stevani, C. V. (2008). Fungi bioluminescence revisited. *Photochem Photobiol Sci, 7*, 170–182.

Desjardin, D. E., Perry, B. A., Lodge, D. J., Stevani, C. V., & Nagasawa, E. (2010). Luminescent Mycena: new and noteworthy species. *Mycologia, 102*, 459–477.

Eberhard, A., Burlingame, A. L., Eberhard, C., Kenyon, G. L., Nealson, K. H., & Oppenheimer, N. J. (1981). Structural identification of autoinducer of *Photobacterium fischeri* luciferase. *Biochemistry, 20*, 2444–2449.

Eckert, R. (1965). Bioelectric control of bioluminescence in the dinoflagellate *Noctiluca*. *Science, 147*, 1140–1145.

Eckstein, J. W., Cho, K. W., Colepicolo, P., Ghisla, S., Hastings, J. W., & Wilson, T. (1990). A time-dependent bacterial bioluminescence emission spectrum in an in vitro single turnover system: energy transfer alone cannot account for the yellow emission of *Vibrio fischeri* Y-1. *Proc Natl Acad Sci USA, 87*, 1466–1470.

Fisher, A. J., Thompson, T. B., Thoden, J. B., Baldwin, T. O., & Rayment, I. (1996). The 1.5-angstrom resolution crystal structure of bacterial luciferase in low salt conditions. *J Biol Chem, 271*, 21956–21968.

Fogel, M., & Hastings, J. W. (1972). Bioluminescence: mechanism and mode of control of scintillon activity. *Proc Natl Acad Sci USA, 69*, 690–693.

Fraga, H. (2008). Firefly luminescence: a historical perspective and recent developments. *Photochem Photobiol Sci, 7*, 146–158.

Fritz, L., Morse, D., & Hastings, J. W. (1990). The circadian bioluminescence rhythm of *Gonyaulax* is related to daily variations in the number of light emitting organelles. *J Cell Sci, 95*, 321–328.

Fuqua, C., & Greenberg, E. P. (2002). Listening in on bacteria: Acyl-homoserine lactone signalling. *Nat Rev Mol Cell Biol, 3*, 685–695.

Gambello, M. J., & Iglewski, B. H. (1991). Cloning and characterization of the *Pseudomonas aeruginosa* lasR gene, a transcriptional activator of elastase expression. *J Bacteriol, 173*, 3000–3009.

Ghiradella, H., & Schmidt, J. T. (2004). Fireflies at one hundred plus: a new look at flash control. *Integr Comp Biol, 44*, 203–212.

Grober, M. S. (1988). Brittle-star bioluminescence functions as an aposematic signal to deter crustacean predators. *Anim Behav, 36*, 493–501.

Haddock, S. H. D., Moline, M. A., & Case, J. F. (2010). Bioluminescence in the sea. *Annu Rev Mar Sci, 2*, 293–343.

Haddock, S. H. D., Rivers, T. J., & Robison, B. H. (2001). Can coelenterates make coelenterazine? Dietary requirement for luciferin in cnidarian bioluminescence. *Proc Natl Acad Sci USA, 98*, 11148–11152.

Harvey, E. N. (1952). *Bioluminescence*. New York: Academic Press.

Hastings, J. W. (1983). Biological diversity, chemical mechanisms and evolutionary origins of bioluminescent systems. *J Mol Evol, 19*, 309–321.

Hastings, J. W. (2007). The Gonyaulax clock at 50: translational control of circadian expression. *Cold Spring Harb Symp Quant Biol, 72*, 141–144.

Hastings, J. W. (2011). Progress and perspectives on bioluminescence: from luminous organisms to molecular mechanisms. In A. Roda (Ed.), *Analytical Chemiluminescence and Bioluminescence: Past, Present, and Future* (pp. 91–112). Cambridge: Royal Society of Chemistry.

Hastings, J. W., & Morin, J. G. (1991). Bioluminescence. In C. L. Prosser (Ed.), *Neural and Integrative Animal Physiology* (pp. 131–170). New York: Wiley Interscience.

Hastings, J. W., Makemson, J., & Dunlap, P. V. (1987). How are growth and luminescence regulated independently in exosymbionts? *Symbiosis, 4*, 3–24.

Hastings, J. W., Potrikus, C. J., Gupta, S., Kurfurst, M., & Makemson, J. C. (1985). Biochemistry and physiology of bioluminescent bacteria. *Adv Microb Physiol, 26*, 235–291.

Head, J. F., Inouye, S., Teranishi, K., & Simomora, O. (2000). The crystal structure of the phosphoprotein aequorin at 2.3 angstrom resolution. *Nature, 405*, 372–376.

Henry, J.-P., Monny, C., & Michelson, A. M. (1975). Characterization and properties of Pholas luciferase as a metalloglycoprotein. *Biochemistry, 14*, 3458–3466.

Herring, P. J. (1982). Luminescence in fishes. *J Oceanogr Mar Biol, 20*, 415–470.

Herring, P. J. (1985a). Review of deep-sea luminescence. In M. S. Laverack (Ed.), *Physiological Adaptations in Marine Animals* (pp. 323–350). Cambridge: Society of Experimental Biology.

Herring, P. J. (1985b). How to survive in the dark: bioluminescence in the deep sea. In M. S. Laverack (Ed.), *Physiological Adaptations in Marine Animals* (pp. 323–350). Cambridge: Society of Experimental Biology.

Herring, P. J. (1987). Systematic distribution of bioluminescence in living organisms. *J Biolum Chemilum, 1*, 147–163.

Herring, P. J. (1990). Bioluminescent communication in the sea. In P. J. Herring, A. K. Campbell, M. Whitfield, & L. Maddock (Eds.), *Light and Life in the Sea* (pp. 245–264). Cambridge: Cambridge University Press.

Herring, P. J. (Ed.), (1978). *Bioluminescence in Action*. New York: Academic Press.

Johnsen, S., Balser, E. J., & Widder, E. A. (1999). Light-emitting suckers in an octopus. *Nature, 398*, 113–114.

Johnson, F. H., Shimomura, O., Saiga, Y., Gershman, G., Reynolds, G. T., & Waters, J. R. (1962). Quantum efficiency of *Cypridina* luminescence with a note on that of *Aequorea*. *J Cell Comp Physiol, 60*, 85–103.

Johnson, C. H., Egli, M., & Stewart, P. L. (2008). Structural insights into a circadian oscillator. *Science, 322*, 697–701.

Johnson, C. H., Inoue, S., Flint, A., & Hastings, J. W. (1985). Compartmentalization of algal bioluminescence: autofluorescence of bioluminescent particles in the dinoflagellate *Gonyaulax* as studied with image-intensified video microscopy and flow cytometry. *J Cell Biol, 100*, 1435–1446.

Li, L., Hong, R., & Hastings, J. W. (1997). Three functional luciferase domains in a single polypeptide chain. *Proc Natl Acad Sci USA, 94*, 8954–8958.

Li, L., Liu, L., Hong, R., Robertson, D., & Hastings, J. W. (2001). N-terminal intramolecularly conserved histidines of three domains in *Gonylaulax* luciferase are responsible for loss of activity in the alkaline region. *Biochemistry, 40*, 1844–1849.

Li, L., Liu, X., Yang, W., Xu, F., et al. (2008). Crystal structure of long-chain alkane monooxygenase (LadA) in complex with coenzyme FMN: unveiling the long-chain alkane hydroxylase. *J Mol Biol, 376*, 453–465.

Liu, Z. J., Vysotski, E. S., Chen, C. J., Rose, J. P., Lee, J., & Wang, B. C. (2000). Structure of the Ca^{2+}-regulated photoprotein obelin at 1.7 angstrom resolution determined directly from its sulfur substructure. *Protein Sci, 9*, 2085–2093.

Lloyd, J. E. (1977). Bioluminescence and communication. In T. A. Sebeok (Ed.), *How Animals Communicate* (pp. 164–183). Bloomington: Indiana University Press.

Lloyd, J. E. (1980). Firefly signal mimicry. *Science, 210*, 669–671.

Lorenz, W. W., McCann, R. O., Longiaru, M., & Cormier, M. J. (1991). Isolation and expression of a cDNA encoding *Renilla reniformis* luciferase. *Proc Natl Acad Sc. USA, 88*, 4438–4442.

Loros, J. J., & Dunlap, J. C. (2001). Genetic and molecular analysis of circadian rhythms in *Neurospora*. *Annu Rev Physiol, 63*, 757–794.

McElroy, W. D. (1947). The energy source for bioluminescence in an isolated system. *Proc Natl Acad Sci USA, 33*, 342–345.

McElroy, W. D., & Hastings, J. W. (1956). Initiation and control of firefly luminescence. In C. L. Prosser (Ed.), *Physiological Triggers* (pp. 80–84). Ronald Press.

McFall-Ngai, M., & Morin, J. G. (1991). Camouflage by disruptive illumination in Leiognathids, a family of shallow-water, bioluminescent fishes. *J Exp Biol, 156*, 119–137.

Mehra, A., Baker, C. L., Loros, J. J., & Dunlap, J. C. (2009). Post-translational modifications in circadian rhythms. *Trends Biochem Sci, 34*, 483–490.

Meighen, E. A. (1991). Molecular biology of bacterial bioluminescence. *Microbiol Rev, 55*, 123–142.

Metzker, M. L. (2005). Emerging technologies in DNA sequencing. *Genome Res, 15*, 1767–1776.

Miller, S. D., Haddock, S. H. D., Elvidge, C. D., & Lee, T. F. (2005). Detection of a bioluminescent milky sea from space. *Proc Natl Acad Sci USA, 102*, 14181–14184.

Morin, J. G., & Hastings, J. W. (1971). Biochemistry of the bioluminescence of colonial hydroids and other coelenterates. *J Cell Physiol, 77*, 303–312.

Morin, J. G. (1983). Coastal bioluminescence: patterns and functions. *Bull Mar Sci, 33*, 787–817.

Morin, J. G., & Cohen, A. C. (1991). Bioluminescent displays, courtship, and reproduction in ostracodes. In R. Bauer, & J. Martin (Eds.), *Crustacean Sexual Biology* (pp. 1–16). New York: Columbia University Press.

Morin, J. G., & Cohen, A. C. (2010). It's all about sex: bioluminescent courtship displays, morphological variation and sexual selection in two new genera of caribbean ostracodes. *J Crustac Biol, 30*, 56–67.

Morse, D., Fritz, L., & Hastings, J. W. (1990). What is the clock? Translational regulation of circadian bioluminescence. *Trends Biochem, 15*, 262–265.

Nakamura, H., Kishi, Y., Shimomura, O., Morse, D., & Hastings, J. W. (1989). Structure of dinoflagellate luciferin and its enzymatic and non-enzymatic air-oxidation products. *J Am Chem Soc, 111*, 7607–7611.

Nealson, K., & Hastings, J. W. (1991). The luminous bacteria. In A. Balows, H. G. Trüper, M. Dworkin, W. Harder, & K. H. Schleifer (Eds.), *The Prokaryotes* (2nd ed.). (pp. 625–639) New York: Springer-Verlag, Vol. I, Part 2, Ch. 25.

Nealson, K. H., & Hastings, J. W. (2006). Quorum sensing on a global scale: massive numbers of bioluminescent bacteria make milky seas. *Appl Environ Microbiol, 72*, 2295–2297.

Nealson, K. H., Platt, T., & Hastings, J. W. (1970). Cellular control of the synthesis and activity of the bacterial luminescent system. *J Bacteriol, 104*, 313–322.

Ng, W. L., & Bassler, B. L. (2009). Bacterial quorum-sensing network architectures. *Annu Rev Genet, 43*, 197–222.

Nicolas, M.-T., Nicolas, G., Johnson, C. H., Bassot, J.-M., & Hastings, J. W. (1987). Characterization of the bioluminescent organelles in *Gonyaulax polyedra* (dinoflagellates) after fast-freeze fixation and antiluciferase immunogold staining. *J Cell Biol, 105*, 723–735.

Ormö, M., Cubitt, A. B., Kallio, K., Gross, L. A., Tsien, R. Y., & Remington, S. J. (1996). Crystal structure of the *Aequorea victoria* green fluorescent protein. *Science, 273*, 1392–1395.

Ow, D. W., Wood, K. V., DeLuca, M., deWet, J. R., Helinski, D. R., & Howell, S. H. (1986). Transient and stable expression of the firefly luciferase gene in plant cells and transgenic plants. *Science, 234*, 856–859.

Parsek, M. R., & Greenberg, E. P. (2005). Sociomicrobiology: the connections between quorum sensing and biofilms. *Trends Microbiol, 13*, 27–33.

Pietsch, T. W. (2009). *Oceanic Anglerfishes*. Berkeley: University of California Press.

Qin, X. M., Byrne, M., & Mori, T. (2010). Intermolecular associations determine the dynamics of the circadian KaiABC oscillator. *Proc Natl Acad Sci USA, 107*, 14805–14810.

Schaefer, A. L., Greenberg, E. P., Oliver, C. M., et al. (2008). A new class of homoserine lactone quorum-sensing signals. *Nature, 454*, 595–599.

Schultz, L. W., Liu, L., Cegielski, M., & Hastings, J. W. (2005). Crystal structure of a pH-regulated luciferase catalyzing the bioluminescent oxidation of an open tetrapyrrole. *Proc Natl Acad Sci USA, 102*, 1378–1383.

Shimomura, O. (2006). *Bioluminescence: Chemical Principles and Methods*. Singapore: World Scientific Publishing Co.

Shimomura, O. (2009). Discovery of green fluorescent protein (GFP) (Nobel Lecture). *Angew Chem Int Ed, 48*, 5590–5602.

Shimomura, O., Johnson, F. H., & Saiga, Y. (1962). Extraction, purification and properties of aequorin, a bioluminescent protein from the luminous hydromedusan, *Aequorea. J Cell Comp Physiol, 59*, 223–240.

Smith, D. S. (1963). Organization and innervation of luminescent organ in a firefly, Photuris Pennsylvanica (Coleoptera). *J Cell Biol, 16*, 323.

Smith, S. M. E., Morgan, D., Musset, B., Cherny, V. V., Place, A. R., Hastings, J. W., & DeCoursey, T. E. (2011). A Voltage-Gated Proton Channel In A Dinoflagellate. *Proc Natl Acad Sci USA, 105*, (in press).

Timmins, G. S., Robb, F. J., Wilmot, C. M., Jackson, S. K., & Swartz, H. M. (2001). Firefly flashing is controlled by gating oxygen to light-emitting cells. *J Exp Biol, 204*, 2795–2801.

Trimmer, B. A., Aprille, J. R., Dudzinski, D. M., et al. (2001). Nitric oxide and the control of firefly flashing. *Science, 292*, 2486–2488.

Tsien, R. Y. (2009). Constructing and exploiting the fluorescent protein paintbox (Nobel Lecture). *Angew Chem Int Ed, 48*, 5612–5626.

Viviani, V. R. (2009). Terrestrial bioluminescence. In K. C. Smith (Ed.), *Photobiological Sciences Online*. Washington, DC: American Society for Photobiology.

Viviani, V. R., Arnoldi, F. G. C., Venkatesh, B., et al. (2006). Active-site properties of Phrixotrix railroad worm green and red bioluminescence-eliciting luciferases. *J Biochem, 140*, 467–474.

Viviani, V. R., Hastings, J. W., & Wilson, T. (2002). Two bioluminescent diptera: the North American *Orfelia fultoni* and the Australian *Arachnocampa flava*. Similar niche, different bioluminescence systems. *Photochem Photobiol, 75*, 22–27.

Wampler, J. E. (1981). Earthworm bioluminescence. In M. A. Deluca, & W. D. McElroy (Eds.), *Bioluminescence and Chemiluminescence* (pp. 249–256). New York: Academic Press.

Wilson, T. (1985). Mechanism of chemiluminescence. In A. Frimer (Ed.), *Singlet Oxygen*, Vol. 2 (pp. 37–57). Boca Raton: CRC.

Wilson, T., & Hastings, J. W. (1998). Bioluminescence. *Annu Rev Cell Dev Biol, 14*, 197–230.

Wood, K. W., Lam, A. Y., Seliger, H. H., & McElroy, W. D. (1989). Complementary DNA coding click beetle luciferases can elicit bioluminescence of different colors. *Science, 244*, 700–702.

Yang, F., Moss, L. G., & Phillips, G. N. (1996). The molecular structure of green fluorescent protein. *Nat Biotechnol, 14*, 1246–1251.

Young, R.E. and Bennett, T.M. (1988). *Cephalopod luminescence*. In M.R. Clarke and E.R. Trueman, (Eds.), The Mollusca, (pp. 241–251). San Diego, CA: Academic Press.

Zhang, J., Campbell, R. E., Ting, A., & Tsien, R. Y. (2002). Creating new fluorescent probes for cell biology. *Nat Rev Mol Biol 3*, 906–918.

Zimmer, M. (2010). Green fluorescent protein: a molecular microscope. In K. C. Smith (Ed.), *Photobiological Sciences Online*. Washington, DC: American Society for Photobiology.

I. EXCITABILITY OF SMOOTH MUSCLES: SOME BASIC FACTS

This Appendix exclusively covers some of the research on smooth muscles by Sperelakis and his outstanding colleagues. This research began with his MS and PhD theses, with the first publications in 1956 and 1958. There are a large number of publications in high-quality refereed journals, with a large number of postdoctoral trainees over several decades. This Appendix should give the reader a firm grasp of many of the fundamentals of the electrical properties of smooth muscles.

IA. Fast Na^+ Channels in Smooth Muscle Cells

Smooth muscle cells are usually thought not to possess *fast Na^+ ion channels*. Instead, the inward depolarizing current for the APs usually is carried by Ca^{2+} ions. However, in some smooth muscle cells, a fast Na^+ current can be demonstrated. In at least one case (pregnant rat uterus), this fast Na^+ current likely plays an important functional role. Three examples of smooth muscle cells in which fast Na^+ current has been demonstrated will be presented here.

The first case is the *pregnant rat uterus*. Inoue and Sperelakis (1991) found that fast Na^+ channels begin to appear in the uterine smooth muscle cells during the *second half of pregnancy* (term is 22 days). The greatest *Na^+ current density*, using whole-cell voltage clamp of isolated single cells, was attained just before delivery (Sperelakis et al., 1992). The Na^+ current density at that time was about equal to, or greater than, the inward Ca^{2+} current. The *Ca^{2+} current density* also increased during the latter part of pregnancy, but the changes were not as pronounced as that for the Na^+ channels (Inoue and Sperelakis, 1991). These investigators concluded that the gain of fast Na^+ channels during pregnancy plays a critical role in insuring *fast propagation* of the APs over the entire uterus to enable simultaneous contraction of the organ to expel the fetus. It was found that protein kinase C stimulates the Ca^{2+} current in the rat myometrial cells during pregnancy (Shimamura et al., 1994).

The second case is the *leiomyosarcoma cell*. This cultured cell line, which is commercially available, was derived from a single fibroid tumor cell in the human uterus. Thus, these cells are derived from uterine smooth muscle cells. Kusaka and Sperelakis (1994a,b), using whole-cell voltage clamp of isolated single cells, found that most of the cells had a substantial fast Na^+ current that was tetrodotoxin (TTX)-sensitive. By varying the amount of serum used in the culture medium, they showed that the current density observed was a function of the amount of serum (Kusaka and Sperelakis, 1994b). Hence, they concluded that some unknown substance in the serum induced fast Na^+ channels. One relevant question is whether these channels play a role in the metastasis of the leiomyosarcoma cells to other sites.

The third case is the *intestinal smooth muscle* cells of the rat colon. Xiong and Sperelakis (1995), using whole-cell voltage clamp of single smooth muscle cells isolated from the ascending colon, found that a substantial fraction of the cells examined had a fast Na^+ current that was TTX-sensitive (Xiong et al., 1993). The amplitude of this inward current was dependent on Na^+ ion concentration of the bathing solution and was not affected by the Ca^{2+} ion concentration. Other portions of the colon had a lower incidence of such cells. It seems likely that the fast current plays a role in non-decremental propagation of the APs and increases the velocity of propagation. Their paper appears to be the first report of fast Na^+ current in intestinal smooth muscle cells.

II. PROPAGATION OF OVERSHOOTING ACTION POTENTIALS IN INTESTINAL SMOOTH MUSCLE

It was observed many years ago that the circular muscle layer of the cat small intestine (ileum) propagates action potentials (APs) at a velocity of about 3–5 cm/s (Prosser and Sperelakis, 1956). These studies were done on isolated rings of circular muscle mounted on a glass rod and suspended in a warm (37°C), moist chamber and using several pairs of recording electrodes and one pair of stimulating electrodes. The propagating APs in the stimulated ring were demonstrated to excite a quiescent adjacent ring when the two rings were pushed into contact for only a few millimeters. This

means that the action currents accompanying the propagating APs were of sufficient intensity to stimulate the quiescent ring. Subsequently, intracellular microelectrode recordings were made (Sperelakis and Prosser, 1958). The average *resting potential* (in good impalements) was about −55 mV and the *maximum rate of rise* of the AP (max *dV/dt*) was usually about 5–6 V/s. The *overshoot* of the AP was to about +5 mV. The *duration of the AP*, measured at 50% amplitude (APD_{50}), was about 30 ms.

However, in many smooth muscle cells, the APs were *undershooting* and small in amplitude. The undershoot is to various degrees. To explain these findings, it was suggested that the *delayed rectifier K^+ conductance* (see Chapter 19) turned on unusually fast in those cells, thus terminating the AP very quickly and causing the undershoot. Evidence for this hypothesis was based on the fact that any agent that slowed and depressed the delayed rectifier K^+ conductance caused the undershooting APs to become overshooting. Such agents include Ba^{2+} ions (ca 0.5 mM), TEA^+ (tetraethylammonium ion) (ca 5 mM) and 5-aminopyridine. Since the usual carrier of the inward current for the AP is Ca^{2+} ion (Xiong et al., 1995a), *elevating the external Ca^{2+}* concentration also increased the amplitude of the APs. See previous section above for evidence that, in some cells, Na^+ ion is also involved in carrying the inward current. Changes in the current densities of the Ca^{2+} and K^+ channels occur during development and aging (Xiong et al., 1995b).

Because, under physiological conditions, many cells fire undershooting APs, the APs tend to *decrement in amplitude and velocity*, and hence die out after a certain distance travelled. This is called *decremental conduction*. Evidence for this could be observed in the ring experiments described in the first paragraph above. If decrement did not occur, then it would be expected that a given ring would continue firing APs once the ring was stimulated a single time. This would be true because the ring circumference was ca 3 cm and, at a propagation velocity of 3 cm/s, it would take ca 1.0 s for excitation to traverse the entire ring once. One second is much beyond the APS_{50} value of ca 30 ms and so the cells should be completely out of their refractory periods.

Intestinal smooth muscle cells, like cardiac muscle and skeletal muscle, possess *K_{ATP} ion channels* (Pluja et al., 1998). These K^+ channels are silent when intracellular ATP concentration is normal, but become active when the ATP concentration is reduced, as during ischemia. In the case of myocardial cells, these channels have been demonstrated to help protect the cells during a period of ischemia (by abbreviating the AP and thereby reducing the Ca^{2+} influx, thus conserving ATP).

III. VASCULAR SMOOTH MUSCLE: PART 1

Vascular smooth muscle (VSM) cells are present in the walls of arteries and veins and they regulate the diameter of the blood vessels by changes in their degree of sustained contraction and hence the peripheral resistance of the vasculature. The latter, in turn, determines the blood pressure, if cardiac output is constant. The degree of *sustained contraction* of the smooth muscle cells (SMCs), or *tonus*, is determined by the *Ca^{2+} influx* through the *slow, L-type Ca^{2+} ion channels*. The greater the Ca^{2+} influx, the greater the tonus, hence the smaller the diameter of the blood vessel. The autonomic innervations to the VSM cells affect their tonus.

In the heart musculature, *cyclic AMP* (cAMP) elevation intracellularly stimulates Ca^{2+} influx through the Ca^{2+} channels and *cGMP* elevation depresses the Ca^{2+} channels, hence influx (Sperelakis et al., 1993). In contrast, in VSM, both *cyclic nucleotides* act in the same direction, namely to depress the activity of the Ca^{2+} channels and hence Ca^{2+} influx (Ousterhout and Sperelakis, 1987; Sperelakis et al., 1993, 1994; Xiong et al., 1994; Xiong and Sperelakis, 1995; Liu et al., 1997a; Sunagawa et al., 1998). One example of inhibition by cAMP is given in Fig. A1. Thus, agents that inhibit the *phosphodiesterase-type 5* (PDE-5) enzyme present in VSM, such as Viagra, result in elevation of cGMP in the cells. This activates the *G-kinase* to a greater extent, which *phosphorylates* various proteins, one of which is the Ca^{2+} channel protein(s). This phosphorylation *inhibits* the channel activity, resulting in vasodilation (Sperelakis and Ohya, 1995). *Tyrosine kinase* is also involved in the regulation of the Ca_L channels of VSM (Liu et al, 1997b).

A number of agents, including some hormones, act via the Ca^{2+} channels to affect the degree of vasoconstriction. For, example, *angiotensin-II* (ang-II) stimulates the Ca^{2+} channels and thereby produces a potent vasoconstriction (Seki et al., 1999). More information about ang-II stimulation is presented in Part 2 below. Attachment to the *cytoskeleton via actin filaments* seems to be required for maximal activity of the Ca_L channels, because disruption of the actin filaments inhibits the Ca^{2+} current (Nakamura et al., 2000).

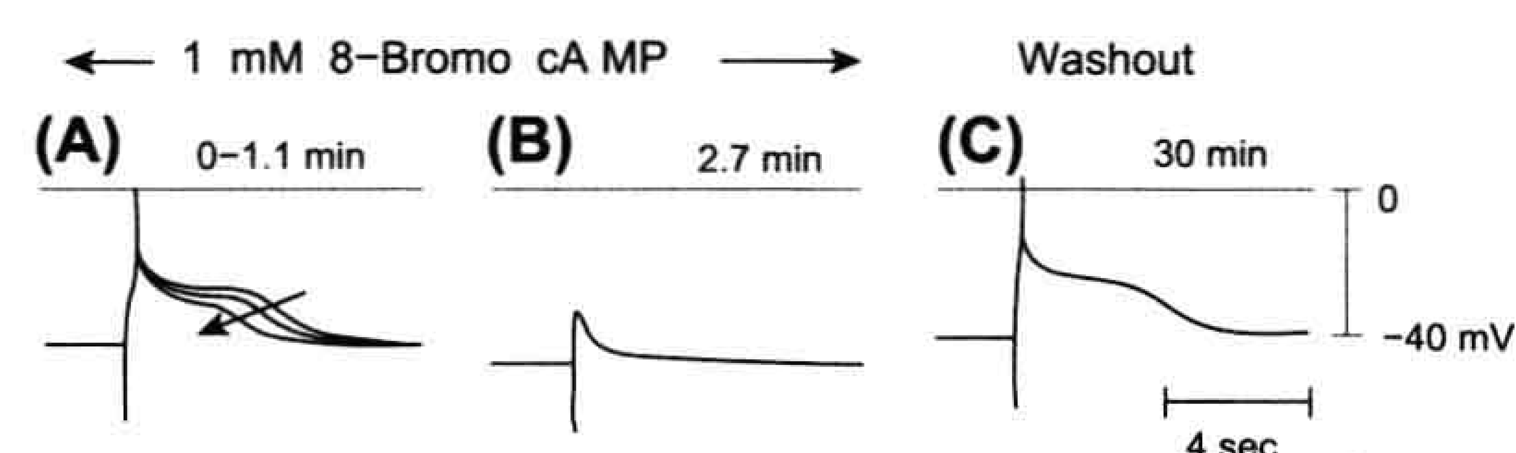


FIGURE A1 Depression and abolition of TEA-induced action potentials (APs) in cultured rat aortic cells by 8-bromo-cAMP (A–C). (A) Superimposed traces of a control AP (in 15 mM TEA) and depression of the AP within 1.1 min after addition of 1.0 mM 8-bromo-cAMP. (B) Abolition of the AP after 2.7 min. (C) Recovery of the AP upon washout for 30 min. (Records A–C were from the same cell.) The stimulation frequency was 0.04 Hz in both experiments. The time and voltage calibrations apply to all records. *(Adapted from Ousterhout and Sperelakis, 1987, with permission.)*

There are a number of types of ion channels in VSM. For example, as in intestinal SMCs stated above, the *K_{ATP} channel* has been demonstrated to be present in VSM cells (Yokoshiki et al., 1997a). The Ca^{2+} channels of VSM cells, as previously shown for myocardial cells, *require ATP to be bound* to them for activity, because it was shown that raising intracellular ATP concentration stimulates the Ca^{2+} current (Ohya and Sperelakis, 1989a,b; Yokoshiki et al., 1997b).

IV. VASCULAR SMOOTH MUSCLE: PART 2

IVA. Resting Potential vs $(K)_o$

When the RP was measured, in VSM cells of guinea pig superior mesenteric artery, as a function of the external K^+ concentration and plotted on a log scale, it was found that the average slope of the curve was 32 mV/decade and not the ca 60 mV/decade observed in myocardial cells or skeletal muscle fibers (Harder and Sperelakis, 1987) (Fig. A2). This means that the *P_{Na}/P_K ratio* (see Chapter 9), is relatively high, e.g. 0.1–0.2 (compared to values of about 0.01–0.05 observed in cardiac muscle and skeletal muscle). For example, a P_{Na}/P_K ratio of 0.17 was obtained for guinea pig superior mesenteric artery under control conditions (Table A1). As shown, in the presence of 1.0 mM Ba^{2+}, which depresses PK, the P_{Na}/P_k ratio became 0.42.

When the curve was extrapolated to zero potential, it gave an estimated *intracellular K^+ concentration* $(K^+)_o$ of 160 mM, a value similar to that obtained for cardiac and skeletal muscles (Fig. A2). When $(K^+)_o$ was lowered below 2 mM, the curve exhibited "fall over", i.e. the RP actually decreased rather than increased. The RP decreased to −32 mV at 0.1 mM K^+. The maximum RP of −54 mV occurred at 2.0 mM. The *fallover of the curve* probably represents the contribution of an *electrogenic pump potential* to the RP (ca 22 mV), because the Na-K pump requires K^+ binding to the outer surface, hence the pump is inhibited at low K_o. (The K_m for K^+ is usually about 2.0 mM). The RPs and input resistances (R_{in}) of several different types of VSM cells is given in Table A1 (Sperelakis and Ohya, 1995).

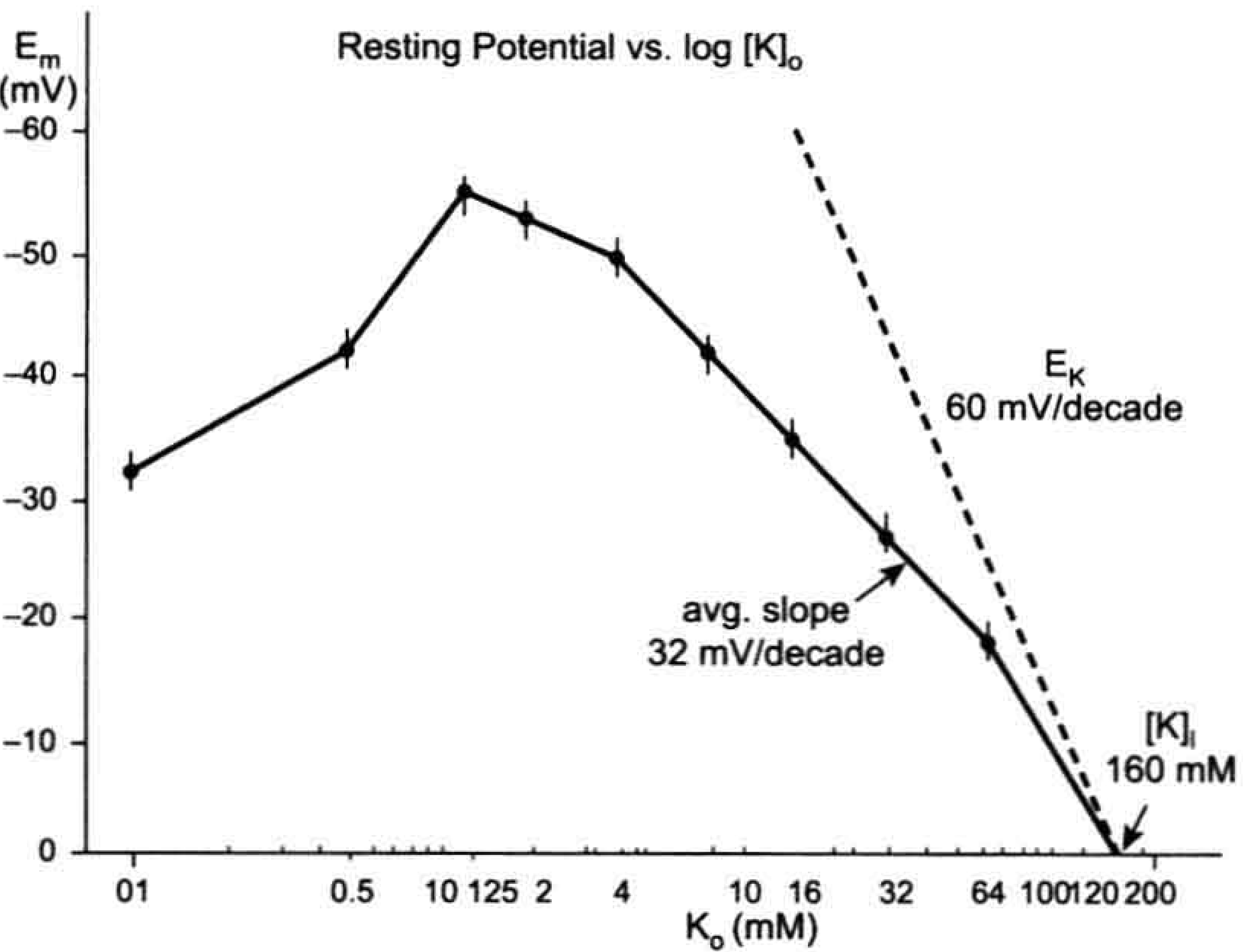


FIGURE A2 Resting potential (E_m) as a function of external K^+ concentration, $[K]_o$ on a log scale, for vascular smooth muscle of guinea pig superior mesenteric artery. The vertical bars represent the mean ±1 SEM for 10–23 impalements in 4–6 muscles. The curve extrapolated to zero potential gives an estimated internal K^+ concentration, $[K]_i$, of 160 mM. The broken line gives the K^+ equilibrium potential (EK), as calculated from the Nernst equation, and has a slope of 60 mV/10-fold change in $[K]_o$. *(From Harder and Sperelakis, 1979, with permission.)*

TABLE A1 Summary of Resting Potentials and Input Resistances of Various Vascular Smooth Muscles

Condition	Resting E_m (mV)	Input Resistance r_{in} (MΩ)	P_{Na}/P_K Ratio
Guinea Pig Superior Mesenteric Artery			
Control	−54 ± 0.6	8.5 ± 0.3	
Ouabain (10^{-5} M)[1]	−46 ± 1.0[a]		0.17
Cl^--free solution	−55 ± 0.6	8.5 ± 0.4	0.42
Ba^{2+} (1.0 mM)	−24 ± 0.8[a]	24.0 ± 1.8*	
Low Na^+ solution	−66 ± 1.3[a]		
Dog Coronary Arteries			
Dog coronary arteries	−56 ± 2	9.0 ± 0.4	
Large diameter	−53 ± 2	10.0 ± 1.0	
Small diameter	−55 ± 1.0		
Small diameter	−54 ± 1.3		

The small coronary arteries were intramural and less than 0.5 mm in diameter; the large coronary arteries were extramural and more than 1.0 mm. Measurements of E_m were made after only 1–5 min exposure to ouabain so that depolarization due to ion shifts would not occur. Data compiled from Harder et al. (1979), Belardinelli et al. (1979), Harder and Sperelakis (1979).

V. HIGH INPUT RESISTANCE AND SHORT LENGTH CONSTANT

As indicated in Table A1, the average input resistance (R_{in}) was 8.5 MOhms in the VSM of guinea pig superior mesenteric artery and 9.0 MOhms in canine coronary artery. This means that current injected intracellularly into one cell does not travel a long distance. Contrary to some reports in the literature, the length constant of intestinal smooth muscle (circular layer), when measured properly, is very short, about the length of one cell (ca 200 μm) (Barr, 1961; Sperelakis and Tarr, 1965). This indicates that there are either no or very few functioning gap-junction channels

between contiguous cells. It was proposed that the intense electric field (EF) that develops in the cell junction when the prejunctional cell fires an AP is the mechanism for the transfer of excitation from cell to cell (Sperelakis and Mann, 1977; Mann and Sperelakis, 1979; Sperelakis et al., 1989; Sperelakis and Ramasamy, 2002).

The **membrane specific resistance R_m** may be calculated from the measured parameters of input resistance (R_{in}), length constant (λ), and fiber radius (α). This was done for smooth muscle, cardiac muscle and skeletal muscle, and the results are summarized in **Table A2.** In those cases in which λ cannot be accurately measured, namely smooth muscle and cardiac muscle [because the cells are short and the end (junctional) membranes have substantial resistance], **equation 1** can be used to calculate R_m, namely the product of R_{in} and fiber membrane surface area (A_s). In the case in which λ can be accurately determined, namely in skeletal muscle (because the multinucleated fibers are very long), **equation 2** may be used to calculate R_m, namely the product of R_{in}, λ, and fiber circumference ($2\pi\alpha$ or πd, where d is the fiber diameter). There is a factor of 2 in equation 2 because the injected current (near the middle of the fiber) spreads in two directions in a long cable. r_m(in Ω-cm) is the membrane resistance of the fiber corrected for unit length (in cm), but not for unit diameter. R_m(in Ω-cm^2) is the membrane resistance corrected for both unit length and unit diameter (to give a fiber circumference of 1.0 cm ($\pi d = 1.0$ cm). The R_M value for squid giant axon is near 1,000 Ω-cm^2.

R_m is sometimes erroneously called the membrane "resistivity". However, the unit of resistivity is always in Ω-cm:

$$\rho_m = R_M/\delta$$

where ρ_m is the true membrane resistivity and δ is the membrane thickness or approximately 0.70×10^{-6} cm). Thus, membrane resistivity would be the resistance of over 10^6 cell membranes stacked in series. A preferred term for R_M is membrane specific resistance.

$$\begin{aligned} R_m &= R_{in} \times A_s \\ &= R_{in} \times \text{circ} \times L \\ &= R_{in} \times \pi\, d\, L \\ \Omega\text{-cm}^2 &= \Omega \times \text{cm} \times \text{cm} \end{aligned} \qquad \text{eq.1}$$

where d is the cell diameter and L is the cell length. If the membrane surface area is adjusted for the two cell ends (junctional membranes), assuming a corrugation factor of 2.0, then equation 1 becomes:

$$R_m = R_{in} \times (\pi dL + 2(\pi\alpha^2 \times 2.0))$$

However since adding the area of the two end membranes raises the total membrane area by less than 1% (in the case of smooth muscle), the values listed in Table A2 are without the end membranes (namely, A_s).

$$\begin{aligned} R_m &= r_m \times \pi d = (2R_{in}\lambda)\pi d \\ \Omega\text{-cm}^2 &= \Omega\text{-cm} \times \text{cm} \end{aligned} \qquad \text{eq.2}$$

R_M of skeletal muscle was also calculated using equation 1 (see Table A2). In this case, the value of A_s was approximated using the λ value, specifically $2\times\lambda$ or $3\times\lambda$. As can be seen in the table, the value of R_M obtained using $2 \times L$ was almost identical to that obtained from equation 2.

TABLE A2 Summary of Measured Parameters Used to Calculate the Membrane Specific Resistance (R_m)

	Smooth Muscle	Cardiac Muscle	Skeletal Muscle
RP (mV)	−55	−80	−79
R_{in} (M Ω)	8.5	10	0.27
λ (mm)	—	—	0.65
α (µm)	3.0	8.0	28.9
r_m (Ω-cm)	—	—	35.5×10^5
R_m (Ω-cm^2)	320	754	637 (eq 2)
			637 ($2\times\lambda$, eq 1)
			956 ($3\times\lambda$, eq 1)
Dimensions (µm)	6.0×200	16.0×150	57.8×10^4
A_s (cm^2)	3.14×10^{-5}	7.54×10^{-5}	23.6×10^{-4} (for $2 \times \lambda$)
			35.4×10^{-4} (for $3 \times \lambda$)

Smooth muscle: generalized smooth muscles
Cardiac muscle: guinea pig ventricular muscles
Skeletal muscle: mouse EDL muscle (extensor digitorum longus). Values listed were taken from Kerr & Sperelakis, 1983, listed below. The R_m value for frog sartorious muscle is considerably higher.

VI. INDUCTION OF APs BY Ba^{2+} AND TEA^+

Guinea pig superior mesenteric artery VSM cells had large RPs, e.g. −54 mV, but usually were inexcitable to electric stimulation. However, addition of agents that depress the *delayed rectifier K^+ conductance*, such as 4-aminopyridine (4-AP), 0.5 mM Ba^{2+} or 5.0 mM TEA^+ (tetraethylammonium ion) rapidly (usually within 5 min) induced APs, undershooting (Ba^{2+}) or overshooting (TEA^+) to ca +5 mV (Fig. A3). The degree of overshoot could be increased by *elevating the external Ca^{2+}* concentration from the standard 1.8 mM to 4.8 mM (Fig. A3). Thus, the inward current for these TEA-induced APs is carried by

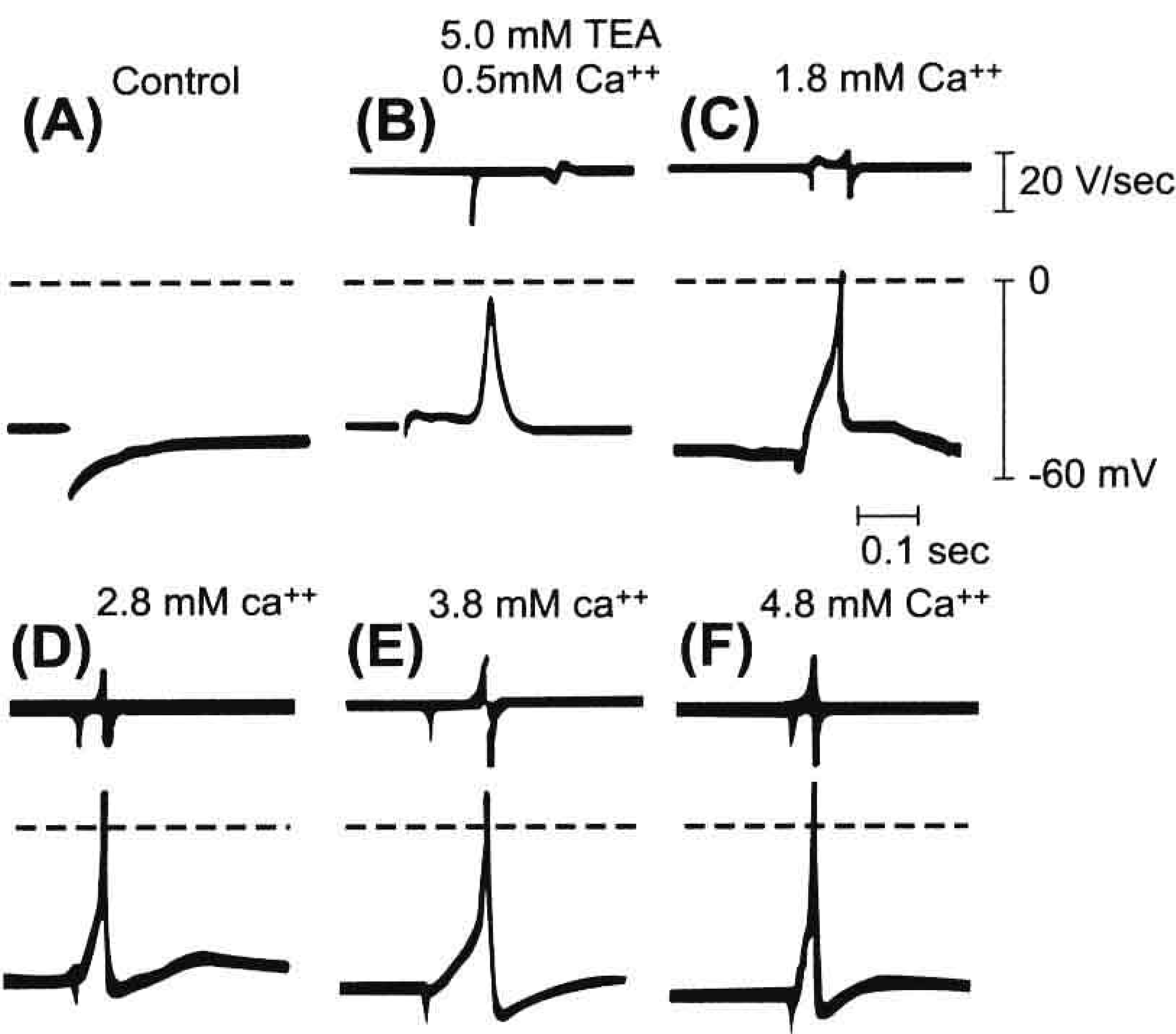


FIGURE A3 Ca^{2+}-dependency of stimulated action potentials (APs) in the presence of TEA^+ in normally inexcitable vascular smooth muscle from guinea pig superior mesenteric artery. All records were taken from one impalement. (A) Control record showing a large RP of −58 mV and lack of spontaneous APs or responses to intense external electrical stimulation (one shock artifact depicted). (B–F) Production of APs (in response to electrical stimulation) after addition of 5 mM TEA, illustrating an increase in amplitude and maximal rate of rise (*dV/dt* max) of APs as $[Ca]_o$ is increased from 0.5 mM (B) to 1.8 mM (C), 2.8 mM (D), 3.8 mM (E) and 4.8 mM (F). The upper trace in (B–F) gives *dV/dt*, the maximal deflection of which is proportional to *dV/dt* max. The horizontal broken line gives the zero potential level. *(Taken from Harder and Sperelakis, 1979, with permission.)*

TABLE A3 Summary of Resting Potentials and Action Potentials of Several Vascular Smooth Muscles

Parameter	Canine Coronary Artery Small Diameter	Canine Coronary Artery Large Diameter	Guinea Pig Superior Mesenteric Artery
Resting E_m (mV)	−53 ± 2	−56 ± 2	−54 ± 1.3
Amplitude of TEA-induced action potentials (mV)	54 ± 1	56 ± 1	59 ± 1
Max *dV/dt* (V/s)	6 ± 1	5 ± 1	6 ± 0.7
Ca^{2+} dependency (mV/decade)	31	30	29

The data are given as the mean ± SE. The duration (at 50% repolarization) of the spikes in the guinea pig was 50–75 ms. From Harder and Speralakis (1979) and Harder and Speralakis (1978), with permission.

Ca^{2+} ions through the voltage-dependent slow L-type Ca^{2+} channels (Ca_L channels). A plot of AP amplitude as a function of the Ca^{2+} concentration (on a log scale), gave a slope of about 30 mV/decade (Table A3) (Sperelakis and Ohya, 1995). A slope of ca 30 mV/decade is what is predicted from the Nernst equation if the divalent cation Ca^{2+} were the sole carrier of the inward current during the rising phase of the AP. These Ca^{2+}-dependent APs could be blocked by Ca channel blockers, such as Mn^{2+} ions and verapamil.

VII. ENHANCEMENT OF THE TEA-INDUCED APs

As stated previously above, many VSM cells do not produce APs in response to electrical stimulation. It appeared that the kinetics of the delayed rectifier K^+ channel conductance is too fast to allow an AP to be elicited. Therefore, an agent, such as TEA^+, is added partially to inhibit and slow this K^+ conductance. The following two studies were carried out in the presence of 10 mM or 5 mM TEA^+, respectively.

The 10 mM TEA-induced APs in cultured VSM cells isolated from rat aorta had overshooting spikes with a pronounced plateau that lasted ca 5 s (Johns and Sperelakis, 1982). Addition of 1.0×10^{-9} M angiotensin-II, a very potent vasoconstrictor, progressively prolonged the plateau component, beginning at ca 5 min and lasting more than 60 min (Fig. A4). At 60 min, the plateau duration was ca 20 s. The spike component did not appear to be affected.

The effect of the cardiac glycoside digoxin was examined on the 5 mM TEA-induced APs of isolated small (ca 0.5 mm) canine coronary arteries (Belardinelli et al., 1979) (Fig. A5). It was found that the amplitude and maximum rate of rise (max *dV/dt*) was greatly enhanced very quickly (ca 2 min). The effects were first noted at 4.0×10^{-9} M and were very prominent at 1.0×10^{-8} M and more-so at 1.0×10^{-7} M. But at higher concentrations, the effects became diminished. This

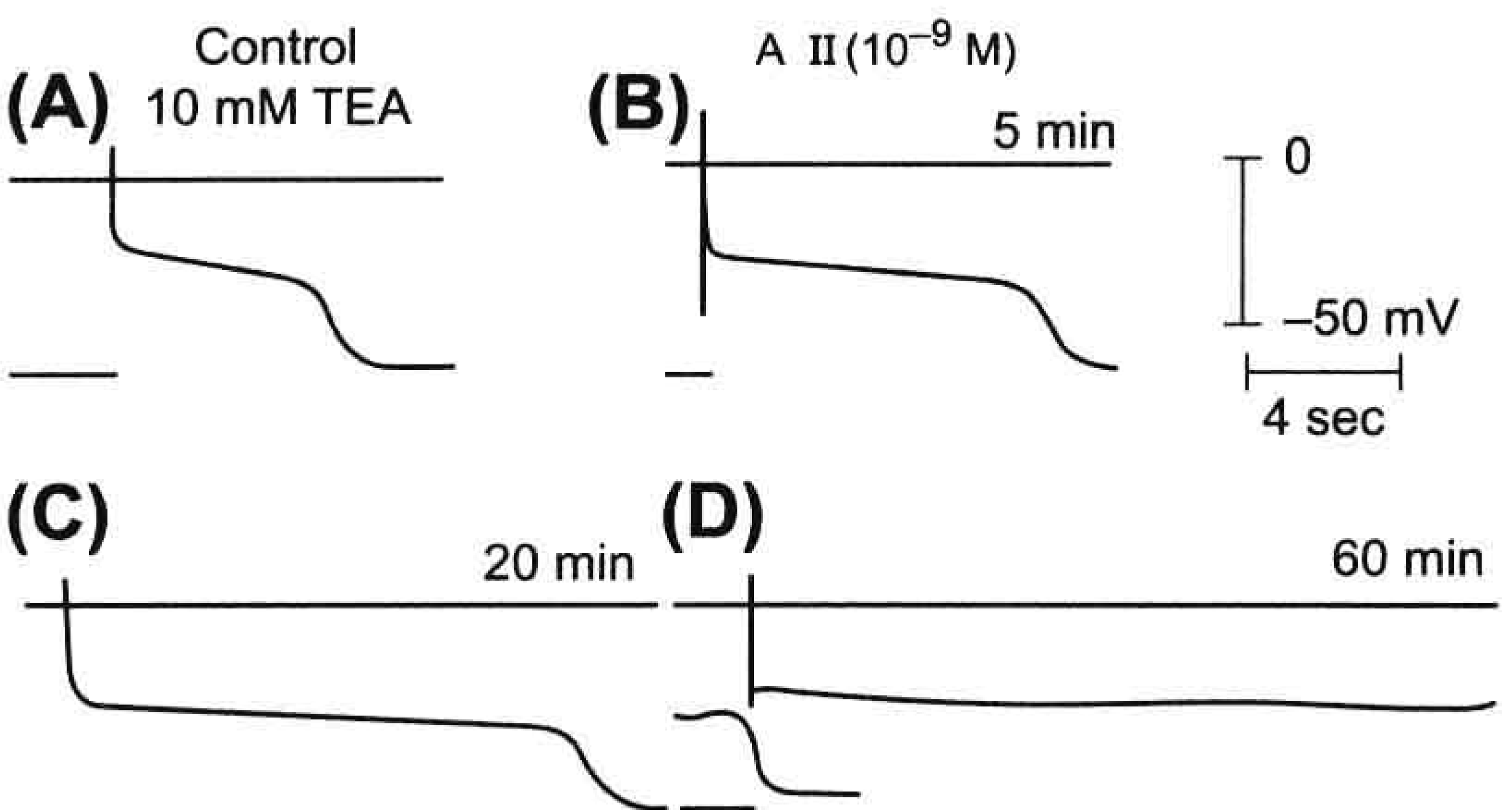


FIGURE A4 Effect of angiotensin (A-II) on the TEA-induced action potential (AP) in a cultured smooth muscle cell from rat aorta. (A) Control AP induced by electrical stimulation in the presence of 10 mM TEA. (B–D) Addition of 10^{-9} M A-II progressively increased the AP duration at 5 min (B), 20 min (C) and 60 min (D). All records were from the same impalement. *(Taken from Johns and Sperelakis, 1982, with permission.)*

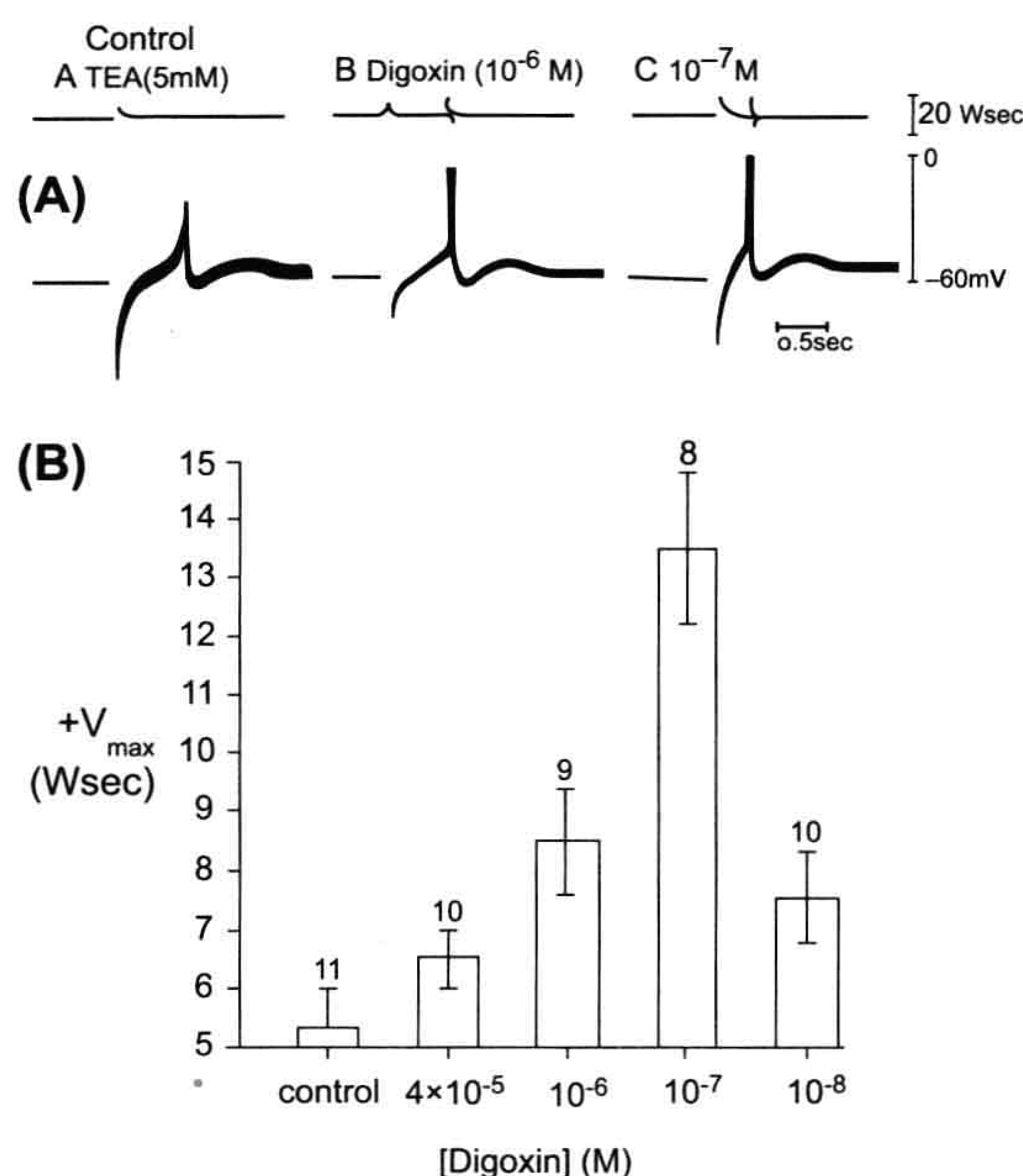


FIGURE A5 (A) Illustration of potentiating effect of digoxin on the amplitude and maximal rate of rise of the action potential (AP). (A) Elicitation of an undershooting AP by electrical stimulation in the presence of TEA (5 mM). (B,C) Records from same cell as in (A) taken within 2 min after the addition of 10^{-8} M (B) and 10^{-7} M (C) digoxin, showing a marked increase in the amplitude and maximal rate of rise of the APs. Upper trace gives *dV/dt*. (B) Summary of data demonstrating the dose-dependency of digoxin on the maximal rate of rise of the AP. The tissue was bathed in 5 mM TEA to allow the elicitation of APs. Each bar gives the mean ± SE for the number of cells impaled (indicated by the number over the bars) in 3–6 coronary arteries. Significant increases in both maximal rate of rise and amplitude occurred at 10^{-8} M and the peak effect occurred at 10^{-7} M. At higher doses of digoxin (10^{-6} M), there was a significant decrease in the maximal rate of rise and amplitude. *(Taken from Belardinelli et al., 1979, with permission.)*

very peculiar action may be involved in some of the toxic side effects of cardiac glycosides.

VIII. EXCITATORY JUNCTION POTENTIALS SOMETIMES GIVE RISE TO APs: ANALOGY WITH SLOW FIBERS OF SKELETAL MUSCLE

The ability of *excitatory junction potentials* (EJPs) to trigger APs in the VSM cells of isolated guinea pig superior mesenteric artery was examined (Ishikawa and Sperelakis, 1987). Repetitive nerve stimulation (rectangular pulses 30 μs in duration and 30 V in amplitude) was applied at a frequency of 1.0 Hz for a total of 11 pulses. Each elicited EJP was about 0.5 s in duration (total) and the amplitude of the EJPs varied between ca 3 mV (first one) and ca 8 mV (last one of train of 11) (Fig. A6). That is, the EJPs exhibited *facilitation*. These EJPs, considered "fast", are produced by ATP, the co-transmitter released with norepinephrine (NE) from the nerve terminals. The ion channel that opens up to produce the fast EJP is a *non-selective cation channel* that allows *both Na^+ and Ca^{++} to enter*, thus producing the depolarizing EJP (Zelcer and Sperelakis, 1982).

In some VSMs, e.g. rabbit ear artery, there are *"slow" EJPS* in addition to the fast EJPs. A slow EJP builds up in amplitude during a short train of stimulations. The slow EJPs are *blocked by NE receptor blockers*, such as phentolamine (an α-adrenergic receptor antagonist). In some cases, the slow EJP emerges out of the declining phase of the fast EJP, but is less than half the amplitude of the fast EJP.

As stated above, a fast EJP often triggers an AP. But even if an AP is not elicited, the small depolarization (e.g. ca 8 mV) produced by the EJP itself is sufficient to bring about some Ca^{2+} influx to raise the *level of tone* of the VSM cell. This would be somewhat analogous to the *slow skeletal muscle fibers*, in which a series of motor end-plates, each producing a localized *end-plate potential* (EPP), brings about a slow contraction of the entire fiber (see Chapter 42). That is, the slow fibers do not normally produce APs.

IX. ELECTRICAL EQUIVALENT CIRCUIT FOR VSM CELLS

The electrical equivalent circuit for arterial VSM cells is given in Fig. A7. Only some of the types of ion channels are depicted. For example, the *fast Na^+ channels* that are found in only some SMCs (see above) are not depicted. Likewise, the *K_{ATP} channels*, discussed above, are not presented. Also not depicted are the *T-type* (or fast transient type) Ca^{2+} channels that have been reported to be present in some VSM cells and in some myocardial cells. Finally, there are several types of *receptor-operated channels* (ROCs) that are not shown. One of these is an ROC that is *non-selective for cations*, allowing Na^+, K^+ and Ca^{2+} to pass through. This channel is activated by *norepinephrine* (NE) and is responsible for the genesis of the depolarizing *excitatory junction potential* (EJP) or *excitatory postsynaptic potential* (EPSP) when the sympathetic nerves are active (see above). There is also an NE-activated ROC, specific for Ca^{2+} ions, that is an important source of Ca^{2+} for contraction. Another NE-activated ROC stimulates *phospholipase C*, via a G-protein, to generate *inositol trisphosphate* (IP_3) and diacylglycerol (DG). The IP_3 acts on the SR to release Ca^{2+}. For more details, please refer to Sperelakis and Ohya (1995).

In Fig. A7, the *conductance pathways* are depicted for both the *resting membrane* (g_K, g_{Na}, g_{Ca} and g_{Cl}) and the *excited membrane* (g'_{Ca}, g'_K, $g_{K(Ca)}$). The arrow through any resistance (excited membrane) means that the *resistance varies with voltage and time*. The $g_{K(Ca)}$ conductance varies

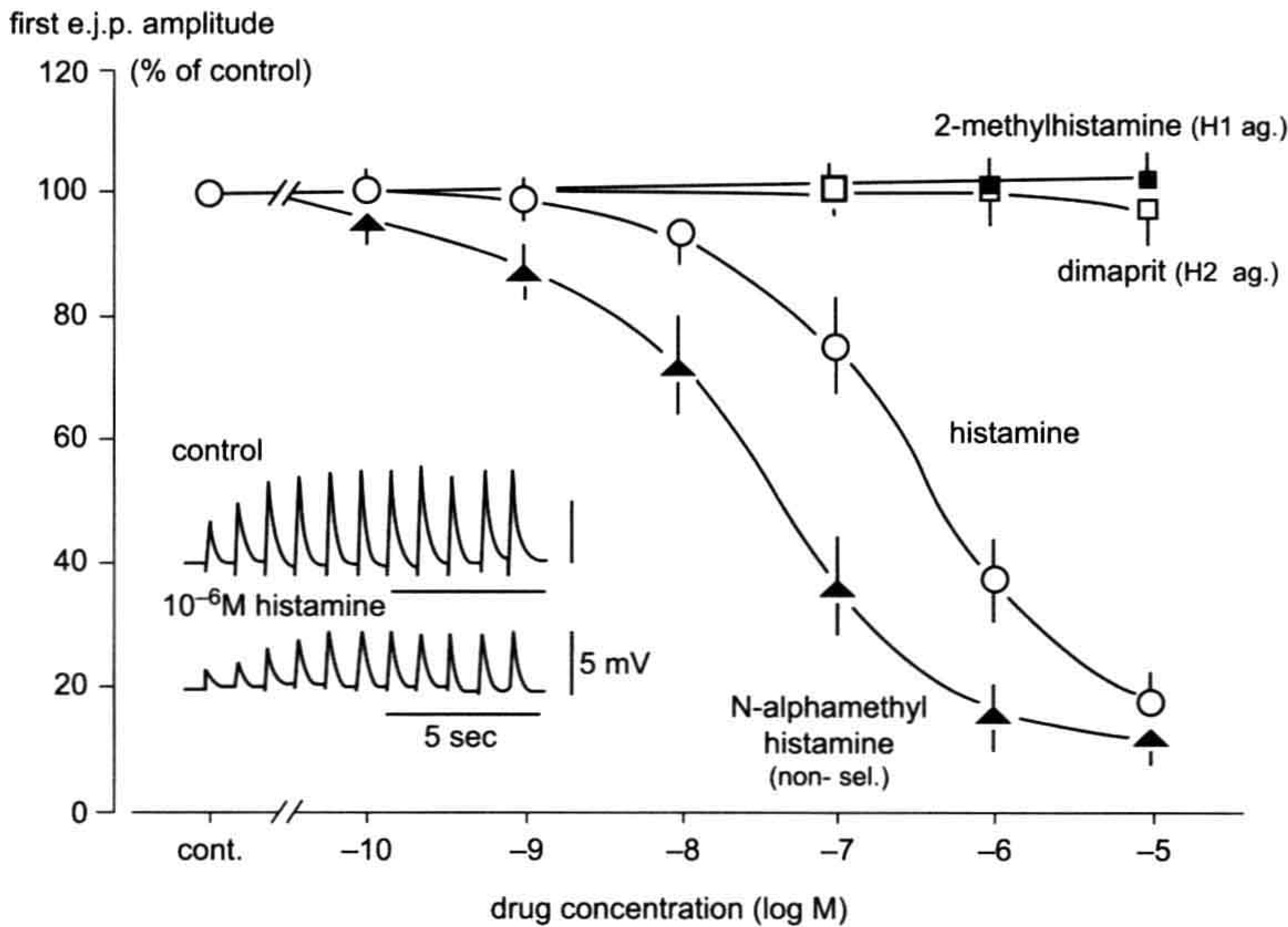


FIGURE A6 Concentration–response curves for the effects of four histamine receptor agonists on neurotransmission in the guinea pig mesenteric artery. The amplitude of the first EJP in a train of stimuli was expressed as a percentage of that in the control. The EJPs were recorded 5–10 min after application of each agonist. The inset shows the inhibitory effect of histamine on the EJPs. The histamine-induced depression of EJP amplitude was not mimicked by 2-methylhistamine (H1 agonist) or dimaprit (H2 agonist). Therefore, it appears that histamine is acting on the H3 receptor. A non-selective histamine derivative, N-α-methyl histamine mimicked the histamine depression with about a 10-fold higher potency than histamine itself. *(Taken from Ishikawa and Sperelakis, 1987, with permission.)*

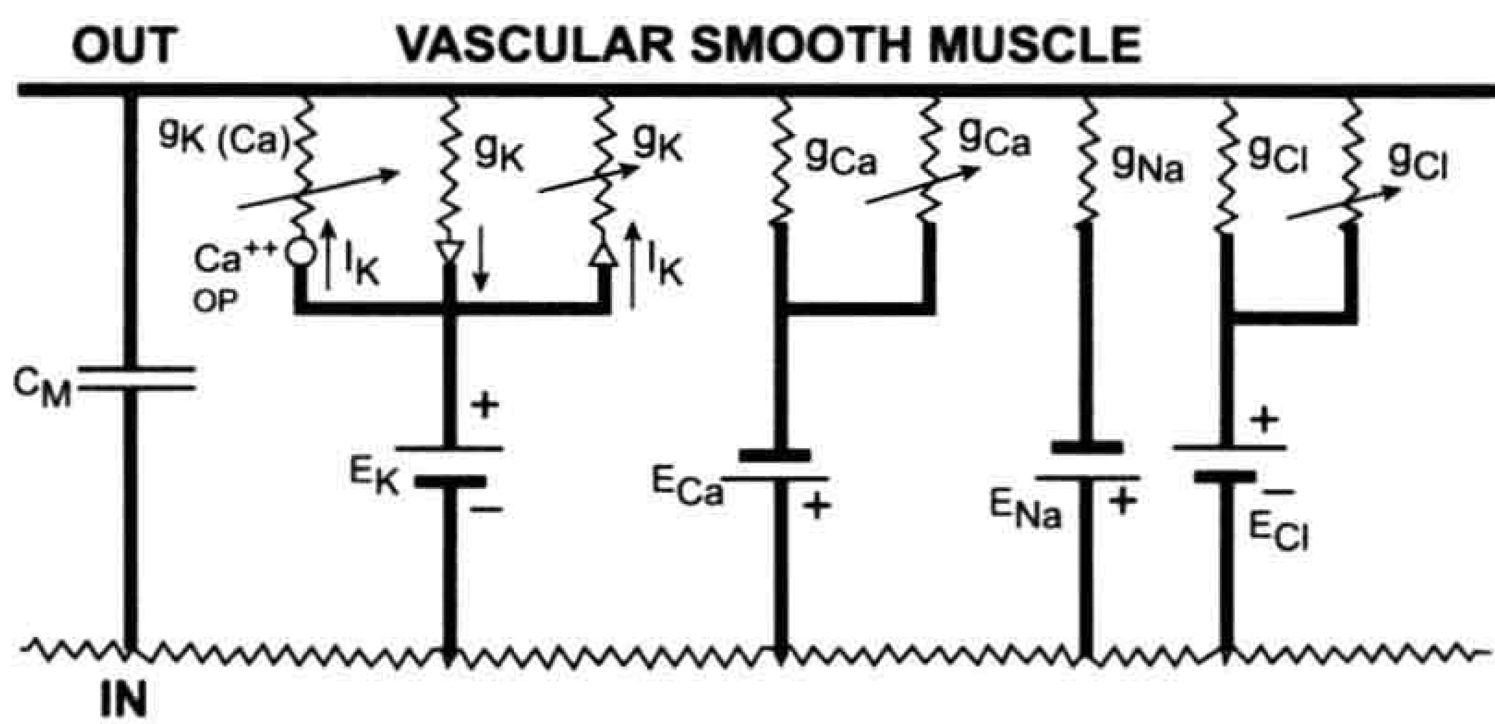


FIGURE A7 Electrical equivalent circuit for the cell membrane of arterial vascular smooth muscle cells. The conductance pathways (channels) are shown both for the resting membrane (g_K, g_{Na}, g_{Ca} and g_{Cl}) and for the excited membrane (g'_{Ca}, g'_K, $g_{K(Ca)}$). The arrow through the resistances (for the excited membrane) represents the fact that the conductance varies with the membrane potential and time, i.e. these are voltage-dependent conductances. $g_{K(Ca)}$ is intracellular Ca^{2+} dependent and voltage dependent, but not time dependent. The equilibrium potentials for the four major ions of concern (E_K, E_{Na}, E_{Ca} and E_{Cl}), as calculated from the Nernst equation for the known ion distributions, are depicted as batteries of differing polarities and magnitudes, as indicated. Ca^{2+} antagonists block the Ca^{2+} channels, whereas TEA^+ and Ba^{2+} block the resting K^+ channels (depress g_K) and depress the kinetics of activation of g_K. One type of voltage-dependent K^+ channel (Ca^{2+} insensitive) allows K^+ to pass more readily outward (outwardly directed rectification or delayed rectification). The AP rising velocity and overshoot is determined by the inward Ca^{2+} current carried through the Ca^{2+} channels. The repolarization of the AP is brought about by a sharp, large increase in g_K and $g_{K(Ca)}$, which are activated by the depolarization and intracellular Ca^{2+}. Inexcitability may be produced when $g_K + g_{K(Ca)}$ is too high. *(Taken from Sperelakis and Ohya, 1995, with permission.)*

with intracellular *free* Ca^{2+} concentration and voltage. The *equilibrium potentials* for the four major ions, as calculated from the Nernst equation, are depicted as batteries, and are in the *polarity* determined by the direction of the concentration gradients. Please refer to the chapters on electrogenesis of the RP and APs for additional information.

The APs, either natural or induced by TEA^+ (partially to suppress the g_K activation), are generally produced by an inward Ca^{2+} current through V-dependent *slow (L-type)* Ca^{2+} *channels* (Ca_L channels). *Repolarization* of the AP is brought about by two major mechanisms. The first is by a sharp, large *increase in* K^+ *conductance* activated by the depolarization, i.e. the V-dependent K^+ channels (Kv) are activated. The second mechanism is by the increase in Ca^{2+} concentration (produced by the large Ca^{2+} influx through the Ca_L channels) that activates the K_{Ca} channel (or $g_{K(Ca)}$ channel).

Nicholas Sperelakis

BIBLIOGRAPHY

Barr, L. (1961). Transmembrane resistance of smooth muscle cells. *Am J Physiol, 200*, 1251–1255.

Belardinelli, L., Harder, D., Sperelakis, N., Rubio, R., & Berne, R. M. (1979). Cardiac glycoside stimulation of inward Ca^{2+} current in vascular smooth muscle of canine coronary artery. *J Pharmacol Exp Ther, 209*, 62–66.

Harder, D. R., & Sperelakis, N. (1978). Membrane electrical properties of vascular smooth muscle from guinea pig superior mesenteric artery. *Pflügers Arch, 378*, 111–119.

Harder, D. R., & Sperelakis, N. (1979). Action potentials in guinea pig arterial smooth muscle by tetraethylammonium. *Am J Physiol/Cell Physiol, 237*, C75–C80.

Inoue, Y., & Sperelakis, N. (1991). Gestational change in Na+ and Ca2+ channel current densities in rat myometrial smooth muscle cells. *Am J Physiol, 260*, C658–C663.

Ishikawa, S., & Sperelakis, N. (1987). A novel class (H3) of histamine receptors on perivascular nerve terminals. *Nature, 327*, 158–160.

Johns, D. W., & Sperelakis, N. (1982). Angiotensin-II depolarization of cultured vascular smooth muscle cells (abstr). *Circulation, 66*, 204.

Kerr L. M. and N. Sperelakis, Membrane alterations in skeletal muscle fibers of the dystrophic mice. *Muscle &* Nerve, 1983, pages 3–13.

Kusaka, M., & Sperelakis, N. (1994a). Fast sodium currents induced by serum in human uterine leiomyosarcoma cells. *Am J Physiol, 267*, C1288–C1294.

Kusaka, M., & Sperelakis, N. (1994b). Veratridine actions on two types of fast Na+ channels in human uterine leiomyosarcoma cells. *Eur J Pharmacol, 271*, 387–393.

Liu, H., Xiong, Z., & Sperelakis, N. (1997a). Cyclic nucleotides regulate the activity of L-type calcium channels in smooth muscle cells from rat portal vein. *J Mol Cell Cardiol, 29*, 1411–1421.

Liu, H., Li, K., & Sperelakis, N. (1997b). Tyrosine kinase inhibitor, genistein, inhibits macroscopic L-type calcium current in rat portal vein smooth muscle cells. *Can J Physiol Pharmacol, 75*, 1058–1062.

Mann, J. E., Jr., & Sperelakis, N. (1979). Further development of a model for electrical transmission between myocardial cells not connected by low-resistance pathways. *J Electrocardiol, 12*, 23–33.

Nakamura, M., Sunagawa, M., Kosugi, T., & Sperelakis, N. (2000). Actin filament disruption inhibits L-type Ca(2+) channel current in cultured vascular smooth muscle cells. *Am J Physiol Cell Physiol, 279*, C480–C487.

Ohya, Y., & Sperelakis, N. (1989a). Modulation of single slow (L-type) calcium channels by intracellular ATP in vascular smooth muscle cells. *Pflügers Arch, 414*, 257–264.

Ohya, Y., & Sperelakis, N. (1989b). ATP regulation of the slow calcium channels in vascular smooth muscle cells of guinea pig mesenteric artery. *Circ Res, 64*, 145–154.

Ousterhout, J. M., & Sperelakis, N. (1987). Cyclic nucleotides depress action potentials in cultured aortic smooth muscle cells. *Eur J Pharmacol, 144*, 7–14.

Pluja, L., Yokoshiki, H., & Sperelakis, N. (1998). Evidence for presence of ATP-sensitive K+ channels in rat colonic smooth muscle cells. *Can J Physiol Pharmacol, 76*, 1166–1170.

Prosser, C. L., & Sperelakis, N. (1956). Transmission in ganglion-free circular muscle from the cat intestine. *Am J Physiol, 187*, 536–545.

Seki, T., Yokoshiki, H., Sunagawa, M., Nakamura, M., & Sperelakis, N. (1999). Angiotensin II stimulation of Ca2+-channel current in vascular smooth muscle cells is inhibited by lavendustin-A and LY-294002. *Pflügers Arch, 437*, 317–323.

Shimamura, K., Kusaka, M., & Sperelakis, N. (1994). Protein kinase C stimulates Ca2+ current in pregnant rat myometrial cells. *Can J Physiol Pharmacol, 72*, 1304–1307.

Sperelakis, N., & Mann, J. E., Jr. (1977). Evaluation of electric field changes in the cleft between excitable cells. *J Theor Biol, 64*, 71–96.

Sperelakis, N., & Ohya, Y. (1995). Electrophysiology of vascular smooth muscle. In N. Sperelakis (Ed.), *Physiology and Pathophysiology of the Heart* (pp. 859–893). Norwell: Kluwer Academic Publishers.

Sperelakis, N., & Prosser, C. L. (1958). Mechanical and electrical activity in intestinal smooth muscle. *Am J Physiol, 196*, 850–856.

Sperelakis, N., & Ramasamy, L. (2002). Modeling electric field transfer of excitation at cell junctions. *IEEE Eng Med Biol Mag, 21*, 130–143.

Sperelakis, N., & Tarr, M. (1965). Weak electronic interaction between neighboring visceral smooth muscle cells. *Am J Physiol, 208*, 737–747.

Sperelakis, N., Inoue, Y., Nozaki, M., & Ishikawa, S. (1989). Neuromuscular transmission at adrenergic nerve terminals with vascular smooth muscle in guinea-pig mesenteric artery. In N. Sperelakis, & H. Kuriyama (Eds.), *Electrophysiology and Ion Channels of Vascular Smooth Muscle and Endothelial Cells* (pp. 3–15). New York: Elsevier.

Sperelakis, N., Inoue, Y., & Ohya, Y. (1992). Fast Na+ channels in smooth muscle from pregnant rat uterus. *Can J Physiol Pharmacol, 70*, 491–500.

Sperelakis, N., Xiong, Z., Haddad, G., & Masuda, H. (1993). Regulation of slow calcium channels of myocardial cells and vascular smooth muscle cells by cyclic nucleotides and phosphorylation. *Review. Mol Cell Biochem, 140*, 103–117.

Sperelakis, N., Tohse, N., Ohya, Y., & Masuda, H. (1994). Cyclic GMP regulation of calcium slow channels in cardiac muscle and vascular smooth muscle cells. *Review. Adv Pharmacol, 26*, 217–252.

Sunagawa, M., Yokoshiki, H., Seki, T., & Sperelakis, N. (1998). Intracellular application of calmidazolium increases Ca2+ current through activation of protein kinase A in cultured vascular smooth muscle cells. *J Vasc Res, 35*, 303–309.

Xiong, Z., & Sperelakis, N. (1995). Regulation of L-type calcium channels of vascular smooth muscle cells. *Review. J Mol Cell Cardiol, 27*, 75–91.

Xiong, Z., Sperelakis, N., & Fenoglio-Preiser, C. (1994). Regulation of L-type calcium channels by cyclic nucleotides and phosphorylation in smooth muscle cells from rabbit portal vein. *J Vasc Res, 31*, 271–279.

Xiong, Z., Sperelakis, N., Noffsinger, A., & Fenoglio-Preiser, C. (1993). Fast Na+ current in circular smooth muscle cells of the large intestine. *Pflügers Arch, 423*, 485–491.

Xiong, Z., Sperelakis, N., Noffsinger, A., & Fenoglio-Preiser, C. (1995a). Ca2+ currents in human colonic smooth muscle cells. *Am J Physiol, 269*, G378–G385.

Xiong, Z., Sperelakis, N., Noffsinger, A., & Fenoglio-Preiser, C. (1995b). Potassium currents in rat colonic smooth muscle cells and changes during development and aging. *Pflügers Arch, 430*, 563–572.

Yokoshiki, H., Katsube, Y., Sunagawa, M., & Sperelakis, N. (1997a). Levosimendan, a novel Ca2+ sensitizer, activates the glibenclamide-sensitive K+ channel in rat arterial myocytes. *Eur J Pharmacol, 333*, 249–259.

Yokoshiki, H., Katsube, Y., & Sperelakis, N. (1997b). Regulation of Ca2+ channel currents by intracellular ATP in smooth muscle cells of rat mesenteric artery. *Am J Physiol, 272*, H814–H819.

Zelcer, E., & Sperelakis, N. (1982). Spontaneous electrical activity in pressurized small mesenteric arteries in hypertensive rats. *Blood Vessels, 19*, 301–310.

Index

A

D

H

I

J

K

L

M

N

Q

R

S

T

U

V

W

X

Z